ICENS

5TH INTERNATIONAL CONFERENCE ON ENGINEERING AND NATURAL SCIENCES

BOOK OF PROCEEDINGS 2019

www.icens.eu

June 12-16 2019 Prague

Organized by

Partners

PROCEEDINGS OF THE
5th INTERNATIONAL CONFERENCE ON ENGINEERING AND NATURAL SCIENCES (ICENS)

12-16 JUNE 2019, PRAGUE, CZECH REPUBLIC

SCIENTIFIC COMMITTEE

1. Prof. Dr. Adisa Parić - University of Sarajevo - Bosnia and Herzegovina
2. Prof. Dr. Ahmet Doğan – Yıldız Technical University - Turkey
3. Prof. Dr. Aleksandar Dimitrov - Ss. Cyril and Methodius University - Macedonia
4. Prof. Dr. Alexander Golub - National University of Kyiv-Mohyla Academy - Ukraine
5. Prof. Dr. Alexander Litvinenko - National University of Food Technologies (Kyiv) - Ukraine
6. Prof. Dr. Anita Grozdanov - Ss. Cyril and Methodius University - Macedonia
7. Prof. Dr. Arslan Saral – Yıldız Technical University - Turkey
8. Prof. Dr. Asif Šabanović – International University of Sarajevo - Bosnia and Herzegovina
9. Prof. Dr. Bekir Erol Ak - Harran University - Turkey
10. Prof. Dr. Cem Şensöğüt - Dumlupınar University - Turkey
11. Prof. Dr. Christos Douligeris - University of Erlangen-Nurnberg - Germany
12. Prof. Dr. Dragutin T. Mihailović - University of Novi Sad - Serbia
13. Prof. Dr. Evgeniy Shtefan - National University of Food Technologies (Kyiv) - Ukraine
14. Prof. Dr. Falko Dressler - University of Paderborn - Germany
15. Prof. Dr. Harry Miller – International University of Sarajevo - Bosnia and Herzegovina
16. Prof. Dr. Houssam Toutanji – Western Michigan University - USA
17. Prof. Dr. Ian F. Akyıldız – Georgia Institute of Technology - USA
18. Prof. Dr. İsmail Usta - Marmara University - Turkey
19. Prof. Dr. Kateryna Derevska - National University of Kyiv-Mohyla Academy - Ukraine
20. Prof. Dr. Liljana Gavrilovska - Ss Cyril and Methodius University - Macedonia
21. Prof. Dr. Lukman Thalib - Qatar University - Qatar
22. Prof. Dr. M. Asghar Fazel – University of Environment - Iran
23. Prof. Dr. Mikhailov Volodymyr - Taras Shevchenko National University of Kyiv - Ukraine
24. Prof. Dr. Mykola Glybovets - National University of Kyiv-Mohyla Academy - Ukraine
25. Prof. Dr. Muammer Koç - Hamad bin Khalifa University - Qatar
26. Prof. Dr. Nadia Bilko - National University of Kyiv-Mohyla Academy - Ukraine
27. Prof. Dr. Özer Çınar – Yıldız Technical University - Turkey
28. Prof. Dr. Perica Paunovik - Ss. Cyril and Methodius University - Macedonia
29. Prof. Dr. Rifat Škrijelj – University of Sarajevo - Bosnia and Herzegovina
30. Prof. Dr. Samir Đug - University of Sarajevo - Bosnia and Herzegovina
31. Prof. Dr. Tanju Karanfil – Clemson University - USA
32. Prof. Dr. Ümit Alver – Karadeniz Technical University - Turkey
33. Prof. Dr. Wolfgang Gerstacker - University of Erlangen-Nurnberg - Germany
34. Prof. Dr. Vladyslav Sukhenko - National University of Life and Environmental Sciences of Ukraine (Kyiv) - Ukraine
35. Prof. Dr. Yılmaz Yıldırım - Bülent Ecevit University - Turkey
36. Prof. Dr. Yousef Haik - Hamad bin Khalifa University - Qatar
37. Assoc. Prof. Dr. Alaa Al Hawari - Qatar University - Qatar
38. Assoc. Prof. Dr. Fatih Ungan - Cumhuriyet University - Turkey
39. Assoc. Prof. Dr. Izudin Dzafic - International University of Sarajevo - Bosnia and Herzegovina
40. Assoc. Prof. Dr. Kateryna Syera - National University of Life and Environmental Sciences of Ukraine (Kyiv) - Ukraine
41. Assist. Prof. Dr. Muhamed Hadziabdic - International University of Sarajevo - Bosnia and Herzegovina
42. Assoc. Prof. Dr. Nusret Drešković - University of Sarajevo - Bosnia and Herzegovina
43. Assoc. Prof. Dr. Polina Vakuliuk - National University of Kyiv-Mohyla Academy - Ukraine
44. Assoc. Prof. Dr. Senija Tahirovic - International University of Sarajevo - Bosnia and Herzegovina
45. Assoc. Prof. Dr. Victor Karamushka - National University of Kyiv-Mohyla Academy - Ukraine
46. Assoc. Prof. Dr. Victoria Konovalova - National University of Kyiv-Mohyla Academy - Ukraine
47. Assoc. Prof. Dr. Yuriy Kravchenko - National University of Life and Environmental Sciences of Ukraine (Kyiv) - Ukraine
48. Assist. Prof. Dr. Fatih Taktak - Uşak University - Turkey
49. Assist. Prof. Dr. Fouzi Tabet - German Biomass Research Center - Germany
50. Assist. Prof. Dr. Haris Gavranovic - International University of Sarajevo - Bosnia and Herzegovina
51. Assist. Prof. Dr. Sasan Rabieh - Shahid Beheshti University - Iran
52. Assist. Prof. Dr. Ševkija Okerić - University of Sarajevo - Bosnia and Herzegovina
53. Dr. Zsolt Hetesi - National University of Public Service, Budapest - Hungary
54. Dr. Zsolt T. Németh - National University of Public Service, Budapest - Hungary

ORGANIZATION COMMITTEE

Chairman of the Conference

Prof. Dr. Özer Çınar – Yıldız Technical University

Members of the Committee

Prof. Dr. Ümit Alver (Co-Chairman) - Karadeniz Technical University - Turkey
Prof. Dr. Mikhailov Volodymyr - Taras Shevchenko National University of Kyiv - Ukraine
Assoc. Prof. Dr. Kateryna Syera - National University of Life and Environmental Sciences of Ukraine (Kiev) - Ukraine
Assoc. Prof. Dr. Lukman Thalib - Qatar University - Qatar
Assoc. Prof. Dr. Yuriy Kravchenko - National University of Life and Environmental Sciences of Ukraine (Kiev) - Ukraine
Assist. Prof. Dr. Sasan Rabieh - Shahid Beheshti University - Iran
Alma Ligata - Zenith Group - Bosnia and Herzegovina
Ismet Uzun - Zenith Group - Bosnia and Herzegovina
Musa Kose - Zenith Group - Bosnia and Herzegovina

WELCOME TO ICENS 2019

On behalf of the organizing committee, we are pleased to announce that the 5th International Conference on Engineering and Natural Sciences (ICENS 2019) will be held from June 12 to 16, 2019 in Prague, Czech Republic. ICENS 2019 provides an ideal academic platform for researchers to present the latest research findings and describe emerging technologies, and directions in Engineering and Natural Sciences issues. The conference seeks to contribute to presenting novel research results in all aspects of Engineering and Natural Sciences.

The conference aims to bring together leading academic scientists, researchers and research scholars to exchange and share their experiences and research results about all aspects of Engineering and Natural Sciences. It also provides the premier interdisciplinary forum for scientists, engineers, and practitioners to present their latest research results, ideas, developments, and applications in all areas of Engineering and Natural Sciences. The conference will bring together leading academic scientists, researchers and scholars in the domain of interest from around the world.

The scientific program will focus on current advances in the research, production and use of Engineering and Natural Sciences with particular focus on their role in maintaining academic level in Engineering and Applied Sciences and elevating the science level.

The conference's goal will to provide a scientific forum for all international prestige scholars around the world and enable the interactive exchange of state-of-the-art knowledge. The conference will focus on evidence-based benefits proven in clinical trials and scientific experiments.

Best regards,

Prof. Dr.Özer ÇINAR

ICENS

5TH INTERNATIONAL CONFERENCE ON ENGINEERING AND NATURAL SCIENCE

12-16 June 2019 Prague

Determining of Fundamental Physical Properties of Various Modified Bitumen With WMA Additives

Bekir Aktas[1], Suayip Aytekin[2], Sevket Aslan[1]

Abstract

Recently, Warm Mix Asphalt (WMA) technologies have becoming important topic due to reduce mixing and compaction temperatures of the asphalt mixture in the world. Thanks to the rapidly developing WMA technologies, the economical use of limited resources is increased and environmental impacts caused by asphalt production can be reduced. In recent years, WMA has started to come to the forefront in terms of asphalt concrete manufacturing especially in countries with high energy requirements. There are studies on WMA in various countries and each country is developing WMA manufacturing procedures which vary according to their conditions. The viscosity of the bitumen used in the production of WMA is reduced and its chemical and physical properties change. In this study, the bitumen modified with 3 different WMA additives were investigated and compared with the pure bitumen in terms of the physical properties such as penetration, specific gravity, softening point, thin film oven test lost, ductility etc.

Keywords: Asphalt Concrete, Warm Mix Asphalt, Additives

1. INTRODUCTION

Asphalt coatings, bituminous hot mixtures (HMA), difficult to perform, laborious and quite expensive applications. Particularly, the energy spent during the heating of bitumen and aggregates is very high. This situation is attributed to the relatively high cost of energy-exporting countries such as Turkey. In addition to this cost, the damage caused to both the environment and the health of the employees during the production of hot mix asphalt and its application to the road is quite high.

New products have been developed to reduce the mixing and compression temperatures of the HMA without compromising the quality of the asphalt pavement. The main purpose of the production of Warm Mix Asphalt (WMA) is to reduce the high temperatures where traditional asphalt mixtures are produced and placed. Although there are many additives produced for this purpose, 3 of these additive products were used in this study.

Warm mix asphalt (WMA) technology has become more and more popular in recent years, reducing energy consumption in asphalt pavement production and its environmental advantages. Studies have shown that the performance of WMA blends has progressively improved [1], [2], [2]–[6].

The main benefits of WMA; the energy consumption required to heat the traditional HMA over 150 oC in the production unit and in the paving area, and the reduction of emissions from gases and odors of fuels burning in the unit and in the paving area, protection of worker health and opening of the road in less time [7]. With the addition of WMA additives, the viscosity of the binder is reduced; in this way, the production and compression temperatures may be lower compared to the values required for the HMA.

WMA has been accepted in at least 45 states in the United States and in many European countries. WMA currently interested in experimental projects and is in active practice in most countries. Large industrial enterprises estimate that 90% of asphalt production facilities will be built on IKA in the next 5 years [2].

---

[1] *Department of Civil Engineering, Erciyes University, Kayseri, Turkey*

[2] *Kayseri 6th Regional Directorate of the General Directorate of Highways, Turkey*

Energy savings can provide economic contributions to countries such as Turkey with energy deficit, increase the performance and lifespan of the pavemen, will minimize reconstruction, maintenance and repair costs. The most important advantage of all these is that it provides much less gas emissions. In 2012, a thesis study in Connecticut, USA, evaluated the suitability of WMA use for these state roads [7].

In this study, 3 different WMA additives were added to 50/70 penetrated bitumen by taking into consideration the suggestions of the manufacturer and the properties of the modified bitumen were compared with the properties of pure bitumen.

2. DIFFERENT WMA ADDITIVES AND CLASSIFICATION

Basically, asphalt additives are considered as three types. These are: organic additives, foam additives and chemical additives [9]. The classes of WMA additives are shown in Table 1.

Table 1. IKA Additive Classes [8]

WMA Additive Type	Various WMA Additives	Company	Definition	Decrease in Production Temperature (° C)
Organic Additives	Asphaltan-B	Romonta GmbH	Refined Montan waxy fatty acid	(20-30 °C)
	Sasobit	Sasol	Fischer-Tropsch waxes	(20-30 °C)
	Licomont BS100	Clariant	Fatty acid amide	(20-30 °C)
WAM-Foam Additives	Plentte Su Enjeksiyonu	Kolo Veidekke ve Shell Bitumen	Bitumen water injection with nozzles	100-120 °C
	Aspha-Min	Eurovia-MHI	Water based zeolite technology	(20-30 °C)
	Advera	PQ Corporation	Water based zeolite technology	(10-30 °C)
Chemical Additives	Evotherm	Mead Westvaco	Anhydrous or aqueous chemical package	85-115 °C
	Cecabase RT	CECA	Chemical package	(30 °C)
	Rediset WMX	Akzo Nobel	Cationic surfactants	(30 °C)

The organic additives have a melting point below the conventional HMA production temperature and are used to reduce the asphalt viscosity. In combination with organic additives, the asphalt viscosity is reduced to a temperature above the melting point to produce asphalt mixtures at low temperatures. Under the melting point, organic additives tend to increase the asphalt stiffness [8].

With the application of WAM-Foam (Foam), it is aimed to reduce the viscosity of the bitumen by using bitumen foaming with water or by various additives. Water spray is foamed by injecting 2% to 5% cold water of bitumen mass at 180 ° C. That is, 0.8 kg of water is added per ton. And in this way, the viscosity of the binder is reduced.

Chemical additives are produced by different companies in many countries with the expansion of WMA production. These additives, which are produced using waste or renewable materials, are widely used in WMA production.

3. EXPERIMENTAL STUDIES

In the study, 3 different WMA additives were used and the related additives were added to the bitumen as indicated by the manufacturer. The additives used are used in the industry under the trade names PAWMA (A1), Licomont BS 100® (A2) and Evotherm M1 (A3). As the additive A1 is in liquid form, it can be directly added to the bitumen without grinding. The bitumen temperature is not changed for the mixture according to the manufacturer's catalog, but the mixture is prepared by reducing the aggregate temperature by 30 ° C. The amount of use is between 0.2% and 0.4% of the bitumen weight. It has been observed that it is extremely practical and easy to use. According to the manufacturer's catalog, the contribution of A2 is 3% of the bitumen, directly into the bitumen and mixed at 160

oC for about 40 minutes. For asphalt concrete mixture, the aggregates are heated to 150 oC and mixed with bitumen for 3-5 minutes. For the addition of A3, the manufacturer recommends that additive should be added to the bitumen at a rate of 0.4% and mixed for about half an hour before the asphalt pavement production. Since it is in liquid format, no additional modification is required in the plant during the mixing process. In preparing the aggregate and bitumen mixture, the bitumen temperature is not changed to dissolve the additive, but the aggregate temperature can be reduced by 30 ° C. This reduces the temperature of the mixture.

Specific gravity, penetration, softening point, thin film oven, elastic return and ductility tests were carried out for the pure bitumen and doped bitumen samples. The results are given separately and a comparison is made.

3.1. Laboratory Test Results

3.1.1. Bitumen Specific Gravity

The results obtained according to the specific gravity test performed in 50/70 penetration bitumen are given in Figure 1.
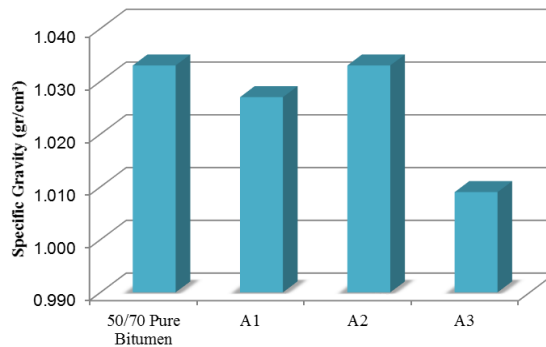
Figure 1. Bitumen Specific Gravity for WMA Additives

According to these results, it was seen that the WMA additives used reduced the bitumen specific gravity by 0.6-2.3%. The results obtained are within the limits of the Highways Specification (1 - 1.1 g / cm3).

3.1.2. Penetration

The results obtained according to the penetration test performed by adding WMA additives to 50/70 penetration bitumen are given in Figure 2.
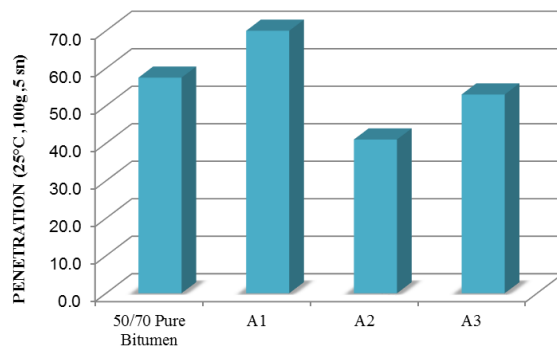
Figure 2. Bitumen Penetrations for WMA Additives

According to these results, it was seen that the WMA additives used had different effects on bitumen penetration. While A1 additive increased bitumen penetration, A2 and A3 reduced bitumen penetration. So A1 softened the bitumen, while A2 and A3 harden the bitumen. The results of the penetration results are within the limits of the Highway Specification values (50-70).

3.1.3. Softening Point

The results obtained according to the softening point test performed by adding WMA additives to 50/70 penetration bitumen are given in Figure 3.
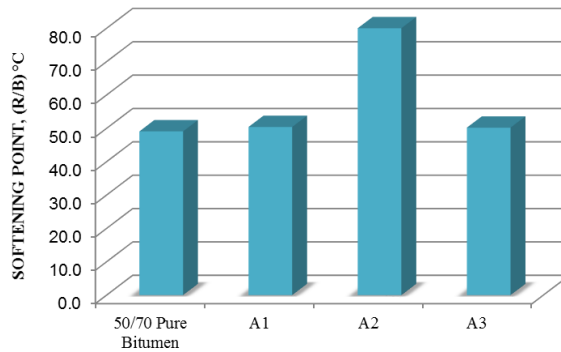
Figure 3. Bitumen Softening Points for WMA Admixtures

Bitumen with a high softening point will show less damage at the same air temperature. According to the results, A1 and A3 additives show a slight increase in softening point while A2 additive increases the softening point by approximately 30 ° C. According to these results, it is seen that especially the A2 additive will have higher resistance at high temperatures.

3.1.4. Thin film Oven Test

The results obtained according to the thin-film oven test performed by adding WMA additives to 50/70 penetration bitumen are given in Figure 4. In this experiment, the mass loss occurring on the asphalt is determined. A mass loss occurs due to aging of the bitumen.
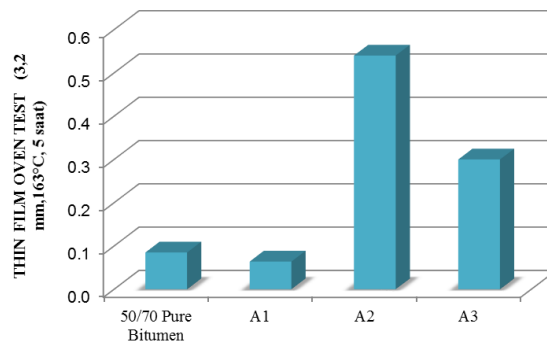
Figure 4. Thin Film Oven Test Results for WMA Additives

In the light of the results obtained, it is seen that the different types of additives used for WMA are lost after heating at different rates. According to these results, it can be said that other additives except for A1 additive increase the mass loss and thus the resistance against aging may be low. However, it is possible to say that some of the WMA additives release water to foam the bitumen and this water is known to vaporize the bitumen by temperature and this loss of water is the result of loss of water rather than aging bitumen.

3.1.5. Penetration After Thin Film Oven Test

The results obtained by the penetration test thin film oven test by adding WMA additives to 50/70 penetration bitumen are given in Figure 5.
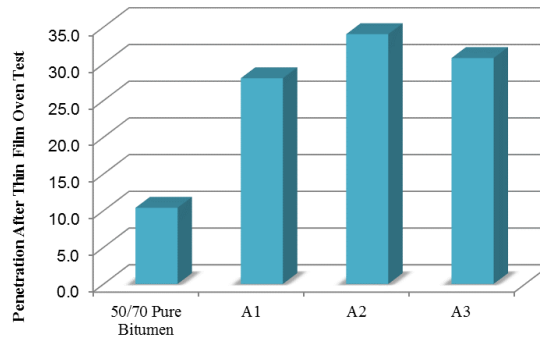
Figure 5. Penetrations after Thin Film Oven Test WMA Additives

These results showed parallel values with thin film oven test. In other words, after heating loss, the additions which have different bitumen aging rates have increased the penetration after heating loss. In other words, bitumen penetration did not decrease too much after a certain period of application in mixtures with WMA additives.

3.1.6. Softening Points Rise and Softening Points After Heating Loss

The results obtained from the softening point rise test after heating loss by adding WMA additives to 50/70 penetration bitumen are given in Figure 6.
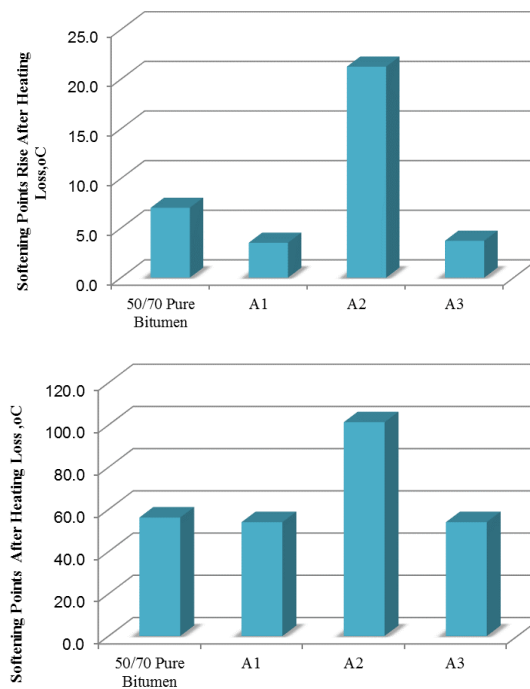
Figure 6. Softening Points (° C) and Softening Point Elevations After Heating Loss for WMA Additives (° C)

According to the results, it is seen that different kinds of additives used for WMA give softening point increases at different rates. Compared to the control sample, A1 and A3 additives caused a lesser increase in softening point,

while A3 contributed to a very high increase. According to these results, it can be said that A3 additive has higher resistance at high temperatures.

3.1.7. Ductility And Average Elastic Return

The results of the ductility and average elastic return test performed by adding WMA additives to 50/70 penetration bitumen are given in Figure 7.
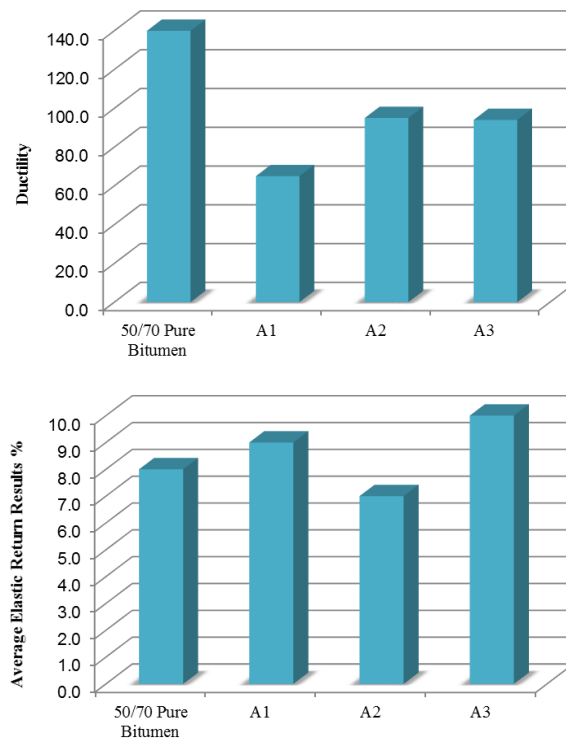
Figure 7. Ductility and Average Elastic Return Results for WM-SMA Admixtures

As ductility increases, adhesion and tensile strength are increased, heat sensitivity and shrinkage at low temperatures are reduced. When the ductility graphy is examined, it is seen that the additives used decrease the ductility value. In the results of elastic return, it is seen that WMA additives increase elastic return except A2. In particular, it is observed that the resilience of restoring the load under the load is increased, and the resilience of the additives is slightly higher in the wheel track.

4. RESULTS

In experimental studies conducted in the laboratory, 3 different WMA additives were added to the 50/70 penetration bitumen by taking into consideration the suggestions of the manufacturer and in the ratio specified in the catalogs and by using the specified method, the properties of modified bitumen were compared with the properties of pure bitumen. Each WMA additive used as a result of the modification made with WMA additives has a different effect on the bitumen properties. As a result of the bitumen experiments, it was observed that the addition of A2 decreased the penetration and increased the softening point. Furthermore, increasing the penetration of the additives used after heating loss can still provide a flexible bituminous mixture at lower temperatures. However, it is likely that the additives will reduce the ductile dust and lead to more shrinkage in cold weather. As the A1 and A3 additives increase elastic return, they will rotate more quickly under load and reduce deformations such as the wheel track.

In the study, only the standard physical properties of modified bitumen were determined and performance tests were not performed. With Superpave performance experiments, the behavior of the bitumen with different modifications, which are different in this way, can be determined at different temperatures.

REFERENCES

[1]   X. Shu, B. Huang, E. D. Shrum, and X. Jia, "Laboratory evaluation of moisture susceptibility of foamed warm mix asphalt containing high percentages of RAP," *Constr. Build. Mater.*, 2012.

[2]   Y. Kim, J. Lee, C. Baek, S. Yang, S. Kwon, and Y. Suh, "Performance evaluation of warm- and hot-mix asphalt mixtures based on laboratory and accelerated pavement tests," *Adv. Mater. Sci. Eng.*, 2012.

[3]   A. Jamshidi, M. O. Hamzah, and Z. You, "Performance of Warm Mix Asphalt containing Sasobit®: State-of-the-art," *Construction and Building Materials*. 2013.

[4]   S. Zhao, B. Huang, X. Shu, X. Jia, and M. Woods, "Laboratory Performance Evaluation of Warm Mix Asphalt containing High Percentages of RAP," *Transp. Res. Rec. J. Transp. Res. Board*, 2012.

[5]   S. Yang, J. Lee, S. Hwang, S. Kwon, and C. Baek, "Development of Warm-Mix Asphalt Additive and Evaluation of Performance," *Transp. Res. Rec. J. Transp. Res. Board*, 2012.

[6]   S. Sargand, M. D. Nazzal, A. Al-Rawashdeh, and D. Powers, "Field Evaluation of Warm-Mix Asphalt Technologies," *J. Mater. Civ. Eng.*, 2012.

[7]   A. K. Bernier, "Laboratory and Field Evaluation of Two Warm-Mix Additives in Conn," 2012.

[8]   M. Sheth, N, "Evaluation of Selected Warm Mix Asphalt," University of Iowa , Civil and Environmental Engineering, 2010.

Results of the new GPS study in the south of Izmir after the 2017 Aegean Sea Earthquakes

Ayca Cirmik[1], Oya Pamukcu[1], Baris Can Malalici[2]

Abstract

High seismic activity was observed in 2017 in the Aegean Sea which includes Izmir and its surroundings. The most important of these are the earthquakes of 12th June and 25th December 2017. On 12th June 2017, an earthquake of magnitude Ml = 6.3 (Mw = 6.2) was occurred in the Aegean Sea (offshore of Karaburun) and it was felt in a wide area. The other important earthquake was occurred on December 25th, 2017 in Izmir Bay (Aegean Sea). The magnitude of this earthquake was recorded as Ml = 4.8 (Mw = 4.6) and the earthquake was felt in Izmir province and its districts. The province of Izmir is located at the western end of the Gediz graben system, which is under the influence of the Western Anatolian extension regime. While normal faulting is observed in east-west direction in Gediz Graben, especially NE-SW, NW-SE and N-S oriented faults are located in the south of Izmir. This region differs within the graben system. The region, which has been attracting attention since the Sigacik earthquake in 2005, has been examined in detail by the Department of Geophysical Engineering of Dokuz Eylul University since 2009 using gravity and GPS methods.

In this study, new GPS measurements were performed at 6 points in the south of Izmir following the earthquakes in 2017. The measurements were carried out between 03/07/2018 and 23/07/2018 within the scope of the Dokuz Eylul University Scientific Research Project No. KB.2018.FEN.010. The new data were evaluated together with the GPS data measured at the same points in 2009-2010 and 2011. As a result of this study, the results obtained from the GPS measurements performed in 2018 were examined together with the results of the measured data in previous years.

Keywords: Izmir, GPS, Earthquake, Aegean Sea

1. INTRODUCTION

The study area has active tectonism and consequently high seismicity [1], [2]. There are 13 active faults in Izmir and its surroundings which have the potential to produce a major earthquake [3]. These are strike-slip and normal faults and are the elements of complex tectonism in the region. Almost all of the faults in the west of the Gediz graben are strike-slip faults. In addition, oblique faults are found in the region, but the dominant movement of these faults is the strike-slip component. The character and regional distribution of the faults indicate that strike-slip deformation dominates the west of the Gediz graben [3].

In 2017, 86 earthquakes occurred with magnitudes greater than 3.5 in the region (Figure 1) [4]. The most important of these earthquakes were occurred on 12th June 2017 and 25th December 2017. The magnitude of the earthquakes occurred on 12th June 2017 was M_l = 6.3 (M_w = 6.2) and occurred offshore of Karaburun in Aegean Sea. The other important earthquake occurred on in Izmir Bay, Aegean Sea with M_l = 4.8 (M_w = 4.6) magnitude. Both of them were felt in wide area, especially in Izmir province and its districts. The study region, which is very seismically active, has studied in detail with gravity and GPS measurements by the Department of Geophysical Engineering of Dokuz Eylul University since 2009.

---

[1] *Dokuz Eylul University, Engineering Faculty, Department of Geophysical Engineering, 35160, Tinaztepe Campus, Buca Izmir, Turkey. ayca.cirmik@deu.edu.tr, oya.pamukcu@deu.edu.tr*

[2] *Dokuz Eylul University, The Graduate School of Natural and Applied Sciences, 35160, Tinaztepe Campus, Buca, Izmir, TURKEY, barismalalici@gmail.com*
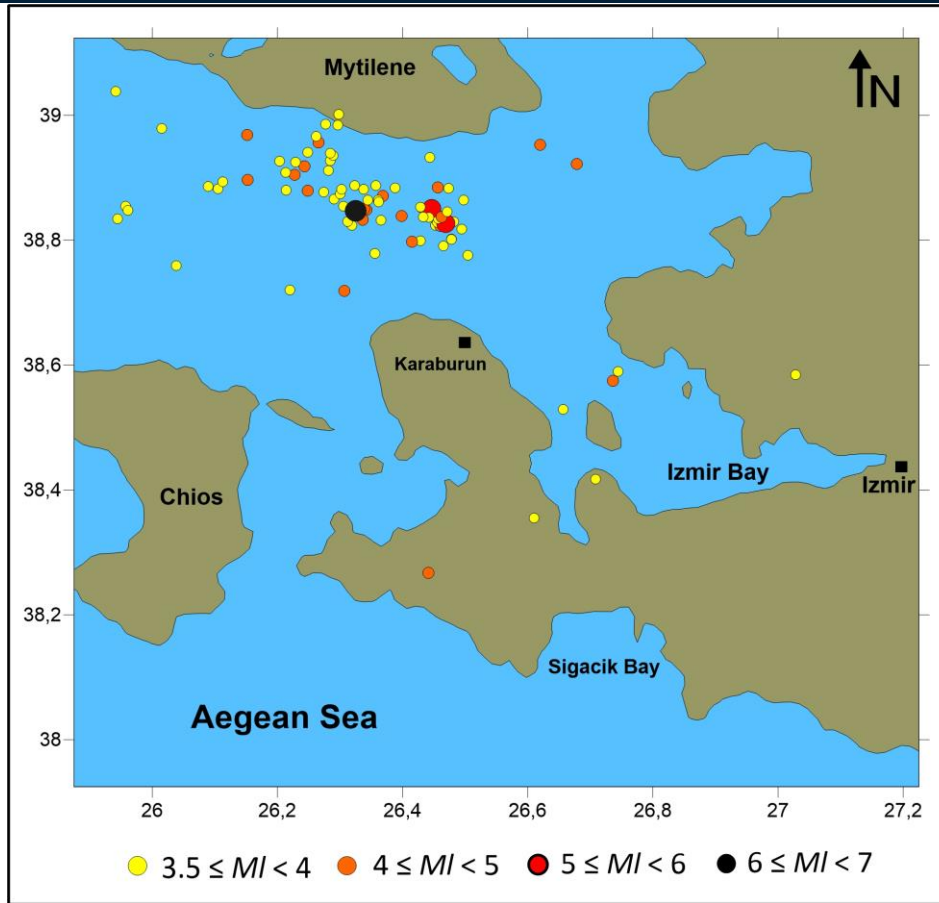
Figure 1. The epicentres of the earthquakes occurred in the study area in 2017.

In this study, the stress-strain distributions in the region were determined with GPS data. In this context, GPS measurements were obtained in 2018 at 6 points in the south of Izmir within the scope of the Dokuz Eylul University Scientific Research Project No. KB.2018.FEN.010. (Figure 2) between the days 184 and 189 (Julian days of 2018). Besides, 2 continuous GPS stations which located at Uzunada Island (Aegean Sea) and Dokuz Eylul University, Tinaztepe Campus were added to the processing. Therefore, new GPS data for 8 GPS stations were processed and combined with GPS data measured in 2009-2010 and 2011 which were obtained within the scope of the TUBITAK Project No. 108Y285). Finally, the strain analysis of the region was carried out and examined together with GPS data measured in 2009-2010 and 2011.

Figure 2. The view of one of the GPS stations of this study.

2.   APPLICATION

The GPS method is widely used in earth sciences in recent years as it offers a large scale and high resolution data set. By modelling and analyzing this data, it is possible to determine the deformation in the region. The deformation, which is the gradient of the displacement area, can be calculated by using GPS velocity vectors and provides important information about the tectonics of the region. In this study, as the first step, the GPS data of 8 GPS stations obtained in 2018 were processed with Gamit/Globk [5] software relative to Eurasia fixed frame and by using ITRF08 and 10 IGS stations as; ISTA, TUBI (Turkey), ZECK (Russia), NICO (Cyprus), MIKL, GLSV (Ukraine), BUCU (Romania), PENC (Hungary), WTZR (Germany) and MATE (Italy). The results were combined with the GPS data based on 2009-2010 and 2011 observation years and GPS velocities were obtained. Then, by using these velocities, the strain analysis was performed by using SSPX software [6] (Figure 3) for 2009-2010-2011 and 2018 observation years and compared with the strain analysis results based on the GPS velocities of 2009-2010 and 2011(Figure 4). Consequently, the extension values were calculated and the changes on the extension were examined based on the data before and after the mentioned 2017 earthquakes.
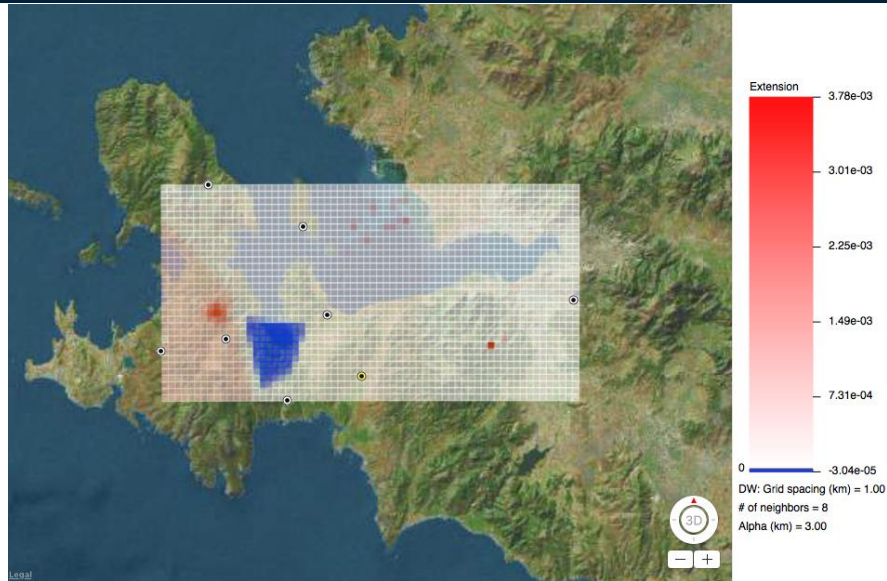
Figure 3 The extension map of the study area based on the GPS velocities of 2009-2010-2011 and 2018 observation data. The points represent the GPS stations.
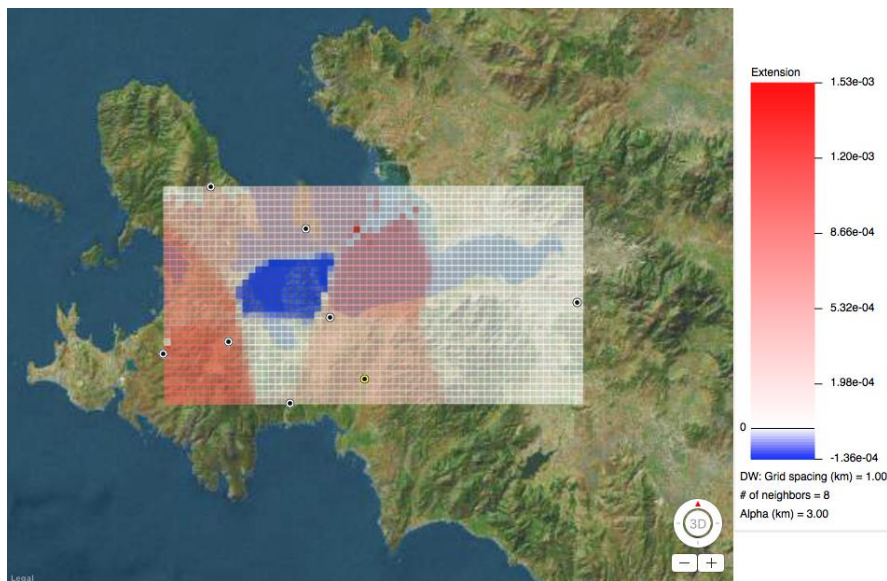
Figure 4. The extension map of the study area based on the GPS velocities of 2009-2010 and 2011 observation data. The points represent the GPS stations

3. RESULTS

In this study, the strain analyses were performed for the GPS data before and after these earthquakes in order to compare deformation changes due to the 2017 earthquakes. Therefore, GPS observations were realized for 6 GPS stations which located around Izmir City and 2 continuous GPS stations were added and were processed together. Then, GPS velocities were obtained for 2009-2010-2011-2018 and strain analysis was realized. According to the strain analysis, the extension was calculated and the extension was monitored at the middle and the western of the study area and the compression was observed between two extensional areas (Figure 3). As the next step, the strain analysis was performed for the GPS velocities based on the observations between 2009 and 2011. In this analysis,

the locations and the amplitudes of the extensions are seen at the same areas with the after earthquake data results (Figure 4). Controversially, the compression area is not located in the same area with the after earthquake data results and it is located offshore and its amplitude is higher than the new GPS data (Figure 4). Consequently, it can be said that while the amplitude and the locations of the extension of the study region are not changes with a great scale with effect of the 2017 earthquakes, the amplitude and location of the compression area was changed. It is noticed that the compression moved to south in the other words, it moved to the land due to effect of 2017 earthquakes.

ACKNOWLEDGMENT

REFERENCES

[1]. D., McKenzie, Active tectonics of the Mediterranean region, Geophys. J.R. Astron. Soc. 30, 109-185, 1972.

[2]. J. F., Dewey and A. C., Şengor, Aegean and surrounding regions: complex multiplate and continuum tectonics in a convergent zone, Geological Society of America Bulletin, 90(1), 84-92, 1979.

[3]. O., Emre, S., Ozalp, A., Dogan, V., Ozaksoy, C., Yildirim, F., Goktas, Active faults and earthquake potential of Izmir and surroundsng region, MTA Geol. Etud Report No: 10754, 2005.

[4] Bogazici University, Kandilli Observatory and Earthquake Research Center Institute (KOERI) Regional Earthquake-Tsunami Monitoring Center, Earthquake catalog (http://www.koeri.boun.edu.tr/sismo/2/earthquake-catalog/)

[5] T.A., Herring, R.W., King, M.A., Floyd, S.C., McClusky, Introduction to GAMIT/GLOBK, Release 10.6. Massachusetts Institute of Technology, Cambridge, 2015.

[6] N., Cardozo, R.W., Allmendinger, SSPX: A program to compute strain from displacement/velocity data, Computers &Geosciences, 35, 1343–1357, 2009.

Numerical Solution of the Time Fractional Korteweg-de Vries Equation by way of Quintic Trigonometric B-spline Integrator

Ozlem Ersoy Hepson[1], Idris Dag[2]

Abstract

An approximate approach is established for getting solutions of the time fractional Korteweg-de Vries (KdV) equation using the quintic trigonometric B-spline collocation and a variant of implicit finite difference method. In the equation, the time fractional derivative is replaced by Caputo fractional derivative which is discretized by use of L_1 finite difference formula and the Crank-Nicolson approximation is engaged to achieve temporal discretization of both the nonlinear and third order terms. After linearization of the nonliner term, spatial discretization is done with quintic trigonometric B-spline collocation method. Time-space integration of the time fractional KdV equation leads to a system of linear algebraic equations whose unknown parameters help us get solutions of the equations at the discrete times. Robustness of the algorithm is shown by studying a test problem.

Keywords: Caputo fractional derivative, collocation method, trigonometric B-spline, time fractional Korteweg-de Vries equation.

1. INTRODUCTION

In various area of science, fractional differential equations (fde) are discovered to model the physical and engineering processes. Nowadays, there is a trend to get analytical and numerical solutions of the fdes. So, many articles come out to give analytical solutions of the fractional equations using some approximate-analytical solutions. Adomian decomposition method [1], the homotopy-perturbation method [2]-[4], residual power series method [5], complex fractional transformation method [6], the local fractional variational iteration method [7]- [8], Lie symmetry analysis [9], functional variable method [10], differential transform method [11] and the local fractional series expansion method [12] are applied to both analytical and approximate-analytical solutions of the fractional Korteweg-de Vries (KdV) equation.

Difficulties exit finding analytical solutions of the fdes. We need efficient numerical methods to get solutions of the fdes. The finite difference approximation of the time fractional KdV equation is given in the study [13]. Collocation method using radial basis functions is built up for numerical solutions of the fractional combined KdV-modified KdV equation. The time fractional KdV equation is

$$\frac{\partial^\alpha u(x,t)}{\partial t^\alpha} + \varepsilon u(x,t)\frac{\partial u(x,t)}{\partial x} + \mu\frac{\partial^3 u(x,t)}{\partial x^3} = f(x,t) \tag{1}$$

where $0<\alpha\leq1$ and the initial data is

$$u(x,0) = g(x) \tag{2}$$

---

[1] *Corresponding author: Eskisehir Osmangazi University, Mathematics & Computer Department, Eskisehir, Turkey, ozersoy@ogu.edu.tr*

[2] *Eskisehir Osmangazi University, Computer Engineering Department, Eskisehir, Turkey, idag@ogu.edu.tr*

and the Dirichlet boundary conditions are

$$u(a,t) = h_1(x), \qquad u(b,t) = h_2(x) \tag{3}$$

over the interval [a,b]. Phenomena of the partial vibrations in lattices, travelling wave and current flow in electrical flow are modeled by the fractional KdV Equation. We use Caputo fractional derivative [14] for time derivative of unknown of the Eq. (1) as follows:

$$\frac{\partial^\alpha u(x,t)}{\partial t^\alpha} = \frac{1}{\Gamma(1-\alpha)} \int_0^t (t-\tau)^{-\alpha} \frac{\partial u(x,t)}{\partial t^\tau} d\tau$$

In this study, Caputo fractional derivative formula can be discretized via L_1 formula [15]:

$$\frac{\partial^\alpha u(t)}{\partial t^\alpha}\Big|_{t_n} = \frac{(\Delta t)^{-\alpha}}{\Gamma(2-\alpha)} \sum_{k=0}^{n-1} \left[(k+1)^{1-\alpha} - k^{1-\alpha} \right] \left[u(t_{n-k}) - u(t_{n-k-1}) \right]. \tag{4}$$

2. QUINTIC TRIGONOMETRIC B-SPLINE COLLOCATION METHOD

A domain $[x_0 = a, x_N = b]$ is divided into finite elements of equal length connected at the nodes x_m, m=0,1,...,N and h=(b-a)/N. The definition of the quintic trigonometric B-splines requires the support of nodes outside problem domain so that the ghost nodes are located outside interval as x_{-3}, x_{-2}, x_{-1}, x_{N+1}, x_{N+2}, x_{N+3}. The quintic trigonometric B-splines (QTBS) $T_m^5(x)$, m = -2 ,..., N+2 defined at the nodes x_m, m=-2, ..., N+2 by

$$
T_m^5(x) = \frac{1}{\theta}
\begin{cases}
\rho_{m-3}^5, & x_{m-3} \leq x < x_{m-2} \\
-\rho_{m-3}^4 \rho_{m-1} - \rho_{m-3}^3 \rho_m \rho_{m-2} - \rho_{m-3}^2 \rho_{m+1} \rho_{m-2}^2 \\
\quad -\rho_{m-3}\rho_{m+2}\rho_{m-2}^3 - \rho_{m+3}\rho_{m-2}^4, & x_{m-2} \leq x < x_{m-1} \\
\rho_{m-3}^3 \rho_m^2 + \rho_{m-3}^2 \rho_{m+1}\rho_{m-2}\rho_m + \rho_{m-3}^2 \rho_{m-1}{}^2 \rho_{m+1} + \\
\rho_{m-3}\rho_{m+2}\rho_{m-2}^2\rho_m + \rho_{m-3}\rho_{m+2}\rho_{m-2}\rho_{m+1}\rho_{m-1} + \\
+\rho_{m+3}\rho_{m-2}^3\rho_m + \rho_{m-3}\rho_{m+2}^2\rho_{m-1}^2 + \rho_{m+3}\rho_{m-2}^2\rho_{m+1}\rho_{m-1} + \\
\quad +\rho_{m+3}\rho_{m-2}\rho_{m+2}\rho_{m-1}^2 + \rho_{m+3}^2\rho_{m-1}^3, & x_{m-1} \leq x < x_m \\
-\rho_{m-3}^2\rho_{m+1}^3 - \rho_{m-3}\rho_{m+2}\rho_{m-2}\rho_{m+1}^2 - \rho_{m-1}\rho_{m+3}^2\rho_m\rho_{m+2} \\
-\rho_{m-3}\rho_{m+2}^3\rho_m - \rho_{m+2}\rho_{m-3}^2\rho_m^2 - \rho_{m+2}\rho_{m-3}\rho_{m+1}\rho_{m-2}\rho_m \\
\quad -\rho_{m+2}\rho_{m-3}\rho_{m+1}^2\rho_{m-1} - \rho_{m+3}^2\rho_{m-1}^2\rho_{m+1} \\
\quad -\rho_{m+3}^2\rho_{m-1}\rho_{m+2}\rho_m - \rho_{m+3}^3\rho_m^2, & x_m \leq x < x_{m+1} \\
\rho_{m-3}\rho_{m+2}^4 + \rho_{m+3}\rho_{m-2}\rho_{m+2}^3 + \\
\rho_{m+3}^2\rho_{m-1}\rho_{m+2}^2 + \rho_{m+3}^3\rho_m\rho_{m+2} + \rho_{m+3}^4\rho_{m+1}, & x_{m+1} \leq x < x_{m+2} \\
-\rho_{m+3}^5, & x_{m+2} \leq x < x_{m+3} \\
0, & \text{else}
\end{cases}
\tag{5}
$$

where

$$\rho_m = \rho(x_m) = \sin\left(\frac{x - x_m}{2}\right), \quad \theta = \sin\left(\frac{h}{2}\right)\sin(h)\sin\left(\frac{3h}{2}\right)\sin(2h)\sin\left(\frac{5h}{2}\right), \quad m = 0\,(1)\,N, \tag{6}$$

form a basis over the the interval [a, b]. U(x, t) denotes an approximate solution to u(x, t) and is interpolated by means of the QTBS as follows

$$U(x,t) = \sum_{m=-2}^{N+2} \delta_m(t) T_m(x), \tag{7}$$

where δ_m are time dependent unknown parameters. u(x, t) is approximated by a collection of N+5 QTBS. QTBS and their first four derivatives are continuous on element [x_{m-3}, x_{m+3}]. This interpolation can be used to approximate

u and the spatial partial derivatives of the function u at the nodes x_m, $m=-2, ..., N+2$. Thus $u(x, t)$ at nodes x_m is found using QTBS in terms of time dependent parameters δ as

$$u_m \approx U_N(t, x_m) = a_1 \delta_{m-2} + a_2 \delta_{m-1} + a_3 \delta_m + a_2 \delta_{m+1} + a_1 \delta_{m+2},$$

$$u'_m \approx \frac{\partial U(t, x_m)}{\partial x} = b_1 \delta_{m-2} + b_2 \delta_{m-1} - b_2 \delta_{m+1} - b_1 \delta_{m+2},$$

$$u''_m \approx \frac{\partial^2 U(t, x_m)}{\partial x^2} = c_1 \delta_{m-2} + c_2 \delta_{m-1} + c_3 \delta_m + c_2 \delta_{m+1} + c_1 \delta_{m+2},$$

(8)

$$u'''_m \approx \frac{\partial^3 U(t, x_m)}{\partial x^3} = d_1 \delta_{m-2} + d_2 \delta_{m-1} - d_2 \delta_{m+1} - d_1 \delta_{m+2}$$

$$u''''_m \approx \frac{\partial^4 U(t, x_m)}{\partial x^4} = e_1 \delta_{m-2} + e_2 \delta_{m-1} + e_3 \delta_m + e_2 \delta_{m+1} + e_1 \delta_{m+2}$$

where the coefficients of the time dependent parameters in (8) is

$$a_1 = \sin^5 \left(\frac{h}{2}\right) / \theta,$$

$$a_2 = 2\sin^5 \left(\frac{h}{2}\right) \cos\left(\frac{h}{2}\right) \left(16\cos^2\left(\frac{h}{2}\right) - 3\right) / \theta,$$

$$a_3 = 2\left(1 + 48\cos^4\left(\frac{h}{2}\right) - 16\cos^2\left(\frac{h}{2}\right)\right) \sin^5\left(\frac{h}{2}\right) / \theta,$$

$$b_1 = (-5/2)\sin^4\left(\frac{h}{2}\right) \cos\left(\frac{h}{2}\right) / \theta,$$

$$b_2 = -5\sin^4\left(\frac{h}{2}\right) \cos^2\left(\frac{h}{2}\right) \left(8\cos^2\left(\frac{h}{2}\right) - 3\right) / \theta,$$

$$c_1 = (5/4)\sin^3\left(\frac{h}{2}\right) \left(5\cos^2\left(\frac{h}{2}\right) - 1\right) / \theta,$$

$$c_2 = (5/2)\sin^3\left(\frac{h}{2}\right) \cos\left(\frac{h}{2}\right) \left(-15\cos^2\left(\frac{h}{2}\right) + 3 + 16\cos^4\left(\frac{h}{2}\right)\right) / \theta,$$

$$c_3 = (-5/2)\sin^3\left(\frac{h}{2}\right) \left(16\cos^6\left(\frac{h}{2}\right) - 5\cos^2\left(\frac{h}{2}\right) + 1\right) / \theta,$$

$$d_1 = (-5/8)\sin^2\left(\frac{h}{2}\right) \cos\left(\frac{h}{2}\right) \left(25\cos^2\left(\frac{h}{2}\right) - 13\right) / \theta,$$

$$d_2 = (-5/4)\sin^2\left(\frac{h}{2}\right) \cos^2\left(\frac{h}{2}\right) \left(8\cos^4\left(\frac{h}{2}\right) - 35\cos^2\left(\frac{h}{2}\right) + 15\right) / \theta,$$

$$e_1 = (5/16)\left(125\cos^4(\frac{h}{2}) - 114\cos^2(\frac{h}{2}) + 13\right)\sin(\frac{h}{2})/\theta,$$

$$e_2 = (-5/8)\sin(\frac{h}{2})\cos(\frac{h}{2})\left(176\cos^6(\frac{h}{2}) - 137\cos^4(\frac{h}{2}) - 6\cos^2(\frac{h}{2}) + 15\right)/\theta,$$

$$e_3 = (5/8)\left(92\cos^6(\frac{h}{2}) - 117\cos^4(\frac{h}{2}) + 62\cos^2(\frac{h}{2}) - 13\right)\left(-1 + 4\cos^2(\frac{h}{2})\right)\sin(\frac{h}{2})/\theta$$

and $\theta = \sin(\frac{5h}{2})\sin(2h)\sin(\frac{3h}{2})\sin(h)\sin(\frac{h}{2})$.

Time derivative part of the KdV equation is discretized by using the L_1 formula defined on the work [16] and spatial derivatives by the Crank-Nicolson method. This discretization gives a time discrete fractional KdV equation:

$$\frac{(\Delta t)^{-\alpha}}{\Gamma(2-\alpha)}(u^{n+1} - u^n) + \frac{(\Delta t)^{-\alpha}}{\Gamma(2-\alpha)}\sum_{k=1}^{n-1}\left[(k+1)^{1-\alpha} + k^{1-\alpha}\right]\left[u^{n-k+1} - u^{n-k}\right] +$$

$$\varepsilon\frac{(uu_x)^{n+1} + (uu_x)^n}{2} + \mu\frac{u_{xxx}^{n+1} + u_{xxx}^n}{2} = F(x, t^{n+1}) \tag{9}$$

After linearization $(uu_x)^{n+1} = u^{n+1}u_x^n + u^n u_x^{n+1} - u^n u_x^n$ is carried out in Eq. (9), approximations in Eq. (7) are replaced in the time discrete Eq. (8) and then collocating at the nodes on the problem domain $[a, b]$. We obtain the system of the fully-discretized fractional KdV in the form of a set of algebraic equations:

$$\left(\left(A + \frac{\varepsilon}{2}L\right)a_1 + \frac{\varepsilon}{2}Kb_1 + \frac{\mu}{2}d_1\right)\delta_{m-2}^{n+1} + \left(\left(A + \frac{\varepsilon}{2}L\right)a_2 + \frac{\varepsilon}{2}Kb_2 + \frac{\mu}{2}d_2\right)\delta_{m-1}^{n+1} + \left(\left(A + \frac{\varepsilon}{2}L\right)a_3\right)\delta_m^{n+1}$$

$$+\left(\left(A + \frac{\varepsilon}{2}L\right)a_2 - \frac{\varepsilon}{2}Kb_2 - \frac{\mu}{2}d_2\right)\delta_{m+1}^{n+1} + \left(\left(A + \frac{\varepsilon}{2}L\right)a_1 - \frac{\varepsilon}{2}Kb_1 - \frac{\mu}{2}d_1\right)\delta_{m+2}^{n+1}$$

$$= \left(Aa_1 - \frac{\mu}{2}d_1\right)\delta_{m-2}^{n+1} + \left(Aa_2 - \frac{\mu}{2}d_2\right)\delta_{m-1}^{n+1} + \left(Aa_3\right)\delta_m^{n+1} + \left(Aa_2 + \frac{\mu}{2}d_2\right)\delta_{m+1}^{n+1} \tag{10}$$

$$+\left(Aa_1 + \frac{\mu}{2}d_1\right)\delta_{m+2}^{n+1} - A\sum_{k=1}^{n-1}\left[(k+1)^{1-\alpha} + k^{1-\alpha}\right]$$

$$\left[\left(\delta_{m-2}^{n-k+1} - \delta_{m-2}^{n-k}\right)a_1 + \left(\delta_{m-1}^{n-k+1} - \delta_{m-1}^{n-k}\right)a_2 + \left(\delta_m^{n-k+1} - \delta_m^{n-k}\right)a_3 +\right.$$

$$\left.\left(\delta_{m+1}^{n-k+1} - \delta_{m+1}^{n-k}\right)a_2 + \left(\delta_{m+2}^{n-k+1} - \delta_{m+2}^{n-k}\right)a_1\right] + F(x, t^{n+1})$$

where

$$K = a_1\delta_{m-2}^n + a_2\delta_{m-1}^n + a_3\delta_m^n + a_2\delta_{m+1}^n + a_1\delta_{m+2}^n \tag{11}$$

$$L = b_1 \delta_{m-2}^n + b_2 \delta_{m-1}^n - b_2 \delta_{m+1}^n - b_1 \delta_{m+2}^n$$

$$A = \frac{(\Delta t)^{-\alpha}}{\Gamma(2-\alpha)}$$

and $U^{n+1} = U(x,(n+1)\,\Delta t)$ represent the solution at the $(n+1)$th time level. Here $t^{n+1} = t^n + \Delta t$, Δt is the time step, superscripts denote n th time level, $t^n = n\,\Delta t$. The equation (10) can be converted into the following matrices system:

$$\mathbf{A}\mathbf{x}^{n+1} = \mathbf{B}\mathbf{x}^n \tag{12}$$

where

$$\mathbf{A} = \begin{bmatrix} \kappa_{m1} & \kappa_{m2} & \kappa_{m3} & \kappa_{m4} & \kappa_{m5} & & \\ & \kappa_{m1} & \kappa_{m2} & \kappa_{m3} & \kappa_{m4} & \kappa_{m5} & \\ & \ddots & \ddots & \ddots & \ddots & \ddots & \\ & & \kappa_{m1} & \kappa_{m2} & \kappa_{m3} & \kappa_{m4} & \kappa_{m5} \end{bmatrix} \quad \mathbf{B} = \begin{bmatrix} \kappa_{m6} & \kappa_{m7} & \kappa_{m8} & \kappa_{m9} & \kappa_{m10} & & \\ & \kappa_{m6} & \kappa_{m7} & \kappa_{m8} & \kappa_{m9} & \kappa_{m10} & \\ & \ddots & \ddots & \ddots & \ddots & \ddots & \\ & & \kappa_{m6} & \kappa_{m7} & \kappa_{m8} & \kappa_{m9} & \kappa_{m10} \end{bmatrix}$$

and

$$\kappa_{m1} = \left(A + \frac{\varepsilon}{2}L\right)a_1 + \frac{\varepsilon}{2}Kb_1 + \frac{\mu}{2}d_1, \quad \kappa_{m2} = \left(A + \frac{\varepsilon}{2}L\right)a_2 + \frac{\varepsilon}{2}Kb_2 + \frac{\mu}{2}d_2,$$

$$\kappa_{m3} = \left(A + \frac{\varepsilon}{2}L\right)a_3, \quad \kappa_{m4} = \left(A + \frac{\varepsilon}{2}L\right)a_2 - \frac{\varepsilon}{2}Kb_2 - \frac{\mu}{2}d_2,$$

$$\kappa_{m5} = \left(A + \frac{\varepsilon}{2}L\right)a_1 - \frac{\varepsilon}{2}Kb_1 - \frac{\mu}{2}d_1, \quad \kappa_{m6} = Aa_1 - \frac{\mu}{2}d_1,$$

$$\kappa_{m7} = Aa_2 - \frac{\mu}{2}d_2, \quad \kappa_{m8} = Aa_3, \quad \kappa_{m9} = Aa_2 + \frac{\mu}{2}d_2, \quad \kappa_{m10} = Aa_1 + \frac{\mu}{2}d_1.$$

The boundary conditions unknown parameters $\delta_m^n = 0$, $U_x(a,\ t)=0$ and $U(b,\ t)=0$ and $U_x(b,\ t)=0$ are used to eliminate parameters δ_{-1}^{n+1}, δ_0^{n+1}, δ_{N+2}^{n+1} and δ_{N+3}^{n+1} from the system (12) so that we have a solvable $(N+5) \times (N+5)$ 5-banded matrix system. This system is solved with Matlab using Thomas algorithm.

To calculate the unknown parameters δ_m^n in the iteration process in Eq. (12), we need to calculate initial unknown parameters δ_m^0 using initial conditions at the nodes

$$u(x_m, 0) = g(x_m), \ m = 0 \ldots N$$

together with the derivatives at boundaries $u_x(x,0) = g'(x)$, $u_{xx}(x,0) = g''(x)$ at boundary points $x = a, b$.

3. NUMERICAL TESTS

In this section, we show the results for time fractional KdV equation via collocation method using quintic trigonometric cubic B-spline functions. We calculate the accuracy of the proposed methods by the error norm

$$L_\infty = |u(x,t) - U(x,t)|_\infty = \max_m |u(x_m,t) - U(x_m,t)|$$

where $u(x,\ t)$ denote exact solution and $U(x,\ t)$ denote numerical solution at time t.

3.1. Problem 1

Firstly, we consider non-fractional problem for testing the algorithm. We use the Eq. (1) with boundary conditions

$$u(a,t) = \frac{1}{3000} t^5 e^{-a^2}, \quad u(b,t) = \frac{1}{3000} t^5 e^{-b^2}, \quad t \geq 0 \tag{13}$$

and the initial condition as

$$u(x,0) = 0, a \leq x \leq b. \tag{14}$$

For this problem *f(x,t)* as follows is given by

$$f(x,t) = \frac{t^5 e^{-x^2}}{25} \left(\frac{1}{\Gamma(6-\alpha)} t^{-\alpha} - \frac{1}{180000} t^2 x e^{-x^2} + \frac{1}{10} x - \frac{1}{15} x^3 \right) \tag{15}$$

and the exact solution of the problem as follows

$$u(x,t) = \frac{1}{3000} t^5 e^{-x^2} \tag{16}$$

We run the programme with the parameters: space step *h=0.05, time step Δt=0.0025, nonlinear constant ε=1, μ=1,* non-fractional order *α=1* up to the terminating time *t=1* on the interval [*-3, 3*]. Numerical solution at time *t=1* and maximum error norm are illustrated in Figs. 1-2. L_∞ error norm is recorded at time *t=1* as 2.0847×10^{-6} exactly seen in Fig. 2.
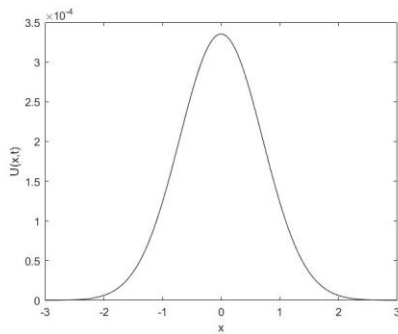
Figure 1. Numerical solution for α=1
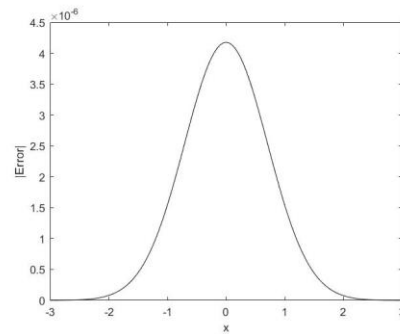
Figure 2. Maximum error norm for α=1

3.2. Problem 2

Secondly, initial condition:

$$u(x,0) = \frac{1}{2} \left[1 - \tanh\left(\frac{|x| - 25}{5} \right) \right]$$

together with boundary conditions:

$$u(-50,t) = u(150,t) = 0, t > 0$$

Will be observed whether or not solutions of fractional KdV Equation produce a train of solitons depending upon the value *α* for the KdV Equation. Computation is done on region *[-50, 150]* up to time *t=800* with parameters *ε=0.2 , μ=0.1, Δt=0.05* and *h=0.4*. Visual representations of the solutions in Figs. 4, 6, 8, 10, 12 are drawn that 10 solitons has been broken up from the given initial condition when integer order *α=1* in KdV equation is used whereas for *α=0.9*, initial condition can not turn into train of soliton solutions as seen in Figs. 3, 5, 7, 9, 11.

Seemingly initial condition started to form waves but can not build up the wave form until running time. Although we had extended the run time of the algorithm, shape of the existing solutions spoiled.
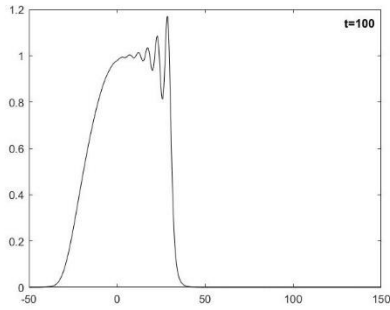
Figure 3. Numerical solutions for α=0.9
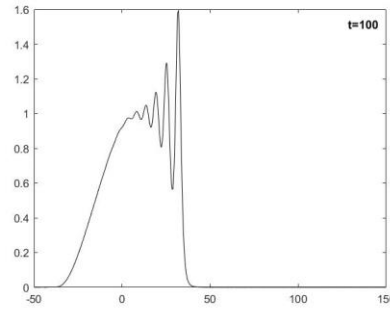
Figure 4. Numerical solutions for α=1
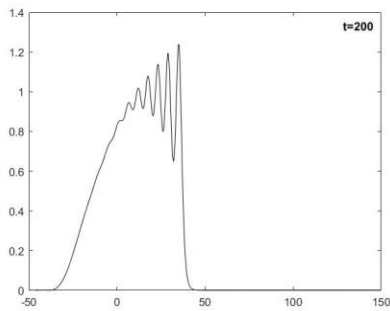
Figure 5. Numerical solutions for α=0.9
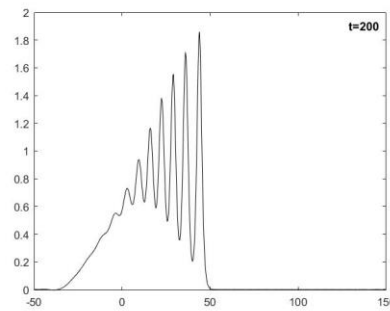
Figure 6. Numerical solutions for α=1
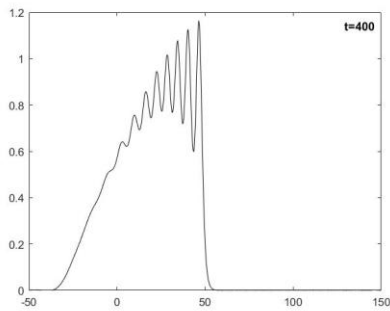
Figure 7. Numerical solutions for α=0.9
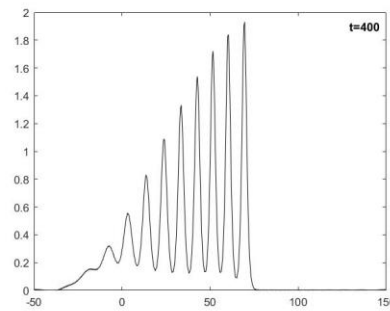
Figure 8. Numerical solutions for α=1
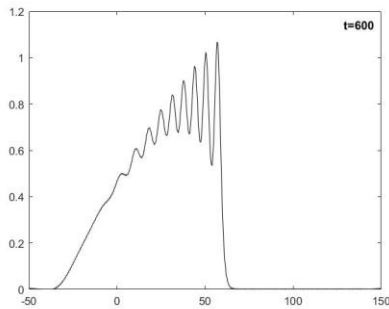
Figure 9. Numerical solutions for α=0.9
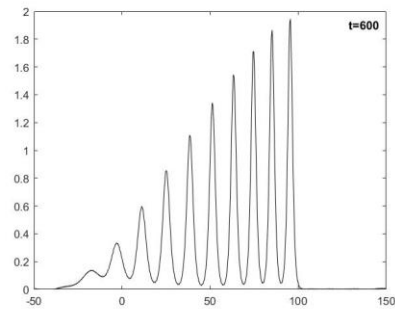
Figure 10. Numerical solutions for α=1
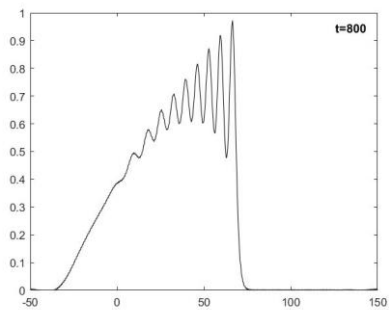
Figure 11. Numerical solutions for α=0.9
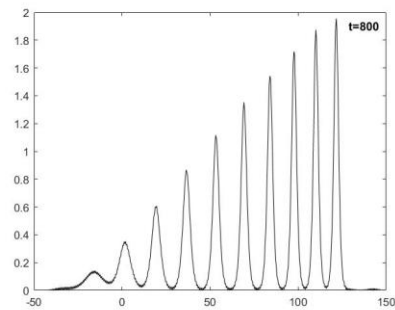
Figure 12. Numerical solutions for α=1

CONCLUSION

An algorithm has been introduced for getting solutions of the time fractional KDV equation. Integration of the time fractional KdV equation is managed by way of quintic trigonometric B-spline collocation method for spatial discretization and Crank-Nicolson formula for the temporal discretization. Fully integration lead to system of algebraic equation. Solution of system gives time parameters so that approximate solution can be obtained using the expression (7). With suggested algorithm, usual solution, evoluation of solitons for the initial condition, can not be managed for using non-fractional derivative order for time fractional KdV although for integer order derivative, algorithm produce solitons correctly.

ACKNOWLEDGMENT

REFERENCES

[1]. S. Momani, "An explicit and numerical solutions of the fractional KdV equation," *Mathematics and Computers in Simulation*, vol. 70, pp. 110–118, 2005.

[2]. O. Abdulaziz, I. Hashim and E. S. Ismail, "Approximate analytical solution to fractional modified KdV equations," *Mathematical and Computer Modelling*, vol. 49, pp. 136–145, 2009.

[3]. Q. Wang, "Homotopy perturbation method for fractional KdV equation," *Applied Mathematics and Computation*, vol. 190, pp. 1795–1802, 2007.

[4]. C. Li, A. Kumar, S. Kumar and X. J.Yang, "On the approximate solution of nonlinear time-fractional KdV equation via modified homotopy analysis Laplace transform method," *J. Nonlinear Sci. Appl.,* vol. 9, pp. 5463–5470, 2016.

[5]. M. Senol and A. Ata, "Approximate solution of time-fractional KdV equations by residual power series method," *BAUN Fen Bil. Enst. Dergisi,* vol. 20(1), pp. 430–439, 2018.

[6]. U. Ghoshsan, T. Raut, S. Sarkar and S. Dasand, "Solution of space time fractional generalized KdV equation, KdV Burger equation and Bona-Mahoney-Burgers Equation with dual power-low nonlinearity using complex Fractional Transformation," *J. Math. Comput. Sci*., vol. 8(1), pp. 114–129, 2018.

[7]. S. A. El-Wakil, E. M. Abulwafa, E. K. El-Shewy and A. A. Mahmoud, "Time-fractional KdV equation for plasma of two different temperature electrons and stationary ion," *Physics of plasmas*, 2011, paper. 18, p. 092116.

[8]. S. Momani, Z. Odibat and A. Alawneh, "Variational Iteration Method for Solving the Space- and Time-Fractional KdV Equation," *Numerical Methods for Partial Differential Equations,* vol. 24(1), pp. 262–271, 2008.

[9]. J. Hu, Y. Ye, S. Shen, and J. Zhang, "Lie symmetry analysis of the time fractional KdV-type equation," *Appl. Math. Comput.,* vol. 233, pp. 439–444, 2014.

[10]. M. Matinfar, M. Eslami and M. Kordy, "The functional variable method for solving the fractiol Korteweg–de Vries equations and the coupled Korteweg–de Vries equations," *Pramana journal of physics,* vol. 85(4), pp. 583–592, 2015.

[11]. M. Kurulay and M. Bayram, "Approximate analytical solution for the fractional modified KdV by differential transform method," *Commun. Nonlinear Sci. Numer. Simul.,* vol. 15(7), pp. 1777–1782, 2010.

[12]. H. K. Jassim and D. Baleanu, "A Novel Approach for Korteweg-de Vries Equation of Fractional Order," J. *Appl. Comput. Mech.,* vol. 5(2), pp. 192-198, 2019.

[13]. A. Yokus, "Numerical solutions of time fractional Korteweg-de Vries equation and its stability," *Commun. Fac. Sci. Univ. Ank. Ser. A1 Math. Stat.* vol. 68(1), pp. 353–361, 2019.

[14]. I. Podlubny, *Fractional Derivative Equations*, Academic Press, San Diego, 1999.

[15]. A. Esen, Y. Ucar, N. Yagmurlu, and O. Tasbozan, "A Galerkin Finite Element Method to Solve Fractional Diffusion and Fractional Diffusion-Wave Equations," *Mathematical Modelling and Analysis,* vol. 18, pp. 260-273, 2013.

[16]. K. Oldham, J. Spanier, *The Fractional Calculus*, AcademicPress, NewYork, 1974.

Free Vibration Analysis of Multi-Carriages Crane Systems with Finite Element Method

Sahin Yildirim [1], Emir Esim[2]

Abstract

External factors affecting the mechanical systems that form the basis of engineering systems can cause resonance. For this reason, it is important to know not only the static characteristics of the systems, but also the dynamic characteristics known as free vibration behavior in order to operate the systems under safe and secure conditions. Since natural frequencies are a parameter that is determined by the mass and flexibility of the objects, the evaluation of the crane system should be evaluated not only as a bridge beam, but also as a whole because the elements are in contact with each other. For this reason, according to the situation of different carriage numbers on the crane system, the movement of the structure in the system together with the load and the different positions of the carriages on the bridge, the modal analysis was performed with ANSYS Workbench 18.1 program which can work according to the finite element method. The results obtained were compared and it was observed that the crane system being the number of carriage change the behavior of the system and the natural frequencies, and the car position had no effect in the crane system.

Keywords: Multi-carriages Crane System, Modal analysis, Free vibration, finite element method

1. INTRODUCTION

Modal analysis is defined as the examination of the dynamic characteristics of a mechanical system. Engineering structures are usually under one or more dynamic impacts during their use Modal analysis is defined as the examination of the dynamic characteristics of a mechanical system. Engineering structures are usually under one or more dynamic impacts during their use. In practice; all machines, vehicles and buildings are subject to dynamic forces leading to vibration. Vibrations are generally; it should be investigated directly for reasons such as causing problems, the structure being completely safe, or the suitability of the desired test conditions. Whatever the reason, the vibration response of the structure needs to be measured in some way, and the factors such as performance and fatigue of the structure can be evaluated [1]. For these reasons, the investigation of the dynamic effects of crane systems has attracted the attention of many researcher and related studies are presented as follows:

In the study by Low, vibration analysis was performed by using eigenfunctions for multiple mass beams. Polynomial approximation mode analysis was compared with both analytical and experimental results. The comparison results yielded valid results for the proposed models [2]. A comparative study of the natural frequencies of the Euler-Bernoilli beam in the case of concentrated mass and mass at any point [3]. Cha has summarized the studies about the approximate and exact analyzes by classifying the widely used analysis approaches related to the free vibrations of linear elastic structures carrying lumped mass at different points in their studies. (eg Lagrange approach, Dynamic Green function approach, Laplace transform, analytical and numerical solution methods) [4], [5], [6]. Karamolla used the finite element method for vibration and displacement analysis against variable loads in tower cranes. The tower realized the displacement of the rod elements forming the crane at the nodes and the modal analysis against the natural frequencies in the whole system [7]. Yildirim and Esim have examined the number of different car numbers on bridged cranes and examined the dynamic effects occurring at the midpoints of the beam according to different working speeds in the case of a beam or double beam in the transportation of the same load using the finite element method[8]. Gasic et al. have studied the effects of the beam on the dynamic

response of the beam by carrying an oscillator with different spring coefficients and according to different velocities [9].

Because natural frequencies are a parameter determined by the mass and flexibility of the objects, the evaluation of the crane system should be done not only as a bridge beam but as a whole as the elements are in contact with each other. In this study, firstly, due to the fact that the crane system has different number of carriages according to the experimental working conditions and the structure moves together with the load, a modal analysis has been performed by taking the whole system into consideration. In order to be able to see the effect of the load in the crane system, which is designed and applied as three carriages, the analyzes were carried out according to the load was at the head of bridge and at the center.

2. FINITE ELEMENT FORMULATION

Dynamic analyzes are used to determine the characteristics of a structure when considering the rigidity and damping of the system under varying loads. Here, as a general approach, it is possible to explain the dynamic characteristic of the system, and the node model dynamic equations can be used in which the system is divided into elements. Since there is a linear relationship between the elements and the node model, the system is divided into many elements and the system becomes a multi-degree of freedom [10]

The vibration model of the structure, which transforms the system into a multi-degree of freedom linear structure, can be expressed by the following equation[11]:

$$\left[m\right]\ddot{x}(t)+\left[c\right]\dot{x}(t)+\left[k\right]x(t)=f(t) \tag{1}$$

Where: [M] is mass matrix; [C] is damped matrix; [K] is stiffness matrix; x (t) is the system displacement response vector; f (t) is the system force vector.

In the finite element model, it is assumed that there is no damping in the vibration systems with multiple degrees of freedom. Therefore Equation 2 can be expressed as follows:

$$\left[m\right]\ddot{x}(t)+\left[k\right]x(t)=0 \tag{2}$$

The fundamental theory of modal analysis in the finite element method uses natural coordinates to change physical coordinates by coordinate transformation.

The dependent equation of motion and the combined equations are converted to independent differential equations. In equation 2, the following equation can be written to convert the coordinates of physics *x(t)* to modal coordinates:

$$x(t)=\left[u\right]\Psi \tag{3}$$

In the above equation, [u] is a modal matrix, Ψ is modal coordinates. If Equation 3 is written in Equation 2, the following equation is obtained:

$$\left[m\right]\left[u\right]\Psi+\left[k\right]\left[u\right]\Psi=0 \tag{4}$$

For the ratio of the non-damping system and the damping system, the modal matrix [u] is considered a modal orthogonal matrix.

$$\left[u\right]^{T}\left[m\right]\left[u\right]=\left[I\right]\ ,\left[u\right]^{T}\left[k\right]\left[u\right]=\lambda \tag{5}$$

If the equation 4 is multiplied by $\left[u\right]^{T}$, the following equation is obtained:

$$\left[u\right]^{T}\left[m\right]\left[u\right]\Psi+\left[u\right]^{T}\left[k\right]\left[u\right]\Psi=0 \tag{6}$$

The following equations can be written from Equation 6.

$$\begin{cases} \ddot{\Psi}+\lambda\Psi=0 \\ \left[k\left\{u\right\}\right]-\lambda\left[m\right]\left\{u\right\}=0 \end{cases} \tag{7}$$

The following equations are obtained when the above equation is solved.

$$\Psi = A.\cos(wt - \varphi) \qquad \lambda = w^2 \tag{8}$$

A and φ arbitrary constants w vibration frequency, while the modal vector is expressed as $\{u\}$.

If Equation 8 is written in Equation 7, the following equation is obtained:

$$\left[k\{u\}\right] - w^2\left[m\right]\{u\} = \{0\} \tag{9}$$

Where, $\left\{w_1^{\ 2}, w_2^{\ 2}....w_n^{\ 2}\right\}$, $\quad \{u\} = \left(u^{(1)}, u^{(2)}...u^{(n)}\right)^T = \Psi$ are defined.

The following equation is obtained from the solution of Equation 9.

$$\{u\}^T\left[k\right]\{u\} = w^2\{u\}^T\left[m\right]\{u\}$$
$$\tag{10}$$

Given the normalization of the modal vector, the following expression can be obtained.
$$\{u\}^T\left[m\right]\{u\} = 1, \qquad \{u\}^T\left[k\right]\{u\} = w^2 \tag{11}$$

A modal matrix is generated by arranging n normalized model vectors, respectively, in a square.

According to the above theory, Equation 7 can be expressed as follows:

$$\ddot{\Psi}_r + w_r^2\Psi_r = \{0\} \qquad (r = 1, 2, ...n) \tag{12}$$

3. MODELING PROCEDURES AND FEA MODEL

When designing the crane system, the design parameters such as lifting capacity, lifting height, bridge span and bridge runaway length should be known. When experimental studies will be carried out later, design parameters and working conditions of the crane system are given in Table 1. According to these parameters, each of the components of the crane system, such as bridge carrier, bridge group, lifting group, which make up the system, requires a separate solid model. Therefore, it is difficult to perform solid modeling of the crane system with ANSYS WORKBENCH software. The solid model of the crane system was created using the SolidWorks program. In this study, based on the dynamic analysis of the multi-carriage crane systems, solid models based on the number of different cars have been realized. For example, the crane system and its components, which are designed as three-car, are shown in Figure 1.
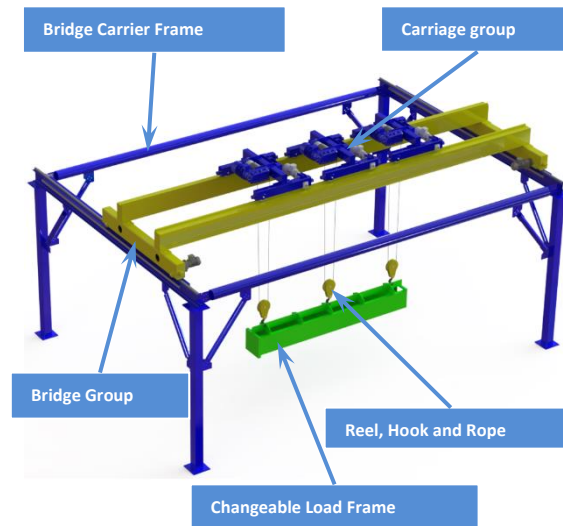
Figure 1. A proposed three- carriages crane system and its components

In order to be able to see the effect of the load position in the crane system, solid models seen in Figure 2 were designed according to the condition of the carriage group and the load at the beginning and middle of bridge. CAD models of different types crane are imported into ANSYS with parasolid file format.

Table 1. Crane Design Parameters

Parameters	Value
Bridge Span	7 m
Lift Height	4 m
Bridge runaway length	5 m
Load Capacity	1600kg
Lifting Speeds	4 m/min
Bridge Motor Power	0,37Kw
Hoist Motor Power	2 Kw
Carriage Motor Power	0,25 Kw
Wire Rope (6*19 Fiber Core)	8 mm
Hook	DIN15401

Model 1   Model 2   Model 3

Model 4   Model 5   Model 6
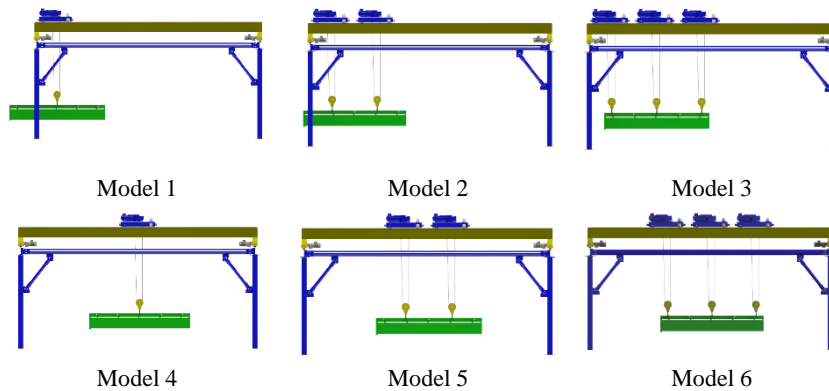
Figure 2. Solid models of crane designed for different carriage numbers for modal analysis

4. MODAL ANALYSIS AND RESULT

Modal analysis is considered as an important step in the design process to predict the vibration characteristics of the designed structure. Therefore, the aim of modal analysis is to determine natural frequencies and behaviors. The basic assumption in modal analysis is that the system is linear and any non-linearity in the system is neglected. In order to calculate the natural frequencies and mode shapes of any structure, the general processing steps were applied within the crane system. The modal analysis process carried out by ANSYS WORKBENCH is as follows[12]:

- After the solid model has been imported in Ansys, element type and material properties are defined for Finite Element Model. In all calculations for different crane types, the materials used in crane design are assumed to be homogeneous and isotropic. Material properties are given in the Table 2.

Table 2. Material properties for modal analysis

Material	Density	Young Modulus	Poisson Ratio
Structural Steel	7850 kg/m3	210 GPa	0.3

- After contact processes have been defined for the structures in contact with each other on the crane system, the crane system is divided into elements. The example of the mesh structure of the crane with 3 cars is given in Figure 4.a. This model consists of 537224 element number and 1577502 node number. The appearance of the boundary conditions of the system is given in Figure 4b.

- After all these definitions, a solution was made to determine the natural frequency and mode shapes of the crane system. These finite element analyses are used to perform computer features; Processor: Intel (R) Core (TM) i7-2600 CPU @ 3.40 GHz 3.40 GHz, Installed memory: 32 GB, System Type: 64 Bit Operating System, Windows version: Windows7 Ultimate.

According to the structural and operating characteristics of the overhead crane, its execution units perform at a low speed running range, so the lower modes play a major role in affecting dynamic characteristics. However, high-frequency modes of the structure have little effect and can be neglected. Therefore, mod shapes corresponding to the first four frequencies were taken into account.
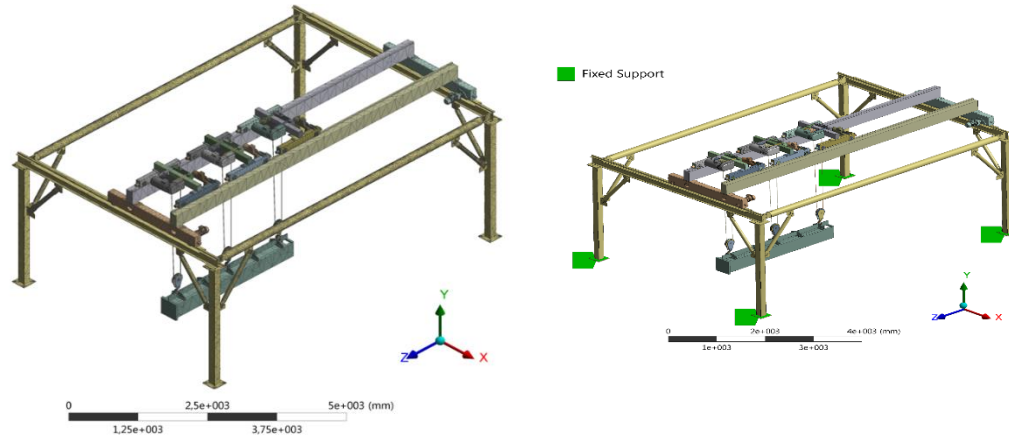
Figure 4 (a) Example of view of mesh structure   (b) Example of applied view of boundary conditions

The mode shapes of the crane system corresponding to the natural frequencies according to the number of different cars and cars at the head of the bridge are given in Figure 5.
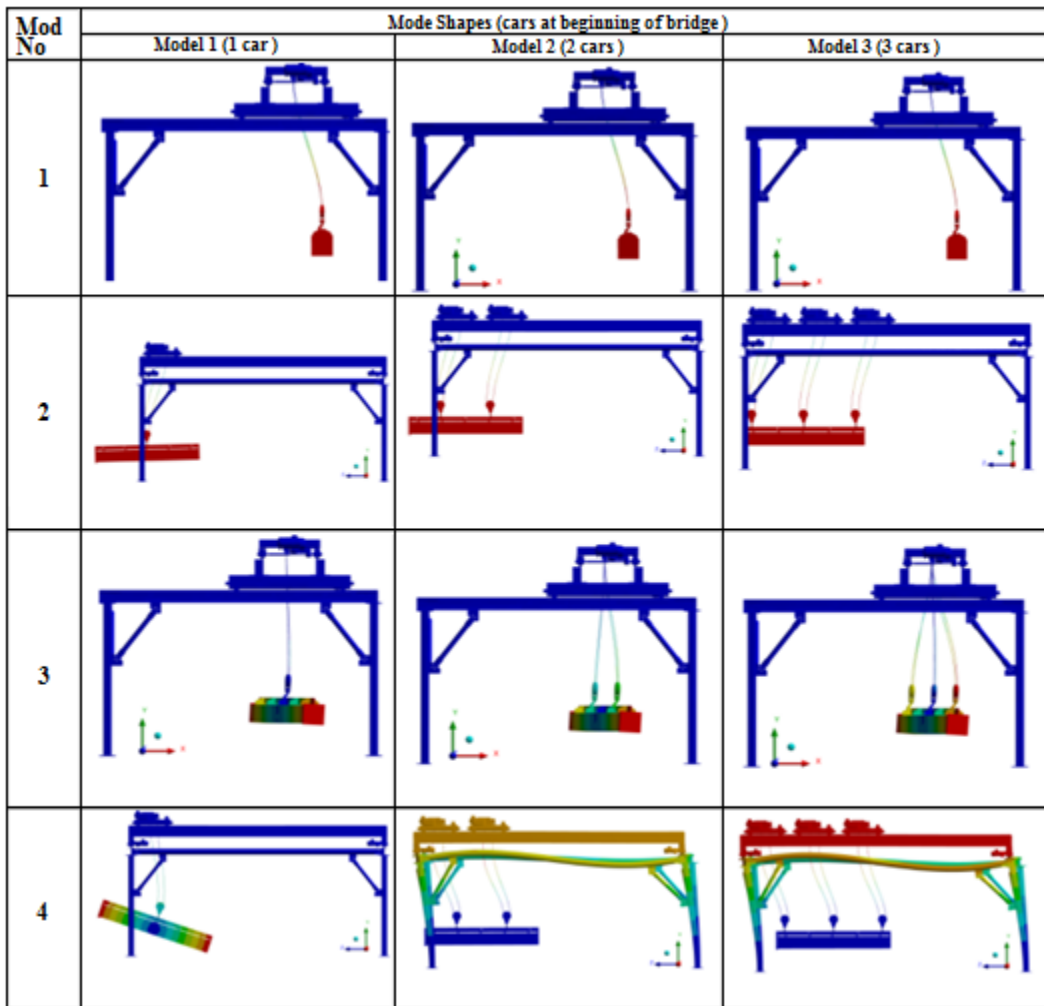
Figure 5. The first Four mode shapes for the different car numbers (cars at the head of the bridge)

Modal behaviors of the crane system in the case of cars running in the middle of the bridge are given in Figure 6. In the same way, different car numbers were taken into consideration. When the graphs are examined, it is seen that the first 3 modal behavior characteristics are similar in different car numbers and in the 4th mode, the behavior is changed for 2 and 3 cars. In the case of 3 cars, it is understood from the corresponding figures that they have more reactions than 2 cars. In general, it is seen that in all modes of a car situation and the first 3 mode behaviors occur on the load and rope, in the 4th mode there are deformations on the beams.

Mod No	Modes Shapes(Cars at the middle of the bridge)		
	Model 4 (1 car)	Model 5 (2Cars)	Model 6 (3 cars)
1			
2			
3			
4			
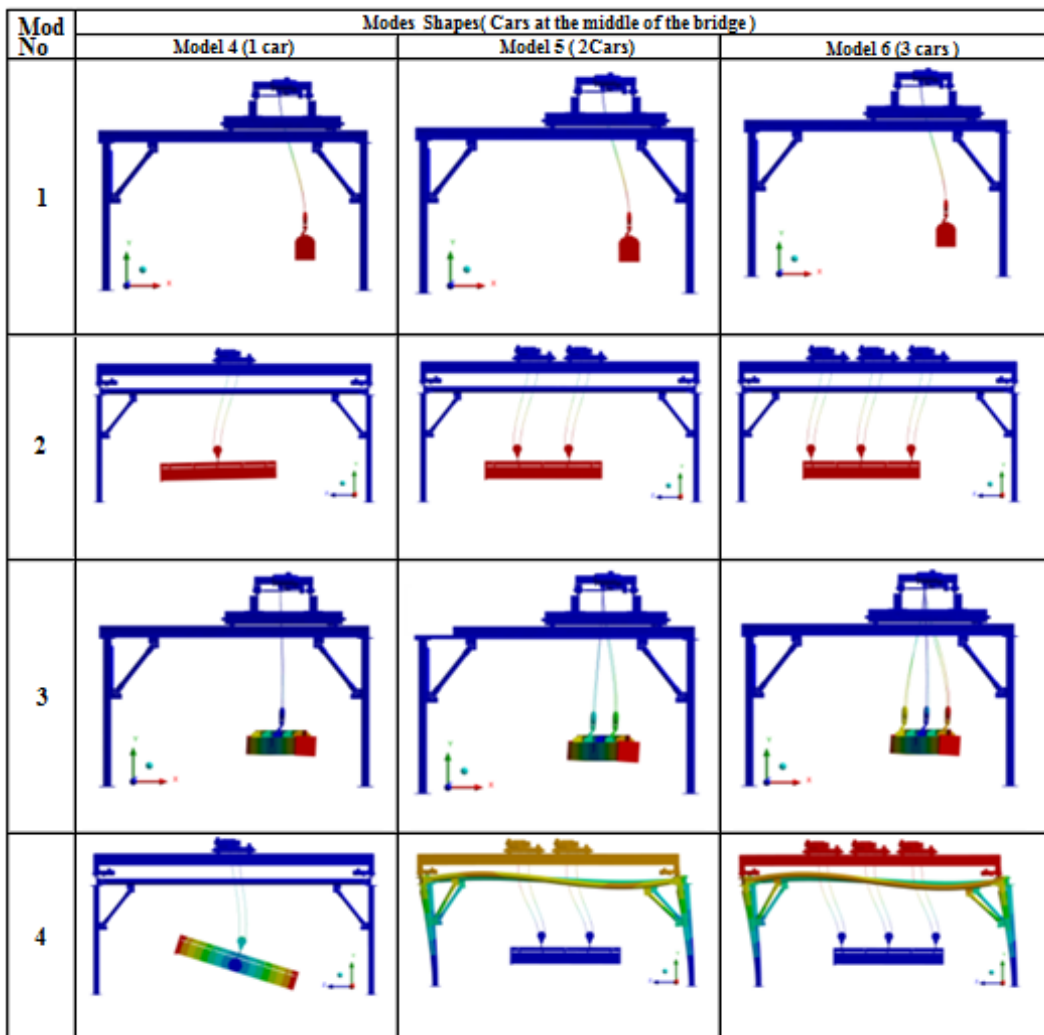
Figure 6. The first four mode shapes for the different car number (cars at the middle of the bridge)

As a result of the study the values of natural frequencies obtained according to different car numbers and the car positions are presented in Table 3.

Table 2. The values of natural frequencies overhead crane system for different car number and car position

	Natural frequency [Hz]					
Mod No	Model 1	Model 2	Model 3	Model 4	Model 5	Model 6
1	3,31E-02	4,66E-02	5,67E-02	3,315E-02	4,65E-02	5,67E-02
2	0,10283	0,16118	0,19672	0,10261	0,16134	0,19655
3	0,91625	1,2804	1,6396	0,92124	1,2934	1,5958
4	1,2343	3,9421	3,6464	1,2228	3,9647	3,6496
5	4,3962	5,6553	5,7244	4,3792	5,6549	5,7112
6	5,0504	5,7642	5,7663	4,9613	5,7565	5,7658
7	5,769	5,7688	5,7713	5,7773	5,7673	5,7669
8	5,8309	5,7858	5,7799	5,8354	5,769	5,7791
9	6,6223	6,2975	5,7808	5,8612	6,2215	5,7801
10	6,6554	6,6089	5,7872	6,6222	6,323	5,7807

It can be seen from this table; the values of natural frequencies generally decrease when the number of carriages number increase. The reason for this result is the increase in the weight of the carriages. The natural frequencies of the crane system will change because the mass will change with the increase in the number of carriages on the crane system. There is an inverse ratio between mass and frequency according to general vibration theory. the results support this situation.

When the mode shapes are examined, it is seen that with the change of the car position, the vibration characteristics occurring in the crane system do not change. In the same way, it is seen that the natural frequency values given in the table are very close to each other. According to the modes of natural frequency changes in order to make the net value of the changes are given in Figure 7.
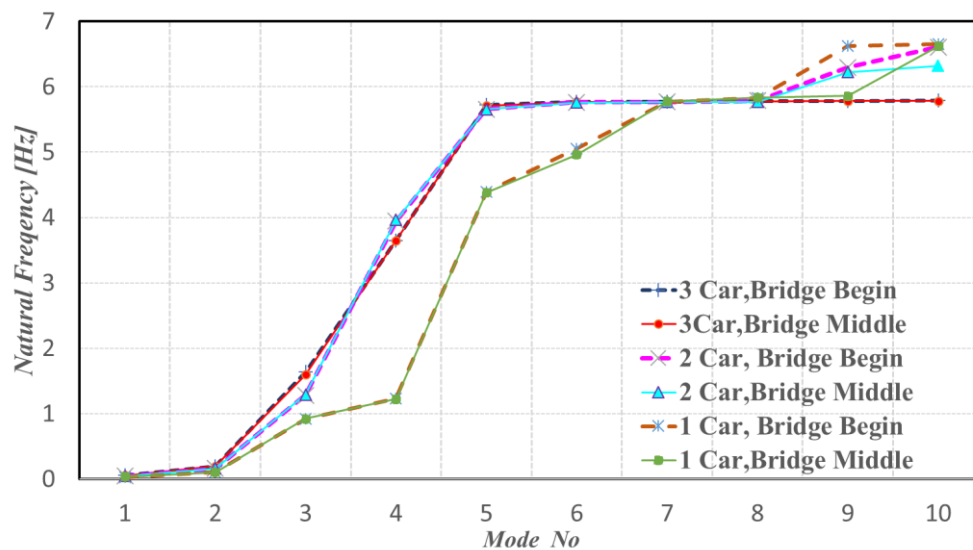
Figure 7. The first four mode shapes for the different car number (cars at the middle of the bridge)

5. CONCLUSION

In this paper the vibration analysis for the double beam overhead crane was investigated to study the influence of different carriages number and different carriages position on the naturel frequency for overhead crane. 3 D model was designed to analyze the vibration characteristics. The modal analysis of the crane system was performed using the finite element method. The conclusions obtained from the present work can be summarized as follows:

- The natural frequencies are reduced due to the change in the number of cars and the mass of the system. The total mass of crane system increases with carriages 'number

- In crane systems, when the cars are evaluated at the beginning of the bridge or in the middle, it is seen that the position does not affect the natural frequencies and characteristic deformations and only one of the locations is enough to take into account when performing the analyzes.

Vibration characteristic information for a multi-carriage crane system is important for achieving a successful design, eliminating excessive and unpleasant stresses, rapid wear and resonance effects in the system. Therefore, it is necessary to investigate the vibration characteristics of the crane system in order to improve performance efficiency and reduce noise. The present study is a preliminary study of the dynamic behavior for the crane system, and the effect of the number of carriages and the position of the carriages on this behavior.

ACKNOWLEDGMENT

REFERENCES

[1]   D. J. Ewins, *Modal Testing: Theory and Practice*: Resarch Studies Press 2000.

[2]   K. H. Low, "An analytical-experimental comparative study of vibration analysis for loaded beams with variable boundary conditions," *Computers & Structures* vol. 65, pp. 97-107, 1997.

[3]   K. H. Low, "A comparative study of the eigenvalue solutions for mass-loaded beams under classical boundary conditions," *International Journal of Mechanical Sciences,* vol. 43, pp. 237-244, Jan 2001.

[4]   P. D. Cha and W. C. Wang, "A novel approach to determine the frequency equations of combined dynamical systems," *Journal of Sound and Vibration,* vol. 219, pp. 689-706, 1999.

[5]   P. D. Cha, "Eigenvalues of a linear elastica carrying lumped masses, springs and viscous dampers," *Journal of Sound and Vibration,* vol. 257, pp. 798-808, 2002.

[6]   P. D. Cha, "A general approach to formulating the frequency equation for a beam carrying miscellaneous attachments," *Journal of Sound and Vibration,* vol. 286, pp. 921-939, 2005.

[7]   M. Karamolla, "Kule Vinclerin Matematik Modellemesi," Doktora Tezi, Fen Bilimleri Enstitusu, Celal Bayar Universitesi Manisa, 2005.

[8]   S. Yildirim and E. Esim, "A New Approach for Dynamic Analysis of Overhead Crane Systems Under Moving Loads," in *CONTROLO 2016*, Cham, 2017, pp. 471-481.

[9]   N. Z. Vlada Gašić, Aleksandar Obradović,Srđan Bošnjak, "Consideration of Moving Oscillator Problem in Dynamic Responses of Bridge Cranes," *FME Transactions* vol. 39, pp. 17-24, 2011.

[10] Z. Wu, C. Xu, J. Zhang, D. Yu, and P. Feng, "Modal and Harmonic Reponse Analysis and Evaluation of Machine Tools," pp. 929-933, 2010.

[11] S. Yildirim and E. Esim, "Design of Neural Network Predictor for Vibration Analysis of a Drill Column Machine During Drilling Plastic Work-Pieces," in *Mechanisms, Transmissions and Applications: Proceedings of the Fourth MeTrApp Conference 2017*, M. I. C. Dede, M. Itik, E.-C. Lovasz, and G. Kiper, Eds., ed Cham: Springer International Publishing, 2018, pp. 269-278.

[12] O. I. Abdullah and J. Schlattmann, "Vibration Analysis of the Friction clutch Disc Using," *Advances in Mechanical Engineering and its Applications (AMEA),* vol. 1, pp. 86-91, 2012.

Some of the quality properties and bioactivity of orange juice fermented with water kefir microorganisms

Selin Kalkan[1], Mustafa Remzi Otag[1]

Abstract

*Water kefir is a homemade fermented beverage based on a sucrose solution with fruit extracts. The aim of this work was to explore the use of orange fruit juice as fermentable substrates to develop new non-dairy fermented beverages. Microbiological (total mesophilic aerobic bacteria, total lactic acid bacteria, Lactococcus spp., total yeast and mold and coliform microorganism), chemical (pH, total soluble matter, titration acidity, density) and physical (color) properties of kefir-like beverages obtained after the fermentation of juice extracted from orange cultivated in Turkey with water kefir microorganisms were investigated. Additionally, total phenolic substance and antioxidant properties were determined of fermented beverages samples. The quantification of total phenolic was performed by using the Folin-Ciocalteu spectrophotometric method. Antioxidant activity was examined by ABTS radical scavenging assay. As results, the pH of fermented sample was found as 4.40±0.21, total soluble matter was 7.50±0.01%, titratable acidity 0.093±0.00 g/L, density was 1.02±0.01, L/a/b color values were 44.33±1.16 / 7.84±0.09/ 44.52±0.81**respectively**, total phenolic contents 92.97±1.34 mg GAE/L and antioxidant activity was of 745.07 µM trolox /g dw. The microorganism concentration of fermented orange juice by using water kefir microorganisms had significantly changed compared to the control group orange juice. The number of total mesophilic aerobic microorganism was determined as 8.79±0.15 log cfu/mL, Lactoccoccus spp. was 8.56±0.37 log cfu/mL, total lactic acid bacteria was 7.67±0.43 log cfu/mL and total yeast and mold were 7.75±0.35 log cfu/mL. Coliform microorganisms have not detected all samples.*

Keywords: Water kefir, orange juice, microbial, total phenolic, antioxidant activity

1. INTRODUCTION

Water kefir grains are a unique starter culture composition mainly used for the production of homemade, sparkling, low alcoholic acidic beverages. Water kefir is a fermented drink made by adding water kefir grains (inoculum) to water, fruit (dried) and sugar mixture [1-3]. The mixture is fermented for 2 to 4 days at room temperature under anaerobic conditions, and then the particles are separated from the fermented liquid to be re-used for the next fermentation process. The fermented liquid is a slightly sweet, acidic, slightly alcoholic and foamy product with a yellowish color and fruity taste and aroma.

The backbone of these grains consists of a polysaccharide matrix (i.e., dextrans) [4]. This microflora differs significantly from that found in dairy kefir grains. However, in contrast to water kefir, the microbiological composition of dairy kefir grains from different countries has been studied intensively [5]. Ward (1892) made the first description of similar grains called "ginger beer plant". Until today various synonyms are known, thus this symbiosis is also called "California bees", "African bees", "Ale nuts", "Balm of Gilead", "Japanese Beer Seeds" or "Sugary kefir grains" [6, 7].

The main microorganisms found in the water kefir are lactic acid bacteria (LAB), yeasts, bifidobacteria, and acetic acid bacteria [1, 3, 8-10]. Different water kefirs contain different species diversity, but it is not yet clear what are the key microorganisms in the fermentation process and how species diversity affects the fermentation process. LAB types, especially *Lactobacillus hilgardii*, are often associated with water kefir fermentation and are thought to be responsible for the growth of water kefir grain due to the production of EPS from sucrose [7, 11]. Recently,

---

[1]*Giresun University, Department of Food Engineering, 28200 Giresun, Turkey.*

Corresponding author: selin.kalkan@giresun.edu.tr

a new species of Bifidobacterium has been found in water kefir, but its importance remains unclear during water kefir fermentation [12]. The main metabolites produced during water kefir fermentation are ethanol, lactic acid, glycerol, acetic acid, and mannitol; the main flavor compounds are 2-methyl-1-propanol, isoamyl alcohol, ethyl acetate, isoamyl acetate, ethyl hexanoate and ethyl octanoate [3].

Currently, the water kefir drink is predominantly carried out at the household level, so the raw materials used to prepare the water kefir drink vary from person to person [3]. From a commercial point of view, the water kefir fermentation process is difficult to control, as it can become unstable, yielding variable end-products. In addition, the water kefir grain growth often decreases, which prevents successful backslopping or upscaling of the production process. To be able to avoid and/or remedy these problems during fermentation and allow the development of a stable commercial production process, a thorough understanding of the water kefir fermentation process is required.

In this study, it was aimed to determine the physical, chemical and microbiological properties of the fermented orange juices using water kefir grains.

2. MATERIALS AND METHODS

2.1. Production of orange juice kefir

In this study, orange juice was fermented with water kefir grains. The fruits were peeled after washing thoroughly and fruit juices were obtained. Water kefir grains to be used in fermentation were provided from Canberk Gida Ihtiyac Mad. Nak. San. ve Tic. Ltd. Sti., (Yenimahalle/ Ankara) as dried. The water kefir grains used in the study were shown at Figure 1.

Figure 1. Water kefir grains

For the production of orange juice kefir, firstly dry water kefir grains were activated. Dry kefir grains were placed in drinking water for 15 minutes for the first fermentation step. Then 40 grams of sucrose and 10 raisins were added to 1 liter of drinking water and added active kefir grains to the mixture. The glass jar sealed with cheesecloth was allowed to pre-fermentation at room temperature for 2 days. After activation of the water kefir cultures, kefir grains were separated from the mixture and added to 10 g of sucrose added orange juice for the second (main) fermentation. The glass jar with orange juice was tightly sealed and allowed to fermentation for 2 days at room temperature. At the end of the main fermentation, the water kefir grains were filtered and separated from fermented orange juice [13].

2.2. Microbiological analyzes

Serial dilutions were prepared to determine the microbiological properties of the control group (orange juice) and fermented orange juice samples with water kefir grains. Cell suspensions were plated and incubated as follows: total mesophilic aerobic bacteria count (TMAB) spread plated on Plate Count Agar (PCA, Merck), incubated aerobically at 37 ºC for 24 h; total coliform group bacteria pour plated on double-layered Violet Red Bile Glucose agar (VRBGA), incubated aerobically at 37 ºC for 24 h; rod LAB pour plated on de Man-Rogosa-Sharpe (MRS) Agar, acidified to pH 5.4 with lactic acid (5 mol/L) and incubated anaerobically at 30 ºC for 48 h; coccus LAB pour plated on M17 Agar, incubated anaerobically at 30 ºC for 48 h; yeasts spread plated on Potato Dextrose (PDA, Merck) Agar, incubated aerobically at 25 ºC for 48 h. Count plates were carried out in duplicate for each independent production [14].

2.2. Physicochemical analyzes

Analyses of pH and soluble solids were performed according to the methodology reported by the Association of Official Analytical Chemistry [15]. Measurements of pH were determined electrometrically using the pH meter FiveEasy Plus™ FP20 (Mettler Toledo, Columbus, Ohio, ABD). Density values of sample and soluble solid content (SSC) was measured using a pycnometer DMA™4100M (Anton Paar, Graz, Austria) and SSC values reported as ^{o}Brix. Total titratable acidity (TTA) was determined by titration of the samples with 0.1 N NaOH to an end point of pH 8.1 and expressed as g/L of citric acid. Total phenolic compounds (TPs) were analysed according to the Folin-Ciocalteu procedure [16] and the results were expressed as mg/L of gallic acid equivalent (GAE). Colour of control and orange juice kefir samples were measured with a colorimeter (Chroma Meter CR-400, Minolta, Osaka, Japan), recording CIElab chromaticity coordinates ($L*$, $a*$, $b*$), where $L*$ is the lightness, $a*$ and $b*$ are color-opponent dimensions, redness and yellowness, respectively [13]. The antioxidant activity was determined as ABTS radical scavenging (μM trolox /g dw).

2.3. Statistical analyzes

The results of microbial and physicochemical analysis of the samples were interpreted using the Windows SPPS 20.0 software statistical package program (SPSS Inc., Chicago, IL, USA) according to the randomized block trial plan. The results of the study were evaluated by using one-way variance analysis.

3.RESULTS AND DISCUSSION

The microbiological and physicochemical analyzes were performed to determine some quality characteristics of orange juice fermented with water kefir and control-orange juice (not fermenting). The results obtained from microbiological analyzes were shown in Table 1.

Table 1. Microbiological properties of orange juice samples (log cfu/mL)

	TMAB	Lactococcus spp.	LAB	Yeast	Total coliforms
Control	3.25 ± 0.20^a	3.50 ± 0.04^a	3.19 ± 0.89^a	3.51 ± 0.18^a	ND*
Fermented orange juice	8.49 ± 0.15^b	8.56 ± 0.37^b	7.67 ± 0.43^b	7.75 ± 0.35^a	ND*

* Mean and std. error; a-b: Different parent icons in the same column indicate a significant difference at p≤0.05; ND: Not determined; TMAB: Total mesophilic aerobic bacteria; LAB: Lactic acid bacteria

As shown in Table 1, the microbiological properties of the fermented orange juice samples are significantly different compared to the control juice (p≤0.05). Water kefir microorganisms caused this difference. Gulitz et al. [1] reported that, mainly, the consortium of water kefir is comprised of 10^8 lactobacilli, 10^6-10^8 acetic acid bacteria and 10^6-10^7 yeasts per gram granules. The LAB of the kefir grains belongs to the following species: Lactobacillus, Lactococcus and Leuconostoc [5]. Gulitz et al. [1] were identified *Lactobacillus nagelii*, *Lactobacillus hordei*, *Lactobacillus hilgardii*, *Lactobacillus casei*, *Leuconostoc mesenteroides* and *Leuconostoc citreum*, as well as two Acetobacter species (*Acetobacter fabarum* and *Acetobacter orientalis*), as stable components of this microbiome using culture-dependent techniques. Leroi and Pidoux [17] have determined synergism between *Lb. hilgardii* and *Saccharomyces florentinus* in water kefir grains. In our study, similar to previous studies, it is found that the number of yeasts and lactic acid bacteria was quite intense in fermented orange juice samples. Coliform group microorganism was not detected in any of the samples.

The physicochemical properties of the samples were summarized in Table 2. As seen in Table 2, the physicochemical properties of the fermented orange juices with water kefir have changed significantly (p≤0.05). Our findings from the research results showed similarity with the results of Randazzo et al. [13].

The antioxidant results of the samples were shown in Figure 2. As shown in Figure 2, the antioxidant activity is higher in fermented orange juice samples than the control group samples.

Table 2. Physicochemical properties of orange juice samples

	pH	Density (g/cm^3)	TTA (g/L citric acid)	SSC (ºBrix)	TP (mg GAL/L)	Color		
						L*	a*	b*
Control	4.04±0.05[a]	1.036±0.00[a]	0.0588±0.00[a]	9.65±0.06[a]	109.07±9.34[a]	35.15±0.45[a]	6.56±0.07[a]	41.66±0.53[a]
Fermented orange juice	4.40±0.21[b]	1.027±0.00[ab]	0.0938±0.00[b]	7.50±0.01[b]	92.97±1.34[b]	43.33±1.16[b]	7.84±0.09[b]	44.52±0.81[b]

* Mean and std. error; a-b: Different parent icons in the same column indicate a significant difference at p≤0.05
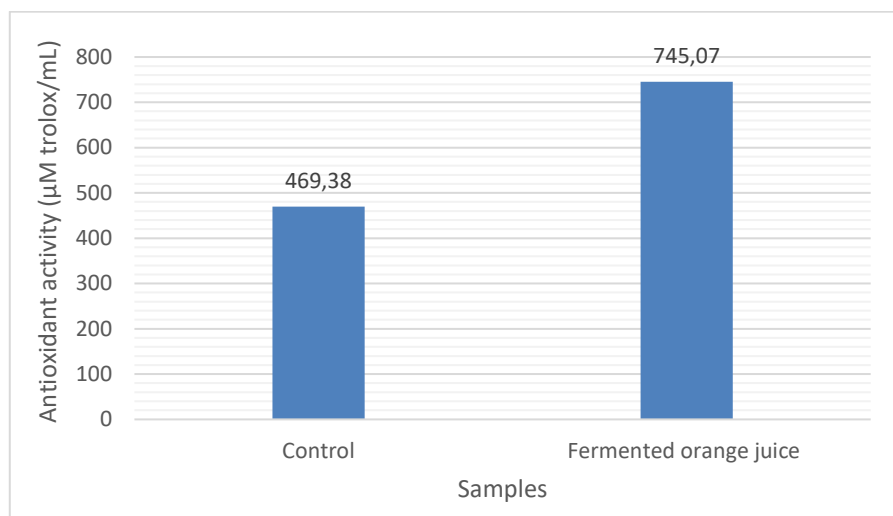
Figure 2. Antioxidant activity of orange juice samples

CONCLUSIONS

The obtained results of this study showed that orange fruit juices can be processed with water kefir microorganisms. Moreover, fermented orange juice can be consumed as an alternative beverage with its suitable microbiological and physicochemical properties.

REFERENCES

[1]. A.Gulitz., J. Stadie, M. Wenning, M. A. Ehrmann, and R. F. Vogel, "The microbial diversity of water kefir", Int J Food Microbiol, vol. 151, pp. 284-288. 2011

[2]. J., Marsh, O. O'Sullivan, C. Hill, R.P. Ross, and P.D. Cotter, "Sequence-based analysis of the microbial composition of water kefir from multiple sources". FEMS microbiology letters, vol. 348(1), pp. 79-85. 2013.

[3]. D. Laureys, De Vuyst, L. "Microbial species diversity, community dynamics, and metabolite kinetics of water kefir fermentation", Appl. Environ. Microbiol., vol 80(8), pp. 2564-2572. 2014.

[4]. H. Neve, K.J. Heller, K. J. "The microflora of water kefir: a glance by scanning electron microscopy", Kieler Milchwirtschaftliche Forschungsberichte, vol. 54(4), pp. 337-349. 2002.

[5]. S. Z. Davidović, M.G. Miljković, M.D. Rajilić-Stojanović, S.I. Dimitrijević-Branković, and D.G. Antonović, "Water Kefir grain as a source of potent dextran producing lactic acid bacteria", Chemical Industry/Hemijska Industrija, vol 69(6)., pp. 595-604, 2015.

[6]. L. F. Kebler,"California Bees", Journal of the Amercian Pharmaceutical Association, vol. 10, pp. 939-943, 1921.

[7]. M. Pidoux, "The microbial flora of sugary kefir grain (the gingerbeer plant): Biosynthesis of the grain from Lactobacillus hilgardii producing a polysaccharide gel". MIRCEN Journal of Applied Microbiology and Biotechnology, vol. 5, pp. 223–238. 1989.

[8]. K.T. Magalhães, G.V. Pereira, D.R. deM. Dias, and R.F. Schwan, "Microbial communities and chemical changes during fermentation of sugary Brazilian kefir", World Journal of Microbiology and Biotechnology, vol. 26(7), pp. 1241–1250. 2010.

[9]. K.T. Magalhães, D.R. Dias, G.V. Pereira, deM., C.R. Campos, G. Dragone, and R.F. Schwan, "Brazilian kefir: structure, microbial communities and chemical composition", Brazilian Journal of Microbiology, vol. 42, pp. 693–702. 2011.

[10]. A.Gulitz, J. Stadie, M. A. Ehrmann, W. Ludwig, and R. F. Vogel, "Comparative phylobiomic analysis of the bacterial community of water kefir by 16S rRNA gene amplicon sequencing and ARDRA analysis", J Appl Microbiol, vol. 114, pp. 1082-1091. 2013.

[11]. F.W. Waldherr, V.M. Doll, D. Meißner, and R.F. Vogel, "Identification and characterization of a glucan-producing enzyme from Lactobacillus hilgardii TMW 1.828 involved in granule formation of water kefir", Food Microbiology, vol. 27(5), pp. 672-678. 2010.

[12]. D. Laureys, M. Cnockaert, L. De Vuyst, and P. Vandamme, P. "Bifidobacterium aquikefiri sp. nov., isolated from water kefir". International journal of systematic and evolutionary microbiology, vol. 66(3), pp. 1281-1286. 2016

[13]. W. Randazzo, O. Corona, R. Guarcello, N. Francesca, M.A. Germana, H. Erten and L. Settanni, "Development of new non-dairy beverages from Mediterranean fruit juices fermented with water kefir microorganisms", Food Microbiology, vol. 54, 40-51. 2016.

[14]. AOAC-Association of Official Analytical Chemistry, In: AOAC - Association of Official Analytical Chemistry (Ed.), Official Methods of Analysis of the Association of Official Analytical Chemistry, seventeenth ed. Washington. 2000.

[15]. FDA. Bacteriolological Analytical Manual. Food and Drug Administration 16 th Edition. AOAC Int. Gaithersburg MD. 1995.

[16]. K. Slinkard, V.L. Singleton, "Total phenol analysis: automation and comparison with manual methods", Am. J. Enol. Vitic. vol. 28 (1), pp. 49-55. 1977.

[17]. F. Leroi, M. Pidoux,"Detection of interactions between yeasts and lactic acid bacteria isolated from sugary kefir grains", Journal of Applied Microbiology, vol. 74(1), pp. 48–53. 1993.

Species List of Zerconid Mites (Acari: Mesostigmata: Zerconidae) of Czech Republic

Mehmet Karaca[1], Rasit Urhan[2]

Abstract

Mites of the family Zerconidae are important members of soil mesofauna in the Holarctic region. Species of this family are free-living predators and their diets include eggs, larvae and immature stages of other mites or springtails, and also nematodes. Systematic of zerconid mites are well-studied in Slovakia and former Czechoslovakia. However, today there is no updated species list for zerconid mites in Czech Republic. As a contribution to the knowledge of acarofauna of this country, current species list of the family Zerconidae is presented herein.

Keywords: Czech Republic, distribution, species list, zerconid mites

1.INTRODUCTION

Czech Republic has a special position on Europe, and located in the middle of this continent (Figure 1). This country has different geomorphological structures and a rich vegetation. Therefore, many animal species from different groups have luck to live in this country. There are many endemic species in terms of both flora and fauna elements. One of these groups is zerconid mites (family Zerconidae) which occur in soil mesofauna of Holarctic region.

Members of this family are known from Holarctic region only [1], [2]. This mites may be colonized in various soil types, in litters, and between moss pads. Zerconids are free-living predators in subclass Acari (Table 1). Their life cycle include four active stages: larvae, protonymph, deutonymph and adults [3]. This small predator mites, fed by eggs, larvae, and nymphs of other mites which live with zerconids in the same environment [4]. Nowadays, over 40 genera and 400 valid species have been recorded from the Holarctic region [5], [6]. Ecological informations (their economic importances and roles in soil decomposition system) about this group is limited for now.

Table 2. Classification of zerconid mites

Regnum	Animalia
Phylum	Arthropoda
Class	Arachnida
Subclass	Acari
Superorder	Parasitiformes
Order	Mesostigmata
Suborder	Monogynaspida
Cohort	Gamasina
Superfamily	Zerconoidea
Family	Zerconidae

---

[1] *Corresponding author: Pamukkale University, Denizli Vocational School of Technical Sciences, Department of Electronic and Automation, 20160, Pamukkale/Denizli, Turkey. karacamehmet@pau.edu.tr*

[2] *Pamukkale University, Faculty of Science and Arts, Department of Biology, 20070, Pamukkale/Denizli, Turkey. rurhan@pau.edu.tr*

Figure 3. Location of Czech Republic on Europe continent [7]

2.MATERIAL AND METHODS

In this paper, species list of zerconid mites of Czech Republic is presented based on two major literature, Halašková (1969) [8] and Mašán & Fenďa (2004) [9]. Zerconid species were compared and current species list was revealed. In addition to species diversity, distribution informations were given for each species.

3.RESULTS AND DISCUSSION

The family Zerconidae is currently reperesented by 3 genera (*Parazercon*, *Prozercon* and *Zercon*), and 25 species in Czech Republic [8], [9]. Most of species are similar to Zerconidae fauna of Slovakia. So far, zerconid mites have been reported from the following regions in the country by Halašková [8]: basins (1-2=Eger, 3=Pilsen), 4=Central-Bohemian Hill Country, forests (5-6=Bohemian), mountains (7-8=Bohemian Central, 16=Foreland of Giant, 17=Giant, 18=Orlice, 27=Rychleby, 29=Oder, 30=Moravian-Silesian Beskydy), plateaus (9=Křivoklát-Radeč, 11=Prague, 13=Jevany), 10=Bohemian Karst, 12=Sázava Valley, 14=Elbe Lowland, 15=Bohemian Paradise, highlands (19-20=Třebová, 21-26=Bohemian-Moravian), 28=Hlučín Hillocks, hills (31=Chřiby, 33=Pavlov) and 32=Lower Moravian Dale (Figure 2). All of these numbers were used for indicate to distribution localities of zerconid mites in Czech Republic.

Species List of Zerconid Mites of Czech Republic

1. Genus: *Parazercon* Trägårdh, 1931
Type Species: *Zercon radiatus* Berlese, 1910
Species: *Parazercon radiatus* (Berlese, 1910)
Distribution in Czech Republic: 1, 2, 5, 7, 17, 19, 22, 25, 27 [8].
Known distribution: Austria, Belarus, British Isles, Canada, Czech Republic, Finland, Germany, Greenland, Latvia, Lithuania, Norway, Poland, Romania, Russia, Slovakia, Sweden, Switzerland, Ukraine, USA [9].
Note: Halašková reported this species as *Parazercon sarekensis* [8].

2. Genus: *Prozercon* Sellnick, 1943
Type Species: *Zercon fimbriatus* C. L. Koch, 1839
Species: *Prozercon carpathofimbriatus* Mašán & Fenďa, 2004
Distribution in Czech Republic: Not mentioned.
Known distribution: Czech Republic, Poland, Slovakia, Turkey [9], [10].
Note: Halašková did not report this species from the country [8].
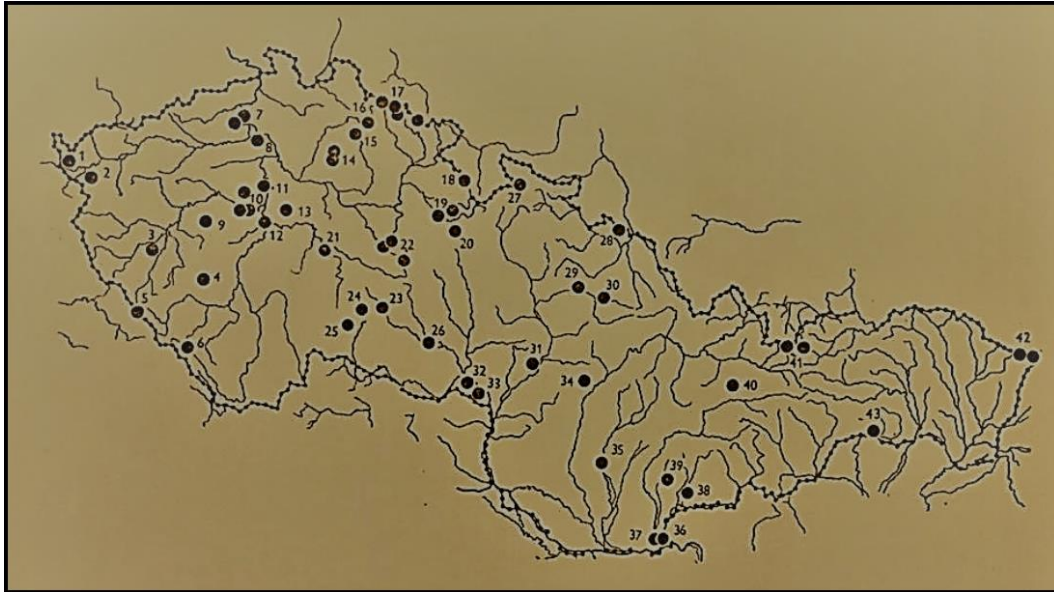
Figure 4. Collection sites for recorded zerconid mites in former Czechoslovakia (Original map of Halaskova, 1969. Not to scale. Today, localities between 1-33 are located in Czech Republic, 34-43 are located in Slovakia)

Species: *Prozercon fimbriatus* (C. L. Koch, 1839)
Distribution in Czech Republic: Not mentioned.
Known distribution: Algeria, Austria, Belgium, British Isles, Bulgaria, Caucasus, Croatia, Czech Republic, France, Germany, Hungary, Italy, Poland, Romania, Slovakia, Spain, Switzerland, Turkey, Ukraine [9], [11].
Note: Halašková did not report this species from the country [8].

Species: *Prozercon kochi* Sellnick, 1943
Distribution in Czech Republic: Not mentioned.
Known distribution: Austria, British Isles, Czech Republic, Finland, Germany, Hungary, Latvia, Poland, Romania, Russia, Slovakia, Sweden, Ukraine [9].

Species: *Prozercon lutulentus* Halašková, 1963
Distribution in Czech Republic: Not mentioned.
Known distribution: Czech Republic, Poland, Slovakia, Spain, Ukraine [9]..
Note: Halašková did not report this species from the country [8].

Species: *Prozercon sellnicki* Halašková, 1963
Distribution in Czech Republic: Not mentioned.
Known distribution: Croatia, Czech Republic, Germany, Latvia, Poland, Slovakia, Ukraine [9], [11].
Note: Halašková did not report this species from the country [8].

Species: *Prozercon traegardhi* (Halbert, 1923)
Distribution in Czech Republic: Not mentioned.
Known distribution: Austria, British Isles, Croatia, Czech Republic, England, Finland, Germany, Hungary, Iceland, Ireland, Latvia, Lithuania, Poland, Romania, Russia, Slovakia, Slovenia, Sweden, Switzerland, Turkey, Ukraine [9], [11].

3. Genus: *Zercon* C. L. Koch, 1836
Type Species: *Zercon triangularis* C. L. Koch, 1836
Species: *Zercon arcuatus* Trägårdh, 1931
Distribution in Czech Republic: 1, 5, 7, 13, 17, 21, 23.
Known distribution: Austria, British Isles, Croatia, Czech Republic, Faroes, Germany, Poland, Romania, Slovakia [9], [12].

Species: *Zercon athiasi* Vincze, 1965
Distribution in Czech Republic: 10.

Known distribution: Croatia, Czech Republic, Hungary, Poland, Slovakia, Ukraine [9], [12].

Species: *Zercon berlesei* Sellnick, 1958
Distribution in Czech Republic: 5, 10, 32.
Known distribution: British Isles, Croatia, Czech Republic, Hungary, Iceland, Italy, Poland, Romania, Slovakia, Spain, Turkey [9], [12].

Species: *Zercon curiosus* Trägårdh, 1910
Distribution in Czech Republic: 4, 30.
Known distribution: Austria, Czech Republic, Finland, Hungary, Iceland, Latvia, Poland, Russia, Slovakia, Sweden, Switzerland, Ukraine [9].

Species: *Zercon gurensis* Mihelčič, 1962
Distribution in Czech Republic: 2, 4, 5, 7, 10, 13, 14, 17, 18, 19, 20, 22, 27, 31, 33.
Known distribution: Austria, Bulgaria, Croatia, Czech Republic, Germany, Poland, Slovakia, Ukraine [9], [11].

Species: *Zercon hercynicus* Halašková, 1969
Distribution in Czech Republic: 5, 6.
Known distribution: Czech Republic [8].

Species: *Zercon hungaricus* Sellnick, 1958
Distribution in Czech Republic: 7, 9, 10, 28, 31, 32.
Known distribution: Austria, Bulgaria, Croatia, Czech Republic, Hungary, Poland, Romania, Slovakia, Turkey, Ukraine [9], [11].

Species: *Zercon italicus* Sellnick, 1944
Distribution in Czech Republic: 5, 6.
Known distribution: Czech Republic, Germany, Italy, Switzerland [8].

Species: *Zercon moravicus* Halašková, 1969
Distribution in Czech Republic: 33.
Known distribution: Bulgaria, Czech Republic, Germany, Slovakia [9].

Species: *Zercon peltatus* C. L. Koch, 1836
Distribution in Czech Republic: 3, 4, 7, 8, 9, 10, 11, 12, 14, 17, 19, 21, 22, 23, 30, 32, 33.
Known distribution: Austria, British Isles, Bulgaria, Croatia, Czech Republic, England, Germany, Hungary, Poland, Romania, Slovakia, Spain, Turkey, Ukraine [9], [11].

Species: *Zercon pinicola* Halašková, 1969
Distribution in Czech Republic: 7, 9, 15, 26.
Known distribution: Austria, Czech Republic, Iceland, Poland, Slovakia, Turkey, Ukraine [9].

Species: *Zercon romagniolus* Sellnick, 1944
Distribution in Czech Republic: 5, 24.
Known distribution: Austria, Croatia, Czech Republic, Italy, Poland, Romania, Slovakia, Switzerland, Ukraine [9], [12].

Species: *Zercon serenus* Halašková, 1969
Distribution in Czech Republic: 4.
Known distribution: Czech Republic, Slovakia [9].

Species: *Zercon spatulatus* C. L. Koch, 1839
Distribution in Czech Republic: 7, 21, 22, 23.
Known distribution: Austria, Croatia, Czech Republic, England, Germany, Hungary, Poland, Spain [8], [11].

Species: *Zercon storkani* Halašková, 1969
Distribution in Czech Republic: 12, 22.
Known distribution: Austria, Croatia, Czech Republic, England, Germany, Hungary, Poland, Spain [8], [12].

Species: *Zercon triangularis* C. L. Koch, 1836
Distribution in Czech Republic: Known from many localities.
Known distribution: Austria, Balcan Peninsula, Belgium, British Isles, Czech Republic, Denmark, Finland, France, Germany, Greenland, Holland, Hungary, Iceland, Ireland, Italy, Latvia, Lithuania, Moldavia, Norway, Poland, Romania, Russia, Slovakia, Spain, Spitzberg, Sweden, Switzerland, Ukraine [8], [9].

Species: *Zercon vacuus* C. L. Koch, 1839
Distribution in Czech Republic: 4, 10, 17, 19, 22.

Known distribution: Austria, Bulgaria, Czech Republic, Germany, Hungary, Poland, Romania, Slovakia, Spain [9].

Species: *Zercon zelawaiensis* Sellnick, 1944
Distribution in Czech Republic: 17.
Known distribution: Czech Republic, England, Russia, Sweden [8].

CONCLUSIONS

The first systematic paper about zerconids in former Czechoslovakia was published by Zerconidae specialist Dr. Vera Halašková in 1969. She recorded 29 zerconid species from the country, 10 of them were presented as new for the science. After split up in 1993, zerconid mites of Slovakia was presented as a book by Mašan & Fend'a in 2004. No zerconid records were given from the country (Czech Republic) after 1969.

Some provinces of Czech Republic is still unstudied in terms of Zerconidae systematic. Further new species and new records of zerconid mites are anticipated with local faunistic investigations (especially in forestland areas) in this country.

ACKNOWLEDGMENT

REFERENCES

[1]. E. E. Lindquist, G. W. Krantz, And D. E. Walter, "Order Mesostigmata, A Manual Of Acarology (Eds: G. W. Krantz And D.E. Walter)", Usa: Texas, Texas Tech University Press, 3rd Ed., 2009.

[2]. P. G. Balan, "To The Knowledge Of The Genus *Prozercon* (Acari, Mesostigmata, Zerconidae)", *Zoologicheskii Zhurnal*, Vol. 71, Pp. 32-38, 1992.

[3]. R. Urhan, "*Prozercon Celali* Sp. Nov. Of Soil Mites (Acari: Zerconidae) From Turkey", *Annales Zoologici*, Vol. 60, Pp. 133–137, 2010.

[4]. G. M. Shereef, M. A. Afifi, And S. H. O. El Bishlawy, " Description, Life Cycle And Feeding Habitats Of *Zercon Adalicus* N. Sp. (Acari, Gamasida, Zerconidae)", *Bulletin Of Faculty Of Agriculture*, Cairo University, Vol. 35, Pp. 1765–1774, 1984.

[5]. R. Urhan, And M. Karaca, "A New Species Of The Genus *Zercon* (Acari, Mesostigmata, Zerconidae) From Kastamonu, Turkey", *Acarological Studies*, Vol. 1, Pp. 3–10, 2019.

[6]. M. Karaca, "*Zercon Kadiri* Sp. N., A New Oligophagous Mite From Eastern Anatolia (Acari: Mesostigmata: Zerconidae)", *Zoology In The Middle East*, Vol. 65, Https://Doi.Org/10.1080/09397140.2019.1627701, 2019.

[7]. (2019) The Geology Website. [Online]. Available: Http://Geology.Com/World/Cia/Map-Of-Europe.Gif

[8]. V. Halašková, "Zerconidae Of Czechoslovakia (Acari: Mesostigmata)", *Acta Universitatis Carolinae-Biologica*, Vol. 3-4, Pp. 175–352, 1969.

[9]. P. Mašán, And P. Fend'a, "Zerconid Mites Of Slovakia", Slovak Academy Of Sciences, Institute Of Zoology, 238 Pp, 2004.

[10]. E. H. Duran, And R. Urhan, "Zerconid Mites (Acari, Zerconidae) In Istanbul, With Four New Records For The Turkish Fauna", *Turkish Journal Of Zoology*, Vol. 41, Pp. 931–939, 2017.

[11]. Z. Ujvári, "New Records Of Zerconid Mites (Acari: Mesostigmata) From Mts. Papuk, Croatia, With Description Of *Zercon Kontschani* Sp. N.", *Opuscula Zoologica Budapest*, Vol. 37, Pp. 63–70, 2006.

[12]. Z. Ujvári, "Zerconid Mites (Acari: Mesostigmata: Zerconidae) From Croatia With Description Of Four New Species", *Journal Of Natural History*, Vol. 44, Pp. 1671–1696, 2010.

Biography: Dr. Mehmet graduated from Institute of Science (Pamukkale University) and obtained the Ph.D. title in 2015. After that, he focused on Zerconidae systematics in different parts of Turkey. Up to now, he published about 25 articles in SCI, SCI-Expanded and other indexed journals. Also he presented 80 notices in national/international congresses, conferences and symposiums. With this studies, 17 new zerconids are described as new for sciences, besides 22 zerconids are recorded as new for Turkish and Iranian acarofauna. He is currently working at Pamukkale University.

Removal of Color and COD from Biologically Treated Textile Effluents by Coagulation-Flocculation, Fenton and Photo-Oxidation (H₂O₂/UV) Methods

Elcin Gunes[1], Gul Kaykioglu[1], Yalcin Gunes[1], Asude Hanedar[1]

Abstract

The textile industry, one of the fastest growing industries in Turkey, is one of the most polluting sectors of the environment. Although it is possible to treat the wastewater of the textile industry by conventional methods, the applied methods are not successful in color removal. In this study, three different treatment technologies (coagulation-flocculation, Fenton and H_2O_2/UV) were studied for color and COD removal in wastewater taken from a textile industrial wastewater treatment plant. Wastewater characteristics were as follows pH: 7.8, conductivity: 934 µS/cm, TSS: 50 mg/L, COD: 200 mg/L, color: 226.1 m^{-1}. Optimum operating conditions for these processes have been determined and evaluated in terms color removal.

In the coagulation-flocculation process, $FeCl_3$ was used as the coagulant and the optimum pH was found to be 5 and the optimum Fe^{3+} dose was found to be 85 mg/L. Color and COD removal rates were 95% and 92% under this conditions. The COD and color removal efficiencies obtained using the Fenton process are 92% and 70%, respectively. The color removal efficiencies in H_2O_2/UV process with 900 mg/L H_2O_2 doses resulted in 98% color and 69% COD removal after 135 minutes. The removal rates increased with time and H_2O_2 doses in H_2O_2/UVC process. Color and COD values were obtained as 11.3 m^{-1} and 16 mg/L, 18.1 m^{-1} and 60 mg/L, 4.5 m^{-1} and 62 mg/L by coagulation-flocculation, Fenton and H_2O_2/UV methods respectively. Compared to the methods used, coagulation-flocculation can be said to be effective, operable and easy to apply for the removal of color and COD from this textile wastewater.

Keywords: *Textile effluents, coagulation-flocculation, color removal, advanced oxidation*

1. INTRODUCTION

The textile industry produces high amounts of wastewater due to the high water consumption for many processes. It contains a wide range of chemicals such as wastewater, acids, alkalis, dyes, hydrogen peroxide, starch, surfactants, auxiliary chemicals and metals [1] [2] . The main pollution source of wastewater comes from dyeing and finishing in this sector [3]. Among the major pollutants in textile wastewater are COD, color, acidity, high suspension solids and other soluble substances. Among the major contaminants in textile wastewaters are BOD, COD, colour, acidity, high suspended solids, metals and other soluble substances [4] [5]. The textile industry includes different dye types with high molecular weight and complex structures and shows very low biodegradability in terms of color removal. For this reason, they are insufficient to provide discharge standards for receiving waters [6]. Textile wastewaters with high colored and organic concentrations threatens the environment when discharged without treatment [7]. The toxicity of dyes and by-products to the nature, mutagenic and carcinogenic effects on humans make it necessary to treat them [8].

It has been widely reported in several studies that biological processes are applied in the treatment of textile wastewater. However, biological treatment processes are limited in the removal of non-biodegradable materials. In addition, organic matter removal and color removal efficiencies are also limited. With different processes of activated sludge following elimination rates could be achieved: about 90%BOD5 40 - 50% COD and 20 -30%

---

colour [3]. In this context, the color removal processes in the treatment of wastewaters containing high amounts of dyestuffs arising from the textile industries are becoming more important in ecological terms [7]. Processes commonly used in color removal from wastewater can be divided into four classes. These include: (i) physical and physicochemical methods such as colagulation-flocculation, ion exchange, adsorption and membrane filtration, (ii) chemical oxidation methods (Fenton, photo-Fenton, ozonation etc.) , (iii) biological methods such as aerobic or anaerobic decomposition, (iv) electrochemical methods such as electrodialysis [7] [9].

In this study, three different treatment technologies (coagulation-flocculation, Fenton and H_2O_2/UV) were studied for color and COD removal in wastewater taken from a textile industrial wastewater treatment plant.The aim of the study was to evaluate the efficiency of coagulation-flocculation, Fenton and photo-oxidation (H_2O_2/UV) processes for the treatment of wastewaters from a textile industriy which is biologically treated.

2. MATERIALS-METHODS

2.1. Analytical Methods

Aerobically pre-treated textile wastewater were taken from a textile finishing industry located in Corlu, Tekirdag.

The samples were collected in 20 L plastic drums and stored at 4ºC. For the wastewater samples, chemical parameters including pH and conductivity were determined in situ by using appropriate sensors, chemical oxygen demand (COD, mg/L) and total suspended solids (TSS, mg/L) were determined according to Standard Methods [10]. The color was measured according to the EN 7887 standard using a thermoelectronic AQUAMATE spectrometer. Three different wavelengths of 436, 525, 620 nm were used.

2.2. Treatment Methods

- #### Coagulation–flocculation process

A series of Jar-test experiments were conducted on wastewater using 1 min rapid mixing at 120 rpm, 20 min slow mixing at 45 rpm and 30 min settling using a polyelectrolyte. Optimum pH and optimum dosages were studied at various pH values and at various coagulant doses at room temperature (25ºC). Ferric chloride was tested as conventional coagulant, and sodium-hydroxide was used for pH adjustment. The samples were allowed to stand for 30 minutes for precipitation. After waiting for 30 min the supernatant was withdrawn for COD and color analyses.

- #### Fenton Process(H_2O_2/Fe^{2+})

Fenton process experiments were conducted with the Jar test method. The pH was adjusted at 3.0±0.2 by adding sulfuric acid. The ferrous and hydrogen peroxide dose optimization studies were carried out at pH:3. The necessary quantities of Fe^{2+} and then H_2O_2 were added simultaneously in the wastewater.   This method was preceded with rapid mixing of the effluent at 120 rpm for 10 min, slow mixing at 45 rpm for 60 min and then standstill for 60 min. After 60 min settling time, the supernatant was treated with 6N NaOH to pH:7-8 to remove residual H_2O_2 and for precipitation of ferro compounds and centrifuged 5 min at 3500rpm. Then physical and chemical characteristics of the treated wastewater were analyzed according to Standard Methods [10].

- #### Photo-oxidation (H_2O_2/UVC)process

For the photo-oxidation (H2O2/UVC) process study 254 nm low pressure mercury vapor lamp (model Hg F15-05, Eurotech) with a nominal power of 12 W (according to the manufacturer) was used. The UV lamp was placed in a 400 mL batch reactor. The pH was adjusted at 3.0±0.2 by adding sulfuric acid. The necessary quantities of H2O2 was added simultaneously in the wastewater. After the required time intervals the pH was adjusted to pH:7 - 8 with 6N NaOH to remove residual H2O2 and for precipitation of ferro compounds and the supernatant was centrifuged 5 min at 3500rpm.

3. RESULTS AND DISCUSSION

- #### Coagulation–flocculation process

In coagulation-flocculation experiments, firstly the optimum pH is determined, then the optimum coagulant doses should be determined. In this study pH 5, 6, 7, 8 and 9 were used for optimum pH studies and $FeCl_3$ was used in experiments. 35 mg/L Fe^{3+} was used in optimum pH study. Color and COD removal efficiencies as a result of optimum pH experiments are given in Figure 1. As seen from the figure, the best removal efficiencies for color and COD were obtained at pH 5. At this pH, 85% and 88% removal efficiencies were obtained for color and COD, respectively. As the Figure 1 shows, as the pH increased, the removal efficiencies decreased.
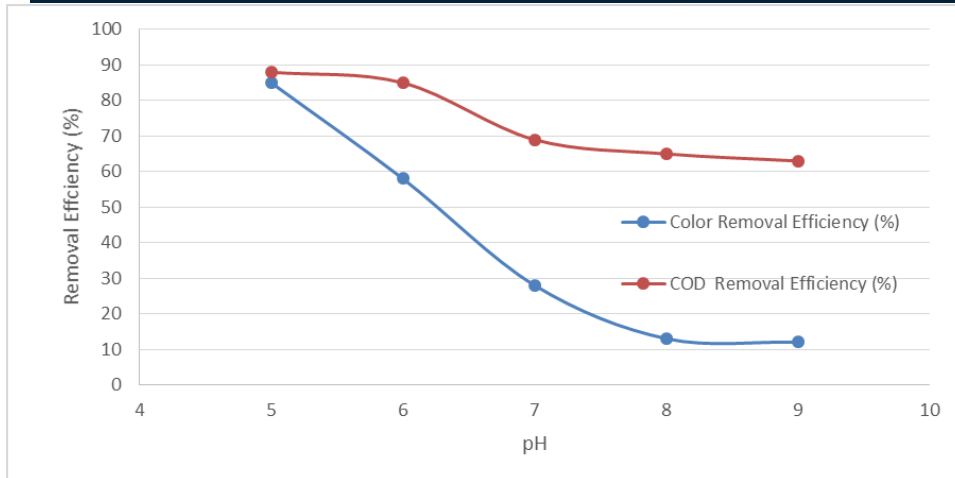
Figure 1. pH effect on COD and color removal efficiencies

The results of optimum dosages study are given in the Figure 2. The best removal rates were obtained at 85 mg/L Fe^{3+} concentrations and the color and COD removal efficiencies at this Fe^{3+} dosages were 95% and 92%, respectively.
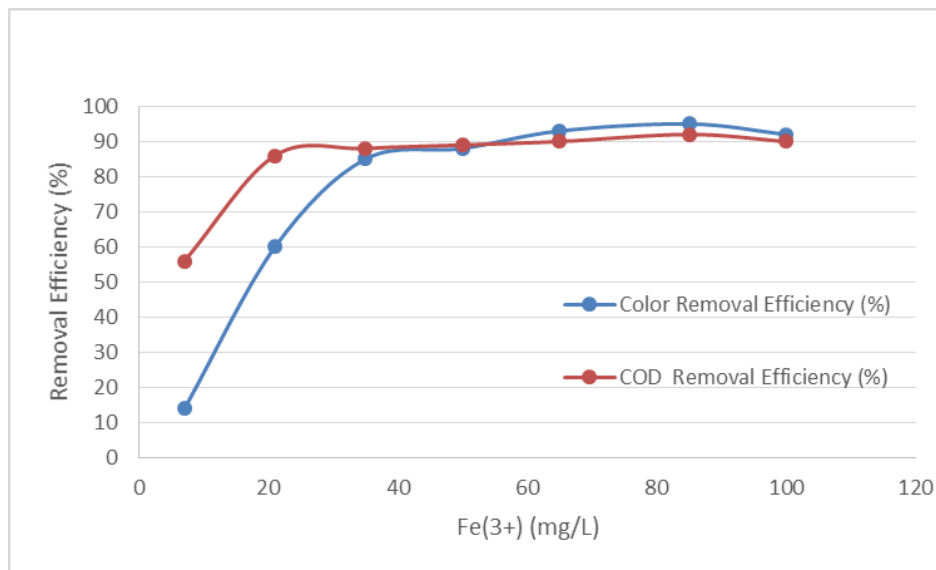
Figure 2. Fe^{3+} effects on COD and color removal efficiencies

- ***Fenton Process (H_2O_2/Fe^{2+})***

Figure 3 shows the effect of Fe^{2+} dosage on the color and COD removal with a fixed amount of 150 mg/L H_2O_2 for the wastewater. As the dosage of Fe^{2+} increased from 50 to 150 mg/L the removal efficiencies increased from 51% to 88% for color removall and 42% to %69 for COD removal. This is because higher Fe^{2+} dosages generate more •OH radicals in Fenton treatment.
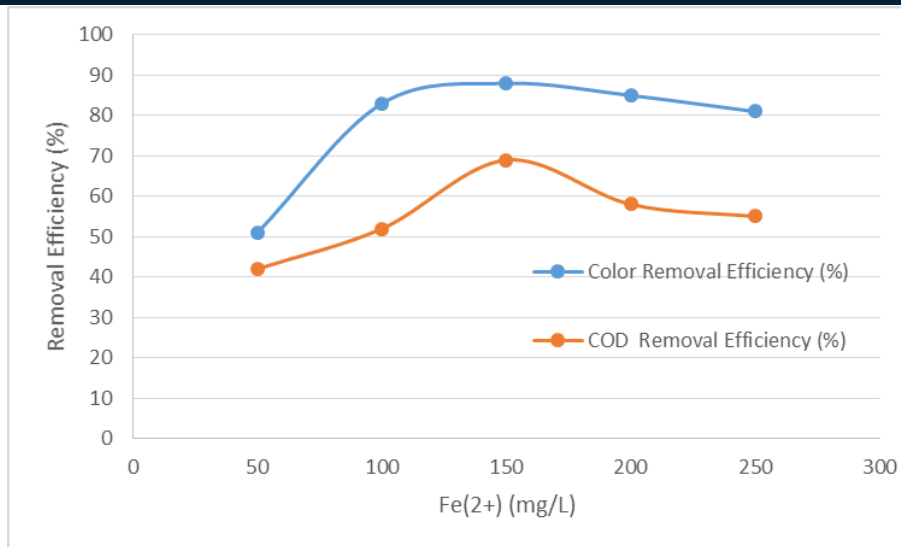
Figure 3. Fe^{2+} effects on COD and color removal efficiencies (150 mg/L H_2O_2)

During the Fenton process, hydrogen peroxide plays a very important role as a source of hydroxyl radical generation [11]. Figure 4 shows the removal of color and COD removal efficiencies for at different H_2O_2 dosages. When the dosage of H_2O_2 increased from 90 to 240 mg/L, the removal efficiency increased from 69% to 92% for color removal and from 57% to 70% for COD removal. As it is known, higher H_2O_2 doses generate more hydroxyl radicals [12] and improved the color and COD removal efficiencies. However, as seen from Figure 1, the color and COD removal efficiencies started to decrease for doses of H_2O_2 over 240 mg/L. This may be explained by the scavenging activity of •OH by reacting with H_2O_2 [13]. The optimum H_2O_2 concentration was determined to be 240 mg/L.
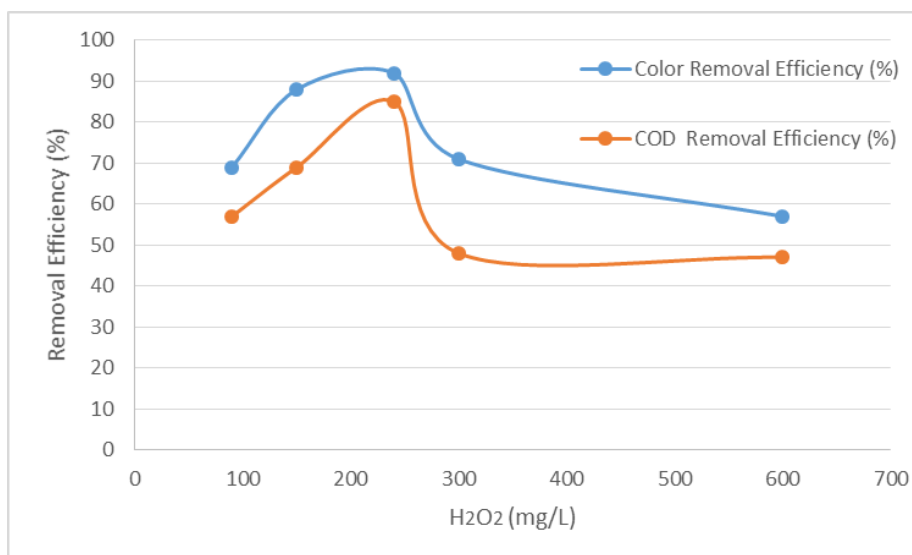
Figure 4. H_2O_2 effects on COD and color removal efficiencies (150 mg/L Fe^{2+})

- ***Photo-oxidation (H_2O_2/UVC)process***

Direct photolysis of H_2O_2 (H_2O_2/UV) produces hydroxyl radicals which can be used for the degradation of organic compounds. For the photo-oxidation process we used 300, 600 and 900 mg/L of H_2O_2 doses. The effect of time and H_2O_2 doses on color removal efficiencies were given on Figure 5 . As it is seen from the Figure 5, after 135 minutes color removal efficiencies for 300, 600, 900 mg/L H_2O_2 concentrations were 87%, 90% and 98% respectively.
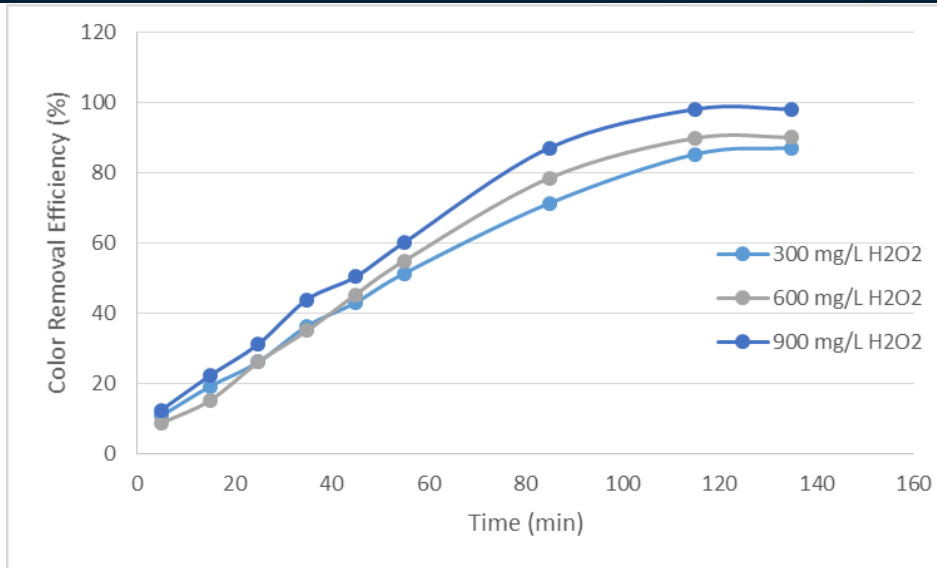
Figure 5.The effect of time and H₂O₂ doses on color removal efficiency

COD removal efficiencies were measured only in 135 minutes. As it can be seen from the Figure 6, at 135 minutes COD removal efficiencies were 65%, 72% and 80% for using of 300, 600 and 900 mg/L H_2O_2 respectively.
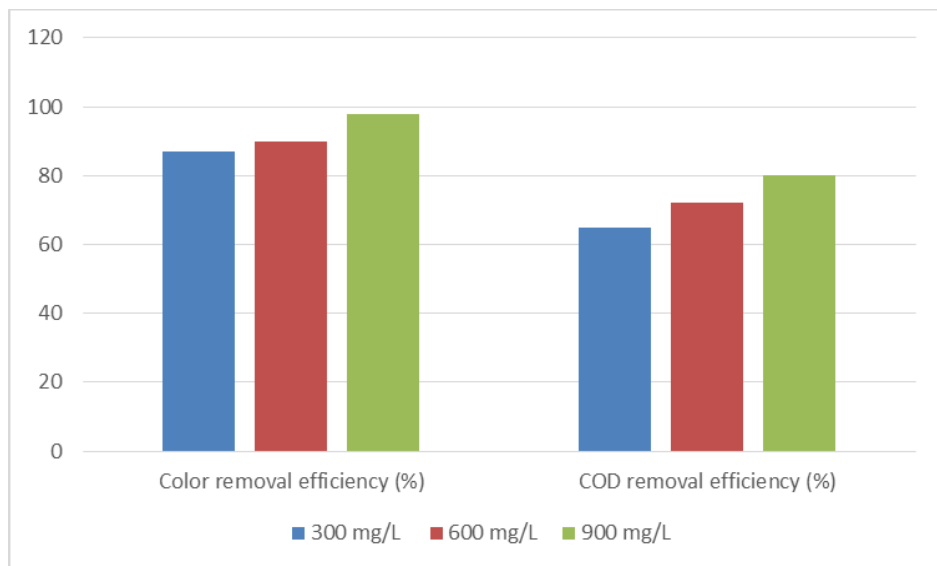
Figure 6. The effect of H₂O₂ doses on color and COD removal efficiencies

CONCLUSION

According to arrangement dated April 24, 2011 in Turkish Water Pollution Control Regulation (TWPCR) discharge standards have been revised for COD and also added standard for color for all textile industries in Thrace Region. It is aimed 2nd class water in 2020 in the region. According to 2nd class water quality in TWPCR COD must be 50 mg/L. According to EN ISO 7887 discharge criteria of the receiving water quality for color parameters must be 15 m⁻¹.So in this study the color and COD removal of a biologically (aerobically) treated textile industrial effluents were investigated. In the study coagulation-flocculation, Fenton and photo-oxidation (H_2O_2/UV) were tested to remove color and COD. The conclusions obtained in the study are summarized below:

- In coagulation-flocculation process optimum pH was found as 5, and optimum dosage of Fe^{3+} was found as 85 mg/L. At this conditions color and COD were measured as 11.3 m^{-1} and 16 mg/L respectively.

- The optimum values of operating parameters during the oxidation of the color and COD by the Fenton's process are Fe^{2+} =150 mg/L, H_2O_2 =240 mg/L. Under these conditions, color and COD values were obtained as 18.1 m^{-1} and 60 mg/L by Fenton process. The experimental results show that the initial concentration of H_2O_2 and Fe^{2+} had great influence on the removal of COD and color by the Fenton's process.

- By employing the photo-oxidation (H_2O_2/UV) process, it was found that this process was also suitable for color and COD removal. Color and COD values were obtained as 4.5 m^{-1} and 62 mg/L by H_2O_2/UV method. In this method, the increase in the time and the increase of the H_2O_2 concentrations increased the removal efficiencies.

When the results are examined it is seen that all methods used may remove color and COD. However, it is seen that coagulation is more efficient in removing COD from these methods. Considering the applicability and easy to operate, it can be said that the coagulation-flocculation process is more feasible.

REFERENCES

[1] C.R. Holkar, A. J. Jadhav, D.V. Pinjari, N.M. Mahamuni, A.B. Pandit (2016). A critical review on textile wastewater treatments: Possible approaches. Journal of Environmental Management 182, 351-366.

[2] J. Paul, A.A. Kadam, S.P. Govindwar et al. (2013). An insight into the influence of low dose irradiation pretreatment on the microbial decolouration and degradation of reactive red-120 dye. Chemosphere 90, 1348-1358.

[3] X.Z. Li & Y. G. Zhao (1997). On-site Treatment of Dyeing Wastewater by a Bio-photoreactor System, Water Science and Technology, Volume 36, Issues 2–3, Pages 165-172.

[4] S. N. Hussain, A. Ahmad, A. Ali, H. Sattar and H. M. A. Asghar (2015). Wastewater Treatment of Textile Industry via Adsorption and Electrochemical Regeneration. International Conference on Advances in Environment Research Volume 87 of IPCBEE (2015) DOI: 10.7763/IPCBEE. 2015. V87. 3.

[5] S. Arslan, M. Eyvaz, E. Gurbulak and E. Yuksel (2016). A Review of State-of-the-Art Technologies in Dye- Containing Wastewater Treatment – The Textile Industry Case. http://dx.doi.org/10.5772/64140.

[6] G.Yildiz. Tore, R.Ata, S.Ozden Celik, S. Kirhan Sesler (2017). ColourRemoval fromBiologically Treated Textile Dyeing Wastewater with Natural and Novel Pre Hydrolysed Coagulants. JOTCSA. 2017; 5(sp. is. 1): 23-36.

[7] O.O.Namal (2017). Tekstil Endustrisi Atiksularinin Aritiminda Kullanilan Proseslerin Arastirilmasi, Nevsehir Bilim ve Teknoloji Dergisi Cilt 6(ICOCEE 2017 Ozel Sayi) 388-396.

[8] TUBITAK KAMAG Projesi (2013). Boyar Madde Iceren Atiksu Aritma Tesislerinin Isletilmesine Yonelik El Kitabi, 109G083 NOLU TUBITAK KAMAG PROJESI.

[9] M. Joshi, R. Bansal, R. Purwar (2004). Colour removal from textile effluents" Indian Journal of Fibre & Textile Research, 29, 239-259.

[10] APHA (2005). Standard Methods for the Examination of Water and Wastewater, 21st ed.

[11] J. Li, Z. Luan, L. Yu, et al (2012). Pretreatment of acrylic fiber manufacturing wastewater by the Fenton process. Desalination,284:62–65.

[12] H.Tekin, O, Bilkay, S.S. Ataberk, et al. (2006). Use of Fenton oxidation to improve the biodegradability of a pharmaceutical wastewater. J Hazard Mater, 136(2):258–265.

[13] F.J. Benitez, J.l.Acero, F.J. Real, et al. (2001) The role of hydroxyl radicals for the decomposition of p-hydroxy phenylacetic acid in aqueous solutions. Water Res, 35(5):1338–1343.

Developing a smart software to calculate similarity factors for time series: T-sim

Ismail Kirbas[1]

Abstract

Today, because of the development and diffusion of sensor technology, measurements are made continuously and the large data obtained is stored in databases. Tracking the behaviour of a specific phenomenon/data in time can produce important information. A large variety of real world applications, such as meteorology, geophysics and astrophysics, collect observations that can be represented as time series. Similarity analysis in time series has become a necessity in many areas. The research on time series includes clustering, classification, similarity search, feature extraction, trend forecasting, and decision support. Similarity measures a fundamental research topic on time series theory. Currently, there is no definitive and uniform description for the similarity of time series, which results in difficulties for relevant research on this topic. In this study, a useful interface has been developed which allows visualization of the different time series on the same screen and calculation of similarity factors. Following the review of the literature, the most accepted similarity factors were determined and a useful and user-friendly software called "T-sim" was developed.

Keywords: Kirbas's relative signal similarity factor, signal similarity, time series, T-sim.

1. INTRODUCTION

Signal comparison and determination of signal similarity are among the processes that need to be performed in many areas today. The analog and digital signals obtained from the sensors give us important clues about what is happening in the outside world. Signal similarity detection is also widely used in in many disciplines, from image processing to the financial sector, and medical device development to pattern recognition [1]–[3].

Although it is applied in many fields, the subject of our study covers the determination of the similarity rate in time series. For this purpose, by making manual and automatic manipulations on two different time series, similarity ratios and geometric distances of the two signals can be easily determined.

Next section gives brief introduction to widely used similarity parameters and their mathematical equations beside a new Kirbas's relative signal similarity ratio (κ).

2. MATERIALS AND METHODS

Clustering of time series is an active research area with a wide range of applications. One of the key components in cluster analysis is to determine an appropriate similarity between two data objects, and several criteria have been proposed in the literature to evaluate the difference between the two-time series [4]–[7].

One of the most basic methods of measuring the similarity between two signals is to take the signals as vectors and calculate the distance between the two vectors geometrically. The equation used for this purpose is the expression given in equation 1, which is referred to as Minkowski distance [5].

$$d_{L_n}(x, y) = \left(\sum_{i=1}^{M} (x_i - y_i)^n \right)^{\frac{1}{n}} \tag{1}$$

---

[1] *Corresponding author: Burdur Mehmet Akif Ersoy University, Department of Computer Engineering, 15100, Burdur, Turkey.*
  ismailkirbas@mehmetakif.edu.tr

Figure 1 shows two different signals, indicated by red and blue colors. The black two-way arrows between the two signals indicate the distance at certain points of the signal.
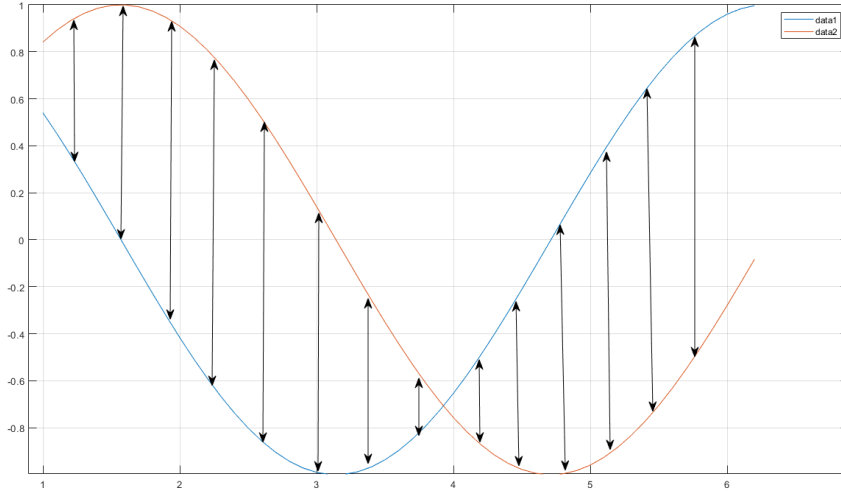
Figure 5.Euclidean distance between two different signals.

In another approach, the similarity ratio is obtained by performing Fourier transform of two series. Equation 2 implies the similarity ratio after this transformation [8].

$$d_{FC}(x,y) = \left(\sum_{i=1}^{M/2} (\hat{x}_i - \hat{y}_i)^2 \right)^{\frac{1}{2}} \tag{2}$$

Another parameter that gives the correlation coefficient between two series is Pearson's correlation factor and it is given in equation 3. $\overline{X_T}$ and $\overline{Y_T}$ represents the average values of serial realizations X_T and Y_T respectively [9].

$$COR(X_T, Y_T) = \frac{\sum_{t=1}^{T}(X_t - \overline{X_T})(Y_t - \overline{Y_T})}{\sqrt{\sum_{t=1}^{T}(X_t - \overline{X_T})^2}\sqrt{\sum_{t=1}^{T}(Y_t - \overline{Y_T})^2}} \tag{3}$$

After the calculated maximum and minimum Euclidean distances between the two series Kirbas's signal relative similarity ratio parameter used for determining the similarity rate based on these values. κ represents Kirbas's relative signal similarity ratio which is given in equation 4.

$$\kappa = 1 - \frac{d_{L_n} - \min(d_{L_n})}{\max(d_{L_n}) - \min(d_{L_n})} \tag{4}$$

κ can take a value between 0 and 1. If its value approaches to 1, signal similarity is maximum in terms of Euclidean distance and signal similarity decreases as the κ value approaches zero.

3. RESULTS AND DISCUSSION

In the developed interface, which is given in Figure 2, there are buttons in the upper right section to load data, normalize the data and calculate the overlap situation where the signal similarity is highest. When the "load" button is pressed, two time series are loaded from the external environment. The overlapped states of the time series are

loaded into the graphic plotting area at the top left of the screen, while the original states of both time series are plotted on the right side of this area.

Figure 6. The screenshot of the developed signal similarity analysis software.

After loading data and drawing graphs, descriptive statistics are calculated for both time series and the calculated values are displayed in the boxes at the bottom of the screen. The calculated main statistic values are series mean, maximum and minimum values, standard deviation, mode and median. In the lower right corner of the screen, there are histogram distributions of two time series. When shifting operations are performed on time series, histogram graphs are recalculated and plotted.

The lag slider position is initially zero and can be moved by the number of elements in the time series. When the lag slider position is increased by 1 unit, the first time series is shifted one unit to the left. With the change of the lag slider position, the upper left graph is redrawn and statistical calculations are repeated. Euclidean distance and Kirbas's signal similarity ratio (κ) between two time series are also recalculated. If the difference between the signal amplitudes is too high, the signals can be normalized by pressing the "normalized" button. Thus, the signal similarity comparison may become more meaningful. Figure 2 shows both time series before the automatic highest similarity calculation process.
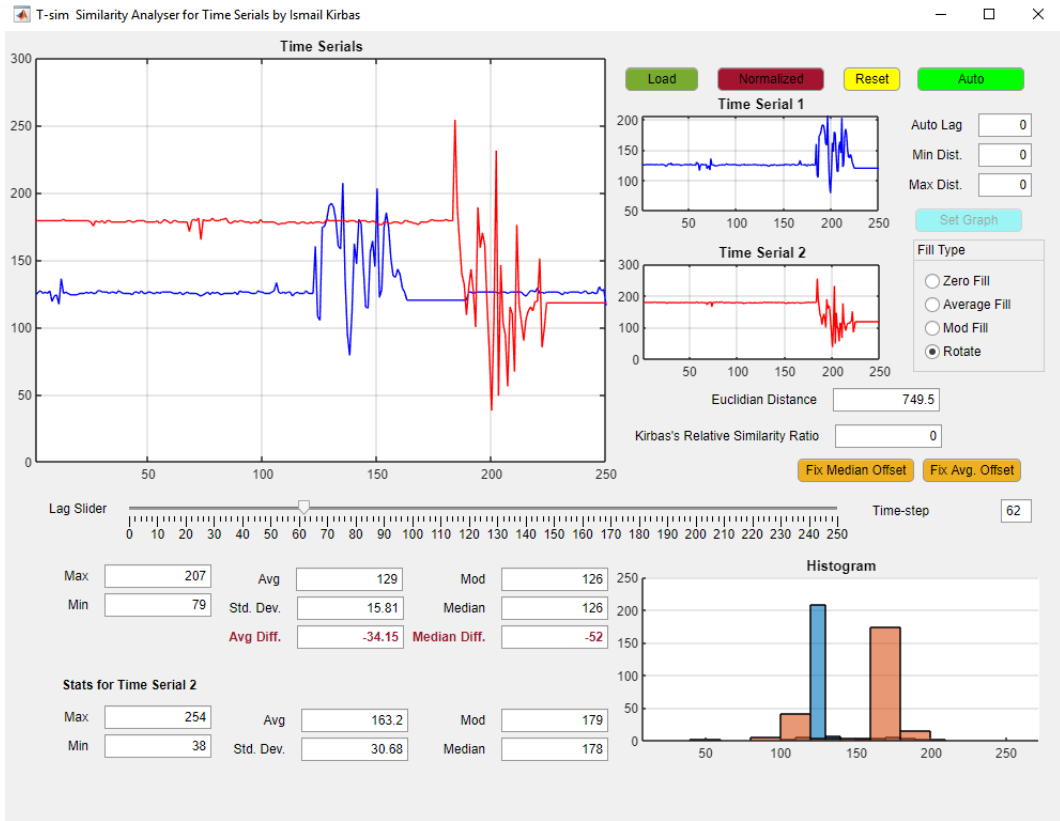
Figure 7. The screenshot before automatic highest similarity finding process.

Four different approaches can be utilized when shifting the signals over each other using the lag slider. You can select which method to scroll with the radio buttons in the fill type section. The first method is to assign zero to the last element of the series each time the series is shifted to the left. The second method assigns the average of the series to the last element in the left shift. The third method assigns the mode value of the series to the last element. The fourth method is different from all the above methods and assigns the value at the beginning of the series as the value of the last element.

When the auto button is pressed, according to the selected fill type method, starting from zero to the last element of the time series is scrolled and after each shift, the distance between the two time series is calculated. The maximum and the minimum distance values between the two time series are calculated and displayed under the auto button in the interface. The shift position value, where the highest similarity value is calculated, is also displayed in the "auto lag" section just below the "auto" button.

Figure 4 shows the new time series graphics after automatic calculation process.
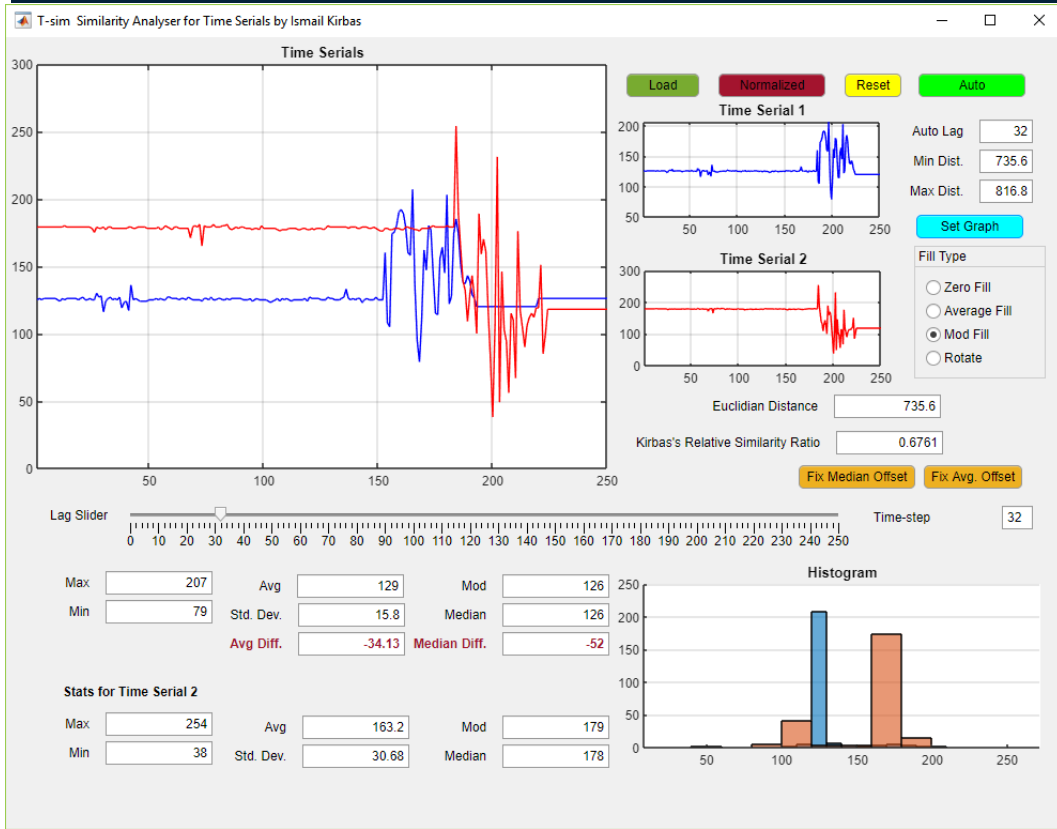
Figure 8. The screenshot after pressing the auto button.

After these calculations, if the "set graph" button is pressed the first time series is drawn again by shifting to the left by the auto lag value. If there is a constant difference between the signal averages or the median values, the "fix median offset" or "fix avg offset" buttons can be used. The median correction is carried out according to the formula in equation 5.

$$d_1(x) = d_1(x) - median(d_1) - median(d_2) \tag{5}$$

The formula given in equation 6 is used for the average correction.

$$d_1(x) = d_1(x) - mean(d_1) - mean(d_2) \tag{6}$$

After the median and average correction, the signals are superimposed on each other on the y-axis. This is confirmed by the overlap in the histogram graph. Figure 5 shows the newest form of both time serials after median correction process.
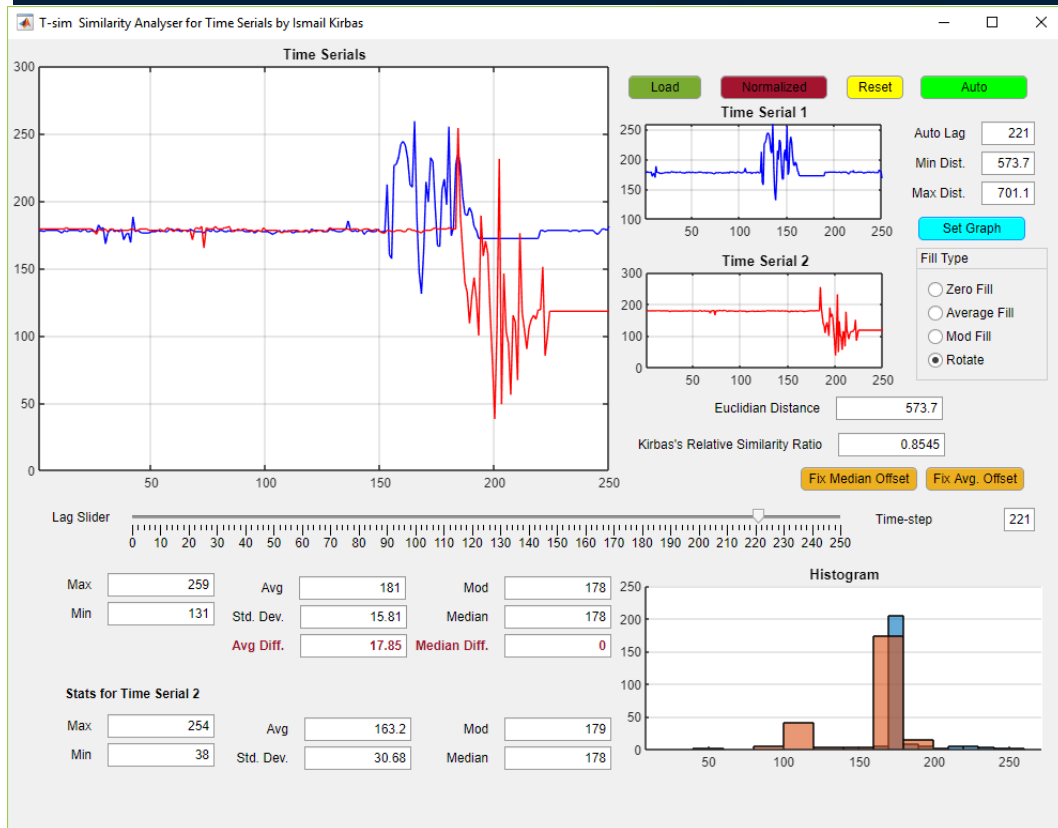
Figure 9. The screenshot after median correction process.

4. CONCLUSIONS

Similarity analysis in time series has become a necessity in many areas. The research on time series includes clustering, classification, similarity search, feature extraction, trend forecasting, and decision support. Similarity measures a fundamental research topic on time series theory. In this study, we developed a smart interface to define similarity ratio between two signals or time series using MATLAB App Designer Tool.

Using this tool, the user can display two different signals on the same screen, examine the basic statistical values for the series, and view the histograms of the series. In addition, the Euclidean distance between the series is calculated and displayed simultaneously. The user can follow the changes in the similarity rate and statistical data by sliding the signals on each other by four different methods. However, the developed software can automatically calculate the time step value which gives the highest similarity ratio.

Kirbas's relative signal similarity ratio κ, which can take values between 0 and 1, is used to express the relative similarity ratio between the signals. For the parameter κ, 1 indicates the highest similarity and 0 indicates the lowest similarity ratio. At the same time, "fix median offset" and "fix average offset" can be used to reset the median and average offset values to make it easier to compare time series with different average and median values.

Many methods and parameters can be used in signal similarity comparison. For the further study, dynamic time wrapping, and similar methods can be studied and the results of these methods may add to the interface.

ACKNOWLEDGMENT

REFERENCES

[1]   I. Kirbas, 'Short-Term Multi-Step Wind Speed Prediction Using Statistical Methods And Artificial Neural Networks', presented at the International Science and Technology Conference, 2016, vol. 1, p. 1064.

[2]   I. Kirbas and M. Peker, 'Signal detection based on empirical mode decomposition and Teager–Kaiser energy operator and its application to P and S wave arrival time detection in seismic signal analysis', Neural Comput. Appl., vol. 28, no. 10, pp. 3035–3045, Oct. 2017.

[3]   I. Kirbas, A. Kerem, I. Kirbas, and A. Saygin, 'Performance Analysis of Time Series Forecasting Models for Short Term Wind Speed Prediction', in III International Conference On Engineering And Natural Science, Budapest, 2016, vol. 1, pp. 2733–2739.

[4]   H. Yin, H. Qi, J. Xu, W. N. N. Hung, and X. Song, 'Generalized Framework for Similarity Measure of Time Series', Math. Probl. Eng., vol. 2014, pp. 1–12, 2014.

[5]   J. Serrà and J. Ll. Arcos, 'An empirical evaluation of similarity measures for time series classification', Knowl.-Based Syst., vol. 67, pp. 305–314, Sep. 2014.

[6]   S. Sengupta, P. Ojha, and H. Wang, 'Effectiveness of similarity measures in classification of time series data with intrinsic and extrinsic variability', p. 6.

[7]   C. Cassisi, P. Montalto, M. Aliotta, A. Cannata, and A. Pulvirenti, 'Similarity Measures and Dimensionality Reduction Techniques for Time Series Data Mining', in Advances in Data Mining Knowledge Discovery and Applications, A. Karahoca, Ed. InTech, 2012.

[8]   E. López-Iñesta, F. Grimaldo, and M. Arevalillo-Herráez, 'Classification Similarity Learning Using Feature-Based and Distance-Based Representations: A Comparative Study', Appl. Artif. Intell., vol. 29, no. 5, pp. 445–458, May 2015.

[9]   P. Montero and J. A. Vilar, 'TSclust: An R Package for Time Series Clustering', J. Stat. Softw., vol. 62, no. 1, 2014.

[10] A. Kerem, I. Kirbas, and A. Saygin, in Performance Analysis of Time Series Forecasting Models for Short Term Wind Speed Prediction, 2016, vol. 1, pp. 2733–2739.

Minimization Of An Unmanned Helicopter Torque Value Using ABC Algorithm

Mehmet Konar[1], Seda Arik[2], Tugrul Oktay [3]

Abstract

One of the important developments that technological innovations add to human life is unmanned aerial vehicles (UAVs). Today, UAVs are used different sizes for different purposes by many users. As UAVs offer a wide range of uses, UAV designs have become a popular application area. UAVs are designed in different sizes with fixed or rotary wing type. One of the issues to be considered in these designs is to determine the optimum torque value of the UAV. In this study, the minimization of the torque value of an unmanned helicopter is discussed. For this purpose, propeller blade parameters that affect the torque value of an unmanned helicopter, i.e. blade length, blade chord width, blade mass density and blade twist angle, are selected as the input parameters. The torque value obtained by using these input parameters is chosen as the output parameter. In the proposed approach, the output parameter values were calculated for certain value ranges of the input parameters, and the input parameter values corresponding to the minimum output parameter were determined. For this purpose, Artificial Bee Colony (ABC) algorithm which is frequently preferred in the literature and offers effective results was used. Thus, the blade parameters required for the minimum torque were determined. The simulation results showed that the ABC algorithm performs very well to calculate the blade parameter values in response to the minimum torque in a short time and with an acceptable error rate. This approach can provide effective performance with less time and less cost using in UAV designs.

Keywords: Helicopters, UAVs, Torque, ABC Algorithm, Optimization.

1. INTRODUCTION

Unmanned aerial vehicles (UAVs) with its technological capabilities meet the requirements of both military and civilian applications. UAV technologies are a multidisciplinary technology that is involved in many fields such as aviation, robotics, electronic hardware and software. Although UAV systems seem to have an ordinary structure today, security protocols and operator requirements have been developed with the technological infrastructure used. UAVs can perform their duties as semi-autonomous or fully autonomous according to the developed operator supports [1].

UAVs are designed in different sizes and types according to task requirements. UAVs are produced in different sizes from the mini size to the size of the manned planes. Large-sized UAVs are usually composed of fixed-wing aircraft, while small-sized UAVs have different types such as fixed and rotary wings. Helicopters and drones are the most widely used types of rotary winged UAVs. While drones can be easily used by many users, helicopters can be used by top-level users due to the need for a good pilotage [2].

The classic UAV helicopter includes two or more rotor blades. One or more rotors drive these rotor blades. By means of the rotor propulsion and blades, the UAV helicopter performs the flight. Rotating rotor blades provide the required lift during flight. Therefore, the optimal design of the rotor propulsion system and blades is an important issue. In this design process, one of the important issue is to perform optimum flight with minimum torque force [3].

---

[1] *Corresponding author: Erciyes University, Department of Aircraft Electrical and Electronics, 38030, Melikgazi/Kayseri, Turkey. mkonar@erciyes.edu.tr*

[2] *Erciyes University, Department of Aircraft Electrical and Electronics, 38030, Melikgazi/Kayseri, Turkey. arikseda@erciyes.edu.tr*

[3] *Erciyes University, Department of Aeronautical Engineering, 38030, Melikgazi/Kayseri, Turkey. oktay@erciyes.edu.tr*

In this study, the minimization of the torque value of an unmanned helicopter was discussed. For this purpose, blade parameters that affect the torque of an unmanned helicopter, that is, the blade length, the blade chord width, the blade mass density and the blade twist angle, were selected as the input parameters. The torque value for these blade parameters was chosen as the output parameter. In the proposed approach, the output parameter values were calculated for certain value ranges of the input parameters and the input parameter values corresponding to the minimum output parameter were determined. For this purpose, the ABC algorithm, which is frequently preferred in the literature, which overcomes many engineering problems and provides effective results, was used. In the study, it is aimed to determine the blade parameter values required for minimum torque.

The first section of the study consists of the introduction and briefly the literature. In the second section, the parameters and method used in the study are explained. The third section consists of simulation results and discussions. In the last section, the results are discussed.

2. PARAMETERS AND METHOD

The helicopter is a rotary wing aircraft, driven by one or more rotors, each containing two or more rotor blades. The advantage of helicopters over fixed-wing aircraft is that they do not require forward acceleration during take-off and can land vertically without the need for a runway [2-4].

The flight principle of helicopters that can take-off and land vertically, and can hover in the air is the same as fixed-wing aircraft. The lift required for the flight is provided by fixed wings in the aircraft, while is provided by rotary rotor blades in the helicopters. The torque generated by the rotor rotates the blades. While rotor blades rotate in the air, a low pressure occurs on the upper surfaces and a high pressure occurs on the lower surfaces. The resulting pressure difference creates the lift. The lift compared to the weight of the helicopter determines the helicopter flight phase such as take-off, landing, or hovering. If the lift is equal to the helicopter weight, hovering phase occurs. If it is large, take-off phase occurs. If it is small, landing phase occurs [5-7].

The aerodynamic structure of the rotor blades play an important role in the generating of the lift giving direction to the helicopter. Some of the most important parameters that determine the aerodynamic structure of the rotor blades are the blade length, the blade chord width, the blade mass density and the blade twist angle. The blade length is the distance from the center of rotation of the rotor blade to the tip of the rotor blades. The blade chord width is the distance between the blade leading edge and the blade trailing edge. Blade mass density refers to the density of the blade material and the twist angle refers to the twisting of the blade from the rotor center to the tip of the blade. By optimizing these blade parameters, the torque required to rotate the helicopter blades can be minimized and the power usage can be optimized [6-10].

In this study, Artificial Bee Colony (ABC) algorithm is used to minimize torque by optimizing helicopter blade parameters. ABC algorithm was developed by Karaboga in 2005 by modeling the food search behavior of real bees [11, 12]. There are three types of bees in this algorithm based on swarm intelligence: employed, onlooker and scout. Synchronously, the ABC algorithm makes global search with scouts and local search with employed and onlooker bees. Due to its quite simple and flexible application, the ABC algorithm with few control parameters is preferred in many optimization problems [13-16].

3. SIMULATION RESULTS AND DISCUSSION

In this section, some features of unmanned helicopter and process used in this study are explained. The unmanned helicopter used in the study is shown in Figure 1. Some features of this helicopter are as follows; main rotor radius is 0.75 m, main rotor chord is 0.045 m and helicopter mass is 5 kg. The block diagram of the proposed method using the blade parameters for unmanned helicopter is given in the Figure 2.

As seen from the block diagram, firstly, input and output parameters were determined. The blade length, the blade chord width, the blade mass density and the blade twist angle were selected as input parameters, torque value was selected as output parameter. Thus, a model with 4 input-single output was created. The values taken as reference were given in Table 1. The optimum input parameter values required to find the minimum torque value were determined by using ABC algorithm. For this purpose, the optimization process was performed by changing reference parameter values by ±5%.

Figure 10. Unmanned helicopter used in the study
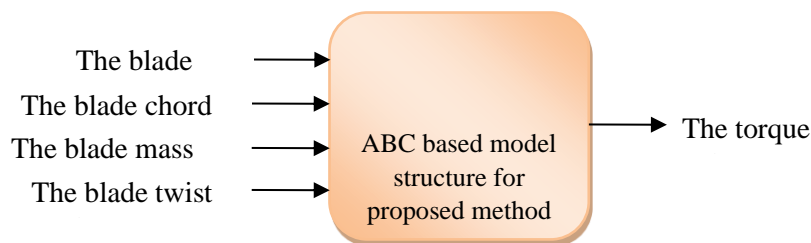
Figure 11. The block diagram of the proposed method

In the optimization process, the values of control parameters for ABC algorithm were chosen as 50-colony size, 2500-iteration numbers and 30 runtime. The parameter values of the best model obtained as a result of optimization process were calculated as 0.7874, 4.5675, 0.1859, -0.1466 for the blade length, the blade chord width, the blade mass density and the blade twist angle, respectively. The torque value for these input parameter values was calculated as 2.3467e-04.

Table 3. The reference values of the input parameters for ABC based model

Input Parameters for Blades	Values	Unit
Length	75	cm
Chord width	4.35	cm
Mass density	0.2	kg/m
Twist angle	-0.14	rad

4. CONCLUSION

In the helicopter, the rotating rotor blades provide the required lift during the flight. Therefore, the optimum determination of rotor torque value and blade parameters values in helicopter designs is an important issue. It is very complicated to calculate the equations in helicopters modeled by complex equation sets. In this study, an ABC algorithm based model was proposed to overcome this problem and to improve the helicopter design used in the study. For this reason, a model with 4 input-single output was formed. While the blade length, the blade chord width, the blade mass density and the blade twist angle, were chosed as the input parameters, the torque value for these blade parameters was selected as the output parameter. Minimum torque value was calculated with ABC algorithm by changing input reference parameter values by ±5%. The torque value for input parameters was determined as 2.3467e-04. When the values obtained from the simulation were compared with the reference values, it was observed that there was a 37% improvement with the proposed model. Obtained results shows that ABC algorithm can be an alternative method for improving helicopter designs or getting a preliminary idea about helicopter design. In addition to all, it was noticed that the increase of the trust/torque ratio should be investigated during this study.

REFERENCES

[1]. R. Austin, "Unmanned Aircraft Systems: UAVS Design, Development and Deployment", pp. 1-15, John Wiley & Sons, 2010.
[2]. G. Avanzini, "Maximum Range for Battery-Powered Aircraft", Journal of Aircraft, vol. 50, no.1, pp. 304-307, 2013.
[3]. J. M. Seddon, S. Newman, "Basic Helicopter Aerodynamics", vol. 40, John Wiley & Sons, 2011.
[4]. J. G. Leishman, "Principles of Helicopter Aerodynamics with CD Extra", Cambridge University Press, 2006.
[5]. G. D. Padfield, "Helicopter Flight Dynamics, Chichester", John Wiley & Sons, 2008.
[6]. T. Oktay, "Constrained Control of Complex Helicopter Models", PhD Dissertation, Virginia Tech, 2012.
[7]. P. Raymer, "Aircraft design: A Conceptual Approach", p.56, American Institute of Aeronautics and Astronautics, Inc., Washington, D.C, 1992.
[8]. T. Oktay and C. Sultan, "Simultaneous Helicopter and Control-System Design", Journal of Aircraft, vol. 50, no. 3, pp. 32-47, 2013.
[9]. B. Mettler, M. B. Tischler and T. Kanade, "System Identification of Small-Size Unmanned Helicopter Dynamics", Annual Forum Proceedings-American Helicopter Society, vol. 2, pp. 1706-1717, 1999.
[10]. C. Sultan, "Proportional Damping Approximation Using the Energy Gain and Simultaneous Perturbation Stochastic Approximation", Mechanical Systems and Signal Processing. vol. 24, pp. 2210-2224, 2010.
[11]. D. Karaboga and B. Akay, "A Comparative Study of Artificial Bee Colony Algorithm", Applied Mathematics and Computation, vol. 214, no. 1, pp. 108-132, 2009.
[12]. D. Karaboga, and B. Akay, "A Powerful and Efficient Algorithm for Numerical Function Optimization: Artificial Bee Colony (ABC) Algorithm", Journal of Global Optimization, vol. 39, pp. 459-471, 2007.
[13]. Bagis and M. Konar, "Comparison of Sugeno and Mamdani Fuzzy Models Optimized by Artificial Bee Colony Algorithm for Nonlinear System Modelling", Transactions of The Institute of Measurement and Control, vol. 38, no. 5, pp. 579-592, 2016.
[14]. Bagis and M. Konar, "ABC and DE Algorithms Based Fuzzy Modeling of Flight Data for Speed and Fuel Computation", International Journal of Computational Intelligence Systems, vol. 11, no. 1, 790-802, 2018.
[15]. S. Arik, I. Turkmen, and T. Oktay, "Redesign of Morphing UAV for Simultaneous Improvement of Directional Stability and Maximum Lift/Drag Ratio", Advances in Electrical and Computer Engineering, vol. 18, no. 4, pp. 57-62, 2018.
[16]. T. Oktay, S. Arik, I. Turkmen, M. Uzun, and H. Celik, "Neural Network Based Redesign of Morphing UAV for Simultaneous Improvement of Roll Stability and Maximum Lift/Drag Ratio", Aircraft Engineering and Aerospace Technology, vol. 90, no. 8, pp 1203-1212, 2018.

BIOGRAPHY

Mehmet Konar is an Assistant Professor at Erciyes University. He received an MS in Aviation from Erciyes University (2010) and a PhD for Electrical and Electronical Engineering at Erciyes University (2017). His main research areas are fuzzy logic theory, optimization methods and unmanned aerial vehicles (UAVs) design and production.

Thermogravimetric Analysis Studies on Sludge in Turkey and World

Hasan Merdun[1], Ismail Veli Sezgin[1], Zakari Boubacar Laouge[1]

Abstract

Thermogravimetric analysis (TGA) is the measuring the weight loss of a sample as a function of the time and/or reaction temperature. TGA is one of the most common techniques used to investigate thermal events and kinetics during combustion or pyrolysis of biomass, coal, or the mixtures of biomass/biomass or biomass/coal. In this study, the studies conducted in Turkey and the world on the TGA of sludge were collected from Web of Science database and presented. These studies were investigated in terms of feedstock parameters (type, particle size, blend ratio, sample amount), TGA parameters (temperature, heating rate, carrier gas/process type, carrier gas amount), and kinetic models or thermodynamic parameters used. The models used in kinetic analyses were introduced and classified based on their important characteristics. The study results showed that sludge alone or mixed with biomass or coal was used in these studies. And also, feedstock and TGA parameters, and kinetic models were very variable in these studies. One of the important results of this study was that there was no study conducted on TGA of sludge in Turkey.

Keywords: sludge, TGA, kinetic models, Turkey

1. INTRODUCTION

The amount of sludge produced from water and wastewater treatment plants has recently increased significantly because of the population growth and then the increase in the consumption ([1], [2], [6]). Sludge is a problematic waste to the environment and it is costly to dispose it properly without damaging the environment ([8], [10]). However, since sludge is an important source of biomass due to its high organic matter content, it has attracted the attention as an energy source or huge energy potential ([4], [5], [12]). The accurate determination of decomposition temperature for thermal processes (combustion or pyrolysis) is important to optimize the process parameters and reduce the conversion cost by decreasing the energy input [10]. The optimum process temperature is commonly determined by thermogravimetric analysis (TGA).

TGA is the analysis of the change in the mass of a sample on heating. TGA measures mass change of a material as a function of temperature or time under a controlled atmosphere. Another way to say that TGA is the measuring the weight loss of a sample as a function of reaction temperature ([23], [24]). Combustion characteristic values, such as ignition temperature, burnout temperature, reaction peak temperature, maximum combustion rate, mean combustion rate, and burning time, could be obtained through TGA ([17], [20], [21]). Also, according to weight loss curves under different temperatures, combustion kinetic parameters such as activation energy, pre-exponential factor, reaction order as well as mechanism function, could be ascertained ([15], [17], [18], [20]). And also, pyrolysis kinetic parameters such as activation energy, pre-exponential factor, and reaction order can be determined by using weight loss curves under different temperatures ([3], [6], [19], [26]).

The objective of this study was to investigate and characterize the studies conducted on the TGA of sludge in Turkey and world by using the data from the scientific research articles collected from the Web of Science database. And also, kinetic models were introduced and classified and thermodynamic parameters used in these studies were mentioned.

---

[1]* Corresponding author: Akdeniz University, Department of Environmental Engineering, 07058, Antalya, Turkey.
  merdun@alumni.clemson.edu

2. MATERIALS AND METHODS

The scientific research articles related to the studies conducted in Turkey and the world on the TGA of sludge by using the key words of "thermogravimetric analysis", "sludge", and "Turkey" were collected from the Web of Science database. The data from these articles were used as materials in this study.

These studies were investigated in terms of different aspect of mainly feedstock and TGA parameters and also kinetic modeling. Specifically, the studies were investigated in terms of feedstock parameters (type, particle size, blend ratio, sample amount), TGA parameters (temperature, heating rate, carrier gas/process type, carrier gas amount), and kinetic models or thermodynamic parameters used. The models used in kinetic analyses were introduced and classified based on their important characteristics.

3. RESULTS AND DISCUSSION

The studies conducted in Turkey and the world on the TGA of sludge were collected from the Web of Science database and investigated in terms of feedstock and TGA parameters in addition to kinetic models or thermodynamic parameters used.

In out of the total 38 studies conducted on TGA of sludge in all over the world as seen in Table 1, studies were conducted by using sludge alone in 4 studies, sludge with biomass in 8 studies, sludge and coal together in 20 studies, sludge with biomass and coal in 4 studies, and sludge with others (heavy oil, oil shale, fly ash) in 2 studies.

In out of total 38 studies, 9 studies were conducted with the feedstock particle size of < 100 μm, 19 studies with 100-200 μm, 4 studies with 200-300 μm, only 1 study with > 300 μm, and 5 studies with ungiven particle size.

A total of 38 studies were distributed in terms of feedstocks blending ratios as 20 studies with the number of ≤ 3 different blending ratios, 11 studies with the number of 3-5 different blending ratios, only 1 study with the number of > 5 different blending ratios, and 6 studies with no given blending ratio.

The amounts of feedstock samples used in TGA of total 38 studies were distributed as 10 studies with 5-10 mg, 12 studies with 10 mg, 3 studies with 10-15 mg, 8 studies with > 15 mg, and 4 studies with no data.

In out of total 38 studies, 8 studies were conducted with the TGA final temperature of the room temperature to 800ºC, 10 studies with the room temperature to 900ºC, 18 studies with the room temperature to 1000ºC, only 1 study with the room temperature to > 1000ºC, and there was no data for 1 study.

A total of 38 studies were distributed in terms of heating rate as 12 studies with a constant heating rate, 2 studies with 2 different heating rates, 12 studies with 3 different heating rates, 8 studies with 4 different heating rates, 2 studies with 5 different heating rates, 1 study with > 5 different heating rates, and no data for the remaining 1 study.

The studies conducted with different carrier gas types were distributed as 10 studies with N_2 representing pyrolysis, 20 studies with air representing combustion, and 8 studies with different ratios of O_2/N_2 or O_2/CO_2 representing partial oxidation or gasification.

A total of 38 studies were distributed in terms of carrier gas flow rate as 5 studies with < 50 mL/min, 11 studies with 50-100 mL/min, 17 studies with 100 mL/min, only 1 study with > 100 mL/min, and there were no data for 4 studies.

The studies were divided into several categories in terms of kinetic models used, pyrolysis or combustion characteristics, and thermodynamic parameters as 19 studies with kinetic models for pyrolysis or combustion, 3 studies with kinetic models and thermodynamic parameters in pyrolysis process, only 1 study with kinetic models and thermodynamic parameters in combustion process, 3 studies with combustion characteristics, 3 studies with kinetic models in combustion process; only 1 study for pyrolysis characteristics, kinetic models, and thermodynamic parameters; only 1 study for combustion characteristics, kinetic models, and thermodynamic parameters; and 6 studies with no modeling attempt.

Table 4. Thermogravimetric analysis studies on sludge in the world

Feedstock Parameters				TGA Parameters				Reference
Type	Size (µm)	Blend (%)	Amount (mg)	Temperature (°C)	Heating Rate (°C/min)	Carrier Gas Type & (mL/min)	Model	
sludge	1000		10	25-800	5, 10, 20	N_2 (200)	CR, ΔH, ΔG, ΔS	[1]
sludge, rice husk	300	0, 30, 50, 70, 100 S	6	25-800	20	N_2	CR, (17 models) ΔH, ΔG, ΔS	[2]
sludge, sawdust, hydrochar	150	1:3, 1:1, 3:1	6	40-900	10, 20, 30,40	N_2 (100)	T_v, T_f, R_v, WR, -R_p, T_m, D_i, FWO, KAS A, ΔH, ΔG, ΔS	[3]
sludge, coal	100	0, 50, 75, 100 C	10	25-900	10	O_2/N_2 (100) O_2/CO_2 (100)		[4]
sludge	200	S, S + SiO$_2$ S + Al$_2$O S + Fe$_2$O$_3$ S + red mud	15	25-900	10, 40	N_2 (100)	DAEM	[5]
sludge	100		6	25-800	5, 10, 20	N_2 (60)	FR, FWO, KAS, Popescu, ΔH, ΔG, ΔS	[6]
textile dyeing sludge, sugarcane bagasse	75	9:1, 8:2, 7:3, 6:4	10	25-1000	10, 20, 30	CO_2/O_2 (50) N_2/O_2 (50)	T_i, T_p, T_b, R_{max}, R_v, D_i, FWO, KAS A, ΔH, ΔG, ΔS	[7]
sludge, heavy oil fly ash	250	0, 20, 30, 40, 100 S	10	25-950	10	air (20)	D_i, S_i	[8]
oily sludge, litchi peels	75	0, 55, 65, 75, 85, 95, 100 S	9	25-1000	10, 20, 30,40	air (50)	T_i, T_p, T_b, -R_p, -R_v, -R_p (ΔT$_{1/2}$), C_i, C_b, D_v, S_i, KAS	[9]
sludge, coal	75	0, 5, 10, 15, 20, 30, 50, 100 S	6	25-900	20	air (80)	T_i, T_b, T_m, C_i, C_b, S_i, CR	[10]
sludge, coal	177	0, 20, 50, 80, 100 S	10	25-1000	20, 40, 60,80	air (100)	D_i, D_b, OFW, CR	[11]
sludge, coal	200			50-950	20, 40	air (60)		[12]
sludge, mushroom, coal	96	0, 25, 50, 75, 100 S/C 0, 25, 50, 75, 100 S/mushr.	9-10	25-1000	20	air (50)	combustion characteristics parameters CR	[13]
sludge	100		25	50-900	20	N_2 (20) O_2/N_2 (20) CO_2/N_2 (20)	AR	[14]
sludge, coffee grounds	74	9:1, 8:2, 7:3, 6:4	10	25-1000	10, 20, 30	air (50)	FWO, KAS	[15]
sludge, microalgae	100		10	25-800	10, 13, 16, 19, 22, 25, 30, 35, 40	N_2 (60)	DAEM	[16]
sludge, oil shale		10, 10, 50, 70, 90 S	10	105-1000	10, 20, 30	air (80)	AR, SR, FWO	[17]
sludge, coal		5S+95C 10S+90C 20S+80C		30-1000	5, 10, 25, 40, 100	air (100)	FWO, VZ	[18]
sludge, coal	178	0, 25, 50, 75, 100 S	6	25-1000	10	N_2 (100)	CR	[19]

paper mill sludge, MSW	177	10, 30, 50, 70, 90 PMS	5	25-1000	10, 20, 30	air (80)	FWO, SR	[20]
sludge, coal	200	2, 5, 10 S	5-10 25	25-1030	10, 25, 40	air (100)	C_i, VZ	[21]

Table 1. Thermogravimetric analysis studies on sludge in the world - Continue

Feedstock Parameters				TGA Parameters				Reference
Type	Size (µm)	Blend (%)	Amount (mg)	Temperature (ºC)	Heating Rate (ºC/min)	Carrier Gas Type & (mL/min)	Model	
sludge, coal	75	25, 50, 75, 85 C	5	25-900	10, 20, 30	N_2 (100)	AR	[22]
sludge, coal 1 coal 2	74	100 C1, 100 C2, 40S60C1 40S60C2 10, 20, 30, 40, 50, 100 S	12	25-1000	20	O_2/CO_2 (60)	combustion property index (S), ignitability property index (C_b), steady combustion property index (G)	[23]
primary& secondary pulp mill sludge, coal	105-210	PS, SS, C, 10PS+90C, 10SS+90C	25	25-925	6, 12, 24, 30	N_2 (100)	VZ	[24]
primary& secondary pulp mill sludge, coal	105-210	10PS+90C, 10SS+90C	25	25-925	6, 12, 24, 30	air (100)	VZ	[25]
lake sludge, coal	200	10, 20, 30, 40, 50 S		25-1200				[26]
sludge, coal	200	0, 20, 40, 60,80,100 S		25-800	30	O_2 (10, 30) N_2 (10, 30)		[27]
wood, oat, sludge, coal		90 C	15	25-1000	10, 40, 100	air (40)		[28]
sludge, coal	200	0, 90, 100C 100 wet S, 100 dry S			40	air	CR	[29]
olive,cotton , olive & peachkernel , pine, cardoon, sludge, coal	250	5, 10, 20 B	20-25	25-850	3, 10, 25, 50, 100	air (45)	D_i, S_i	[30]
sludge, animal manure, organic MSW	105-210		25	25-630	5, 10, 25, 50	air (100)	VZ	[31]
sludge, coal	250	10, 20, 50 S	5-10	25-1000	10, 20, 30	N_2/O_2 (100)	FR-Carroll	[32]
sludge, coal, coal gangue	200 S 74 C 200 CG	10, 20, 70 S	10	25-1000	40 S 10, 20, 40	N_2/O_2 (100)		[33]
sludge, straw, coal	200 74 C	10, 20, 70 S	10	25-1000	40 S 10, 20, 40	N_2/O_2 (100)	FWO, KAS	[34]
sludge 1, sludge 2, coal		2, 5,10 S1 2, 5,10 S2	25	25-1000	5, 10, 25, 40	air (100)	FWO, VZ	[35]
sludge, coal		2, 5, 10 S	25	25-1000	5, 10, 25, 40	air (100)	OFW, VZ	[36]

61

sludge 1, sludge 2, sludge 3, coal	200	0, 10, 50, 100 S	10	25-800	10	air	AR	[37]
sludge 1, sludge 2, sludge 3, coal		0, 1, 5, 50, 100 C	25	25-1000	15	air (50)		[38]

B: Biomass, C: Coal, S: Sludge, T_v: Initial decomposition temperature, T_f: Final temperature, R_v: Average weight loss rate, WR: pyrolysis residue mass, $-R_p$ or R_{max}: Maximum weight loss rate, $-R_p$ ($\Delta T_{1/2}$): Temperature interval at the half value of $-R_p$, T_m: Temperature at the maximum weight loss rate, T_i: Ignition temperature, T_b: Burnout temperature, T_p or T_m: Peak temperature, D_i: Ignition index, D_b: Burnout index, D_v: Volatile matter release index, S_i: comprehensive combustibility index, C_i: Ignition or combustibility index, C_b: Burnout index. CR: Coats-Redfern, FWO: Flynn-Wall-Ozawa, OFW: Ozawa-Flynn-Wall, KAS: Kissinger-Akahira-Sunose, DAEM: Distributed Activation Energy Model, FR: Friedman, AR: Arrhenius, SR: Starink, VZ: Viyazovkin, A: Pre-exponential factor or frequency factor, ΔH: Changes in enthalpy, ΔG: Gibbs free energy, ΔS: Entropy.

The TGA data were used in the kinetic modeling of a given feedstock by using a variety of kinetic modeling approaches (Table 1). There are many methods in the investigation of solid phase kinetics. Generally, these methods are divided into two main groups as model-fitting and model-free. Each of main groups are also divided into two sub-groups as iso-thermal and non-isothermal. These kinetic models/methods are used in the calculation of activation energy (E) and pre-exponential factor (A).

Thermodynamic parameters such as pre-exponential factor (A), changes in enthalpy (ΔH), Gibbs free energy (ΔG), and entropy (ΔS) can be calculated by using the TGA.

Table 5. The methods used in the investigation of solid phase kinetics [39]

Model-fitting		Model-free	
Isothermal	Non-Isothermal	Isothermal	Non-Isothermal
Conventional	Differential	Standard	Kissinger
	Freeman-Carroll	Friedman	Flynn-Wall-Ozawa
	Coats-Redfern	AIC	Vyazovkin and AIC
			Kissinger-Akahira-Sunose

4. CONCLUSIONS

This study presented the studies conducted on the TGA of sludge in Turkey and world and collected from the Web of Science database. These studies were presented based on the feedstock parameters (type, particle size, blend ratio, sample amount), TGA parameters (temperature, heating rate, carrier gas/process type, carrier gas amount), and kinetic models or thermodynamic parameters used. The results showed that the studies had variable values of both feedstock and TGA parameters. Different kinetic models, pyrolysis and combustion characterization indexes, and thermodynamic parameters were used in the studies. These results suggest that different studies may require different feedstock and TGA parameters in addition to different modeling approaches.

ACKNOWLEDGMENT

REFERENCES

[1]. Naqvi, S.R., Tariq, R., Hameed, Z., Ali, I., Naqvi, M., Chen, W.H., Ceylan, S., Rashid, H., Ahmad, J., Taqvi, S.A., Shahbaz, M., 2019, Pyrolysis of high ash sewage sludge: Kinetics and thermodynamic analysis using Coats-Redfern method, Renewable Energy, 131, 854-860.

[2]. Naqvi, S.R., Hameed, Z., Tariq, R., Taqvi, S.A., Ali, I., Niazi, M.B.K., Noor, T., Hussain, A.,Iqbal, N., Shahbaz, M., 2019, Synergistic effect on co-pyrolysis of rice husk and sewage sludge by thermal behavior, kinetics, thermodynamic parameters and artificial neural network, Waste Management, 85, 131-140.

[3]. Ma, J., Luo, H, Li, Y., Liu, Z., Li, D., Gai, C., Jiao, W., 2019, Pyrolysis kinetics and thermodynamic parameters of the hydrochars derived from co-hydrothermal carbonization of sawdust and sewage sludge using thermogravimetric analysis, Bioresource Technology, 282, 133-141.

[4]. Lei, K. Zhang, R., Ye, B., Cao, J., Liu, D., 2019, A study of sewage sludge/coal co-combustion by thermogravimetric analysis and single particle co-combustion method, Energy & Fuels, xx, xxxx-xxxx.

[5]. Yang, J., Xu, X., Liang, S., Guan, R., Li, H., Chen, Y., Liu, B., Song, J., Yu, W., Xiao, K., Hou, H., Hu, J., Yao, H., Xiao, B., 2018, Enhanced hydrogen production in catalytic pyrolysis of sewage sludge by red mud: Thermogravimetric kinetic analysis and pyrolysis Characteristics, International Journal of Hydrogen Energy, 43, 7795-7807.

[6]. Naqvi, S.R., Tariq, R., Hameed, Z., Ali, I., Taqvi, S.A., Naqvi, M., Niazi, M.B.K., Noor, T., Farooq, W., 2018, Pyrolysis of high-ash sewage sludge: Thermo-kinetic study using TGA and artificial neural networks, Fuel, 233, 529-538.

[7]. Xie, W., Wen, S., Liu, J., Xie, W., Kuo, J., Lu, X., Sun, S., Chang, K., Buyukada, M., Evrendilek, F., 2018, Comparative thermogravimetric analyses of co-combustion of textile dyeing sludge and sugarcane bagasse in carbon dioxide/oxygen and nitrogen/oxygen atmospheres: Thermal conversion characteristics, kinetics, and thermodynamics, Bioresource Technology, 255, 88-95.

[8]. Li, X., Miao, W., Lv, Y., Wang, Y., Gao, C., Jiang, D., 2018, TGA-FTIR investigation on the co-combustion characteristics of heavy oil fly ash and municipal sewage sludge, Thermochimica Acta, 666, 1-9.

[9]. Liu, C., Liu, J., Sun, G., Xie, W., Kuo, J., Li, S., Liang, J., Chang, K., Sun, S., Buyukada, M., Evrendilek, F., 2018, Thermogravimetric analysis of (co-)combustion of oily sludge and litchi peels: combustion characterization, interactions and kinetics, Thermochimica Acta, 667, 207-218.

[10]. Wang, Z., Hong, C., Xing, Y., Li, Y., Feng, L., Jia, M., 2018, Combustion behaviors and kinetics of sewage sludge blended with pulverized coal: With and without catalysts, Waste Management, 74, 288-296.

[11]. Niu, S., Chen, M., Li, Y., Song, J., 2018, Co-combustion characteristics of municipal sewage sludge and bituminous coal, Journal of Thermal Analysis and Calorimetry, 131, 1821-1834.

[12]. Li, Y., Yang, D., Qu, M., Suo, L., Sun, W., 2018, Experimental investigation on co-combustion kinetics and gas emission law of sewage sludge–bituminous coal, International Journal of Energy Research, 42, 4097-4107.

[13]. Chen, GB, Chatelier, S., Lin, H.T., Wu, F.H., Lin, T.H., 2018, A study of sewage sludge co-combustion with Australian Black Coal and Shiitake substrate, Energies, 11, 3436, 1-25.

[14]. Hernandez, A.B., Okonta, F., Freeman, N., 2017, Thermal decomposition of sewage sludge under N_2, CO_2 and air: Gas characterization and kinetic analysis, Journal of Environmental Management, 196, 560-568.

[15]. Chen, J., Liu, J., He, Y., Huang, L., Sun, S., Sun, J., Chang, K., Kuo, J., Huang, S., Ning, X., 2017, Investigation of co-combustion characteristics of sewage sludge and coffee grounds mixtures using thermogravimetric analysis coupled to artificial neural networks modeling, Bioresource Technology, 225, 234-245.

[16]. Soria-Verdugo, A., Goos, E., Morato-Godino, A., García-Hernando, N., Riedel, U., 2017, Pyrolysis of biofuels of the future: Sewage sludge and microalgae-Thermogravimetric analysis and modelling of the pyrolysis under different temperature conditions, Energy Conversion and Management, 138, 261-272.

[17]. Lin, Y., Liao, Y., Yu, Z., Fang, S., Ma, X., 2017, The investigation of co-combustion of sewage sludge and oil shale using thermogravimetric analysis, Thermochimica Acta, 653, 71-78.

[18]. Park, J.M., Keel, S., Yun, J., Yun, J.H., Lee, S.S., 2017, Thermogravimetric study for the co-combust ion of coal and dried sewage sludge, Korean Journal of Chemical Engineering, 34(8), 2204-2210.

[19]. Mu, L., Chen, J., Yao, P., Zhou, D., Zhao, L., Yin, H., 2016, Evaluation of co-pyrolysis petrochemical wastewater sludge with lignite in a thermogravimetric analyzer and a packed-bed reactor: Pyrolysis characteristics, kinetics, and products analysis, Bioresource Technology, 221, 147-156.

[20]. Hu, S., Ma, X., Lin, Y., Yu, Z., Fang, S., 2015, Thermogravimetric analysis of the co-combustion of paper mill sludge and municipal solid waste, Energy Conversion and Management, 99, 112-118.

[21]. Li, H., Li, Y., Jin, Y., 2015, Co-combustion analyses of coal and sewage sludge with high moisture content, Energy Sources, Part A: Recovery, Utilization, and Environmental Effects, 37, 1896-1903.

[22]. Xiao, P., Xu, L., Wang, X., Chang, Z., 2015, Co-pyrolysis characteristics of coal and sludge blends using thermogravimetric analysis, Environmental Progress and Sustainable Energy, 34, 1780-1789.

[23]. Zhang, Y., Zhang, L., Duan, F., Jiang, X., Sun, X., Chyang, C.S., 2015, Co-combustion characteristics of sewage sludge with different rank bituminous coals under the O_2/CO_2 atmosphere, Journal of Thermal Analysis and Calorimetry, 121, 729-736.

[24]. Coimbra, R.N., Paniagua, S., Escapa, C., Calvo, L.F., Otero, M., 2015, Thermogravimetric analysis of the co-pyrolysis of a bituminous coal and pulp mill sludge, Journal of Thermal Analysis and Calorimetry, 122, 1385-1394.

[25]. Coimbra, R.N., Paniagua, S., Escapa, C., Calvo, L.F., Otero, M., 2015, Combustion of primary and secondary pulp mill sludge and their respective blends with coal: A thermogravimetric assessment, Renewable Energy, 83, 1050-1058.

[26]. Xia, J., Li, H., 2014, Co-pyrolysis charateristics study of Dianchi Lake sludge and coal, Advanced Materials Research, 860-863, 518-521.

[27]. Yu, L.Y., Li, P.S., 2014, Thermogravimetric analysis of coal and sludge co-combustion with microwave radiation dehydration, Journal of the Energy Institute, 87, 220-226.

[28]. Magdziarz, A., Wilk, M., 2013, Thermogravimetric study of biomass, sewage sludge and coal combustion, Energy Conversion and Management, 75, 425-430.

[29]. Li, H., Li, Y., Jin, Y., 2012, Analyses of coal and sewage sludge co-combustion using Coats-Redfern model, Advanced Materials Research, 518-523, 3271-3274.

[30]. Vamvuka, D., Sfakiotakis, S., 2011, Combustion behaviour of biomass fuels and their blends with lignite, Thermochimica Acta, 526, 192-199.

[31]. Otero, M., Sanchez, M.E., Gómez, X., Morán, A., 2010, Thermogravimetric analysis of biowastes during combustion, Waste Management, 30, 1183-1187.

[32]. Yanfen, L., Xiaoqian, M., 2010, Thermogravimetric analysis of the co-combustion of coal and paper mill sludge, Applied Energy, 87, 3526-3532.

[33]. Hanmin, X., Xiaoqian, M., Kai, L., 2010, Co-combustion kinetics of sewage sludge with coal and coal gangue under different atmospheres, Energy Conversion and Management, 51, 1976-1980.

[34]. Xiao, H., Ma, X., Lai, Z., 2009, Isoconversional kinetic analysis of co-combustion of sewage sludge with straw and coal, Applied Energy, 86, 1741-1745.

[35]. Otero, M., Calvo, L.F., Gil, M.V., Garcia, A.I., Moran, A., 2008, Co-combustion of different sewage sludge and coal: A non-isothermal thermogravimetric kinetic analysis, Bioresource Technology, 99, 6311-6319.

[36]. Otero, M., Gomez, X., Garcia, A.I., Moran, A., 2007, Effects of sewage sludge blending on the coal combustion: A thermogravimetric assessment, Chemosphere, 69, 1740-1750.

[37]. Folgueras, M.B., Diaz, R.M., Xiberta, J., Prieto, I., 2003, Thermogravimetric analysis of the co-combustion of coal and sewage sludge, Fuel, 82, 2051-2055.

[38]. Otero, M., Diez, C., Calvo, L.F., Garcia, A.I., Moran, A., 2002, Analysis of the co-combustion of sewage sludge and coal by TG-MS, Biomass and Bioenergy, 22, 319-329.

[39]. Khawam, A., Application of solid-state kinetics of desolvation, PhD Thesis, University of Lowa, USA, 2011.

BIOGRAPHY

Dr. Hasan Merdun is currently serving as a faculty member at the Department of Environmental Engineering, Akdeniz University in Antalya, Turkey. His research interests include renewable energy, waste-to-energy, clean energy production, biomass, bioenergy, thermochemical conversion of biomass to biofuels, pyrolysis and gasification technologies, upgrading of biofuels, useful chemicals production from waste, and global warming and climate change. His research mission is to add value to the national and global bioenergy sector by applying an integrated biorefinery approach for the development of renewable energy technologies.

Cesme –Urla (Izmir-Turkey) evaluation of new microgravity data

Oya Pamukcu[1], Baris Can Malalici[2]

Abstract

The study area which in the southwest of Izmir, has a very complex tectonic structure. Western Anatolia and the Aegean Sea, where the study area is located, is a complex tectonic mechanism with north-south extension. Regionally, Western Anatolia and the Aegean Sea are bounded by the North Anatolian Fault Zone in the north and Hellenic-Cyprus Arc in the south. The study area is limited to Cesme (in the west), Seferihisar and Urla (in the east), Gulbahce Bay (in the north) and Sigacik Bay (in the south). Regional main tectonic structures are Karaburun Fault, Gulbahce Fault and Uzunkuyu Intrusive.

Past studies in the region have suggested that the area should be investigated in more detailed and emphasized that the tectonic structures in the region should be examined in detail. In the light of these suggestions, Dokuz Eylul University Scientific Research Project No. 2018.KB.FEN.010 was built and microgravity studies were conducted to determine the tectonic elements in the study area. Different data processing techniques were applied to the measured microgravity data and the study area was examined in detail.

Keywords: Izmir, Western Anatolia, microgravity, Gulbahce, Sigacik

1. INTRODUCTION

The study area is located west of Izmir city centre (Figure 1). In this area, the Karaburun Peninsula, Izmir Bay and Urla Basin are separated from each other as structural and morphological. West Anatolia and Aegean Sea where the study area is located (Figure 1) have a complex tectonism that shows North-South oriented extension [1]-[2]. The formation occurred by North-south extension from Piliocene to present day in West Anatolia which is bounded by North Anatolian Fault Zone in the North and Helen-Cyprus Arc in the south is based upon the deformation related to the tectonic escape [3]. In the study area, Paleozoic-Mesozoic carbonates (Karaburun platform), Neogene volcanics and sedimentary rocks, Upper Cretaceous-Paleocene Bornova flysch zone and Quaternary alluvium units constitute the main geological structures [4], [5]-[6].

Figure 1. The location of the study area (Google Earth) and the main faults in the region [3], [7]-[8].

[1] *Dokuz Eylul University, Engineering Faculty, Department of Geophysical Engineering, 35160, Tinaztepe Campus, Buca Izmir, Turkey. ayca.cirmik@deu.edu.tr, oya.pamukcu@deu.edu.tr*

[2] *Dokuz Eylul University, The Graduate School of Natural and Applied Sciences, 35160, Tinaztepe Campus, Buca, Izmir, TURKEY, barismalalici@gmail.com*

In order to examine the tectonic structure in the area, gravity measurements were made in the region and the measurement area are given in Figure 1. This study was conducted within the scope of Dokuz Eylul University Scientific Research Project No. 2018.KB.FEN.010. The data obtained from the surveys were evaluated together with TUBITAK (The Scientific and Technological Research Council of Turkey) project No.108Y285 data. When evaluating the data, firstly gravity corrections (latitude, free-air, Bouguer and terrain corrections) were made and Bouguer Gravity map was obtained. Then, the polynomial fitting method was applied to the data set.

2. APPLICATIONS

In Geophysics, various corrections are applied to the data obtained from field studies. The data obtained by these corrections cannot be used directly in interpretation. Therefore, some data processing techniques are needed. Since gravity data includes regional and residual effects, it is necessary to eliminate these effects according to the study purpose in order to make a reliable interpretation. Various data processing techniques are available to differentiate between regional and residual effects. In this study, polynomial fitting method was preferred.

Polynomial fitting method is the process of extracting the appropriate mathematical function from the data in order to distinguish regional and residual anomalies. In this process, the mathematical function presents the regional effect and the deviations from this surface reveal the residual effect. On the basis of the method, it is assumed that the residual values are randomly distributed (common variance = 0) and the residual sum of all data is zero [9]. Equation (1) means that the sum of the squares of the differences between the observation values and the function to be calculated is the smallest. With this approach, the polynomial coefficients that determine the function to be determined are determined [9].

$$\sum_{i=1}^{n} R_i^2 = \sum_{i=1}^{n}(G_i - T_i)^2 = \text{smallest}$$
(1)

Here, G_i observation values, T_i trend values, R_i are residual values. Polynomial fitting can be applied from normal polynomials given in Equation (2) and by using orthogonal polynomials given in Equation (3). In the Polynomial fitting method applied to the potential field data, orthogonal polynomials are generally preferred [9].

$$T(x,y) = A_{00} + A_{10}x + A_{01}y + A_{11}x + \cdots + A_{pq}x^p y^q$$
(2)

$$T(x,y) = E_{00} + E_{10}P_{10}(x,y) + \cdots + E_{pq}P_{pq}(x,y) \tag{3}$$

The coefficients in Equation (2) and (3) are found by solving the matrix system given in Equation (4) with the least squares. The desired degree of function is calculated by the established equation system [9].

$$\begin{bmatrix} n & \sum x_i \\ \sum x_i & \sum x_i^2 \end{bmatrix} \cdot \begin{bmatrix} A_0 \\ A_1 \end{bmatrix} = \begin{bmatrix} \sum G_i \\ \sum x_i G_i \end{bmatrix} \tag{4}$$

Polynomial fitting method was applied to the Bouguer gravity values by using the specified theoretical infrastructure. The residual anomalies of 1st and 5th degree obtained by Polynomial fitting method are given in Figure 2.
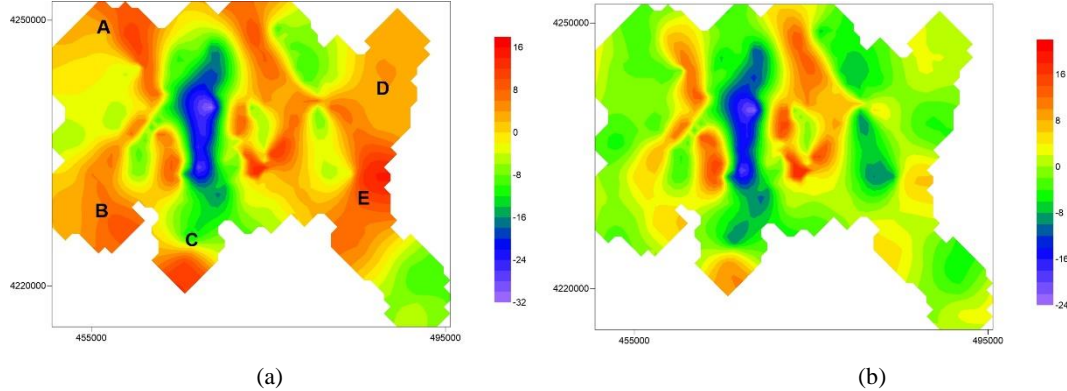
Figure 2. The residual anomalies of 1st and 5th degree obtained by Polynomial fitting method

RESULTS

Polynomial fitting, which is important regional residual separation method, provides ease of interpretation, especially in complex areas. The residual anomalies of 1st and 5th degree obtained by Polynomial fitting method are given in Figure 2. The first degree polynomial fitting Bouguer anomaly map in Figure 2a and the 5th degree polynomial fitting Bouguer anomaly map in Figure 2b are seen. Because the function is more linear, the 1st degree anomaly values have the effects of deep structures. On the other hand, when the 5th degree residual anomaly map is examined, it is simplified because it was effected shallow structures relative to 2a. There are approximately north-south extending anomalies on both maps (Figure 2a-b). When we compared to Figure 2a and b the anomalies which were shown with A, B, C, D and E in Figure 2a are due to different depth structures.

ACKNOWLEDGMENT

REFERENCES

[1]. McKenzie, D. (1972). Active tectonics of the mediterranean region. Geophysical Journal International, 30(2), 109–185.
[2]. Dewey, J. F., and Sengor, A. C. (1979). Aegean and surrounding regions: complex multiplate and continuum tectonics in a convergent zone. Geological Society of America Bulletin, 90(1), 84–92.
[3]. Uzel, B., and Sozbilir, H. (2008). A first record of strike-slip basin in western Anatolia and its tectonic implication: the Cumaovasi basin as an example. Turkish Journal Earth Science, 17, 559–591.
[4]. Goktas, F. (2016). Ildir Korfezi guneyindeki bolgenin Neojen stratigrafisi Cesme Yarimadasi, Bati Anadolu. Geological Bulletin of Turkey, 59 (3), 299–321.
[5]. Sozbilir, H., Sumer, O., Uzel, B., Ersoy, Y., Erkul, F., Inci, U., Helvaci, C. and Ozkaymak, C. (2009). 17-20 Ekim 2005-Sigacik Korfezi (Izmir) depremlerinin sismik jeomorfolojisi ve bolgedeki gerilme alanlari ile iliskisi, Bati Anadolu. Geological Bulletin of Turkey, 52 (2), 217–238.
[6]. Uzel, B., Sozbilir, H. and Ozkaymak, C. (2012). Neotectonic evolution of an actively growing superimposed basin in western Anatolia: The inner bay of Izmir, Turkey. Turkish Journal of Earth Sciences, 21, 439-471.
[7]. Emre, O., Ozalp, S., Dogan, A., Ozaksoy, V., Yildirim, C. and Goktas¸, F. (2005). Izmir Yakin Cevresinin Diri Faylari ve Deprem Potansiyelleri. General Directorate of Mineral Research and Exploration Report no. 10754.
[8]. Cirmik, A., Dogru, F., Gonenc, T., and Pamukcu, O. (2017b). The Stress/Strain Analysis of Kinematic Structure at Gulbahce Fault and Uzunkuyu Intrusive (Izmir, Turkey). Pure and Applied Geophysics, 174, 1425–1440.
[9]. Akcig Z, ve Pinar R. (2000). Gravite ve manyetik arama yontemleri. Izmir: Dokuz Eylul University Press.

Prediction of Traffic Parameters in Turkey Using with Grey Prediction Method

Mahmut Aytekin[1], Bekir Aktas[2]

Abstract

Traffic accidents on highways are one of the most common reason of the deaths and injuries in the world. The World Health Organization (WHO) announced that in 2018, 1,35 million people lost their lives in traffic accidents. In Turkey, the main transportation is provided by highways and as a result of this, the number of vehicles and traffic accidents are increasing rapidly due to population growth and economic developments. Due to the number of vehicles experienced and the increase in traffic accidents, it has become an inevitable necessity to make future predictions for reducing traffic accident increasing and planning safety in highways. There are many accident prediction methods developed differently in road safety planning and policies. Grey prediction models are simple, adaptable, better able to cope with sudden parameter changes and do not require much data points for forecast updates. In this study, the predictions for the future using the data of traffic accidents and some accident parameters between 2008 and 2017 were made by using Grey Prediction Model GM(1,1) and Rolling Grey Prediction Model RGM(1,1) and the results of the prediction methods were tested by using performance tests.

Keywords: *GM(1,1), grey prediction, grey systems, rolling grey prediction, traffic accident data*

1. INTRODUCTION

Thousands of people die and get injured every year in the traffic accidents that occur in our country. As a result of traffic accidents, families are divided and people are disabled. This reveals the social dimension of the event. Furthermore, when we evaluate the treatment processes of the injured and the financial losses that occurred after the accidents, we see that the accidents caused a serious economic loss to the country's economy.

Highways have a great importance in the load and passenger transportation of our country. In Turkey, 95% of the freight transport and 92% of the passenger transport is on the highways and this causes the high risk of traffic accidents on the roads. In 1998, 458.661 traffic accidents occurred in Turkey. In 2006, the number of traffic accidents increased by 59% and reached 728.756. In 2017, there was a 262% increase compared to 1998 and the number of traffic accidents was 1.202.716 [1,2].

In the world, projects are designed to reduce the loss of life and property in traffic accidents. In this context, the European Union has signed "Vision Zero" in order to reduce the deaths in traffic accidents [3].

There are a wide variety of prediction models in the literature, first proposed by Professor Julong Deng in 1982, the grey system theory is a model capable of predicting the inherent flaws of traditional statistical methods and estimating the behavior of an uncertain system with a limited amount of data. In summary, the main aim of the grey system theory is to produce more accurate prediction data in inadequate data cases [5].

It is very important to investigate the latest data to reduce the loss of life and financial in traffic accidents and to determine and strategize the measures to be taken to estimate the number of future vehicle number and the accidents that occur. In this study, grey prediction method and rolling grey prediction method were used to produce predictions with great accuracy in cases with little data for future predictions.

---

[1] *Kilis 7 Aralik University, Vocatinoal School of Thecnical Sciences, 79000, Kilis,, Turkey. mahmutaytekin@.edu.tr*

[2] *Corresponding author: Erciyes University, Department of Civil Engineering, 38280, Talas/Kayseri, Turkey. baktas@erciyes.edu.tr*

2. GREY SYSTEM THEORIES

Many social, economic, agricultural, industrial, ecological, biological, etc. while systems are named by taking into account the characteristics of the classes of objects, grey systems are labeled using the color of the respective systems. We use "black" to indicate unknown information, "white" to show fully known information, and "grey" to indicate information that is partially known and partially unknown. According to this, systems with fully known knowledge are known as white, systems with completely unknown information as black and partially known and partially unknown information systems as grey [6].

The grey model is shown as dynamic grey differential equation model with GM(N, H) model. where "N" is the degree of the grey differential equation, and "H" is the number of variables. The most widely used model among all grey models is the GM(1,1) model [6-8].

2.1 Grey Model (1,1)

The grey model GM(1,1) consists of the basic steps described in detail below [6].

1. Generation of $y^{(0)}$ raw data sets with at least four positive parameters of the prediction time series.

$y^{(0)} = (y^{(0)}(1), y^{0)}(2), y^{(0)}(3),…, y^{(0)}(n)); (n{\geq}4)$

2. $y^{(1)})$ is generated from the $y^{(0)}$ series by using the first degree total production operator.

$y^{(1)}(k) = \sum_{i=1}^{k} y^{(0)}(i)$; (k=1,2,…,n)

3. Using the first degree average production operator $z^{(1)}$ background sequence is created.

$z^{(1)}(k)= 0.5y^{(1)}(k)+ 0.5y^{(1)}(k-1)$; (k=2,3,…,n)

4. Define the grey differential equation

Grey differential equation is generated as follows: $y^{(0)}(k) + az^{(1)}(k) = b$

The matrix representation of Parameters [a.b], $\hat{a}$, B and Y values is shown below.

$\hat{a}=\begin{bmatrix} a \\ b \end{bmatrix}$

$$B=\begin{bmatrix} -Z^{(1)}(2) & 1 \\ -Z^{(1)}(3) & 1 \\ -Z^{(1)}(4) & 1 \\ ………… & 1 \\ -Z^{(1)}(n) & 1 \end{bmatrix},$$

$$Y=\begin{bmatrix} y^{(0)}(2) \\ y^{(0)}(3) \\ y^{(0)}(4) \\ … \\ y^{(0)}(n) \end{bmatrix},$$

$Y= B\hat{a}$

$B^{T}Y=B^{T}B\hat{a}$

$\hat{a}=\begin{bmatrix} a \\ b \end{bmatrix} = (B^{T}B)^{-1}B^{T}Y$

5. Calculation of grey differential equation

$\frac{dy^{(1)}(k)}{dk} + ay^{(1)}(k) = b$ equality is solved and the prediction model is obtained.

$\hat{y}^{(1)}(k+1) = (y^{(0)}(1) \, e^{-ak} + \frac{b}{a}(1 - e^{-ak})$

$\hat{y}^{(0)}(k+1) = (1 - e^{a})(y^{(0)}(1) - \frac{b}{a}) e^{-ak}$

Then, using the prediction model, the prediction values are generated [6].

2.2 Rollign Grey Model RGM(1,1)

Rolling Grey Model RGM (1,1) is based on the data of the sequence to generate GM (1,1). For example, while the fifth predict data is predicted from the first four values, the first value is subtracted from the model when calculating the sixth value and the values of 2,3,4 and 5 are included in the model. Prediction is performed by creating a new model. This process repeats to the last element. The number of data to be used can be selected by trial and error. Prediction can be made by selecting the model that gives the lowest error rate. This model is based on the fact that the value to be predicted is not likely to be the closest to it [9,10].

2.3 Performance Tests of the Prediction Model

There are many performance tests in the literature applied to prediction models. In this study, small error probability (accuracy parameter) (P), relative error (RE) and mean relative error (MRE) were used.

Error: $\varepsilon(k) = y^{(0)}(k) - \hat{y}^{(0)}(k)$

Relative Error: $\Delta_k = \frac{|\varepsilon(k)|}{y^{(0)}(k)}$

Mean Relative Error: $\overline{\Delta} = \frac{1}{n}\sum_{k=0}^{n}\Delta_k$

The following steps are followed when determining the small error probability (P);

Firstly, the error rate $\delta^{(0)}(k)$ for each element of K is determined.

$\delta^{(0)}(k) = (\frac{y^{(0)}(k) - \hat{y}^{(0)}(k)}{y^{(0)}(k)}) \times 100\%, \ (k=2,3,\dots,n)$

After the error rate is determined, the parameter P is calculated as follows.

$P = \frac{\sum_{k=2}^{n}(1 - |\delta^{(0)}(k)|)}{n-1}$

Table 1. The performance tests used in the model [6]

Accuracy Scale	Performans Parameters	
	Relative error, Δ	Small error probability, P
Wonderful	0,01	0,95
Qualified	0,05	0,80
Reluctant	0,10	0,70
Unqualified	0,20	0,60

In most applications published in the field of grey systems to date, the most commonly used is the relative error and small error probability criterions. If the relative error is close to 0, the predict is so realistic and accurate. Similarly, if the P parameter is close to 1, the predict is so realistic and accurate [6].

3. PREDICTION OF TRAFFIC ACCIDENTS IN TURKEY WITH GREY PREDICTION GM(1,1) AND ROLLING GREY PREDICTION RGM(1,1) MODELS

In this part of the study, traffic accident statistics published by Turkish Statistical Institute (TUIK) were used. With the help of these data, future predictions were made in between 2008 and 2013 years about the number of vehicles registered in traffic, the number of total traffic accidents, the number of dead-injured traffic accidents, the number of material damaged traffic accidents, and the number of persons who lost their lives in accidents. The data between 2008-2012 was used as a model for the establishment of a "raw data set" while the data between 2013-2017 was used after the installation stage. Forecast data in 2018-2022 the data in 2013-2017 were produced using raw data instead, and performance tests were not performed because the actual data did not exist.

The number of vehicles registered to traffic by years, model values and model performance parameters are shown in Table 2. The data for the number of vehicles registered in the traffic, the grey prediction data generated and the rolling grey prediction data produced are graphed in Figure 1.

Table 2. Real values and model values of vehicles registered to traffic by years

	Year	Real Value	Grey Model GM(1,1)				Rolling Grey Model RGM(1,1)			
			Model Value	P	RE Δ,%	MRE $\overline{\Delta}$,%	Model Value	P	RE Δ,%	MRE $\overline{\overline{\Delta}}$, %
Model setup stage	2008	13 765 395								
	2009	14 316 700								
	2010	15 095 603								
	2011	16 089 528								
	2012	17 033 413	k=5				k=5			
After model setup stage	2013	17 939 447	18 054 535		0,64		18 054 535		0,64	
	2014	18 828 721	19 143 595		1,67		19 037 147		1,11	
	2015	19 994 472	20 298 348	0,98	1,52	1,72	19 867 552	0,99	0,63	0,20
	2016	21 090 424	21 522 757		2,05		21 021 926		0,32	
	2017	22 218 945	22 821 023		2,71		22 264 259		0,20	
Prediction of future years	2018		23 498 464				23 498 464			
	2019		24 822 560				24 767 242			
	2020		26 221 266				26 135 606			
	2021		27 698 787				27 582 296			
	2022		29 259 563				29 082 187			

Figure 1. Real values and produced model values for the number of vehicles registered in traffic (2013-2017 years)

Table 2. when examined, it is observed that the number of vehicles registered to traffic will increase in both models. When the performance tests were evaluated, grey prediction and rolling grey prediction models were found to produce predictions with great accuracy.

The number of traffic accidents and prediction data produced according to years are given in Table 3. The data obtained for the total number of traffic accidents between 2013 and 2017 obtained from Table 3., grey predicted data and rolling grey predicted data are presented graphically in Figure 2.

Table 3. Real values and model values for total traffic accidents by years

	Year	Real Value	Grey Model GM(1,1)				Rolling Grey Model RGM(1,1)			
			Model Value	P	RE Δ,%	MRE $\overline{\Delta}$,%	Model Value	P	RE Δ,%	MRE $\overline{\overline{\Delta}}$, %
Model setup stage	2008	950 120								
	2009	1 053 346								
	2010	1 106 201								
	2011	1 228 928								
	2012	1 296 634	k=5				k=5			
After model setup stage	2013	1 207 354	1 400 014		15,96		1 400 014		15,96	
	2014	1 199 010	1 505 868		25,59		1 302 014		8,59	
	2015	1 313 359	1 619 726	0,62	23,33	33,60	1 189 390	0,93	9,44	4,96
	2016	1 182 491	1 742 192		47,33		1 264 930		6,97	
	2017	1 202 716	1 873 918		55,81		1 235 327		2,71	
Prediction of future years	2018		1 195 192				1 195 192			
	2019		1 183 736				1 140 428			
	2020		1 172 392				1 148 558			
	2021		1 161 156				1 117 281			
	2022		1 150 027				1 094 305			
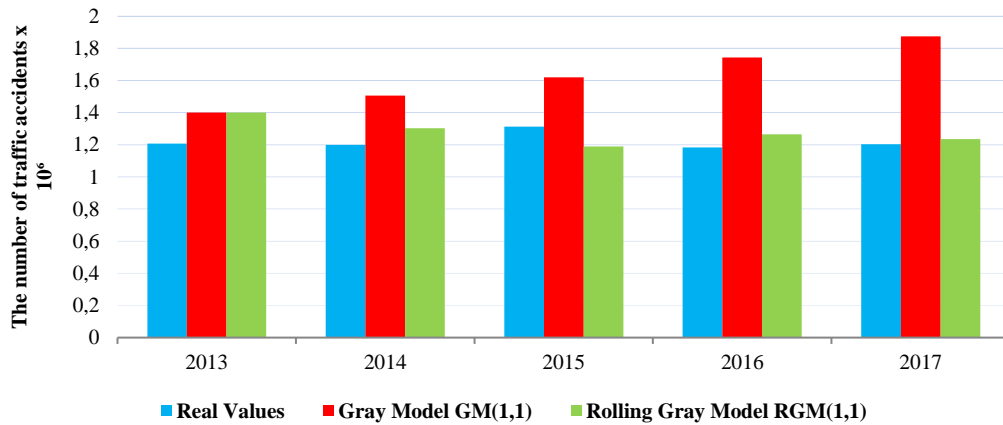
Figure 2. Real values and produced model values for the number of traffic accidenst (2013-2017 years)

When the predictions of the number of accidents in the following years are examined according to Table 3, it is observed that there will be a decrease in the number of accidents in the following years. According to the results, the rolling grey prediction model has fewer error percentages and better accuracy scores.

The real values number of traffic accidents with death-injury and their prediction data are given in Table 4. The grey prediction data and the rolling grey prediction data for the number of traffic accidents with death-injury between the years of 2013-2017 obtained from Table 4. are presented graphically in Figure 3.

Table 4. Real values and model values for traffic accidents with death-injury by years

	Year	Real Value	Grey Model GM(1,1)				Rolling Grey Model RGM(1,1)			
			Model Value	P	RE Δ,%	MRE $\overline{\Delta}$,%	Model Value	P	RE Δ,%	MRE $\overline{\overline{\Delta}}$, %
Model setup stage	2008	104 212								
	2009	111 121								
	2010	116 804								
	2011	131 845								
	2012	153 552	k=5				k=5			
After model setup stage	2013	161 306	168 753		4,62		168 753		4,62	
	2014	168 512	189 025		12,17		183 359		8,81	
	2015	183 011	211 731	0,75	15,69	21,20	184 830	0,95	0,99	5,18
	2016	185 128	237 165		28,11		192 030		3,73	
	2017	182 669	265 654		45,43		196 871		7,74	
Prediction of future years	2018		191 030				191 030			
	2019		195 735				190 957			
	2020		200 556				194 011			
	2021		205 495				198 254			
	2022		210 556				199 849			
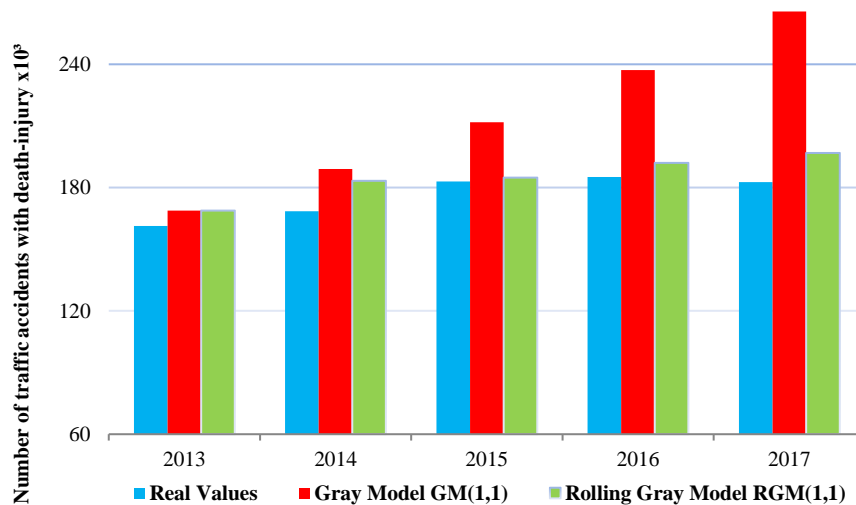
Figure 3. Real values and produced model values for the number of traffic accidents with death-injury (2013-2017 years)

When the predictions of the number of traffic accidents with death-injury in the following years are examined according to Table 4, it is observed that there will be a increase in the number of accidents with death-injury in the following years. It has been observed that the rolling grey prediction model has less error percentages and better accuracy scores than the grey prediction model.

The real values number of traffic accidents involving material loss only and their prediction data are given in Table 5. The grey prediction data and the rolling grey prediction data for the number of traffic accidents involving material loss between the years of 2013-2017 obtained from Table 5. are presented graphically in Figure 4.

Table 5. Real values and model values for traffic accidents involving material loss by years

	Year	Real Value	Grey Model GM(1,1)				Rolling Grey Model RGM(1,1)			
			Model Value	P	RE Δ,%	MRE $\overline{\Delta}$,%	Model Value	P	RE Δ,%	MRE $\overline{\overline{\Delta}}$, %
Model setup stage	2008	845 908								
	2009	942 225								
	2010	989 397								
	2011	1 097 083								
	2012	1 143 082	k=5				k=5			
After model setup stage	2013	1 046 048	1 232 154		17,79		1 232 154		17,79	
	2014	1 030 498	1 318 870		27,98		1 121 874		8,87	
	2015	1 130 348	1 411 688	0,59	24,89	36,15	1 007 764	0,93	10,84	5,08
	2016	997 363	1 511 039		51,50		1 073 625		7,64	
	2017	1 020 047	1 617 382		58,56		1 039 815		1,94	
Prediction of future years	2018		1 004 698				1 004 698			
	2019		989 246				950 516			
	2020		974 032				955 357			
	2021		959 052				921 861			
	2022		944 302				898 428			
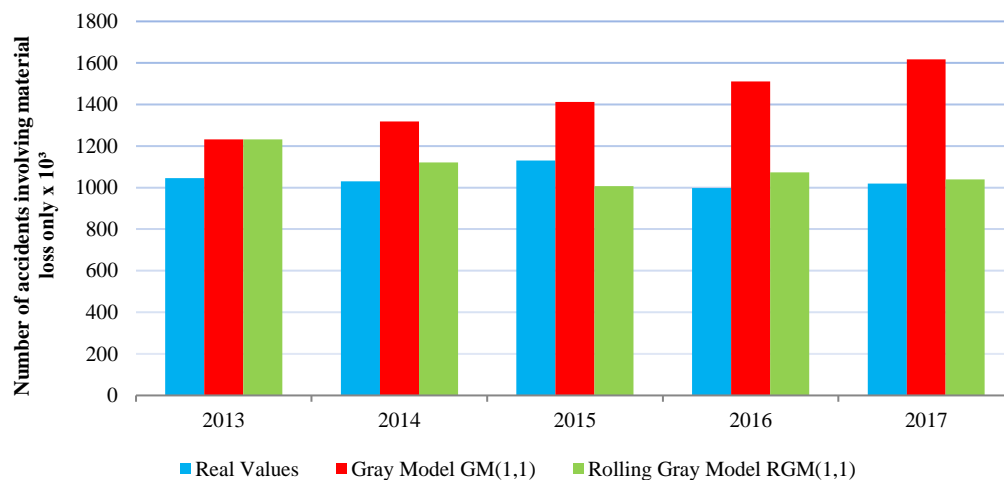
Figure 4. Real values and produced model values for the number of traffic accidents involving material loss only (2013-2017 years)

The future predictions of traffic accidents involving material loss only were produced shows in Table 5. Despite the increase in the number of vehicles in the number of accidents in the coming years, a decrease is expected. Compared to prediction models, the rolling grey prediction model was found to be more effective than the grey prediction model.

The real values number of people dying in a traffic accident and their prediction data are given in Table 6. The grey prediction data and the rolling grey prediction data for the number of people dying in a traffic accident the years of 2013-2017 obtained from Table 6. are presented graphically in Figure 5.

Table 6. Real values and model values for people dying in a traffic accident by years

	Year	Real Value	Grey Model GM(1,1)				Rolling Grey Model RGM(1,1)			
			Model Value	P	RE $\Delta,\%$	MRE $\overline{\Delta},\%$	Model Value	P	RE $\Delta,\%$	MRE $\overline{\overline{\Delta}},\%$
Model setup stage	2008	4 236								
	2009	4 324								
	2010	4 045								
	2011	3 835								
	2012	3 750	k=5				k=5			
After model setup stage	2013	3 685	3 524		4,37		3 524		4,37	
	2014	3 524	3 356		4,77		3 544		0,57	
	2015	7 530	3 195	0,55	57,57	37,20	3 456	0,73	54,10	0,54
	2016	7 300	3 043		58,32		8 658		18,60	
	2017	7 427	2 898		60,98		10 146		36,61	
Prediction of future years	2018		9 443				9 443			
	2019		11 056				9 592			
	2020		12 946				10 889			
	2021		15 158				12 216			
	2022		17 748				13 212			
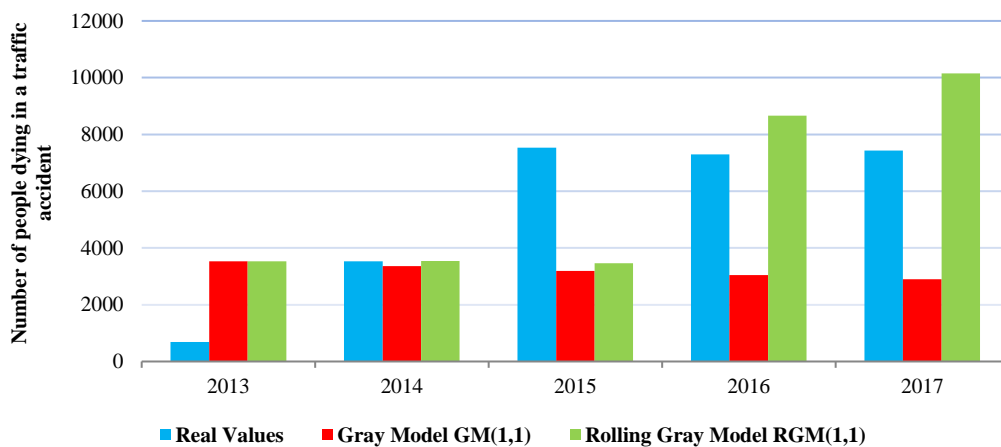
Figure 5. Real values and produced model values for the number of people dying in a traffic accident (2013-2017 years)

When the data obtained from Table 6. is analyzed, it is seen that the number of people dying in a traffic accident in the next years will increase with a certain amount every year. The rolling grey prediction model was found to be good compared to the grey prediction model.

4. CONLUSIONS

The purpose of this study is to determine the effectiveness of grey prediction and rolling grey prediction models in case of insufficient data. For this reason, number of traffic accidents, number of traffic accidents involving material loss only, number of traffic accidents with death-injury, number of dying people and total number of vehicle accidents occurred between the years 2008-2017, were produced prediction data for the future. The data between 2008-2012 were used as raw data and the data between 2013-2017 were used as real data and the predicted data were produced for use as benchmark for 2013-2017. Produced grey prediction and rolling grey prediction data were tested using performance tests such as relative error, mean relative error, and accuracy parameter.

According to the results, it was seen that the rolling grey prediction model had less error percentages and better accuracy scores than grey prediction model. For this reason, it can be seen that the use of the rolling grey prediction model will be more useful for producing prediction data for the number of vehicles and accidents in traffic.

When the predicted data are evaluated, it was determined that there would be a decrease in the total number of accidents, but the number of deaths and injuries in the specified years would increase. Considering the increased number of vehicles, the importance of increasing safety in the highways and planning related to this issue has been re-demonstrated in this study. Although there is not much data in terms of modeling, it has been determined that grey prediction models used in this study can be successfully applied in order to make some predictions.

REFERENCES

[1].   TUIK- News Bulletin, "*Road Traffic Accident Statistics Report*," 2017.
[2].   T.C. Sayistay Baskanligi, "*Traffic Auditing Prevention Activities Performance Audit Report (Decision 5216/1*)," Ankara: T.C. Sayistay Baskanligi, 2008.
[3].   R. S. Hosse, U. Becker, H. Manz*, "Grey Systems Theory Time Series Prediction applied to Road Traffic Safety in Germany,"* IFAC-PapersOnLine vol. *49-3, pp. 231-236, 2016.*
[4].   J. Deng, "*Introduction of Grey System Theory*," Journal of Grey System, vol. 1-1, pp.1-24, 1989.
[5].   K. L. Wen, "*Grey Systems: Modeling and Prediction*," Yang's Scientific Research Institute, USA, 2004.
[6].   S. Liu, Y. Lin, "*Grey Information: Theory and Practical Applications*," Springer, Vol. 11-21, 2006. DOI: 10.1007/978-3-642-16158-2
[7].   J. L. Deng, "*The control problems of grey systems*," System & Control Letters, Vol. 5: pp. 288-294, 1982.
[8].   J. L. Deng, "*Grey forecasting and decision*," Huazhong University of Science and Technology Press, 1986.
[9].   E. E. Basakin, M. Ozger, N. E. Unal, "*Water Consumption Model of Istanbul City by Grey Prediction Method*," Journal of Polytechnic, DOI: 10.2339/politeknik.422727, 2018.
[10]. B. Guner, E. Tacyildiz, "*Forecasting Traffic Accidents in Turkey by Rolling-Gm(1,1) Mechanism*," Journal of Social and Technical Researches, Vol.13, pp59-71, 2017.

Where is the Northern boundary of Western Anatolia?

Ayca Cirmik[1]

Abstract

Western Anatolia is one of the most seismically active and normal-fault-dominated extending regions in the world and is currently experiencing an approximately N–S continental extension. The tectonic system which is dominated with normal fault system replaces to the strike-slip system in the north of Western Anatolia. There is a boundary which is called as North Aegean Region (NAR) between these two different systems. However, the location of this boundary has not been explained, exactly.

In this study for investigating the northern boundary of Western Anatolia, GPS data were analyzed with Gamit/Globk software relative to the Anatolian block system. According to the Anatolia block solutions, GPS vectors represented different directional movements. The GPS vectors locate in the north of this boundary which obtained by GPS solutions move to the north, on the other hand, the south vectors move to the west and southwest. Finally, this boundary which obtained by GPS solutions were correlated with the geological features of the study region. Therefore, it is found that this boundary pointed to the Northern boundary of Western Anatolia, namely NAR.

Keywords: Western Anatolia, North Aegean Region, GPS

1. INTRODUCTION

Western Anatolia locates in the N-S directional extensional system and is one of most important regions which have seismic activity in the world [1]. Western Anatolia has a complex tectonic structure and includes different tectonic structural elements such as E–W trending basins and the active normal faults which bounded these basins and the NE-SW trending basins [1]. Additionally, the extension and movement of Western Anatolia includes high importance for the tectonic deformation for Aegean region. But, the answer of the question; where the Western Anatolia region begins or ends is not clear. Therefore, in this study, the GPS data was used and its relation with geological structures was given for pointing out the northern boundary of Western Anatolia.

In this study, the GPS data of two national projects, namely, Multi-Disciplinary Earthquake Researches in High Risk Regions of Turkey Representing Different Tectonic Regimes" (TURDEP) and "Continuously Operating Reference Stations-Turkey" (CORS-TR) (Fig. 1) were used. The GPS data were processed by using GAMIT/GLOBK software [2] respect to the Eurasia fixed frame. Then, the Anatolian block fixed frame solutions were calculated for investigating the interplate motions of the study area.

An elastic block model in Africa-Arabia-Eurasia continental collision zone for representing the recent-day plate motions (respect to Euler vectors), regional deformation within the interplate zone, and slip rates for major faults were put forward by [3]. The block boundaries were defined by mapped faults, seismicity, and historic earthquakes. The Euler Vectors were calculated respect to Eurasia for determining the block model. Euler vectors relative to Eurasia for the Anatolian block fixed reference frames are 30.8°N, 32.1°E, with angular velocity, 1.231°/Myr. [3]. In this study, Anatolian block fixed velocity vectors were calculated by using Euler vectors [3] which present interplate motions (Fig. 2). Therefore, the directions of the velocities were obtained and the northern boundary of Western Anatolia was presented.

2. APPLICATION

For determining the deformation and interplate motions of Western Anatolia, the data of GPS stations located at Western Anatolia were used of TURDEP and CORS-TR projects. The data of TURDEP and CORS-TR projects were reached from TUBITAK (Marmara Research Center, Earth and Marine Science Institute) and General Directorate of Land Registry and Cadastre (Map Department), respectively.

In this context, firstly, 10 continuous GPS stations of TURDEP Project; AKHT (Akhisar, Manisa), BDMT (Bademli, Izmir), BORT (Borlu, Manisa), CALT (Cal, Denizli), ESMT (Esme, Usak), IZMT (Izmir, City Center), KRCT (Karacasu, Aydin), KRPT (Karpuzlu, Aydin), TRBT (Torbali, Izmir) and TRGT (Turgutlu, Manisa) and 11 continuous GPS stations of CORS-TR projects; AYD1 (Aydin, City Center), BALK (Balikesir, City Center), CESM (Cesme, Izmir), DEIR (Demirci, Manisa), DENI (Denizli, City Center), HARC (Harmancik, Bursa), IZMI (Izmir, City Center), KIKA (Kirkagac, Manisa), MUGL (Mugla, City Center), SALH (Salihli, Manisa), USAK (Usak, City Center) (Fig. 1) were processed by using GAMIT/GLOBK software for the days between $180^{th} – 195^{th}$ (as Julian days) of 2009-2010-2011 years.
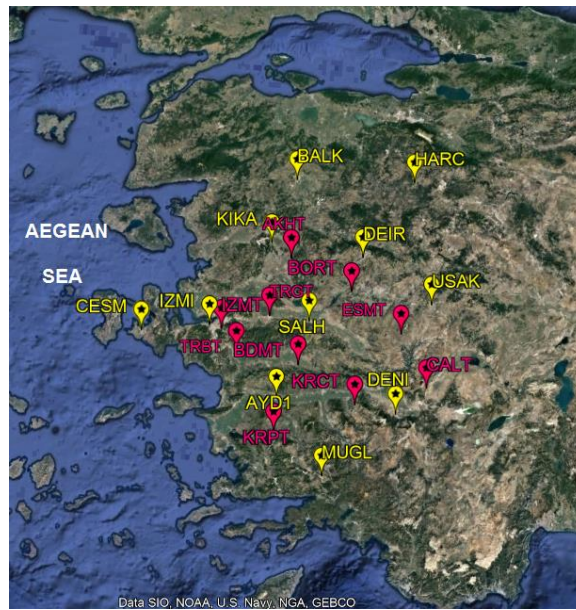
Fig. 1. The locations of the GPS stations. Pink and yellow marks represent TURDEP and CORS-TR project stations, respectively. This figure is created by using [4].

As the next step, for understanding the interplate motion of the Western Anatolia, by using the velocities of the stations respect to Eurasia, the Anatolian block fixed frame solutions were calculated. In this process, the Anatolian block fixed velocities were obtained (Fig. 2) by using Euler vectors calculated by [3].
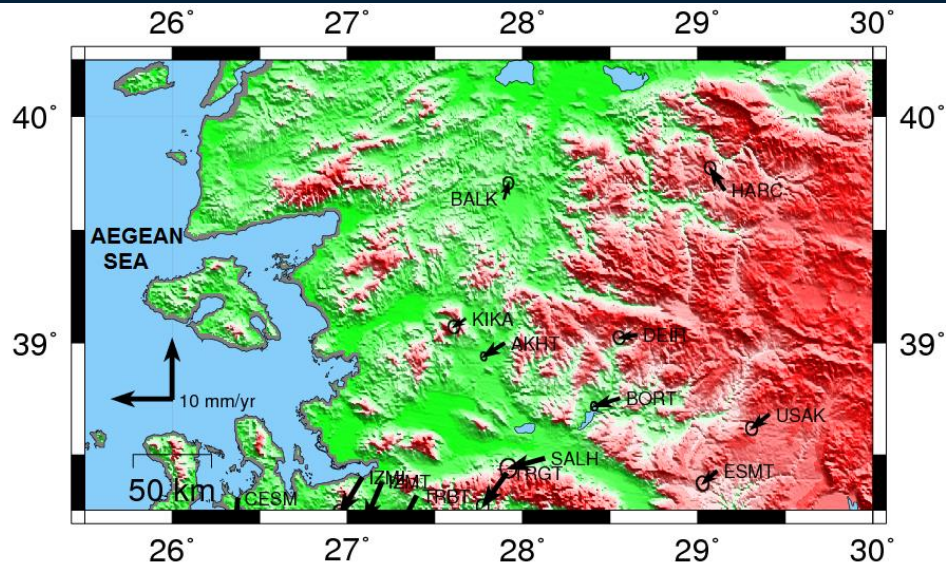
Fig 2. The Anatolian block fixed solutions of Western Anatolia.

3. RESULTS

The Anatolian Block solutions were calculated respect to the Euler vectors for stations of TURDEP and CORS-TR projects (Fig. 2). The directions of the velocity vectors of the GPS stations locate between 38.5° and 39° latitudes are towards to SW. On the other hand, the directions of the velocity vectors of the GPS stations (BALK and HARC) locate between 38° and 39° latitudes are towards to N which are the opposite directions respect to the other stations.

Western Anatolia is dominated with normal faults, North Aegean Region is dominated with the strike-slip faults [5]. Therefore, there is a boundary but its location is not clear which separate Western Anatolia and North Anatolian Regions from each other. Therefore, the northern boundary of Western Anatolia which separates these regions can be located horizontally between the stations BALK-HARC and KIKA-DEIR, approximately at 39.5° latitude. Besides, this finding is consistent with the Northern boundary of Western Anatolia which was given by in tectonic models of [6], [7], [8], [9].

ACKNOWLEDGEMENT

REFERENCES

[1]. E., Bozkurt, Neotectonics of Turkey—a synthesis. Geodinamica Acta 14, 3–30, 2001.

[2]. T.A., Herring, R.W., King, M.A., Floyd, S.C., McClusky, Introduction to GAMIT/GLOBK, Release 10.6. Massachusetts Institute of Technology, Cambridge, 2015.

[3]. R., Reilinger, et al., GPS constraints on continental deformation in the Africa-Arabia-Eurasia continental collision zone and implications for the dynamics of plate interactions, J. Geophys. Res. 111, B05411, 2006.

[4]. http://www.earth.google.com

[5]. C., Ozkaymak, H., Sozbilir, B., Uzel, Neogene–Quaternary evolution of the Manisa Basin: Evidence for variation in the stress pattern of the Izmir-Balikesir Transfer Zone, western Anatolia, J. Geodynamics 65, 117-135, 2013.

[6]. D.P., McKenzie, Active tectonics of the Alpine–Himalayan belt: the Aegean Sea and surrounding regions, Geophys. J. Roy. Astro. Soc. 55, 217–254, 1978.

[7]. J.F., Dewey, A.M.C., Sengor, Aegean and surrounding regions: complex multiple and continuum tectonics in a convergent zone. Geol. Soc. Am. Bull. 90, 84–92, 1979.

[8]. H., Sozbilir, T., Emre, Supradetachment basin and rift basin developed during the neotectonic evolution of the Menderes Massif. In: 49th Geological Congress of Turkey Abstracts, Ankara, 30–31, 1996.

[9]. I., Cemen, E. J., Catlos, O., Gogus, C., Ozerdem, Postcollisional extensional tectonics and exhumation of the Menderes Massif in Western Anatolia extended terrane, Turkey. Geol. Soc. Am. Sp. Pub. 409, 353–379, 2006.

The Cubic Trigonometric B-spline Galerkin Method for the Fisher Equation

Ozlem Ersoy Hepson[1], Idris Dag[2]

Abstract

A computational algorithm based on the cubic trigonometric B-spline Galerkin is set up to find numerical solutions of the Fisher equation. Fully-integration of the Fisher equation is managed by use of the Crank-Nicolson scheme for the temporal discretization and the Galerkin method for spatial discretization. The trial function in the Galerkin method is formed with combination of the cubic trigonometric functions and test function is taken to be the trigonometric function well. Resulting 7-banded system of algebraic equations is solved to get numerical solutions of the Fisher equation at discrete points over problem domain. The robustness of the algorithm is exhibited on studying test problems.

Keywords: cubic trigonometric B-spline, Fisher equation, Galerkin method.

1. INTRODUCTION

A paper of Schoenberg [1] was described in its current form of spline functions. Since then variety of polynomial and non-polynomial splines are defined to solve problems, such as spline functions can be used to interpolate data or to form an approximation function for numerical solutions of the differential equations. Since a spline function of degree *n* is a continuous functions with *n-1* continuous derivatives, we can set up smooth functional approximation. Thus we can fulfil continuity condition up to order of the given differential equations. Propagation of an advantageous gene in population was introduced in form of the Fisher equation (FE) by Fisher [2], which is a nonlinear parabolic partial differential equation given by

$$\frac{\partial u(x,t)}{\partial t} = \lambda \frac{\partial^2 u(x,t)}{\partial x^2} + \beta u(x,t)\big(1 - u(x,t)\big), \qquad -\infty < x < \infty, t > 0 \tag{1}$$

where λ is diffusion coefficient and β is reaction coefficient. It consists of term u_t, linear diffusion term u_{xx} and nonlinear reaction term $u(1-u)$. This equation has been found to model physical, chemical and biological phenomena involving diffusion and nonlinear growth, for instance, neutron population in nuclear reactions [3], flame propagation in any medium [4]. The initial and different boundary conditions for FE (1) are given as

$$u(x,0) = f(x), \qquad x \in (-\infty, \infty), \tag{2}$$

$$\lim_{x \to -\infty} u(x,t) = 1, \quad \lim_{x \to \infty} u(x,t) = 0, \tag{3}$$

or
$$\lim_{x \to \pm\infty} u(x,t) = 0. \tag{4}$$

In the literature, conditions (2) and (3) are known as nonlocal conditions, while conditions (2) and (4) are local conditions.

Numerous numerical and approximate-analytical methods have been composed to have solutions of the FE. Here in, we only mention about the spline related methods. The collocation methods are set up to integrate the FE fully

[1] Corresponding author: Eskisehir Osmangazi University, Mathematics & Computer Department, Eskisehir, Turkey, ozersoy@ogu.edu.tr

[2] Eskisehir Osmangazi University, Computer Engineering Department, Eskisehir, Turkey, idag@ogu.edu.tr

by using cubic B-spline, extended cubic B-splines, trigonometric B-splines and exponential cubic B-splines in spatial direction and finite difference approximation in time direction in studies [5]- [10]. Recently, the fourth order cubic B-spline collocation method is build up for getting numerical solutions of the FE [11]. Numerical solution of the FE is obtained by establishing the Galerkin method based on quadratic, quartic and exponential B-splines [12]-[14]. A numerical method for solving the generalized Burgers-Fisher equation using the derivative of the cubic B-spline quasi interpolation to integrate the spatial derivative of the equation together with forward difference scheme for the temporal discretization is constructed [15]. The quintic B-spline collocation method is proposed to get solution of the Fisher equation in the study [16]. The formulation of spline difference method is described to solve the FE in [17]. FE is solved by employing the differential quadrature method that uses the cubic B-spline in [18].

Our aim in the paper is to construct the cubic trigonometric B-spline Galerkin scheme for solving the FE. Integration of the FE is achieved by employing the Galerkin method for spatial discretization and the Crank-Nicolson method for temporal discretization.

2. CUBIC TRIGONOMETRIC B-SPLINE GALERKIN METHOD

The evenly spaced nodes, $a=x_0<x_1<\cdots<x_N=b$ with distance between nodes $h=(b-a)/N$, are considered to partition the problem domain $[a, b]$. Over these nodes and external nodes x_{-3}, x_{-2}, x_{-1}, x_{N+1}, x_{N+2}, x_{N+3} outside problem domain, cubic trigonometric B-spline basis $C_m(x)$, $m=-1...N+1$ can described in the following form [9] over the interval $[a, b]$:

$$C_m(x) = \frac{1}{c_h}\begin{cases} c^3(x_{m-2}), & x \in [x_{m-2}, x_{m-1}] \\ c(x_{m-2})\big(c(x_{m-2})\hat{c}(x_m) + \hat{c}(x_{m+1})c(x_{m-1})\big) + \hat{c}(x_{m+2})c^2(x_{m-1}), & x \in [x_{m-1}, x_m] \\ c(x_{m-2})\hat{c}^2(x_{m+1}) + \hat{c}(x_{m+2})\big(\hat{c}(x_{m-1})\hat{c}(x_{m+1}) + \hat{c}(x_{m+2})c(x_m)\big), & x \in [x_m, x_{m+1}] \\ \hat{c}^3(x_{m+2}), & x \in [x_{m+1}, x_{m+2}] \\ 0, & otherwise \end{cases} \tag{5}$$

where $c(x_m) = sin\big(\frac{x-x_m}{2}\big)$, $\hat{c}(x_m) = sin\big(\frac{x_m-x}{2}\big)$, $c_h = sin\big(\frac{h}{2}\big)sin(h)sin\big(\frac{3h}{2}\big)$. The cubic trigonometric B-spline function set $\{C_m(x)\}_{m=-1}^{N+1}$ is twice continuously differentiable. Thus smooth approximate solution can be obtained for the differential equations of order two. Formulation of an approximate solution $U(x,t)$ to analytical solutions $u(x,t)$ is in the form

$$U(x,t) = \sum_{m=-1}^{N+1} \varphi_m(t)C_m(x) \tag{6}$$

where φ_m and $C_m(x)$ are time dependent parameters and trigonometric B-splines recursively. The approximate solution $U(x,t)$ and its derivative at nodes x_m can be obtained in terms of time dependent parameters φ_m using Eqs. (5)-(6):

$$U(x_m,t) = \alpha_1\varphi_{m-1}(t) + \alpha_2\varphi_m(t) + \alpha_1\varphi_{m+1}(t)$$
$$U'(x_m,t) = \beta_1\varphi_{m-1}(t) - \beta_1\varphi_{m+1}(t) \tag{7}$$
$$U''(x_m,t) = \gamma_1\varphi_{m-1}(t) + \gamma_2\varphi_m(t) + \gamma_1\varphi_{m+1}(t)$$

where

$$\alpha_1 = sin^2\big(\tfrac{h}{2}\big)csc(h)csc\big(\tfrac{3h}{2}\big), \alpha_2 = \frac{2}{1+2cos(h)}, \beta_1 = -\tfrac{3}{4}csc\big(\tfrac{3h}{2}\big), \gamma_1 = \frac{3\big((1+3cos(h))csc^2\big(\tfrac{h}{2}\big)\big)}{16\big(2cos\big(\tfrac{h}{2}\big)+cos\big(\tfrac{3h}{2}\big)\big)}, \gamma_2 = -\frac{3cot^2\big(\tfrac{h}{2}\big)}{2+4cos(h)}. \tag{8}$$

To implement the Galerkin procedure, Eq. (1) is multiplied by the weight function $w(x)$ and integration of the expression from a to b gives:

$$\int_a^b w(x)\left(\frac{\partial u(x,t)}{\partial t} - \lambda\frac{\partial^2 u(x,t)}{\partial x^2} - \beta u(x,t)\big(1 - u(x,t)\big)\right)dx = 0 \tag{9}$$

The approximate solution U is interpolated within each element by

$$U^e = C_{m-1}(x)\varphi_{m-1}(t) + C_m(x)\varphi_m(t) + C_{m+1}(x)\varphi_{m+1}(t) + C_{m+2}(x)\varphi_{m+2}(t) \tag{10}$$

where quantities $\varphi_j(t)$ and $C_j(x)$, $j = m-1, m\ \ m+1, m+2$ are element parameters and element shape functions respectively. Since the weak form Eq. (9) is valid on the whole region, particularly it is valid over the typical element $[x_m, x_{m+1}]$:

$$\int_{x_m}^{x_{m+1}} w(x)\left(\frac{\partial u(x,t)}{\partial t} - \lambda\frac{\partial^2 u(x,t)}{\partial x^2} - \beta u(x,t)\big(1 - u(x,t)\big)\right)dx = 0. \tag{11}$$

We use transformation $\xi = x - x_m$ to be independent from the local coordinates so that Eq. (10) takes the form

$$\int_0^h w(\xi)\frac{\partial u(\xi,t)}{\partial t}d\xi - \lambda\int_0^h w(\xi)\frac{\partial^2 u(\xi,t)}{\partial \xi^2}d\xi - \beta\int_0^h w(\xi)u(\xi,t)d\xi + \beta\int_0^h w(\xi)u^2(\xi,t)d\xi = 0 \tag{12}$$

Over the sample element $[0, h]$, B-spline shape functions can be found in terms of the local coordinate ξ as:

$$C_{m-1} = \frac{1}{\theta}sin^3\left(\frac{h-\xi}{2}\right),$$

$$C_m = \frac{1}{\theta}\left(sin\left(\frac{\xi+2h}{2}\right)sin^2\left(\frac{\xi-h}{2}\right) + sin\left(\frac{\xi-2h}{2}\right)sin\left(\frac{\xi+h}{2}\right)sin\left(\frac{\xi-h}{2}\right) + sin^2\left(\frac{\xi-2h}{2}\right)sin\left(\frac{\xi}{2}\right)\right),$$

$$C_{m+1} = \frac{1}{\theta}\left(sin^2\left(\frac{\xi+h}{2}\right)sin\left(\frac{h-\xi}{2}\right) + sin\left(\frac{\xi+h}{2}\right)sin\left(\frac{2h-\xi}{2}\right)sin\left(\frac{\xi}{2}\right) + sin\left(\frac{3h-\xi}{2}\right)sin^2\left(\frac{\xi}{2}\right)\right),$$

$$C_{m+2} = \frac{1}{\theta}sin^3\left(\frac{\xi}{2}\right), \tag{13}$$

where $\theta = sin\left(\frac{h}{2}\right)sin(h)sin\left(\frac{3h}{2}\right)$. Substituting Eq. (10) to Eq. (12), we have

$$\sum_{j=m-1}^{m+2}\left[\int_0^h C_i C_j d\xi\right]\dot{\varphi} - \lambda\sum_{j=m-1}^{m+2}\left[\int_0^h C_i C_j'' d\xi\right]\varphi$$

$$-\beta\sum_{j=m-1}^{m+2}\left[\int_0^h C_i C_j d\xi\right]\varphi + \beta\sum_{k=m-1}^{m+2}\sum_{j=m-1}^{m+2}\left(\int_0^h C_i C_k C_j\, d\xi\right)\varphi = 0 \tag{14}$$

where $\cdot$ and $'$ denotes time and space derivative respectively. If we take

$$A_{ij}^e = \int_0^h C_i C_j d\xi, \quad B_{ij}^e = \int_0^h C_i C_j'' d\xi, \quad C_{ikj}^e = \sum_{k=m-1}^{m+2}\left(\int_0^h C_i C_k C_j d\xi\right) \tag{15}$$

where $i, j, k = m\text{-}1, m, m\text{+}1$, A^e and B^e are element matrices with the dimension 4×4 and $C^e(\varphi^e)$ is the element matrix with the dimension $4\times4\times4$. Eq. (14) can be written in the matrix form

$$A\dot{\varphi}^e + \left(-\lambda B^e - \beta A^e + \beta C^e(\varphi^e)\right)\varphi^e \tag{16}$$

where $\varphi^e = (\varphi_{m-1}, \varphi_m, \varphi_{m+1}, \varphi_{m+2})^T$. Assembling contribution from all element matrices A^e, B^e and C^e in Eq. (16) gives global matrix equation in the form:

$$A\dot{\varphi} + \left(-\lambda B - \beta A + \beta C^e(\varphi)\right)\varphi = 0 \tag{17}$$

where the matrices **A**, **B** and **C** are obtained by combining element matrices and $\boldsymbol{\varphi} = (\varphi_{-1}, ..., \varphi_{N+1})^T$.

If we use the Crank-Nicolson formula for φ and $\dot{\varphi}$ and the nonlinear term φ in Eq. (17) is approximated by the following formula based on Taylor series

$$(\varphi^2)^{n+1} = 2\varphi^n \varphi^{n+1} - (\varphi^n)^2. \tag{18}$$

After the nonlinear term is linearized using the formula (18), it gives recurrence relation between the sequential time levels:

$$\left[A - \frac{\Delta t}{2} \lambda B(\varphi_k^n) - \frac{\Delta t}{2} \beta A(\varphi_k^n) + \Delta t \beta C(\varphi_k^n) \right] \varphi^{n+1} \tag{19}$$

$$= \left[A + \frac{\Delta t}{2} \lambda B(\varphi_k^n) + \frac{\Delta t}{2} \beta A(\varphi_k^n) \right] \varphi^n$$

The system (19) consists of *N+1* linear equation in *N+3* unknown parameters. To make solvable the system, boundary conditions are used to eliminate φ_{-1}, φ_{N+1} from the system (19) which then becomes a solvable matrix equation for the unknown $\varphi_0^{n+1}, ..., \varphi_{N+1}^{n+1}$. A seven band final system of equation can be solved using Matlab.

3. NUMERICAL TESTS

Numerical method described in the previous section is tested on three problems for getting solutions of the Fisher's equation in order to demonstrate the robustness and numerical accuracy. The maximum error norm (L_∞) and relative error norm (rel)

$$L_\infty = \left| u(x,t) - U(x,t) \right|_\infty = \max_m \left| u(x_m, t) - U(x_m, t) \right| \tag{20}$$

and

$$rel = \sqrt{\frac{\sum_{m=1}^{N+1} |U_m^{n+1} - U_m^n|^2}{\sum_{m=1}^{N+1} |U_m^n|^2}} \tag{21}$$

are used to measure error between the analytical *(u)* and numerical *(U)* solutions.

o   ***Strong Reaction***

Ablowitz and Zepetella in [19] suggested the solution of the (1) in the following form:

$$u(x,t) = \left(1 + \exp\left(\sqrt{\frac{\beta}{6}} x - \frac{5\beta}{6} t \right) \right)^{-2} \tag{22}$$

The numerical solution of Eq. (1) with initial condition (22) with *t=0* and boundary conditions *u(a,t)=1, u(b,t)=0* over the problem domain *[-0.2,0.8]* has been found for *N=40* with *Δt=0.0001* at times *t=0.002, 0.003, 0.004, 0.005,0.006, 0.007* seen in Fig. 1, at times *t=0.001, 0.002, 0.003, 0.004, 0.005* seen in Fig. 2 agreeing with same parameters in the study [10].
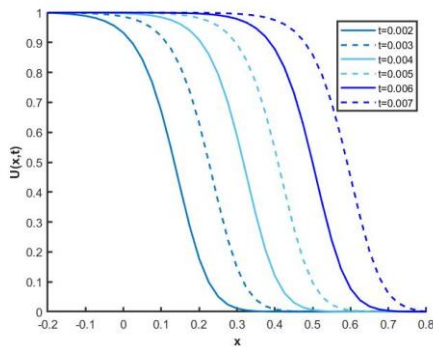
Figure 1. Numerical solutions for $\beta=2000$
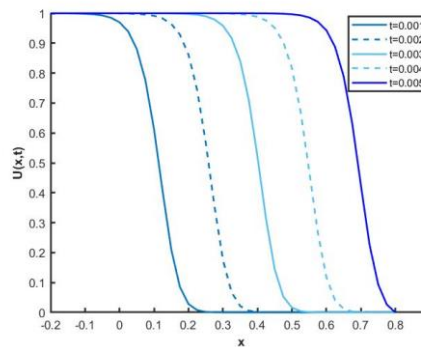
Figure 2. Numerical solutions for $\beta=5000$

For $\lambda=1$, $\beta=10000$, $N=64$, $\Delta t=5\times10^{-6}$ and $x\in[-0.2,0.8]$, results are presented in Table 1 to compare with findings [9], [10], [13], [14], [16], [21].

Table 1. Maximum error norms at some different times for the strong reaction

Method	t=0.0005	t=0.0015	t=0.0025	t=0.0035
Present Method	2.10×10^{-4}	1.12×10^{-3}	2.35×10^{-3}	3.63×10^{-3}
p=1, [14]	5.67×10^{-5}	8.76×10^{-4}	2.10×10^{-3}	3.38×10^{-3}
various p, [14]	7.83×10^{-4} (p=0.002530)	7.89×10^{-4} (p=0.002530)	7.89×10^{-4} (p=0.002530)	8.71×10^{-4} (p=0.002530)
[9]	1.02×10^{-2}	1.49×10^{-1}	3.24×10^{-1}	4.78×10^{-1}
p=1, [10]	1.10×10^{-2}	1.49×10^{-1}	3.44×10^{-1}	5.08×10^{-1}
various p, [10]	3.54×10^{-3} (p=0.00000300)	7.63×10^{-2} (p=0.00000192)	2.04×10^{-2} (p=0.00000089)	1.52×10^{-2} (p=0.00000089)
[16]	2.05×10^{-4}	2.30×10^{-3}	5.49×10^{-3}	9.04×10^{-3}
[13]	2.55×10^{-3}	1.62×10^{-1}	8.65×10^{-2}	6.98×10^{-2}
CN [21]	1.03×10^{-2}	1.25×10^{-1}	2.80×10^{-1}	4.48×10^{-1}
ASD [21]	1.07×10^{-2}	4.93×10^{-2}	9.37×10^{-2}	9.44×10^{-1}
FPS [21]	3.13×10^{-6}	3.90×10^{-6}	7.82×10^{-5}	3.42×10^{-1}
DSC [21]	6.28×10^{-6}	1.98×10^{-6}	4.46×10^{-6}	6.22×10^{-6}

o   ***Initial Pulse Profile***

Secondly, the initial pulse profile

$$u(x, 0) = sech^2(10x) \tag{23}$$

is chosen as the initial condition for our first numerical experiment together with boundary condition *U(-50, t) = 0* and *U(50, t) = 0*. In numerical calculations, the constants in Eq. (1) are selected as *λ = 0.1* and *β = 1*. The space and time increments *h = 0.025* and *Δt = 0.05* are used respectively. The algorithm is run up to time *t = 40* over the domain [*-50, 50*]. Solutions of *U* at times *t = 0, 0.2, 0.4, 0.6, 0.8, 1* are depicted over the interval [*-2, 2*] in Fig. 3, in which diffusion dominates the reaction so that peaks decreases and becomes flatted. *U* values at larger periodic times *t = 0, 1, 2, 3, 4, 5* in Fig. 4 are drawn over the interval [-6, 6], from which we see that after the solution reaches the shorter form, then it grown up until *U* reaches *1* at about time *t = 6*, it means that gradually reaction dominates the diffusion. Finally for larger periodic times *t = 0 , 10, 20, 30, 40, 50* solutions are graphed in the interval [*-50, 50*] in Fig. 5, the peak reaches the initial peak value *U = 1* and keep this value *U = 1* on the top as time advances, propagation continues with flat top to the right and left symmetrically.
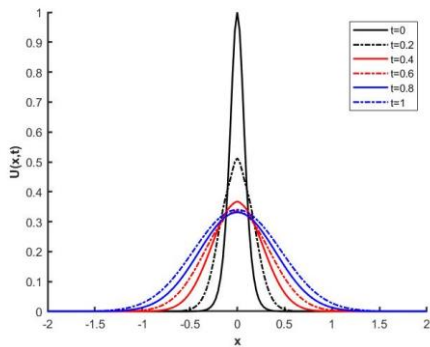
Figure 3. Solutions at early times.
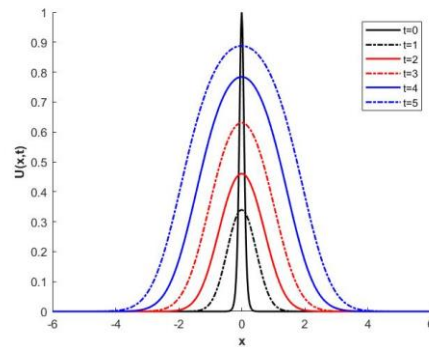
Figure 4. Short-time behavior.
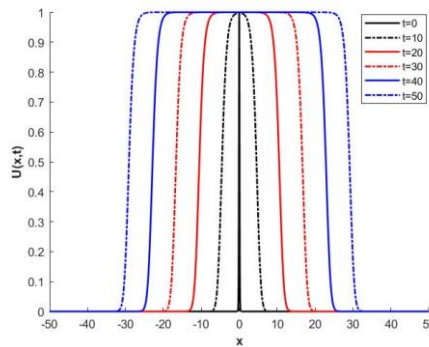
Figure 5. Long-time behavior.

In the Table 2 errors at some different times for initial pulse profile is documented for *λ = 0.1, β = 1, N = 64, Δt = 0.05* and *x* ∈ [*-50, 50*].

Table 2. Relative error norms at some different times for the initial pulse profile

Method	t=5	t=10	t=15	t=20	t=40
Present	1.190×10^{-2}	6.939×10^{-3}	7.860×10^{-3}	5.002×10^{-3}	3.396×10^{-3}
p=1, [10]	1.180×10^{-3}	1.665×10^{-2}	1.870×10^{-2}	4.515×10^{-2}	2.218×10^{-2}

various p, [10]	7.730×10^{-3}	1.364×10^{-3}	9.087×10^{-4}	6.412×10^{-4}	2.730×10^{-8}
	(p=1.4235)	(p=0.1773)	(p=1.92731)	(p=1.35700)	(p=0.59194)
[13]	1.386×10^{-2}	7.860×10^{-3}	6.054×10^{-3}	5.090×10^{-3}	3.434×10^{-3}

o *Initial Step Profile*

Lastly, the Fishers equation is studied with local boundary condition (4) and initial condition with straight top and sharp sides given by:

$$u(x,0) = \begin{cases} e^{10(x+1)}, & x < -1 \\ 1, & -1 \le x \le 1 \\ e^{-10(x-1)}, & x > 1 \end{cases} \qquad (24)$$

In this test problem, the parameters are chosen as $\lambda = 0.1$, $\beta = 1$, $\Delta t = 0.05$ and $N = 40$. Graphical solutions at some times are illustrated in Fig. 6 over the spatial interval [*-6, 6*] seen slight diffusion at the bottom and top part of the solutions near at $x = -1$ and $x = 1$ change in shape from stepness to smoothness and as time advances wave fronts forms and started moving in opposite direction depicted at some times in Fig. 7 over the interval [*-30, 30*].

With selection of parameters $\lambda = 0.1$, $\beta = 0.1$ the diffusion and reaction are clearly distinguished effectively in Fig. 8 and Fig. 9. So that solutions are drawn at early time for the interval [*-6, 6*] at $t = 0, 1, 2, 3, 4, 5$ top part goes down and bottom becomes spreaded and also are drawn for [*-30, 30*] at $t = 5, 10, 15, 20, 25, 30$ later times reaction is seen to be more influential. In Fig. 8, effects of diffusion and reaction are very small. Near the corners diffusion is more effective and it causes decays slightly there.
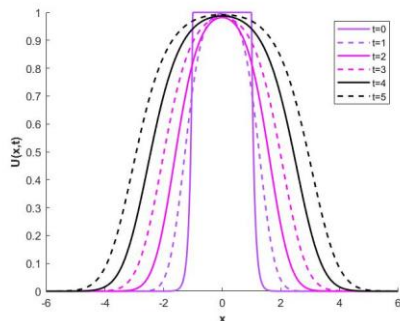
Figure 6. Time dependent profile versus for λ=0.1, β=1   *Figure 7. Time dependent profile versus for λ=0.1, β=1*
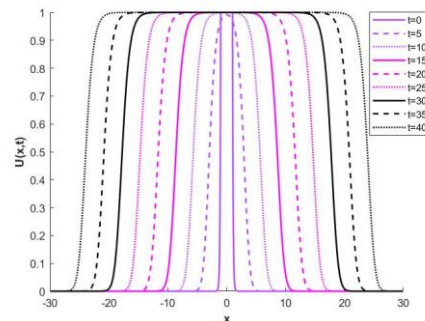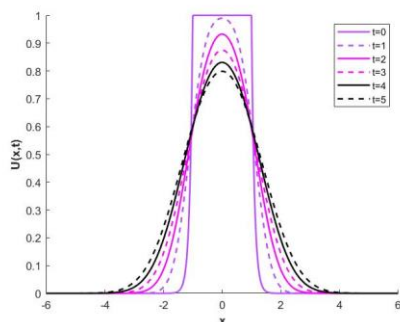
Figure 8. Time dependent profile versus for λ=0.1, β=0.1   *Figure 9. Time dependent profile versus for λ=0.1, β=0.1*
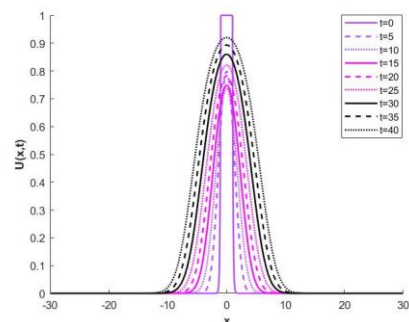
In the Table 3, relative error norms at some different times for the initial step profile is documented for *λ=0.1, β=1, h=0.025, Δt=0.05* and *x*∈[*-50,50*

Table 3. Relative error norms at some different times for the initial step profile

Method	t=5	t=10	t=15	t=20	t=40
Present	9.514×10^{-3}	6.946×10^{-3}	5.620×10^{-3}	4.822×10^{-3}	3.340×10^{-3}
p=1, [10]	1.033×10^{-3}	7.458×10^{-3}	5.967×10^{-3}	5.088×10^{-3}	3.490×10^{-3}
[13]	9.435×10^{-3}	6.917×10^{-3}	5.614×10^{-3}	4.825×10^{-3}	3.352×10^{-3}

CONCLUSION

A simple and straightforward Galerkin method based on cubic trigonometric B-spline functions is developed for solving the FE. Results of the proposed method is compared with numerical results of the studies referenced [9], [10], [13], [14], [16], [21]. It is found that the suggested method presents similar results with the exponential B-spline Galerkin method with the free parameter of a value *p = 1* and better than the polynomial B-spline collocation methods. Usability of the cubic trigonometric b-splines is exhibited for the Galerkin method.

ACKNOWLEDGMENT

REFERENCES

[1]. J. Schoenberg, "Contributions to the problem of approximation of equidistant data by analytic functions," *Quart. Appl. Math*. vol. 4, pp. 45-99 and pp. 112–141, 1946.

[2]. R. A. Fisher, "The wave of advance of advantageous genes," *Ann. Eugenics,* vol. 7, pp. 355–369, 1937.

[3]. J. Canosa, "Diffusion in nonlinear multiplicative media," *J. Math. Phys.,* vol. 10, pp. 1862–1868, 1969.

[4]. J. B. Zeldovich and D. A. Frank-Kamenetzk, "A theory of thermal propagation of flame," *Acta Physicochimica,* vol. 9(2), pp. 341–350, 1938.

[5]. O. Ersoy and I. Dag, "The extended B-spline collocation method for numerical solutions of Fisher equation," *AIP Conference Proceedings*, 2015, paper. 1648, p. 370011.

[6]. R. C. Mittal and R. K. Jain, "Numerical solutions of nonlinear Fisher's reaction–diffusion equation with modified cubic B-spline collocation method," *Mathematical Sciences,* vol. 7(12), pp. 1–10, 2013.

[7]. R.C. Mittal and S. Dahiya, "A study of quintic B-spline based differential quadrature method for a class of semi-linear Fisher-Kolmogorov equations," *Alexandria Engineering Journal,* vol. 55, pp. 2893–2899, 2016.

[8]. H. S. Shukla and M. Tamsir, "Extended modified cubic B-spline algorithm for nonlinear Fisher's reaction-diffusion equation," *Alexandria Engineering Journal,* vol. 55, pp. 287–2879, 2016.

[9]. O. E. Hepson and I. Dag, "The Numerical Approach to the Fisher's Equation via Trigonometric Cubic B-spline Collocation Method," *Communications in Numerical Analysis,* vol. 2, pp. 91–100, 2017.

I. Dag and O. Ersoy, "The exponential cubic B-spline algorithm for Fisher equation," *Chaos, Solitons and Fractals,* vol. 86 , pp. 101–106, 2016.

[10]. R. Rohila and R. C. Mittal, "Numerical study of reaction diffusion Fisher's equation by fourth order cubic B-spline collocation method," *Mathematical Sciences,* vol. 12, pp. 79–89, 2018.

A. Sahin, I. Dag and B. Saka, "A B-spline algorithm for the numerical solution of Fisher's equation," *Kybernetes*, vol. 37(2), pp. 326–342, 2008.

[11]. Dag , A.Sahin and A. Korkmaz, "Numerical Investigation of the Solution of Fisher's Equation via the B-Spline Galerkin Method," *Numerical Methods for Partial Differential Equations,* vol. 26(6), pp. 1483–1503, 2010.

[12]. M. Z. Gorgulu and I. Dag, "Exponential B-splines Galerkin Method for the Numerical Solution of the Fisher's Equation," *Iran J Sci Technol Trans Sci*, vol. 42, pp. 2189–2198, 2018.

[13]. C. G. Zhu and W. S. Kang, "Numerical solution of Burgers-Fisher equation by cubic B-spline quasi-interpolation," *Applied Mathematics and Computation,* vol. 216, pp. 2679–2686, 2010.

A. Sahin, O. Ozmen, "Usage of Higher Order B-splines in Numerical Solution of Fisher's Equation," International Journal of Nonlinear Science, vol. 17(3), pp. 241–253, 2014.

[14]. M. Aghamohamadi, J.Rashidinia and R. Ezzati, "Tension spline method for solution of non-linear Fisher equation," *Applied Mathematics and Computation,* vol. 249, pp. 399–407, 2014.

[15]. M. Tamsir, N. Dhirman and V. K. Srivasta, "Cubic trigonometric B-spline differential quadrature method for numerical treatment of Fisher's reaction diffusion equations," *Alexandria Engineering Journal,* vol. 57(3), pp. 2019-2026, 2018.

[16]. M. Ablowitz and A. Zepetella, "Explicit solution of Fisher's equation for a special wave speed," *Bull. Math.,* vol. 41(6), pp. 835–840, 1979.

[17]. R. C. Mittal and G. Arora, "Efficient numerical solution of Fisher's equation by using B-spline method," *International Journal of Computer Mathematic,* vol. 87(13), pp. 3039–3051, 2010.

[18]. S. Zhao and G. W. Wei, "Comparison of the discrete singular convolution and three other numerical schemes for solving Fisher's equation," *SIAM J Sci Comput.,* vol. 25, pp. 127–147, 2003.

Harmonic Response Analysis of Double Bridge Crane System on Multi Carriages

Sahin Yildirim [1], Emir Esim[2]

Abstract

In crane systems, force changes occur in ropes especially when the load is lifted. Considering these forces, one approach using harmonic response to analyze the characteristics of full model crane system which is modelled with bridge carrier, bridge group, car, load and rope is proposed in this paper. The forces to be lifted on the ropes were calculated and applied to the crane system. Also, dynamic theory and modeling method of multi-degree of freedom system are introduced. Based on these parameters, a virtual dynamic model is established to match the actual one. ANSYS Workbench 18.1 program was used to determine the correct dynamic characteristics of the crane system under these conditions. Moreover, studies of harmonic response are carried out to get the explicit characteristics of each part in the model. In addition, recommendations are made for future improvement studies.

Keywords: Multi-carriages Crane System, Modal analysis, Harmonic response analysis, finite element method

1. INTRODUCTION

When designing a mechanical system, it is necessary to determine the characteristics of the system and to test the qualifications. Therefore, dynamic analysis methods such as modal analysis, harmonic analysis, and passive analysis are used to determine the characteristics of the systems. The definition of modal parameters is a prerequisite for understanding the dynamic properties. The vibration is related to the oscillating movement of dynamic systems. All bodies with mass and elasticity may vibrate at a specific natural frequency. The resonance phenomenon occurs if the natural frequency of the structural system matches the dynamic load frequency, which may cause the structure to deteriorate. In order to avoid such a malfunction, it is essential to examine the vibrational behavior of the system and in fact it is absolutely necessary. Vibration in mechanical systems is a serious problem for engineers for more than a century. therefore, many investigators have examined the modal parameter and the vibration problems caused by these parameters [1], [2].

Some studies on the crane and beams can be presented as follows: Abu Hilal has studied the forced vibration of Euler Bernoulli beams based on Green's functions [3]. Wu has performed the dynamic analysis of the 3-dimensional portal crane by using the finite element model and experimental model analysis [4].Malgaca et al have applied dynamic strain measurements of the overhead crane and compared the SEM model with the experimental stress values for the beam [5]. The plane vibration analysis of the portal crane with a capacity of 2x400 tons was realized by Sahin by both mathematical and finite element methods and compared the results [6]. In a study by Gurgoze, an alternative formulation was developed for the frequency equation of the Euler Bernoilli beam with several springs and mass systems along the beam [7]. in another study by Gurgoze and Erol, they examined the vibration analysis of the beam in the case of the addition of a viscous damping and spring system [8]. Gasic and Petkovic have studied the determination of eigenfrequencies of overhead cranes in vertical plane. It is assumed that the individual members of the frame are managed by the transverse vibration theory of the Euler-Bernoulli beam. The exact values of the natural frequencies were determined by mathematical software. FEM verification of 2 types of gantry crane structure was performed [9]. Modal and harmonic response analyses were performed with experimental and FEM in order to analyze the dynamic characteristics of whole machine tools [10]. Yildirim and

Esim modeled a drill column machine and performed hormonic vibration analysis through the finite element method. In addition, in this study, they performed the performance analysis of the drill column machine by analyzing the vibration parameters obtained with finite elements with artificial neural networks[11] . Yongfeng Zheng at al have studied   dynamic of the four-link combination boom portal crane. ANSYS software is used to create a FEM model of a four bar portal crane and performed a modal analysis to evaluate the dynamic properties and provide a theoretical reference for the light design of the four link mechanisms [12].

Any changes to be made to meet the design criteria on the structures change the structural characteristics of the structure such as natural frequency, shape and deformation distribution. Therefore, such analyzes have to be repeated for each changed prototype structure. In such cases, calculating the effects of the change using the mathematical model of the structure would eliminate the need for costly changes and vibration tests on the actual structure. Due to the change in the number of cars and the load on the crane system, the dynamic characteristics of the crane system change. Because of these reasons, in this study, the studies on determining the frequency response of the crane system in case of change of load according to the number of different cars on double bridge overhead crane.

2.   FREQUENCY RESPONSE FUNCTION THEORY

Dynamic analyzes are used to determine the characteristics of a structure when considering the stiffness and damping of the system under varying loads. Here, as a general approach, it is possible to explain the dynamic characteristic of the system, and the node model dynamic equations can be used in which the system is divided into elements. Since the system is divided into many elements by accepting a linear relationship between the elements and the node model, the system is transformed into a multi-degree of freedom[13]

The vibration time dependent model of the multi-degree of freedom system is expressed as follows:

$$[m]\ \ddot{x}(t)+[c]\ \dot{x}(t)+[k]\ x(t)=f(t) \tag{5}$$

The expression of the system in the Laplace form is given as follows:

$$\left([m]\ s^2+[c]\ s+[k]\right)\ x(s)=f(s) \tag{6}$$

Where; $[m]$ is the mass matrix, $[c]$ is the damping matrix, and $[k]$ is the stiffness matrix. The matrix of mass and stiffness matrix are symmetrical matrix, the damping matrix is defined as non-symmetrical due to the nonlinear structure [14].

The mechanical impedance of this multi-degree of freedom system is expressed as follows:

$$z(s)=[m]\ s^2+[c]\ s+[k] \tag{7}$$

If the mechanical impedance matrix is written in the dynamic equation, the following equation is obtained;

$$z(s)=\frac{f(s)}{x(s)} \tag{8}$$

The transfer function of the system can be defined by the inverse of the impedance matrix:

$$H(s)=z^{-1}(s) \tag{9}$$

The system's response to the frequency under the effect of a dynamic load in a sinusoidal drive is characterized as a harmonic response. This is called a kind of forced vibration, which makes it possible to learn how the structure is affected. Under the harmonic loading, the dynamic equation is defined as follows:

$$x(s)=z^{-1}(s)f(s)=H(s).f(s) \tag{10}$$

Where x (s) can be calculated if the transfer function and the applied force are known.

3. MODELING AND FEA MODEL

The crane system consists of many substructures such as bridge carrier, bridge, lifting group. In these structures, it is a combination of many parts. therefore, the design of the crane system becomes complex. It is very difficult to create and model these solid models with ANSYS WORKBENCH software. In addition, the crane system should be modeled according to different car numbers. For this reason, different models of the crane system have been created by using Solidworks software. The appearance and components of one of the crane models used in the analyzes are given in Figure 1. These solid models were created in order to perform an analysis under different conditions and were transferred to the ANSYS software in Parasolid format provided by SOLIDWORKS software for ANSYS.
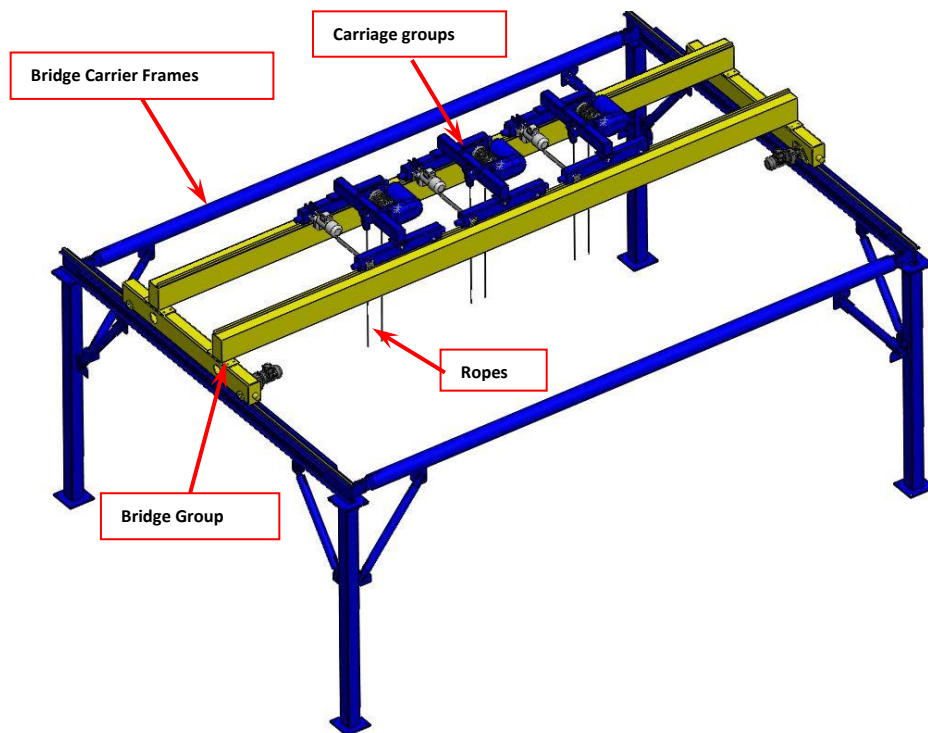
Figure 12. Designed and controlled   proposed three- carriages crane system and its components

In order to be able to see the effect of the different carriages number and different load condition in the crane system, solid models seen in Figure 2 were designed. Authors showed that the features of the system did not change according to the position of the load in crane systems by the previous study, free vibration analysis. For this reason, in order to examine the effects of the change in the number of cars in the crane system and the change in the load, the requirement that the load is removed from the center of the crane system is taken into consideration.

| Model 1 | Model 2 | Model 3 |
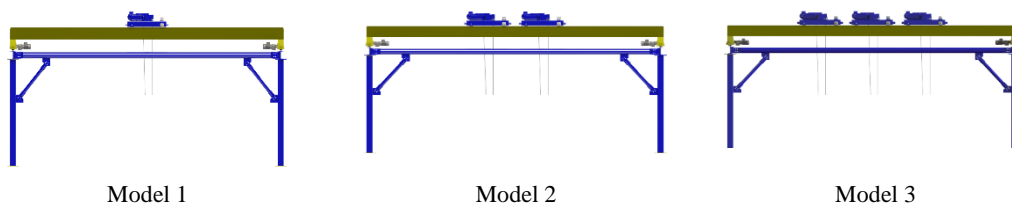
Figure 13. Solid models of proposed crane designed for different carriage numbers for harmonic analysis

4. HARMONIC ANALYSIS AND RESULT OF PROPOSED MULTI- CARRIGES CRANE

Simulation of the crane system and the determination of the frequency response experimentally are more meaningful to analyze the dynamic characteristics. Therefore, more studies on harmonic response are made. Each structure has modal qualities that cannot be eliminated. These modal structures do not affect the working process

at the same level. Therefore, reducing these failures and knowing the values that will lead to modal behavior help to take these values into account by providing some advantages.

The crane system is particularly subject to a strain during the lifting of the load. Harmonic analyzes were performed using the ANSYS Workbench 18.1 program to determine the response of the crane system to this challenge. In this analysis, except for the applied force, the analysis procedures for the modal analysis were performed in harmonic analysis. As in the case of modal analysis, the models of the crane system were modeled according to the different car numbers and transferred to the ANSYS program. The models used are bridge carrier, bridge, car and rope-hook group. In order to apply the load, the hook group was neglected, and a forced load was applied on the rope. harmonic analysis process executed by ANSYS Workbench as in modal analysis after the program is assigned to the solid model are as follows:

- After imported the solid models to the program, the materials of each component which form the crane system are defined. structural steel with a modulus of elasticity of 210 GPa, a poison ratio of 0.3 and a density of 7850kg /m^3 was selected as a material

- Due to the fact that the crane system does not have high operating frequencies, harmonic analysis of the crane system has been carried out considering the accuracy of 1Hz solution in the frequency range 0-200Hz.

- For the realization of the crane system model, contact of the crane components with each other is described. Then, the network structure was divided into a finite number of elements. For example, the mesh model of the crane model with 3-car model is given in Figure 3.
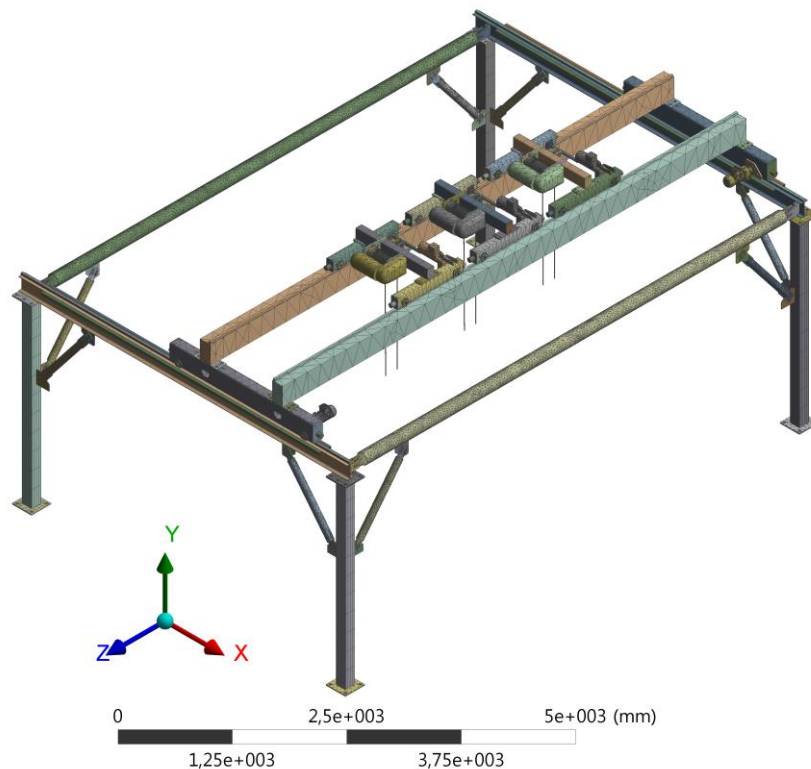
Figure 3. View of the network structure of the proposed crane with 3 cars for harmonic analysis

For harmonic analysis, it is assumed that the crane system is fixed to the ground from the plates located under the bridge carrier which is in contact with the ground. At the same time, the hook was omitted from the rope and hook group for the application of forced force on the crane system, and at the same time the rope was divided into two to apply the load; The forces were applied to the end of the ropes according to the size of the load to be lifted. The initial and boundary conditions of the crane system and the load applied for harmonic analysis are detailed in Figure 4.

Harmonic analysis was performed in order to obtain the frequency response of the crane system under the applied forces after all the definitions were made for the harmonic analysis. In order to make comparison in crane system, as in free vibration analysis, analyzes were carried out considering different car numbers and two different loads on the crane system. It was also assumed that the cars were lifted from the middle of the beams on the crane.
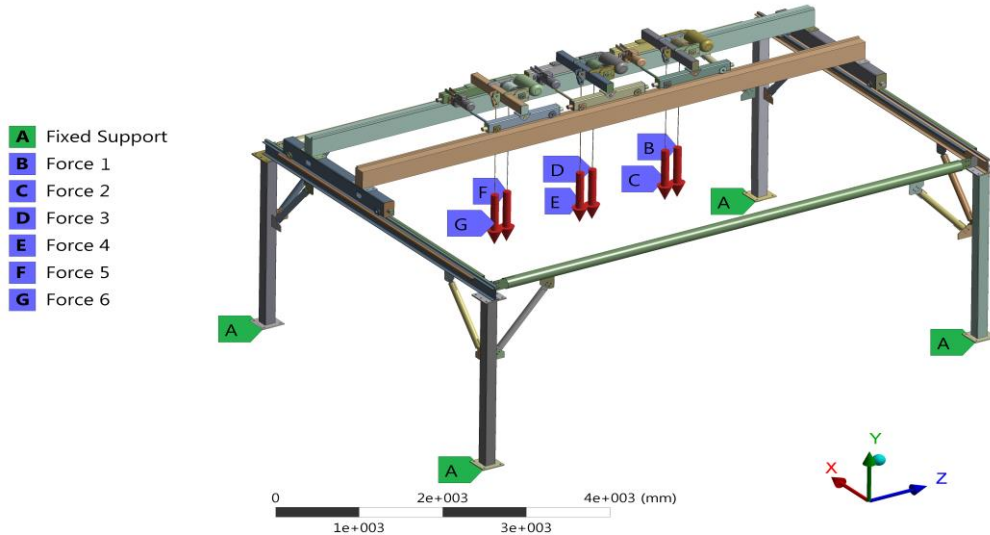
Figure 4. View of the loading applied with boundary conditions for harmonic analysis of the proposed crane system

In these analyzes, results can be obtained from many points of the crane system. However, the reaction of the midpoints in the bridge beams of the crane systems is an important parameter considered in crane constructions. For this reason, the acceleration results in response to the frequency occurring in the middle of the bridge beams are taken into consideration. The effects of the crane system on the crane system according to the above-mentioned working conditions are presented in graphs.

Considering the number of trolleys on the crane system, the load being lifted at 430kg and in the middle of the bridge, the frequency response of beams is given in Figure 5.
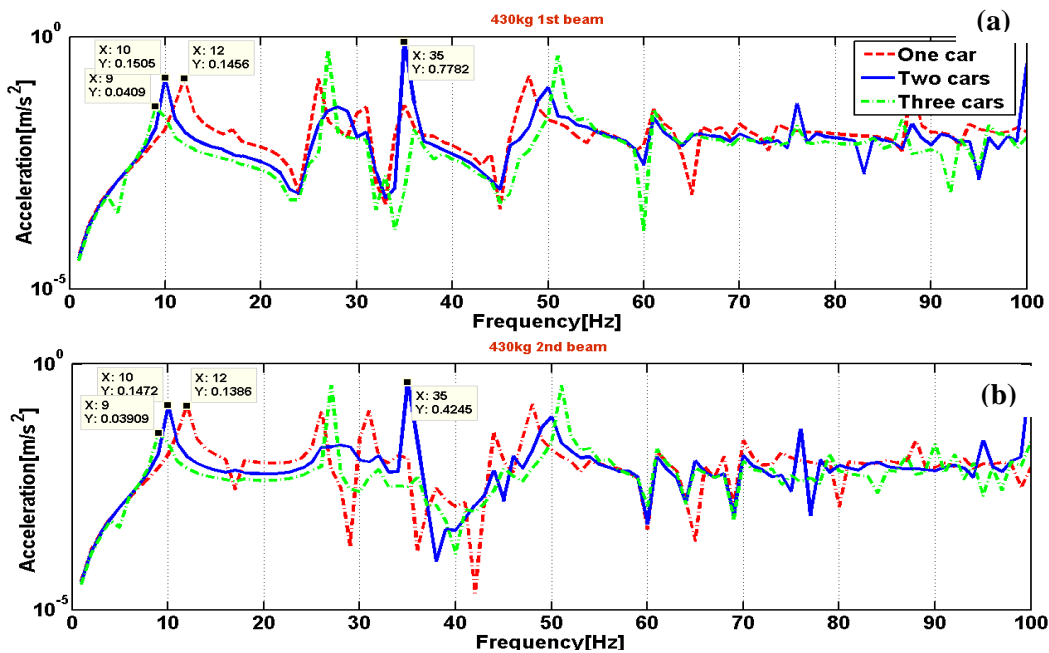
Figure 5. Frequency response of crane beams in case of carts in the middle of bridge and lifting of 430 kg load (a)1ˢᵗ beam (b) 2ⁿᵈ beam

In the case of cars in the middle of the bridge, it is understood that a variable number of cars cause different modes to be formed on the beams while modes occur around the same frequencies. While the effects of the carriages on both beams occur at the same frequencies, it is understood that there is only a difference in amplitude.

When the load is increased to 1540kg and lifted from the middle of the bridge, acceleration changes of the beams according to the frequency in different car numbers are shown in Figure 6.
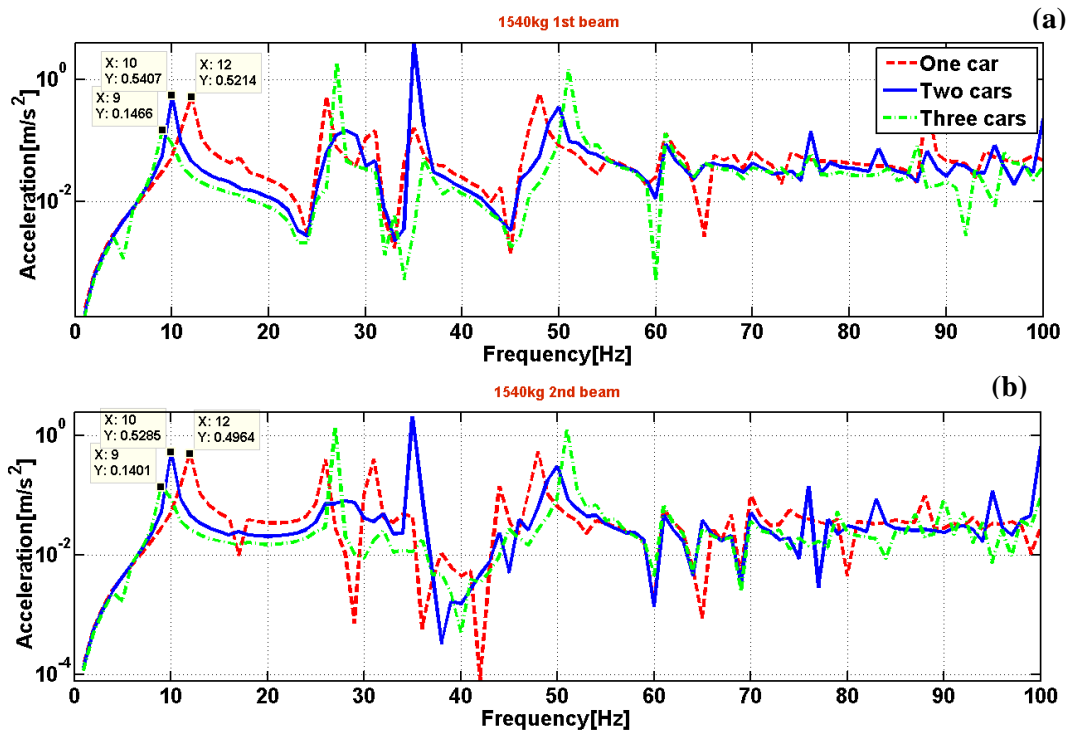
Figure 6. Frequency response of crane beams in case of carts in the middle of bridge and lifting of 1540 kg load (a)1st beam (b) 2nd beam

When it is evaluated in terms of beams, it is understood from the graphs that there is a reaction with different amplitudes at the same frequencies. For example, when a trolley case is examined, it is understood that the first frequency value of first beam and second beam reacts at 12Hz around 0.5214m/s^2 and 0.4964 m/s^2 respectively. When compared to a load of 430kg for the same position, it is understood that the same vibration characteristic occurs for both beams, but their amplitude is increased with respect to the load.

CONCLUSION

In this study, harmonic response analysis was performed using ANSYS to evaluate the performance of a proposed three cars crane system. Harmonic response explains in detail how modal characteristics actually affect vibration. Performing only modal analyzes is insufficient to determine the system behavior clearly.

In the proposed crane systems, the study of the frequency response has been utilized for the cranes which are included in the system with rope and load and which have more than one car. Investigation of the effect of rope, load and cart on the natural frequency of the system makes a significant contribution in this regard.

In addition, as it can be depicted from the frequency response analysis, it is seen that there are different behaviors between beams in double bridge crane systems. Since different amplitudes are encountered at the same frequencies, this situation should be taken into consideration in crane design.

ACKNOWLEDGMENT

REFERENCES

[1] D. J. Inman, *Engineering Vibration* Englewood Cliffs, NJ, USA: Prentice-Hall, 2007.

[2] C. W. d. Silva., *Vibration and Shock Handbook*: aylor & Francis Group, 2005.

[3] M. Abu-Hilal, "Forced vibration of Euler–Bernoulli beams by means of dynamic Green functions," *Journal of Sound and Vibration,* vol. 267, pp. 191-207, 2003.

[4] J. J. Wu, "Finite element analysis and vibration testing of a three-dimensional crane structure," *Measurement,* vol. 39, pp. 740-749, 2006.

[5] Malgaca L., Kara C., and Demirsoy M., "Dinamik Sekil Degistirme Olcumu ve Bir Tavan Vincinde Uygulamasi," presented at the VII. Ulusal Olcumbilim Kongresi, MMO Tepekule Kongre ve Sergi Merkezi IZMIR, 2008.

[6] T. Sahin, "2x400 Ton Portal Krenin Matematiksel ve Sonlu Elemanlar Yontemiyle Duzlem Titresim Analizi," Yuksek Lisans Tezi, Fen Bilimleri Enstitusu, Istanbul Teknik Universitesi, Istanbul, 2015.

[7] M. Gurgoze, "On the alternative formulations of the frequency equation of a Bernoulli–Euler beam to which several spring-mass systems are attached in-span," *Journal of Sound and Vibration,* vol. 217, pp. 585-595, 1998/10/29 1998.

[8] M. Gurgoze and H. Erol, "On the eigencharacteristics of longitudinally vibrating rods carrying a tip mass and viscously damped spring-mass in-span," *Journal of Sound and Vibration,* vol. 225, pp. 573-580, 1999.

[9] A. O. Vlada GAŠIĆ, Zoran PETKOVIĆ, "Mathematical modelling of the in-plane vibrations of portal cranes with fem verification," 2009.

[10] Z. Wu, C. Xu, J. Zhang, D. Yu, and P. Feng, "Modal and Harmonic Reponse Analysis and Evaluation of Machine Tools," pp. 929-933, 2010.

[11] S. Yildirim and E. Esim, "Takim tezgâhlarinda yapay sinir agi kullanilarak performans analizi," presented at the Uluslararasi Katilimli 17. Makina Teorisi Sempozyumu(UMTS 2015), Izmir, 2015.

[12] Y. Zheng, Y. Hu, B. Wu, P. Yi, and J. Liu, "Finite Element Modal Analysis of Four-link Combination Portal Crane," 2015.

[13] R. W. Clough and J. Penzien, *Dynamics of Structures*. New York: McGraw-Hill, 1993.

[14] S. S. Rao, *Mechanical Vibrations* United State of America: Prentice Hall 2011.

The Use of Probiotics Microorganisms in Cheese

Selin Kalkan[1]

Abstract

Probiotics are live microbial food additives that provide beneficial effects on host health by providing and improving intestinal microbial balance. Probiotic-containing products have become primary choice for the consumer because of their health attributes. Therefore, the market for such products has rapidly grown. Many different strains and species of lactobacilli and bifidobacteria have been used commercially as probiotics. It is well known that Lactobacillus acidophilus has health-promoting effects and antagonistic activity against food-borne disease agents. To date, the most popular food systems used as carriers of probiotic bacterial cultures are fresh fermented products such as yogurt and fermented milk. Cheese may offer certain advantages over yogurt-type products in terms of delivery of viable probiotics, such as the higher pH of the cheese, the higher fat content and more solid consistency of cheese may offer protection to the probiotics in the gastrointestinal tract. In the studies focusing on the expanding probiotic product class, very few researchers and dairy companies have worked on the production of cheese varieties that contain a high number of probiotic cultures. In this review, some examples of the studies on development strategies of probiotic cheese and the inclusion of probiotics in cheese are discussed.

Keywords: Probiotics, cheese, dairy technology

1. INTRODUCTION

Live microorganisms that have a positive effect on the health of the host organism when they are consumed sufficiently are defined as probiotics [1]. Probiotic microorganisms reach the intestines by preserving their vitality in the mouth, digestive system, upper respiratory tract, and urogenital system because of their consumption. The microorganism cultures show a biological effect on the intestinal wall by developing in the gastrointestinal tract [2, 3].

Today, the most commonly used probiotics are Lactobacillus spp. The reason for this is that they have been used in the first scientific theories to investigate the positive effects of probiotics [4]. *Lactobacillus*, *Streptococcus*, *Enterococcus*, *Leuconostoc*, *Pediococcus*, and *Bifidobacterium* spp. are frequently used. In addition, yeasts such as Saccharomyces cerevisiae and bacterial species such as *Bacillus* spp. (exp. *B. clausii*) also used as probiotics [5]. *E. faecalis* and *E. faecium* species were found in the majority of food, human and animal isolates.

Yogurt and fermented milk beverages, which are the most emphasized foods on the development of probiotic dairy products, are freshly consumed and their shelf life is short. Compared to these products, identification of probiotic cultures in cheeses with a longer ripening time and shelf life or research on the enrichment of cheese in this type of culture provides the potential for improving the health and quality of the product.

In this review, critical points about probiotic cheese production and quality are discussed in the light of the available literature. In the last part, the results of the research on the production of probiotic cheese are given.

2. CHEESES AS A CARRIER OF PROBIOTICS MICROORGANISMS

Cheese contributes to the prolonged viability of probiotic microorganisms in their production and storage compared to other products when considering pH, oil content, oxygen level, and storage conditions [6-8]. In general, cheeses (4.8-5.6 pH) have a very high pH compared to fermented milk (3.7-4.3 pH) and provide a more stable environment supporting the long-term viability of acid-sensitive probiotic microorganisms. In addition, cheese has higher buffering capacity than yogurt. [7, 9]. The metabolic activity of the bacteria in cheese creates an anaerobic

---

[1] *Corresponding author: Giresun University, Department of Food Engineering, 28200, Giresun, Turkey.*
  selin.kalkan@giresun.edu.tr

environment that supports the development and viability of anaerobic probiotic microorganisms within a few weeks of ripening in cheese. In addition, the relatively high fat content of the cheese matrix and cheese provides protection against probiotic bacteria throughout the gastrointestinal tract [8].

Careful selection of the strains to be used in the production of probiotic cheese is critical in protecting and maintaining the viability of probiotic bacteria in the cheese matrix. Interactions between probiotic bacteria and starter microorganisms used in production can change the viability of probiotics within the product and may negatively affect product properties.

Probiotic bacteria are used successfully in the production of many types of cheese. The success of adding probiotic bacteria to cheeses depends on factors such as the species and strain used, the activity of lactic acid bacteria used in production, cheese composition, production and maturation conditions. In practice, probiotic microorganisms most commonly encountered for use in cheese production are Bifidobacteria, Lactobacilli and Enterococci.

3.   APPLICATIONS OF PROBIOTIC CHEESE

In the studies focusing on the expanding probiotic product range, some researchers and dairy enterprises have studied the production of cheese varieties that contain a high number of probiotic cultures. Studies on probiotic cheese production are summarized in Table 1.

Table 1. Some studies of probiotic cheese production

Type of cheese	Probiotic bacteria strain	Reference
Cheddar	*Bifidobacterium* spp.	10
Cottage and White brined cheese	*B. infantis* , *B. bifidum*	11
Cresceza	*B. bifidium, B. longum, B. infatis*	12
Goat cheese	*B. lactis, L. acidophilus*	13
Cheddar	*L. paracasei* NFBC 38 and NFBC 364, *L. salivarius* NFBC 321 and NFBC 48	14
Cheddar	*Enterococcus faecium* PR 88	15
Cheddar	*Enterococcus faecium* Fargo 688	16
Cheddar	*L. paracasei* NFBC 338	16
Cheddar	*Bifidobacterium* spp.	17
Goat cheese	*B. bifidium* Bb02, *B. longum* Bb46	18
White brined cheese	*L. acidophilus* LA-5, *B. bifidum* BB-02	19
White brined cheese	*L. acidophilus*	20
Minas fresh cheese	*L. paracasei*	21
Cheddar	*L. acidophilus, L. casei, L. paracasei, B. bifidobacterium*	22
Ras cheese	*L. reuteri, L. casei, L. gasseri*	23
Turkish white cheese	*L. fermentum* AB5-18 and AK4-120, *L. plantarum* AB16-65 and AC18-82	24
Feta cheese	*L. casei*	25
Cheddar	*Enterococcus faecium* PR 88	26
Quarg cheese	*L. casei* NCDC 298, *L. acidophilus* NCDC 15	27
Minas fresh cheese	*L. acidophilus*	28

4.   CONCLUSION

Producing cheeses containing probiotics will enable competition among dairy producing companies and increase the production of more nutritious and physiological quality dairy products. Generally, different types of cheese are consumed at least once a day (especially breakfast) in different regions of the world. Therefore, the use of cheeses as a carrier of probiotics is an important and effective approach. For successful use of probiotic bacteria in cheese, may possibly because probiotics maintain their vitality throughout the shelf life of the product and do not adversely affect the composition, flavor, texture and other sensory properties of the cheese.

REFERENCES

[1]. FAO/WHO, Guidelines for the evaluation of probiotics in foods. Food and Agriculture Organization of the United Nations and World Health Organization Expert Consultation Report. Food and Agricultural Organization of the United Nations and World Health Organization Working Group Report (online), 2002.

[2]. P. Kanmani, R. Satish Kumar, N. Yuvaraj, K Paari, V. Pattukumar and V. Arul, "Probiotics and its functionally valuable products-a review", *Critical Rev in Food Sci and Nutr*, vol. 53(6), pp. 641–58, 2013.

[3]. B. Turchi , S. Mancini, F. Fratini, F. Pedonese, R. Nuvoloni, F. Bertelloni, and D. Cerri, "Preliminary evaluation of probiotic potential of *Lactobacillus plantarum* strains isolated from Italian food products", *World J of Micro and Biotec*, vol. 29(10), pp. 1913–1922, 2013.

[4]. A.C. Ouwehand, S. Salminen, and E. Isolauri, " Probiotics: an Overview of Beneficial effects". *Antonie van Leeuwenhoek*. vol. 82, pp. 279-289, 2002.

[5]. D. Song, S. Ibrahim, and H. Saeed, "Recent Application of Probiotics in Food and Agricultural Science". Chapter 1, 1-35. 2012.

[6]. C. Stanton, G. Gardiner, H. Meehan, K. Collins, G. Fitzgerald, P.B. Lynch, and R.P. Ross R P. "Market Potential for Probiotics". *Am. J. Clin. Nutr.* vol. 73 (Suppl.), pp. 476-483, 2001.

[7]. R.P. Ross, G. Fitzgerald, K. Collins, and C. Stanton, "Cheese Delivering Biocultures-probiotic Cheese". *Aust. J. Dairy Technol*. vol. 57, pp. 71-78, 2002.

[8]. T.R. Boylston, C.G. Vinderola, H.B. Ghoddusi, and J.A. Reinheimer, "Incorporation of Bifidobacteria Into Cheeses: Challenges and Rewards". *Int Dairy J*. vol. 14 (5), pp. 375-387, 2004.

[9]. G. Gardiner, C. Stanton, P.B. Lynch, J.K. Collins, G. Fitzgerald, and R.P. Ross , "Evaluation of Cheddar Cheese as a Food Carrier for Delivery of a Probiotic Strain to the Gastrointestinal Tract", *J. Dairy Sci.,* vol. 82, pp. 1379-1387.

[10]. P. Dinekar, V. V. Mistry, "Growth and Viability of *Bifidobacterium bifidum* in Cheddar cheese". *J. Dairy Sci*. vol. 77, pp. 2854-2864, 1994.

[11]. H.B. Ghoddusi, R.K. Robinson, "The test of time", *Dairy Ind. Int.*, vol. 61, pp. 21-28, 1994.

[12]. M. Gobbetti, A. Corsetti, E. Smacchi, A. Zocchetti, and M. De Angelis, "Production of Crescenza Cheese by Incorporation of Bifidobacteria", *J. Dairy Sci.*, vol. 81, pp. 37-47, 1998.

[13]. A.M.P. Gomes, F.X. Malcata, "Development of Probiotic Cheese Manufactured From Goat Milk: Response Surface Analysis Via Technological Manuipulation". *J. Dairy Sci*. vol. 81, pp. 1492-1507, 1998.

[14]. G. Gardiner, R.P. Ross, J.K. Collins, G.F. Fitzgerald, and C. Stanton "Development of a Probiotic Cheddar Cheese Containing Human-Derived *Lactobacillus paracasei* strains", *Appl. Environ. Microbiol.*, vol. 64, pp. 2192-2199, 1998.

[15]. G.E. Gardiner, R.P. Ross, J.M. Wallace, F.P. Scanlan, PPJM Jagers, G.F. Fitzgerald, J.K. Collins, and C. Stanton, "Influence of a Probiotic Adjunct Culture of *Enterococcus faecium* on the quality of Cheddar cheese". *J. Agric. Food Chem*. 47: 4907-4916. 1999.

[16]. C. Stanton, R.P. Ross. "New Probiotic Cheddar Cheese". End of Project Report. ISBN: 1 84170 122 X, ARMIS No. 4266, DPRC No. 29. Irish Agriculture and Food Development Authorty, Dairy Products Research Centre Teagasc, Moorepark, Fermoy, Co., Cork, Ireland. 2000.

[17]. S. Brearty, Mc P. Ross, G.F. Fitzgerald, J.K. Collin, J.M. Wallace, C. Stanton, "Influence of two Commercially Avaliable Bifidobacteria Cultures on Cheddar Cheese". *Int. Dairy J*. vol. 11(8), pp. 599-610, 2001.

[18]. M.R. Corbo, M. Albenzio, M. De Angelis, A. Sevi, and M. Gobbetti, "Microbiological and Biochemical Properties of Canestrato Pugliese Hard Cheese Supplemented With Bifidobacteria". *J. Dairy Sci.* vol. 84, pp. 551-561, 2001.

[19]. M. Yilmaztekin, B.H. Ozer, and F. Atasoy, "Survival of Lactobacillus acidophilus LA-5 and Bifidobacterium bifidum BB-02 in white-brined cheese". *Int J of Food Sci and Nutr.*, vol. 55, pp. 53-60, 2004

[20]. A. Kasimoglu, M. Goncuoglu, and S. Akgun , "Probiotic white cheese with *Lactobacillus acidophilus"*. *Int. Dairy J*, vol. 14, pp. 1067–1073, 2004.

[21]. F.C.A. Buriti, J. S. da Rocha, E.G. Assis, and S.M.I. Saad, "Probiotic potential of Minas fresh cheese prepared with the addition of Lactobacillus paracasei". *Lebensm.-Wiss. u.-Technol.*, vol. 38, pp. 173–180, 2005.

[22]. L. Ong, A. Henriksson, and N.P. Shah, "Chemical analysis and sensory evaluation of Cheddar cheese produced with Lactobacillus acidophilus, Lb. casei, Lb. paracasei or Bifidobacterium sp.", *Int. Dairy J*, vol. 17, pp. 937–945, 2007.

[23]. N. Dabiza, K. El-Deib, "Biochemical evalutation and microbial quality of Ras cheese supplemented with probiotic strains". *Polish J of Food and Nutr Sci*. 57(3): 295-300, 2007.

[24]. G. B. Kilic, H. Kuleasan, I. Eralp, A.G. Karahan, "Manufacture of Turkish Beyaz cheese added with probiotic strains", *LWT - Food Sci and Techn*, vol. 42, pp. 1003–1008, 2009.

[25]. R. Mahmoudi, H. Tajik, A. Ehsani, A.A. Farshid, P. Zare, and M. Hadian, "Effects of Mentha longifolia L. essential oil on viability and cellular ultrastructure of Lactobacillus casei during ripening of probiotic Feta cheese", *Int J of Dairy Techn*. vol. 66(1), pp. 77-82, 2013.

[26]. K.M. Amine, C.P. Champagne, Y. Raymond, D. St-Gelais, M. Britten, P. Fustier, S. Salmieri, and M. Lacroix, " Survival of microencapsulated Bifidobacterium longum in Cheddar cheese during production and storage". *Food Cont,* vol. 37, pp. 193-199, 2004.

[27]. K.S. Kadiya, S.K. Kanawjia, and A.K. Solanki, "Survival of free and encpsulated probiotic bacteria and their effect on the sensory properties of Quarg cheese"**.** *Int. Jo of Fermented Foods*. vol. 3(1), pp. 61-76, 2014.

[28]. T.L. Felicio, E.A. Esmerino, V.A.S. Vidal, L.P. Cappato, R.K.A. Garcia, R.N. Cavalcanti, M.Q. Freitas, C. A. Conte Junior, M.C. Padilha, M.C. Silva, R.S.L. Raices, D.B. Arellano, H.M.A Bollini, M.A.R Pollonio, and A.G. Cruz, "Physico-chemical changes during storage and sensory acceptance of low sodium probiotic Minas cheese added with arginine", *Food Chem.*, vol. 196, pp. 628–637, 2016.

A New Record of the Family Zerconidae (Acari: Mesostigmata) from Turkey: *Prozercon rekaae* Ujvári, 2008

Rasit Urhan[1], Mehmet Karaca[2], Elif Hilal Duran[3], Busra Aksu[3], Kamil Bilki[3]

Abstract

Mites of the family Zerconidae collected from Dikili County (Izmir province) at February 15, 2019 were evaluated. Collected samples were placed into plastic bags, labelled and transferred to acarology laboratory. Samples were placed into combined Berlese funnels and mites were extracted for 5–7 days. Then, mites were separated under a stereo-microscope. Collected zerconid mites were placed in 60% lactic acid for clearing and their identifications were made using a light-microscope. Finally, all zerconid mites were put in stock bottles which contain 70 % alcohol and 1- 3 drops glycine. Among them, Prozercon rekaae was recorded for the first time from Turkey. Also, measurements of different body parts, drawings and geographic distribution of specimens were given.

Keywords: Acari, Izmir, new record, *Prozercon rekaae*, systematic, Turkey

1. INTRODUCTION

Today, kingdom Animal contains approximately 1,5 million species identified under 40 phyla. Among them, phylum Arthropoda (arthropods) have 1,250 million species, constitutes 80 % of all animal species. In this phylum, Arachnida (arachnids) is a large class of invertebrates, including about 110 thousand species, including mites, ticks and spiders [1].

Mites are the richest group of all arachnids in terms of species diversity and abundance of individuals. To date, over 50 thousand mite species have been identified around the world and it is presumed that there are over 1 million mite species that have not yet been discovered [2].

Zerconids (family Zerconidae) is one of the richest mite groups in various types of forest ecosystems and their distribution is confined to the Holarctic region [3]. Today, systematic and ecological studies on zerconids are still in progress. Also, number of new zerconid species increases day by day, especially with local faunistic studies.

In Turkey, the family Zerconidae represent by 2 genera (*Prozercon* and *Zercon*) and 119 species [3]-[6]. Of these, genus *Prozercon* is the second richest genus both in Turkey and the Holarctic region. Species records of the genus were given from different habitats (mostly from moss and litters of pine, oak and juniper trees) in this country before. In order to reveal Zerconidae fauna of Coastal Aegean Region of Turkey, litter and moss samples which collected from Dikili county (Izmir province) were investigated.

2. MATERIAL AND METHODS

Litters of *Quercus* sp. (oak) and *Pyrus* sp. (wild pear) trees, and also moss samples were collected from different habitats in Nebiler village (39˚ 12.825′N, 26˚ 58.120′E, 361 m a.s.l.), Dikili county, Izmir province (Figure 1).

---

[1] Corresponding author: Pamukkale University, Faculty of Science and Arts, Department of Biology, 20070, Pamukkale/Denizli, Turkey. rurhan@pau.edu.tr

[2] Pamukkale University, Denizli Vocational School of Technical Sciences, Department of Electronic and Automation, 20160, Pamukkale/Denizli, Turkey. karacamehmet@pau.edu.tr

[3] Pamukkale University, Institute of Sciences, Department of Biology, 20070, Pamukkale/Denizli, Turkey. elifhilalduran@hotmail.com, baksu13@posta.pau.edu.tr, kamilbilki@gmail.com

Samples with mites were put into plastic bags and carried to acarology laboratory of Pamukkale University (Turkey). Then, collected samples were placed into Berlese funnels. During 5-7 days, zerconid mites were separated under stereomicroscope (Nikon SZM 745T). 60 % lactic acid and glycerine were used for cleaning and easier visibility of zerconid mites. Their identifications were made with a lightmicroscope (Olympus SZ51). Lastly, zerconids were labelled and put in stock bottles which contain 70 % alcohol and 1-3 drops glycine.
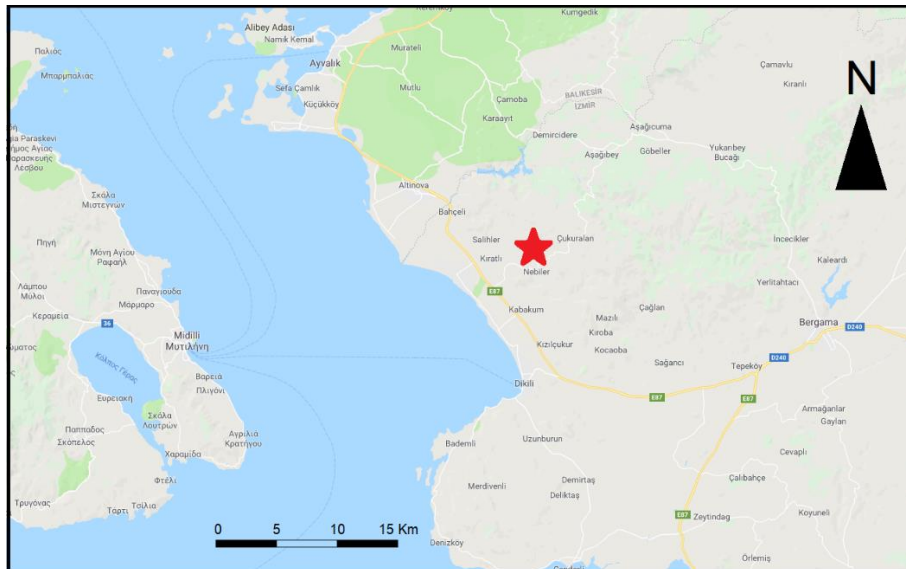
Figure 14. Sampling area of Prozercon rekaae (Nebiler village, Dikili county, Izmir province) [7]

The examined specimens were deposited in Acarology Laboratory of Pamukkale University (Denizli province, Turkey). Morphological terminology, idiosomal chaetotaxy, and poroidotaxy used in the descriptions follow those of [8]-[11]. All measurements are given in micrometers (μm).

3. RESULTS AND DISCUSSION

Among identified zerconid species, 2 male specimens of *Prozercon rekaae* were found. Females and immature stages (deutonymphs and protonymphs) were not detected. After identification process, different body parts of *Prozercon rekaae* were measured (Table 1) and its drawings were given (Figures 2A-B). Also, geographic distribution of this species was discussed based on current literatures.

3.1 Description of Male Specimens

Dorsal side: 20 pairs of different setae present on podonotum (j row with 6 pairs, z row with 2 pairs, s row with 5 pairs, r row with 7 pairs). Seta j1 finely barbed. Remaining setae in j series, also setae z1-z2, s1-s5 and r2 short, smooth and needle-like. Marginal setae r1 and r3-r7 elongated and plumose. 23 pairs of different setae present on opisthonotum (J row with 6 pairs, Z row with 5 pairs, S row with 4 pairs, R row with 8 pairs). Setae J1, Z1, S1 and marginal R setae short, smooth and needle-like. Setae J2-J5 slightly pilose, and not reach to bases of following setae. Setae Z2-Z4 slightly pilose, and not reach to bases of following setae. Setae J6, Z5 and S2-S4 long, plumose and brush-like. Setae S2-S4 reach to margin of opisthonotum (Figure 2A).

Pores and dorsal cavities: Three pairs of pores presented on podonotum. Pores *po*1 located below of *s*1, *po*2 on line connecting *j*4 and *s*3 (closer to *s*3), *po*3 located between *s*4 and *z*2 (closer to *s*4). Podonotum covered by irregular tile-like pattern. Four pairs of pores present on opisthonotum. Pores *Po*1 located anteromedially to base of Z1, *Po*2 located between *Z*2 and *S*1, *Po*3 located between Z4 and S3 (closer to Z4), *Po*4 near insertion of S4. Opisthonotal shield with irregular tile-like pattern in the anterior region and punctate pattern in the posterior region. Dorsal cavities general size and appearance saddle-like, well sclerotized, and axes parallel to that of the body (Figure 2A).
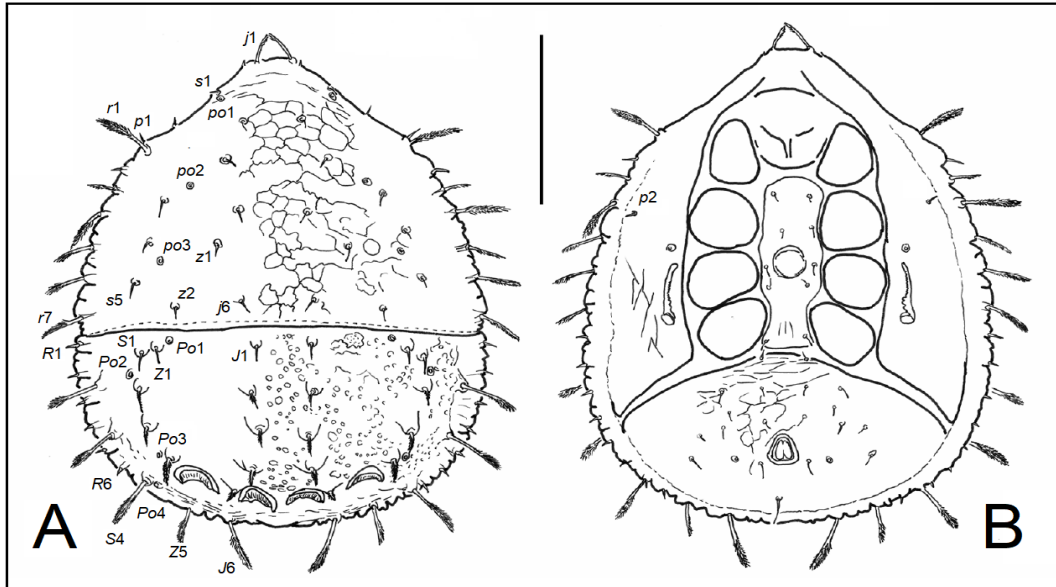
Figure 15. Dorsal (A) and ventral (B) views of male of Prozercon rekaae (Original drawings of Ujvári, 2008. Some body parts are designated. Scale bar 100 μm)

Ventral side: Shape, chaetotaxy of ventral shields, and shapes of peritremes typical for genus Prozercon. Peritremal setae p1 and p2 short, smooth, and needle-like. Lateral ends of peritremal shield reach seta R4. Adgenital shields absent. Ventroanal shield with 9 pairs of setae. Anterior margin of ventroanal shield with 2 setae, postanal seta is single. All of them short, smooth, and needle-like (Figure 2B).

3.2 Measurements of Specimens

Lenghts of idiosoma (excluding gnathosoma) 275-288 μm, widths 218-225 μm (n=2).

Measurements of opisthonotal setae and longitudinal distances between their bases were given in Table 1. Values as mean, in micrometers.

Table 6. Lengths of opisthonotal setae and the distances between their bases in J, Z, and S rows of Prozercon rekaae (♂).

Seta	♂♂	Seta	♂♂	Seta	♂♂
J1	9	Z1	10	S1	10
J1-J2	29	Z1-Z2	25	S1-S2	28
J2	13	Z2	12	S2	26
J2-J3	24	Z2-Z3	25	S2-S3	30
J3	13	Z3	16	S3	30
J3-J4	20	Z3-Z4	23	S3-S4	35
J4	13	Z4	18	S4	34
J4-J5	16	Z4-Z5	28		
J5	9	Z5	19		
J5-J6	21				
J6	30				
J6-J6	59				

3.3. Known Distribution

According the published literature, this species reported from Crete island (Greece) before [12] and this is the first record from Turkey (Figure 3).

4. CONCLUSIONS

According to distribution area of *Prozercon rekaae* in Aegean Sea, most probably this species may be found on some Greek islands (e.g. Lesvos, Chios, Samos, Kos, Rhodes and other islands with miscellaneous dimensions of this country) and some coastal region of Turkey (e.g. Fethiye, Marmaris, Bodrum, Kusadasi, Cesme, Ayvalik) in subsequent investigations.

Setal and morphological characters of Turkish specimens of *Prozercon rekaae* very similar to type specimens. The lengths and widths of our specimens are approximately the same size as type specimens.

Figure 16. Known distribution of Prozercon rekaae [7]

ACKNOWLEDGMENT

REFERENCES

[1]. Z.-Q. Zhang, "Animal biodiversity: An outline of higher-level classification and survey on taxonomic richness", *Zootaxa*, vol. 3148, pp. 1–237, 2011.

[2]. S. Dogan, and N. Ayyildiz, "New species of *Neophyllobius* (Acari, Camerobiidae) and description of *Cryptognathus ozkani* (Acari, Cryptognathidae) male from Turkey", *Biologia*, vol. 58, pp. 121–132, 2003.

[3]. M. Karaca, "*Zercon kadiri* sp. n., a new oligophagous mite from Eastern Anatolia (Acari: Mesostigmata: Zerconidae)", *Zoology in the Middle East*, vol. 65, https://doi.org/10.1080/09397140.2019.1627701, 2019.

[4]. R. Urhan, and M. Karaca, "A new species of the genus *Zercon* (Acari, Mesostigmata, Zerconidae) from Kastamonu, Turkey", *Acarological Studies*, vol. 1, pp. 3–10, 2019.

[5]. R. Urhan, E. H. Duran, and M. Karaca, "The diversity of zerconid mites (Acari, Zerconidae) in Akdag National Park (Denizli/Turkey)", *International Journal of Scientific and Technological Research*, vol. 4, pp. 509–517, 2018.

[6]. R. Urhan, and E. H. Duran, "A new record of genus *Zercon* (Acari, Zerconidae) for Turkish fauna: *Zercon saphenous* Błaszak, 1974", *International Journal of Scientific and Technological Research*, vol. 5, pp. 24–28, 2019.

[7]. (2019) The Google Maps website. [Online]. Available: http://www.google.com.tr/maps/

[8]. M. Sellnick, "Die familie Zerconidae Berlese", *Acta Zoologica Academiae Scientiarum Hungaricae*, vol. 3, pp. 313–368, 1958.

[9]. V. Halašková, "Zerconidae of Czechoslovakia (Acari: Mesostigmata)", *Acta Universitatis Carolinae-Biologica*, vol. 3–4, 175–352, 1969.

[10]. C. Błaszak, "Zerconidae (Acari, Mesostigmata) Polski", Monografie Fauny Polski, 315 pp, 1974.

[11]. P. Mašán, and P. Fend'a, "Zerconid mites of Slovakia", Slovak Academy of Sciences, Institute of Zoology, 238 pp, 2004.

[12]. Z. Ujvári, "Zerconid mites (Acari: Mesostigmata: Zerconidae) from Crete, Greece, with description of two new species", *Opuscula Zoologica Budapest*, vol. 39, pp. 99–108, 2008.

Biography: Dr. Rasit Urhan graduated from Faculty of Science (Ataturk University) and obtained the Ph.D. title in 1995. After that, he focused on Zerconidae systematics in Turkey and he defined many new species and new records of zerconid mites from the country. Up to now, he published over 50 articles in SCI and SCI-Expanded journals and described over 75 new zerconid species. He is currently working at Pamukkale University.

Investigation of Predictive Performance of LSTM Artificial Neural Networks on Brownian Time Series

Ismail Kirbas[1]

Abstract

The data sets that the data changes over time are called time series. Time series analysis is used in a wide area ranging from biomedical, agricultural, energy systems to forecasting and predicting of financial markets. In time series analysis, data must be measured over time at consistent intervals to identify patterns that form trends, cycles, and seasonal variances. In order to make successful predictions in time series analysis, it is important and difficult to determine the relationships between the data. If this association can be formulated correctly, it is possible to estimate future values by looking at historical data.

The Long Short-Term Memory (LSTM) approach, which constitutes the subject of our study, can produce successful results in estimation of sequential data. In order to examine the performance of LSTM models in different data sets, three different Brownian time series were produced in our study and multi-step estimations were made for these time series. The python keras library and matlab software were used to create the LSTM model. RMSE and R parameters were used to compare model performances and the obtained values were examined in detail.

Keywords: Brownian time series, LSTM neural networks, multi-step prediction, time series prediction.

1. INTRODUCTION

Time series is a well-defined set of data points measured at consistent time intervals over a period of time. Time series analysis is the use of statistical methods to analyse time series data and to draw meaningful statistics and characteristics about the data. Time series is a wide range of applications that can be used for all time-varying measurements and data. Nowadays, time series analysis methods can be applied for all data, which can be expressed as a series although it is not time dependent.

Time series is the subject of many disciplines. Meteorologists try to predict the future by looking at historical data. Health professionals want to determine whether there is an anomaly by examining the change of parameters such as blood pressure body temperature and pulse over time. Financial experts try to determine the future value of commodity and stock markets. Energy producers examine past consumption data and make projections for the future. When planning their expenditures and budgets, states and governments have to examine and interpret the previous time series [1]–[6].

There are many statistical models developed for use in time series estimation [7], [8]. However, the subject of our study is the use of artificial neural network (LSTM) which is an increasingly popular method of machine learning. LSTM is a kind of a recurrent neural network, which outperforms traditional RNNs in many application areas such as speech recognition, handwriting recognition, language modelling and polyphonic music modelling.

2. MATERIALS AND METHODS

At the entrance of this section, explanation of Brownian noise and its mathematical formula is given. Then the components and the internal structure of the LSTM network were examined in detail.

---

[1] *Corresponding author: Burdur Mehmet Akif Ersoy University, Department of Computer Engineering, 15100, Burdur, Turkey.*
ismailkirbas@mehmetakif.edu.tr

2.1. Brownian Time Series

In uncorrelated uniform noise, the values in the series are completely independent of the previous and subsequent values. However, in Brownian noise type, each value is the sum of the previous value and a random value. The Brownian expression is an analogy from the Brownian motion and is usually explained by a random walk [7].

Brownian motion is often described using a random walk, a mathematical model of a path in which the distance between steps is characterized by a random distribution. In one-dimensional random walk, the particle moves up or down a random amount each step. The particle position at any point in time is the sum of the previous steps [9].

Brownian noise is referred to as brown noise in some texts, but it is also called red noise in literature. This noise can be generated by transient integration of white noise [10]. When $dW(\tau)$ represents white noise, the integral of white noise gives the Brownian motion. The corresponding equivalence is given in equation 1.

$$W(t) = \int_0^t \frac{dW(\tau)}{d_\tau} dt \tag{1}$$

The power spectrum intensity of this noise is constant and when F represents the Fourier transform, it gives equation 2 equation.

$$S_0 = \left| \mathcal{F}\left[\frac{dW(t)}{d_t} \right](w) \right|^2 = constant \tag{2}$$

The power spectrum equation of Brownian noise is given in equation 3.

$$S(w) = |\mathcal{F}[W(t)](w)|^2 = \frac{S_0}{w^2} \tag{3}$$

Within the scope of the study, 5 different brownian noisy time series, each consisting of 500 samples, were produced. Figure 1 shows all 5 time series together.

Figure 1. Five different Brownian time series with 500 values.

Basic statistical data related to the time series produced is given in Table 1. In order to make a fair comparison, attention was paid to minimize the similarity between the series.

Table 1. Basic statistical data for five different Brownian time series.

	Serial 1	Serial 2	Serial 3	Serial 4	Serial 5
Min	-1.007	-20.177	-50.751	-35.490	-16.692
Max	27.489	-0.132	5.419	3.589	6.847
Mean	13.915	-8.549	-15.288	-18.181	-2.813
Median	14.947	-7.568	-8.642	-17.536	-2.479
Mode	-1.007	-20.177	-50.751	-35.490	-16.692
Std Dev.	6.556	4.773	14.770	10.908	4.995
Range	28.497	20.044	56.169	39.079	23.540

2.2. LSTM Neural Network Models

LSTM networks are the deepest neural networks created to prevent vanishing gradient problems while training deep neural networks. Their depth is due to the spread of their layers over time. LSTM is a generalized version of the gated recurrent unit. It has more gates than the gated recurrent unit, so it is more flexible. Processing load and memory requirements are also higher, but these make LTSM generally more efficient [11].

Sequence is often used in learning and processing problems. Using sequential to sequential structure, sequential output can be generated from sequential input, for machine translation or dialog systems. However, a single class output can be generated from sequential input.

The Long Short Term Memory (LSTM) network consists of the neural network elements shown in Figure 2.
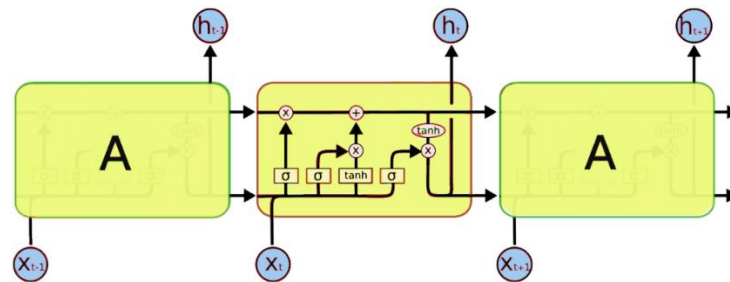
Figure 2. LSTM neural network structure.

In this structure, x_t represents inputs, and h_t expresses the output values; the internal structure of each cell is given in Figure3.
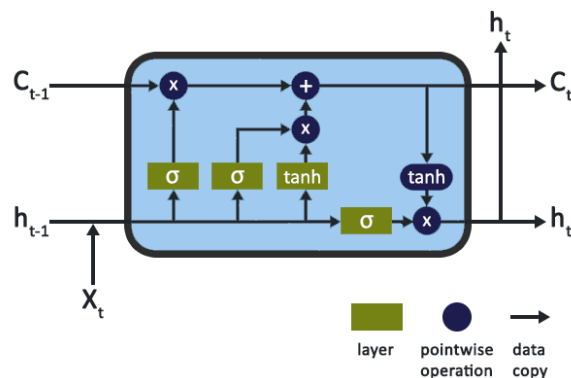
Figure 3. Basic structure of the LSTM network element.

Cells are connected to each other by h_t and C_t outputs. The most important concept for LSTM is the state of the cell, and this information is transmitted to each other between cells with C_t data embedded on the top of the cell.

The cell state is like a kind of conveyor belt and is carried along the entire chain. Cells may make small changes to this information. There are gates inside the cells. These gates contain a sigmoid function and open and close the sigmoid function according to the output value. Then the gate output value and C_t value are subjected to multiplication. The sigmoid function outputs can take values between 0 and 1, while a value of zero closes the information transition and moves a value across the entire information.

The first thing the LSTM cell needs to decide is to report the cell status. This decision is made by the forget gate layer. The forget gate layer generates a value between 0 and 1 for each C_{t-1} by looking at H_{t-1} and x_t. 1 means that data is stored and 0 means that it will be forgotten. Equation 4 is the mathematical expression of the process performed by forget gate layer.

$$f_t = \sigma(W_f \cdot [h_{t-1}, x_t] + b_f) \tag{4}$$

The next step is about whether to record the new information in the cell state. Input gate layer decides which value to update. Equation 5 describes input gate layer and it represents output of the input gate layer.

$$i_t = \sigma(W_i \cdot [h_{t-1}, x_t] + b_i) \tag{5}$$

A non-linear function layer (tanh) which is given in equation 6, generates a vector of new candidate values, $\widetilde{C}_t$ that could be added to the state.

$$\widetilde{C}_t = \tanh(W_c \cdot [h_{t-1}, x_t] + b_C) \tag{6}$$

The old cell state is then updated and the C_t value representing the new cell state is determined. Equation 7 shows the equation for obtaining the new C_t value.

$$C_t = f_t * C_{t-1} + i_t * \widetilde{C}_t \tag{7}$$

Finally, to ensure that the output value is between -1 and 1 and filter the output, the output functions specified in eq. 8 and eq. 9 are used respectively.

$$o_t = \sigma(W_o \cdot [h_{t-1}, x_t] + b_o) \tag{8}$$

$$h_t = o_t * \tanh(C_t) \tag{9}$$

Thus, h_t output value of LSTM cell is determined. The LSTM artificial neural network used in the study was developed using Matlab Deep Learning toolbox [12]. The first 450 data in the time series were used for the training of the neural network. The artificial neural network predicted the last 50 values.

Network training parameters are as follows maximum number of iterations 250, learning rate 0.001, hardware resource single CPU, learning rate schedule piecewise, training data 90%, predicting data 10%, number of hidden neuron 200, initial learning rate 0.005, learning rate drop period 125, and finally learn rate drop factor is 0.2. The average network training time for each time series is about 1 minute.

3. RESULTS AND DISCUSSION

In Figure 4, blue straight line indicates the actual value of the time series, while the orange line shows non- updated network prediction and the updated network prediction values are shown in red lines. When the figure is examined, it is seen that there is a harmony between the red line and the blue line. The dissimilarity rate in the orange line appears to be higher.
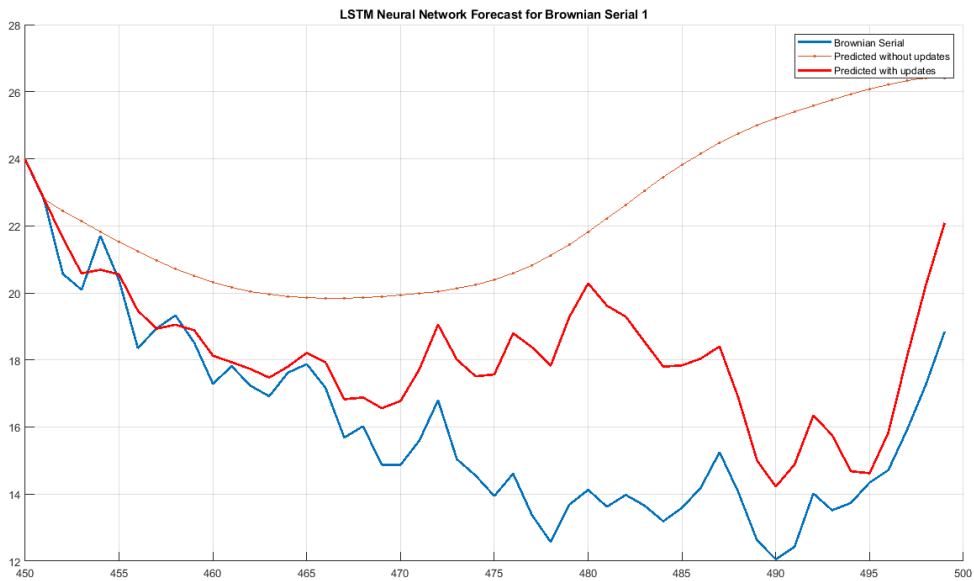
Figure 4. LSTM neural network predictions for the first time serial.

Figure 5 shows the real and artificial neural network estimation values of the second time series. It is noticeable that the estimation error is lower than the first time series.
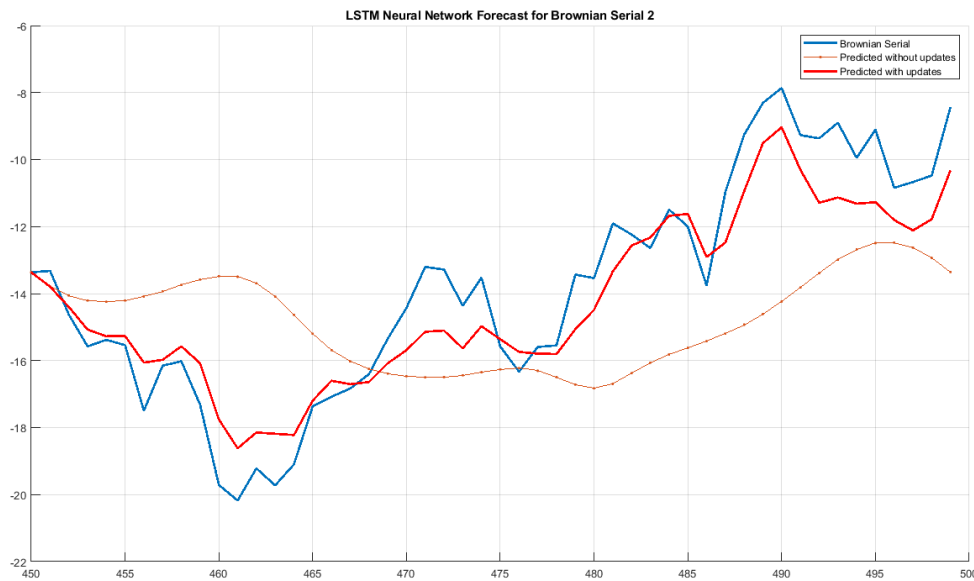
Figure 5. LSTM neural network predictions for the second time serial.

Figure 6 shows the actual and predicted values for the third time series. The red and blue lines appear to be compatible with each other when the orange line is straight.
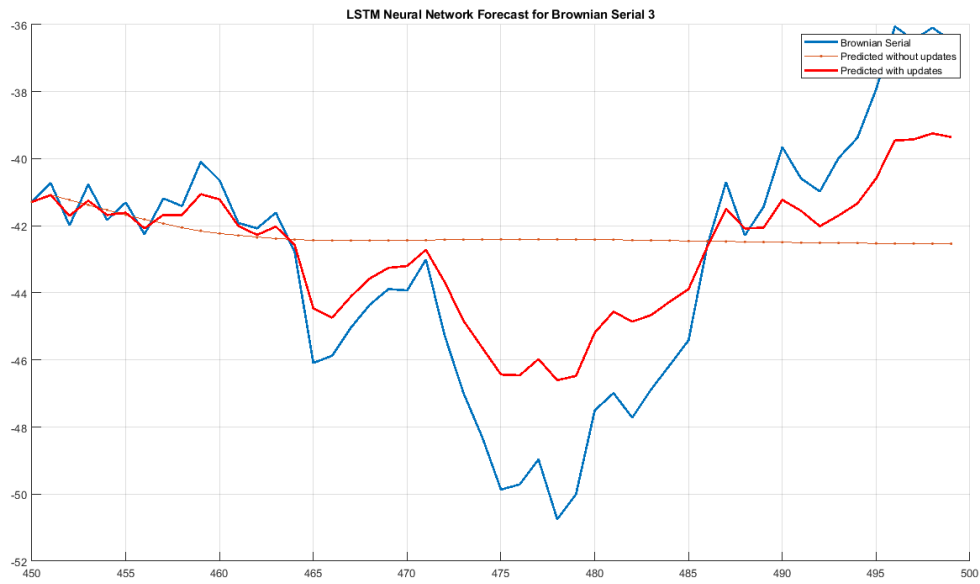
Figure 6. LSTM neural network predictions for the third time serial.

Similarly, figure 7 shows the real and predictive data for time series 4, while figure 8 represents the actual and predictive values for the last time series graphically.
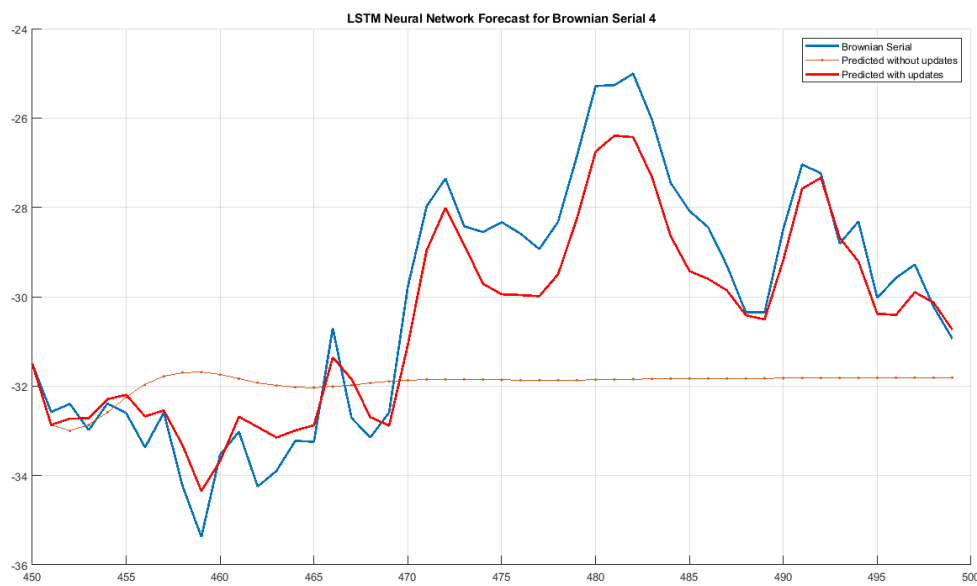
Figure 7. LSTM neural network predictions for the fourth time serial.
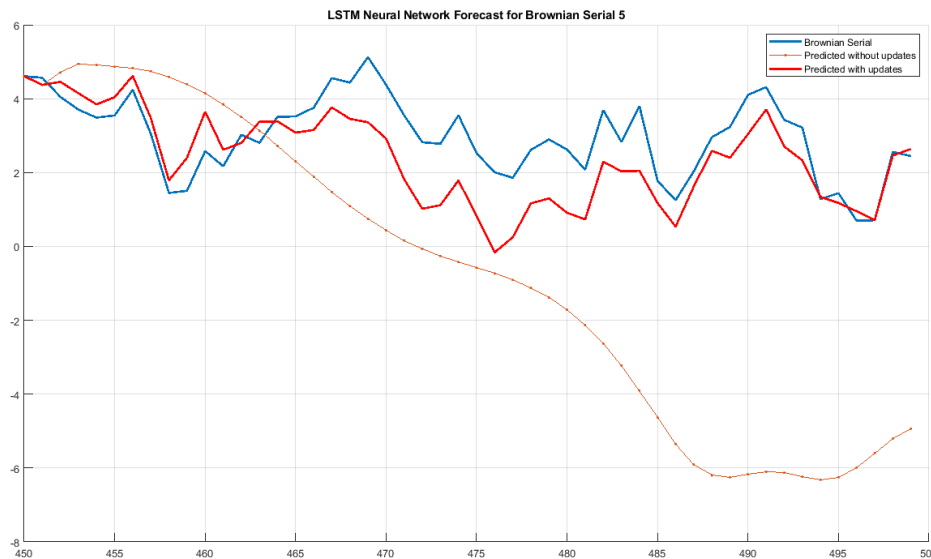
Figure 8. LSTM neural network predictions for the fifth time serial.

RMSE (Root Mean Squared Error) and R error metrics were used to determine the error rate between the actual values and the artificial neural network predictions. Equation 7 is used to calculate the RMSE error rate, while equation 8 is used for R value. The RMSE value should be close to zero while the R value is close to 1, indicating that the estimation error is low. A RMSE value of zero indicates no prediction error.

$$RMSE = \sqrt{\frac{\sum_{i=1}^{n}(Y_i - \widehat{Y_i})^2}{n}} \tag{7}$$

$$r = \frac{n(\sum y_i \widehat{y_i}) - (\sum y_i)(\sum \widehat{y_i})}{\sqrt{[n\sum y_i{}^2 - (\sum y_i)^2][n\sum \widehat{y_i}{}^2 - (\sum \widehat{y_i})^2]}} \tag{8}$$

Table 2 shows the prediction error rates of the artificial neural network and network training time for each time series.

Table 2. Error rates and processing times for multi-step prediction of LSTM artificial neural network.

	Serial 1	Serial 2	Serial 3	Serial 4	Serial 5
RMSE (without updates)	7.442	3.715	3.951	2.733	5.313
RMSE (with updates)	3.008	1.652	1.895	1.288	1.214
R-squared (with updates)	0.844	0.990	0.998	0.998	0.926
Training time (seconds)	51	55	50	60	59

No significant difference is observed when comparing the training time values. But, the RMSE value of Serial 2 and Serial 3 is quite close, while Serial 4 has the lowest estimation error. The biggest error is made for the first series and it is followed by series 5. R value can also be reviewed similar comments. The lowest error was made for Serial 4, while the highest incorrect estimate was made for the first one.

4. CONCLUSIONS

Within the scope of this study, the concept of future value estimation is discussed in time series, which is increasingly important in our daily lives. Firstly, an LSTM artificial neural network consisting of 200 neurons was developed using Matlab Deep Learning toolbox. Five different time series have been produced in order to measure the performance of the network fairly. 90 percent of the time series was used to train the network. The estimation results obtained are compared with the graphs. RMSE and R values were examined as predictive success criteria. Performance results are given in Table 2. In general, the results obtained appear to be quite satisfactory after network update operation. A value of R above 0.85 may also be considered successful. Accordingly, all multi-step estimates appear to be within acceptable limits. It is possible to achieve more successful results by changing the hyper parameters of the LSTM network. For the further study, hyper parameter optimization can be examined.

REFERENCES

[1] M. Khanna, N. K. Srinath, and J. K. Mendiratta, 'Feature Extraction of Time Series Data for Wind Speed Power Generation', in *2016 IEEE 6th International Conference on Advanced Computing (IACC)*, 2016, pp. 169–173.

[2] A. Kerem, I. Kirbas, and A. Saygin, in *Performance Analysis of Time Series Forecasting Models for Short Term Wind Speed Prediction*, 2016, vol. 1, pp. 2733–2739.

[3] R. H. Shumway and D. S. Stoffer, *Time series analysis and its applications: with R examples*, 3rd ed. New York: Springer, 2011.

[4] I. Kirbas, 'Short-Term Multi-Step Wind Speed Prediction Using Statistical Methods And Artificial Neural Networks', presented at the International Science and Technology Conference, 2016, vol. 1, p. 1064.

[5] I. Kirbas, 'Istatistiksel metotlar ve yapay sinir aglari kullanarak kisa donem cok adimli ruzgâr hizi tahmini', *Sak. Univ. J. Sci.*, vol. 22, no. 1, pp. 24–38, Feb. 2018.

[6] I. Kirbas, 'NAR based forecasting interface for time series analysis: T-seer', in *IV International Conference on Engineering and Natural Science (ICENS)*, Kiev Ukraine, 2018, vol. 1, pp. 144–149.

[7] I. Kirbas, 'Brownian Gurultulu Zaman Serilerinde ARIMA Tahmin Modellerinin Performanslarinin Incelenmesi', in *MAS International Conference on Mathematics-Engineering-Natural & Medical Sciences-IV*, Antalya - Turkiye, 2019, pp. 32–41.

[8] K. Yunus, T. Thiringer, and P. Chen, 'ARIMA-Based Frequency-Decomposed Modeling of Wind Speed Time Series', *IEEE Trans. Power Syst.*, vol. 31, no. 4, pp. 2546–2556, Jul. 2016.

[9] A. Downey, *Think DSP Digital Signal Processing in Python*, vol. 1. Needham, Massachusetts: Green Tea Press, 2014.

[10] 'Brownian noise', *Brownian noise*, 18-Mar-2019. [Online]. Available: https://en.wikipedia.org/wiki/Brownian_noise. [Accessed: 21-Mar-2019].

[11] J. Chung, C. Gulcehre, K. Cho, and Y. Bengio, 'Empirical Evaluation of Gated Recurrent Neural Networks on Sequence Modeling', *ArXiv14123555 Cs*, Dec. 2014.

[12] 'MATLAB Deep Learning Toolbox', *MATLAB*. [Online]. Available: https://www.mathworks.com/help/deeplearning/index.html. [Accessed: 09-Jun-2019].

Studies on Thermochemical Conversion of Sludge for Bioenergy Production in Turkey and World

Hasan Merdun[1], Zakari Boubacar Laouge[1] , Ismail Veli Sezgin[1]

Abstract

The use of water or wastewater treatment sludge in energy recovery has attracted great attention in recent years by using thermochemical conversion methods such as combustion, pyrolysis, gasification, and liquefaction. In this study, the studies conducted in Turkey and the world on the conversion of sludge into biofuels or bioenergy by using thermochemical conversion methods were collected from Web of Science database and presented. These studies were investigated in terms of feedstock type, sludge type, sludge treatment, thermochemical conversion processes, catalyst usage, and products. A total of 151 scientific research articles collected from literature were used in the study. The study results showed that in 106 studies sludge were used alone, where as in the remaining 45 studies sludge was co-processed with either biomass or coal. Different catalysts were used in only 33 studies during the conversion processes. Sludge types, sludge treatments, conversion processes, and products showed variations in these studies. The studies conducted in Turkey on sludge conversion into biofuels or bioenergy were very limited compared to the studies in the world.

Keywords: sludge, thermochemical, bioenergy, Turkey

1. INTRODUCTION

The depletion of fossil fuels and their inverse effects on the environment caused sludge to be an alternative energy source to fossil fuels. Anaerobic digestion is generally used to recover energy from domestic/municipal sewage sludge in Turkey, but it is actually not sufficient to apply only current technologies related to high treatment yield, product recovery, emission generation, etc. for sustainable sludge management. Therefore, different methods/technologies need to be compared with each other in terms of different criteria [1]. In a study performed with SWOT analysis for a sustainable municipal sewage sludge management in Greece, pyrolysis was the optimal thermochemical conversion method compared to incineration and gasification [2]. The use of water or wastewater treatment sludge in energy recovery has attracted great attention in recent years by using thermochemical conversion methods such as combustion, pyrolysis, gasification, and liquefaction [3-6]. Sludge can be used alone as feedstock in the conversion process and also together with different biomasses or coal, the process named as co-combustion, co-pyrolysis, or co-gasification [7-9].

Combustion is the rapid reaction of biomass or organic material and oxygen to obtain thermal energy and flue gas (CO_2, H_2O) [10]. Pyrolysis is thermal decomposition of biomass or organic material at temperatures between 400 and 650°C in the absence of oxygen under atmospheric pressure to produce solid (biochar), liquid (bio-oil), gas mixture [11]. Gasification is thermal decomposition of biomass or organic material at temperature 700-1000°C with limited oxidizing agent (air, O_2, CO_2, steam or mixture of these) under atmospheric pressure to produce biochar and gas mixture (H_2, CO, CO_2, CH_4, C_2H_4, C_2H_6, etc.) [12]. Liquefaction is a high pressure (150 bar) process with moderate temperatures (250-400°C) to obtain mainly liquid product (bio-oil) [13].

The objective of this study was to investigate the studies conducted on thermochemical conversion of sludge into biofuels or bioenergy in Turkey and world by using the data from the scientific research articles collected from the Web of Science database.

---

[1]*Corresponding author: Akdeniz University, Department of Environmental Engineering, 07058, Antalya, Turkey.
 merdun@alumni.clemson.edu*

2. MATERIALS AND METHODS

The scientific research articles related to the studies conducted in Turkey and the world on thermochemical conversion of sludge into biofuels or bioenergy by using the key words of "thermochemical", "sludge", "pyrolysis", gasification", "combustion", and "Turkey" were collected from the Web of Science database. The data from these articles were used as materials in this study.

These studies were investigated in terms of feedstock (sludge, sludge and biomass, sludge and coal), sludge type (WWTP, WWTP anaerobic, WWTP aerobic, other), sludge treatment (thermally dried, anaerobic digestion, air dried, dehydration, aerobic digestion, no data), thermochemical conversion processes (pyrolysis, co-pyrolysis, gasification, co-gasification, combustion, co-combustion), catalyst (with catalyst, without catalyst), and products (biochar, bio-oil, gas, biochar and bio-oil, bio-oil and gas, biochar and bio-oil and gas, chemicals, energy, no data). A total of 151 research articles collected from literature were used in the study.

3. RESULTS AND DISCUSSION

The scientific research articles including the studies conducted in Turkey and the world on thermochemical conversion of sludge were collected from the Web of Science database and investigated in terms of different aspects. There were only 8 studies conducted in Turkey on thermochemical conversion of sludge into different products, whereas the remaining 143 studies were conducted in other countries.

The number of studies conducted on thermochemical conversion of sludge for bioenergy production in Turkey and world based on feedstock is shown in Figure 1. In significant number (106) of studies, sludge was used as feedstock, but only 12 studies used sludge and coal together.

The distribution of studies based on the sludge type is presented in Figure 2. Very significant number (133) of studies used raw sludges of wastewater treatment plants (WWTPs), whereas a few studies used sludges of WWTPs after anaerobically and aerobically treated.

The number of studies conducted on thermochemical conversion of sludge for bioenergy production in Turkey and world based on feedstock is illustrated in Figure 3. Sludges are treated by using different techniques before using in thermochemical conversion processes to reduce their high water contents and therefore improve the technical and economical conversion efficiency of the processes. Thermally drying (the number of 78) was the main application in the sludge treatment. The sludge treatment methods of anaerobic digestion, air drying, and dehydration were used in the decreasing order in the studies. There was no information on the sludge treatment in 22 studies.

The number of studies on the conversion of sludge into different products by using different thermochemical conversion processes is displayed in Figure 4. The most applied (number of 64) process was pyrolysis and then gasification (the number of 40). Co-pyrolysis and co-combustion methods were used relatively less, but combustion and co-gasification were applied in a few studies.

The distribution of studies based on the catalyst usage is presented in Figure 5. It was interesting that in only 33 studies different catalysts were used in the thermochemical conversion of sludge into different products.

The number of studies conducted on thermochemical conversion of sludge for bioenergy production in Turkey and world based on products is shown in Figure 6. In 36 out of 151 studies, gas was obtained as the product and bio-oil (number of 29) was the second highest product obtained in the studies. Useful chemicals were produced in 15 studies. There was no data on the product in 25 studies.

4. CONCLUSIONS

The scientific research articles related to the studies conducted in Turkey and the world on thermochemical conversion of sludge into different products were collected from the Web of Science database and investigated based on different parameters such as feedstock type, sludge type, sludge treatment technique, thermochemical conversion method, catalyst usage, and products obtained. Only 8 studies out of total 151 studies were conducted in Turkey. The results were interesting and showed that the studies were significantly variable in terms of each parameter. The significant number of studies used sludge alone as the feedstock, raw sludge of WWTP as the sludge type, thermally dried sludge as the sludge treatment, pyrolysis as the thermochemical conversion method, no catalyst in the conversion studies, and produced bio-oil and gases. These results may guide a scientist or researcher in defining appropriate values of these parameters for techno-economic and environmentally-friendly future studies on thermochemical conversion of sludge.
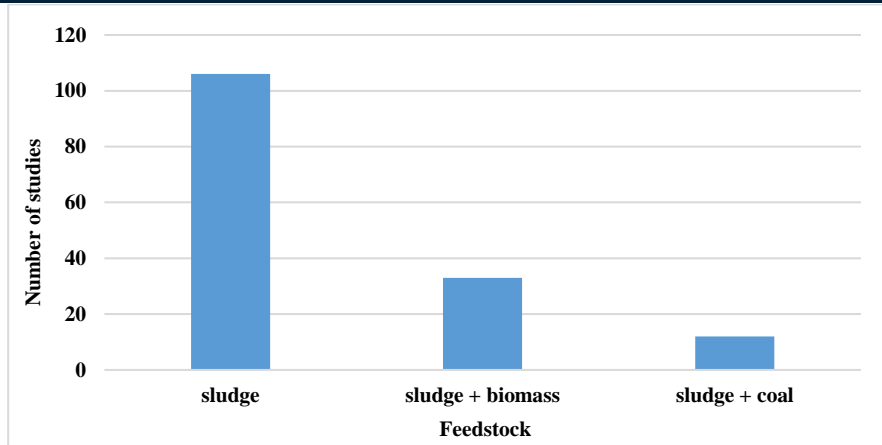
Figure 1. The number of studies conducted on thermochemical conversion of sludge for bioenergy production in Turkey and world based on feedstock
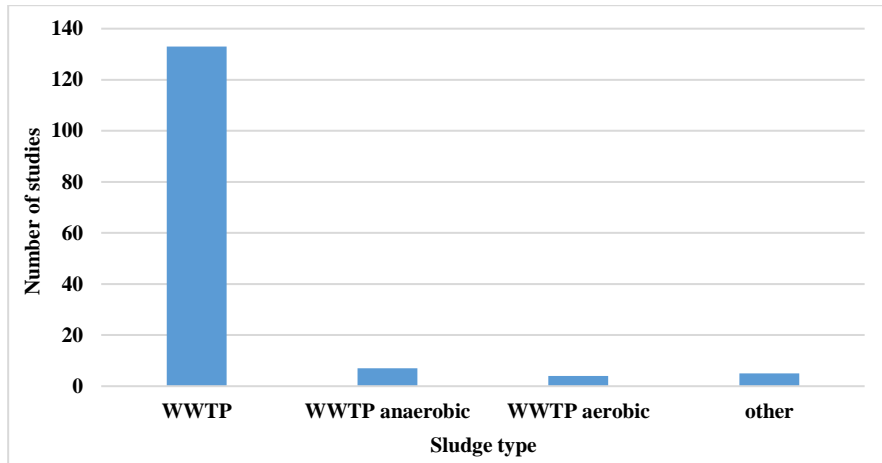
Figure 2. The number of studies conducted on thermochemical conversion of sludge for bioenergy production in Turkey and world based on sludge type
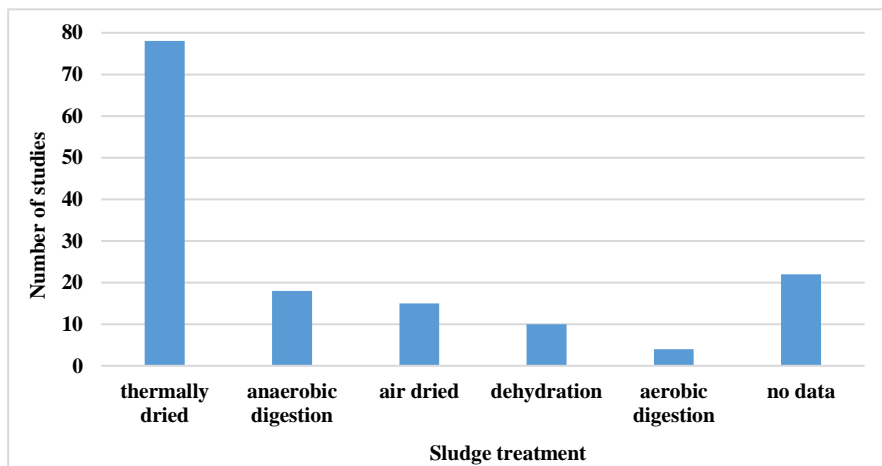
Figure 3. The number of studies conducted on thermochemical conversion of sludge for bioenergy production in Turkey and world based on sludge treatment
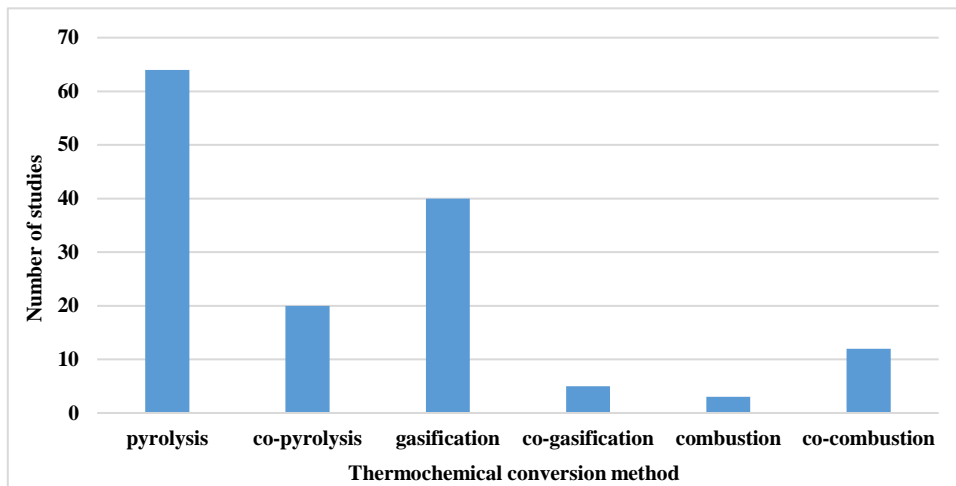
Figure 4. The number of studies conducted on thermochemical conversion of sludge for bioenergy production in Turkey and world based on thermochemical conversion method
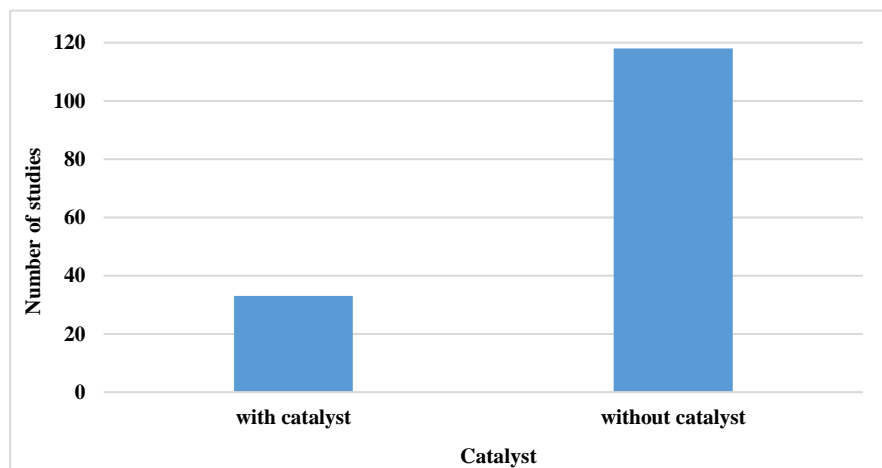
Figure 5. The number of studies conducted on thermochemical conversion of sludge for bioenergy production in Turkey and world based on catalyst used in the studies
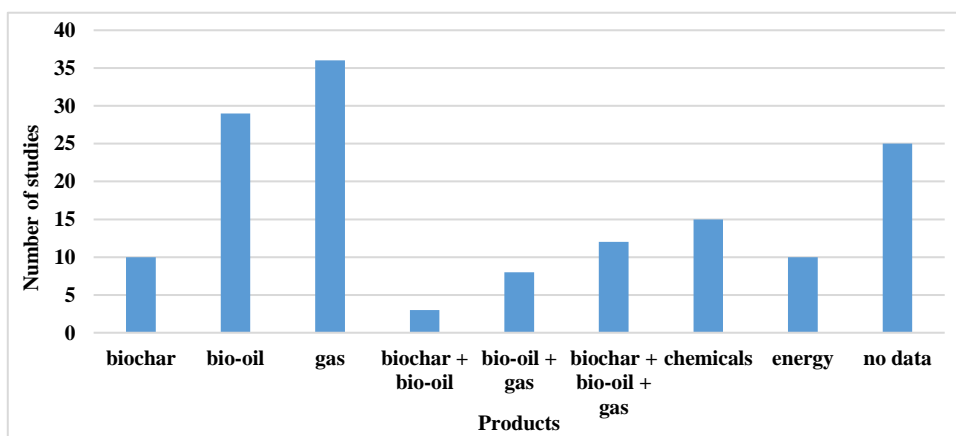
Figure 6. The number of studies conducted on thermochemical conversion of sludge for bioenergy production in Turkey and world based on products

REFERENCES

[1]. Adar, E., Karatop, B., Ince, M., Bilgili, M.S., 2016, Comparison of methods for sustainable energy management with sewage sludge in Turkey based on SWOT-FAHP analysis, Renewable and Sustainable Energy Reviews, 62, 429-440.

[2]. Samolada, M.C., Zabaniotou, A.A., 2014, Comparative assessment of municipal sewage sludge incineration, gasification and pyrolysis for a sustainable sludge-to-energy management in Greece, Waste Management, 34, 411-420.

[3]. Coimbra, R.N., Paniagua, S., Escapa, C., Calvo, L.F., Otero, M., 2015, Combustion of primary and secondary pulp mill sludge and their respective blends with coal: A thermogravimetric assessment, Renewable Energy, 83, 1050-1058.

[4]. Barry, D., Barbiero, C., Briens, C., Berruti, F., 2019, Pyrolysis as an economical and ecological treatment option for municipal sewage sludge, Biomass and Bioenergy, 122, 472-480.

[5]. Choi, Y.K., Ko, J.H., Kim, J.S., 2018, Gasification of dried sewage sludge using an innovative three-stage gasifier: Clean and H_2-rich gas production using condensers as the only secondary tar removal apparatus, Fuel, 216, 810-817.

[6]. Qian, L., Wang, S., Savage, P.E., 2017, Hydrothermal liquefaction of sewage sludge under isothermal and fast Conditions, Bioresource Technology, 232, 27-34.

[7]. Akdag, A.S., Atak, O., Atimtay, A.T., Sanin, F.D., 2018, Co-combustion of sewage sludge from different treatment processes and a lignite coal in a laboratory scale combustor, Energy, 158, 417-426.

[8]. Xu, X, Zhao, B., Sun, M., Chen, X., Zhang, M., Li, H. Xu, S., 2017, Co-pyrolysis characteristics of municipal sewage sludge and hazelnut shell by TG-DTG-MS and residue analysis, Waste Management, 62, 91-100.

[9]. Akkache, S., Hernandez, A.B., Teixeira, G., Gelix, F., Roche, N., Ferrasse, J.H., 2016, Co-gasification of wastewater sludge and different feedstock: Feasibility study, Biomass and Bioenergy, 89, 201-209.

[10]. Richardson, Y., Blin, J., Julbe, A., 2012, A short overview on purification and conditioning of syngas produced by biomass gasification: Catalytic strategies, process intensification and new concepts, Progress in Energy and Combustion Science, 38, 765-781.

[11]. Bridgwater, A.V., 2012, Review of fast pyrolysis of biomass and product upgrading, Biomass & Bioenergy, 38, 68-94.

[12]. Bridgwater, A.V., 2012, Review of fast pyrolysis of biomass and product upgrading, Biomass & Bioenergy, 38, 68-94.

[13]. Zhong, C., Wei, X., 2004, A comparative experimental study on the liquefaction of wood, Energy, 29, 1731-1741.

BIOGRAPHY

Dr. Hasan Merdun is currently serving as a faculty member at the Department of Environmental Engineering, Akdeniz University in Antalya, Turkey. His research interests include renewable energy, waste-to-energy, clean energy production, biomass, bioenergy, thermochemical conversion of biomass to biofuels, pyrolysis and gasification technologies, upgrading of biofuels, useful chemicals production from waste, and global warming and climate change. His research mission is to add value to the national and global bioenergy sector by applying an integrated biorefinery approach for the development of renewable energy technologies.

Parameter determination applications for magnetic anomalies between Bayburt – Bitlis (Turkey)

Oya Pamukcu[1], Ayca Cirmik[1]

Abstract

It is difficult to determine the location and depth of the structure which is investigated due to the solution in natural potential areas. In the investigation of geophysical anomalies, more accurate results are obtained by using more than one parameter determination methods.

In this study, the normalized full gradient and power spectrum methods were applied to the model and measured magnetic anomalies. By using the normalized full gradient method, vertical and horizontal structural transitions which cause magnetic anomalies were investigated. The basis of the normalized full gradient method is based on the downward continuation of the magnetic data. As the first application, these methods were applied to theoretical magnetic prism model anomalies, then to magnetic data of the region between Bayburt - Bitlis (Turkey).

As a result, the horizontal changes of possible structures in the study area were investigated with the normalized full gradient method and these results were compared with the power spectrum results.

Keywords: Bayburt, Bitlis, magnetic anomaly, parameter determination methods

1. INTRODUCTION

The aim of the study is to examine the structures causing magnetic anomaly by different parameter determination methods. In this context, the results were examined by applying parameter determination methods to the magnetic anomalies which were first produced from theoretical models and then measured from the field.

In this study, the normalized full gradient (NFG) method was applied to magnetic anomalies of Prism model. The normalized full gradient (NFG) method is one of the methods used to determine the single point location of potential fields ([1], [2], [3], [4], [5], [6], [7], [8], [9], [10]).

Theoretical magnetic anomalies were calculated for prism model with different slope values in the first stage of the application. Then, these anomalies were investigated by applying NFG and the vertical and horizontal structure transitions that caused the anomaly. Finally, NFG method was applied to magnetic anomalies measured from the between Bayburt and Bitlis (Turkey). At the other step of the application, the same data was applied to the power spectrum method. Studies on the application of power spectra to potential data were developed by [11], by [12] and by [3].

As a result, the upper and lower depths of the prism model in were successfully found by the NFG method. In addition, the results of the NFG and power spectrum methods were compared with the theoretical results. In Bayburt – Bitlis (Turkey) field anomaly study, source structures for possible magnetic anomaly were interpreted.

---

[1] *Dokuz Eylul University, Engineering Faculty, Department of Geophysical Engineering, 35160, Tinaztepe Campus, Buca Izmir, Turkey.*
oya.pamukcu@deu.edu.tr
ayca.cirmik@deu.edu.tr

2. METHODS AND APPLICATIONS

2.1 NFG Method

The two dimensional NFG operator $G(x_i, z_j)$ is defined as [4];

$$G(x_i,z_j) = \frac{\sqrt{\left[\left(\frac{\partial N(x_i,z_j)}{\partial x}\right)^2 + \left(\frac{\partial N(x_i,z_j)}{\partial z}\right)^2\right]^\nu}}{\frac{1}{M}\sum_{i=1}^{M}\sqrt{\left[\left(\frac{\partial N(x_i,z_j)}{\partial x}\right)^2 + \left(\frac{\partial N(x_i,z_j)}{\partial z}\right)^2\right]^\nu}} \tag{1}$$

where, $N(x_i, z_j)$ is the function of the geophysical field, M is the number of observation points and ν is called the degree of the NFG operator which controls the peak amplitude value and peak anomaly width of the NFG sections. The denominator of equation (1) is the mean value of the full gradient computed over M observation points, which makes the full gradient value dimensionless. Since NFG values are close to 1 in areas off the anomalous body, the contour values greater than 1 are known as maxima and those smaller than 1 are accepted as minima.

2.2 Power Spectrum Method

Fourier Transform of an f(x) function

$$F(w) = \int_{-\infty}^{\infty} f(x).e^{-iwx}dx \tag{2}$$

can be obtained by using the (2). If the real part of F(w) is P(w) and the imaginary part is iQ(w);

$$F(w) = P(w) + iQ(w) \tag{3}$$

$$E(w) = (F(w))^2 = (P^2 + Q^2) \tag{4}$$

equation (4) is the power spectrum of the f(x). The average depth of the underground structures are calculated as h; ([12]).

$$\overline{h_i} = \frac{\ln E(w_{i+1}) - \ln E(w_i)}{2(w_{i+1} - w_i)} \tag{5}$$

2.3 Applications

In the first step using the formula of [13], theoretical prism model anomaly was calculated as; the lower depth is 25 m, upper depth is 5 m, and width is 5 m and inclination is 30^0 (Figure 1). NFG method was applied to the magnetic anomaly values shown in Figure 1 (Figure 2). As shown in Figure 2, the upper depth of the structure began to appear in the 10th harmonic. The upper depth of the structure were determined in the 15th harmonic. Finally, the power spectrum method was applied to the same anomaly values (Figure 3).

In the field application of the study, five cross-section anomalies obtained from the magnetic map of the between Bayburt-Bitlis (Turkey) were used (Figure 4). The NTG method was applied to the profiles in Figure 4. When the NFG results of Profile 1 (Figure 5) were examined, the structure was found in 6th harmonic.
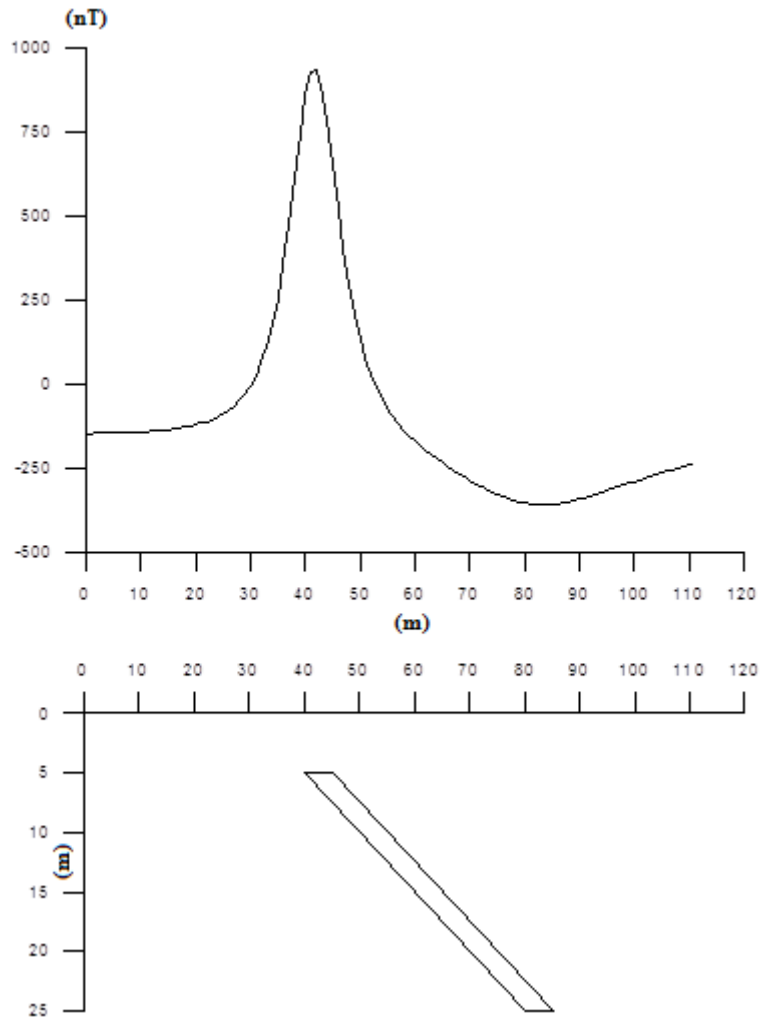
Figure 1. The prism model and its magnetic anomaly
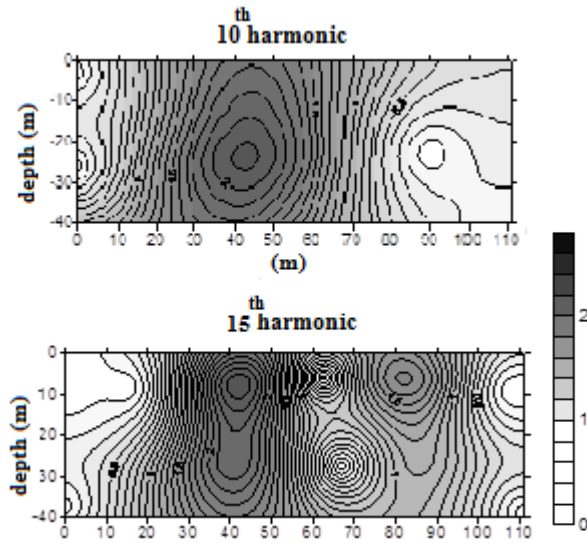
Figure 2. The NFG results of the magnetic anomaly values shown in Figure 1.
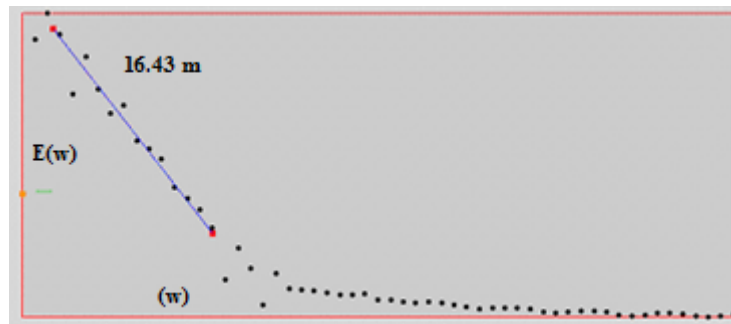
Figure 3. The power spectrum values of the theoretical prism model
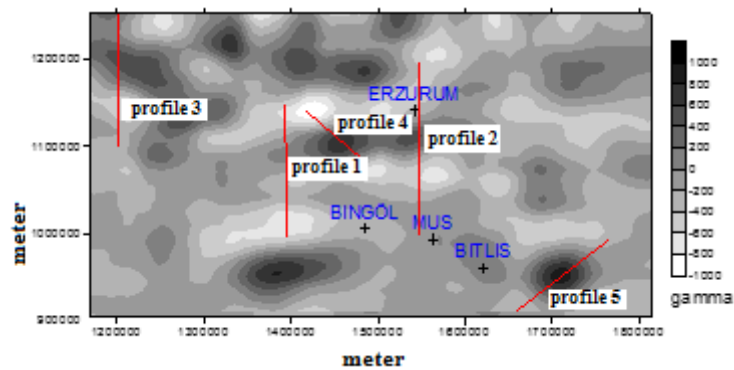
Figure 4. Magnetic map of the study area and the profiles used in the study.
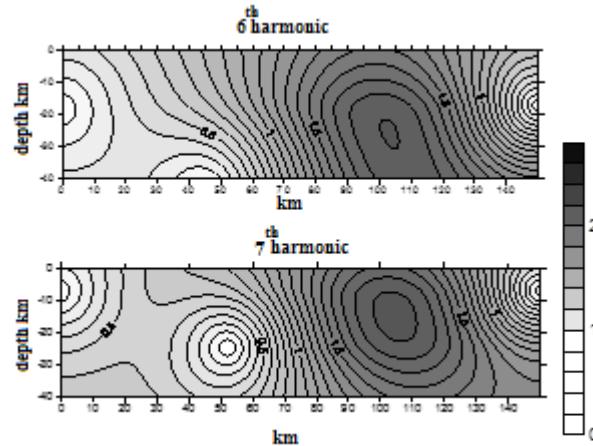
Figure 5. NFG results of the Profile 1 shown in Figure 4

RESULTS

If prism model was inclined, the depths of the upper and lower depths and location of the structure were more successful with the NFG method. The lower depth of structure was determined in the lower harmonics; the upper depth of structure was determined in the higher harmonics. In power spectrum applications, average depths of the structures were obtained. The results of NFG and power spectrum methods [14] applied to the magnetic anomalies of the field data were consistent with each other. As the result of the study, NFG results in all applications were more advantageous in determining the location and depth of the structure.

REFERENCES

[1] Berezkin, V.M., and Buketov, A.P. (1965). Application of the harmonical analysis, for the interpretation of gravity data. Applied Geophysics, 46, 161-166

[2] Berezkin, V.M., (1967). Application of the total vertica gradient of gravity for determination of the depths of the gravity sources. Expl Geohp, No:13, Nedra, Moscow

[3] Eliseeva, I.S., (1982). Methodical rules for the study of the distribution of density inhomogenities in earth's crust based on the results obtained from gravity. Min. Of Geology. VINI Geofizica, Moscow

[4] Berezkin, V. M., and Skotarenko S.S., (1983). Application for research anticline and nonanticline oil-gas structures using the gravity prospecting. Neftegeofizica. 131-139.

[5] Berezkin, V.M., (1988) The full gradient method in geopyhsics. Nedra, Moscow.

[6] Eliseeva, I.S., (1995)., Methodical recommendations for the interpretation of gravity and magnetic data by means of the quasi-singular points method. Institute for oil and gas exploration, VNIIGeofizika, Geoinfomark, Moscow.

[7] Lindner, H., and Scheibe, R., 1977: Interpretationstechnik fur gravimetrische und magnetische Felder. Freiberger Forschungshefte, DV fur Grundstoffindustrie, Leipzig.

[8] Ciancara, B., and Marcak, H., (1979). Geophysical anomaly interpretation of potential fields by means of singular points method and filtering. Geophysical Prospecting. 27,251-260

[9] Pasteka, R., and Seiberl, W. (1992). Die Auswertung polreduzierter Magnetfelddaten anhand des totalen Feldgradienten. Geophysic, 133-143

[10] Pamukcu, O., Gonenc, T., Cirmik, A., Pamukcu, C., and Erturk, N. (2019). The Geothermal Potential of Buyuk Menderes Graben Obtained by Combined 2.5-D Normalized Full Gradient Results. Pure and Applied Geophysics, Doi: 10.1007/s00024-019-02227-y

[11] Bhattacharyya, B.K., (1966). Continuous spectrum of the total magnetic field anomaly due to a rectangular prismatic body. Geophysics, 31, pp. 97-121.

[12] Spector, A., and Bhattacharyya, B. K. (1966). Energy density spectrum and autocorrelation function of anomalies due to simple magnetic models. Geophysical Prospecting, 14(3), 242-272.

[13] Telford, W.M., Geldart, L.P., Sheriff, R.E., and Keys, D.A., (1976). Applied geophysics. Cambridge University Press, Cambridge, London.

[14] Pamukcu, O. (2004). Investigation of geodynamical structure of Eastern Anatolia by geophysical data (Doctoral dissertation, Ph. D. Thesis, Izmir: Dokuz Eylul University Graduate School of Natural and Applied Sciences, 98 (in Turkish).

Exponential B-spline Solution for the Time Fractional Burgers' Equation

Ozlem Ersoy Hepson[1], Idris Dag[2]

Abstract

A numerical approach is described to get the solution of the time fractional Burgers' equation. The Caputo formulation of the time fractional derivative is discretized using the implicit difference scheme, temporal discretization of the nonlinear and second order term is carried out using the Crank-Nicolson method. After linearization of nonlinear term using Taylor method, spatial discretization is managed by use of the exponential cubic B-spline based interpolation integrator. The presented collocation method gives a system of linear algebraic equation at time steps. A computational experiment is performed to show feasibility and accuracy of the suggested algorithm.

Keywords: Caputo formulation, collocation method, exponential cubic B-spline, time fractional Burgers' equation.

1. INTRODUCTION

The Fractional Calculus has been an active area for scientists since communications about the noninteger order differentiation through letter by famous two mathematicians G.W. Leibnitz and L' Hospital (1695). After the introduction of the Fractional Calculus, contributions have been done by many scientist such as Euler, Laplace, Fourier, Lacroix, Abel, Riemann, Liouville, Caputo and et al. The during the last three decades, studies on the fractional calculus have gained acceleration due to be finding applications in disciplines such as fluid flow, rheology, reaction, diffusion, relaxation, oscillation, anomalous diffusion, reaction-diffusion, turbulence, electric network, physics, chemistry, waves, dynamic problems and recently in statistical distribution theory. Some of these events are modelled by use of fractional differential equations (fDE). Thus many scientist have been working out to find analytical and numerical solutions of fDE. The space fractional form of the Burgers' equation has been shown to model unidirectional propagation of weakly nonlinear acoustic waves through a gas-filled pipe and [1] and losses of nonlinear waves arising in acoustics. Analytical solution of the space fractional Burgers' equation (fBE) is given by applying Adomian decomposition method [2]. In the later studies [3]-[4], the same method is engaged to get both analytical and numerical solutions of both time and space fBE. Another approximate-analytical methods, variational iteration method, differential transformation method, homotopy perturbation method, homotopy analysis method, invariant subspace method, expansion method and residual power series method are also used to have solutions of the fBE in the works [5]- [13]. Solutions mentioned above are mostly obtained in form of the series. Standard numerical methods has started to apply fBE for finding numerical solution of the wide range of boundary and initial conditions: The cubic B-spline based collocation method and quadratic B-spline Galerkin method are presented for some problems of the fBE [14]-[15]. Iterative reproducing kernel method for numerical solution of fBE is presented [16]. Chebyshev wavelet based unified finite difference method is established for solving the fBE [17]. Cubic parametric spline functions are used to develop numerical method for approximating solutions of the tie fBE [18]. Solutions of two-dimensional time fBE are given as a results of applying the discontinuous Galerkin method to spatial variables and a finite difference scheme to temporal variables [19]. In this study we consider the time fBE

$$\frac{\partial u^{\mu}(x,t)}{\partial t^{\mu}} + u(x,t)\frac{\partial u(x,t)}{\partial x} - v\frac{\partial^2 u(x,t)}{\partial x^2} = f(x,t), \tag{1}$$

---

[1] Corresponding author: Eskisehir Osmangazi University, Mathematics & Computer Department, Eskisehir, Turkey, ozersoy@ogu.edu.tr

[2] Eskisehir Osmangazi University, Computer Engineering Department, Eskisehir, Turkey, idag@ogu.edu.tr

where v is a viscosity parameter, $0<\mu\leq 1$ and together with the initial data

$$u(x,0) = g(x) \tag{2}$$

and the Dirichlet boundary conditions

$$u(a,t) = h_1(x), \qquad u(b,t) = h_2(x) \tag{3}$$

is studied over the interval $[a,b]$. Caputo fractional derivative has the following form:

$$\frac{\partial^{\mu} u(x,t)}{\partial t^{\mu}} = \frac{1}{\Gamma(1-\mu)} \int_0^t (t-\tau)^{-\mu} \frac{\partial u(x,t)}{\partial t^{\tau}} \, d\tau \tag{4}$$

In this study, Caputo fractional derivative formula can be discretized via L_1 formula given in the reference [20]:

$$\frac{\partial^{\mu} u(t)}{\partial t^{\mu}}\Big|_{t_n} = \frac{(\Delta t)^{-\mu}}{\Gamma(2-\mu)} \sum_{k=0}^{n-1} \left[(k+1)^{1-\mu} - k^{1-\mu} \right] \left[u(t_{n-k}) - u(t_{n-k-1}) \right]. \tag{5}$$

One of the nonlinear form of the polynomial B-splines known as exponential B-splines are introduced by McCartin [21] and similar properties of both polynomial and exponential B-splines are shown to exits. Computer aided design, curve and surface approximation and fitting are performed by way of these splines. Recently the numerical methods have been set up using the exponential B-splines for solving the differential equations [22]-[25]. The free parameters of exponential splines cause to produce the determination of various bell-shaped forms. Sometimes use of best free parameters in the numerical methods result in good approximation for approximation of data or finding solution of differential equations having the steep behavior.

In this paper, an algorithm using exponential cubic B-spline collocation finite element method is established for obtaining the numerical solutions of the time fBE equation using the L_1 discretization formula of the fractional derivative of Caputo means and the Crank-Nicolson formula.

2. EXPONENTIAL CUBIC B-SPLINE COLLOCATION METHOD

Partition the interval $[a,b]$ at equally distributed knots as:

$$\pi: a = x_0 < x_1 < \cdots < x_N = b$$

with mesh spacing $h=(b-a)/N$. The exponential cubic B-splines, $B_m(x)$, at knots at the points of π with additional external knots x_m, $m=-3, -2, -1, N+1, N+2, N+3$ outside problem domain can be given as

$$B_m(x) = \begin{cases} b_2\left((x_{m-2} - x) - \dfrac{1}{\rho}\sinh(\rho(x_{m-2} - x)) \right), & x \in [x_{m-2}, x_{m-1}] \\[2mm] a_1 + b_1(x_m - x) + c_1 \exp(\rho(x_m - x)) + d_1 \exp(-\rho(x_m - x)), & x \in [x_{m-1}, x_m] \\[2mm] a_1 + b_1(x - x_m) + c_1 \exp(\rho(x - x_m)) + d_1 \exp(-\rho(x - x_m)), & x \in [x_m, x_{m+1}] \\[2mm] b_2\left((x - x_{m+2}) - \dfrac{1}{\rho}\sinh(\rho(x - x_{m+2})) \right), & x \in [x_{m+1}, x_{m+2}] \\[2mm] 0, & \text{otherwise} \end{cases} \tag{6}$$

where

$$a_1 = \frac{\rho h \, c}{\rho h \, c - s}, \quad b_1 = \frac{\rho}{2} \frac{c(c-1) + s^2}{(\rho h \, c - s)(1-c)}, \quad b_2 = \frac{\rho}{2(\rho h \, c - s)},$$

$$c_1 = \frac{1}{4} \frac{\exp(-\rho h)(1-c) + s(\exp(-\rho h)-1))}{(\rho h\, c - s)(1-c)}, d_1 = \frac{1}{4} \frac{\exp(\rho h)(c-1) + s(\exp(\rho h)-1))}{(\rho h\, c - s)(1-c)}$$

and $c = cosh(ph)$, $s = sinh(ph)$, p is a free parameter. Each exponential cubic B-spline $B_m(x)$ has continuous first and second order derivatives defined in the interval $[x_{m-2}, x_{m+2}]$ so that smooth approximation can be obtained for fBE. Since $B_m(x)$, $m = -1...N+1$ forms a basis for the functions defined over the interval $[a, b]$ [21], combination of the exponential cubic B-splines is used to form the approximation for numerical methods. The functional and derivative values of the exponential cubic B-splines are summarized in Table 1.

Table 1. Values of $B_m(x)$ and its principle two derivatives at the knot points

x	x_{m-2}	x_{m-1}	x_m	x_{m+1}	x_{m+2}
B_m	0	$\dfrac{s-ph}{2(phc-s)}$	1	$\dfrac{s-ph}{2(phc-s)}$	0
B'_m	0	$\dfrac{p(1-c)}{2(phc-s)}$	0	$\dfrac{p(c-1)}{2(phc-s)}$	0
B''_m	0	$\dfrac{p^2 s}{2(phc-s)}$	$-\dfrac{p^2 s}{phc-s}$	$\dfrac{p^2 s}{2(phc-s)}$	0

Over the sub element $[x_m, x_{m+1}]$ the variation of $U(x, t)$ is expressed as separation of variables in the form of the exponential cubic B-spline shape functions $B_m(x)$ and time parameters $\delta_m(t)$ as

$$U(x,t) = \sum_{j=m-1}^{m+2} \delta_j(t) B_j(x) \tag{7}$$

Use of values of the exponential cubic B-splines and its derivatives using Eqs. (6)-(7) at knots x_m gives an approximate solution for the unknown $u(x, t)$ in terms of time parameters $\delta_m(t)$ as

$$U(x_m, t) = \frac{s-ph}{2(phc-s)}\delta_{m-1} + \delta_m + \frac{s-ph}{2(phc-s)}\delta_{m+1},$$

$$U'(x_m, t) = \frac{p(1-c)}{2(phc-s)}\delta_{m-1} + \frac{p(c-1)}{2(phc-s)}\delta_{m+1}, \tag{8}$$

$$U''(x_m, t) = \frac{p^2 s}{2(phc-s)}\delta_{m-1} - \frac{p^2 s}{phc-s}\delta_m + \frac{p^2 s}{2(phc-s)}\delta_{m+1}.$$

Temporal discretization of the time fBE is managed by using L_1 formula for time derivative term and Crank-Nicolson formula for other terms so that one reach the time discretized time fBE equation:

$$\frac{(\Delta t)^{-\mu}}{\Gamma(2-\mu)}(u^{n+1} - u^n) + \frac{(\Delta t)^{-\mu}}{\Gamma(2-\mu)}\sum_{k=1}^{n-1}\left[(k+1)^{1-\mu} + k^{1-\mu}\right]\left[u^{n-k+1} - u^{n-k}\right] +$$

$$\frac{(uu_x)^{n+1} + (uu_x)^n}{2} - \nu\frac{u_{xx}^{n+1} + u_{xx}^n}{2} = F(x, t^{n+1}) \tag{9}$$

The nonlinear term $(uu_x)^{n+1}$ in Eq. (9) is converted to linear forms by using the following linearization formula [26] based on Taylor series:

$$(uu_x)^{n+1} = u^{n+1}u_x^n + u^n u_x^{n+1} - u^n u_x^n$$

and substituting local approximation and its derivatives at the knots (8) leads to the system of the fully discretized algebraic equation set

$$\left(\left(A+\frac{L}{2}\right)\alpha_1 + \frac{K}{2}\beta_1 - \frac{v}{2}\gamma_1\right)\delta_{m-1}^{n+1} + \left(\left(A+\frac{L}{2}\right)\alpha_2 - \frac{v}{2}\gamma_2\right)\delta_{m}^{n+1} + \left(\left(A+\frac{K}{2}\right)\alpha_1 - \frac{K}{2}\beta_1 - \frac{v}{2}\gamma_1\right)\delta_{m+1}^{n+1}$$

$$= \left(A\alpha_1 + \frac{v}{2}\gamma_1\right)\delta_{m-1}^{n} + \left(A\alpha_2 + \frac{v}{2}\gamma_2\right)\delta_{m}^{n} + \left(A\alpha_1 + \frac{v}{2}\gamma_1\right)\delta_{m+1}^{n} \tag{10}$$

$$-A\sum_{k=1}^{n-1}\left[(k+1)^{1-\mu} + k^{1-\mu}\right]\left[\left(\delta_{m-1}^{n-k+1} - \delta_{m-1}^{n-k}\right)\alpha_1 + \left(\delta_{m}^{n-k+1} - \delta_{m}^{n-k}\right)\alpha_2 + \left(\delta_{m+1}^{n-k+1} - \delta_{m+1}^{n-k}\right)\alpha_1\right] + F(x, t^{n+1})$$

where

$$K = \alpha_1\delta_{m-1}^{n} + \alpha_2\delta_{m}^{n} + \alpha_1\delta_{m+1}^{n}, \quad L = \beta_1\delta_{m-1}^{n} - \beta_1\delta_{m+1}^{n}, \quad A = \frac{(\Delta t)^{-\mu}}{\Gamma(2-\mu)}$$

and

$$\alpha_1 = \frac{s - ph}{2(phc - s)}, \quad \alpha_2 = 1, \quad \beta_1 = \frac{p(1-c)}{2(phc - s)}, \gamma_1 = \frac{p^2 s}{2(phc - s)}, \quad \gamma_2 = -\frac{p^2 s}{phc - s}.$$

There are $N+3$ unknown parameters

$$\mathbf{d}^{n+1} = (\delta_{-1}^{n+1}, \delta_{0}^{n+1}, \dots, \delta_{N+1}^{n+1})$$

in the system (10) consisting of only $N+1$ linear equations. In order to equalize the numbers of equations and unknowns, we have to eliminate δ_{-1}^{n+1} and δ_{N+1}^{n+1} by manipulating the appropriate boundary conditions as follows

$$\delta_{-1}^{n+1} = \frac{1}{\alpha_1}(u_0 - \alpha_2\delta_{0}^{n+1} - \alpha_1\delta_{1}^{n+1}), \quad \delta_{N+1}^{n+1} = \frac{1}{\alpha_1}(u_N - \alpha_1\delta_{N-1}^{n+1} - \alpha_2\delta_{N}^{n+1})$$

After this elimination, we can solve the system (10) using Thomas algorithms for the solution of 3 banded matrix via Matlab.

3. NUMERICAL TESTS

In this section, we show the results for time fBE. We calculate the accuracy of the proposed methods by calculating the error norm

$$L_\infty = |u(x,t) - U(x,t)|_\infty = \max_m |u(x_m,t) - U(x_m,t)| \tag{12}$$

where $u(x,t)$ denote exact solution and $U(x,t)$ denote numerical solution at time t.

a. **Problem 1**

Firstly, we use the Eq. (1) with boundary conditions

$$u(0,t) = t^2, \ u(1,t) = et^2, t \geq 0 \tag{12}$$

and the initial condition as

$$u(x,0) = 0, 0 \leq x \leq 1. \tag{13}$$

For this problem *f(x, t)* as follows is given by

$$f(x,t) = \frac{2t^{2-\mu}e^x}{\Gamma(3-\mu)} + t^4 e^{2x} - vt^2 e^x \tag{14}$$

and the exact solution of the problem as follows

$$u(x,t) = t^2 e^x. \tag{15}$$

The program is run with parameters free parameter *p=1*, the number of nodes *N=40, 80* and time steps *Δt =0.002, 0.001, 0.0005, 0.00025*. Errors of results of suggested algorithm are documented in Table 2 to make comparison with ones given for the cubic B-spline collocation method [15] and the quadratic B-spline Galerkin method [14]. When the number of the knots is kept fixed as *N=40* and fractional order of the fBE vary and vice versa, L_∞ are documented in Table 3. It is seen from the Tables 2-4 that the presented method produces similar results with the polynomial B-spline-based methods. Fractional and non-fractional solutions of the FBE are exhibited in Fig.1. Fractional solutions are shown to approach non-fractional solutions according value of the fractional derivative orders. Error of the non-fractional solutions are high since the alteration of the non-fractional solution is higher than the fractional solution eyed in Fig. 2.

Table 2. Error norms for μ=0.5 up to the terminating time t=1

Δt	Present Method p=1, N=80	[14] p=1, N=80	Present Method p=1, N=40	[15] p=1, N=40
0.002	8.1034×10^{-4}	9.3661×10^{-4}	8.0980×10^{-4}	6.4200×10^{-4}
0.001	4.0335×10^{-4}	5.3023×10^{-4}	4.0363×10^{-4}	2.6541×10^{-4}
0.0005	2.0118×10^{-4}	3.2830×10^{-4}	2.0132×10^{-4}	2.1188×10^{-4}
0.00025	1.0042×10^{-4}	1.3312×10^{-4}		

Table 3. Error norms for N=40 and Δt=0.00025 up to the terminating time t=1

μ	Present Method p=1	[14]	[15]
0.1	1.0670×10^{-4}	2.3583×10^{-4}	2.7294×10^{-4}
0.25	1.0453×10^{-4}	2.3264×10^{-4}	2.5862×10^{-4}

0.75	9.8794×10^{-5}	2.2452×10^{-4}	1.2456×10^{-4}
0.9	1.0842×10^{-4}	2.3256×10^{-4}	6.6682×10^{-5}

Table 4. Error norms for μ=0.5 and Δt=0.00025 up to the terminating time t=1

N	Present Method p=1	[14]	[15]
10	1.0166×10^{-4}	2.2966×10^{-3}	3.1012×10^{-3}
20	1.0052×10^{-4}	6.2501×10^{-4}	8.1284×10^{-4}
40	1.0049×10^{-4}	2.2735×10^{-4}	2.0949×10^{-4}
80	1.0042×10^{-4}	1.3312×10^{-4}	6.9208×10^{-5}

We run the programme accomplished with the parameters *μ=0.5, N=40, Δt=0.00025* and various *t*. According to these parameters, numerical solutions and error norms are documented in Figures 1-2 respectively.
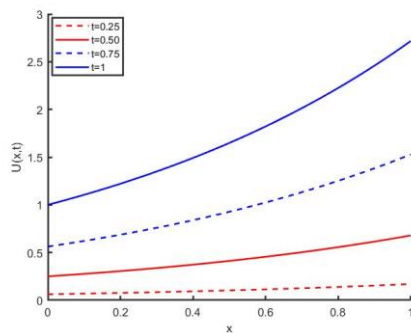
Figure 1. Numerical solutions for Problem 1
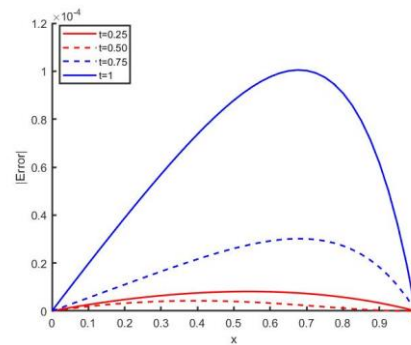
Figure 2. Error norms for Problem 1

b.   Problem 2

Secondly, we use the Eq. (1) with boundary conditions

$$u(0,t) = t^2, \ u(1,t) = -t^2, t \geq 0 \tag{16}$$

and the initial condition as

$$u(x,0) = 0, \ 0 \leq x \leq 1. \tag{17}$$

For this problem *f(x,t)* as follows is given by

$$f(x,t) = \frac{2t^{2-\mu} \cos(\pi x)}{\Gamma(3-\mu)} - \pi t^4 \cos(\pi x) \sin(\pi x) - \nu \pi^2 t^2 \cos(\pi x) \tag{18}$$

and the exact solution of the problem as follows

$$u(x,t) = t^2 \cos(\pi x). \tag{19}$$

Table 5. Error norms for μ=0.5 and N=80 up to the terminating time t=1

Δt	*Present Method p=1*	*[14]*	*[15]*
0.002	*2.4138×10^{-4}*	*1.7564×10^{-4}*	*2.3978×10^{-4}*
0.001	*1.0603×10^{-4}*	*7.7491×10^{-5}*	*1.0035×10^{-4}*
0.0005	*3.8391×10^{-5}*	*2.8460×10^{-5}*	*3.0679×10^{-5}*

Table 6. Error norms for N=40 and Δt=0.00025 up to the terminating time t=1

μ	*Present Method p=1*	*[14]*	*[15]*
0.1	*4.9413×10^{-6}*	*6.455×10^{-6}*	*2.2129×10^{-5}*
0.25	*5.0500×10^{-6}*	*5.257×10^{-6}*	*2.0782×10^{-5}*
0.75	*6.0696×10^{-6}*	*3.443×10^{-6}*	*8.187×10^{-6}*
0.9	*7.7727×10^{-6}*	*4.065×10^{-6}*	*7.886×10^{-6}*

Table 7. Error norms for μ=0.5 and Δt=0.00025 up to the terminating time t=1

N	*Present Method p=1*	*[14]*	*[15]*
10	*1.8194×10^{-3}*	*7.3109×10^{-4}*	*2.4155×10^{-3}*
20	*4.3564×10^{-4}*	*2.7331×10^{-4}*	*5.8358×10^{-4}*
40	*8.4709×10^{-5}*	*6.3233×10^{-5}*	*1.2049×10^{-4}*
80	*5.3302×10^{-6}*	*4.192×10^{-6}*	*1.6164×10^{-5}*

Results are documented in Table 5-7 in which, to observe the variation of error norms and effects of the some parameters, time increment, fractional order and the number of knots are changed while the other parameters remain fixed. All outcomes show that once more the exponential cubic B-spline Galerkin method produce same results with polynomial based B-spline finite element method. We run the programme accomplished with the parameters *μ=0.5, N=80, Δt=0.00025* and various *t*. Solutions are graphed at some time and error changes can also be observed in Fig 3-4.
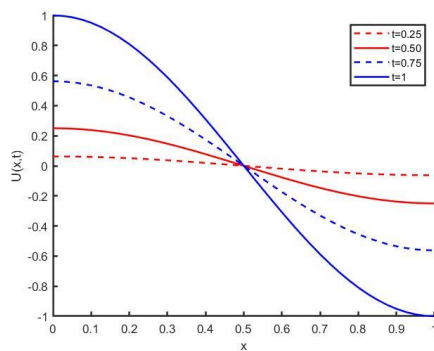
Figure 3. Numerical solutions for Problem 2
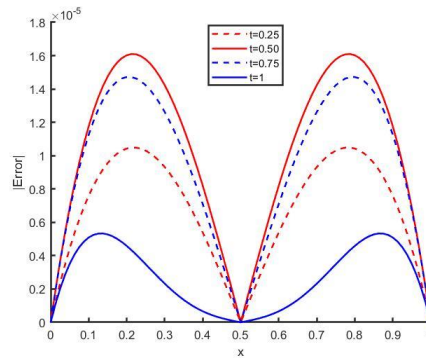
Figure 4. Error norms for Problem 2

4. CONCLUSION

Approximation consisting of combination of exponential cubic B-splines can shown to be used with the finite element method for solving FBE. It is seen from the errors that the use of nonpolynomial B-spline for finite element method cause to poduce less effect on getting higher accuracy for solution of FBE. It can be viewed that smooth fractional solutions depending on fraction order happen around the non-fractional solution.

ACKNOWLEDGMENT

REFERENCES

[1]. N. Sugimoto, "Burgers equation with a fractional derivative; Hereditary effects on non-linear acoustic waves," *J. Fluid Mech.*, vol. 225, pp. 631–53, 1991.

[2]. M. El-Shahed, "Adomian decomposition method for solving Burgers equation with fractional derivative," *J Fac Cal.,* vol. 24, pp. 23–28, 2003.

[3]. S. Momani, "Non-perturbative analytical solutions of the space and time fractional Burgers equations," *Chaos, Solitons & Fractals,* 28(4), 930–937, 2006.

[4]. Q. Wang, "Numerical solutions for fractional KdV-Burgers equation by adomian decomposition method," *Appl. Math. Comput.,* vol. 182 (2), pp. 1048–1055, 2006.

[5]. M. Inc, "The approximate and exact solutions of the space- and time-fractional Burgers equations with initial conditions by variational iteration method," *J.Math.Anal.Appl.,* vol. 345(1), pp. 476–484, 2008.

[6]. J. Biazar and H. Aminikh, "Exact and numerical solutions for non-linear Burger's equation by vim," *Math. Comput. Model,* vol. 49, pp. 1394–1400, 2009.

[7]. K. M. Saad, E. H. F. Al-Sharif, "Analytical study for time and time-space fractional Burgers' equation," *Advances in Difference Equations*, vol. 2017(300), pp. 1–15, 2017.

[8]. A. Yildirim and S. T. Mohyud-Din, "Analytical Approach to Space- and Time-Fractional Burgers Equations," *Chin. Phys. Lett.,* 2010, paper. 27(9), p. 090501.

[9]. M. Kurulay, "The approximate and exact solutions of the space-and time-fractional Burgers equations," *Int. J. Res. Rev.Appl. Sci.* vol. 3(3), pp. 257–263, 2010.

[10]. M. S. Rawashdeh, "A reliable method for the space-time fractional Burgers and time-fractional Cahn-Allen equations via the FRDTM," *Advances in Difference Equations,* vol. 2017(99), pp. 1–14, 2017.

[11]. N. A. Khan and A. Ara, "Numerical solutions of time-fractional Burgers equations, A comparison between generalized differential transformation technique and homotopy perturbation method," *International Journal of Numerical Methods for Heat & Fluid Flow*, vol. 22(2), pp. 175–193, 2012.

[12]. P. A. Harris and R. Garra, "Analytic solution of nonlinear fractional Burgers-type equation by invariant subspace method," *Nonlinear Studies,* vol. 20(4), 2013.

[13]. A. Yokus and D. Kaya, "Numerical and exact solutions for time fractional Burgers' equation," *J. Nonlinear Sci. Appl.,* vol. 10, pp. 3419–3428, 2017.

[14]. A. Esen and O. Tasbozan, "Numerical solution of time fractional Burgers equation," *Acta Univ. Sapientiae, Mathematica*, vol. 7(2), pp. 167–185, 2015.

[15]. A. Esen and O. Tasbozan, "Numerical Solution of Time Fractional Burgers Equation by Cubic B-spline Finite Elements," *Mediterr. J. Math.,* vol. 13, pp. 1325–1337, 2016.

[16]. M. Giyas, S. O. Saldir and F. Erdogan, "Numerical solution of time-fractional Burgers equation in reproducing kernel space," arXiv:1805.06953v1, 2018.

[17]. O. Oruc, A. Esen and F. Bulut, "A unified finite difference Chebyshev wavelet method for numerically solving time fractional Burgers' equation," *American Institue of Mathematical Sciences,* vol. 12(3), pp. 533–54, 2019.

[18]. T. S. El-Danaf and A. R. Hadhoud, "Parametric spline functions for the solution of the one time fractional Burgers' equation," *Applied Mathematical Modelling,* vol. 36, pp. 4557–4564, 2012.

[19]. W. Cao, Q. Xu and Z. Zheng, "Solution of two-dimensional time-fractional Burgers equation with high and low Reynolds numbers," *Advances in Difference Equations,* vol. 2017(338), pp. 1–14, 2017.

[20]. A. Esen, Y. Ucar, N. Yagmurlu and O. Tasbozan, "A Galerkin Finite Element Method to Solve Fractional Diffusion and Fractional Diffusion-Wave Equations," *Mathematical Modelling and Analysis,* vol. 18, pp. 260–273, 2013.

[21]. B. J. McCartin, "Theory of exponential splines," *Journal of Approximation Theory,* vol. 661, pp. 1–23, 1991.

[22]. R. Mohammadi, "Exponential cubic B-spline collocation method for numerical solution of the generalized regularized long wave equation," *Chin. Phys. B,* vol. 24(5), pp.1–14, 2015.

[23]. O. Ersoy and I. Dag, "The exponential cubic B-spline algorithm for Korteweg-de Vries Equation," *Advances in Numerical Analysis*, Article ID 367056, pp. 1–8, 2015.

[24]. O. Ersoy and I. Dag, "Numerical solutions of the reaction diffusion system by using exponential cubic B-spline collocation algorithms," *Open Physics,* vol. 13, pp. 414–427, 2016.

[25]. O. Ersoy and I. Dag, "The Exponential Cubic B-Spline Collocation Method for the Kuramoto-Sivashinsky Equation," *Filomat,* vol. 30(3), pp. 853–861, 2016.

[26]. S. G. Rubin and R. A. Graves, "A cubic spline approximation for problems in fluid mechanics," Nasa TR R-436, Washington, DC, 1975.

Physical Parameters of Cruise Port Identity

Seyma Bayazit[1], Tuncay Kuleli[2]

Abstract

In this study, port identity was examined for cruise ports. The port identity which was pointed out in the literature before due to its importance for cruise port-destination development. However; any common definition for the port identity in cruise related literature has not been found according to a deep-peer literature review. It is derived from desk-study based investigation, despite identity concept defined in different studies with different points of view it consists of two main components: physical (tangible) and intangible components. Within this respect, the aim of this research is to determine physical parameters which form the port identity for any cruise port. To do this, cruise tourism characteristics, identity literature and author's observations and stakeholders' evaluations were utilized. A case study was handled. As a result, destination points-of-interest (POIs) and tourism-based maritime transportation characteristics give main parameters which form cruise port identity such as natural places, endemic places, land network connections, touristic information desks. Using those defined parameters, the port identity was defined and determined for a real cruise port-destination named Bodrum Cruise Port where located in the Aegean-Med Coast of Turkey.

Keywords: Cruise tourism, Port Identity, Cruise Port, Port-destination development

1. INTRODUCTION

Cruise tourism is one of the emerging ocean industries considering its long-term potential for innovation, employment creation and economic growth in travel and tourism market (Organization for Economic Co-operation and Development [1]. As a part of maritime and coastal tourism industries, cruise tourism is the fastest growing sector of tourism industry, increasing 7.2% annually since 1990 [2]. Currently, more than 400 cruise ships have sailed with 27.2 million passengers during 2018 [3].

There is a wide range of itinerary choices in the cruise market, currently more than 2000 cruise destinations exist. Among cruise regions the Caribbean (40 % market share) and the Mediterranean (30 % market share) are the most popular ones. Characteristics of cruise passengers are varied therefore, there are segmentation such as budged, premium, luxury etc. However, there is a common feature of cruisers that each seek unique experiences in port destinations.

The importance of the port identity has been highlighted many times in the literature [4], [5], [6], [7], [8], [9]. However, it has not defined well. As an important function of the port identity, it can be used for «differentiating» a specific cruise port destination among others. The port identity can be used as a tool for land-use policies in such cruise destinations, if it is defined by physical, measurable and comparable criteria. Therefore, in this study, the «port identity» notion was defined by its own physical factors representing with weight factors as parameters determined considering group decision making process.

2. RESEARCH AREA

Research area was a part of the a coastal region of Bodrum which is a district of Mugla Province in the Aegean Region, on the Bodrum Peninsula surrounded by the Gulf of Gulluk in the north and the Gulf of Gokova in the south. According to [10], the geographical position of Bodrum is located on the southern end of the Aegean Sea between the Gulfs of Mandalya and Kerme. Bodrum is an ancient city founded in the Gulf. It is connected to the

---

[1] *Corresponding author: Bandirma Onyedi Eylul University, Maritime Faculty, Department of Maritime Transportation and Management Engineering, 10200, Bandirma/Balikesir, Turkey. sbayazit@bandirma.edu.tr*

[2] *Mugla SK University, Bodrum Maritime Vocational School, Department of Transportation Services, kulelituncay@mu.edu.tr*

province of Mugla and has only a land border with Milas district. The Aegean and the Mediterranean embrace [10]. Bodrum is a settlement built on Halicarnassus, one of the most famous cities of antiquity, at the junction of the Mediterranean and the Aegean [11]. The geographic location of selected area is shown in the Figure 1.
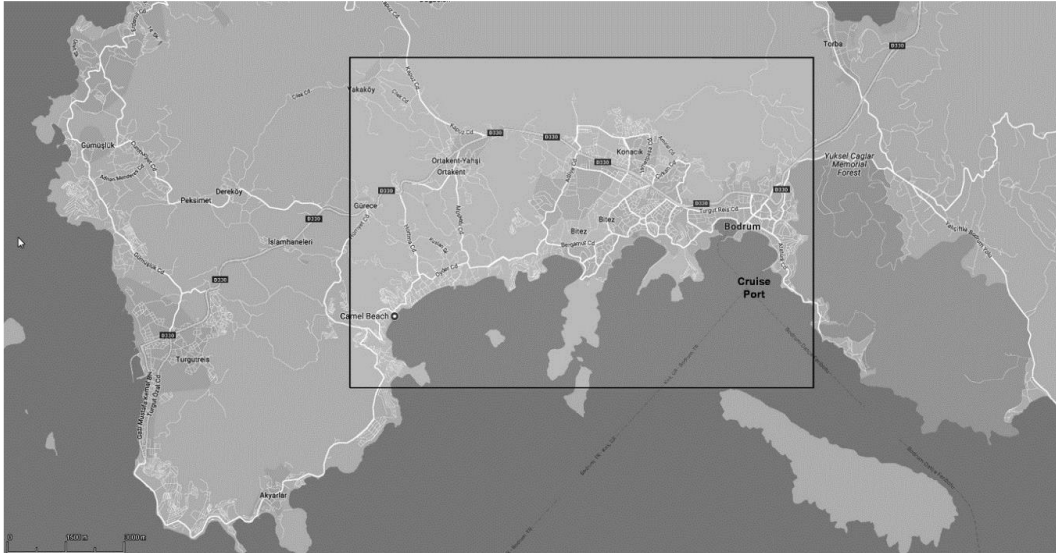
Figure 1. *Bodrum Cruise Port-Destination, Eagean Coast of Turkey (Google.earth, authors)*

3.   MATERIALS AND METHODS

For defining the port identity criteria for cruise ports followings are carried out:

- a peer-view literature relating place identity, cruise ports, cruise industry was reviewed.
- Secondary data was analyzed.
- Field observations were used in the research area which is located in Bodrum, Turkey.
- In the research area, a group of cruise stakeholders' was determined via stakeholder analysis.
- A questionnaire and interview was conducted with those stakeholders in order to define the criteria.
- Questionnaire study was conducted with the same group for determining factor weights of each criteria.

Main methods used for defining criteria and determining port identity for the researh area are as follows:

➢ Pairwise comparision (1-9 scale) according to Saity's AHP method

Materials , programs, softwares are used as:

➢ Stakeholder questionnaires
➢ Office programs.

3.1. Stakeholder Analysis

Stakeholder analysis, a stage of the logical framework approach (LWA), is a method used to identify and categorize relevant parties that may be related to the research topic [12]. Groups of individuals, groups, institutions or organizations that affect or are affected by a solution are defined as stakeholders (practitioners, facilitators, beneficiaries, or competitors) [13]. DMO (Destination Management Organization) theory developed by [14] and different cruise port-destinations were utilized in stakeholder analysis [14]. In addition to this, field observations and interviews were used for defining cruise port destination stakeholders in this study. This can be varied among different destinations because each would have its own features. Therefore, stakeholder analysis is expected to be done considering issues such as beneficiaries, influencers, positive effectors, negative effectors etc.

3.2 Pairwise comparision with Saity's AHP

According to the AHP method proposed by [15] the comparable priorities determined by making pairwise comparisons on 1-9 scale are calculated according to the formulas shown in equation 1 based on the row-based geometric mean method (RGM). The results are then normalized according to equation 2 [16].

$$p_i = r_i / \sum_{i=1}^{N} r_i$$
(1)

$$r_i = exp\left[\frac{1}{N}\sum_{j=1}^{N} ln(a_{ij})\right] = \left(\prod_{l=1}^{N} a_{ij}\right)^{1/N}$$
(2)

ri   : row i result value

pi   : priorities

N   : number of factors

aij   : pairwise comparison matrix (NxN)

Although the AHP method is consistent by having a certain systematic in itself, the validity of the individual evaluations made by the decision-makers depends on the consistency in the personal comparisons. The consistency of the individual evaluations made for prioritizing the criteria is measured by the degree of consistency (CR) [15] in order to determine whether the judgments made are reasonable. In order to be considered consistent, the consistency index should be less than 0.10 (CR≤0.10) [15]. Otherwise, the discrepancy will be excessive and unacceptable.

4.RESULTS

As a result of this study, following factors were found regarding as cruise port identity physical parameters:

- ❖ Historical-cultural places
- ❖ Natural places
- ❖ City center
- ❖ Traditional food and drinks places
- ❖ Coasts and beaches
- ❖ Endemic places
- ❖ Sport facilities
- ❖ Touristic information desks
- ❖ Bazaar market
- ❖ Malls
- ❖ Networks (roadways etc.)

According to the result of participants (public, private and NGOs partners of the destination) from several institutions regarding their stakeholder participation for cruise tourism in the region cruise port idenity factors which is above mentioned were evaluated via pairwise comparision. Results show that group decision is reach 0,027 consistency rate which is acceptable / reasonable according to Saaty 1980 [17], [18]. The importance order of each factors are shown in the Table 1.

Table 1. Normalized weights of cruise port identity factors

Port Identity Criteria	Normalized Eigen Values (Factor Weights)
Historical cultural places	0.2515
Natural places	0.2048
Endemic places	0.1862
Traditional food and drinks places	0.0800
Beaches coasts	0.0760
Sport facilities	0.0560
City center	0.0510
Touristic information desk	0.0360
Bazaar & local markets	0.0360
Shopping centers	0.0230
Networks (roads etc)	«1.0»

According to the Table 1. each factors has its own importance level regarding to the Stakeholder evaluations. One exception is networks among others. Since transportability is a main issue in travel and tourism industry especially in such cruise port destinations, the factor weight of it is not need to evaluate by individuals. So, it took "1" point which means that it should have the top level of importance among others.

CONCLUSION

As conclusion, cruise port identity was defined considering eleven factors. As a result of stakeholder analysis, defined cruise destination stakeholders from different public, private and NGOs' institutes and individuals such as ministry, maritime association, tour operators, maritime trade unions etc. were determined prioritization weights of each factors. Weight factors of each factors were used as a parameter in order to achieve group decision making outputs. Using those defined parameters, the port identity was defined and determined for a real cruise port-destination named Bodrum Cruise Port where located in the Aegean-Med Coast of Turkey. Regarding joint group decision level of each individual evaluation which is called consensus level was found 83 per cent. It can be derived from study results that stakeholders of selected cruise port-destination are agreed in defining cruise port identity by a common way. Outputs are expected to give rise to multi-criteria and multi-stakeholder approaches in cruise literature for future studies.

ACKNOWLEDGMENT

REFERENCES

[1]. The Organisation for Economic Co-operation and Development (OECD) (2016). The Ocean Economy in 2030, OECD Publishing, Paris.
[2]. Klein, R.A. (2011). Responsible Cruise Tourism: Issues of Cruise Tourism and Sustainability. Journal of Hospitality and Tourism Management, 18, 107–116.
[3]. Cruise Lines International Association Europe (CLIA) (2017a). 2018 Cruise industry Outlook.
[4]. Broeze, F. (1985). Port Cities. The Searching for an Identity. *Journal of Urban History, 11* (2), 209-225.

[5]. Hooydonk, E. V. (2009). Port City Identity & Urban Planning. Asociación para la Colaboración entre Puertos y Ciudades // Association for the Collaboration between Ports & Cities (RETE), PORTUS (Rete Publications), 18. 16-23.

[6]. The Organisation for Economic Co-operation and Development (OECD) (2015). The Competitiveness of Global Port-Cities: Synthesis Report.

[7]. Guney Ege Kalkinma Ajansi (GEKA) (2014). TR32 Duzey 2 Bolgesi Bolge Plani 2014-2023.

[8]. Port Everglades Final Art Master Plan. (2009). Art and, Moment and Transformation, Art in Flux.

[9]. Mccarthy, J.P. & Romein, A. (2012). Cruise Passenger Terminals, Spatial Planning and Regeneration: The Cases Of Amsterdam and Rotterdam. European Planning Studies, 2033-2052.

[10]. Koc, A. (1973). Bodrum. Cografya, Tarih, Folklor ve Turizm. Milas: Yeni Milas Matbasi.

[11]. Kiper, H. P. (2004). Kensel Kureselesme Surecinde Kentlerin Tarihsel-Kulturel Degerlerinin Korunmasi -Turkiye-Bodrum Ornegi- (Ph.D thesis).

[12]. Ortengren, K. (2004), Swedish Agency for International Development Cooperation (SIDA), The Logical Framework Approach, A Summary of the Theory Behind the LFA Method.

[13]. Barbera, G. (2004). Project Cycle Management and Logical Framework.

[14]. Sheehan, L.R. & Ritchie J.R.B. (2005). Destination stakeholders exploring identity and salience. Annals of Tourism Research, 32 (3), 711–734.

[15]. Saaty, T. L. (1980). *The Analytical Hierarchy Process*. McGraw-Hil, New York.

[16]. Goepel, K.D. (2013). Implementing the Analytic Hierarchy Process as a Standard Method for Multi-Criteria Decision Making In Corporate Enterprises – A New AHP Excel Template with Multiple Inputs, Proceedings of the International Symposium on the Analytic Hierarchy Process.

[17]. Roszkowska, E. (2013). Rank Ordering Criteria Weighting Methods–A Comparative Overview. Optimum Studia Ekonomiczne NR, 5 (65), 15-33.

[18]. Franek, J. and Krestaa ,A. (2014). Judgment scales and consistency measure in AHP. Procedia Economics and Finance, 12, 164-173.

Investigation of Some Physical Properties of Dual-Core Multi-Twist Slub Yarns

Nida Yildirim[1], Munevver Ertek Avci[2], Huseyin Gazi Turksoy[3]

Abstract

Denim fabrics are the most widely used type of fabrics for clothing and consumption of it is increasing all over the world. It is a well-known fact that companies operating in the denim sector are challenged every day. To be innovative in scopes such as to use new materials, to develop new technologies, to improve production processes and to develop environmentally friendly solutions during the dye-finishing phase has great importance in this highly competitive sector. There are many parameters that can affect the characteristics and performance of denim fabric within the scope of innovations. In this study, dual-core multi-twist slub yarns have been developed to give both functional and visual effects to denim fabrics. Unevenness, hairiness, tenacity and breaking elongation properties of these yarns were analyzed. Experimental results have indicated that slub type is a statistically significant factor for unevenness and hairiness values and it is not a statistically significant factor for tenacity and breaking elongation values.

Keywords: *Denim Fabric, Hybrid Yarns, Dual-Core Slub Yarn, Multi-Twist Slub.*

1. INTRODUCTION

Denim fabric is considered among the most popular fabrics for clothing market. Denim fabrics have adjectives such as comfortable, risky, adventurous, relaxing, glamorous, attractive, aggressive, smart, casual, funny, dynamic, energetic, fashionable, practical, creative… universal. Denim can also be define not only as a style in fashion but also as something more: a lifestyle [1,2].

It is a well-known fact that companies operating in the denim sector are challenged every day. The only way to survive in harsh competitive conditions is the constant search for innovation. A wide variety of materials and production techniques are used in the design and development of different aesthetic denim fabrics with improved functional properties.

Expectations from denim fabrics vary according to gender. While women prefer weft resembling elasticity jeans (stretch, super stretch), men prefer rigid and comfort jean fabrics (low elasticity). Stretchable properties to jean fabrics are gained with various core-spun yarns which contain elastane filaments [3-5]. The core-spun yarn is a kind of hybrid yarns that generally manufactured at modified ring frame, by placing elastane to the center while yarn is being produced out of cotton or other staple fibers. An advanced version of the core-spun yarn production method is the dual-core yarn production method. In dual-core production method, two core threads (one of them is elastane filament) are fed into the center to benefit from the properties of three different textile materials at the same time [6-8]. In addition, nowadays, it has been observed that the use of slub yarn in denim fabric production has also been widespread with the effect of fashion trends such as vintage, authentic in recent years for different appearance and surface effects [9,10]. In this study, innovative dual-core slub hybrid yarns for denim fabrics is produced and then the various physical properties of these yarns were evaluated comparatively.

2. MATERIALS AND METHODS

In this study, three different types of dual-core multi-twist slub yarns having three different slub versions were produced. Dual-core yarn samples without slub were also produced as a control group. The count of yarn samples was Ne 10.4. 55 dtex T400® with 1.06 draft, 78 dtex elastane with 3.5 draft and cotton fibers (30% Turkmen

---

[1] Corresponding author: Karadeniz Technical University, Trabzon Vocational School, Trabzon, Turkey. nidayildirim@ktu.edu.tr

[2] Calik Denim R&D Center, Malatya, Turkey, Munevver.ErtekAvci@calikdenim.com

[3] Erciyes University, Department of Textile Engineering, Kayseri, Turkey, hgazi@erciyes.edu.tr

Sawgin, 50% Urfa Roller, 20% USA Sawgin) were used in the production of dual-core multi-twist slub yarn samples. The yarn samples were produced on the Marzoli MDS1 ring spinning machine modified with Pinter dual-core and Marzoli slub system (Figure 1).
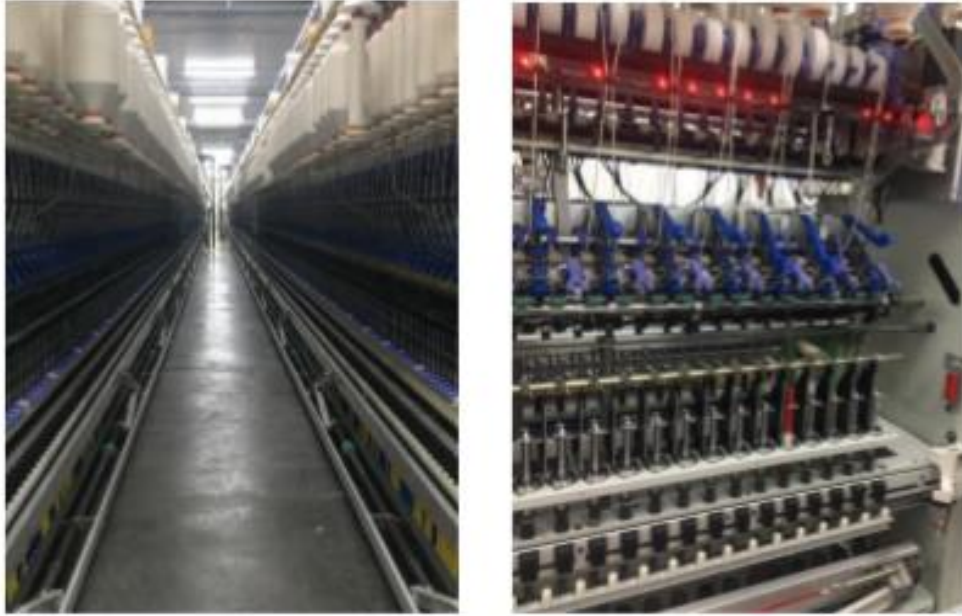
Figure 1. Marzoli MDS1 ring spinning machine.

The production parameters and codes of the yarn samples were summarized in Table 1. Dual-core multi-twist slub yarns were coded as 'MDC' and dual-core yarns without slub were coded as 'DC'. The technical visuals (simulative images of fabrics) created with the Amsler WinPK® II EP5000 program of the yarns produced by the dual-core slub method in the ring spinning system were given in Figure 2.

Table 1. Production parameters of yarn samples.

Sample Code	Spindle speed (rpm)	Twist (tpm)	Twist coefficient (α_e)	Type of Slub
MDC 1	7500	460-510-560	3,6 - 4 - 4,4	(Slub MTV1)
MDC 2	7500	460-510-560	3,6 - 4 - 4,4	(Slub MTV2)
MDC 3	7500	460-510-560	3,6 - 4 - 4,4	(Slub MTV3)
DC	8500	560	4,4	-

The parameters of the multi-twist slub versions (MTV) were defined as the followings:

- Slub MTV1; 460-510-560 tpm, with equal density distribution
- Slub MTV2; 510-560 tpm, density reduced by 25% and balanced final number with 460 T/M density
- Slub MTV3; 460 tpm density increased by 25%, balanced final number with 510-560 T / M density

(a)

(b)

(c)
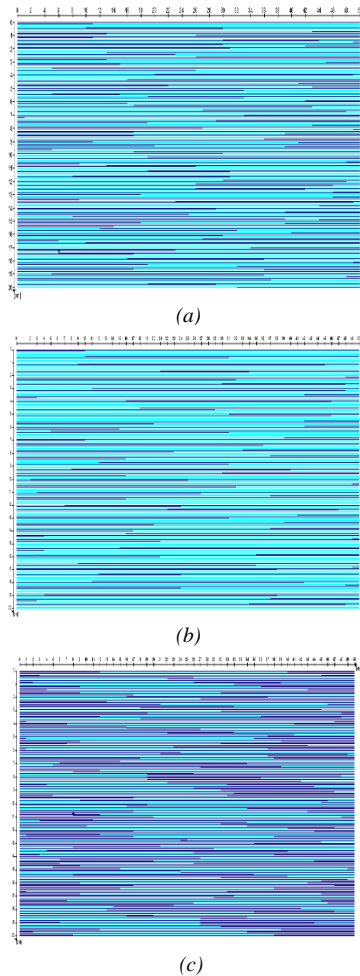
Figure 2. Simulative images of fabrics for Slub MTV1 (a), MTV 2 (b) and MTV 3 (c)

All yarn samples were conditioned in the testing laboratory under standard atmospheric conditions of 20±1C and 65±2% R.H. for 24h. Unevenness and hairiness tests of yarn samples were measured on Uster Tester 5 device with the testing speed of 400 m/min throughout 1 minute. Yarn tenacity and breaking elongation were determined on Uster Tensorapid 4 Tester. The number of breaking for each test is 500. The test length is 500 mm and the test speed is 400 m/min. For each yarn sample, three tests were performed and the averages were reported.

3. RESULTS AND DISCUSSIONS

Unevenness, hairiness, tenacity and breaking elongation properties of MDC and DC yarns were evaluated comparatively. Test results were analyzed by using one-way replicated analysis of variance (ANOVA), and the means were compared by DUNCAN tests at 0.05 level using SPSS 13.0 statistical package software. The average yarn unevenness values of the DC and MDC yarn samples are shown in Figure 3. According to ANOVA results, the effect of slub types on the unevenness value of yarn samples is found statistically significant. (P_t=0.009).
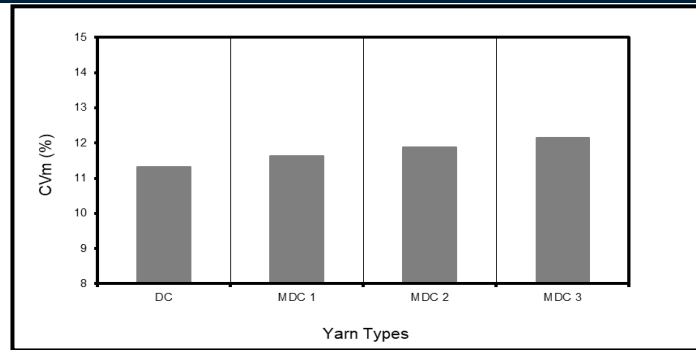
Figure 3. The average unevenness results of yarn samples.

The multiple comparison of factor levels for unevenness test results according to the DUNCAN test of yarn samples are shown in Table 2. According to the DUNCAN test results, there is a statistically significant difference between the yarn unevenness values of MDC 2 and MDC 3 coded dual-core slub yarns with DC yarns. In addition, it is observed that there is not statistically significant between unevenness values of yarns produced with different slub types. It is thought that this situation is related to the selected slub types and if the different twisting density (gap between the slits) are selected, statistically significant differences between slub types can be obtained.

Table 2. DUNCAN results for unevenness values of yarn samples.

Process	S	Subset	
Yarn Type			
DC	5	11,310	
MDC 1	5	11,766	11,766
MDC 2	5		11,876
MDC 3	5		12,164
Sig.		0,051	0,188

The average hairiness values of yarn samples are given in Figure 4. According to ANOVA results, the effect of slub types on hairiness values of yarn samples is found statistically significant ($P_t=0.019$).
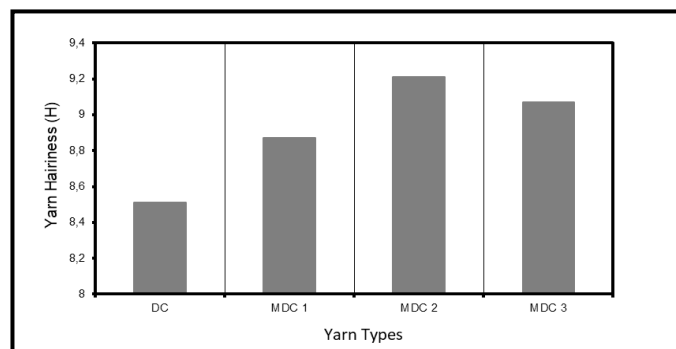
Figure 4. The average hairiness results of yarn samples.

According to DUNCAN test results; only difference between the hairiness values of MDC 2 yarns with DC yarns is found statistically significant (Table 3).

Table 3. DUNCAN results for hairiness values of yarn samples.

Process	S	Subset	
Yarn Type			
DC	5	8,514	
MDC 1	5	8,634	8,634
MDC 3	5	9,072	9,072
MDC 2	5		9,216
Sig.		0,063	0,051

The average yarn tenacity values and breaking elongation values of DC and MDC yarns respectively are given in Figure 5 and Figure 6. According to ANOVA results; the slub type is not statistically significant factor for tenacity values (P_t=0.060) and breaking elongation (P_t=0.406) values of yarn samples.
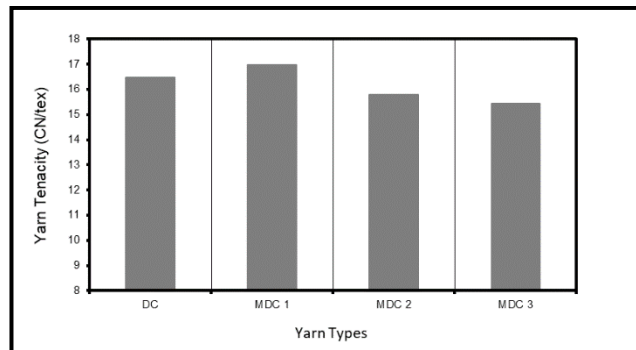
Figure 5. The average tenacity results of yarn samples.
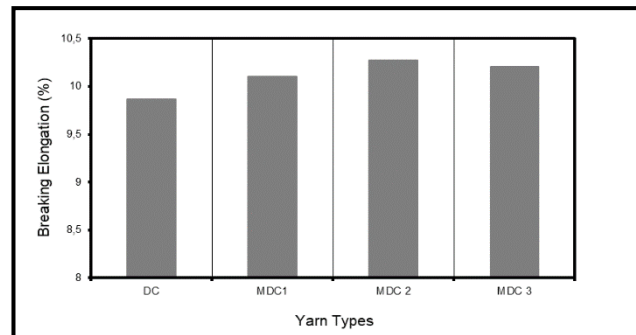
Figure 6. The average breaking elongation results of yarn samples.

4.CONCLUSION

In the study, the production of dual-core slub yarns with different multi-twist slub types in the modified ring spinning system was carried out, and then the various physical properties of the yarn samples were evaluated comparatively. Results have indicated that slub type is a statistically significant factor for unevenness and hairiness values and it is not a statistically significant factor for tenacity and breaking elongation values.

REFERENCES

[1]. Archroma's denim specialist team, 2014. "Archroma Denim Book". Spain.
[2]. Tantawy, S.E., Sabry, M. and Bakry, M. 2017. The effect of different weft yarn production technique on the pilling property of jeans fabrics, *International Design Journal*, 7(3), 161–169.
[3]. Kumar, S., Chatterjee, K., Padhye, R., Nayak. R. 2016. Designing and development of denim fabrics: part 1 - study the effect of fabric parameters on the fabric characteristics for women's wear, *Journal Textile Science Engineering*, vol.6, pp. 265.

[4]. Nayak, R., Padhye, R., Gon, D.P. 2010. Sewing performance of stretch denim, *Journal of Textile and Apparel Technology and Management*, vol. 6, pp. 1-9.

[5]. Jaouachi, B., Hassen, M.B., Sahnoun, M., Sakli, F. 2010. Evaluation of wet pneumatically spliced elastic denim yarns with fuzzy theory, *The Journal of Textile Institute*, vol. 101, pp.111-119.

[6]. Paul, R. Denim manufacture, finishing and applications, In: Woodhead Publishing, pp. 599, 2015.

[7]. Ertas, O., G., Zervent Unal B., and Celik, N., 2016. Analyzing the Effect of the Elastane-Containing Dual-Core Weft Yarn Density on the Denim Fabric Performance Properties, *The Journal of The Textile Institute*, Cilt 107, No. 1, 116–126. DOI: 10.1080/00405000.2015.1016319.

[8]. Zhanga, T., Guoa, M., Chenga, L., Yua, Y., Tanga H., and Lib, S., 2016. Investigation on Production, Analytical Models, and Characteristics of Monofilaments/Staple fibers Composite Yarn, *The Journal of The Textile Institute*, 107(5), 589–595. DOI: 10.1080/00405000.2015.1052675.

[9]. Altas, S., Ozgen, B., 2015. Optimization of slub yarn tensile strength with Taguchi techniques, *Industria Textila*, vol 66 /6 , pp 335-339.

[10]. Ray, N.C., Mukhopadhyay, A., Midha, V.K., 2016. Response of Slub Characteristics on Tensile Properties og Injected Slub Yam, *Journal of The Institution of Engineers (India): Series E,* 97(1), pp 47-53.

Restoration Ecology of the Last Native *Potamogeton praelongus* Population in the Czech Republic Using the Knowledge of Other Localities in its World Distribution

Zuzana Kozelková[1], Romana Prausová[1], Zina Tomášová[1]

Abstract

At the beginning of the 1990s the macrophyte aquatic species Potamogeton praelongus grew in about 20 different localities in the Czech Republic. Since 1997, the species has been growing only in its last native locality, the Orlice River Oxbow near Hradec Králové (East Bohemia). Optimal conditions for this species are to be found in the northern part of its distribution range. Our study of its ecological requirements, seed germination, clonal growth, long-term monitoring of the Czech population, and observations of some localities in Norway, Sweden and Poland have been used for the P. praelongus Rescue Programme established in 2003. Currently, comprehensive interventions for the restoration of the last native locality are in progress. To decrease the trophic status of the water the bottom muddy substrate and organic litterfall have been excavated. Reduction of trees and riparian vegetation on the banks of the river oxbow was carried out to decrease the amount of litterfall and mainly to decrease the shade level of the water surface. A sedimentation reservoir was built on Stříbrný Stream above the outfall into the river oxbow to reduce the rapid transport of sandy substrate from Stříbrný Stream. To preserve the new close-to-natural river bed, a free zone without any interventions has been created.

Keywords: ecology, *Potamogeton praelongus*, rescue programme, restoration

1. INTRODUCTION

Potamogeton praelongus (Long-stalked Pondweed) is a submerged perennial aquatic plant with a long perennial rhizome [1].

The distribution of P. praelongus is classified as circumpolar and suboceanic. The species mainly grows in the boreal climatic zone [2]. There is only one locality in the Czech Republic out of about 20 historically known ones with its natural occurrence today. This is the temporarily protected Orlice River Oxbow protected area by the Stříbrný Pond in Hradec Králové (TPA in the text below). Several micropopulations have been established in the Protected Landscape Area in the Kokořínsko and Máchův kraj regions [3].

Potamogeton praelongus occurs in lakes, river floodplains (river oxbows, pools), moderately flowing water, ponds, and reservoirs. It grows especially in unpolluted, mesotrophic, 0.2–2.0 m deep waters in humic or sandy soils, clayish, muddy or peaty beds [4]. In northern countries, it grows in streams and lakes with high water transparency and mainly gravel bottoms in water columns up to several meters deep (approx 4 m). In the CR, it usually grows in oxbows or backwater pools in 0.2–0.7 m water columns, where it requires a moderate shade level preventing overheating [5]. This species is basophilic [6 - 8]. There are high values of conductivity (200–300 μS.cm^{-1}) in all Czech localities [5]. In northern localities, the values of conductivity are significantly lower [6 - 7]. Total alkalinity higher than 1.2 mekv.l^{-1} is beneficial for this species [9]. In all Czech localities, *P. praelongus* grows in neutral to slightly alkaline water, meso- to eutrophic (determined by N and P concentrations),

with (NO^{2-}) N concentration ranging between 0 and 14 mg.l-1 and (PO$_4^{3-}$) P concentration between 30 and 1000 μg.l^{-1}, and calcium concentration between 50 and 60 mg.l^{-1} [5].

Eutrophication and its consequences are the most important factors in surviving or extinction of *P. praelongus* in the CR because they cause significant changes of its habitats. Decreasing water transparency and a disbalance of relationships between aquatic macrophytes, alga and, cyanobacteria are the most intensive factors. *P. praelongus* is not sufficiently competitive as are natant macrophyte *Nuphar lutea* or the *Caliergonella cuspidata* expansive moss, both overgrowing eutrophicated sites [3]. Filamentous algae cover the leaf surface of *P. praelongus*, decrease gas exchange and increase pH on the leaf surface. Parts of the shoots covered with algae necrotize and a smelly muddy black substrate of organic material forms on the bottom [10].

Potamogeton praelongus is included in the Red List of IUCN (International Union for Conservation of Nature and Natural Resource) in the LC category (least concern) of species protection. In the EU Red List the species is included in the same category of endangerment [11]. According to Act No. 114/1992 Coll., on nature conservation and landscape protection, the species is listed as critically threatened in the CR. It is included in the same category in the Red List of vascular plants [12] and in the Red Book of the CR [13].

The primary aim of this research was to study site conditions in *Potamogeton praelongus* optimal biotopes, its tolerance to different stress factors in northern countries (Norway, southern Sweden and Poland), and its linkage to species diversity of vascular plants. Since *P. praelongus* grows in extreme ecological conditions in the Czech Republic, the second aim was to find a solution how to restore the last native site for this species in the CR.

2. MATERIALS AND METHODS

2.1. Field data collection

Potamogeton praelongus sites were studied in four European countries in 2014–2016 in the span of 50–67° of latitude and 10–23° of longitude). The study covered localities in the Czech Republic, southern Sweden, Norway and Poland (Figure 1).
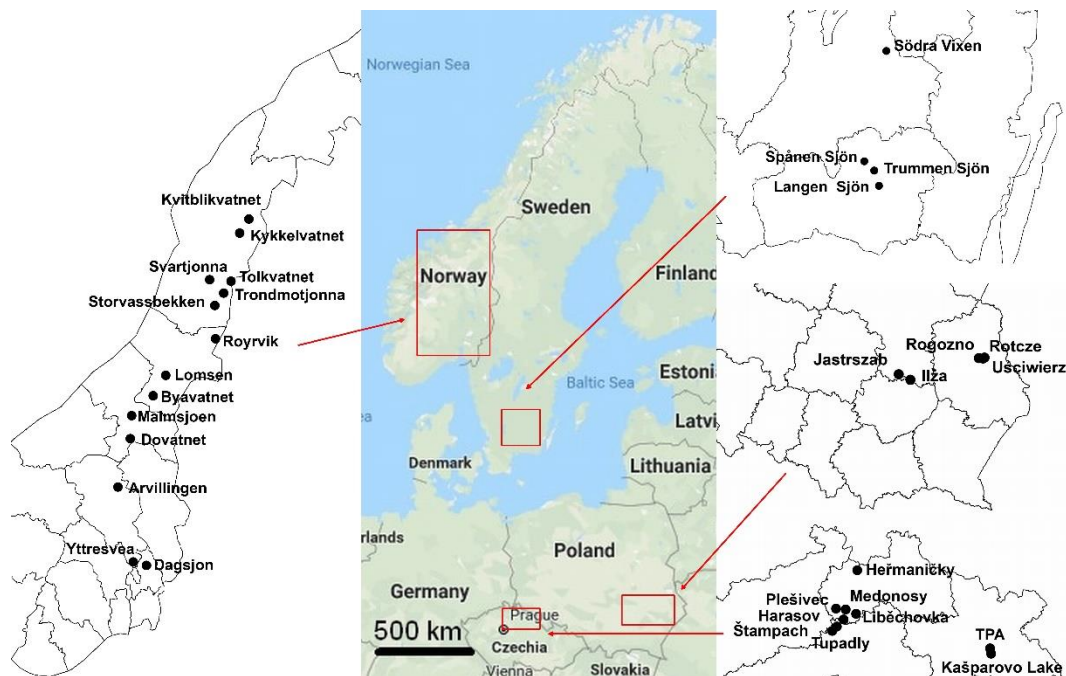
Figure 1. Localities examined in 2014–2016

For GPS location, Garmin e-Trex H with high sensitivity was used. Habitat conditions were measured by portable devices for measuring water temperature, conductivity, pH, dissolved oxygen content (Hach HQ 30d), water transparency (Secchi desk), and illumination (luxmeter Voltrcarft LX-1108). Shade level (%) was calculated as the difference between 100% and the ratio (%) of the illumination (lx) of the *P. praelongus* site to the illumination

(lx) of an open, fully lighted place. Site conditions recorded in all the localities were used for comparison between Czech and Nordic localities.

Potamogeton praelongus and other species of vascular plants were observed and identified in the pools (from a boat) and in the littoral zones. Undetermined species were gathered and submitted to specialists for identification (A. Hájek, M. Hroneš, Z. Kaplan). The nomenclature of vascular plant species according to Danihelka et al. [14], The Plant List [15] was used. According to our experience gained in other countries and long-term observations of all Czech sites with native and reintroduced *P. praelongus* micropopulations we made a plan for the restoration of the species' last native site (Orlice River oxbow).

2.2. Statistical evaluation

Environment data were statistically evaluated by PCA. The environment conditions have been characterized by water temperature, pH, water transparency, shade level, conductivity, water depth and dissolved oxygen content. Environment conditions were used as logarithmically transformed response data. Floristic data of vascular plants were evaluated using DCA without any transformation. A presence or absence of the species was recorded 1 or 0 respectively and exported to the statistical programme. All multivariate data were tested in Canoco 5 programme[16].

3. RESULTS AND DISCUSSION

3.1. Water characteristics of studied sites

The studied localities significantly differ in their site conditions. The first two axes show 80% of data variability (Fig. 2).

All Czech and two Polish localities (Iłżanka and Jastrząb) are the most antropogenic in the whole set being studied. Czech sites are too shaded. During observations made in July, the water temperature of all Czech and two Polish sites was 16–26°C and electrical conductivity was 192–410 µS.cm^{-1}. Populations in all these localities (and also the Norwegian Kvitblikvatnet site) occur in 0.26–1.05 m deep water with a transparency of 0.26–0.62 m.

Other Polish localities (Rogóźno, Rotcze, Uśćiewierz) together with most of the Norwegian lakes belong among sites characterized by a high dissolved oxygen content, water transparency of 1.1–3.6 m, and a high pH value. The highest dissolved oxygen content and the highest pH value were detected in Jastrząb lido, the recreationally most exploited locality among all the localities studied in Poland.

All Swedish localities are characterized by water temperature 15.5–17.2°C, pH 7.4–8.05, electrical conductivity 54.7–144.7 µS.cm^{-1}, and shade level 8–43% during observation in July. These localities had a very good water transparency (1.1–3.6 m). Only one Norwegian locality (Dovatnet) was similar (water temperature 12.9°C, pH 8.2, conductivity 22.5 µS.cm^{-1}, and shade level 31%). Some *P. praelongus* lake localities were more shaded by woody vegetation around the lakes (Dovatnet 31%, Langen 35%, Trummen 43%).

In Norway, where the largest number of localities was studied and the highest span of site conditions and species diversity was observed, most localities belong to mesotrophic sites. The lowest electric conductivity was measured in Kvitblikvatnet (18 µS.cm^{-1}) and Dovatnet (22.5 µS.cm^{-1}). The highest conductivity was measured in Yttre Svea (140 µS.cm^{-1}), Lomsen (138.5 µS.cm^{-1}), Storvassbekken (130.4 µS.cm^{-1}), Malmsjoen Lakes (114.6 µS.cm^{-1}).
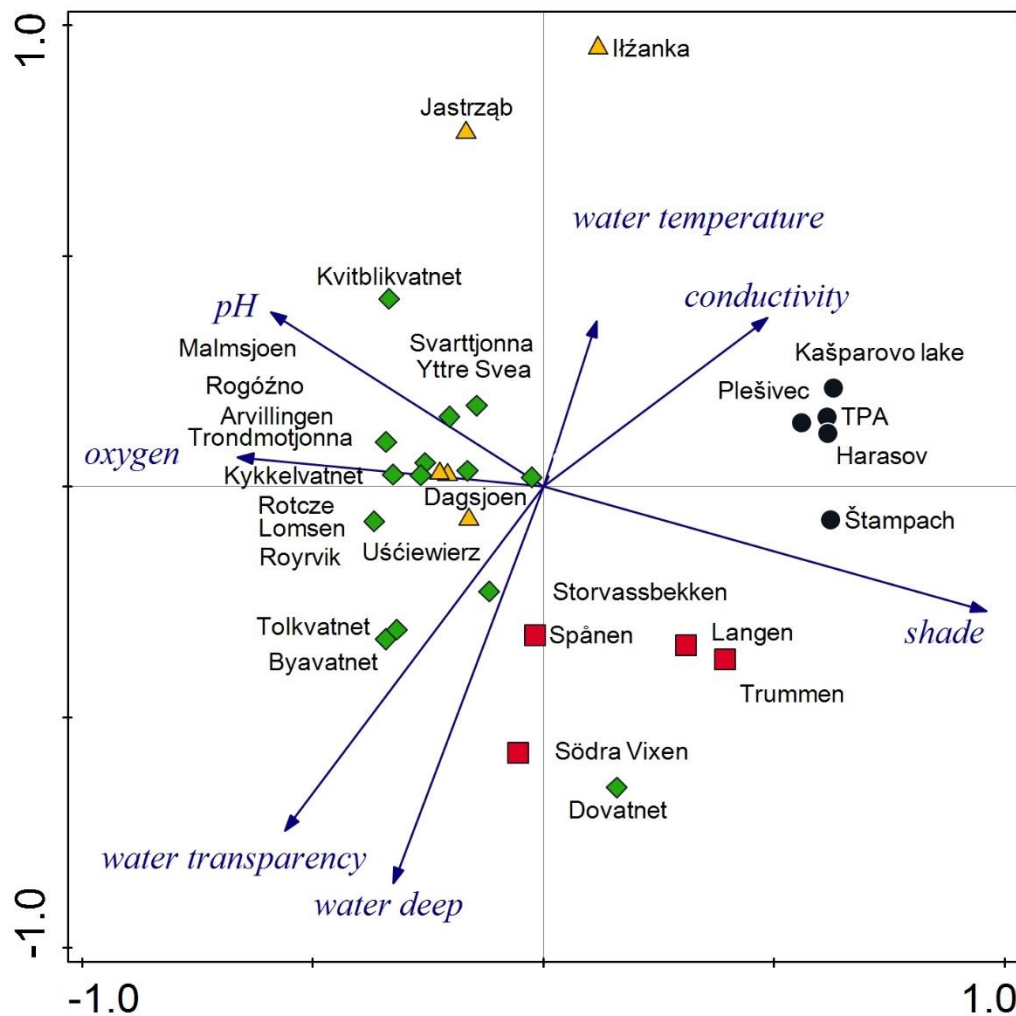
Figure 2. PCA plot, comparison of localities with P. praelongus in the Czech Republic (black), central Poland (yellow), Norway (green) and Southern Sweden (red), with the first axis affecting 57% of data variability and the first two axes taken together affecting 80% of data variability.

3.2. Plant diversity of studied sites

Different site conditions in the studied localities also cause differences in the composition of species (Fig. 3). Eutrophic sites are represented by Czech and two Polish localities (Iłżanka lagoon and Jastrząb lido). *Potamogeton praelongus* grows there together with *Nuphar lutea*, *Persicaria amphibia*, *Ceratophyllum demersum*, *Elodea canadensis*. In Czech localities, eutrophication comes from the surrounding agricultural landscape and intensive fishing. The Polish Jastrząb lido locality is exposed to the recreation burden. Iłżanka lagoon is surrounded by several houses, gardens and an agricultural landscape.

Polish localities of Rogóźno and Uśćiewierz are slightly eutrophic sites and are indicated by *Nymphaea candida*, *Hydrocharis morsus-ranae*, *Myriophyllum spicatum*, *Utricularia australis, Stratiotes aloides,* growing together with *P. praelongus*. All these localities are affected by fishing and recreation.

Eutrophic Trummen Lake in Southern Sweden is located in the vicinity of Växjo city and its current eutrophication is caused by local waste discarded in the past by a hospital and several factories.

In the oligotrophic locality of Sodra Vixen in Sweden, *Isoëtes lacustris*, *Littorella uniflora* and *Lobelia dortmanna* were observed. The other two Swedish lakes, Langen and Spånen, can be characterised as mesotrophic. In both these localities, *P. praelongus* grows together with *P. lucens*, *P. natas*, *Nymphaea alba*, *Nuphar lutea* etc.

Most Norvegian localities belong to mestrophic sites. The lowest electric conductivity was measured in Kvitblikvatnet and the Dovatnet lakes, where oligotrophic species *Isoëtes lacustris* and *Utricularia minor* grow.
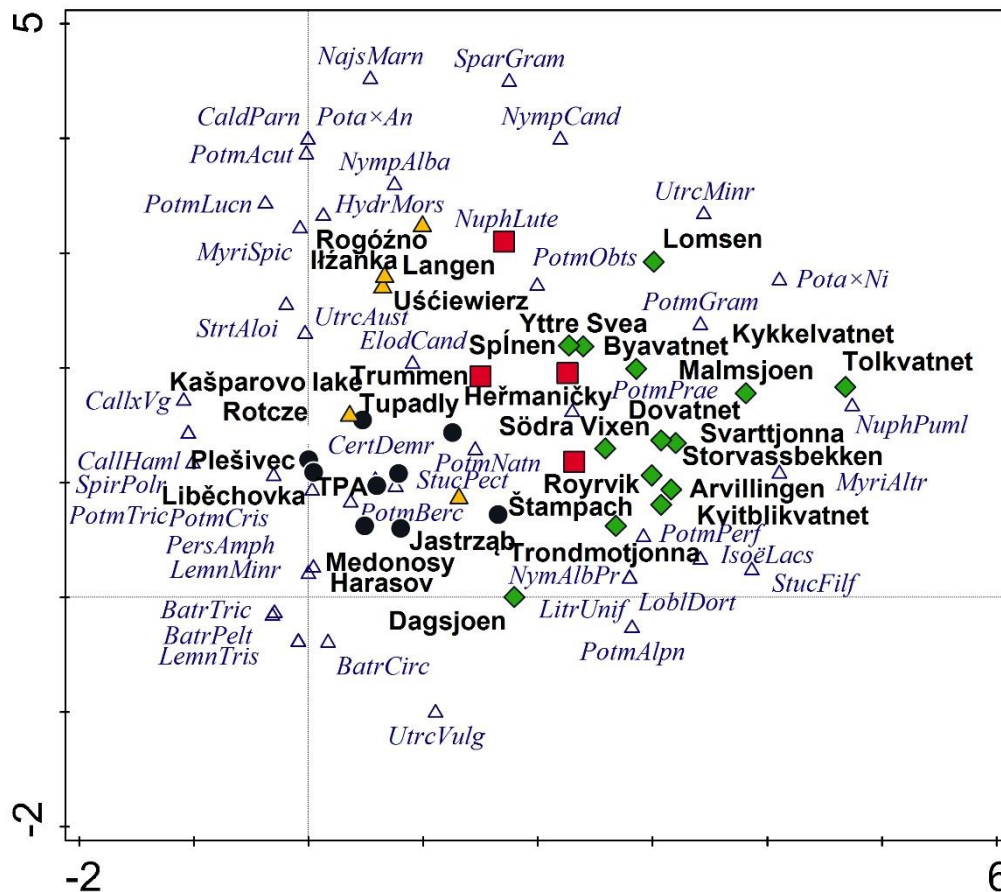
Figure 3. DCA plot, species diversity of vascular plants in localities of P. praelongus in the Czech Republic (black), central Poland (yellow), Norway (green) and Southern Sweden (red). There are only 50% of species shown in this graph according to their importance,the first axis affecting 11% of data variability, the first two axes taken together affecting 18% of data variability.

Abbreviations of taxa names: *Batrachium circinatum* (*BatrCirc*), *Batrachium peltatum* (*BatrPelt*), *Batrachium trichophyllum*(*BatrTric*), *Caldesia parnassifolia* (*CaldParn*),*Callitriche hamulata* (*CallHaml*), *Callitriche × vigens* (*Call×Vg*), *Ceratophyllum demersum* (*CertDemr*), *Elodea canadensis* (*ElodCand*), *Hydrocharis morsus-ranae* (*HydrMors*), *Isoëtes lacustris* (*IsoëLacs*), *Lemna minor* (*LemnMinr*), *Lemna trisulca* (*LemnTris*), *Littorella uniflora* (*LitrUnif*), *Lobelia dortmanna* (*LoblDort*), *Myriophyllum alterniflorum* (*MyriAltr*), *Myriophyllum spicatum*(*MyriSpic*), *Najas marina* (*NajsMarn*), *Nuphar lutea* (*NuphLute*), *Nuphar pumila* (*NuphPuml*), *Nymphaea alba* (*NympAlba*), *Nymphaea alba* var. *purpurea* (*NymAlbPr*), *Nymphaea candida* (*NympCand*), *Persicacaria amphibia* (*PersAmph*), *Potamogeton acutifolius* (*PotmAcut*), *Potamogeton alpinus* (*PotmAlpn*), *Potamogeton × angustifolius* (*Pota×An*), *Potamogeton berchtoldii* (*PotmBerc*),*Potamogeton crispus* (*PotmCris*), *Potamogeton gramineus* (*PotmGram*), *Potamogeton lucens* (*PotmLucn*), *Potamogeton natans* (*PotmNatn*), *Potamogeton × nitens* (*Pota×Ni*), *Potamogeton obtusifolius* (*PotmObts*), *Potamogeton perfoliatus* (*PotmPerf*), *Potamogeton praelongus* (*PotmPrae*), *Potamogeton trichoides* (*PotmTric*), *Sparganium gramineum* (*SparGram*), *Spirodela polyrhizza* (*SpirPolr*), *Stratiotes aloides* (*StrtAloi*), *Stuckenia filiformis* (*StucFilf*),

Stuckenia pectinata (*StucPect*), *Utricularia australis* (*UtrcAust*), *Utricularia minor* (*UtrMinr*), *Utricularia vulgaris* (*UtrcVulg*)

3.3 Restoration of *the* last native locality of *Potamogeton praelongus* in the Czech Republic

Local environmental conditions, such as conductivity, water transparency, presence of invasive species, spatial gradients, elevation and climate have a big impact on macrophyte communities, and it is necessary to use the spatial aggregation of environmental and connectivity factors in the landscape scale approach to lake management [17]. Response of aquatic plants to environmental factors has been a frequently discussed problem during the past decades [18] - [19]. Difficulties concerning eutrofication resulting in high phytoplankton biomass and low summer water transparency are known not only from densely populated Central Europe, but also from the Nordic part of Europe [6], [20].

Many activities are pursued in the framework of the *Potamogeton praelongus* Rescue Programme [21]: monitoring of the populations and site-specific habitat factors in its localities, monitoring of the biodiversity and plant communities, management of biotopes with *P. praelongus*, rescue cultivations, in vitro cultures, gene banks, selection of potential localities and planting for reintroductions, and also popularisation of the rescue programme and presentation of the results.

Currently, particular interventions for the restoration of the Orlice River Oxbow near Stříbrný rybník Pond have been carried out (Fig. 4). Mud excavation was done in the entire oxbow (particular areas No. 1, 4, 5, 6, 7) except for the intact zones, leaving a 5–10 cm layer of sediment. Prior to the excavation, endangered aquatic macrophytes (*Potamogeton praelongus*, *P. alpinus*) were removed and temporarily grown in artificial pools. The mud excavation is intended to decrease the trophic status of the water and bottom substrate, which is a source of nutrients, especially of nitrogen and phosphorus, and allow better contact between the water column and the alkaline bedrock. A temporary lagoon for the excavated mud was established in particular area No. 8. Expansive species covers (*Nuphar lutea*, *Phalaris arundinacea*, *Glyceria maxima*) were removed during mud excavation to improve the competitive ability of *P. praelongus* and other precious species.

Reduction of the riparian vegetation with the aim to decrease the shading of the water surface and the amount of litterfall contributing to mud generation and water transparency decline was conducted during the autumn in particular areas No. 2

The new close-to-natural river bed created in the thick layer of the gravel deposit layer in the oxbow part below the outfall of the Stříbrný Stream (southern part of particular area No. 4) was considered as a preserved part with spontaneous restoration. There were only young individuals of trees removed and a small pool formed in the shaded and clogged oxbow part below the outfall of the Stříbrný Stream.

The functioning of the sedimentation reservoir on the Stříbrný Stream above its outfall into the oxbow was checked and regular removal of sediment and organic litterfall deposits from the reservoir was carried out in coopertion with the Hradec Králové municipality.

There are important targets for the future: 1. to remove pollution sources from the upper part of the oxbow (the TPA), which lie in the cottage area, 2. to remove pollution in the oxbow (the TPA) caused by the outlet from the Stříbrný Pond (regular monitoring and checking of the chemical parameters of the water below the outfall from the Stříbrný Pond, and preservation of important parameters suitable for organisms bound to the TPA), 3. to protect aquatic macrophytes from herbivorous fish and aquatic birds (to stop herbivorous fish husbandry and long-term residence of aquatic birds in the oxbow and on the Orlice River, to put up barriers against organisms browsing aquatic macrophytes).

Figure 4. Eight particular areas of the last native locality of Potamogeton praelongus in the Czech Republic, where interventions were carried out at the beginning of 2019: 1. upper part of oxbow, 2. riparian vegetation and trees, 3. Stříbrný Stream estuary, 4. spontaneously restored part of the oxbow, 5. muddy part with P. alpinus, Nuphar lutea, 6. part with P. praelongus, 7. lower part of the oxbow, 8. temporary lagoon for excavated mud

CONCLUSION

The sites of Potamogeton praelongus studied in four countries (Czech Republic, Poland, Norway and Sweden) varied in water depth, transparency, conductivity, temperature, and shade level. Nordic localities provide optimal site conditions for this aquatic species because of the high number of large and deep lakes in the non-intensively managed landscape and natural sources. Eutrophication and its consequences are the most important factors in the survival or extinction of P. praelongus not only in the CR but also in the whole of Central Europe.

The aim of the last native site of *Potamogeton praelongus* restoration is to decrease the trophic level by mud excavation and efficient protection of the site against pollution from various sources, build a semi-natural sedimentation dam (permeable for migrating animals) to eliminate sediment from Stříbrný Stream, and to reduce competitive macrophytes, riparian vegetation and shading trees. Differentiation of the water depth is important for a permeable protection of endangered macrophytes against ducks and other aquatic birds. Resting zones should be established for in-situ experiments.

ACKNOWLEDGMENT

REFERENCES

[1]. Z. Kaplan, *Potamogeton L. - rdest* (Potamogeton L – Long – stem Pondweed). In J. Chrtek (jun.), Z. Kaplan, J. Štěpánková, Eds. Flora of the Czech Republic 8. Academia (Prague): 330–378. 2010.

[2]. E. Hultén, The circumpolar plants. vol. 1. Vascular cryptogams, conifers, mono-cotyledons. Kungl. Sven. Vetenskap. Handl. Ser. 4, 8 (5): 1–280, 1964.

[3]. R. Prausová, Ed., *Potamogeton praelongus Wulfen*. Gaudeamus, University of Hradec Králové, 1–223. ISBN 978-80-7435-669-8, 2017.

[4]. [4]. S. J. Casper, and H.D. Krausch, *Sußwasserflora von Mitteeuropa*. Bd. 24, VEB Gustav Fischer Verlag (Stuttgart – New York), 1981.

[5]. R. Prausová, L. Adamec, M. Kitner, K. Pásek, and V. Dvořák, *The Conservation of Long-stalked Pondweed (Potamogeton praelongus) in the Czech Republic*. Příroda (Prague) 32: 17–37. http://www.ochranaprirody.cz/res/archive/239/029985.pdf?seek=1435738314, 2014

[6]. T. Rintanen, *Changes in the flora and vegetation of 113 Finnish lakes during 40 years*. Annales Botanici Fennici 33 (2): 101–122. ISSN 0003-3487, 1996.

[7]. M. Voge, *Ecological studies on water plants of 14 sites around Kangerlussuaq, southern West Greenland, with special regard to Potamogeton (Hamburg)*: 1–42. http://www.solo-tauchen.de/PDF/www04.pdf, 2002.

[8]. M. Mäemets, K. Palmik, M. Haldna, D. Sudnitsyna, and M. Melnik, *Eutrophication and macrophyte species rischness in the large shallow North-European Lake Peipsi*. Aquatic Botany 92: 273 – 280, 2010.

[9]. Š. Husák, and L. Adamec, *Rescue cultivation of threatened species of aquatic and wetland species at Institute of Botany of the Czech Academy of Sciences in Třeboň*. Příroda (Prague) 12: 7–26, 1998.

[10]. R. Prausová, P. Sikorová, and. L. Šafářová, *Generative reproduction of long stalked pondweed (Potamogeton praelongus Wulfen) in the laboratory*. Aquat. Bot. 120: 268–274. https://doi.org/10.1016/j.aquabot.2014.09.005, 2015.

[11]. M. Bilz, S.P. Kell, N. Maxted, and R.V. Lansdown, *European Red List of Vascular Plants*. Publications Office of the European Union (Luxembourg): 1–130. https://portals.iucn.org/library/sites/library/files/documents/RL-4-016.pdf, 2011.

[12]. V. Grulich, *Red list of vascular plants of the Czech Republic*. Preslia 84: 631–645, http://www.preslia.cz/P123Grulich.pdf, 2012.

[13]. J. Čeřovský, V. Feráková, J. Holub, Š. Maglocký, and F. Procházka, Eds., *Red Book of threatened and rare species of plants and animals in the CR and SR*. Vol. 5. Vascular Plants. Príroda a. s. (Bratislava): 1–456, 2001.

[14]. J. Danihelka, J. Chrtek, and Z. Kaplan, Eds., Checklist of vascular plants of the Czech Republic. Preslia 84: 647–811. https://www.preslia.cz/P123Danihelka.pdf/, 2012.

[15]. The Plant List, Version 1.1. Published on the Internet; http://www.theplantlist.org/ (accessed 1st January 2013), 2013.

[16]. C. J. F. Ter Braak, and P. Šmilauer, Canoco reference manual and user's guide: software for ordination, version 5.0. Microcomputer Power. (Ithaca, USA): 1–496, 2012.

[17]. M. T. O´Hare, K. A. Hutchinson, and R. T. Clarke, *The drag and reconfiguration experienced by five macrophytes from a lowland river*. Aquat Bot 86 (3): 253–259, https://doi.org/10.1016/j.aquabot.2006.11.004, 2012.

[18]. P. Lacoul, and B. Freedman, *Environmental influences on aquatic plants in freshwater ecosystems*. Environ. Rev. 14: 89–136. https://doi.org/10.1139/a06-001, 2006.

[19]. G. Bornette, and S. Puijalon, *Response of aquatic plants to abiotic factors: a review*. Aquat Sci 73(1): 1–14. https://doi.org/10.1007/S00027-010-0162-7, 2011.

[20]. H. Mäemets, and L. Freibert, *Coverage and depth limits of macrophytes as tools for classification of lakes*. Proc Estonian Acad Sci Biol Ecol. 56: 124–140. http://eap.ee/public/Ecology/2007/issue_2/bio-2007-2-4.pdf, 2007.

[21]. R. Prausová, J. Janová, and L. Adamec, *Rescue of the critically endangered long-stalked pondweed (Potamogeton praelongus) in the Czech Republic*. Acta Biol Slov. 54: 43–54, 2011.

A Review Investigation on Experimental Heat Transfer Enhancement Method by Using Twisted Tape

Toygun Dagdevir[1], Orhan Keklikcioglu[2] and Veysel Ozceyhan[3]

Abstract

Heat transfer enhancement is a critical and important phenomenon to save energy and cost, reduce size of the systems and protect the environment from the waste energy effects. Passive heat transfer enhancement method is the most used method since it does not require an energy input to the system. Twisted tape, coiled wire, dimpled surface are the most commonly used methods of the passive heat transfer enhancement method. In this paper, a detail review investigation is conducted on experimentally heat transfer enhancement method by many various configurations of the twisted tape. Addition to geometrical properties such as width, pitch, thickness, different processes implemented such as separated from the inner wall, perforated, center-cleared, jagged twisted tapes effects on thermal and hydraulic performance are examined and discussed. It is observed that the use of twisted tape is quite effectively method for heat transfer enhancement in a tube, since it generates swirl flow through the tube and destruct the thermal boundary layer. Moreover, another advantageous of the use of twisted tape is that to supple low pressure drop penalty compared with other inserts. It is concluded that the twisted tape will continue to use to improve heat transfer in energy conversion systems with more effective configurations.

Keywords: Twisted tape, Heat transfer enhancement, Pressure drop, Performance evaluation criteria

1. INTRODUCTION

Heat exchangers are commonly used in many industrial processes such as steam generation, chemical processes, energy conversation systems, food industries, waste heat recovery etc. Increase in the efficiency of the heat exchanger provides energy and cost savings. There are two methods to improve the efficiency of the heat exchangers: active method and passive method. There is an external energy requirement in the active method like vibration, electric or magnetic field [1]. However, the passive methods do not require any energy input to the system. Rough surfaces [2], coiled tubes [3], extended surfaces [4], corrugated tubes [5], and various inserts (twisted tapes, coiled wires, nozzles) [6, 7, 8] to the flow tube are mainly passive methods.

2. TWISTED TAPE INSERTS

This paper is a review research of using twisted tape on heat transfer and hydraulic performance investigations since from 2007 to 2018. Many heat transfer enhancement investigations by using several twisted tape configuration are available in literature. It is estimated that Smithberg is one of the first twisted tape users to use heat transfer enhancement method in 1961. [9]. Geometrical structure of typical twisted tape is illustrated in Fig. 1. In addition to various typical twisted tape configurations (different y, w and y/w ratios), several different twisted tape configuration is derived to more enhance heat transfer.

---

[1] *Corresponding author: Erciyes University, Department of Mechanical Engineering, 38039, Melikgazi/Kayseri, Turkey.*
  toygun@erciyes.edu.tr

[2] *Erciyes University, Department of Mechanical Engineering, 38039, Melikgazi/Kayseri, Turkey,*
  keklikcioglu@erciyes.edu.tr

[3] *Erciyes University, Department of Mechanical Engineering, 38039, Melikgazi/Kayseri, Turkey, ozceyhan@erciyes.edu.tr*
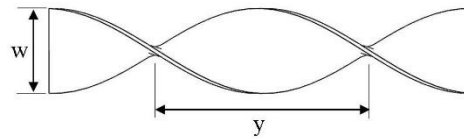
Figure 1. Typical twisted tape

To examine the effects of the inserts like twisted tape on heat transfer and flow characteristics an experimental setup is established by researchers. The experimental setups are generally established with consideration of a straight horizontal tube under constant heat flux, because almost all heat exchangers comprise the straight horizontal tube. Results on heat transfer enhancement by using twisted tapes having different structural properties in literature are summarized in Table 1. Table 1. shows the twisted tapes are used generally for turbulent flow conditions. However, the highest PEC or η is obtained for the lowest considered Re number. At the same time, over the range investigated in Table 1, the PEC / η is obtained higher than unity for almost all investigations.

3. CONCLUSION

To determine the heat transfer performance and hydraulic performance, some researchers used performance evaluation criteria (PEC). In other hand, some researchers used only heat transfer efficiency (η) to determine the performance of the heat exchangers equipped with twisted tape inserts. The literature review showed that used twisted tape in a tube provides high thermal performance, but increase the pressure drop penalty comparison with smooth tube. However, increase in heat transfer performance generally surpasses the increase in pressure drop penalty. Main reason of used twisted tape inserts in a tube is that generating swirl flow through the tube and gets more energy from the heated wall. Moreover, it is purposed to destruct the thermal and hydraulic boundary layer by various modification on the twisted tape.
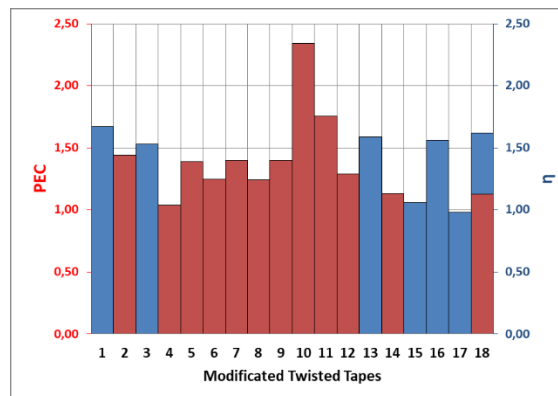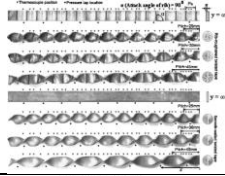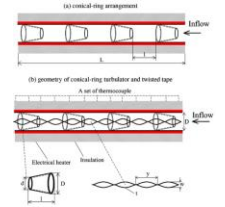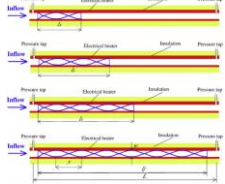
Figure 2. Best performance evaluation criteria (PEC) and heat transfer enhancement (η) results of the considered investigation in literature.
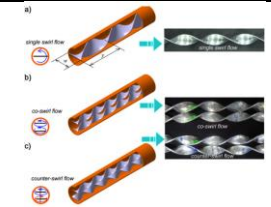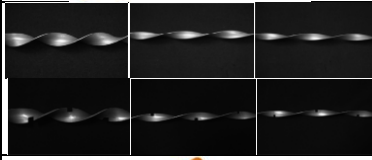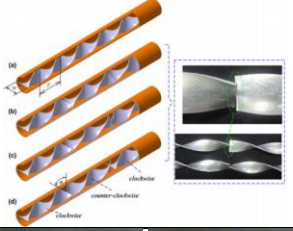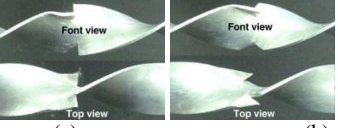
Over the considered investigations examined, the highest PEC value is obtained by Suresh et al with helical screw tape insert flowing Cuo/water nanofluid volume fraction (φ) of 0.1%. Actually, one of the reasons of this significant result is used CuO nanofluid. Increase in thermal conductivity of the fluid with addition of metal nanoparticle to base fluid, heat transfer dramatically enhances with/without insert. On the other hand, the Fig. 2 shows that PEC/η results reached to maximum 1.6 for the other investigations. As a conclusion, inserts generating swirl flow and destructing the thermal boundary layer enhance the heat transfer and improve the heat exchanger performance. Moreover, the used nanofluid is a promising method to improve heat exchanger performance in future.
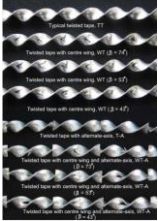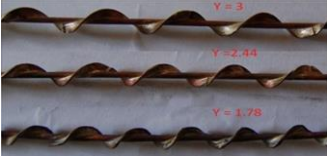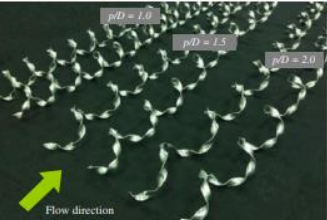
Table 2. Summary results of used twisted tape having various modifications on heat transfer enhancement in literature
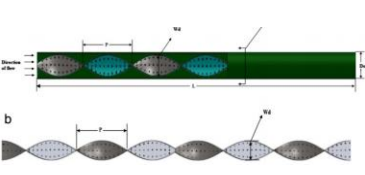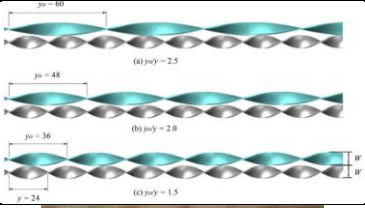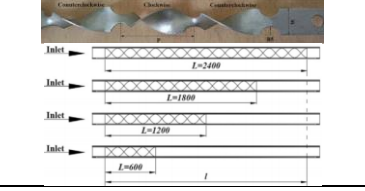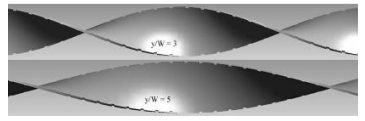
No	Year	Authors	Insert type	Illustration	Operating conditions	Best PEC/ η	Observation
1	2007	S. W. Chang, Y. J. Jan, J. S. Liou [10]	Serrated twisted tape		Working fluid: Water $5000 \leq Re \leq 25000$ $1.56 \leq TR \leq 2.81$	**PEC=1.67** for Re=5000, Smooth twisted tape, TR=1.56	The twisted tape showed better thermo-hydraulic performance results comparing with the serrated twisted tape. Increase in twist ratio (TR) cause to decrease in the PEC values.
2	2007	P. Promvonge, S. Eiamsa-ard [11]	Conical-ring and twisted tape		Working fluid: Air $6000 \leq Re \leq 26000$ $3.75 \leq TR \leq 7.5$	**η=1.44** for Re=6000, Conical-ring and twisted tape, TR=3.75	The enhancement efficiency decreases with the increase of Reynolds numbers and the decrease of twist ratio. This indicates that the conical-ring in combination with the twisted-tape is not beneficial in terms of energy saving at higher Reynolds number.
3	2008	P.Promvonge [12]	Twisted tape and wire coil turbulators		Working fluid: Air $3000 \leq Re \leq 18000$ $4 \leq TR \leq 6$ $4 \leq CR \leq 8$	**PEC=1.53** for Re=3745, CR=4, TR=4	The combined twisted tape and wire coil turbulator should be used instead of using a single one only. Moreover, to obtain the best performance, lowest values of coil spring pitch (CR) and twist ratio (TR) and Re number should be selected.
4	2009	S. Eiamsa-ard, C. Thianpong, P. Eiamsa-ard, P. Promvonge [13]	Short-length twisted tape		Working fluid: Air $4000 \leq Re \leq 20000$ $TR = 4$ $0.29 \leq LR \leq 1.0$	**η=1.04** for Re=4000, TR=4, LR=1	Although the shorter twisted tape presents lower pressure drop, heat transfer performance reduces as well. The heat transfer enhancement efficiency is obtained higher than unity only for the full-length twisted tape at lowest Re number.
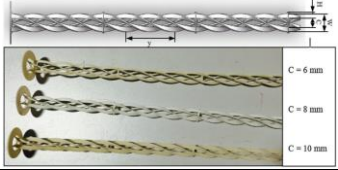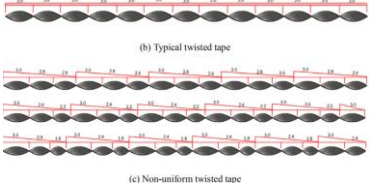
5	2010	S. Eiamsa-ard, C. Thianpong, P. Eiamsa-ard [14]	Twin twisted tape		Working fluid: Water $3700 \le Re \le 21000$ $2.5 \le TR \le 4.0$ Co-swirl and counter-swirl flow	**η=1.39** for Re=3700, Counter-swirl flow, TR = 2.5	Counter-swirl tape provides heat transfer more efficiently than the co-swirl tape, because counter swirl flow increases intensity of vortex strength.
6	2010	P. Murugesan, K. Mayilsamy and S. Suresh [15]	Square-cut twisted tape		Working fluid: Water $2000 \le Re \le 12000$ $2 \le TR \le 6$	**η=1.25** for Re=3000, Square twisted tape, TR = 2	STT provides an additional disturbance to the fluid in the vicinity of the tube wall and vorticity behind the cuts and thus leads to a higher heat transfer enhancement in comparison with plain tube and PTT.
7	2010	S. Eiamsa-ard and P. Promvonge [16]	Alternate clockwise and counter-clockwise twisted tape		Working fluid: Water $3000 \le Re \le 27000$ $3 \le TR \le 5$	**η=1.4** for Re=3000, counterclockwise, θ=90°, TR = 3	The periodic change of swirl direction from clockwise to counterclockwise directions and vice versa, causes the sudden change of fluid arrangement, giving better fluid mixing and uniform temperature. The higher twist angle offers the larger difference of plane direction for the adjacent twist lengths, providing more effective disturbance to the flowing fluid.
8	2010	S. Eiamsa-ard, K. Wongcharee, P. Eiamsa-ard, C. Thianpong [17]	Delta-winglet twisted tape	(a)　　　　　(b) straight delta-winglet　b) oblique delta-winglet	Working fluid: Water $3000 \le Re \le 27000$ $3 \le TR \le 5$ Depth of wing cut ratio (d/W)=0.11, 0.21, 0.32	**η=1.24** for Re=3000 Oblique delta-winglet d/W=0.32 TR=3	Oblique delta-winglet twisted tape more disturbed and increase degree of turbulence intensity than straight delta-winglet twisted tape.

9	2010	S. Eiamsa-ard, K. Wongcharee, P. Eiamsa-ard, C. Thianpong [18]	Centre wings and alternate-axes twisted tape		Working fluid: Water $5200 \leq Re \leq 22000$ TR = 3 (β = 43°, 53° and 74°)	**$\eta=1.4$** for Centre wings and alternate-axes twisted tape (WT-A) Re=3000 β = 74° TR=3	Combine reasons of the WT-A are : 1) common swirling flow by the twisted tape 2) a vortex generated by the wing 3) a strong collision of the recombined streams behind each alternate point.
10	2011	S. Suresh, K.P. Venkitaraj, P. Selvakumar [19]	Helical screw tape		Working fluid: Al_2O_3/water and CuO/water nanofluid $4900 \leq Pe \leq 13500$ $1.78 \leq TR \leq 3$ $\varphi=0.1\%$	**$\eta=2.34$** for Pe=4900 TR=1.78 CuO/water $\varphi=0.1\%$	Insertion of helical screw tape causes to excellent fluid mixing and an efficient redevelopment of the thermal/hydrodynamic boundary layer.
11	2012	H. Bas and V. Ozceyhan [20]	Twisted tape inserts placed separately from the tube wall		Working fluid: Air $5132 \leq Re \leq 24989$ $2 \leq TR \leq 4$ $0 \leq$ Clearance ratio (c/D) ≤ 0.0357	**PEC=1.756** for Re=5183 TR=2 c/D=0.0178	The twist ratio is more effective on heat transfer enhancement than the clearance ratio. The twisted tapes are placed separately from the tube wall to obtain only heat transfer increase depending on laminar sublayer destruction near the tube wall. So, the effect of increased heat transfer surface area is eliminated.
12	2013	K. Nanan, K. Yongsiri, K. Wongcharee, C. Thianpong, S. Eiamsa-ard [21]	Helically twisted tapes		Working fluid: Air $6000 \leq Re \leq 20000$ TR=3 $1 \leq$ Pitch Ratio (PR) ≤ 2	**$\eta=1.29$** for co-swirl flow helically twisted tape PR=2 Re=6000	Using helically twisted tape enhance the heat transfer considerably. Because the effect of the secondary flow–induced inserts, leading to the better mixing between the fluids near the tube wall and the core region.

13	2013	M.M.K. Bhuiya, M.S.U. Chowdhury, M. Saha, M.T. Islam [22]	Perforated twisted tape		Working fluid: Air $7200 \leq Re \leq 49800$ TR=3 $1.6\% \leq$ Porosity $(R_p) \leq 14.7\%$	**PEC=1.59** for Re=7200 R_P=4.5%	The perforated twisted tape inserts generated swirl flow or secondary flow offering a longer flowing path of fluid flow through the tube; intensive mixing of fluid and pressure gradient might be created along the radial direction. Due to the tangential velocity component and lower flow cross-sectional area, the mixing of fluid between the fluids at the wall region and fluid at the core region was induced by the generated centrifugal force had significant ability to enhance the heat transfer rate.
14	2015	S. Eiamsa-ard, K. Kiatkittipong, W. Jedsadaratanachai [23]	Overlapped dual twisted-tapes		Working fluid: TiO$_2$/water nanofluid $5400 \leq Re \leq 15200$ $1.5 \leq y_o/y \leq 2.5$ $0.07\% \leq \varphi \leq 0.21\%$	**η=1.13** for Re=5400 TR=1.5 TiO$_2$/water φ=0.21%	Thermal performance factor increased as yo/y of O-DTs decreased. This implies that by decreasing yo/y, the augmentation of the heat transfer was more pronounced than pressure drop penalty. The thermal performance factor of O-DTs tended to decrease with the increase of Reynolds number.
15	2016	C. Man, J. Yao, C. Wang [24]	Counter-clockwise, semi-circular cutted with various length twisted tapes		Working fluid: Water $11000 \leq Re \leq 27000$ $600 \leq L \leq 2400$	**PEC=1.06** for Re=11000 L=600	Twisted tape did not have obvious advantages compared to the plain tube in the experimental conditions. Twisted tape is actually more suitable for laminar and weak turbulent operating conditions
16	2018	R.M. Sarviya and V. Fuskele [25]	Twisted tape insert having continuous cut edges		Working fluid: Water $3000 \leq Re \leq 19000$ $3 \leq y/W \leq 5$	**PEC=1.56** for Re=3000 y/W=3	The continuous cut edges cause the flow to spiral along the tube length and disturb the entire flow field that leads to higher heat transfer rate. removal of viscous sub-layer near tube wall is presumed to take place due to the additional turbulence generated by the continuous cut edges of R-CCTT and thus leading to a superior heat transfer improvement than TT.

17	2018	Y. He, L. Liu, P. Li, L. Ma [26]	Cross hollow twisted tape inserts		Working fluid: Water 5600 ≤ Re ≤ 18000 6 ≤ hollow width (C) ≤ 10	**PEC=0.98** for Re=5600 C=10 mm	The tube fitted with cross hollow twisted tape inserts may not achieve the expected energy saving under turbulent flow. However, the tube with tape inserts is advantageous in terms of energy saving when Re is low.
18	2018	S. Eiamsa-arda, K. Wongcharee [27]	Non-uniform twisted tape		Working fluid: Ag/Water nanofluid 5210 ≤ Re ≤ 18000 1.8 ≤ y/W ≤ 3.010 0.007% ≤ φ ≤ 0.03%	**PEC=1.62 η=1.125** for Re=5210 y/W=3.0>2.4>1.8 φ=0.03%	The enhancing devices are more promising for energy saving at lower Reynolds numbers. The thermal performance factors associated with the use of non-uniform twisted-tapes (N-TT) with twist ratios (y/W) in series of 3.0>2.8>2.6, 3.0>2.6>2.2 and 3.0>2.4>1.8 were higher than those associated with the use of the typical twisted tape by around 1.3%, 3.0% and 4.6%, respectively.

ACKNOWLEDGEMENT

REFERENCES

[1] M. Omidi, M. Farhadi, M. Jafari, "A comprehensive review on double pipe heat exchangers", *Applied Thermal Engineering*, vol. 110, pp. 1075-1090, 2017.

[2] K. Nilpueng, S. Wongwises, "Experimental study of single-phase heat transfer and pressure drop inside a plate heat exchanger with a rough surface", *Experimental Thermal and Fluid Science*, vol. 68, pp. 268-275, 2015.

[3] M. Wang, M. Zheng, M. Chao, J. Yu, X. Zhang, L. Tian, "Experimental and CFD estimation of single-phase heat transfer in helically coiled tubes", *Progress in Nuclear Energy,* vol. 112, pp. 185-190, 2019.

[4] T. Dixit, I. Ghosh, "An experimental study on open cell metal foam as extended heat transfer surface", *Experimental Thermal and Fluid Science*, vol. 77, pp. 28-37, 2016.

[5] C.Qi, Y. Wan, C. Li, D. Han, Z. Rao, "Experimental and numerical research on the flow and heat transfer characteristics of TiO2-water nanofluids in a corrugated tube" *International Journal of Heat and Mass Transfer,* vol. 115, pp. 1072-1084, 2017

[6] N. Piriyarungrod, S. Eiamsa-ard, C. Thianpong, M. Pimsarn, K. Nanan, "Heat transfer enhancement by tapered twisted tape inserts", *Chemical Engineering and Processing: Process Intensification,* vol. 96, pp. 62-71, 2015.

[7] K. Abdul Hamida, W. H. Azmi, R. Mamat, K. V. Sharma, "Heat transfer performance of TiO_2–SiO_2 nanofluids in a tube with wire coil inserts", *Applied Thermal Engineering*, vol. 152, pp. 275-286, 2019.

[8] P. Promvonge, S. Eiamsa-ard, "Heat transfer enhancement in a tube with combined conical-nozzle inserts and swirl generator", *Energy Conversion and Management*, vol. 47, pp. 2867-2882, 2006.

[9] E. Smithberg, "An Investigation into the Heat Transfer and Friction Characteristics of Round Tubes with Twisted Tape Swirl Promoters", D. Eng. Sc. Thesis, Department of Mechanical Engineering, New York University, New York, N. Y., May, 1961.

[10] S. W. Chang, Y. J. Jan, J. S. Liou, "Turbulent heat transfer and pressure drop in tube fitted with serrated twisted tape", *International Journal of Thermal Sciences*, vol. 46, pp. 506-518, 2007

[11] P. Promvonge, S. Eiamsa-ard, "Heat transfer behaviors in a tube with combined conical-ring and twisted-tape insert", *International Communications in Heat and Mass Transfer*, vol. 34, pp. 849-859, 2007.

[12] P. Promvonge, "Thermal augmentation in circular tube with twisted tape and wire coil turbulators", *Energy Conversion and Management*, vol. 49, pp. 2949-2955, 2008.

[13] S. Eiamsa-ard, C. Thianpong, P. Eiamsa-ard, P. Promvonge, "Convective heat transfer in a circular tube with short-length twisted tape insert", *International Communications in Heat and Mass Transfer*, vol. 36, pp. 365-371, 2009.

[14] S. Eiamsa-ard, C. Thianpong, P. Eiamsa-ard "Turbulent heat transfer enhancement by counter/co-swirling flow in a tube fitted with twin twisted tapes", *Experimental Thermal and Fluid Science*, vol. 34, pp. 53-62, 2010

[15] P. Murugesan, K. Mayilsamy and S. Suresh, "Turbulent Heat Transfer and Pressure Drop in Tube Fitted with Square-cut Twisted Tape", *Fluid Flow And Transport Phenomena*, vol. 18, pp. 609-617, 2010.

[16] S. Eiamsa-ard and P. Promvonge, "Performance assessment in a heat exchanger tube with alternate clockwise and counter-clockwise twisted-tape inserts", *International Journal of Heat and Mass Transfer*, vol. 53, pp. 1364-1372, 2010.

[17] S. Eiamsa-ard, K. Wongcharee, P. Eiamsa-ard, C. Thianpong, "Heat transfer enhancement in a tube using delta-winglet twisted tape inserts", *Applied Thermal Engineering*, vol. 30, pp. 310-318, 2010.

[18] S. Eiamsa-ard, K. Wongcharee, P. Eiamsa-ard, C. Thianpong, "Thermohydraulic investigation of turbulent flow through a round tube equipped with twisted tapes consisting of centre wings and alternate-axes", *Experimental Thermal and Fluid Science*, vol. 34, pp. 1151-1161, 2010.

[19] S. Suresh, K.P. Venkitaraj, P. Selvakumar, "Comparative study on thermal performance of helical screw tape inserts in laminar flow using Al2O3/water and CuO/water nanofluids", *Superlattices and Microstructures*, vol. 49, pp. 608-622, 2011.

[20] H. Bas and V. Ozceyhan, "Heat transfer enhancement in a tube with twisted tape inserts placed separately from the tube wall", *Experimental Thermal and Fluid Science*, vol. 41, pp. 51-58, 2012.

[21] K. Nanan, K. Yongsiri, K. Wongcharee, C. Thianpong, S. Eiamsa-ard, "Heat transfer enhancement by helically twisted tapes inducing co- and counter-swirl flows", *International Communications in Heat and Mass Transfer*, vol. 46, pp. 67-73, 2013.

[22] M.M.K. Bhuiya, M.S.U. Chowdhury, M. Saha, M.T. Islam, "Heat transfer and friction factor characteristics in turbulent flow through a tube fitted with perforated twisted tape inserts", *International Communications in Heat and Mass Transfer,* vol. 46, pp. 49-57, 2013.

[23] S. Eiamsa-ard, K. Kiatkittipong, W. Jedsadaratanachai, "Heat transfer enhancement of TiO2/water nanofluid in a heat exchanger tube equipped with overlapped dual twisted-tapes, *Engineering Science and Technology, an International Journal*, vol. 18, pp. 336-350, 2015.

[24] C. Man, J. Yao, C. Wang, "The experimental study on the heat transfer and friction factor characteristics in tube with a new kind of twisted tape insert", *International Communications in Heat and Mass Transfer*, vol. 75, pp. 124-129, 2016.

[25] R.M. Sarviya, Veeresh Fuskel, "Heat Transfer and Pressure Dropina Circular Tube Fitted with Twisted Tape Insert Having Continuous Cut Edges", *Journal of Energy Storage*, vol. 19, pp. 10-14, 2018.

[26] Y. He, L. Liu, P. Li, L. Ma, "Experimental study on heat transfer enhancement characteristics of tube with cross hollow twisted tape inserts", Applied Thermal Engineering, vol. 131, pp. 743-749, 2018.

[27] S. Eiamsa-arda, K. Wongcharee, "Convective heat transfer enhancement using Ag-water nanofluid in a micro-fin tube combined with non-uniform twisted tape", *International Journal of Mechanical Sciences,* vol. 146, pp. 337-354, 2018.

Bending Behaviour of Carbon Fiber-Epoxy-CNT Composites: A Theoretical Approach

Umut Caliskan[1,2], Constantinos Soutis[2]

Abstract

The exceptional mechanical properties of carbon nanotubes (CNT), combined with their low density, offer scope for the development of nanotube reinforced composite materials. In the present study, three point bending analysis of the carbon fibre-epoxy-carbon nanotubes (CF/Ep/CNT) were investigated numerically. Halpin-Tsai model was employed to evaluate the material properties of two-phase composite consisted of uniformly distributed and randomly oriented carbon nanotubes through the epoxy resin matrix. Afterwards, the structural properties of carbon nanotubes reinforced polymer matrix, which is assumed as a matrix, and then, reinforced with continuous long carbon fibres, they are calculated by a fibre micromechanics approach. The influence of weight percentage of carbon nanotubes and fibre orientation angle on the bending characteristics of the CF/Ep/CNT composite plate is discussed in detail. A parametric modelling plug-in for bending analysis of composites is established using ABAQUS-Python scripting language.

Keywords: Nanocomposites, Carbon Nanotubes, Micromechanical Model, Three point bending.

1. INTRODUCTION

The exceptional mechanical properties of the CNTs, combined with their low density, offer scope for the development of fibre reinforced composite materials with superior thermos-mechanical behaviour. Multiscale laminated nanocomposite materials made of carbon fiber/polymer/carbon nanotubes offer high specific strength and stiffness, mechanical properties that are often required in high performance structural applications. Kim et al. [1] fabricated and characterised carbon fibre-reinforced epoxy composites modified with carbon nanotubes (CNTs). They used high-energy sonication to disperse CNTs in the resin, followed by infiltration of fibre preform with the resin/CNT mixture. They also studied the effects of sonication time on the mechanical properties of ''multiscale" composites, which contain reinforcements at varying scales. They used a combination of Halpin–Tsai equations and woven fiber micromechanics in hierarchy to predict the mechanical properties of multiscale composites. Arani et al. [2] investigated modelling and vibration analysis of carbon nanotubes/ fiber/ polymer composite microplates. Halpin-Tsai model was used to evaluate the material properties of two-phase composite consisted of uniformly distributed and randomly oriented carbon nanotubes through an epoxy resin matrix. They also calculated the structural properties of the nano reinforced polymer in the presence of E-Glass fibre using a micromechanics approach. The influences of various parameters such as the weight percentage of single-walled carbon nanotube, aspect ratio, and size effect on the vibration characteristics of microplate were discussed in detail. Their results indicated that the stability of Carbon nanotubes/fiber/polymer composite microplates can be improved by adding appropriate amount of carbon nanotubes. Kalaitzidou et al. [3] focused on the reinforcing efficiency of nanomaterials and the role of the reinforcement's dispersion and orientation on the nanocomposite's flexural and tensile modulus. They founded that graphite platelets are the best reinforcement in terms of flexural modulus whereas PAN-based carbon fibres cause the largest improvement in the tensile modulus. The importance of good dispersion within the polymer matrix and of perfect contact between the two phases was emphasised comparing the experimental modulus data to theoretical predictions by the Halpin-Tsai and Tandon-Weng

---

[1] *Corresponding author: Erciyes University, Department of Mechanical Engineering, 38039, Melikgazi/Kayseri, Turkey.*
ucaliskan@erciyes.edu.tr ; umut.caliskan@manchester.ac.uk

[2] *Northwest Composites Centre, School of Materials, University of Manchester, Oxford Road, Manchester, M13 9PL, UK.*
constantinos.soutis@manchester.ac.uk

models. Yung et al. [4] investigated nanocomposites consisting of an epoxy matrix filled with silicate clay particles. The properties of intercalated clusters of clay platelets were calculated by a rule of mixtures based on a parallel platelet system. The modified composite theory of Halpin–Tsai was applied to calculate the modulus of the nanocomposite as a function of the clay concentration for various parametric variations, including the exfoliation ratio, the particle/matrix stiffness ratio E_f/E_m, the particle volume fraction φ_f, and the particle aspect ratio L/t. The modified composite theory satisfactorily captured the stiffness behaviour of the polymer/clay composites. Sharma and Shukla [5] investigated the macro scale IM700 carbon fibre (CF) with amino modified multi-wall carbon nanotubes (MWCNT-NH2) within LY-556 epoxy matrix to produce three-phase, multi-scale composites. They used to high frequency probe sonication method for homogenous dispersion of CNTs. Mechanical characterisation of the multiscale composites fabricated by hand layup process included tensile, flexure and inter-laminar shear stress tests. The addition of small amounts of MWCNTs (up to 1.5 %wt) for the fabrication of multiscale composites resulted in a maximum enhancement in tensile strength of 23% , flexural modulus of 35%, flexural strength of 5% and ILSS of 7%. They characterised CF/epoxy composites (without CNTs) for comparison with MWCNT-NH2/CF/epoxy composites. Luo et al. [6] investigated a modified rule of mixtures for the experimentally observed nonlinear variation of tensile strength. A modified Halpin–Tsai model was presented to predict the Young's modulus of multiscale reinforced composites with both micron-sized and nano sized reinforcements. In the composites, both micron-sized fillers-carbon fibres and nano-sized fillers rubber nanoparticles and carbon nanotubes were added into the epoxy resin matrix. They used mechanical experiments and scanning electron microscopy observations to study the effects of the micro-sized and nano-sized reinforcements and their combination on tensile and toughness properties of the composite. The results showed that the combined use of multiscale reinforcements had synergetic effects on both the strength and the toughness of the composites. Montazeri et al. [7] fabricated MWNT/ epoxy composite samples by sonication technique using untreated and acid-treated multi-walled carbon nanotubes (MWNT). The effect of MWNT addition and their surface modification on the mechanical properties were investigated. Modified Halpin–Tasi equation was used to evaluate the Young's modulus and tensile strength of the MWNT/epoxy composite samples by the incorporation of an orientation as well as an exponential shape factor in the equation. There was a good correlation between the experimentally obtained Young's modulus and tensile strength values and the modified Halpin–Tsai theory. The fracture surfaces of MWNT/epoxy composite samples were analysed by scanning electron microscope. Rafiee et al. [8] investigated the nonlinear free vibration of carbon nanotubes/fiber/polymer composite (CNTFPC) multi-scale plates with surface-bonded piezoelectric actuators. They derived the governing equations of the piezoelectric nanotubes/fibre/polymer multi scale laminated composite plates based on first-order shear deformation plate theory (FSDT) and von Kármán geometrical nonlinearity. Halpin–Tsai equations and fibre micro mechanics were used in hierarchy to predict the bulk material properties of the multi scale composite. The carbon nano tubes were assumed to be uniformly distributed and randomly oriented through the epoxy resin matrix. The effects of the applied constant voltage, plate geometry, volume fraction of fibres and weight percentage of single-walled carbon nanotubes (SWCNTs) and multi-walled carbon nanotubes (MWCNTs) on the linear and nonlinear natural frequencies of the piezoelectric nanotubes/fiber/polymer multiscale composite plate were investigated through a detailed parametric study. In the present study the emphasis is on the numerical simulation of the flexural response of a CF/Ep/CNT composite plate; achievements and limtations are discussed. Manta et al. [9] validated recently developed numerical method that simulates the electrical response of a graphene/polymer nanocomposite with experimental data. Their approach was based on the multiscale method and consists of a unit cell and a representative volume element (RVE), accounting for aligned and randomly distributed nanoparticles. At the unit cell level, the material nano characteristics (filler geometry, constituent electrical and interfacial properties) were integrated into a local resistance algebraic matrix. The material architecture was then modelled at the micro-level (RVE) by a user-defined distribution of the unit cell electrical properties. A statistical sample was studied and the average electrical response was compared with measurements for direct (DC) and alternate current (AC). The model was proven to be an effective, flexible and time-efficient tool to design and optimize advanced nanocomposite systems. Gresil et al. [10] presented a quantitative dispersion characterisation method using non-contact infrared thermography mapping that measures the thermal diffusivity (α) of the graphene nanocomposite and related α to a dispersion index. The main advantage of the proposed method was its ability to evaluate dispersion over a large area at reduced effort and cost, in addition to measuring the thermal properties of the system. The actual resolution of this thermal mapping reached 200 μm per pixel giving an accurate picture of graphene nanoplatelets (GNP) dispersion. The post-dispersion treatment showed an improvement in directional thermal conductivity of the composite of up to 400% increase at 5 wt% of GNP. The Maxwell-Garnet effective medium approximation was proposed to estimate thermal conductivity that compare favourably to measured data.

2. MODELLING METHOD

Mechanical properties of nanostructured materials can be determined by a select set of computational methods. These modelling methods span a wide range of length and time scales, as shown in Figure 1. For the smallest length and time scales, Computational Chemistry techniques are primarily used to predict atomic structure using first-principles theory. For the largest length and time scales, Computational Mechanics is used to predict the mechanical behaviour of materials and engineering structures. Computational Chemistry and Computational

Mechanics modelling methods are based on thoroughly established principles that have been developed in science and engineering. However, the intermediate length and time scales do not have general modelling methods that are as well-developed as those on the smallest and largest time and length scales. Therefore, multiscale modelling techniques are employed, which take advantage of Computational Chemistry and Computational Mechanics methods simultaneously for the prediction of the structure and properties of materials.
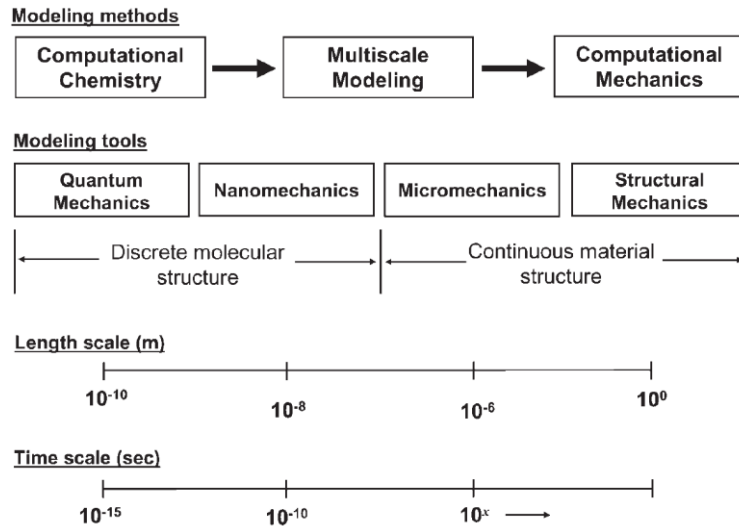
Figure 1. Various length and time scales used in determining mechanical properties of polymer nanocomposites [11].

Figure 2 is a schematic that details the relationship of specific modeling techniques in Computational Mechanics and Computational Chemistry. The continuum-based methods primarily include techniques such as the Finite Element Method (FEM), the Boundary Element Method (BEM), and the micromechanics approach developed for composite materials. Each of these continuum and molecular based modeling methods are described below.
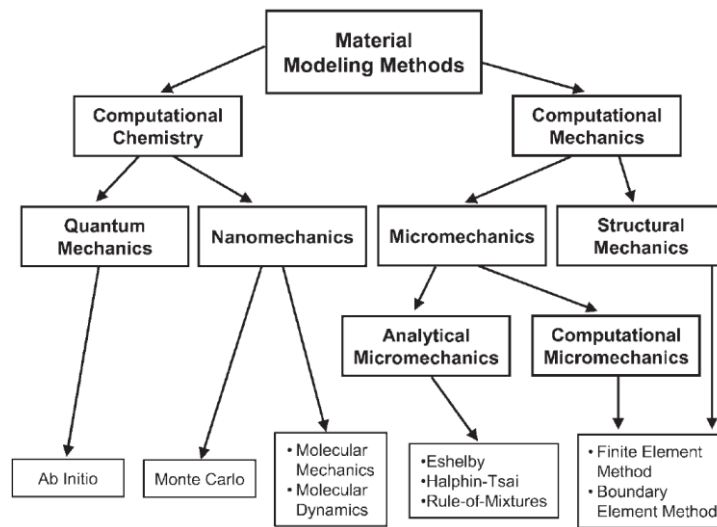
Figure 2. Diagram of material modelling techniques [11].

o   ***Theoretical formulation***

These modelling methods assume the existence of continuum for all calculations and generally do not include the chemical interactions between the constituent phases of the composite. These methods can be classified as either analytical or computational. It is assumed that the three-phase CNTs/fiber/polymer multiscale laminated composite plate host is made from a mixture of isotropic matrix (epoxy resin), CNTs and fibers (E-glass) with different alignments for each lamina through the thickness. The carbon nanotube composites are regarded as isotropic, as the CNTs are assumed to be uniformly distributed and randomly oriented through the matrix. The effective material properties of the three-phase CNTs/fiber/polymer multiscale laminated composite can be predicted according to a combination of Halpin–Tsai scheme and micromechanics approach via two steps in the hierarchy as shown in Figure 3.
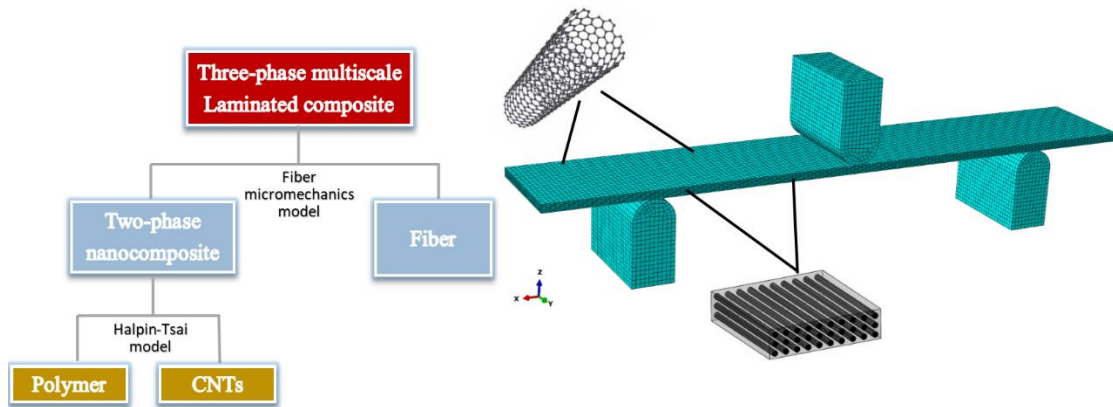
Figure 3. Hierarchy of the three-phase fiber/polymer/CNT multiscale composite and finite element model.

The elastic material properties of the nanocomposite can be predicted by combining first CNT and polymer using the Halpin-Tsai model to form two phase nanocomposite. The effective material properties of the two phase nanocomposite are known to be isotropic and can be predicted by using the below given equations. The tensile modulus of nanocomposites according to the Halpin-Tsai model can be expressed as: [2],

$$E^{MNC} = \frac{E^{MER}}{8}\left[5\left(\frac{1+2B_{dd}V_{CN}}{1-B_{dd}V_{CN}}\right) + 3\left(\frac{1+2\left(\frac{l^{CN}}{d^{CN}}\right)B_{dL}V_{CN}}{1-B_{dL}V_{CN}}\right)\right] \tag{1}$$

Where,

$$B_{dl} = \frac{\left(\frac{E_{11}^{CN}}{E^{MER}}\right)-\left(\frac{d^{CN}}{4t^{CN}}\right)}{\left(\frac{E_{11}^{CN}}{E^{MER}}\right)+\left(\frac{l^{CN}}{2t^{CN}}\right)} \tag{2}$$

$$B_{dl} = \frac{\left(\frac{E_{11}^{CN}}{E^{MER}}\right)-\left(\frac{d^{CN}}{4t^{CN}}\right)}{\left(\frac{E_{11}^{CN}}{E^{MER}}\right)+\left(\frac{d^{CN}}{2t^{CN}}\right)} \tag{3}$$

Where,

E_{11}^{CN} = Young's modulus of CNTs,

V_{CN} = volume fraction of CNTs,

l^{CN} = length of CNTs,

d^{CN} = outer diameter of CNTs,

t^{CN} = thickness of CNTs,

V_{MER} = volume fraction of isotropic epoxy resin matrix,

E^{MER} = Young's modulus of isotropic epoxy resin matrix.

From the above formulations the volume fraction of CNTs could be expressed as,

$$V_{CN} = \frac{w^{CN}}{w^{CN} + (\rho^{CN}/\rho^{MER}) - (\rho^{CN}/\rho^{MER})w^{CN}}$$

(4)

Where,

w^{CN} = mass fraction of CNTs,

ρ^{CN} = mass density of CNT,

ρ^{MER} = mass density of epoxy resin matrix.

And the Poisson's ratio and mass density of nanocomposite could be expressed as

$$v^{MNC} = v^{MER}$$
(5)

$$\rho^{MNC} = V_{CN}\rho^{CN} + V_{MER}\rho^{MER}$$
(6)

Where,

v^{MER} = Poisson's ratio of epoxy matrix,

v^{MNC} = Poisson's ratio of nanocomposite.

The shear modulus of matrix phase can be calculated by:

$$G^{MER} = \frac{E^{MER}}{2(1+v^{MER})}$$
(7)

The elastic properties of the microplate can be determined by Micromechanics approach as follows [2]

$$E_{11} = E_{11}^f V^f + E^m V^m$$
(8)

$$\frac{1}{E_{22}} = \frac{V^f}{E_{22}^f} + \frac{V^m}{E^m}$$
(9)

$$\frac{1}{G_{12}} = \frac{V^f}{G_{12}^f} + \frac{V^m}{G^m}$$
(10)

$$\rho^C = \rho^f V^f + \rho^m V^m$$
(11)

$$\rho^C = \rho^f V^f + \rho^m V^m$$
(12)

$$v_{12} = v_{12}^f V^f + v^m V^m$$
(13)

Where E_{11} and E_{22} are longitudinal and transverse Young's moduli, respectively. Also, G_{12} is in plane shear modulus.

The three-point bending flexural test provides values for the modulus of elasticity in bending E_f, flexural stress σ_f, flexural strain ε_f and the flexural stress–strain response of the material. The main advantage of a three-point flexural test is the ease of the specimen preparation and testing.

Calculation of the flexural stress σ_f,,

$$\sigma_f = \frac{3FL}{2bd^2}$$

(14)

Calculation of the flexural strain ε_f,

$$\varepsilon_f = \frac{6Dd}{L^2}$$

(15)

Calculation of the flexural modulus E_f,

$$E_f = \frac{L^3 m}{4bd^3}$$

(16)

in these formulae the following parameters are used:

σ_f, Stress in outer surface at midpoint, (MPa)

ε_f, Strain in the outer surface, (mm/mm)

E_f, Flexural Modulus of elasticity, (MPa)

F, Load at a given point on the load deflection curve, (N)

L, Support span, (mm)

b, Width of test beam, (mm)

d, Depth or thickness of tested beam, (mm)

D, Maximum deflection of the centre of the beam, (mm)

m, The gradient (i.e., slope) of the initial straight-line portion of the load deflection curve, (N/mm)

o   ***Finite Element Model***

In this study, three point bending analysis of the carbon fiber-epoxy-carbon nanotubes were investigated numerically. Halpin-Tsai model was utilised to evaluate the material properties of the two-phase nano modified composite consisted of uniformly distributed and randomly oriented carbon nanotubes in an epoxy resin matrix. The effects of the weight fraction of CNTs (2, 4, 6, 8 and 10%) and fibre orientation angle (0º, 45º and 90º) were also investigated. The 3D solid finite element (C3D8R) and orthotropic material model were used to simulate the response of the 8-ply composite laminate, as shown in Fig.3. Material properties of carbon fibre, epoxy resin and CNTs are presented in Table 1.

The supports related with three-point bending model was modelled as rigid body behaviour. The encastered boundary condition was applied to the bottom supports. Ten millimetres displacement was applied to the top apparatus (loading point) after pre-studies. So, the maximum force and displacement were calculated under these conditions. The hourglass control was also used for the finite elements of core material as another option to avoid excessive element distortions and calculate numerical integrations accurately. The mechanical contact between composite plate and rigid supports was simulated by surface to surface contact algorithm in ABAQUS [12].

Table 1. Material properties of carbon fibre, epoxy resin and CNTs

Symbol	Value	Unit	Description
Single-walled carbon nanotubes			
t^{CN}	0.34x10⁻⁹	m	Thickness of carbon nanotubes
d^{CN}	1.4x10⁻⁹	m	Outer diameter of carbon nanotubes
l^{CN}	25x10⁻⁹	m	Length of carbon nanotubes
w^{CN}	2,4,6,8,10	%	Weight percentage of carbon nanotubes
ρ^{CN}	1350	kg/m³	Mass density of carbon nanotubes
E_{11}^{CN}	2x10¹²	kg/m²	Young's modulus of carbon nanotubes
v^{MNC}	0.33		Poisson's ratio of carbon nanotubes

Epoxy resin polymer matrix

ρ^{MER}	1294	kg/m^3	Mass density of epoxy resin matrix
E^{MER}	3x10^9	Pa	Young's modulus of epoxy resin matrix
v^{MER}	0.33	kg/m^2	Poisson's ratio of epoxy resin matrix

Carbon fibre

V^f	0.55	%	Fiber volume ratio
ρ^f	1743	kg/m^3	Density of carbon fibres
E_{11}^f	259.1x10^9	kg/m^2	Longitudinal Young's modulus
E_{22}^f	13.9x10^9	kg/m^2	Transverse Young's modulus
G_{12}^f	50.9x10^9	kg/m^2	In-plane shear modulus
G_{23}^f	8.2x10^9	kg/m^2	Out-of-plane shear modulus
v_{12}^f	0.26		In-plane Poisson's ratio,
v_{23}^f	0.3		Out-of-plane Poisson's ratio

3.   RESULTS

There are several articles in the literature discussing the Halphin-Tsai Model and CNTs. These researches are about generally on the mechanical properties of fiber-epoxy-CNTs. The accuracy of the Halphin-Tsai Model for CNTs has been validated in the literature by experimental data. In this study, three point bending behaviour of CF composite plates reinforced with CNTs was investigated by using three-dimensional non-linear finite element method for different weight percentage of CNTs and fibre angle in the ABAQUS/Standard [10]. The composite plate is made of 8 of unidirectional (UD) carbon fibre plies. Three different fibre orientations of 0º, 45º and 90º and five different weight percentage of CNTS as 2, 4, 6, 8 and 10% were assumed for the composite plate.
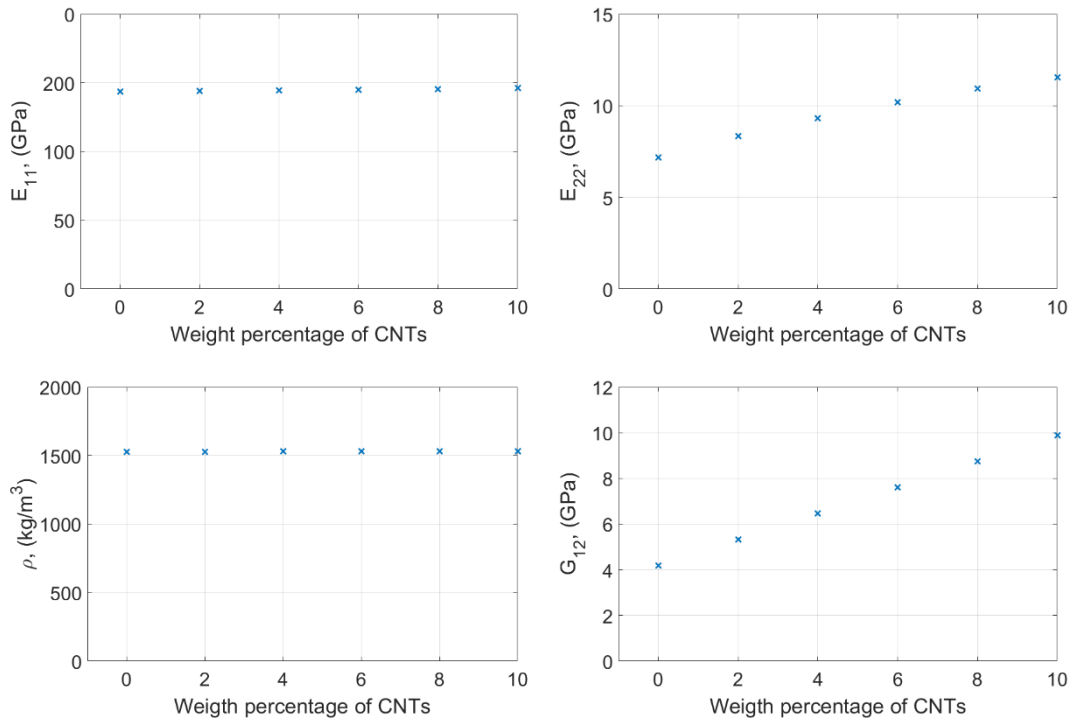
Figure 4. The effect of fibre angle and weight fraction of CNTs on the mechanical properties of carbon fibre-epoxy-CNTs composites

Figure 4 shows the variation of mechanical properties as function of percentage weight of CNTs in terms of E_{11}, E_{22}, G_{12} and ρ. The carbon fibre exhibits quite high strength in the longitudinal direction. There is no significant change with the addition of CNTs in longitudinal elastic modulus and density. However, for the transverse direction, there is significant change. This is also the case for the in-plane shear modulus.

The effect of the fiber angle and weight fraction of CNTs on the force-displacement variation of the carbon fiber-epoxy-CNTs composites under three-point bending is shown in Figure 5. As the weight fraction of CNTs is increased, the force levels increase. However, the changing of maximum forces is quite less for the composite plates with 0° fiber angle. The reason of this case, the longitudinal mechanical properties with CNTs remain almost same. The maximum forces of the 0° fiber angle composite plates with 0, 2, 4, 6, 8 and 10% CNTs are 1333, 1367, 1401, 1433, 1465 and 1497 N, respectively. The corresponding displacement to the maximum forces is about 9.29 mm. For the 45° fiber angle with different weight fraction of CNTs, the maximum forces are 205, 242.7, 278.1, 313.4 and 347.5, respectively. The corresponding displacements are 9.66, 9.59, 9.59, 9.51 and 9.51, respectively. As the fiber angle is increased, the maximum forces decreased and the corresponding displacements increased. As the composite plate with 90° fiber angle is considered, the maximum forces on the composite plates with weight fraction of 0, 2, 4, 6, 8 and 10% CNTs are 84.41, 97.93, 111.3, 123.5, 134.8 and 145.2, respectively and the corresponding displacements are about 9.81 mm for all plates. As the fiber angle is increased from 0° to 90°, the maximum force changes form 1400 N to 100 N. As the weight fraction of CNTs is increased, the maximum forces are increased. These cases are more apparent in the composite plates with 45° and 90° fiber angle. Because, the mechanical properties of the composite plate in the transverse direction change with increasing weight fraction of CNTs.

Fiber angle =0°

Fiber angle =45°

Fiber angle =90°

Fiber angle =0°, 45°, 90°
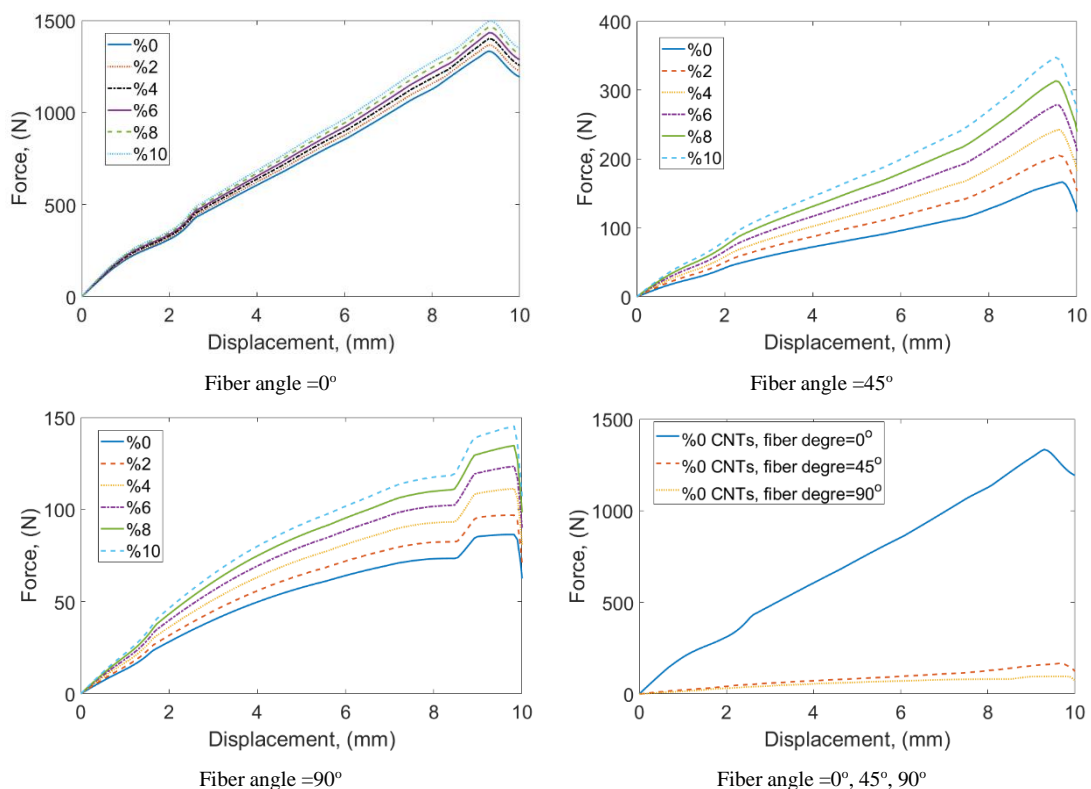
Figure 5. The effect of fibre angle and weight fraction of CNTs on the force-displacement of the carbon fiber-epoxy-CNTs composites under three-point bending.

Table 2. The effect of the fibre angle and weight fraction of CNTs on the flexural stress, stain and modulus of the carbon fibre-epoxy-CNTs composites under three-point bending

	σ_f (GPa)			ε_f			E_f (GPa)		
	0°	45°	90°	0°	45°	90°	0°	45°	90°
0%	1.99	0.25	0.13	0.01	0.01	0.01	179.3	21.5	11.1
2%	2.05	0.31	0.15	0.01	0.01	0.01	183.9	26.7	12.5
4%	2.10	0.36	0.17	0.01	0.01	0.01	188.5	31.6	14.1
6%	2.15	0.42	0.19	0.01	0.01	0.01	192.8	36.2	15.7
8%	2.20	0.47	0.20	0.01	0.01	0.01	197.1	41.2	17.2
10%	2.25	0.52	0.22	0.01	0.01	0.01	201.4	45.7	18.5

Table 2 shows the effect of the fiber angle and weight fraction of CNTs on the flexural stress, stain and modulus of the carbon fiber-epoxy-CNTs composites under three-point bending. The flexural stress in the middle region of composite plate increases with increasing weight fraction of CNTs. However, flexural strain remains same. Because, all displacements similar for all maximum forces. The flexural stresses and modulus change for composite plate with 0° fiber angle from 1.99 GPa to 2.25 GPa and from 179.3 GPa and 201.4 GPa, respectively, for the composite plate with 45° fiber angle from 0.25 GPa to 0.52 GPa and from 21.5 GPa to 45.7 GPa, respectively, for the composite plate with 90° fiber angle from 0.13 GPa to 0.22 GPa and from 11.1 GPa to 18.5 GPa for the weight fraction from 0 to 10% CNTs, respectively. The changing fiber angle affected all results quite more. It is seen more apparent in Table 2.

Figure 6 shows the effect of the fiber angle and weight fraction of CNTs on the Von-Misses stress distribution of the carbon fiber-epoxy-CNTs composites under three-point bending. The Von-Misses stresses are similar the flexural stresses. Stress distribution is on the fiber direction. The increasing weight fraction of CNTs affected quite more Von-Misses stress values for the composite plate with 90° fiber angle.

Fiber angle = 0°, 0% CNTs

Fiber angle = 0°, 10% CNTs

Fiber angle = 45°, 0% CNTs

Fiber angle = 45°, 10% CNTs

<div align="center">

Fiber angle = 90º, 0% CNTs   Fiber angle = 90º, 10% CNTs

</div>
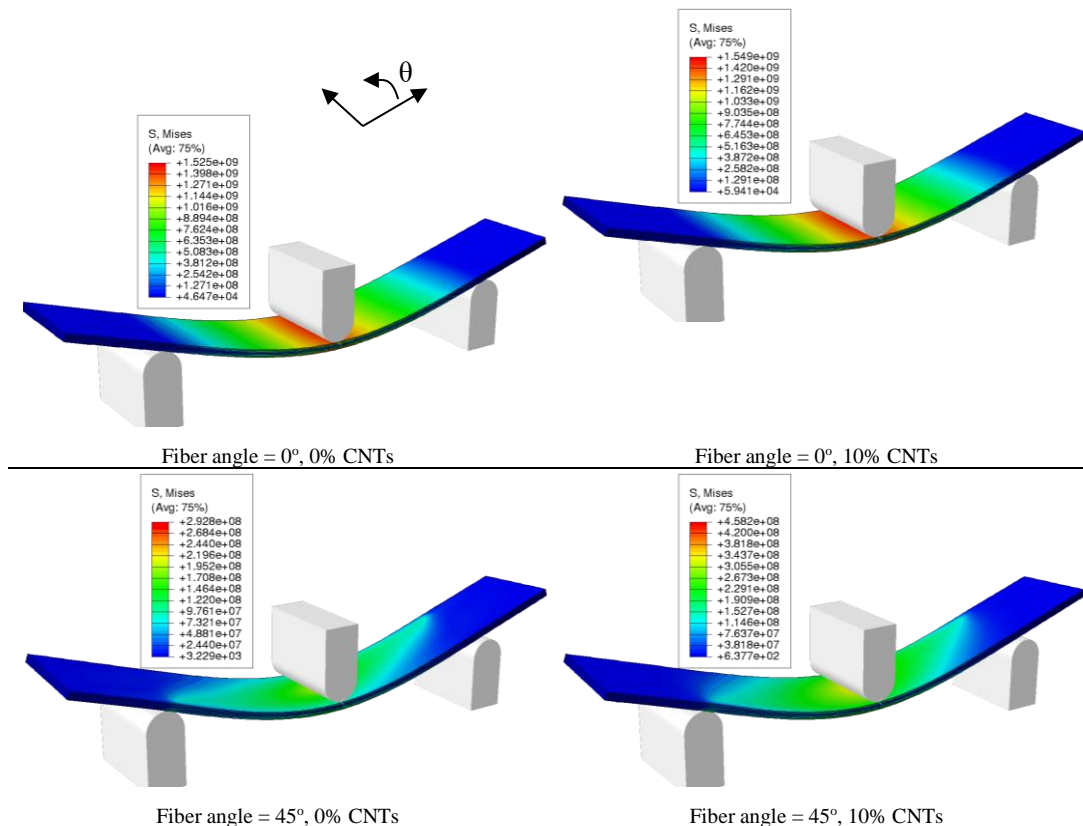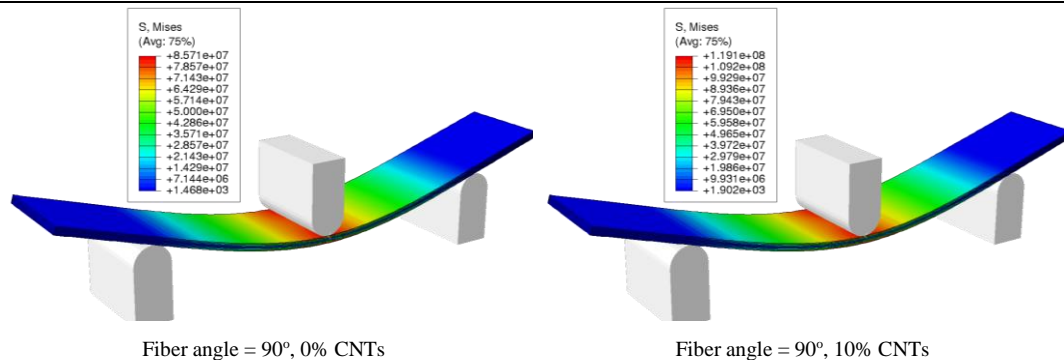
Figure 6. Effect of fibre angle and %wt of CNTs on the Von-Misses stress distribution of the carbon fibre-epoxy-CNTs composites under three-point bending.

REFERENCES

[1] M. Kim, Y.B. Park, O. I. Okoli and C. Zhang, "*Processing, characterization, and modeling of carbon nanotube-reinforced multiscale composites," Composites Science and Technology,* vol. 69, pp. 335-342, 2009.

[2] G. Arani, B.A. Zarei and E. Haghparast, *"Application of Halpin-Tsai Method in Modelling and Size-dependent Vibration Analysis of cnts/fiber/polymer Composite Microplates", Journal of Computational and Applied Mechanics,* vol. 47, pp. 45-52, 2016.

[3] K. Kalaitzidou, H. Fukushima, H. Miyagawa and L. T. Drzal, *"Flexural and tensile moduli of polypropylene nanocomposites and comparison of experimental data to halpin-tsai and tandon-weng models", Polymer Engineering and Science,* vol. 47, pp. 1796-1803, 2007.

[4] K. C. Yung, J. Wang and T. M. Yue, "*Modeling young's modulus of polymer-layered silicate nanocomposites using a modified halpin–tsai micromechanical model*", *Journal Of Reinforced Plastics and Composites,* vol. 25, pp. 847-861, 2006.

[5] K. Sharma and M. Shukla, "*Experimental Study of Mechanical Properties of Multiscale Carbon Fiber-Epoxy-CNT Composites*", *Advanced Materials Research*, Vols. 383-390, pp. 2723-2727, 2012.

[6] Z. Luo, X. Li, J. Shang, H. Zhu and D. Fang, "*Modified rule of mixtures and Halpin–Tsai model for prediction of tensile strength of micron-sized reinforced composites and Young's modulus of multiscale reinforced composites for direct extrusion fabrication*", "*Advances in Mechanical Engineering*", vol. 10, pp. 1-7, 2018.

[7] A. Montazeri, J. Javadpour, A. Khavandi and A. Tcharkhtchi and A. Mohajeri, "*Mechanical properties of multi-walled carbon nanotube/epoxy composites*", *Materials and Design,* vol. 31, pp. 4202-4208, 2010.

[8] M. Rafiee, X. F. Liu, X. Q. He and S. Kitipornchai, "*Geometrically nonlinear free vibration of shear deformable piezoelectric carbon nanotube/fiber/polymer multiscale laminated composite plates*", *Journal of Sound and Vibration,* vol. 333, pp. 3236-3251, 2014.

[9] A. Manta, M Gresil, and C Soutis, "*Simulated electrical response of randomly distributed and aligned graphene/polymer nanocomposites*", *Composite Structures,* vol. 192, pp. 452-459, 2018.

[10] M. Gresil, Z. Wang, Q. A. Poutrel and C. Soutis, "*Thermal Diffusivity Mapping of Graphene Based Polymer Nanocomposites*", *www.nature.com/scientificreports,* vol. 7, pp. 5536, 2017.

[11] P. K. Valavala and G. M. Odegard, "*Modeling techniques for determination of mechanical properties of polymer nanocomposites*", Reviews On Advanced Materials Science, vol. 9, pp. 34-44, 2005.

[12] ABAQUS/Standart (Version 2019), User's manual, Finite Element Software. Available from: http://www.simulia. Com

Influence of Current Type and Shielding Gas on Weld Beads of TIG-Welded ANSI 304 Stainless Steel

Simge Gencalp Irizalp[1], Gaye Ceren Emre[2]

Abstract

In this study, the effects of shielding gas and current type on tungsten inert gas welded ANSI 304 stainless steel were investigated. Tungsten inert gas (TIG) welding is widely used in any structural applications of this steel. TIG welding is preferred in stainless steel because of its high quality weldments and its lower equipment investment. By using the TIG welding method, which is widely used in the stainless steel industry, it is critical to obtain a good appearance of weld joints as well as the weld beam which has full penetration and good mechanical properties. In this study, pulsed current and conventional continuous current were used as the current type and Ar and He gases were used as the shielding gas. Penetration, microstructure and hardness were examined. Weld bead width was increased when current values increased from 50A to 70A. The conventional continuous current results in better penetration than the pulsed current, as well as increasing the weld bead width. The effects of helium and argon gases on the weld bead varied with the current. The conventional continuous current has a more uniform weld line than the pulsed current. As a result, both the current type and the shielding gas effects are thought to be responsible for increasing the efficiency of the weld and improving the appearance of the stainless steel weld joints.

Keywords: TIG welding, shielding gas, ANSI 304 stainless steel, weld morphology

1. INTRODUCTION

Austenitic stainless steels are widely used in the sheet metal industry and in the nuclear, chemical and medical industries as well as in high-performance pressure vessels. Moreover, mostly they have superior corrosion resistance and plastic deformability properties. They have outstanding properties compared to other structural steels. The preferred welding method for stainless steel is frequently TIG for its low cost and easy application. [1]. TIG welding is widely used in the construction of buildings and in the aerospace, automotive, chemical and electronic industries [2]. It is an electric arc welding process, and well known that fusion energy produced between tungsten electrode and work piece. The arc region is protected by inert gases or mixed gases from the negative impact of the environment [3-4]. The weldability of this steel type, which is so widely used and has good properties, is always interesting and continuous to be investigated. As is known, material properties are directly associated with microstructure. The fabrication of weldments can also be performed using conventional continuous current or pulsed current. Pulsed current welding is a joining technology, which is a variant of the conventional continuous current welding utilized in a wide range of applications. Some studies have reported that the pulsed current TIG welding has numerous advantages [5-9]. The difference between pulsed current and continuous current welding is usually due to the heat input. In pulsed current welding, total heat input to the weld is reduced. A decrease in the total heat input results in a reduction of the weld bead width, and also the residual stress, distortion, humping and porosity defects decreases. Continuous current gas tungsten arc welding is widely employed technique in many fields. The current type directly affects the microstructure, and so the material properties. In the fusion welding process, three different zones are observed at the welding: fusion zone or weld zone, heat affected zone and base metal. In conventional continuous current welding, fusion zones generally display coarse columnar dendrites because of the cooling behavior during the solidification of the weld metal [9]. Pulsed current welding modifies the grain morphology. It aims to minimize residual stress and defects by inducing

---

[1] *Corresponding author: Manisa Celal Bayar University, Department of Mechanical Engineering, 45140, Yunusemre/Manisa, Turkey.* simge.gencalp@cbu.edu.tr

[2] *Manisa Celal Bayar University, Department of Mechanical Engineering, 45140, Yunusemre/Manisa, Turkey,* gaye.ceren@hotmail.com

a controlled heat input. Shielding gas is critical, especially for a better penetration and independent of internal layer defects [10].

Researches have shown that the low heat input brings the uniform weld bead contour, less residual stress and distortion [9, 11]. As well as a number of metallurgical properties related to welding beam increase the mechanical performance of the welded material, such as the refining of the grain structure of the fusion zone, a narrow heat affected zone, a narrow weld beam and control of the segregation. This paper described the effect of two different protective gases (Argon and Helium) and the effect of the current types (continuous and pulsed) on the metallurgical and mechanical properties of the TIG welded ANSI 304 stainless steel joint.

2. EXPERIMENTAL PROCEDURE

ANSI 304 austenitic stainless steel plates with the dimensions 100x100x2mm were used for welding experiments. Chemical composition of the as received material according to the certificate was given in Table 1. Autogenous bead-on-plate welding procedure was fabricated without filler metal addition in single pass operation along the center of the plates. High purity (99.99%) Argon and high purity (99.99%) Helium gases were used as two different shielding gases with a flow rate 12 lpm. The welding procedure was carried out under both constant current mode (conventional continuous current TIG welding-CCTIG) and pulse current mode (pulsed current TIG welding-PCTIG). In constant mode, the welding process is carried out at a constant current value. The pulsed current welding is a joining technology where constant welding current is changed. In pulsed current mode, the welding current varies quickly between two levels. The high current level is known as pulse current, while the low current level is called as background current [7, 8, 12]. The pulsed current mode used in this study was defined in Figure 1. The welding parameters used in this investigation were shown in Table 2. Welded samples were cut as shown in Figure 2. Weld bead widths were measured in stereo microscope (SM). Samples were moulded from the sampling area as shown in Figure 2 for optical microscope (OM) examinations. For metallographic examinations, a sample of facet was set to include the base metal, HAZ and fusion zone. The moulded samples were polished metallographically. After polishing, they were etched in "15cc HCl+10cc HNO_3+10cc acetic acid+2/3 drops glycerine" solution to reveal the microstructures. The microstructural characterization of the weldments was carried out by an optical microscope (Nikon Eclipse LV150N). Microhardness test was performed in both longitudinal direction (from base metal to weld metal) with a load of 500g by Vickers indenter (Future-Tech Corp FM-700).

Table 1. Chemical composition of ANSI 304 austenitic stainless steel

C	Si	Mn	P	S	Cr	Ni	Fe
0.08	0.75	2.00	0.045	0.030	18-20	8-10.5	Balance
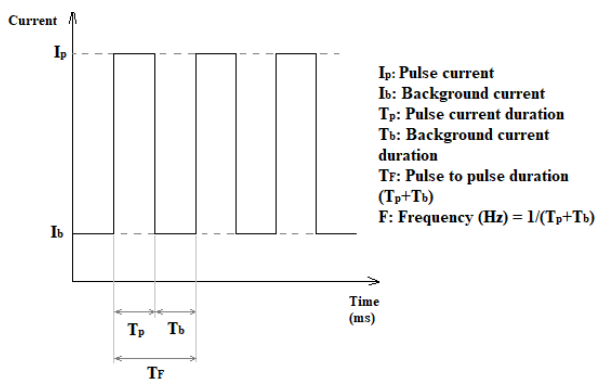
Figure 1. Pulsed current mode
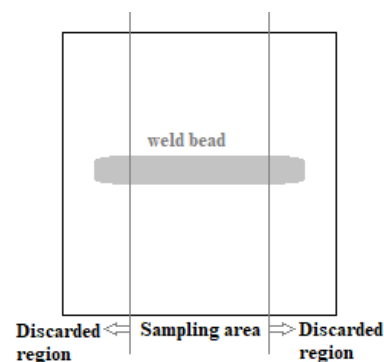
Figure 2. Schematic illustration of welded sample and showing the location of cross-sectioning and sampling area

3. RESULTS AND DISCUSSION

3.1. *Effect of pulsed current on heat input*

The total welding time was the range of 52-55 s. And length of weld bead was set at 64-65 mm. Accordingly, the average welding speed of repeated welding operations 1.2±0.05 mm/s. For the calculation of the heat input (Q), the relationship used for CCTIG was $Q = \left(\frac{V \times I}{s}\right)\eta$, where V is the voltage, I is the current, s is the welding speed and η is the welding efficiency ($\eta = 0.90$) [9, 13]. The calculated values of heat input were given in Table 2. The heat input during welding and the cooling rate after welding strongly affect the weld bead morphology [1, 9]. In constant current process, the higher heat input was 784 J/mm and the lower heat input was 560 J/mm; in pulsed current process, when average heat input was calculated, the higher heat input was 560 J/mm and the lower heat input was 448 J/mm. As the heat input increased, cooling rate decreased as a result of increase in peak temperature. Fast cooling rates associated with the low heat inputs.

Table 2. Average heat input values calculated by welding parameters

	Current (A)	Pulse to pulse duration (ms)	Voltage (V)	Avr. welding speed (mm/s)	Heat input (J/mm)
CCTIG	50	-	13	1.2	560
	70	-	13	1.2	784
PCTIG	50-30	20	13	1.2	560-336
	70-30	20	13	1.2	784-336

3.2 *Macrostructural Examinations*

Figure 3 showed the weld bead morphology under pure He and pure Ar shielding gas with a different current mode and values. The weld bead surface was clean and well protected in the He shielding gas in comparison with Ar shielding gas. Under the pure Ar shielding, the weld bead surface was relatively dirty and oxidized. The bead surface using He shielding gas was better and smoother.

Macrostructural examinations of the cross-section of CCTIG and PCTIG welds were performed. The macrographs were shown in Figure 4 and 5. In Figure 4, the macrographs illustrated cross sectional profile of the CCTIG weld beads. In Figure 5, the macrographs illustrated cross sectional profile of the PCTIG weld beads. The weld bead dimensions were seen in the macrographs and they were penetration depth and weld bead width. To achieve a good welding result, the weld bead should have a full penetration and a narrow bead width. Penetration depth (P), bead width (W) and W/P values were listed in Table 4.
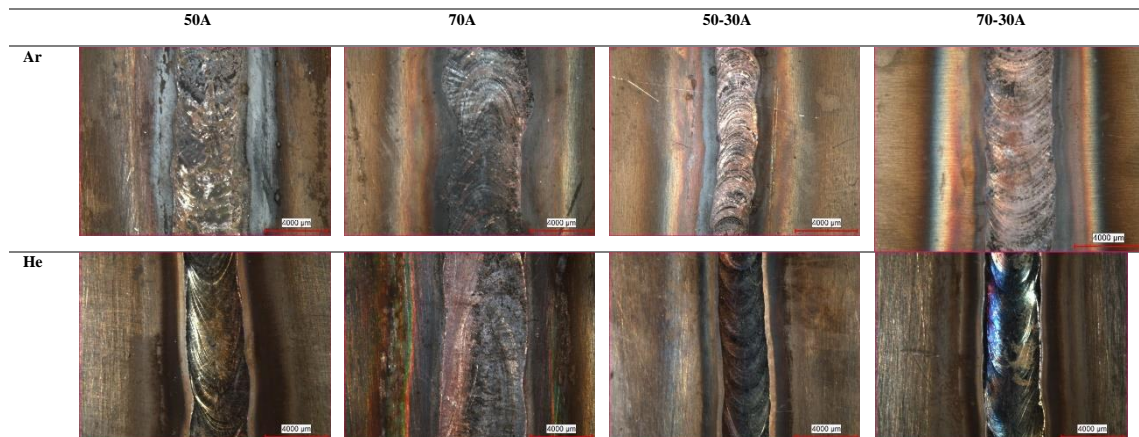
Figure 3. Macrostructures of the weld beads

Table 4. Weld bead dimensions

	50A Ar	50A He	70A Ar	70A He	50-30A Ar	50-30A He	70-30A Ar	70-30A He
Bead Width (W) (μm)	3710.1	4115.9	4782.6	6376.8	2318.8	2840.5	3652.1	3768.1

Penetration (P) (µm)	F	1151	F	F	1138	1307	983	1281
W/P	1.85	3.57	2.39	3.18	2.08	2.17	3.71	2.94

*F: Full

50A Ar	70A Ar	50A He	70A He
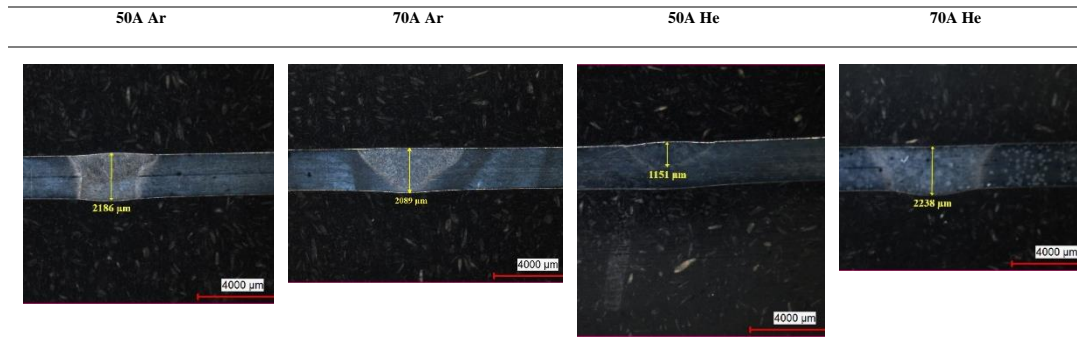
Figure 4. Cross sectional profiles of CCTIG welds

50-30A Ar	70-30A Ar	50-30A He	70-30A He
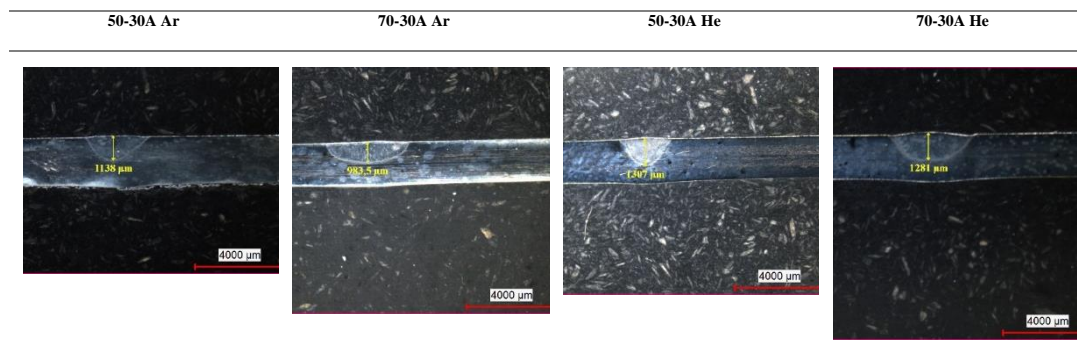
Figure 5. Cross sectional profiles of PCTIG welds

3.2.1. Effect of pulsed current on bead profile

According to Figure 4 and 5, full penetration was achieved only CCTIG welding. It was observed that bead width expanded with the increase of heat input. In PCTIG welding, the penetration achieved was almost 50-60% (Table 4). In PCTIG welding, a narrower weld bead was obtained as the heat input fluctuated. The temperature gradient is fluctuant in the heat input fluctuations. This situation narrows the bead width. The narrowest welded beam was obtained in 50-30A in He shielding and the largest was obtained in 70A in He shielding (Table 4). In terms of penetration, the heat input at the CCTIG welding is at a constant level. As the heat input increases, the peak temperature increases and this brings about a larger melting area.

3.2.2. Effect of shielding gas on bead profile

When Ar shielding gas was used, full penetration was achieved in both low heat input and high heat input in CCTIG joints. In the CCTIG joints using He shielding gas, full penetration was achieved at high heat input. In this study, no full penetration was achieved in any of the PCTIG welding parameters. When observing at the bead surfaces which obtained argon and helium shielding, the more dirty and oxidized surface of argon-shielded weld beam was remarkable. There was an oxidized surface appearance when argon was used. This layer was noticeable in the microstructure shown in Figure 6. It is estimated that this layer is an oxide layer. This oxide layer plays an important role to prevent oxygen transfer and so to prevent the dissolution of oxygen in the weld pool. So, oxygen in the weld pool plays an important role in changing the weld appearance [14]. A large temperature gradient will generate a strong Marangoni convection. $\partial\sigma/\partial T$ is associated with surface tension and temperature. The surface produced fluid flow on the pool surface is also called Marangoni convection. The effect of temperature gradient on weld shape and penetration depends on $\partial\sigma/\partial T > 0$ or $\partial\sigma/\partial T < 0$. When $\partial\sigma/\partial T < 0$, W/P ratio increases and when $\partial\sigma/\partial T > 0$, W/P ratio decreases [14]. In recent literature, investigating the effects on weld shape and

penetration of TIG welding with activated flux has become an interesting research topic. Activated flux has been used to increase the oxygen content on weld surface and to achieve deep penetration [15-17]. When the oxide layer is taken from the point of Marangoni convection, it increases the surface tension and forms a deeper weld pool; moreover, a large temperature gradient with the increase of heat input constitutes the strong Marangoni convection [14]. However, the temperature gradient is fluctuant in the heat input fluctuations. This situation narrows the bead width. In the He shielding with a 70A current, heat input was high, which increased the amount of melting, but this melting was spread over a wider area than the Ar shielding. This increases the W/P ratio and so reduces the welding performance. When the difference between the Ar and He shielding gases was itemized: (i) The W/P ratio increased when the He was used as shielding gas whereas it decreased when the Ar was used; (ii) In CCTIG welding, He shielding gas brought about wider bead width whereas in PCTIG welding, Ar brought about narrower bead width; (iii) Even with low heat input in CCTIG welding, Ar shielding brought about a great penetration and narrow bead, as a result of increased surface tension with oxide film based on Marangoni convection principle; (iv) Ar is heavier than the atmosphere and He is lighter, this situation may be increase the penetration. The average hardness values of ITAB for 70A CCTIG mode was 188.6 HV in Ar shielding and 174.5 HV in He shielding. When the hardness values were taken into account, the hardness obtained from Ar shielding gas was relatively higher than the He shielding gas. Fusion zone microstructures were given in Figure 7. When the effect of shielding gas was examined microstructurally, it was determined that a more homogenous grain structure was achieved in Ar.
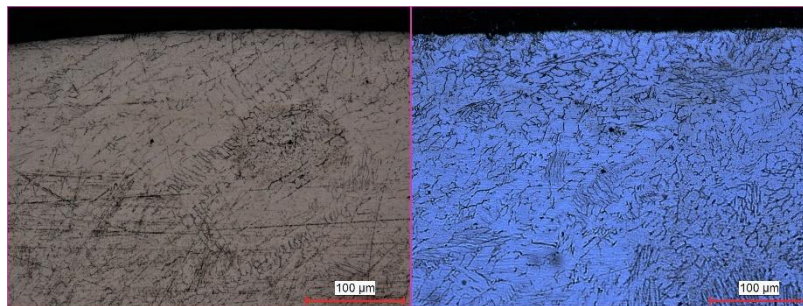
Figure 6. The cross-section microstructure of (a) He and (b) Ar shielded PCTIG welded specimens

3.3. Grain Structure Examinations

The fusion zone was quite evident in microstructures. The microstructures showed both a dendritic structure and a cellular structure as well as a fine cellular structure. These structures were indicated by arrow on the Figure 7. The coarser columnar dendritic structure was observed in CCTIG welding especially in higher heat input conditions. The coarse columnar dendritic structure with a small amount of cellular dendrites was also observed in CCTIG in lower heat input conditions. In PCTIG welding, the fine cellular structure and partly the fine columnar dendritic structure were obtained. In PCTIG welding and lower heat input conditions, the fine cellular grain structure constituted the general microstructure. As a result of rising heat input with 70-30A, it was noticed that columnar dendritic growth occurred in partly. In pulsed current mode, the pulsed arc promoted the cooling in a reduced time and in this case the temperature gradient decreased. And then a fine cellular dendritic structure occured. In 50-30A pulse current, the temperature dropped at a reduced time due to lower heat input and so fine cellular structure occured. The microstructures were proof of that.

In lower heat inputs, cooling rate was relatively higher and this resulted in finer dendrite size; at higher heat inputs, cooling rate was slower resulting in coarser dendrites. When the microstructural effect of the shielding gas was examined, it was determined that a more homogenous and finer grain structure was achieved in the welds produced under Ar gas [18].

3.4. Interfacial Microstructure Examinations

The weld interface microstuructures were examined in Figure 8. The micrographs at the interface between weld metal and base metal showed the presence of δ-ferrite stringers in all weldments. In this study, no additional filler metal was used and autogenous welding procedure was performed. Therefore, there is no element with different melting points. δ-ferrite stringers zone is wider due to the high heat input at constant current than the pulsed current mode. Moreover, in the weldments produced in the pulsed current mode, no grain coarsening was observed due to the controlled heat input at the joints. The grain growth was different at various zones of the weld. Vermicular (skeletal) δ-ferrite, parallel (lathy) ferrite and polygonal ferrite were showed in Figure 7. The interface microstructure revealed the presence of ferrite stringers at the HAZ. Base metal of ANSI 304 showed

the typical austenite grain and grain boundaries. Formation of delta ferrite stringers in the austenitic grains was observed at the HAZ of the ANSI 304 for all the weldments, which are in agreement with Naffakh et al. [19], Arivarasu et al. [6]. The presence of clusters of δ-ferrite at the HAZ of ANSI 304 was observed. In lower heat input, the presence of vermicular δ-ferrite near the HAZ was observed. In PCTIG, it was evident from the micrographs that the PCTIG weldments had produced small and lesser amounts of ferrit stringers and there was an equiaxed growth in the HAZ region. Higher heat cycles are required to get the austenite to ferrite transformation. HAZ thermal cycle is normally quite rapid, since the lower heat cycle is induced in PCTIG, the degree of ferrite formation is low. Ferrite stringers formed along the grain boundary of HAZ would limit grain growth and further minimize the HAZ weakness [6].
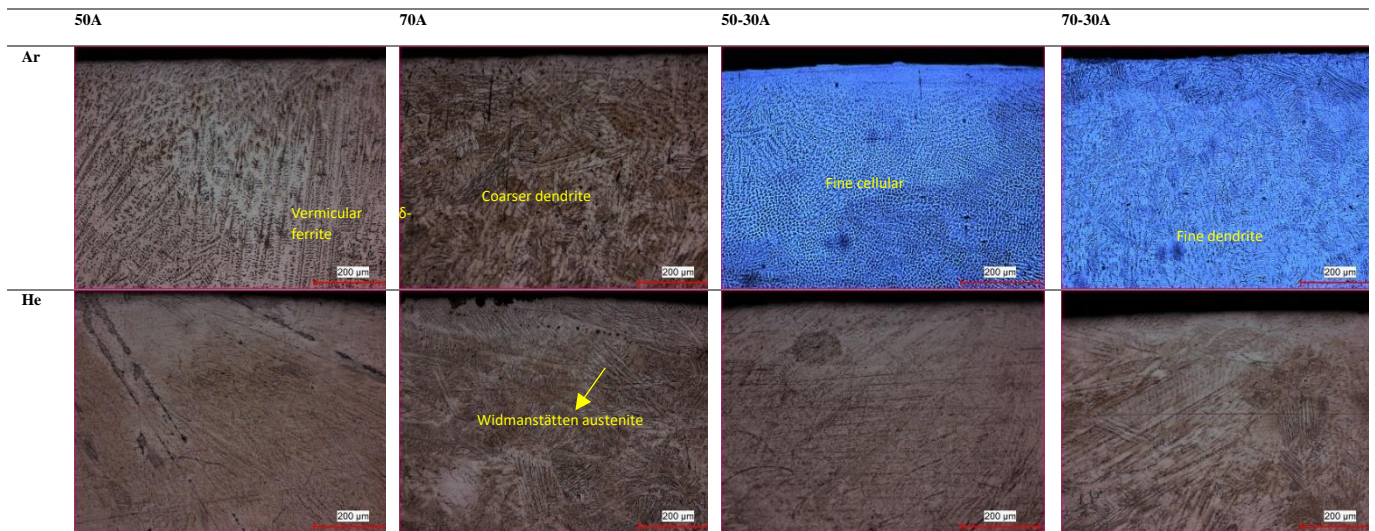
Figure 7. Microstructures of center of the cap side of the fusion zone
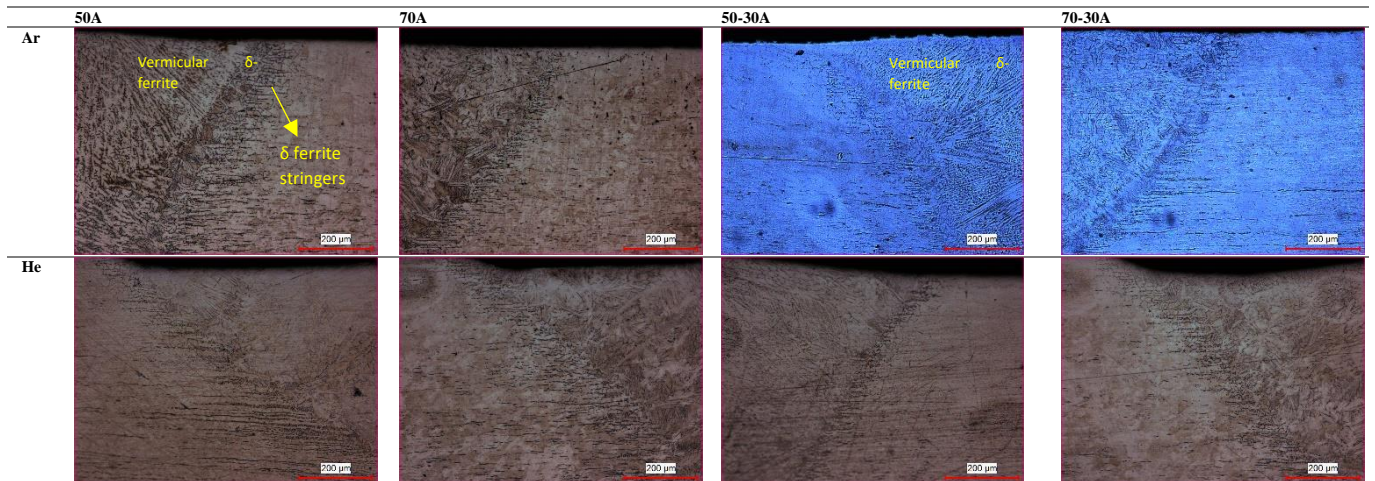
Figure 8. Microstructures of interface between weld and base metal

3.5. Hardness

The presence of vermicular ferrite and/or delta ferrite stringers in γ-phase at the HAZ of ANSI 304 contributed for better strength [6]. The fusion zone has higher cooling rate resulting in no reduced hardness. . The controlled heat input causing the faster cooling rate during PCTIG welding process, which contributed for grain refinement. The grain refinement contributed to a greater strength. When examined the fusion zone microstructure, the presence of the nominal values of ferrite and austenite is increased the strength [20]. A typical fully austenitic

structure was seen in base metal microstructure, and also some samples have partly austenitic structure with stringers delta ferrite. Vermicular ferrite stringers in γ phase contributed to the better strength property. As a result of this, The base metal average hardness of each sample was not the same. This alloy had a Vickers microhardness value equal to 190±21.5HV0.5.

During the welding, due to the high cooling rate, in the HAZ, stringers of delta ferrite inside the austenitic matrix was observed. The presence of delta ferrite can reduce the growth of grains in the HAZ and this prevented the weakening of mechanical properties in HAZ. No hardness reduction occurs in the HAZ due to ferrite stringers (Figure 9). Furthermore, there is no grain growth behavior in the HAZ. Casalino et al. [21] stated that the presence of delta ferrite affected ANSI 304 properties, the corrosion resistance increased due to high chromium amount and fatigue resistance decreased because δ-ferrite between the Widmanstätten austenite plates is one of the reasons for formation of sub-surface cracks in FZ [22, 23]. Long austenite plates are Widmanstätten austenite. When the middle region of the weld metal was examined, Widmanstätten austenite was formed in the fusion zone in the weldments of 70A and 70-30A current. Figure 10 showed the detailed microstructure of 70-30 A and He shielding welded joint. The coarser structure of the Widmanstätten austenite is noteworthy in helium shielding. The grain boundary and Widmanstätten austenite plates require a relatively small driving force, and as a result can occur at higher temperatures [20, 24, 25]. Accordingly, it was observed that these structures formed in the high heat input. Low heat inputs result in a very fast cooling rate during the weld thermal cycle. These fast cooling rates suppress the austenite nucleation and form almost fully ferritic high temperature microstructures (as shown in Figure 7 -50A and 50-30A welding currents-) [26]. It was observed that delta ferrite was comminuted in the HAZ of PCTIG weldments because the heat produced during PCTIG was immediately dissipated compared to CCTIG weldments. Ferrite transformation from austenite requires large heat inputs reported by Arivarasu et al. [6] and Lippold et al. [27]. The formation of ferrite stringers along the grain boundaries in the HAZ limited the grain growth. This also prevents the liquation cracking in the HAZ region [6]. As a result, it eliminates the mechanical weaknesses that can develop in HAZ.
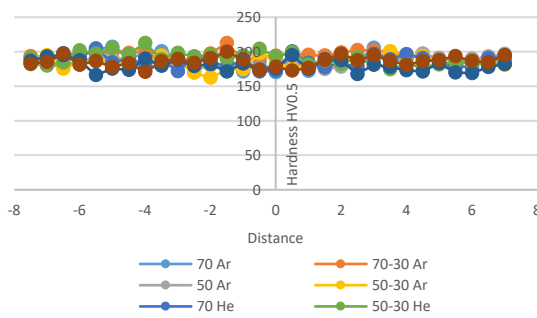
Figure 9. Hardness Profile of the welded samples
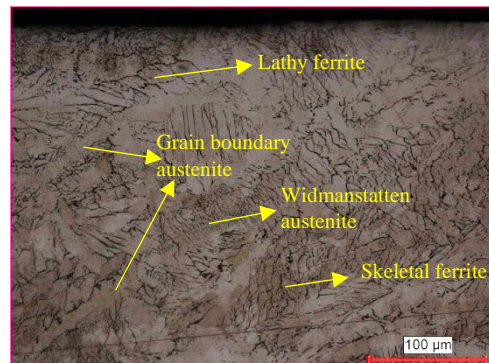
Figure 10. High magnification microstructure of cap region of the PCTIG weld metal (70-30A, He shielding)

4. CONCLUSION

The following results could be drawn from the various tests and analysis and they were summarized as follows:

(1) TIG autogenous weldments of ANSI 304 stainless steel were performed from both constant current and pulsed current modes no additional filler metals and pure Ar and pure He shielded. A more homogenous grain structure was achieved in the Ar shielded weldments.

(2) The coarser grain structure was observed in CCTIG weldments. CCTIG welding has higher heat input condition. PCTIG welding has lower heat input condition, and so the fine grain structure constituted the general weld metal microsturucture. In the pulsed current mode, the grain coarsening was not observed due to controlled heat input at the joints.

(3) δ-ferrite stringers was shown at the interface between weld metal and base metal in all weldments. The δ-ferrite stringers region was wider in the constant current mode due to the high heat input than the pulsed current mode.

(4) The presence of δ-ferrite stringers can reduce the grain growth in the HAZ and so this prevented the weakening of mechanical properties in HAZ. The grain boundary and Widmanstätten austenite plates were observed in the high heat input. Because these phases require a relatively small driving force,

and so as a result can occur at higher temperatures. Low heat inputs result in a very fast cooling rate during the weld thermal cycle. These fast cooling rates suppress the austenite nucleation and form almost fully ferritic high temperature microstructures.

ACKNOWLEDGMENT

REFERENCES

[1]. Karunakaran, N., *Effect of pulsed current on temperature distribution, weld bead profiles and characteristics of GTA welded stainless steel joints*, International Journal of Engineering and Technology, 2(12), 2012.

[2]. DebRoy, T., & David, S. A., *Physical processes in fusion welding*, Reviews of modern physics, 67(1), 85, 1995.

[3]. Devakumar, D., & Jabaraj, D. B.,*Research on gas tungsten arc welding of stainless steel-An overview*, International Journal of Scientific & Engineering Research, 5(1), 1612,2014.

[4]. Yilmaz, R., & Tehci, T., *Ostenitik Paslanmaz Celiklerin TIG Kaynaginda Kaynak Akimi ve Kompozisyonun Nufuziyete Etkisi*, Sakarya University Journal of Science, 16(1), 53-61,2012.

[5]. Farahani, E., Shamanian, M., & Ashrafizadeh, F.*, A comparative study on direct and pulsed current gas tungsten arc welding of alloy 617*, International Journal on Manufacturing and Material Science, 2(1), 1,2012.

[6]. Arivarasu, M., Ramkumar Kasinath, D., & Natarajan, A.*, Effect of continuous and pulsed current on the metallurgical and mechanical properties of gas tungsten arc welded AISI 4340 aeronautical and AISI 304 L austenitic stainless steel dissimilar joints*, Materials Research, 18(1), 59-77,2015.

[7]. Yousefieh, M., Shamanian, M., & Saatchi, A., *Optimization of the pulsed current gas tungsten arc welding (PCGTAW) parameters for corrosion resistance of super duplex stainless steel (UNS S32760) welds using the Taguchi method*, Journal of Alloys and Compounds, 509(3), 782-788,2011.

[8]. Yousefieh, M., Shamanian, M., & Saatchi, A.*, Influence of heat input in pulsed current GTAW process on microstructure and corrosion resistance of duplex stainless steel welds*, Journal of Iron and Steel Research International, 18(9), 65-69,2011.

[9]. Karunakaran, N., & Balasubramanian, V., *Effect of pulsed current on temperature distribution, weld bead profiles and characteristics of gas tungsten arc welded aluminum alloy joints*, Transactions of Nonferrous Metals Society of China, 21(2), 278-286,2011.

[10]. Huang, H. Y., *Effects of shielding gas composition and activating flux on GTAW weldments*, Materials & Design, 30(7), 2404-2409,2009.

[11]. Shinoda T, Ueno Y and Masumoto I, *Effect of pulsed welding current on solidification cracking in austenitic stainless steel welds*, Transac. of the Japan Welding Soc., 1990, Vol. 21, :18-23.

[12]. Indira Rani, M., & Marpu, R. N. , *Effect of pulsed current tig welding parameters on mechanical properties of J-joint strength of AA6351*, The International Journal of Engineering And Science (IJES), 1(1), 1-5.

[13]. Peng, D., Shen, J., Tang, Q., Wu, C. P., & Zhou, Y. B., *Effects of aging treatment and heat input on the microstructures and mechanical properties of TIG-welded 6061-T6 alloy joints*. International Journal of Minerals, Metallurgy, and Materials, 20(3), 259-265,2013.

[14]. Lu, S. P., Fujii, H., & Nogi, K. *Weld shape comparison with iron oxide flux and Ar–O2 shielding gas in gas tungsten arc welding*, Science and technology of welding and joining, 9(3), 272-276,2004.

[15]. Shyu, S. W., Huang, H. Y., Tseng, K. H., & Chou, C. P. *Study of the performance of stainless steel A-TIG welds*. Journal of Materials Engineering and Performance, 17(2), 193-201, 2008.

[16]. Tathgir, S., & Bhattacharya, A. *Activated-TIG welding of different steels: influence of various flux and shielding gas*. Materials and Manufacturing Processes, 31(3), 335-342, 2016.

[17]. Huang, H. Y. *Effects of shielding gas composition and activating flux on GTAW weldments*. Materials & Design, 30(7), 2404-2409, 2009.

[18]. Sharma, S., Taiwade, R. V., & Vashishtha, H., *Effect of continuous and pulsed current gas tungsten arc welding on dissimilar weldments between hastelloy C-276/AISI 321 austenitic stainless steel*, Journal of Materials Engineering and Performance, 26(3), 1146-1157,2017.

[19]. Naffakh H, Shamanian M and Ashrafizadeh F., *Microstructural evolutions in dissimilar welds between AISI 310 austenitic stainless steel and Inconel 657*, Journal of Materials Science, 45(10):2564-2573,2010.

[20]. Ramkumar, K. D., Choudhary, A., Aggarwal, S., Srivastava, A., Mohan, T. H., & Arivazhagan, N., *Characterization of microstructure and mechanical properties of continuous and pulsed current gas tungsten arc welded superaustenitic stainless steel*. Journal of Materials Research, 30(10), 1727-1746,2014.

[21]. Casalino, G., Angelastro, A., Perulli, P., Casavola, C., & Moramarco, V., *Study on the fiber laser/TIG weldability of AISI 304 and AISI 410 dissimilar weld*, Journal of Manufacturing Processes, 35, 216-225,2018.

[22]. Sharifitabar, M., Halvaee, A., & Khorshahian, S., *Microstructure and mechanical properties of resistance upset butt welded 304 austenitic stainless steel joints*, Materials & Design, 32(7), 3854-3864,2011.

[23]. Hong, H. U., Rho, B. S., & Nam, S. W.*, A study on the crack initiation and growth from δ-ferrite/γ phase interface under continuous fatigue and creep-fatigue conditions in type 304L stainless steels*, International journal of fatigue, 24(10), 1063-107,2002.

[24]. Ramkumar, K. D., Bajpai, A., Raghuvanshi, S., Singh, A., Chandrasekhar, A., Arivarasu, M., & Arivazhagan, N.*, Investigations on structure–property relationships of activated flux TIG weldments of super-duplex/austenitic stainless steels*. Materials Science and Engineering: A, 638, 60-68,2015.

[25]. Tseng, K. H., & Hsu, C. Y., *Performance of activated TIG process in austenitic stainless steel welds*, Journal of Materials Processing Technology, 211(3), 503-512,2011.

[26]. du Toit, M., & Naudé, J. *The influence of stabilization with TITANIUM on the HEAT-AFFECTED ZONE SENSITIZATION of 11 to 12% chromium ferritic stainless steels under low heat input welding conditions*. Welding in the World, 55(3-4), 38-47, 2011.

[27]. Lippold JC and Koteki DJ., *Welding metallurgy and weldability of stainless steels*, 2nd ed. New Jersey: John Wiley & Sons,2005.

A Review of Combined Heat Transfer Enhancement Methods Using Nanofluids and Inner Ribs

Orhan Keklikcioglu[1] , Toygun Dagdevir[2], Veysel Ozceyhan[3]

Abstract

Heat transfer enhancement is a process of increasing the heat transfer rate and thermohydraulic performance of a system using various methods. These different methods are grouped mainly under two techniques, passive and active. The technique of application of inner ribs, such as twisted tapes, coiled or tangled wires, and nozzle turbulators, and nanofluids are among the passive heat transfer enhancement method that has been commonly studied in recent years. The methods of heat transfer enhancement are employed for developing the heat transfer without affecting the overall realization of the systems significantly, and it covers a wide range of areas where heat exchangers are used. Using of inner ribs in flow region increase both convective heat transfer and fluid friction because of inducing the turbulence and promoting the swirl flow. Additionally, nanoparticles enhance the thermal properties of base fluids that causes the increment of heat transfer rate without causing major frictional forces in thermal systems. To obtain the thermo-hydraulic performance of a thermal system, both heat transfer and fluid friction characteristics should be investigated. For this reason, the present study represents a comprehensive review that focused on combined heat transfer enhancement methods with nanofluid and inner ribs used in the flow region.

Keywords: Inner rib, nanofluid, heat transfer, pressure drop, heat transfer enhancement

1. INTRODUCTION

Over the past decades, in accordance with the developing technology, efforts to control energy consumption have accelerated. Due to many reasons, such as the insufficiency of energy resources and the high cost, researchers have endeavored to increase the efficiency of thermal systems and to reduce the size and therefore the energy consumption rates.

Controlling or enhancing heat transfer and thus avoiding energy consumption is not only important for complex engineering systems, but it is also a serious issue covering all systems that consume energy used in our daily life. For this reason, heat transfer enhancement methods have been developed to prevent heat loss from the thermal systems. The methods of heat transfer enhancement mainly based on three different techniques; passive, active and compound. Active techniques that require external power input and passive techniques do not require any additional energy to improve the thermo-hydraulic performance of the system. In addition, two or more passive and active techniques can be used together and called compound technique.

The methods of heat transfer enhancement are employed for developing the heat transfer without affecting the overall realization of the systems significantly, and it covers a wide range of areas where heat exchangers are used. Using of inner ribs in flow region increase both convective heat transfer and fluid friction because of inducing the turbulence and promoting the swirl flow. Additionally, nanoparticles enhance the thermal properties of base fluids that causes the increment of heat transfer rate without causing major frictional forces in thermal systems. Heat transfer fluids such as water, ethylene glycol or oil limit the performance of heat exchangers [1]. For this reason, researchers started to investigate alternative fluids which have better thermophysical properties when they used in heat exchangers. In this way, nanofluids were also discovered. Nanofluids are suspension containing nanoparticles and thermal conductivities of nanofluids are significantly higher than those of base liquids [2].

In this study, it is aimed to present an overview of passive heat transfer enhancement methods using nanofluid as a working fluid. The used passive techniques and nanofluids are briefly presented in accordance with the effect on heat transfer and pressure drop penalty. Moreover, the details and overall enhancement ratio of investigated studies are given in tables to provide a comparative approach to the reader.

2. ENHANCEMENT TECHNIQUES

2.1. *Passive techniques*

Passive techniques include surface or geometric modifications in the flow region. They increase both the heat transfer coefficients and pressure drop. The most used passive techniques are coiled tubes, corrugated tubes, swirl devices(twisted tapes, coiled wires, conical rings, vortex rings, etc.) and rough surfaces. Additionally, fluid additives such as nanoparticle is one of the most widely used methods of passive heat transfer enhancement method.
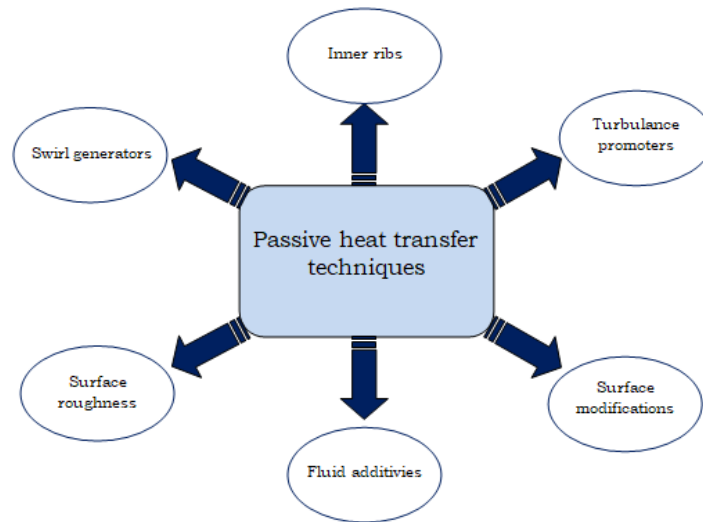
Figure 17. Schematics of passive techniques

2.2. *Active techniques*

Active techniques are provided to improve the heat transfer as a result of the power given to the fluid; it presents a more practical approach due to the absence of additional inserts. The most commonly used active techniques are mechanical methods, surface and fluid vibration, electrostatic field.

2.3. *Compound techniques*

A compound technique consists of a combination of active or passive technique. It can be used to create a greater impact by combining factors that affect system performance. Preliminary studies on the compound passive augmentation technique of this kind are quite encouraging

3. EVALUATION OF HEAT TRANSFER ENHANCEMENT

The basics of Performance Evaluation Criteria (PEC) was determined for the fixed geometry criteria (FG) which were related with on heat transfer and friction factor characteristics of various augmentation techniques in Ref. [3].

The fixed geometry criteria is used for many passive techniques which include various types of inner ribs or inserts in the tube. The investigations of heat transfer enhancement with passive techniques are generally conducted at the same pumping power in accordance with the fixed geometry criteria. Thus comparison of results for the tube with inserts and without inserts can be carried out in ease. The Nusselt Number can be written below as to calculate the thermal performance of the system,

$$Nu = \frac{hD}{k}$$

(1)

And the Reynolds number for fluid is

$$\mathrm{Re} = \frac{UD}{\nu}$$

(2)

The friction factor, f is calculated as follows, for the fully developed isothermal flow;

$$f = \frac{\Delta P}{\frac{1}{2}\rho U^2 \frac{L}{D}}$$

(3)

where U represents the mean fluid velocity in the tube.

The heat transfer rate and friction factor of the smooth tube and smooth tube fitted with inserts are evaluated under the same pumping power as below [4];

$$(\dot{V}\,\Delta P)_s = (\dot{V}\,\Delta P)_a$$

(4)

$$(f\,\mathrm{Re}^3)_s = (f\,\mathrm{Re}^3)_a$$

(5)

$$\mathrm{Re}_s = \mathrm{Re}_a (f_a/f_s)^{1/3}$$

(6)

The overall enhancement ratio (OER) is the parameter which usually used in heat transfer augmentation to determine the performance of different variations of heat exchangers. The parameter can be written as in Eq. (7) for the same pumping power based on the fixed geometry criteria [4].

$$\eta = \frac{h_a}{h_s}\Big|_{pp} = \frac{Nu_a}{Nu_s}\Big|_{pp} = \left(\frac{Nu_a}{Nu_s}\right)\left(\frac{f_s}{f_a}\right)^{1/3}$$

(7)

4. HEAT TRANSFER ENHANCEMENT WITH COMBINATION OF INNER RIBS AND NANOFLUIDS

This paper focuses on reviewing the recent investigations about the heat transfer enhancement with inner ribs which are widely used as a passive technique in tubular flow together with the nanofluids as a working flow.
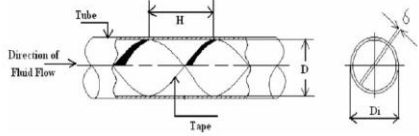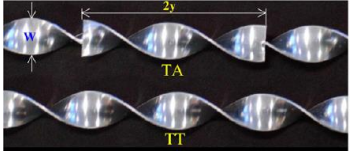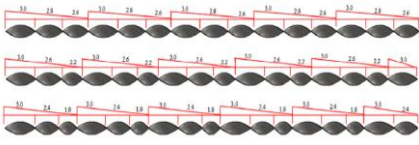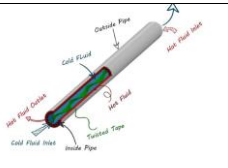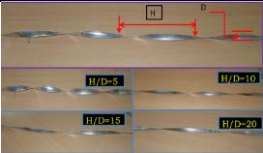
4.1. Twisted tapes

The twisted tapes produced in various configurations and frequently used in flow applications in the tube, to disrupt the flow region and cause turbulence to increase heat transfer. Sundar and Sharma [5] investigated the convective heat transfer coefficient and friction factor data at various volume concentrations for flow in a plain tube and with twisted tape insert was determined experimentally for Al2O3 nanofluid. Experiments were conducted in the Reynolds number range of 10,000–22,000 with tapes of different twist ratios in the range of 0 < H/D < 83. The results showed that the heat transfer coefficient and friction factor of 0.5% volume concentration of Al2O3 nanofluid with twist ratio of five is 33.51% and 1.096 times respectively higher compared to flow of water in a tube. Heat transfer and pressure drop of CuO/water nanofluid with twisted tape inserts were explored by K. Wongcharee and S. Eimsa ard. [6]. The results demonstrated that using CuO nanofluid with the twisted alternate axis (TA) obtain a higher Nusselt number and thermal performance, and the twisted tape in alternate axis was about 89% more effective than typical twisted tape. In another study K. Wongcharee and S. Eimsa ard. [7] presented an experimental study of convective heat transfer enhancement using combined techniques of non-uniform twisted-tapes Ag-water nanofluid. The effects of the twist ratios of non-uniform twisted-tapes (y/W in three series, 3.0 > 2.8 > 2.6, 3.0 > 2.6 > 2.2 and 3.0 > 2.4 > 1.8), tube and tape arrangements (counter and co-current arrangements), nanofluid concentrations (ϕ of 0.007, 0.016 and 0.03% by volume) on thermal performance of micro-fin tube were determined. It was reported that the maximum enhanced heat transfer rate of 112.5% and the thermal performance factor of 1.62 were achieved for the best configuration. Karimi et. al [8] studied the effect of Alumina/water nanofluid and twisted tape on the hydrodynamic and thermal performance of

the double tube heat exchanger. A two-phase mixture model was employed to simulate alumina-water nanofluid flow inside a double tube

heat ex-changer with twisted tape inserts with various pitch ratios and materials. The results revealed that the use of twisted tape and alumina particles in water increased the Nusselt number up to 22% and 30%, respectively.

Table 7. Various samples of twisted tape inserts

Authors	Fluid	Type	Flow region	OER	Sample of twisted tape inserts
Sundar and Sharma [5]	Al_2O_3 nanofluid	twisted tape inserts	10,000≤Re≤22,000 Turbulence	-	
K. Wongcharee and S. Eimsaard. [6]	CuO-water nanofluid	twisted alternate axis	830≤Re≤1990 Laminar	5.53	
K. Wongcharee and S. Eimsaard. [7]	Ag-water nanofluid	non-uniform twisted tape	5210 ≤Re≤15,420 Turbulence	1.62	
Karimi et. al [8]	Alumina/water nanofluid	twisted tape	250≤Re≤2250 Laminar 3000≤Re≤9000 Turbulance	1.49	
Prasad and Gupta [9]	Al_2O_3- water nanofluid	twisted tape	3000 ≤Re≤30,000 Turbulence	1.25	
Eiamsa-ard and Kiatkittipong [10]	TiO_2-water nanofluid	multiple twisted tape inserts	5400 ≤Re≤15,200 Turbulence	1.59	
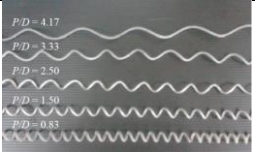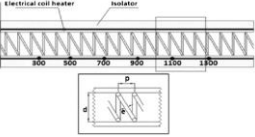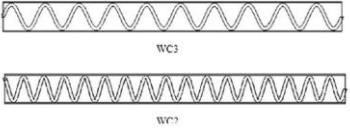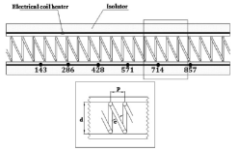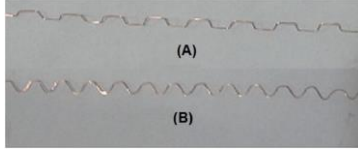
Prasad and Gupta [9] studied to enhance the rate of heat transfer of Al_2O_3 nanofluid in a U-tube heat exchanger with twisted tape insert for the Reynolds number ranging from 3000 to 30,000. Eiamsa-ard and Kiatkittipong [10] investigated the enhancement of thermal performance in a heat exchanger with multiple twisted tape. TiO2/water nanofluid was used in the experiment as working fluid. They reported that the tube inserted the multiple twisted tapes showed superior thermal performance factor when compared with a plain tube or the tube inserted a single twisted tape.

4.2. Wire coils

The wire coil inserts are widely used in thermal systems to increase the efficiency of the systems in terms of heat transfer. Moreover, using of wire coil is recommended if the pressure is an important parameter in the system[11].

Hamid et al.[12] studied the thermal hydraulic performance of TiO2-SiO2 nanofluids with wire coil inserts for Reynolds number from 2300 to 12,000. The TiO2-SiO2 nanofluids were prepared by using the two-step method for volume concentrations of 0.5–3.0%. The wire coil inserts are designed at various ratios of pitch over diameter (P/D) in the range of 0.83–4.17. The heat transfer performance of nanofluids was enhanced for a maximum of 254.4% at 2.5% volume concentration of TiO2-SiO2 nanofluids and 1.50 pitch ratio of the wire coil. Behabadi et al.[13] studied the effect of different parameters such as Reynolds number, nano-particle concentration, wire diameter and coil pitch on heat transfer coefficient and pressure drop. Multi-walled carbon nanotubes (MWCNTs) in distilled water and wire coils in different pitch were used for the investigation. The results revealed that 85% increase in heat transfer coefficient and 475% penalty in pressure drop was observed at the highest Reynolds number inside the wire coil inserted a tube with the highest wire diameter. Chougule et al. [14] investigated heat transfer and friction factor characteristics of CNT/water nanofluid flowing through a uniformly heated horizontal tube with and without wire coil.

Table 2. Various samples of wire coil inserts

Authors	Fluid	Type	Flow region	OER	Sample of wire coil inserts
Hamid et al.[12]	TiO2-SiO2 nanofluids	wire coil inserts	2300≤Re≤12,000 Turbulence	2.06	
Behabadi et al.[13]	MWCNT–water nano-fluid	wire coil inserts	10,000≤Re≤20,000 Turbulance	5.53	
Chougule et al. [14]	CNT/water Nanofluid	wire coil inserts	600≤Re≤2280 Laminar	-	
Chandrasekar et al. [15]	Al2O3/water nanofluid	wire coil inserts	600≤Re≤2275 Laminar	-	
Saeedinia et al.[16]	CuO-Base oil nanofluid	coiled wire	20≤Re≤105 Laminar	-	
K. Goudarzi and H. Jamali [17]	Al2O3-EG nanofluid	wire coil inserts	18,500 ≤Re≤22,700 Turbulence	1.09	
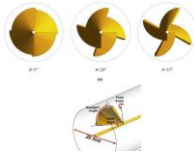
Chandrasekar et al. [15] investigated the convective heat transfer and pressure drop characteristics of Al2O3/water nanofluid in the fully developed laminar region of pipe flow with and without wire coil inserts. Saeedinia et al.[16] carried out an experimental study on the heat transfer and pressure drop characteristics of CuO/Base oil nanofluid laminar flow in a smooth tube with different wire coil inserts. The effect of variety
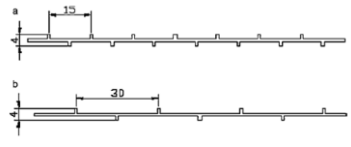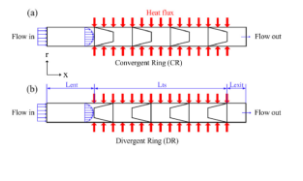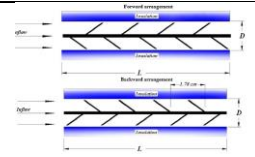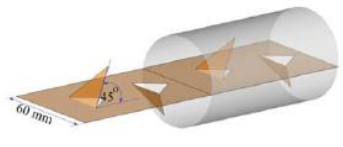
parameters including Reynolds number, wire diameter, coil pitch, nanofluid concentration on thermohydraulic performance was investigated. They reported that a 45% increase in heat transfer coefficient and 63% penalty in pressure drop was conducted for the optimum configuration. K. Goudarzi and H. Jamali [17] studied the effect of Aluminum Oxide (Al2O3) in Ethylene Glycol (EG) as nanofluid and wire coil on heat transfer enhancement of car radiator. In the study, two different wire coils insert with different geometry and nanofluids with volume concentrations of 0.08%, 0.5% and 1% were investigated. The results indicated that the use of coils inserts enhanced heat transfer rates up to 9%.

4.3. Various inserts (conical and longitudinal strips, conical rings, baffles and wings)

Aliabadi et al. [18] investigated three concentrations of Cu nanoparticles: 0.0%, 0.1%, and 0.3% by volume, six different shapes of inserts: perforated-tape, jagged-tape, twisted-tape, helical-screw, vortex-generator, and offset-strip and seven volumetric flow rates: 2.0, 2.5, 3.0, 3.5, 4.0, 4.5, and 5.0 l/min in a tube to conduct the effect of the parameters on thermal performance. Test results indicated that the thermal hydraulic performance of the tube was strongly related to the shape of inserts. It was found that the tube fitted with the vortex-generator insert offered the highest values of the heat transfer coefficient and pressure drop. Sundar et al. [19] studied the enhancement of effectiveness oof solar flat plate collector using Al2O3/water nanofluids and with longitudinal strip inserts. The experiments were conducted in the Reynolds number range from 5000 to 13,500, longitudinal strip inserts of aspect ratios (AR) equal to 1, 1.5 and 3, volume concentrations of 0.1% and 0.3%. Khodabandeh et al. [20] studied the thermohydraulic performance of a tube with the water–Ag nanofluid and twisted conical strip inserts. Three twist and two geometry angles were considered for the one-blade and two-blade configurations and thermo hydraulic characteristics of the water–Ag nanofluid with a concentration of 3% in a circular tube was investigated. Suresh et al. [21] studied the convective heat transfer and friction factor characteristics in a circular tube with spiraled rod inserts with two different pitch. Distilled water and Al2O3/water nanofluids with three different volume fractions were selected as working fluid and Al2O3 nanoparticles were synthesized by using a chemical precipitation method. With the contribution of the spiraled rod and using Al2O3/water nanofluid in the tube, the Nusselt number showed an increase of about 10–48% compared to the Nusselt numbers obtained with the plain tube. Mohammed et al. [22] investigated the effect of four nanofluids types (Al2O3, CuO, SiO2, and ZnO) and conical ring inserts on the thermohydraulic performance of a circular tube, numerically. Single phase and two-phase mixture analyses were carried out separately. The results revealed that the highest performance enhancement criteria is provided by the divergent ring inserts with 365%. SiO2-water nanofluids have achieved the highest heat transfer enhancement in terms of Nusselt number and the friction factor.

Table 3. Various samples of different type of inserts

Authors	Fluid	Type	Flow region	OER	Sample of various inserts
Aliabadi et al. [18]	Cu–water nanofluid	perforated-tape, jagged-tape, twisted-tape, helical-screw, vortex-generator, and offset-strip	2.0, 2.5, 3.0, 3.5, 4.0, 4.5, and 5.0 l/min	3.5	
Sundar et al. [19]	Al2O3 water nanofluids	longitudinal strip inserts	5000 ≤Re≤13,500 Turbulence	1.84	
Khodabandeh et al. [20]	Ag-water nanofluid	novel conical strip inserts	100≤Re≤1500 Laminar	-	

Suresh et al. [21]	Al2O3/ water nanofluid	spiraled rod inserts	2500≤Re≤6000 Turbulence	-	
Mohammed et al. [22]	Al2O3, CuO, SiO2, and ZnO-water nanofluids	convergent and divergent conical rings inserts	2000 ≤Re≤10,000 Turbulence	3.65	
Rathnakumar et al. [23]	CNT/water nanofluid	helical screw louvered rod inserts	10,000≤Re≤27,500 Turbulence	1.23	
Singh et al. [24]	CuO water base nanofluids	the baffles	1000≤Re≤12,000	1.3	
S. Eiamsa-ard and K.Wongcharee [25]	TiO2-Water Nanofluid	Semi-Circular Wing Tapes	8000≤Re≤15,000 Turbulence	1.98	

Rathnakumar et al. [23] investigated the thermal performance in a tube with helical screw louvered rod inserts using water and carbon nanotube (CNT)/water nanofluids of 0.1%, 0.2% and 0.5% volume concentration under turbulent flow condition. It was concluded that the maximum thermal performance factor value of 1.23 was found with the use of CNT/ water nanofluid of 0.5% volume concentration with twist ratio of 1.78 in the backward arrangement. Singh et al. [24] studied the enhancement in the heat transfer characteristics of CuO-water base nanofluids with two different volume fractions by inserting the baffles in the annulus of the double pipe heat exchanger. The results showed that in comparison to the distilled water, copper oxide nanofluids with baffles shows more heat transfer enhancement. S. Eiamsa-ard and K.Wongcharee [25] investigated the effect of using of semi semi-circular wing tapes and TiO2-water nanofluids in a corrugated tube on thermal performance. The experiments were carried out with three difeerent TiO2 concentrations (0.05 to 0.15% by volume), semi-circular wing tapes with three wing angles (45 to 75°), and two wing arrangements, and Reynolds numbers between 8000 and 15,000. The highest thermal enhancement factor of 1.98 was obtained by the use of the combined devices in the parallel pattern at wing angle of 75°, the concentration of TiO2-water nanofluid of 0.15% by volume and Reynolds number of 8000.

5. CONCLUSIONS

In this review, recent and important researches on increasing the heat transfer performance by using the inner ribs in the tube flow are included. It is observed that heat transfer and pressure drop increased in most of the work done for the inner ribs. The main objective to design a heat exchanger should be enhance the heat transfer without causing more pressure drop. For this reason, inner ribs can be used together with the nanofluid flow to eliminate the pressure drop penalty on OER. Most of the researchers oriented to find better configuration of internal ribs to determine the minimum pressure drop and the maximum heat transfer. The configuration and physical properties of inserts are the most important parameter to enhance the overall thermohydraulic performance of a heat exchanger.

REFERENCES

[1]. W. Yu, H. Xie, and D. Bao, "Enhanced thermal conductivities of nanofluids containing graphene oxide nanosheets," Nanotechnology, vol. 21, pp. 7, 2009.

[2]. H. Zhu, C. Zhang, S. Liu, Y. Tang, Y. Yin, "Effects of nanoparticle clustering and alignment on thermal conductivities of Fe3O4 aqueous nanofluids," Applied Physics Letters., vol. 89, 2006.

[3]. R.L. Webb, Performance evaluation criteria for use of enhanced heat transfer surfaces in heat exchanger design. Int. Jou. of Heat and Mass Trans. vol.24, pp.715-726, 1981.

[4]. S. Eiamsa-ard, P. Promvonge, Thermal characteristics in round tube fitted with serrated twisted tape. Appl. Therm. Eng. 2010

[5]. L. Syam Sundar, K.V. Sharma, Turbulent heat transfer and friction factor of Al2O3 Nanofluid in circular tube with twisted tape inserts, International Journal of Heat and Mass Transfer, vol. 53, pp. 1409–1416, 2010.

[6]. Wongcharee, K., Eiamsa-ard, S., Enhancement Of Heat Transfer Using CuO/Water Nanofluid And Twisted Tape With Alternate Axis. Int. Comm. Heat and Mass Transf., vol. 38, pp. 742:748,2011.

[7]. Smith Eiamsa-ard, Khwanchit Wongcharee, Convective heat transfer enhancement using Ag-water nanofluid in a micro-fin tube combined with non-uniform twisted tape, International Journal of Mechanical Sciences, vol. 146, pp. 337–354, 2018.

[8]. Ali Karimi, Abdullah A.A.A. Al-Rashed, Masoud Afrand , Omid Mahian, Somchai Wongwises, Amin Shahsavar, The effects of tape insert material on the flow and heat transfer in a nanofluid-based double tube heat exchanger: Two-phase mixture model, International Journal of Mechanical Sciences, vol.156, pp. 397–409, 2019.

[9]. P.V. Durga Prasad, A.V.S.S.K.S. Gupta, Experimental investigation on enhancement of heat transfer using Al2O3/water nanofluid in a u-tube with twisted tape inserts. Int. Comm. Heat and Mass Transf. vol.75, pp.154-161, 2016.

[10]. Smith Eiamsa-ard, Kunlanan Kiatkittipong, Heat transfer enhancement by multiple twisted tape inserts and TiO2/water nanofluid. Appl. Therm. Eng., vol. 70, pp. 896:924, 2014.

[11]. L. Wang, B. Sundén, Performance comparison of some tube inserts, Int. Commun. Heat Mass Transf., vol. 29, pp. 45–56, 2002.

[12]. K. Abdul Hamid, W.H. Azmi,∗, Rizalman Mamat, K.V. Sharma, Heat transfer performance of TiO2–SiO2 nanofluids in a tube with wire coil inserts, Applied Thermal Engineering vol.152, pp. 275–286,2019.

[13]. M.A. Akhavan-Behabadi, Mohamad Shahidi, M.R. Aligoodarz, An experimental study on heat transfer and pressure drop of MWCNT–water nano-fluid inside horizontal coiled wire inserted tube, International Communications in Heat and Mass Transfer, vol. 63, pp.62–72, 2015.

[14]. S. S. Chougulea, Vishal V. Nirgudea, Prajakta D. Ghargeb, Mayank Modaka, S. K. Sahu, Heat Transfer Enhancements of Low Volume Concentration CNT/water Nanofluid and Wire Coil Inserts in a Circular Tube. Energy Procedia, vol. 90, pp.552-558, 2016.

[15]. M. Chandrasekar, S. Suresh, A. Chandra Bose, Experimental studies on heat transfer and friction factor characteristics of Al2O3/water nanofluid in a circular pipe under laminar flow with wire coil inserts, Experimental Thermal, and Fluid Science vol. 34, pp.122–130, 2010.

[16]. M. Saeedinia, M.A. Akhavan-Behabadi, M. Nasr, Experimental study on heat transfer and pressure drop of nanofluid flow in a horizontal coiled wire inserted tube under constant heat flux, Experimental Thermal and Fluid Science, vol. 36, pp. 158–168, 2012.

[17]. K. Goudarzi, H. Jamali, Heat transfer enhancement of Al2O3-EG nanofluid in a car radiator with wire coil inserts, Applied Thermal Engineering, vol. 118, pp. 510–517, 2018.

[18]. M. Khoshvaght-Aliabadi, H. Shabanpour, A. Alizadeh, O. Sartipzadeh, Experimental assessment of different inserts inside straight tubes: Nanofluid as working media, Chemical Engineering and Processing, vol. 97, pp.1–11,2015.

[19]. L. Syam Sundar, A. Kirubeil, V. Punnaiah, Manoj K. Singh, Antonio C.M. Sousa, Effectiveness analysis of solar flat plate collector with Al2O3 water nanofluids and with longitudinal strip inserts, International Journal of Heat and Mass Transfer vol.127, pp.422–435,2018.

[20]. Erfan Khodabandeh, Mehdi Bahiraei, Ramin Mashayekhi, Bahram Talebjedi, Davood Toghraie, Thermal performance of Ag–water nanofluid in tube equipped with novel conical strip inserts using two-phase method: Geometry effects and particle migration considerations, Powder Technology, vol. 338, pp. 87–100,2018.

[21]. S. Suresh, P. Selvakumar, M. Chandrasekar, V. Srinivasa Raman, Experimental studies on heat transfer and friction factor characteristics of Al2O3/water nanofluid under turbulent flow with spiraled rod inserts, Chemical Engineering and Processing, vol. 53,pp.24– 30,2012.

[22]. Hussein A. Mohammed, Ibrahim A.M. Ali Abuobeidab, Hari B. Vuthalurua, Shaomin Liua, Two-phase forced convection of nanofluids flow in circular tubes using convergent and divergent conical rings inserts, International Communications in Heat and Mass Transfer, vol. 101, pp.10–20, 2019.

[23]. P. Rathnakumar, S. Mohamed Iqbal, Jee Joe Michael, S. Suresh, Study on performance enhancement factors in turbulent flow of CNT/water nanofluid through a tube fitted with helical screw louvered rod inserts, Chemical Engineering & Processing: Process Intensification, vol.127, pp. 103–110,2018.

[24]. Swati Singh, Gurpreet Singh and Amit Singla, Experimental Studies on Heat Transfer Performance of Double Pipe Heat Exchanger with using Baffles and Nanofluids, Indian Journal of Science and Technology, vol 9(40),2016.

[25]. Smith Eiamsa-ard & Khwanchit Wongcharee, Experimental Study of TiO2-Water Nanofluid Flow in Corrugated Tubes Mounted with Semi-Circular Wing Tapes, Heat Transfer Engineering, vol. 39:1, pp. 1-14,2018.

Overview Of Project Management In Construction Sector

Feyza Gurbuz[1], Gizem Erdinc[1]

Abstract

In generally, Project Management is defined as the application of meeting the project requirements and available sources. On the other hand, each projecthas different needs and sources. So, this diversity needs dissimilar applications and technics and these applications create the project management literature in the sector used. This study is prepared to understand the literature onproject management in the construction industry. We discussed the studies about the construction industry and project management application written in the recent past.Shortcomings of the studies examined under these headings were identified and are noted in the results section. The papers mostly published between 2014-2018. So, the aim of this study is to guide to study is prepared in order to eliminate the deficiency in the literature.

Keywords: *Construction project management, project management skills, project management*

1. INTRODUCTION

Project Management is a phenomenon that has been going on for many years and its content has not changed much. In other words, using time, money, manpower, machinery and equipment in the most efficient way is defined as efforts to complete the purpose in the best time with the most appropriate budget.Today, it is not the changing objective, but the tools and the methodology of these tools[1].

In this study, various project management application studies (recently written), which are prepared for the construction sector in the literature, are considered and introduced under some titles: 'Key Success Factors in Project Management ?', 'Project Management Concept in Turkey', 'Disadvantages and Deficiencies of Classical Methods', 'Different Applications of Critical Path Method', 'Optimization in Project Management', 'Fuzzy Logic in Project Management', 'Simulation in Project Management'. The deficiencies of these studies have been identified and stated in the results section.

2. LITERATURE REVIEW

In this section, the studies which are mainly published between 2014-2018 and which contain application studies are examined and given under the following headings.

2.1. *Key Success Factors in Project Management*

In the studies discussed under this heading, the reasons for failing to succeed in project management in the construction sector and the reasons for failure are explained.In this context, Varejao et al. [2] investigated the main success factors in Project Management. According to this study, they applied surveys to medium and large companies operating in construction and software sectors and evaluated the results; The most important reason for the failure of project management in the construction sector is that it is difficult to accurately measure performance and manage success.The reason for this is not only the complexity of the project but also a large number of suppliers.

Varajao et al. [2] show that; in the literature on the success criteria of project management in the construction sector; according to Atkinson [3] the time, cost and scope criteria, and Chan and Chan [4] the health and risk criteria should be included in the project management. In addition, some criteria should be examined closely for successful project management. Detailed information is given in Table 1.

---

[1] *Erciyes University, Industrial Engineering Department, Kayseri, Turkey feyza@erciyes.edu.tr*

In addition to the inferences given in Table 1, according to Varajao et al. [2], project management examines the similarities and differences between the construction and software sector. In two areas, the following two factors were identified as success criteria: 'project planning' and 'well-defined objectives and needs'.In addition, it is stated that the effectiveness/efficiency of the project manager is very effective in project management in both areas.

Tablo 1. Success Requirements and Failure Causes in Project Management

Success requirements in project management	Reasons for failure in project management
Examining the importance of time, cost and scope criteria[3]	Failure to accurately measure performance in the construction sector[2]
Examination of the importance of health and risk criteria[4]	It is difficult to manage successin the construction industry[2]
The importance of human factor and the contribution of human to project success[5]	Including many suppliers[2]
Examining competency, commitment, communication criteria [6]	
Understanding the importance of internal management[8]	

Cano and Saenz [9] pointed out that the use of project management simulations increased with the development of project management. For this reason, according to Cano and Saenz [9], education in this area has become mandatory.Experience is essential for successful project management, and this can only happen with practice.The simulation gives the opportunity to practice in the abstract sense in the field of project management. It calls as Experimental Learning. This provides the project manager with personal experience while providing information for the entire company.However, according to Randel and Wellington [10], the following factors are necessary for an effective project simulation: team size, the ethnic unity of team members, initial statements and previous academic achievements.

2.2. *Project Management Concepts in Turkey*

As mentioned in the introduction, getting to know the sector closely is one of the most important factors for successful project management. In this context, Islamoglu [11] tried to understand and review 'The project management concept in the construction industry in Turkey' and 'The role of the project manager'.In this context, he found theconstruction and project management company that represents the number of 30-35 percent in Turkey.Among the projects examined in these companies, the project has served with project management services for projects with a total construction area of 3 million m2 or more or 25 companies with at least one international projector with at least 50 employees.At the end of his observations and analysis, Islamoglu pointed out that unfortunately,*the culture of project management has not yet settled in Turkey* and that *effective management practices are not possible*.In order to determine why effective project management could not be carried out, it applied the survey prepared by the companies to the companies and obtained the following results.

The reason for the lack of effective project management made in Turkey[11];

- Lack of project management perspective and awareness
- Lack of regulations, laws, and accreditation on project management
- The need to provide construction project management services without employer intervention
- Ignorance of investors in Turkey
- The employer does not provide the necessary support for the project management team in the field
- Establishing the issue of authorization by entering into bilateral relations with other stakeholders

In another of the current studies in our country, Karaman and Son [12] stated that one of the most important functions of project management is the monitoring and control of the process.According to Karaman and Son [12], the projected Earned Value Analysis (KDA) in project management is a well-known management system that combines cost, timing, and technical performance.This analysis is a very important technique to measure and control the performance and progress of a project and is used in various sectors.It is also used in the management process of comprehensive construction projects, as it is a widely used project control technique and provides a quantitative measurement of business performance. This analysis allows calculation of cost and timing variances and performance indices and estimates project cost and schedule duration.In this study, Karaman and Son [12] evaluated some work items of a completed construction project according to Earned Value Analysis and analyzed the results of time and cost performances.

2.3. *Disadvantages and Deficiencies of Classical Methods*

After the conceptual requirements and deficiencies of the project management are discussed and the situation in our country is examined, the classical project management techniques and deficiencies that constitute the technical part of the project management are explained.It is seen that many engineering projects have resulted in different than in practice.Ballesteros-Perez et al. [13] claimed that the main reason for this difference was poor planning control.Unfortunately, according to Ballesteros-Peres et al.[13], the classical methods which are the Critical Path Method (CPM), the Program Evaluation and Review Technique (PERT) and the Gantt Chart (Gantt Chart), theydo not fully calculate the project durations and give project managers optimistic estimates. Optimistic estimations lead to incorrect scheduling and lead to different results from the planning phase of the project, especially in terms of project completion time.This study, as shown in Table 2, demonstrated the particularly disadvantageous disadvantages of the classical methods CPM, PERT and Gantt Chart methods and discussed with practical evidence how critical the disadvantages can be, even for a project manager.In order to make an accurate and effective estimation, computer simulations are needed rather than a statistical point of view[13].

Table 2. Disadvantages and Deficiencies of Classical Methods

Method	Disadvantages and Deficiencies
Gannt Chart	1-Inability to define relationships between activities (for example time-cost relationship cannot be determined) - therefore not suitable for projects involving repetitive activities 2- To be able to show a single probability scenario
Cpm	1-Rather than being a method, CPM can be claimed to be the concept of monitoring the critical activities of the project manager 2- CPM is based on the assumption that the activities scheduled are always present and that their duration is known.3- CPM is not a good predictor when activity duration is uncertain
PERT	1-In the method used to find the mean and standard deviation calculated in the equation, activity times are considered to be appropriate for beta distribution, while μ and r obtained in the next step can only be expressed with normal distribution 2- Exaggeration of project duration distribution 3- Based on the assumption that timed activities are always available and their duration is known

In addition to Table 2 disadvantages of Critical Path Method according to expert opinions [14]:

- Unable to automate shared resource variables (for example work team) between work packages

- Unable to show the variable resource level and duration during work package during application

- Not being able to model the exact needs for all work packages

- Unable to show the limitations of how many people can work in a workspace

- Unable to show the difficulty in controlling congestion due to work packages applied in several areas

2.4. *Different Applications of Critical Path Method*

Although many researchers find it incomplete and inaccurate, the most common method in the construction sector is the Critical Path Method.Many researchers have combined the Critical Path Method solution with different approaches and contributed to the literature.For example, Aziz et al. [15] developed a model which is the Critical Path Method but combines this with the multipurpose genetic algorithm.In this method developed for optimization of time, cost and quality for mega projects, the optimum resource utilization calculation was made for the mentioned triple optimization.The aim here is to provide practical support to project managers who aim to increase quality while minimizing the waiting concurrently.Aziz and his friends [15] with their Smart Critical Path Method System, aimed to improve the following 4 factors:Improving resource utilization, decreasing construction time, reducing construction costs, measuring and improving product quality.

Although the Critical Path Method is a suitable method for programming original projects, it is insufficient in the programming of repetitive or linear construction projects, including multiple units, multi-story housing, roads, pipelines, canals or similar units[16].According to Okmen [16], it is necessary to maintain resource continuity between units while providing logical sorting between activities in construction projects involving repeating units.Otherwise, depending on the resources remaining inactive, projects are completed longer than necessary.

2.5. *Optimization in Project Management*

One of the areas that has become popular in recent years and which has entered the focal point of many researchers is project management optimization.Some of the works carried out on project management by the concept of optimization, which can be defined as the most appropriate use of available resources, are as follows:Tareghian et al. [17] studied a project of 45 activities and optimized the project in terms of time an cost and quality criteria.In the optimization model, a purpose function has been written for each criterion and the problem is solved by using 3 binary integer programming and using LINGO program together with model constraints.The problem was solved in 10 different modes and the modes were selected randomly. As the last stage of the study, the number of modes taken into consideration was tried to be reduced.

Salimi et al. [18] claimed that there is a need for simulation during the analysis and planning of the project due to the uncertainty and variability of the projects.They emphasized that a trade-off between cost and time criteria, which is the most common criteria in project management, in other words, is a close relationship and that this relationship is the key element for optimization.However, as the scope of a project grows, the uncertainty and complexity of the project have increased, and Salimi and his friends have created a simulation-based model and have obtained the optimum solution by using the NSGA-II optimization algorithm.In order to reduce the processing time of the solution, they used the High-Performance Computing (HPC) application simultaneously.

Tatar and Kaplan [19], who is believed to be one of the richest studies on project management optimization, presented an application for subcontractorused in the construction sector.In the project of construction of a logistics center by using Genetic Algorithm (GA) and Monte Carlo Simulation, cost quality optimization and risk assessment model has been formed for a period of subcontractor selection.The subcontractor data obtained by constructing activities, work program and project data within the scope of the model were evaluated with the mentioned software.In order to determine the optimum sub-contractor sequence to be used in the project, the Evolver software working with GA was used.Time, cost and quality data included in the optimization study were added to the risk factor effect with the help of @Risk software working with MCS.It is stated that there may be positive and negative deviations in total project duration, cost and quality values in the simulation results.The results are expected to provide a different approach to subcontractor selection.It is thought that the changes between time, cost and quality criteria will be better interpreted. The aim of this study is to raise awareness of the risks and uncertainties.

2.6. *Fuzzy Logic in Project Management*

If we look at the uncertainty and variability of the construction sector, it should be the Fuzzy Logic and its Applications that can be used to manage this sector.Fuzzy Logic approach, which provides the ability to express qualitative and variable expressions mathematically, also has many examples of construction project management.The first of these, Gorener and Sabuncuoglu [20], studied the problem of contractor selection problem with a multi-criteria decision making (MCDM) problem, which included quantitative and qualitative characteristics.Choosing a contractor with the desired characteristics in the construction sector is an important requirement in project success.In this context, Gorener and Sabuncuoglu [20] proposed an approach that includes the Analytic Hierarchy Process (AHP) and Technique for Order of Preference by Similarity to Ideal Solution(TOPSIS) methods to be used in contractor selection.With the AHP, the importance of the selection criteria was determined and the appropriate contractor alternatives were evaluated with the TOPSIS method.An example of an application from the construction industry has also been given for the proposed approach.

Durucasu et al. [21] aimed to show how the critical path and completion time of a real construction project can be calculated with fuzzy operating times and to compare the α-cut and center of gravity methods that are commonly used in the literature.In the study, the periods related to the activities were determined as triangular fuzzy numbers instead of exact numbers and the network diagram were visualized with Graphviz software.A network type mathematical programming model was developed with AMPL algebraic modeling language to determine project completion time with the critical path.The critical path and completion time of the project were compared with the α-cutting approach and the center of gravity, which is one of the widely used rinse techniques.In addition, the accuracy of time was tested by the Yager method, which is one of the sorting methods of fuzzy numbers.Durucasu et al. [21] suggest the importance of the study of fuzzy numbers instead of exact numbers instead of the exact numbers of the fuzzy CPM method instead of the classical CPM method commonly used in the literature.

2.7. *Simulation in Project Management*

In order to achieve the highest business value in project management, the approach that provides effective use of limited resources and demonstrates this can be called project management simulation.As mentioned above, completing a project in the right way requires more than anything else.But experience means money and time. Simulation techniques and applications that give an idea to the project managers about the various situations are not found before.In this context,The logic of Bayhan et al.[21] work: In machinery intensive construction projects, which are becoming more common nowadays, it is of great importance to estimate the efficiency of each building machine in order to determine the machine costs that make up a large part of the project cost. Using stochastic simulation models, they tried to predict the production efficiency of construction machinery on site under certain constraints. According to Bayhan and his friends, unit price analysis of machine-intensive work items can be detailed and used in bids. In addition, by analyzing the productivity values obtained from the model, the project can be controlled by comparing the planned and actual progress of the project.In this study, Bayhan et al. [22] performed estimated efficiency calculations of future projects using stochastic models that were previously performed but not outdated.Respectively; To determine the variables affecting productivity, the mathematical formulation of the effect of variables, to determine the range of possible results, to complete the statistical and probability calculations and to perform computer-aided planning study with the prescribed Monte Carlo simulation.The yield-time cost table of a job with machine-intensive horizontal work program was created with the data obtained from the model.Bayhan et al. [22] in their study, the data obtained as a result of the analysis, the most important two parameters in the construction business, time and cost ratios will help determine the determination.

Unlike other studies, Sevim and Gurcanli [23] emphasized that the construction industry has separated from other sectors due to the high level of labor and a large number of suppliers.Security-based design and planning are one of the newpoints of researchers working in the field of project management. Elimination and substitution according to the risk control pyramid are the first two steps required to reduce the risk.In this context, Sevim and Gurcanli [23] have developed a new algorithm with the desire to perform elimination and substitution steps. In the construction industry, project planning and implementation have calculated a risk (R) value for each activity in the schedule obtained by the Primevara program, which is one of the frequently used project management programs.It is recommended that this algorithm should be redesigned or revoked according to this risk value with an algorithm lower or higher than any value, and this algorithm should be used as software and used with Primavera.

3. CONCLUSION

In this study, some studies which have various applications about project management in the construction sector are examined.In this review study aimed at understanding the construction sector project management literature, it is aimed to see the shortcomings of the current studies. Therefore, the following inferences were found from the studies examined.

Firstly, it can be said that the human factor is very effective in project success and abstract criteria such as competence, commitment, and communication should be included in the steps of project management.Furthermore, it can be said that the Critical Path Method is not a good predictor inthe resource level and duration of the work package during the application is not fixed,difficult to control congestion due to work packages applied in several areas

In the programming of repetitive or linear construction projects containing many units of the same or similar, such as residential buildings, roads, pipelines, conduits, etc.In these cases, it has been understood that more effective methods should be developed than the Critical Path Method.

REFERENCES

[1]. Avenal, A.,Why Construction Project Management Should be includedas aseparate undergraduate Program and what topics should cover?, 4.PYYK,Eskisehir, 20, 2014.
[2]. Varajao, J., Dominguez, C., Ribeiro, P., Paiva, A., Critical success aspects in project management: similarities and differences between the construction and the software industry, Tehnički vjesnik 21(3), 583-589, 2014.
[3]. Atkinson, R., Project Management: Cost, time, and quality, two best guesses and a phenomenon, it is time to accept other success criteria, International Journal of Project Management, 17(6), 77-82,1999.
[4]. Chan, A. P. C., Chan, A. P. L., Key performance indicators for measuring construction success, Benchmarking: an International Journal, 11(2), 203-221, 2004.
[5]. Belout, A., Gauvreau, C., Factors influencing project success: the impact of human resource management, International Journal of Project Management. 22(1), 1-11, 2004.
[6]. Nguyen, L. D., Oguniana, S. O., Xuan Lan, D. T., A Study on Project Success Factors in Large Construction Projects in Vietnam, Engineering, Construction and Architectural Management, 11(6), 404-413, 2004.
[7]. Doloi, H., Lim, M. Y., Measuring performance in Construction Projects-A critical Analysis with an Australian Perspective, RICS, London, 2007.
[8]. Teixeira, R., Caracterizacão da prática da gestão de projectos de desenvolvimento de software, Perspectiva das empresas versus perspectiva dos prestadores de servicos, University of Trás-os-Montes e Alto Douro, Master's thesis, Vila Real, 2009.
[9]. Cano, J.L.,Saenz, M.J., Project Management Simulation Laboratory: Experimental Learning And Knowledge Acquisition, Production Planning and Control,14(2),166-173,2003.
[10]. Randel, J.,Morris, B.A.,Wetzel, C.D., Whitehill, B.V.,The Effectiveness of Games for Educational Purposes: A Review of Recent Research, Simulation, and Gaming: An International Journal of Theory, Practice, and Research(Sage Publications), 23, 261-276, 1992.
[11]. Islamoglu, A., Detection Of Profiles Of Construction Project Management Companies That Have Operations In Turkey, Master Thesis, Istanbul TechnicalUniversity,Institute of Science and Technology,2015.
[12]. Karaman, E., Son, S., Performance evaluation of construction project with earned value analysis method, Journal BAUN Institute of Science and Technology, 20(1), 287-295, 2018.
[13]. Ballesteros-Pérez, P., Larsen, G., González-Cruz, M., Do Projects Really End Late? On The Shortcomings Of The Classical Scheduling Techniques, Journal Of Technology And Science Education, 8(1), 17-33, 2018.
[14]. Hu, D., Mohamed, Y., Taghaddos, H., Hermann, U., A Simulation-Based Method For Effective Workforce Planning Of Industrial Construction Projects, Construction Management and Economics, 36(6), 328-347, 2018.
[15]. Aziz, R. F., Hafez, S. M., Abuel-Maged, Y. R., Smart Optimization For Mega Construction Projects Using Artificial Intelligence, Alexandria Engineering Journal, 53(3), 591-606, 2014.
[16]. Okmen, O., Critical Routing of Construction Projects with Repeatitive Units,4.PYYK,Eskisehir, 2016.
[17]. Tareghian, H.R., Taheri S.H., On The Discrete Time, Cost And Quality Trade-Off Problem, Applied Mathematics And Computation, 181,1305–1312, 2006.
[18]. Salimi, S., Mawlana, M., Hammad, A., Performance Analysis Of Simulation-Based Optimization Of Construction Projects Using High-Performance Computing, Automation in Construction, 8, 158-172, 2018.
[19]. Tatar, G.,Kaplan, B., Genetic Algorithm and Monte Carlo Simulation with the Time of Subcontractor Selection in a Construction Project - Cost-Quality Optimization and Risk Assessment,Master Thesis,Istanbul TechnicalUniversity,Institute of Science and Technology, 2014.
[20]. Gorener, A., Sabuncuoglu, A.O., Decision Making Through the Fuzzy TOPSIS Method: Contractor Selection in Construction Projects, Research in Bussiness and Social Science, 5(2), 2016.
[21]. Durucasu, H., Karamasa, C., Ican, O., Yesilaydin,G., Gulcan,B., Project Scheduling by means of Fuzzy CPM Method: An Implementation in Construction Sector, Ege Academic Review, 15(4), 449-466, 2015.

[22]. Bayhan, H.G.,Kanra, Y.C.,Demir, M.C.,Kar, H.,Gurcanli G.E., Estimation of Production Efficiency of Work Machines at Site with Stochastic Simulation Model, 4.PYYK,Eskisehir, 2016.

[23]. Sevim, M.,Gurcanli, G.E., A Semi-Automated Rule-Based Approach for Safety Based Scheduling, 5.PYYK,Kuzey Kibris, 83-91, 2018.

Analysis Of Quality Errors During The Bed Production Process

Feyza Gurbuz[1], Hande Madenoglu[1]

Abstract

Today, it is very important to be able to deliver the products at desired time and required quality in order to respond customers quickly and meet consumers' expectations due to increasing current consumption. Businesses should make much more effort to stay competitive. On the other hand, businesses pay special attention to quality defects that cause defective products and faulty production, and negatively affect operational efficiency. It is equally important to be able to respond customers quickly and deliver the products at the required quality. It is also very important to work on quality defects in order to increase customer satisfaction and operational efficiency. This paper aims to be a case study by analyzing the quality defects in the production line of a mattress enterprise. In addition to analysis of quality defects, failure mode and effects analysis (FMEA) and galvanic skin response methods were also used in the study.

Keywords: Analysis of Quality Defects, Failure Mode and Effects Analysis (FMEA)

1. INTRODUCTION

In today's conditions, as a result of the increase in customer request, demands and the development of consumer awareness, competition among firms have increased. In addition to these, access to all kinds of companies and procurement from companies has become much easier with the development of technology. Under these conditions, the importance of quality is emerging for the survival of business in a competitive environment. Quality is one of the most important factors determining the competitiveness of the business. Variability in quality creates customer dissatisfaction, which leads to financial loss. In order to avoid these variations, investing in quality seems to be costly in the first place by companies. However, as a result of investment in quality, costs such as scrap, reprocessing and customer loss will be reduced by avoiding defective production. If defective production is minimized or reduced, profit will increase with customer satisfaction.

In this thesis, the quality analysis study was carried out on a bed production line of a company that is engaged in furniture production in Kayseri. Statistical methods such as pareto analysis, fishbone diagram, cause and effect matrix used in quality and process improvement were used in the study. In addition to these methods, the factors causing the error were identified and risk assessment was made by using Failure Mode and Effects Analysis (FMEA) method.

Competition, which is a necessity of today's conditions, has brought about the concept of quality. Quality in terms of speciality and qualification comes from the Latin Word " qualis ". In defining quality, it can be generally defined as suitability for use, consumer satisfaction and expediency[1]. The features of the product such as being durable, ergonomic and being able to perform the expected functions give information about the quality sufficiency of that product. The quality of a country's services and products indicate the level of development of that country. Product and service quality is the level of meeting the identified and probable needs [2]. In this century, the importance of quality has been understood by the executives and studies on quality have been started with the quality departments in this rising competitive environment.

Customer satisfaction has been one of the leading parameters in this process. This has led to the necessity of detecting the faulty product before going to the customer. Analysis and various techniques have started to be used with the detection of quality errors.

Failure Mode and Effects Analysis (FMEA) technique is a method used to identify and eliminate the problems that are present or likely to occur in the system and support the minimization of errors. HTEA generally has four types: system, design, process and service.

Baysal et al. (2002) applied an example of FMEA in the automotive sector to set an example for the process type [3]. Cevik and Aran analyzed the faults encountered during production in a company producing pistons with HTEA technique. [4]. Eryurek and Tanyas (2003), in addition to the HTEA technique, they also used Simple-Sum Weighting and Electre methods and made analysis considering the cost element. [5]. Ozfirat (2014) used HTEA technique on occupational health and safety by making an application in mining sector. He used fuzzy prioritization method in addition to FMEA technique and stated that the results would be more realistic.[6]. Soykan et al. (2014) conducted studies for grading infectious disease risks in health institutions in order to show that the HTEA technique, which is mostly used in the production sector, can be used in the health sector. [7]. Scheu et al. (2019) used the FMEA method on wind turbine systems to reduce maintenance costs and increase the usability of products. The objectives of the study are to prioritize the system and to identify and monitor the parameters causing the error in particular [8]. Kudlac et al. (2017), using FMEA and Saaty method together, they conducted a study to analyze and evaluate the logistics chain by using customer request.

The aim of these methods is to eliminate the main restriction that may affect productivity in order to ensure the efficient operation of the logistics chain and to identify a suitable carrier targeted. [9]. Ahire and Relkar (2012) investigated the relationship between total equipment effectiveness (TEE) and FMEA technique [10].

2. METHOD

The methods, which are used to analyze the data and collected in favor of the study as having a scientific basis, are explained in the sub-headings.

2.1 Pareto Analysis

Pareto analysis is one of the statistical process control techniques. Pareto analysis provides a sorting of importance for the causes or errors discussed. It assists at setting priorities. Specifically, when detecting quality errors, it shows the percentage sorting of errors and determines which errors should be dealt with. Pareto analysis is a technique that shows the causes of errors in a product or system as unimportant and more important by graphical method [11].

2.2. 5N Analysis

5N analysis is one of the quality tools. It is used to identify the causes of the error. It provides the root cause by asking consecutively what, where, when, how and how many questions to the problem to be studied [12].

2.3. Fishbone Diagram

It is a quality tool used to find the causes of errors and to determine the factors that affect the errors. Fishbone diagram is prepared by identifying the factors affecting quality error and other factors affecting these reasons [13].

2.4. Cause- effect Matrix

The cause-effect matrix is the scoring of the factors affecting the error obtained by the fishbone diagram method and establishing an order of importance. Scoring is made for each factor by forming a group by the people who are in the process and masters the subject. As a result of scoring, factors with high significance are determined [14-15].

2.5. Failure Mode and Effects Analysis (FMEA)

The HTEA technique is a method that focuses on existing errors and identifies possible errors, classifies the types of errors according to their risks, and makes plans to prevent errors [16].

HTEA targets are as follows [17].

- To meet expectations by identifying potential product and process defects
- To identify potential consequences
- To Identify potential causes of errors
- To Establish a continuous control system
- To Determine risk levels in systems or processes
- To reduce the risks that may occur

3. FINDINGS

In order to identify the errors that occur in the production lines, a team consisting of the personnel working in the quality unit and the operators working in the production line is constituted. The quality errors encountered were determined and data were collected. As a result of the obtained data, the most common error was determined by creating a pareto graph. As a result of the pareto graph, the most commob error is the quilting removal error.

By applying 5N analysis, quilting removal error was questioned in detail and the root cause was determined. Answers were given with brainstorming by the constituted group.

- WHAT: Quilting removal
- WHERE: Upper and lower quilting
- WHEN: During the quilting weaving
- HOW: By not merging the upper thread and the lower thread while quilting
- HOW MUCH: 23270 pieces in production 286 piecess / 1.23%
- WHO: Operator, quality

In order to detect the quilting removal error, a fishbone diagram was made with the team formed and the factors that could cause the error were determined.
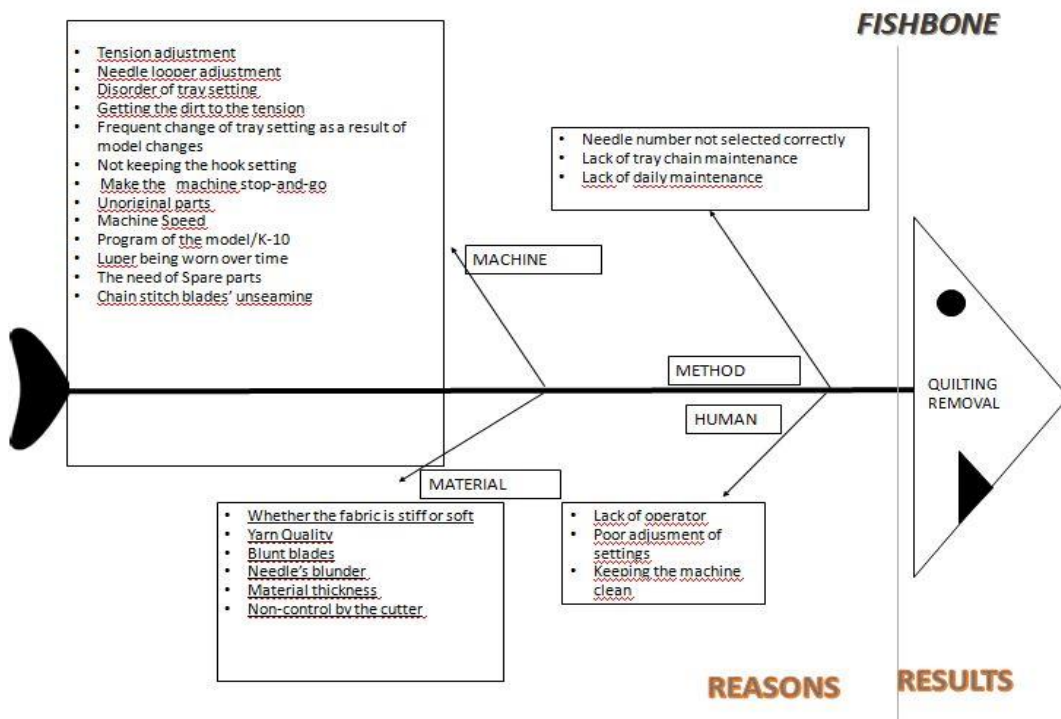
Figure 1. *Fishbone diagram for quilting removal error*

After establishing the Fishbone diagram, root causes detected by three persons, one maintainer, one operator and the person who mended the quilting errors, were scored. After the scoring, order of priority was done by using 'Cause-Effect Matrix' . As a result of the sorting, the points to be focused were determined.

- Disorder of tray setting,
- Needle and looper adjustment,
- Not keeping the machine clean,
- Frequent change of tray setting as a result of model changes,
- Material thickness,
- Unoriginal parts,
- The need of spare parts.

Then, pareto analyzes were carried out according to model, machine and operator. As a result of Pareto analysis, the most errors were found in three models. When the models called Dushess, Majestat and Tesla were analyzed, it was found that the models were produced only on the quilting machine called K-10. In order to determine the attachment to the machine, it was decided to make an error pareto analysis according to the machine. As a result of the analysis, it was found that the error rate was mostly in K-10 quilting machine. After the result, it was decided to make an error pareto analysis according to the bed models produced in K-10 quilting machine.

For K-10 machine, it was decided to make analyzes by considering operator and shift factors and the effect of variables such as operator and shift on the occurrence of error was analyzed. As a result of the pareto analysis, it was observed that the errors in the night shift increased. The quilting machine employs two people: operator and cutter. Pareto analysis and boxplot graphs were made according to operator and cutter.

Then, the error graph was obtained according to the quilting model. The quilting patterns were determined as two groups as pointed 's' and round' y 'corners. It was found that the error rate number increased in pointed corner models.

Quilting thickness is another factor affecting the error. For quilting thickness, pareto graph was made. It was observed that the number of errors increased in products with a high thickness.

As a result of these studies, the most common mistake was found in the night shift. For the operator and the cutter, the names with the most errors were determined. Then, the effect of the model and the thickness of the model on the error has been studied and it was found that more errors occurred in the models with thicker and pointed corners.

In addition to the studies, HTEA was applied and the risk factors for quilting removal were classified according to their risk.

Table 1. HTEA Quilting Removal Error Study

Failure Mode and Effects Analysis (HTEA)										
Process activity	Potential Error Type	Potential effects of the error	violence	class	Potential reasons of the error /Mechanisms	Possibility	Existing controls		Detection	ROS
							Prevention	Detection		
BED QUILTING	Quilting Removal	Customer Returns. Rework	6		Rope tension adjustment	5	NOT	%100 Inspection	7	210

WEAVING PROCESS		Costs Unproductivity Late Delivery			Needle looper adjustment	8	NOT			336
					Disorder of tray setting	8	NOT			336
					Getting the dirt to the tension	4	NOT			168
					Because of remodelling, changing the tray settings frequently	8	NOT			336
					Not keeping the hook setting	6	NOT			252
					Make the machine stop-and-go	2	NOT			84
					Unoriginal parts	7	NOT			294
					Machine Speed	3	NOT			126
					Program of the model	9	NOT			378
					Luper being worn over time	5	NOT			210
					The need of Spare parts	8	NOTX			336
					Chain stitch blades' unseaming	2	NOT			84
					Lighting	7	NOT			294
					Needle number not selected correctly	2	NOT			84
					Lack of tray chain maintenance	6	NOT			252

					Lack of Daily maintenance	6	NOT		252
					Whether the fabric is stiff or soft	5	NOT		210
					Yarn Quality	4	NOT		168
					Blunt blades	7	NOT		294
					Needle's blunder	7	NOT		294
					Material thickness	7	NOT		294
					Non-control by the cutter	7	NOT		294
					Lack of operator	7	NOT		294
					Poor adjusment of settings	8	NOT		336
					Keeping the machine clean	7	NOT		294

Following are the main factors that should be taken as a result of the applied HTEA.

- Needle looper adjustment
- Disorder of tray setting
- Excessive model changes
- Unoriginal parts
- Program of the model
- The need of Spare parts
- Lighting
- Blunt blades
- Needle's blunder
- Material thickness
- Non-control by the cutter
- Lack of operator
- Poor adjustment of settings
- Not keeping the machine clean

Precaution studies that have been started to be done or recommended to be done in order to prevent the factors that cause the quilting removal specified above are as follows.

For the needle looper adjustment and disorder of tray setting problems, setup documents have been prepared to enable the operators to make standard adjustments on quilting machines.

For the blunt blades and the needle's blunder, a report was prepared for the determination of the blade and needle change times and their routine changes.

For the fact that the parts are not original, it was negotiated with the purchasing unit and studies were started to obtain the original parts

In case of the program factor of the model, the software of the drawings made by the R & D unit is entered into the machine in more than one way. As a result of this situation, wrong production is made by selecting the wrong program. R & D unit was negotiated and revisions were made to the software of the machine program.

For the lighting factor, the company was informed about the insufficient light situation about which the operators complained.

It was decided to provide training to the employees for the reasons such as failure of the cutter to control, inadequate of operators and poor adjustment of the settings. Detailed setting reports have been prepared in order to facilitate the adjustment of operators

For the material thickness factor, it was informed that the test design should be done by taking into consideration rope tension adjustment according to the thickness and density of the filling material.

In order to keep the machine clean, a report was prepared on how long the cleaning took time and how to clean and the operators were informed about them.

4.   CONCLUSION

In this study, the quality errors in the bed manufacturing process of the furniture factory in Kayseri were analyzed. Statistical quality control methods were used in the analyzes. Besides these methods, failure mode and effects analysis was done and the criteria that caused the error were determined carefully first.

As a result of these studies, the most common quilting removal error was tackled and the studies were carried out on this error. Brainstorming was carried out with a team including quality team and captione machine operators, fishbone diagram was formed and analyzes were made on the factors that could cause error. The main factors causing the error were determined by quality control methods. In order to prevent the error before occuring, failure mode and effects analysis was done. As a result of failure mode and effects analysis, the factors whose ros value is greater than 250 and the factors which have to be corrected and taken precaution, were determined.

Quilting removal error is mostly seen in K-10 machine. The K-10 machine has been considered as a pilot area where remedial studies have been carried out. The reason for the error is especially intensified under two headings. These are the problems experienced in making machine settings and the inexperience of operators and cutters working on the machine, and lack of sufficient training. These issues have been discussed in particular and priority has been given to recovery studies, which are defined as the form of machine setup documents and training of operators. In order to prevent and minimize the quilting removal error, necessary works have been started or recommendations have been made in the business mentioned in the findings section.

In addition to this study, the stress factor on the employees will be discussed and the effect of the stress on the error will be investigated. For this study, the device called galvanic skin reaction will be used.

REFERENCES

[1]. Boran, S., 2008. Toplam kalite yonetimi. Sakarya Universitesi Uzaktan Egitim Ders Notu, (Hafta 1)

[2]. Cakar, T., Serdar, T., 2002. Kalite yonetim sistemleri. SAU Fen Bilimleri Enstitusu Dergisi, 6 (2): 87-91.

[3]. Baysal, M., Caniyilmaz, E., Eren, T., 2002. Otomotiv yan sanayinde hata turu ve etkileri analizi. Teknoloji, 5 (1-2): 83-90.

[4]. Cevik, O., Aran, G., 2009. Kalite iyilestirme surecinde hata turu etkileri analizi ve piston uretiminde bir uygulama. SU IIBF Sosyal ve Ekonomik Arastirmalar Dergisi, 8 (16): 241-265.

[5]. Eryurek, O., Tanyas, M., 2003. Hata turu ve etkileri analizi yonteminde maliyet odakli yeni bir karar verme yaklasimi. Itu Dergisi, 2 (6): 31-40.

[6]. Ozfirat, P., 2014. Bulanik onceliklendirme metodu ve hata turu ve etkileri analizini birlestiren yeni bir risk analizi yontemi. Gazi Univ. Muh. Mim. Fak. Der., 29 (4): 755-768.

[7]. Soykan, Y., Kurnaz, N., Kayik, M., 2014. Saglik isletmelerinde hata turu ve etkileri analizi ile bulasici hastalik risklerinin derecelendirilmesi. Organizasyon Ve Yonetim Bilimleri Dergisi, 6 (1): 172-183.

[8]. Scheu, M., Tremps, L., Smolka, U., Kolios A., Brennan F., 2019. A systematic failure mode effects and criticality analysis for offshore wind turbine systems towards integrated condition based maintenance strategies. Ocean Engineering, 176: 118-133.

[9]. Kudlac, S., Stefancova, V., Josef, M., 2017. Using hte saaty method and the fmea method for evaluation of constraints in logistics chain. Procedia Engineering, 187: 749-755.

[10]. Ahire, C., Relkar, A., 2012. Correlating failure mode effect analysis (fmea) & overall equipment effectiveness (oee). Procedia Engineering, 38 :3482-3486.

[11]. Gokdeniz, I., 2005. Uretim sektorundeki iscilerin orgut ici stres kaynaklari ve mobilyacilik sektorunde bir uygulama. Selcuk Universitesi Sosyal Bilimler Enstitusu Dergisi, (13): 163-172.

[12]. Dayan, T., Figlali, A., 2018. Hata turu etkileri analizi ve kalite araclari kullanilarak bakir profil uretim verimliliginin artirilmasi. Kocaeli Universitesi Fen Bilimleri Dergisi, 1 (2): 67-76.

[13]. Seker, S., 2014. Sebep etki diyagramlari. YBS Ansiklopedi, 1 (4): 2-6.

[14]. Vardar, Y., 2012. Kobiler icin problem cozme teknikleri. Fethiye Ticaret ve Sanayi Odasi El Kitapcigi.

[15]. Caglar, M., Kurt, M., 2015. Alti sigma yaklasimi ve savunma sanayi sektorunde bir uygulama. Endustri Muhendisligi Dergisi, 27 (3): 13-24.

[16]. Yucel, O., 2007. Konfeksiyon uretiminde hata turu ve etkileri analizi. Tekstil ve Konfeskiyon, 2: 126-131.

[17]. Ceber, Y., 2010. Hata Turu Ve Etkileri Analizi Yonteminin (FMEA) Uretim Sektorunde Uygulamasi. Dokuz Eylul Universitesi, Sosyal Bilimler Enstitusu, Yuksek Lisans Tezi, Izmir, 110 s.

A Study on the Dyeing of Wool by using Linden Flower (Tilia)

Huseyin Benli[1], M.Ibrahim Bahtiyari[2],Fazlihan Yilmaz[2]

Abstract

The linden flowers are widely used for different aims because of their active substances but in this study, linden flowers with the leaves were researched as a natural source in dyeing of woolen fabrics. The linden that collected in season were dried, and then, used directly (without a previous extraction) in dyeing of fabrics at boiling temperature for 60 minutes. In the research, four separate metal salts: copper sulfate, iron sulfate, potassium dichromate and alum were used as mordant materials in the simultaneously dyeing procedure. The color efficiencies (K/S) and CIE L*a*b* results of the naturally dyed samples were determined and in addition to this, dyed woolen fabrics were tested in terms of fastness properties too. Consequently, it has been seen that satisfactory colors and fastnesses can be obtained by dyeing the woolen fabrics with linden.

Keywords: Natural dyes, woolen fabric, linden, dyeing, color

1. INTRODUCTION

The natural dyes, that can be obtained from animals or vegetable materials, are non-toxic, non-allergic and non-carcinogenic also these dyes without chemical processes but during the manufacturing of synthetic dyes, many carcinogenic chemicals are used [1]. Natural dyes, which were pushed during the last sixty years into the background by synthetic dyes, are recently again becoming object of consumer interests because of the awareness of possible risks during production of synthetic dyes [2].

In this study, Linden flowers, as natural colorant, are used in dyeing of wool fabrics. Turkey is one of the few areas in the world which is rich in terms of biodiversity. Linden flowers are widely used in medical and cosmetic industries due to the active substances they comprise [3]. A lot of phenolic compounds are in the herbal materials. Phenolic or polyphenols are secondary plant metabolites generally found in edible plants and have always been of interest because of their biological functions. These compounds presence an aromatic ring with one or more hydroxyl groups and their structures may vary from a simple phenolic molecule to a complex polymer with high-molecular mass [4].

Many researchers reported that linden flowers (esp. Tilia *tomentosa*) have got a lot of phenolic compounds such as Luteolin, Quercetin, Apigenin, Naringenin, Gallic acid, Myricetin, Kaempferol in Figure 1 [4], [5], [6].

| Quercetin | Kaempferol | Luteolin | Apigenin |
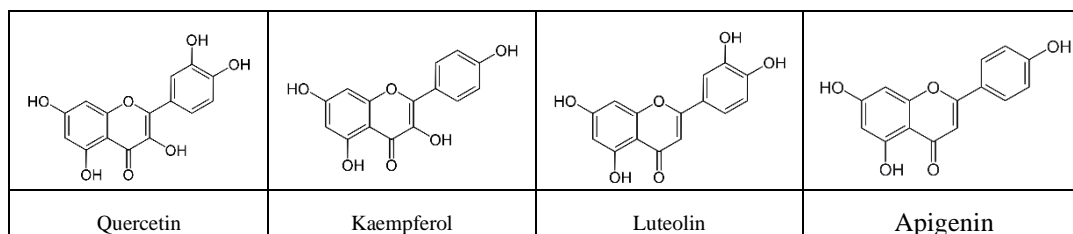
Figure 1. Some chemical structures of Linden

---

[1] Corresponding author: Kayseri University, Mustafa Cikrikcioglu Vocational School, 38280, Kayseri, Turkey. hbenli@kayseri.edu.tr

[2] Erciyes University, Department of Textile Engineering, 38039, Kayseri, Turkey, ibahtiyari@yahoo.com

2. MATERIALS AND METHODS

2.1. Materials

Linden flowers (Figure 2) with the leaves were collected in spring in Kayseri province and then they were dried in the shade and then grinded before use. These dried forms of this herbal source was directly used in dyeing processes of pretreated wool fabrics.

Figure 2. The dried linden flowers and leaves

2.2. Methods

In the study, we have tested four different mordanting agents and we have used these mordants (3% (w/w) iron (II) sulfate, 3% (w/w) copper (II) sulfate, 3% (w/w) potassium dichromate or 20% (w/w) alum) during the dyeing so simultaneously mordanting and dyeing was applied. In other words, the fabric, mordanting agent and the grinded linden flower and leaves (in the same amount with the fabric weight) were all together added to the bath and dyeing was managed at boiling temperature for 60 minutes as detailed in our previous study [7]. Washing processes were carried out following dyeing and the fabrics were then allowed to dry at room temperature.

To analyze the obtained colors a spectrophotometer (Konica Minolta 3600d) was used and the CIE $L*a*b*$ values were measured. In the CIE $L*a*b*$ space, $L*$ indicates lightness; colors with $a*>0$ represent redness, and those with $a*<0$ greenness; $b*>0$ indicates yellowness, and $b*<0$ blueness [8]. Moreover the color efficiencies (K/S) of the samples were measured by the spectrophotometer as well. In addition, the washing fastness with ISO 105-C10 [9], rubbing fastness with ISO 105-X12 [10] and light fastness with ISO 105-B02 [11] were evaluated too.

3. RESULTS AND DISCUSSION

The colors obtained from wool fabrics dyed with linden were collected in Table 1. It was observed that the color of the dyed samples were shifting depending on the used mordanting agents. As seen from the Table 1 after dyeing with linden flowers and leaves; khaki colors by using copper (II) sulfate, gray colors by using iron (II) sulfate, beige/pale yellow colors by using alum, and yellow/buff colors by using potassium dichromate could be obtained. Furthermore, the spectral measurements for the dyed wool samples were confirmed the color shifts caused by the change of mordants.

From the Table, it can be easily said that the lightest color was obtained from wool sample naturally dyed by using alum mordanting agent. In that case, the highest b* value ($b*$=32.2) was obtained as well and the color was yellow. On the other hand, the darkest color was obtained from the sample dyed by using iron (II) sulfate ($L*$=49.74) and the lowest redness ($a*$=0.1) was obtained in this case. In case of using potassium dichromate as mordanting agent the color is in light beige/buff shade and the hue angle was 84.51.

Table 1. Scanned photos, color fastness and CIE L*a*b* values of dyed samples.

Mordant agent	Dyed sample	CIE $L*a*b*$		Fastness properties				
				Rubbing		Washing		Light
				Wet	Dry	Sta.	C.C.	
$CuSO_4.5H_2O$		$L*$	53.7	4/5	5	5	5	4/5
		$a*$	1.68					
		$b*$	25.11					
		$C*$	25.17					
		h^o	86.18					
		K/S	6.84					
$FeSO_4.7H_2O$		$L*$	49.74	5	5	5	5	3
		$a*$	0.1					
		$b*$	7.74					
		$C*$	7.74					
		h^o	89.28					
		K/S	3.91					
$KAl(SO_4)_2.12H_2O$		$L*$	78.38	5	5	5	5	3/4
		$a*$	-1.46					
		$b*$	32.2					
		$C*$	32.24					
		h^o	92.59					
		K/S	2.68					
$K_2Cr_2O_7$		$L*$	66.81	5	5	5	5	4
		$a*$	2.64					
		$b*$	27.47					
		$C*$	27.59					
		h^o	84.51					
		K/S	2.96					

Sta.: Staining on cotton; C.C.: Color Change

The color efficiencies (*K/S*) of the dyed wool samples were analyzed too. It was observed that the highest color efficiency was obtained from the dyeings with copper (II) sulfate and the lowest color efficiencies were observed from the natural dyeing by using alum. The values were 6.84 and 2.68 respectively.

The dyed wool samples were analyzed in terms of fastness as well. For the light fastness, the best result was obtained by using copper (II) sulfate as a mordanting agent and in that case the light fastness was 4/5 point. On the other hand, in the use of potassium dichromate, alum, iron (II) sulfate, the obtained light fastness values were been 4, 3/4, 3 respectively. So it can be told that the type of metal element can affect the light fastness and changed it.

Moreover, it was observed that for the all dyed wool samples, the washing and the rubbing fastness were very good (the fastness values were 5 nearly for all samples).

4. CONCLUSIONS

In this study, instead of synthetic dyes linden flowers and leaves were used in dyeing of wool fabrics. For this aim this herbal source were firstly dried and then used directly in dyeing of wool with four different mordant. We have found that the tested herbal source can be suitable for the coloration of the wool and by changing the mordants different colors with different light fastnesses could come out.

As a result, it is thought that it can be used in coloration of wool fabrics and can find different opportunities in coloration of different textile materials as well. Therefore, when take into account satisfactory fastness properties too, in the further works, it is recommended to investigate the usability of linden in dyeing of synthetic fibers such as polyester, polyamide, polyacrylonitrile.

REFERENCES

[1]. N. Pruthi, G. D. Chawla, and S. Yadav, "Dyeing of silk with barberry bark dye using mordant combination," *Natural Product Radiance,* vol. 7, pp. 40-44, Jan. 2008.

[2]. K. H. Prabhu, and A. S. Bhute, "Plant based natural dyes and mordnats: A Review," *Journal of Natural Product and Plant Resources,* vol.2, pp. 649-664, Nov. 2012.

[3]. G. Tuttu, S. Ursavas, and R. Soyler, "Harvest Amounts and Ethnobotanical Uses of the Linden Flowers in Turkey," *Anatolian Journal of Forest Research,* vol.3, pp. 60-66, Jul. 2017.

[4]. S. Kivrak, T. Gokturk, and I. Kivrak, "Determination of Phenolic Composition of Tilia Tomentosa Flowers Using UPLC-ESI-MS/MS," *Int. J. Sec. Metabolite,* Vol. 4, pp. 249-256, Aug. 2017.

[5]. H. Matsuda, K. Ninomiya, H. Shimoda, and M. Yoshikawa, "Hepatoprotective Principles from the Flowers of Tilia argentea (Linden): Structure Requirements of Tiliroside and Mechanisms of Actiony," *Bioorganic & Medicinal Chemistry*, Vol.10, pp. 707–712, Mar. 2002.

[6]. A. Oniszczuk, and R. Podgórski, "Influence of different extraction methods on the quantification of selected flavonoids and phenolic acids from Tilia cordata inflorescence," *Industrial Crops and Products*, vol.76, pp. 509–514, Dec. 2015.

[7]. H. Benli, M. I. Bahtiyari, and F. Yilmaz, "The Dyeing of Wool Fabrics with Barberry Shrub Branches," in *Proc. ICENS 4th International Conference on Engineering and Natural Science,* 2018, p. 155.

[8]. K. J. Smith, *Colour order systems, colour spaces, colour difference and colour scales,* 2nd ed., R. McDonald, Ed. *Colour Physics for Industry,* Bradford, England: JSDC, 1997.

[9]. ISO 105-C10:2006 Textiles - Tests for color fastness - Part C10: Color fastness to washing with soap or soap and soda, Test Condition:Test A(1), International Organization for Standardization, Geneva Switzerland, 2006.

[10]. ISO 105-X12:1993 Textiles–tests for color fastness. Part X12: color fastness to rubbing, International Organization for Standardization, Geneva Switzerland, 1993.

[11]. ISO 105-B02:1994 Textiles - Tests for color fastness-Part B02: Color fastness to artificial light: Xenon arc fading lamp test, International Organization for Standardization, Geneva, Switzerland, 1994.

The Dyeing of Cotton Yarns by using Safflower (Carthamus tinctorius L.)

Huseyin Benli[1], M.Ibrahim Bahtiyari[2],Fazlihan Yilmaz[2]

Abstract

Nowadays, many scientists have been making intense efforts to produce environmentally friendly products in almost every branch. It is possible to see such efforts in the textile industry too. Especially, in the literature, also it is possible to meet by chance intensive studies onto clean textile dyestuffs and green applications. As part of this purpose, a research study was carried out on the dyeing of cotton yarns by using the Safflower plant. One of the most important expectations of this study will be not only the identification of environmentally friendly natural dyes but also to become widespread of usability too. In research, five different metal salts were used to make the dyeing more efficient. Addition to this, dyeing was conducted without use of mordanting agents. All the dyeing applications were carried out for one hour at boiling temperature according to meta-mordanting method. The color efficiencies (K/S) and CIE L*a*b* results of the dyed samples were determined and yarns were tested in terms of fastness properties as well. As a result, it has been seen that satisfactory colors and fastnesses can be obtained by dyeing the cotton yarns with Safflower plant.

Keywords: Textile, cotton, yarn, safflower, natural dyes, green application

1. INTRODUCTION

Recently, scientists have been working intensively on textile dyes. Some of these studies focused on natural colorants. Especially in recent years, herbal based colorants have become very popular. Many plant sources have flavon-based structures and can exhibit dye properties for textile materials. The use of natural dyes for textile materials is increasing due to awareness of environment, ecology, and pollution control [1]. Safflower can be one of these vegetable based dye source.

Safflower (Carthamus tinctorius L.) is a plant that has been cultivated since ancient times [2]. It has been grown for centuries, primarily for its colorful petals to use as food coloring and flavouring agent [3], as vegetable oils in the Far East, Central and Northern Asia, and European Caucasian [4]. Safflower, one of the oil-seed plants, is a single-year plant and can be cultivated as winter and summer [5]. It is reported that Safflower has been used in the Middle East, India and Africa for purgative and alexipharmic (antidote) effects, as well as in a medicated oil, to promote sweating and cure fevers [3]. Nowadays, it is possible to see that the Safflower plant is used for many different purposes. For example; vegetable oil can be obtained from them [6], can be used as raw material in biodiesel production [7], [5], and can be used in the dyeing of woolen textile materials (carpet-weaving industries) [3]. In addition, the Safflower plant could also be used in varnish, feed and pharmaceutical industry [7], [3]. The water-soluble yellow dye, carthamidin (Figure 1-(a)) can be obtained from safflower florets [3]. In this study, Safflowers, as natural colorant, are used in dyeing of cotton yarns.

---

[1] *Corresponding author: Kayseri University, Mustafa Cikrikcioglu Vocational School, 38280, Kayseri, Turkey.*
  hbenli@kayseri.edu.tr

[2] *Erciyes University, Department of Textile Engineering, 38039, Kayseri, Turkey, ibahtiyari@yahoo.com*

2. MATERIALS AND METHODS

2.1. Materials

The bleached 100% cotton yarns (Ne 40/1) were used in this study. Safflower (Figure 1-(b)) were provided from Kayseri province and then they were dried in the shade and then grinded before using. These dried forms of the plants were directly used in dyeing processes.

(a)	(b)
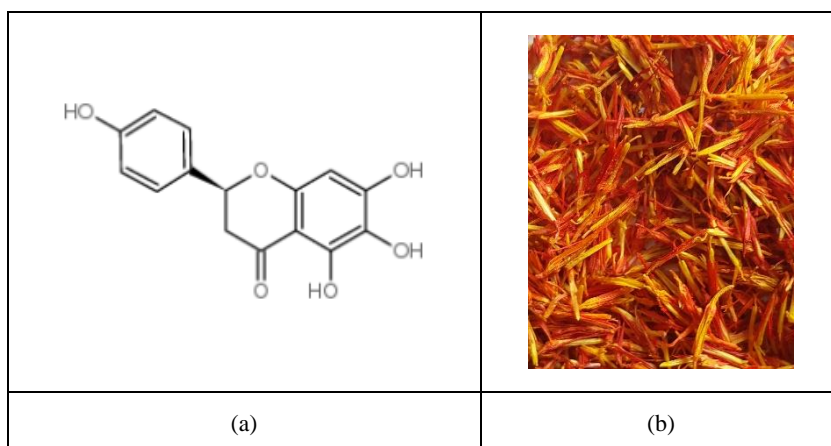
Figure 1. (a) Chemical structure of carthamidin [8] and (b) the dried Safflowers

2.2. Methods

In the all experiments, as mordanting agents, 3% (w/w) iron (II) sulfate, copper (II) sulfate, potassium dichromate, stannous (II) chlorate or 20% (w/w) alum were used. Furthermore, dyeing was carried out without using any mordant agent too. During the experiment, meta-mordanting method was applied. So the cotton yarn, mordanting agent and the grinded safflowers (in the same amount with the yarn weight) were all together added to the bath. In the experiments, the dyeing diagram used in our previous study and shown in Figure 2 has been carried out [9]. After dyeing, a cold rinsing, a washing in boiling with soap, a warm washing and then drying at room temperature were carried out respectively.
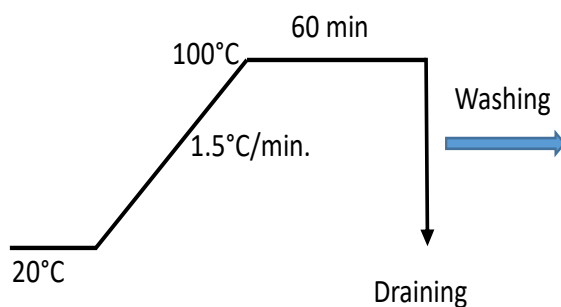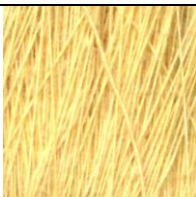
Figure 2. Dyeing diagram for cotton yarn
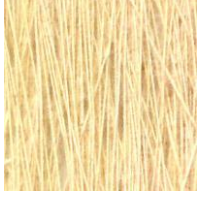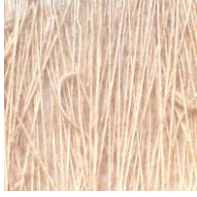
After dyeing processes, all the dyed yarns were tested in terms of *K/S* and CIE *L*a*b** values by using Konica Minolta 3600d spectrophotometer. The washing fastness with ISO 105-C10 [10] and light fastness with ISO 105-B02 [11] were investigated too.

3. RESULTS AND DISCUSSION

The colors obtained from cotton yarns dyed by using safflowers are shown in Table 1. As seen from the Table 1, through different the mordanting agents, the colors of the dyed yarns have been varied too. In addition, cotton yarns were dyed without the use of any mordanting agents too.

*Table 1. Scanned photos, color fastness and CIE L*a*b* values of dyed samples*

Mordant agent	Dyed sample	CIE $L*a*b*$		Fastness properties		
				Washing		Light
				Sta.	C.C.	
No-mordant		$L*$	81.82	5	5	4
		$a*$	4.08			
		$b*$	5.35			
		$C*$	6.73			
		h^o	52.65			
		K/S	0.29			
$CuSO_4.5H_2O$		$L*$	66.27	5	5	3/4
		$a*$	3.81			
		$b*$	1.23			
		$C*$	4			
		h^o	17.93			
		K/S	0.94			
$FeSO_4.7H_2O$		$L*$	67.39	5	5	3
		$a*$	1.18			
		$b*$	13.26			
		$C*$	13.31			
		h^o	84.9			
		K/S	1.54			
$KAl(SO_4)_2.12H_2O$		$L*$	79.33	5	5	3
		$a*$	1.41			
		$b*$	32.56			
		$C*$	32.59			
		h^o	87.52			
		K/S	2.25			

$K_2Cr_2O_7$		$L*$	75.1	5	5	3
		$a*$	0.39			
		$b*$	19.98			
		$C*$	19.99			
		h^o	88.89			
		K/S	1.43			
$SnCl_2$		$L*$	72.88	5	5	3
		$a*$	1.04			
		$b*$	13.33			
		$C*$	13.37			
		h^o	85.54			
		K/S	1.12			
Sta.: Staining on cotton yarn; C.C.: Color Change						

So, after dyeing by using safflowers violet colors by using copper (II) sulfate, brown colors by using iron (II) sulfate, yellow colors by using alum, light pink colors by using tin (II) chlorate, and beige colors by using potassium dichromate were obtained, and also pinkish orange colors by without the use of any mordanting agents were obtained.

Furthermore, the spectral measurements for the dyed cotton yarns were done too. In the CIE $L*a*b*$ space, $L*$ indicates lightness; colors with $a*> 0$ represent redness, and those with $a*< 0$ greenness; $b*> 0$ indicates yellowness, and $b*< 0$ blueness [12].

When the color efficiency (K/S) of cotton yarns dyed using safflowers are examined; Table 1 shows that different color efficiency can be obtained by using different mordant agents. The color efficiency of cotton yarns dyed using safflowers were changing as; non-mordanted < mordanted with Cu < mordanted with Sn < mordanted with Cr < mordanted with Fe < mordanted with Al, respectively. For the all of the dyed samples, the highest $L*$ value (81.82) was obtained from dyeing without mordant and the lowest $L*$ value (66.27) was obtained from dyeing by using copper (II) sulfate.

All dyed cotton yarns were tested for fastness properties too. The obtained results were very good especially in terms of washing fastness and were in the range of 4-5 points. The light fastness results were determined within the range of 3-4 points and all results are being satisfactory.

4. CONCLUSIONS

Safflower plant used in many different fields has been used for coloring of bleached cotton yarns as a source of natural dyes in this study. It has been observed that bleached cotton yarns can be colored by using safflower in terms of color fastness and color tones obtained. By using different mordants totally different colors were obtained and light colors were observed without the use of mordant material too.

REFERENCES

[1]. A. Davulcu, H. Benli, Y. Sen, and M. I. Bahtiyari, "Dyeing of cotton with thyme and pomegranate peel," *Cellulose,* vol. 21, pp. 4671-4680, Dec. 2014.

[2]. J. R. Smith, "Safflower", AOCS Press, Champaign, Illinois, 1996.

[3]. (1996) The bioversityinternational website. [Online]. Available: www.bioversityinternational.org

[4]. N. Camas, C. Cirak, and E. Esendal, "Seed Yield, oil content and fatty acids composition of safflower (carthamus tinctorius L.) Grown in northern Turkey conditions," *J. Fac. of Agric.*, vol. 22, 98-104, Jun. 2007.

[5]. T. Eryilmaz, C. Cesur, M. K. Yesilyurt, and E. Aydin, "Aspir (Carthamus tinctorius L.), Remzibey-05 Tohum Yagi Metil Esteri: Potansiyel Dizel Motor Uygulamalari icin Yakit Ozellikleri," *Turk Tarim ve Doga Bilimleri Dergisi*, vol.1, pp. 85–90, Jun. 2014.

[6]. D. Katar, I. Subasi, and Y. Arslan, "Effect of Different Maturity Stages in Safflower (Carthamus tinctorius L.) on Oil Content and Fatty Acid Composition," *Suleyman Demirel Universitesi Ziraat Fakultesi Dergisi*, vol. 9, pp. 83-92, Jun. 2014.

[7]. H. Karabas, "Ulkemiz Islahci Cesitlerinden Remzibey-05 Aspir (Carthamus tinctorius L.) Tohumlarindan Uretilen Biyodizelin Yakit Ozelliklerinin Incelenmesi," *Journal of Agricultural Faculty of Uludag University*, vol. 27, pp. 9-17, Feb. 2013.

[8]. H. Obara, J. Onodera, and F. Yamamoto, "The Synthesis of 4',5, 6, 7- and 4', 5, 7, 8-Tetrahydroxyflavanone and Their Comparison with Carthamidin and Isocarthamidin," *Chemistry Lett., Published by the Chemical Society of Japan*, p. 915-916, Jun. 1973.

[9]. H. Benli, M. I. Bahtiyari, and F. Yilmaz, "The Dyeing of Wool Fabrics with Barberry Shrub Branches," in *Proc. ICENS 4th International Conference on Engineering and Natural Science,* pp. 155, 2018.

[10]. ISO 105-C10:2006 Textiles - Tests for color fastness - Part C10: Color fastness to washing with soap or soap and soda, Test Condition:Test A(1), International Organization for Standardization, Geneva Switzerland, 2006.

[11]. ISO 105-B02:1994 Textiles - Tests for color fastness-Part B02: Color fastness to artificial light: Xenon arc fading lamp test, International Organization for Standardization, Geneva, Switzerland, 1994.

[12]. K.J. Smith, *Colour order systems, colour spaces, colour difference and colour scales,* 2nd ed., R. McDonald, Ed. *Colour Physics for Industry,* Bradford, England: JSDC, 1997.

Aerodynamic Optimization of Rotating Diffuser for Horizontal Axis Wind Turbine

Safak Dogru[1], Oktay Yilmaz [1], Ali Can Koyuncuoglu [1]

Abstract

Energy costs are increasing, and environmental pollution is becoming more and more serious all over the world. In recent years, there has been a trend towards renewable energy sources. The use of wind energy, which is a renewable energy source, has gained more importance in recent years. As a result, wind turbine systems, one of the wind power electricity generation techniques, have developed rapidly in the last few decades. This research focused on improving the performance of an experimentally validated conventional 3-blade horizontal axis wind turbine with an optimum rotating diffuser. In order to understand performance augmentation effects of a rotating diffuser on the wind turbine, the effects of the diffuser shape on the increased wind speed and flow uniformity just around the turbine rotor were investigated by computational fluid dynamics (CFD) analyses. The rotating diffuser is shaped based on GOE431 *airfoil. The numerical results have shown that flow uniformity and the wind speed through the rotating diffuser was greatly influenced by the chord length and angle of attack of the airfoil used. The design of rotating diffuser is investigated with the response surface optimization method for maximum wind speed with good flow uniformity around the rotor. In this study, an optimum rotating diffuser with power coefficient well beyond the Betz limit has been developed for a conventional horizontal wind turbine with a rotor diameter of 0.90 m.*

Keywords: Wind Turbine, CFD, Response Surface Optimization, Rotating Diffuser, Betz Limit

1. INTRODUCTION

Many countries in the world use wind turbines to generate electricity through renewable energy sources and use this environmentally friendly system. Due to the increase in energy demand and population growth in the world, the use of wind energy, which is one of the leading renewable energy sources, has gained more importance in recent years.

Among the renewable energy sources, the most popular issue in the world for the time being is the efforts to make maximum use of wind energy. The main reason for this is that the wind is an easily accessible source. Researches, PhD theses and graduation projects are studies on increasing the usability of the existing systems at maximum level and bringing differences with the innovation work. There exist lots of studies concentrated on wind turbine with diffuser [1-4]. Productivity, portability, ease of use and minimum cost can be considered to be advantages of wind energy renewable energy systems. When we consider these systems, electrical energy from wind prevents pollution in the atmosphere with zero carbon dioxide emission.

With increasing use of wind energy and increasing interest in renewable energy in the world, number of wind energy systems has started to increase.

Especially, numerical investigations are carried out for flow fields around flanged diffusers to develop small wind turbines by Abe and Ohya [4] and Phillips et al. [3]. Hansen et al. [5] showed that Betz limit can be exceeded with the relative increase in mass flow through the rotor.

In the Krogstad and Adaramola [6] study, the model tested is a three-bladed horizontal axis type wind turbine with an upstream rotor of 0.90 m diameter. Also, in this study, the wind turbine geometry is the same as Krogstad and Adaramola [6].

As can be understood from the literature review, small horizontal axis wind turbine can properly be used with diffuser. However, many researchers have worked on the use of stationary diffuser. The purpose of this study is to investigate the effect of rotating diffuser on turbine performance.

2. METHODS

2.1 Validation and Computational Fluid Dynamics

ANSYS Fluent R2019 R1 has been used for present case. Second order upwind scheme was used for spatial discretization and coupled algorithm was used for velocity-pressure coupling. In order to resolve viscous sublayer, RANS - SST k-ω turbulence model has been used. Whole analyses have been performed as steady state pressure based, and proper mesh resolution has been used for near wall and volume mesh.

At the beginning of the study, validation has been performed for wind turbine of which experimental performance characteristics are provided in detail by Krogstad and Adaramola [6] with study performed in the wind tunnel of Department of Energy and Process Engineering at The Norwegian University of Science and Technology. A large set of experimental datum is published, and for the validation has been carried out with comparison of the power coefficient and thrust coefficient.

Firstly, mesh independence tests were carried out for 6 different meshes at 9 m/s free wind speed for open rotor wind turbine as shown in Figure 1. Proper number of mesh was 2.8 million elements.
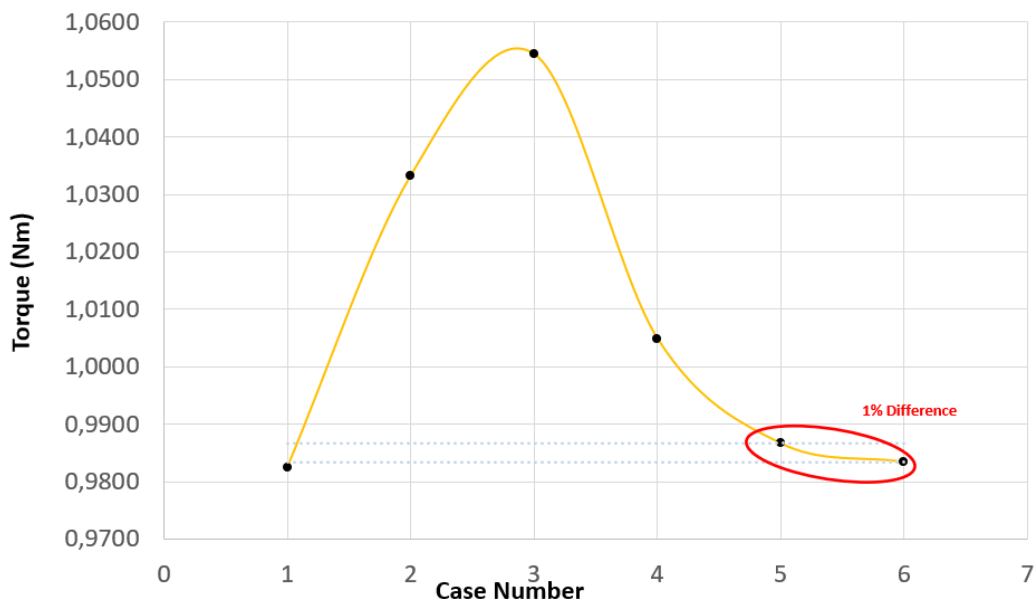
Figure 1. Mesh independence study for Open Rotor Turbine in CFD

For the validation, CFD results compared with experimental data. The CFD results exhibit very close agreement with experimental data except high TSR values. Power coefficient (C_P) and thrust coefficient (C_T) can be found depending on different tip speed ratios (TSR) in Figures 2 and 3.

$$C_P = \frac{2T\Omega}{\rho\pi R^2 U_\infty^3} \tag{1}$$

Where T is torque generated by rotor, Ω is rotor angular speed, ρ is density of air, R is radius of rotor, U_∞ is freestream velocity of air.

$$C_T = \frac{2D}{\rho\pi R^2 U_\infty^2}$$

(2)

Where D is drag force.
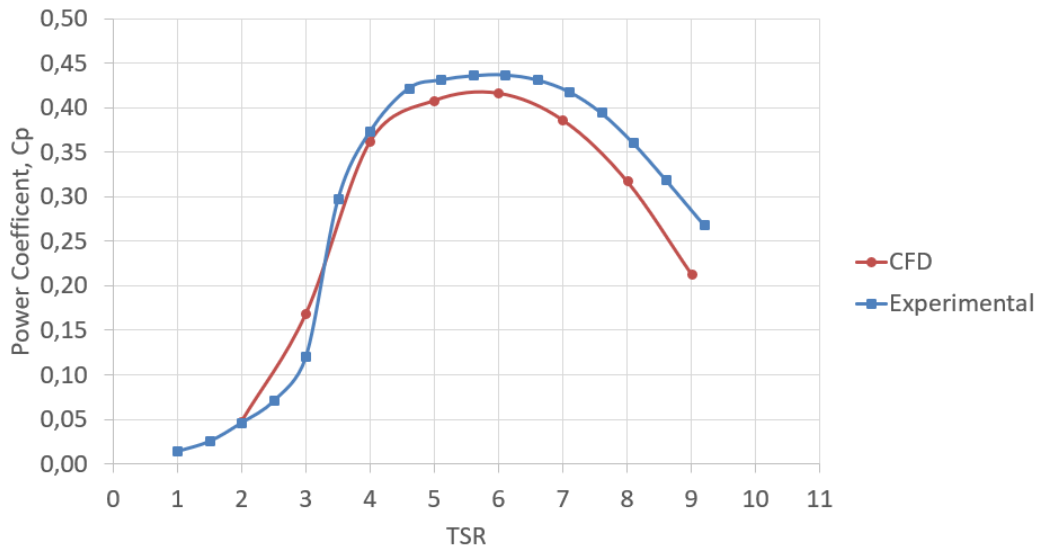
Figure 2. Comparison of power coefficients from CFD and the experiments
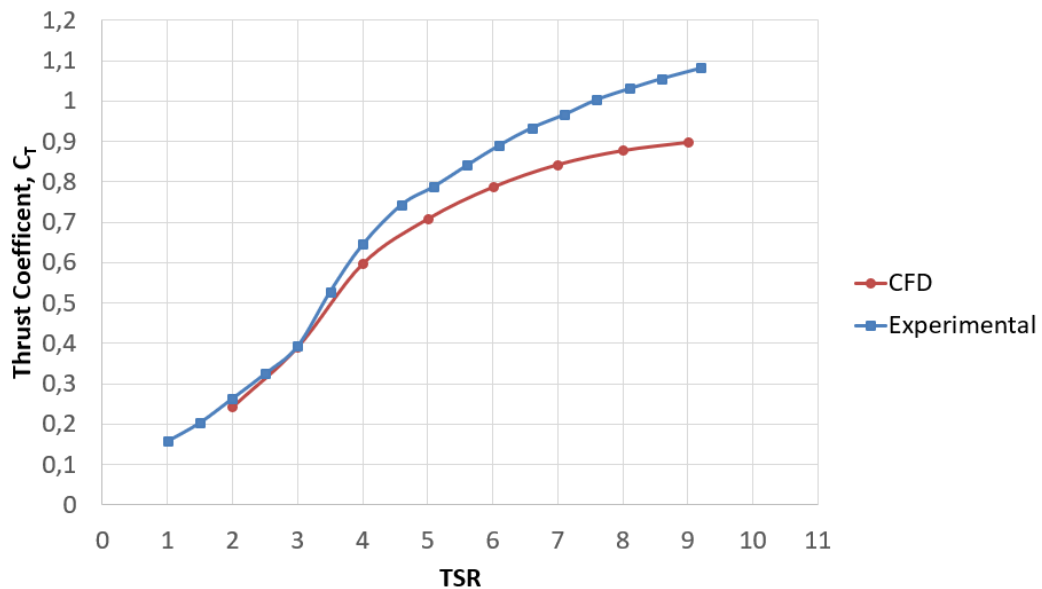
Figure 3. Comparison of trust coefficients from CFD and the experiments

2.2. Optimization

For this validated wind turbine, a diffuser based on an asymmetrical GOE431 airfoil has been optimized with response surface optimization method.

Uniform wind velocity of 9 m/s is set at the inlet boundary of the computational domain which is the same as one that in experimental study of the tested turbine. Also, the computational model is prepared as 2D axisymmetric swirl in order to represent rotating diffuser in CFD. It is shown in the Figure 4 and Figure 5.

A mesh independence assessment was carried out by analyzing mass flow rate of diffuser for several mesh configurations which have increasing number of computational cells. The mesh independence results can be seen in Figure 6 showing minimized differences. Proper number of mesh elements is 0.2 million.
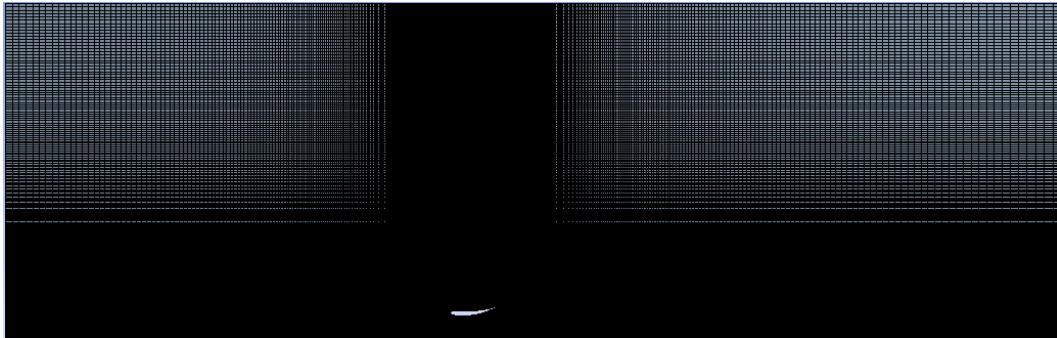
Figure 4. 2D Axisymmetric swirl model and mesh
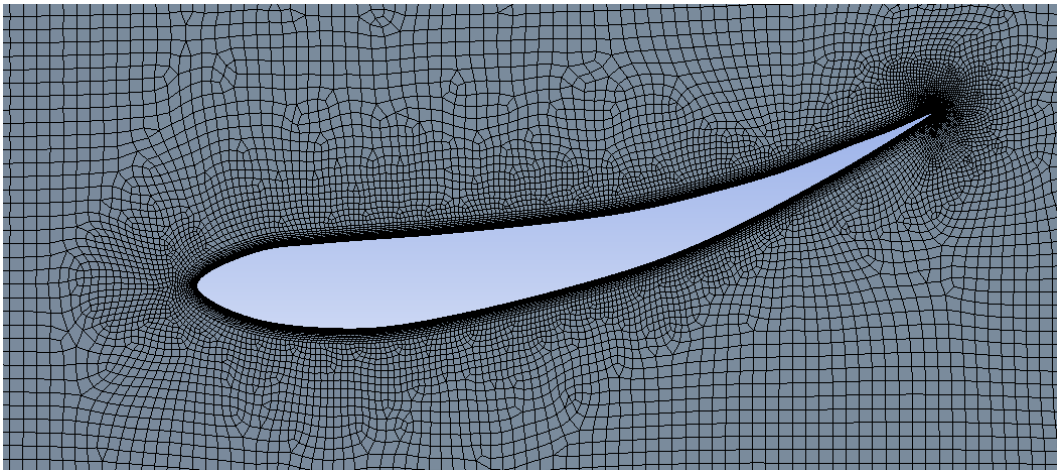
Figure 5. Near wall mesh resolution ($y^+ \cong 1$)

Figure 6. Mesh independence study for diffuser optimization

Two different parameters have been selected to be optimized. These parameters are the chord length and angle of attack of the diffuser airfoil. Chord length range is from 0.2 m to 0.7 m, and angle of attack range is from 2° to 20°. The goal is to maximize the mass flow rate while maintaining velocity distribution as uniformity as possible at the rotor plane. Parameters are calculated from the exit of the diffuser. The summary of parameters can be seen in Table 1.

Table 8. Optimization conditions and objectives

Parameter	Type	Lower Bound	Upper Bound	Objective
Chord Length (m)	Input	0,2	0,7	-
Angle of Attack (°)	Input	2	20	-
Mass Flow Rate (kg/s)	Output	-	-	Maximum
Uniformity of Velocity	Output	-	-	Maximum

Response surface method employed with high sensitivity. The response surface method is based on kriging interpolation, and prediction of response surface has highly accurate results. The response surfaces can be found in Figure 7.

Mass Flow Rate   Uniformity of Velocity
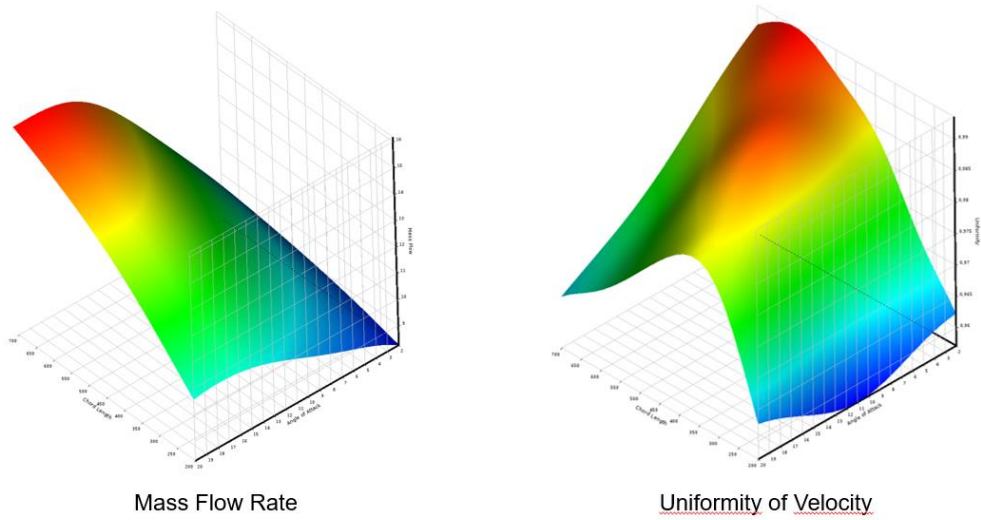
Figure 7. Response surface of mass flow rate and uniformity of velocity

As a result of the optimization procedure, optimal design point is 0.472 m chord length and 13.1° angle of attack as shown in Table 2 below.

Table 9. Optimization results of parameters

Parameter	Type	Lower Bound
Chord Length (mm)	Input	472
Angle of Attack (°)	Input	13,1
Mass Flow Rate (kg/s)	Output	13,47
Uniformity of Velocity	Output	0,988
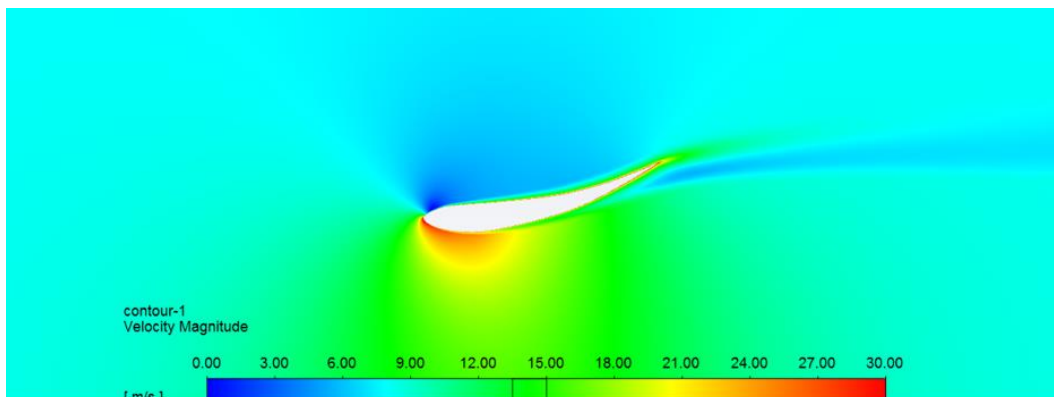
Figure 8. Optimal geometry and velocity contour

2.3. Rotor with diffuser

The same mesh configuration was also used for the two cases, leading to 2.8 million elements for the open rotor and 7.6 million for the rotor with diffuser cases.

3. RESULTS AND DISCUSSION

The rotor with rotating diffuser is not suitable for application. Numerical analysis results showed us that the turbine needs a huge torque to rotate. There is excessive friction between the air and the diffuser which prevents the turbine from rotating as illustrated in Figure 9.
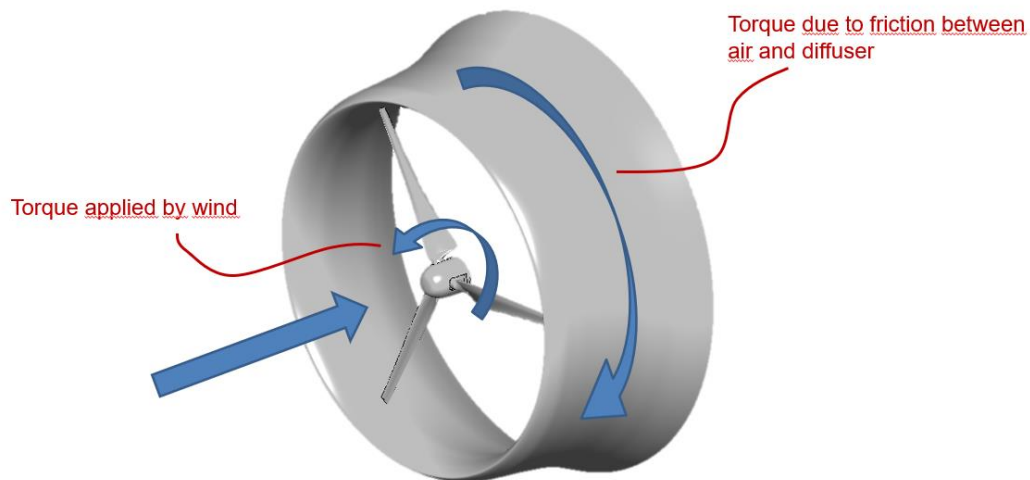
Figure 9. Rotating Diffuser

Therefore, the study was continued with stationary diffuser, and tip clearance was adjusted as 5 mm. The open rotor wind turbine is compared with rotor with stationary diffuser. Power coefficient (C_P) and thrust (C_T) coefficients versus TSR are depicted in Figures 10 and 11. These graphics show that the same TSR does not have similar trend between the open rotor and rotor with diffuser. In proper operation of the rotor with diffuser, maximum C_P is expected to be in the higher range of TSR. Blade twist angle must be optimized to achieve higher efficiency in a wider range of TSR.
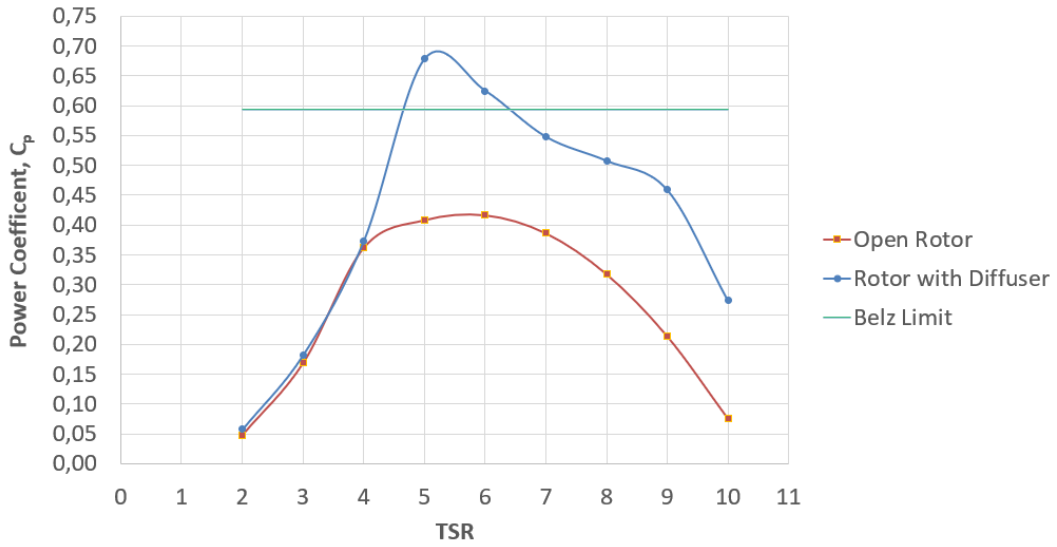
Figure 10. Comparisons of power coefficients of ''Open Rotor'' and ''Rotor with Diffuser''
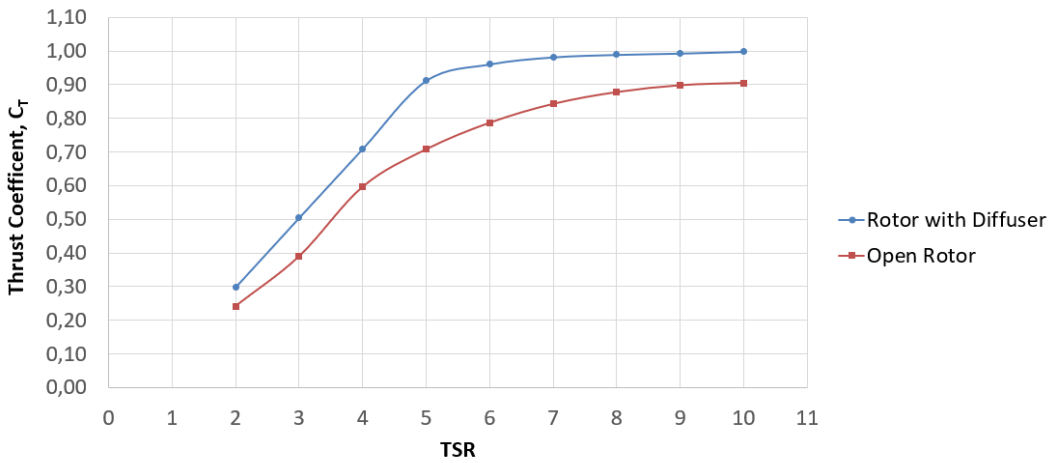
Figure 11. Comparisons of thrust coefficients of ''Open Rotor'' and ''Rotor with Diffuser''

Also, comparison of mass flow rates of blank, only diffuser, open rotor and rotor with diffuser are shown in the Figure 12 below.

Parameter	Mass Flow Rate (kg/s)
Blank	7,014
Diffuser	10,788
Open Rotor	5,652
Rotor with diffuser	6,015

Figure 12. Mass flow rates of geometries

4. CONCLUSIONS

In this study, first, a wind turbine of which geometry and performance charts are well-documented is validated by CFD. Then characteristics of a wind turbine with diffuser are investigated by an engineering approach. The power and thrust coefficients are calculated by computational fluid dynamics. This will be a guideline for the proper design of wind turbine with diffuser. It can be concluded that rotating diffuser is not effective as stationary diffuser due to its huge friction surface with air. The diffuser should have large size of chord length to increase mass flow rate, and this is a contradiction. Therefore, the engineering approach will continue to be applied to the use of stationary diffuser to increase the power generated from the wind.

For the further works, shape optimization will be applied on airfoil. Even, different airfoil shape will be added on optimization process. Also, tip clearance of the turbine and diffuser will be worked on. Rotor blade twist angle will be considered to increase the efficiency.

ACKNOWLEDGEMENTS

REFERENCES

[1]. B.L. Gilbert, K.M. Foreman Experiments with a diffuser-augmented model wind turbine. Journal of Energy Resources Technology vol 105, p. 46–53, 1983.

[2]. O. Igra Research and development for shrouded wind turbines. European Wind Energy Conference EWEC84, Hamburg, pp. 236–245, 1984.

[3]. D.G. Phillips, P.J. Richards, R.G.J. Flay, CFD modelling and the development of the diffuser augmented wind turbine, Proceedings of the Computational Wind Engineering, pp. 189–192, 2000.

[4]. K. Abe, Y. Ohya, An investigation of flow fields around flanged diffusers using CFD, Journal of Wind Engineering and Industrial Aerodynamics, pp. 315-330, 2004.

[5]. M. O. L. Hansen, N. N. Sørensen, R. G. J. Flay, Effect of Placing a Diffuser around a Wind Turbine, Wind Energy, vol 3, pp. 207–213, 2000.

[6]. P. A. Krogstad and M. S. Adaramola, Performance and near wake measurements of a model horizontal axis wind turbine, Wind Energy, vol 15, pp. 743–756, 2012.

Risk Management in Complex Power Facilities

Natalija Petrova[1], Vangel Fustik[2]

Abstract

The subject of research presented in this paper is development and application of methodologies for managing technical risks in the complex power facilities. The vulnerabilities (threats), the uncertainties and faults of the power facilities and its' equipment, as well as the interruptions in the power system are analyzed. The main objective is defining an convenient methodology for providing the opportunity for analysis and providing acceptable reliability of the technical system, i.e. reducing the number of interruptions to a minimum, optimizing the utilization of the available potential and ensuring safe working procedures. According to the methodology and necessary analyzes, risk management is realized by setting margins that determine the acceptability of risk exposure and reducing the likelihood of occurrence of events that have a potential threat to reduce the reliability of the systems. Furthermore, the methodology of a fault tree and a log events for quantitative risk assessment in the power plants will be applied, as well as the use of the Baes networks for decision making for the treatment of the technical risks. As a result, it is expected that risk management techniques will enable successful management of the risks, faults and activities associated with the identified risks in order to ensure safe and reliable functioning of the plants and facilities as a whole. An overview is given to the operation of the protection and management systems that often reach a high level of specificity as they are affected by the equipment or the characteristics of the plants (substations, power plants, lines) and it is necessary that experts who know the process study them well. In addition, companies that have specific expertise need to quantify and accurately represent them. These risks have economic impact on the performance of companies and therefore their assessment and risk management is of highest necessity.

Keywords: risk management, power facilities, faults, interruptions

1. INTRODUCTION

Risk management is logical and sistematic approach for identification, analysis, evaluation, monitoring and communication of the risks in projects in a way that the loses of the company will be minimized and possibilities maximized [1], [2]. Identified risks have economic impact on the performance of companies and therefore their assessment and risk management is of highest necessity [3], [4].

The scope of research presented in this paper is development and application of methodology for managing technical risks in the complex power facilities.

The focus of the analysis are: vulnerabilities (threats), the uncertainties and faults of the power facilities and its' equipment, as well as the interruptions in the power system are analyzed.

The main objective is defining an convenient methodology for providing the opportunity for analysis and providing acceptable reliability of the technical system.

That way the number of interruptions will be reduced to a minimum, optimizing the utilization of the available potential and ensuring safe working procedures.

2. THE METHODOLOGY APPLIED

Risk management is realized by setting margins that determine the acceptability of risk exposure and reducing the likelihood of occurrence of events that have a potential threat to reduce the reliability of the systems [5-7].

---

[1] Corresponding author: University Saints Cyril and Methodius, Faculty of Electrical Engineering and Infromation Technologies, Skopje, North Macedonia, npetrova@feit.ukim.edu.mk

[2] University Saints Cyril and Methodius, Faculty of Electrical Engineering and Infromation Technologies, Skopje, North Macedonia

The methodology of a fault tree and a log events for quantitative risk assessment in the power plants will be applied, as well as the use of the Baes networks for decision making for the treatment of the technical risks.

Risk management techniques will enable successful management of the risks, faults and activities in order to ensure safe and reliable functioning of the plants and facilities as a whole.

High level of specificity as they are affected by the equipment or the characteristics of the plants (substations, power plants, lines) and it is necessary that experts who know the process study them well.

3. RESULTS

Tipes of analyzed risk are:

- Financial risk (investment, ROI, IRR, NPV)
- Legal risks (legal procedures, environ. restrictions, policy)
- Natural and physical risks
- Human workmanship risks, knowledge,
- Technical risks;
- Security risks etc.

Applied methods – Qualitative [8-11]:

- Probability Analysis
- Delphi Method
- Monte Carlo Method
- SWOT
- Brainstorming

Applied methods – Quantitative [8-11]:

- Expected Monetary Value – EMV
- Sensitivity analysis
- Decision tree
- Modeling and simulation
- Expert evaluation
- Range estimation

The results are presented on figures 1, 2, 3 and 4.
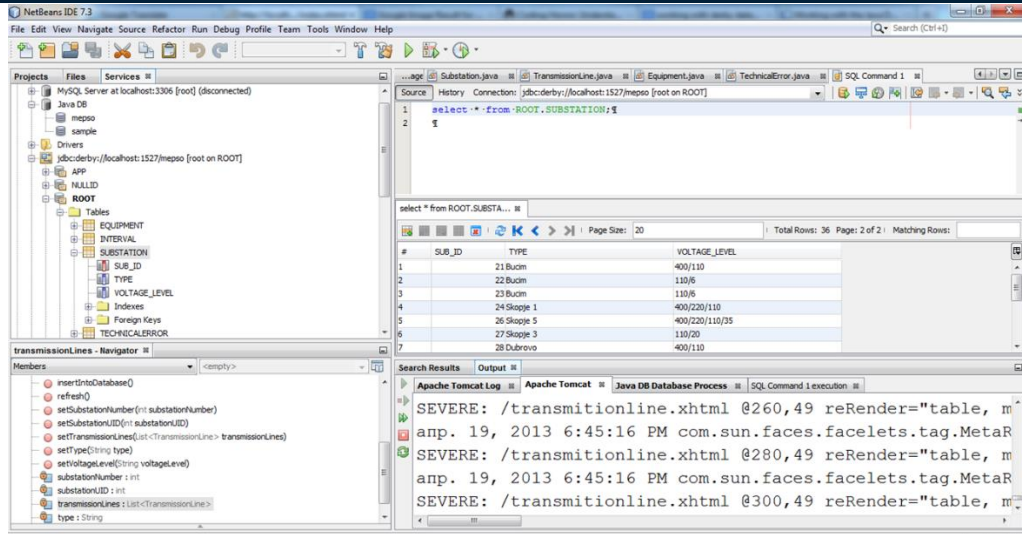
Figure 1. Risk analysis for complex facility – a case study
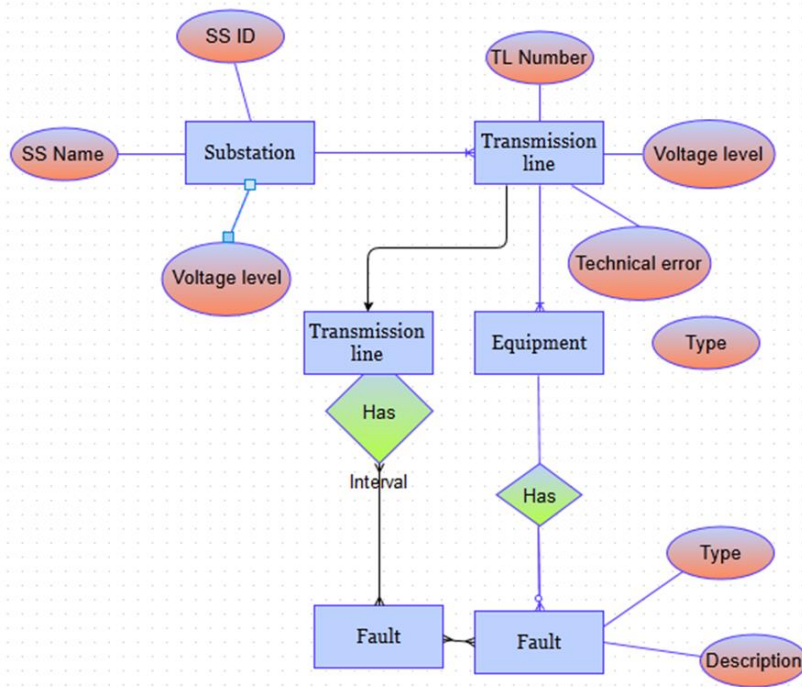
Figure 18. Entity-relationship diagram (ER)
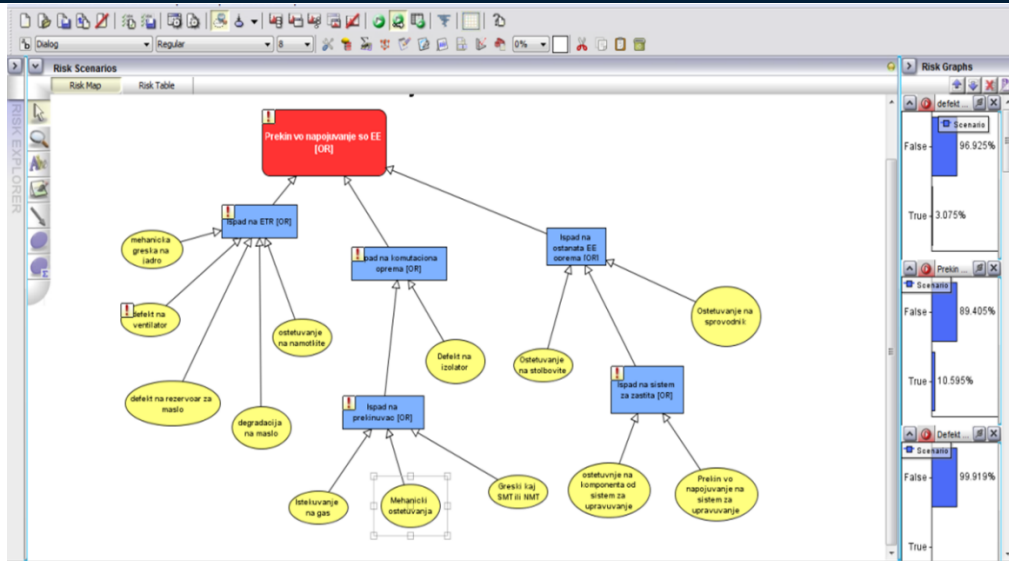
Figure 3. Baesian model – network diagram for electricity delivery interruption in substation
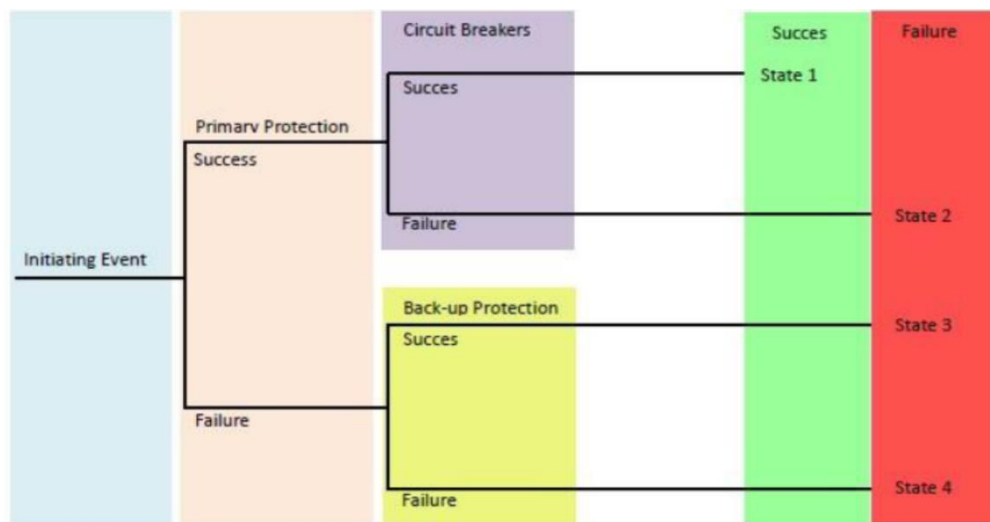
Figure 4. The Tree of events for line interuption

4. CONCLUSION

In power system the technical risks could be of different origin, depending on the applied technology, voltage levels and arrangement. The could occur by various reasons and different probability and different impact on the equipment and functionality of the entire facility.

An application of the Risk management is inevitable to predict such risks and to make risk plane for adequate risk response.

The applied methodology depends on the: project phase, risk management strategy and treated variables such as Time, Quality or Costs. Each facility has its' own specific features and a considerable knowledge and experience in the field is necessary, as well as, the theory and practice of risk management.

REFERENCES

[1].   PMI, „Project Management Book of Knowledge", Edition 2010.
[2].   Identifying and Managing Project Risk: Essential Tools for Failure-Proofing Your Project, Tom Kendrick, AMACOM © 2003.
[3].   N. Petrova, N. Kiteva Rogleva, V. Fustik, „Managing Renewable Energy Projects Including Risk Analysis", MESTE, Belgrade, may 2018.
[4].   R. Max Wideman, „Project and Program Risk Management – Guide to Managing Project Risks and Oppurtunities", PMI, Pennsylvania, USA, 1992.
[5].   The Essentials of Risk Management, by Michel Crouhy (Author), Dan Galai (Author), Robert Mark (Author), 2014.
[6].   A Practical Guide to Risk Management, by Thomas S. Coleman (Author), 2011.
[7].   Practical Methods of Financial Engineering and Risk, by Rupak Chatterjee (Author), 2014.
[8].   Thamhain, H. J. (2013). Managing risks in complex projects. Project Management Journal, 44(2), 20–35.
[9].   Browning, T. R. (2019). Planning, Tracking, and Reducing a Complex Project's Value at Risk. Project Management Journal, 50, 71–85.
[10].   Avery, G. (2016). Leading high-risk projects: servant leadership lessons from the 1953 Mount Everest Expedition. Paper presented at PMI® Global Congress 2016—EMEA, Barcelona, Spain. Newtown Square, PA: Project Management Institute.
[11].   Gumz, J. (2012). Risk on complex projects: a case study. Paper presented at PMI® Global Congress 2012—EMEA, Marsailles, France. Newtown Square, PA: Project Management Institute.

An Overview About Software Metric Tools

Zeynep Behrin Guven Aydin[1], Ugur Osman Yucel[1], Ruya Samli[2]

Abstract

Measurement in a software is a basic process applied from the first part to the last part of the Software Development Life Cycle. Since it's impossible to express the quality of the software in an abstract manner objectively, the quality of the software needs to be concretized. In software engineering, measurement is difficult and not precise. However, any measure is better than zero measure. Software Metric Tools are the most basic measurement tools for measuring the quality of software. In this paper software metric tools are explained:

Keywords: software metric tools

1. INTRODUCTION

A measurement is the process of assigning numbers or symbols to the properties of real-world entities defined by clearly defined rules. Therefore, measurement requires assets, properties, and rules to assign values to properties.According to the IEEE Standards Glossary, the measurement process is defined as the quantitative measure of the degree to which a system, component, or process has a specific characteristic. The word "metric" is a French-based word that means ''measured in terms of meters or meter-based metrics.''

Metrics allow software to be evaluated in many ways. These assessments help develop quality software [1]. Many measurements have been proposed in the literature to capture and measure the structural quality of object-oriented code and design in particular. Software Metric Tools are the most basic measurement tools for measuring the quality of software.

In the literature; There are many traditional paid or free software testing tools such as Radar, QuickBugs, Bugtrack, ZeroDefect, Roundup and Abuky, and object-oriented software testing tools such as Sonargraph, Understand, Findbugs, Metrics, PMD and Coverity have been developed.

2. SOFTWARE METRIC TOOLS

Software metrics are the most basic measurement tools that can be used to measure the quality of software. There are many tools used to measure software metrics.

2.1. Understand

Understand is a static analysis tool focused on source code comprehension, metrics, and standards testing. It is designed to help maintain and understand large amounts of legacy or newly created source code. It provides a cross-platform, multi-language, maintenance-oriented IDE (interactive development environment)

The source code analyzed may include C, C++, C#, Objective C/Objective C++, Ada, Assembly, Visual Basic, COBOL, Fortran, Java, JOVIAL, Pascal/Delphi, PL/M, Python, VHDL, and Web (PHP, HTML, CSS, JavaScript, and XML).

[1] Maltepe University, Department of Software Engineering, 34220, Maltepe/Istanbul, Turkey. zeynepguven@maltepe.edu.tr

[2] 2 Istanbul University – Cerrahpasa, Department of Computer Engineering, Avcilar/Istanbul TURKEY

It offers code navigation using a detailed cross-referencing, a syntax-colorizing "smart" editor, and a variety of graphical reverse engineering view [2].

Understand is a customisable integrated development environment (IDE) that enables static code analysis through an array of visuals, documentation, and metric tools.[3] It was built to help software developers comprehend, maintain, and document their source code. It enables code comprehension by providing flow charts of relationships and building a dictionary of variables and procedures from a provided source code.[4]

In addition to functioning as an integrated development environment, Understand provides tools for metrics and reports, standards testing, documentation, searching, graphing, and code knowledge. It is capable of analyzing projects with millions of lines of code and works with code bases written in multiple languages.[5] Developed originally for Ada, it now supports development in several common programming languages.[6] Integration with the Eclipse development environment is also supported.

Understand has been used globally for government, commercial, and academic use. It is used in many different industries to both analyze and develop software. Specific uses include a variety of applications: code validation for embedded systems,[5] software litigation consulting,[6] reverse engineering and documentation,[7] and source code change analysis.[8]
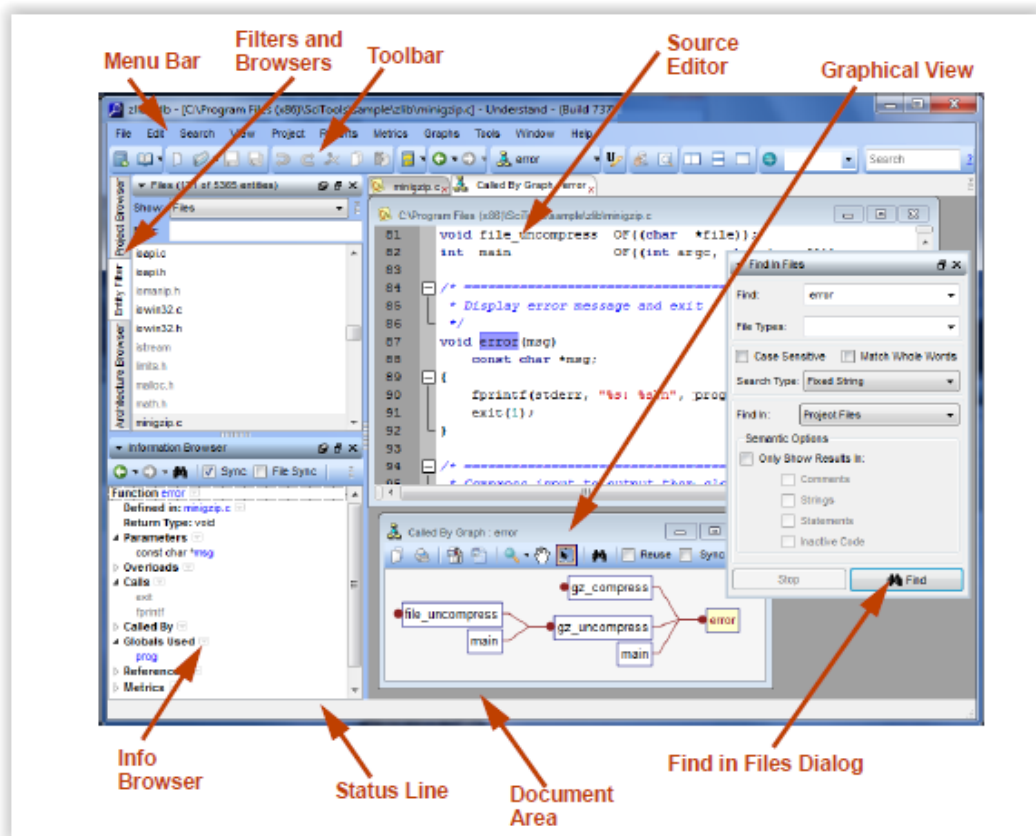
Figure 9-Understand Tool

2.2. Sonargraph

Sonargraph is a powerful static code analyzer that allows you to monitor a software system for technical quality and enforce rules regarding software architecture, metrics and other aspects in all stages of the development process. The Sonargraph platform supports Java, C#, Python 3 and C/C++ out of the box and includes powerful features like a Groovy based scripting engine and a DSL (domain specific language) to describe software architecture [9]

Sonargraph is a commercial tool for static code analysis of software written in Java, C#, C or C++. By parsing the source code it builds an in memory dependency and metrics model of the analyzed code. The model

dependencies can then be visualized graphically so that the user is able to understand the structure of the system. Moreover, the tool allows the definition of a logical architecture model (intended structure of the software) based on a domain specific language designed for software architecture. By comparing the logical model with the real dependency structure Sonargraph finds and list all architecture violations (deviations from the intended structure).

Moreover, Sonargraph computes a wide range of software metrics that help the user to pinpoint problematic code sections and to estimate the overall technical quality of his project. It also helps with finding duplicated blocks of code, which are usually considered undesirable. A Groovy based scripting engine allows the user to compute user defined metrics and to create customized code checkers [10].
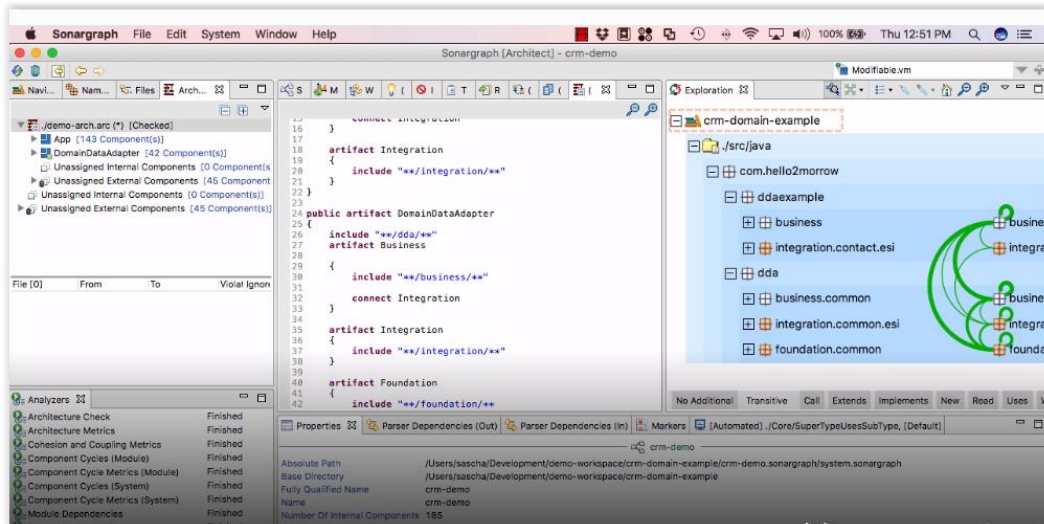
Figure 10-Sonargraph Tool

2.3. Findbugs

FindBugs is an open-source static code analyzer created by Bill Pugh and David Hovemeyer which detects possible bugs in Java programs [11][12]. Potential errors are classified in four ranks: (i) scariest, (ii) scary, (iii) troubling and (iv) of concern. This is a hint to the developer about their possible impact or severity [13]. FindBugs operates on Java bytecode, rather than source code. The software is distributed as a stand-alone GUI application. There are also plug-ins available for Eclipse, [14] NetBeans, [15] IntelliJ IDEA, [16][17][18] Gradle, Hudson, Maven, [18]Bamboo[19] and Jenkins.[20] Additional rule sets can be plugged in FindBugs to increase the set of checks performed.[21] A successor to FindBugs, called SpotBugs, has been created.

Findbugs is an open source tool for static code analysis of Java programs. It scans byte code for so called bug pattern to find defects and/or suspicious code [22].
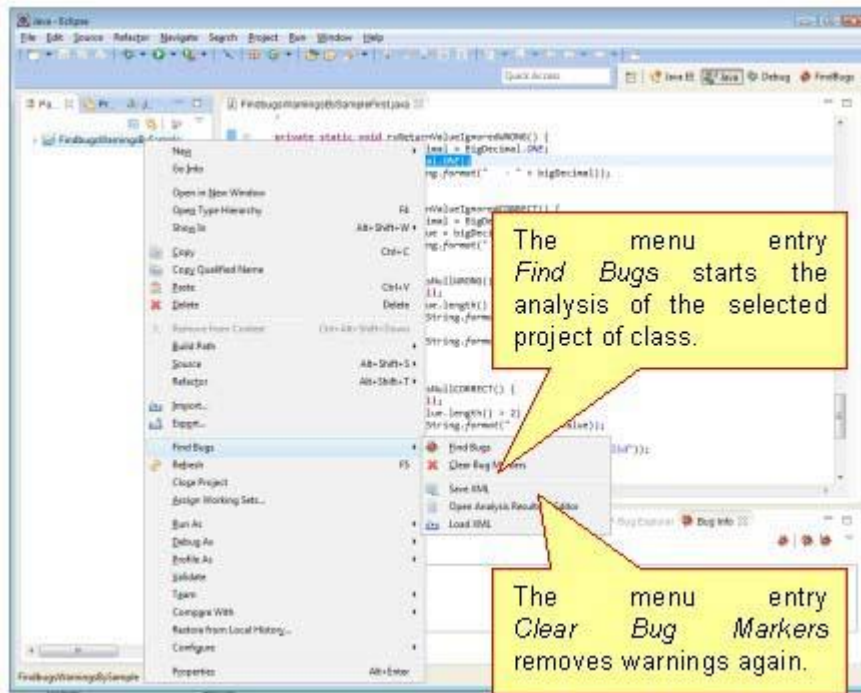
Figure 11-FindBug Tool

2.4. Metrics

Metrics is another open source program developed as an extension to the Eclipse project. The Java program in the Eclipse development environment can run in an integrated format, automatically measuring many commonly used software metrics and reporting to the developer. Metrics such as the number of static functions, the depth of derivation, dependency, complexity of functions, and the number of abstraction are just a few of them. Metrics also has the ability to graphically show dependencies in the software. In this way, it is possible for the developers to analyze the dependencies in the software better visually.[23]
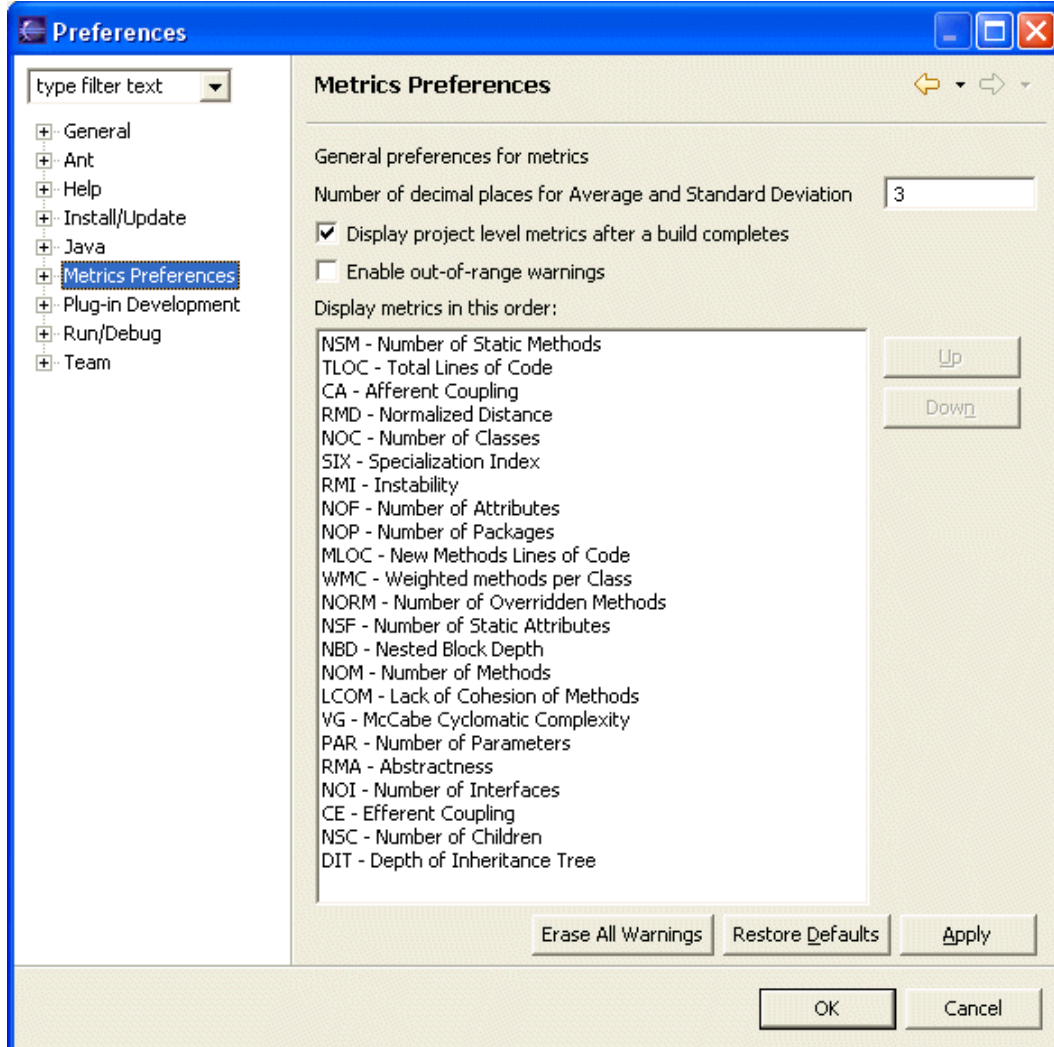
Figure 12-Metric Tool

2.5. PMD

PMD is a static source code analyzer. It finds common programming flaws like unused variables, empty catch blocks, unnecessary object creation, and so forth. It's mainly concerned with Java and Apex, but supports six other languages. It supports Java, JavaScript, Salesforce.com Apex and Visualforce, PLSQL, Apache Velocity, XML, XSL.

Additionally it includes CPD, the copy-paste-detector. CPD finds duplicated code in Java, C, C++, C#, Groovy, PHP, Ruby, Fortran, JavaScript, PLSQL, Apache Velocity, Scala, Objective C, Matlab, Python, Go, Swift and Salesforce.com Apex and Visualforce [24].

2.6. Coverlipse

Coverlipse is an open source Eclipse plugin that examines the overlap relationship between implementation and software code and requirements and test cases. The program analyzes the overlap relationships between these three basic stages of software development, revealing gaps between them [25].

2.7. Checkstyle

Checkstyle[1] is a static code analysis tool used in software development for checking if Java source code complies with coding rules. The CheckStyle program is another open source software tool that deals with format rather than software structure. It helps developers work in accordance with code writing standards by performing format analysis on existing Java code. This software, where the institution can create its own writing standards, also has some generally accepted international writing standards[26].

2.8. SDMetrics

SDMetrics is a commercial program that can perform various visual and numerical analyzes on UML design documents, not on code. By analyzing the design of the software before the design phase, ie the development phase, the program can reveal many nonconformities about dependency and complexity. Early detection at this stage can also be significant in terms of cost.

SDMetrics is a software design quality measurement tool for the UML. It measures structural design properties such as coupling, size, and complexity of UML models. SDMetrics also checks design rules to automatically detect incomplete or incorrect design, and adherence to style guidelines such as circular dependencies or naming conventions [27]
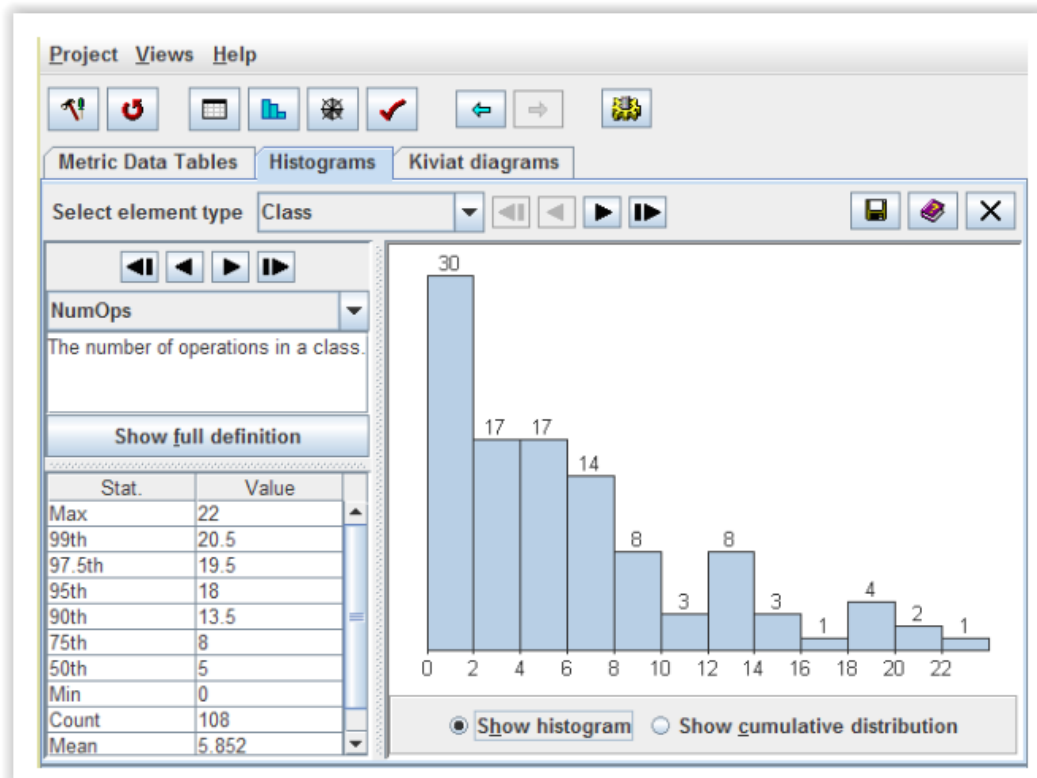
Figure 13-SDMetrics Tool

2.9. Coverity

Coverity is a brand of software development products from Synopsys, consisting primarily of static code analysis tools and dynamic code analysis services. The tools enable engineers and security teams to find defects and security vulnerabilities in custom source code written in C, C++, Java, C#, JavaScript and more[28].

CONCLUSION

In this paper software metric tools are explained detailed. Some popular open source and commercial tools that can be used especially in the scope of quality studies of object oriented software are introduced. These tools are designed to improve software quality.They can make some of the measurements needed in the studies automatically and quickly and make the quality analysis studies quite easy.

REFERENCES

[1] Ertemel, H.O., "Nesneye dayali yazilim gelistirmede kalite olcutlerinin incelenmesi", Yuksek Lisans Tezi, Yildiz Teknik Universitesi Fen Bilimleri Enstitusu, Istanbul, (2009).

[2] https://scitools.com/documents/manuals/pdf/understand.pdf

[3] Dragomir, Mircea (1 December 2015). "Understand". Softpedia.com. Softpedia. Retrieved 7 December 2015.

[4] Martin, George (March 2011). "The Project-Ready Designer". No. 248. Circuit Cellar. p. 57. Retrieved 8 December 2015.

[5]Adkins, Francis; Jones, Luke (24 April 2015). "Machine Assisted Semantic Understanding" (PDF). INSuRE. Northeastern University. Retrieved 4 December 2015.

[6]Loren, Lydia; Johnson-Laird, Andy. "Computer Software-Related Litigation"(PDF). FCLR.org. Federal Courts Law Review. Retrieved 7 December 2015.

[7] Richard, Brett (24 May 2013). "Source Code Analyzers as a Development Tool". Flurry.com. Yahoo Developer Tools. Retrieved 7 December 2015.

[8] Phillips, Michael; Mok, Amy. "Spacecraft Flight Software Design Pattern Discovery" (PDF). Johns Hopkins Applied Physics Laboratory. Lockheed Martin Corporation. Retrieved 7 December 2015.

[9] Eshow, Michelle (1 June 2014). "RTMA Source Code Change Analysis" (PDF). Aviation Systems Division. NASA. Retrieved 7 December 2015.

[9] https://www.hello2morrow.com/products/sonargraph

[10] https://www.wikiwand.com/en/Sonargraph

[11]https://www.ibm.com/developerworks/java/library/j-findbug1/

[12] https://www.ibm.com/developerworks/java/library/j-findbug2/

[13] Markus, Sprunck. "Findbugs – Static Code Analysis of Java". Retrieved April 24, 2013.

[14] http://findbugs.sourceforge.net/downloads.html

[15]https://netbeans.org/kb/docs/java/code-inspect.html

[16]https://code.google.com/archive/p/idea-findbugs/

[17]https://code.google.com/archive/redirect/a/code.google.com/p/findbugs

[18]idea?movedTo=http:%2F%2Fandrepdo.github.io%2Ffindbugs-idea%2F

[19]https://qaplug.com/

[20]https://gleclaire.github.io/findbugs-maven-plugin/

[21]http://fb-contrib.sourceforge.net/

[22] http://www.methodsandtools.com/tools/findbugs.php

[23] http://metrics.sourceforge.net/

[24] https://pmd.github.io/latest/index.html

[25] http://coverlipse.sourceforge.net/index.php

[26] https://checkstyle.sourceforge.io/index.html

[27] https://www.sdmetrics.com/PRMar2011.html

[28] https://www.wikiwand.com/en/Coverity

A Survey About Object-Oriented Software Metrics

Ugur Osman Yucel[1], Zeynep Behrin Guven[1], Ruya Samli[2]

Abstract

In the literature; there are object-oriented metric sets such as Chidamber & Kemerer, Brito e Abreu (also known as MOOD Metric Set) and Bansiya & Davis (also known as QMOOD Metric Set). These metrics include the degree of complexity in a class, the distance of the class to the root of the inheritance, the number of sub-classes directly derived from a class, the number of methods that can be triggered by this object if the methods of an object are invoked, the ratio of visible methods to all methods, the ratio of accessible qualities in all classes defined in the system to all qualifications, the ratio of the number of methods with heritability in all classes defined in the system to the number of all methods, for the class C, the ratio of the different multiform situations to the maximum possible multi-state situations, depth of inheritance tree values of all classes, the measure of similiarity, the number of classes that accept a class as a parameter, the number of derived methods in all classes defined in the system, the ratio of all methods and number of methods of the class.

***Keywords:** Software Engineering, Software Measurement, Software Metrics*

1. INTRODUCTION

In real life, people can't live without measuring objects. Thanks to measurement, they know how much money they have, their weight or current time. According to those measurements' results, they will plan their future. Software measurement is just like real life measurement. It is important for every step in the Software Development Life Cycle. Software developers can plan the future of project based on the measurement results. This study is a survey of Object-Oriented Software Metrics. Purpose of this project is to let people to understand metrics' meanings and why we use them.

2. OBJECT-ORIENTED PROGRAMMING SOFTWARE METRICS

In this chapter, three most popular object-oriented metric set will be examined. As it mentioned above, metrics of Chidamber & Kemerer Software Metric Set, MOOD Metric Set and QMOOD Metric Set will be described below.

2.1. Weighted Methods per Class (WMC)

WMC belongs to Chidamber & Kemerer Software Metric Set. Rather than use Cyclomatic Complexity they assigned each method a complexity of one making WMC equal to the number of methods in the class[1] [3]. This metric shows the complexities of all classes. By using WMC, project team can estimate their effort to develop those classes.

2.2. Depth of Inheritance Tree (DIT) :

DIT metric is also belongs to Chidamber & Kemerer Software Metric Set. In trees, depth means the maximum lenght between a child node and root [1]. Inheritance tree shows the structure of classes. Root is the superclass and child nodes are the subclasses.

---

[1] *Maltepe University, Faculty of Engineering and Natural Sciences, Department of Software Engineering, Maltepe/Istanbul TURKEY*

[2] *Istanbul University – Cerrahpasa, Department of Computer Engineering, Avcilar/Istanbul TURKEY*

2.3 Number of Children (NOC) :

NOC is a member of Chidamber & Kemerer Software Metric Set. This metric measures how other classes used to create another class [1] . It is the number of classes derived from a class. Every class has its own NOC value.

2.4 Coupling Between Object Classes (CBO) :

CBO metric is a member of Chidamber & Kemerer Software Metric Set . Coupling means that an object use property or message of an object which belongs to another class. This metric is the sum of objects like that.

2.5 Response for a Class (RFC) :

This metric is from Chidamber & Kemerer Software Metric Set. This is the number of methods which will be executed when a message sent to a class by an object [1]. If RFC will increase, testing and debugging will be more complex.

2.6 Lack of Cohesion in Methods (LCOM) :

LCOM is a member of Chidamber & Kemerer Software Metric Set. Cohesion metric examines how the methods of a class have relation with the others [6] . High cohesion is always better than lower ones.

2.7 Method Hiding Factor (MHF) :

This metric belongs to Brito e Abreu's metric set which can be called as MOOD Metric Set. In this metric, hiding means encapsulation [4] . So this metric examines how methods are encapsulated.

$$\text{MHF} = 1 - (\text{Visible Methods} - (\text{Total Number of Classes} - 1)). \tag{1}$$

2.8 Attribute Hiding Factor (AHF) :

This metric is also belongs to MOOD Metric Set. As it can be easily seen, this metric examines how attributes are encapsulated [4].

$$\text{AHF} = 1 - (\text{Visible Attributes} - (\text{Total Number of Attributes} - 1)) . \tag{2}$$

2.9 Method Inheritance Factor (MIF) :

MIF is a member of MOOD Metric Set. This metric is the division of inherited methods to the total number of methods [2]. Its range is between 100-0. It is better to be not too low or too high. MIF should get an optimal value. According to the creator of the MOOD who is Fernando Brito e Abreu , acceptable MIF values should be lower than %80. [4]

$$\text{MIF} = \text{number of inherited methods} / \text{total number of methods}$$
(3)

2.10   Attribute Inheritance Factor (AIF) :

AIF is also a member of MOOD Metric Set. This metric is the division of inherited attributes to the total number of attributes [2]. If a child class redefines it superclass' attribute, this attribute will be an inherited attribute.

$$\text{AIF} = \text{number of inherited methods} / \text{total number of attributes} \tag{4}$$

2.11   Polymorphism Factor (POF) :

POF belongs to the MOOD Metric Set. This metric represents the actual number of possible different polymorphic situations[4]. Polymorphism Factor is the division of overrided methods to the maximum possible overrided methods. Its range is between 100-0. If POF is equalls to 100, all of the possible methods are overrided in derived classes. If POF is equals to 0, none of those methods are overrided.

2.12   Coupling Factor (COF) :

COF is the last of MOOD Software Metrics. Coupling Factor is the division of couplings between classes to the maximum possible number of couplings [4]. An example will be given here to understand what is coupling. There are two classes which are C1 and C2. If C1 calls C2's methods or accesses C2's variables, it can be said that C1 is coupled to C2. However, C2 is not coupled to C1. There is one way relationship between them. This metric's range is between 100-0.

2.13 Average Number of Ancestors (ANA) :

This metric is member of the QMOOD Metric Set which is created by Bansiya and Davis. This metric is the number of classes among all paths from the root to all classes in a structure [5]. This metric gives people an opinion about inheritance structure of the project.

2.14 Cohesion Among Methods of Class (CAM) :

This metric is also a member of the QMOOD Metric Set. CAM can be calculated by using summation of the intersection of parameters a method with the maximum independent set of all parameter types in the class [6]. Its range is between 1-0. Maximum value is the best case and minimum value is the worst case.

2.15 Class Interface Size (CIS) :

CIS is one of the QMOOD Metrics. Class interface size is the number of public methods in a class [5].

2.16   Data Access Metric (DAM):

This metric belongs to the QMOOD Metric Set. DAM is the division of private methods to the all methods [7] . Not only privates, but also protected methods will be counted while calculating DAM [5] . Its range is between 1-0. Higher DAM values are more desired.

2.17   Direct Class Coupling (DCC) :

DCC is from the QMOOD Metric Set. This is the number of classes which have relationship with another class [5]. Relationship can be everything like derivation, message passing or attribute declarations etc…

2.18   Measure Of Aggregation (MOA) :

This metric is a member of QMOOD Metric Set. This metric checks the data types [5] . If data types are user defined classes, then value of MOA will increase [7]. MOA is the number of data declarations which has a user defined type.

2.19   Measure of Functional Abstraction (MFA) :

MFA is from the QMOOD Metric Set. This metric is the division of number of inherited methods to total number of methods. Its range is between 1-0.

2.20   Number of Methods (NOM) :

This is the count of all methods in a class.

CONCLUSION

Finally, this study is a review of Object Oriented Programming metrics in the literature. Correct determination of metrics in a software is important for the understanding of the software. Especially in Object Oriented Programming, this is more crucial. For the future studies, performance evaluation of these metrics is planned.

REFERENCES

[1].   S. R. Chidamber and C. F. Kemerer, ―A Metrics Suite for Object Oriented Design,‖ IEEE Transactions on Software Engineering, Vol. 20, No. 6, pp. 476–493, 1994.

[2].   F. B. Abreu, ―The MOOD Metrics Set‖, In Proc. ECOOP'95, Workshop on Metrics, 1995.

[3].   Virtual Machinery - Sidebar 3 - WMC, CBO, RFC, LCOM, DIT, NOC - 'The   Chidamber and Kemerer Metrics' http://www.virtualmachinery.com/sidebar3.htm

[4].   e Abreu, F. Brito, and Walcelio Melo. "Evaluating the impact of object-oriented design on software quality." *Proceedings of the 3rd international software metrics symposium*. IEEE, 1996.

[5].   J. Bansiya and C.G. Davis, ―A Hierarchical Model for Object-Oriented Design Quality Assessment‖, IEEE Transactions on Software Engineering, Vol. 28, No. 1, 2002

[6].   Sandhu, Parvinder, and Hardeep Singh. "A Critical Suggestive Evaluation of CK Metric." *PACIS 2005 Proceedings* (2005): 16.

[7].   Goyal, Puneet Kumar, and Gamini Joshi. "QMOOD metric sets to assess quality of Java program." *2014 International Conference on Issues and Challenges in Intelligent Computing Techniques (ICICT)*. IEEE, 2014.

Investigation Of Computer Aided Programs In Landscape Architecture In A Planted Design Process: A Case Study Of Duzce University Botanic Garden

Engin Eroglu[1], Ezgi Bulbul Kurt[1], Sertac Kaya[1]

Abstract

Computers are effective in all areas of our life as well as in landscape architecture profession group. With the convenience of computers to our lives, the benefit cannot be ignored. In landscape architecture, traditional presentation techniques are gradually replaced by computer-aided programs. In this study; The aim of this course is to determine the effects of rapidly developing and developing computer and communication technologies on the landscape architecture design process, especially the importance and necessity of the current two dimensional (2D) and three dimensional (3D) programs in visual presentation techniques, while the advantages and disadvantages of computer technology it is examined. In addition, the difficulties and requirements of visualization technology, landscape and environmental planning has been examined the potential to apply. In the study, presentation techniques (traditional presentation technique or computer aided presentation techniques) and preferred programs used in the design process were evaluated with examples in the Duzce University Botanical Garden field study. Firstly, scientific researches and current applications in the literature have been evaluated and then, in order to get expert opinions, a questionnaire study was conducted for some firms and presentation techniques and the results were evaluated in terms of general and international validity. According to the obtained results, traditional application techniques are introduced in the design phase and presentation techniques and calculation section are used to save time and go to computer aided design phase. Due to the fact that computer programs are more preferred in terms of presentation and ease of use, the botanical garden activities in the campus have been supported by 2D and 3D studies through computer aided programs and re-survey work has been done. According to the results, presentation techniques, aesthetic perception, intelligibility, impressiveness, the visuality of vegetative design has been highlighted and accepted by people more realistic.

Keywords: *Landscape design, Landscape visualization, Planting design, 3D program*

1. INTRODUCTION

People always aim to work with the concern of making the environment, beautification, development and more livable. Landscape architecture is also based on this philosophy and aims to create more livable cities for people. The purpose of the design space in these professional studies is important in terms of shaping the design and placing it on the land.

In landscape architecture studies, plants are both aesthetic and functional design elements. If necessary, these conditions should be visualized in terms of the comprehensibility of the plant composition and ideas should be supported by two-dimensional and three-dimensional expression techniques.

The drawing is a method that best describes and supports the designer's thoughts in the landscape architecture profession. Two-dimensional and three-dimensional perspective drawing technique should be used to provide the person with the opportunity to present and understand the thoughts.

Computer-based architectural visualization programs are used both to accelerate the design process and to evaluate the spatial relationships in which a designer reflects his / her ideas in the best way possible. The spaces

[1]* Corresponding author: Duzce University, Department of Landscape Architecture, 81620, Duzce, Turkey.
  ezgisbk@gmail.com

are first created on a model, then objects are added to this work, material dressing and light adjustments are made. In this way, the spaces arranged in computer environment can be defined as realistic visually [1].

While the visualization technique brought by the traditional drawing technique is a much more demanding and time consuming work in general terms, it has been observed that landscape architects, architects, designers and people dealing with this discipline have developed their creative aspects using this technique. The aim of this study is to investigate the positive or negative effects of computer aided design programs in the landscape architecture profession in the study process and applied to the botanical garden within the main campus boundaries of Duzce University.

2. MATERIALS AND METHOD

2.1. Materials

The botanical garden, located in the main campus boundaries of Duzce University, which has the same name in Duzce, located in the western Black Sea region of the Black Sea Region, is the main material of this study (Figure 1). Project drawings and plan visualizations in this study were drawn with AutoCAD 2018 and Adobe Photoshop CC 2019 programs; SketchUp 2018 and Lumion 7.5 programs were used for perspective visualizations.
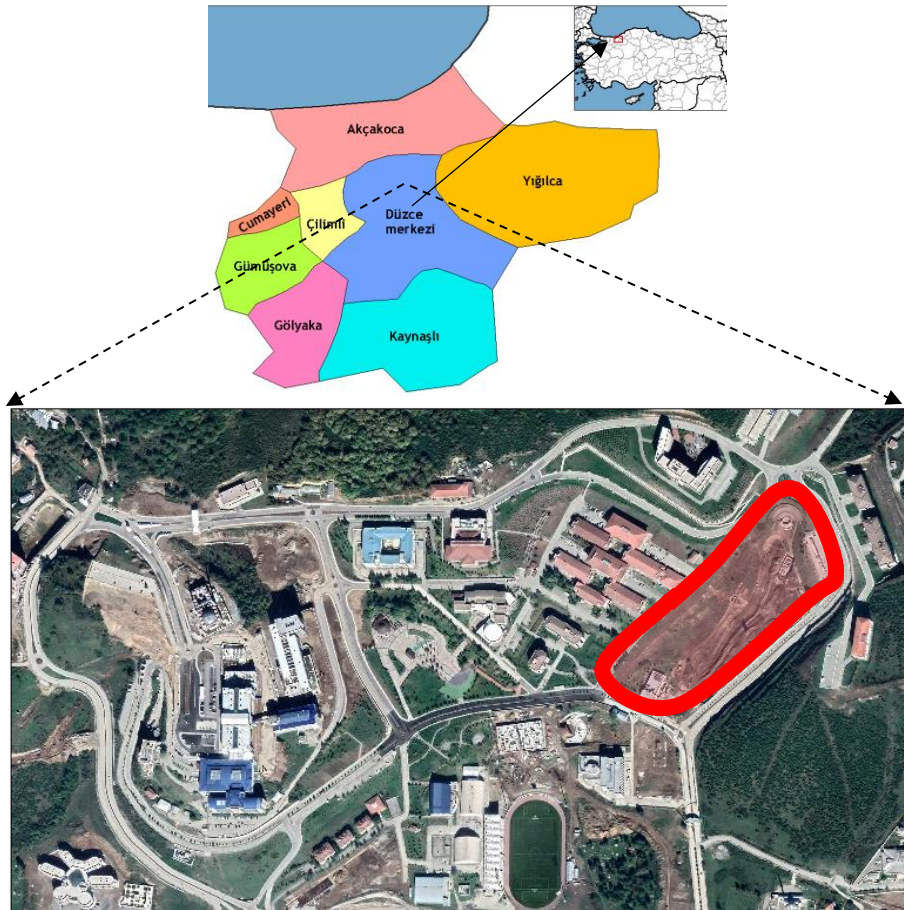
Figure 1. Study Area: Botanical Garden in Duzce University Campus.

2.2. Method

Working process; the literature surveys were conducted in the form of determination of the project area, on-site observation, photo-taking, survey study and statistical evaluation of the survey results. In order to obtain a clear and correct result, a questionnaire study was carried out and it was tried to determine whether the hypothesis was correct, wrong or how much was correct.

The Duzce University Botanical Garden project, which was chosen as the study area, was evaluated by two surveys. The first survey conducted on landscape architecture university students and landscape architecture firms were designed to investigate the positive or negative effects of traditional drawing techniques and computer aided design programs on the process of landscape architecture.

According to the data obtained from the results of the first survey, computer-aided design programs were preferred more than the traditional drawing technique and this was the content of the second survey. The second survey consisted of computer aided programs based on the values obtained from the results of the first survey conducted and the visuals made using these programs.

In the second survey, a project plan was drawn in AutoCAD, which was selected as the most used program, and visualized in Adobe Photoshop and modeled in SketchUp, rendered in 3D, and visualized in Lumion.

Images were obtained using computer-aided programs and two-dimensional (2D) in the second survey, 4 plan, three-dimensional (3D) studies in the work of 20 perspective by presenting the perspective, examining within certain parameters and people were asked to put out the effect they leave on. The survey study was categorized as 2D plan visuals and 3D perspective visuals.

According to the results of the second survey, mean value analysis (Table 1 and Table 2), the computer-aided statistical program SPSS 20.0 package program with the help of the frequency analysis was explained in detail and explained.

RESULTS AND DISCUSSIONS

According to the results of the questionnaire applied to the participants; As shown in Table 1, visuals 2 and 4 are more aesthetic and perceptible than images 1 and 3 and have a positive effect on individuals as a texture and color effect, and attracted more attention from the participants by creating a sense of wonder.

Table 1. Evaluation of parameters by individuals on 2D plan visuals (S: SketchUp, L: Lumion)

MEAN VALUE ANALYSIS						
Program Name	Visual Number	Aesthetic	Perceptible	Impressive /Interesting	Positive Color Effect	Curiosity Perception in Place
S	G1	3,53	3,74	3,47	3,65	3,58
L	G2	4,00	4,14	4,03	4,08	4,03
S	G3	3,51	3,56	3,56	3,53	3,55
L	G4	4,12	4,23	4,15	4,18	4,13

Image 1 and 2 and 3 and 4 are the twin visuals among themselves and have emerged as a result of the use of AutoCAD and Adobe Photoshop programs and revealed different feelings for the participants.

Images 2 and 4 In Adobe Photoshop, more realistic effects, plants, grass surface texture, hard ground and flooring, light-shade studies and the possibility of material diversity have made the images more quality, understandable and realistic (Figure 2).

1   2   3   4
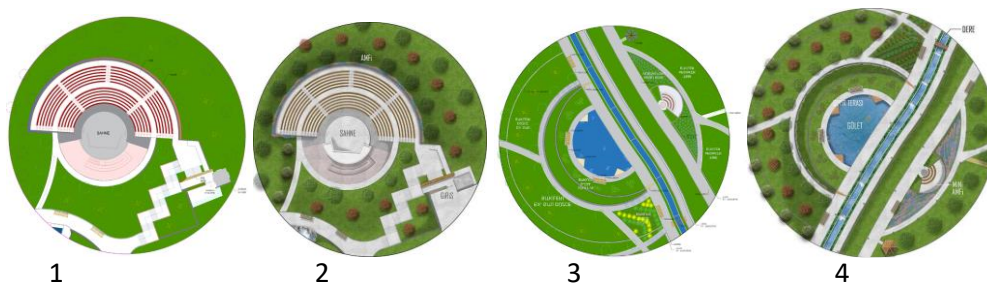
Figure 2. 2-D Images

Table 2. Evaluation of parameters by individuals on 2D plan visuals (S: SketchUp, L: Lumion)

MEAN VALUE ANALYSIS

Program	Visual No	Natural	Aesthetic	Perceptible	Regular	Feeling of Trust	Impressive/ Interesting	Positive Color Effect	Planting Dimension	Vegetable Texture	Vegetable Form	Mobility	Continuity	Curiosity Perception in Place
S	**G5**	3,32	3,5205	3,8995	3,8950	3,7032	3,5616	3,5571	3,4932	3,4155	3,4429	3,3973	3,4475	3,4292
L	**G6**	4,43	4,5160	4,4977	4,4247	4,4429	4,5297	4,5068	4,5114	4,5205	4,5023	4,4703	4,3927	4,5068
S	**G7**	3,27	3,3744	3,7169	3,8356	3,5799	3,4064	3,4292	3,4201	3,3562	3,3881	3,4018	3,5616	3,3836
S	**G8**	3,79	3,7397	3,9817	3,9361	3,8493	3,7397	3,7626	3,8630	3,7854	3,8265	3,7489	3,8447	3,7671
L	**G9**	4,16	4,2785	4,3653	4,3470	4,2283	4,2557	4,3059	4,2511	4,2100	4,2146	4,2603	4,2603	4,2511
L	**G10**	4,22	4,3470	4,3699	4,4110	4,3516	4,3151	4,3607	4,3014	4,2922	4,3014	4,2329	4,2420	4,2420
S	**G11**	3,44	3,5845	3,8493	3,7808	3,6530	3,5571	3,6119	3,5525	3,5662	3,5845	3,6530	3,6210	3,5662
S	**G12**	3,39	3,4292	3,6575	3,6986	3,5571	3,3973	3,4064	3,5023	3,4384	3,4749	3,3836	3,4703	3,3425
L	**G13**	4,12	4,2100	4,2283	4,2100	4,1918	4,1963	4,2100	4,2055	4,2055	4,1735	4,2100	4,1963	4,2055
S	**G14**	3,63	3,6712	3,8676	3,8721	3,7489	3,6347	3,7215	3,7397	3,7534	3,7352	3,7352	3,7352	3,6804
S	**G15**	3,41	3,4612	3,6804	3,6712	3,5936	3,4749	3,4795	3,5479	3,5205	3,5251	3,4932	3,5799	3,5068
L	**G16**	4,48	4,5205	4,4658	4,5023	4,4612	4,5068	4,4886	4,4612	4,4886	4,4658	4,4658	4,3927	4,4749
L	**G17**	4,12	4,2557	4,2968	4,3151	4,2237	4,2283	4,2694	4,2420	4,1963	4,1918	4,1872	4,1918	4,2374
S	**G18**	3,42	3,4384	3,5479	3,5479	3,4384	3,3973	3,4292	3,4977	3,5297	3,5068	3,4977	3,5342	3,5068
S	**G19**	3,54	3,6027	3,7489	3,7352	3,6667	3,5205	3,5023	3,5708	3,6073	3,5936	3,5388	3,6073	3,5434
L	**G20**	4,35	4,4155	4,3744	4,3607	4,3607	4,3425	4,3744	4,3059	4,3288	4,2922	4,2831	4,3014	4,3607
L	**G21**	3,84	3,8904	4,0091	3,9498	3,8630	3,8721	3,9406	3,8950	3,9269	3,8995	3,8995	3,8721	3,8995
L	**G22**	4,42	4,4475	4,4155	4,3607	4,4064	4,4521	4,4795	4,4338	4,4292	4,4247	4,4018	4,3516	4,3836
S	**G23**	3,34	3,3653	3,5662	3,5662	3,5342	3,3379	3,4201	3,4018	3,4155	3,4247	3,3653	3,4201	3,3699
L	**G24**	4,40	4,4658	4,4749	4,4703	4,4110	4,4201	4,4658	4,4384	4,4475	4,4338	4,3516	4,3790	4,3881

According to the data obtained from the survey results, visuals made using SketchUp program showed an average score of 3.37-3.95 points, whereas visuals made using Lumion program showed results between 3.86 and 4.52 points, and the visuals made in Lumion program were more real. close feeling. Visual number 7 in the SketchUp

program received the lowest value in the average value analysis table, while visual number 6 received the highest score.

SketchUp program is not very realistic when it is taken in the desired light-shadow settings in outdoor solar works, image 7 are not preferred because it does not come in effect, does not stand aesthetically and does not look natural. The inadequate plant diversity effected vegetation texture and form, did not provide mobility and did not cause curiosity. For this reason, image 7 was not impressive.
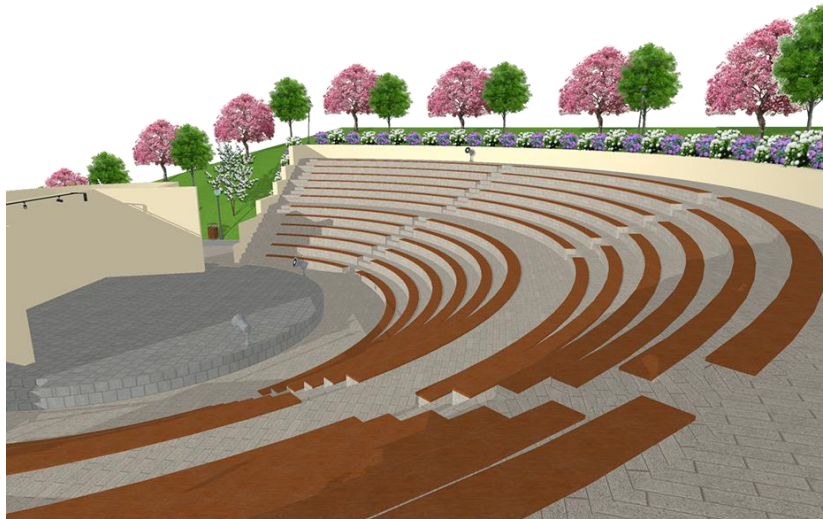
Figure 3. The lowest value image according to Average Value Analysis Table (Image 7)

The visual average value analysis Image 7 in the SketchUp program received the lowest value, while the visual number 6 received the highest score. According to Bernasconi et al. [2], Grass fields and trees considerably improve the quality of urban landscapes and visual quality 6 affects participants. Also according to Yao et. al. [3], the variety of vegetation and rich color differences increased the visual quality. The Lumion program's plant library, the variety of material content and effective settings have been observed to increase the perception of reality in the field. When we look at the total result, the studies obtained in Lumion program attracted more attention of individuals in terms of visual quality and preferred.

Figure 4. Highest Value According to Average Value Analysis Table (Image 6)

CONCLUSIONS

Computer aided drawing techniques; It is observed that it is preferred to gain speed in time, to obtain more data in a shorter time. But in the design phase, traditional drawing techniques are preferred because they use the lines more freely and reliably. According to the hypothesis, computer-aided design programs were predicted to be in

front of the traditional drawing techniques and to be completely broken off by hand drawing technique. According to the findings of the research, it is concluded that both techniques have taken their places at various stages of the project and make their users feel more comfortable at these stages. In later stages, traditional drawing techniques are replaced by computer aided drawing techniques.

In order for any design product to be clearly expressed, it is understood that the location of three-dimensional images is very important. As a result of the researches, it was determined that computer aided drawing tools improved the design process and made the project more mature. For this reason, modeling programs not only limit the imagination, but also provide solutions to the designer in order to produce different alternative

solutions. Thus, the projects can have alternative design proposals in a short time, appear more realistic and make the presentation more successful.

REFERENCES

[1]. S. M. Ervin, H. H. Hasbrouck, "Landscape Modeling Digital Techniques for Landscape Visualization", *Landscape and Urban Planning*, 2001.

[2]. Bernasconi, C., Strager, M.P., Maskey, V., Hasanmyer, M., Assessing Public Preferences for Design and Environmental Attributes of An Urban Automated Transportation System. Landscape and Urban Planning, 90: 155–167. 2009.

[3]. Yao Y., Zhu X., Xu Y., Yang H., Wu X., Li Y., Zhang Y. Asessing The Visual Quality of Green Landscaping in Rural Residential Areas: The Case of Changzhou, China. Environmental Monitoring and Assessment, Volume 184 (2), 951-967, 2011.

Determination of Some Physical and Chemical Properties of Kiwi Fruit Grown in Trabzon Region During Different Ripening Periods

Mustafa Otag[1]

Abstract

The aim of this study is to reveal some physical and chemical changes in the structure of a Hayward kiwi cultivar grown in Trabzon region during the ripening period. In order to determine physical properties, titratable acid, pH, total soluble solids (TSS) analyzes were performed, total phenolic content and antioxidant activity analysis were performed to determine changes in chemical properties of fruit during ripening period. The quantification of total phenolics was performed by using the Folin-Ciocalteu spectrophotometric method. Antioxidant activity was examined by 1-diphenyl-2-picrylhydrazyl (DPPH) radical scavenging assay.

As a physical properties, pH, titratable acidity and total soluble solid analysis results were found in range of 3.49-4.02, 3,12% -0.63%, 1.80 -12.00 °Bx, respectively. Total phenolics and DPPH radical scavenging results were found to vary in the range of 408.21 mg GAE /L-110.56 mg GAE/ L, 66.9% -18.88%, respectively.

The concentration of total soluble solids increased as a result of the conversion of organic acids into sugar in kiwi fruit with the maturation of fruit. The titratable acidity decreased due to the breakdown of organic acids, but an increase in pH was observed due to the decrease in acidity. Reductions in the amount of phenolic compounds were determined by the breakdown of important compounds, for example organic acids. In general, ripe kiwifruits in this study showed lower antioxidant capacities than their unripe counterparts, which might be ascribed to decreases in the total phenolic content during ripening. Antioxidant capacity had a higher linear correlation coefficient with total phenolic contents . The results above suggest that kiwifruits at various maturity stages are a valuable source of phenolics and antioxidants for industrial application and consumer health benefit.

Keywords: Kiwi fruit, Hayward, Ripening, Total phenolic, antioxidant activity

1. INTRODUCTION

Fruit and vegetables contain significant levels of biologically active components with physiological and biochemical functions which benefit human health [1].

Kiwi (*Actinidia deliciosa*) or kiwifruit is a plant belongs to genus Actinidia in the family Actinidiaceae. The most known female varieties of kiwi fruit known to have more than 12 species are Hayward, Bruno, Abbott, Allison, Monty, Vincent, and male varieties are Matua and Tomuri [2].

Kiwifruit is native to north-central and eastern China. Kiwifruits were originally called Tang Yao. The first recorded description of the kiwifruit dates to 12th century China during the Song dynasty. As it was usually collected from the wild and consumed for medicinal purposes, the plant was rarely cultivated or bred. In 1960 it changed its name and was renamed the Chinese Gooseberries [3]. Cultivation of kiwifruit spread from China in the early 20th century to New Zealand, where the first commercial plantings occurred. The fruit became popular with British and American servicemen stationed in New Zealand during World War II [4].

According to FAO 2017, Kiwi cultivation is 4 million tons worldwide. China has the first place in the world, Italy has the second place and New Zealand has the third place while in recent years our country Turkey has risen to eighth place [5].

In Turkey, the region where the most kiwi cultivation is done is the Black Sea Region, and the province where the production is made the most is Yalova.

Ripening of kiwifruit is associated with changes in respiration, texture, carbohydrates, organic acids, ethylene production and volatile compounds, which give the characteristic aroma [6].

Kiwifruit is harvested unripe and ripening can be initiated by exposure to exogenous ethylene. Ethylene triggers rapid and dramatic changes in fruit firmness, and advances ripening and subsequent senescence. The simple gas ethylene is an endogenous regulator of a variety of stress responses and developmental processes. During ripening, several structural and biochemical changes occur in fruit that confer specific organoleptic qualities, such as modifications in the external aspect, texture and flavor of the fruit. Several studies have already demonstrated that ethylene controls most of the events associated with the fruit ripening process [7].

As one of the most popular fruits today, kiwifruit is also well-known for an excellent source of antioxidants. All these antioxidant compounds have strong antioxidant functions that enable them to scavenge free radicals or suppressing formation of free radicals in vitro and in vivo. It has been considered that a network of bioactive compounds with different physicochemical properties may function in a synergistic way to protect human from chronic diseases, cardiovascular diseases, cancer, and delaying aging [8].

The objectives of this study were to determine the changes in the total phenolic content, antioxidant activity, physicochemical profile throughout the developmental stages of kiwifruits.

2. MATERIALS AND METHODS

2.1 Materials

Hardy kiwifruit cultivar 'Hayward' were harvested in 2018 at 13 different maturity stages from a mature commercial vineyard Dernekpazari, Trabzon, Turkey. Approximately, 1 kg of kiwifruit (Hayward cultivar) were picked from the mature green stage in June 22th to December 21st, fruits were picked every 15 days. 15 to 20 immature fruits and 7 to 9 mature fruits were picked from the same tree and peeled as thinly as possible. The collected kiwifruits were frozen and stored at -20 ° C until the experiments and analyses to be performed.

2.2. Extraction for physicochemical and spectrophotometric analysis

The kiwifruits were hand peeled, followed by removal of seeds and cores. The products were homogenized at 10°C for 3 min in a Waring Blender.

For spectrophotometric analysis, 10 g fresh homogenized sample was extracted with 80% ethanol using sonication for 30 min at 40 °C. The extracts were then filtered and dried using a rotary evaporator at 40 °C. After concentration, 80% ethanol solvent was added to adjust the final volume to 10 mL total phenolic content (TPC), and antioxidant activity determination.

2.3. Physicochemical analyzes

Analyses of pH and soluble solids were performed according to the methodology reported by the Association of Official Analytical Chemistry [9]. Measurements of pH were determined electrometrically using the pH meter FiveEasy Plus™ FP20 (Mettler Toledo, Columbus, Ohio, ABD). Soluble solid content (SSC) was measured using a pycnometer DMATM4100M (Anton Paar, Graz, Austria) and SSC values reported as oBrix. Total titratable acidity (TTA) was determined by titration of the samples with 0.1 N NaOH to an end point of pH 8.1 and expressed as % of citric acid. The color of whole cherry skin was determined by Hunter Lab Colorimeter (Hunterlab MiniScan EZ 4000L, USA) based on the CIELab color space, after calibration with the white and black glass standards.

2.4. Total Phenolic Content

The total phenolic content (TPC) was determined according to the adapted Folin–Ciocalteu colorimetric method [10]. 0.5 mL of cherry fruit extract obtained at 70% ethanol was mixed with 2.5 mL of Folin-Ciocalteu reagent (10% (v/v)) and 2 mL of sodium carbonate solution (7.5% (w/v)). The mixture was stirred and kept at room temperature for 1h in the dark place. The absorbance of sample against blank was determined at 725 nm using UV-Visible Spectrophotometer (Hach DR6000, Lange GmbH, 189 Germany). The TPC of the samples was expressed as mg of gallic acid equivalents (GAE) per gram of dry weight (dw) by using Gallic acid calibration curve obtained for the concentrations of 40–400 mg/L.

2.5. Antioxidant Activity

The free radical scavenging activity of ethanol extract of Cherry fruits was determined by DPPH• assay described by Engin et al.[11] with minor modifications. Briefly, 1 mM solution of DPPH• in methanol was prepared. Then, five separate test tubes were added to 600 μL of DPPH• and extraction solutions at specific concentrations (20, 40, 60, 80, 100 μL) were added and complete with methanol as volume 6 mL. The reaction mixture was mixed in the vortex mixer and kept in the dark at the room temperature for 30 min. After 30 min keeping of reaction, the absorbance of the mixture was read against a blank at 517 nm by a UV-VIS spectrophotometer (Hach DR6000, Lange GmbH, 189 Germany). The scavenging of DPPH radicals by the samples was calculated according to the following equation:

DPPH activity (%) = [1 - (absorbance of sample − absorbance of blank)/absorbance of control] × 100.

2.6. Statistical analyzes

Experimental data were analyzed by analysis of variance (ANOVA) using a statistical program SPSS (Version 16). Duncan's multiple range tests was employed to establish the multiple comparison of mean values. Mean values were considered significantly different when $p < 0.05$. Each experiment was performed in triplicate.

3. RESULTS AND DISCUSSION

The physicochemical properties (SSC, pH, titratable acidity) of the kiwifruit were summarized in Table 1.

Table 1. Physicochemical properties of kiwifruit samples at different ripening stages

Developmental Stages	SSC (ºBrix)	TTA (%, citric acid)	pH
June 22th	1,81±0,08i	0,849±0,02j	3,49±0,01j
July 6th	2,48±0,14hi	0,817±0,05i	3,52±0,02j
July 20th	2,54±0,07h	0,792±0,08hi	3,53±0,03j
August 3rd	3,09±0,05g	0,778±0,02hi	3,57±0,01i
August 17th	3,27±0,11g	0,751±0,01h	3,60±0,03h
August 31th	3,65±0,04f	0,734±0,03gh	3,63±0,02h
September 14th	4,17±0,08e	0,715±0,02g	3,67±0,04g
September 28th	4,92±0,03d	0,689±0,06f	3,81±0,02f
October 12th	5,51±0,06d	0,604±0,09e	3,86±0,01e
October 26th	5,79±0,14d	0,627±0,05d	3,92±0,02d
November 9th	10,08±0,08c	0,554±0,01c	3,98±0,01c
November 23th	10,54±0,03b	0,407±0,05b	4,06±0,05b
December 21th	12,16±0,04a	0,318±0,02a	4,13±0,03a

* Values as mean±SD. Values within a column followed by the different letter are significant (P<0.05)

As seen in Table 1, significant increase for total soluble solids and pH degree existed in selected kiwifruits in relation to ripening stages. Early in the ripening process, a much slower increase in soluble solids content was observed. The Brix degree was 5,79. After ripening for 15 days, and was approaching optimum eating quality, it was observed that the changes in soluble solids were accelerated. This change represents almost 67% of the total change. On the other hand titratable acidity decreased considerably during ripening considering first and last date, respectively. The organic acids were metabolized by the fruit during the ripening process, resulting in decrease in total acidity and rise in pH value.

The total phenolic content results of the samples were shown in Figure 1. As shown in Figure 1, total phenolic content of kiwifruits decreased significantly from first date to last date. In September, samples highest decrease in polyphenolic content as compared to other stages.
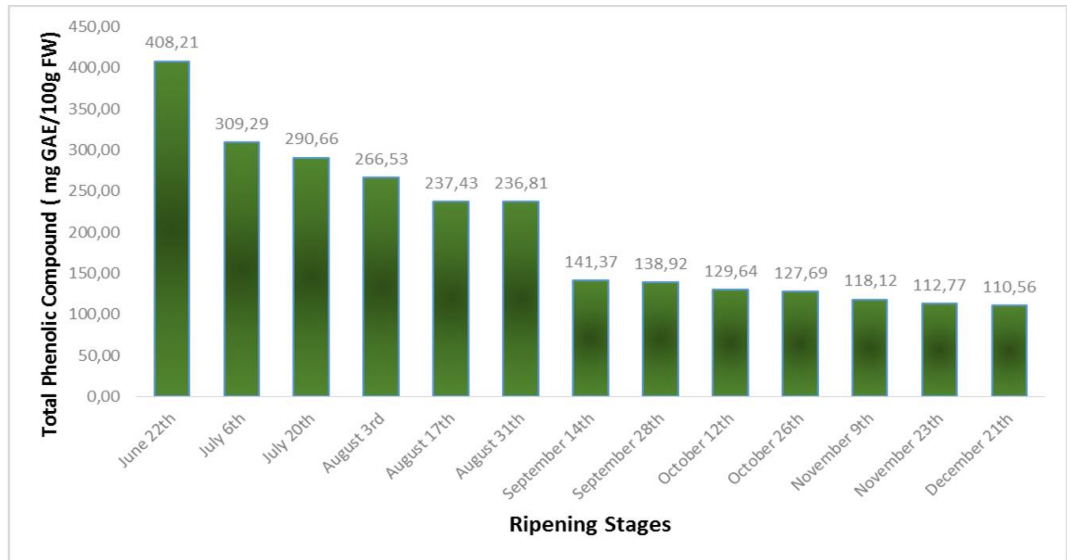
Figure 1. Total phenolic content of kiwifruit samples at different ripening stages

The antioxidant results of the samples were shown in Figure 2. As shown in Figure 2, The DPPH antioxidant activity decreased from 69.954 to 18.882 % fruit throughout the development of fruits. Free radical scavenging activities were measured via the DPPH radical scavenging assays. The kiwifruit had significantly higher radical scavenging activities at the start of fruit development, but it decreased as the fruit matured. Total antioxidant activity is highly correlated with total polyphenol content.
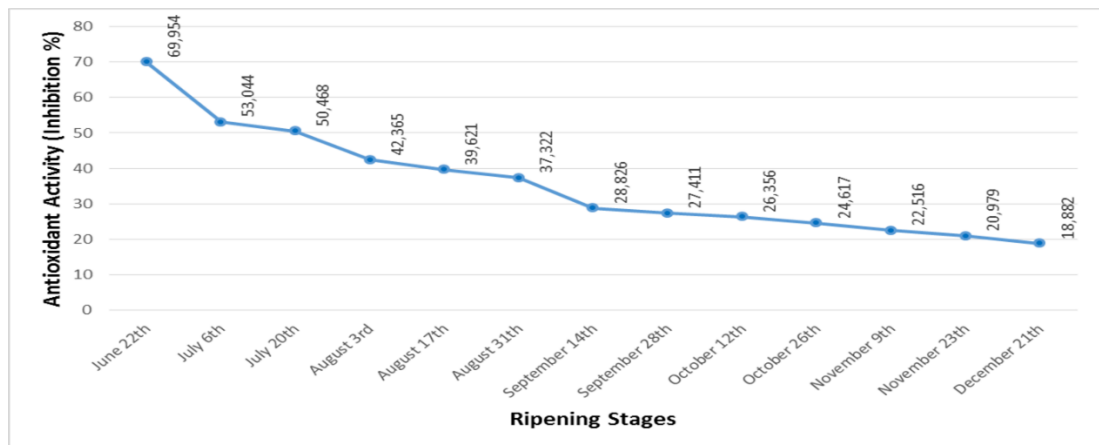
Figure 2. Antioxidant activity of kiwifru samples at different ripening stages

4. CONCLUSIONS

The physicochemical and bioactive properties measured serve to design the equipment used in ripening processing and to improve the quality of kiwifruit ('Hayward'). The following conclusions are drawn from the investigation on chemical and physical properties of kiwifruits:

Total phenolic content and the total antioxidant values were higher at early stages of maturity than at mature period, whereas pH and total soluble solid contents were higher at early stage of ripening period than at physiological maturity. These results are consistent with the results observed for total phenolic content. There were strong correlations between antioxidant capacity and total phenolic content. The contents of bioactive compounds, antioxidant capacity are significantly higher that could be a valuable addition to known disease preventing diets.

REFERENCES

[1]. N.S. Hariram, and S.W. Park, "Edible berries: Bioactive components andtheir effect on human health". *Nutrition,* vol. 30, pp. 134-144, 2014.

[2]. I. Parameswaran, and V.K. Murthi, "Comparative study on Physico and phyto-Chemical analysis of Persea Americana and Actinidia deliciosa". *Int. J. Sci. Res. Pub.*, vol. 4, pp. 2250-3153, 2014.

[3]. N. Patlolla, S. Poojitha, S. Reddy, V. Rao and E. Margaret, "Effect of Polyphenolic Components of Kiwi on Plant and Human DNA", *Int. J. Mol. Genet.,* vol. 7, pp. 1-10, 2016.

[4]. C.A. Schroeder and W.A. Fletcher, "The Chinese Gooseberry(Actinidia chinensis) in New Zealand", Eco. Bot., vol. 21, pp.81-92, 1967.

[5]. FAO, 2017. FAO statistical database. Available at:http://www.fao.org/statistics/en/

[6]. O.W. Mitalo, W.O. Asiche, Y. Kasahara, Y. Tosa, S. Tokiwa, K. Ushijima, "Comparative analysis of fruit ripening and associated genes in two kiwi fruit cultivars ('Sanuki Gold' and 'Hayward') at various storage temperatures. *Postharvest Biol Technol.*, vol. 147, pp. 20-28. 2019.

[7]. M.D.C. Antunes, "The role of ethylene in kiwifruit ripening and senescence", *Stewart Postharvest Rev.,* vol. 2, pp 1-8, 2007.

[8]. D. Guorong, L. Mingjun, M. Fengwang, and L. Dong, "Antioxidant capacity and the relationship with polyphenol and Vitamin C in Actinidia fruits", *Food Chem.,* vol. 113, pp. 557-562, 2009.

[9]. AOAC-Association of Official Analytical Chemistry, In: AOAC - Association of Official Analytical Chemistry (Ed.), Official Methods of Analysis of the Association of Official Analytical Chemistry, seventeenth ed. Washington. 2000.

[10]. K. Slinkard, V.L. Singleton, "Total phenol analysis: automation and comparison with manual methods", *Am. J. Enol. Vitic*. vol. 28 (1), pp. 49-55. 1977.

[11]. M.S. Engin, S. Kalkan, S. Cay, A. Guder, M.R. Otag, G. Gur, and A. Kablan, 1DPPH Radical Scavenging, Phenolic and Antimicrobial Activity of Momordica charantia and Rheum ribes". *Res J Pharm Biol Chem Sci.,* vol. 9, pp. 447-458, 2018.

Evaluation of physicochemical properties and bioactive compounds during ripening of Giresun Sweet Cherry *(Prunus avium L.)* variety

Mustafa Remzi Otag[1], Selin Kalkan[1]

Abstract

This study was carried out to determine the changes in physicochemical and bioactive properties of Giresun sweet cherry (Prunus avium L.) fruit collected from Piraziz district of Giresun province during ripening. In this study, as a physical properties, the pH value, soluble solids (TSS), titration acidity and color values of the cherry fruit and bioactive properties of the total phenolic content and Antioxidant Activity values were determined by periodically analyzing of fruit during ripening. The quantification of total phenolics was performed by using the Folin-Ciocalteu spectrophotometric method. Antioxidant activity was examined by ABTS radical scavenging assay. During the ripening of the sweet cherry fruits collected in the harvest of 2017/2018, pH change was 3.56-4.32, total soluble solids 2.54- 15.64%, titratable acidity 0.855-0.348 g/L, a/b color value 0.08-0.22, total phenolic contents 495.42-641.83 mg GAE/L, antioxidant activity was found in the range of 61.35-115.58 mg trolox equivalent /100 g dw.

The pH change of fresh cherry was determined to increase due to maturation. In parallel with the increase in pH, it was determined that there was a significant decrease in total acidity values. During the ripening of cherry fruit, it was determined that total soluble solids (Bx) values increased due to the enhancement in sugar concentration in the fruit structure. The distinct red color of the cherry is associated with the anthocyanin content. Anthocyanins are water-soluble natural colorants that give a wide range of colors ranging from pink, red, purple and blue to the fruit. Anthocyanins have a strong antioxidant effect as well as their coloring properties. It has been determined that there is a significant increase in antioxidant activity values due to the increase in such phenolic compounds within the cherry fruit.

Keywords: Sweet cherry, ripening, color, total phenolics, antioxidant activity

1. INTRODUCTION

Cherry is one of the most popular fruits growing in temperate climate regions. Cherries are within the Rosaceae family and belong to the genus *Prunus*, subspecies Cerasus and section Eucerasus. There are three main species of cherry fruits referenced in this section; sweet (*Prunus avium*), and tart or sour (*Prunus cerasus*), and ground (*Prunus fruticosa Pall.)* cherries. Among the three species, of global trading importance are sweet and tart cherries [1].

The softness and color of the skin influences consumer acceptance of cherry cultivars as well as fruit weight. The color of the skin is the most important indicator of the quality and maturity of fresh cherries and depends on the anthocyanidin content [2].

Sweet cherry (Prunus avium L.) is a deciduous tree originated around the Black and Caspian Seas. The sweet cherry is apparently native in some parts of northern Turkey. It was reported that the center of diversity of sweet (Prunus avium) and sour (P. cerasus) cherry is around Asia Minor, northern Iran, Iraq, Syria, Ukraine, and other countries south of the Caucasus Mountains. The earliest description of the cherry comes from Theophrastus in ca. 300 BC. The name Theophrastus used for the cherry was 'kerasos'. The Greek kerasia may have originated

---

[1]*Giresun University, Department of Food Engineering, 28200 Giresun, Turkey.*

* Corresponding author: mustafa.otag@giresun.edu.tr

from the name of the town Kerasun on the Black Sea (possibly Giresun, today) and cerasus became the species name [3].

According to FAO Statistical Database (2017)[4], cherry production in the world was realized in approximately 416.485 ha area. Turkey, the United States, Iran, Uzbekistan, Chile, Italy, and Spain are the most important sweet cherry producing countries approximately 62% of world sweet cherry production. Turkey is one of the main cherry producers in the world, with a production of 627,000 ton in FAO Statistical Database (2017) which represents 25% of the total in the World production.

Maturity at harvest is an important factor affecting quality perception and the rate of change of quality during postharvest handling. Variability in the maturity of sweet cherries is related to several factors, including crop load, fruit to leaf ratio, location on the tree and exposure to light. Maturity indices can be determined in many ways, including estimation of the duration of development; measurement of size, weight, or density; physical attributes such as color, firmness and moisture or solids content; other chemical attributes such as starch, sugar, or acid content; or morphological evaluation [5].

The objectives of this study were to describe and compare physicochemical attributes (soluble solids, pH and titratable acidity) total phenolic content and antioxidant activity) of Giresun sweet cherry cultivar at different developmental stages.

2. MATERIALS AND METHODS

2.1. Materials

The cherry fruits used in the study were collected from six different trees from an orchard in Kargi Village in Piraziz district of Giresun province from May to the third week of June of 2017-2018 harvest year. Cherry fruits were picked at commercial maturity on the basis of fruit color. Fruits were classified into four developmental stages as follow: green (immature), yellow, orange, and red (mature); May 4th) (immature), May 19th (yellow), June 3rd (pink) and June 18th (red) of the twenty-eighteen (2018) crop year. The sampling was performed with consistent procedure by randomly picking up from the top, central and bottom part of trees.

The collected cherries were packed in plastic bags (0.5 kg) frozen and stored at -20 °C until the experiments and analyses to be performed.

2.2. Extraction for physicochemical and spectrophotometric analysis

The cherry fruits were stoned and homogenised with a manual blender. Mashed (10 g) fruit was dissolved with 40 ml of twice distilled water for 20 min at room temperature. The extracted sample was centrifuged at 15,000 g for 5 min at 10°C (Centurion Scientific K3 centrifuge, UK).The supernatant was filtered through a 0.45 μm syringe filter, transferred into a vial and used for analyses.

For spectrophotometric analysis, 10 g fresh homogenized sweet cherry sample was extracted with 80% ethanol using sonication for 30 min at 35 °C. The extracts were then filtered and dried using a rotary evaporator at 40 °C. After concentration, 80% ethanol solvent was added to adjust the final volume to 10 mL total phenolic content (TPC), and antioxidant activity determination.

2.3. Physicochemical analyzes

Analyses of pH and soluble solids were performed according to the methodology reported by the Association of Official Analytical Chemistry [6]. Measurements of pH were determined electrometrically using the pH meter FiveEasy Plus™ FP20 (Mettler Toledo, Columbus, Ohio, ABD). Soluble solid content (SSC) was measured using a pycnometer DMATM4100M (Anton Paar, Graz, Austria) and SSC values reported as oBrix. Total titratable acidity (TTA) was determined by titration of the samples with 0.1 N NaOH to an end point of pH 8.1 and expressed as g/L of malic acid. The color of whole cherry skin was determined by Hunter Lab Colorimeter (Hunterlab MiniScan EZ 4000L, USA) based on the CIELab color space, after calibration with the white and black glass standards.

2.4. Total Phenolic Content

The total phenolic content (TPC) was determined according to the adapted Folin–Ciocalteu colorimetric method [7]. 0.5 mL of cherry fruit extract obtained at 70% ethanol was mixed with 2.5 mL of Folin-Ciocalteu reagent

(10% (v/v)) and 2 mL of sodium carbonate solution (7.5% (w/v)). The mixture was stirred and kept at room temperature for 1h in the dark place. The absorbance of sample against blank was determined at 725 nm using UV-Visible Spectrophotometer (Hach DR6000, Lange GmbH, 189 Germany). The TPC of the samples was expressed as mg of gallic acid equivalents (GAE) per gram of dry weight (dw) by using Gallic acid calibration curve obtained for the concentrations of 40–400 mg/L.

2.5. Antioxidant Activity

The antioxidant activity was determined by ABTS method of Re et al. [8] with slight modifications. The ABTS radical cation (ABTS*+) was generated by the reaction of 5 mL of aqueous ABTS solution (7 mM) with 88µL of potassium persulfate (2.45 mM). The mixture was kept in the dark for 16 h before use that results blue–green ABTS+ radical solution. After adjusting the initial absorbance of ABTS+ radical solution to 0.700 ± 0.05 at 734 nm by diluting with ethanol, the fruit extracts or a reference substance (Trolox) was added in different concentrations to 2 mL of ABTS+ radical solution. The decrease of absorbance at 734 nm was measured every minute during 6 minutes using UV-Visible Spectrophotometer (Hach DR6000, Lange GmbH, 189 Germany). The results were expressed as Trolox equivalent antioxidant capacity (TEAC) (µM trolox/g dry weight of sample) by using Trolox calibration curve.

2.6. Statistical analyzes

Experimental data were analyzed by analysis of variance (ANOVA) using a statistical program SPSS (Version 16). Duncan's multiple range tests was employed to establish the multiple comparison of mean values. Mean values were considered significantly different when $p < 0.05$. Each experiment was performed in triplicate.

3. RESULTS AND DISCUSSION

The physicochemical properties (SSC, pH, titratable acidity and color parameters) of the samples were summarized in Table 1.

Table 1. Physicochemical properties of cherry samples at different ripening stages

Developmental Stages	SSC (ºBrix)	TTA (g/L malic acid)	pH
Immature	2,54±0,01d	0,855±0,05a	3,56±0.01d
Phase 1	9,32±0,02c	0,731±0,05b	4,05±0.02c
Phase 2	13,31±0,04b	0,516±0,02c	4,13±0.04b
Phase 3	15,64±0,07a	0,348±0,06d	4,32±0.01d

* Values as mean±SD. Values within a column followed by the different letter are significant (P<0.05

As seen in Table 1, there were some significant differences in TSS between the immature stage and Phase 3 stage for cherry fruits. Brix values increased from 2.54 of immature stage to 15.64 for Phase 3 stage. Significant increase for total soluble solids and pH degree existed in cherries in relation to maturity stages. The increase in total soluble solids (TSS) is related to sugar accumulation, since the majority of soluble solids in cherries are glucose and fructose. On the other hand, titratable acidity (TA) decreased considerably during ripening, varying from 0.855 g/L to 0.348 g/L considering immature and phase 3 stages. The reduction in acidity is attributed to dilution by the increase in the berries weight, oxidative respiration and contribution of cations associated with climatic conditions that contribute to the degradation of these compounds.

The color properties of the samples were shown in Figure 2. As shown in Figure 2, with respect to external color parameters, the luminosity (L*) and b* (indicator of yellow-blue changes) showed the highest values at early stages of development and a linear decrease until Phase 3 of development, from which the values remained significantly unchanged until the end of the ripening. Contrarily, parameter a* increased sharply from immature

stage to Phase 2, at which the maximum a* value was detected, and then a continuous diminution was observed (Figure 1).
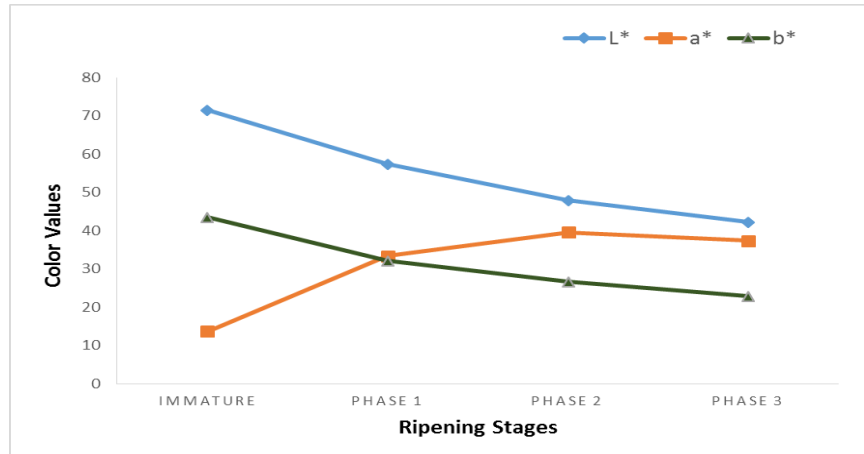
Figure 2. Color parameters of cherry samples at different ripening stages

The total phenolic content results of the samples were shown in Figure 3. As shown in Figure 3, total phenolic content of Giresun cherries increased significantly from immatue stage to Phase 3 stage. This increase is thought to result mainly from the accumulation of anthocyanins and conversion of phenolic acids to salt forms.

Those cultivars with higher phenolics content will have higher quality. In addition, taking into account data from harvest dates, a highly positive correlation was found between total anthocyanins and total phenolics concentration using a polynomial quadratic equation.
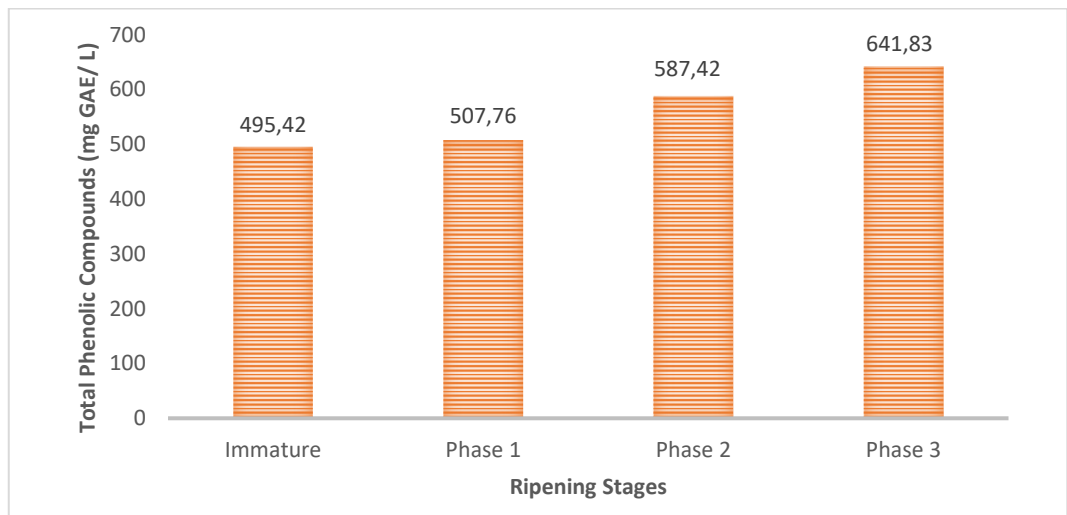
Figure 3. Total phenolic content of cherry samples at different ripening stages

The antioxidant results of the samples were shown in Figure 4. As shown in Figure 4, The DPPH antioxidant activity increased from 61.35 to 115.58 mg TE/100 g fruit throughout the development of fruits.

These results are consistent with the results observed for total phenolic content. There were strong correlations between antioxidant capacity and total phenolic content
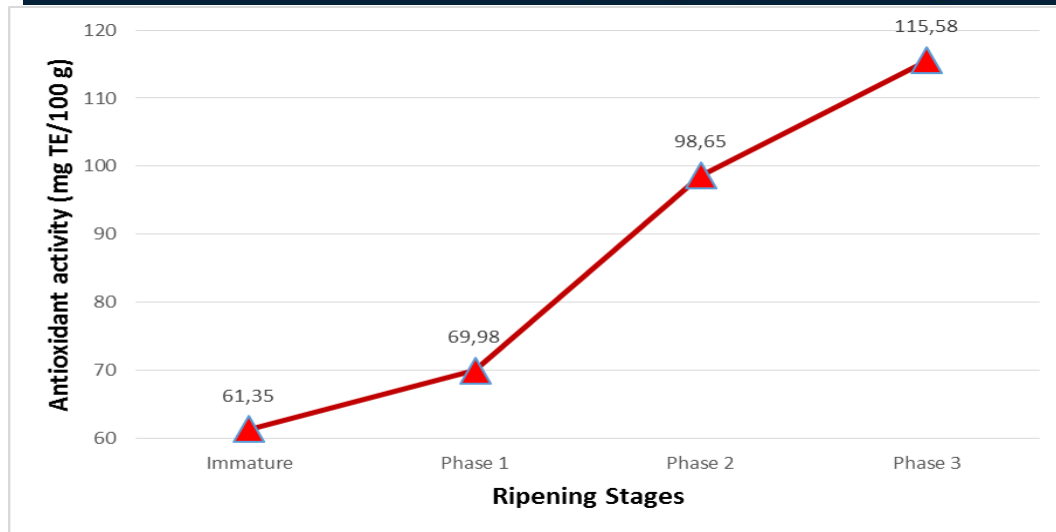
Figure 4. Antioxidant activity of cherry samples at different ripening stages

4. CONCLUSIONS

The obtained results of this study demonstrate that total phenolic content and antioxidant activities change during fruit development in Giresun cherry used in this trial. The demonstration that Giresun cherry fruits present high antioxidant activity, regardless the fruit developmental stage, is expected to stimulate the wider use of Giresun cherry fruits by the food industry as a source of bioactive human health promoters phytochemicals.

REFERENCES

[1]. V. Usenik, J. Fabčič, F. Stampar, "Sugars, organic acids, phenolic composition and antioxidant activity of sweet cherry (Prunus avium L.)". *Food Chem.,* vol.107, pp. 185-192, 2008.
[2]. A. Nawirska-Olszańska, J. Kolniak-Ostek, M. Oziembłowski, A. Ticha, R. Hyšpler, "Comparison of old cherry cultivars grown in Czech Republic by chemical composition and bioactive compounds". *Food Chem.,*vol. 228, pp.136-142, 2017.
[3]. F. Blando, B.D. Oomah, "Sweet and sour cherries: Origin, distribution, nutritional composition and health benefits". *Trends in Food Sci. & Technol.,* vol. 86, pp. 517-529, 2019.
[4]. FAO, 2017. FAO statistical database. Available at:http://www.fao.org/statistics/en/
[5]. G.B. Celli, A.B. Pereira-Netto, and T. Beta, "Comparative analysis of total phenolic content, antioxidant activity, and flavonoids profile of fruits from two varieties of Brazilian cherry (Eugenia uniflora L.) throughout the fruit developmental stages". *Food Res. Int.,* vol. 44, pp. 2442-2451, 2011.
[6]. AOAC-Association of Official Analytical Chemistry, In: AOAC - Association of Official Analytical Chemistry (Ed.), Official Methods of Analysis of the Association of Official Analytical Chemistry, seventeenth ed. Washington. 2000.
[7]. K. Slinkard, V.L. Singleton, "Total phenol analysis: automation and comparison with manual methods", *Am. J. Enol. Vitic*. vol. 28 (1), pp. 49-55. 1977.
[8]. R. Re, N. Pellegrini, A. Proteggente, A. Pannala, M. Yang, and C.Rice-Evans, "Antioxidant activity applying an improved ABTS radical cation decolorization assay". *Free Radic Biol Med.*, vol. 26, pp. 1231-1237, 1999.

Heat Transfer and Pressure Drop Augmentation of a Helically Coiled Tube with Using Graphene Nanoplatelet-Water Nanofluid

Orhan Keklikcioglu[1], Toygun Dagdevir[2], Veysel Ozceyhan[3]

Abstract

In the present study, to investigate the effect of GnP-water nanofluid mass fraction on heat transfer and fluid friction characteristics in a helically coiled heat exchanger tube a numerical study is carried out. The impact of various mass fraction (0.5, 0.75, 1.00 %) of GnP-water nanofluid on Nusselt number and friction factor is studied for Reynolds number ranging from 7000 to 13000. The numerical solution procedure includes the investigation of heat transfer and pressure drop characteristics with using finite volume method with the Transition SST model is based on the coupling of the SST k-ω transport equations to solve the continuity, momentum, energy and turbulence equations in three-dimensional domain. The use of GnP-water nanofluids with in the coiled heat exchanger tubes leads to increase in heat transfer and pressure drop over the smooth tube. The Nusselt number increases with the increment of the nanofluid concentrations and Reynolds number. In conclusion, to enhance heat transfer, Graphene nanoplatelet-water nanofluids can be widely applied wherever helically coiled heat exchangers are used.

Keywords: Graphene nanoplatelet, nanofluid, heat transfer, pressure drop, helically coiled heat exchanger

1. INTRODUCTION

In recent years, with the adaptation of nanotechnological engineering applications to complex systems, the use of nanofluids rapidly spreading in systems operating under thermal load or in the recycling of thermal load. It is noteworthy that nanoparticle-containing base fluids are used instead of fluids such as water, mono ethylene glycol, propylene glycol, oil, which are the basic heat transfer fluid.

Nanofluids are suspension containing nanoparticles and thermal conductivities of nanofluids are significantly higher than those of base liquids [1]. Such fluids are now being used and developed to provide thermal load and temperature control in nuclear power plants, automotive industry, processors used in computer systems, defense systems, aerospace systems, heat exchangers, heating, cooling and ventilation systems. The most notably property of nanofluid is enhanced the heat transfer rate relatively and increase the pressure drop and pumping power slightly.

Many studies have conducted the advantages of nanofluids over base fluids by using SiO2, TiO2, Al2O3, CuO nanofluids. However, only limited researches have been performed about the thermohydraulic performance of graphene-water nanofluids. In recent years, it has been observed that the thermal and hydraulic performances of the nanofluids containing graphene nanoparticles are examined in the smooth tube and they are mostly covered between 2014 and 2018. In this context, in a study conducted in 2014, Ghozatloo et al. [2] studied the contribution of the graphene-water fluid in three different weight ratios (0.05%, 0.075, 0.1) to the heat transfer in a flat heat exchanger tube. According to the results of the study, it was found that the thermal conductivity of graphene-water nanofluids increased in the range of 12.6% to 29.2% and the heat transfer coefficient in laminar flow conditions was improved by 23.9%. Mehrali et al. [3] performed a thermal performance analysis at laminar flow conditions using a graphene-water nanofluid having a concentration of 0.025-0.1% in a test tube applied constant heat flux to the surface. As a result of this study, it was stated that the use of graphene nanoparticle increased thermal conductivity in the range of 12-28% and the highest thermal performance coefficient was 1.15. Zanjani et al. [4] reported using a graphene nanoparticle with a 0.02% volume ratio, increasing the heat transfer coefficient in water base fluid by 14.2% in the 1850 Reynolds number. Selvam et al. [5] performed an experimental study in

which a 70:30% mixture of water: ethylene glycol was used as a refrigerant in a car radiator. In this study, by adding a graphene nanoparticle at a ratio of 0.1-0.5% volumetric to the base fluid, a 104% improvement in heat transfer was obtained. Selvam et al. [6] in another study conducted in 2017, they investigated the increase in heat transfer by adding 0.1%, 0.2, 0.3, 0.4, and 0.5% of the graphene nanoparticle into the water: ethylene glycol mixture in the experimental study under laminar, transition and turbulent flow conditions. In 2018, Vallejo et al. [7] investigated the thermophysical properties of nanofluid with addition of 0.25, 0.50, 0.75 and 1.0 weight percent of graphene nanoparticle to propylene glycol-water mixture. They reported that the thermal conductivity of the fluid increased with increasing weight ratio, resulting in an improvement in the thermal conductivity value of up to 16% in a 1.0% weight ratio mixture.

In this study, thermal and hydraulic effect of grapheme nanoplatelet-water in a helical tube numerically investigated. Gholamalizadeh et al. [8] used the same helical tube to investigate the variety of coiled wire inserts on heat transfer and pressure drop penalty in the tube flow. In the light of this study, in our study, the analysis conducted with three different volume fractions (φ=0.5, 0.75 and 1 %) of grapheme nanoplatelet-water nanofluid, three different mass flow rate ranging from 0.05 to 0.1. Constant wall temperature of 60 °C is applied on the outer surface of the test tube. It is assumed that the flow is under developed turbulent condition. The primal aim of this study to investigate the effect of different volume fractions of graphene nanoplatelet-water on heat transfer rate and friction factor coefficient at different mass flow rate.

2.1. NUMERICAL METHODOLOGY

2.1 Design, boundary conditions and numerical procedure

As illustrated in Fig.1 a helically coiled tube heat exchanger that was used in Ref. [8] with different variations of insert created in 3D. The helically coiled tube geometry composed of the tube diameter (D_t) of 0.01m, the coil pitch (P) of 0.02 m, the coil diameter (D_c) of 0.08 m and six coil turns. The total tube length is 1.518 m and the surface area is 0.0476 m^2. Ref. [8] it is investigated the heat transfer and pressure drop characteristics of a helically coiled tube with different coiled wire configurations. The heat transfer and pressure drop analysis were carried out in the mass flow rate of 0.05, 0.075 and 0.1 kg/s by using graphene-water nanofluids at volumetric ratios of 0.5, 0.75, 1% in the helical pipe.
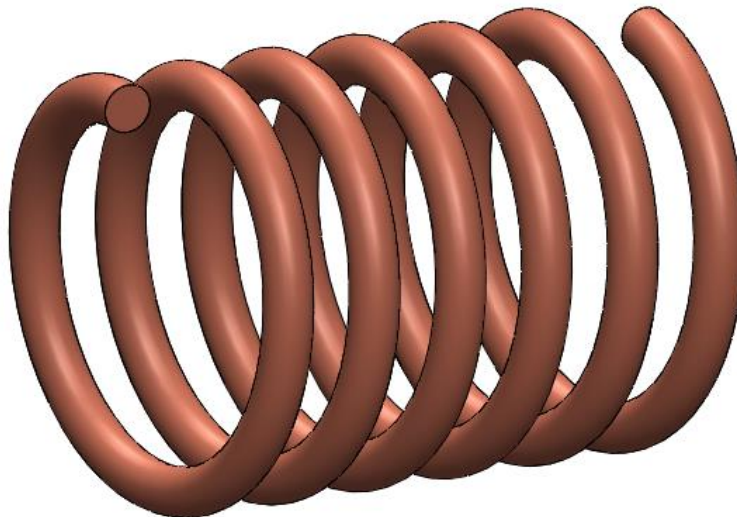
Figure 1. Geometry of smooth helical tube

Three different Reynolds numbers of 6366.2, 9549.3 and 12732.4 used with respect to the mass flow rate of 0.05, 0.075 and 0.1 kg/s. Constant wall temperature of 60 °C is applied on the outer surface of the test tube and it is assumed nanofluid entered the test tube in 10 °C. It is accepted that the velocity vectors are uniform and normal to inlet surface, and there is no gauge pressure in helically coiled tube outlet.

In this study the single phase model has been applied in the modeling of nanofluid. The three-dimensional continuity, momentum and energy of Navier-Stokes equations are solved by using a finite volume method and the SIMPLE algorithm scheme is applied to examine the effects of turbulent flow on heat transfer and friction characteristics. Second order upwind discretization schemes were chosen on all the transport equations. The

Transition SST k-*w* turbulence model was selected. In order to compute data with high accuracy, the residual sum was computed and set for each iteration and the convergence criterion was less than 10^{-6} for all equations.

2.2 Validation of numerical study and grid independence check

For validation of the numerical study, the obtained results of Nusselt number and fiction factor of smooth helically coiled tube with water for this study compared to the results of Ref. [8.]. As seen in Table 1. compared Nusselt number and friction factor values show a good agreement with results of Ref. [8].

Table 1. Comparison between Ref. [8] and this study results of Nusselt number and friction factor

m(kg/s)	Reynolds	Nu$_t$ Ref.[8]	f$_t$ Ref.[8]	Nu (This study)	f (This study)	Deviation (%) Nu	f
0.05	6366.2	73.1	0.054	75.83	0.059	3.73	9.25
0.075	9549.3	81.9	0.040	85.96	0.044	4.96	10
0.1	12732.4	92	0.036	99.44	0.041	8.09	13.88
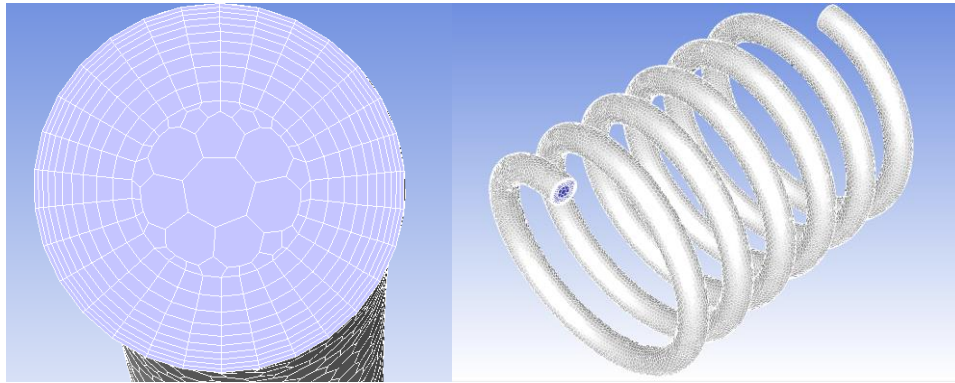
Figure 2. Mesh structure of smooth helical tube

A careful check for grid independence is required for ensuring the validity and accuracy of numerical methodology. For this purpose, detailed grid indepence tests were conducted and according to the grid models. As in Fig 2 mesh models of helical tube was created with 710654, 1244586 and 1956875 cell numbers. After 1244586 cell numbers, Nusselt number has increased less than 2% conjunction with accrual of cells number.

2.3 Thermo-physical Properties of Nanofluid

To determine thermo physical properties of nanofluid, the following equations were presented by researchers. The thermal efficiency of nanofluids can be determined by the heat transfer coefficient which is a function of a number of thermo-physical properties such as density, specific heat, thermal conductivity and viscosity.

The density of nanofluid expressed by B.C. Pak and Y.I. Cho [9]:

$$\rho_{nf} = (1 - \varphi)\rho_{bf} + \varphi\rho_{np} \quad (1)$$

Specific heat of nanofluid determined by Buongiorno J. [10]:

$$Cp_{nf} = \frac{(1-\varphi)\rho_{bf}Cp_{bf} + \varphi\rho_{np}Cp_{np}}{\rho_{nf}} \quad (2)$$

For calculation the thermal conductivity of nanofluid Eq. 3 which was developed by Hamilton and Crosser [11] was used.

$$k_{nf} = k_{bf} \frac{[k_{np}+(n-1)k_{bf}-(n-1)\varphi(k_{bf}-k_{np})]}{[k_{np}+(n-1)k_{bf}+\varphi(k_{bf}-k_{np})]} \ (3)$$

Dynamic viscosity was also calculated from the following equation,

$$\mu_{nf} = \mu_{bf}(123\varphi^2 + 7.3\varphi + 1) \ (4)$$

Nanofluids composed from a base fluid and nanoparticles. The thermo-physical properties of nanofluids calculated with using the above equations. In order to calculate, thermo-physical properties of graphene-water nanofluid, density, specific heat, dynamic viscosity and thermal conductivity of graphene and water as given in Table.2.

Table 2. Thermo-physical properties of the nanoparticles graphene and water at T = 300 K.

Thermo-physical properties	Graphene[12]	Water
ρ (kg/m^3)	2200	998.2
C (j/kgK)	643	4182
μ (kg/ms)	-	1.003E-03
k (W/mK)	3000	0.6

2.4 Calculation Heat Transfer and Friction Factor

The heat energy transfer to the fluid;

$$Q = m.c.(T_o - T_i) \ (5)$$

The convective heat transfer coefficient through the channel is defined as;

$$h = \frac{Q}{(T_{iw}-T_b)A} \ (6)$$

Here, T_{iw} and T_b represent the inner wall temperature of the numerical method and bulk temperature of the fluid. A represents the surface area of the tube.

The Nusselt and Reynolds numbers can be calculated from;

$$Nu = \frac{hD}{k} \ (7)$$

where k is the conductive heat transfer coefficient of fluid.

$$Re = \frac{UD}{v} \ (8)$$

where D is hydraulic diameter, U is velocity, v is kinematic viscosity.

The friction factor is defined as;

$$f = \frac{\Delta P}{\frac{1}{2}\rho.U^2\frac{L}{D}} \ (9)$$

3. RESULTS AND DISCUSSIONS

In this section, thermal energy transfer and pressure drop were investigated by using the graphene nanoparticle in different volume fractions in a helical heat exchanger tube. Firstly, the smooth tube analyzes were compared to a study performed previously (Ref. [8]) at 0.05, 0.075 and 0.1 kg /s for three input mass flow rates, and validation was performed with maximum deviation value of 8.09 and 13.88 % for Nusselt number and friction factor, respectively. In the second stage, the effect of different volume fractions of graphene-water nanofluids and Reynolds numbers on heat transfer and pressure drop were performed.

Table 3. Effect of GnP-water nanofluid volume fractions on Nusselt number and friction factor.

$m(kg/s)$	$Reynolds$	$\varphi(\%)$	Nu_s	f_s	Nu_{nf}	f_{nf}	$Variation(\%)$	
							Nu	f
0.05	6366.2	0.5	75.83	0.059	89.76	0.063	18.37	6.78
0.075	9549.3	0.5	85.96	0.044	99.95	0.047	16.28	6.82
0.1	12732.4	0.5	99.44	0.041	115.13	0.044	15.78	7.32
0.05	6366.2	0.75	75.83	0.059	99.48	0.069	31.19	16.95
0.075	9549.3	0.75	85.96	0.044	111.24	0.052	29.41	18.18
0.1	12732.4	0.75	99.44	0.041	126.84	0.050	27.55	21.95
0.05	6366.2	1	75.83	0.059	108.21	0.077	42.70	30.51
0.075	9549.3	1	85.96	0.044	121.05	0.060	40.82	36.36
0.1	12732.4	1	99.44	0.041	138.18	0.057	38.96	39.02

The variation of Nusselt number and friction factor characteristics for different volume concentration of graphene nanoplatelet-water nanofluid in the smooth helical tube is given in Table 3. The Nusselt number increases with the increment of volume fraction with reference to the base fluid. The highest Nusselt number of 138.18 observed for φ=1% volume fraction at Reynolds number of 12732.4. The friction factor decreases with the increasing of the Reynolds number. As seen in Table 3. friction factor results show an ascending trend with the increment of volume fractions. To evaluate the variation in terms of pumping power, 0.05 mass flow rate, 0.5 volume fraction and 6366.2 Reynolds number model is advantageous.

Table 4. Total temperature and pressure contours for Reynolds number of 9549.3 versus volume fractions 0.5, 0.75 and 1%

	Reynolds=9549.3, φ=0.5 %	*Reynolds=9549.3, φ=0.75 %*	*Reynolds=9549.3, φ=1 %*
Total temperature (K)			
Total pressure (Pa)			
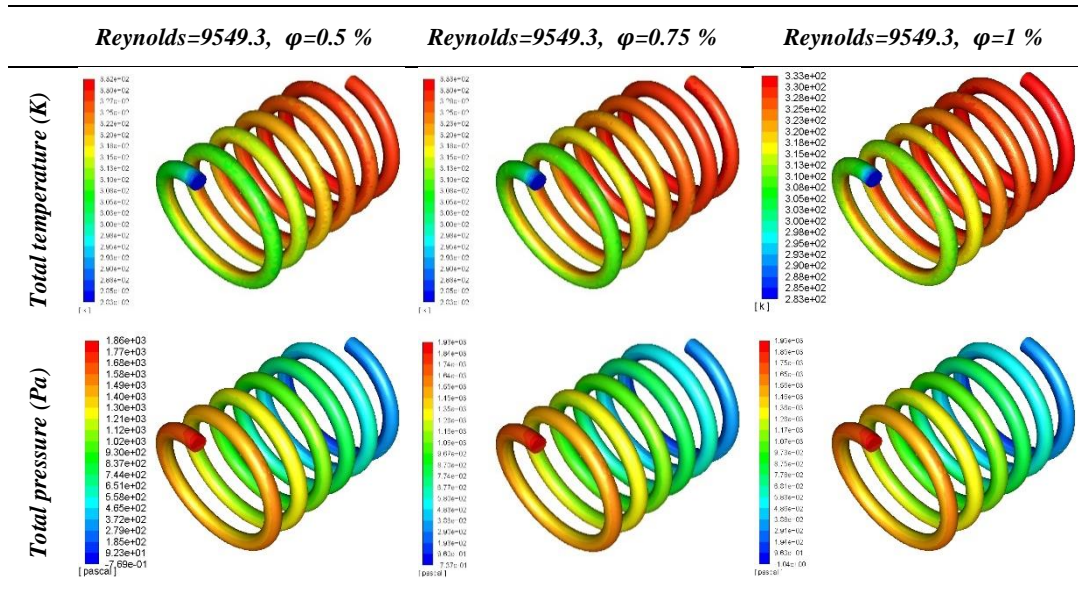
As can be seen in Table 4. using of nanofluid improved the thermal characteristics of helical tube. With the increment of volume fraction, the nanofluid in helical tube reaches the high temperature more rapidly than lower volume fraction model. On the other hand, high volume fraction causes the considerable pressure drop in helical tube. As understood in Table 4. The pressure drop value increases with the increment of volume fraction at a constant Reynolds number.

4. CONCLUSIONS

The present study represents the heat transfer enhancement of graphene nanoplatelet-water nanofluids in a smooth helical tube. A previous model was used and validated in accordance with smooth tube using water fluid. A 3D model of the helical tube was created and meshed to investigate parameters of three Reynolds number 6366.2, 9549.3 and 12732.4, three graphene nanoplatelet volume fractions (φ=0.5, 0.75 and 1 %). The Nusselt number increases with the increment of volume fraction with reference to the base fluid. The highest Nusselt number of 138.18 observed for φ=1% volume fraction at Reynolds number of 12732.4. Friction factor results show an ascending trend with the increment of volume fractions. The lowest friction factor of 0.044 observed for φ=0.5 % volume fraction at Reynolds number of 12732.4. According to the numerical investigation results, the graphene nanoplatelet-water nanofluid introduced a good performance to enhance the heat transfer rate; therefore, it can be more effective in heat transfer applications.

ACKNOWLEDGMENT

REFERENCES

[1]. H. Zhu, C. Zhang, S. Liu, Y. Tang, Y. Yin, Effects of nanoparticle clustering and alignment on thermal conductivities of Fe3O4 aqueous nanofluids, Applied Physics Letters., vol. 89, 2006.

[2]. Ahmad Ghozatloo, Alimorad Rashidi, Mojtaba Shariaty-Niassar, Convective heat transfer enhancement of graphene nanofluids in shell and tube heat exchanger, Experimental Thermal and Fluid Science, vol. 53, pp.136–141, 2014.

[3]. Mohammad Mehrali, Emad Sadeghinezhad, Marc A. Rosen, Amir Reza Akhiani, Sara Tahan Latibari, Mehdi Mehrali, Hendrik Simon Cornelis Metselaar, Heat transfer and entropy generation for laminar forced convection flow of graphene nanoplatelets nanofluids in a horizontal tube, International Communications in Heat and Mass Transfer, vol. 66, pp. 23–31,2015.

[4]. Hossein Akhavan-Zanjani, Majid Saffar-Avval, Mohsen Mansourkiaei, Farhad Sharif, Mohammad Ahadi, Experimental investigation of laminar forced convective heat transfer of Graphene-water nanofluid inside a circular tube, International Journal of Thermal Sciences, vol.100, pp.316-323,2016.

[5]. C. Selvam, R. Solaimalai Raja, D. Mohan Lal, Sivasankaran Harish, Overall heat transfer coefficient improvement of an automobile radiator with graphene based suspensions, International Journal of Heat and Mass Transfer, vol. 115, pp.580–588, 2017.

[6]. C. Selvam, T. Balaji, D. Mohan Lal, Sivasankaran Harish, Convective heat transfer coefficient and pressure drop of water-ethylene glycol mixture with graphene nanoplatelets, Experimental Thermal and Fluid Science, vol. 80, pp. 67–76, 2017.

[7]. J.P. Vallejo, J. Pérez-Tavernier, D. Cabaleiro, J. Fernández-Seara, L. Lugo, Potential heat transfer enhancement of functionalized graphene nanoplatelet dispersions in a propylene glycol-water mixture. Thermophysical profile, J. Chem. Thermodynamics, vol. 123, pp.174–184, 2018.

[8]. Ehsan Gholamalizadeh, Ebrahim Hosseini, Mohammadreza Babaei Jamnani, Ali Amiri, Ali Dehghan saee, Ashkan Alimoradi, Study of intensifcation of the heat transfer in helically coiled tube heat exchangers via coiled wire inserts, International Journal of Thermal Sciences, vol. 141, pp. 72–83, 2019.

[9]. B. C. Pak, Y. I. Cho, Hydrodynamic and heat transfer study of dispersed fluids with submicron metallic oxide particles. Experimental Heat Transfer. vol. 11, pp. 151-170, 2007.

[10]. J. Buongiorno, Convective transport in nanofluids. ASME J. Heat Transfer, vol. 128, pp.240-250, 2006.

[11]. R.L. Hamilton, O.K. Crosser, Thermal conductivity of heterogeneous two component systems, I and EC Fundam., vol.1 (3), pp.187–191, 1962.

[12]. C. Selvam, D. Mohan Lal, Sivasankaran Harish, Thermal conductivity and specific heat capacity of water–ethylene glycol mixture-based nanofluids with graphene nanoplatelets, Journal of Thermal Analysis and Calorimetry, vol.129(2), pp. 947-955, 2017.

Multi-Scale Modelling of Mechanical Behaviour of Graphene-Reinforced Composites

Umut Caliskan[1,2], Constantinos Soutis[2]

Abstract

A multi-scale representative volume element (RVE) for simulating the mechanical behaviour of a graphene-enhanced polymer is proposed in this study. The RVE integrates nanomechanics and continuum mechanics, thus bridging the length scales from the nano- through to macro scale. The mechanical response of both armchair and zigzag graphene is described by a finite element (FE) model based on molecular mechanics. At the graphene sheet and matrix interface a simplification is introduced, perfect bonding is assumed. The C-C bonds of the graphene sheet in the analysis are described by beam elements with nodal translations and rotations in a space frame configuration, representing its atomic structure. The effect of geometric parameters of graphene platelet on the tensile response of the nanocomposite RVE is investigated.

Keywords: Graphene, multi-scale analysis, molecular mechanics, representative volume element.

1. INTRODUCTION

Graphene sheets are considered to be the thinnest, strongest and stiffest materials currently in use. Earliest work on these carbon-based materials can be traced back to 1960s. However, only during the last decade few-layers of graphitic planes nanostructures have been produced and characterised [1]. Epoxy polymers are well known because of their excellent adhesion, considerable mechanical and high electrical insulating properties with relatively good chemical resistance. Epoxy is now widely used in various applications ranging from microelectronics to aerospace structures. Ayatollahi et al. [2] presented multiscale modelling for the nonlinear properties of a polymer/single wall carbon nanotube (SWNT) nanocomposite under tensile, bending and torsional loading. They developed a finite element (FE) model based on the theory of molecular mechanics to predict the mechanical properties of both armchair and zigzag SWNTs. The equivalent beam element was then used to build a cylindrical representative volume element (RVE) where the effects of the interphase between SWNT and the polymer on mechanical response could be studied. Their results showed that while the interphase had a small effect on the nanocomposite stiffness, the ratio of (SWNT length)/(RVE length) dramatically affected its stiffness. Khalili and Haghbin [3] investigated the role of nanotubes specifications on the nonlinear tensile behaviour of nanocomposites using multi-scale material modelling. They also studied the effect of diameter, chirality and volume fraction of nonlinearly modelled SWCNTs on their composites. Multi-scale modelling was applied to assemble various RVEs composed of different SWCNTs embedded in the polymer. Attained stress-strain curves of nanocomposites revealed that using Armchair SWCNTs rather than Zigzags made nanocomposites tougher in tensile loading. Also the diameter of CNT had an inverse effect on the stress-strain curves. Using CNTs with smaller diameter, regardless of the chirality and type, made nanocomposites stronger in tension. Furthermore, the effect of diameter was more obvious in higher volume fraction of CNTs. Tserpes et al. [4] investigated a multi-scale representative volume element for modelling the tensile behaviour of carbon nanotube-reinforced composites. A progressive fracture model based on the modified Morse interatomic potential was used for simulating the behaviour of the isolated carbon nanotubes and the FE method for modelling the matrix and building the RVE. The effect of interfacial shear strength on the tensile behaviour of the nanocomposite was also

studied. Stiffness was found to be unaffected, while tensile strength to significantly decrease with decreasing the interfacial shear strength. Khalili and Haghbin [5] applied multi-scale material modelling to investigate the effect of major design parameters of reinforcing agents in single-walled carbon nanotube (SWCNT) reinforced nanocomposites in impact loads. They also studied the influence of diameter, chirality and volume fraction (VF) of SWCNTs on impact behavior of different representative volume elements (RVEs) of nanocomposites. They modeled SWCNTs through beam elements in space frame structures in finite element modeling (FEM) software based on their atomic structures in molecular mechanics. The various RVEs were exposed to a tensile impact load and the obtained responses were analyzed to evaluate the effective design parameters of SWCNTs in the nanocomposite structures. The results in the form of strain energy density and axial strain oscillations of RVEs in a time period after impact demonstrate a great improvement in the impact behavior of nanocomposites due to adding SWCNTs in matrix. Applying SWCNTs with smaller diameter in RVEs caused a better impact strength in nanocomposites. Guo et al. [6] proposed a new multiscale simulation method for analyzing the mechanical properties of graphene-reinforced composites. The atomistic and the macroscopic scales are combined in the proposed finite element modeling approach. In the nanoscale analysis, a space frame structure of graphene was selected, the carbon atoms were described as nodes, and the carbon–carbon covalent bonds were represented with nanoscale beams. The macroscopic homogeneous isotropic model of the matrix and the interface was included in the representative volume element of the composites. The effect of graphene volume fraction and different inclined angles on the mechanical properties of the composites was investigated under axial tension. The simulation results showed that with the increase in the graphene volume fraction, the Young's modulus of the composites was increased significantly. The Young's modulus of the composites was highly dependent on the size of graphene. Mortazavi et al. [7] developed a multiscale scheme using molecular dynamics (MD) and finite element (FE) methods for evaluating the effective thermal conductivity of graphene epoxy nanocomposites. The proposed hierarchical multiscale approach included three different scales. First, MD simulations were used for the investigation of thermal conduction in graphene epoxy assembly at atomic scale. Their results suggested that thermal conductivity of single layer graphene decline by around 30% in epoxy matrix for two different hardener chemicals. Parashar and Mertiny [8] stuied the fracture characteristics of graphene-modified polymer nanocomposites. A three-dimensional representative volume element-based multiscale model was developed in a finite element environment. Graphene sheets were modeled in an atomistic state, whereas the polymer matrix was modeled as a continuum. Fracture characteristics of graphene/polymer nanocomposites were investigated in conjunction with the virtual crack closure technique. The results demonstrate that fracture characteristics in terms of the strain energy release rate were affected for a crack lying in a polymer reinforced with graphene. Ahmadia et al. [9] investigated the behavior of L-shaped samples made of multi-scale carbon nanotube/carbon fiber reinforced polyethylene under the bending test by using the extended finite element method. The mechanical properties of the multi-scale composite were obtained by a stochastic finite elementmode. Initially, molecular dynamics simulations were used to compute the mechanical properties of nanotubes at the nanoscale. Then, by using the finite element method, the properties of the carbon nanotube/polyethylene nanocomposite are obtained. Considering the mechanical properties of the matrix as the properties of nanotube reinforced polyethylene, the carbon fibers were included into the composites in the next scale. Kumar and Srivastava [10] aimed to evaluate and compare the effective elastic properties of CNT- and graphene-based nanocomposites using 3-D nanoscale representative volume element (RVE) based on continuum mechanics using finite element method (FEM). Different periodic displacement boundary conditions were applied to the FEM model of the RVE to evaluate various elastic constants. The effects of the matrix material, the volume fraction and the length of reinforcements on the elastic properties were also studied. Results predicted were validated with the analytical and/or semi empirical results and the available results in the literature. Although all elastic stiffness properties of CNT- and graphene-based nanocomposites were found to be improved compared to the matrix material, but out-of-plane and in-plane stiffness properties are better improved in CNT- and graphene-based nanocomposites, respectively. It was also concluded that long nanofillers (graphene as well as CNT) are more effective in increasing the normal elastic moduli of the resulting nanocomposites as compared to the short length. Manta et al. [11] validated recently developed numerical method that simulates the electrical response of a graphene/polymer nanocomposite with experimental data. Their approach was based on the multiscale method and consists of a unit cell and a representative volume element (RVE), accounting for aligned and randomly distributed nanoparticles. At the unit cell level, the material nano characteristics (filler geometry, constituent electrical and interfacial properties) were integrated into a local resistance algebraic matrix. The material architecture was then modelled at the micro-level (RVE) by a user-defined distribution of the unit cell electrical properties. A statistical sample was studied and the average electrical response was compared with measurements for direct (DC) and alternate current (AC). The model was proven to be an effective, flexible and time-efficient tool to design and optimize advanced nanocomposite systems. Gresil et al. [12] presented a quantitative dispersion characterisation method using non-contact infrared thermography mapping that measures the thermal diffusivity (α) of the graphene nanocomposite and related α to a dispersion index. The main advantage of the proposed method was its ability to evaluate dispersion over a large area at reduced effort and cost, in addition to measuring the thermal properties of the system. The actual resolution of this thermal mapping reached 200 μm per pixel giving an accurate picture of graphene nanoplatelets (GNP) dispersion. The post-dispersion treatment showed an improvement in directional thermal conductivity of the composite of up to 400% increase at 5 wt% of GNP. The Maxwell-Garnet effective medium approximation was proposed to estimate thermal conductivity that compare favourably to measured data.

2. THEORY AND MODELLING TECHNIQUE

2.1. Geometry of Graphene Sheets

Graphene sheet is a lattice of hexagonal bonds between carbon atoms in which every atom is bonded to the three nearest neighbours via very strong covalence bonds of length 1.421 Å. Many of Graphene sheets mechanical and electrical properties particularly depend on the direction and the length of vector that describes the atomic arrangement of bonds. This vector, namely chiral vector or chirality index C_h, is generated from the two a_1 and a_2 primitive vectors of the unit cell in the graphene sheet. The chiral vector is made up of **n** units of a_1 and **m** units of a_2, i.e. (Fig. 1) [5]:

$$C_h = n\vec{a}_1 + m\vec{a}_2, \qquad bn \geq m \tag{1}$$

Chirality index that is specified by (**n, m**) is representing the length and direction of chiral vector on graphene sheet. Regarding the chiral index, three types of graphene sheets are defined. The Armchair graphene sheets are defined by (n, n) and the Zigzag graphene sheets by (n, 0). Other ones with different chirality indices are Chiral graphene sheets.
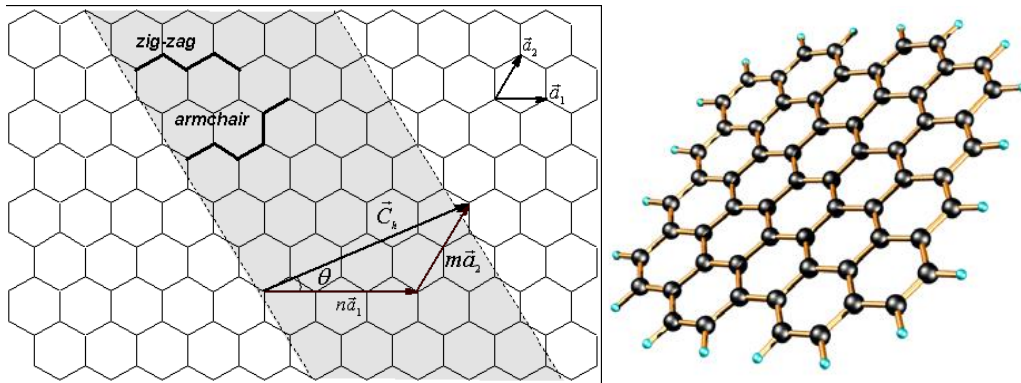
Figure 1. Schematic diagram of graphene sheet, Zigzag and Armchair directions are highlighted.

2.2. Molecular Structural Mechanics Modelling

In computational nanoscience, the energy of a system including several hundred to billions atoms is evaluated using interatomic potentials. The total potential energy function of an n-body nanostructure, always understood to refer to the configurational potential energy that can be expressed in terms of coordinates of its constituent atoms. The simplest way is to express this energy as a cluster expansion involving two- and three-body, etc., potential energy functions as follows [5],

$$H_I = \frac{1}{2!}\sum_i \sum_{j \neq i} V_2(r_i, r_j) + \frac{1}{3!}\sum_i \sum_{j \neq i} \sum_{k \neq i,j} V_3(r_i, r_j, r_k) + \dots \tag{2}$$

where V_n are n-body interatomic potential functions. The potentials are functions of atomic coordinates, but in practice they are expressed in terms of interatomic distances. Thus potential energy depends on interatomic separation and also the angles between the bonds connecting individual atoms.

In molecular mechanics, graphene sheets are considered as a great molecule including carbon atoms. Therefore, its potential energy function is expressed in the form of steric potential energy, which depends solely on the relative position of nuclei of carbon atoms. The general form of a nanostructure force-field is expressed such as [5]:

$$U = \sum U_r + \sum U_\theta + \sum U_\emptyset + \sum U_W + \sum U_{vdw} \tag{3}$$

where U_r is the bond stretching, U_θ is the bond angle bending, $U_\emptyset$ is the dihedral angle torsion, U_W is the out of plane torsion and U_{vdw} is the non-bonded Van der Waals interactions in molecule.

The molecular mechanics modelling method is aimed to simulate atomic properties of GNP structure as a space frame in classical structural mechanics. For this reason carbon atoms in graphene sheets are regarded as the joints in the frame and carbon bonds as load carrying beam elements correspondingly, Figure 2. Simple harmonic

functions and Amber force-field is applied to describe potential energy terms in molecular mechanics as follows [5]:

$$U_r = \frac{1}{2}k_r(r - r_0)^2 = \frac{1}{2}k_r(\Delta r)^2 \tag{4}$$

$$U_\theta = \frac{1}{2}k_\theta(\theta - \theta_0)^2 = \frac{1}{2}k_\theta(\Delta\theta)^2 \tag{5}$$

$$U_\tau = \frac{1}{2}k_\tau(\tau - \tau_0)^2 = \frac{1}{2}k_\tau(\Delta\tau)^2 \tag{6}$$

where k_r, k_θ, k_τ are the bond stretching force, bond angle bending force and torsional resistance constant, respectively, and the symbols Δr, $\Delta\theta$ and $\Delta\tau$ represent the bond stretching increment, the bond angle change and the angle change of bond twisting, respectively. Where in structural mechanics, the strain energy of a uniform beam element representing a carbon bond with the length L, due to deformations is expressed as follows [5]:

$$U_A = \frac{1}{2}\int_0^L \frac{N^2}{EA}dL = \frac{1}{2}\frac{N^2 L}{EA} = \frac{1}{2}\frac{EA}{L}(\Delta L)^2 \tag{7}$$

$$U_T = \frac{1}{2}\int_0^L \frac{T^2}{GJ}dL = \frac{1}{2}\frac{T^2 L}{GJ} = \frac{1}{2}\frac{GJ}{L}(\Delta\beta)^2 \tag{8}$$

$$U_M = \frac{1}{2}\int_0^L \frac{M^2}{EI}dL = \frac{2EI}{L}\alpha^2 = \frac{1}{2}\frac{EI}{L}(2\alpha)^2 \tag{9}$$

Where U_A, U_T and U_M are the strain energies of a beam element due to the pure axial force N, the pure bending moment M and the pure torsion T, respectively. In association, ΔL, α and $\Delta\beta$ are the axial stretching deformation, the rotational angle at the ends of the beam and the relative rotation between the ends of the beam, respectively. Now by setting a direct relation between the strain energies in structural mechanics, in Eqs. (7)–(9), and potential energies in molecular mechanics, Eqs. (4)–(6), assuming same deformations, the elastic (Young's modulus E and shear modulus G) and geometrical properties of the beam elements (length L and cross-section area A) are obtained by by[5]:

$$\frac{EA}{L} = k_r, \qquad \frac{EI}{L} = k_\theta, \qquad \frac{GJ}{L} = k_\tau, \tag{10}$$
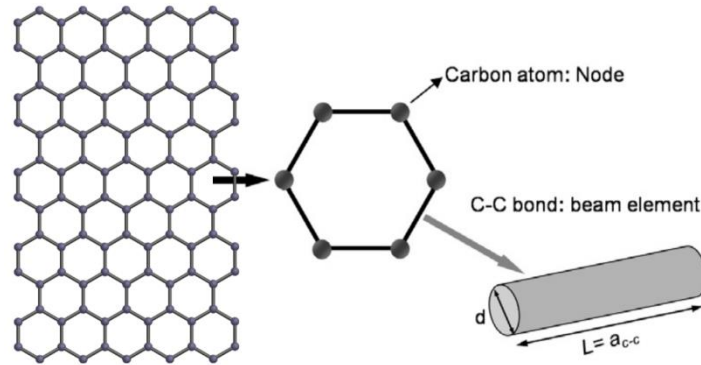
Figure 2. Simulation of a graphene sheet as a space-frame structure.

For convenience, the beam elements are considered of a circular cross section. By knowing the molecular mechanics parameters from Amber force field, E, G and diameter (*d*) of the beam elements are ready to be applied in structural mechanics modelling through the following relations [5]:

$$d = 4\sqrt{\frac{k_\theta}{k_r}}, \qquad E = \frac{k_r^2 L}{4\pi k_\theta}, \qquad G = \frac{k_r^2 k_\tau L}{8\pi k_\theta^2} \tag{11}$$

$$k_r = 938 \ kcal \ mol^{-1} \ A^{-2} = 6.52 \times 10^{-7} \ N \ nm^{-1}$$

$$k_\theta = 126 \ kcal \ mol^{-1} \ rad^{-2} = 8.76 \times 10^{-10} \ N \ nm^{-1} \ rad^{-2} \tag{12}$$

$k_\tau = 40 \, kcal \, mol^{-1} \, rad^{-2} = 2.78x10^{-10} \, N \, nm^{-1} \, rad^{-2}$

This formulation was applied in finite element method through solving the system of matrices which are derived for a circular two-node beam elements. Each node has six degrees of freedom (DOF), three translational (x, y, z) and three rotational degrees of freedom (DoF).

2.3. Modelling Graphene Sheet and Assembling Representative Volume Element (RVE)

In this study, linear Euler–Bernoulli beam elements with six DoF are used for applying molecular structural modelling. This element is based on known elastic parameters such as E and G and also on diameter which are obtained from molecular structural modelling method. The beam elements are applied to a space-frame structure that is geometrically modelled through coordinates of carbon atoms in its molecular structure. The coordinates are achieved by using a nanomaterial modeling program. After that, the beam elements are situated between two pertinent carbon atoms regarding the chirality of graphene sheets. The four different graphene sheets are used in this study. Fig. 3 shows a using graphene sheets in ABAQUS [13] and Table 1 shows the geometric dimension and properties of graphene sheets using in this study.

| a) Armchair (6,6) | b) Zigzag (10,0) | c) Armchair (12,12) | d) Zigzag (20,0) |
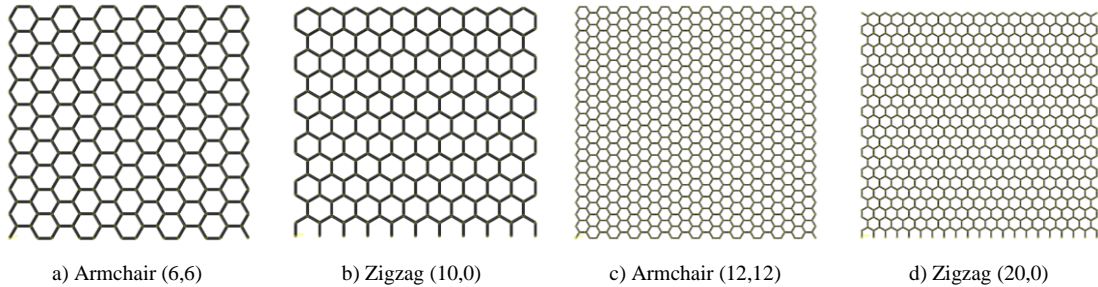
Figure 3. The modeled graphene sheets in ABAQUS.

The main principle in multi-scale material modelling of nanocomposites is to assemble a RVE as a representative of the material system to be analysed. In the numerical simulation of a GNP/polymer nanocomposite, the nano particle is modelled more accurately by molecular mechanics, while the polymer part, which has rather less significant effect on composite strength and stiffness, is represented by common solid elements in FEM as a continuum.

Table 1. The geometric dimension and properties of graphene sheets.

Graphene	Dimensions (nm)		Number of Atoms
	Length (y)	Width (x)	
1 (6,6)	2.3392	2.4157	240
2 (10,0)	2.3478	2.4612	242
3 (12,12)	4.8041	4.9735	960
4 (20,0)	4.6893	4.9224	923

Epoxy	Dimensions (nm)		
	Length (y)	Width (x)	Thickness (z)
4%, (6,6), GNP	2.3392	2.4157	3.6
8%, (6,6), GNP	2.3392	2.4157	1.8
12%, (6,6), GNP	2.3392	2.4157	1.2
4%, (10,0), GNP	2.3478	2.4612	3.5
8%, (10,0), GNP	2.3478	2.4612	1.75
12%, (10,0), GNP	2.3478	2.4612	1.168
4%, (12,12), GNP	4.8041	4.9735	3.525
8%, (12,12), GNP	4.8041	4.9735	1.763
12%, (12,12), GNP	4.8041	4.9735	1.175
4%, (20,0), GNP	4.6893	4.9224	3.477
8%, (20,0), GNP	4.6893	4.9224	1.738
12%, (20,0), GNP	4.6893	4.9224	1.159

In this study, the polymer is assumed as a linear elastic material with Young's modulus of 3 GPa and Poisson's ratio of 0.3. Linear cubic eight node elements with six DoF per each node in space are used to mesh the polymer portion in FEM. In order to investigate the effect of GNP parameters, different arrangement of RVEs are modelled. The RVEs consist of four different dimensions of Armchair and Zigzag GNP embedded in diverse amount of polymer. GNPs are located at the middle of RVE with the same length as the polymer. Volume fraction of GNP is calculated by ABAQUS and the thickness of GNP is taken equal to the interlayer space in graphite sheets, i.e., 0.34 nm. Figure 4 shows a RVE including GNP and encircling polymer that is modeled in ABAQUS [13].
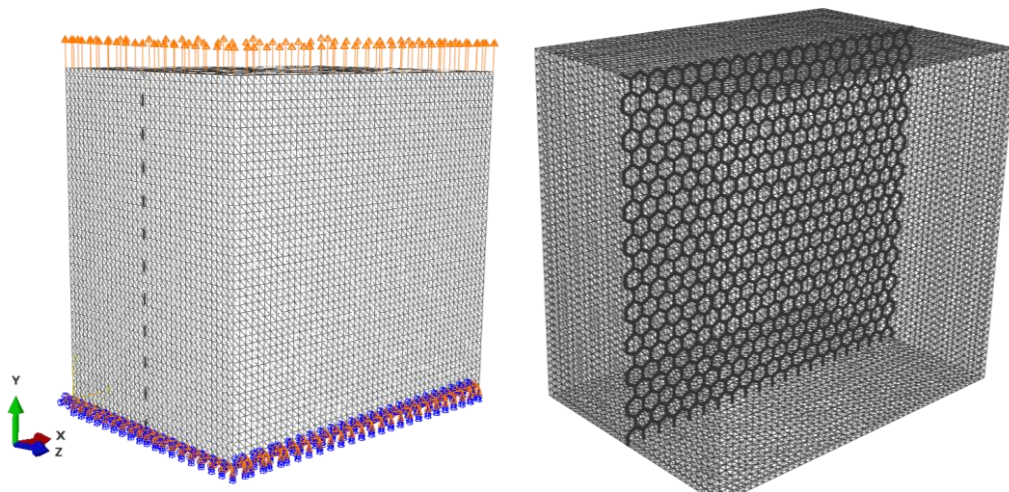
Figure 4. A modelled RVE in ABAQUS consist of graphene sheet and polymer.

The interaction between GNP and surrounding polymer is a critical point in multi-phase material modelling. Hence, ''embedded element'' as a capability in ABAQUS, is used to model the interface in RVE. This ability is successfully used for reinforcing agents in multi-phase structures. In analysing procedure, one end of each RVE was fully constrained and an incremental axial displacement is applied to another end until gaining 10% strain. This method is commonly used in evaluating the tensile behaviour of RVEs [14]. Considering the nonlinearity of the beam elements in GNP, allowed the analysis to have nonlinear results in general. Normal stress is calculated based on total reaction forces in the fixed extremity and obtained from software outputs.

In the present study, to investigate the effect of GNP parameters on tensile behaviour of nanocomposites, four types of GNPs including (6, 6), (12, 12) Armchair and (10, 0), (20, 0) Zigzag GNPs are inserted in the polymer in 4%, 8% and 12% volume fractions. Armchair (6, 6) and Zigzag (10, 0) GNPs are in an nearly equal length, and also it is the same for (12, 12) and (20, 0) graphene sheets.

3. RESULTS

Multi-scale material modelling was used to investigate the role of graphene sheets specifications on the tensile behaviour of nanocomposites. Particularly, the effect of chirality and volume fraction of nonlinearly modelled GNPs is studied on their composites. Multi-scale modelling is applied to assemble various RVEs composed of different GNPs embedded in polymer. Graphene sheets are modelled in continuum mechanics based on their atomic structures in the case of space frame structures. Elements in this structure are defined in such a way to resemble carbon bonds characteristics in molecular mechanics. Polymer portion of RVE is modelled as a linear elastic continuum material, regarding the modelling convenience.

Twelve RVEs consisting two Armchair GNPs (6,6), (12,12) and two Zigzags (10,0), (20,0), each one in 4, 8 and 12 percent VF are analysed in separate stepwise procedures. Its noticeable that (6,6) and (10,0) GNPs are two different kinds GNPs with nearly equal length (2.3 nm). The same way is valid for two other mentioned GNPs in length of about 4.6 nm. The volume fraction of GNP in RVEs is 8% unless specified otherwise in studying the effect of VF on tensile behaviour.

a)   Armchair, 8% GNPs

b)   Zigzag, 8% GNPs

c)   Armchair and Zigzag, 8% GNPs
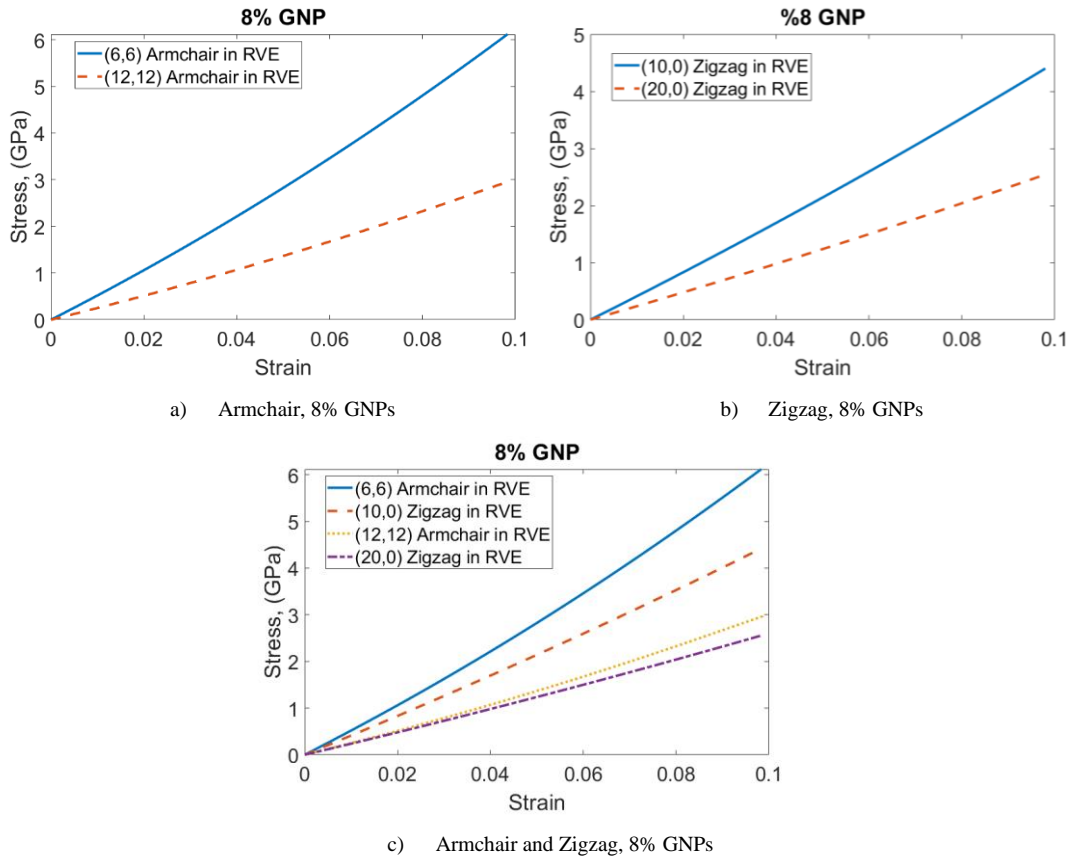
Figure 5. The effect of GNPs chirality on the tensile behaviour of RVE

In order to investigate the effect of embedded GNPs chirality on tensile behaviour of nanocomposites, Armchair and Zigzag GNPs were compared separately. Figure 5a shows the stress-strain curves of RVEs including Armchair GNPs in different dimensions (both in same volume fraction). On the other side, Figure 5 b shows the same curves for inserted Zigzag GNPs in RVEs. It illustrates that using GNPs with lower dimensions in RVEs will strengthen the nanocomposites in tension. A similar behaviour also observed in Zigzag GNPs. The stress-strain curves of four RVEs in one diagram is presented in Figure 5c. It can be concluded that using RVEs including Armchair GNPs results superior curves in nanocomposites. It means more strength and toughness in tensile loadings especially in higher strains (in both dimension ranges).

In Figure 6a the stress-strain curves of 4, 8 and 12 percent VF of Armchair GNPs included RVEs, and in Figure 6b for Zigzag GNPs included is depicted. The figures are expressing that higher amount of GNP in RVE will improve the tensile behaviour of nanocomposite. It is clear that in a same VF using smaller dimensions GNPs in RVE will result superior curves. The important point is that the improvement in tensile behaviour of nanocomposites due to dimensions of GNPs in higher VFs is greater. Thus, it could be deduced that the effect of GNP dimension on tensile behaviour of nanocomposites is influenced by the amount of GNP in it. In order to investigate the dependency of chirality effect to the volume fraction of GNP, stress-strain curves of two equal dimensions Armchair and Zigzag GNPs are superposed in Fig 6c. The diagram declares that the influence of chirality of GNP on tensile behaviour of nanocomposite is not dependent to volume fraction of embedded GNP.

a)   Armchair GNPs, (6,6), (12,12)

b)   Zigzag GNPs, (10,0), (20,0)

c)   Armchair and Zigzag GNPs, (6,6), (10,0)
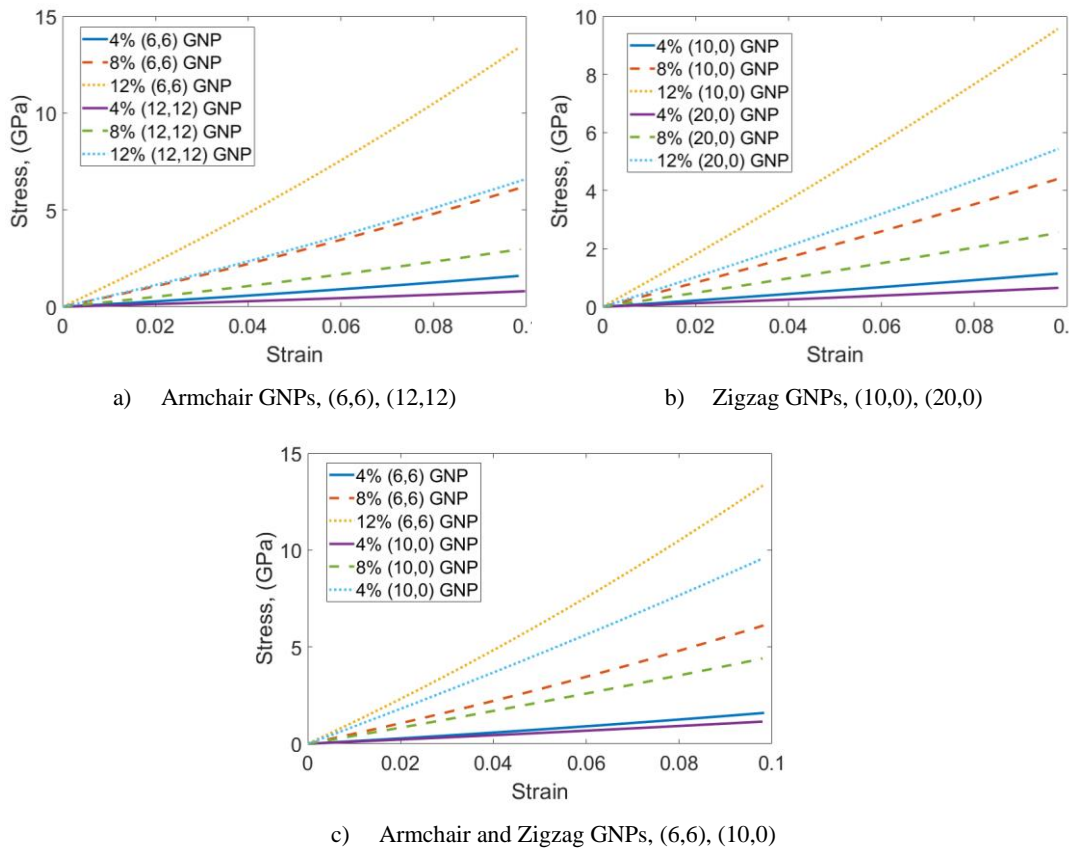
Figure 6. The effect of chirality and volume fraction of GNPs on the tensile behaviour of RVE

4. CONCLUSION

The effect of chirality, dimension and volume fraction of GNPs on tensile behaviour of their nanocomposites is investigated. Multi-scale material modelling in ABAQUS software is used to simulate the tensile loading on a representative volume element of GNP/polymer nanocomposite. GNPs are modelled based on their atomic structures through modified Morse PEF in molecular mechanics as space frame structures. Different amount of Armchair and Zigzag GNPs in different dimensions are assembled by composing GNP and polymer in RVEs. The obtained nonlinear stress-strain curves of RVEs show the dependency of nanocomposites tensile behaviour on volume fraction, chirality and dimensions of embedded GNPs. It is shown that using GNPs with smaller dimensions in RVEs will strengthen the nanocomposites in tension. In addition, using RVEs with Armchair GNPs, it results in higher strength and toughness under tensile loading, especially at higher applied strains. Moreover, adding a larger amount of GNP in RVE will improve the tensile strength of the nanocomposite, something that may not happen in a physical experiment, since the uniform dispersion of nanoparticles is of paramount importance. Finally, for a given amount of GNPs in RVEs, but of smaller dimension GNPs will significantly improve tensile strength of the nanocomposite, especially in higher volume fraction of GNPs.

REFERENCES

[1] Y. Chandra, F. Scarpa, R. Chowdhury, S. Adhikari and J. Sienz, "Multiscale hybrid atomistic-FE approach for the nonlinear tensile behaviour of graphene nanocomposites", Composites: Part A, vol. 46, pp. 147-153, 2013.

[2] M.R. Ayatollahi, S. Shadlou and M.M. Shokrieh, "Multiscale modeling for mechanical properties of carbon nanotube reinforced nanocomposites subjected to different types of loading", Composite Structures, vol. 93, pp. 2250-2259, 2011.

[3] S.M.R. Khalili and A. Haghbin, "Multi-scale modeling of nonlinear tensile behavior in single-walled carbon nanotube reinforced nanocomposites", International Journal of Modeling and Optimization, vol. 1, pp. 199-204, 2011.

[4] K.I. Tserpes, P. Papanikos, G. Labeas, and Sp.G. Pantelakis, "Multi-scale modeling of tensile behavior of carbon nanotube-reinforced composites", Theoretical and Applied Fracture Mechanics, vol. 49, pp. 51-60, 2008.

[5] S.M.R. Khalili and A. Haghbin, "Investigation on design parameters of single-walled carbon nanotube reinforced nanocomposites under impact loads", Composite Structures, vol. 98, pp. 253-260, 2013.

[6] Z. Guoa, L. Songa, G.B. Chaib, Z. Lia, Y. Lia, and Z. Wanga, "Multiscale finite element analyses on mechanical properties of graphene-reinforced composites", Mechanics of Advanced Materials and Structures, vol. 0, pp. 1-8, 2018.

[7] B. Mortazavi, O. Benzerara, H. Meyer, J. Bardon and S. Ahzi, "Combined molecular dynamics-finite element multiscale modeling of thermal conduction in graphene epoxy nanocomposites", Carbon, vol. 60, pp. 356-365, 2013.

[8] A.Parashar and P. Mertiny, "Multiscale model to investigate the effect of graphene on the fracture characteristics of graphene/polymer nanocomposites", Nanoscale Research Letters, vol. 7, pp. 595, 2012.

[9] M. Ahmadi, R. Ansari and S. Rouhi, "Fracture behavior of the carbon nanotube/carbon fiber/polymer multiscale composites under bending test – a stochastic finite element method", Mechanics of Advanced Materials and Structures, vol. 0, pp. 1-9, 2018.

[10] D. Kumar and A. Srivastava, "Elastic properties of CNT- and graphene-reinforced nanocomposites using RVE", Steel and Composite Structures, vol. 21, pp. 1085-1103, 2016.

[11] A. Manta, M Gresil, and C Soutis, "Simulated electrical response of randomly distributed and aligned graphene/polymer nanocomposites", Composite Structures, vol. 192, pp. 452-459, 2018.

[12] M. Gresil, Z. Wang, Q. A. Poutrel and C. Soutis, "Thermal Diffusivity Mapping of Graphene Based Polymer Nanocomposites", www.nature.com/scientificreports, vol. 7, pp. 5536, 2017.

[13] ABAQUS/Standart (Version 2019), User's manual, Finite Element Software. Available from: http://www.simulia. Com

[14] S.J.V. Frankland, V.M. Harik, G.M. Odegard, D.W. Brenner, T.S. Gates, "The stress–strain behavior of polymer–nanotube composites from molecular dynamics simulation". Compos Sci Technol vol. 63 pp. 1655–16661, 2003.

Optimal Design of Shell and Tube Heat Exchanger by Using Net Saving and Saving Cost Ratio Objectives in Waste Heat Recovery System

Ibrahim Kaya[1], Yasin Ust[2]

Abstract

This study presents an optimal design of the shell and tube heat exchanger used for an example case in waste heat recovery system (WHRS) according to multi objective functions using two different optimization methods. The optimization methods are genetic algorithm and univariate search method. By this way, accuracy of the methods will be compared each other. The decision variables in the optimization, namely design parameters, are number of shell, length of tube, number of tube, baffle spacing ratio, tube pitch ratio, tube inner diameter, tube angle, tube arrangement and hot fluid side. The constraints in the optimization are the pressure losses on both sides and the bounds on the design parameters. Objective functions in the optimization are money saved (saving) from waste energy and saving – cost ratio. Finally, the effects of lost exergy cost on the design parameters will be examined towards the end of this study.

Keywords: Energy, Waste Heat Recovery, Heat Exchanger Optimization, Shell and Tube Heat Exchanger, Thermo – Economy Optimization

1. INTRODUCTION

Global energy demand is increasing with the growth of human population and global economy. However, our non-renewable energy resources are limited as well these are gradually decreasing. Furthermore, waste heat recovery has become one of the popular topics in order to reduce greenhouse gas emissions and increase energy savings with increasing environmental parametric. Waste heat recovery normally is carried out by means of heat exchangers. However, due to a heat exchanger having many design parameters, finding the best parameters for user constraints can be a robust optimization problem. Some of the studies in the relevant literature on this subject are presented below and summarized in Table 1.

Demir et al. [1] developed a model for determining the type and area of heat exchangers that provide maximum net savings with certain thermo - economic parameters. In this model, they introduced a new dimensionless number that can be applied to all heat exchangers, and this number depends on both thermo - economic parameters and certain types of heat exchangers. In this model, the heat exchanger area can be determined by providing the most net savings based on defined thermo - economic parameters. In the developed model, the cost of heat exchanger is merely investment cost and has been accepted that the cost of heat exchanger is changed linearly with total area of the heat exchangers.

Agra [2] developed a new model that provides the type and heat transfer surface area of the heat exchanger, by providing the maximum net savings in certain thermo - economic parameters and defined savings - investment ratio. In the model developed, Agra introduced a new dimensionless number called saving effectives which is multiplying of saving - investment ratio and investment - saving potential ratio. This dimensionless number can

be applied to all heat exchangers. In the developed model, the cost of the heat exchanger is defined as merely the cost of the investment and accepted that linear relationship with heat transfer area which is similar to [1].

Ust et al. [3] performed a thermo-economic performance optimization for a single-pass counter-flow heat exchanger. In their work, only heat transfer in finite temperature differences was taken into consideration as irreversibility, and the objective function was defined as the heat transfer rate per unit total cost by considering the loss exergy and investment costs. Then, the results of the parametric analysis were showed by non-dimensioning the objective function. After parametric analysis, the dimensionless objective function was optimized according to the heat exchanger efficiency (ε) and number of transfer units (NTU).

Eryener [4] carried out the thermo-economic optimization of the baffle spacing in shell and tube heat exchanger in a constant heat duty and a constant heat transfer surface area cases. The objective function in the study was defined to minimize the sum of heat exchanger capital cost and exergy demolition cost and the decision variable was defined the ratio of baffle spacing to shell diameter. The cost of the pumping is therefore reflected to the cost of exergy destruction. The Bell - Delaware method is used to determine heat transfer coefficient and pressure loss at the shell side. He used the graphical method as an optimization method.

Caputo et al. [5] proposed a method that minimizes cost in body tube heat exchangers for defined heat duty by using genetic algorithm (GA). They demonstrated the results comparatively in three case from the related literature to prove the accuracy of their method. In their study, The Kern method is used to determine heat transfer coefficient and pressure loss at the shell side. The objective function was defined summing of capital and operation costs of heat exchanger and the decision variables were shell diameter, tube outside diameter and baffle spacing. According to their results, total costs decreased by more than 50%. Therefore, they suggested GA for heat exchanger optimization.

Gosselin et al. [6] optimized the cost of the shell and tube heat exchangers which satisfy defined heat duty in two case in relevant literature with GA. In their study, they explained in detail the design and optimization processes of the heat exchanger. The objective function in their study was the cost summing of capital and operation costs. The decision variables were considered as the pitch ratio, tube layout pattern, number of tube passes, baffle spacing at center, baffle spacing at inlet - outlet, baffle cut, tube to baffle diameter clearance, shell to baffle diameter clearance, tube bundle outer diameter, shell diameter, tube outer diameter in the optimization problem. The Bell - Delaware method is used to determine heat transfer coefficient and pressure loss at the shell side. It should be noted that decision variables were discrete. The constraints in the optimization problem were considered as pressure losses and lower – upper bounds on decision variables. They also showed that optimization results were dramatically changed by adding a maintenance-related constraint (the increase in surface coefficient) to the optimization problem.

Fesanghary et al. [7] optimized an air-cooled condenser by minimized the total cost using Harmony Search method (HS). The objective function in the optimization problem is the total cost which is summing capital and operating costs. The decision variables were considered as tube outside diameter, air velocity, fin height, number of tubes per row, number of tube passes, tube material, tube length. In their study, global parametric analysis (GSA) carried out to measure the effectiveness of decision variables on objective function before the optimization process. In this way, the decision variables being very little effect on the objective function were turned into constant parameter so the complexity of the optimization process has been reduced. They showed the accuracy of HS and compared the results with the GA results. As a result, they proposed HS with GSA for thermal optimization problems.

Fesanghary et al. [8] optimized shell and tube heat exchanger from by using GSA and HS. In their study, objective functions was minimization of summing of capital and operation costs and decision variables were shell diameter, tube diameter, pitch ratio, tube layout, length ratio, baffle cut, baffle spacing ratio, number of sealing strips and material type and. They showed the accuracy of HS and compared the results with the GA results. As a result, similar to [7], they proposed HS with GSA for thermal optimization problems.

Gutierrez et al. [9] presented an approach to the GA for optimal design of the shell and tube heat exchanger. They used a compact formulation of the Bell - Delaware method to describe the shell side flow pattern in the proposed approach. The objective function in the optimization problem is the total cost which is summing capital and operating costs. The optimization variables were considered as tube side pressure loss, shell side pressure loss, baffle cut, number of tube passes, standard inside, outside tube diameters and pitch, tube pattern arrangement, hot fluid allocation, number of sealing strings, tube bundle type, ratio inlet and outlet baffle spacing. They demonstrated the results comparatively in two case from the related literature to prove the accuracy of their method. They emphasized that the GA has easier access to the global solution than the gradient methods. As a result, GA are often more efficient in providing global optimum solutions compared to other standard optimization methods that are often confined to local optimal solutions when applied to non-convex models.

Najafi et al. [10] carried out multi-objective optimization of a plate and fin heat exchanger by using GA. The objective functions in the optimization problem were the heat transfer rate and the annual cost of heat exchanger. The decision variables in the optimization problem were the design parameters with lower and upper bounds. As a result, together with their parametric analysis, they showed the Pareto Front being the optimal solution set.

Thibault et al. [11] presented minimization of heat transfer area and pumping power with the Pareto Front solutions for the shell and tube heat exchanger. The nine decision variables in the optimization problem were tube layout pattern, number of tube passes, baffle spacing, baffle cut, tube-to-baffle diametrical clearance, shell-to baffle diametrical clearance, tube length, tube outer diameter, and tube wall thickness. They used the fast and elitist non-dominated sorting GA (NSGA-II) available in the multi-objective GA module of MATLAB. They showed results comparatively with the case study from the relevant literature for confirming their results. Moreover they presented effect of decision variables being continuous or discrete on the results. According to their results, discrete decision variables are not significant in Pareto - Front but cause a significant difference in objective functions.

Sanaye and Hajabdollahi [12] carried out multi – objective optimization with NSGA – II for shell and tube heat exchanger. They used the Bell - Delaware method for the heat transfer coefficient and pressure loss at shell side. The objective functions in optimization problem were maximization the effectiveness and minimization the cost of the heat exchanger. The cost was defined as summing of capital and operation costs. The seven decision variables in optimization problem tube arrangement, tube diameter, tube pitch ratio, tube length, tube number, baffle spacing ratio and baffle cut ratio. The results of the studies are; tube pitch ratio, tube length, number of tube and baffle spacing ratio were found to be important design parameters leading to a conflict between effectiveness and total cost. On the other hand, the tube arrangement has no effect on the objective functions.

Rao and Patel [13] introduced a modified version of the TLBO (teaching-learning-based optimization) algorithm in their study, and performed a multi-purpose optimization of the GA – optimized plate – fin and shell and tube heat exchangers. Similarly to [12], the objective functions in optimization problem were maximization the effectiveness and the cost of the heat exchanger. Optimization results using modified TLBO were compared with those obtained using genetic GA. They demonstrated the advantage of the modified TLBO algorithm in terms of speed and accuracy when compared to the GA approach of the proposed algorithm for such a thermodynamic optimization.

Table 10. Summary of some studies about optimization of heat exchangers.

Researcher	Heat Exchanger Type	Method	Decision Variable	Objective Function(s)
Demir et al. [1]	Parallel, Counter, Shell and Tube, Cross Flow	Mathematical Model	NTU	Net Saving
Agra [14]	Parallel, Counter, Shell and Tube, Cross Flow	Mathematical Model	NTU	Net Saving
Ust et al. [3]	Counter Flow	Mathematical Model	Effectivity – Number of Transfer Units	Non – Dimensional Number About Exergy And Capital Cost
Eryener [4]	Shell and Tube	Graphical	Ratio Of Baffle Spacing to Shell Diameter	Summing of Capital and Exergy Demolition Cost
Caputo et al. [5]	Shell and Tube	GA	Shell Diameter, Tube Outside Diameter and Baffle Spacing	Summing of Capital and Operation Costs
Gosselin et al. [6]	Shell and Tube	GA	Pitch Ratio, Tube Layout Pattern, Number Of Tube Passes, Baffle Spacing at Center, Baffle Spacing at Inlet - Outlet, Baffle Cut, Tube to Baffle Diameter Clearance, Shell to Baffle Diameter Clearance, Tube	Summing of Capital and Operation Costs

			Bundle Outer Diameter, Shell Diameter, Tube Outer Diameter	
Fesanghary et al. [7]	Compact Heat Exchanger (Tube and Fin)	GSA – HS	Tube Outside Diameter, Air Velocity, Fin Height, Number of Tubes per Row, Number Of Tube Passes, Tube Material, Tube Length	Summing of Capital and Operation Costs
Fesanghary et al. [8]	Shell and Tube	GSA – HS	Shell Diameter, Tube Diameter, Pitch Ratio, Tube Layout, Length Ratio, Baffle Cut, Baffle Spacing Ratio, Number of Sealing Strips and Material Type	Summing of Capital and Operation Costs
Gutierrez et al. [9]	Shell and Tube	GA	Tube Side Pressure Loss, Shell Side Pressure Loss, Baffle Cut, Number of Tube Passes, Standard Inside, Outside Tube Diameters And Pitch, Tube Pattern Arrangement, Hot Fluid Allocation, Number of Sealing Strings, Tube Bundle Type, Ratio Inlet and Outlet Baffle Spacing	Summing of Capital and Operation Costs
Najafi et al. [10]	Compact Heat Exchanger (Plate and Fin)	GA	Cold and Hot Fluid Side Lengths, Height Of The Fin, Fin Frequency, Fin Thickness, Lance Length of The Fin, Number of Fin Layers for Hot and Cold Sides	Heat Transfer Rate and Summing of Capital and Operation Costs
Thibault et al. [11]	Shell and Tube	NSGA-II	Tube Layout Pattern, Number Of Tube Passes, Baffle Spacing, Baffle Cut, Tube-To-Baffle Diametrical Clearance, Shell-To Baffle Diametrical Clearance, Tube Length, Tube Outer Diameter, and Tube Wall Thickness	Heat Transfer Area and Pumping Power
Sanaye and Hajabdollahi [12]	Shell and Tube	NSGA-II	Tube Arrangement, Tube Diameter, Tube Pitch Ratio, Tube Length, Tube Number, Baffle Spacing Ratio and Baffle Cut Ratio	Effectiveness and Cost
Rao and Patel [13]	Plate-Fin – Shell and Tube Heat	TLBO	Relevant Design Parameters	Effectiveness and Cost

In this study, multi – objective optimization for shell and tube heat exchanger will be performed by using GA and universe search method for an example case in waste heat recovery system (WHRS). The decision variables in the optimization, namely design parameters, are tube length, number of tubes, tube arrangement, tube angle, pitch ratio, number of shell, hot fluid side, tube inside diameter and baffle spacing ratio. The constraints in the optimization are the pressure losses on both sides and the bounds on the design parameters. The objective functions in the optimization are money saved from waste energy (saving) and saving – cost ratio. Finally, the effects of lost exergy cost on the design parameters will be examine towards the end of this study.

2. SYSTEM MODELLING

Mathematical model was written in Matlab [15] environment and fluid's thermophysical properties were called from Refprop's function [16]. In this way, the fluid properties at the outlet of the heat exchanger can be accurately calculated by using the iterative method. In this study, the effectiveness (ε) – NTU method [17] is used for thermal analysis of shell and tube heat exchanger and its formulation is shown below.

$$c = C_{min} / C_{max} \qquad (1)$$

$$A = Ns \cdot Nt \cdot pi \cdot do \cdot L \qquad (2)$$

$$NTU = U_o A / C_{min} \qquad (3)$$

$$U_o = \left(\frac{d_o}{d_i h_{in}} + R_{fi} \frac{d_o}{d_i} + d_o \frac{\ln(d_o / d_i)}{2k} + R_{fo} + \frac{1}{h_{out}} \right)^{-1} \qquad (4)$$

$$\varepsilon = 2 \left\{ 1 + c + \sqrt{1+c^2} \frac{1 + \exp\left[-NTU\sqrt{1+c^2} \right]}{1 - \exp\left[-NTU\sqrt{1+c^2} \right]} \right\}^{-1} \qquad (5)$$

$$\dot{Q} = \varepsilon C_{min} \left(T_{h1} - T_{c1} \right) \qquad (6)$$

2.1. The Heat Transfer Coefficient Correlations

The Nusselt correlations used in the shell and tube side respectively are shown below. It's note that the Kern method [18] is used for shell side heat transfer coefficient.

$$Nu_s = 0,36 \left(\frac{D_e G_s}{\mu} \right)^{0,55} \left(\frac{C_p \mu}{k} \right)^{1/3} \left(\frac{\mu_b}{\mu_w} \right)^{0,14} \qquad (7)$$

$$Nu = 1,86 \left(\frac{\text{Re} \Pr di}{L} \right)^{1/3} \left(\frac{\mu}{\mu_s} \right)^{0,14} , \ \text{Re} \leq 3 \times 10^3 \ \text{for tube side and laminer} \qquad (8)$$

$$Nu = \frac{(f/8)(\text{Re} - 1000) \Pr}{1 + 12,7 (f/8)^{0,5} (\Pr^{2/3} - 1)} , \ 3 \times 10^3 \leq \text{Re} \leq 5 \times 10^6 \ \text{for tube side and turbulence} \qquad (9)$$

$$f = \frac{64}{\text{Re}} , \ \text{Darcy friction factor for tube side and laminer} \qquad (10)$$

$$\frac{1}{\sqrt{f}} = -2 \log \left(\frac{\varepsilon / D}{3,7} + \frac{2,51}{\text{Re}\sqrt{f}} \right), \ \text{Darcy friction factor for tube side and turbulence} \qquad (11)$$

2.2. The Pressure Loss Correlations

The Pressure loss correlations used in the shell and tube side respectively are shown below .It's note that the Kern method [18] is used for the pressure losses.

$$f_s = \exp \left(0.576 - 0.19 \ln \text{Re}_S \right) \qquad (12)$$

$$\Delta P_s = \frac{f_s G_s^2 D_s}{2 \rho D_e B_r (\mu_w / \mu_b)^{0,14}} , \ \text{for shell side} \qquad (13)$$

$$\text{Re}_s = \frac{G_s D_e}{\mu} , \ \text{for shell side} \qquad (14)$$

$$\Delta P_t = \left(\frac{L}{d_i} f + 4 \right) \rho u_m^2 , \ \text{for tube side} \qquad (15)$$

2.3. The Economic Parameters and Objective Functions

The current value method will be used for the cost calculations during the economic life of the heat exchanger. Real interest rate (r), real fuel price rate (e_r) and present worth factor (*PWF*) [1] including interest rate (i), fuel price rate (fr) and inflation rate (g) are shown below. In this study, considering objective functions are net saving from waste energy and saving – cost ratio. The cost calculation of heat exchanger are summing of capital and operation costs. In addition, to show the effect of exergy destruction on the decision variables, the lost exergy cost will be put in place of the operating cost. For lost exergy cost, dead state temperature is accepted 293.15 K.

The capital cost correlation [19], operation and lost exergy costs formulation and the objective functions are presented in below:

$$r = \frac{i - g}{1 + g} \tag{16}$$

$$e_r = \frac{fr - g}{1 + g} \tag{17}$$

$$PWF = \left[\frac{1}{r - e_r}\right]\left[1 - \left(\frac{1 + e_r}{1 + r}\right)^n\right], for\ r \neq er \tag{18}$$

$$PWF = \left[\frac{n}{1 + e_r}\right], for\ r = e_r \tag{19}$$

$$IC = \delta_M \delta_P \delta_T\, 3.28 \times 10^4 \left(\frac{A}{80}\right)^{0.68} \tag{20}$$

$$OC = PWF \cdot ec \cdot op \left(\frac{\Delta P_t\, \dot{m}_t}{\rho_t \eta_t} + \frac{\Delta P_s\, \dot{m}_s}{\rho_s \eta_s}\right) \tag{21}$$

$$EC = PWF \cdot ec \cdot op \cdot \left(\dot{X}_{pumps} + \dot{X}_{he}\right) \tag{22}$$

$$\dot{X}_{pumps} = \frac{\Delta P_{loss,s}\, \dot{m}}{\rho_s}\left(\frac{1}{\eta_{p,s}} - 1\right) + \frac{\Delta P_{loss,t}\, \dot{m}}{\rho_t}\left(\frac{1}{\eta_{p,t}} - 1\right) \tag{23}$$

$$\dot{X}_{he} = \left(E_{s1} + E_{t1}\right) - \left(E_{s2} + E_{t2}\right) \tag{24}$$

$$TC_1 = IC + OC \tag{25}$$

$$TC_2 = IC + EC \tag{26}$$

$$Saving = 3600 \cdot PWF \cdot \dot{Q} \cdot op \cdot FP / \eta_b Hu \tag{27}$$

$$NS_1 = Saving - TC_1 \tag{28}$$

$$NS_2 = Saving - TC_2 \tag{29}$$

$$SC_1 = Saving / TC_1 \tag{30}$$

$$SC_2 = Saving / TC_2 \tag{31}$$

$$F_1 = w \frac{NS_1}{NS_{1,max}} + (1 - w)\frac{SC_1}{SC_{1,max}} \tag{32}$$

$$F_2 = w \frac{NS_2}{NS_{2,max}} + (1 - w)\frac{SC_2}{SC_{2,max}} \tag{33}$$

3. CASE STUDY

The System used for WHRS shows in Figure 2 and the constant parameters and the decision variables with constrains about shell and tube heat exchanger are present in Table 2 and Table 3 respectively. Hot fluid mass flow rate and temperature are inspired by marine engine cooling water. Similarly, Lower heating value and fuel price are determined according to marine diesel oil. Tube and shell materials of heat exchanger are chosen monel (thermal conductivity 66 W/m²K [20]) and carbon steel respectively. Therefore, δ_M, δ_P and δ_T accepted as 2.1, 1 and 1 according to [19]. In addition, tube wall thickness is accepted as 3 mm. The pressure losses on both sides constrains are accepted as *20 kPa*. It is note that when pressure loss at tube or shell side exceed *20 kPa*, the mathematical model formed in Matlab environment will return zero values for objective functions.

Table 2. The constant parameters

Parameters	Values
Hot fluid	Water
Cold fluid	Water
Hot fluid mass flow rate kg/s	5
Cold fluid mass flow rate kg/s	2
Hot fluid inlet temperature °C	90
Cold fluid inlet temperature °C	20
Hot fluid inlet pressure kPa	140
Cold fluid inlet pressure kPa	140
Life time (n) years	15
Electrical energy (ec) cost $/kwh	0.1
Total Operation hours (op) h	105192
Interest rate (i)	0.1
Inflation rate (g)	0.08
Fuel price rate (fr)	0.14
PWF	7.1677
Tube Material	Monel 400
Shell Material	Carbon Steel
Tube wall thickness mm	3
Tube wall conductivity W/m²K	66
δ_M	**2.1**
δ_P	**1**
δ_T	**1**
Inner fouling factor (R_{fi}) W/m²K	**0.0001**
Outer fouling factor ($\underline{R_{fo}}$) W/m²K	**0.0002**
Pumps efficiency	**0.7**
Lower heating value (Hu) j/kg	42700000
Fuel price (FP) $/kg	0.45

Table 3. The decision variables with constrains

	Low Bound	Upper Bound	Continuous/Discrete
Number of Shell, N_s	1	5	**Discrete**
Length of Tube, L *m*	0.5	4	**Continuous**
Number of Tube N_t	50	200	**Discrete**
Baffle Spacing Ratio B_r	0.01	0.25	**Continuous**
Tube Pitch Ratio P_r	1.0001	2	**Continuous**
Tube Inner Diameter d_i *mm*	5e-3	20e-3	**Continuous**
Tube Angle	1 (45° or 90°)	2 (30° or 60°)	**Discrete**
Tube Arrangement	1 (Square)	2 (Triangle)	**Discrete**
Hot Fluid Side	1 (Shell Side)	2 (Tube Side)	**Discrete**

4. RESULT AND DISCUSSION

In this section, parametric analysis, univariate search method (USM) and GA optimization will be carried out for the case study. Parametric analysis is carried out for determining effect of the decision variable on the objectives. Thus, the relationship between objective functions and decision variables can be noticed.

4.1. Parametric Analysis

Figure 1 and Table 5 shows how decision variables affect the objectives. It's note that the objectives are conflicting in most cases. Constant decision variables at parametric analysis are Ns: 3, L: 2 m, Nt: 100, Br: 0.1, Pr: 1.25, di: 20 mm, tube angle: 90°, tube arrangement: square and hot fluid side: shell side.
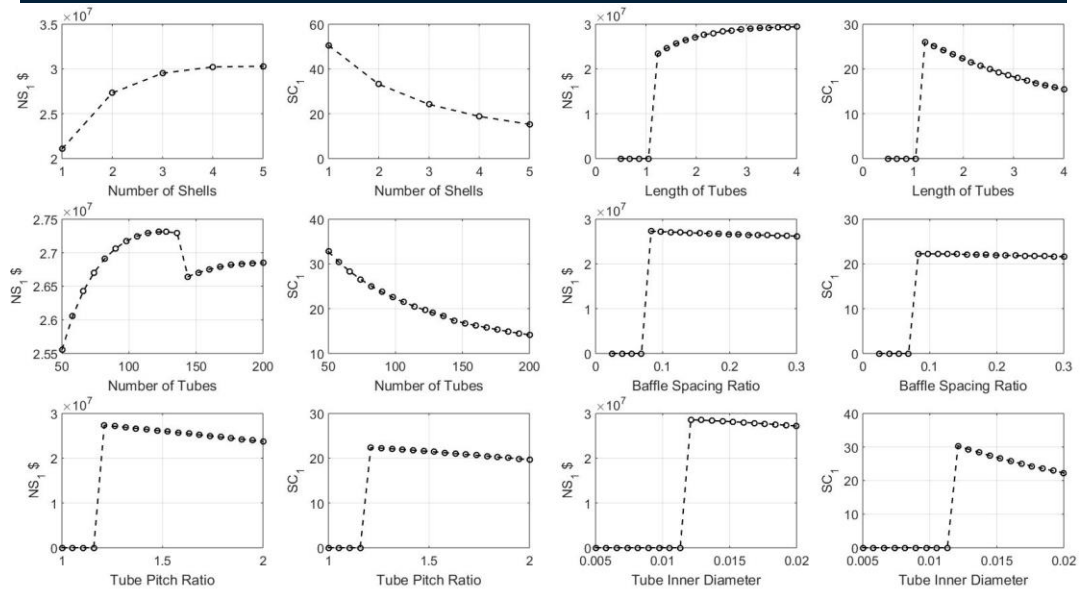
Figure 1. Parametric analysis for Ns, L, Nt, Br, Pr and di decision variables

As can be seen from Figure 1, gradient-based optimization methods are not applied due to sharp turns in some regions. Thus, heuristic methods are considered suitable for this optimization problem.

Table 4. Parametric analysis for tube angle, arrangement and hot fluid side

	Value	*NS_1 \$*	*SC_1*
Tube Angle	1 *(45° or 90°)*	2.7195e7	22.2711
	2 *(30° or 60°)*	2.7239e7	22.2977
	Difference	4.3808e4	0.0266
Tube Arrangement	1 *(Square)*	2.7195e7	22.2711
	2 *(Triangle)*	2.7347e7	22.3299
	Difference	1.5157e5	0.0588
Hot Fluid Side	1 *(Shell Side)*	2.7195e7	22.2711
	2 *(Tube Side)*	2.9262e7	23.9854
	Difference	2.0652e6	1.7143

4.2. Optimizations with Univariate Search Method and Genetic Algorithm

Univariate search method is a method that performs optimization individually in the vector of decision variables iteratively. In this way, one-dimensional optimization methods can be applied to multiple dimensions. In this study, bisection method is used in univariate search method. Although bisection method is slower than gradient methods, its probability of divergence is very low. The Bisection method used in USM scans with *8* points in each iteration and the maximum number of iterations is *20* and the relative error rate is *1e-6*. In the USM, a decision variable must give the same value 3 times for convergence and the maximum number of iterations is *20* relative and the error rate is *1e-6*. The initial values are the same as the values in the parametric analysis. GA is a population-based optimization method, which results in better results for global result, especially in non-convex functions, although it is rather slow compared to gradient methods or USM. In this study, the default settings in the Matlab optimization toolbox are used except for population size (150) and parallel computing. Single objective optimization results of both methods are shown in Table 5 respectively.

Table 5. Single objective optimization results of both methods

	Max. NS_1		Max. SC_1		Max. NS_2		Max. SC_2	
	USM	*GA*	*USM*	*GA*	*USM*	*GA*	*USM*	*GA*
N_s	3	4	1	1	3	4	3	3

L m	4	2.4170	1.1230	1.2037	4	3.3514	2.7148	2.9151
N_t	66	90	66	50	66	27	66	60
B_r	0.0291	0.2137	0.25	0.25	0.0291	0.2491	0.0373	0.2461
Pr	1.2492	1.0674	1.0457	1.0608	1.2499	1.0402	1.25	1.0432
d_i, mm	20	13.6338	12.9143	14.1701	20	17.5934	20	15.4860
T. Angle	1	2	1	2	1	2	1	2
T. Arr.	1	2	1	2	1	2	1	2
Hot F. Side	2	2	2	2	2	2	2	2
ΔP_t, kPa	6.3442	19.6121	8.1454	9.5960	6.3443	19.7656	5.2319	19.8692
ΔP_s, kPa	17.1662	16.9567	15.8347	15.3991	17.1719	17.0248	17.2141	17.2066
U_m, $W/m^2 K$	1043.6	1446.3	1696.6	1753.1	1043.1	1067.3	1418.7	1532.5
ε_m	0.9728	0.9852	0.4761	0.4479	0.9728	0.9868	0.9499	0.9604
A, m^2	57.2273	45.4689	3.7058	3.2466	57.2273	46.8339	38.8408	30.4733
IC, $	5.1147e5	3.5970e5	1.6785e5	1.5341e5	5.1147e5	3.6701e5	3.9298e5	3.3321e5
OC / EC, $	1.2845e4	2.5641e4	1.3982e4	1.5195e4	4.5597e6	4.5038e6	4.6645e5	4.6328e6
NS, $	3.0393e7	3.0897e7	1.5422e7	1.4510e7	2.5842e7	2.6442e7	2.5333e7	2.5895e7
SC	20.6429	22.0981	85.8124	87.0560	5.2386	5.4277	5.3333	5.5975
Time, min.	9.5314	81.2348	1.5449	3.4745	9.8926	55.7815	7.6381	143.9682

As can be seen from Table 5, although the USM responds faster, GA gives better results for each objective function. In addition, although USM and GA give similar results for most objective functions, they give quite different values for decision variables. In line with these results, GA method will be used at the optimization of multi-objective functions. Table 6 – 11 shows the pressure losses, effectiveness and the average heat transfer coefficient of each shell of the heat exchangers. Another issue to be noted is that as the number of shells increases, heat exchanger efficiency increases because the shells are connected cross flow form.

Table 6. Pressure losses, overall heat coefficients and effectiveness for NS_1 according to USM

Ns	1	2	3	4	5
ΔP_t, kPa	2.1011	2.1085	2.1346	-	-
ΔP_s, kPa	5.9665	5.6419	5.5579	-	-
U_o, W/m²K	1081.0	1061.8	998.6	-	-
ε	0.7571	0.7551	0.7468	-	-

Table 7. Pressure losses, overall heat coefficients and effectiveness for NS_1 according to GA

Ns	1	2	3	4	5
ΔP_t, kPa	4.8776	4.8833	4.8996	4.9516	-
ΔP_s, kPa	4.4598	4.2193	4.1505	4.1271	-
U_o, W/m^{2}K	1482.4	1474.8	1453.7	1390.6	-
ε	0.7252	0. 7245	0. 7224	0. 7146	-

Table 8. Pressure losses, overall heat coefficients and effectiveness for NS_2 according to USM

Ns	1	2	3	4	5
ΔP_t, kPa	2.1011	2.1086	2.1346	-	-
ΔP_s, kPa	5.9684	5.6437	5.5597	-	-
U_o, W/m^{2}K	1080.6	1061.4	998.2	-	-
ε	0.7571	0.7551	0.7467	-	-

Table 9. Pressure losses, overall heat coefficients and effectiveness for NS_2 according to GA

Ns	1	2	3	4	5
ΔP_t, kPa	4.9171	4.9223	4.9376	4.9886	-
ΔP_s, kPa	4.4792	4.2345	4.1668	4.1443	-
U_o, W/m^{2}K	1516.7	1509.5	1489.1	1426.2	-
ε	0.7343	0.7337	0.7319	0.7248	-

Table 10. Pressure losses, overall heat coefficients and effectiveness for SC_2 according to USM

Ns	1	2	3	4	5
ΔP_t, kPa	1.7358	1.7407	1.7554	-	-
ΔP_s, kPa	5.9738	5.6689	5.5715	-	-
U_o, W/m^{2}K	1104.5	1081.9	1021.7	-	-
ε	0.6930	0.6891	0.6769	-	-

Table 11. Pressure losses, overall heat coefficients and effectiveness for SC_2 according to GA

Ns	1	2	3	4	5
ΔP_t, kPa	6.5878	6.6081	6.6733	-	-
ΔP_s, kPa	5.9814	5.6592	5.5660	-	-
U_o, W/m^{2}K	1592.0	1571.1	1509.1	-	-
ε	0.7178	0.7158	0.7085	-	-

The optimization results of the multi – objective functions according to the different weights in eq. 32 and 33 are shown in detail in Tables 12 and 13 and the Pareto Front curves are shown in Figure 3. As noted, the Figure 3a has a softer curve than Figure 3b. It's mean that Figure 3a yields more reliable results than Figure 3b.

Table 12. Multi objectives NS_1 - CS_1 optimization results of GA method

w	0.1	0.2	0.3	0.4	0.5	0.6	0.7	0.8	0.9
Ns	1	1	1	1	1	1	2	3	3
L m	1.3335	1.5086	1.7494	2.0783	2.5500	3.1972	2.9315	3.1016	3.3530
Nt	50	50	50	50	50	50	58	52	62
Br	0.25	0.25	0.25	0.25	0.2500	0.2500	0.2484	0.2487	0.2489
Pr	1.0555	1.0496	1.0438	1.0384	1.0329	1.0275	1.0380	1.0397	1.0380
di, mm	14.0981	14.0203	13.9406	13.8891	13.8089	13.7589	14.3347	16.5903	15.5353
T. Angle	2	2	2	2	2	2	2	2	2
T. Arr.	2	2	2	2	2	2	2	2	2
H.F. Side	2	2	2	2	2	2	2	2	2
NS_1, $	1.5463e7	1.6623e7	1.7994e7	1.9530e7	2.1215e7	2.2831e7	2.8673e7	3.0474e7	3.0695e7
SC_1	86.9070	86.3187	85.0163	82.6751	78.7942	73.2479	44.9944	31.1738	27.6415

Table 13. Multi objectives NS_2 - CS_2 optimization results of GA method

w	0.1	0.2	0.3	0.4	0.5	0.6	0.7	0.8	0.9
Ns	3	3	3	3	3	3	4	4	4
L m	2.9154	2.9154	2.9154	3.0743	3.0745	3.0745	2.9652	3.0361	3.0780
Nt	60	60	60	64	64	64	50	52	54
Br	0.2461	0.2461	0.2461	0.2489	0.2489	0.2489	0.2291	0.2347	0.2469
Pr	1.0432	1.0432	1.0432	1.0411	1.0411	1.0411	1.0487	1.0467	1.0439
di, mm	15.4871	15.4872	15.4871	15.1639	15.1635	15.1635	17.9250	17.6721	17.4414
T. Angle	2	2	2	2	2	2	2	2	2
T. Arr.	2	2	2	2	2	2	2	2	2
H.F. Side	2	2	2	2	2	2	2	2	2
NS_2, $	2.5895e7	2.5895e7	2.5895e7	2.6048e7	2.6049e7	2.6049e7	2.6369e7	2.6403e7	2.6423e7
SC_2	5.5975	5.5975	5.5975	5.5897	5.5897	5.5897	5.5214	5.5002	5.4811
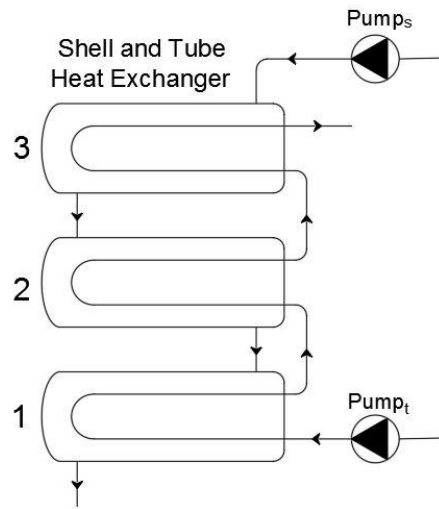
Figure 2. System schema for 3 shells heat exchanger and pumps
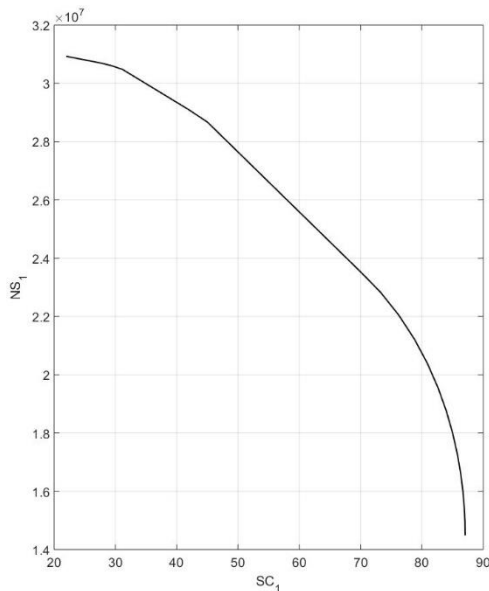
Figure 3. (a) Pareto Front for $SC_1 - NS_1$ objectives   *(b) Pareto Front for $SC_2 - NS_2$ objectives*
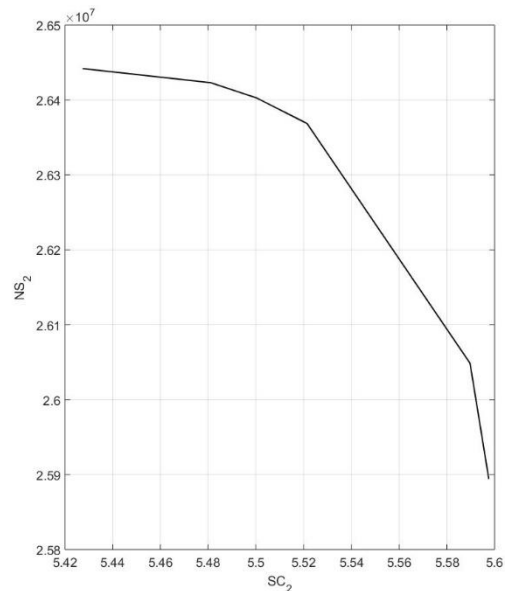
5. CONCLUSIONS

In this study, multi-objective optimization of the shell and tube heat exchanger was performed for an example case. The decision variables in the optimization are tube length, number of tubes, tube arrangement, tube angle, pitch ratio, number of shell, hot fluid side, tube inside diameter and baffle spacing ratio. The constraints in the optimization are the pressure losses on both sides and the bounds on the design parameters. The objective functions in the optimization are money saved from waste energy (saving) and saving – cost ratio. In addition, the effects of lost exergy cost replaced by the operation cost on the design parameters was demonstrated. As a result, the following results were obtained;

- Although the genetic algorithm was slower than USM, it gave better results. From this result, it can be make inference that the USM converges to the nearest local optimum to the given initial point.

- It has been shown that the lost exergy cost in NS objective function has no significant effect on the decision variables but it has a significant effect on the decision variables in SC objective function.

- As shown in the parametric analysis, the number of shells increases as NS objective function value increases, but SC objective function value decreases. This inference was confirmed in the optimization results.

- As seen in the optimization results, heat exchanger efficiency was higher in the NS objective function than in the SC objective function.

In this study, a single heat exchanger type and identical heat exchangers were used. In addition to this and similar study in the future, it may be interesting to optimize the heat exchanger network with different types and non-identical heat exchangers.

NOMENCLATURE

A	Heat transfer surface area (m2)	R_{fi}	Internal fouling factor (m^{2}K/W)
c	Heat capability rate	R_{fo}	External fouling factor (m^{2}K/W)
C	Heat capability (kW/°C)	SC	Saving Cost Ratio
D_e	Equivalent diameter (m)	T	Temperature °C
ec	Electrical cost	TC	Total cost ($)
ep	Equivalent roughness (m)	u_m	Overall velocity inside tubes (m/s)
EC	Lost exergy cost ($)	U	Overall heat transfer coefficient (W/m^{2}K)
d_i	Inner diameter (m)	w	Weight
d_o	Outer diameter (m)	$\dot{X}$	Lost exergy (kW)
f	Darcy friction factor		*Subscripts*
fr	Fuel prize rate	*1*	Considering OP
f_s	Friction factor	*2*	Considering EC
F	Non – dimensional objective function	*c1*	Cold fluid inlet
FP	Fuel prize ($)	*h1*	Hot fluid inlet
g	Inflation	*he*	Heat exchanger
G_s	Mass velocity (kg/m^{2}s)	*i*	Inner
Hu	Lower heat Value (kj/kg)	*m*	Mean / Overall
i	Interest	*o*	Outer
IC	Investment / Capital cost ($)	*r*	Rate
n	Life time of system	*s*	Shell side
N_b	Number of baffles	*t*	Tube side
N_P	Number of the tube passes	M	Material
N_s	Number of shells	P	Pressure
N_t	Number of tubes	T	Temperature
NS	Net saving ($)		
NTU	Number of transfer units		*Greek Symbols*
Nu	Nusselt number	δ	Correction factor
op	Total operation hours (h)	η	Pumps efficiency
OP	Operation cost ($)	ε	Effectiveness
P	Pressure (kPa)	μ	Dynamic viscosity (kg.m/s)
PWF	Present worth factor	ρ	Density (kg/m^3)
Pr	Prandtl number		
$\dot{Q}$	Heat transfer rate (W)		

REFERENCES

[1] I. Teke, O. Ağra, S. O. Atayilmaz, and H. Demir, "Determining the best type of heat exchangers for heat recovery," *Appl. Therm. Eng.*, vol. 30, no. 6–7, pp. 577–583, 2010.

[2] O.¨ Ağra, "Sizing and selection of heat exchanger at defined saving-investment ratio," *Appl. Therm. Eng.*, vol. 31, no. 5, pp. 727–734, 2011.

[3] B. Sahin, Y. Ust, I. Teke, and H. H. Erdem, "Performance analysis and optimization of heat exchangers: a new thermoeconomic approach," *Appl. Therm. Eng.*, vol. 30, no. 2–3, pp. 104–109, 2010.

[4] D. Eryener, "Thermoeconomic optimization of baffle spacing for shell and tube heat exchangers," *Energy Convers. Manag.*, vol. 47, no. 11–12, pp. 1478–1489, 2006.

[5] A. C. Caputo, P. M. Pelagagge, and P. Salini, "Heat exchanger design based on economic optimisation," *Appl. Therm. Eng.*, vol. 28, no. 10, pp. 1151–1159, 2008.

[6] P. Wildi-Tremblay and L. Gosselin, "Minimizing shell-and-tube heat exchanger cost with genetic algorithms and considering maintenance," *Int. Agric. Eng. J.*, vol. 31, pp. 867–885, 2007.

[7] A. R. Doodman, M. Fesangary, and R. Hosseini, "A robust stochastic approach for design optimization of air cooled heat exchangers," *Appl. Energy*, vol. 86, no. 7–8, pp. 1240–1245, 2009.

[8] M. Fesanghary, E. Damangir, and I. Soleimani, "Design optimization of shell and tube heat exchangers using global parametric analysis and harmony search algorithm," *Appl. Therm. Eng.*, vol. 29, no. 5–6, pp. 1026–1031, 2009.

[9] J. M. Ponce-Ortega, M. Serna-González, and A. Jiménez-Gutiérrez, "Use of genetic algorithms for the optimal design of shell-and-tube heat exchangers," *Appl. Therm. Eng.*, vol. 29, no. 2–3, pp. 203–209, 2009.

[10] H. Najafi, B. Najafi, and P. Hoseinpoori, "Energy and cost optimization of a plate and fin heat exchanger using genetic algorithm," *Appl. Therm. Eng.*, vol. 31, no. 10, pp. 1839–1847, 2011.

[11] S. Fettaka, J. Thibault, and Y. Gupta, "Design of shell-and-tube heat exchangers using multiobjective optimization," *Int. J. Heat Mass Transf.*, vol. 60, no. 1, pp. 343–354, 2013.

[12] S. Sanaye and H. Hajabdollahi, "Multi-objective optimization of shell and tube heat exchangers," *Appl. Therm. Eng.*, vol. 30, no. 14–15, pp. 1937–1945, 2010.

[13] R. V. Rao and V. Patel, "Multi-objective optimization of heat exchangers using a modified teaching-learning-based optimization algorithm," *Appl. Math. Model.*, vol. 37, no. 3, pp. 1147–1162, 2013.

[14] I. Teke, O. Agra, H. Demir, and S. O. Atayilmaz, "Sizing, selection, and comparison of heat exchangers considering the lowest saving-investment ratio corresponding to the area at the tag end of the heat exchanger," *Energy*, vol. 78, pp. 114–121, 2014.

[15] MathWorks: https://www.mathworks.com/products/matlab.html.

[16] NIST: https://www.nist.gov/

[17] Cengel Yunus A., *Book - Heat and Mass Transfer Fundamentals and Applications 5Th*, vol. 136, no. 1. 2007.

[18] Donald Q. Kern, "Process Heat Transfer.Pdf." p. 871, 1950.

[19] S. Robin, *Chemical Process Design and Integration*, vol. 68, no. 11. New Work: Wiley, 2014.

[20] A. P. Sadik KAKAC, Hongtan LIU, *HEAT EXCHANGERS Selection, Rating, and Thermal Design*, Third Edit. CRC Press.

Exergetic Performance Analysis To Compare Of Two Different Oxy Fuel Combustion Power Plant

Yasin Ust[1], Ibrahim Ozsari[1]

Abstract

The carbon capture storage (CCS) and oxy fuel combustion systems become more important due to global warming with the trends of green energy solutions. Oxy-fuel combustion is the process of burning a fuel using pure oxygen instead of air as the primary oxidant. In this article, exergetic performances of two different oxy-fuel combustion power plants have been investigated. These are Clean Energy System (CES) Cycle and MATIANT Cycle. Different fuel kinds have been used in CES cycle and MATIANT Cycle to investigate the energetic and exergetic performances. Temperature, pressure, specific enthalpy, specific entropy and specific exergy of each state points have been determined for each cycles. Also, the net power, exergy destruction and exergy efficiency of the components such as Compressors, Combustion Chamber, Turbines, Recuperator, Condenser and Pumps have been presented. The results demonstrate that one cycle is advantageous in terms of energy but disadvantageous in terms of exergy destruction.

Keywords: *Exergy, Oxy Fuel Combustion Cycle, Thermodynamic analysis, Zero emission*

1. INTRODUCTION

In addition to the increasing energy need in recent years, the search for an environmentally friendly system has gained a great importance due to the global warming crisis and the increase in the penalties and sanctions against the formation of pollutant emissions. In order to be effective in the fight against global warming and climate change, intensive studies are carried out on carbon dioxide capture, transportation and storage. Three basic technologies are used to keep carbon dioxide concentrations resulting from the combustion of fuels at the intended emission values. These are post-combustion capture, pre-combustion capture and oxy-combustion systems.[1] Oxy-fuel combustion technology is a thermodynamic cycle in which the fuel is burned in a combustor with an oxidant stream of substantially pure oxygen. If we burn fuel with pure oxygen in oxy-fuel combustion power cycles, very high temperatures will occur. In today's technology, two different solutions have been found in these oxy-combustion power cycles in order to reduce material strength temperatures. They are used as a diluent in CO_2 semi-closed oxy-combustion combined cycle (SCOC-CC), MATIAT and NET Power cycles, and H_2O is used as diluent in Graz and CES cycles [2]–[7].

Mamaghani et al. [8] studied to model a molten carbonate fuel cell-gas turbine hybrid plant from energetic, exergetic, economic and environmental standpoints and to optimize the system through a multi-objective optimization scheme. Mahto and Pal [9] carried out thermodynamic and thermoeconomic analysis of simple combined cycle power plant with gas turbine blade cooling by means of fogging. Rao and Francuz [10] supplied identification and assessment for advanced performance improvements of combined cycles in coal based power systems. Yang et al. [11] performed exergetic performance analysis and optimization of an endoreversible intercooled regenerative Brayton cogeneration plant. Alhussan et al. [12] compared the cycle characteristics of the Brayton cycle with those of the Otto and Carnot cycles. Ramakrishnan and Edwards [13] used an irreversibility minimization approach to provide maximum efficiency characteristics of a regenerative gas turbine for heat and work production based on three different unconventional methods. Fernández-Villacé and Paniagua [14] proposed a methodology to assess exergetic effectiveness, propulsive efficiency, total loss and subcomponent losses of a combined cycle engine. Singh and Kaushik [15] offered an assessment and

thermoeconomic optimization for a Brayton–Rankine–Kalina combined triple power cycle using Specific Exergy Costing methodology. Objective function was the minimization of the total cost rate of all components of the plant studied on. Al-Sulaiman and Atif [16] performed a thermodynamical comparison study for different supercritical carbon dioxide Brayton cycles combined with a solar power tower. It was stated that regenerative Brayton cycle shows comparable performance to the recompression Brayton cycle in Dhahran. Gonca and Ozsari [17] carried out an exergetic performance analysis of a gas turbine with two intercoolers and two reheaters operating with different type fuels and investigated the performance characteristics of the turbine. Abusoglu and Kanoglu [18] presented a detailed and comprehensive analysis for the exergetic and thermoeconomic evaluation of the diesel engine powered cogeneration systems.

In this study, an exergetic performance analysis of two oxy-fuel combustion power plant (CES and MATIANT cycles) has been carried out and CES and MATIANT cycles have been compared in terms of their energetic and exergetic performances.

2. THEORICAL MODEL
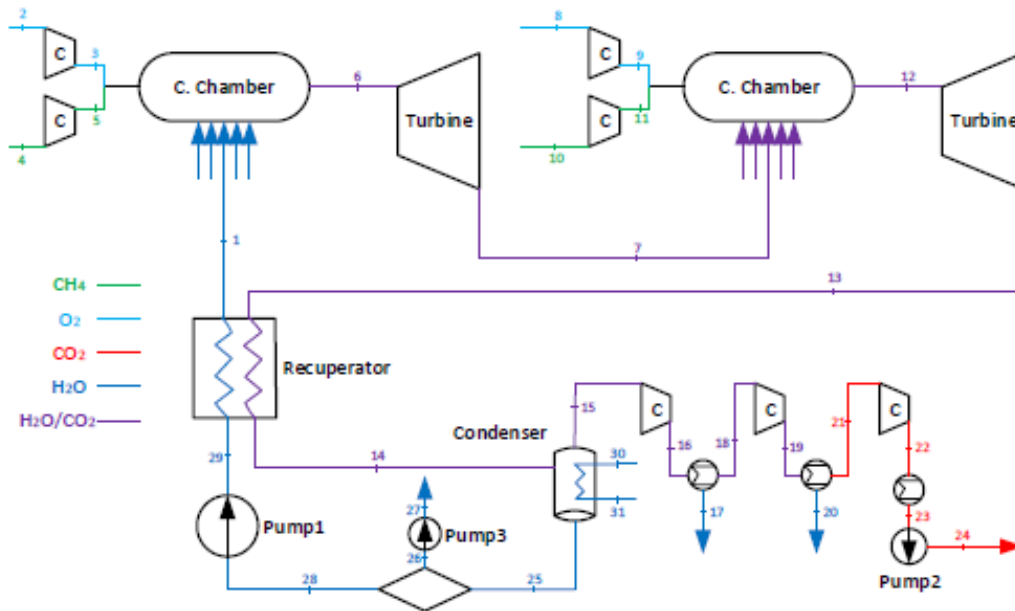
Figure 1. Flowsheet diagram of the CES cycle

Thermodynamic simulations were carried out with the assumptions which are listed below;
Isentropic efficiency of compressors are 0.88,
Isentropic efficiency of pumps are 0.80,
Isentropic efficiency of the turbines are 0.90,
Mechanical efficiency is 0.99,
O_2 and CH_4 delivery temperature 15 ^0C,
O_2 and CH_4 delivery pressure 5 bar and
Combustor pressure drop is 3%.
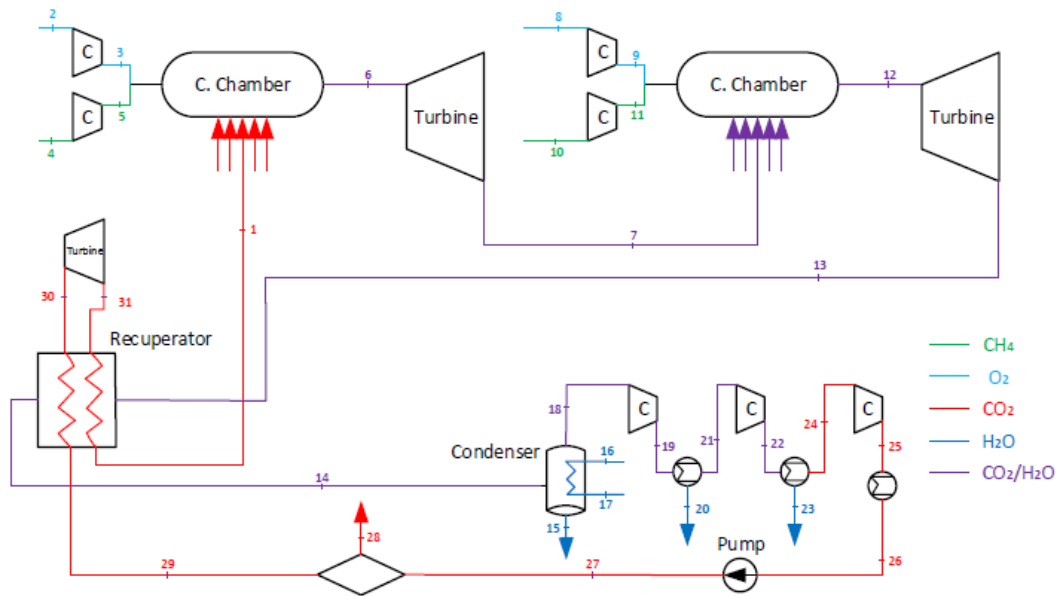
Figure 2. Flowsheet diagram of the MATIANT cycle

In this study, an exergetic performance analysis has been conducted for CES and MATIANT oxy fuel combustion power plant cycles. The CES cycle and MATIANT cycle schematics and T-s diagrams are shown in Fig. 1, Fig. 2 and Fig. 3 respectively. Effective power, exergy efficiency, exergy destruction and ecological coefficient of performance have been evaluated using power plant design parameters.
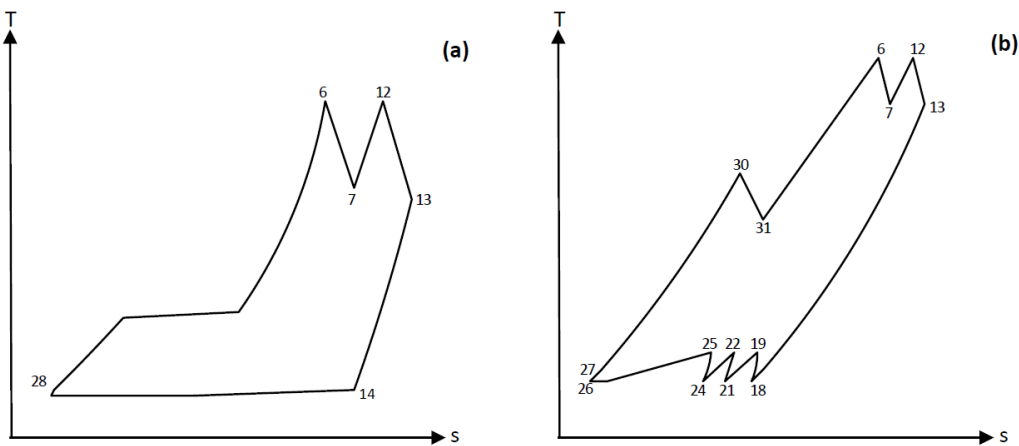
Figure 19. (a) T–s diagram of the CES cycle   (b) T–s diagram of the MATIANT cycle

In the numerical model, pressure and expansion ratios can be stated as follows:

$$r_c = \frac{P_3}{P_2} = \frac{P_5}{P_4} = \frac{P_9}{P_8} = \frac{P_{11}}{P_{10}}$$ (1)

$$r_t = \frac{P_6}{P_7} = \frac{P_{12}}{P_{13}}$$ (2)

Values of the each state points are obtained using Engineering Equation Solver (EES) software [19]–[22]. Compressor and turbine temperatures are:

$$T_{c,o} = T_{c,i} \left[1 + \frac{1}{\eta_c} \left(r_c^{\frac{k-1}{k}} - 1 \right) \right] \tag{3}$$

$$T_{t,o} = T_{t,i} \left[1 - \eta_t \left(1 - (r_t)^{\frac{1-k}{k}} \right) \right] \tag{4}$$

Where k exponent depends on specific heats and is calculated as below:

$$k_i = \frac{c_{p,i}}{c_{v,i}} \tag{5}$$

$$\dot{Q}_{in} = \dot{Q}_{f,c} - \dot{Q}_{ht} = \dot{m}_T \left[\int_{T_{CC1,i}}^{T_{CC1,o}} C_p \, dT + \int_{T_{CC2,i}}^{T_{CC2,o}} C_p \, dT \right] \tag{6}$$

Where $Q_{f,c}$ is the heat released by combustion; Q_{ht} is the heat loss by heat transfer into cylinder wall and they are given as below:

$$\dot{Q}_{f,c} = \eta_c \dot{m}_f H_u \tag{7}$$

$$\dot{Q}_{ht} = h_{tr} A_{sur} (T_{me} - T_w) = h_{tr} A_{sur} \left(\frac{T_7 + T_6}{2} - T_w \right) \tag{8}$$

$$\dot{m}_f = \frac{m_f N}{60} \tag{9}$$

Where, η_c is combustion efficiency and it can be taken as 0.98, T_w is the turbine wall temperature, m_f is time-dependent fuel mass and it can be expressed as follows:

$$m_f = m_{wf} \phi F_{st} \tag{10}$$

$$A_{sur} = \frac{4V_T}{b} \tag{11}$$

Where ϕ and b are equivalence ratio and turbine bore (inner diameter). F_{st}, V_T and m_{wf} are stoichiometric fuel air ratio, total volume of the turbine and the working fluid mass per cycle (kg).
They are calculated as follow:

$$F_{st} = \frac{\xi \times (12.01 \times \alpha + 1.008 \times \beta + 16 \times \gamma + 14.01 \times \delta)}{MA_{wf}} \tag{12}$$

$$V_T = \frac{\pi b^2}{4} L = m_T v_{max} \tag{13}$$

Where $\alpha, \beta, \gamma, \delta$ are atomic numbers of carbon, hydrogen, oxygen, nitrogen in fuel, respectively. ξ is molar fuel-air ratio [20]:

$$\xi = \frac{0,21}{\left(\alpha - \frac{\gamma}{2} + \frac{\beta}{4} \right)} \tag{14}$$

$$m_T = m_{wf} + m_f + m_{o_2} \tag{15}$$

The enthalpy, entropy and exergy of the each state point is obtained as follow:

$$h_{(i)} = f \left(T_{(i)}, P_{(i)} \right) \tag{16}$$

$$s_{(i)} = f \left(T_{(i)}, P_{(i)} \right) \tag{17}$$

$$ex_{(i)} = \left(h_{(i)} - h_0 \right) - T_0 \left(s_{(i)} - s_0 \right) \tag{18}$$

In the present model, power, energy efficiency, exergy efficiency and the ecological coefficient of performance (ECOP) could be stated as follow:

$$P_{ef} = \dot{Q}_{in} - \dot{Q}_{out} \tag{19}$$

$$\eta = \frac{W_{net}}{Q_{in}} \tag{20}$$

$$W_{spesific} = \frac{W_{net}}{m_T} \tag{21}$$

$$ECOP = \frac{W_{net}}{T_0 \dot{S}_{gen}} = \frac{P_{ef}}{X_{total}} \tag{22}$$

$$\varepsilon = \frac{ex_{total} - X_{total}}{ex_{total}} \tag{23}$$

Where ex_{total} is the total exergy input into the system and it can be written as below:

$$ex_{total} = \dot{m}_f \psi \tag{24}$$

Where ψ is specific exergy of the fuel (CH_4)

Where X_{total} is total exergy destruction of the gas turbine and it is obtained from below equation:

$$X_{total} = X_{compressors} + X_{c.chambers} + X_{turbines} + X_{pumps} + X_{recuperator} + X_{condenser} \tag{25}$$

Where $X_{compressors}$, $X_{c.chambers}$, X_{pumps}, $X_{turbines}$, $X_{recuperator}$, $X_{condenser}$ are the exergy destructions of the compressors, combustion chambers, turbines, pumps, recuperator, condenser, respectively.
They are expressed as follow:

$$X_{compressor,i} = \dot{m}_{wf,i} \left[\left(h_{i,o} - h_{i,i} \right) - \left(ex_{i,o} - ex_{i,i} \right) \right] \tag{26}$$

$$X_{C.Chamber,1-2} = \dot{m}_f \psi - \left[\dot{m}_{T,1} \left(ex_{1,o} - ex_{1,i} \right) + \dot{m}_{T,2} \left(ex_{2,o} - ex_{2,i} \right) \right] \tag{27}$$

$$X_{turbine,i} = \dot{m}_{T,i} \left[\left(ex_{i,i} - ex_{i,o} \right) - \left(h_{i,i} - h_{i,o} \right) \right] \tag{28}$$

$$X_{pump,i} = \dot{m}_{wf,i} \left[\left(h_{i,o} - h_{i,i} \right) - \left(ex_{i,o} - ex_{i,i} \right) \right] \tag{29}$$

$$X_{condenser} = \left[\left(ex_{cold,o} - ex_{cold,i} \right) - \left(ex_{heat,i} - ex_{heat,o} \right) \right] \tag{30}$$

$$X_{recuperator} = \left[\left(ex_{cold,i} - ex_{cold,o} \right) + \left(ex_{heat,i} - ex_{heat,o} \right) \right] \tag{31}$$

In this study, the exergy efficiency of the each system component is found as below:

$$\varepsilon_{comp,i} = \frac{ex_{i,o} - ex_{i,i}}{h_{i,o} - h_{i,i}} \tag{32}$$

$$\varepsilon_{c.chambers} = \frac{\dot{m}_T \left[\left(ex_{1,o} - ex_{1,i} \right) + \left(ex_{2,o} - ex_{2,i} \right) \right]}{\dot{m}_f \psi} \tag{33}$$

$$\varepsilon_{turb,i} = \frac{\left(h_{i,i} - h_{i,o} \right)}{\left(ex_{i,i} - ex_{i,o} \right)} \tag{34}$$

$$\varepsilon_{comp,i} = \frac{ex_{i,o} - ex_{i,i}}{h_{i,o} - h_{i,i}} \tag{35}$$

$$\varepsilon_{recuperator} = \frac{ex_{cold,o} - ex_{cold,i}}{ex_{heat,i} - ex_{heat,o}} \tag{36}$$

$$\varepsilon_{recuperator} = \frac{\dot{m}_{cond,f}\left(ex_{cold,o} - ex_{cold,i}\right)}{\dot{m}_{wf}\left(ex_{heat,i} - ex_{heat,o}\right)} \tag{37}$$

3. RESULT AND DISCUSSION

In this study, an exergetic performance analysis of two oxy-fuel combustion power plant (CES and MATIANT cycles) has been carried out and CES and MATIANT cycles have compared in terms of their energetic and exergetic performances.

Table 1. Chart of calculated results for different statement points for CES cycle

	Working fluid	Temperature T (K)	Pressure P (Bar)	Specific Enthalpy h (kj/kg)	Specific Entropy s (kj/kg K)	Specific Exergy ex (kj/kg)
1	H_2O (f)	556	106,6	1249,6	3,0811	363,9
2	O_2	288	5	260,63	5,9577	120,2
3	O_2	725	100	687,49	6,0659	515,9
4	CH_4	288	5	883,26	5,7599	239
5	CH_4	613	100	1756,3	6,1859	989,4
6	CO_2-H_2O	1250	97	4155,3	7,308	2142
7	CO_2-H_2O	811	10,78	3220,6	7,3179	1115
8	O_2	288	5	260,63	5,9577	120,2
9	O_2	359	10	325,77	5,9802	178,9
10	CH_4	288	5	883,26	5,7599	239
11	CH_4	345	10	1010,5	5,807	352,7
12	CO_2-H_2O	1250	9,7	3942,3	7,9417	1749
13	CO_2-H_2O	795	0,97	2998,6	7,9559	709
14	CO_2-H_2O	331	0,105	2165,3	7,2752	71,7
15	CO_2-H_2O	300	0,1	813,27	4,047	206,1
16	CO_2-H_2O	539	1,05	1074,6	4,1432	27,53
17	H_2O (f)	300	1	112,65	0,39306	1,108
18	CO_2-H_2O	566	1	812,15	3,4901	91,12
19	CO_2-H_2O	1010	8,88	1335,4	3,7422	541,8
20	H_2O (f)	300	8,44	113,34	0,39286	1,852
21	CO_2	300	8,44	500,38	2,3251	114,9
22	CO_2	535	75	710,95	2,4437	291,3
23	CO_2	300	71,25	276,92	1,2524	200,3
24	CO_2	345	300	333,9	1,3349	233,6
25	H_2O (f)	300	0,1	112,57	0,39309	1,018
26	H_2O (f)	300	0,1	112,57	0,39309	1,018
27	H_2O (f)	300	1	112,65	0,39306	2,008
28	H_2O (f)	300	0,1	112,57	0,39309	1,018
29	H_2O (f)	301	112,2	127	0,40375	11,19
30	H_2O (f)	288	1	62,45	0,2223	0,09
31	H_2O (f)	300	1	112,7	0,3931	1,108

Table 1. and Table 2. show the working fluids, temperature, pressure, specific enthalpy, specific entropy and specific exergy of the statement points. As expected, the specific enthalpy, specific entropy and specific exergy increase with increasing temperature. The maximum temperatures are seen at the turbine inlets. The minimum temperature is seen at the condenser inlet.

Table 2. Chart of calculated results for different statement points for MATIANT cycle

	Working fluid	Temperature T (K)	Pressure P (Bar)	Specific Enthalpy h (kj/kg)	Specific Entropy s (kj/kg K)	Specific Exergy ex (kj/kg)
1	CO_2	973	38,58	1218,1	2,8132	1102
2	O_2	288	5	260,63	5,9577	120,2
3	O_2	547,3	40	505,38	6,0204	346,9
4	CH_4	288	5	883,26	5,7599	239
5	CH_4	476,5	40	1341	5,9015	656
6	CO_2-H_2O	1200	38,8	1781,6	4,0585	1394
7	CO_2-H_2O	964,9	7,76	1439,2	4,0828	958
8	O_2	288	5	260,63	5,9577	120,2
9	O_2	358,3	10	325,11	5,9784	178,7
10	CH_4	288	5	883,26	5,7599	239
11	CH_4	341,6	10	1002,4	5,7833	351,4
12	CO_2-H_2O	1200	9,7	1900,2	4,5805	1363
13	CO_2-H_2O	906	1,21	1492,7	4,6589	845,5
14	CO_2-H_2O	376	1,05	696,87	3,2704	449,6
15	H_2O (f)	300	1	112,65	0,39306	1,105
16	H_2O (f)	288	1	62,45	0,2223	0,09
17	H_2O (f)	300	1	112,7	0,3931	1,108
18	CO_2	300	1	507,43	2,7446	411,6
19	CO_2	430,5	4,4	624,89	2,7901	515,9
20	H_2O (f)	300	4	112,93	0,39298	1,408
21	CO_2	300	4	504,64	2,4762	486,1
22	CO_2	430,5	17,6	619,12	2,5182	588,5
23	H_2O (f)	300	17	114,13	0,39262	2,711
24	CO_2	300	17	491,62	2,1718	560,7
25	CO_2	430,5	74,8	593,03	2,1988	654,4
26	CO_2	300	71,25	265,99	1,2085	612,5
27	CO_2	346	299,3	336,02	1,3413	644,3
28	CO_2	346	300	335,94	1,3408	644,4
29	CO_2	346	299,3	336,02	1,3413	644,3
30	CO_2	873	284,3	1092,8	2,7396	998,4
31	CO_2	600,6	40,61	871,1	2,8249	752,1
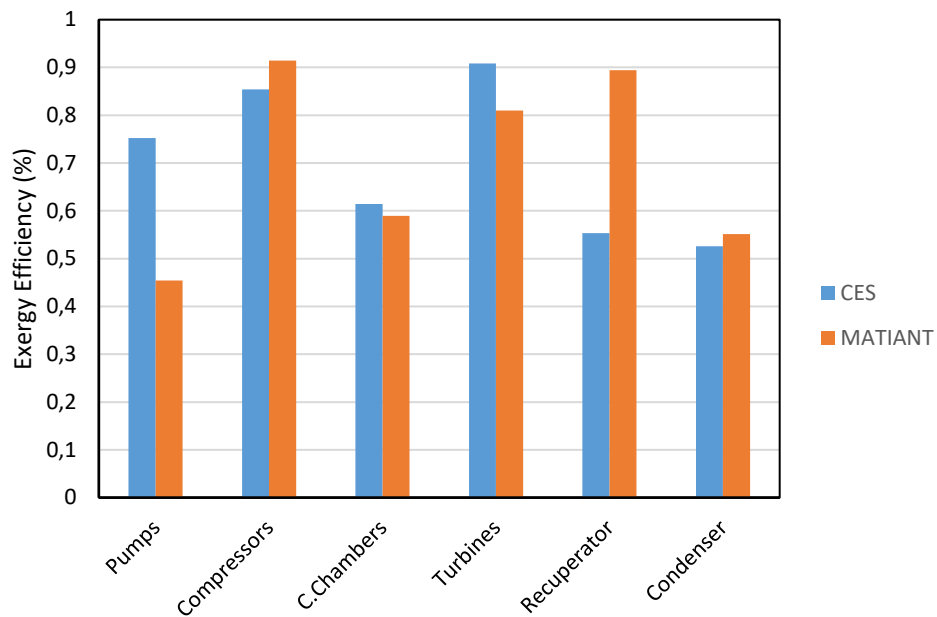
Figure 4. Comparison of two oxy combustion cycles components exergy efficiency

Exergy efficiencies of the main components of the MATIANT cycle and the CES cycle was presented in the Figure 4 for pumps, compressors, combustion chambers, turbines, recuperator and condenser. Exergy efficiencies were similar in compressor, combustion chamber, turbine and condenser but very different in recuperator and pump. In the MATIANT cycle, when carbon dioxide was introduced into the pump in the liquid phase, the increase in pressure and supercritical phase in the exit increased exergy destruction. Therefore, the exergy efficiency decreased. On the other hand, exergy destruction of these components was exhibited in figure 5. It is concluded that the exergy destruction in CES cycle is approximately 3 times higher in the MATIANT cycle. In the case of separate examination of the components, the compressor 3.55, combustion chamber 2.65, turbine 3.3 recuperator 3.68, the condenser have 3.76 times more exergy destruction. In both cycles, the most exergy destruction was observed in the combustion chamber.
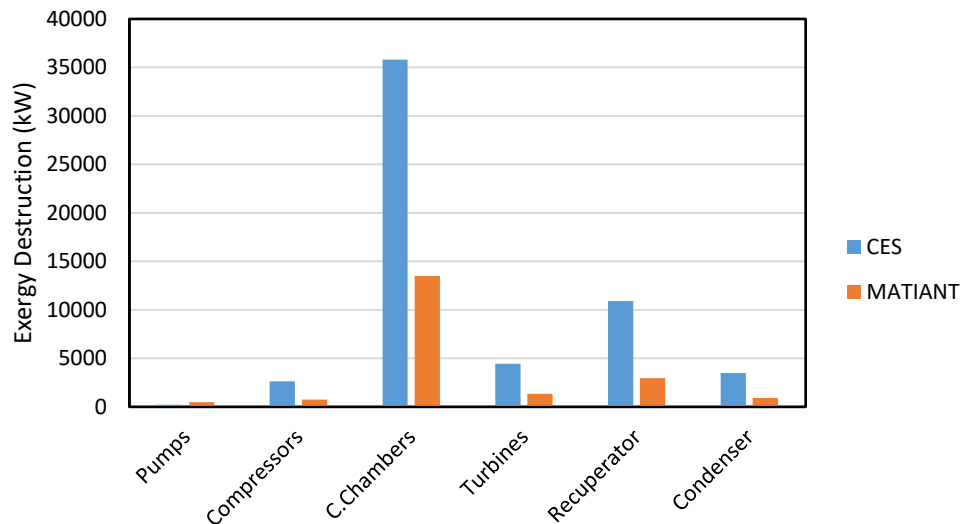
Figure 5. Comparison of two oxy combustion cycles components exergy destruction
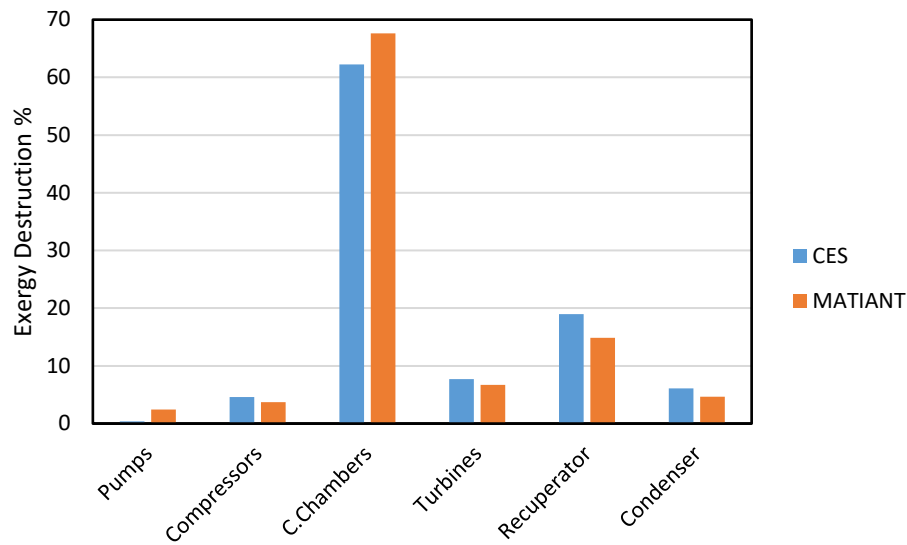
Figure 6. Comparison of two oxy combustion cycles components exergy destruction percentage

Since there is a situation as in Figure 5, it would be more accurate to compare the ratio of exergy destruction to total exergy destruction. For this reason, in Figure 6, exergy destruction rates are shown in two oxy-fuel power plants. According to the CES cycle of the MATIANT cycle, a higher exergy destruction percentages was obtained in the pump and combustion chamber components. The CES cycle for other components has a higher percentage ratio. In another aspect, the energy and exergy studies of these two oxy-combustion power cycles are presented in Figure 7. When we compared two oxy-combustion power plants in terms of work, heat, specific work and exergy destruction; the values obtained from the CES cycle were 2.79, 2.82, 2.5 and 2.88 times higher than the MATIANT cycle values, respectively. MATIANT cycle have seen to be approximately 1 point higher in terms of thermal efficiency and exergy efficiency. That is, the MATIANT cycle efficiency is 40%, while the CES cycle is 39%. Likewise, the exergy efficiencies are 40.35% and 39.58% respectively.
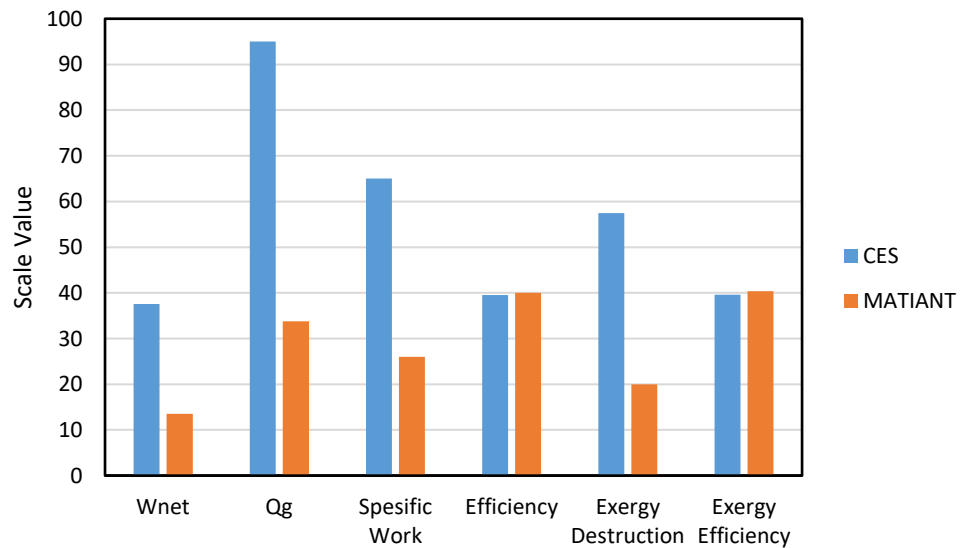
Figure 7. Comparison of two oxy combustion power plant energetic and exergetic results

Table 3. Chart of calculated results for using fuel kinds

Fuel	Formula	LHV (kj/kg)	Chem. Exergy (kj/kg)	CES - ECOP	MATIANT - ECOP
Methane	CH_4	50050	51591,5	0,6230	0,6432
Ethane	C_2H_6	47520	49839,0	0,5895	0,6082
Propane	C_3H_8	46357	48897,4	0,5827	0,6011
Octane	C_8H_{18}	44427	47194,8	0,5826	0,6009
Decane	$C_{10}H_{22}$	44240	47036,0	0,5814	0,5997

As you seen in Table 3. illustrates the chemical formula, lower heating value, chemical exergy, and ecological coefficient of performance (ECOP) of investigated fuels such as methane, ethane, propane, octane, decane. From methane to decane, carbon and hydrogen increase, lower heating value and chemical exergy decrease. It should be pointed out that the ecological coefficient of performance (ECOP) decreases as exergy destruction increases. When comparing two oxy-fuel combustion power plants in terms of the ECOP, the MATIANT cycle is seen to be slightly superior for these 5 different fuels.

4. CONCLUSION

Energetic and exergetic performance analysis of two oxy-fuel combustion power plant (CES and MATIANT cycles) has been carried out and CES and MATIANT cycles have been compared in terms of their energetic and exergetic performances in this study. The results showed that, specific enthalpy, specific entropy and specific exergy increase with increasing temperature. Compressors and turbines have the highest exergy efficiency and combustion chamber have the maximum exergy destruction ratio. Exergy efficiencies were similar in compressor, combustion chamber, turbine and condenser for two oxy-fuel combustion power plants. On the other hand, exergy destruction in CES cycle is approximately 3 times higher in the MATIANT cycle. According to the CES cycle of the MATIANT cycle, a higher exergy destruction percentages was obtained in the pump and combustion chamber components. The CES cycle for other components has a higher percentage ratio. When we compared two oxy-combustion power plants in terms of work, heat, specific work and exergy destruction; the values obtained from the CES cycle were 2.79, 2.82, 2.5 and 2.88 times higher than the MATIANT cycle values, respectively. MATIANT cycle have seen to be approximately 1 point higher in terms of thermal efficiency and exergy efficiency. That is, the MATIANT cycle efficiency is 40%, while the CES cycle is 39%. Likewise, the exergy efficiencies are 40.35% and 39.58% respectively. Finally, it has been seen that as the carbon and hydrogen number increase in a fuel, lower heating value and chemical exergy decrease. When two oxy-fuel combustion power plants are compared in terms of ECOP, the MATIANT cycle is seen to be more advantageous than CES cycle for all the fuels used in the study.

ACKNOWLEDGMENT

NOMENCLATURE

A   heat transfer area (m2)

b   bore (m)

C_v constant volume specific heat (kJ/kg.K)

C_p constant pressure specific heat (kJ/kg.K)

FA   fuel-air ratio

FTT   finite-time thermodynamics

h_{tr} heat transfer coefficient (W/ m^2K)

Hu   lower heat value of the fuel (kJ/kg)

ICE   Internal combustion engines

l   loss

m   mass (kg)

$\dot{m}$ time- dependent mass rate (kg/s)

N   engine speed (rpm)

P   pressure (bar), power (kW)

$\dot{Q}$ rate of heat transfer (kW)

r pressure and expansion ratios

R   gas constant (kJ/kg.K)

T   temperature (K)

v   specific volume (m^3/kg)

V   volume (m^3)

Greek letters

α cycle temperature ratio, atomic number of carbon

β pressure ratio, atomic number of hydrogen

δ atomic number of nitrogen

ϕ equivalence ratio

γ atomic number of oxygen

λ cycle pressure ratio

ψ cut-off ratio

η efficiency

ρ density (kg/m3)

Subscripts

wf   working fluid

c   combustor, combustion

ef   effective

f   fuel

ht   heat transfer

i   inlet, point series

o   outlet

in   input

l   loss

max   maximum

me   mean

min   minimum

mix   mixture

out   output

sur   surface

st   stoichiometric

t   total, turbine

REFERENCES

[1]. J. Mletzko, S. Ehlers, ve A. Kather, "Comparison of Natural Gas Combined Cycle Power Plants with Post Combustion and Oxyfuel Technology at Different CO2 Capture Rates", Energy Procedia, c. 86, ss. 2-11, Oca. 2016.

[2]. George Tsatsaronis ve Mathias Penkuhn, "Exergy Analysis of the Allam Cycle", 5th Int. Symp. – Supercrit. CO2 Power Cycles March 28-31 2016 San Antonio Tex.

[3]. R. Scaccabarozzi, M. Gatti, ve E. Martelli, "Thermodynamic Optimization and Part-load Analysis of the NET Power Cycle", Energy Procedia, c. 114, ss. 551-560, Tem. 2017.

[4]. R. Scaccabarozzi, M. Gatti, ve E. Martelli, "Thermodynamic analysis and numerical optimization of the NET Power oxy-combustion cycle", Appl. Energy, c. 178, ss. 505-526, Eyl. 2016.

[5]. Y. Zhao, J. Chi, S. Zhang, ve Y. Xiao, "Thermodynamic study of an improved MATIANT cycle with stream split and recompression", Appl. Therm. Eng., c. 125, ss. 452-469, Eki. 2017.

[6]. B. S. Choi, M. J. Kim, J. H. Ahn, ve T. S. Kim, "Influence of a recuperator on the performance of the semi-closed oxy-fuel combustion combined cycle", Appl. Therm. Eng., c. 124, ss. 1301-1311, Eyl. 2017.

[7]. N. Ferrari, L. Mancuso, J. Davison, P. Chiesa, E. Martelli, ve M. C. Romano, "Oxy-turbine for Power Plant with CO2 Capture", Energy Procedia, c. 114, ss. 471-480, Tem. 2017.

[8]. A. H. Mamaghani, B. Najafi, A. Shirazi, ve F. Rinaldi, "Exergetic, economic, and environmental evaluations and multi-objective optimization of a combined molten carbonate fuel cell-gas turbine system", Appl. Therm. Eng., c. 77, ss. 1-11, Sub. 2015.

[9]. D. Mahto ve S. Pal, "Thermodynamics and thermo-economic analysis of simple combined cycle with inlet fogging", Appl. Therm. Eng., c. 51, sy 1-2, ss. 413-424, Mar. 2013.

[10]. A. D. Rao ve D. J. Francuz, "An evaluation of advanced combined cycles", Appl. Energy, c. 102, ss. 1178-1186, Sub. 2013.

[11]. B. Yang, L. G. Chen, ve F. R. Sun, "Exergetic performance optimization of an endoreversible variable-temperature heat reservoirs intercooled regenerated Brayton cogeneration plant", J. Energy Inst., c. 89, sy 1, ss. 1-11, Sub. 2016.

[12]. K. Alhussan, M. Assad, ve O. Penazkov, "Analysis of the actual thermodynamic cycle of the detonation engine", Appl. Therm. Eng., c. 107, ss. 339-344, Agu. 2016.

[13]. S. Ramakrishnan ve C. F. Edwards, "Maximum-efficiency architectures for heat- and work-regenerative gas turbine engines", Energy, c. 100, ss. 115-128, Nis. 2016.

[14]. V. Fernández-Villacé ve G. Paniagua, "On the exergetic effectiveness of combined-cycle engines for high speed propulsion", Energy, c. 51, ss. 382-394, Mar. 2013.

[15]. O. K. Singh ve S. C. Kaushik, "Thermoeconomic evaluation and optimization of a Brayton–Rankine–Kalina combined triple power cycle", Energy Convers. Manag., c. 71, ss. 32-42, Tem. 2013.

[16]. F. A. Al-Sulaiman ve M. Atif, "Performance comparison of different supercritical carbon dioxide Brayton cycles integrated with a solar power tower", Energy, c. 82, ss. 61-71, Mar. 2015.

[17]. G. Gonca ve I. Ozsari, "Exergetic Performance Analysis of a Gas Turbine with two Intercoolers and two Reheaters Fuelled with Different Fuel Kinds", Conf. Adv. Mech. Eng. Istanb. 2016, May. 2016.

[18]. A. Abusoglu ve M. Kanoglu, "Exergetic and thermoeconomic analyses of diesel engine powered cogeneration: Part 1 – Formulations", Appl. Therm. Eng., c. 29, sy 2-3, ss. 234-241, Sub. 2009.

[19]. "EES Academic Professional Edition, (2014), V.9.701-3D, USA, F-Chart Software." .

[20]. Ferguson CR., Internal combustion engines – applied thermosciences., New York: John Wiley & Sons Inc.; 1986.

[21]. Ibrahim Dincer ve Marc A. Rosen, Exergy, Energy, Environment And Sustainable Development, Second Edition. Elsevier, 2013.

[22]. YA Cengel ve MA Boles, Thermodynamics: an engineering approach, Fifth Edition. McGraw-Hill Education, 2006.

Load Shaping Based Privacy Protection in Smart Grids: An Overview

Cihan Emre Kement[1, 2]

Abstract

Fine-grained energy usage data collected by Smart Meters (SM) is one of the key components of the smart grid (SG). While collection of this data enhances efficiency and flexibility of SG, it also poses a serious threat to the privacy of consumers. Through techniques such as nonintrusive appliance load monitoring (NALM), this data can be used to identify the appliances being used, and hence disclose the private life of the consumer. Various methods have been proposed in the literature to preserve the consumer privacy. This paper focuses on load shaping (LS) methods, which alters the consumption data by means of household amenities in order to ensure privacy. An overview of the privacy protection techniques, as well as heuristics of the LS methods, privacy measures, and household amenities used for privacy protection are presented in order to thoroughly analyze the effectiveness and applicability of these methods to smart grid systems. Finally, possible research directions related to privacy protection in smart grids are discussed.

Keywords: Advanced metering infrastructure, battery load hiding, load shaping, privacy metrics, smart grid privacy, smart meters.

1. INTRODUCTION

Rapid changes in the technology towards the end of the 20th and the beginning of the 21st century imposed changes in the people's lives as well as their energy consumption. Daily life becomes more and more dependent on electricity, due to the digital transformation and new products such as plug-in electric vehicles (PEVs). Today's electric grid is expected to meet the increasing consumer demand as well as to be more reliable, efficient, scalable and secure. In order to fulfill these expectations, *smart grids* (SGs) are being developed, where the energy flow is coupled with a two-way information flow between the components of

the grid structure. The information flow throughout the SG has many advantages. Distribution system operators (DSOs) can quickly detect failures or shortages, whereas electricity generators (EGs) can monitor the electricity usage data in order to tune electricity production and hence increase efficiency. The latter is made possible by *advanced metering infrastructure* (AMI), where fine-grained electricity usage of consumers are collected with the help of smart meters (SMs).

Although the high-granularity consumption data is very useful for both the supply and demand sides, it also contains very detailed information about the consumers' private lives. By using nonintrusive appliance load monitoring (NALM) techniques, the power signature of a house can be disintegrated into the individual appliances [1]-[7]. Therefore, sensitive information such as the number of residents, daily consumption patterns of the residents and whether the house is vacant or not can be inferred from the collected data.

In order to protect the consumers' privacy, many methods such as load shaping (LS), adding noise to the consumption data, differential privacy, data aggregation and cryptographic measures have been proposed in the literature. Among these, LS methods stand out as they hide the details of electricity usage while providing the utility company (UC) with the true consumption data.

The remainder of this paper is as follows: first, some background information about the AMI and NALM techniques, as well as different notions of privacy in the case of SGs are provided. Then, various privacy protection methods are categorized, indicating their advantages and disadvantages, followed by the LS methods

---

[1] ASELSAN Inc., 06172 Yenimahalle/Ankara, Turkey. cekement@aselsan.com.tr

[2] TOBB University of Economics and Technology, Department of Electrical and Electronics Engineering, 06510 Cankaya/Ankara, Turkey. ckement@etu.edu.tr

in detail. The means used for LS are explained, along with their limitations. Then, various privacy measures proposed are reviewed. Finally, future research directions for LS based privacy protection in SGs are proposed. Concluding remarks are provided in the conclusion section.

2. BACKGROUND INFO

2.1. Advanced Metering Infrastructure (AMI)

AMI is an integrated system of communication networks and SMs which enables the two-way communication between consumers and UCs [8]. This two-way communication comes with many advantages. It enables DSOs to automatically detect outages, which would be otherwise reported by customers. UCs can learn a lot more detail about the electricity usage trends of their consumers. By using this information, UCs can increase their efficiency. Furthermore, UCs can provide real-time electricity prices to consumers, who can use this information to reduce their electricity bills by shifting their electricity usage to off-peak hours. This is an example of demand side management (DSM), a scheme where the electricity usage of consumers is changed by UCs by using various incentives.

2.2. Nonintrusive Appliance Load Monitoring (NALM)

NALM is a process for inferring which appliances have been used from the aggregated electricity load profile. Originally invented by Hart et al. [9] in 1985, today NALM is a family of methods all of which use different properties of the load signature in order to distinguish between electric appliances accurately.

NALM uses unique power signatures of appliances such as the (real and reactive) power levels, operation duration and periodicity to identify them. Appliances can in general be divided into three categories; namely ON/OFF appliances (such as a light bulb), Finite State Machine (FSM) appliances (such as refrigerators and washing machines) and continuously variable appliances (such as light dimmers and sewing machines). Unique properties of these appliance categories are utilized for an effective identification.

2.3. Notions of Privacy

Privacy threats that are introduced with the SG can be interpreted in different ways. As described earlier, NALM techniques can reveal the appliance usage data. However, some of this data can be of less importance in terms of privacy. For example; usage data of a toaster machine and a kettle can be interpreted as the resident being hungry, but how private this information is to the resident? These scenarios lead to different notions of privacy. NIST guidelines [11] listed some of the information which can be sensitive to the consumers as in Table 1. Some of these can be interpreted through the usage of metered load data.

Table 11. Sensitive information made available by SGs [11].

Information	Description
Name	Name responsible for the account.
Address	Location to which service is being taken.
Meter Reading	kW, kWh power consumption collected at 15-60 minute intervals during the current billing cycle.
HAN	In-home electrical appliances.
Lifestyle	When the home is occupied and it is unoccupied, when occupants are awake and when they are asleep, how many various appliances are used, etc.
DER	The presence of on-site generation and/or storage devices, operational status, net supply to or consumption from the grid, usage patterns.

To protect privacy, one approach can be to hide every electric signature regardless of its source. However, this approach can be inefficient as some of these signatures can be of less importance. Some researchers propose to hide only high frequency events [12]. The claim is that low frequency events such as refrigerators reveal less information about the private life of the consumer, while spikes in the load signatures can be of more personal

appliances. Another privacy measure tries to prevent occupancy detection. The logic behind it is that the occupancy of consumer is an important information in terms of privacy, since it can be used for burglary by adversaries. For similar reasons, the number of the occupants and their genders can also be of importance.

3. PRIVACY PROTECTION METHODS

3.1. Noise Addition and Differential Privacy

Adding noise to the metered data is one of the privacy measures which is studied widely in the literature [13]-[20]. Most of these approaches try to achieve or maximize the *differential privacy* (DP), which is a statistical representation of the difference between the original and distorted data.

The main disadvantage of the noise addition is that it causes a mismatch between the metered load and the actual load. This prevents DSOs from rapidly and accurately reacting to outages, and UCs from producing accurate billing services as well as scheduling energy production in a precise manner. Therefore, noise-added consumption data undermines the very benefits of the SG. Access to the real metered data is crucial for setting accurate electricity prices as well as scheduling the energy production for better efficiency.

3.2. Data Aggregation and Cryptography

Data aggregation is another major method which aims to send aggregated multi-house power signatures to the UC so that an individual house's power signature can be hidden. Methods of homomorphic encryption are widely utilized in these studies [21]-[29].

The main drawback of these methods is the computational complexity of cryptographic techniques. Also, there is a need for a Trusted Third Party (TTP) for aggregation or encryption of multiple house data. This shifts the privacy concerns towards TTPs. Furthermore, metering multi-house power signatures can harm certain house-specific DSM applications, where each house is provided with individual incentives for changing their electricity usage patterns.

3.3. Data Anonymization and Downsampling

Data anonymization methods mainly focus on using pseudonyms instead of the customer IDs in order to protect their privacy [29], [30]. However, this approach does not protect customers from an adversary monitoring the electricity just outside of their houses.

Downsampling can simply be defined as reducing the frequency of metering energy data, so that high-frequency electric usage is hidden under the time-aggregated metered data. This method is shown to reduce the effectiveness of NALM methods [31] However; downsampling also hides the real-time electricity usage from the UCs and DSOs, reducing the effectiveness of the DSM applications and causing late responses to the failures.

3.4. Load Shaping

Load Shaping (LS) methods differ from the other approaches by sending the actual electricity usage data frequently and per-house basis. Therefore, LS eliminate the shortcomings of other methods. LS methods use household amenities (such as batteries, PEVs, RESs, shiftable appliances) in order to mask the real energy consumption of consumers. In the next section, the existing LS techniques are presented.

4. LOAD SHAPING BASED PRIVACY PROTECTION TECHNIQUES

4.1. Best Effort (BE)

Initially proposed by Kalogridis et al. [32], the Best Effort (BE) method tries to keep the load demand of the house as steady as possible with the help of a Rechargeable Battery (RB). This method results in a completely flat metered load if the capacity of the RB is big enough.

Three different privacy metrics are proposed in [32]: Relative Entropy (or Kullback-Leibler Divergence), clustering analysis and regression analysis. The efficiency of the method is evaluated by using these three metrics.

4.2. Non-intrusive Load Leveling (NILL)

McLaughlin et al. [33] proposed a LS method which uses a household RB to mask the appliance load signatures. Unlike BE method, where the metered load exposes appliance signatures when the battery is empty or full, NILL aims to maintain a steady load no matter the amount of energy stored in the RB. To achieve this, NILL adopts three target load levels. The algorithm chooses one of these levels according to the charging state of the battery. If the battery is close to full capacity and the load is below the steady state load K_{ss}, NILL chooses the *high recovery* state K_H which sets the target metered load to a lower value. Therefore, the appliance load signatures are still masked, while the battery is not overcharged. Similarly, in *low recovery* state, the target metered load is set to a higher value so that the battery is charged while a constant metered load is maintained. The algorithm updates its K_{ss} each time a low recovery or high recovery state is visited.

In [33], privacy performance is measured by the number of features, i.e. changes in the energy consumption between adjacent time slots, and empirical entropy.

4.3. Tolerable Deviation (TD)

Tolerable Deviation (TD) strategy aims to keep the metered load *within* a certain limit of a target load. Introduced in [34], the idea is that small amounts of change in the metered load do not leak information about the appliances, and hence do not violate privacy.

In the study, the authors propose two different metrics for privacy: Number of (non-tolerable) changes in the metered load, and the mutual information between the actual load and the metered load [34].

4.4. Stepping

Stepping method in [35] also utilizes a RB for LS. Similar to BE and NILL, this technique maintains a flat load until it is forced to change it. The change in the metered load is only allowed as a multitude of a certain step size.

The privacy performance of the stepping algorithms in [35] is measured in terms of the mutual information metric.

5. AMENITIES USED FOR LOAD SHAPING

5.1. Renewable Energy Sources (RESs)

5.1.1. Photovoltaic Energy (PVE)

Photovoltaic energy (PVE) is one of the major sources of clean electricity. With the expansion of smart grid, more and more distributed PVE plants are expected to be integrated to the grid. With the decreasing cost of photovoltaic panels, the number of PVE producing houses is expected to increase [36].

In addition to reducing the electricity bill, PVE can also be used to mask some of the household energy usage. One shortcoming is, however, is the unpredictability of the PVE production. If the house is not equipped with a rechargeable battery (RB) or the capacity of the RB is not large enough, PVE can only be used as it is generated.

5.1.2. Wind Energy (WE)

Another common RES which can be used for LS is wind energy. Wind energy is produced from the natural air flow by using a turbine to convert mechanical energy into electrical energy. WE accounts for more than one percent of the overall electricity production worldwide [36]. SG enables distributed WE production by consumers. Therefore, WE can be used by households to mask the changes in their load demand. However, similar to PVE, WE is also unpredictable and in the absence of a RB it can only be used to mask the load at the instant it is generated.

5.2. Rechargeable Batteries (RB)

Household batteries are expected to be a fundamental part of the Smart Homes (SHs) of the SGs. They can be used for privacy, as well as they are used for storing excess energy from RESs and for storing energy when it is cheaper in order to reduce the bill of the consumers.

However, using RBs impose a certain cost on the consumers [12]. They require a long time for an acceptable return of investment [37]. Also, the depreciation period of RBs are around 20 years [37], therefore it is not a one-time investment. Considering the installment and maintenance costs of RBs as well as their charging/discharging

inefficiency are important when consumers invest in RBs either for profit or for privacy. Also, one should note that the capacity of RB has an impact of the effectiveness of LS methods. In order for LS methods to work efficiently, a large capacity RB is generally needed.

5.3. Shiftable Appliances

Appliances in a household can be categorized into four types: time-shiftable, power-shiftable, time and power shiftable, and non-shiftable [38]. The operation time slots of time-shiftable appliances can be changed for load shaping in order to improve privacy at the cost of reducing the comfort of consumers. Similarly, power-shiftable appliances' power consumption can be modified to achieve the desired privacy. Note that some appliances such as Plug-in Electric Vehicles (PEVs) can be both time-shiftable and power-shiftable.

5.4. Plug-in Electric Vehicles (PEVs)

PEVs differ from the other (time and power shiftable) appliances in a house because they can draw energy from the grid *and* provide electricity for the other appliances thanks to their large-capacity internal batteries. Therefore, they can be used to shape the metered load for privacy just like a RB [39]. One important downside of using PEVs for privacy is that their primary purpose is different from that of RBs. A house can drain its RB for the purpose of cheap energy or privacy; however it may not be able to do so with PEVs because PEVs need to be sufficiently charged when the consumers need to use them.

5.5. Thermal Energy Storages - Combined Heat and Power

Majority of households are equipped with a form of thermal energy storage (TES), which is used either for heating or for supplying hot water to the house [40]. Therefore, TESs that are driven by electricity can be used as a thermal battery to hide load signatures. TESs are generally well-insulated, and hence energy efficient. However, a disadvantage of using TESs is that they convert energy in one direction only (electric energy to heat energy). Therefore, they can only be used to increase the load for certain time slots.

To mitigate the shortcomings of TESs, combined heating and power (CHP) devices are proposed in the literature [40]. The main advantage of CHPs is that they can generate both power and heat from various sources such as RESs and natural gas. In [40], cooling capability is also added to the CHP and the system is called combined cooling, heating and power unit (CCHP).

6. PRIVACY PERFORMANCE METRICS

6.1. Information Theoretic Metrics

6.2. Mutual Information (MI)

In information theory, the mutual information (MI) is a metric between two sets of data which quantifies how much information of a set of data can be obtained by observing the other. In case of smart grid privacy, the mentioned two sets of data are the metered load and the actual load. Many studies including [34], [35] and [41] utilize the MI as a performance metric. However, the rationale behind using MI as a metric is not clear, as NALM methods use various techniques such as edge detection and clustering to identify individual appliances, and having a lower MI does not always guarantee that the load signatures of appliances are hidden.

6.3. Relative Entropy (RE)

Also known as Kullback-Leibler Divergence (KLD), relative entropy (RE) is also a metric which is used to distinguish a probability distribution from another. It measures the expected number of bits (of data) lost between a distribution and another distribution, which is the approximation of the first one. In case of measuring privacy, the first distribution is the actual load and the second distribution is the metered load. Thus, KLD gives us the information lost by changing the actual load with the metered load. Many studies including [32] and [42] use RE as a performance metric.

6.4. Statistical Metrics and Correlation Coefficients

6.5. Mean Square Error (MSE)

In statistics, mean square error (MSE) measures the average of the squared distances between a set of data and its estimation. In the smart grid literature, it is used as a privacy metric where the set of data is the actual consumption and the estimation is the metered load [43]. Although it measures the distance between the metered and the actual load, a high MSE does not guarantee a high privacy, as privacy is not directly related with the distance between the two sets of data.

6.6. Coefficient of Determination (CoD)

Various correlation coefficients (CCs) such as Fisher correlation coefficient (FCC), Matthews correlation coefficient (MCC) and Pearson correlation coefficient (PCC) are also used for measuring privacy in smart grids [32], [44]. Similar with the CoD, CCs also measure the relationship between two sets of data. The difference between CCs and the CoD is that correlation coefficients measure the linear correlation between two variables. In case of smart grid privacy, they are used to measure the correlation between the metered load and the actual load.

6.7. Empirical Metrics

6.8. Number of Changes (NoC)

Since NALM methods generally look for the changes in the load signature and match them with the change in the load caused by individual appliances, some of the studies use the number of changes (NoC) in the load signature between each time slot in order to measure the performance of their methods [10], [33]. In this case, 0 is the best possible outcome, which indicates a completely flat load. The more changes there are in the load, the worse the method's performance in terms of privacy is. However, this metric is not able to measure privacy directly, as are all the previously mentioned metrics.

6.9. Cluster analysis

Cluster analysis is the grouping a set of data such that the data in the same group are more similar to each other, compared to the data from the other groups. In [32], cluster analysis is used to measure the privacy, where clustering is made by using the changes in the actual load data first and then by using the changes in the metered load; and the number of correct classifications in the latter one is counted. The more correct classifications there are, the worse the performance is.

6.10. Combined Metrics

In [7], a combination of three performance metrics, namely NoC, CoD and RE, is used to derive a combined performance metric. This approach can be beneficial for an accurate measurement of privacy, as none of the metrics alone can guarantee an accurate measurement. However, further analysis is needed to assess if using the combination of more than one metrics yields in a more accurate measurement of privacy than those obtained by using one of the singular metrics.

7. POSSIBLE RESEARCH DIRECTIONS FOR PRIVACY IN SMART GRIDS

7.1. Definition of Privacy

As discussed in this paper, there are various information that can be inferred from monitoring the load demand of the consumers. Some of these information can be sensitive to a type of consumer, whereas another consumer may not be interested in protecting them. Therefore, which information is important to which type of customer should be assessed and the research should focus on protecting these particular information. This is where sociology and power systems engineering disciplines can join forces. An example study in the field of sociology is presented in [47], where authors try to assess which type of information that people want to be protected against adversaries in case of SGs.

7.2. Commercial Privacy vs. Residential Privacy

Another issue that should be addressed is the privacy needs of commercial or industrial consumers and residential customers. An industrial or commercial company might want to hide different information compared to the residential users (such as shift hours, product design changes etc.). Also, their adversaries can be very different than that of residential consumers (such as rival companies, intelligence agencies, etc.). Therefore, privacy for commercial and industrial customers should be considered separately from the residential ones.

7.3. One Privacy Measure for All

The literature on smart grid privacy does not use a single privacy measure as discussed earlier. This is partly because none of the existing metrics is able to accurately measure protection against NALM techniques. Coming up with an accurate privacy measure for smart grid privacy methods is an open research area.

7.4. Opting out of Smart Grid

The acceptance of the smart grid by the public is an important issue, as this new technology arises new questions in peoples' minds, especially in terms of privacy [48]. Some EU countries such as Netherlands integrate an option for the consumers to "opt-out" from smart grid, which means they can turn on and off smart grid functionality as they want [49]. This flexibility comes with complexity in both the design and the operation of the smart grid. Current literature assumes that all of the consumers are part of the smart grid scheme. Therefore, the issues that arise with dynamic customers are yet to be addressed by the research community.

8. CONCLUSION

Smart grid comes with many advantages, thanks to its ability to convey both power and information between its constituents. Detailed power usage data of consumers enable a more efficient power production as well as customized and more profitable services for the consumers. On the other hand, high frequency metered load data can be used by adversaries to break it down to individual appliance usage data, which can be used against the consumers' consent. Therefore, there are many techniques proposed in the literature to mitigate this privacy problem.

This paper presented an overview of existing privacy protection techniques, as well as the means that can be used for ensuring privacy and the privacy metrics. A categorization of existing techniques was provided along with their advantages and disadvantages. The privacy metrics used in the literature and the logic behind using them were explained. Household amenities that can be used for load shaping and hence providing privacy were presented. Possible research directions concerning privacy protection in smart grids were also provided in order to shed light upon the future of the topic.

REFERENCES

[1]. D. Alahakoon and X. Yu, "Smart electricity meter data intelligence for future energy systems: A survey," *IEEE Trans. Ind. Informat.*, vol. 12, no. 1, pp. 425–436, Feb. 2016.

[2]. P. McDaniel and S. McLaughlin, "Security and privacy challenges in the smart grid," *IEEE Sec. Priv.*, vol. 7, no. 3, pp. 75–77, May. 2009.

[3]. F. G. Marmol, C. Sorge, O. Ugus, and G. M. Perez, "Do not snoop my habits: preserving privacy in the smart grid," *IEEE Commun. Mag.*, vol. 50, no. 5, pp. 166–172, May. 2012.

[4]. S. Uludag, S. Zeadally, and M. Badra, *Techniques, Taxonomy, and Challenges of Privacy Protection in the Smart Grid.* Springer, Oct.2015, pp. 343–390.

[5]. M. A. Lisovich, D. K. Mulligan, and S. B. Wicker, "Inferring personal information from demand-response systems," *IEEE Sec. Priv.*, vol. 8, no. 1, pp. 11–20, Jan. 2010.

[6]. Z. Wang and G. Zheng, "Residential Appliances Identification and Monitoring by a Nonintrusive Method," *IEEE Trans. Smart Grid*, vol. 3, no. 1, pp. 80–92, Mar. 2012.

[7]. C. E. Kement, H. Gultekin, B. Tavli, T. Girici, and S. Uludag, "Comparative analysis of load-shaping-based privacy preservation strategies in a smart grid," *IEEE Trans. Ind. Informat.*, vol. 13, no. 6, pp. 3226–3235,Dec. 2017.

[8]. R. R. Mohassel, A. Fung, F. Mohammadi, and K. Raahemifar, "A survey on advanced metering infrastructure," *International Journal of Electrical Power & Energy Systems*, vol. 63, pp. 473–484, 2014.

[9]. G. W. Hart, "Prototype nonintrusive appliance load monitor," in *MIT Energy Laboratory Technical Report, and Electric Power Research Institute Technical Report*, 1985.

[10]. G. W. Hart, "Nonintrusive appliance load monitoring," *Proc. IEEE*, vol. 80, no. 12, pp. 1870–1891, 1992.

[11]. V. Y. Pillitteri and T. L. Brewer, "Guidelines for smart grid cybersecurity," Tech. Rep., 2014.

[12]. G. Giaconi, D. Gunduz, and H. V. Poor, "Privacy-aware smart metering: Progress and challenges," *IEEE Signal Processing Magazine*, vol. 35, no. 6, pp. 59–78, 2018.

[13]. J. Zhao, T. Jung, Y. Wang, and X. Li, "Achieving differential privacy of data disclosure in the smart grid," in *IEEE INFOCOM 2014-IEEE Conference on Computer Communications.* IEEE, 2014, pp. 504–512.

[14]. Z. Zhang, Z. Qin, L. Zhu, J. Weng, and K. Ren, "Cost-friendly differential privacy for smart meters: Exploiting the dual roles of the noise," *IEEE Transactions on Smart Grid*, vol. 8, no. 2, pp. 619–626, 2016.

[15]. Z. Yang, P. Cheng, and J. Chen, "Differential-privacy preserving optimal power flow in smart grid," *IET Generation, Transmission & Distribution*, vol. 11, no. 15, pp. 3853–3861, 2017.

[16]. E. Liu and P. Cheng, "Mitigating cyber privacy leakage for distributed dc optimal power flow in smart grid with radial topology," *IEEE Access*, vol. 6, pp. 7911–7920, 2018.

[17]. R. Pal, P. Hui, and V. Prasanna, "Privacy engineering for the smart micro-grid," *IEEE Transactions on Knowledge and Data Engineering*, vol. 31, no. 5, pp. 965–980, 2019.

[18]. H. Cao, S. Liu, Z. Guan, L. Wu, and T. Wang, "Achieving differential privacy of data disclosure from non-intrusive load monitoring in smart grid," in *International Symposium on Cyberspace Safety and Security*. Springer, 2017, pp. 32–42.

[19]. X. Lou, R. Tan, D. K. Yau, and P. Cheng, "Cost of differential privacy in demand reporting for smart grid economic dispatch," in *IEEE INFOCOM 2017-IEEE Conference on Computer Communications*. IEEE, 2017, pp. 1–9.

[20]. P. Barbosa, A. Brito, and H. Almeida, "A technique to provide differential privacy for appliance usage in smart metering," *Information Sciences*, vol. 370, pp. 355–367, 2016.

[21]. S. Tonyali, K. Akkaya, N. Saputro, A. S. Uluagac, and M. Nojoumian, "Privacy-preserving protocols for secure and reliable data aggregation in iot-enabled smart metering systems," *Future Generation Computer Systems*, vol. 78, pp. 547–557, 2018.

[22]. H. Chun, K. Ren, and W. Jiang, "Privacy-preserving power usage and supply control in smart grid," *Computers & Security*, vol. 77, pp. 709–719, 2018.

[23]. M. Bae, K. Kim, and H. Kim, "Preserving privacy and efficiency in data communication and aggregation for ami network," *Journal of Network and Computer Applications*, vol. 59, pp. 333–344, 2016.

[24]. S. Tonyali, R. Munoz, K. Akkaya, and U. Ozgur, "A realistic performance evaluation of privacy-preserving protocols for smart grid ami networks," *Journal of Network and Computer Applications*, vol. 119, pp. 24–41, 2018.

[25]. U. B. Baloglu and Y. Demir, "Lightweight privacy-preserving data aggregation scheme for smart grid metering infrastructure protection," *International Journal of Critical Infrastructure Protection*, vol. 22, pp.16–24, 2018.

[26]. H. J. Jo, I. S. Kim, and D. H. Lee, "Efficient and privacy-preserving metering protocols for smart grid systems," *IEEE Transactions on Smart Grid*, vol. 7, no. 3, pp. 1732–1742, 2015.

[27]. S. Tonyali, O. Cakmak, K. Akkaya, M. M. Mahmoud, and I. Guvenc, "Secure data obfuscation scheme to enable privacy-preserving state estimation in smart grid ami networks," *IEEE Internet of Things Journal*, vol. 3, no. 5, pp. 709–719, 2015.

[28]. M. F. Balli, S. Uludag, A. A. Selcuk, and B. Tavli, "Distributed multi-unit privacy assured bidding (pab) for smart grid demand response programs," *IEEE Transactions on Smart grid*, vol. 9, no. 5, pp. 4119–4127, 2018.

[29]. A. Abdallah and X. Shen, "Lightweight security and privacy preserving scheme for smart grid customer-side networks," *IEEE Transactions on Smart Grid*, vol. 8, no. 3, pp. 1064–1074, 2015.

[30]. Y. Gong, Y. Cai, Y. Guo, and Y. Fang, "A privacy-preserving scheme for incentive-based demand response in the smart grid," *IEEE Transactions on Smart Grid*, vol. 7, no. 3, pp. 1304–1313, 2015.

[31]. G. Eibl and D. Engel, "Influence of data granularity on smart meter privacy," *IEEE Trans. Smart Grid*, vol. 6, no. 2, pp. 930–939, Mar.2015.

[32]. G. Kalogridis, C. Efthymiou, S. Z. Denic, T. A. Lewis, and R. Cepeda, "Privacy for smart meters: Towards undetectable appliance load sig-natures," in *Proc. IEEE Int. Conf. Smart Grid Commun. (SmartGrid-Comm)*, 2010, pp. 232–237.

[33]. S. McLaughlin, P. McDaniel, and W. Aiello, "Protecting consumer privacy from electric load monitoring," in *Proc. ACM Conf. Comput. Commun. Security (CCS)*, Oct. 2011, pp. 87–98.

[34]. B. Ge and W. T. Zhu, "Preserving user privacy in the smart grid by hiding appliance load characteristics." ser. Lecture Notes in Computer Science, G. Wang, I. Ray, D. Feng, and M. Rajarajan, Eds., vol. 8300.Springer, 2013, pp. 67–80.

[35]. W. Yang, N. Li, Y. Qi, W. Qardaji, S. McLaughlin, and P. McDaniel, "Minimizing private data disclosures in the smart grid," in *Proc. ACM Conf. Comput. Commun. Security (CCS)*, Oct. 2012, pp. 415–427.

[36]. M. Liserre, T. Sauter, and J. Y. Hung, "Future energy systems: Integrating renewable energy sources into the smart power grid through industrial electronics," *IEEE industrial electronics magazine*, vol. 4, no. 1, pp. 18–37, 2010.

[37]. M. Naumann, R. C. Karl, C. N. Truong, A. Jossen, and H. C. Hesse, "Lithium-ion battery cost analysis in pv-household application," *Energy Procedia*, vol. 73, pp. 37–47, 2015.

[38]. F. B. Saghezchi, F. B. Saghezchi, A. Nascimento, and J. Rodriguez, "Game theory and pricing strategies for demand-side management in the smart grid," in *Proc. Int. Symp. Commun. Syst. Netw. Digtl. Sign. Proc. (CSNDSP)*, 2014, pp. 883–887.

[39]. K. Mets, T. Verschueren, W. Haerick, C. Develder, and F. De Turck, "Optimizing smart energy control strategies for plug-in hybrid electric vehicle charging," in *2010 IEEE/IFIP Network Operations and Management Symposium Workshops.* IEEE, 2010, pp. 293–299.

[40]. F. Brahman, M. Honarmand, and S. Jadid, "Optimal electrical and thermal energy management of a residential energy hub, integrating demand response and energy storage system," *Energy and Buildings*, vol. 90, pp. 65–75, 2015.

[41]. G. Giaconi, D. Gunduz, and H. V. Poor, "Smart meter privacy with an energy harvesting device and instantaneous power constraints," in *Proc. IEEE Int. Conf. Communications (ICC)*, Jun. 2015, pp. 7216–7221.

[42]. G. Kalogridis, R. Cepeda, S. Z. Denic, T. Lewis, and C. Efthymiou, "ElecPrivacy: Evaluating the privacy protection of electricity management algorithms," *IEEE Trans. Smart Grid*, vol. 2, no. 4, pp. 750–758, Dec. 2011.

[43]. G. Giaconi, D. Gunduz, and H. V. Poor, "Joint privacy-cost optimization in smart electricity metering systems," *arXiv preprint arXiv: 1806.09715*, 2018.

[44]. Z. Chen and L. Wu, "Residential appliance DR energy management with electric privacy protection by online stochastic optimization," *IEEE Trans. Smart Grid*, vol. 4, no. 4, pp. 1861–1869, Dec. 2013.

[45]. D. Chen, S. Kalra, D. Irwin, P. Shenoy, and J. Albrecht, "Preventing occupancy detection from smart meters," *IEEE Trans. Smart Grid*, vol. 6,no. 5, pp. 2426–2434, Sep. 2015.

[46]. J. Koo, X. Lin, and S. Bagchi, "Rl-blh: Learning-based battery control for cost savings and privacy preservation for smart meters," in *2017 47th Annual IEEE/IFIP International Conference on Dependable Systems and Networks (DSN)*. IEEE, 2017, pp. 519–530.

[47]. C. Horne, B. Darras, E. Bean, A. Srivastava, and S. Frickel, "Privacy, technology, and norms: The case of smart meters," *Social science research*, vol. 51, pp. 64–76, 2015.

[48]. T. Krishnamurti, D. Schwartz, A. Davis, B. Fischhoff, W. B. de Bruin, L. Lave, and J. Wang, "Preparing for smart grid technologies: A behavioral decision research approach to understanding consumer expectations about smart meters," *Energy Policy*, vol. 41, pp. 790–797, 2012.

[49]. S. Zhou and M. A. Brown, "Smart meter deployment in europe: A comparative case study on the impacts of national policy schemes," *Journal of Cleaner Production*, vol. 144, pp. 22–32, 2017

Optimization of Coating Process Parameters for Color Difference of Denim Fabrics Abraded by Flexing and Abrasion Method

Sumeyye Ustuntag[1], Munevver Ertek Avci[2], Huseyin Gazi Turksoy[1]

Abstract

In this study, it was aimed to optimize various coating process parameters for color difference of denim fabrics abraded by Flexing and Abrasion Method using Taguchi method. The squeeze pressure, the viscosity of the coating fluid, the fabric passing speed, the drying temperature and the weft density were selected as control parameters. An L27 (3^5) orthogonal design was chosen as experimental plan. In the evaluations with Taguchi Method, analyses of the signal to noise ratio (S/N) and variance (ANOVA) were used. Based on the S/N ratio, it was found that the optimum levels of the coating parameters for color difference were 17 picks/cm weft density, 160 °C drying temperature, 50 dPa.s viscosity, 3 bar squeeze pressure, 30 m/min fabric passing speed. According to ANOVA method, the weft density was found as the most effective parameter on color difference. Moreover, the color difference after abrasion of coated denim fabrics under optimum conditions was found to be decreased 1.62 times.

Keywords: Denim Fabric, Color Difference, Flexing and Abrasion Method, Taguchi Method.

1. INTRODUCTION

The denim market is highly competitive and is driven by volume and not necessarily by niches. Thus, success for companies in the denim market needs to be driven by aspects such as process optimization and marketing profile. Future trends also signal the use of different kinds of finishing technologies to differentiate among fabrics. Finishing of denim fabrics can provide aesthetic as well as functional properties. There are countless dry and wet processes in denim garment processing to achieve fading, excellent handle and unique looks. The coating process, which is one of the finishing processes of denim fabric, is simple to apply but provides a fast surface treatment for specific effects such as brightness, smoothness and leather appearance. Coating form a thin layer on the denim surface and thus change the surface attributes of the treated fabric. The coating process can be applied either on a small area or on the whole denim surface. Generally, coating process of a denim garment is performed by using any of the methods of knife, foam and rotary screen coating [1].

Denim fabrics, which are largely coated for aesthetic purposes, are subject to wear in many ways during use. When abrasion occurred, coating on the fabric surface will be rubbed out and color differences occur on the fabric surface. While the color difference due to the usage of classical denim fabrics is an expected situation, the color differences due to wear in coated denim fabrics are not desired by consumers. The present study is focused on optimizing the various coating process parameters for color difference after abrasion of denim fabrics by Flexing and Abrasion Method.

Lower prices and saving time are very important for engineering the denim fabrics and producing them. Because a basic need is to make fabrics cheaper and to save time, optimization have a significant role in the manufacture of denim fabrics. Taguchi method provides a simple, efficient and systematic approach to optimize designs for performance, quality, and cost. Therefore, Taguchi method was used in this study for optimization of coating processes.

1.1. Description of the Taguchi method

---

[1] *Corresponding author: Erciyes University, Department of Textile Engineering, 38280, Talas/Kayseri, Turkey. sumeyyeustuntag@erciyes.edu.tr*

[2] *Calik Denim R&D Center, Malatya/Turkey, munevver.ertekavci@calikdenim.com*

Taguchi method is one of the most commonly used statistical methods for process optimization with minimum number of experimental runs [2]. In recent years, the rapid growth of interest in the Taguchi method has led to numerous applications of the method in a world-wide range of industries, including textile [3-9]. Taguchi involves the stages of system design, parameters design, and tolerance design. System design involves the application of scientific and engineering knowledge required in manufacturing a product; parameter design is employed to find optimal process values for improving the quality characteristics; and tolerance design consists of determining and analyzing tolerances in the optimal settings recommended by parameter design [10, 11]. The parameter design is a key step in the Taguchi method to achieving high quality without increasing cost and so, the parameter design is adopted in this paper, to reduce the color difference that occurs after abrasion of the coated denim fabrics.

The use of the parameter design in the Taguchi method to optimize a process with multiple performance characteristics includes the following steps [12]. First, performance characteristics are identified and process parameters to be estimated are selected. Second, it is decided that how many number of parameter levels there are and what kind of mutual effects are possible for the process parameters. Next, appropriate orthogonal array (OA) is selected and process parameters are assigned to the orthogonal array. After that, experiments are ready to be run based on the arrangement of the orthogonal array. Then, performance statistics (signal to noise - S/N ratio) are calculated. After the calculations, experimental results are analyzed with the help of S/N ratio and a statistical analysis of variance (ANOVA) is performed to see which process parameters are statistically significant [9]. Following is the selection of the optimal levels of process parameters. Finally, optimal process parameters are verified through the confirmation experiment [13].

2. MATERIALS AND METHODS

In this study, Minitab Version 16.0 software package was used to the parameter design of Taguchi method. The most important stage in the Taguchi method is the identification of control factor. The factors selected for optimization are squeeze pressure, the viscosity of the coating fluid, the fabric passing speed, drying temperature and weft density. Each parameter was investigated at three levels to study the non-linearity effect of the process parameters (Table 1). L27 the orthogonal array table (Table 2) was chosen to determine experimental plan; five factors with three levels.

Table 1. Control factors and levels for the experimental design.

Code	Factors	Levels		
		1	2	3
A	Weft density (picks/cm)	14	17	20
B	Drying temperature (°C)	120	140	160
C	Viscosity (dPa.s)	30	50	70
D	Squeeze pressure (Bar)	3	5	7
E	Fabric passing speed (m/min)	10	20	30

After determining the control factors and their levels, three denim fabric samples were manufactured with 3/1 Z twill structure by Calik Denim Inc. Ne 8.2/1 ring yarn were used as the warp yarn with a density of 17 ends/cm for all fabric samples. Ne 10.4/1 ring core-spun yarns (%95 cotton and % 5 Elastane-70 dtex) were used as weft yarn with three different densities (14, 17 and 20 picks/cm). Depending on the Taguchi experiment design, the coating of the denim fabrics was applied by the Rotary Screen Coating Method. A standard coating pat used in the mill was used for the coating of the denim fabrics.

The denim fabrics were abraded with Flexing and Abrasion Tester (Figure 1) according to ASTM D 3885 standard. Samples prepared according to the relevant standard were abraded only in weft direction with 4 repetitions at 500 cycles. In this device, the fabric is rubbed with metal rod by making back and forth movement with the help of lower jaw. After the fabrics have been abraded, their color differences were tested by Minolta CM 3600D model spectrophotometer (Figure 2) and the following formula (Formula 1) were used to calculate the color difference (ΔE) of the fabrics.

$$\Delta E = \sqrt{[(\Delta L^*)^2 + (\Delta a^*)^2 + (\Delta b^*)^2]} \tag{1}$$
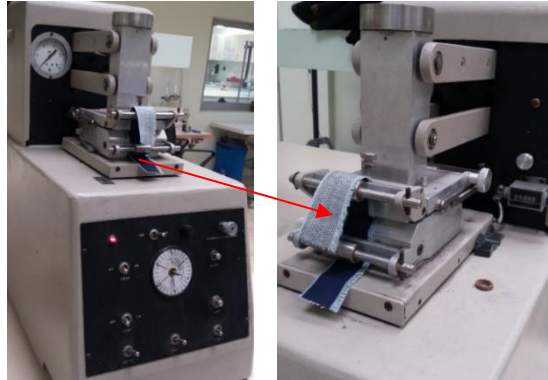
Figure 1. Flexing and Abrasion Tester

Figure 2. Spectrophotometer

3. RESULTS AND DISCUSSION

In the Taguchi method, the experimental results are transformed into a signal-to-noise ratio (S/N ratio), which represents the ratio of sensitivity to variability. Maximum S/N ratio signifies minimum effect of random noise factors and vice versa. Therefore, the higher the S/N ratio, the better is the quality. The method of calculating the S/N ratio depends on whether the response parameter is "nominal-the-best", "larger-the-better", or "smaller-the-better" [14]. In this study, the color difference was classified under the response type "smaller-the-better", because the high value of color difference is not a desirable feature in terms of coated denim fabrics. The formula used for the calculation of the S/N ratio are given in Formula 2.

$$\frac{S}{N} = -10 \log \left[\frac{1}{n} \sum_{i=1}^{n} y_i^2 \right] \tag{2}$$

where y_i denotes the data obtained from experiments; n represents the number of experiments. The experimental layout, average color difference values and the calculated S/N ratios for all tests are given in Table 2.

Table 2. L27 the orthogonal array, average ΔE values and S/N ratios.

Order	Parameters					Colour Difference (ΔE)	S/N Ratio (dB)
	A	B	C	D	E		
1	1	1	1	1	1	9.22	-19.33
2	1	1	1	1	2	8.98	-19.08
3	1	1	1	1	3	8.05	-18.13
4	1	2	2	2	1	8.72	-18.82
5	1	2	2	2	2	9.80	-19.84
6	1	2	2	2	3	9.85	-19.89
7	1	3	3	3	1	9.92	-19.96
8	1	3	3	3	2	9.07	-19.25
9	1	3	3	3	3	7.99	-18.08
10	2	1	2	3	1	7.54	-17.60
11	2	1	2	3	2	7.87	-17.96
12	2	1	2	3	3	8.04	-18.12
13	2	2	3	1	1	7.92	-17.99
14	2	2	3	1	2	8.06	-18.15
15	2	2	3	1	3	8.03	-18.11
16	2	3	1	2	1	8.47	-18.57
17	2	3	1	2	2	8.22	-18.33
18	2	3	1	2	3	7.51	-17.53
19	3	1	3	2	1	8.44	-18.53
20	3	1	3	2	2	8.76	-18.87
21	3	1	3	2	3	8.61	-18.74
22	3	2	1	3	1	9.56	-19.61
23	3	2	1	3	2	8.56	-18.66
24	3	2	1	3	3	9.14	-19.24
25	3	3	2	1	1	7.99	-18.08
26	3	3	2	1	2	7.94	-18.02
27	3	3	2	1	3	7.89	-17.96

Subsequently, the response table and response graph were formed for each control factor using Minitab 16 software as demonstrated in Tables 3 and Figure 3, respectively. Response Table shows mean response value above different levels for each parameter. The factor levels corresponding to the maximum average effect are selected as the optimum level. In response table, the delta value is calculated by subtracting the largest value from the lowest from among the values in each column. A higher delta value means that the difference at the selected level for a given factor is highly pronounced.
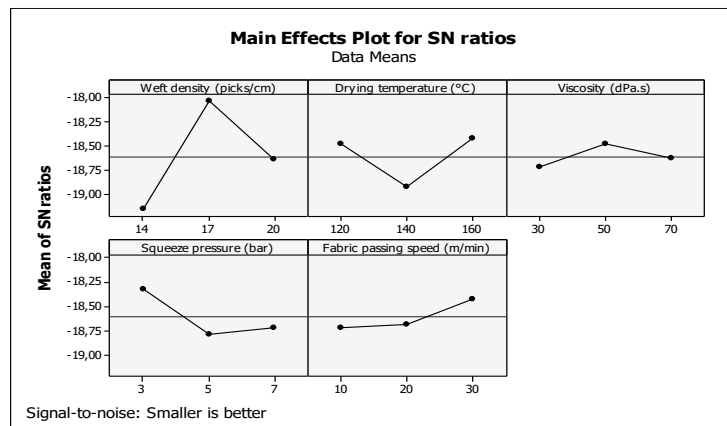
Figure 3. Main effects plot for S/N of ΔE output

Table 3. Response table for the S/N ratio of ΔE output

Factors	Average S/N, dB				
	Level 1	Level 2	Level 3	Delta	Rank
A	-19.15	-18.04*	-18.64	1.11	1
B	-18.48	-18.92	-18.42*	0.50	2
C	-18.72	-18.48*	-18.63	0.24	5
D	-18.32*	-18.79	-18.72	0.48	3
E	-18.72	-18.68	-18.42*	0.30	4

*: Optimum parameter level.

According to Figure 3 and Table 3, the optimum levels of the coating parameters for color difference are 17 picks/cm weft density, 160 °C drying temperature, 50 dPa.s viscosity, 3 bar squeeze pressure, 30 m/min fabric passing speed. Also, it was found that the most effective input parameter is weft density (A) and second effective input parameter is drying temperature (B) (Table 3). In one of our previous studies [15], the coating process parameters was optimized for the color difference of coated denim fabrics abraded by Martindale Abrasion and Pilling Tester based on Lissajous movement. As a result of this study, it was found that the most effective input parameter is drying temperature (B) and second effective input parameter is weft density (A). As can be seen from this result, the wear on the fabric surface varies depending on different abrasive devices.

The optimum levels of the input parameters are determined by conducting ANOVA analysis. Contribution values are calculated using the sum of squares values in the ANOVA table. Contribution of each factor value is a percentage value for the process effect. The bigger this value on the output of that parameter is understood to be effective at that rate.

Table 4. ANOVA table for S/N ratio of ΔE output

Factor	df	Sum of squares (SS)	Mean square (MS)	F-value	P	Percentage contribution (%)
A	2	5.5667	2.7834	10.80	0.001	42.93
B	2	1.3517	0.6759	2.62	0.103	10.42
C	2	0.2722	0.1361	0.53	0.600	2.10
D	2	1.1823	0.5911	2.29	0.133	9.12
E	2	0.4713	0.2356	0.90	0.421	3.63
Residual	16	4.1225	0.2577			31.80
Total	26	12.9667	-	-	-	100

Table 4, ANOVA analysis for S/N ratio of color difference is given. According to the result of ANOVA, only the weft density has a statistical effect on color difference after abrasion. Also, statistical results showed that the contribution rates of A, B, C, D and E factors are 42.93, 10.42, 2.10, 9.12 and 3.63% for the color difference of coated denim fabrics, respectively.

3.1. Confirmation tests

The confirmation experiment is the final step of the design of an experiment. If the optimum levels determined as a result of the analysis are not present in the experimental design, we need to calculate the predicted value of the S/N ratio at the optimum levels. The predicted value of the S/N ratio at the optimum levels is calculated as:

$$\eta_0 = \eta_m + \sum_{i=1}^{j} (\eta_i - \eta_m) \tag{3}$$

where, η_m is total mean of S/N ratio, j is the number of factors, and η_i are the multiple S/N ratios corresponding to optimum factor levels. The predicted S/N ratio of optimum design is found to be -17.24 dB for color difference. If the S/N is known and we want to learn about the result expected that will make the S/N, the procedure is to

back-transform S/N to find the performance value expected [5]. When the predicted S/N was placed into Formula 2, the predicted color difference values of the optimum design was obtained as 7.18 (ΔE).

Table 5. Comparison between initial coating parameters and optimal coating parameters

	Initial coating parameters	*Optimal coating parameters (prediction)*	*Difference*
Optimal Level	A1B1C1D1E1	A2B3C2D1E3	d
ΔE	9.22	7.18	2.04
S/N ratio	-19.33	-17.24	1.89

The decrease in color difference with the optimum levels determined in the study is determined according to the initial levels (A1B1C1D1E1) in the experimental design. The S/N ratio of the initial design (S/N_i) is -19.13, as can be seen from Table 2. The difference (d) is obtained between the S/N ratio of the initial design (S/N_i) and the predicted S/N ratio of the optimal design (S/N_0), as shown Table 5. Depending on the d value, the recovery rate is calculated using the formulas given below. Based on this calculation, the recovery rate for the color difference of abraded coated denim fabrics under optimum conditions was found to be 1.62.

$$d = \frac{S}{N_i} - \frac{S}{N_o}$$

$$d = -10 \log L_i - (-10(\log L_o))$$

$$\frac{L_o}{L_i} = 10^{\frac{d}{10}}$$

(4)

4. CONCLUSIONS

In this study, the optimum coating conditions was determined for the color difference of denim fabrics after abraded with Flexing and Abrasion Method, using Taguchi method. With the S/N and ANOVA analyses, the optimal combination of the process parameters and the levels of importance of the coating parameters were determined. As a result of the study, the optimum levels of the coating parameters for color difference was found as 17 picks/cm weft density, 160 °C drying temperature, 50 dPa.s viscosity, 3 bar squeeze pressure, 30 m/min fabric passing speed. Also, it was found that the highly effective parameters on color difference after abrasion was weft density and the contribution rate of the weft density was 42.93%. Moreover, the color difference after abrasion of coated denim fabrics under optimum conditions was found to be decreased 1.62 times.

REFERENCES

[1]. R. Paul, "Denim Manufacture, Finishing and Applications", *Woodhead Publishing Series in Textiles: Number 164*, Elsevier, pp. 1-599, 2015.
[2]. K. Shaker, M. Umair, M. Maqsood, Y. Nawab, S. Ahmad, A. Rasheed, M. Ashraf and A. Basit, "A Statistical Approach for Obtaining the Controlled Woven Fabric Width", *AUTEX Research Journal,* Vol. 15, No 4, pp. 275-279, 2015.
[3]. H. Lai, Y. Chang, H. Chang, "A robust design approach for enhancing the feeling quality of a product: a car profile case study", *International Journal of Industrial Ergonomics*, 35, pp. 445-460, 2004.
[4]. J. J. Jung, S. Kim, C. K. Park, "Optimization of Digital Textile Printing Process using Taguchi Method", *Journal of Engineered Fibers and Fabrics,* 11, pp. 51-59, 2016.
[5]. S. Mavruz, R. T. Ogulata, R. T, "Taguchi Approach for the Optimisation of the Bursting Strength of Knitted Fabrics" *FIBRES & TEXTILES in Eastern Europe*, 18, pp. 78-83, 2010.
[6]. M. Maqsood, T. Hussain, N. Ahmad, Y. Hawab, "Multi-response optimization of mechanical and comfort properties of bi-stretch woven fabrics using grey relational analysis in Taguchi method", *The Journal of The Textile Institute*, 108:5, pp. 794-802, 2017.
[7]. N. Ahmad, S. Kamal, Z.A. Raza, T. Hussain, F. Anwar, "Multi-response optimization in the development of oleo-hydrophobiccotton fabric using Taguchi based grey relational analysis", *Applied Surface Science*, 367, pp. 370-381, 2016.
[8]. K. Shabaridharan, A. Das, "Analysis of thermal properties of multilayered fabrics by full factorial and Taguchi method", *The Journal of The Textile Institute,* Vol. 105, No. 1, pp. 29-41, 2014.

[9]. W. H. Yang, Y. S. Tarng, "Design optimization of cutting parameters for turning operations based on the Taguchi method", *Journal of Materials Processing Technology*, 84, pp. 122-129, 1998.

[10]. N. Tosun, C. Cogun, G. Tosun, "A study on kerf and material removal rate in wire electrical discharge machining based on Taguchi method", *Journal of Materials Processing Technology*, 152, pp.316-322, 2015.

[11]. S. Gunes, E. Manay, E. Senyigit, V. Ozceyhan, "A Taguchi approach for optimization of design parameters in a tube with coiled wire inserts", *Applied Thermal Engineering*, 31, pp. 2568-2577, 2011.

[12]. E. Oguz, B. Keskinler, C. Celik, Z. Celik, "Determination of the optimum conditions in the removal of Bomaplex Red CR-L dye from the textile wastewater using O3, H2O2, HCO3 − and PAC", *Journal of Hazardous Materials B131,* pp. 66-72, 2006.

A. B. Engin, O. Ozdemir, M. Turan, A. Z. Turan, "Color removal from textile dyebath effluents in a zeolite fixed bed reactor: Determination of optimum process conditions using Taguchi method", *Journal of Hazardous Materials,* 159, pp. 348-353, 2008.

[13]. A: Ghosh, P. Mal, A. Majumdar, D. Banerjee, "An Investigation on Air and Thermal Transmission Through Knitted Fabric Structures Using the Taguchi Method", *AUTEX Research Journal*, Vol. 17, No 2, pp. 152-163, 2007.

[14]. H. G. Turksoy, S. Ustuntag, M. E. Avci, "Optimization of Coating Process Parameters for Color Difference After Abrasion of Denim Fabrics by Using Taguchi Method", *ICONTEX 2019- 2. International Congress of Innovative Textiles,* 17-18.04.2019, Vol. 2, pp. 188-195.

Anfis Based Longitudinal Controller Design of a Fixed Wing UAV

Saban Ulus[1], Ikbal Eski[2]

Abstract

In this study, adaptive neuro-fuzzy inference system called ANFIS structure was investigated for longitudinal control of a fixed wing unmanned aerial vehicle (UAV). ANFIS control is one of the modern control techniques which is based on artificial neural networks (ANN) and the structure of the system is based on Takagi-Sugeno fuzzy inference system. In this conference paper, ANFIS control method was studied in order to design a longitudinal controller architecture of a fixed wing UAV. Reference model and aerodynamic parameter values of the UAV were obtained from the literature for this specific UAV model. According to the simulation data taken from PID controller structure in MATLAB®, ANFIS training and testing data were obtained and trained data were used for longitudinal aircraft dynamics such as pitch attitude hold characteristics. Hybrid and back-propagation optimization algorithms were applied to have optimum training performance. ANFIS structure was also simulated together with PI and PID controllers in Simulink. In this analysis, results have been satisfying in terms studies of the fixed wing UAV control and ANFIS and PID hybrid methods had more suitable results.

Keywords: ANFIS, fixed wing UAV, longitudinal control, PID, pitch attitude.

1. INTRODUCTION

Unmanned Aerial Vehicles (UAV) are known as a remotely controlled vehicles (RC) or drones and their communication is provided by using both ground and air control stations known as telemetry modules. UAV applications are getting more attention day by day and application areas are getting wider for daily life activities and army applications. UAV models have two main types such as multi-copter designs and fixed wing UAV designs. The design types of the UAVs used in some applications have some advantages and disadvantages according to their flight and task conditions. For example; multi-rotor UAV models can be used in a small area by having a capability of vertical take off and landing and they are used in mapping, photography, spraying and light weight transportation and slower than fixed wing UAV models. In contrast, fixed wing UAV models are mostly chosen in different flight conditions where flight zones need to have a large area to maneuver aircraft stably and fixed wing models have the ability of more payload transportation, more spraying area for agricultural applications, mapping, and ability to reach higher altitude etc. So many research and experimental works on this area have been studied in the literature [1], [2],[3],[4],[5].

According to the application areas of UAVs, it is necessary to choose a proper design to task and it is very important to have quick and stable flight while doing their task from take off position until landing position. In another words, to achieve a stable flight condition, control system structure design and UAV control surfaces must work in a well-suited condition while their real time flight duration. In this research, Artificial Neuro-Fuzzy Inference System (ANFIS) structure have been investigated for longitudinal dynamics of the fixed wing UAV model. Artificial Intelligence (AI) techniques has become very popular in so many research areas and applications [6], [7]. Marichal et al. [8] studied on vibration reduction at the vision system of a rotary-wing UAV by using neuro-fuzzy approach. Researchers used a scaled helicopter dynamic model and obtained simulation data from its fuselage. It was noted that proposed method had satisfactory results in vibration reduction. AL-Saedi et al. [9], studied on PID controller design for trajectory tracking of a flexible hydraulically driven parallel robot machine by using ANFIS and Fuzzy Logic approach. ANFIS and Fuzzy was more efficient than classical control techniques in their parallel robot mechanism. In another study, Kurnaz et al. [10] described an ANFIS model to achieve an autonomous flight controller of a UAV. Three fuzzy logic modules were developed to control the

position of the UAV in three-dimensional space. Research group observed that proposed model indicated the capability of the approach to achieve the performance criteria.

In this paper, Section 2 gives material and methodology section and in the next section ANFIS controller and longitudinal dynamics are explained for the given system. Section 3.3 shows results and comments. Conclusion part is presented in section 4.

2. MATERIAL AND METHODS

In this section, UAV type and its geometrical properties was identified. A UAV model named "Ultrastick-25e" was chosen as a reference model to implement a controller structure. To obtain the dynamic equations and state-space matrix representations of the UAV model, its' aerodynamic parameter estimations and geometrical specifications were taken from literature. The UAV model has a fixed wing shape and wingspan was 1.2 m long. The gross weight of the model was 1.9 kg. Table 1 represents the values of the given UAV model [11].
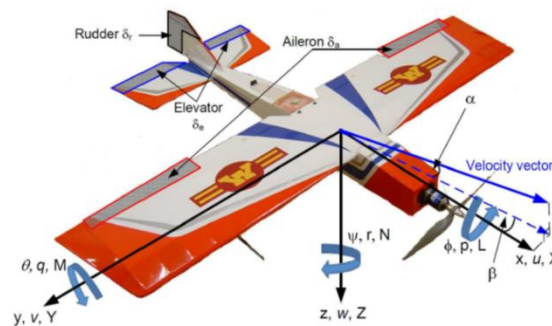
Figure 1. Reference UAV model "Ultrastick 25e" for controller structure [11]

In the previous studies of this UAV model, PID type controller was implemented and represented at the 4th ICENS symposium [12]. In this study, ANFIS based controller structure was investigated to control the UAV in longitudinal directions by using elevator and throttle deflection control inputs. Pitch angle and pitch rate, downward velocity and airspeed versus throttle and elevator inputs were simulated by using MATLAB® and SIMULINK® program.

Table 12. Specifications of the reference UAV type [11]

Parameter	Specification	Value
S	Wing reference area	0.32 m^2
b	Wingspan	1.27 m
$\bar{c}$	Wing Chord	0.25 m
m	Gross weight	1.9 kg
I_x	Roll moment of inertia	0.0894 kg.m^2
I_y	Pitch moment of inertia	0.144 kg.m^2
I_z	Yaw moment of inertia	0.162 kg.m^2
I_{xz}	Product of inertia	0.14 .m^2

2.1. Dynamic Equations and Transfer Functions at Longitudinal Directions

Aircraft equations of motions (EOM) are defined in the x, y, z direction in the space and all the equations are derived from Newtons' principal laws. It is important to obtain dynamic EOMs to define and control UAV according to a mathematical base. Another important thing to have an accurate dynamic model of the UAV is to get and acquire correct aerodynamic parameters. Aerodynamic characteristics of the specified model was taken

from the previous studies [11]. Longitudinal EOMs and some aerodynamic calculations were obtained from Nelson 2nd edition book [13].

Equations in (1) is related to the aircraft EOMs. The subscripts a, g, c, p, d in eq. (1) mean as aerodynamics, gravitational, control surfaces, thrust and atmospheric disturbance effects respectively.

$$m.(\overset{g}{u}+qw-rv) = X_a + X_g + X_c + X_p + X_d$$

$$m.(\overset{g}{v}+ru-pw) = Y_a + Y_g + Y_c + Y_p + Y_d$$

$$m.(\overset{g}{w}-qu+pv) = Z_a + Z_g + Z_c + Z_p + Z_d$$

$$L = I_x.\overset{g}{p}-(I_y-I_z)qr-I_{xz}(pq+\overset{g}{r}) = L_a + L_g + L_c + L_p + L_d \qquad (1)$$

$$M = I_y.\overset{g}{q}+(I_x-I_z)pr+I_{xz}(p^2-r^2) = M_a + M_g + M_c + M_p + M_d$$

$$N = I_z.\overset{g}{r}+(I_x-I_z)pq+I_{xz}(qr-\overset{g}{p}) = N_a + N_g + N_c + N_p + N_d$$

3. ARTIFICIAL NEURO-FUZZY CONTROLLER APPROACH

Neuro-fuzzy approaches and artificial intelligence methods have great importance and getting more attention day by day. In this study, ANFIS controller design was investigated to control the UAV longitudinal dynamics such as pitch angle, pitch rate and downward and forward speeds. ANFIS model is based on data modelling and training-testing processes. It is possible to use ANFIS graphical interface or by coding in MATLAB. ANFIS can have the capacity of learning nonlinear system structures quickly with artificial neuro-fuzzy approach. It is based on Sugeno structure and Takaghi-Sugeno-Kang was first introduced the Sugeno structure in 1985. Output function is either linear or constant in Sugeno type apart from Mamdani type model. The ANFIS technique was introduced by Jang in 1993 [14].

3.1. Anfis Structure

The entire process of ANFIS structure is given in this section. Figure 2 clearly shows the Sugeno type rule base with 2 inputs and 1 output. Inputs can have different membership function type such as Gauss, Gbell-shaped, triangular etc. and output function is either linear or constant value.
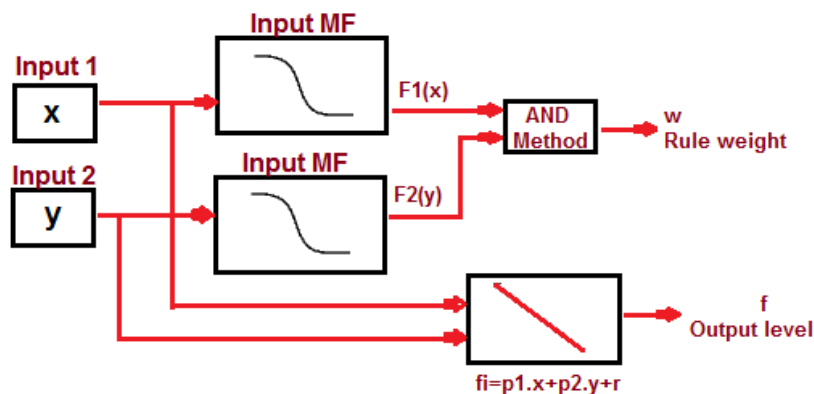
Figure 2. ANFIS Sugeno Rule Base Structure

The general structure of ANFIS is given in Figure 3. In the first layer, it has 2 inputs as x, y and the output are defined as $fi = p_i.x + q_i.y + r_i$. Each rule has own weight to create the output fi and it is based on AND rule. p_i, q_i, r_i are the design parameters for training process. Rules can be described like below;

312

Rule 1: If x=A₁ and y=B₁ then $f_1 = p_1.x + q_1.y + r_1,$ (2)

Rule 2: If x=A₂ and y=B₂ then $f_2 = p_2.x + q_2.y + r_2,$ (3)
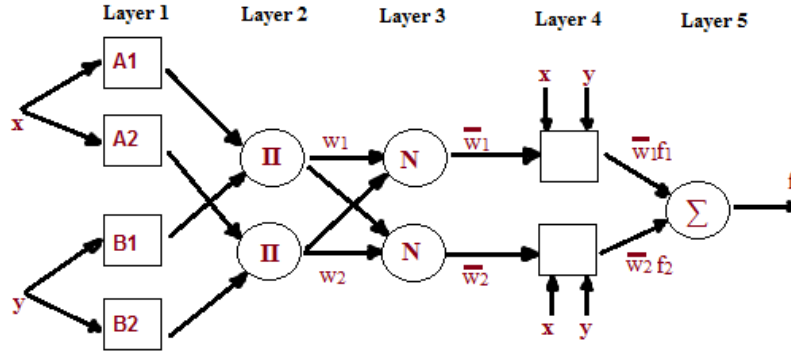
Figure 3. ANFIS structure with 2 inputs and 1 output

The ANFIS structure has five layers. O_i^j defines the **i$_{th}$** node and **j$_{th}$** layer output.

- **Layer 1:** In the first layer, each node is defined by node function.

$$O_i^1 = \mu_{A_i}(x) \qquad for \ i = 1,2 \tag{4}$$

"x" is the input and Ai is a linguistic symbol that indicates membership functions like Gauss, triangular etc.

- **Layer 2:** This layer calculates weight strength of each rule product.

$$O_i^2 = w_i = \mu_{A_i}(x)*\mu_{B_i}(y) \qquad for \ i = 1,2 \tag{5}$$

- **Layer 3:** This is the normalization process of each rule weights.

$$O_i^3 = \bar{w_i} = \frac{w_i}{w_1 + w_2} \qquad for \ i = 1,2 \tag{6}$$

- **Layer 4:** In this layer, each i$_{th}$ rule contribution is calculated.

$$O_i^4 = \bar{w_i}*f_i = \bar{w_i}.(p_i*x + q_i*y + r_i) \tag{7}$$

- **Layer 5:** In the last layer, each single node contributes and calculates total contribution of each rule.

$$O_i^5 = \sum_i \bar{w_i}*f_i = \frac{\sum_i w_i*f_i}{\sum_i w_i} \tag{8}$$

In this level of study, ANFIS structure was applied by using grid portioning method and sub-clustering method to start training process. For this reason, it was used genfis1, genfis2 and genfis3 commands in MATLAB®. Gauss and triangular MFs were used for input MF types. In the simulations, several trials were done by using 3 MFs up to 10 MFs for inputs. ANFIS results were chosen according to most close and fast response to step function for proposed control system. Figure 4 depicts the training algorithm structures for the system with two inputs and five MFs grid partitioning and two sub-cluster examples.

a)   *b)*
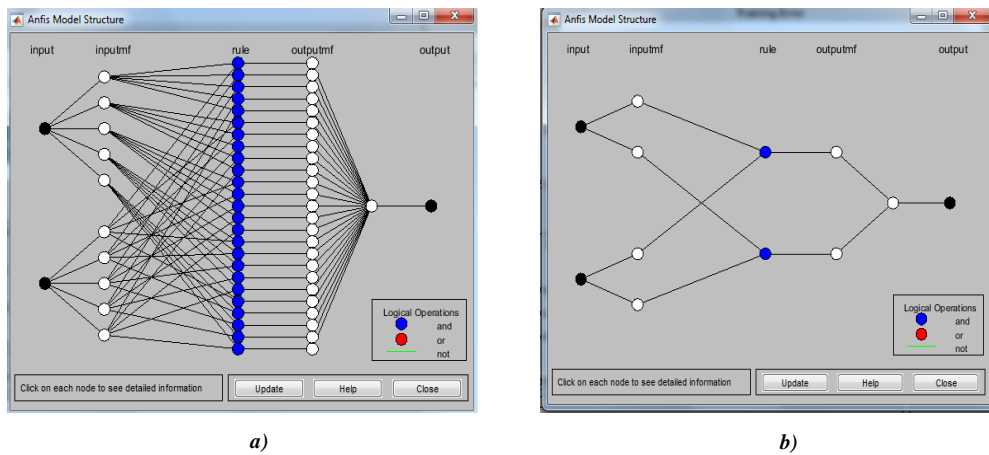
*Figure 4. Training methods for ANFIS **a)** Grid-Partioning, 2 input – 5 MF **b)** Sub-Clustering method*

3.2. Longitudinal Control of the UAV with ANFIS and ANFIS-(PI&PID) Structure

For the given UAV model, PID feedback response data were obtained and trained by using neuro-fuzzy approach as explained in previous section. For training process, it was used 85% of all obtained data and 15% of all data were selected for testing process. All inputs in the range for training and testing process were shuffled and normalized between 0 and 1. Different epoch numbers were selected for each process because of no more decreasing error. In general, 100 epochs were enough for training process.

ANFIS-PID structure is shown in Figure 5 to control the system longitudinal dynamics. Both ANFIS and PI or PID settings were used parallel to each other to create a control output for system. PID parameters such as K_p, K_i, K_d were settled according to classical Ziegler-Nichols method.
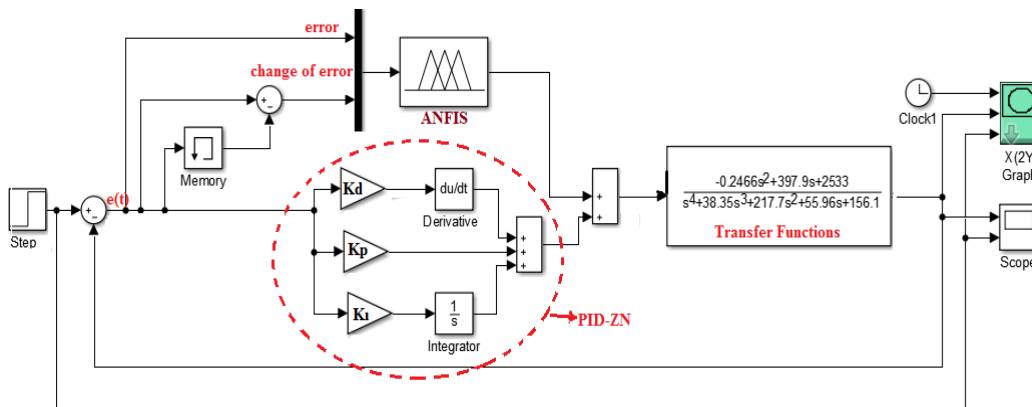
Figure 5. Parallel ANFIS and PID structure to control system dynamics

3.3. Results and Discussions

In the results section, some of the longitudinal dynamics such as pitch angle, pitch rate and airspeed in the x direction were analyzed and step response graphics were obtained for both ANFIS and PID structures together. ANFIS, ANFIS-PI and ANFIS-PID controller responses have been investigated and obtained graphics were shown in Figure 6-7-8-9. Step input was used for evaluating each control inputs of throttle and elevator.

Figure 6 represents the step response of the UAV pitch angle. ANFIS-PID response has no steady state error and too fast with less overshoot then PID-ZN results. ANFIS controller itself has big a steady state error and it is not enough for controller.
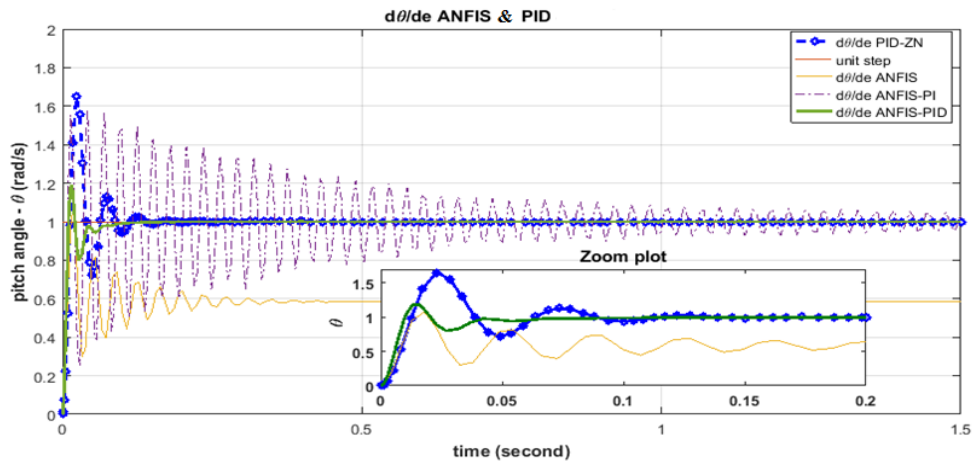
Figure 6. Pitch angle controller step response with elevator deflection input

In the next graphic, it is clear to see that ANFIS-PID step response has no steady state error, no overshoot and it has faster settling time PID-ZN. In addition to that, ANFIS-PI has a little overshoot but slower than ANFIS-PID result. Figure 7 gives pitch angle controller step response with respect to throttle input.
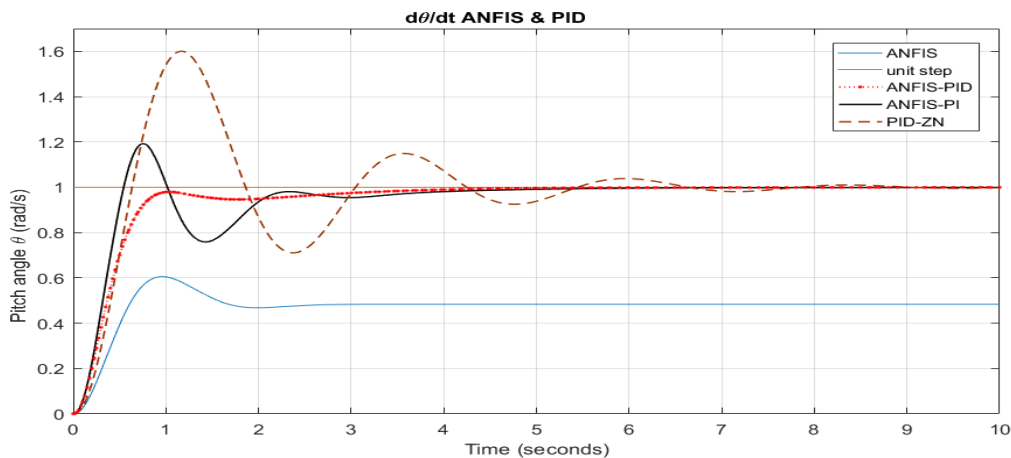
Figure 7. Pitch angle controller step response with throttle input

Airspeed control was analyzed in terms of elevator deflection input and throttle input. It is shown in Figures 8-9. Even if, ANFIS-PI has more overshoot and slower settling time, ANFIS-PID has a small overshoot and less steady-state error with less settling time in Fig. 8.
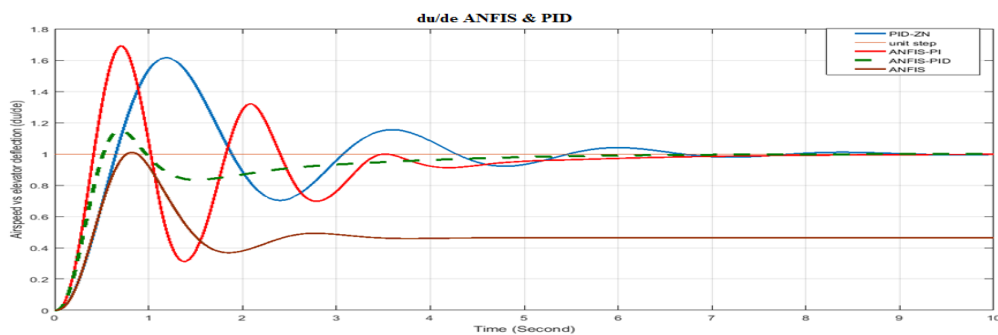
Figure 8. Airspeed step response with elevator deflection input

Figure 9 clearly shows that proposed ANFIS-PID and ANFIS-PI responses had no overshoot and very quick settling time with no steady state error.
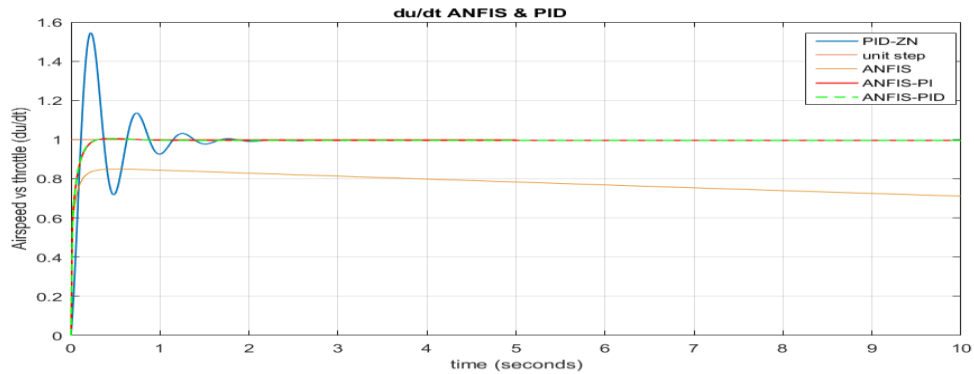
Figure 9. Airspeed step response with throttle input

Table 1 gives a detailed step response table which was obtained from simulation results in this study. In Table 1, only ANFIS-PID and PID-ZN responses were located in. As seen in the table, ANFIS-PID had more effective results instead of using only PID-ZN controller. Settling time, overshoot and steady state error have been decreased in the simulations by using hybrid controller approach.

Table 13. ANFIS and PID Step Responses of UAV at longitudinal direction

Transfer Function	ANFIS-PID							PID-Ziegler Nichols				
	Rise Time	Peak Time (s)	Peak Value	Overshoot (%)	Settling Time (s)	Steady state error		Rise Time	Peak Time	Peak Value	Overshoot (%)	Settling Time (s)
d⊖/de	0.01	0.018	1.18	18	0.03	0		0,03	0,03	1,65	65	0.15
d⊖/dt	0.7	1.1	1.0	No	3	0.01		0,6	01198	1,6	60	7,5
du/de	0.22	0.71	1.0	No	5	0		0,3	1.2	1,6	60	6,5
du/dt	0.08	0.2	1.18	No	0.022	0.002		0,1	0,13	1,5	50,0	1,069
dq/de	0.01	0.03	1.05	5	0.05	0.02		0,008	0,020	1,092	10,603	0,035
dq/dt	0.04	0.08	1.06	6	0.098	0		0,026	0,069	1,435	43,581	0,337
dw/de	0.035	0.06	1.06	6	0.038	0		0,008	0,019	1,147	16,329	0,034
dw/dt	0.3	0.5253	1.024	2.4	0.55	0.02		0,182	0,502	1,502	50,151	2,344

CONCLUSION

Neuro-fuzzy approach was implemented to control longitudinal dynamics of a UAV model called "Ultra-stick 25e" which is already exist in the literature. The UAV model was investigated, and dynamic equations were derived from aerodynamic derivatives of the specified model. 40 km/h flight speed condition was applied to the EOMs and state space representation of the UAV model was created. In the neuro-fuzzy approach, ANFIS structure was applied and valuable training results were selected to use in the control system in SIMULINK®.

This paper proposes an ANFIS-PID and ANFIS-PI type controllers. In addition, ANFIS controller was also analyzed alone in the system. Simulation results clearly shows that ANFIS controller usage brought some advantages over classical PID-ZN method for given conditions of the aircraft at the longitudinal directions. Because of nonlinearity in the systems, ANFIS can have better performance and it contributed by decreasing overshoot, settling time and steady state error when it was applied with parallel to PID in the control system. It is apparent that hybrid approach can have better performance in this control architecture.

ACKNOWLEDGMENT

REFERENCES

[1]. H. Zhu, Y. Lan, W. Wu, Hoffmann, W. C., Y. Huang, X. Xue et al., "Development of a PWM Precision Spraying Controller for Unmanned Aerial Vehicles", *Journal of Bionic Engineering*, 7 (3), 276-283, 2010.

[2]. S.K. Seelan, S. Laguette, G.M. Casady, G.A. Seielstad, "Remote sensing applications for precision agriculture: A learning community approach", *Remote Sensing of Environment*, 88 (1), 157-169, 2003.

[3]. R. Godwin, T. Richards, G. Wood, J. Welsh, S. Knight, "An economic analysis of the potential for precision farming in UK cereal production", *Biosystems Engineering*, 84 (4), 533-545, 2003.

[4]. J. Suomalainen, N. Anders, S. Iqbal, G. Roerink, J. Franke, P. Wenting, et al., "A lightweight hyperspectral mapping system and photogrammetric processing chain for unmanned aerial vehicles, *Remote Sensing*, 6 (11), 11013-11030, 2014.

[5]. A. M. Samad, N. Kamarulzaman, M.A. Hamdani, T.A. Mastor, K.A. Hashim, "The potential of unmanned aerial vehicle (UAV) for civilian and mapping application", in 2013 IEEE 3rd International Conference on System Engineering and Technology, Shah Alam, Malaysia, 2013, paper. 313.

[6]. Y. Arya and N. Kumar, "BFOA-scaled fractional order fuzzy PID controller applied to AGC of multi-area multi-source electric power generating systems," *Swarm and Evolutionary Computation*, vol. 32, pp. 202-218, 2017

[7]. U. Caydas, A. Hascalik, and S. Ekici, "An adaptive neuro-fuzzy inference system (ANFIS) model for wire-EDM," *Expert Systems with Applications*, vol. 36, pp. 6135-6139, 2009.

[8]. G.N. Marichal, M.T. Rodriguez, A. Hernandez, S.C. Rivera, P. Campoy, "Vibration reduction for vision systems on board unmanned aerial vehicles using a neuro-fuzzy controller", *Journal of Vibration and Control*, vol. 20 (15), pp. 2243-2253, 2014.

[9].   M. I. Al-Saedi, H. Wu, and H. Handroos, "ANFIS and Fuzzy tuning of PID controller for trajectory tracking of a flexible hydraulically driven parallel robot machine", *Journal of Automation and Control Engineering*, vol. 1, pp. 70-77, 2013

[10]. S. Kurnaz, O. Cetin, and O. Kaynak, "Adaptive neuro-fuzzy inference system based autonomous flight control of unmanned air vehicles", *Expert Systems with Applications*, vol. 37, pp. 1229-1234, 2010

[11]. Paw, "Synthesis and validation of flight control for UAV", Phd. Thesis, Faculty of the Graduate School of the University of Minnesota, December 2009.

[12]. S. Ulus, I. Eski, "Lateral and longitudinal dynamics control of a fixed wing UAV by using PID controller", 4th. International Conference on Engineering and Natural Sciences (ICENS), Kyiv,Ukraine, 02-06 May 2018, paper 994.

[13]. Nelson R. C., Flight Stability and Automatic Control, 2nd ed., Mc. Graw Hill International Editions Aerospace Sciences and Tech. series, Singapore, 1998.

[14]. J.S.R. Jang, "ANFIS:adaptive-network-based fuzzy inference system," *IEEE Trans. Systems, Man, and Cybernetics*, vol. 23(3), pp. 665-684, 1993.

Gear Fault Modelling by Using Acoustic Measurements and Artificial Neural Networks

Saban Ulus[1], Memduh Suveren[2]

Abstract

Rotating machine elements in mechanical systems such as gears and bearings have a major impact to maintain machine power transmission and machine working life in a healthy situation. Some mechanical failures including cracked tooth and pitting faults especially in gears may have a crucial effect on system failure and safety. However, fault condition monitoring (FCM) at rotating machine parts was studied mostly by using classical vibration monitoring in the literature. In this study, acoustic measurement results were obtained experimentally from a single stage gearbox. Experiments were performed by measuring different running speeds, loading conditions and fault characteristics under dry friction conditions of gears. According to results, an artificial neural network (ANN) design for predicting and modelling different possible faults of the system was created. Acoustic results were evaluated by using training data, test data and validation data. This work shows that ANN design represents a good accordance with experimental results and specify predictable information about fault varieties occurred at gearbox.

Keywords: Acoustic, artificial neural networks, fault condition monitoring, fault modelling, gears

1. INTRODUCTION

In recent years, artificial neural networks and artificial intelligence techniques have been found in many areas of our academic and daily lives. As a result of advances in technology it has become possible to see artificial intelligence applications in many areas. Therefore, artificial neural networks, fuzzy logic, genetic algorithm applications etc. can be used in predictive maintenance techniques of machines and modeling of the systems. Rotational moving mechanisms can be seen in many areas and many machines. In the power transmission systems of the machines, gear wheels are of great importance in transmitting movement and changing direction. Failure of such machine elements during the operation of the system may affect the entire production line and can also pose a great danger in terms of safety in case of failure of components such as in helicopter gearboxes. In general, most of the failure cases of the gear systems occur because of the defects such as tooth breakage, pitting, cracked tooth root. Some defects can develop without giving any symptoms if it was not measured by any sensor or measuring devices. Therefore, it is very important to measure and follow the conditions of the machinery systems before their failure and stoppage of the systems.

In the literature, there are so many works about condition monitoring of the systems such as classical vibration monitoring [1], [2], [3], acoustic emission [4], [5] thermography analysis [6], oil debris analysis [7] etc. ANN architectures are also investigated by the researchers in a wide range of applications nowadays. Chen et al. [8], presented a paper which was related to implementation of deep learning for fault identification and fault classification in gearboxes. Researchers applied 20 different test case combinations each included 12 different basic conditions. They measured time-domain signals and frequency domain signals and it was noted that proposed method was highly reliable in FCM. Kane and Andhare [9], studied on gear fault diagnosis by using ANN and application of psychoacoustics. They analyzed faulty and good gear conditions by acquiring data from a gearbox test rig. ANN for gearbox system and psychoacoustic features was the ability that they could have the potential for the end of line prediction of gearbox. Ulus et al. [10] investigated fault condition of different gears at different loading conditions, different running speeds by using acoustic emission measurements. Statistical

results such as root means square, crest factor and kurtosis were analyzed, and it was noted that acoustic measurements had some advantages over classical techniques.

This paper is organized as follows; Section 2 gives an experimental system perspective and methods for fault classification for gears. Results and discussion part are given in Section 3 and in the final section, conclusion is presented in Section 4.

2. EXPERIMENTAL SYSTEM AND METHODS

Gears have a vital role in most machineries because of transmitting power, changing direction of the motion and need for continuous production processes. Some of the most used gear types in the industry are spur and helical gears. In this experimental work, spur and helical gears were used for gear fault analysis. The experimental system had single stage gearbox and loading disc to implement different load conditions. It was used 3 KW and 3 phase electric motor to control the running speed of the shaft and to run at different running speeds. In Figure 1, experimental test rig is shown, and it has a microphone unit to obtain acoustic signals from the gear sound resource.
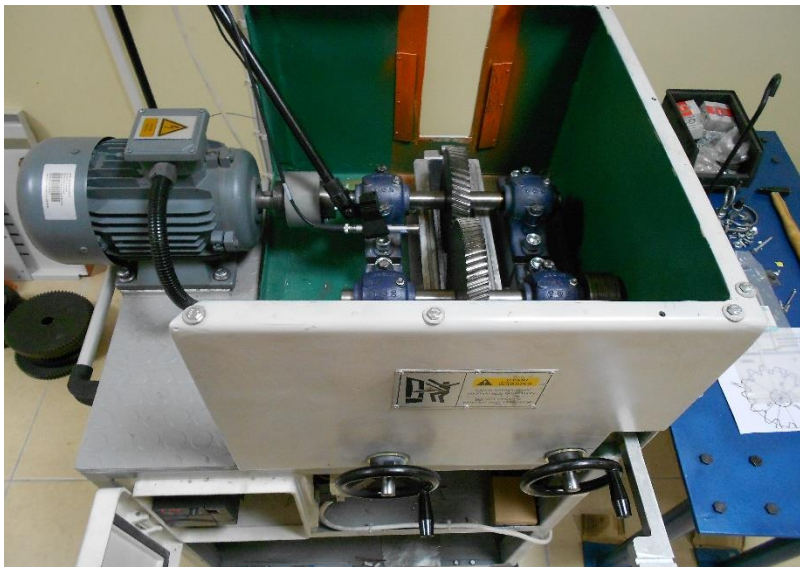
Figure 1. Experimental gearbox system

In the experiments, used gears had a module of 3 and pinion gears had 51 teeth while driven gear's tooth number was 70. System was run at dry friction condition and a Bruel-Kjaer (B&K) free-field 4189-A-021 microphone unit was located near the meshing gear position. In Table 1, spur and helical gear specifications are given. Because the shaft centers of the spur and helical gears were different, the bearing locations were produced as adjustable sliding mechanism.

Table 1. Gear Specifications used in the experiments

	Helical Gear		Spur Gear	
Parameters	**Pinion**	**Driven Gear**	**Pinion**	**Driven Gear**
Num. Of Teeth	51	70	51	70
Module	3 mm	3 mm	3 mm	3 mm
Shaft Angle	90°	90°	90°	90°
Addendum	3 mm	3 mm	3 mm	3 mm
Dedendum	3,5 mm	3,5 mm	3,5 mm	3,5 mm

Pitch Circle Diameter	162,82 mm	223,48 mm	153 mm	210 mm
Face Width	25,1 mm	25,1 mm	25,1 mm	25,1 mm
Direction	Right	Left		
Pressure Angle	20°	20°		
Helix Angle	20°	20°		

In the experiments, a cracked tooth root profile was created artificially at the driven gear tooth. Figure 2 shows the type of the gear fault evaluated in the system.

Figure 2. The artificially created cracked tooth defect

Measurements were completed by using a Bruel-Kjaer (B&K) portable multi-channel vibration and sound pulse analyzer and obtained data in the time domain was converted to frequency domain by the analyzer that capable to use Fast Fourier Transform. Frequency data between 0-3200 Hz was obtained and evaluated in the ANN structure for fault classification.

2.1 ANN METHODOLOGY FOR FAULT DIAGNOSIS

The methodology of this study is to determine the gear sound data for different input characteristics of the gear system. Acoustic data generated by the gear system was obtained by using ANN structure depending on different input conditions such as operating speed, gear type, operating frequency and loading conditions. The ANN structure of the gear system depending on the different input characteristics is shown in Figure 3.
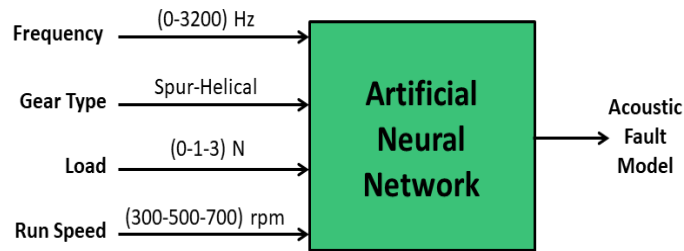
Figure 3. The ANN structure of gear system

This experimental study was carried out for 18 different cases for 2 different gear types (Spur, Helical), 3 different load amounts (0N, 1N, 3N) and 3 different operating speeds (300rpm, 500rpm, 700rpm). In addition, acoustic data of the gear system for all cases were obtained at frequencies in the range 0 to 3200Hz. All data as the input of ANN was normalized and adjusted to a range of 0 to 1. In the gear type, spur gear was implemented as 0 while helical gear was 1. For the running speed, 300, 500, 700 rpm speeds were normalized to 0, 0.5, 1 respectively. Similarly, frequency and load values were normalized to a range of 0 to 1.

In the next step, fault detection process was performed according to acoustic sound data by using Matlab® software. In Matlab® program, 6 different scenarios including 2 different training algorithms and 3 different training functions for each case were examined. Figure 4 shows the network structures of Feed Forward Back Propagation (FFB) and Cascade Forward Back Propagation (CFB) training algorithms used in Matlab®. Based on our previous experience [11], two hidden layers were used in both algorithms with 30 neurons in each layer

as shown at Figure 4. In addition, the performance of Levenberg Marquardt (LM), Bayesian Regulation (BR) and Scaled Conjugate Gradient (SCG) training functions in fault detection were examined for each training algorithm.
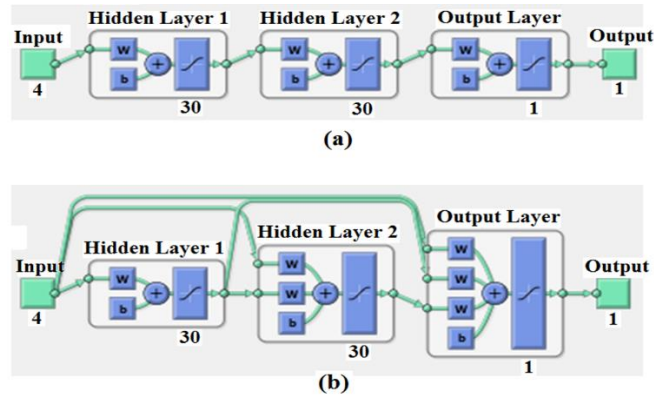
Figure 4. (a) FFB Train Algorithm Structure (b) CFB Train Algorithm Structure

In order to perform a performance analysis for each scenario, 85% of the data was used to train the ANN network and 15% was used to test the performance for each scenario. In addition, the test and train data were randomly selected for each scenario at the beginning and each was given 10 minutes to find the results.

3. RESULTS

In order to find acoustic fault detection model of the gearbox system, experimental studies were performed for 2 different gear types. In the experimental system, which was established by using spur and helical gear, sound data were obtained with acoustic sensors. Also, the system was operated in dry friction conditions without oil.

Table 2. shows the network training results obtained according to gear type, load amount and working speed. Here, two different training algorithms such as FFB and CFB were applied for ANN training and test results according to different training functions such as LM, BR, SCG. For each scenario, the program was run 10 times and a total of 60 runs were performed. As a result, the average values of these scenarios are shown in Table 2. In each scenario, Root Mean Square (RMS), mean and standard deviation (Std) values were compared.

Table 2. Six different ANN scenario results

Algorithms		Train			Test		
		LM	BR	SCG	LM	BR	SCG
FFB	RMS	3,739	3,779	4,005	4,017	3,992	4,194
	Mean	2,930	2,973	3,136	3,149	3,117	3,275
	Std	2,323	2,334	2,491	2,494	2,494	2,619
CFB	RMS	3,941	3,802	4,152	4,134	4,015	4,347
	Mean	3,073	2,988	3,241	3,212	3,145	3,365
	Std	2,467	2,351	2,596	2,601	2,496	2,751

When the results given in the table are examined, the best results are found in FFB algorithm. While the LM algorithm gives good results at the training data, the BR algorithm appears in front of the LM with a slight difference at the test data. When the total performance in the test and training is examined, it is seen that LM and BR are very close to each other. For this reason, the speed of the algorithms was compared in the Table 3 and their net performances were determined.

Table 3. Number of running epochs in the 10 minutes

	FFB	**CFB**
LM	891	591
BR	787	544
SCG	28260	47440

When the table was examined, it is seen that how many epochs the algorithms have solved in equal time. It is clear the fastest training function using more epochs in 10 minutes was SCG. This was followed by LM and BR respectively. In addition, it is seen that LM and BR functions were faster in FFB in terms of training algorithms. When the results given in both tables are combined, it is seen that the LM function was slightly ahead of BR function. For this reason, Motivation was on FFB training algorithm and LM function. For this scenario, the best and worst results were investigated, and the results are given in Table 4.

Table 4. Best and worst neuron results for FFB+LM scenario

		RMS	**Mean**	**Std**
Best	**Train**	3,695	2,906	2,283
	Test	3,886	3,047	2,413
Worst	**Train**	3,803	2,980	2,363
	Test	4,143	3,250	2,570

In case of the best and worst neuron results for the FFB + LM scenario, it is seen that the results were close and the mean difference for the train and test at the best and worst neuron was 5% and 8% respectively. This result shows that the selected algorithms worked stable. Figures 5 and 6 show the test results for the best state of the ANN approach (combination of FFB and LM). In Figure 5, 40 randomly selected data were used to illustrate better visualization of the figures rather than show all data. In Figure 6, we obtained test results, in case of selection of helical gear, 1N load and 500 rpm running speed over all frequencies
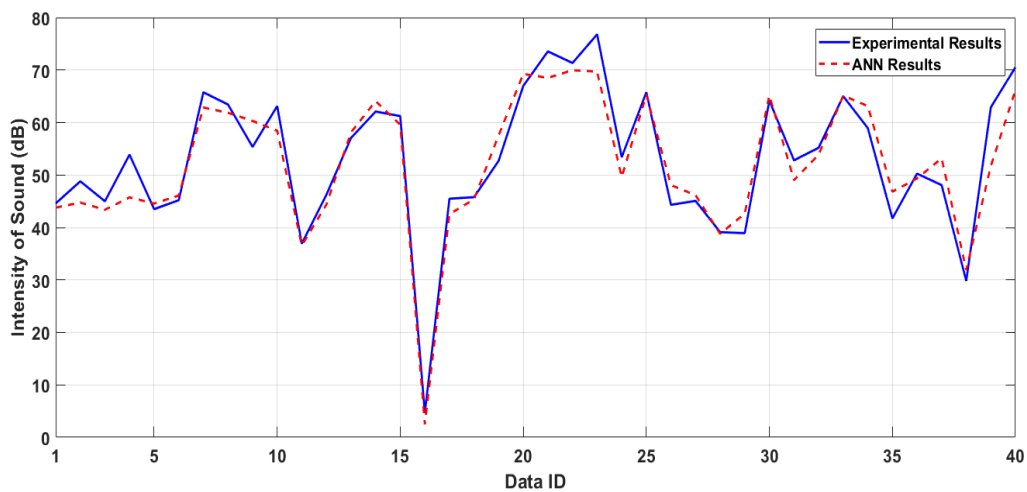
Figure 5. Random test data results for LM+FFB Scenario
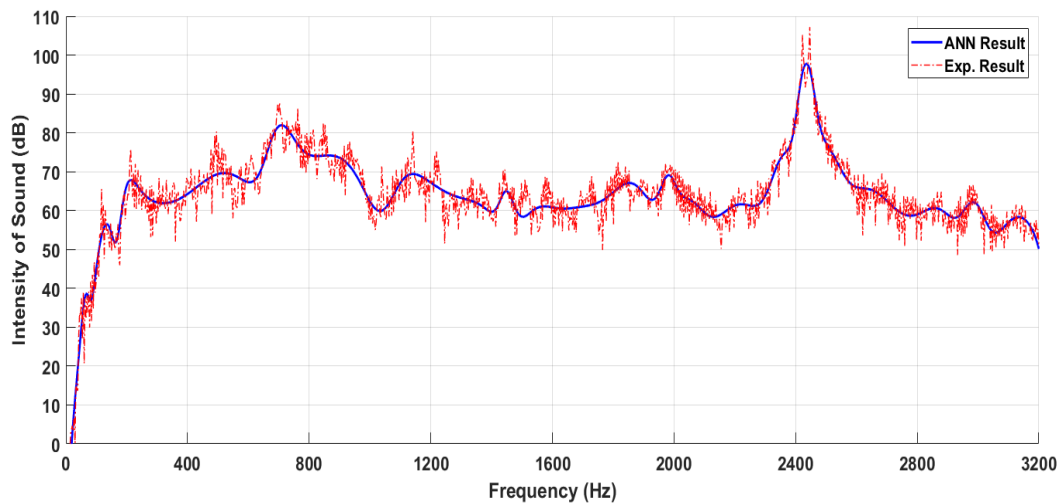
Figure 6. Test data results for Helical gear, 1N load and 500rpm running speed over all frequencies at LM+FFB Scenario

Figure 5 and 6 clearly show that the FFB + LM scenario models the acoustic fault detection system so experimental and ANN results have a good combination and accuracy between them.

4. CONCLUSIONS

In this paper, we discussed the problem of fault classification in the gear systems which have different fault conditions, different running speeds and different loading conditions. One of the most seen gear faults, cracked tooth root fault was chosen for experiments. ANN structure was a tool for classification gear faults and models. Spur and helical gears were run at 3 different running speeds which was 300 rpm, 500 rpm, 700 rpm respectively. To obtain data, acoustic signals were acquired and used for training process in the ANN structure.

In the training process, 85% of all 19206 data were used for analysis. Rms, mean and standard deviation were calculated for different scenarios. In the results, it is concluded that FFB algorithm was more accurate than CFB algorithm results in terms of both training and testing processes. Even so, CFB results and resulting train and test errors were not so big and CFB error was also in acceptable range. While FFB-LM scenario gave less error for training, FFB-BR scenario was better for accuracy in testing results. SCG scenario was the fastest one even if, it had bigger training and test error. Figure 5 and 6 show that the accuracy how well fitted to the experimental results.

As a result, it is clearly seen that ANN is able to classify faulty or normal gears by using acoustic emission and frequency data. ANN may be usable for early diagnosis of system faults without operator knowledge.

ACKNOWLEDGMENT

REFERENCES

[1]. Z. Cheng, N. Hu, X. Zhang, "Crack level estimation approach for planetary gearbox based on simulation signal and GRA", *Journal of Sound and Vibration, vol. 331, pp. 5853-5863, 2012*.
[2]. S. Choi, C. Li, "Estimation of gear tooth transverse crack size from vibration by fusing selected fear condition indices", Measurement Science and Technology, VOL. 17, PP.2395–2400, 2006.
[3]. P.L. Dempsey, D.G. Lewicki, D.D., Le, "Investigation of current methods to identify helicopter gear health", in Aerospace Conference by the IEEE and AIAA, Big Sky, Montana, NASA/TM—2007-214664, 2007, paper 01.
[4]. A. Saxena, A. Saad, "Evolving an artificial neural network classifier for condition monitoring of rotating mechanical systems", *Applied Soft Computing*, Vol. 7., pp. 441-454, 2007.
[5]. Y.H.Ali, R.A. Rahman, R.I.R. Hamzah, "Acoustic emission signal analysis and artificial intelligence techniques in machine condition monitoring and fault diagnosis: A review", *Jurnal Teknologi*, vol. 69(2), pp.121-126, 2014.
[6]. A.M.D. Younus and B.S. Yang, "Intelligent fault diagnosis of rotating machinery using infrared thermal image," *Expert Systems with Applications*, vol. 39(2), pp. 2082–2091, 2012.

5TH INTERNATIONAL CONFERENCE ON ENGINEERING AND NATURAL SCIENCE
12 - 16 June 2019 Prague

[7]. C. Li and M. Liang, "Extraction of oil debris signature using integral enhanced empirical mode decomposition and correlated reconstruction", *Measurement Science and Technology*, vol. 22(8), 2011.

[8]. Z.Q. Chen, C. Li, R.V. Sanchez, "Gearbox fault identification and classification with convolutional neural networks", *Shock and Vibration,* vol. 2015, Article ID. 390134, 2015. http://dx.doi.org/10.1155/2015/390134

[9]. P.V. Kane and A.B. Andhare, "Application of psychoacoustics for gear fault diagnosis using artificial neural network", *Journal of Low Frequency Noise, Vibration and Active Control",* vol. 35(3), pp. 207-220, 2016.

[10]. S. Ulus, S. Erkaya, "An experimental study on gear diagnosis by using acoustic emission techniques", *International Journal of Acoustics and Vibration,* vol. 21(1), pp. 103-111, 2016. http://dx.doi.org/10.20855/ijav.2016.21.1400

[11]. S. Ulus, M. Suveren, S. Erkaya, "A vibration-based fault model of gear systems using neural predictor", *Conference on Advances in Mechanical Engineering, Journal of Thermal Eng.,* YTU, Istanbul, 10-13 May2016, paper 426.

Investigation of the Effect of Diameter Size Distribution of Bond Mill Balls on the Determination of the Bond Work Index

Vedat Taylan Engin[1], Ceren Uygun[2], Mehmet Tanriverdi[2]

Abstract

Comminution is one of the irreplaceable operations in many industrial processes. It is used not only producing fine or finest material for the next industrial step but also used liberation of the minerals before subsequent mineral processing operations. On the other hand, comminution is the most expensive operation of the process. Therefore, scientific and technological studies on comminution technology are increasing. In comminution; the most important thing is the effective use of energy. To design crushing and grinding machinery, Bond Work Index Method can be used.

In this study, Aydin region feldspar ore was used. It was crushed using a jaw crusher with a gap size of 4 mm. A roll crusher was used as a secondary crusher to crush material below 3.35 mm (100%). Following the Bond Standard Test Procedure, applied for two different samples with the same properties. One of the tests was used that exact diameter (nominal) Bond balls and, the other test was used that abraded balls (not on the exact diameter).

The purpose of this study is to the evaluation of any differences between these two tests conducted with different ball size distributions.

Keywords: Bond Work Index, Bond Mill, Bond Mill balls, Bond Mill ball diameter size distributions.

1. INTRODUCTION

Comminution is an operation in many industrial processes such as mineral processing, cement, ceramic, food and pharmaceutical industries. It is usually carried out in various stages, starting with primary crushing and ending with the finest size reduction. On the other hand, comminution is the most expensive operation of the process. Therefore, scientific and technological studies on grinding technology are increasing. The most important thing in grinding is effective to use of energy [1].

The Bond work index is a physical property that is different for each mineral. For this reason, Bond grinding test is required for each ore. Bond grindability testing is the most commonly used method in the design of grinding circuits in an ore preparation plant, in sizing mills, in determining power requirements and in evaluating mill performances. BWI (Bond Work Index) is an important step in mineral characterisation. It is a guide in decreasing energy consumption and increasing comminution efficiency, and it gives satisfactory results in industrial applications [2].

The standard Bond grinding media consists of 285 balls with a total weight of 20125 g. In this study, the two Bond tests were compared, which applied for same Feldspar ore, with the standard Bond ball diameter and standard ball numbers and with abraded ball diameter and different ball numbers. The main goal of this study is the determination of any differences between the results of these two tests conducted with different ball size distributions.

---

[1] *Corresponding author: Dokuz Eylul University, Department of Miningl Engineering, 35390, Buca/Izmir, Turkey.*
  taylan.engin@deu.edu.tr

[2] *Dokuz Eylul University, Department of Miningl Engineering, 35390, Buca/Izmir, Turkey,* ceren.bursa@deu.edu.tr

2. MATERIAL AND METHODS

Feldspar samples taken from KALTUN Mining (area of Cine-Milas) Mugla / Turkey, were used in this study. In the experimental studies, the standard Bond test procedure was applied as two different ball size distribution. One of the tests named nominal ball charge, the other is abraded ball charge (Figure 1.). The difference between these two tests is that the size distribution of Bond Mill balls as given in Table 1.

Table1. Size distributions of the grinding media (balls) of the two Bond Tests (All the parameters are the same except for the size distribution)

Original Bond Mill Ball Charge			Nominal Ball Charge			Abraded Ball Charge		
Ball diameter (mm)	Weight (kg)	Number of balls	Ball diameter (mm)	Weight (kg)	Number of balls	Ball diameter (mm)	Weight (kg)	Number of balls
38.10	8.800	43	40.00	11.295	43	38.10	8.516	38
31.75	7.209	67	30.00	7.403	67	30.00	7.251	66
25.40	0.672	10	25.00	0.640	10	25.40	1.065	16
19.05	2.012	71	20.00	2.315	71	19.05	1.989	71
15.87	1.432	94	15.00	1.297	94	15.80	1.519	94
Total	20.125	285	Total	22.950	285	Total	20.340	285
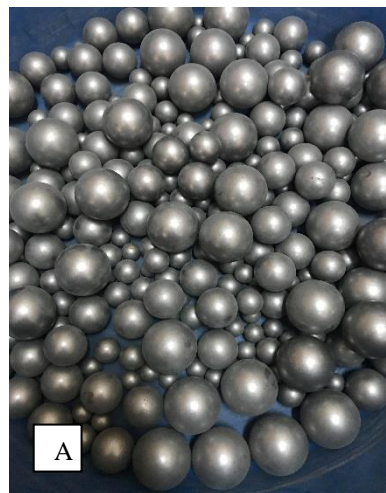
Figure 1. (a)   Nominal ball charge, (b) Abraded ball charge

2.1. The test of standard ball mill Bond grindability

According to Bond Work Index Method, the feed sample is prepared by stage crushing to pass a 3.35 mm screen [3]. The Bond grindability tests were conducted dry feed materials in a standard ball mill (30.5 x 30.5 cm) (Figure 2.) [5]. Then, screen analysed with standard screens and packed into a 700 cm^3 graduated cylinder and weighted this sample. It is calculated that the bulk density of the material (Table 2.).

Table 2. Physical properties of each Feldspar sample

	Sample name	Volume (cm^3)	Charge weight (g)	Bulk Density (g/cm^3)
Nominal Ball Charge	Feldspar	700	1335.07	1.907
Abraded Ball Charge	Feldspar	700	1312.31	1.874

Figure 2. Bond ball mill

It has a revolution counter and works at 70 rpm. The first grinding cycle usually begins to run for 100 revolutions. The test procedure takes from 6 to 10 grinding cycles with the required amount of material for the whole procedure being approximately 10 kg [6-7]. The work indices were determined at a test sieve size of 100 μm. Bond grindability tests were conducted with both nominal ball charge and abraded ball charge. Sieve analysis was performed for each cycle. The Bond work index values (W_i) are calculated from equation 1 below.

$$W_i = \frac{44.5}{P_i^{0.23} G_{bp}^{0.82} [\frac{10}{\sqrt{P_{80}}} - \frac{10}{\sqrt{F_{80}}}]} ; \left(\frac{kwh}{st}\right) \tag{1}$$

W_i= Bond work index (kwh / t)

P_i= Test sieve mesh size (μm)

G_{bp}= Weight of the test sieve fresh undersize per mill revolution (g/ rev)

F_{80}= Sieve mesh size passing 80% of the feed before grinding (μm)

P_{80}= Opening of the sieve size passing 80% of the last cycle test sieve undersize product (μm) [4]

For each sample F_{80}, P_{80}, G_{bp} and W_i values are given in Table 3.

Table 3. The values of F_{80}, P_{80}, G_{bp} and W_i of each sample

	Total grinding cycle	P_i (μm)	F_{80} (μm)	P_{80} (μm)	G_{BP} (g/rev)	W_i (kwh/t)
Nominal Ball Charge	6	106	1900	91	1.4186	15.35
Abraded Ball Charge	9	106	1700	88	1.3722	15.68

3. RESULTS AND DISCUSSION

Defining work index (W_i), is "as the total work input in kw-hr per ton required to reduce the material from theoretically infinite particle size to product of normal distribution, 80% of which passes 100 microns, this reduction being performed under the same conditions and assuming the material characteristic to be the same as those prevailing during actual reduction over a finite size range in the machine being considered" [8].

When the circulating load is 250 %, product sieve undersize equal to 1/3.5 of the total material in the mill. Then the particle size distribution balance is provided and, G_{bp} value calculated as the average of the last three G_{bp} value.

In this study, the original Bond Mill ball charge is 20.125 kg, the nominal ball charge is 22.950, and abraded ball charge is 20.340 kg. These charge's size distributions are given in Table 1. Nominal ball charge's average G_{bp} value (1.4186) is bigger than the abraded ball charge (1.3722). But W_i value has not changed enough to affect the result.

4. CONCLUSIONS

In this study, headsamples and all the operations in the experiments were tried to make a standard. And interpreting the experimental data, it was accepted that every operations were done the same standard or too close to each other. The results obtained with these assumptions are as follows.

- Although there is a 200 μm difference between the F_{80} values of the two tests, the P_{80} values are very close to each other. At the same time, there was no significant change in W_i values due to the small change in G_{bp} values.

- The average nominal ball size is 32.93 mm; average abraded ball size is 31.02 mm. Wi values come close to each other. There was no significant change in W_i value despite about 2 mm drop in average ball diameters.

- The Bond Work Index test made with abraded balls has more cycles than made with nominal balls. So at the nominal ball charge G_{bp} value that must be done for real value with less cycle than the abraded ball charge.
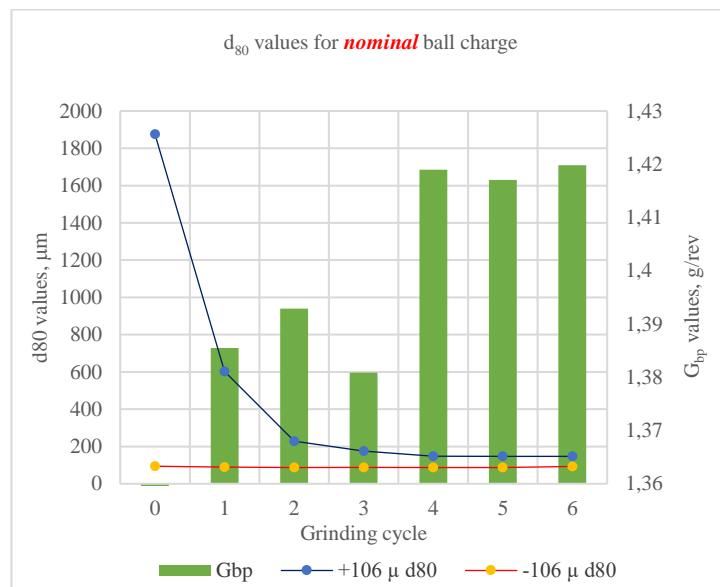
Figure 3. d80 values for nominal ball charge

- When examined at the graphs, it can be seen the d_{80} values of -106 μm and +106 μm sieve analyzes made at the end of each round. As is seen, there is no significant difference between the two tests in terms of d_{80} values (Figure 3-4).

- For nominal ball charge, $Gb_{bp\ avg}$ is bigger than the abraded ball charge.

- For this feldspar, about 2 mm abrasion is not affected the W_i value. In the next studies, the lower limit of abrasion that not affect the W_i values will be investigated.
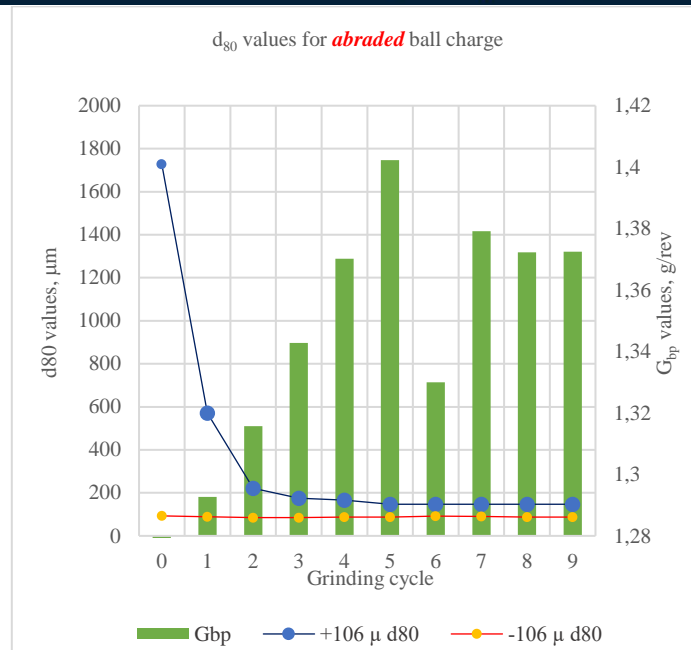
Figure 4. d₈₀ values for abraded ball charge

REFERENCES

[1]. V. Deniz, "Relationships between Bond's grindability (G_{bg}) and breakage parameters of grinding kinetic on limestone", *Powder Technology*, vol. 139, pp. 208–21, Jan. 2004.

[2]. B.A. Rodriguez, G. G. Garcia, " Product size distribution function influence on interpolation calculations in the Bond ball mill grindability test" International Journal of Mineral Processing, vol. 157, pp. 16-20, Sept. 2016.

[3]. E. Kaya, P.C. Fletcher, P. Thompson, "Reproducibility of Bond grindability work index", Minerals and Metallurgical Processing, vol. 20, pp. 140-142, August 2003

[4]. F.C. Bond, W.L. Maxson, " Standard grindability tests and calculations." Trans. Soc. Min. Eng., AIME vol. 153, pp. 362-372, 1943.

[5]. H. Ipek, Y. Ucbas, C. Hosten, " The bond work index of mixtures of ceramic raw materials." Minerals Engineering, vol. 18, pp. 981-983, February 2005.

[6]. H.H. Gharehgheshlagh, " Kinetic grinding test approach to estimate the ball mill work index", Physicochemical Problems Mineral Processing, vol. 51(1), pp. 342-352, 2016.

[7]. V. Deniz, H. Ozdag, " A new approach to Bond grindability and work index: dynamic elastic parameters" Minerals Engineering, vol. 16, pp. 211-217, 2003.

[8]. J. A. Holmes, "A Contribution to the study of communition- A modified from of Kick's Law," Trans. Instn. Chem. Engrs., vol. 35, p. 125, 1957.

Beneficiation of Nigde Ulukisla Region Oxidized Coarse Size (9.51/4.75 mm) Lignites

Vedat Taylan Engin[1], Ilknur Cocen[2], Ebru Tufan[2]

Abstract

From within, at the animal and plant residues into the soil occur decomposition and microbial degradation on the organic matter due to biological and physicochemical phenomena. Decomposition and microbial degradation of these tissues are defined as humification. Organic matter humification occurs with the help of microorganisms. The most important nutrition of organic matter is the groups of carbon. Humic, fulvic and hymatomelanic acids, formed as the resulting products of decomposition and microbial degradation, are long-lasting organic substances.

In this study, a jigging test conducted with 9.51/4.75 mm size fraction. With using the concentrate product of the jig test, upgraded and derived humic acid, fulvic acid and hymatomelanic acid.

Keywords: Oxidized lignites, jigging, total humic acid, free humic acid, fulvic acid.

1. INTRODUCTION

With geological times, plant and animals residues under the high temperature and pressure formed coal. As the temperature and pressure increased, the pores in the coal were reduced, the impurities were removed, the ash content of the coal decreased, and the heating content was increased. The degree of carbonization increases with increasing temperature and pressure. Coals can be classified as peat, lignite, hard coal and anthracite. Leonardite and oxidised lignite formed by lignite oxidation with atmospheric conditions. They haven't completed the process of coalification exposed to high oxidation condition and eventually reached to high humic acid content. Besides, leonardite has low heating content as fuel; it has a high content of humic acid and humic acid derivatives. Less mature coals, including oxidised lignite and leonardite, may contain a significant amount of molecules with acidic functional groups.

The organic matter extracted from soils or sediments with such reagents as $NaOH$ and $Na_4P_2O_7$ are usually fractioned based on solubility characteristics. The fractions commonly obtained include humic acid, soluble in alkali, insoluble in acid; fulvic acid, soluble in alkali soluble in acid; hymatomelanic acid, alcohol soluble part of humic acid, humin insoluble in alkali. A complete fractionation scheme is given in Fig. 1 [1].

By the end of the nineteenth century, it had been firmly established that humus was a complex mixture of organic substances that were mostly colloidal and weakly acidic properties [1].

Humic acid presence in an aqueous solution can significantly enhance the water solubility of a hydrophobic organic compound. This solubilization in solutions is often attributed to the presence of micelles. The structure of humic acids is such that it allows them to function as surfactants with the ability to bind both hydrophilic and hydrophobic materials [3]. Besides humates are widely used in agriculture as growth promoters and organic fertilizers [4], horticulture, cosmetics, drilling industry filter systems products [6].

---

[1] *Corresponding author: Dokuz Eylul University, Department of Mining Engineering, 35390, Buca/Izmir, Turkey.*
taylan.engin@deu.edu.tr

[2] *Dokuz Eylul University, Department of Mining Engineering, 35390, Buca/Izmir, Turkey. ilknur.cocen@deu.edu.tr*

Humus

Extract with alkali

Insoluble humin   Soluble

Treat with acid

(Precipitated)   (Not precipitated)

Extract with alcohol   humic acid   fulvic acid

Hymatomelanic acid

Extract with alkali

Redissolve in base and add electrolyte

(Precipitated)   (Not precipitated)

Gray humic acid   Gray humic acid
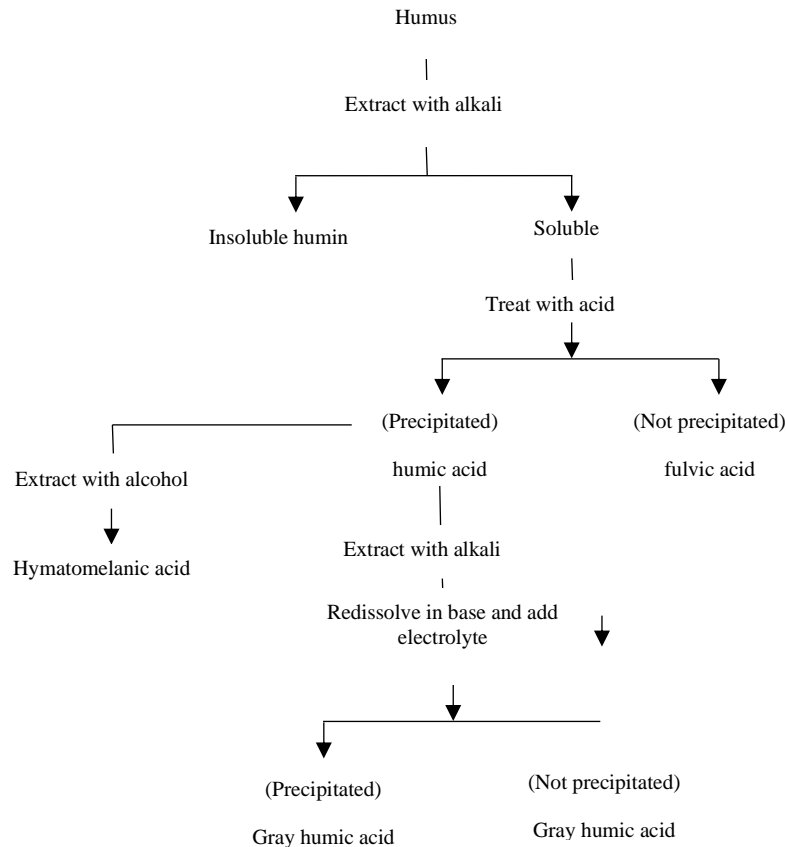
Figure 20. Scheme for the fractionation of humic substances [1]

Fulvic acids are lower molecular weight than humic acids, and soil derived materials are larger than aquatic materials. They are soluble in water at all ph values [1]. Increasing the concentration of extracted fulvic acid in water led to a sharp decrease in its surface tension [3]. Moreover, it is an important material for the medical industry.

Humin is black in colour and it is comparatively more aromatic as compared to humic acid, fulvic acid and hymatomelanic acid. It also has comparatively weaker water retaining, sorbing, and metal-binding properties than the other humic substances [3].

It is well known that humic acids from oxidized lignite, leonardite and peat pronounced biological activity, which is related to their participation in ion transfer, an affinity for biological membranes, effects on the activity of enzymes, etc. Hymatomelanic acids as an important constituent of humic substances also exhibit biological activity, and they can find use in the medical practice as antipyretics immunocorrecting agents [7].

The first task of the getting humic substances is to separate organic matter from the impurities with using gravity concentration techniques (shaking table, MGS multi-gravity separator), can be separated impurities from macerals included humic substances. This process is a pre-concentration treatment. In this pre-concentration treatment, a large part of humin removed from humus as tailing.

2. MATERIAL AND METHODS

In this paper, headsample from Nigde Ulukisla Hacibekirli region oxidized lignite (9.51/4.75 mm) upgraded with single compartment jig. Jigging is to separate minerals with significant differences in specific gravity. The light and heavy particles have separated by using their abilities to penetrate and oscillating fluid bed supported on a screen. A pulsating current of water by a plunger dilates the material so that the heavier, smaller particles penetrate

the interstices of the bed and the larger high specific gravity particles fall under a condition of hindered settling. The process and the bedding of the jig are schematically described in Figure 2 [8].

(a)   (b)a
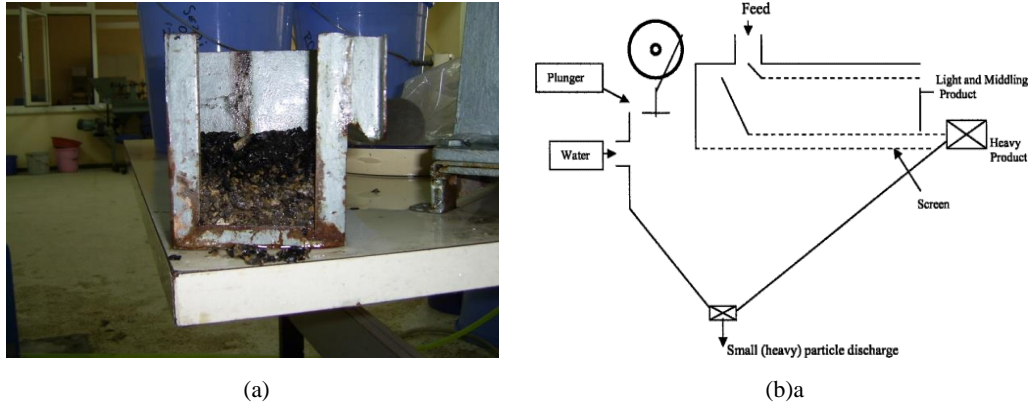
Figure 2. (a) Bedding of single compartment jig (b) Plunger type jig a schematic representation [8]

Jig pulsation by the belt mechanism rotates as 1200 rpm. And using with the concentrate of the jig; extraction prosses was applied for getting the derivatives of leonardite (humin, humic acid, fulvic acid, hymatomelanic acid). The prosses of getting the derivative of leonardite is given in Figure 3.
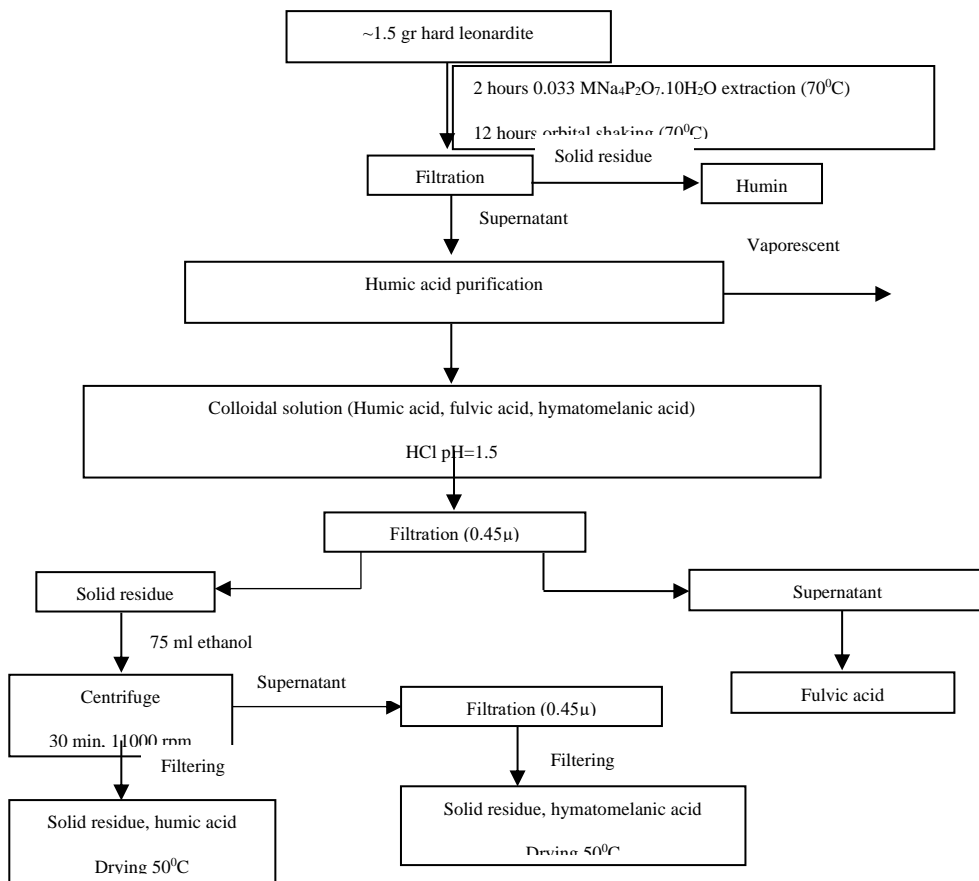
Figure 3. Extraction-evaporation process for getting humic acid derivatives

3. RESULTS AND DISCUSSION

The concentration of the headsample was done with jigging. Jigging test results are given in Table 1.

Table1. Jigging test results with respect to ash%, combustible% and THA%

Products	Weight (%)	Ash (%)	Combustible (%)	THA (%)	Yield (%) Yanabilir	Kul	THA
Concantrate	35.67	12.06	87.94	63.39	41.43	17.70	44.41
Middling	27.07	17.01	82.99	56.52	29.68	18.95	30.06
Tailing	37.26	41.32	58.68	34.88	28.89	63.35	25.53
Headsample	100.00	24.30	75.70	50.91	100.00	100.00	100.00

According to Table 1, the total humic acid value is upgraded from 50.91% (headsample) to 63.39% (jig concentrate), with 35.67% weight recovery. It means, the headsample of the extraction, upgraded as total humic acid content, and the tailing was eliminated (impurities).

In the extraction-evaporation process (Figure 3), about 1.5 gr jig concentrate was used. Extraction evaporation process results are given in Table 2.

Table2. Extraction-evaporation process results

Products	Weight (gr)	Weight (%)
Headsample	1.5226	100.00
Humin	1.2998	85.37
Humic acid	0.2198	14.44
Hymatomelanic acid	0.0030	0.19

4. CONCLUSIONS

In this laboratory work, employing jig was investigated through upgrading the Nigde Ulukisla oxidized coarse (9.51/4.76 mm) lignites. The results of the study as follows.

1. The headsample with 50.91% total humic acid contents was upgrading to 63.39% total humic acid contents, with 35.67% weight recovery and 44.41% total humic acid yield.

2. The tailing has 34.88% total humic acid content with 37.26% weight recovery and 25.53% total humic acid yield.

3. Experimental studies, when evaluated as ash content, concentrate has 12.06% ash, but this sample is oxidised lignite and low calorific value and high moisture content.

4. In the extraction- evaporation process, the humic acid yield (wt-%) is 14.44, and the humin yield (wt-%) is 85.37%.

5. Considering the formation of the coal, the mineral matter in this sample, collect in the jig tailings extraction for obtaining humin, can be done to the jig tailing. So humin yield as weight % can be higher than the jig concentration extraction process.

6. Concerning the experimental work results, from 1 kg Nigde Ulukisla region oxidised lignites, getting 627.40 gr jig concentrate with 60% total humic acid content. And, with using this concentrate can be obtained about 90 gr pure humic acid.

REFERENCES

[1]. F. J. Stevenson, Humus Chemistry Genesis, Composition, Reactions, 1st ed, United States of America, 1982.

[2]. M.P. Skhonde, A. A. Herod, T.J. van der Walt, W. L. Tsatsi and K: Mokoena, "The effect of thermal treatment on the compositional structure of humic acids extracted from South African bituminous coal," Int. J. Miner. Process, vol. 81, pp. 51–57, August 2006.

[3]. R. Khanna, S P. Agarwal, R.K. Khar, Humic Substances in Drug Development, 1st ed, India, 2009.

[4]. A. Ya. Zherebker, Y. I. Kostyukevich, A. S. Kononikhin, E. N. Nikolaev, and I. V. Perminova, "Molecular compositions of humic acids extracted from leonardite and lignite as determined by fourier transform ion cyclotron resonance mass spectrometry," Mendelev Communications, vol. 26, pp. 446-448, 2016.

[5]. J. O. Grimalt, and C. Saiz-Jimenez, "Lipids of soil humic acids. I. The hymatomelanic acid fraction," The Science of Total Environment., vol. 81/82, pp. 409-420, 1989.

[6]. M. Stefanova, L. Gonsalvesh, S. Marinov, J. Czech, R. Carleer, and J. Yperman, "Reductive pyrolysis of Miocene aged lignite humic acids, Bulgaria," Fuel, vol. 165, pp.324-330, 2016.

[7]. I. V. Efimova, S,. L. Khil'ko, O. V. Smirnova, V. S. Berezhnoi, and V. I. Rybachenko, "Antioxidant properties of hymatomelanic acids from brown coal," Solid Fuel Chemistry, vol. 47, No. 4, pp.193-196, 2013.

[8]. S. Ramachandra Rao, Ed., Resource Recovery and Recycling From Metallurgical Wastes, ser. Waste Managements. Oxford, England: Elsevier, 2006, vol. 7.

Numerical Investigation Of Zno-Water Nanofluid Flow In A Spiral Coil

Tugba Tepe[1], Kamil Arslan[2], Recep Ekiciler[3]

Abstract

In this study, ZnO-water nanofluid flow in a spiral coil was numerically analyzed. Different nanoparticle volume fractions of nanofluid (1.0%, 2.0%, 3.0% and 4.0%) were used. The study was conducted under turbulent flow regime. Constant temperature boundary condition was applied on the coil surface. The effects of using ZnO-water nanofluid as a working fluid in a spiral coil on convective heat transfer characteristics were determined in detail. Variations of convective heat transfer rate and Darcy friction factor with Reynolds number were analyzed. Also, the formation of secondary flows and temperature fluctuations in the coil were investigated with the velocity and temperature distributions. The 3.0% nanoparticle volume fraction of the ZnO-water nanofluid was obtained as the most effective working fluid for this case.

Keywords: CFD, Spiral coil, ZnO-water nanofluid

1. INTRODUCTION

Convective heat transfer plays an important role for industrial heating or cooling operations. Especially, due to the issues of efficient using of energy an important topic nowadays, increased interest in studies on heat transfer. Studies have been carried out for a long time in order to improve convective heat transfer. It is realized from studies that it can be developed convective heat transfer with changing the flow geometry or boundary conditions or improving the fluid thermophysical properties.

Improving the heat transfer performance of fluids used for convective heat transfer took place one of the most studied topics recently. One technique used to improve the performance of heat transfer fluids adding the solid particles which have higher thermal conductivity than the thermal conductivity of the fluids. Until now, this type of fluid and solid particles comprising the use of suspensions of solid particles millimeters in size is in question. As a result of the recent studies new discovery of nanofluids which have 10-50 nanometer-sized solid particles in suspension, led to increase the studies about this subject. The most important reason, even very small concentrations of nanoparticles, surprisingly nanofluids have high thermal conductivity values.

Today, metals, oxides, carbides, or nano-carbon tubes are generally used as nanoparticle in nanofluids. In the main fluid, water, ethylene glycols, cooling fluids or engine oil used often in the heat exchangers as fluid are used. It is expected that using the nanofluids for increasing heat transfer due to the high thermal conductivity of nanofluids will increase in the future.

Nanofluid is a fact that more than simply expressing mixture of liquid-solid. Some of the special characteristics of nanofluids are counted that their suspensions have distribution to be equivalent, stable, accumulation of solid particles demonstrate low levels and the lack of chemical changes. The most important parameter in determining the character of nanofluids is heat transfer coefficient. It is expressed in the studies that question of significant increase of conduction heat transfer coefficient in nanofluids depends on factors such as the Brownian movement of solid particles, liquid solid joint, which comes to the surface of the liquid layering at the molecular level, the nature of the heat transfer mechanism and the effect of nanoparticle accumulations.

---

[1]Karabuk University, Department of Mechanical Engineering, 78050, Karabuk, Turkey, *tuba78.1991@gmail.com*

[2]Corresponding author: Karabuk University, Department of Mechanical Engineering, 78050, Karabuk, Turkey, *kamilarslan@karabuk.edu.tr*

[3]Gazi University, Department of Mechanical Engineering, 06570, Ankara, Turkey, *recepekiciler@gazi.edu.tr*

Nanofluids occur from the suspension of solid nanoparticles, dimensions are in nm, in the base fluid. In the previous investigations, nanofluids have been found to provide much better heat transfer enhancement than the conventional fluids. This increase depends on the nanoparticle size, nanoparticle size distribution, the volume fraction of nanoparticles, temperature, pH, thermal conductivity of nanoparticles and base fluids [1]. The most important feature of nanofluids is that the thermal conductivity which is higher than expected or even theoretical estimates. Compared to the base fluid, the thermal conductivity of the nanofluid strongly depends on the temperature. The large surface area of the nanoparticles allows much more heat transfer. At the same time, the viscosities of the nanofluids are also higher than those of the base fluids. Previous studies have been reported that the nanofluids stabilize for months when using nanostructured stabilizing materials. Also, using nanofluids reduces pump power. Reduce the friction coefficient. It saves cost and energy of the engineering systems. Concequently, nanofluids are used in new and critical applications in electricity, nuclear applications, biomedical instruments and equipments, transport and industrial refrigeration systems.

Curved tubes are widely used in various industrial applications in order to enhance the convective heat transfer. Spiral coils are the well-known types of curved tubes which have been used in a wide variety of applications, such as heat recovery processes, air conditioning and refrigeration systems, chemical reactors, food and dairy processes. Nevertheless, the heat transfer characteristics of nanofluid flow in spirally coiled heat exchangers have rarely been investigated in literature.

Mohammed and Narrein [2] have numerically investigated the effects of using different geometric parameters and nanofluid combination on the flow and heat transfer characteristics in a coiled tube heat exchanger. Nusselt number was evaluated in terms of the heat transfer rate, pressure drop efficiency and performance index, and the results showed that some geometric parameters such as spiral radius and inner pipe diameter affect the performance under laminar flow conditions. It was found that the heat exchanger type produces better results than counterflow configuration. Aly [3] conducted a computational fluid dynamics study to investigate the heat transfer and pressure drop characteristics of water-based Al_2O_3 nanofluid flow in a coiled tube heat exchanger. The k-ε turbulence model was used in the study. It was determined that nanofluid behaved differently depending on the water and selected parameter. In addition, when compared with the same radius of curvature and Dean numbers, it was found that the heat transfer coefficient increases with increasing the volume fraction of the nanoparticles and coil diameter, and the friction factor increases with increasing the curvature ratio. Keklikcioglu and Ozceylan [4] conducted an experimental study for the thermo-hydraulic performance of a circular-sectioned pipe with coiled wire inserts placed on the inner wall of the tube. As a result, the wound wire sections caused a significant increase in both the heat transfer rate and the smooth tube due to the void spacing and voids in the friction factor. As a result, laminar boundary layer degradation has been shown to be effectively enhanced using such helical wire sections. Akhavan-Behabadi et al. [5] investigated experimentally to increase the heat transfer in the thermal inlet region of a nanofluid stream in vertical spiral conduits. As a result of this experiment; the use of helical wound tubing instead of flat wound tubing significantly improves the heat transfer rate because nanofluid flows have a higher Nusselt numbers. Akbaridoust et al. [6] have demonstrated the variations of heat transfer coefficient and friction factor of Al_2O_3-water and Cu-water nanofluid flow in a spiral coil under laminar flow condition. The wall temperature was kept at constant temperature. Experiments were performed for two types of nanoparticles in water and different volumetric ratios. It has been found that the thermal conductivity of Cu-water nanoparticles is about 18% higher than the Al_2O_3-water nanoparticles at a volumetric ratio of 2.23%. Finally, it has been also obtained that the spiral coil application is very effective in improving the thermal performance. Narrein [7] numerically investigated the various types of nanofluids on heat transfer and fluid flow properties in a spiral tube heat exchanger. The results show that nanofluids can improve the thermal properties and performance of heat exchangers. The Nusselt number was obtained at the highest rate when using CuO-water nano-fluid. Sasmito et al. [8] conducted a numerical study to investigate the heat transfer performance of planar spiral channels with various cross-sections such as rectangular, square, triangular, trapezoidal, and semicircular. Results are compared with the straight lengths of the same cross-sections. The effects of Reynolds number and Prandtl number on the convective heat transfer are discussed for various geometries. Kurnia et al. [9] carried out study about the heat transfer performance of three configurations of square cross-section spiral channels. It was obtained that the secondary flow due to the curvature has a significant effect on the flow behavior and the heat transfer performance in ducts. Suresh et al. [10] examined the convective heat transfer in a flat and helical tubes under turbulent flow condition. As a result; it was found that Nusselt number of helical tube is 19% higher than the Nusselt number obtained from the straight tube. Furthermore, the pressure loss of the helical tube is slightly higher than that of straight tube. Hashemi and Akhavan-Behabadi [11] investigated the pressure drop and heat transfer properties for nanofluid flow in a horizontal coiled pipe. It was showed that nanofluids have better heat transfer properties than base fluids in the presence of a spiral tube. Humunic and Humunic [12] investigated the heat transfer characteristics of a spiral tube heat exchanger under laminar flow conditions. It was showen that the

CuO nanoparticles added to pure water at 2% volumetric ratio increased the heat transfer rate about 14%, however; the pressure drop began to increase as the higher nanoparticle concentrations led to higher viscosity.

In this study, nanofluid flow in spiral coils was analyzed numerically. ZnO-water was used as the working fluid with different nanoparticle volume fractions (1.0%, 2.0%, 3.0%, 4.0%). The study was carried out under turbulent flow regime ($8\times10^3<Re<1.9\times10^4$). The average Nusselt numbers and the average Darcy friction factors that can be used to predict the flow and heat transfer performance in the spiral coil were obtained for each nanoparticle volume fraction. In addition, velocity and temperature profiles and secondary flows were analyzed in detail. As a result of the study, the effects of the nanofluid flow with different nanoparticle volume fractions on the flow and heat transfer characteristics of fluid flow in spiral coil were determined.

2. NUMERICAL ANALYSIS

The ZnO-water nanofluid flow in spiral coil was numerically modeled in this study. The spiral coil geometry used in the numerical study is shown in Figure 1. Inner diameter and curvature ratio of the spiral coil are 8 mm and 0.04, respectively. The number of coil turns is 5 and pitches of spirally coiled tube is 20 mm. ZnO-water nanofluid with different nanoparticle volume ratios (1.0%, 2.0%, 3.0%, 4.0%) was used as the working fluid. The study was carried out under turbulent flow conditions. A fixed surface temperature was applied to the surface of the spiral channel.
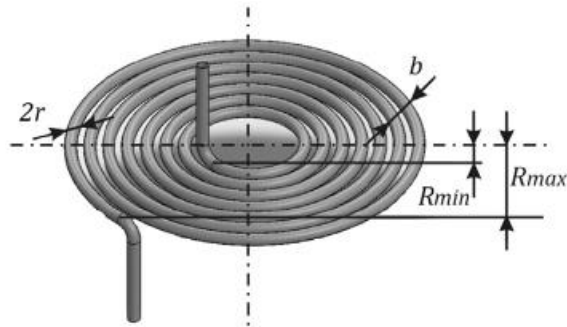
Figure. 1. Schematic view of spiral coil

The governing equations for continuity, momentum, energy, and turbulence are given as:

Continuity:
$$\nabla \cdot \vec{u} = 0$$
(1)

Momentum:
$$\nabla \cdot \left(\rho \vec{u}\vec{u}\right) = -\nabla P + \nabla \cdot (\bar{\bar{\tau}})$$
(2)

Energy:
$$\nabla \cdot (\vec{u}\rho h) = \nabla \left(k_{eff}\nabla T\right)$$
(3)

The Standard k-ε model was used for modeling of the turbulent flow. The k and ε equations can be defined as:

k-equation:
$$\frac{\partial}{\partial x_i}(\rho u_i k) = \frac{\partial}{\partial x_i}\left[\left(\mu + \frac{\mu_t}{\sigma_k}\right)\frac{\partial k}{\partial x_i}\right] + G_k - \rho\varepsilon$$
(4)

ε-equation:

$$\frac{\partial}{\partial x_i}(\rho u_i \varepsilon) = \frac{\partial}{\partial x_i}\left[\left(\mu + \frac{\mu_t}{\sigma_\varepsilon}\right)\frac{\partial \varepsilon}{\partial x_i}\right] + \frac{\varepsilon}{k}(c_1 G_k - c_2 \rho \varepsilon)$$ (5)

where $\bar{\bar{\tau}}$, k_{eff}, μ_t and G_k are defined, respectively, as

$$\bar{\bar{\tau}} = (\mu + \mu_t)\left[\left(\nabla \vec{u} + \nabla \vec{u}^T\right) - \frac{2}{3}\nabla \cdot \vec{u}\vec{I}\right]$$

(6)

$$k_{eff} = K + c_p \mu_t / Pr_t$$ (7)

$$\mu_t = c_\mu \rho k^2 / \varepsilon$$

(8)

$$G_k = \mu_t \frac{\partial u_i}{\partial x_j}\left(\frac{\partial u_i}{\partial x_j} + \frac{\partial u_j}{\partial x_i}\right)$$

(9)

Turbulence model constants were taken as: Pr_t=0.85, σ_k=1.0, σ_ε=1.3, c_μ=0.09, c_1=1.44, c_2=1.92.
The continuity, momentum, energy, and turbulence equations were solved with boundary conditions. The fluid enters the coil with uniform velocity and uniform inlet temperature, i.e.,

u=0, v=0, w=W_{in}, T=T_{in}, k=0.005W_{in}^2, ε=$C_\mu k^{1.5}$/0.03R (10)

No-slip boundary condition and constant wall temperature boundary condition were used on the coil surface,

u=0, v=0, w=0, T_s=310K, k=0, $\partial \varepsilon / \partial n$=0 (11)

At the outlet of the test section, the pressure outlet boundary condition of ANSYS FLUENT 18.2 [13] was used, i.e.

$\partial u / \partial z = 0$, $\partial v / \partial z = 0$, $\partial w / \partial z = 0$, $\partial T / \partial z = 0$, $\partial k / \partial z = 0$, $\partial \varepsilon / \partial z = 0$ (12)

The thermophysical properties of ZnO-water nanofluid were determined using Eqs. (13-16) [14-15]:

$$\rho_{nf} = (1 - \phi)\rho_f + \phi \rho_p$$
(13)

$$c_{p,nf} = \frac{\left[\phi(\rho_p . c_{p,p})\right] + \left[(\rho_f . c_{p,f})(1 - \phi)\right]}{\rho_{nf}}$$ (14)

$$\mu_{nf} = \mu_f(1 + 2.5\phi)$$
(15)

$$k_{nf} = k_f\left[\frac{k_p + k_f(n-1) - \left[\phi(n-1)(k_f - k_p)\right]}{k_p + k_f(n-1) + \phi(k_f - k_p)}\right]$$

(16)

In Eq. (16), n is the empirical shape factor given by $3/\psi$, and ψ is the nanoparticle sphericity, defined as surface area of a sphere (with the same volume as the given nanoparticle) to the surface area of the nanoparticle. For spherical nanoparticle, the value of n is 3 [16]. The thermophysical properties of pure water and ZnO nanoparticle are presented in Table 1 [17].

Reynolds number, average Nusselt number and average Darcy friction factor are defined as, respectively,

$$Re = \frac{W_i \cdot D_h}{\nu}$$
(17)

$$Nu = \frac{h \cdot D_h}{k}$$
(18)

$$f = \frac{\Delta P(D_h / L)}{\rho W_i^2 / 2}$$
(19)

Average convective heat transfer coefficient in Eq. (18) is obtained as follows [18]:

$$h = \frac{q_s''}{(T_s - (T_i + T_o)/2)}$$
(20)

Table 1. The thermophysical properties of pure water and ZnO nanoparticle

Thermophysical Property	Pure Water	ZnO
Density, ρ [kg·m-3]	997	5600
Specific heat, c_p [J·kg-1·K-1]	4179	692
Thermal conductivity, k [W·m-1·K-1]	0.613	8.4
Dynamic viscosity, μ [N·s·m-2]	0.000885	-

Computations were performed for fully turbulent flow region. Fully turbulent flow has been assumed in the case of Re>10^4 [19]. The Standard type of k-ε turbulence model with enhanced wall treatment was used for discretization of the turbulence equation. The effect of molecular viscosity was taken negligible. The Reynolds averaged Navier-Stokes and energy equations are solved numerically in conjunction with transport equations for turbulent flow. Near wall regions were fully resolved for average y^+ values nearly 1.0 in all the calculations, sufficiently resolving the laminar sub-layer (i.e. $y^+ \leq$4-5). In the present study, tridiagonal cells were created with a fine mesh near the surface of the coil (Figure 2). Close to wall, the number of grid points or control volumes were increased to enhance the resolution and accuracy. Steady segregated solver is used with second order upwind scheme for convective terms in the mass, momentum, energy, and turbulence equations. For pressure discretization, the standard scheme has been employed while the SIMPLE-algorithm has been used for pressure-velocity coupling discretization.
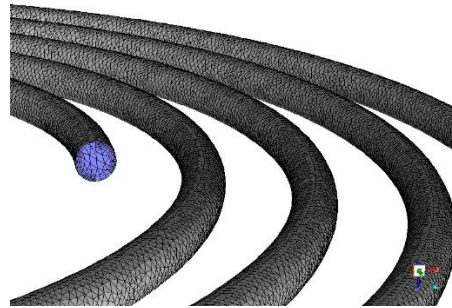
Figure 2. Mesh distribution of the spiral coil

To assure the accuracy of the results presented, a grid independence study was conducted using eight different grid sizes changing from 526735 to 1357812 for Re=1.9x10^4 to study the effects of grid size. This study was performed by refining the grid size until the variation in both average Nusselt number and average Darcy friction factor were less than 1.0 %. The grid size 1355035 points was obtained for optimum grid size. No convergence problems were observed. To obtain convergence, each equation for mass, momentum, turbulence and energy equation has been iterated until the residual falls below 1x10^{-6}.

3. RESULTS AND DISCUSSION

The results were presented in convective heat transfer rate and pressure drop in a coil. After the determination of temperature fields in the spiral coil, the convective heat transfer coefficients were calculated. In addition, Darcy friction factor was estimated as the non-dimensional form of pressure drop. Numerical results obtained under steady-state condition were presented in Figure 3 through Figure 6. The flow velocity and temperature distributions, the average Nusselt numbers and average Darcy friction factors were presented in this study to highlight the influence of the nanofluid on thermal performance of flowing in spiral coil.

Velocity distribution at the outlet of the coil can be shown in Figure 3 for nanoparticle volume fraction of 4.0% and different Reynolds numbers. It is seen in this figure that velocity profile changes with changing Reynolds numbers and maximum velocity moves towards to exterior surface of the coil because of the centrifugal effect.

| Re=8x10^3 | Re=1.4x10^4 | Re=1.9x10^4 |

Velocity Magnitude

0.00e+00   4.12e-01   8.25e-01   1.24e+00   1.65e+00   2.06e+00   2.47e+00 2.75e+00

[m/s]
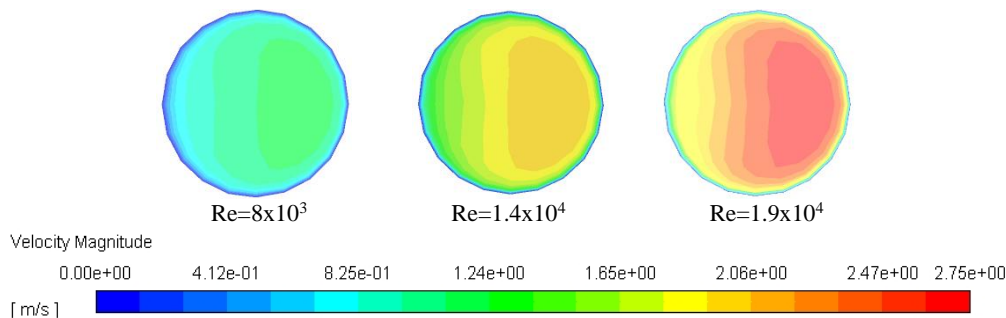
Figure 3. Isovel contours of velocity magnitude at the outlet of the coil for different Reynolds numbers

Figure 4 shows the velocity distribution along the spiral coil at different locations (turns) for Re=19051 and 4.0% nanoparticle volume fraction. It can be seen that velocity profile repeats itself after second turn into spiral coil and it reaches the hydrodynamically fully developed condition after that location. At the same locations and conditions, temperature profiles have been compared with each other and it is obtained that thermally fully developed condition is reached after fourth turn into the spiral coil (Figure 5).

Variation of average Nusselt number and average Darcy friction factor with Reynolds number are presented in Figure 6a and 6b for different nanoparticle volume fractions, respectively. It is obtained that increasing Reynolds number increases the average Nusselt number; however, decreases the average Darcy friction factor. Also, the condition of using ZnO-water nanofluid of 3.0% nanoparticle volume fraction gives the highest convective heat transfer performance. On the other hand, the value of average Darcy friction factor does not varied with addition of nanoparticles in water.

Velocity Magnitude

| 0.00e+00 | 4.12e-01 | 8.25e-01 | 1.24e+00 | 1.65e+00 | 2.06e+00 | 2.47e+00 2.75e+00 |

[m/s]
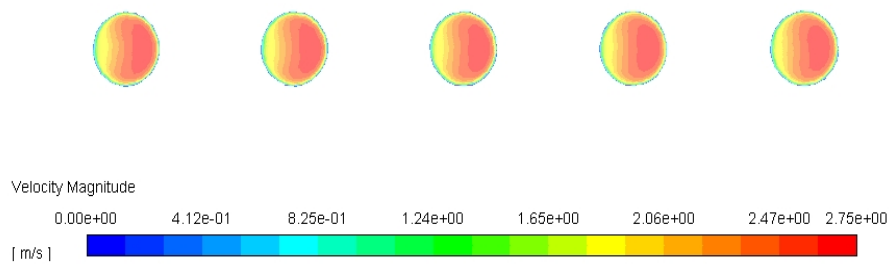
Figure 4. Isovel contours of velocity magnitude along the coil at different locations

Static Temperature

| 3.00e+02 | 3.02e+02 | 3.03e+02 | 3.05e+02 | 3.06e+02 | 3.08e+02 | 3.09e+02 3.10e+02 |

[k]
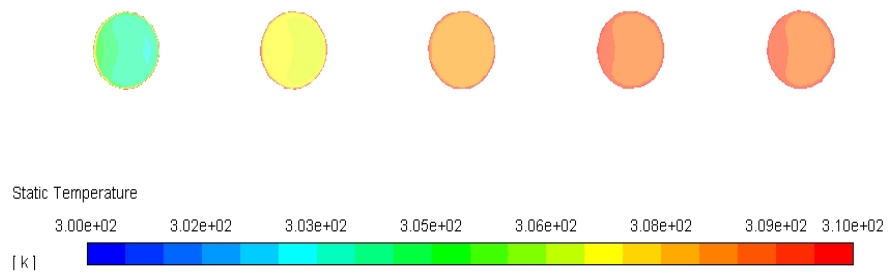
Figure 5. Isovel contours of temperature magnitude along the coil at different locations
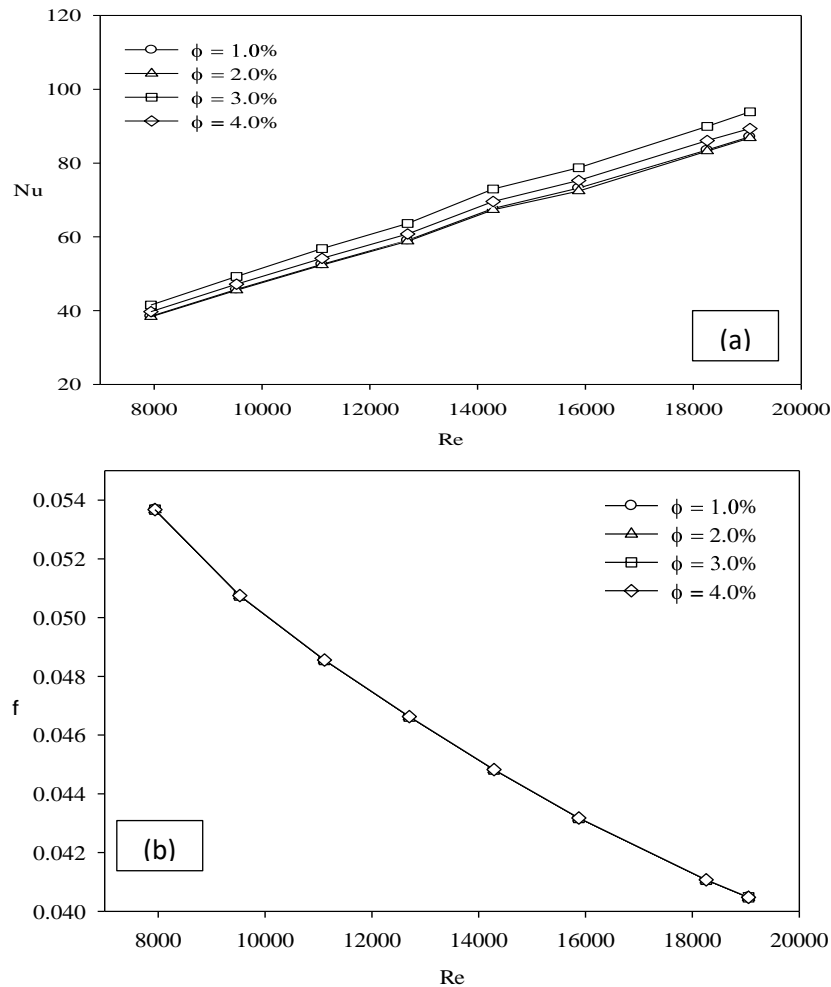
Figure 6. Variation of (a) average Nusselt number and (b) average Darcy friction factor; with Reynolds number for different nanoparticle volume fractions

4. CONCLUSIONS

Heat transfer and fluid friction of water based ZnO nanofluid flowing inside the spiral coil with different nanoparticle volume fractions were numerically investigated in this study. The hydrodynamically and thermally developing three-dimensional steady turbulent flow conditions in a spiral coil were carried out. Reynolds number was changing from 8×10^3 to 1.9×10^4. Results were given in Figure 3 to Figure 6. The results of numerical computations are presented in terms of average Nusselt numbers and average Darcy friction factors. It is obtained in this study that increasing the Reynolds number increases the average Nusselt number. On the other hand, average Darcy friction factor decreases with increasing Reynolds number. Also, 3.0% nanoparticle volume fraction of ZnO-water nanofluid has the highest average Nusselt number. The value of average Darcy friction factor does not change with addition of nanoparticles in water.

NOMENCLATURE

c_p	specific heat, $[Jkg^{-1}K^{-1}]$
f	average Darcy friction factor, [-]
h	average heat transfer coefficient in the coil, $[Wm^{-2}K^{-1}]$
k	thermal conductivity, $[Wm^{-1}K^{-1}]$
L	axial length of the coil, [m]
Nu	average Nusselt number, [-]
ΔP	pressure drop along the coil, [Pa]
P	pressure, [Pa]
q''	steady-state rate of convective heat flux, $[Wm^{-2}]$
Re	hydraulic diameter based Reynolds number, [-]
r_i	inner radius of the coil, [m]
T	fluid temperature, [K]
T_b	mean bulk temperature in the coil, [K]
T_w	surface temperature of the coil, [K]
T_i	inlet nanofluid temperature, [K]
U_i	inlet nanofluid velocity, [m/s]
U	mean velocity in the coil, [m/s]
x, r, Θ	cylindrical coordinates, [-]
V	axial velocity, [m/s]

Greek symbols

ϕ	particle volume fraction, [-]
ν	kinematic viscosity, $[m^2s^{-1}]$
μ	dynamic viscosity, $[Nsm^{-2}]$
ρ	density, $[kgm^{-3}]$

Subscript

nf	nanofluid
p	nanoparticle
f	base fluid

REFERENCES

[1]. Hadadian M., Samiee S., Ahmadzadeh H., Goharshadi E.K. "Nanofluids for Heat Transfer Enhancement – A Review", *Phys. Chem. Res*., 2013,1(1), 1-33.

[2]. Mohammed H.A., Narrein K. "Thermal and hydraulic characteristics of nanofluid flow in a helically coiled tube heat exchanger", *International Communications in Heat Mass Transfer*, 2012, 39, 1375-83.

[3]. Aly W. "Numerical study on turbulent heat transfer and pressure drop of nanofluid in coiled tube-in-tube heat exchangers", *Energy Conversion and Management*, 2014, 79, 304-316.

[4]. Keklicioglu O., Ozceylan V. "Experimental investigation on heat transfer enhancement of a tube with coiled-wire inserts installed with a separation from the tube wall", *International Communications in Heat and Mass Transfer*, 2016, 78, 88-94.

[5]. Akhavan-Behabadi M.A., Fakoor-Pakdaman M., Ghazvini M. "Experimental investigation on the convective heat transfer of nanofluid flow inside vertical helically coiled tubes under uniform wall temperature condition'', *International Communications in Heat Mass Transfer*, 2012, 39, 556-64.

[6]. Akbaridoust F., Rakhsha MA., Saffar-Avval M. "Experimental and numerical investigation of nanofluid heat transfer in helically coiled tubes at constant wall temperature using dispersion model", *International Journal of Heat and Mass Transfer*, 2013, 58, 480-91.

[7]. Narrein K., Mohammed H.A."Influence of nanofluids and rotation on helically coiled tube heat exchanger performance", *Thermochimica Acta*, 2014, 564,13-23.

[8]. Sasmito A.P., Kurnia J.C., Mujumdar A., Sadashiv W.W. "Numerical analysis of laminar heat transfer performance of in-plane spiral ducts with various cross-sections at fixes cross-section area", *International Journal of Heat and Mass Transfer*, 2012, 55, 5882-5890.

[9]. Kurnia J.C., Sasmito A.P., Akhtar S., Shamim T., Arun S.M. "Numarical investigation of heat transfer performance of various coiled square tubes for heat exchanger application", *International Conference on Applied Energy*, 2015, 75, 3168-3173.

[10]. Suresh S., Chandrasekar M., Sekhar SC. "Experimental studies on heat transfer and friction factor characteristics of CuO/water nanofluid under turbulent flow in a helically dimpled tube", *Experimental Thermal and Fluid Science*, 2011, 35, 542-9.

[11]. Hashemi SM., Akhavan-Behabadi MA. "An empirical study on heat transfer and pressure drop characteristics of CuO-based oil nanofluid flow in a horizontal helically coiled tube under constant heat flux", *International Communications in Heat Mass Transfer*, 2012, 39, 144-51.

[12]. Humunic G., Humunic A. "Heat transfer characteristics in double tube helical heat exchangers using nanofluids" *International Journal of Heat and Mass Transfer*, 2011, 54, 4280-7.

[13]. Jiang, W., Ding, G., & Peng, H. "Measurement and model on thermal conductivities of carbon nanotube nanorefrigerants" *International Journal of Thermal Sciences*, 2009, 48(6), 1108-1115.

[14]. Moraveji, M. K., & Ardehali, R. M. "CFD modeling (comparing single and two-phase approaches) on thermal performance of Al_2O_3/water nanofluid in mini-channel heat sink" *International Communications in Heat and Mass Transfer*, 2013, 44, 157-164.

[15]. Moraveji, M. K., Darabi, M., Haddad, S. M. H., & Davarnejad, R. "Modeling of convective heat transfer of a nanofluid in the developing region of tube flow with computational fluid dynamics" *International communications in heat and mass transfer*, 2011, 38(9), 1291-1295.

[16]. Peng, H., Ding, G., Jiang, W., Hu, H., & Gao, Y. "Heat transfer characteristics of refrigerant-based nanofluid flow boiling inside a horizontal smooth tube" *International Journal of Refrigeration*, 2009, 32(6), 1259-1270.

[17]. Jwo, C. S., Jeng, L. Y., Teng, T. P., & Chang, H. "Effects of nanolubricant on performance of hydrocarbon refrigerant system" *Journal of Vacuum Science & Technology B: Microelectronics and Nanometer Structures Processing, Measurement, and Phenomena*, 2009, 27(3), 1473-1477.

[18]. Vajjha, R. S., & Das, D. K. "Experimental determination of thermal conductivity of three nanofluids and development of new correlations" *International Journal of Heat and Mass Transfer*, 2009, 52(21-22), 4675-4682.

[19]. Kakac, S., Liu, H., & Pramuanjaroenkij, A. "Heat exchangers: selection, rating, and thermal design" *CRC press*, 2002.

Testing of Rosa canina L. in Coloring of Cotton Fabrics

M.Ibrahim Bahtiyari[1], Fazlihan Yilmaz[2], Huseyin Benli[3]

Abstract

In this study, the fruit of the rose hip (Rosa canina L.) plant was used in the dyeing of cotton fabrics and thus the coloration of cotton fabrics with a natural source has been tried to be investigated. For this aim; the dried fruits of rose hip were firstly milled and added to the dye bath containing only water and fabric and mordanting agents. The dyeing temperature was set as 120ºC. By this, it was planned to make dyeing and extraction simultaneously. The liquor ratio was set as 1:65 and during dyeings 6 different mordant were used, also dyeings without use of any mordant has been tested too. After the dyeings, the washed/rinsed and dried samples were evaluated in terms of fastness to washing/light and the colors obtained. As a conclusion, it was observed the fruits of rose hip can be used in dyeing of cotton fabrics.

Keywords: Cotton, rose hip fruit, Rosa canina L., color

1. INTRODUCTION

The art of applying color in fabrics has been known for a long time. Historical records of the use of natural dyes extracted from vegetables, fruits, flowers, insects and also fish date back to 3500 BC [1]. However with the introduction of synthetic dyes, the world of textiles has been totally changed, on the other hand the effluent load produced by synthetic dyes causes serious threats [2]. The environmental and health related problems due to the use of synthetic dyes has increased research on re-introduction of natural dyes [3]. Nowadays, natural dyes have been gaining importance. They are considered as renewable resources whose potential deserves to be studied in order to optimize their production and development [4].

In this study, it was aimed to examine the coloration of cotton fabrics by the use of rose hip fruits. *Rose hip* (Rosa canina L.) is a member of the botanical family Rosaceae [5]. It is also known as wild rose and native of the European Mediterranean region [6]. The Rosa genus (Rosaceae family) comprises numerous species and varieties, including rose hip plants which are grown in many areas of the world, including Europe, Africa, and Middle and West Asia [7]. Rose hips constitute a recently domesticated small fruit crops [8]. They have been found to contain higher amounts of various bioactive compounds than several other fruits and berries [9].

2. MATERIALS AND METHODS

2.1. Materials

In dyeing processes pretreated cotton woven fabrics were used and as a source of dyestuff the dried rose hip fruits after grinding were used. In figure 1 the dried rose hips before and after grinding were given.

---

[1] *Corresponding author: Erciyes University, Department of Textile Engineering, 38039, Kayseri, Turkey, ibahtiyari@yahoo.com*

[2] *Erciyes University, Department of Textile Engineering, 38039, Kayseri, Turkey, fazlihanyilmaz@erciyes.edu.tr*

[3] *Kayseri University, Mustafa Cikrikcioglu Vocational School, 38280, Kayseri, Turkey. hbenli@kayseri.edu.tr*

a) before grinding	**b)** after grinding
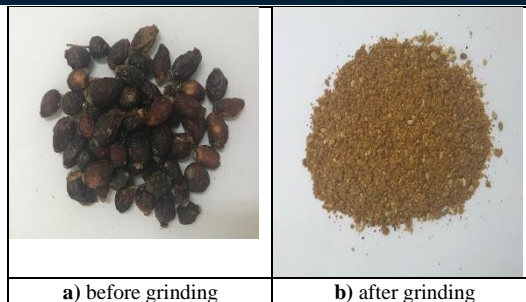
Figure 1. Dried rose hip fruits

2.2. Method

In dyeing of textile materials 6 different mordanting agents: (copper (II) sulfate ($CuSO_4.5H_2O$), tin (II) chloride ($SnCl_2.2H_2O$), iron (II) sulfate ($FeSO_4.7H_2O$), potassium dichromate ($K_2Cr_2O_7$), Zinc Chloride ($ZnCl_2$) or alum ($KAl(SO_4)_2.12H_2O$)) were simultaneously used during the dyeing. The mordant concentrations in dyeing baths were 4% for copper, tin, iron, *chromium,* and zinc based mordants and 25% for alum mordant. Meanwhile not mordanted but dyed samples were tested as well.

Dyeing was carried out at 120ºC with a procedure shown in figure 2. The liquor ratio was adjusted to 1:65 and the natural dye source (rose hip fruits) was used directly without any previous extraction process. In dyeing experiments, natural dye source and fabric were used with equal weight (1:1). Moreover to test the effect of dyeing temperature, the dyeing experiments without using any mordant were also performed at 100ºC too.
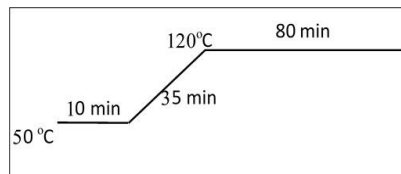
Figure 2. Dyeing procedure

After dyeing, the rinsed/washed and dried samples were then tested in terms of color efficiencies/yield (K/S) and color values (CIE L*a*b*) with a spectrophotometer (Konica Minolta CM-3600d). Moreover, the washing fastness with ISO 105-C10 standard in test condition of Test A (1) [10] and light fastness with ISO 105-B02 standard [11] were evaluated too.

3. RESULTS AND DISCUSSION

In the first part of the study, 6 different mordanting agent were investigated in dyeing with rose hip fruits. Besides, the unmordanted dyeings were also performed too.

From the Figure 3 in which the photos of the dyed samples were presented, it was observed that after dyeing of cotton fabrics with rose hip, brown colors in different shades were obtained depending on the mordanting agent type.

No mordant	Mordant type					
	$CuSO_4.5H_2O$	$SnCl_2.2H_2O$	$FeSO_4.7H_2O$	$K_2Cr_2O_7$	$KAl(SO_4)_2.10H_2O$	$ZnCl_2$

Figure 3. The photos of the dyed samples

Addition to the evaluation of the photos of the samples, the colors and color efficiencies of the fabrics were measured and collected as well. The CIE L*a*b* and K/S values obtained as a result of the dyeing processes were presented in Table 1.

As seen from the table it was observed that the rose hip can also be used without any mordanting agent and in that case L*=76.74; a*=5.81; b*=9.93 and h^0= 59.67 (the color was light brown). By the use of different mordants,

as told the color shades were changed but the highest shift in the color was obtained in the use of potassium dichromate in that case $h^0 = 74.43$ and the redness of the color was lowest.

Table 1. CIELab (L, a*, b*, C* and h°) and K/S values of the samples dyed at 120ºC*

Mordant type	CIE L*a*b* (D65)					
	K/S	L*	a*	b*	C*	hº
No mordant	0.57	76.74	5.81	9.93	11.51	59.67
Copper (II) sulfate	0.74	73.78	6.58	11.8	13.51	60.85
Tin (II) chloride	0.65	75.61	6.55	12.3	13.93	61.97
Iron (II) sulfate	0.61	74.55	4.97	9.07	10.34	61.3
Potassium dichromate	0.47	78.86	2.81	10.09	10.47	74.43
Alum	0.68	74.4	6.42	11.77	13.41	61.41
Zinc Chloride	0.57	75.83	5.78	9.84	11.41	59.59

On the other hand, the color efficiencies (color yields) were examined too. The highest color efficiency has been obtained from the dyeing with copper (II) sulfate and in that case K/S (color efficiency) was 0.74 and L* value was 73.78. The lowest color efficiency (K/S) was 0.47 and it was obtained from the dyeing with potassium dichromate.

In the second part of the study the effect of dyeing temperature on the obtained colors were also tested by making dyeings at 100-120 ºC with the unmordanted dyeing processes.

*Table 2. CIE L*a*b* and K/S values of the samples dyed without use of any mordants at 100ºC and 120ºC*

Dyeing Temperature	Mordant type	CIE L*a*b* (D65)					
		K/S	L*	a*	b*	C*	hº
120ºC	No mordant	0.57	76.74	5.81	9.93	11.51	59.67
100ºC	No mordant	0.35	83.52	2.24	9.64	9.9	76.92

It was found that the darker shades and higher color efficiencies come out in dyeings at 120ºC. The K/S was 0.57 in dyeing at 120ºC but this value was 0.35 in dyeing at 100ºC without use of any mordant. From this findings it can be told that by dyeing at higher temperature; the extraction of the dyestuff from the herbal source and dyeing of the cotton more efficiently managed.

Additionally, the fastness of the dyed colors to the washing and artificial light has been analyzed and presented in table 3.

Table 3. The fastnesses of the dyed samples with rose hip at 120ºC

Mordant Agent	Light	Washing	
No mordant	2	C.C.	4-5
		Sta.	5
CuSO$_4$.5H$_2$O	3-4	C.C.	5
		Sta.	5
SnCl$_2$.2H$_2$O	3	C.C.	5
		Sta.	5
FeSO$_4$.7H$_2$O	3-4	C.C.	4-5
		Sta.	5
K$_2$Cr$_2$O$_7$	3-4	C.C.	5
		Sta.	5
KAl(SO$_4$)$_2$.10H$_2$O	3	C.C.	4-5
		Sta.	5
ZnCl$_2$	3	C.C.	5
		Sta.	5
Sta.:Staining on cotton; C.C.:Color Change			

When the light fastness results in Table 3 were taken into consideration, it was seen that limited values can come out and depending on the mordant type the light fastness can be differed. Generally K$_2$Cr$_2$O$_7$, FeSO$_4$.7H$_2$O and CuSO$_4$.5H$_2$O mordants have ensured better light fastnesses. On the other hand, the lowest light fastness was obtained in sample dyed without use of any mordant.

In terms of washing fastness in all cases prefect results were found as seen from the table. In other words very good values were obtained both in terms of color change and staining of the reference fabric.

4. CONCLUSIONS

In the study, the use of rose hip fruit as a source of natural dyes for cotton fabrics' dyeing was investigated. As a result of the study, it was determined that rose hip fruit could color cotton fabrics. In addition, good fastness to washing but limited fastness to artificial light were obtained. In context of the study, the effect of mordants on obtained colors and fastnesses were tested and the positive effect of dyeing at higher temperature has been announced too.

REFERENCES

[1]. N. T. Vila, "Natural dyeing of silk with eucalyptus leaves extract" Global Journal of Researches in Engineering: C Chemical Engineering, vol. 18 (1), pp. 1-10, 2018.

[2]. S. Adeel, F. U. Rehman, K. M. Zia, M. Azeem, S. Kiran, M. Zuber, M. Irfan, M. A. Qayyum, "Microwave – supported green dyeing of mordanted wool fabric with arjun bark extracts" Journal of Natural Fibers, DOI: 10.1080/15440478.2019.1612810, pp. 1-15, 2019.

[3]. M. Gorjanc, M. Mozetic, A. Vesel, R. Zaplotnik, "Natural dyeing and uv protection of plasma treated cotton" The European Physical Journal D, vol. 72:41, pp. 1-6, 2018.

[4]. M. Souissi, A. Guesmi, A. Moussa, "Valorization of natural dye extracted from date palm pits (phoeniz dactylifera) for dyeing of cotton fabric. Part 2 : Optimization of dyeing process and improvement of colorfastness with biological mordants" Journal of Cleaner Production, vol. 204, pp. 1143-1153, 2018.

[5]. C. Turkben, V. Uylaser, B. Incedayi, I. Celikkol, "Effects of different maturity periods and processes on nutritional components of rose hip (Rosa canina L.)", Journal of Food, Agriculture & Environment, vol. 8(1), pp. 26-30, 2010.

[6]. B.N. Pirone, M.R. Ochoa, A.G. Kesseler and A. De Michelis, "Chemical Characterization and Evolution of Ascorbic Acid Concentration During Dehydration of Rosehip (Rosa eglanteria) Fruits", American Journal of Food Technology, vol. 2(5), pp. 377-387, 2007.

[7]. G. Fascella, F. D'Angiolillo, M. M. Mammano, M. Amenta, F. V. Romeo, P. Rapisarda, G. Ballistreri, "Bioactive compounds and antioxidant activity of four rose hip species from spontaneous Sicilian flora" Food Chemistry, vol. 289, pp. 56-64, 2019.

[8]. M. Uggla, K. E. Gustavsson, M. E. Olsson, H. Nybom, "Changes in colour and sugar content in rose hips during ripening" The Journal of Horticultural Science and Biotechnology, vol. 80 (2), pp. 204-208, 2005.

[9]. S. C. Andersson, K. Rumpunen, E. Johansson, M. E. Olsson, "Carotenoid content and composition in rose hips (rosa spp) during ripening, determination of suitable maturity marker and implications for health promoting food products" Food Chemistry, vol. 128, pp. 689-696, 2011.

[10]. ISO 105-C10:2006, Textiles–Tests for color fastness - Part C10: Color fastness to washing with soap or soap and soda, Test Condition: Test A (1), International Organization for Standardization, Geneva, Switzerland, 2006.

[11]. ISO 105-B02:1994, Textiles - Tests for color fastness-Part B02: Color fastness to artificial light: Xenon arc fading lamp test, International Organization for Standardization, Geneva, Switzerland, 1994.

Shallow and Deep Convolutional Neural Network Models for Classification of VNIR Wheat Samples

Kemal Ozkan[1], Sahin Isik [2], Busra Yavuz[2]

Abstract

Recently, the use of machine learning systems in the agricultural industry has increased tremendously for particular tasks. In this study, we have performed Shallow and VGG16 deep learning models on a new VNIR dataset in order to classify wheat samples. There are 40 classes and 200 instances per each class. While the performance shallow model has reached an accuracy of 80.13%, the VGG16 model is 91.13%. According to the results of obtained by simulations, deep learning methods were found to be more successful than parametric dependent based ones.

Keywords: deep learning models, wheat classification, VNIR imaging

1. INTRODUCTION

In particular, wheat is a very important plant for human nutrition and supplying food resources for population growth. Additionally, wheat grain is a basic nutrient of approximately 50 countries as regards to its convenient nutritive value. In Turkey, the wheat cultivation area is almost 7.7-9 million hectares and production rate is about 20 million tons. In our country, annual rate of average consumption per person is 200-250 kg, which accounts for 20 million tons of wheat should be produced when considering 80 million people. In order to achieve this production rate, about 2 million tons of kernels per 20 kg of seedlings are needed every year which accounts for approximately 9.5 million hectares of land. However, wheat production in Turkey is based mostly on dry farming with a production rate of average 20 million tons. In general, from 20 million tons, 10 million tons of wheat production are reserved for bread and 1 million tons of wheat production are used for other bakery products.

Apart from production rate, the quality of the wheat also has a great prominence. The quality of wheat kernels can be influenced by genetic or environmental factors, which may result in a great financial loss. Therefore, economical supports are greatly required to encourage producing qualified products. To meet world standards, objective systems are required for correct classification and accurate price policies in wheat industry. Thus, it is necessary to integrate the machine learning based systems for wheat classification.

Moreover, accurate identification of the wheat varieties is effective in specifying the quality degree of the produced wheat cultivar. For this reason, reliable methods should be developed for the identification and classification of wheat varieties. With this aim, we have developed a new wheat dataset, which is Visible Near Infrared (VNIR, wavelength 400-1100nm). A total of 8000 images were obtained, from 40 wheat varieties, in which each class have 200 images.

Other studies have been established on the same direction. As an example of them is the study of [1], attempted to develop a wheat identification system based on the color and NIR cameras with a purpose of classifying healthy and moderately damaged wheats. They extracted the characteristic six statistical features (maximum, minimum, mean, median, standard deviation and variance) and histogram features of the significant wavelength images of hyperspectral data and forward them to three statistical classifiers (linear, quadratic and Mahalanobis). When the NIR hyperspectral image features were combined with the best 10 color image features, they obtained the highest

average accuracy of 95.3-99.3% in the classification of healthy and damaged wheat grains. Authors of [2] has also benefited from hyperspectral imaging in order to estimate the geographic origin of wheat grains and flour samples produced in different regions of Chile with NIR imaging and chemo metric methods. In given study, the spectral data obtained with NIR camera were analyzed by using Discriminate Partial Smallest Squares (DPLS). In referred study, they correctly classified 76% of the wheat grain samples and accurately identified the 90% to 96% of the wheats according to their geographical origins. In the study of [3], the authors investigated the classification of wheat varieties by using different pattern properties of images. In total, 120 grey level wheat kernel images considered based on the standardized lighting conditions (fluorescent light). The whole set of 131 textural features have been derived from LBP (Local Binary Pattern), LSN (Local Similarity Number), LSP (Local Similarity Pattern), gray level, GLRM (Gray Level Run Length Matrix) and GLCM (Gray Level Co-occurrence Matrix). They achieved 84% accuracy in case of the experimental stage. Again, the study of [4] performed three experiments to define the best combination of spectral pretreatment method. The aim was to classify different contaminants, which are seven foreign substances (barley, canola, corn, flaxseed, oats, rye and soybean), six types of dockages (broken wheatgrass, buckwheat, straw, wheat spikelets, stones and wild oats) and 2 different animal wastes (deer and rabbit wastes). When the NIR imaging and SVM, NB and k-NN classifiers were used for the classification of wheat, $79.0 \pm 0.8\%$, $60.9 \pm 0.8\%$ and $90.1 \pm 0.6\%$ accuracy were obtained respectively. In the study of [5], the authors strived to classify thirty different cereals and nineteen different dries using Near Infrared Spectroscopy (NIRS) in their studies. A total of 276 spectra were defined as a mixed class of hazelnut from a data set consisting of 384 spectra.

The rest of the paper is organized as follows. Section II shows technical information about developed CNN based prediction models. Section III presents information about our VNIR dataset and includes experimental results. Finally, in the last section, a conclusion is given about proposed methods.

2. METHODS AND TOOLS

2.1.Shallow and Deep CNN Models

With its ability to produce an effective performance for task-oriented image and video processing applications, the CNN-based deep learning attracts great interest from particular experiments on medicine, automotive, marketing, agriculture and industry in terms of efficient use of labor force in manufacturing and equipment. The most widely known study on deep learning is the study of AlexNet [6]. They utilized a large, deep convolutional network to separate up to 1000 different high-resolution images in the ImageNet. The AlexNet architecture has 60 million parameters and 650,000 neurons, 5 convolution layers and 1000-way softmax. They achieved 37.5% and 17.0% error rates in the Top 1 and Top 5 test dataset.
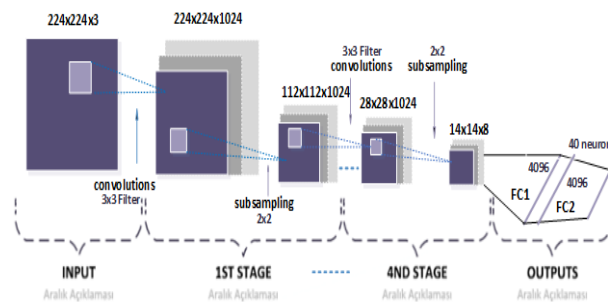
Figure 1: Proposed Shallow Model

By considering its robustness, the CNN-based deep learning has been integrated into predictive frameworks that are related to agriculture, taxonomy and plant analysis. The study of [7] focused on the classification of white beans, red beans and soy beans by using CNN methodology and achieved nearly 97% overall accuracy rate. In another study [8] empirical efforts attempted to identify diseases stated on particular plant types by comparing different deep learning architectures. The study of [9] investigated the potential ability of a particular CNN model for disease detection from rice images as the performance of developed model validated with a 95.48% accuracy rate.

In our study, we explored the generalized characteristics of deep and shallow CNN models for wheat classification. The proposed classification framework consists of two different independent models, the VGG16 and a shallow CNN model. Compared to shallow model, the VGG16 –a pre-trained model on more than one million images of ImageNet dataset- is a stratified CNN architecture with 16 convolutional layers as well as 2 fully connected layers. Technically, the VGG16 performed on 1000 object categories and it consists a total of 41

layers including Max Pooling, Fully Connected Layer, Relu Layer, Dropout Layer and Softmax classifier. The VGG16 transforms a processed image into the discriminative features, which are represented with Fully Connected Layers. To reduce an efficient and effective CNN model, we have also developed a light CNN architecture. The reason to develop an alternative shallow CNN is explained that consuming less memory resources and improving the computational time. Despite the fact that adding more layers allows for easier representation of interactions within input data and learned features, however, it is subjected to some constraints imposed by tradeoffs between computation and accuracy for a deeper architecture. By considering such factors, we have conducted experiments on a light a CNN on the basis of achieving successful identification scores and efficient allocation of resources. The Table 1 shows the layers or our proposed Shallow model. Again, the Table 2 presents the hyper-parameters setting, which are batch-size, learning rate, epoch number for both of deep and CNN models.

Table 1: The layers of our proposed Shallow model

Layers	# of filters	Filter Size
Conv1	1024	(3,3)
Conv2	1024	(3,3)
Max-Pool	-	(2,2)
Conv3	1024	(3,3)
Max-Pool	-	(2,2)
Conv4	1024	(3,3)
Max-Pool	-	(2,2)
Conv5	1024	(3,3)
Max-Pool	-	(2,2)
FC1	4096	-
Dropout	50%	
FC2	4096	-
Dropout	50%	

Both of Shallow and VGG16 models were trained on 8 GPUS. A single GPU has 16 GB memory. Code is implemented on python Keras library with Tensor flow backend.

Table 2: Hyper parameters of trained CNN algorithms

	Shallow	VGG16
Learning Rate	1e-3	1e-4
Batch Size	16	16
Epochs	500	200
Optimizer	SGDM	SGDM

2.2. Wheat Identification Framework

The proposed identification framework is represented with Fig. 2. One can observe that the Shallow and VGG16 models were trained by using augmented training data. The capability of the system was evaluated by making experiments of 1600 test instances. While the 150 instances of each class were reserved for training, 10 instances for validation and remaining ones used in case performance evaluation through accuracy and F-measure metrics. As its demonstrated in Table 1, we considered the Stochastic Gradient Descent with Momentum (SGDM) as an optimization function. Also, the epochs are 500 and 200 for Shallow and VGG16.
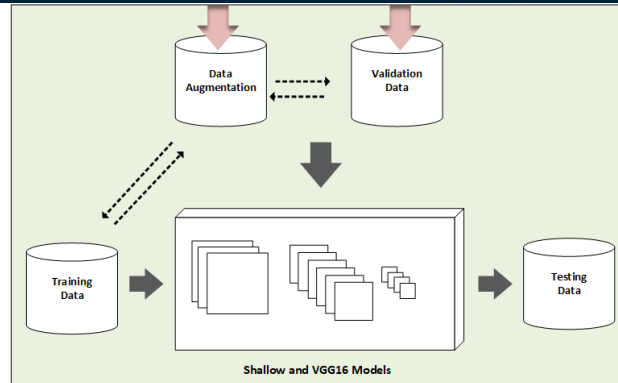
Figure 2: Wheat Classification Framework

3. EXPERIMENTS

3.1. VNIR Dataset

VNIR multi-spectral image cameras have a wide range of applications in remote sensing, imaging spectroscopy and robotic agriculture. With the special lens and NIR rays involved in the camera, it is possible to detect changes and details that the human eye cannot recognize on the surface of the product. The wheat sample kernels were obtained from a Visible Near Infrared (VNIR) imaging system in a controlled environment. A special VNIR camera was located at a distance of 30 cm above wheat samples to obtain optimum quality in the experimental environment. Its wavelength range is between 400 and 1100 nm, and covers the area of 9x7 cm², which is the dimension of the container for wheat samples.

To compensate the sudden light effects, two 100 W halogen light sources were used on the right and left sides to ensure homogeneous distributed lighting. Each captured wheat image has dimensions of approximately 640 x 512. To increase the data size, an augmentation process was applied by dividing an image into four quadrants. Thus, each class includes 200 instances and 8000 instances have obtained from 40 classes. While 6000 of this data set were used for training simulation, 400 for validation and the remaining 1600 images were used for test simulation. Labels of 40 wheat classes have shown in Table 3.

Table 3: Labels of 40 wheat types

Ahmetaga	Altay2000	Atay85	Aytin	Bayraktar2000
Bezostaja	Cesit1252	Cetiner	Dagdas	Ekiz
Energo	Es26	Esperia	Flamura85	Gelibolu
Gerek79	Harmankaya	Izgi	KateA1	Kirac
Kirgiz	Kunduru	Mesut	Michelangelo	Midas
Mufitbey	Nacibey	Pehlivan	Porsuk	Reis
Renan	Selimiye	Sonmez	Soyer	Sultan95
Suzen	Tosunbey	Yelken	Yildiz	Yunus

3.2. Results and Discussions

To assess the robustness of deep learning tools for wheat label forecasting, we evaluate the performance based on the accuracy and F-measure scores. The performance of Shallow and VGG16 have concurrently performed for benchmark comparison.

Table 4: Performance comparison of our Shallow and VGG16 models with other studies

Method Name	Accuracy (%)
Shallow (our)	80.13
VGG16 (Our)	91.13

[1] Singh et. al.	99.30
[2] Martin et. al.	76.00
[7] Grinblat et. al.	97.00

Table 4 presents proposed models classification results in comparison to other studies. Since each method was developed for different classification task and completely different datasets, it is not fair to compare our results with results of these methods. However, we show a general insight into their potential capability on wheat identification. Although the result of [7] is higher than our proposed methods, but, in reality, the VGG16 is much more effective when comparing the number of wheat cultivars. While the proposed study is conducted on 40 wheat cultivars, the [7] considers only 3 beans types.

In case of softmax classifier, the labels of test samples have determined by activation probability returned from the CNN models. There are 1600 test samples in total. Upon inspecting the obtained results in Table 3, one can say that there are 318 samples misclassified by Shallow model. On the other side, the VGG16 is capable to correctly determine wheat labels with a 0.09% error rate, which accounts for 142 misclassified wheat samples.
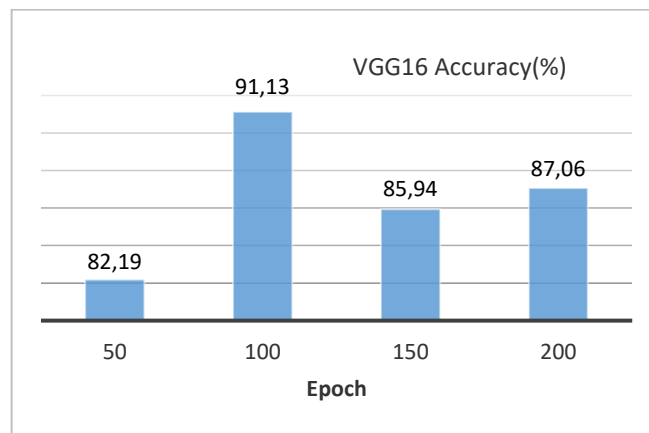
Figure 3: Accuracy of VGG16 per 50 epochs

The performance of VGG16 is given in Fig. 3 by reporting, prediction results per 50 epochs. One can observe from the Fig. 3 that the VGG16 gives best classification results in 100th epoch, which is noted as 91.13% accuracy rate. There is fluctuation in accuracy rates between 100 and 200 epochs.
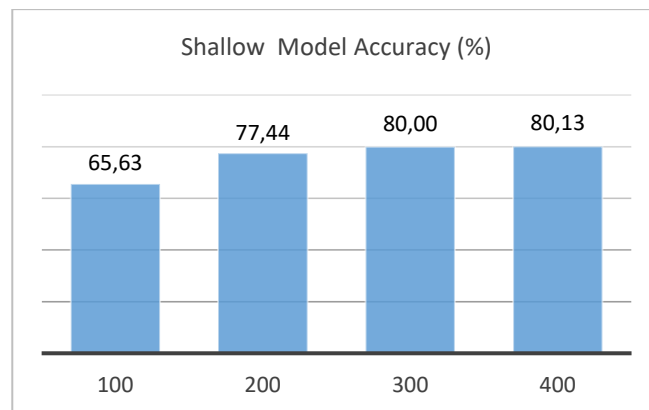
Figure 4: Accuracy of Shallow Model per 100 epochs

Again, the prediction capability of our Shallow model is shown in Fig. 4. Clearly, we can say that the Shallow CNN model is not able to produce a satisfying classification performance as good as VGG16 model. This is not interesting as regards to widely known fact that is, the deeper means the better in terms of classification. The performance gap between Shallow and VGG16 model is approximately 11% in terms of wheat kernel identification.

4. CONCLUSIONS AND FUTURE WORK

In this study, we analyzed the impact of deep and shallow, deep learning models for wheat cultivar classification. For this purpose, the shallow and VGG16 models were conducted on 40 wheat types. Experimental simulation results indicate that the VGG16 gives an impressive performance when integrated for wheat type detection. A new VNIR dataset constructed by using a special camera, capturing bands between 400 and 1100 nm. On the basis of valuable accuracy rate of 91.13%, one can emphasize that the deep learning models give accurate categorization results without using any parameter engineering.

ACKNOWLEDGMENT

REFERENCES

[1]. C. Singh, D. Jayas, J. Paliwal, N.J.J.o.S.P.R. White, Detection of insect-damaged wheat kernels using near-infrared hyperspectral imaging, 45 (2009) 151-158.

[2]. M.I. González-Martín, G.W. Moncada, C. González-Pérez, N.Z. San Martín, F. López-González, I.L. Ortega, J.-M.J.F.c. Hernández-Hierro, Chilean flour and wheat grain: tracing their origin using near infrared spectroscopy and chemometrics, 145 (2014) 802-806.

[3]. R. Ronge, M. Sardeshmukh, Comparative analysis of Indian wheat seed classification, Advances in Computing, Communications and Informatics (ICACCI, 2014 International Conference on, IEEE2014, pp. 937-942.

[4]. L. Ravikanth, C.B. Singh, D.S. Jayas, N.D.J.B.E. White, Classification of contaminants from wheat using near-infrared hyperspectral imaging, 135 (2015) 73-86.

[5]. S. Ghosh, P. Mishra, S.N.H. Mohamad, R.M. de Santos, B.D. Iglesias, P.B.J.B.E. Elorza, Discrimination of peanuts from bulk cereals and nuts by near infrared reflectance spectroscopy, 151 (2016) 178-186.

[6]. A. Krizhevsky, I. Sutskever, G.E. Hinton, Imagenet classification with deep convolutional neural networks, Advances in neural information processing systems2012, pp. 1097-1105.

[7]. G.L. Grinblat, L.C. Uzal, M.G. Larese, P.M.J.C. Granitto, E.i. Agriculture, Deep learning for plant identification using vein morphological patterns, 127 (2016) 418-424.

[8]. E.C. Too, L. Yujian, S. Njuki, L.J.C. Yingchun, E.i. Agriculture, A comparative study of fine-tuning deep learning models for plant disease identification, (2018).

[9]. Y. Lu, S. Yi, N. Zeng, Y. Liu, Y.J.N. Zhang, Identification of rice diseases using deep convolutional neural networks, 267 (2017) 378-384.

Visual Features with Common Vector Approach on Recommendation Systems

Kemal Ozkan[1], Caner Balim[2]

Abstract

Recommendation systems help customers to discover item from predicting the theirs's opinions of each items. But if it is a new item or if there is no feedback about it, recommender systems have difficulties in these items. This problem is also called the cold start problem. To overcome cold start issue, some recommender systems use additional information, such as review text, purchase history, visual information etc. In this short paper we propose an image-based model that creating more accurate predictions and help to cold start issue, for recommendation system. We use SURF, SIFT, SHAPE, COLOR, LBP and GIST features for image description in our system. Further we combine image features with common vector analysis to one descriptor. The model is validated with experiments on two real-world datasets (Amazon.com and Tradesy.com). Then we compare our method to other existing studies. According to the experiment results, our proposed method was achieved more than 79% accuracy rate.

Keywords: Image-based recommender system, implicit feedback, common vector approach, recommendation systems

1. INTRODUCTION

The Recommendation systems (RS) which play significant role recommends commercial items by evaluating from historical feedback from users. These systems help people for to discover items like clothes, music, news etc. With the rapid increase of e-commerce, RS have playing an important role helping customers interact with large amounts of content. Further, many companies like Netflix, Ali Baba etc. have been using RS to aim customers by recommending products or services.

RS has at least two elements which are users and items. Bobadilla et al, cited that RS can categorized into three classes [1]: collaborative filtering (CF) methods, content-based (CB) methods and hybrid methods.

- Collaborative filtering methods: CF methods [2,3] use the past activities or preferences, such as user ratings on items, without using user or item content information.

- Content-based methods: These approaches do not interest other user's history. It recommends items which have similar content to our history. Figure 1 shows both CF and CB filtering sample.

- Hybrid methods: Hybrid methods [4] offer recommendations by taking pros from CB and CF-based methods.

[1] Corresponding author: Eskisehir Osmangazi University, Department of computer Engineering 26140, Meselik/Eskisehir, Turkey. kozkan@ogu.edu.tr

[2] Afyon Kocatepe University, Sandikli Vocational School,Department of Computer Programming, Sandikli/Afyonkarahisar, Turkey, cnrblm@gmail.com
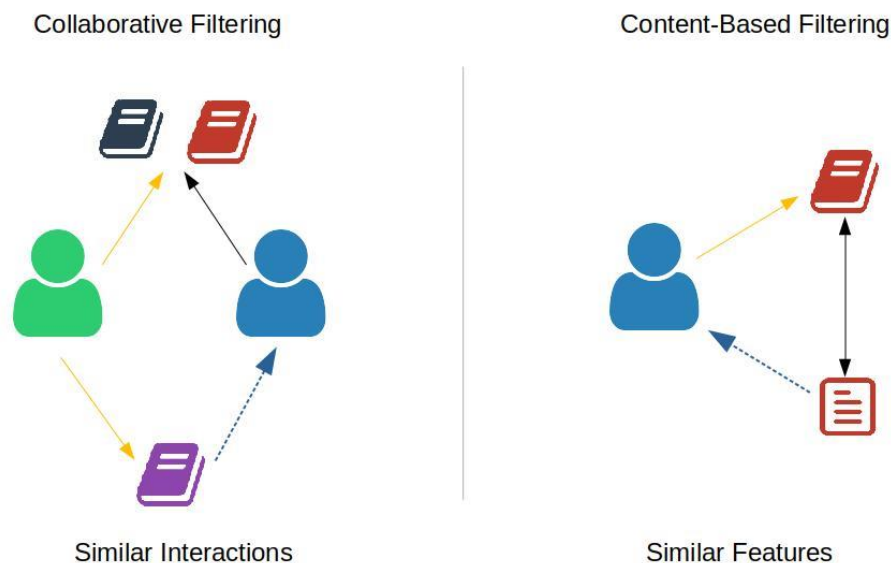
Figure 1: Sample of CF and CB recommendation

The Most widely implemented technology on recommender systems is CF method. There are two kinds of data available for CF:

--Explicit feedback: Rating, like or scores

--Implicit feedback: Not as obvious in terms of preference, such as a click or view

In the conventional CF approach, a user-item matrix is created, which shows an example of the valuations that users give to items. Due to the size of data in real-time applications, the matrix dimensions can be very high and sparse. One of the most popular approaches to modeling this data using latent features is based on matrix factorization [5].

Most time customers don't provide ratings and scores in real time applications. So, the RS doesn't know scores of the item. This may lead cold start issue which no user history about items. Because of this issue, researchers focus implicit data solutions. Customers want to have enough insight into the details of the item in real time applications. Besides the item's attribute, benefits and price, the item's image is among the issues that most consumers are very careful. For this reason, image-based recommendation systems have been developed.

There are recently developed image-based solutions in the literature. Pliakos and Kotropoulos (2015) designed a recommender system by utilizing the visual features and textual information from tourism related images [6]. In order to measure similarity of the images in the collection, GIST descriptor and GPS data used on their system.

Kalantidis et al. proposed an approach for learning the relationships between apparel and events (birthday parties, funerals etc.) to recommend appropriate items [7].

McAuley et al. (2015) proposed Image-based Recommendation (IBR) algorithm which recommends stylistically similar items to users [8]. They use nearest-neighbor search for prediction step.

He et al. (2016) proposed Visual Bayesian Personalized Ranking (VBPR) algorithm by combine with visual features which learning from Convolutional Neural Network (CNN), into matrix factorization [9].

In this work, we create a recommendation system that using visual features for describing images. First, we extract visual features (SIFT, SURF, SHAPE, COLOR, LBP, GIST) from all images in datasets. Then, these features are combined with common vector approach to one vector. Then we incorporate these vectors for the task of personalized ranking on implicit feedback datasets. As a result of the experiments, it has been observed that the cold start issue which are the general problem of the recommender systems, can be reduce and users can be offered more accurate personalized recommendations.

2. COMMON VECTOR APPROACH

Common vector approach (CVA) is a subspace method and it used to find unique vector from feature vector. This unique vector is also called common vector. CVA can be divided into two case: insufficient $(n \geq m)$ and sufficient case $(n < m)$. m represents the number of vectors in the class, and n represents the size of the vector. In a group of feature vectors, it is assumed that each vector consists of a common and difference vector as

$$a_i = a_{i,diff} + a_{com}, i = 1,2,\ldots,m$$
(1)

where a_{com} is common vector and a_{diff} is difference vector of the class. Only insufficient case of CVA is described in the following.

First, a random reference vector, $\vec{a_i}, (i = 1,2,\ldots,m-1)$, are used to create the differences of feature vectors. Then the difference vectors belonging to the processed data is obtained by:

$$\vec{b_1} = \vec{a_2} - \vec{a_1}$$
$$\vec{b_2} = \vec{a_3} - \vec{a_1}$$
$$\cdot$$
$$\cdot$$
$$\cdot$$
$$\vec{b_{m-1}} = \vec{a_m} - \vec{a_1}$$
(2)

Once $(m - 1)$ difference vectors are obtained, the difference subspace (B) for i-th class can be calculated by gathering the difference vectors.

$$B = \{\vec{b_1}, \vec{b_2}, \ldots\ldots, \vec{b_{m-1}}\}$$
(3)

In the next stage, the Gram-Schmidt orthogonalization procedure is applied to B_i to obtain the orthonormal basis.

$$\vec{d_1} = \vec{b_1}\vec{z_1} = \frac{\vec{d_1}}{\|\vec{d_1}\|} = \frac{\vec{b_1}}{\|\vec{b_1}\|}$$
$$\vec{d_2} = \vec{b_2} - \langle\vec{b_2}, \vec{z_1}\rangle\vec{z_1}\vec{z_2} = \frac{\vec{d_2}}{\|\vec{d_2}\|}$$
$$\cdot$$
$$\cdot$$
$$\cdot$$
$$\vec{d_{m-1}} = \vec{b_{m-1}} - \sum_{i=1}^{m-2}\langle\vec{b_{m-1}}, \vec{z_1}\rangle\vec{z_1}\vec{z_2} = \frac{\vec{d_{m-1}}}{\|\vec{d_{m-1}}\|}$$
(4)

When the orthonormal basis is computed, the difference vectors $a_{i,diff}$ can be obtained by the projection of any sample a_i

$$\overline{a_i} = \sum_{k=1}^{m-1}\langle\vec{a_i}, \vec{z_k}\rangle\vec{z_k}, i = 1,2,\ldots,m$$
(5)

At last, subtracting the $a_{i,diff}$ from any vector a_i, gives a common vector.

$$\vec{a_{com}} = \vec{a_i} - \overline{a_i}, i = 1,2,\ldots,m$$
(6)

3. PROPOSED SYSTEM

In real applications, the user-item matrix is very large and extremely sparse. Latent factor approach has been used in recent years in order to solve the size problem and the problem of sparse structure [10]. The general approach in the latent factor model is to describe each user and item as a vector relative to the user and the item's latent vector.

If the user is desired to be formulated as the preference / vote estimate for a given item, the interaction between the user and the hidden factor vectors obtained from the item; γ_i, the hidden factor vector for item i and γ_u the hidden factor vector for user u can be defined:

$$x_{u,i} = \langle \gamma_u, \gamma_i \rangle$$
$$(7)$$

Since the user's voting on the item cannot be excluded from this interaction, the bias of the user and the item itself must also be used to estimate votes [3]. In this context, a general expression can be created by adding bias terms to the interaction part of the user's rating/ score estimation formula. In the below equation, α, β_u and β_i, respectively indicate the global offset and the bias value for the user and the item.

$$x_{u,i} = \alpha + \beta_u + \beta_i + \langle \gamma_u, \gamma_i \rangle$$
$$(8)$$

Image feature extraction can be both laborious and faulty in image-based solutions. He et al. (VBPR), used the descriptors obtained from the AlexNet [11], which was the winner of the large-scale Visual Recognition Competition (ImageNet) in 2012 for obtain descriptors from the item images. AlexNet has two fully connected layers with 4096 outputs. In this study, this problem has been overcome with features which frequently used in pattern recognition and image access problems [12]. In this context, for each image in the datasets, Scale Invariant Feature Transform (SIFT) [13], Adaptive Color Feature [14], Speeded-Up Robust Features (SURF) [15], Local Binary Pattern (LBP) [16], Shape Base Robust Feature [17] and GIST Feature [18] are obtained. Each feature consists of 4096-sized vector. These feature vectors are combined for represent the image (4096×6). Thus, the 4096×6-sized feature matrix was created for each image.

For a fair comparison with VBPR, we used 4096 size feature vectors in experiments. Principal Component Analysis (PCA) is most commonly used data reduction method. CVA is a data reduction technique like PCA. They are very similar in many ways. But CVA's data reduction in a fundamentally different way. CVA composes latent variable from all variables. This latent variable cannot be measured from a single variable. So, in order to better describe the image, each feature vectors were combined with CVA to create an image descriptor.

The formula is represented by the addition of the D-dimensional vector representing the visual properties associated with the item:

$$x_{u,i} = \alpha + \beta_u + \beta_i + \langle \gamma_u, \gamma_i \rangle + \langle \theta_u, \theta_i \rangle$$
$$(9)$$

Due to the high dimensionality of the features (4096), dimensionality reduction techniques (PCA) was used and the feature vector size reduce Kx1 size in VBPR. So, the model has been finalized with the addition of the term visual bias β_v and E which is linear transformation matrix.

$$x_{u,i} = \alpha + \beta_u + \beta_i + \langle \gamma_u, \gamma_i \rangle + \langle \theta_u, E(f_i) \rangle + \langle \beta_v, f_i \rangle$$
$$(10)$$

As a result, As a result, our proposed method for predicting the user's opinions of each items basically consist of visual factors and latent (non-visual) factors. Proposed method is presented in Figure 2.
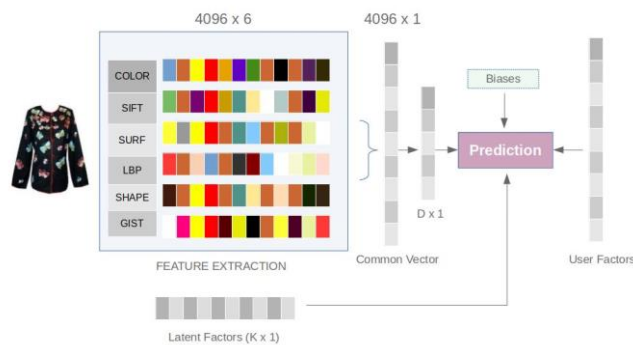
Figure 2: Proposed Algorithm

4. EXPERIMENTS

We conduct several experiments to test the performance of proposed algorithm. Based on our experiments on the features that we described in Section 3. In Section 4.1, we present the dataset that we used in our experiments. Section 4.2. introduces performance metrics and Section 4.3. presents the experimental results.

4.1. Dataset

In order to present performance of our algorithm, we evaluated our model on two datasets (Amazon.com and Tradesy.com) [8, 9]. Amazon.com dataset includes Women's Clothing, Men's Clothing and Cell Phones Accessories. In addition, we use Tradesy.com dataset which have product information sold, liked and purchased by users. See Table 1 for more information about the datasets.

Table 1: Dataset after pre-processing

	User	Item	Feedback
Amazon Woman	99748	331173	854211
Amazon Men	34323	100654	260352
Amazon Phones	113900	192085	964477
Tradesy.com	19823	166526	410186
Total	267683	790438	2489226

4.2. Performance Metrics

All data are divided into pieces which include training (P_u) validation (V_u) and testing (T_u) from using a random item is selected for each selected user u. The predicted ranking value is calculated on the T_u set for the AUC (Area Under ROC Curve).

$$AUC = \frac{1}{|U|}\sum_u \frac{1}{|E(u)|}\sum_{(i,j)\in E(u)} \delta\left(x^{\hat{}}_{u,\iota} > x^{\hat{}}_{u,j}\right)$$
(11)

where the evaluation / prediction pair set for the user u and items (i, j) are defined as follows.

$$E(u) = \{(i,j) \vee (u,i) \in T_u \wedge (u,j) \notin (P_u \cup V_u \cup T_u)\}$$
(12)

and (b) is an indicator function that returns 1 if b is true. In all cases we report the performance on the test set T for the hyper parameters that led to the best performance on the validation set V.

4.3. Results

The model is evaluated on two datasets. We also compare our method with existing methods. In the overall evaluation process, the latent factor size was determined as 20.

4.3.1. Comparison of Visual Features

In this subsection, we evaluate the performance of our work through visual features. Table 2 shows visual feature performance with proposed algorithm.

Table 2: Comparison of Visual Features

	Amazon Woman	Amazon Men	Amazon Phones	Tradesy.com
Color	0.69	0.66	0.78	0.68
GIST	0.71	0.69	0.77	0.68
LBP	0.7	0.69	0.77	0.68
SHAPE	0.68	0.66	0.77	0.69

SIFT	0.71	0.7	0.77	0.68
SURF	0.69	0.67	0.77	0.69

4.3.2. Comparison of VBPR

We further compare our method with VBPR. Table 3 shows results with VBPR on same datasets.

Table 3: Comparison with VBPR

	VBPR	Proposed Method
Amazon Woman	0.78	0.8
Amazon Men	0.78	0.79
Amazon Phones	0.81	0.8
Tradesy.com	0.78	0.79

As a result of experiments, it was seen that it would be better to creating a descriptor with CVA instead of using only the features of the image for recommendations. Also, a lot of factors such as color, pattern and shape of the item were effective, when a user will choose an item. So, classification purposes approach may insufficient for item recommendations.

5. CONCLUSIONS AND FUTURE WORK

With the rapid increase of e-commerce, monitoring of the items purchased by a person and suggesting items to persons are considered an important area of study in computer science. RS have playing an important role helping customers interact with large amounts of content. In this paper, we explored on the current RS techniques and suggested a new method which using visual descriptors of items for RS based on implicit feedback. For the purpose of judging its performance evaluation, we used two different real-world datasets. The evaluation result shows that our method has outperform results.

In this study, only one item image was used for each item. In future, it is planned to add the item images as well as user profile information to the proposed model.

ACKNOWLEDGMENT

REFERENCES

[1]. J. Bobadilla, F. Ortega, A. Hernando, and A. Gutiérrez, "Recommender systems survey," Knowledge-based systems, vol. 46, pp. 109–132, 2013.
[2]. S. Rendle, C. Freudenthaler, Z. Gantner, and L. Schmidt-Thieme, "Bpr: Bayesian personalized ranking from implicit feedback," in Proceedings of the twenty-fifth conference on uncertainty in artificial intelligence. AUAI Press, 2009, pp. 452–461.
[3]. Y. Koren and R. Bell, "Advances in collaborative filtering," in Recommender systems handbook. Springer, 2015, pp. 77–118.
[4]. L. Hu, J. Cao, G. Xu, L. Cao, Z. Gu, and C. Zhu, "Personalized recommendation via cross-domain triadic factorization," in Proceedings of the 22nd international conference on World Wide Web. ACM, 2013, pp. 595–606.
[5]. R. M. Bell, Y. Koren, and C. Volinsky, "The bellkor solution to the netflix prize," KorBell Teams Report to Netflix, 2007.
[6]. K. Pliakos and C. Kotropoulos, "Building an image annotation and tourism recommender system," International Journal on Artificial Intelligence Tools, vol. 24, no. 05, p. 1540021, 2015.
[7]. Y. Kalantidis and Y. Avrithis, "Locally optimized product quantization for approximate nearest neighbor search," in Proceedings of the IEEE Conference on Computer Vision and Pattern Recognition, 2014, pp. 2321–2328.

[1]. J. McAuley, C. Targett, Q. Shi, and A. Van Den Hengel, "Image-based recommendations on styles and substitutes," in Proceedings of the 38th International ACM SIGIR Conference on Research and Development in Information Retrieval. ACM, 2015, pp. 43–52.

[2]. R. He and J. McAuley, "Vbpr: visual bayesian personalized ranking from implicit feedback," in Thirtieth AAAI Conference on Artificial Intelligence, 2016.

[3]. A. Karpathy and L. Fei-Fei, "Deep visual-semantic alignments for generating image descriptions," in Proceedings of the IEEE conference on computer vision and pattern recognition, 2015, pp. 3128–3137.

[4]. A. Krizhevsky, I. Sutskever, and G. E. Hinton, "Imagenet classification with deep convolutional neural networks," in Advances in neural information processing systems, 2012, pp. 1097–1105.

[5]. Z. Kurt and K. Özkan, "An image-based recommender system based on feature extraction techniques," in 2017 International Conference on Computer Science and Engineering (UBMK). IEEE, 2017, pp. 769–774.

[6]. D. G. Lowe, "Distinctive image features from scale-invariant keypoints," International journal of computer vision, vol. 60, no. 2, pp. 91–110, 2004.

[7]. W.-T. Chen, W.-C. Liu, and M.-S. Chen, "Adaptive color feature extraction based on image color distributions," IEEE Transactions on image processing, vol. 19, no. 8, pp. 2005–2016, 2010.

[8]. H. Bay, A. Ess, T. Tuytelaars, and L. Van Gool, "Speeded-up robust features (surf)," Computer vision and image understanding, vol. 110, no. 3, pp. 346–359, 2008.

[9]. M. Heikkilä, M. Pietikäinen, and C. Schmid, "Description of interest regions with local binary patterns," Pattern recognition, vol. 42, no. 3, pp. 425–436, 2009.

[10]. X. Wang, B. Feng, X. Bai, W. Liu, and L. J. Latecki, "Bag of contour fragments for robust shape classification," Pattern Recognition, vol. 47, no. 6, pp. 2116–2125, 2014.

[11]. A. Oliva and A. Torralba, "Modeling the shape of the scene: A holistic representation of the spatial envelope," International journal of computer vision, vol. 42, no. 2, pp. 145–175, 2001.

An Innovative Solution for Abrage Fault Detection on Yarn Bobbin and Fabric Surface

H.Ibrahim Celik [1], Elif Gultekin[1], L.Canan Dulger [2], H.Ibrahim Sunbul[3], Harun Kani[3]

Abstract

New developments in machine vision and automation technologies provide more accurate and sensitive process control and quality inspection in each stage of the production line. Development in industry 4.0 technology and image processing techniques have been used in many textile industry areas in last decay. However, many processes that are achieved manually and subjectively exist in yarn production stages. The abrage fault inspection is one of them. During the yarn production, the fiber content of the yarn must be preserved from blending of other foreign materials and fibers. Abrage fault control is achieved by the human eye on both the yarn package and the fabrics under UV light. This process is very time consuming and tiring. The available method contains the high potential for the risk of missdetection and overlooking. In this study, a machine vision system for automatic inspection of yarn bobbin and fabric abrage defect is presented. The prototype system is introduced and properties of its components are investigated. The optimum image acquisition parameters that are useful for abrage inspection were also determined.

Keywords: Abrage fault, Image processing, Machine vision, Yarn Fault

1. INTRODUCTION

Abrage fault is detected on the bobbin after the yarn production and on the fabric before the read-made process. Nowadays, this fault control is currently performed by the human eye both on the yarn package and the fabric. The yarn bobbins are placed in a creel prior to packing and transported to a room illuminated by UV light, where the bobbins are individually controlled by human eye. If considering the average daily production capacity of 15 tons of yarn, approximately 7500/day bobbins are controlled manually. Four workers are to be employed at least. This process is time consuming and tiring. When the number of bobbins to be checked daily is considered, the risk of overlooked bobbin is high. On the other hand, the automated process flow in fully automated spinning mills is interrupted by visual evaluation. If the abrage faults cannot be detected either on the yarn package or on the fabric surface, it will be eventuated as defective (second quality) end-use textile product. This situation is being reflected as a serious problem for the manufacturers and cause very high reclamation costs. In order to perform this operation automatically, a machine vision system based on the inspection of different fiber contents in yarn bobbin from their different reflectance values under the same lightening conditions is proposed

Studies on image processing applications to fiber characterization generally concentrated on the determination of the geometric properties of the fibers such as diameter, length, fineness and crimp. In the literature survey, it is also distinguished that the studies on image processing applications to yarn characteristic are generally about determination of yarn hairiness, yarn twist, yarn unevenness, and yarn defects (thick, thin, and neps) [1-21]. In order to detect the foreign fiber or material content in staple fiber lint, some studies have been conducted. In these studies, different machine vision systems were proposed for automatic detection of foreign fibers [22-27]. J.Silvestre et al. conducted a study to determine the abrage faults caused by the mixing of the different types of fibers on the yarn spool (cops) by using the different reflectance properties of the fibers the under the UV light [28]. Celik [29] presented a prototype machine vision system for abrage fault detection and an image processing

---

algorithm was built. A simple prototype system was manufactured and the abrage regions of the bobbin samples were detected successfully.

When a yarn bobbin including foreign material is used for fabric production, it will cause different appearance after finishing or dyeing processes. It is also a critical fabric fault. The fabric abrage is also detected on industrial fabric quality inspection machines by human eyes under UV lightening. This detection process is achieved manually by the workers. Success of manual inspection process completely depends on worker concentration and experience. The studies on the determination of fabric characteristics are mostly focused on objective quality and performance evaluation such as fabric defect detection, fabric defect classification, pilling and wrinkle resistance evaluation [31-41].

In this study, a prototype vision inspection system was developed to acquire image frames of the yarn bobbin and fabric samples for image analyzing. The image acquisition parameters and components of the system were also investigated.

2. DESIGN OF ABRAGE INSPECTION SYSTEM

A prototype vision inspection system is developed to acquire image frame of the yarn bobbin and fabric samples for analyzing (Figure 1). The system consists of a lightening unit, a CMOS camera system, cabin and compter. A top-lightening unit is developed and manufactured. The lightening unit consist of UV fluorescent lamps is positioned to top of cabin. The camera system is placed in the middle of the lightening unit. Since the image quality is influenced by many environmental factors, a closeable cabin frame is designed for yarn bobbin positioning. For positioning the bobbin and fabric sample a suitable apparatus is designed at the bottom of the system. The distance of the bobbin or fabric sample to camera can be adjusted by using the apparatus so that the camera field of view can be edited according to the sample size. A simple screw system is used for sample distance adjustment.
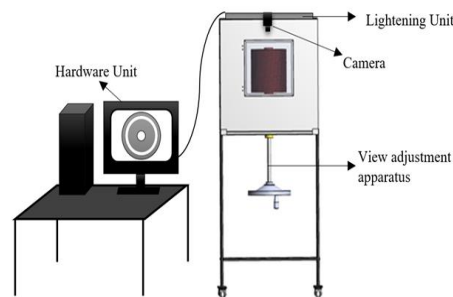
Figure 1. A prototype machine vision inspection system

3. IMAGE ACQUISITION PARAMETERS

In the machine vision systems, the quality and characteristics of the image have a significant effect on the system success. Before, a robust image processing algorithm, high quality image frames must be acquired. Otherwise, the target success cannot be achieved, although the algorithm is robust. Conditions such as lighting, motion blur, camera resolution, and compression of images taken while storing are factors that affect image quality. Therefore, the images taken with the camera are digitized and transferred to a computer environment and then improved using various noise cleaning and image enhancement filters [30]. So, the effect of the image acquisition parameters are viewed on the yarn bobbin fault inspection.

According to the lighting conditions, to obtain high image quality, the parameters in the camera software interface (Pylon5) were analyzed (Figure 2). The related camera parameters; Light Source Pre-set, Gain, Gamma and Exposure time etc. have been adjusted until the required image frame was obtained. Different camera parameters were tried for abrage inspection tests, it was seen that these parameters are very effective on determining the abrage fault [42].
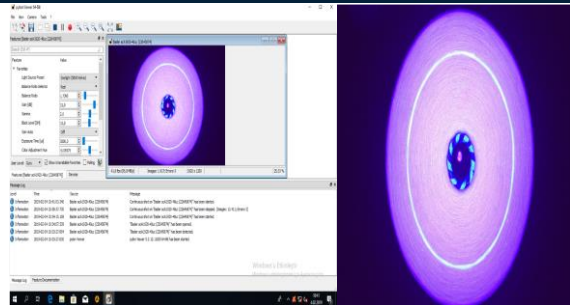
Figure 2. The effect of some camera parameters on image frame.

3.1. The Light Source Pre-set

The light source preset parameter provides correction of color bursts caused by certain light sources. Depending on the specific color temperature, the light used to produce the image may cause color changes in the image. So the selecting correct corresponding color source preset is important. These light sources are;

Off: Without any light source preset, it remains connected to the light from the full illumination.

Daylight 5000K: Corrects color bursts caused by daylight illumination with a color temperature of approximately 5000 Kelvin.

Daylight 6500K: Corrects color bursts caused by daylight illumination with a color temperature of approximately 6500 Kelvin.

Tungsten 2800K: Corrects color shifts caused by tungsten lighting with a color temperature of 2500-3000 Kelvin.

Experiments on light source adjustment are shown in Figure 3.
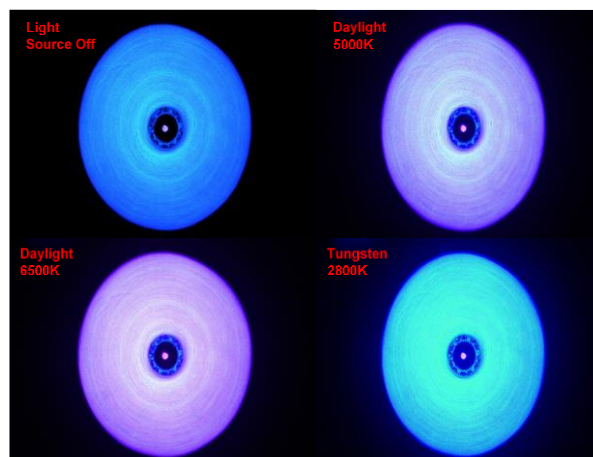
Figure. 3. Effect of preset light source on image enhancement

3.2. Gain

The gain feature of the camera allows us to increase the brightness of the images coming out of the camera. Increasing this increases all pixel values of the image. Related trials are shown in Figure 4.
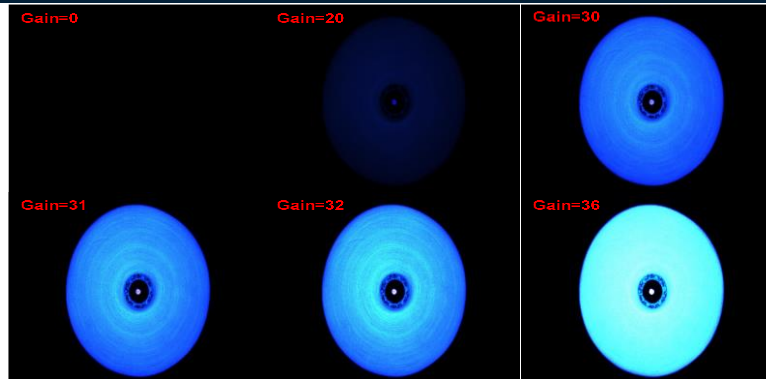
Figure 4. Effect of Gain parameter on image enhancement

3.3. Gamma

Gamma (*Y*) effect allows to optimize the brightness of acquired images to display on the monitor. The range of values of the gamma parameter is 0 to ≈4. Experiments on gamma adjustment are shown in Figure 5.

Gamma = 1: The overall brightness remains unchanged.

Gamma <1: The overall brightness increases.

Gamma> 1: The overall brightness decreases.
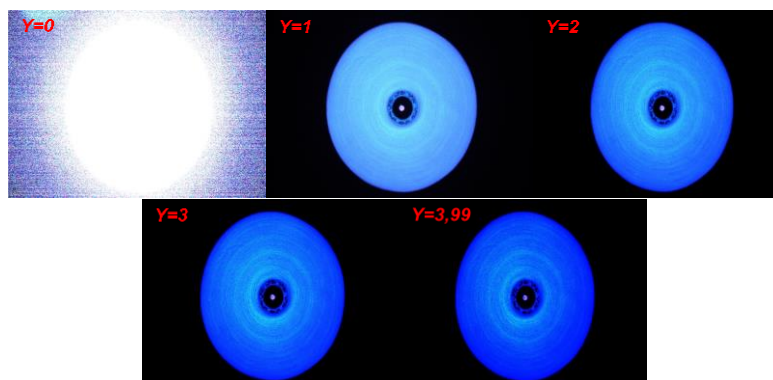
Figure 5. Effect of Gamma (Y) parameter on image enhancement

3.4. Exposure Time

The exposure time camera feature determines how long the image sensor is exposed to light during image acquisition. Experiments on setting the exposure time are shown in Figure 6.
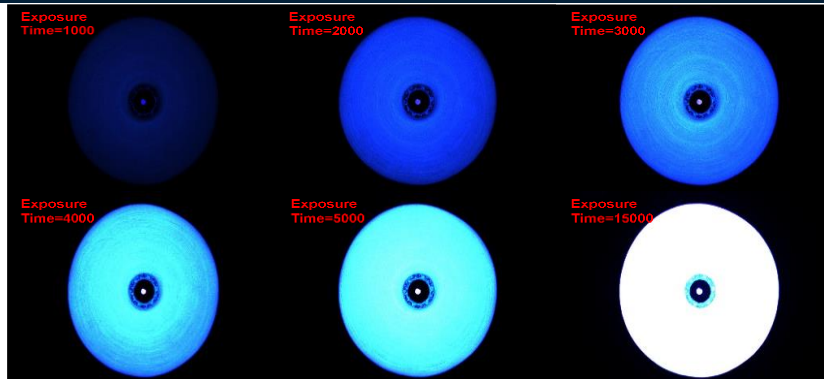
Figure 6. Effect of Exposure Time parameter on image enhancement

Apart from these settings, ***Blance White, Color Adjustment*** and ***Brightness and Contrast*** settings should also be examined to improve the image quality.

3.5. Balance White

Balance White camera feature allows to manually correct color shifts so that white objects appear white in images acquired. The following adjustment choices can be tried.

Balance ratio = 1: The intensity of the color remains unchanged.

Balance ratio > 1: The intensity of the color is increased relative to the other two colors.

Balance ratio < 1: The intensity of the color is decreased relative to the other two colors.

3.6. Color Adjustment

Color Adjustment camera feature allows to adjust the hue and saturation of individual colors in images. Hue and saturation separately for each primary and secondary color in the RGB color space (red, green, blue, yellow, cyan, and magenta). Diagram shows (Figure 7) how changing hue and saturation of the color red affects the colors of images.
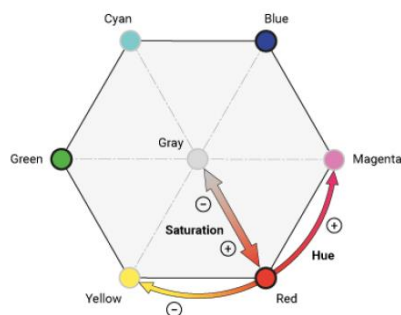
Figure 7. Diagram of hue and saturation of the color red affects the colors of images.

The following effects become apparent:

Decreasing the hue changes all red colors (i.e., colors with a predominantly red component) towards yellow.

Increasing the hue changes all red colors towards magenta.

Decreasing the saturation decreases the colorfulness of all red colors. At minimum, all red colors will be replaced by gray.

Increasing the saturation increases the colorfulness of all red colors. At maximum, all red colors are replaced by 100 % red.

3.7. Brightness and Contrast

Brightness and Contrast camera feature allows to adjust the tonal values of your images. Adjusting the contrast changes the degree of difference between light and dark areas in the image. The more contrast you apply, the more pronounced the difference will be. Increasing or decreasing the contrast, increases or decreases the gradient of the linear function. The difference between this two adjustments is shown Figure 8.
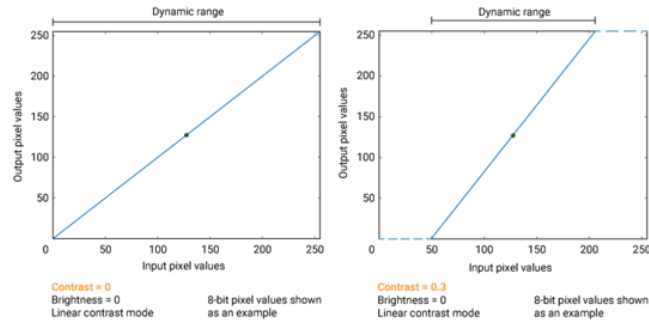
Figure 8. Effect of Contrast mode on the image

Adjusting the brightness allows to lightening or darkening the image by increasing or decreasing its tonal values.

Increasing the brightness moves the pivot point towards the upper left. This means that the image will appear lighter.

Decreasing the brightness moves the pivot point to the lower right. This means that the image will appear darker.

The Figures 9 below show examples with the Brightness Contrast mode selected.
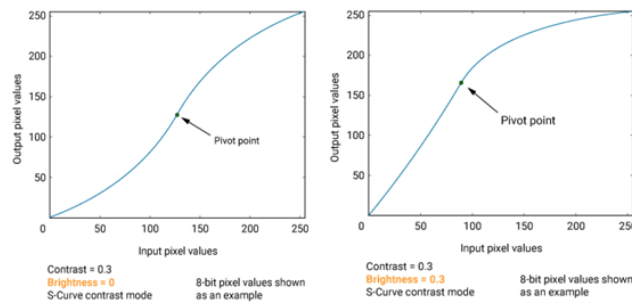
Figure 9. Effect of Brightness parameter on image

4. CONCLUSION

In this study, a suitable machine vision system for bobbin and fabric abrage fault detection as an industrial application was explained. In order to obtain high quality images, the parameters in the camera interface were investigated and the adjustments that are effective in obtaining high quality image frames were presented. Thus, the machine vision system created by using the correct illumination system with high resolution camera was suitable on an online production line. However, the fault check process in the manual yarn package can be determined by an automatic and objective evaluation. This machine vision system will greatly affect the production flow in a fully automated spinning mill. Proposed system can be adapted to industrial systems and run in real-time. By this way, the yarn manufacturing efficiency and yarn quality can definitely be improved.

ACKNOWLEDGEMENT

REFERENCES

[1]. C.A. Glasbey, D. Hitchcock, A.J.F. Russel, and H. Redden, "Towards the Automatic Measurement of Cashmere-fibre Diameter by Image Analysis," *Journal of Textile Institute*, vol. 85, pp. 301-307. Feb.1994.

[2]. B.P. Baxter, M.A. Brims, and T.B. Taylor, "Description and Performance of the Optical Fibre Diameter Analyzer (OFDA)," *Journal of Textile Institute,* vol.83, pp.507-526, Dec. 1992.

[3]. N. Dehghan, M.A. Tavanaie, and P. Payvandy, "Morphology study of nanofibers produced by extraction from polymer blend fibers using image processing," *Korean Journal of Chemical Engineering*, vol. 32(9), pp. 1928-1937, Sep.2015.

[4]. M.A. Lieberman, C.K. Bragg, and S.N. Brennan, "Determining Gravimetric Bark Content in Cotton with Machine Vision," *Textile Research Journal*, vol. 68, pp. 94-104, Feb. 1998.

[5]. T.J. Kang, and S.C. Kim, "Objective Evaluation of the Trash and Color of Raw Cotton by Image Processing and Neural Network," *Textile Research Journal*, vol.72, pp. 776-782, Sep. 2002.

[6]. Y.R. Shiau, I.S. Tsai, and C.S. Lin, "Classifying Web Defects with a Back-propagation Neural Network by Color Image Processing," *Textile Research Journal*, vol.70, pp. 633-640, Jul. 2000.

[7]. D.H. Wu, *"A Study* of The Analysis of Fibre Cross Sections by Image Processing," *Journal of the China Textile Institute,* vol.4, pp. 81-89, 1994.

[8]. B. Xu, B. Pourdeyhimi, and J. Sobus, "Fiber Cross-sectional Shape Analysis Using Image Processing Techniques," *Textile Research Journal*, vol. 63, pp. 717-730, Dec. 1993.

[9]. S. Zheng, Z.Y. Zou, W. Shen, and L. Cheng, "A Study of the Fiber Distribution in Yarn Cross Section for Vortex-Spun Yarn," *Textile Research Journal*, vol. 82(15), pp. 1579-1586, May 2012.

[10]. T.J. Kang, and J.Y. Lee, "Filament Crimp in Three Dimensions Measured by Image Analysis and Fractal Geometry," *Textile Research Journal*, vol. 71, pp. 112-116, Feb. 2001.

[11]. X.H. Wang, J.Y. Wang, J.L. Zhang, H.W. Liang, and P.M. Kou, " Study on The Detection of Yarn Hairiness Morphology Based on Image Processing Technique," in Ninth International Conference on Machine Learning and Cybernetics, Qingdao, 2010, paper 11(14), p. 2332-2336.

[12]. M. Kuzanski, "The Algorithms of The Yarn Shape Detection and Calculation of The Protruding Fibres Length," *MEMSTECH,* **2008,** paper 21(24), p. 98-100.

[13]. A. Fabijanska, and L.J. Strumillo, "Image Processing and Analysis Algorithms for Yarn Hairiness Determination," *Machine Vision and Applications*, vol. 23, pp. 527-540, May 2012.

[14]. B.G. Xu, C. Murrells, and X.M. Tao, "Automatic Measurement and Recognition of Yarn Snarls by Digital Image and Signal Processing Methods," *Textile Research Journal*, vol. 78(5), pp. 439-456, May 2008.

[15]. A. Guha, C. Amarnath, S. Pateria, and R. Mittal, "Measurement of yarn hairiness by digital image processing," *Journal of Textile Institute,* vol. 101(3), pp. 214-222, Feb. 2010.

[16]. V. Carvalho, P. Cardoso, M. Belsley, R.M. Vasconcelos, and F. O. Soares, "Development of a Yarn Evenness Measurement and Hairiness Analysis System," *32nd Annual Conference on IEEE Industrial Electronics*, 2006, p.3621-3626.

[17]. H. Asgari, F. Mokhtari, M. Latifi, and M. Amani-Tehran, "Characterizing cotton yarn appearance due to yarn-to-yarn abrasion by image processing," *Journal of Textile Institute,* vol. 105(5), pp, 477-482, Sep. 2014.

[18]. Y.A. Ozkaya, M. Acar, and M.R. Jackson, "Yarn twist measurement using digital imaging," *Journal of the Textile Industry,* vol. 101(2), pp. 91-100, Jul. 2009.

[19]. W. Yang, D. Li, L. Zhu, Y. Kang, and F. Li, "A New Approach For Image Processing In Foreign Fiber Detection," *Computers and Electronics in Agriculture,* vol.68(1), pp. 68-77, Aug. 2009.

[20]. S. Roy, and A. Sengupta, "Determination of the Diameter Spectrogram and Neps for Yarn Parameterization using Image Processing" *International Journal of Electrical, Electronics and Computer Engineering,* vol. 2(2), pp. 72-76, Dec. 2013.

[21]. A.S. Nateri, F. Ebrahimi, and N. Sadeghzade, "Evaluation of yarn defects by image processing technique," *Optik-International Journal for Light and Electron Optics,* vol. 125(20), pp. 5998-6002, Oct. 2014.

[22]. C.A. Lawrence, *Fundamentals of spun yarn technology,* CRC Press LLC, Inc.;Boca Raton London New York Washington, D.C., 2003, pp 34-35.

[23]. D. Li, W. Yang, and S. Wang, "Classification Of Foreign Fibers In Cotton Lint Using Machine Vision and Multi-Class Support Vector Machine," *Computers and Electronics in Agriculture,* vol. 74(2), pp. 274-279, Nov. 2010.

[24]. Z. Su, Y.G. Tian, and C. Gao, "A Machine Vision System For On-Line Removal Of Contaminants In Wool," *Mechatronics,* vol. 16(5), pp. 243-247, Jun. 2006.

[25]. D. Yuhong, L. Yongheng, J. Xiuming, C. Wenchao, and G. Donghan, "Research Of Foreign Fibers In Cotton Yarn Defect Model Based On Regression Analysis," *Journal of Textile Institute,* vol. 107(9), pp. 1089-1095, Sep. 2015.

[26]. W. Xinhua, W. Shu, X. Laiqi, S. Baoguo, and L. Meijin, "Identification Of Foreign Fibers Of Seed Cotton Using Hyper-Spectral Images Based On Minimum Noise Fraction," *Transactions of the Chinese Society of Agricultural Engineering,* vol.30(9), pp.243-248, 2014.

[27]. A. Pai, H. Sari-Sarraf, and E.F. Hequet, "Recognition Of Cotton Contaminants Via X-Ray Microtomographic Image Analysis," *IEEE Transactions On Industry Applications,* vol. 40(1), pp. 77-85, Feb. 2004.

[28]. J. Silvestre, R. Perez, and J. Mufnoz, "Systems integration of a mixed fibre detection process in raw yarn packages by computer vision" *in 2005 IEEE Conference on Emerging Technologies and Factory Automation,* 2005, p. 1-4.

[29]. H.I. Celik, H "Development of a machine vision system for yarn bobbin inspection," *Industria Textila,* vol.67(5), pp. 292-296, 2016.

[30]. Gonzalez, R. C. In *Digital Image Processing Using Matlab-Gonzalez Woods & Eddins* 2004, pearson.

[31]. X. Yang, G. Pang, and N. Yung, *"A review of automatic fabric defect detection techniques,"* in *Proceedings-Vision, Image Signal Process*, 2005, paper 152(6), p.715-723.

[32]. D.A. Karras, "Improved defect detection in textile visual inspection using wavelet analysis and support vector machines," *International Journal on Graphics, Vision and Image Processing,* vol. 5(4), pp. 41-47, Apr. 2005.

[33]. A. Serdaroglu, A. Ertuzun, and A. Ercil, "Defect detection in textile fabric images using subband domain subspace analysis," *Pattern Recognition and Image Analysis*, vol. 17(4), pp. 663-674, Dec. 2007.

[34]. M.B. Goswami, and K.A. Datta, "Detecting defects in fabric with laser-based morphological image processing," *Textile Research Journal*, vol 70(9), pp. 759-762, Sep. 2000.

[35]. C.J. Kuo, and C.J. Lee, "A back-propagation neural network for recognizing fabric defects," *Textile Research Journal*, vol. 73(2), pp. 147- 151, Feb. 2003.

[36]. T.J. Kang, D. H. Cho, and H.S.A. Whang, "New objective method of measuring fabric wrinkles using a 3-D projecting grid technique," *Textile Research Journal*, vol. 69(4), pp. 261-268, Apr. 1999.

[37]. T.J. Kang, S.C. Kim, I.H. Sul, J.R. Youn and K. Chung, "Fabric surface roughness evaluation using wavelet-fractal method: Part I: wrinkle, smoothness and seam pucker," *Textile Research Journal*, vol 75(11), pp. 751-760, Nov. 2005.

[38]. K.L. Jensen, and M. Carstensen, *"Fuzz and pills evaluated on knitted textiles by image analysis," Textile Research Journal*, vol. 72(1), pp. 34-50, Jan. 2002.

[39]. A. Cherkassky, and A. Weingberg "Objective evaluation of textile fabric appearance part 1: basic principles, protrusion detection, and parameterization," *Textile Research Journal*, vol. 80(3), pp. 226-265, Sep. 2010.

[40]. K. Hanbay, M.F. Talu, and O.F. Ozguven, "Fabric defect detection systems and methods—A systematic literature review," *Optik*, vol. 127(24), pp. 11960-11973, Dec. 2016.

[41]. H.I. Celik, L.C. Dulger, and M. Topalbekiroglu, "Development of a machine vision system: real-time fabric defect detection and classification with neural networks," *Journal of Textile Institute,* vol. 105(6), pp. 575-585, Sep. 2014.

[42]. User Manuel for Basler Camera- Pylon User Guide

An Application of Enterprise Risk Management and Internal Control in the Construction Sector: Joint Project Management Portal

Aynur Kazaz[1], Gokcen Arslan[1], Serdar Ulubeyli[2]

Abstract

The complex structure of the construction sector necessitates of expertise of the combination different areas and many uncertainties in its structure make construction projects vulnerable to risks. One-off and unique production of construction projects diversifies and increases the risks. These risks, in large numbers and varieties, constitute an obstacle for the project to reach its basic objectives such as quality, cost and time and to complete it successfully. When the attitude of the construction sector towards the risks is examined; it is seen that risks are ignored assuming that they are insignificant to affect project success adversely.However, it is known that the risks that seems small and unimportant at the beginning of the project will lead to unsuccessful results in the advanced stages for the institutions if the measures are not taken.The negative results encountered not only leave the project and the project owner firmly difficult, but also create a domino effect at the macro level and thus damage the country's and even the world's economy. This situation becomes more important especially for developing countries where the construction sector is one of the leading sectors of the economy and it makes the use of risk management in the sector inevitable.

Risk management is a proactive management approach based on taking necessary measures against elements that may cause negative results by anticipating elements that may prevent the project from being successful. When the studies in the field of risk management are examined, the basic steps of risk management are risk identification, risk analysis, determination of responses to risks, control and recording of risks. It is emphasized that risk management must be repeated throughout the project period and has an active role in the project management process.

Within the scope of the study, literature review on risk management in the construction sector has been conducted and the results of different studies have been examined. The results of the study were evaluated by comparing each other and the risk profile of the construction sector in Turkey was tried to be determined.

The identified risk profile showed that risk management in the sector should be integrated with the concepts of internal control and corporate risk management. For this purpose, the Joint Project Management Portal, a web-based software, has been developed. Within the scope of the study, it is aimed to improve the software by researching the contributions of the software to the companies operating in the sector. It is considered that the data to be obtained as a result of the joint work with the firms will be the source of many studies in this area.

Keywords: Risk Management, Risk in the Construction Sector, Entertainment Risk Management

1. RISK AND RISK MANAGEMENT IN CONSTRUCTION SECTOR

In the business world, risk is an inevitable element for all sectors and brings unsuccessful results if not managed properly. However, the complexity of the construction sector requires a combination of different areas of expertise and its structure contains many uncertainties; Compared to other sectors, it makes the sector more

[1] Corresponding author: Akdeniz University, Department of Civil Engineering, 07070, Konyaalti/Antalya, Turkey. akazaz@akdeniz.edu.tr

[1] Akdeniz University, Department of Civil Engineering, 07070, Konyaalti/Antalya, Turkey. gokcenarslan@akdeniz.edu.tr

[2] Bulent Ecevit University, Department of Civil Engineering, Zonguldak, Turkey. ulubeyli@beun.edu.tr

vulnerable to risks. The fact that technological developments have given a great impetus to the competition in the construction sector and the production of construction projects as one-off diversifies the risks associated with the sector. The various classifications of these risks are shown in Table 1.

Table 14. Various risk classifications of the construction sector

Research Date	Researcher	Classifications of Risks
1985	Perry ve Hayes	Physical Risks Environmental Risks Design Risks Logistics Risks Financial Risks Building Risks
1990	Albahar	Natural Disaster Risks Environmental Risks Design Risks Logistics Risks Financial Risks Building Risks
1994	Tas	Management Risk Market Risk Legal and Regulation Risk Interest Risk Currency Risk
1996	Abdou	Financial Risks Risks due to Duration Design Risks
2001	Chapman	Environmental risks Market Risk Risks due to Owners Project Risks
2015	Eker	*Internal Risks* Owner's Risks Designer Risks Contractual Risks Subcontractor Risks *External Risks* Financial Risks Regulation Risks Policy Risks Environmental risks
2016	Kusan and Others	**Internal Risks** *Production Risks* *Product Management Risks* *Construction Economics Risks* *Resource Risks* *Design Risks* *Technical Risks* *Construction Site Risks* *Contractual Risks* *Contract Management Risks* *Contract Economy Risks* *Scale of a contract Risks* *Partnership Risks* *Conditions of Contract and Penal Sanction Risks* **External Risks** *Politics Risks* *Financial Risks* *Regulative and Bureaucracy Risks*

These risks, in large numbers and varieties, prevent the achievement of the main objectives such as the completion of the project in the planned time, not exceeding the estimated costs and reaching the targeted quality. This makes it necessary to analyze the risks in detail in all projects that are targeted to success and to determine and implement the necessary methods to minimize the potential negative effects. The need to analyze the risks and to show the required attitude against the risks by companies makes effective and successful risk management inevitable.

Risk management is often used in construction projects in the areas of security, cost and time management. In addition, risk management can be used in bid decision making, feasibility studies, market research, performance development, emergency management and at every stage of the project life cycle. [1].

In construction projects, the target is generally defined as function, cost, time and quality limits. For this reason, the most important risks encountered in construction are facing these limits and this situation is considered as failure. However, the risks do not always consist of negative outputs. Opportunities may also be a risk, but the fact that most risks are negative outputs pushes individuals to think that risks are only negative [2].

The fact that the construction project activities are very open to change throughout the process, can be easily affected from the changes in the macro environment, has many components and teams within the construction process and the specific characteristics of each project; it causes many controllable and uncontrollable risks within the construction projects. This situation leads to a variety of scenarios, making risk management in the construction industry challenging, complex and tedious. [3].

As is evident from the literature reviews, time and money are very valuable for every industry, while the competitive and high profit-targeted structure of the construction sector requires effective time and cost management in projects. Efficient use of labor, equipment, materials, cash and time can only be achieved by effective project management. The basic requirements of successful project management are accurate planning and effective communication between units. However, in all stages of the structure supply chain, construction project notifications are weak, incomplete and inconsistent. The acceptance of different terminologies by the project team causes them to be unable to communicate in a common language. This situation leads to losses during the transfer of information and the lack of information raises uncertainties and risks. For effective implementation of risk management in projects, it is necessary to determine a common terminology between the units and to maintain communication on the same language. The project team and the risk management experts need to come together, identify risks through brainstorming and similar methods, analyze them and decide the response to the risks. By gathering the experiences gained as a result of the encountered risks in a pool and storing them in an accessible area along with their effects and resources, it will provide a great advantage for future projects.

2. RISK MANAGEMENT PROFILE OF THE TURKISH CONSTRUCTION SECTOR

The construction sector's complex, highly competitive structure, which requires expertise from many disciplines, makes risk management even more important for the construction sector compared to other sectors. The importance of the subject has led researchers to carry out various studies on risk and risk management in the construction sector. Within the scope of this study, the risk profile of the Turkish Construction Sector has been tried to be examined.

Within the scope of a master thesis, Sener conducted a survey on the risk management practices of 40 people in different occupations and duties in the Turkish Construction Sector. As a result of the survey, it is seen that the firms have little knowledge about risk analysis methods and risk management. It is stated that the reasons for not applying the risk management in the construction sector are; lack of knowing how the risks are managed in construction projects, lack of professional knowledge and considering the risk management process as a waste of time. As a result of the study, it is observed that Turkish contractors and subcontractors use basically two main methods to eliminate risks. The first one preferred to minimize the uncertainty. This can be understood from the fact that they prefer to work with subcontractors or manufacturers they have already worked with and want to keep good dialogue with the employer. It is seen that they prefer risk sharing as second method by adding special substances to contracts or by making All Risk insurance. [4].

As a result of Zabun's master thesis, which was published in 2012; It is seen that project managers predict different risks in line with their experiences and exhibit different attitudes towards these risks. As a result of the examination of 4 projects identified as case studies; project risks are classified under two main headings as

predicted and unpredictable risks. Among the predictable risks, the factors that affect the project to the highest extent are stated as the applicability of the architectural project, insufficiency of the contractor firm, material and construction quality and programming factors. In unpredictable risks; It is seen that the construction phase mistakes and the low labor performance due to the contractor have the highest impact on the project. [5].

Scope of Eker's work in 2015, established risks that may apply to the construction industry, which is then the project goals of these risk factors were classified according to their source; The effects of cost, time, quality and environment-work safety and its relationship with the project process were investigated. The risk classification for the construction sector of our country is shown in Table 1. Table 2 shows the internal and external risk factors affecting the cost, time, quality and environment-work safety negatively.

Table 2. Internal and External Risk Factors Affecting Project Goals Negatively

Basic Project Objectives	Internal Risks Affecting Project Targets Negatively	External Risks Affecting Project Targets Negatively	Risks Affecting Project Targets Negatively in Total
Cost	Designs requiring superior-High technology	War	War
Time	Work stoppage all or partly	War	War
Quality	Use of unsuitable construction methods	War	Using inadequate methods
Environment-Work Safety	Failure to take necessary and adequate occupational safety measures	Occupational Accidents	Failure to take necessary and adequate occupational safety measures
All Projects Targets	Inadequate and inexperienced field team	War	War

As a result of the studies conducted, it has been revealed that the cost target is most adversely affected by designer and policy-based risks, where the time target affected adversely by policy-related risks. It is also revealed that quality target is negatively affected by the contractor risks where the contractor-related risks impacts negatively environmental-work safety. In addition, it was stated that the most affected process was the construction process based on the project processes, and this was thought to be due to the lack of sufficient time and budget for the feasibility and design processes. [6].

In his study, Turker determined the cost of a building construction project for three different situations where risks were not taken into consideration, risks were avoided, and risks were not prevented. Within the scope of the study, three different situations were analyzed and compared with each other. In the results of working; When the risks were taken into account and the measures were not taken, it was seen that the project cost increased by 12% and the project completion time increased by 34% compared to the planned values. In the case of the management of risks and response plans to the project, it is stated that the effect of the risks on the cost decreased by 45% and the duration effect decreased by 42%. [7].

It is understood from the studies that risk is an inevitable phenomenon in construction projects and risk management is very important in terms of project goals and corporate prestige. It is understood from the studies about the risk management in Turkish construction sector that the risks of the project are mainly due to the fact that the design and feasibility processes are not given due importance, and that the source of the risks is largely contractor and policy based.

3. ENTERPRISE RISK MANAGEMENT

According to the COSO Treadway Commission on enterprise risk management, the most widely accepted definition is; "Enterprise risk management is a process, effected by an entity's board of directors, management

and other personnel, applied in strategy setting and across the enterprise, designed to identify potential events that may affect the entity, and manage risk to be within its risk appetite, to provide reasonable assurance regarding the achievement of entity objectives." [8].

In contrast to the traditional risk management approach that risk management undertakes by specific units or individual units within the organization, the Enterprise Risk Management approach addresses the situation in a much wider perspective and deals with the risks and opportunities that affect the creation and protection of corporate value. Enterprise Risk Management enables a strategic analysis of all business-wide risks and build up a risk profile. [9].

In Enterprise Risk Management practices, executives should not expect to have various benefits in a short period of time. The benefits from corporate risk applications can be gained immediately in some areas, while in some areas, earnings are provided in a longer period [10]. The advantages of the institutions together with the establishment of the Enterprise Risk Management system are shown in Table 3.

Table 3. Advantages of Enterprise Risk Management for Companies [11].

	Advantages of Enterprise Risk Management for Companies
1	Improves readiness for changes
2	Reduces operational losses
3	Makes it possible to comply with regulations and respond to risks
4	Predicts uncertainties about performance targets
5	Provides confidence in the systematic risk assessment process
6	Eliminates excess and unnecessary activities
7	Combines the response to the risks
8	Regulates risk transaction cost
9	Determines how much of the risk is tolerated
10	Aligns the organization's business plans with risk management
11	Provides the reliability of the risk assessment process
12	Provides management of all risks in the organization
13	Improves fund and resource allocation
14	Configures risk taking according to self-assessments
15	Protects brand value and reputation.

4. THE CONCEPT OF INTERNAL CONTROL

In today's world the need for accurate and reliable information resulting from the multiplicity and complexity of the transactions formed by the operations of the enterprise has made internal control and external audit indispensable. Internal control is a set of policies and procedures; to achieve the desired results of an enterprise, business policies and government programs, to comply with the identified corporate goals and objectives, to protect the programs from wastage, fraud and mismanagement, to obtain reliable and timely information, to protect and report these information and when necessary to be used in reception mechanisms. [12].

The definition adopted by COSO, which is known by regulatory authorities and audit firms all over the world, is: "In the broadest sense, it is the entity that is affected by the board of directors, senior management and other staff in a business or other organization;

• Efficiency and productivity of operations

• Reliability of financial reporting

• Compliance with then-current legislation and other regulations

It is a process established to provide reasonable assurance for the purposes of the three groups which can be classified as.

There are many factors in the selection and effective implementation of the control methods and techniques of the enterprise. Evaluation of these factors is necessary to evaluate the control methods and techniques. Internal control cannot be expected to achieve its objectives unless an entity has the necessary elements to establish an appropriate and effective internal control system. [13].

As shown in Figure 1, internal control was used in the COSO model; It consists of five interconnected elements.

These:

- Control environment

- Risk assessment

- Control activities

- Information and communication

- Monitoring Activities
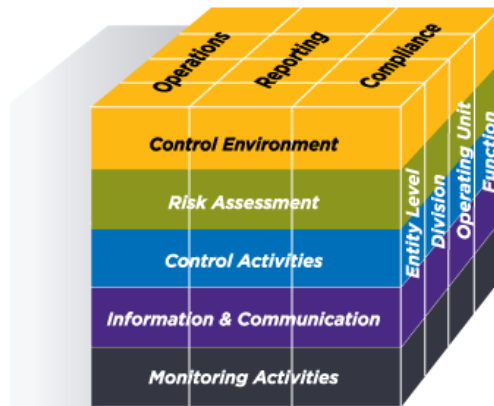
Figure 1. COSO Internal Control Model Elements

5. INTEGRATION OF ENTERPRISE RISK MANAGEMENT AND INTERNAL CONTROL TO CONSTRUCTION SECTOR

It is a fact that risk management is inevitable for construction projects, but only risk management is not sufficient for corporate companies to achieve their strategic plans. In order to institutionalize risk management, a common risk profile and risk appetite should be determined. The management to be carried out on the determined risk profiles should be implemented by all the levels in the institution.

Enterprise risk management shapes the future of companies in line with their strategic plans. However, the evaluation of the acquired experiences and performances also necessitates the supervision of the projects that have been done and are being made. Financial and managerial information should be independently tested for accuracy, reliability, timing, and compliance with standards, policies and procedures.

The institutions operating in the construction sector; because of the long-term, complex and unique nature of the construction projects, it is clear that the need to manage the internal control and enterprise risk management concepts. In line with this requirement, web-based software has been developed for construction companies. It is aimed to synchronize the organization, contract, project, process, risk, internal control and performance management of the companies with the Joint Project Management Portal developed, and to obtain project and company risk maps with interactive inputs by recording project-based experiences.

o   ***Joint Project Management Portal***

Joint Project Management Portal, a web-based software; software consists of seven modules, as shown in Figure 2, including organization management, contract management, project management, process management, risk management, internal control management and performance management.
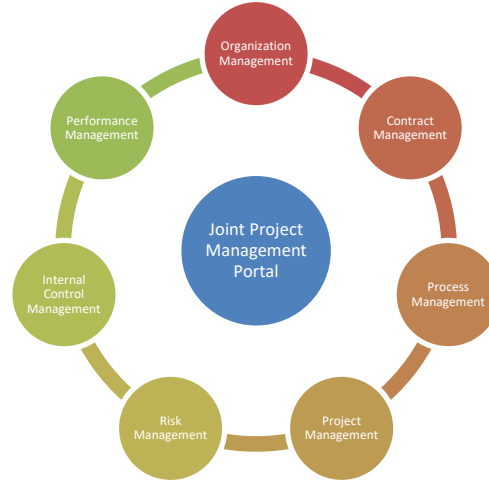
Figure 2. Joint Project Management Portal Modules

The screenshots of the seven main modules and sub-modules of the portal are shown in Figures 3 and 4 below for a better understanding of the software.
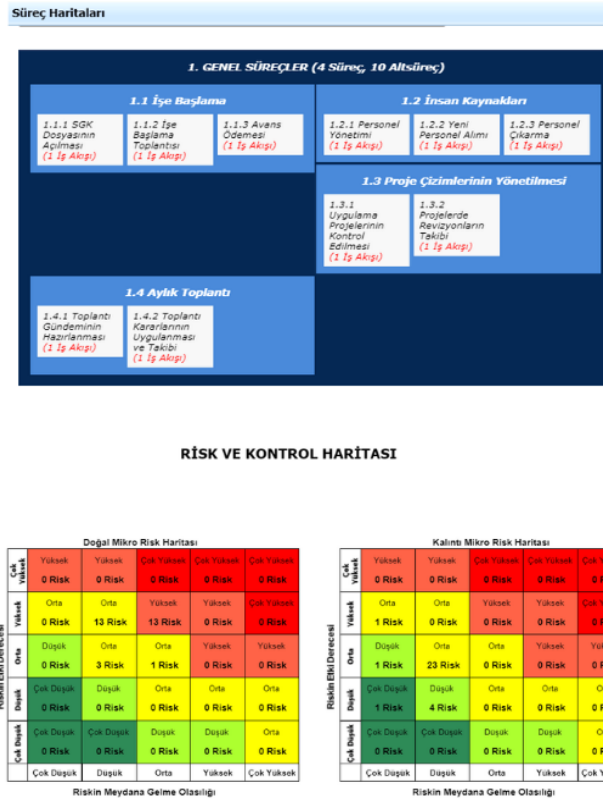
Figure 3. A Screenshot of Process and Risk Maps

Figure 4. A Screenshot of Organization Management Module

Within the scope of the portal, it is aimed to ensure the synchronization between the modules, to prevent miscommunication, to provide dynamism between the units by creating an interactive environment, to ensure process control by monitoring the project processes, to integrate the risks analyzed on a project basis with the company risks, to ensure the compliance with the risk appetite and to increase the efficiency through performance management.

CONCLUSION AND SUGGESTIONS

The unique nature of the construction projects makes the risk inevitable for the sector and brings risk management to a very important position in terms of achieving project objectives and sustainability of institutions. In the literature, it is understood from the studies conducted in the Turkish construction sector that the risks of the project are mostly due to the design and feasibility processes not being given importance, and that the source of the risks is largely contractor and policy-based. As a result of the studies, it is understood that risk reactions are generally ignoring the risks or applying to All Risk insurance and the information about the risk management of the company managers is insufficient. This situation makes the Turkish construction sector vulnerable to risks and makes it an obstacle to sustainability of companies and to increase their efficiency.

It is known that risk management is necessary but inadequate for the construction companies in the way of institutionalization. It is necessary to check the compliance of the project-based risk management practices with the strategic plans of the companies and to implement the proactive management model in every section from the top to the lowest level of the company.

In line with the proactive management model required for the construction companies in the path of institutionalization, a web-based software was developed within the scope of this study. It is foreseen that the software will be a guiding framework for the institutionalization of the construction companies. A result analysis will be carried out according to the data to be obtained as a result of the cooperation to be made with the contractor construction companies and the contribution of the outputs to the companies in terms of risk management will be evaluated.

As a result of the widespread use of the software program mentioned above by the contractor construction companies, it is thought that the awareness level of the risks in construction sector and the key measures to be taken against these risks will increase and the data obtained from the software will shed light on the new researches.

ACKNOWLEDGMENT

REFERENCES

[1]. Han S. H., Kim D.Y., Kim H. and Jang W.S., A Web-based Integrated System for International Project Risk Management, Automation in Construction, 17(3), 342-356, 2008.
[2]. Baloi, D. ve Price, A. D. F., Modelling global risk factors affecting construction cost performance, International Journal of Project Management, 2003, 21, 261-269
[3]. Dikmen I, Birgonul M T, Anac C, Tah J H M, Aouad G, Learning From Risks: A Tool For Post-Project Risk Assessment, Automation in Construction, 2008, 18(1), 42-50
[4]. Sener B, Perception of The Risk for Construction Companies and The Risk Reducing Precautions, M.S. Thesis, Istanbul Kultur University, Institute of Science, Istanbul, Turkey, 2012.
[5]. Zabun A., Case Studies About Risk Management During The Progress Of Project Construction, M.S. Thesis, Istanbul Technical University, Graduate School of Science Engineering and Technology, Istanbul, Turkey, 2012.
[6]. Eker, D., The Relationship Of Risk Factors In Construction Projects With The Project Process And Project Goal, M.S. Thesis, Istanbul Technical University, Graduate School of Science Engineering and Technology, Istanbul, Turkey, 2015.
[7]. Turker M., A Simulation Based Risk Management Model Which Cost, Schedule and Risk are Considered as Together in Construction Projects, Journal of Selcuk-Technic, Volume 14, Number:2, 2015.
[8]. COSO, Enterprise Risk Management-Integrated Frmaework Executive Summary Framework, 2004.
[9]. Thornton, G., An ERM Framework: Developing Effective Risk Management, Corporate Governor Series, 2003.
[10]. Bozkurt, C., Risk, Enterprise Risk Management and Internal Audit, Denetisim Dergisi, s.17-30., 2010.
[11]. Akcakanat O., Enterprise Risk Management and Process of Enterprise Risk Management, Suleyman Demirel University The Journal of Visionary, C.4, S.7. s.30-46, 2012.
[12]. Keskin, D., Internal Control System Control Self-Assessment, Beta Basim Yayim, Istanbul, 2006.
[13]. Duman, O., Accounting and Reporting, Ankara: Tesmer Yayinlari, 2008.

A Case Study of Productivity Improvement by using Cloud-based Process Planning Tools

Filip Mitrevski[1], Pece Mitrevski[2]

Abstract

The paper presents a case study in the development and application of a time study in the production of complex wiring systems for the automotive industry, and discusses the use of cloud-based process planning tools used for the purpose of productivity improvement. The motivation is the necessity to address the issue of productivity per shift between the employees and the management of a company, vis-à-vis questions of productivity. One of the most apparent conclusions is that the time of producing a unit of product is directly proportional to the number of stages in the production pipeline and the time spent at each of them. Nevertheless, to achieve productivity improvements in manufacturing companies, application of new technologies or adoption of mass production may not always be feasible. The most practical approach is to focus on the work process itself – that is to say, review and redesign the operations and apply automation and mechanization. In such cases, productivity assessment using industrial engineering techniques is employed for evaluating the present situation and identifying the potential for increased productivity, whereas additional industrial engineering methods are applied to develop improvement prospects. In view of the fact that the modern industry requires next generation of manufacturing systems to be intelligent, flexible, and interoperable, as well as to offer better performance with lower cost, the wide popularity of the cloud computing paradigm brings the opportunity to manufacturing systems with high scalability, productivity and agility, and provides practical implementations with elastic investment solutions. Since the manufacturing resources and capabilities are provided in a service-oriented architecture as cloud services, some practical models of cloud-based systems are investigated, and distributed process planning services are recommended in a so-called cloud manufacturing system.

Keywords: Process Planning, Efficiency study, Time study, Management analysis, Cloud, Manufacturing System.

1. INTRODUCTION

Process planning is an activity which identifies methods and processes to be used for the manufacture of a part or a product [1]. Its functions may include some or all of the following: selection of operations, sequencing of operations, selection of machines, selection of tools, definition of setup requirements, calculation of parameters, tool path planning, expected manufacturing cost calculation, etc.

The widespread use of Computer Aided Process Planning (CAPP) in modern manufacturing enterprises significantly improves the efficiency of process planning for parts. However, both the organization and management of process planning are typically carried out in a conventional manner, resulting that the overall efficiency of process planning and fast response are somewhat restricted. Aiming at improving process planning efficiency, process planning workflow systems have been introduced [2], putting the related process work into automation – all the related documents and tasks are on the move according to the defined flow, and coordination among participants is achieved.

The fourth industrial revolution brings more flexibility and agility in manufacturing, as a result of a series of advancements in evolving technology domains [3]. For example, production lines' setup times decrease, thus enabling prototyping and iterative production. Consequently, business models change and manufacturing organizations are obliged to innovate, because of the ability to produce customer-driven designs. Businesses must become more agile and respond to dynamic market situation, in order to be competitive in the next manufacturing

---

[1] University "Ss. Cyril and Methodius", Faculty of Computer Science and Engineering, 1000, Skopje, Republic of North Macedonia. *fmitrevski@gmail.com*

[2] Corresponding author: University "St. Kliment Ohridski", Faculty of Information and Communication Technologies, 7000, Bitola, Republic of North Macedonia. *pece.mitrevski@fikt.edu.mk*

age. Increasingly obvious is the shift to collaborative environments, which calls for a service dominant logic, where service is the application of knowledge and skills. In such circumstances, increasing number of organizations outsource resources, capabilities, and/or expertise, and focus on their core competencies.

Having in mind all the advantages of cloud computing as a prominent and popular computing paradigm (e.g. high accessibility, reliability, scalability, elasticity, low set-up costs, as well as ease of maintenance), if one can significantly improve the efficiency and quality of planning algorithms in the cloud, the cloud-based process planning tools can be regularly used by all users and may fundamentally change the application landscape [4]. The remainder of this paper is organized as follows: Section 2 reviews related work towards collaborative process planning for sustainable manufacturing environments. In Section 3 we provide a comparison of a handful of cloud-based process planning tools that offer "free trial" or "freemium" pricing options. A case study in the development and application of a time study in the production of complex wiring systems for the automotive industry, and discussion on the use of cloud-based process planning tools used for the purpose of productivity improvement, are presented in Section 4. Finally, Section 5 concludes the paper with some recommendations for distributed process planning services in a cloud manufacturing system.

2. RELATED WORK: TOWARDS COLLABORATIVE PROCESS PLANNING

A collaborative environment supported by Computer-Aided software (CAx) and networks is a clear trend of the modern production system in recent years [5]. Data files from computer-aided software applications, e.g. Computer-Aided Design (CAD), Computer-Aided Process Planning (CAPP), Computer Aided Manufacturing (CAM), and Computer Numerical Controller (CNC), have gradually replaced conventional paper-based technical documents. In order to support the complex interactions between stakeholders like multiple departments, providers and contractors, these data files are exchanged over the network, while manufacturers aim to provide shorter response time and higher agility to the fast-changing market and dynamic task assignments.

The CAPP-4-SMEs project [6] was aimed at enhancing the competitiveness of European companies, particularly SMEs, in sustainable manufacturing environment by adopting cloud and service-oriented computing approaches (which are the new-generation supplement, consumption, and delivery model for the over-the-Internet provision of dynamically scalable resources and utility computing), as a service platform to:

- support SMEs to move away from developing and maintaining resource-intensive and standalone CAPP systems, and
- migrate to portable CAPP services accessible and configurable over the Internet.

Using the services of cloud manufacturing and knowledge-based process planning, distributed engineering teams can create process plans collaboratively (i.e. Collaborative Process Planning), as illustrated in Figure 1. The knowledge about manufacturing operations, tools and machines contains information about: what operations to use for a certain feature with required tolerances, which tools are most appropriate, and on which machine to perform these operations [7]. Part of this knowledge are data on the particular arrangement of machines and tools among different manufacturing cells.
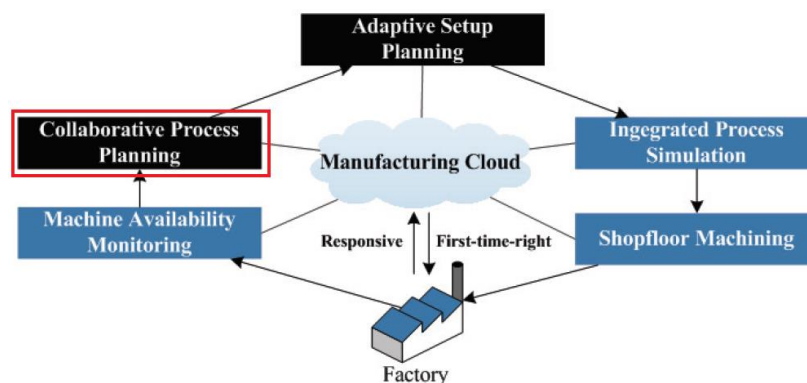
Figure 1. Process Planning-centric Cloud Manufacturing service model (Source: Xi Vincent Wang et al., 2017, p. 41)

Using a client/server architecture, exposed as an HTTP-based Web Service on the server side, and as an Application Programming Interface (API) on the client-side, a prototype implementation of a fast and scalable service that moves planning search to a distributed system has been developed in [8], as shown in Figure 2.
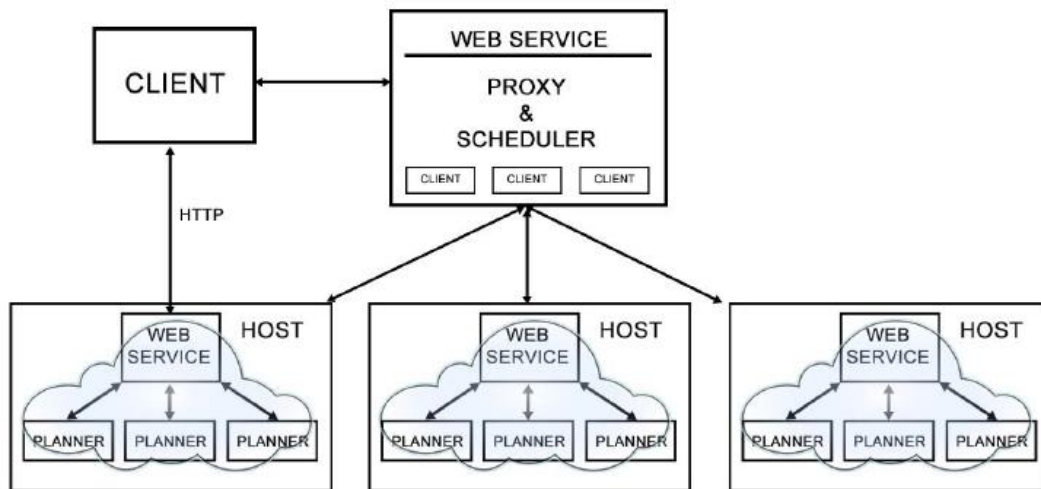
Figure 2. Clients requesting a solution from a specified planning host or via a Proxy & Scheduler that optimizes throughput
(Source: Thompson and Voorhis, 2014, p. 494)

Using the client-side API, a client sends a planning request to the server or a specific planning host, while the planning host, in turn, solves the problem (or generates error messages) and returns a response to the client. Each planning host can run multiple instances of the planning software, created in response to planning requests received via a conventional RESTful (REpresentational State Transfer) Web Service. New (virtual) hosts can be launched or destroyed programmatically, and computational capacity can be algorithmically expanded or contracted in response to demand – it is a feature of typical IaaS (Infrastructure as a Service) cloud facilities. In order to decide when to launch new planning (virtual) hosts or destroy unneeded ones, Proxy & Scheduler uses information about each host's system load and the available computational resources, in addition to the aggregate throughput of planning requests and responses.

3. A COMPARISON OF SELECTED CLOUD-BASED PROCESS PLANNING TOOLS

The section discusses the use of cloud-based process planning tools used for the purpose of productivity improvement, i.e. a handful of Production Scheduling Software tools that offer "free trial" or "freemium" pricing options (provided free of charge, but money (premium) is charged for additional features), material requirements planning (MRP) and/or scheduling features, as well as web-based deployment.

When a manufacturing company can no longer efficiently plan its production with an Excel spreadsheet, **FrePPLe** [9] provides an easy and cost-effective way to boost the planning process to a new level. FrePPLe leverages an open source business model as a unique differentiator in the market of Advanced planning and scheduling (APS) tools.

Cybertec offers a complete range of APS (Advanced Planning and Scheduling) software, in a single solution: **CyberPlan** [10]. This solution supports all the needs of your manufacturing company, from demand planning to finite capacity scheduling. CyberPlan is the solution needed to improve service level, increase productivity and decrease costs.

Delfoi Planner [11] is a transparent, web-based Advanced Planning and Scheduling (APS) software which uniquely includes also manufacturing execution (MES) functionalities. The advanced planning and scheduling software is well suited for discrete and project type manufacturing, service and maintenance operations. Delfoi Planner can be easily integrated into ERP systems using robust and proven interfaces. The most significant benefits for using Delfoi Planner are drastically reduced lead times (the time between the initiation and completion of a production process).

Infor CloudSuite Industrial (SyteLine) [12] is a true mixed mode application for engineer to order, configure to order, highly repetitive, service-based manufacturers and more for both discrete and process markets. Based on a 30-year history, the solution helps manage complexity and growth while gaining performance improvement in customer service, productivity and cost control. One can choose from either on-premises or cloud deployment options.

Table 1. A comparison of selected cloud-based process planning tools

	FrePPLe	CyberPlan	Delfoi Planner	Infor CloudSuite Industrial (SyteLine)
Best For	When a company runs into the limits of an Excel-based planning process, FrePPLe offers an easy and cost-effective way to bring the planning process to a new level of capability and maturity.	Manufacturing companies from each sector (chemical, food and beverage, industrial machinery, metal and mechanical, plastic and rubber, metal forging and stampings, electronic equipment and components).	Machine building, aerospace, plastics and rubber, consumer goods, and food industry.	Metal/plastic fabricators, machinery/equipment, medical device, automotive, aerospace/defense, electronics, furniture, windows/doors, food/beverage, paint/coatings, distributors. 2 tier ERP support.
Product Features	• Automated Scheduling • Capacity Planning • Change Management • MRP • Scheduling • What-if Analysis	• Automated Scheduling • Capacity Planning • Change Management • MRP • Quality Management • Scheduling • What-if Analysis	• Automated Scheduling • Capacity Planning • Change Management • MRP • Quality Management • Scheduling • What-if Analysis	• Automated Scheduling • Capacity Planning • Change Management • MRP • Quality Management • Scheduling • What-if Analysis
Platform	Cloud / Windows	Cloud / Windows	Cloud / Android	Cloud / Windows

4. A CASE STUDY OF PRODUCTIVITY IMPROVEMENT

The section presents a case study in the development and application of a time study in the production of complex wiring systems for the automotive industry, and discusses the use of cloud-based process planning tools used for the purpose of productivity improvement. The motivation is the necessity to address the issue of productivity per shift between the employees and the management of a company, vis-à-vis questions of productivity.

According to [13], "productivity improvement measures can be roughly classified into four groups: (1) redesign of operations, (2) automation and mechanization, (3) use of mass production, and (4) application of new technology – each of which can be effective in specific situations". Opportunities to apply appropriate new technology may be few, and not many products can be made in volumes large enough to justify mass production (with increased diversification of customer demands resulting in more product models). Focusing on the work process itself is usually the most effective approach, as soon as productivity improvements in manufacturing companies are concerned. Improvements are usually made through measures belonging to the first two groups: redesign of the operations, and application of automation and/or mechanization.

Work measurement has been defined by British Standard Institution as "the application of techniques designed to establish the time for a qualified worker to carry out a specified job at a defined level of performance" [14]. On the other hand, work measurement is also called time study and is essential for both planning and control of operations [15]. Time study is a direct and continuous observation of a task, using a timekeeping device to record the time taken to accomplish a task [16] and it is often used when: [17]

- There are repetitive work cycles of short to long duration,
- Wide variety of dissimilar work is performed, or
- Process control elements constitute a part of the cycle.

The Industrial Engineering Terminology Standard, defines time study as "a work measurement technique consisting of careful time measurement of the task with a time measuring instrument, adjusted for any observed variance from normal effort or pace and to allow adequate time for such items as foreign elements, unavoidable or machine delays, rest to overcome fatigue, and personal needs" [18].

Our study focuses on a sample production line (Figure 3) in the manufacturing of complex wiring systems for the automotive industry, in a local plant of one of the global leaders in the supply of electrical systems, cables and plastic components. Fundamentally, the whole organization of the production area and the process flow closely

resemble pipelined execution in a superscalar processor, i.e. a CPU that implements instruction-level parallelism within a single processor by simultaneously dispatching multiple instructions to different execution units.
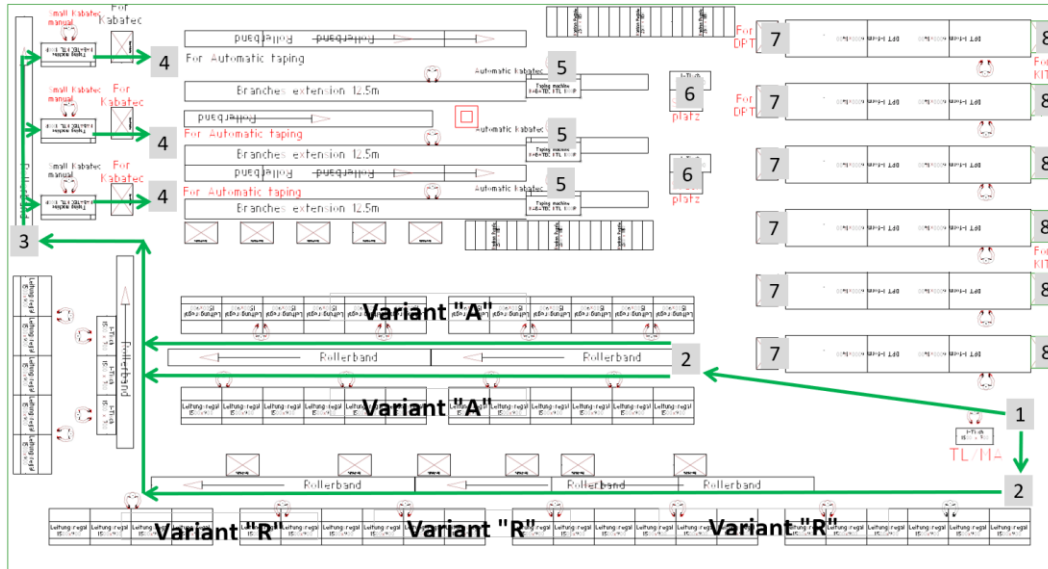
Figure 3. Sample production line workflow

One of the most apparent conclusions is that the time of producing a unit of product is directly proportional to the number of stages in the production line and the time spent at each of them (Table 2):

Table 2. Process flow in the sample production area

#	Stage
1	Line order printing and delivery to the corresponding racks
2	Gathering of wires and material for modules – variant A or R, according to line order
3	Taping on a standard table-top machine with an open winding head
4	Workmanship of modules
5	Taping on a machine for complex cable harnesses with successive winding steps
6	Plugging wires into corresponding housings
7	Dimensional checking of the harnesses
8	Complete harnesses

A browser-based planner can choose the latest possible time to manufacture (based on an order) and the software calculates automatically the point of time when a particular work stage has to begin at the latest. For instance, Delfoi Planner allows for "backward scheduling" to target delivery date, "forward scheduling" from earliest start date, as well as complete "re-scheduling" with new start and/or end date. In this particular case, a saving of approximately 30% in total time (Tables 3 and 4) and man power (Table 5) per production cycle was obtained through an iterative planning process (a cycle of agreement, execution, and assessment).

Table 3. Time study for variant "A"

Variant "A" Steps	Proposed time per step [min]	Total time per operation [min]	Target / Shift	Total time [min]	Man-power
Plug wires	5.75				
Coiling	3.17	11.17	240	2680.20	6.2
Walking	2.25				
Taping on a table-top machine	4.61	4.61	240	1107.00	2.6
Tape, spot tape and route on cable board	6.39	6.39	240	1533.90	3.6
Place on wire shelfs	4.44	4.44	240	1065.60	2.5
Taping on a machine for complex cable harnesses	3.82	3.82	240	916.50	2.1
Plug wires into housings	0.97				
Divide wires	2.11	4.35	240	1044.90	2.4
Strip wires	0.61				
Collect wires and place grommet	0.67				

Route harnesses for dimensional checking	3.58				
Add clips	13.60	18.33	240	4398.84	10.2
Pack	1.15				

Table 4. Time study for variant "R"

Variant "R" Steps	Proposed time per step [min]	Total time per operation [min]	Target / Shift	Total time [min]	Man-power
Plug wires	2.64				
Coiling	2.22	6.10	80	487.80	1.1
Walking	1.25				
Taping on a table-top machine	3.40	3.40	80	272.20	0.6
Tape, spot tape and route on cable board	3.71	3.71	80	296.60	0.7
Place on wire shelfs	2.51	2.51	80	200.80	0.5
Taping on a machine for complex cable harnesses	3.30	3.30	80	263.80	0.6
Plug wires into housings	0.37				
Divide wires	2.37	3.92	80	313.60	0.7
Strip wires	0.82				
Collect wires and place grommet	0.36				
Route harnesses for dimensional checking	1.51				
Add clips	2.38	5.05	80	403.84	0.9
Pack	1.16				

Parameters like number of personnel, different types of skills, time period, etc. are part of manpower planning, i.e. the process of estimating the optimum number of people required for completing a project, task or a goal within time (Table 5).

Table 5. Manpower planning

	Manpower TOTAL
Plug wires	
Coiling	7
Walking	
Taping on a table-top machine	3
Tape, spot tape and route on cable board	4
Place on wire shelfs	3
Taping on a machine for complex cable harnesses	3
Plug wires into housings	
Divide wires	3
Strip wires	
Collect wires and place grommet	
Route harnesses for dimensional checking	
Add clips	11
Pack	

5. CONCLUSION AND RECOMMENDATION

Cloud computing can play an important part in the evolution of manufacturing to "Industry 4.0", as clouds are becoming actual hosting platforms for manufacturing data and software stacks, including applications, with full visibility into everything that comes to pass in the production area. As a benefit of deploying cloud-based solutions, manufacturers can count on standard cloud services, allowing them to pay attention on business-critical functions, decrease capital expenses for hardware/software, pilot and start quickly, enjoy operational flexibility (making it easier to scale up or down as demand changes), as well as to reduce IT management costs [19].

Advanced scheduling software reduces production lead times drastically, minimizes work in progress and improves delivery accuracy. Cloud-based solutions are, generally speaking, easy to deploy and they enhance transparency of planning between production units (multi-site) and sales departments and other interest groups of a company – globally.

Popular features among the best cloud-based production scheduling software include capacity planning, change management, material requirements planning, quality management and scheduling, whereas pricing options vary between free trial, freemium, monthly/annual subscription, and one-time license. We have shown that, by the use of a browser-based HTML5 solution, along with its interface support in mobile and tablets on Android, Windows 8 and iOS, the time spent rescheduling a production plan can be reduced from hours to minutes.

From a more general perspective, in an integrated Web-based Distributed Process Planning system (Web-DPP) [20], dispersed working groups are engaged in a collaborative environment, allowing the team members to share real-time information. As a recommendation for researchers and practitioners, one should note that research efforts on process planning have recently shifted to Cloud-based Distributed Process Planning (Cloud-DPP) [5] based on function-block (FB) technology, in which FBs are either utilized at data level, or exchanged among stakeholders as services, or comprise a dynamic runtime system consisting of both local FBs and remote FBs executed in the cloud. Undoubtedly, the course of moving manufacturing organizations to the cloud is in progress right now – specifically, for companies with the right vision.

REFERENCES

[1]. Tien-Chien Chang, *Expert Process Planning for Manufacturing*, Menlo Park, CA: Addison-Wesley, Inc., 1990.

[2]. Yingying Su, Wanshan Wang, Jianrong Wang, and Shuang Liang, "Research on the Workflow System of Collaborative Process Planning", in *Proc. International Conference on Computer Science and Software Engineering*, 2008.

[3]. Kerem Kayabay, Mert Onuralp Gokalp, P. Erhan Eren, and Altan Kocyigit, "A Workflow and Cloud Based Service-Oriented Architecture for Distributed Manufacturing in Industry 4.0 Context", in *Proc. IEEE 11th International Conference on Service-Oriented Computing and Applications*, 2018.

[4]. Qiang Lu, You Xu, Ruoyun Huang, Yixin Chen, and Guoliang Chen, "Can Cloud Computing be Used for Planning? An Initial Study", in *Proc. Third IEEE International Conference on Cloud Computing Technology and Science*, 2011.

[5]. Xi Vincent Wang, Mohammad Givehchi, and Lihui Wang, "Manufacturing system on the cloud: a case study on cloud-based process planning", *Procedia CIRP*, vol. 63, pp. 39-45, 2017.

[6]. (2013) CAPP-4-SMEs: Collaborative and Adaptive Process Planning for Sustainable Manufacturing Environments. [Online]. Available: www.capp-4-smes.eu.

[7]. Dusan N. Sormaz and Behrokh Khoshnevis, "Knowledge Representation for Automated Process Planning", in *Proc. IEEE International Symposium on Assembly and Task Planning (ISATP '95)*, 1995.

[8]. Tommy Thompson and Dave Voorhis, "Planning in the Cloud: Massively Parallel Planning", in *Proc. IEEE/ACM 7th International Conference on Utility and Cloud Computing*, 2014.

[9]. (2019) Production Planning – frePPLe Open Source Supply Chain Planning Tool webpage on FrePPLe. [Online]. Available: https://frepple.com/features/production-planning/

[10]. (2019) Advanced Planning Scheduling Software / Cyberplan webpage on Cybertec. [Online]. Available: https://www.cybertec.it/en/software-advanced-planning-scheduling/

[11]. (2019) Advanced Planning and Scheduling – Delfoi Planner webpage on Delfoi. [Online]. Available: https://www.delfoi.com/web/products/delfoi_planner/en_GB/advanced-planning-and-scheduling/

[12]. (2019) CloudSuite Industrial (SyteLine) / Manufacturing Cloud Software for SMB webpage on Infor. [Online]. Available: https://www.infor.com/products/cloudsuite-industrial

[13]. Shoichi Saito, "Case Study: Reducing Labor Costs Using Industrial Engineering Techniques" (Chapter 2.9), in *Maynard's Industrial Engineering Handbook*. The McGraw-Hill Companies, 2004.

[14]. (2019) Work Measurement: Definition, Objectives and Techniques webpage on Economics Discussion. [Online]. Available: http://www.economicsdiscussion.net/engineering-economics/work-measurement-definition-objectives-and-techniques/21707

[15]. Satish Keru Raut, Kedar M. Relekar, and Vikas Sarjerao Dhane, "A Case Study of Productivity Improvement by using IE Tools", *International Journal of Innovations in Engineering Research and Technology*, vol. 1, no. 1, Nov. 2014.

[16]. Mikell P. Groover, *Automation, Production Systems, and Computer-Integrated Manufacturing*, 3rd ed. Prentice Hall, 2007.

[17]. Gavriel Salvendy, Ed., *Handbook of Industrial Engineering: Technology and Operations Management*, 3rd ed., John Wiley & Sons, Inc., 2001.

[18]. (2019) Z94.17 – Work Design and Measurement Terminology webpage on Institute of Industrial & Systems Engineers. [Online]. Available: https://www.iise.org/Details.aspx?id=2606

[19]. Mazin Yousif, "Manufacturing and the Cloud", *IEEE Cloud Computing*, vol. 3, no. 4, July-Aug. 2016.

[20]. Lihui Wang and Mohammad Givehchi, "Web-DPP: An Adaptive Approach to Planning and Monitoring of Job-Shop Machining Operations", in *Proc. 7th CIRP International Conference on Digital Enterprise Technology*, 2011.

Re-engineering Information Management Processes and IT Infrastructure: a Survey on ICT Adoption and E-Government Development in WB6 Countries

Ana Sekulovska - Jovkovska[1], Pece Mitrevski[2]

Abstract

The provision of public services and IT infrastructure is one of the main tasks of national administrations. The development of new communication technologies and the emerging importance of the Internet is obliging national authorities to provide a growing number of services online. This, in turn, means that citizens require IT infrastructure and skills to take advantage of electronic services on offer. This paper aims to demonstrate the willingness of ministries in Western Balkans Six (WB6) countries to re-engineer information management processes and IT infrastructure for services to citizens, business stakeholders and to other MDAs (ministries, departments and agencies). To measure the development of national e-Government capacities, the United Nations has generated the E-Government Development Index (EGDI) as a composite indicator that consists of three equally weighted indices – Online Service Index; Telecommunication Infrastructure Index; and Human Capital Index. Conversely, the World Economic Forum is introducing the new Global Competitiveness Index 4.0 (GCI), with a total of 98 indicators, organized into 12 pillars – Institutions; Infrastructure; ICT adoption; Macroeconomic stability; Health; Skills; Product market; Labour market; Financial system; Market size; Business dynamism; and Innovation capability. The focus of this comparative study is on one of the GCI components, i.e. "ICT adoption" (Pillar 3) and the rankings of WB6 countries in e-Government development against the performance of others. Dropping a few positions does not imply that a country had underperformed, nor does higher ranking mean better or more desirable outcomes, especially when it refers to countries belonging to the same EGDI level. The main objective is to raise awareness of stakeholders on key issues in e-Governance implementation to ensure rich content, sustainable service management and efficient use of ICT in support of current efforts in institutional, economic and administrative reform programs.

Keywords: IT Infrastructure, Information Management, Public Policy, ICT Adoption, E-Government Development, WB6 Countries

1. INTRODUCTION

Electronic Government (e-Government) refers to "the use by the Government of web-based Internet applications and other information technologies, combined with processes that implement these technologies, to – (a) enhance the access to and delivery of government information and services to the public, other agencies, and other Government entities; or (b) bring about improvements in Government operations that may include effectiveness, efficiency, service quality, or transformation" [1]. A transformational and participatory e-Government [2] is expected to "cause or permit the relationship between citizens and governments to fundamentally change in positive ways, generally producing much more citizen-centric and responsive government and thereby increasing citizen trust in government dramatically" [3]. All things considered, e-Governance initiatives are similar across the world – providing one-stop service to their stakeholders is the main effort of most of the Governments in their interoperable e-Government systems [4]. Successful e-Government should be able to move people online who are not already there, attract citizens who are already connected online, and enable the transformation to e-

Government at three levels: Government-to-Government (G2G), Government-to-Business (G2B), and Government-to-Citizen (G2C) [5].

An information management process is the method an organization uses to: acquire or retrieve information, organize information, and maintain information [6]. As an upgrade, "the ability of two or more systems or components to exchange information and then use the information that has been exchanged", is one of the first standardized definitions of interoperability, published by IEEE back in 1990 [7]. The concept of interoperability has evolved with the evolution of society: in serving their citizens, government administrations continually face new challenges, and e-Government interoperability is an area of strategic importance [8]. Improving the ability to navigate the information- and knowledge-based economy was an investment of multinational organizations, companies, and other large enterprises at local, regional, and national level. Although founded on technical aspects of data collection and retrieval, interoperability is inherently multidimensional and can counteract barriers to information exchange. In open government, information can be straightforwardly exchanged between an organization and its constituent parts – this shift toward open government has been led by transformative ICT adoption in public organizations. Collaboration is a key principle in open government, relied on and fostered by interoperability as a back-office ICT function. Achieving open government is still essential to achieving any level of "smart government" (including smart and digital cities), even though the differences in maturity levels and evolution of these changes remain challenge while moving forward.

Having in mind that e-Government is the use of Information and Communication Technology and its application by the government for the provision of information and basic public services to their citizens, its main objective is to provide more responsible and accountable services online. Therefore, governments and organizations need to know the e-readiness level to implement e-Government [9]. E-readiness is a measuring tool of national or large sized organization readiness to provide quality e-services, and can be used to evaluate the quality of ICT infrastructure, as well as the ability of consumers, businesses and government to utilize ICT to their benefit [10].

In order to demonstrate the willingness of ministries in Western Balkans Six (WB6) countries to re-engineer information management processes and IT infrastructure for services to citizens, business stakeholders and to other MDAs (ministries, departments and agencies), the remainder of this paper is organized as follows: Section 2 reviews related work towards measuring the development of national e-Government capacities. In Section 3 we perform a correlation analysis between the "ICT adoption" pillar of the World Economic Forum's Global Competitiveness Index (GCI) and the e-Government Development Index (EGDI) 2018, confirming a hypothesis that WB6 countries that have more successfully adopted ICT, better perform in e-Government development. Discussion on the key issues in e-Governance implementation is the main concern in Section 4, whereas Section 5 concludes the paper.

2. RELATED WORK: TOWARDS MEASURING THE DEVELOPMENT OF NATIONAL E-GOVERNMENT CAPACITIES

Numerous e-Government projects have been implemented and various approaches (focusing mainly on technical aspects of inter-organizational communication) have been proposed for the design and the development of architecture to deliver e-Government services to citizens – initiatives, frameworks, reference models, architectures, etc. [11]. Relevant European initiatives, frameworks and roadmaps to develop interoperability of enterprise applications and software are presented in ATHENA, IDEAS, INTEROP NoE, and other EU-funded projects. ECOLEAD has directly addressed issues on Collaborative Networking performance, whereas the eGOV project, the FASME project, the EU-PUBLI.com project and the eGovSM project support the automation of administrative processes involving several administrations and allowing the reuse of data. For example, the eGovSM is formalized using a set of XML Schema models in order to support the realization of an interoperable system.

To address the problem of e-Government fragmentation and ensure that e-Government could deliver the next generation of public services to citizens and businesses, in 2009, the European Commission (EC) issued Decision No. 922/2009/EC – a mandate to establish the Interoperability Solutions for European Public Administrations (ISA) program [12]. In December 2010, the EC adopted the European Interoperability Strategy (EIS) and the European Interoperability Framework (EIF) [13], which has four main contributions: a set of underlying interoperability principles; an interoperability model composed of technical, semantic, organizational, and legal interoperability levels; a public service model; and 25 recommendations to guide European public services development. The ISA program, which ended in December 2015, created the European Interoperability Reference Architecture (EIRA) (Figure 1).
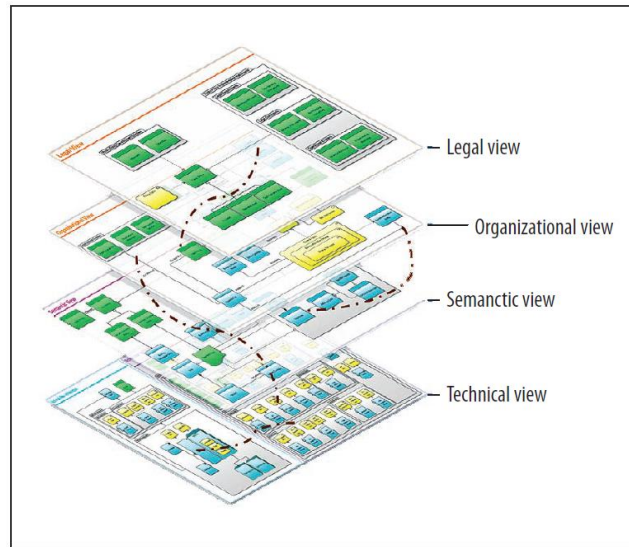
Figure 1. Four layers of the European Interoperability Reference Architecture (EIRA) (Source: Bovalis et al., 2014, p. 28)

To measure the development of national e-Government capacities, the United Nations has generated the E-Government Development Index (EGDI) [14] as a composite indicator that consists of three equally weighted indices – Online Service Index (OSI); Telecommunication Infrastructure Index (TII); and Human Capital Index (HCI). Conversely, the World Economic Forum is introducing the new Global Competitiveness Index 4.0 (GCI) [15], with a total of 98 indicators, organized into 12 pillars – Institutions; Infrastructure; ICT adoption; Macroeconomic stability; Health; Skills; Product market; Labour market; Financial system; Market size; Business dynamism; and Innovation capability. The scope of the GCI 4.0 and its 12 pillars captures the extent and complexity of the competitiveness ecosystem. The results suggest that "the quality of the overall ecosystem is as good as the quality of its weakest component. It is therefore not surprising that the most competitive economies tend to perform well on all pillars, whereas the least competitive economies tend to struggle in all areas".

As far as Western Balkan (WB) countries are concerned, the focus of a recent comparative study [16] was to examine the level of development of e-Government in WB countries and to compare it with the EU countries, in order to cover the geographical gap in past research. The analysis is based on a number of e-Government survey reports conducted by the United Nations between 2003 and 2018 – the data were extracted and distilled from survey reports on both regions, in order to perform a trend analysis and descriptive comparison. More precisely, the study makes a comparison of EGDI and its components.

However, UN's data on e-Government, e-services or e-participation do not cover Kosovo[*] (in line with United Nations Security Council Resolution 1244). Using the Unified Theory of Acceptance and Use of Technology (UTAUT), the intention of Kosovo's citizens to adopt e-Government was measured in [17] by representing e-Government as behavioral intention to adopt it. The study concludes that the complexity of the e-Government platforms should be reduced and more user-friendly software should be developed, which can be easily used by individuals who are less competent on using internet services, and that the government should try to raise awareness of e-Government existence and benefits.

3. CORRELATION OF E-GOVERNMENT DEVELOPMENT INDEX (EGDI) 2018 AND THE ICT ADOPTION

According to [14], in 2018, there are more countries with values between 0.50 and 1.00, or High- and Very-High-EGDI. Consequently, the cumulative percentage of countries with High and Very-High levels of e-Government development has reached 58%, nearly two-thirds of the United Nations Member States. Moreover, 40 countries scored "Very-High", with EGDI values in the range of 0.75 to 1.00, as compared to only 29 countries in 2016 (Figure 2).

In addition, the United Nations has identified 32 countries that are landlocked developing countries (LLDCs), which have the additional obstruction as countries with limited access to the sea. Namely, they rely on bordering countries for access to important telecommunication infrastructures, and their access to the international market depends on their neighboring countries, as well. This, in turn, increases the cost of trading. The African region is

represented with 16, followed by Asia with 12 and the Americas with 2 and Europe with 2. North Macedonia, as a country belonging to the Southern Europe sub-region, has been ranked fourth among the Top 10 Landlocked Developing Countries for e-Government.
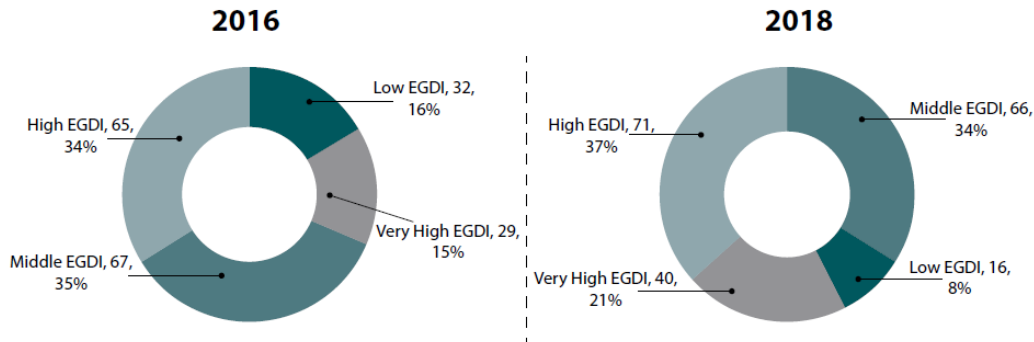
Figure 2. Number of countries grouped by E-Government Development Index (EGDI) in 2016 and 2018 (Source: United Nations E-Government Survey, 2018, p. 84)

Table 1. Rankings of WB6 countries in e-Government development against the performance of others

Very High EGDI 2018 (Greater than 0.75)	High EGDI 2018 (Between 0.50 and 0.75)	Middle EGDI 2018 (Between 0.25 to 0.50)	Low EGDI 2018 (Less than 0.25)
40 countries	71 countries (including Albania, Bosnia and Herzegovina, Montenegro, North Macedonia, and Serbia)	66 countries	16 countries

The focus of this comparative study is on one of the GCI components, i.e. "ICT adoption" (Pillar 3) and the rankings of the Western Balkan countries (WB6 – Albania, Bosnia and Herzegovina, Montenegro, North Macedonia, Serbia, and Kosovo[*]) in e-Government development against the performance of others. It is relevant to repeat that the E-Government Development Index is a normalized broad relative index, and dropping a few positions in rankings does not necessarily imply that a country had underperformed in the survey period, nor does higher ranking always mean better or more desirable outcomes, especially if it refers to a country belonging to the same EGDI level (High – between 0.50 and 0.75 – for the WB6 countries) (Table 1). Every country should determine the level and extent of its digital government objectives based on its specific national development context, capacity, strategy and programs, and never on an arbitrary assumption of its future position in the ranking. EGDI is a powerful and reliable benchmarking tool for development, but only if it is used as a snapshot performance indicator, and not "an award" conferred to worldwide leadership positions or outstanding advancements against the performance of others.

The correlation of EGDI and the global competitiveness of countries, assessed by the World Economic Forum in its Global Competitiveness Report 2015-2016, shows that "countries that have performed in e-Government development are more competitive" [18] (Figure 3).
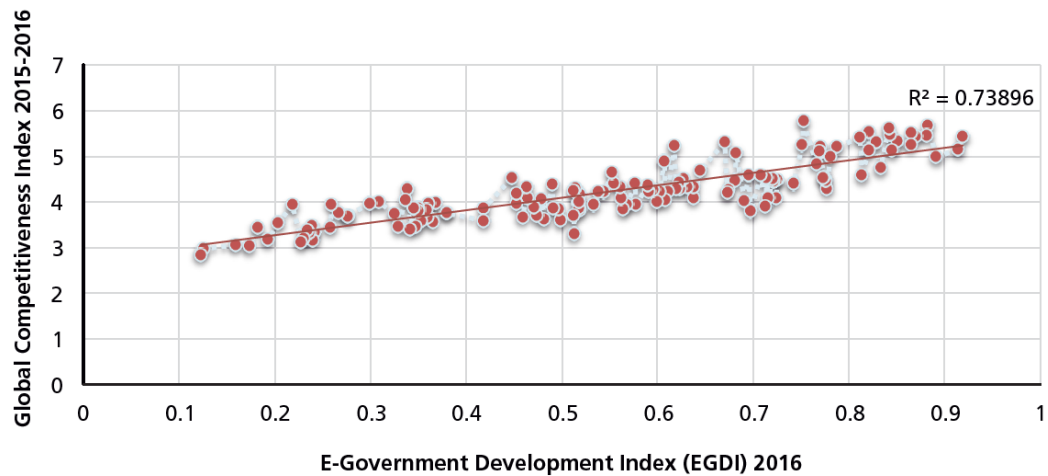
Figure 3. Correlation of E-Government Development Index (EGDI) 2016 and the global competitiveness (2015-2016)
(Source: United Nations E-Government Survey, 2016, p. 125)

In a similar fashion, we raise the following question: how does the ICT adoption score (i.e. Pillar 3) of the World Economic Forum's Global Competitiveness Report 2018 correlate with the EGDI 2018 for the WB6 countries (Table 2)?

Table 2. EGDI 2018 vs. ICT adoption for WB6 countries

WB6 Country	ICT adoption score 2018	EGDI 2018
Albania	52.3	0.6519
Bosnia and Herzegovina	45.8	0.5303
Montenegro	57.1	0.6966
North Macedonia	54.0	0.6312
Serbia	56.9	0.7155
Kosovo[*]	(not covered by the UN's data on e-government, e-services or e-participation)	
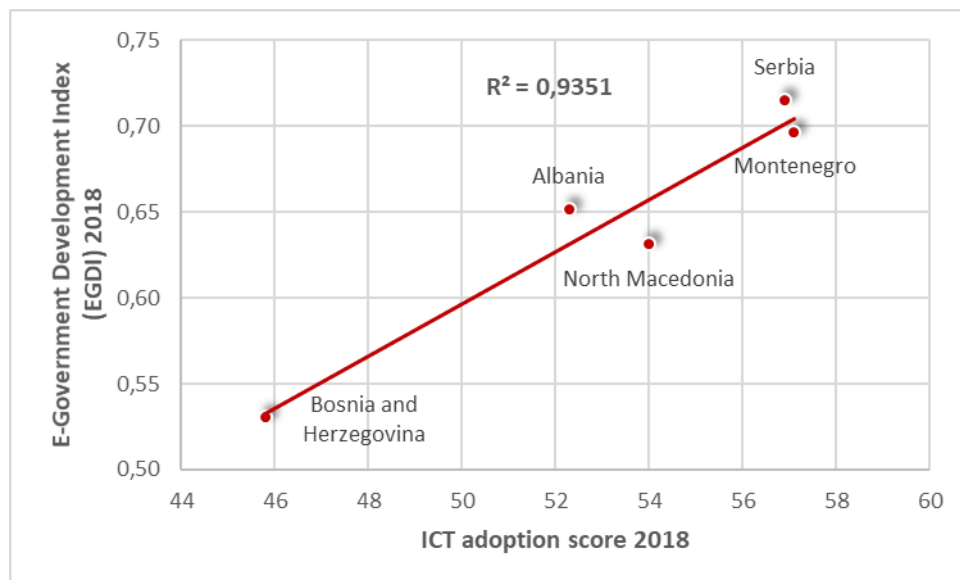
Figure 4. Correlation of ICT adoption score and the E-Government Development Index (EGDI) 2018

In this particular case, the correlation coefficient between the two data sets (R = 0.967009; R^2 = 0.9351) shows a strong uphill (positive) linear relationship, i.e. the countries that have adopted ICT to a larger extent, better perform in e-Government development (Figure 4).

4. DISCUSSION ON SOME KEY ISSUES IN E-GOVERNANCE IMPLEMENTATION

The ability for a country to benefit from ICT depends on an enabling environment that includes the following [19]: mature technical infrastructure in various government departments; civil service willing to re-engineer, share information and treat citizen as customers; legal framework that fosters public confidence and supports a government mandate to conduct transaction online; political commitment from managers; aware citizens that understand their rights. Although not many countries are entirely prepared on all the aforementioned dimensions, this should not discourage them from "starting small" through pilot projects used to result in changes in public sector performance.

Citizens prefer online transactions for most services, as it has been revealed by many survey results (e.g. on average a citizen's level of digital preferences accounts for more than 80% [20]). Furthermore, citizens primarily favor classic online channels, i.e. online forms and e-mail, but they indicate preferences for multi-channel (Mobile app, Live chat), as well.

In respect to service delivery channels, most entities provide classic online channels, i.e. online forms on websites as well as e-mails, while only a small number provide a mobile application for citizens to transact services online. Thus, instead of establishing an interplay, citizens' preferences are not matched by government supply – there is "a large gap between the citizens' level of digital preferences and the level of digitalization" [20].

Performance expectancy, i.e. the degree to which the user expects that using the system will help him or her to attain gains in job performance, positively influences a person's perceived likelihood or subjective probability that he or she will engage in a given behavior. In other words, with the belief that using ICT will improve their job performance, employees of government organizations are more likely to adopt ICT [21].

5. CONCLUSIONS

Widespread ICT adoption can be a growth facilitator and can be used to initiate the necessary changes to make it happen. Nevertheless, translating an ambitious dream into practical steps that fit a specific national development context, capacity, strategy and programs, is not a simple task. Governments must ensure effective coordination of different ICT initiatives across ministries and government agencies, and should be proactive in converging these ICT initiatives towards common national priorities.

It is becoming more and more clear that for a country to put ICT in effective use, it must be e-ready in terms of infrastructure and accessibility of ICT to the overall population. Therefore, efforts must be made to find ways to improve e-readiness of countries and communities by re-engineering information management processes and services between government agencies, departments or organizations (G2G), between subjects of public administration and enterprises (businesses) (G2B), as well as citizens (G2C), especially in queries, payments, form-filling, bookings and various types of registrations that they require to function. The correlation analysis of the ICT adoption score and the EGDI of WB6 countries shows that countries that have adopted ICT to a larger extent, better perform in e-Government development.

REFERENCES

[1]. (2002) E-Government Act of 2002. [Online]. Available: https://www.govinfo.gov/content/pkg/PLAW-107publ347/pdf/PLAW-107publ347.pdf

[2]. Hun Myoung Park, "Should E-government Be Transformational and Participatory? An Essay on E-government in the Utilitarian Mode of Information Technology Use", in *Proc. 48th Hawaii International Conference on System Sciences*, 2015.

[3]. Coursey and D.F. Norris, "Models of E-government: Are They Correct? An Empirical Assessment", *Public Administration Review,* vol. 68, no. 3, pp. 523-536, 2008.

[4]. Paul and V. Paul, (2012, October). "The e-Government interoperability through Enterprise Architecture in Indian perspective", in *Proc. 2012 World Congress on Information and Communication Technologies (WlCn)*, pp. 645-650, IEEE, 2012.

[5]. R. O. Shannak, "The Difficulties and Possibilities of EGovernment: The Case of Jordan", *Journal of Management Research*, vol. 5, no. 2, pp. 189-204, 2013.

[6]. (2019) Glossary webpage on Experian Limited. [Online]. Available: https://www.experian.co.uk/business/glossary/information-management-process/

[7]. *IEEE Standard Computer Dictionary: A Compilation of IEEE Standard Computer Glossaries*. New York: IEEE, 1990.

[8]. Carlos E. Jiménez, Agusti Solanas, and Francisco Falcone, "E-Government Interoperability: Linking Open and Smart Government", *IEEE Computer*, 2014.

[9]. Shreedhar Marasini and Subarna Shakya, "E-readiness To Implement E-government: An overview study in HR domain in Nepal", in *Proc. 2015 International Conference on Green Computing and Internet of Things (ICGCloT)*, 2015.

ICENS — 5TH INTERNATIONAL CONFERENCE ON ENGINEERING AND NATURAL SCIENCE — 12-16 June 2019 Prague

[10]. Pornchai Chanyagorn and Bundid Kungwannarongkun, "ICT Readiness Assessment Model for Public and Private Organizations in Developing Country", *International Journal of Information and Education Technology*, vol. 1, no. 2, pp. 99-106, 2011.

[11]. Mohamed Mahmoud El Benany and Omar El Beqqali, "SOA Based E-Govemment Interoperability – BPEL Orchestration Approach", in *International Workshop "Wireless Technologies and Distributed Systems" (WITS)*, IEEE, 2015.

[12]. Konstantinos Bovalis, Vassilios Peristeras, Margarida Abecasis, Raul-Mario Abril-Jimenez, Miguel Alvarez Rodríguez, Corinne Gattegno, Athanasios Karalopoulos, Ioannis Sagias, Szabolcs Szekacs, and Suzanne Wigard, "Promoting Interoperability in Europe's E-Government", *IEEE Computer*, Oct. 2014.

[13]. European Commission, "Towards Interoperability for European Public Services", *Communication from the Commission to the European Parliament, the Council, the European Economic and Social Committee and the Committee of the Regions*, COM 744, 2010.

[14]. (2018) United Nations E-Government Survey 2018. [Online]. Available: https://publicadministration.un.org/egovkb/Portals/egovkb/Documents/un/2018-Survey/E-Government%20Survey%202018_FINAL%20for%20web.pdf

[15]. (2018) World Economic Forum's The Global Competitiveness Report 2018. [Online]. Available: http://www3.weforum.org/docs/GCR2018/05FullReport/TheGlobalCompetitivenessReport2018.pdf

[16]. Nikola Levkov, "Comparative Study on E-Government Indicators between Western Balkan Countries and the EU Countries", *Annual of the Faculty of Economics – Skopje*, vol. 53, pp. 219-232, 2018.

[17]. Marigona Geci, Burim Prenaj, Adelina Zeqiri, and Behare Sholla. "Adoption, Diffusion and Use of E-Government Services in Kosovo", in *Proc. 1st International Scientific Conference "Knowledge Based Society as a Strategy for Faster Economic Growth"*, Faculty of Economics, University of Prishtina, 2017.

[18]. (2016) United Nations E-Government Survey 2016. [Online]. Available: http://workspace.unpan.org/sites/Internet/Documents/UNPAN97453.pdf

a. Okoronkwo Matthew and N. Agu Monica, "E-Readiness Assessment of Enugu State, Nigeria", *Asian Journal of Information Management*, vol. 5, pp. 25-34, 2011.

[19]. Lea Thiel, "The Interplay between E-Government Service Adoption Preferences and E-Government Service Delivery in Germany", in *Proc. 49th Hawaii International Conference on System Sciences*, 2016.

[20]. Yihong Zhan, Ping Wang and Shouxin Xia, "Exploring the Drivers for ICT Adoption in Government Organization in China", in *Proc. Fourth International Conference on Business Intelligence and Financial Engineering*, 2011.

Effect of Fiber Blend Ratio on Yarn Packing Density

H.Ibrahim Celik[1], Gulistan Canli[1]

Abstract

Both synthetic and natural fibers cannot be produced by adapting themselves to the area in which they are used. By combining these synthetic and natural fibers, desired characteristic features can be acquired within the same structure. The distribution and uniformity of the fibers in the cross-sections of blended yarns in textile materials are important in determining the structural, functional, mechanical and visual properties of the products. The distribution of the different fibers in the cross-section of the blend yarns has an important effect. Also, the packing density is a very significant parameter because it determines the characteristics of the yarn such as feeling, dyeing, temperature and volume. For this purpose, 30/1 Ne ring yarns with three different twist coefficients; 3.5 α, 4.0 α, 4.5α and three cotton/acrylic blend ratios; 40/60, 50/50, 75/25 were produced to analyze the effect of fiber blend ratio and twist coefficient on yarn packing density. The yarn packing density values were determined by using an image processing algorithm. The results were discussed and statistically evaluated.

Keywords: Yarn Packing Density, Blend Ratio, Twist Coefficient, Image Processing, Cotton, Acrylic

1. INTRODUCTION

Today, it is mentioned that yarns are made in order to take advantage of the charging properties of different fibers in the same final product. Both synthetic and natural fibers cannot be produced by adapting themselves to the area in which they are used, but by combining these synthetic and natural fibers, desired characteristic features can be acquired within the same structure. The yarn structure characteristics and fiber distribution within the cross-section have significant effect on both yarn and fabric performance properties. When the previous studies were searched, it was seen that there are many studies on the structural properties of yarns and yarn performance properties. In particular, there are many papers in which different methods are proposed for measuring fiber migration, yarn packing density and yarn diameter properties. However, these studies have mostly focused on yarns that made of a single fiber type.

Hussain U. et al. presented the effect of spinning variables on packing density of cotton yarn [2]. The study revealed that the raise in yarn count, TPI and spindle speed lead to increase of yarn packing density. Zou Z. et al. presented effect of some variables on the fiber packing pattern in a yarn cross-section for vortex spun yarn [3]. The results demonstrated that the fiber fineness, yarn count, distance from the front roller nip point to the hollow spindle, nozzle pressure and yarn delivery speed are all significant parameters for yarn hairiness and fiber packing density in a vortex spun yarn cross-section. Kilic M. et al. presented a study on comparing the packing densities of yarns samples produced with ring spinning, compact spinning and vortex spinning systems. The packing densities were measured by using image analysis method [4]. Result showed that compact yarns have the highest packing densities while vortex yarns have the lowest. However, differences between the packing densities of ring and compact yarns are not found statistically significant. Results displayed that the packing density values are parallel to yarn density values. Taheri M. et al. presented a study on investigating the effect of yarn count twist factor on the packing density and wicking height of lyocell ring-spun yarns [5]. The results showed that the correlation factor between the predicted and measured wicking height was 0.98 indicating the capability of the presented model to predict the wicking height of lyocell ring-spun yarns. Kumar A. et al. presented impact of yarn extension on packing density of ring yarn [6]. It was emphasized that the radial packing density of the yarn is not regular across the cross-section of the yarn. It is not maximum close the yarn axis, rather it is maximum at

---

[1] *Corresponding authors: Gaziantep University, Textile Engineering Department, Gaziantep, Turkey, hcelik@gantep.edu.tr, canligulistan@gmail.com*

some length from the yarn axis. Zheng S. et al. presented a paper of the fiber distribution in yarn cross-section for vortex spun yarn [7]. According to the research, it was understood that the density of fiber packing in vortex yarn is lower both in the center and on the surface than in the conventional ring yarn. In bamboo / cotton blended vortex yarns, it is stated that bamboo fibers are more easily distributed in the yarn core. Ishtiaque S. M. et al. presented a study on the effect of process parameters on packing density of open-end and core-sheath friction spun yarns [8]. It was concluded that core-sheath friction yarns have greater packing density but lower yarn diameter and helix angle than open-end friction yarns. Yilmaz D. et al. introduced packing density of compact yarns [9]. The outcomes of packing density values of compact yarns produced via three different compact yarn spinning systems, namely Rieter K44, Suessen Elite and Zinser Air- Com-Tex700, find out that there are no remarkable differences among these systems, with regard to yarn packing density values. Kumar A. et al. introduced paper on influence of spinning operation variables on the packing density of air-jet, ring and rotor yarns using the Taguchi method [10]. It was concluded that a decrease in the rotor spinner and an increase in draft in the air-jet raises the packing density of the severally yarns. Jiang X.Y. et al. introduced a study on the assignation the cross-sectional packing density of rotor spun yarns [11]. Tyagi G.K. and Kaushik R.C.D. introduced radial packing density and related features of polyester DEF-3 yarns [12]. Kumar Sinha S. et al. presented a paper about the packing density of modified ring spun yarn [13].

In the scope of study, the effects of fiber blend ratios and twist coefficient on yarn packing density of blended yarns were investigated. For this aim, cotton ring spun yarns with three different twist coefficients; 3.5α, 4.0α, 4.5α and three different cotton/acrylic blend ratios; 40/60, 50/50, 75/25 were produced. On the other hand, an image processing algorithm was developed to determine yarn packing density. Thus, it is aimed to easily and precisely determine the packing density characteristics of the yarn from yarn cross-section images with the developed algorithm. The yarn packing density results were analyzed statistically.

2. MATERIAL AND METHOD

In this study, Ne 30/1 ring spun yarn samples with 3 different blend ratios, 3 different twist factors were produced. The blend ratios were determined as 75/25%, 50/50%, 40/60% cotton/acrylic. The twist factors were determined as α=3.5, 4 and 4.5. Thus, totally 9 yarn samples were produced by using conventional ring spinning machine (Zinser 351). The fiber properties used in yarn sample production are submitted in Table 1. The physical properties of yarn samples are given in Table 2.

Table 1. Fiber properties

Fiber Properties	Cotton (American)	Acrylic (Dralon)
Fiber Fineness	5.21 g/inch	1.3 ± 0.2 dtex
Breaking Elongation	5.10%	23 ± 5 %
Strength	30.6 g/tex	≥ 25 cN/tex
Radiance	76.6	Bright
Moisture	6.60%	-
C-Grade	30-1	898
U Index	81.8	-
SF-Value	8.4	2.4

Table 2. Yarn Physical Properties

S. No	Blend Ratio % (Co/Acry)	Ne	Twist Ratio (α)	U%	CVm %	Thin -50%	Thick +50%	Neps +200%	Elong. (%)	Strng. (cN/tex)	H.	Dia. (mm)	Density (g/cm³)
Y.S.1	40/60%	30/1	3.5	11.99	15.53	16.30	268.80	580.00	8.08	13.18	8.86	0.24	0.43
Y.S.2	40/60%	30/1	4	12.13	15.59	11.30	303.80	665.00	7.31	12.59	7.86	0.23	0.47
Y.S.3	40/60%	30/1	4.5	11.96	15.33	10.00	245.00	617.50	7.74	13.86	7.02	0.22	0.52
Y.S.4	50/50%	30/1	3.5	11.20	14.35	2.50	168.80	372.50	13.32	5.77	8.29	0.24	0.43
Y.S.5	50/50%	30/1	4	11.07	14.12	2.50	146.30	385.00	6.85	13.45	7.19	0.23	0.48
Y.S.6	50/50%	30/1	4.5	12.01	15.40	8.80	278.80	518.80	7.29	13.69	6.66	0.22	0.52
Y.S.7	75/25%	30/1	3.5	13.12	17.03	12.50	475.00	738.80	5.68	9.99	8.95	0.26	0.37
Y.S.8	75/25%	30/1	4	13.52	17.41	11.30	470.00	792.50	6.05	13.30	8.13	0.24	0.43
Y.S.9	75/25%	30/1	4.5	13.42	17.31	23.80	515.00	833.80	6.28	14.03	7.18	0.23	0.48

There are several methods in literature to determine the packing density. The yarn packing density can be determined by using three different methods; direct method, secant method and tracer fiber method.

In this study, direct method was used. To apply the direct method, yarn cross-section views under microscope must be acquired. For this aim, the yarn samples were placed into a resin and solidified separately. Some special molds were used to solidify the samples. The yarn cross-section slices were taken by using Microtome device (Figure 1). To calculate an average packing density value, 9 yarn molds were prepared form each sample.

Figure 1. Microtome and yarn sample mold views on microtome device

Firstly, the samples prepared in the mold were placed on the microtome device. Then section thickness adjustment was done on the microtome. In this study the optimum thickness, obtained from the results of many trials, was determined as 16µm. After the sections were taken at the specified thickness, they were examined under a microscope and yarn cross-section images were taken (Figure 2). Cross-sectional images were analyzed with image processing software that prepared on MATLAB.
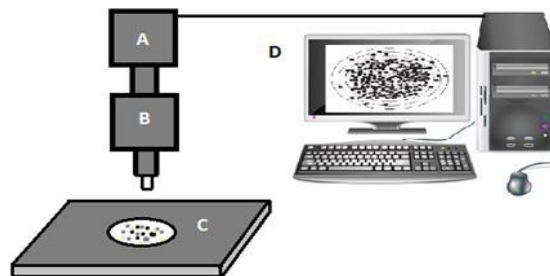
Figure 2. Schematic diagram of the image-acquisition system (A) Camera (Leica DM1000), (B)Optical Microscope, (C) Yarn Cross-Section Sample, (D) Computer,

In order to determine the desired yarn structure properties from cross-section views, an image processing algorithm was developed in MATLAB environment. Since the spaces between fibers in yarn cross-section will be determine, it was thought that these spaces can be detected in accordance with the light intensity value differences at fibers and spaces. For this aim, an image processing algorithm based on noise removing filters, low pass filters and binarization was developed (Figure 3).

Figure 3. Yarn packing density algorithm

First of all, the size adjustments for yarn cross-section image frames were made on MATLAB. The image frame in RGB (Figure 4.a) form was converted to gray level. The noising removing operation was achieved by using Gaussian filter. The Gaussian filter was used for image smoothing as low-pass filter. Then, the image frame was converted to binary form (Figure 4.b). In order to determine the yarn packing density exactly, morphological closing was applied to fill in the spaces in fiber lines (Figure 4.c). Closing is the name given to the morphological operation of dilation followed by erosion with the same structuring element.
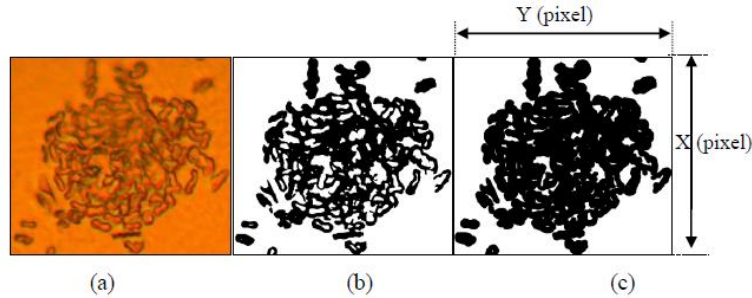
Figure 4. Packing Density Views of Yarn Cross-sections, (a)Microscope view, (b) Binary view, (c) Morphological Closed view

The yarn total cross-section area is calculated by selecting the maximum axis of the binary image size as the diameter of the yarn (Figure 4.c). Finally, the ratio of total black pixes to total pixels in yarn cross-section was calculated as yarn packing density.

3. RESULTS AND DISCUSSION

Packing density measurement results are given in Figure 5. As seen from Figure 5, there is a consistency between cotton content and packing density of the yarn samples among all twist coefficients. As the cotton content of the yarn increase, the packing density of the yarn sample also increase. This result means that cotton fibers are located very close to each other with lower spaces. The result can be attributed to the cross-section geometry of acrylic and cotton fibers (Figure 6). The cotton fibers have higher roughness and spaces. This situation allows more compact placement of cotton fibers. On the other hand, the acrylic fiber has less roughness and spaces. The packing capacity of the fibers also depends on their bending rigidity and compressibility characteristics. Since the cotton fiber has lower bending rigidity than acrylic, higher packing density was obtained with higher cotton content.
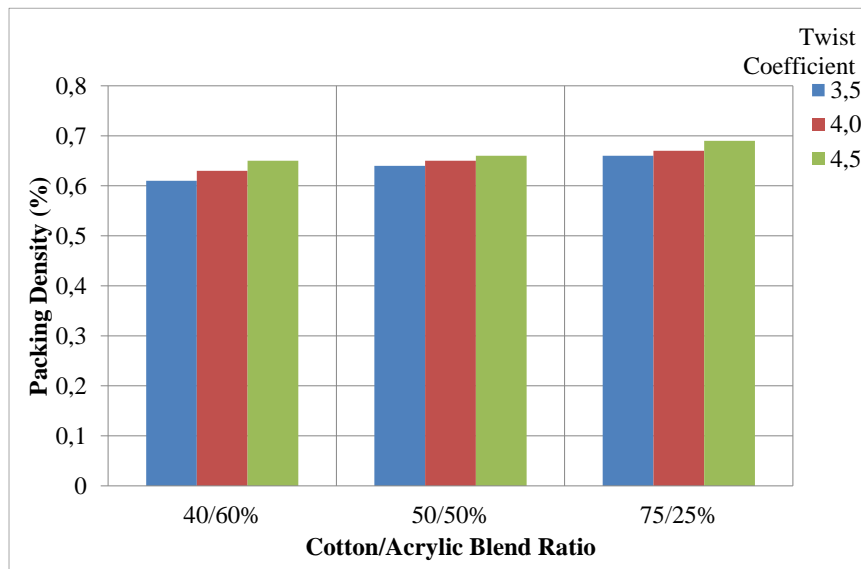
Figure 5. Packing density of yarn samples
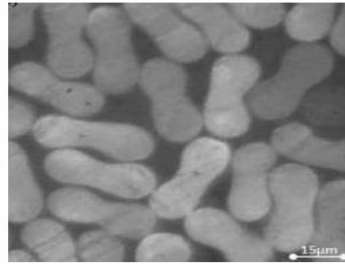
Figure 6. a) Acrylic fibers view   b) Cotton fibers view
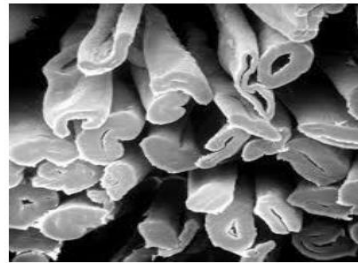
Similarly, as the twist factor increases, the packing densities of all blend ratios also increase. There is also consistency between twist coefficient and packing density. This result can be explained with decreasing effect of twist coefficient on yarn diameter (Table 2). Due to higher radial force of higher twist per unit length, the yarn diameter decreased as the twist coefficient increased. Thus, the lower yarn diameter provides higher packing density because of lower area per unit fiber amount. This property provides a tighter yarn structure.

Packing density and fiber density are the main factors determining yarn diameter. Yarn diameter will be higher with fibers of lower density because of higher fiber diameter. Finer fibers compact better than coarser fibers and result in lower yarn diameter. Further, coarser fibers offer greater resistance to bending during twisting leading to higher diameter. Longer fibers result in lower diameter because of reduced hairiness and better compaction.

ANOVA results for fiber blend ratio and twist coefficient are given in Table 3. As given in Table 3, both of the independent parameters; twist factor (p= 0.000) and blend ratio (p= 0.000) has statistically significant effect on yarn packing density values, in 95% confidence interval. It can be analyzed that the blend ratio has higher (F = 17.840) and twist coefficient (F=12.4).

Table 3. Yarn packing density ANOVA results

Tests of Between-Subjects Effects						
Dependent Variable:	**Packing Density**					
Source	**Type IV Sum of Squares**	**df**	**Mean Square**	**F**	**Sig.**	**Partial Eta Squared**
Corrected Model	.536[a]	26	0.021	3.77	0.000	0.111
Intercept	324.368	1	324.368	59285.142	0.000	0.987
Blend Ratio	0.195	2	0.098	17.84	0.000	0.044
Twist Factor	0.136	2	0.068	12.4	0.000	0.031
Blend Ratio * Twist Factor	0.019	4	0.005	0.884	0.473	0.004
Total	329.189	810				

CONCLUSIONS

From the statistical analysis, it was determined that twist factor and blend ratio have significant effect on yarn packing density. It was seen that as the cotton ratio increases, the yarn packing density value also increases. This result was attributed to the cotton cross-section characteristic and lower bending rigidity.

It was also determined that the twist coefficient has significant effect on yarn packing density. The higher twist factor leads to higher packing density. This result was attributed to the increasing twist radial force and so lower yarn diameter. According to ANOVA results, it was analyzed that the cotton/acrylic blend ratio has higher effect that twist coefficient.

REFERENCES

[1]. Balasubramanian, N., (2014) Yarn diameter, specific volume & packing density. The Indian Textile J, 8(11), 1-28.

[2]. https://www.researchgate.net/publication/304792966 12.04.2018.

[3]. Hussain, U., Sarwar, A., Shafqat, A. R., Muzaffar, M., Iqbal, M., Zahra, N. & Hussain, T. (2014). Effect of spinning variables on packing density of cotton yarn. Indian Journal of Fibre & Textile Research, 39, 434-436

[4]. Zou, Z., Zheng, S., Cheng, L., Xi, B., & Yao, J. (2014). Effect of Some Variables on the Fibre Packing Pattern in a Yarn Cross-section for Vortex Spun Yarn. Fibres & Textiles in Eastern Europe. 2(104), 40-46.

[5]. Kilic, M., Buyukbayraktar, R.B., Kilic, G.B., Aydin, S., Eski, N. (2014). Comparing the packing densities of yarns spun by ring, compact and vortex spinning systems using image analysis method. Indian Journal of F. & Tex. Res. 39, 351-357.

[6]. Taheri, M., Vadood, M., Johari, M.S. (2013). Investigating the Effect of Yarn Count and Twist Factor on the Packing Density and Wicking Height of Lyocell ingspun Yarns. Fibers and Polymers, 14 (9), 1548-1555.

[7]. Kumar, A., Ishtiaque, S.M., Das, A. (2012). Impact of Yarn Extension on Packing Density of Ring Spun Yarn. Fibers and Polimers. 13(8), 1071-1078.

[8]. Zheng, S.M., Zou, Z.Y., Shen, W., Cheng, L.D. (2012). A Study of the Fiber Distribution in Yarn Cross Section for Vortex-spun Yarn. Textile Research Journal, 82(15), 1579–1586.

[9]. Ishtiaque, S.M., Das, A., Vishnoi, P. (2011). Influence of process parameters on packing density of open-end and core-sheath friction spun yarns. Indian Journal of Fibre & Textile Research, 36, 152-157.

[10]. Yilmaz, D., Goktepe, F., Goktepe, O., (2007). Packing Density of Compact Yarns. Tex. Res. J., 77(9), 661-667.

[11]. Kumar, A., Ishtiaque, S.M., Salhotra, K.R. (2006). Study of Effect of Spinning Process Variables on the Packing Density of Ring, Rotor and Air-jet Yarns Using Taguchi Method. AUTEX Research Journal, 6(3), pp. 122-135.

[12]. Jiang, X.Y., Hu, L., Cheng K.P.S. (2005). Determining the Cross-Sectional Packing Density of Rotor Spun Yarns. Textile Res. J. 75(3), 233-239.

[13]. Tyagi, G.K., Kaushik, R.C.D. (2000). Radial Packing Density and Related Properties of Polyester DREF-3 Yarns. Indian Journal of Fibre & Textile Research, 25, 20-24.

[14]. Sinha, S.K., Kumar, P., Ghosh, S., (2016). A Study on the Packing Density of Structurally Modified Ring Spun Yarn. Fibers and Polymers, 17(11), 1898-1907.

Triaxiality in N=32 Isotones with Covariant DFT

Tuncay Bayram[1,2], Serkan Akkoyun[3]

Abstract

Investigation for deformation and collective modes of nuclei is hot topic in nuclear physics both experimentally and theoretically. Recent two decades more information on shape of nuclei far from nuclear stability line has been obtained via heavy-ion evaporation-reactions by many lab. Accurate excitation energies, their ratios and transition strengths are used for investigation of geometrical shape of nuclei. On the other hand there can be found experimental difficulties for yielding neutron rich and proton rich nucleus and successful theoretical model studies can help for better understanding of shape of these nuclei. Nuclei along the N = Z region, between proton number Z = 28 to Z = 50 is known as to exhibit rapid shape changes and some nuclei have been determined as to be having triaxial symmetry. By regarding this point, covariant density functional theory with density dependent interactions (DD-ME2) have been employed for N=32 isotones starting from Ni to Se nucleus in the present study. For this purpose, potential energy surfaces of each nucleus have been carried out to discussing shape of nucleus in this isotonic chain. 64Ge has been found as to exhibit triaxiality in its ground state as in agreement with experimental indications. Also, detailed discussion on the shape of other nuclei in this isotonic chain is presented in this study. Furthermore some nuclear properties of considered nuclei such as binding energy, charge radii and quadrupole moments are given in detail.

Keywords: *Triaxiality, Shape evolution, Covariant DFT, N=32 isotones*

1. INTRODUCTION

Nuclei can have different geometrical shapes such as spherical, deformed and γ-soft rotor in their ground states [1]. Also, nuclei can exhibit shape coexistence and transitional behavior. Furthermore new critical point symmetries called E(5) and X(5) have been introduced by means of quantum phase transitions and they can be occur ongoing from spherical to γ-soft and from spherical to deformed shape, respectively [2,3]. These topics are attractive for studying in nuclear physics research. An excellent review on deformation and collective modes of nuclei can be found in [4]. In particular, accurate determination of some energy levels and electric quadrupole transition probabilities of nuclei are required for experimental identification of deformation and collective mode of nuclei. Also, some geometric and algebraic nuclear models for studying on deformation of nuclei are useful [1]. Furthermore relativistic and non-relativistic mean field models can be used for analyzing of deformation of nuclei as in these studies [5] and [6]. In these studies potential energy surface (PES) obtained for each nuclei by using relativistic and non-relativistic nuclear model calculations have been used for determination collective mode of nuclei. The PES in the β and γ plane is useful tool for identification of deformation or shape of nuclei.

Nuclei along the N = Z region, between proton number Z = 28 to Z = 50 is known to exhibit rapid shape changes and shape-coexistence phenomena. Starting from the low Z values, the ground-state shape evolves from spherical for ^{56}Ni, triaxial in ^{64}Ge, to oblate for the ^{68}Se, ^{72}Kr [7]. In particular, an investigation on N=32 isotonic chain can be an interesting study by means of deformation or collective modes of nuclei. By considering this point, we have employed relativistic mean field (RMF) approach ([8] and references therein) with a density-dependent interaction on N=32 isotonic chain starting from Ni (Z=28) to Se (Z=34) nucleus. For each nuclei, PES have been obtained within the framework of RMF model. In the present study obtained PESs have been used to identification of deformation of nuclei interested by taken into account experimental observables.

[1] Corresponding author: Karadeniz Technical University, Department of Physics, 61080, Ortahisar/Trabzon, Turkey. t.bayram@ktu.edu.tr

[2] Istituto Nazionale di Fisica Nucleare, Laboratori Nazionali di Legnaro, I-35020 Legnaro (PD), Italy.

[3] Cumhuriyet University, Department of Physics, Sivas, Turkey.

2. METHOD

In the present study we have employed RMF theory with a density dependence for carrying out PES of N=32 isotones. In this model nucleons in nuclei interact with each other via exchange of various mesons [9]. There can be found different kinds of RMF model by means of handling interaction such as non-linear, density-dependent and point coupling ([10] and references there in). Density dependence of RMF theory makes calling of it as covariant density functional theory. In the present study, density-dependent version of RMF model with DD-ME2 interaction [11] has been used. Therefore we are restricting ourselves to brief RMF model by considering only density-dependent version of RMF model in this section.

The RMF model starts with a Lagrangian density given by

$$\mathcal{L} = \bar{\psi}(i\gamma.\partial - m)\psi + \frac{1}{2}(\partial\sigma)^2 - \frac{1}{2}m_\sigma^2\sigma^2 - \frac{1}{4}\boldsymbol{\Omega}_{\mu\nu}\boldsymbol{\Omega}^{\mu\nu} + \frac{1}{2}m_\omega^2\omega^2 - \frac{1}{4}\vec{\boldsymbol{R}}_{\mu\nu}\vec{\boldsymbol{R}}^{\mu\nu} + \frac{1}{2}m_\rho^2\vec{\rho}^2 - \frac{1}{4}\boldsymbol{F}_{\mu\nu}\boldsymbol{F}^{\mu\nu} - g_\sigma\bar{\psi}\sigma\psi - g_\omega\bar{\psi}\gamma.\omega\psi - g_\sigma\bar{\psi}\gamma.\vec{\rho}\vec{\tau}\psi - A\frac{1-\tau_3}{2}\psi. \quad (1)$$

In this equation, bold types symbols represent space vectors while symbols with arrows represent isospin vectors. m_σ, m_ω and m_ρ-are masses of σ, ω and ρ mesons, respectively. The mass of nucleons are represented with m. When variation principle apply on equation (1), two set of coupled equation called RMF equation are obtained. These equations are Dirac and Klein-Gordon like equations for nucleons and mesons, respectively. These equations can be solved in a self-consistent way. Numerical recipes and details on how nuclear properties of finite nuclei such as binding energy, deformation and root mean square charge radii can be found in [12].

In the present study we have obtained PES of N=32 nuclei. For this purpose we have used constrained RMF model calculations which means that we have obtained binding energies by fixing β and γ degree of freedoms separately.

3. RESULTS AND DISCUSSION

For checking of nuclear models, one of the best ways is checking of its prediction on ground-state binding energies of nuclei. In the present study we have employed RMF calculations with DD-ME2 interaction for N=32 isotones ^{60}Ni, ^{61}Cu, ^{62}Zn, ^{63}Ga, ^{64}Ge, ^{65}As and ^{66}Se. For these calculations initial gaps for neutrons and protons $\Delta_n = 4.8/N^{1/3}$ and $\Delta_p = 4.8/Z^{1/3}$ formulas have been used, respectively. In these formulas N and Z represents neutron numbers and proton numbers of nuclei interested, respectively. The calculated ground-state binding energies of considered nuclei are listed in Table 1 together with experimental data taken from [13]. As it can be seen in Table 1, our results are in agreement with experimental data. Maximum deviation between our results and experimental data is about 10 keV. It should be noted that we do not represent experimental errors because experimental data errors are less than their last digits.

Table 15. The calculated binding energies of ^{60}Ni, ^{61}Cu, ^{62}Zn, ^{63}Ga, ^{64}Ge, ^{65}As and ^{66}Se. (in unit of keV) with RMF+DD-ME2 in the present study and experimental data taken from [13].

	^{60}Ni	^{61}Cu	^{62}Zn	^{63}Ga	^{64}Ge	^{65}As	^{66}Se
This Work	518.975	524.609	533.099	528.758	541.082	534.135	543.333
Experiment	526.846	531.646	538.119	540.787	551.144	545.753	547.800

For discussing of ground-state shapes of N=32 isotones we have carried out their PESs by using covariant mean field approach with DD-ME2 interaction. For this purpose we have put restriction for β and γ deformation parameters to calculation of binding energies. In our calculations we have used 170 fixed points to carry out for each PES. The scale of β is between 0 and 0.55 while scale of γ is between 0° and 60°. In the PECs calculated lowest ground-state energy has been set as 0. Thus differences of binding energies obtained for ground-sate and for fixed deformation have been used to figure out PES on β-γ plane. From Figure 1, ^{60}Ni nucleus can be identify as having slightly oblate deformed shape because it has lowest ground-state around β=0.15 and γ=60°. The obtained PESs for ^{62}Zn and ^{66}Se show clear γ independency and they can be signed as γ-soft nuclei. On the other hand, somehow similar PESs have been obtained for ^{61}Cu, ^{63}Ga, ^{64}Ge and ^{65}As nuclei in the Figure 1. These PESs have lowest energy around β=0.25 and γ=30° which means that these nuclei are possible candidates for to be triaxial nuclei.
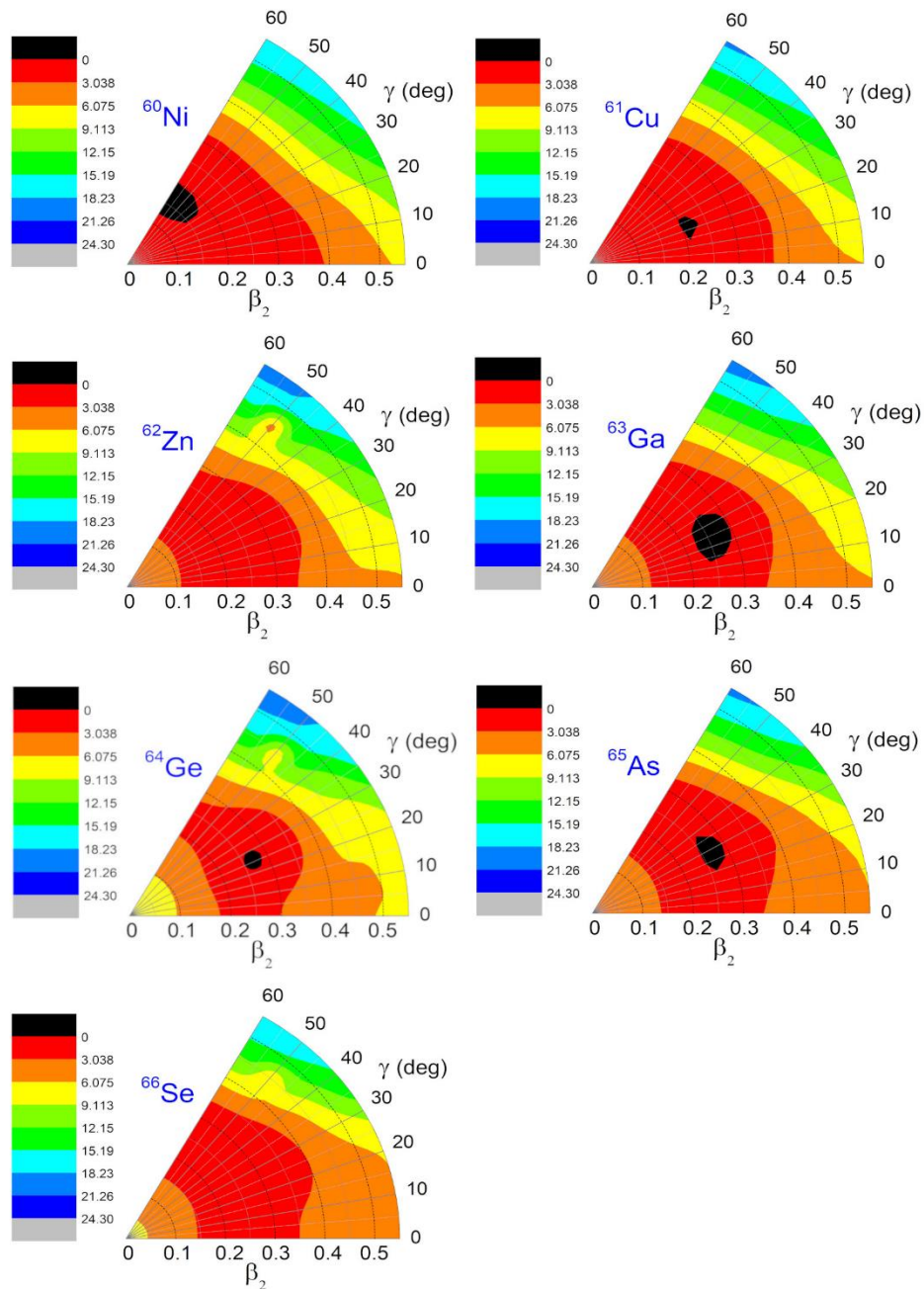
Figure 1. The calculated PES of N=32 isotones by using RMF+DD-ME2. See text for details.

[64]Ge nucleus has pay attention because it has equal number of neutrons and protons. It has been pointed out as triaxial nuclei in [14] and this confirmed by using Recoil Doppler Shift (RDS) technique [15] experimentally. Our results also confirm the results of those [14] and [15] for [64]Ge nucleus.

Nuclear spectroscopy knowledge is an important tool for determination of deformation of nuclei. Some available energy levels of even-even nuclei [16] considered in this work are listed in Table 2. Experimental errors were not presented because their value is lower than the last digits of presented values. Rate of transition energies for

certain levels and reduced electric quadrupole transition rates are used mainly. Rate of electric transition levels from 4_1^+ to 0_1^+ and from 2_1^+ to 0_1^+ ($R_{4/2} = E(4_1^+ \rightarrow 0_1^+)/E(2_1^+ \rightarrow 0_1^+)$) is one of the fundamental quantity for this task. 2, 3.33 and 2.5 values of $R_{4/2}$ are related with spherical, axially deformed and γ-soft nuclei, respectively [4]. For ^{60}Ni, ^{62}Zn and ^{64}Ge, the experimental values from Table 1 are 1.88, 2.29 and 2.28, respectively. These results indicate that ^{62}Zn and ^{64}Ge nuclei can be possible triaxial nuclei. These results are matching with our results for the case of ^{64}Ge nucleus. It should be noted that ^{62}Zn nucleus can be seen as γ-soft nuclei in our PES results obtained from RMF+DD-ME2 calculations. These results shows that triaxiality in nuclei can be found at/around N=32. More precise experimental results and extended calculations by using excited states of nuclei can be employed for deeper understanding shape of nuclei in the considered region.

Table 2. List of experimental transition levels of ^{60}Ni, ^{62}Zn and ^{64}Ge nuclei

Nuclei	2_1^+ (keV)	4_1^+ (keV)	2_2^+ (keV)	0_2^+ (keV)	0_3^+ (keV)	6_1^+ (keV)
^{60}Ni	1332.51	2505.75	2158.63	2284.80	3317.83	4265.0
^{62}Zn	953.84	2186.06	1804.67	2341.95	3042.90	4347.9
^{64}Ge	901.70	2052.60	1578.70	-	-	3406.7

4. CONCLUSIONS

Covariant density functional theory with DD-ME2 interaction has been employed to carry out potential surfaces of N=32 isotones. The calculated ground-state binding energies of ^{60}Ni, ^{61}Cu, ^{62}Zn, ^{63}Ga, ^{64}Ge, ^{65}As and ^{66}Se have been found in agreement with experimental data. The obtained potential energy surfaces indicates that ^{60}Ni nucleus has slightly oblate shape, ^{62}Zn and ^{66}Se nuclei have γ-soft character while ^{61}Cu, ^{62}Zn, ^{63}Ga and ^{64}Ge can be possible candidate for triaxial nuclei. Furthermore this work shows the significance of studying N=32 isotones by means of triaxiality.

REFERENCES

[1]. W. Greiner and J. A. Maruhn, *Nuclear Models*, Berlin, Germany: Springer-Verlag, 1996.
[2]. F. Iachello, "Dynamic symmetries at the Critical Point", *Physical Review Letters*, vol. 85, pp. 3580, Oct. 2000.
[3]. F. Iachello, "Analytic Description of Critical Point Nuclei in a Spherical-Axially Deformed Shape Phase Transition", *Physical Review Letters*, vol. 87, pp. 052502, July 2001.
[4]. R. F. Casten and E. A. McCutchan, "Quantum phase transitions and structural evolution in nuclei", *J. Phys. G: Nucl. Part. Phys.*, vol. 34, pp. R285-R320, May 2007.
[5]. T. Bayram, "An investigation on shape evolution of Ti isotopes with Hartree-Fock-Bogoliubov Theory", *Modern Physics Letters A*, vol. 28, no. 1250162, Aug. 2012.
[6]. T. Bayram and S. Akkoyun, "An analysis of E(5) shape phase transitions in Cr isotopes with covariant density functional theory", *Physica Scripta*, vol. 85, no. 065201, 2013.
[7]. J. W. Negele and E. W. Vogt Ed., *Advances in Nuclear Physics*. New York, Springer-Verlag, 2001, vol. 26.
[8]. T. Bayram and A. H. Yilmaz, "Table of Ground State Properties of Nuclei in the RMF Model", *Modern Physics Letters A*, vol. 23, n. 1350068, May 2013.
[9]. J. D. Walecka, "A theory of highly condensed matter", *Annals of Physics*, vol. 83, pp. 491-529, Apr. 1974.
[10]. T. Bayram, S. Akkoyun and S. Senturk, "Adjustment of Non-linear Interaction Parameters for Relativistic Mean Field Approach by Using Artificial Neural Networks", *Physics of Atomic Nuclei*, vol. 81, pp. 288-295, June 2018.
[11]. G. A. Lalazissis, T. Niksic, D. Vretenar and P. Ring, "New relativistic mean-field interaction with density-dependent meson-nucleon couplings", *Physical Review C*, vol. 71, no. 024312, Feb. 2005.
[12]. T. Niksic, N. Paar, D. Vretenar and P. Ring, "DIRHB-A relativistic self-consistent mean-field framework for atomic nuclei", *Computer Physics Communications*, vol. 185, pp. 1808-1821, June 2014.
[13]. M. Wang, G. Audi, F. G. Kondev, W. J. Huang, S. NAimi, X. Xu, "The AME2016 atomic mass evaluation", *Chinese Physics C*, vol. 41, no. 030003, March 2017.
[14]. P. J. Ennis, C.J. Lister, W. Gelletly, H. G. Price, B.J. Varley, P. A. Butler, T. Hoare, S. Cwiok and W. Nazarewicz, "Triaxiality and isospin-forbidden E1 decays in the N=Z nucleus ^{64}Ge", *Nuclear Physics A*, vol. 535, pp. 392-424, Dec. 1991.
[15]. K. Starosta et al., "Shape and Structure of N=Z ^{64}Ge: Electromagnetic Transition Rates from the Application of the Recoil Distance Method to a Knockout Reaction, *Physical Review Letters*, vol. 99, no. 042503, July 2007.
[16]. NuDat 2.7 (2019). Available: https://www.nndc.bnl.gov/nudat2/

Determination of some energy transitions of Ga products after photonuclear reaction

Serkan Akkoyun[1,2], Tuncay Bayram[3]

Abstract

Nuclear spectroscopy is an important tool for deeper understanding of nuclear structure and dynamics of nuclear system. One of the easy way to investigate atomic nuclei is photonuclear reaction. Target nucleus is bombarded by bremsstrahlung photons which can be generated from a medical linear electron accelerator. For the photon energy in the order of 10-20 MeV, the number of reaction channel is limited. Therefore, the gamma spectrum is relatively clear and the use of particle or neutron detectors are not highly needed. In this study the bremsstrahlung photons with endpoint energy of 14 MeV have been used for activating Ga target. The some energy transitions of product nuclei belonging to the low neutron/proton reaction exit channels have been measured via HPGe detectors. The results are in good agreement with the literature values.

Keywords: *Photonuclear reaction, Ga, bremsstrahlung, HPGe*

1. INTRODUCTION

Nuclear reaction activated by photon is named as photonuclear reactions. They have an importance in nuclear physics studies [1-3]. The target materials are bombarded by photons and can be absorbed by a nucleus in the target if the cross section is high enough. The excited nucleus after this process emits a particle or photons. The character of this interaction is pure electromagnetic. In the giant resonance region of about 15-30 MeV energy, photonuclear reaction cross sections are large. Therefore by these reactions table nuclei might be transmuted to short-lived or stable nuclei. The experimental studies on these reactions have begun in 1934 [4], but existing data is still deficient. In order to fill the deficiency, systematic studies for photonuclear reactions on different target materials should be performed. The advantages of the reaction by photon activation are determination of the multiple element simultaneously, non-destructive structure of the process, requiring no time-consuming chemical separation procedure, deeper penetrating capability of the photon into the target [5]. The most detailed experiment performed for the determination of the half-lives and energy levels by using photonuclear reactions have been done in 1966 [6]. The photonuclear data are useful for determination of neutron binding energy, identification of nuclear energy levels, nuclear deformations and half-life of the isotopes. They are also important for the application of radiation protection, dosimetry, calculation of absorbed dose, designing radiation shielding and activation analyses [7].

The Gallium, used as a target in this work, has two stable isotopes. Both are used in nuclear medicine and nuclear physics. ^{69}Ga is used for production of the radioisotope ^{68}Ge. This isotope is used for so-called ^{68}Ge /^{68}Ga generator which is used as positron emission tomography isotope. ^{71}Ga has also an astrophysical importance. It is used to study the behavior of solar neutrinos and in nuclear magnetic resonance studies. In this study we have used natural Ga as a target which is bombarded by bremsstrahlung photon from clinical linac. Previously most of the transitions have been measured in this reaction [8]. In the present study we have investigated weak peaks belonging to the transitions in product nuclei from same experiment.

2. EXPERIMENT

The experiment is composed of two main stages. First one is irradiation of the target material and the second one is measurement of residual activity. The Elekta TM Synergy TM medical linear accelerator has been used for the

[1] *Corresponding author: Cumhuriyet University, Department of Physics, Sivas, Turkey. sakkoyun@cumhuriyet.edu.tr*

[2] *Istituto Nazionale di Fisica Nucleare, Laboratori Nazionali di Legnaro, I-35020 Legnaro (PD), Italy.*

[3] *Karadeniz Technical University, Department of Physics, 61080, Ortahisar/Trabzon, Turkey.*

activation of the target. The primary electron beam which is generated by a gun with 50 keV energy is accelerated into a copper cavity by 3 GHz radio frequency with about 5MW peak power. The average electron current was about 30 μA at electron energy of 18 MeV. The electrons are stopped by hitting the tungsten target. By slowing down the electrons, bremsstrahlung photons are produced. The resulting photon beam is uniform forward focused because of its flattening and collimating with filters.

The gallium metal target consists of ^{69}Ga and ^{71}Ga stable isotopes mixture with 60.11% and 39.89% natural abundances, respectively. Gallium target was liquid in room temperature as during the experiment (melting point of 29.8 ℃). The total weight of the sample was 10 g in a small isinglass case. The target was placed 58 cm away from the source and bombarded by bremsstrahlung photons with 18 MeV endpoint energy. The irradiation time was one hour. The clinical linac is capable to provide sufficient photon intensity for the reaction [9-14]. In this study, we have focused on the energies whose values are slightly above the neutron threshold. The neutron/proton separation energies for ^{69}Ga and ^{71}Ga isotopes are about 10.3/6.6 and 9.3/7.9 MeV, respectively. Because of the activation energy from the photons is enough for the Ga target, both photo-neutron reaction (γ,n) and photo-proton reaction (γ,p) are possible. Other reaction can take place with less probability. Since there are lots of neutrons appear in the experimental area, it is also possible to neutron capture reaction with low probability. After irradiation of the target which causes activation, the ^{67}Ga, ^{68}Ga, ^{70}Ga and ^{72}Ga radioactive isotopes have been generated by various reactions. Due to the short half-lives of the isotopes (67 minutes for ^{68}Ga, 20 minutes for ^{70}Ga and 14 hours for ^{72}Ga), the total counting time were taken about 72 hours which corresponds 6-7 half-lives for the minimization of the errors. The total counting time has been taken about 72 hours. In Figure 1, we have shown the gamma spectrum from activated Ga target which is measured by HPGe detector.
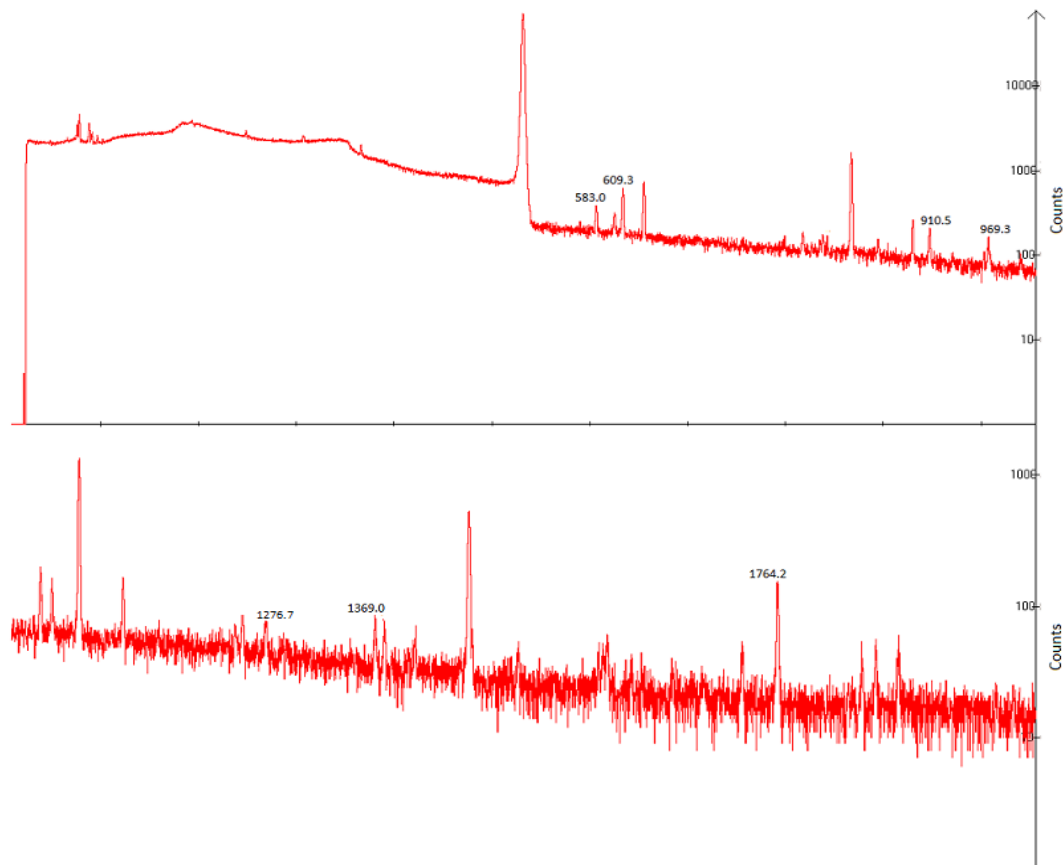
Figure 1. Gamma ray spectrum of products after photo activation of Ga target.

3. RESULTS AND DISCUSSION

In the previous work belonging to the analysis of the same reaction, most of the intense gamma transitions have been observed and published [8]. In this study, we have analyzed the weak peaks in gamma spectrum from the reaction which was not investigated previously by this reaction. The reaction paths are given below by the number from 1 to 4.

In the first reaction, stable ^{69}Ga isotope absorbs the gamma-rays and undergoes photo-neutron reaction by emitting one neutron. After electron capture process, ^{68}Zn emits gamma rays by the gamma decay. We have observed one weak peaks belonging to the transition in this isotope. We have also observed two peaks from the transition in ^{68}Ga radionuclide. In the second reaction, ^{69}Ga stable isotope emits two neutrons with very less probability and transform to ^{67}Ga radionuclide. We observed three peaks in gamma spectrum which most probably belongs to this radionuclide. In third reaction, stable ^{71}Ga isotope absorbs the gamma-rays and undergoes photo-neutron reaction by emitting one neutron. After electron capture process, excited ^{70}Zn emits gamma rays from the transitions between its levels. We have measured one peak from this isotope. Also from ^{70}Ga, one peak appears in measured gamma spectrum. In the last reaction, a transition in ^{72}Ga from one neutron capture reaction has been observed. In Table 1, we have compared our measurements to the available experimental values [15].

1: $^{69}Ga + \gamma \longrightarrow {}^{68}Ga + n$

$\qquad {}^{68}Ga \longrightarrow {}^{68}Zn^* + e^+ + \nu$

2: $^{69}Ga + \gamma \longrightarrow {}^{67}Ga + 2n$

3: $^{71}Ga + \gamma \longrightarrow {}^{70}Ga + n$

$\qquad {}^{70}Ga \longrightarrow {}^{70}Zn^* + e^+ + \nu$

4: $^{71}Ga + n \longrightarrow {}^{72}Ga + \gamma$
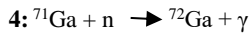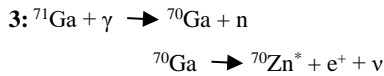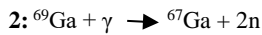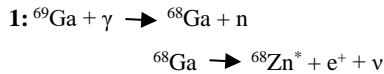
Table 1. List of observed and literature transition energies from Ga activation

Nuclei	Path	Energy (keV)	Literature Energy (keV)
^{68}Ga	2^- to 1^+	583.0	583.8
^{68}Ga	$1,2,3^+$ to 1^+	609.0	608.9
^{70}Zn	8^+ to 6^+	860.5	860.3
^{67}Ga	$5/2^-$ to $3/2^-$	910.5	910.9
^{70}Ga	$1,2^-$ to $1,2^+$	969.3	969.5
^{68}Zn	$1^-,2^+$ to 3^-	1276.7	1276.9
^{67}Ga	$27/2^-$ to $27/2^+$	1368.8	1368.8
^{67}Ga	$5/2^-$ to $5/2^-$	1764.9	1765.2

CONCLUSIONS

The weak gamma-ray transition energies of the daughter nucleus from photonuclear reaction on gallium target have been identified in agreement with the literature values. Maximum and minimum differences between observed and literature energies are between 0.3 and 0 keV. The average difference is 0.28 keV. Our aim was not only obtaining more sensitive and accurate energy values for the transitions, but also to show the usefulness of the method and clinical linear accelerator in determination of the energies of the isotopes.

REFERENCES

[1] C. Segebade, H.-P. Weise and G. J. Lutz, Photon Activation Analysis (Walter de Gruyter and Co, Berlin, 1987).
[2] K. Strauch, Ann. Rev. Nucl. Sci. 2 (1953) 105.
[3] IAEA-TECDOC-1178, Handbook on Photonuclear Data for Applications CrossSections and Spectra (IAEA Nuclear Data Section, 2000).
[4] J. Chadwick and M. Goldhaber, Nature 134 (1934) 237.
[5] J. Green, S. Zaijing, D. Wells and H. Maschner, AIP Conf. Proc. 1336 (2011) 497.
[6] Y. Oka, et al., J. Nucl. Sci. Tech., vol. 4, no. 7, pp. 346 352, 1967.
[7] Y. O. Lee, T. Fukahori and J. Chang, J. Nucl. Sci. Technol. 35 (1998) 685.
[8] S. Akkoyun, et al., Int. J. Mod. Phys. E, 25 (2016) 1650045.
[9] P. Mohr, S. Brieger, G. Witucki and M. Maetz, Nucl. Instrum. Methods A 580 (2007) 1201.
[10] M. Tatari and A. H. Ranjbar, Ann. Nucl. Energy 63 (2014) 69.
[11] M. Roig, V. Panettieri, M. Ginjaume and A. Sanchez-Reyes, Phys. Med. Biol. 49 (2004) N243.
[12] J. H. Chao, M. T. Liu, S. A. Yeh, S. S. Huang, J. M. Wu, D. Y. L. Chang, F. Y. Hsu, C. Y. Chuang, H. Y. Liu and Y. C. Sun, Appl. Radiat. Isot. 67 (2009) 1121.
[13] T. Fujibuchi, S. Obara, H. Sato, M. Nakajima, N. Kitamura, T. Sato, H. Kumada, T. Sakae and T. Fujisaki, Prog. Nucl. Sci. Technol. 2 (2011) 803.
[14] A. Alfuraih, M. P. W. Chin and N. M. Spyrou, J. Radioanal Nucl. Chem. 278 (2008) 681.
[15] NuDat 2.7 (2019). Available: https://www.nndc.bnl.gov/nudat2/

The Effect of Core-spun Yarn Type and Layout of These Yarns in the Fabric on Stiffness Properties of Denims

Esin Sarioglu[1]

Abstract

Denim fabrics are preferred that serve highly comfortable to wear for daily use. This comfort term can be emphasized as highly elastic and recovery, shape retention, better fitting to the body, etc. To enable these properties, elastic yarns are widely used as filling. Furthermore, giving elasticity to the fabric, yarns can be produced with different yarn construction design such as one component core-spun or dual core-spun yarns. In this study, three types of core-spun yarns were produced; elastic core-spun yarn (single core-spun yarn), filament core-spun yarn (single core-spun yarn) and filament+elastane core-spun yarn (dual core-spun) on modified ring spinning frame. For this purpose, elastane, Polyethylene terephthalate/ Polytrimethylene terephthalate (PET/PTT) bicomponent filament were used as core material; cotton fiber was used as sheath fiber for ring spun core yarn production at the same parameters. These yarns and uncovered PET/PTT bicomponent filament were utilized as filling in order to manufacture 3/1 twill construction denim fabrics at the different filling layout in the fabric. Stiffness properties were determined in accordance with the related standard. Results were evaluated statistically via analysis of variance. It was found that filling yarn types and filling yarn layout in the fabric had a statistically significant effect on the stiffness properties of denim fabrics at the 0.05 significance level. Moreover, it can be concluded that there was no statistically difference between the stiffness properties of denim fabrics made of elastane core-spun yarn and PET/PTT bicomponent dual core-spun yarns.

Keywords: *dual core-spun yarn, elastic core-spun yarn, denim fabric, stiffness.*

1. INTRODUCTION

In the clothing industry, denim has a wide acceptance with high potential uses as a fashion trend all over the world. Generally, denims are woven with a construction of 3/1 twill and they consist of indigo dyed warp yarns interlaced with gray weft yarns. On the other hand, denim sector needs to continuously improve fabric properties to meet consumer needs such as flexible, shape-retention, low abrasion resistance, and comfort to wear in use at all times. High competitive potential in this sector pushes the companies to offer opportunities of different fiber, functional yarns use which contribute fabric properties. One of the best offered way which response to these requirements is using core-spun yarns. These yarns are produced by wrapping sheath fibers around filament or staple fiber core with a certain twist. Besides using of elastic core-spun yarn, filament core-spun yarns are also widely used in order to enhance some characteristics of fabric i.e. durability, esthetic and functional properties. With technological progress and rising demands to obtain durable and long lifetime fabric, now the use of multicomponent core-spun (dual core-spun) yarns which enables elasticity and durable at the same time is available. In other words, dual core-spun yarn consists of two core components; filament and elastane. Several studies have been concerned the effect of dual core-spun yarn on yarn and fabric performance [1-7].

Fabric drape is defined as the ability of a fabric (a circular specimen of known size) to deform when suspended under its own weight in specified conditions [8]. Drape ability of a fabric is combined effect of several factors such as stiffness, flexural rigidity, weight, thickness, etc. Stiffness is an attribute of the fabric hand, for example, one of the most important factors determining the draping quality of the fabric, for example, soft fabric drapes which are closer to the body-forming ripples, while stiff fabric drapes away from the body [9-10]. This study concerns the effect of filling yarn type and filling yarn layout in fabric on stiffness properties of denim fabric.

---

[1] *Gaziantep University, Faculty of Fine Arts, Department of Fashion and Textile Design, 27310 Sehitkamil/Gaziantep, Turkey, sarioglu@gantep.edu.tr*

For this purpose, single and dual core-spun yarns with PET/PTT bicomponent filament and elastane core material were produced. In addition, these core-spun yarns were used as filling with uncovered PET/PTT bicomponent filament at the different layout. Stiffness properties were determined and results were evaluated statistically.

2. MATERIALS AND METHOD

This study conducted about the investigation on filling yarn type and filling yarn layout on denim fabric stiffness properties. For this aim, three types of filling yarns were produced as core-spun yarns. Core-spun yarn production included single core part (PET/PTT bicomponent filament and elastane) and dual core (PET/PTT bicomponent filament and elastane feeding at the same time). These core materials mentioned were wrapped by cotton fiber in order to obtain core-spun yarns.

As sheath fiber cotton fiber with 4.8 micronaire filament fineness, 29.33 fiber length, 30.6 g/tex strength and 5.6% elongation was used. As core material, elastane Invista spandex brand with 78 dtex linear density was used. As another core material, PET/PTT bicomponent filament with 55 linear density was chosen for its most widely used for dual core-spun yarn production. In this study, two different PET/PTT bicomponent filaments were selected; one for core material of core-spun yarn, the other used as uncovered for filling yarn in denim fabric. Properties of PET/PTT bicomponent filaments used for core-spun yarn and denim fabric production are submitted in Table 1.

Table 1. Properties of PET/PTT bicomponent filaments used for core-spun yarn and denim fabric

Properties	Core-spun yarn PET/PTT bicomponent filament	Denim fabric PET/PTT bicomponent filament
Linear density (dtex)	55	165
Number of filaments	7	68
Strength (gf/den)	4	4
Elongation (%)	17	22
Potential crimp (%)	63	67

Modified ring spinning frame was used for core-spun yarn production and the schematic representation of ring frame and single and dual core-spun yarn views are illustrated in Figure 1. It is possible to produce single and dual core-spun yarns on the same machine with applying some modification on the machine. The feeding of two core material, an extra creel mechanism was added at the top of the machine. Table 2 indicates single and dual core-spun yarn production parameters.
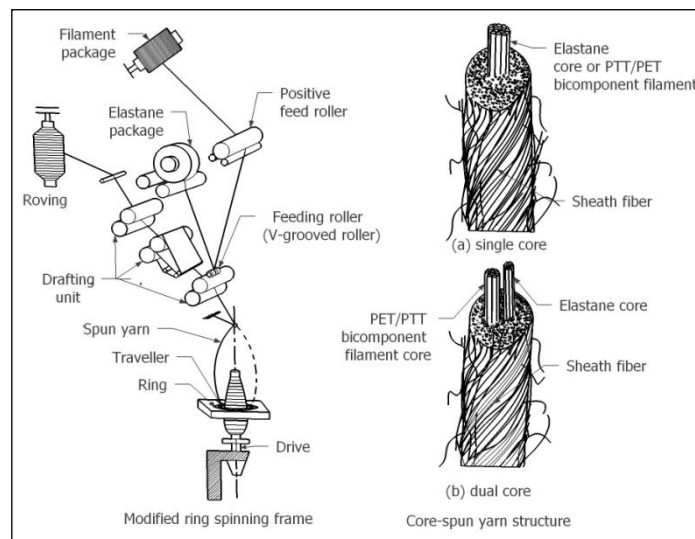
Figure 1. Schematic representation (a) single and (b) dual core-spun yarn production and

view of single and dual core-spun yarn structure

Three different core-spun yarn samples were produced and used as filling yarns for denim production. Besides, core-spun yarn samples and an uncovered PET/PTT bicomponent filament were arranged as different filling layout which is given in Table 3. As an example for filling yarn layout in denim fabric is shown in Figure 2. As seen in Figure 2, in order of 2 filling represents uncovered PET/PTT bicomponent filament and 6 filling represents core-spun yarn (PET/PTT bicomponent core-spun yarn, PET/PTT bicomponent filament+elastane dual core-spun yarn and elastane core-spun yarn).

Tablo 2. Core-spun yarn production parameters

Core-spun yarn type/ Production parameters	PET/PTT bicomponent filament+elastane dual core-spun yarn	PET/PTT bicomponent filament core-spun yarn	Elastane core-spun yarn
Roving count (Ne)	0.70	0.70	0.70
Yarn count (Ne)	18	18	18
Elastane draft ratio	3.62	-	3.62
PET/PTT bicomponent filament draft ratio	1.08	1.08	-
Twist (tpm)	760	760	760
Spindle speed (rpm)	12.160	12.160	12.160

Tablo 3. Filling yarn layout in the denim fabric

No	Filling yarn layout	Abbreviation
1	**1** uncovered F+**2** PET/PTT bicomponent filament core-spun yarn	
2	**1** uncovered F+**2** PET/PTT bicomponent filament+spandex dual core-spun yarn	1F:2CY
3	**1** uncovered F+**2** Elastane core-spun yarn	
4	**1** uncovered F+**4** PET/PTT bicomponent filament core-spun yarn	
5	**1** uncovered F+**4** PET/PTT bicomponent filament+spandex dual core-spun yarn	1F:4CY
6	**1** uncovered F+**4** Elastane core-spun yarn	
7	**1** uncovered F+**6** PET/PTT bicomponent filament core-spun yarn	
8	**1** uncovered F+**6** PET/PTT bicomponent filament +spandex dual core-spun yarn	1F:6CY
9	**1** uncovered F+**6** Elastane core-spun yarn	
10	**2** uncovered F+**2** PET/PTT bicomponent filament core-spun yarn	
11	**2** uncovered F+**2** PET/PTT bicomponent filament +spandex dual core-spun yarn	2F:2CY
12	**2** uncovered F+**2** Elastane core-spun yarn	
13	**2** uncovered F+**4** PET/PTT bicomponent filament core-spun yarn	
14	**2** uncovered F+**4** PET/PTT bicomponent filament +spandex dual core-spun yarn	2F:4CY
15	**2** uncovered F+**4** Elastane core-spun yarn	
16	**2** uncovered F+**6** PET/PTT bicomponent filament core-spun yarn	
17	**2** uncovered F+**6** PET/PTT bicomponent filament+spandex dual core-spun yarn	2F:6CY
18	**2** uncovered F+**6** Elastane core-spun yarn	
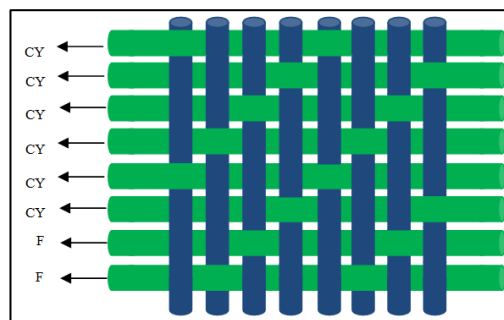
Figure 2. Regarding with from 16th to 18th denim fabric sample filling yarn layout:

F:Uncovered PET/PTT bicomponent filament, CY:core-spun yarn

In the production of denim fabric, indigo dyed Ne 14/1 100% cotton yarn was used as warp yarn and fabric construction was chosen as 3/1 twill weave for its most commonly produced. Picanol brand weaving machine with 550 m/min speed produced 18 different types of denim fabrics at the same production parameters such as

number of warp yarn: 3880, warp sett: 28 ends/cm, filling sett: 20 picks/cm, number of reed: 70 dents/10 cm, number of warp yarn threaded in one dent:4. After weaving, fabric face singeing and standard finishing processes were performed to all denim fabric samples at the same condition. Before stiffness test, all fabric samples were conditioned at standard atmosphere condition at 20±2 °C and 65± 4% for 24 hours [11]. The stiffness properties of the fabric samples were determined in accordance with ASTM D4032 standard [12]. The dimension of fabric sample was 102mm x 204mm. The sample is folded at half point; center the sample hopper. The two measuring buttons are pressed simultaneously and the button is pressed until the fabric falls down from the sample chamber. Machine air pressure control was 3.24 kPa (47 PSI). The stiffness values in the test result were determined in kgf.

For statistical analysis SPSS package program was used to assess the effect size and significance of filling yarn type and filling yarn layout in the denim fabric on stiffness properties at 95% confidence interval. Moreover, in order to evaluate multiple comparison of filling yarn type and filling yarn layout in the fabric, Student-Newman-Keuls multiple comparison was achieved at 0.05 significance level.

3. RESULT AND DISCUSSION

The structural parameters of denim fabrics are given in Table 4. The stiffness test results for denim fabrics are shown in Figure 3.

Table 4. Structural properties of denim fabrics

No	Core Material	Filling layout	Warp sett (ends/cm)	Filling sett (picks/cm)	Weight (g/m²)
1	PET/PTT bicomponent filament		36.6	21.8	249.2
2	PET/PTT bicomponent filament+elastane	1F:2CY	44	22.4	298.6
3	Elastane		42.2	22.6	301.8
4	PET/PTT bicomponent filament		36.4	21.2	257.6
5	PET/PTT bicomponent filament+elastane	1F:4CY	42.6	22	287.2
6	Elastane		42	21.8	296.8
7	PET/PTT bicomponent filament		36.2	21.4	251.6
8	PET/PTT bicomponent filament+elastane	1F:6CY	42	21.8	304.6
9	Elastane		41.4	21.6	296.4
10	PET/PTT bicomponent filament		37.6	22.16	258.4
11	PET/PTT bicomponent filament+elastane	2F:2CY	43	20	298
12	Elastane		43.8	22.4	292.2
13	PET/PTT bicomponent filament		36.6	21	244
14	PET/PTT bicomponent filament+elastane	2F:4CY	41.2	21	277.8
15	Elastane		42.4	21.4	278.8
16	PET/PTT bicomponent filament		36.6	20.8	244.6
17	PET/PTT bicomponent filament+elastane	2F:6CY	42.2	21.2	288.8
18	Elastane		42.6	21.2	281.8
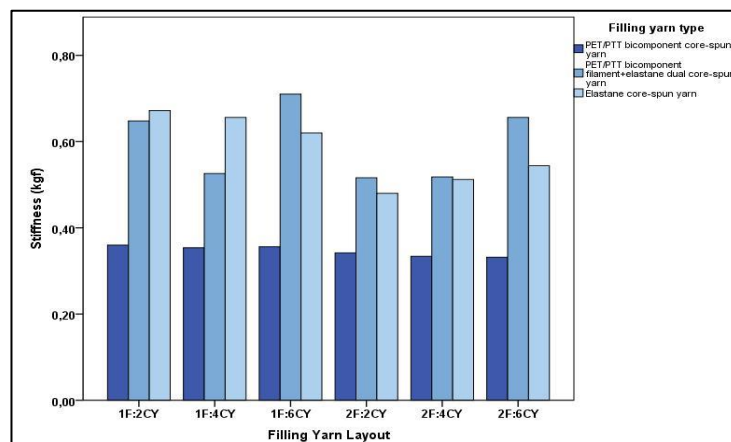
Figure 3. Stiffness results of denim fabrics

Drape ability with regards to stiffness of denim fabric with PET/PTT bicomponent filament core spun yarn, using 1F filling have worse stiffness properties than 2F filling layout. It can be said that increasing the number of filament is the key factor to improve drape ability. However, using high number of the PET/PTT bicomponent core-spun yarn helps to eliminate stiffness by enabling to obtain softer fabric. On the other hand, for 1F design 1F:2CY fabric shows higher stiffness than 1F:4CY denim fabric with PET/PTT bicomponent filament+elastane dual core-spun yarn, but, after that the stiffness value gets the highest point for 1F:6CY fabric. The similar results obtained for 2F layout of filling yarn. In addition using 2F design reduces stiffness values of the denim fabric. The stiffness values of denim fabrics with elastane core-spun yarn for 1F design, increasing the number of elastane core-spun yarn in the layout of filling yarns helped to decrease the stiffness of fabric. It is an expected result that elastane core-spun yarns are more elastic which leads to fabric easily formed. On the other hand, for 2F design, stiffness values decreased with respect to 1F design. From 2F:2CY to 2F:6CY stiffness of fabric increased by increasing the number of the elastane core-spun yarn in the filling yarn layout.

Analysis of variance statistical test result for stiffness is illustrated in Table 5. All parameters (filling yarn type and filling yarn layout in the fabric) and interactions have significant effect on air permeability. It can be said that filling yarn type and filling yarn layout in the denim fabric explain the stiffness with high adjusted R-squared value of 83.6%.

Table 5. Analysis of variance test results for stiffness values of denim fabrics

Source	Sum of Squares	df	Mean Square	F	Sig.
Corrected Model	1.519[a]	17	0.089	27.746	0.000*
Intercept	23.185	1	23.185	7200.353	0.000*
Filling yarn type	1.173	2	0.587	182.149	0.000*
Filling yarn layout	0.185	5	0.037	11.488	0.000*
Filling yarn type * filling yarn layout	0.161	10	0.016	4.995	0.000*
Error	0.232	72	0.003	-	-
Total	24.936	90	-	-	-
Corrected Total	1.751	89	-	-	-
a. R Squared = 0.868 (Adjusted R Squared = 0.836)					

Table 6. Student-Newman-Keuls[a,b] multiple comparison stiffness test results for filling yarn type, The error term is Mean Square (Error) = 0.003, a. Uses Harmonic Mean Sample Size = 30.000, b. Alpha = 0.05

Filling yarn type	N	Subset 1	Subset 2
PET/PTT bicomponent core-spun yarn	30	0.3463	
Elastane core-spun yarn	30		0.5807
PET/PTT bicomponent filament+elastane dual core-spun yarn	30		0.5957
Sig.		1.000	0.309

Table 6 indicates multiple comparison of filling yarn type according to the stiffness values of denim fabrics. It can be said that denim fabrics produced from PET/PTT bicomponent core-spun yarn has the lowest stiffness value. In addition, there is difference between PET/PTT bicomponent core-spun yarn and other types of core-spun yarns at 0.05 significance level. On the other hand, it was found that there is no difference obtained from the stiffness values of denim fabrics with elastane core-spun yarn and PET/PTT bicomponent filament+elastane dual core-spun yarn. Student-Newman-Keuls multiple comparison stiffness test results for filling yarn layout is given in Table 7. As seen in Table 7, denim fabric with 2F:2CY and 2F:4CY filling yarn layouts have similar stiffness values, and differ from the other filling layout types. On the other hand, it was found that there is no difference between the rest of the fabrics with different filling yarn layout.

Table 7. Student-Newman-Keuls[a,b] multiple comparison stiffness test results for filling yarn layout, The error term is Mean Square (Error) = 0.003, a. Uses Harmonic Mean Sample Size = 15.000, b. Alpha = 0.05

Filling yarn layout	N	Subset 1	Subset 2
2F:2CY	15	0.4460	
2F:4CY	15	0.4547	
2F:6CY	15		0.5107
1F:4CY	15		0.5120
1F:2CY	15		0.5600

1F:6CY	15		0.5620
Sig.		0.6770	0.0720

CONCSLUSION

As a conclusion of this study, results can be summarized as follows;

- PET/PTT bicomponent filament core-spun yarn improved draping quality of denim fabric with lowest stiffness value. PET/PTT bicomponent filament core-spun yarn differs from PEET/PTT bicomponent filament+elastane dual core-spun and elastane core-spun filling yarn types.

- In general, the worst draping property (highest stiffness) was obtained from denim fabric including PET/PTT bicomponent filament+elastane dual core-spun yarns.

- Filling yarn type and filling yarn layout have statistically significant effect on stiffness values of denim fabric.

- Denim fabrics from PET/PTT bicomponent filament core-spun yarn have lowest stiffness value.

REFERENCES

[1]. O. Babaarslan, E. Sarioglu, H.I. Celik, M. Ertek Avci, "Denim Fabrics woven with dual core-spun yarns," Engineered Fabrics, Ed:Mukesh Kumar Singh, IntechOpen, 2018, Chapter 2, 19-39,DOI: 10.5772/intechopen.80286.
[2]. O.B. Ertas, B.Z. Unal, N. Celik, "Analyzing the effect of the elastane-containing dual-core weft yarn density on the denim fabric performance properties," The Journal of the Textile Institute, 2016, vol.107, pp.116-126.
[3]. T. Bedez Ute, "Analysis of mechanical and dimensional properties of the denim fabrics produced with double-core and core-spun weft yarns with different weft densities," Journal of the Textile Institute, 2018, vol.109, pp.1-7.
[4]. T. Hua, N.S. Wong, W.M. Tang, "Study on properties of elastic core-spun yarns containing a mix of spandex and pet/ptt bi-component filament as core," Textile Research Journal, 2018, vol.88, pp.1065-1076.
[5]. A. Telli, Y. Dasan, O. Babaarslan, S. Karaduman, "Usage of core and dual-core yarns containing tungsten for electromagnetic shielding," Advance Research in Textile Engineering, 2017, vol.2, pp.1-7.
[6]. H.G. Turksoy, N. Yildirim, "Effect of process variables on the properties of dual-core yarns containing wool/elastane," Industria Textila, 2018, vol.69, pp.352-356.
[7]. H.G. Turksoy, S. Ustundag, "Elastic hybrid yarns for denim fabrics," Industria Textila, 2015, vol.66, pp.306-313.
[8]. British Standards Institution Textiles (2008) Test method for nonwovens. Determination of drape ability including drape coefficient. London: BSL.
[9]. https://www.sciencedirect.com/topics/engineering/drapability.
[10]. S.H. Eryuruk, F. Kaloglu, S.K. Bahadir, C. Saricam, S. Jevsnik, "The evaluation of stiffness and drape behaviour of wool fabrics," Journal of Textile and Engineer, 2015, vol. 22, pp.24-32.
[11]. ISO 139:2005-Textiles -Standard atmospheres for conditioning and testing.
[12]. ASTM D4032-08(2016)-Standard Test Method for Stiffness of Fabric by the Circular Bend Procedure.

Biography

Esin Sarioglu was born in 1980 in Gaziantep Turkey. She graduated from the Textile Engineering Department, Gaziantep University, in 2004. She received MSc Degree in 2008 from the Textile Engineering Department, Gaziantep University, and PhD Degree in 2015 from the Textile Engineering Department, Cukurova University, Turkey. In 2006, she joined Textile Engineering Department, Gaziantep University, as a research assistant. In 2018, she started to work in Department of Fashion and Textile Design in Gaziantep University as Assistant Professor. Her current research interests include recycling in textile industry, yarn technology, weaving technology, woven fabrics and textile quality. Esin Sarioglu can be contacted at: sarioglu@gantep.edu.tr

Application of Principal Component Analysis to Determine the Effect of Process Parameters on the Pyrolysis Product Yields

Aysun Ozkan[1], Kemal Ozkan[2], Zerrin Gunkaya[3], Ece Yapici[3], Hasret Akgun[3], Mufide Banar[3]

Abstract

Experimantal results are effected by the process conditions. There are mathematical models to determine the relationship between yields and process parameters. One of those models is principal component analysis (PCA). PCA is a dimension-reduction tool that can be used to reduce a large set of variables to a small set that still contains most of the information in the large set. The objective of this study was to determine the effect of process parameters (material, heating rate, temperature and catalyst) on the yields of pyrolysis products (solid, liquid and gas). Two different waste material were used: low density polyethylene (LDPE) and composite LDPE (C/LDPE). Other process parameters are 5-10-20 °C/min for heating rates, 400-600-800°C for temperature, waste clay-zeolite-sludge from ceramic wastewater treatment plant for catalysts. Waste samples were individually pyrolyzed in a fixed bed reactor by using the forementioned process parameters. Finally, the pyrolysis product distributions were monitored using PCA technique.

Keywords: C/LDPE, LDPE, PCA, Pyrolysis

1. INTRODUCTION

Plastics play an important role in our daily life and our increasing dependence to plastics is associated with their versatility, lightness and low production cost compared to other classic materials such as wood, concrete and metal. The packaging industry is the largest consumer of plastic materials (39.7% of the total production of plastics) [1]. In 2017, 3.8 million thousand tons of 9.6 million tons produced plastics were used for packaging materials in Turkey [2]. Beside the packaging industry, plastics are now considered the key material in numerous sectors such as construction, medical, engineering applications, automotive, food and others [3].

Several properties such as barrier to water vapor, gas, flavor and light, and flexibility or rigidity, are required for the production of food packaging materials. Thus, the food packaging industry needs to develop multilayer films [4]. Aluminum is used wide range in packaging materials. For example, composite laminates multilayered with aluminum foil and polymeric films are used for frozen foods, vacuum packaging for coffee, Tetra Pak for beverages, and containers for instant soups. Composites mainly consist of polyethylene terephthalate (PET), polyethylene (PE), polypropylene (PP) and nylon films. Aluminum plays an important role in these laminates by protecting the food from oxygen, moisture gain or loss, sun light and ultraviolet radiation effect, and loss of flavor [5]. In spite of these advantages, the recycling of such kind of material is very difficult and not able to separate by hand. C/LDPE (composite/low density polyethylene) is one of the packaging materials that is located in the plastic/aluminum class and coded with 90 according to Turkish Regulation of Packaging Waste Control. Because of plastic content is more than aluminum content, code of package is abbreviated as LDPE.

Packaging waste is managed by different techniques including, reducing, reusing, recycling, energy recovery and disposal at landfill sites [6-7]. Only 15–20 % of total plastic waste can be recycled by conventional recycling

---

[1]*Corresponding author: Eskisehir Technical University, Department of Environmental Engineering, 26555, Iki Eylul Campus, Eskisehir, Turkey. aysunozkan@eskisehir.edu.tr*

[2]*Eskisehir Osmangazi University, Faculty of Engineering and Architecture, Department of Computer Engineering, Eskisehir, Turkey, kozkan@ogu.edu.tr*

[3]*Eskisehir Technical University, Department of Environmental Engineering, 26555, Iki Eylul Campus, Eskisehir, Turkey. zcokaygil@eskisehir.edu.tr*

methods such as sorting and grinding [8-9]. Beyond this level, the plastic becomes contaminated with materials like soil, dirt, aluminum foils, food wastes and paper labels [10]. At this point, pyrolysis process is a method that can be used for separating the materials in such wastes and converting them into valuable products. Pyrolysis process converts plastic waste into liquid oil, solid residue and gases via thermal decomposition [11]. Therefore, the pyrolysis process depends on series of factors such as temperature, residence time, heating rates, feedstock composition and use of catalyst [12-13]. In literature, there are several studies regarding to the pyrolysis of LDPE with some other plastic types and some catalysts.

Since a large number of variables are involved in the pyrolysis experiments, there is required to apply a technique to interpret the multivariate data such as the principal components analysis (PCA). PCA is commonly used to reduce data [14] and to extract a small number of latent factors (principal components - PCs) for analyzing relationships among samples or variables. The objective of this study was to detect correlations between process parameters (material, heating rate, temperature and catalyst) and the yields of pyrolysis products (solid, liquid and gas). Two different waste material were used: LDPE and C/LDPE. Other process parameters are 5-10-20°C/min for heating rates, 400-600-800°C for temperature, waste clay-zeolite-sludge from ceramic wastewater treatment plant for catalysts. Waste samples were individually pyrolyzed in a fixed bed reactor by using the forementioned process parameters. Finally, the pyrolysis product distributions were monitored using PCA technique.

2. MATERIALS AND METHODS

2.1. Material Characterization

Two different waste materials (LDPE and C/LDPE) and three different catalysts (waste clay, zeolite, sludge from ceramic wastewater treatment plant) were used (Figure 1) Analytical samples of waste materials and catalysts were prepared, and the moisture, ash, volatile matter and fixed carbon content of these samples were carried out according to ASTM D-3173-85, ASTM D-3174-82, ASTM D-3172-73 and ASTM D-3175-82, respectively. The elemental composition (C, H, N and S) of the waste materials were determined using a Leco TruSpec CHN and S (USA).
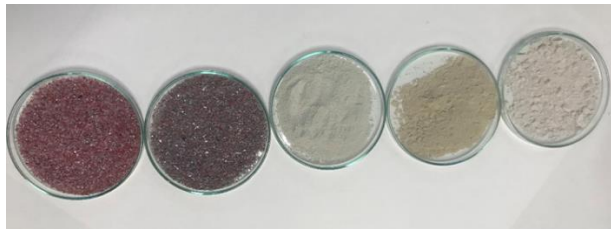
Figure 1. LDPE, C/LDPE, waste clay, zeolite, and, waste sludge (from left to the right)

2.2. Pyrolysis Experiments

Firstly, the pyrolysis experiments were carried out under atmospheric pressure at 400-600-800°C with 5-10-20°C/min heating rates in a fixed bed stainless steel reactor (Figure 2). All of the experiments were conducted in typical runs, in which 10 g of sample were placed in the reactor. As a result of the pyrolysis process, solid, liquid, and gas phases were produced. The liquid phase was collected in a cold trap maintained at approximately 0°C using ice. The solid and liquid product yields were determined gravimetrically for each experiment. The gas yields were determined by the mass difference. All the yields were expressed on a dry basis and the average yields of at least three experiments were used. Then, the optimum heating rate and temperature values were determined that yielded the maximum gas product. At these optimum conditions, the pyrolysis were realized in the presence of 5%, 10%, 15% (by weight) catalysis (waste clay, zeolite, and sludge from ceramic wastewater treatment plant addition).

Figure 2. Pyrolysis system

2.3. *Principal Component Analysis (PCA)*

PCA, which forms the basis of Multivariate Analysis, is an analysis that provides significant convenience in reducing and interpreting a large number of dependent variables to as few linear components as possible. The main objective of this analysis is based on the determination of new variables with fewer independent components that allow the separation of the original variance-covariance or correlation matrix without much loss of information.

A principal component analysis is concerned with explaining the variance-covariance structure of a set of variables through a few linear combinations of these variables. Its general objectives are data reduction and interpretation. Although p components are required to reproduce the total system variability, often much of this variability can be accounted for by a small number k of the principal components. If so, there is (almost) as much information in the k components as there is in the original p variables. The k principal components can then replace the initial p variables, and the original data set, consisting of n measurements on p variables, is reduced to a data set consisting of n measurements on k principal components [15]. Principal component analysis is a method applied to express the information expressed in the data set in an alternative form and there is no dependent variable. All variables in the data set serve the same purpose in. Any one of them is not chosen to explain the others. Principal component analysis is known as a dimension reduction method rather than a technique for re-expressing the data set. This is because re-expression of the data set usually allows size reduction [14].

The PCA method begins with determining of a covariance matrix Σ for a d-dimensional (for this work 6: LPDE or C/LPDE, heating rate, temperature, catalyst type, catalyst amount and pyrolysis products (solid, liquid and gas product)) and n-sample (for this work 36) dataset $X=[x_1,x_2,\ldots,x_n]$:

$$\Sigma = \frac{1}{n}\sum\left(x_i - \bar{x}\right)\left(x_i - \bar{x}\right)^T = \frac{1}{n}XX^T$$

(1)

The term $\bar{x}$ represents the average value. The eigenvalues and eigenvectors of the covariance matrix are found by the eigenvalue-eigenvector separation method. Eigenvalue with the highest value is selected (in this study the value is taken as 3) and the P transformation matrix is created using the r eigenvector vector corresponding to these eigenvalues. The data matrix obtained in experimental studies (for this study; dimensions of 6 x 36) was reduced by dimensioning the above mentioned P transformation matrix to be drawn in the 3-D graphic.

3. RESULTS AND DISCUSSION

The moisture, ash, volatile matter, and fixed carbon content, and elemental composition of the materials are given in Table 1.

Table 1. Proximate and elemental analyses results

		LDPE	C/LDPE	Clay	Zeolite	*Sludge*
Moisture (%)		0.05	<0.001	1.99	1.05	1.16
Ash (%)		1.05	18.37	68.50	89.19	89.85
Volatile matter (%)		98.62	80.71	29.38	9.45	8.95
Fixed carbon (%)		0.28	0.92	0.13	0.31	0.04
Elemental analysis	C	75.69	65.68			
	H	11.25	10.23			
	O*	11.96	5.22			
	N	<0.001	0.56			
	S	<0.001	<0.001			

* by mass difference

The solid, liquid and gas product yields (wt %) obtained from waste LDPE and C/LDPE pyrolysis without catalysts are presented in Table 2. According to the Table 2, the maximum gas product yields were obtained at 20°C/min and 600°C for LDPE (58.2%) and C/LDPE (47.6%).

Table 2. Pyrolysis product yields for LDPE and C/LDPE

Experiment no	Waste material	Heating rate, °C/min	Temperature, °C	Solid product, %	Liquid product, %	Gas product, %
1	LDPE	5	400	30.7	26.9	42.4
2	LDPE	5	600	6.3	72.2	21.5
3	LDPE	5	800	2.3	85.9	11.9
4	LDPE	10	400	5.3	65.6	29.1
5	LDPE	10	600	3.2	72.96	24.2
6	LDPE	10	800	2.0	74.4	23.7
7	LDPE	20	400	3.2	52.4	44.4
8	LDPE	20	600	4.6	37.1	**58.2**
9	LDPE	20	800	2.2	41.0	56.8
10	C/LDPE	5	400	31.3	32.9	35.8
11	C/LDPE	5	600	5.8	71.3	22.9
12	C/LDPE	5	800	6.2	60.2	33.6
13	C/LDPE	10	400	19.9	45.5	34.6
14	C/LDPE	10	600	6.1	55.7	38.1
15	C/LDPE	10	800	6.6	49.6	43.8
16	C/LDPE	20	400	21.3	38.5	40.1
17	C/LDPE	20	600	5.8	46.5	**47.6**
18	C/LDPE	20	800	7.1	59.1	33.8

Pyrolysis results with catalysts at 20°C/min and 600°C were given in Table 3. The highest gas product is obtained with adding 0.5 g zeolite for LDPE (62.6%) and 1 g zeolite for C/LDPE (69.8%).

Table 3. Pyrolysis product yields for LDPE and C/LDPE with catalyst addition

Experiment no	Waste material	Catalyst	Amount of catalyst (g)	Solid product, %	Liquid product, %	Gas product, %
1	LDPE	Waste clay	0.5	1.0	51.6	47.4
2	LDPE	Waste clay	1	1.2	36.5	62.2
3	LDPE	Waste clay	1.5	1.1	47.0	51.9
4	LDPE	Zeolite	0.5	1.1	36.4	**62.6**
5	LDPE	Zeolite	1	0.5	44.2	55.2
6	LDPE	Zeolite	1.5	0.7	43.0	56.4
7	LDPE	Waste sludge	0.5	0.5	46.1	53.4
8	LDPE	Waste sludge	1	1.9	41.7	56.4
9	LDPE	Waste sludge	1.5	1.3	54.5	44.2
10	C/LDPE	Waste clay	0.5	5.5	43.9	50.6
11	C/LDPE	Waste clay	1	5.8	28.3	65.8
12	C/LDPE	Waste clay	1.5	6.6	40.6	52.9
13	C/LDPE	Zeolite	0.5	5.5	47.4	47.0
14	C/LDPE	Zeolite	1	3.3	26.8	**69.8**
15	C/LDPE	Zeolite	1.5	5.6	25.5	68.8
16	C/LDPE	Waste sludge	0.5	6.7	28.1	65.2
17	C/LDPE	Waste sludge	1	5.7	44.7	49.6
18	C/LDPE	Waste sludge	1.5	6.3	35.9	57.8

The variances of principal components (PC) obtained using data from Table 2 and 3 are given in Table 4. According to the table, the first three components explain 99% of the total variability. Figure 3 illustrates the reduction of solid, liquid and gas product outputs to 3 basic components. In this figure, blue colors indicate C/LPDE, red colors indicate LDPE. Values indicated by (*), (+), (o) and (□) symbols are non-catalyst, waste clay, zeolite and waste sludge catalyst states (0, 5; 1; 1.5), respectively. PCA illustrates that the yields of pyrolysis products have a response to the process parameters. According to the results; the effect of temperature on solid product yields is lower than that of liquid product and gas product. The effect of heating rate on product yields is less than the temperature. The effect of temperature on the yield of gas products in the absence of catalyst is less than that of in the presence of catalyst.

Table 4. The variances of principal components

	Solid product			Liquid product			Gas product		
	Eigenvalue	Variance	Cumulative variance	Eigenvalue	Variance	Cumulative variance	Eigenvalue	Variance	Cumulative variance
PC1	412	84.47	84.47	415	67.59	67.59	422	67.25	67.25
PC2	45	9.22	93.69	166	27.15	94.74	174	27.75	95
PC3	30	6.18	99.87	30	4.91	99.65	29	4.64	99.64
PC4	1.1	0.12	99.99	1.2	0.21	99.86	0.14	0.21	99.85
PC5	0.7	0.01	100	0.7	0.14	100	0.012	0.15	100
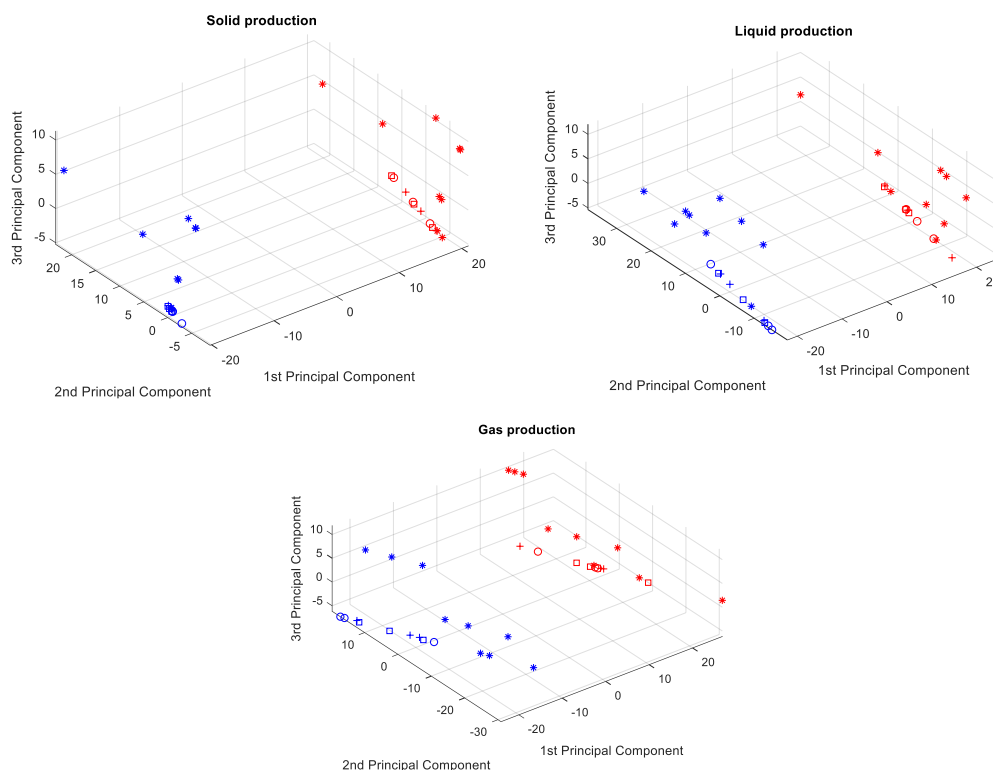
Figure 3. PCA analysis results

CONCLUSION

Since a large number of variables were involved in the pyrolysis experiments, the principal components analysis (PCA) is a technique to interpret the multivariate data obtained. In this study, PCA was used to detect correlations between process parameters and the yields of pyrolysis products. The highest gas product is obtained at 600 C with 20C/min heating rate. The highest gas product is obtained with adding 0.5 g zeolite for LDPE and 1 g zeolite for C/LDPE. In further studies; the effect of process parameters on pyrolysis results with more variables, like alkane content of liquid product, will be determined, since PCA technique is promising in multivariable data analysis.

ACKNOWLEDGMENT

REFERENCES

[1]. An analysis of European plastics production, demand and waste data, Plastics Europe, 2018.
[2]. Turkish Plastics Sector Monitoring Report (original in Turkish), PRDEF (Turkish Plastics Manufacturers Research, Development and Educational Foundation; in Turkish PAGEV), 2017.
[3]. S. M. Al-Salem, A. Antelava, A. Constantinou, G. Manos & A. Dutta, A review on thermal and catalytic pyrolysis of plastic solid waste (PSW), Journal of Environmental Management, 197, 177-198, 2017.
[4]. S. L. Fávaro, A. R. Freitas, T. A. Ganzerli, A. G. B. Pereira, A. L. Cardozo, O. Baron, E. C. Muniz, E. M. Girotto, and E. Radovanovic, "PET and aluminium recycling from multilayer food packaging using supercritical ethanol," J. of Supercritical, Fluids, vol. 75, pp.138–143, Dec, 2012.
[5]. A. K. Kulkarni, S. Daneshvarhosseini and H. Yoshida, "Effective recovery of pure aluminium from waste composite laminates by sub- and super-critical water," J. of Supercritical Fluids, vol. 55, pp. 992–997, Sep. 2010,

[6]. O. K. M. Ouda, S. A. Raza, A. S. Nizami, M. Rehan, R. Al-Waked, N. E. Korres, Waste to energy potential: a case study of Saudi Arabia, Renew. Sustain. Energy Rev. 61, 328e340, 2016.

[7]. Y. Sadef, A. S. Nizami, S. A. Batool, M. N. Chaudhary, O. K. M. Ouda, Z. Z. Asam, K. Habib, M. Rehan, A. Demibras, Waste-to-energy and recycling value for developing integrated solid waste management plan in Lahore, Energy Sources Part B 11, 571e581, 2016.

[8]. M. S. Khan, Z. Kaneesamkandi, Biodegradable waste to biogas: renewable energy option for the Kingdom of Saudi Arabia. Int. J. Innovation Appl. Stud. 4 (1), 101–113, 2013.

[9]. M. N. Siddiqui, H. H. Redhwi, Pyrolysis of mixed plastics for the recovery of useful products, Fuel Process, Technol. 90, 545–552, 2009.

[10]. A. S. Nizami, O. K. M. Ouda, M. Rehan, A. M. O. El-Maghraby, J. Gardy, A. Hassanpour, S. Kumar, I. M. I. Ismail, The potential of Saudi Arabian natural zeolites in energy recovery technologies, Energy 108, 162e171, 2015.

[11]. D. Chen, L. Yin, H. Wang, & P. He, Reprint of: pyrolysis technologies for municipal solid waste: a review. Waste Management, 37, 116-136, 2015.

[12]. N. Miskolczi, A. Angyal, L. Bartha, I. Valkai, Fuels by pyrolysis of waste plastics from agricultural and packaging sectors in a pilot scale reactor, Fuel Process. Technol., 90, 1032e1040, 2009.

[13]. R. Miandad, M. A. Barakat, A. S. Aburiazaiza, M. Rehan, & A. S. Nizami, Catalytic pyrolysis of plastic waste: A review. Process Safety and Environmental Protection, 102, 822-838, 2016.

[14]. R. A. Johnson, W. W. Dean, Applied Multivariate Statistical Analysis, Fifth Edition, Prentice-Hall, Inc., New Jersey, 2002.

[15]. B.B. Jackson, Multivariate Data Analysis an Introduction, Richard, D. Irwin, Inc., Ilnois, 2004.

BIOGRAPHY

Aysun Ozkan is an associate professor in the Environmental Engineering Department at Eskisehir Technical University, where she has been a faculty member since 2000.

Ozkan completed her undergraduate and PhD at Anadolu University. Her research interests lie in the area of solid and hazardous waste management.

For additional information, please see https://akademik.eskisehir.edu.tr/aysunozkan

Life Cycle Assessment of Waste Composite Packaging Pyrolysis

Aysun Ozkan[1], Kubra Cebeci Topbas[2], Ece Yapici[2], Zerrin Gunkaya[2], Mufide Banar[2]

Abstract

Composite/Low-density polyethylene (C/LDPE) packages are used for food packaging of varied products (soup, instant coffee, etc.). Although the consumption rate of these packaging type has been increasing, their recycling is so difficult due to their complex nature. With this motivation, the aim of this study is to investigate the environmental effects of C/LDPE waste recovery by pyrolysis through life cycle assessment (LCA). The system boundary includes laboratory scaled pyrolysis in a fix bed stainless steel reactor and material/energy/emission flows. The functional unit was defined as 10 g of waste C/LDPE entering the pyrolysis process. Inventory data has been collected through onsite measurements, materials usage and Ecoinvent software database. The LCA calculations were carried out using licensed SimaPro 8.5 software. At the impact assessment step, the CML-IA method was applied for the selected impact categories (abiotic depletion, global warming, toxicity, acidification and eutrophication).

Keywords: C/LDPE, environmental impacts, life cycle assessment (LCA), pyrolysis, waste composite packaging.

1. INTRODUCTION

The packaging industry is the largest consumer of plastic materials. In 2017, 3.8 million tons of 9.6 million tons produced plastics were used for packaging materials in Turkey [1]. Different properties, such as barriers to gas, light, flavour and water vapour, as well as flexibility, are essential for the production of food packages. These properties may be obtained by combining different polymers [2]. Aluminium is widely used in packaging laminates. Aluminium plays a significant role in these laminates by preventing the food from the effect of oxygen, moisture gain or loss, sunlight and ultraviolet radiations, and flavour loss [3]. Despite these advantages, the recycling of such kind of material is quite difficult and cannot be separated by hand. At present, waste plastics are mainly treated with mechanical recycling, chemical recycling, incineration and dispose on landfill. Chemical recycling, on the other side, can be used to recover petrochemical components of waste plastics, to remanufacture plastics, and to make other synthetic chemicals [4]. Pyrolysis, as one of the chemical recycling method, is believed to be one of the best thermal alternatives for waste Composite/Low-density polyethylene (C/LDPE) packages [5].

Life cycle assessment (LCA) methodology is generally regarded as one of the best environmental management tools that can be used to compare alternative eco-performances of recycling/recovery systems. It views the environment as a whole, including indirect releases, energy and material consumption, emissions in the environment, and waste disposal and follows each activity from the extraction of raw materials to the return of wastes to the ground (cradle-to-grave approach) [6]. The main objective of this study is to investigate the environmental effects of C/LDPE waste recovery by pyrolysis through LCA.

2. MATERIALS AND METHODS

This study was conducted according to ISO 14040 and ISO14044 standards developed by the International Organization for Standardization (ISO). This LCA study compromises the four stages according to the ISO

[1] Corresponding author: Eskisehir Technical University, Department of Environmental Engineering, 26555, Iki Eylul Campus, Eskisehir, Turkey. aysunozkan@eskisehir.edu.tr

[2] Eskisehir Technical University, Department of Environmental Engineering, 26555, Iki Eylul Campus, Eskisehir, Turkey. kcebeci@eskisehir.edu.tr

standards: The goal and scope definition (functional unit, system description and system boundaries), Life cycle inventory (data collection), Life cycle impact assessment and Interpretation.

○ *Goal and scope definition*

The goal of this study is to determine the environmental effects of waste C/LDPE recovery through pyrolysis by LCA method. The functional unit was defined as 10 g of waste C/LDPE entering the pyrolysis process.

▪ *System description*

The pyrolysis experiments were carried out under atmospheric pressure at 600°C with a 20°C/min heating rate in a fixed bed stainless steel (380 S) 240 cm³ reactor. 10 g of sample was placed in the reactor. As a result of the pyrolysis process, liquid, solid and gas phases were produced. In these conditions, the yield of the solid, liquid and gas product were found to be 5.8±0%, 46.5±0.1% and 47.6±0.1%, respectively.

▪ *System boundaries*

Cradle-to-gate system boundaries were applied which includes laboratory scaled pyrolysis of waste C/LDPE in a fix bed stainless steel reactor and material/energy/emission flows. The system boundaries that were considered in this LCA analysis are shown in Figure 1, based on the system description. The total environmental impact, regarding waste C/LDPE pyrolysis, consists of 3 components: indirect impact caused by energy and the material production stage, direct impact caused by waste C/LDPE pyrolysis, and impacts avoided by valuable products (recycled material and energy).
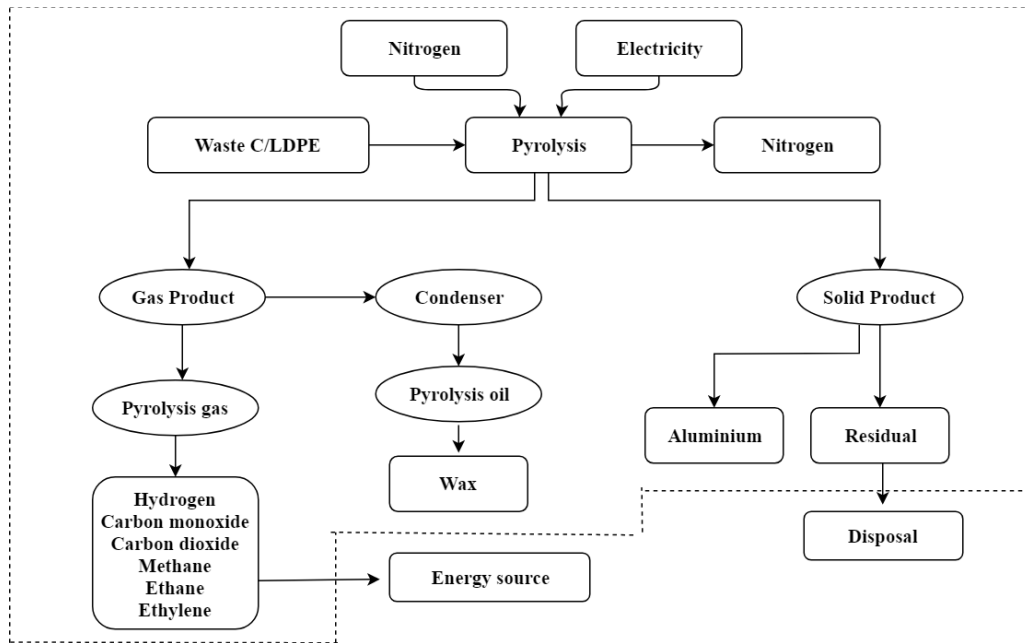
Figure 1. System Boundary

○ *Life cycle inventory*

For the life cycle inventory, the data was distinguished into two parts as primary and secondary data. Primary data on the input (electricity) and output (pyrolysis gas composition and pyrolysis products) were mainly obtained from the onsite measurements and materials usage. Before starting the pyrolysis experiment, the reactor was placed for 5 minutes along with nitrogen gas at a flow rate of 750 mL/sec. In total, 266.625 g of nitrogen was consumed. During pyrolysis, the LDPE in the composite package is decomposed to the gas phase, and the gas becomes wax by condensing again. The liquid product contains aliphatic and aromatic hydrocarbons that can be used to obtain wax. To obtain 4.65 g of wax formed after pyrolysis, the liquid product collected in the liquid collection containers was washed with an average of 66.5 g of dichloromethane (DCM) solvent. The average amount of electricity required for production was 5.65 kWh per 10 g of waste C/LDPE. Emissions and recovered quantities of aluminium and wax were calculated by mass balance. The analyses of the gases collected in the gas

bags during the pyrolysis were carried out in the Petkim Petrochemical Holding laboratory using GC-FID and GC-TCD systems (Table 1). The gas product obtained from the process can be further used for heat production. The aluminium content of the pyrolysis solid product was determined gravimetrically by burning off the organic content of the product in a muffle furnace for 30 minutes at 900°C and was obtained as to be 88.70%. Therefore, high aluminium content of solid product is promising in terms of recovery of pure aluminium. According to the results of the gravimetric analysis, the recovered quantity of aluminium is 0.514 g. The summary of the primary data is given in Table 2.

Table 1. Component of gas product

Compound	% (as volume)
Hydrogen (H_2)	2.03
Carbon dioxide (CO_2)	31.03
Carbon monoxide (CO)	25.39
Methane (CH_4)	12.33
Ethane (C_2H_6)	9.82
Ethylene (C_2H_4)	19.41

Table 2. Primary inventory data on experimental work (on reference flow basis)

Pyrolysis process per 10 g of C/LDPE	Quantities
Input	
Waste C/LDPE	10 g
Nitrogen (N_2)	266.625 g
Dichloromethane	66.5 g
Energy consumption	
Reactor	3.6 kWh
Evaporator	0.05 kWh
Muffle furnace	2 kWh
Output	
Nitrogen (N_2)	266.625 g
Hydrogen (H_2)	0.006 g
Carbon dioxide (CO_2)	2.068 g
Carbon monoxide (CO)	1.092 g
Methane (CH_4)	0.304 g
Ethane (C_2H_6)	0.45 g
Ethylene (C_2H_4)	0.84 g
Aluminium	0.514 g
Wax	4.66 g
Residual	0.066 g

SimaPro 8.5 software was used to develop unit process by using primary data and to link the primary to the secondary data. Secondary data was gathered from the EcoInvent (v.3.0.3) database which is embodied in SimaPro 8.5. In addition to the secondary data obtained from Ecoinvent, electricity production data was gathered from Gunkaya et al. (2016) [7]. This electricity mix data was modified based on the electricity mix of Turkey in 2018 (30.5% natural gas, 22.7% hydroelectric, 36% coal (mainly coal, imported coal and lignite), 6.2% for wind, 2.3% geothermal).

o   *Life cycle impact assessment*

At the impact assessment step, the CML-IA method, embodied in SimaPro 8.5, was applied for the selected impact categories: abiotic depletion (element) potential (ADPe), abiotic depletion (fossil fuels) potential (ADPff), global warming potential (GWP), acidification potential (AP), eutrophication potential (EP) and human toxicity potential (HTP). Normalization results were also calculated using the EU25+3, 2000 calculation method under the CML-IA baseline (v3.00) method.

3. RESULTS AND DISCUSSION

Characterization and normalization results are given in Table 3. According to normalization results, ADPff, GWP and AP are the dominant impact indicators of the waste C/LDPE pyrolysis.

Table 3. Characterization and normalization results.

Impact category	Characterization		Normalization
	Unit	Amount	
ADPe	kg Sb eq.	0.00156	2.58E-10
ADPff	MJ	54400	1.55E-09
GWP	kg CO_2 eq.	5830	1.12E-09
HTP	kg 1.4-DB eq.	401	8.02E-10
AP	kg SO_2 eq.	62.2	3.69E-09
EP	kg PO_4 eq.	3.55	1.92E-10

Distribution of the characterization results to the input processes is shown in Figure 2, according to which, among all the impact categories, the environmental impact resulting from electricity consumption is observed to be overwhelming (93.7%-96.4%) compared to other process components (pyrolysis, nitrogen production, dichloromethane production).
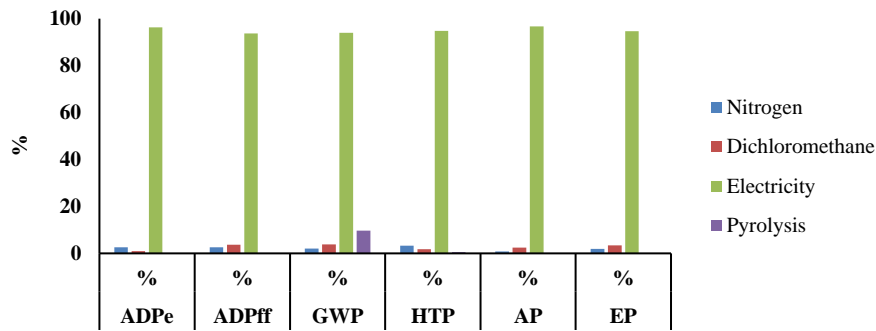
Figure 2. Distribution of characterization results to the input processes

Environmental effects avoided by recovery of Al and wax as a result of pyrolysis process are presented in Figure 3. From figure, it is found that Al recovery provides more environmental benefits than wax in all the impact categories.
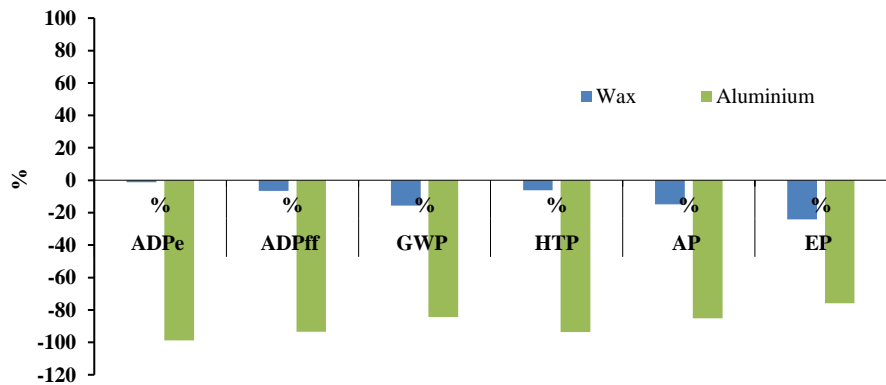
Figure 3. Avoided characterization results by valuable products

The parameters that cause ADPe effects of waste C/LDPE pyrolysis are given in Figure 4. According to Figure 4a, ADPe effect category is mostly caused by copper, chromium and molybdenum elements. It is seen that, in the background, these elements are in the structure of the materials used in the construction phase of the power plants. The avoided ADPe parameters by recovery of Al and wax as a result of pyrolysis is given in Figure 4b. As can

be seen from the figure, due to the avoided virgin copper element usage, Al recovery has an important role in avoiding ADPe effect.

(a)

(b)

Figure 4. ADPe impact of 10 g of waste C/LDPE pyrolysis: a) distribution of characterization results to the input processes, and b) avoided characterization results by valuable products

Figure 5 (a) shows that coal consumption has the highest amount in the ADPff impact category. The ADPff impact can be decreased by wax recovery (Figure 5 (b)). In this context, a significant decrease will be observed, especially in the use of crude oil and coal.

(a)

(b)

Figure 5. ADPff impact of 10 g of waste C/LDPE pyrolysis: a) distribution of characterization results to the input processes, and b) avoided characterization results by valuable products

The main pollutants causing the GWP effect of the pyrolysis of the waste C/LDPE material are CO_2 and CH_4, and the effects are 93.2% and 6.6%, respectively (Figure 6 (a)). This significant impact of CO_2 emissions on GWP is due to the burning of coal in electricity generation. Figure 6b shows that wax recovery was found to have a larger contribution than Al recovery to avoiding GWP effect. This contribution can be made especially by preventing the release of CO_2 emissions.

(a)　　　　　　　　　　　　(b)

Figure 6. GWP (100 a) impact of 10 g of waste C/LDPE pyrolysis: a) distribution of characterization results to the input processes, and b) avoided characterization results by valuable products

The pollutant components that cause the toxic effect on humans are the emissions of Cr^{+6}, Se, Mo, Ni, As and Cd that emerge during the generation of electricity (Fig. 7 (a)). These emissions are due to the disposal of high-carbon ferrochrome process, coal mines and coal-fired power plants during the construction of wind turbines used in electricity generation. Al and wax recovery are not given graphically because of their insignificant amounts in HTP impact category.

Figure 7 (b) shows that the main cause of eutrophication of waste C/LDPE pyrolysis is the emissions of nitrogen and phosphate released during the mining of lignite and NO_x blasting into the air due to the combustion of fossil fuels for electricity generation. Al and wax recovery are not given graphically because of their insignificant amounts in EP impact category.

(a)　　　　　　　　　　　　(b)
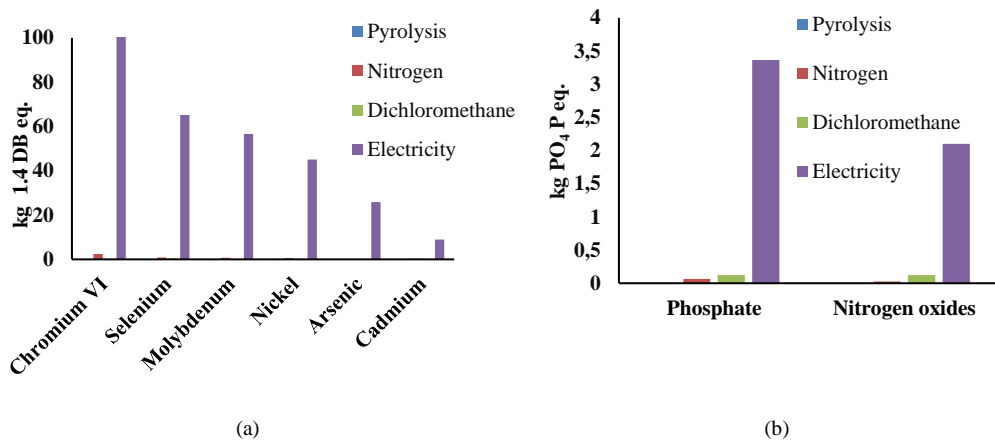
Figure 7. Distribution of characterization results to the input processes: a) HTP impact of 10 g of waste C/LDPE pyrolysis, and b) EP impact of 10 g of waste C/LDPE pyrolysis

Figure 8 (a) shows that the SO_2 and NO_x emissions released during the production of the electricity are the major pollutants that cause the acidification potential (%83.6 and %13, respectively). These emissions are caused by the burning of coal and natural gas used in electricity generation. According to Figure 8 (b), wax recovery will have a significant role on the reduced acidification effect due to the avoided SO_2 and NO_x emissions.
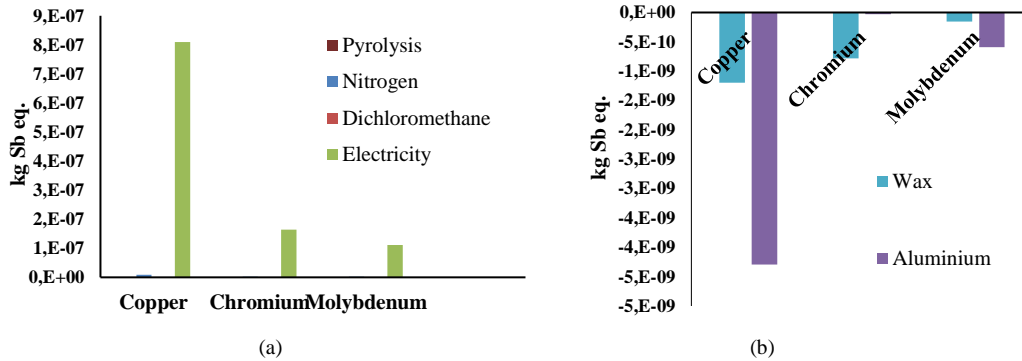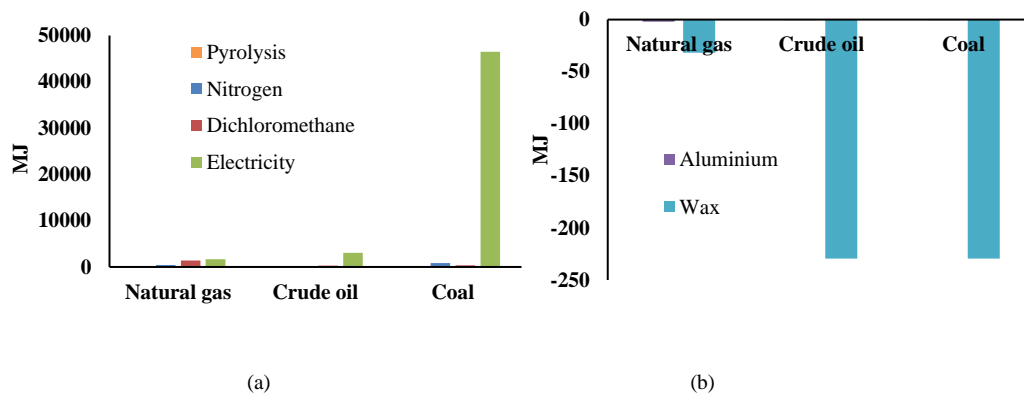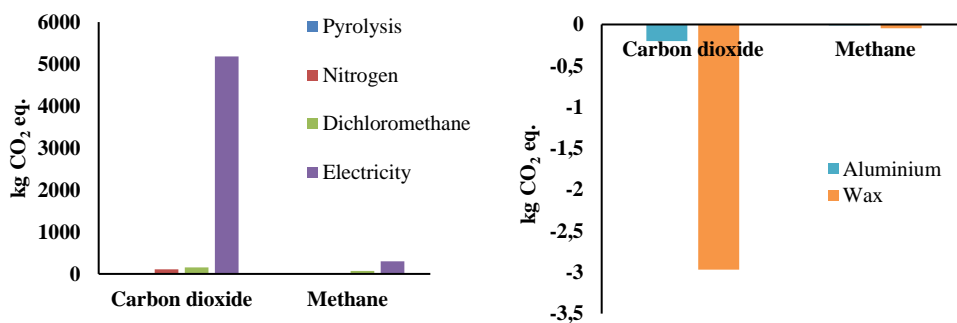

(a)　　　　　　　　　　　　(b)
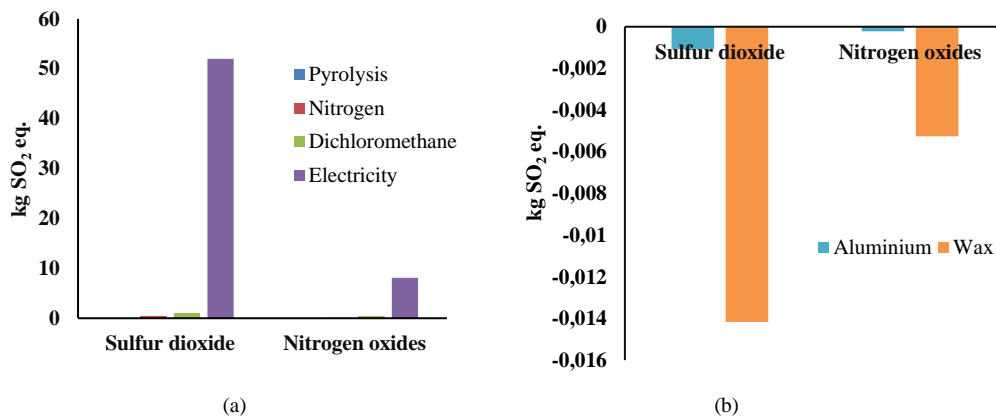
Figure 8. AP impact of 10 g of waste C/LDPE pyrolysis: a) distribution of characterization results to the input processes, and b) avoided characterization results by valuable products

ICENS 5TH INTERNATIONAL CONFERENCE ON ENGINEERING AND NATURAL SCIENCE 12-16 June 2019 Prague

CONCLUSION

In this study, environmental impacts of waste C/LDPE pyrolysis were determined by using LCA. Pyrolysis process produces valuable materials, such as gases, solids and oils that can be used in energy and material applications. Generally, pyrolysis is an energy intensive process. Therefore, electricity use is the most influential contributor among all environmental impact categories. Replacement of fossil fuels by various sources of renewable energy (photovoltaic, wind power, etc.) in Turkey's electricity production is quite likely to reduce these environmental impacts. This is the first LCA study on waste C/LDPE pyrolysis in Turkey. Therefore, the findings of this study are likely to be of assistance for decision-makers and practitioners by providing a framework to better understand the major environmental effects of waste C/LDPE pyrolysis and its conversion to useful products.

ACKNOWLEDGMENT

REFERENCES

[1]. Turkish Plastics Sector Monitoring Report (original in Turkish), PRDEF (Turkish Plastics Manufacturers Research, Development and Educational Foundation; in Turkish PAGEV), 2017.
[2]. S.L. Fávaro, A.R. Freitas, T.A. Ganzerli, A.G.B. Pereira, A.L. Cardozo, O. Baron, E.C. Muniz, E.M. Girotto, and E. Radovanovic, "PET and aluminium recycling from multilayer food packaging using supercritical ethanol," J. of Supercritical. Fluids, vol. 75, pp.138–143, Dec. 2012.
[3]. A.K. Kulkarni, S. Daneshvarhosseini and H. Yoshida, "Effective recovery of pure aluminium from waste composite laminates by sub- and super-critical water," J. of Supercritical Fluids, vol. 55, pp. 992–997, Sep. 2010.
[4]. J. Gong, J. Liu, Z. Jiang, J. Feng, X. Chen, L. Wang, E. Mijowska, X. Wen and T. Tang, "Striking influence of chain structure of polyethylene on the formation of cup-stacked carbon nanotubes/carbon nanofibers under the combined catalysis of CuBr and NiO," Applied Catalyst B, vol.147, pp. 592– 601, Aug. 2013.
[5]. M. Banar, "Life Cycle Assessment of Waste Tire Pyrolysis", Fresenius Environmental Bulletin, vol. 24, pp. 1215-1225, Jan. 2015.
[6]. F. Perugini, M. L. Mastellone, and U. Arena, "A Life Cycle Assessment of Mechanical and Feedstock Recycling Options for Management of Plastic Packaging Wastes", Environmental Progress, vol.24, pp.137-154, July 2005.
[7]. Z. Gunkaya, A. Ozdemir, A. Ozkan, and M. Banar, "Environmental Performance of Electricity Generation Based on Resources: A Life Cycle Assessment Case Study in Turkey," Sustainability, vol. 8 (1097) pp. 1-14. Oct. 2016.

BIOGRAPHY

Aysun Ozkan is an associate professor in the Environmental Engineering Department at Eskisehir Technical University, where she has been a faculty member since 2000.

Ozkan completed her undergraduate and PhD at Anadolu University. Her research interests lie in the area of solid and hazardous waste management.

For additional information, please see https://akademik.eskisehir.edu.tr/aysunozkan

The Air Pollutant Emission Factor Development for Automobile Fuels

Ali Can [1], Aysegul Filiz [2]

Abstract

The population increases and development of industries are causing an excessive consumption of earth resources. Therefore, the natural resources have already reached an irreversible point which causes an adverse effect on the earth future. However, human's sensitivity is not the same as solving these environmental problems as it is created by them. Therefore, the environmental disasters dimensions have caused people to adapt to these problems. One of the most important problems is the air pollution due to the high rate consumption of fuels by households, transport and industrial sectors.

In this study, the emission factor of CO_2, CH_4, N_2O pollutants from road vehicles will be investigated by using instantaneous fuel consumption on the roads in different velocities and gears. Direct GHGs pollutant emissions are calculated and it is used for the emission calculations for daily case study done for the highway roads connecting center of Karabuk province and Safranbolu district.

The emission factor of CO_2, CH_4, N_2O pollutants from road vehicles will be investigated by using instantaneous fuel consumption on the roads in different velocities and gears. Direct GHGs pollutant emissions are calculated and it is used for the emission calculations for daily case study done for the highway roads connecting center of Karabuk province and Safranbolu district. This improved EFs can be used for the Tier 2 methodologies for the National Emission Inventory (NIR) calculations of Turkey. According to the study, the daily CO_2 equivalent emission is calculated as 257 ton. The annual emission from this highway is 93 million ton CO_2 eq. emission.

Keywords: CO_2, CH_4, N_2O pollutants, Road Transport, Emission Factor

1. INTRODUCTION

The rapid growth of the world population and high rate industrial development are consuming excess resources of the earth. This consumption of natural resources has already reached a level, which is irreversible at the beginning of 21st century. However, human beings are not at the same attitude toward to solve these problems. Therefore, the environmental disasters that have occurred in recent years have caused people to adapt not only to these expected problems but also the worse future scenarios [1].

The most important source of air pollutants is the energy consumption resulting from the use of fuels. Energy consumption is essential for human well-being. Energy and economy are the two important factors that form the most important development building blocks of countries which cannot be thought independently. Therefore, the energy consumption cannot be decreased due to economical factors [2]. The increase in energy consumption is increasing pollutant emissions and air pollution. The air pollution is causing economic, environmental and social pressure on the earth [3].

The most important component of the fresh air concentration is oxygen. By means of ozone depletion, degradation of atmospheric gases components, and the change in the current density of oxygen are the effects of pollution which is highly felt by people [4].

When the air pollutant causes are examined, it is seen that a significant ratio is caused by transportation [5]. Despite the increase in the number of used vehicles, it is estimated that their impact on the ecosystem is balanced by technological development. It is also expected to be reduced further by new technological improvements [6].

---

[1]*Corresponding author: Karabuk University, Department of Mechanical Engineering, 78050, Karabuk, Turkey. alican@karabuk.edu.tr*

[2]*Karabuk University, Department of Mechanical Engineering, 78050, Karabuk, Turkey, aysegulfiliz1@gmail.com*

The increase in the number of motor vehicles for the transportation sector every year has caused to increase in air pollution to a certain level in our country. The effect of emissions from motor vehicles on the atmosphere is the same as the average rates seen in other countries around the world, which is in the range of 25% -40% [7].

Alternative bio-liquid fuel production for transport vehicles is reducing air emissions. Advanced technology such as Catalytic Converters and Renewable Energy Source Execution are the tools for Turkey, like the world countries by involving in priority of air pollution and climate change. Particulate matter, sulfur oxides, nitrogen oxides, VOC emissions etc. due to exhaust emissions not to exceed the limit values of pollutants is the building block of this struggle [8].

Gasoline, diesel and LPG are used in transport vehicles. The emissions from the consumption of these fuels cause anair pollution from the exhaust. Fuel consumptions by vehicles source create pollutants. These pollutants are listed as carbon monoxide (CO), carbon dioxide (CO_2), hydrocarbons (HC), nitrogen oxides (NO_x) and particulate matter (PM). Motor vehicles have a share of carbon monoxide (CO) emissions of 40-90%, nitrogen oxide (NOx) emissions of 20-70% and hydrocarbon (HC) emissions of about 40-50%. These pollutants also cause a variety of diseases such as heart and circulatory system disorders, asthma, bronchitis and lung cancers [9].

The parameters such as vehicle model, age, engine volume, tire diameter and slope of the road, vehicle operating speed, engine operating temperature, fuel type, fuel quality and user habits directly affect the air pollutant emissions. While the inefficient combustion is occurring, then the carbon monoxide (CO) pollutant is higher and the amount of nitrogen oxide (NO) is lower. If the NO emission is observed more than the CO emission due to nitrogen oxidation caused by the increasing temperature, the vehicle will start to accelerate [5]. CO is the result of ineffective combustion. The formation of CO gas from motor vehicles is due to the lack of sufficient oxygen in the fuel-air mixture reaction. Carbon monoxide is affected by the engine running at low speeds. This pollutant increases in the free state of engine, while the motor starts to accelerate to a certain level, the CO emission decreases [10, 11]. Timely maintenance of the vehicles, efficient use of fuel, regular checks of the vehicle, not carrying passengers or cargo over capacity are improving vehicle performance and reducing air pollution rates [5]. Nitrogen oxides (NOx) is consisting, nitric oxide (NO) and nitrogen dioxide (NO_2). These gases emerge as a result of chemical combustion reaction and increase with high pressure and temperature. Nitrogen in air has an absolute relationship to emission [12]. The two most important factors in NO_x formation in motor vehicles are the air/fuel ratio in the engine combustion chamber and the temperature values of engine combustion chamber. To prevent the temperature and pressure in the combustion chamber as low as possible, the reduction of NO_x gases in the chamber [13].

Methane gas (CH_4), as a component of natural gas, is an important pollutant gas if it is released into the atmosphere. CH_4 is harmful, because the effect of its global warming is high due to CH_4 enthalpy value. It also has properties such as being poisonous, explosive or suffocating when reacting with other gases [14, 15].

Volatile organic compounds (NMVOC) are referred to as non-methane volatile organic compounds. NMVOC is including butane, propane compounds, which are causing the depletion of ozone and other oxidants in the atmosphere together with the nitrogen oxides. The paint application is spreading high NMVOC to the atmosphere [16]. The damages of air pollution emissions are summarized in the below figure 1 [17]. Although, these emissions are studied within the study, only CO_2, CH_4 and N_2O are evaluated in this article.

This study will close a significant gap in air pollution calculations in Karabuk province by determining emission factors (EFs) of air pollutants. The study has been constructed on the busiest highway chosen between Karabuk province and Safranbolu districts. Later the collected and estimated EFs are used to determine the air pollutant emissions from the road of Karabuk.

In this study, the pollutants EFs for CO_2, CH_4, N_2O from transport vehicles of Karabuk province is investigated by measuring instantaneous fuel consumptions. Hourly pollution emissions are calculated. The calculation of road-based emissions will reveal the impact of transport-related emissions in Karabuk. This study is quite different from the studies conducted in the region. It will reveal the emission factors at the point scale along the way for the selected region.

It will also lead to the development of transport sector emission factors. Another benefit of the study is the national sector emission methodology in National Inventory Report submitted to the UNFCCC annually will be increased to IPCC T2 level for road transportation by using the EFs calculated within this study.
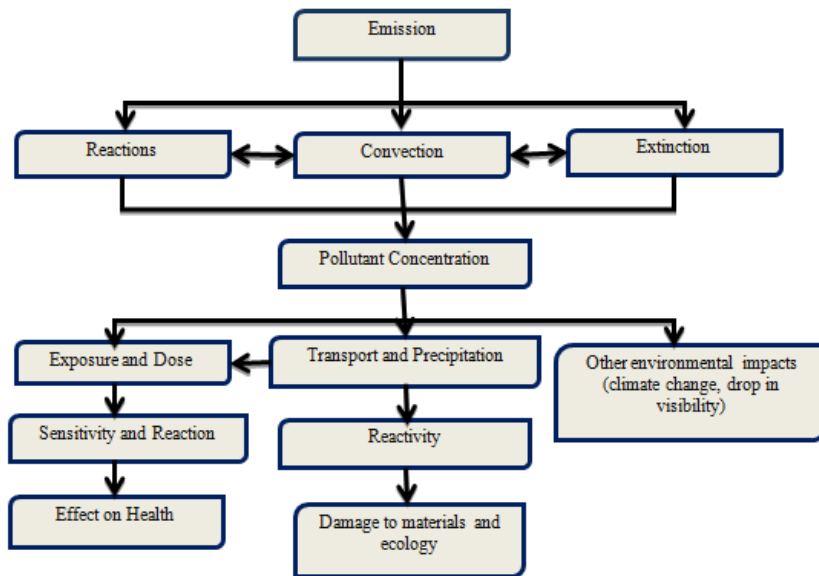
Figure 1.Air Pollution and its Problems [17]

Air pollution includes five main headings. These are called pollutant sources, source types, pollutant, receiver and carrier (medium) [18, 19]. Within this study, the pollutant source is road transport vehicles; source types are listed as automobiles, minibus, bus and truck; pollutants are CO_2, CH_4, N_2O; receivers are people and close regions to roads; carrier is wind causing convection during puff emission from road vehicles.

2. METHODOLOGY

This study was carried out between Karabuk Terminal Junction in Karabuk province (1st Point) to Safranbolu center (7th point) in Safranbolu district. The total distance between the two points is 8.14 km (Figure 2). Altitude changes due to inclined and straight roads along the way. The emission rate makes a difference on inclined and straight roads due to fuel consumptions. The determined altitude for each point was given below. The lowest altitude is 261 m and the highest altitude is 503 m as seen in Figure 3.
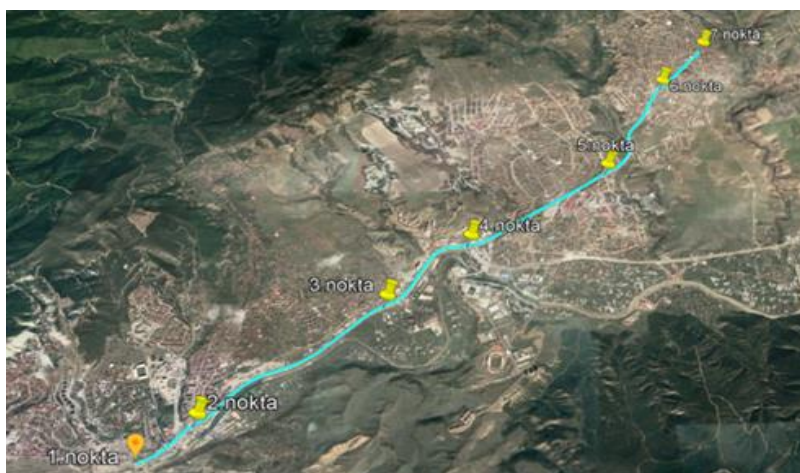
Figure 2. Satellite Image for Study Area.
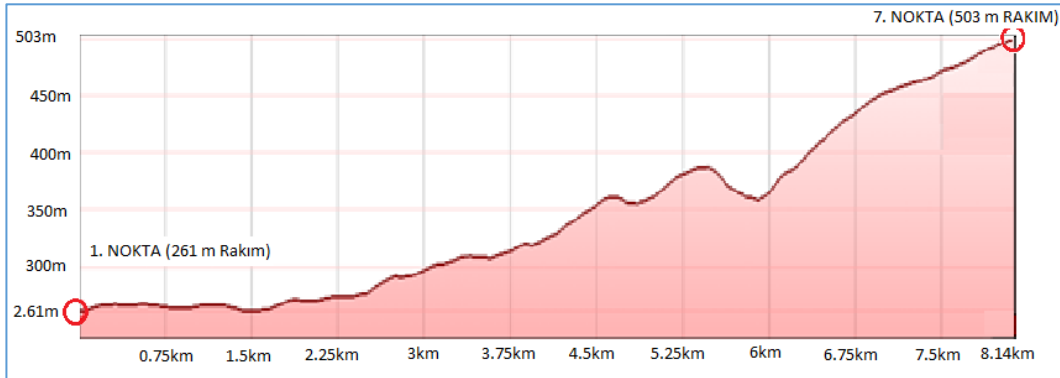
Figure 3. The altitudes of selected road for EF determinations

The instantaneous fuel consumptions, gears and speed of vehicles are recorded for diesel and gasoline car as seen in Figure 4 by cam recording. Basically, the productions of emission factors are only a section of modeling study. But in this article, only productions of EFs are described. The instantaneous LPG measurements are not made, however, the gear changes and related to the gear, speed panel on the same road are also recorded, the instantaneous LPG consumption is estimated by speed and gear compared with gasoline and diesel. All these data are used for improving of EFs.

The IPCC [20] and EMEP/CORINAIR [21] EFs are also used for improving speed related EF's (Table 1.). By using table 1, the energy conversion is made.

Figure 4. The instantaneous fuel consumption cam recorded from vehicles' panel

Table 16. The fuel emission factor due to consumption [20, 21]

Yakit	CO_2(tC/TJ)	CH_4 (kG/TJ)	N_2O(kG/TJ)
LPG	17.2	50	0.1
Gasoline	18.9	20	0.6
Diesel	20.2	5	0.6

A polynomial nonlinear regression model [22] is also determined by the Eq. (1):

$$y = b + c_1 X + c_2 X^2 + c_3 X^3 + \cdots + c_n X^n \qquad (1)$$

$c_{1,,,}c_n$: constant

And the R-squared (R^2) values which are a statistical measures of how close the variables are fitted to the models. The closest R^2 values to unity are considered as acceptable. R^2 is also known as the coefficient of determination and it is calculated as in Eq. (2):

$$R^2 = 1 - \frac{SSE}{SST} \; ; \text{ where } \; SSE = \sum(Y_i - \hat{Y}_i)^2 \text{ and } SST = (\sum Y_i^2) - \frac{(\sum Y_i)^2}{n} \qquad (2)$$

R^2 : R squared value
SSE   : sum of squares of the residual error
SST   : treatment sum of squares
n   : Observation numbers
Y_i : Observation value
$\hat{Y}_i$: Fitted value

3. RESULT AND DISCUSSION

In this study, the emission factor of CO_2, CH_4, N_2O pollutants from road vehicles will be investigated by using instantaneous fuel consumption on the roads in different velocities and gears. Direct GHGs pollutant emissions are calculated and it is used for the emission calculations for 24 hours of a case study done for the highway roads connecting center of Karabuk province and Safranbolu district.

As a result by many measurements, the following figures were obtained. The instantaneous and speed depended fuel consumptions and EFs are obtained according to 3 different car and 25 voyage 15-20 minutes duration. As seen in Figure 5, the carbon emission factor is very high at low speed due to inefficient burning of fuels. However, it is decreasing with increasing speed until 60-70 km/h, then again it is increasing due to high rate of fuel consumption. The polynomial model is also given within the each figure. The statistical evaluation of these models is also gives us high rate R square values, which means the models is highly matched with the measured values.
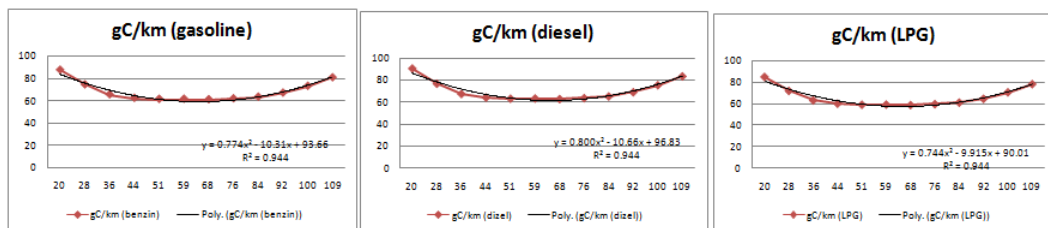
Figure 5. The C speed depended EFs for gasoline, diesel and LPG

The studies were also extended for obtaining CH_4 and N_2O. The CH_4 EFs are calculated differently for fuel types. The LPG is emitting high rate CH_4 to the atmosphere because of inefficient burning and fugitive emission during the pressure decreases of fuel consumption in the motor section. However, the diesel is 3 times lower compared to the gasoline due to the fluidity properties of fuels. In the following figures, the models for estimating speed depended EFs are given with high rate of R squared values.
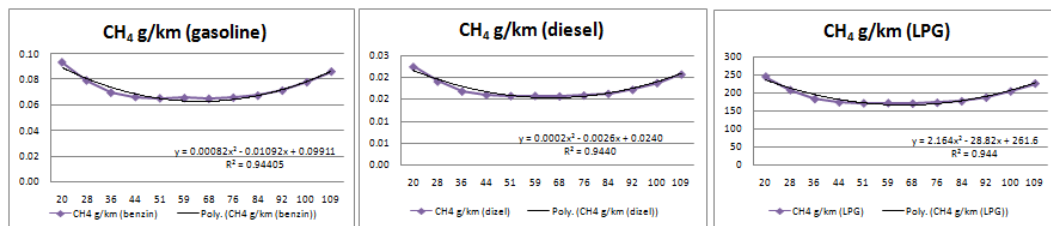
Figure 6. The CH_4 speed depended EFs for gasoline, diesel and LPG

The N_2O emissions from gasoilne and diesel are the same. The main reason is the oxidation of atmospheric nitrogen. The emission from LPG is higher due to gas burning properties of motor with the high rate feeding of atmospheric air to the system. Otherwise the efficiency is decreasing comparable quantity. In all models, the high rate R-squared values are obtained.
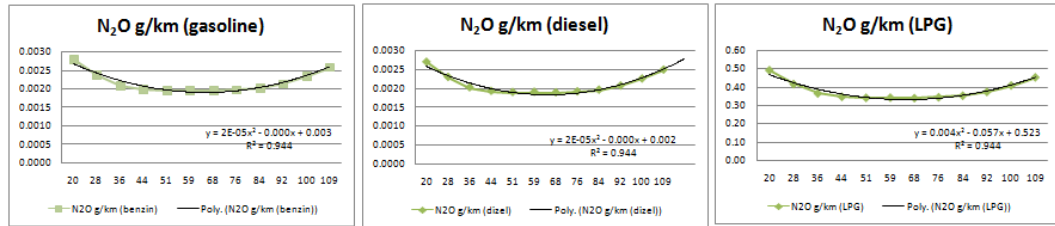
Figure 7. The N_2O speed depended EFs for gasoline, diesel and LPG

By using all these EFs, the cam recording transport vehicles Table 2 are multiplied and the average direct GHGs are calculated as given in Table 3.

According to the Table 2., automobile fuel types are estimated by Turkish Statistical Institute, Transportation Statistic Databases values [23].According to these statistics, approximately 26% of cars is using gasoline and the remaining 35% and 36% respective percent values are belonging to the diesel and LPG.

Table 2. Average number of cars passing on the road

Vehicle types	Automobile			Minibus, Van	Autobus, Truck
Fuel types	Gasoline	Diesel	LPG	Diesel	Diesel
daily vehicles number counted on the study area	4374	5966	6472	3336	848

And according to these vehicle numbers, the GHGs emission factor (EF), study area average EF, study area GHGs emissions are given in Table 3-5.

Table 3. Average GHGs Emission Factor

Emission Factor (EF)	Automobile			Minibus, Van	Autobus, truck
Fuels Type	Gasoline	Diesel	LPG	Diesel	Diesel
gC/km	68.6600	70.9000	65.9000	70.9000	70.9000
CO_2 g/km	251.7533	259.9667	241.6333	259.9667	259.9667
CH_4 g/km	0.0726	0.0175	191.5500	0.0175	0.0175
N_2O g/km	0.0022	0.0021	0.3831	0.0021	0.0021

The following table is obtained by counting daily automobile, minibus, van, otobus and truck times the EF given in Table 3. Depending on daily truck and bus numbers, the emissions from diesel consumptions of bus and trucks on the selected road are low. However, the unit basis emissions are always the highest for these vehicles.

Table 4. Study Area Emission Factor

Selcted Area EF	Automobile			Minibus, Van	Autobus, truck
Fuels Type	Gasoline	Diesel	LPG	Diesel	Diesel
ton C/km	0.300	0.423	0.426	0.237	0.060
ton CO_2/km	1.101	1.551	1.564	0.867	0.220
ton CH_4/km	0.000318	0.000104	1.239688	0.000058	0.000015
ton N_2O/km	0.00000962	0.00001253	0.00247938	0.00000701	0.00000178

The total daily CO_2 equivalent emission is calculated as 257 ton for the highway roads connecting center of Karabuk province and Safranbolu district. The calculated results are given below Table 5.

Table 5. Study Area GHGs Emissions

Study Area Emission	Automobile			Minibus, Van	Autobus, truck	Total CO_2 Eq. Emission (ton/day)
Fuels Type	Gasoline	Diesel	LPG	Diesel	Diesel	
ton C	2.403	3.384	3.412	1.892	0.481	-
ton CO_2	8.810	12.409	12.511	6.938	1.764	42.43
ton CH_4	0.003	0.001	9.918	0.000	0.000	208.35
ton N_2O	0.000077	0.000100	0.019835	0.000056	0.000014	6.23
TOTAL						257.01

4. CONCLUSION

The emission factor of CO_2, CH_4, N_2O pollutants from road vehicles will be investigated by using instantaneous fuel consumption on the roads in different velocities and gears. Direct GHGs pollutant emissions are calculated and it is used for the emission calculations for daily case study done for the highway roads connecting center of Karabuk province and Safranbolu district. Depending on daily truck and bus numbers, the emissions from diesel consumptions of bus and trucks on the selected road are low. However, the unit basis emissions are always the highest for these vehicles. These improved EFs can be used for the Tier 2 methodologies for the National Emission Inventory (NIR) calculations of Turkey. According to the study, the daily CO_2 equivalent emission is calculated as 257 ton. The annual emission from this highway is 93 million ton CO_2 eq. emission.

Acknowledgements

REFERENCES

[1]. Chen, B., Song, Y. and Kwan, M., "How do people in different places experience different levels of air pollution? Using worldwide Chinese as a lens", Environmental Pollution Elsevier Journal, 874-883 (2018).

[2]. Demirarslan, K. O., "Kocaeli ili korfez ilcesi konut kaynakli CO ve NOx emisyon dagilimlarinin farkli modeller yardimiyla degerlendirilmesi", Dogal afetler ve cevre dergisi, Cilt:1 Sayi:1-2 Sayfa:66-73 (2015).

[3]. Erdogan, E., "Sanayi kaynakli hava kirliliginde modellerin kullaniminin karar verme surecindeki rolu", Yuksek Lisans Tezi, Istanbul Teknik Universitesi Fen Bilimleri Enstitusu, Istanbul, 3-25 (2012).

[4]. Kudal, S., "Hava kirliliginin cevresel ve mekansal modellenmesi, analizi ve tematik haritalarla gorsellestirilmesi", Yuksek Lisans Tezi, Yildiz Teknik Universitesi Fen Bilimleri Enstitusu, Istanbul, 3-18 (2009).

[5]. Coskun, A., "Sehir atmosferinde tasit emisyonlarindan kaynaklanan hava kirliliginin belirlenmesi", Yuksek Lisans Tezi, *Marmara Universitesi Fen Bilimleri Enstitusu*, Istanbul, 23-59 (2008).

[6]. Cuci, Y., Polat Ergun, E., "Gaziantep'in trafik kaynakli hava kirliliginin belirlenmesi", *KSU Muhendislik Bilimleri Dergisi*, 18(2), (2015).

[7]. TUIK. Turkiye Istatistik Kurumu, "Ulusal Seragazi Emisyon Envanteri Raporu 1990-2017",http://www.tuik.gov.tr (2018).

[8]. Elbir, T., Bayram, A., Kara, M., Altiok, H., Seyfioglu, R. ve Ergun, P., Simsir S.,"Izmir kent merkezinde karayolu trafiginden kaynaklanan hava kirliliginin incelenmesi", *DEU Muhendislik Bilimleri Dergisi*, Izmir, Cilt 12 Sayi 1 1-17 (2010).

[9]. Taosheng J., "Application of GIS to modified models of vehicle emission dispersion", *Atmospheric Environment Elsevier Journal*, 6326-6333 (2005).

[10]. Kilic, A., "Gemilerden kaynaklanan egzoz yayilimlari ve dagilim modellemesi", Yuksek Lisans Tezi, *Istanbul Teknik Universitesi Fen Bilimleri Enstitusu*, Istanbul, 1-3 (2006).

[11]. Snyder, G. M., Venkatram, A., and Heist, K. D., Petersen, B. W., "Rline: a line source dispersion model for near-surface releases", *Atmospheric Environment Elsevier Journal*, 748-756, (2013).

[12]. Venkatram, A., Isakov, V., and Thoma, E., Baldauf, R., "Analysis of air quality data near roadways using a dispersion model", *Atmospheric Environment Elsevier Journal*, 9481-9497, (2007).

[13]. Sorusbay, C., Ergeneman, M ve Pekin, M.A., "Karayolu ulasimindan kaynaklanan sera gazi emisyonlari: Turkiyedeki durumun degerlendirilmesi", Istanbul Teknik Universitesi (2009)

[14]. Rajaeifara M.A, Ghanavatib H., Dashtid B.B., Heijungse R., Aghbashlof M., Tabatabaeib M. Electricity generation and GHG emission reduction potentials through different municipal solid waste management technologies: A comparative review. Renewable and Sustainable Energy Reviews Vol 79. 414–439. (2017).

[15]. Rios M., Kaltschmitt M., 2016. Electricity generation potential from biogas produced from organic waste in Mexico. Renewable and Sustainable Energy Reviews Vol 54. p. 384-395.(2016)

[16]. JRC, Reference documents under the IPPC Directive and the IED. Surface Treatment Using Organic Solvents. Web addresses: http://eippcb.jrc.ec.europa.eu/reference/ date:10.05.2019 (2019)

[17]. Sofuoglu, A., "Hava kirliligi", Izmir Yuksek Teknoloji Enstitusu, [Online]. Available https://www.tubitak.gov.tr/tubitak_content_files/vizyon2023/csk/EK-6.pdf, (2018).

[18]. Hanna, R, S., Briggs, A, G., and Hosker, P, R., "Handbook on Atmospheric Diffusion", *Technical Information Center U.S Department of Energy*, 25-35, (1982).

[19]. Holnicki, P., Kaluszko, A., and Trapp, W., "An urban scale application and validation of the Calpuff model" *Atmospheric Pollution Research Elsevier Journal*, 393-402, (2016).

[20]. IPCC Greenhouse Gas Inventory Reference Manual – IPCC Guidelines for National Greenhouse Gas Inventories - Intergovernmental Panel on Climate Change, (2006).

[21]. EEA greenhouse gas - data viewer. [Online]. Available: http://www.eea.europa.eu/data-and-maps/data/data-viewers/greenhouse-gases-viewer date: 12.01.2019. (2019)

[22]. Draper N.R., Smith H. Apllied Regression Analysis. 1-70. (1966)

[23]. TurkStat, - TUIK - Transportation Statistics Databases (2004-2016). [Online]. Available: http://tuikapp.tuik.gov.tr date:09.12.2018.(2018)

The Air Pollutant (PM, SO₂, NO, NO₂, NOₓ, O₃ and CO) concentrations dispersion measures by statistical evaluations

Ali Can[1]

Abstract

The air pollutant measurements are important and they are usually evaluated by indexing. However, the statistical evaluation on data spread from the center gives many tendency and more meaningful on the dispersion. Measures of dispersion or variability in data sets include the sample range, variance, standard deviation, coefficient of variation and interquartile range. In this study, the Karabuk province air pollutant station data for the year 2017 and 2018 are studied and it is evaluated by using statistical approaches. The main aim is to determine the air pollutant conditions within the province. Because of high emissions within this industrialized city, the pollutant concentrations spreaded among in a sample range in other words differences between smallest and largest values of the sample. This study is considered seasonal and annual basis. The main finding of the study is the emission is spreading entire year. However, during the winter season, it was increasing with the household consumption of fuels. But the seasonal emissions variations are also gives us a signal of the main affection of industries on the Karabuk air.

The annual evaluation of pollutant has shown that pollutants are dispersed in a small clustered and its tightly closed around the mean. However, this comment is not valid for SO₂ and there is some extreme values. The SO₂ values have to be evaluated for Karabuk province due to high rate emissions especially for winter seasons. The main reason is supposed to be the high rate consumption of coal by emission sources.

Keywords: Air Pollutant, Statistical Dispersion, Variability in Data, Sample Range

1. INTRODUCTION

The irreversible effect of air pollution on the environment is creating a pressure on the industries to find an immediate solution for their emissions or to decrease it on a level which is not harmful for human beings, animal and plant life [1]. The air has been polluted while the emission emitted from the plumes and disappeared with the wind. If the meteorological conditions are not suitable for the emission dispersion, then the limitation of wasted emissions onto atmosphere will decrease its inverse effects [2]. The inverse effect of pollution is controlled to the some level with the technological improvement [3]. The pollution control is required until quality criteria, which seems very high for the pollutant creators but it is strict that this level is not enough for future generations. Beyond the standards, the pollution prevention is necessary due to many adverse effects of their aggregation properties on the air [4].

The air pollutant in the atmosphere is increasing and the local studies have shown that the effect of long-range air transport is varying due to the different aspect in the regions. The meteorology, geographical aspect, persistence in the air, climate and seasons have big effect in the air pollution [5, 6, 7].

The entire inverse affect of these pollutant are evaluated by using measures of central tendency which are more meaningful if accompanied by information on how the data spread out from the center [8]. Therefore, the pollutant can be commented with its evaluations whether the pollutant can be decreased or increased with the extreme values by numbers of non-detected results [9].

---

[1]*Corresponding author: Karabuk University, Department of Mechanical Engineering, 78050, Karabuk, Turkey.*
 alican@karabuk.edu.tr

The statistical, mathematical or graphical approach can be used for air pollutant data analyses [10], [11]. The biggest problem in time series analyses is the missing data. In this study, the gathered data from MEU [12] is analyzed and any missing pollutants in a day is also cause the other pollutants not to be considered in the analyses.

In this study, the Karabuk province air pollutant station data for the year 2017 and 2018 are studied and it is evaluated by using statistical approaches. The main aim is to determine the air pollutant conditions within the province. Because of high emissions within this industrialized city, the pollutant concentrations speeded among in a sample range in other words differences between smallest and largest values of the sample. This study is considered seasonal (3 month data) and annual basis.

2. METHODOLOGY

Measures of central tendency are more meaningful if accompanied by information on how the air pollutant data spread out from the center. Measures of data dispersion or variability as a set include the calculation of sample range, variance, standard deviation, coefficient of variation, and the interquartile range [8; 13]. These calculations are simple statistical calculations for the data evaluations. However, the combining evaluations are giving us the dispersion [8; 14].

In this study, the followings is going to be calculated for the air pollutants: These are,

- Range: This is the difference between the largest and smallest result from the data set.

- Variance. This is a measurement of the dispersion or deviation of results from the mean of a data set.

- Standard Deviation. This is the square root of the sample variance, it has the same unit of measure as the original data.

- Coefficient of Variation (CV). This is sometimes called the relative standard deviation (RSD), a unitless measure equal to the standard deviation divided by the mean.

- Interquartile Range. This is the difference between the 75th and 25th percentiles, it measures the central 50% of the results in the data set.

- Sample Range. The simplest measure of dispersion to compute is the sample range. The sample range (R) is the difference between the largest value and the smallest value of the sample:

$$R = X_{(l)} - X_{(s)} \qquad (1)$$

Where $X_{(l)}$ is the largest order value and $X_{(s)}$ is the smallest order value. The range is considering extreme values.

- Sample Variance. The sample variance measures the dispersion or deviation of results from the mean of a data set.

$$s^2 = \frac{\sum_{i=1}^{n} X_i^2 - n\bar{X}^2}{n-1} \qquad (2)$$

A large sample variance implies that there is a large spread among the data, that the data are not clustered tightly around the mean. A small sample variance implies that there is little spread among the data, and that most of the data are near the mean. Like the mean, the sample variance is affected by extreme values and by a large number of non-detected results.

- Sample Standard Deviation. The sample standard deviation has the same unit of measure as the original data. The sample standard deviation (s) is the square root of the sample variance:

$$s = \sqrt{s^2} \qquad (3)$$

- Sample Coefficient of Variation. The CV or RSD is a unitless measure that allows the comparison of dispersion across several sets of data because it is scaled to the mean. The sample CV is the sample standard deviation divided by the sample mean:

$$CV = \frac{s}{\bar{X}} \qquad (4)$$

And the CV is often expressed as percentage

$$\%RSD = \frac{s}{\bar{X}} 100\% \qquad (5)$$

- Sample Interquartile Range (IQR). When extreme values are present, the interquartile range may be more representative of dispersion in the data than the standard deviation. This range is not heavily influenced by extreme values because it measures the spread within the center portion of a data set, rather than include the most extreme values as does the range. As a result, it is useful when the data include a large number of non-detects. The 25th and 75th percentiles of the data difference (x0.25 and x0.75 respectively) give the IQR value. Then,

$$IQR = X_{0.75} - X_{0.25} \qquad (6)$$

3. RESULT AND DISCUSSION

The data is evaluated according to the methodology described in the paper. The examples are given for the seasonal evaluation of particulate matter, sulphur dioxide and carbon monoxide in the following Table 1. According to the table, the seasonal variation is showing that the spread of data around the average values are sometimes dangerous and over the standard pollution values. But the most important evaluation is the distribution. If the distribution is seems in big range and the data is spread in a big interquartile range (IQR), then the pollutant will be followed due to its dangerous effect on environment according to the standard values.

Table 17. PM10, SO$_2$ and CO Dispersion with Statistical Evaluation

YEAR	SEASON	parameter	RANGE	IQR	VARIANCE	STD DEV.	COEFF. VAR.(RSD)
2017	1	PM10	121.98	44.80	876.01	29.60	0.43
2017	2	PM10	85.82	34.23	506.88	22.51	0.49
2017	3	PM10	113.51	18.83	360.42	18.98	0.49
2017	4	PM10	65.13	24.03	258.91	16.09	0.40
2018	1	PM10	91.59	13.77	260.84	16.15	0.44
2018	2	PM10	75.04	15.79	212.61	14.58	0.39
2018	3	PM10	75.04	7.33	212.61	14.58	0.39
2018	4	PM10	58.80	13.38	129.62	11.38	0.34
2017	1	SO2	74.58	16.17	215.55	14.68	0.66
2017	2	SO2	39.25	8.16	68.47	8.27	0.89
2017	3	SO2	22.61	4.66	13.62	3.69	0.73
2017	4	SO2	289.18	39.86	2625.97	51.24	1.17
2018	1	SO2	184.59	20.47	630.43	25.11	0.90
2018	2	SO2	55.78	18.47	179.49	13.40	0.70
2018	3	SO2	55.78	6.37	179.49	13.40	0.70
2018	4	SO2	344.16	28.07	1769.93	42.07	1.18
2017	1	CO	2849.13	892.61	314803.62	561.07	0.48
2017	2	CO	3558.09	474.00	280749.96	529.86	0.57
2017	3	CO	1345.68	418.79	76483.21	276.56	0.33
2017	4	CO	3446.23	995.40	583463.45	763.85	0.60
2018	1	CO	2120.87	569.70	201677.56	449.09	0.50
2018	2	CO	1431.54	421.88	65822.62	256.56	0.38
2018	3	CO	1431.54	242.08	65822.62	256.56	0.38
2018	4	CO	3744.40	762.90	586397.13	765.77	0.65

The standard deviation (STD) and interquartile range (IQR) are also describing the deviation of measured pollutant values as seen in following Figures 1-8. In Figure 1, the PM10 dispersion is showing that the average values are after the 3rd season is almost the same. The dispersion is changing considerably from season to season. In the3rd, 5th, 6th, 7th and 8th season, the PM10 values are very close to each other.

On the other hand, in the 1st, 2nd and 4th season, the PM10 values are distributed in a big IQR. These seasons have to be detail observed for over measured PM10 values. Throughout the two years, the seasonal IQR and the average concentration is decreasing. For SO$_2$ values, the IQR dispersion is less than standard deviation except for 7th season. Therefore, it can be commented as the values is distributed in a wide range due to excluding of extreme values and the standard deviation figure is showing that there is some extreme minimum and maximum values on the series.
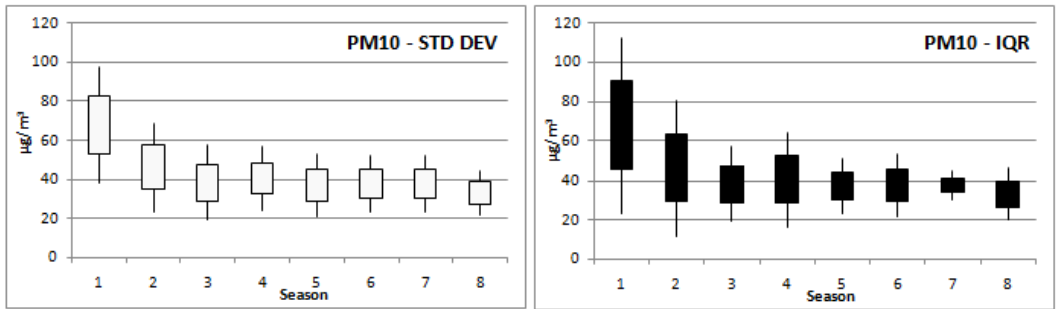
Figure 1. PM10 dispersion measures
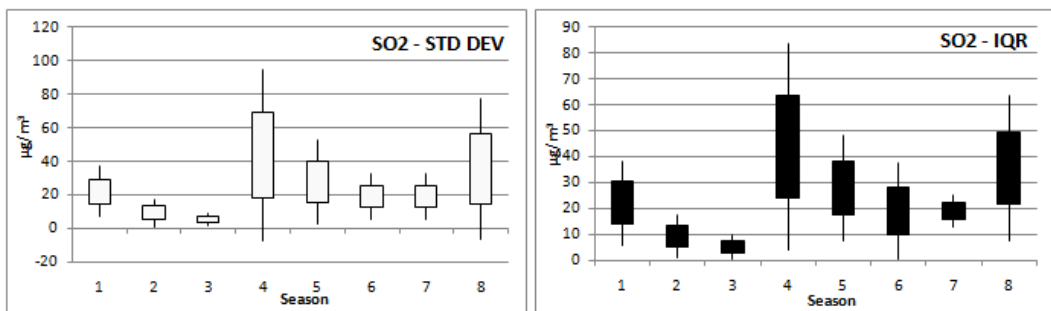
Figure 1. SO₂ dispersion measures

The entire CO values except for 7th season is dispersed in a wide IQR rather than STD. Therefore, the values are spread wider and it means there is an environmental problem on the measurement due to continous emission on Karabuk province. The CO means inefficient burning of fuels.
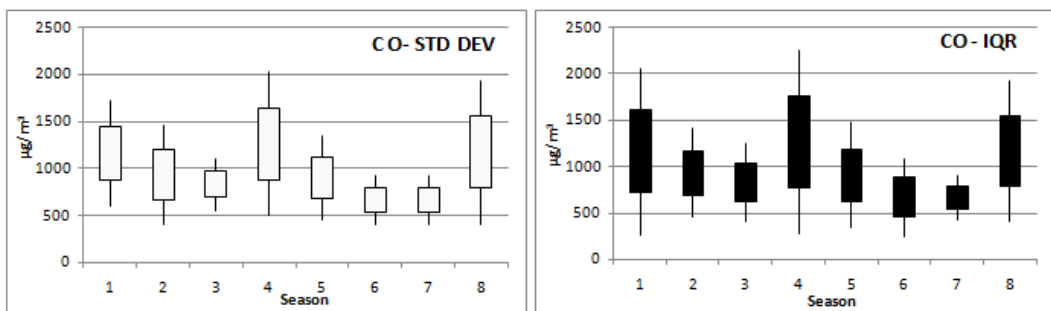
Figure 2. CO dispersion measures

The NO_x is the aggregation of NO and NO_2. The NO_x concentration is highly emitted from the burning of fuels with air. The air is containing 78% of nitrogen and its oxidation is causing high rate NO_x emissions. According to the IQR, during the winter season, there is a high rate NO_x concentration and in the summer the concentration is decreasing (Figure 4). Because in winter, the dispersion is very high and extreme values for the IQR results is not noticeable compared with the STD figures.
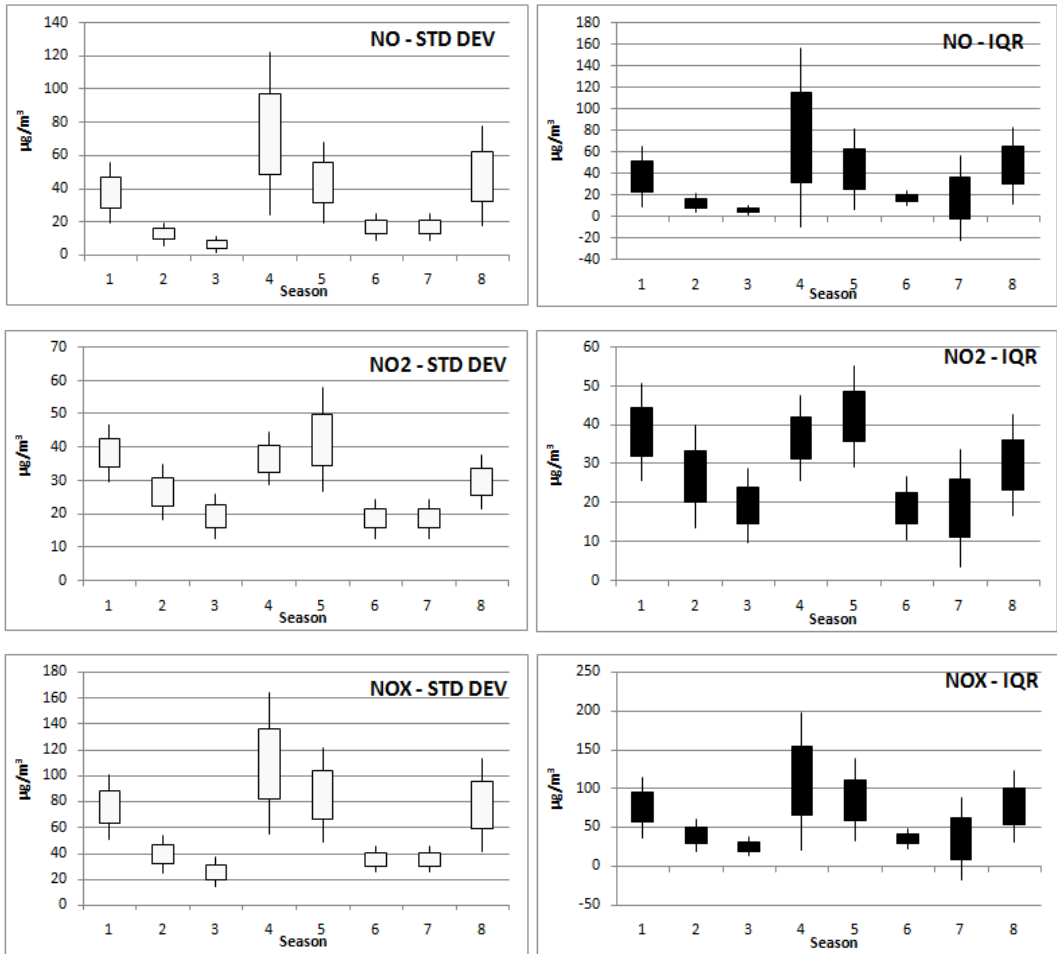
Figure 3. NO, NO₂ and NOₓ dispersion measures

The ozone (O3) concentration IQR is showing very stable figures (Figure 6). The concentration is not changing noticeable due to low concentrations. However, the values are doubled after season 5th.
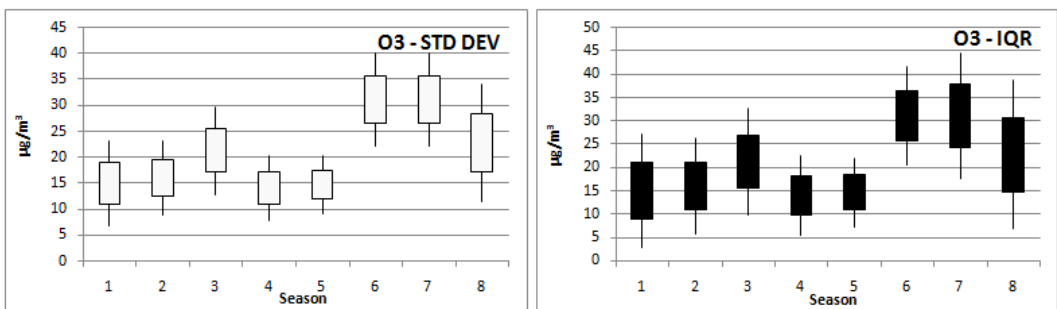
Figure 4. O₃ dispersion measures

The annual Figures are also showing some fluctuations and extreme values. The Figures 7 has shown that rather than SO₂, the pollutant are dispersed in a small clustered and its tightly closed around the mean. However, it is not the case for SO₂ and there is some extreme values and it is also concluded in the seasonal evaluation. Therefore, the sample variance is affected by extreme values and by large number of non-detected results which have to be evaluated according to the standard pollution values.

When extreme values are present, the IQR may be more representative of dispersion in the data than the standard deviation. This range is not heavily influenced by extreme values because it measures the spread within the center portion of a data set, rather than include the most extreme values.
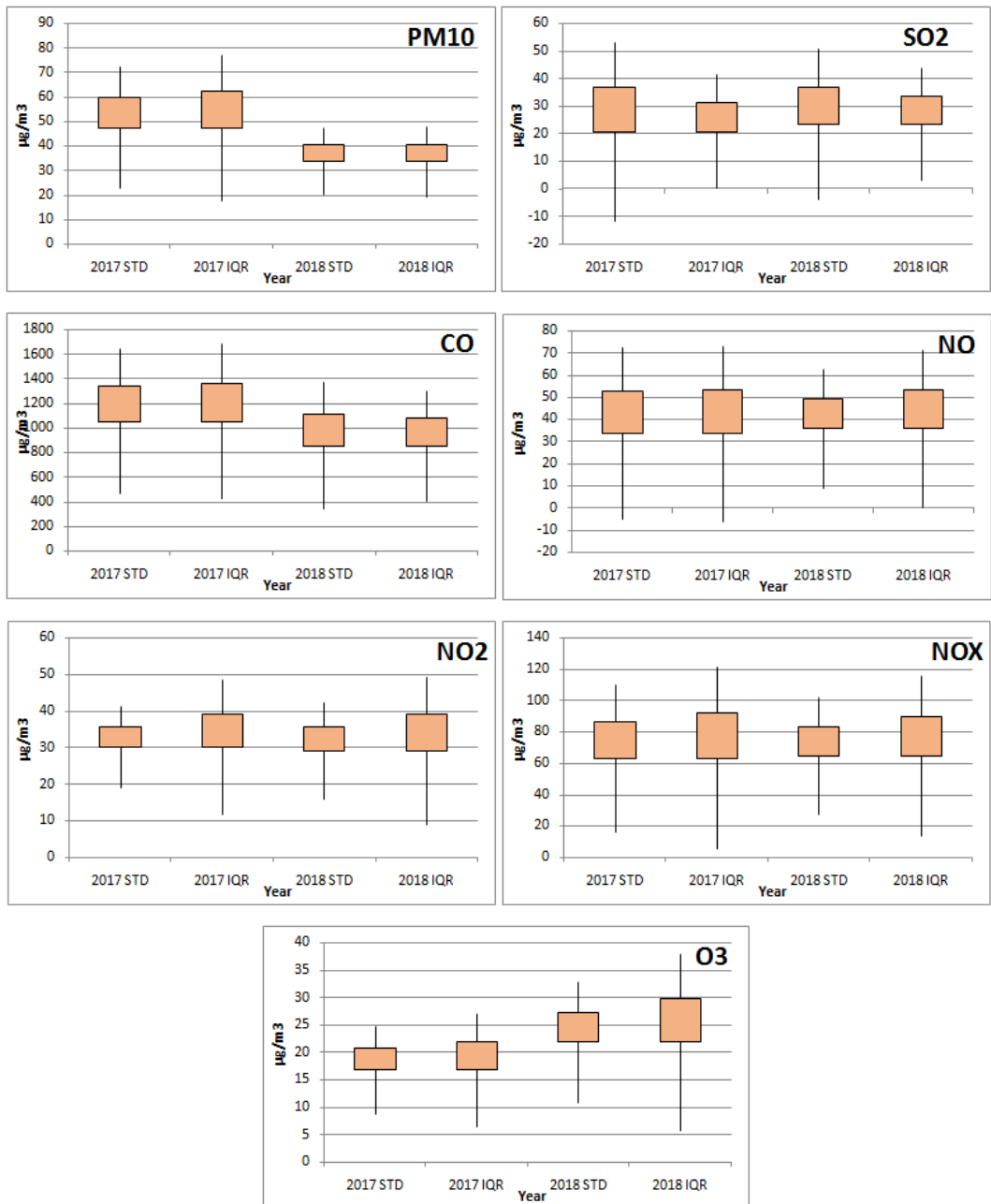
Figure 5. The Pollutant dispersion measures

CONCLUSION

If extreme values are present, the IQR may be more representative of dispersion in the data than the standard deviation. The annual evaluation of pollutant has shown that pollutants are dispersed in a small clustered and its tightly closed around the mean. However, this comment is not valid for SO_2 and there is some extreme values. This result is also concluded in the seasonal evaluation. Therefore, the sample variance is affected by extreme

values and by large number of non-detected results which have to be evaluated according to the standard pollution values. The SO_2 values have to be evaluated for Karabuk province for high rate emissions especially for winter seasons. The main reason is supposed to be industrial and household emissions with the high rate consumption of coal.

REFERENCES

[1]. Boubel R.A., Fox D.L., Turner D.B., Stern A.C., Fundamentals of Air Pollution – Academic Press, Third Addition, P.3-33, 1994.

[2]. Vesilind P.A., Environmental Pollution and Control – Department of Civil Engineering Duke University – North Caroline - Ninth printing, 1980. P.111-182.

[3]. Wang L.K., Pereira N.C., Hung Y., Advanced Air and Noise Pollution Control – Volume 2 – Handbook of Environmental Engineering. 2004. P.1-12.

[4]. Vallero D., Fundamentals of Air Pollution – Fourth Edition – Civil and Environmental Engineering Department - Duke University – North Caroline. 2007. P.659-677.

[5]. Meraz M., Rodriguez E., Femat R., Echeverria J.C., Alvarez-Ramirez J., 2015. Statistical persistence of air pollutants (O_3, SO_2, NO_2 and PM10) in Mexico City. Physica A 427. (2015).p.202-217.

[6]. Poberznik M., Strumbelj E., 2016.The effects of air mass transport, seasonality, and meteorology on pollutant levels at the Iskrba regional background station (1996-2014). Atmospheric Environment 134 (2016)p.138-146.

[7]. Qu Y., An J., He Y., Zheng J. 2016. An overview of emissions of SO2 and NOx and the long-range transport of oxidized sulfur and nitrogen pollutants in East Asia. Journal of Environmental Science p.13–25.

[8]. Kottegoda, N.T., Rosso, R., 2008. Applied statistics for civil and environmental engineers, Blackwell. Second Edition.p.3-38.

[9]. USEPA, 2007. Guidance on the Use of Models and Other Analyses for Demonstrating Attainment of Air Quality Goals for Ozone, PM2.5.

[10]. Guyet T., Nicolas H., 2016. Long term analysis of time series of satellite images. Pattern Recognition Letters 70 (2016).p.17–23.

[11]. Perepu S. K., Tangirala A. K., 2016. Reconstruction of missing data using compressed sensing techniques with adaptive dictionary-Journal of Process Control 47 (2016)p.175–190.

[12]. MEU., 2019. Ministry of Environment and Urbanization. Air Quality Monitoring Network. web address: http://www.havaizleme.gov.tr/ Default.ltr.aspx date: 15.04.2019.

[13]. Fox, J., 2016. Applied regression analysis and generalized linear models (3rd ed.). p.82-368.

[14]. Corps, U.S.A., 2008. Environmental statistics – Environmental Quality. EM 1110-1-4014. p. D.10-D.14.

Detection of Phishing Emails with Text Classification

Zeynep Orman[1], Rasim Savci[1], Sibel Senan[1]

Abstract

Phishing attacks are widespread nowadays, and are used to obtain personal information by e-mails that are often sent from known websites, internet service providers or banks that cause many financial and moral damages for individuals and institutions. The prevention of these attacks is vital for information security. In this study, the content of phishing e-mails is examined by using Natural Language Processing (NLP) methods and phishing e-mails are determined with machine learning techniques. The data set used in this study is obtained by combining PhishingCorpus for phishing e-mails and CSDMC2010 HAM sets for clean e-mails and 2500 samples are taken from both datasets. 20% of the dataset is reserved for testing. Word representations are taken from the content of the e-mails in the training dataset, and machine learning models are trained by forming feature vectors from the text content of the e-mails. The best result is obtained with the Multilayer Perceptron model, with a correct classification of 97.3% on the test data set.

Keywords: natural language processing, machine learning, phishing

1. INTRODUCTION

Nowadays, with the spread of computers and the Internet, shopping, education, state affairs and many more work have been started to be realized online and in electronic environment. For this reason, almost every individual requires to use these technologies. These developments in technology bring many benefits as well as some security threats. Computers and Internet, which have become the tools used by everyone, have made IT security to be more important than ever. Ideally, it may be appropriate for users to maintain their own security while dominating the use of computers, but in practice it is often not possible for people in different occupational groups to be advanced users. In addition, by making instant mistakes, even advanced computer users can be affected by the attacks which are using human weaknesses such as phishing. Therefore, security applications are inevitable.

Phishing are the attacks that are based on fooling and capturing sensitive information from a targeted person or institution by impersonating another person or institution by a variety of methods. The attacker attempts to send the phishing tools that he has developed or acquired (for example, fake web site scripts) to the user by uploading them to the Internet. For this purpose, attackers can send personal or collective scam e-mails or use methods such as using search engines, entering content into existing legal websites and placing fake links to these sites, and man-in-the-middle phishing [1]. Attackers can easily get the information entered into phishing e-mails or web site links. These attacks are widespread in recent years and are not only violating the privacy of individuals, but also causing financial damages to individuals and institutions, and moreover, leading to loss of reputation. According to the Internet Crime Report [2] of the FBI's IC3 unit for 2017, the number of victims of phishing and similiar attacks is 25,344 and the total cost is about $29.7 million. Figure 1 indicates the basic stages of a typical phishing attack.

[1] Corresponding author: Istanbul University-Cerrahpasa, Department of Computer Engineering, 34320, Avcilar/Istanbul, Turkey. ormanz@istanbul.edu.tr

```
┌─────────────────────┐        ┌─────────────────────┐
│  Attacker uploads   │ ────▶  │ The attacker asks the│
│  Phishing tools to  │        │  users to enter their│
│     Internet        │        │ information with a fake│
│                     │        │ site by accessing the│
└─────────────────────┘        └─────────────────────┘
         ▲                               │
         │                               ▼
┌─────────────────────┐        ┌─────────────────────┐
│ The victim's information is │ │ The targeted victim enters│
│  obtained by the attacker. The│◀─│ his information via e-mail│
│ attacker uses this information for│ │   or a fake link    │
│ malicious purposes such as │   │                     │
│   phishing or theft.│         │                     │
└─────────────────────┘        └─────────────────────┘
```
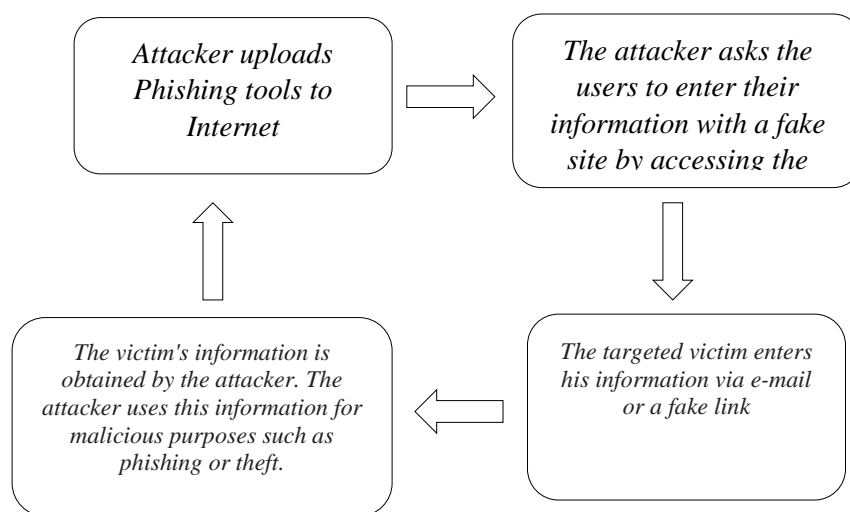
Figure 1. Stages of phishing attacks

The phishing detection can be integrated into conventional security solutions such as anti-viruses, firewalls, spam detectors, and intrusion detection systems, as well as it can also be developed as a separate application. Although it is possible to implement it both on a host and network basis, host-based implementation would be more appropriate when considering the problems that occur because of the man-in-the-middle style solutions in security protocols such as SSL, TLS.

Some of the studies on phishing detection examine e-mails, while others are concerned with the structure of the URLs and the content of the web pages. The most common vector of these attacks is the e-mails. By examining the e-mails, one can work with more features than other approaches. However, in the URL approach, phishing attacks that occur with other vectors can also be detected. In this study, we consider the e-mail examination approach to detect phishing attacks. Therefore, only the previously published studies in the literature that are using this approach are reviewed. Bergholz et al. [3] used adaptive-trained dynamic Markov Chain and class-thread models to determine the characteristics to be selected when classifying phishing e-mails by machine learning. It was stated in the paper that besides the basic features, the classification made with the use of the advanced features extracted in this way leads to less faulty classification than previous studies. They used Support Vector Machine (SVM) as the main classification algorithm. The obtained f-score was 99.46% according to the selected features with their dataset. Weider et al. [4] used a heuristic approach to detect phishing e-mails. They examined the subjects and content of incoming e-mails separately. They measured whether the specific areas on the subject line match with each other and the similarities between them. For the content, they applied text filters determined by their experience and tried to detect some abnormalities in the URLs. They assigned predetermined weight values to all features and scored each of them. The system which they named as PhishCatch can detect 80% phishing emails. Khonji et al. [5] proposed a method which was called as lexical URL analysis. In this URL token examination method, they combined subject-based and body-based features and Javascript-based features to the existing textual features. Random Forest machine learning method was performed on the PhishingCorpus ve SpamAssassin datasets. As a result, they obtained accuracy between 98.98% and 99.47% and sensitivity between 98.81% and 99.37%. The reason for these good results is the lexical URL analysis method. Kumar et al. [6] addressed the phishing problem with data mining approaches and they developed the DC scanner method for scanning and examining the data. They used a rule-based system that examines the HTML codes of the URLs within the e-mail, website domain names, domain name registration details and script codes associated with the URLs. They also suggested that websites should be designed based on a set of basic rules to improve the results. Patil et al. [7] attempted to detect phishing emails by using SVM and Hidden URL Detection Algorithm. They benefited from the BigData technology and the Hadoop platform. They found the frauds by examining the URLs in the mail content and determine the structures such as forms by examining the HTML elements with the proposed algorithm. In order to evaluate the result of this study, the system performance was examined and the method they used was found to be applicable. Peng et al. [8] identified phishing attacks by examining the text content of e-mails in semantic terms using NLP and machine learning methods. Sentences that asks for sensitive information are assumed to be dangerous. A blacklist containing the harmful word pairs (verb-direct object) was automatically generated from the training set with supervised learning techniques. The method used in this study

also examined the urgency tone and general welcome statements in messages, as well as performing a malicious link analysis. 95% accuracy and 91% sensitivity were obtained as the result of the study.

In this paper, we implement text classification for the detection of phishing e-mails. Some of the well-known machine learning algorithms that are Bayesian Networks, SVM, J48 Decision Tree, Random Forest, K-Nearest Neighbor (K-nn) and Multilayer Perceptron are used to train and test the feature vectors and their performance are compared in terms of accuracy, sensitivity and f-score. The remainder of this paper is organized as follows. Section II examines the details of the datasets used in this evaluation and also describes the methods used for phishing detection. Section III evaluates the obtained results and compares the performance of different machine learning models in terms of accuracy, sensitivity and f-score. Finally we summarize, conclude and outline plans for the future direction of this study in Section IV.

2. DATASET AND METHOD

There were basically two different approaches for keeping users away from phishing sites in the past. One of them is the URL filtering. This method creates a blacklist and the web sites are examined if they are in this list or not. However, because the number of phishing sites is constantly increasing, it is very difficult to prepare and update such a list. The other approach is to use heuristic methods. These methods try to predict phishing sites based on the developers' experience. Although they can detect new phishing sites, detection rates are not suitable for practical use. Therefore, a need for a new approach was born, and in recent years, machine learning methods have been used to detect these types of attacks [9].

Since the main vector of phishing methods are the e-mail messages [10], for the detection of phishing attacks, the contents of the e-mails were examined with NLP methods in this study. Word embedding was used for word representations as presented in [11] and word vectors were created from the contents of the e-mails in the training set. As the dataset, we used PhishingCorpus[12] for the phishing e-mails and the HAM e-mails of CSDMC2010[13] for the clean e-mails. A set of double-class and labeled data was created with 2500 entries from both data sets. E-mails were pre-processed by deleting the headers and subject section and leaving only the content. The dataset was then converted to the appropriate format for the model. 80% of the dataset was reserved for training and 20% for testing.

Skipgram model was preferred when creating the word vectors and the vector size was chosen to be 100. The e-mail content in the training and test datasets was converted into a feature vector by using the average values of the word vectors. Fasttext [14] implementation presented in [11] was used for the word representations. Finally, machine learning models were trained with the part of the feature vectors that were formed for the training, and were tested with those formed for testing.

2.1. Word Representations

In most of the word embedding methods, the words that make up the text are vectorized. Thus, words are represented by numerical values in the vector. One of the most common ways of using word embedding is the Word2Vec [15] method. In this method, the words to create the vector are determined and then all the words in the corpus are given numerical values according to the relationship with these determined words and the word vectors are created. In the resulting vector space, the vectors of related (context sharing) words are close to each other. In this way semantic meaning is caught. The Word2vec approach is further developed in [11] and the words are expressed as a series of n-grams. This means better processing for the less common words.

There are generally two methods for creating word vectors as stated in [14],[15] and [16] that are Continuous Bag of Words (CBOW) and Skipgram. In CBOW, depending on the width of the selected window, it is attempted to predict the word itself from the next words that define the context. The order of these words does not affect the prediction. In Skipgram, by using a word, it is attempted to estimate the word contexts around it. Those who are closer to the word have a higher weight. While CBOW runs faster, Skipgram gives better results for less common words. In this study, we used the Skipgram method with n-gram length as 3-6 and the vector size as 100.

3. EXPERIMENTAL RESULTS

Different machine learning models that are Bayesian Networks, SVM, J48, Random Forest, K-nn, Multilayer Perceptron were used to train the dataset. The tests were performed with Weka [17] program. Default parameters are used for models. For K-NN, k was automatically determined between 1 and 7. Accordingly, accuracy, sensitivity and f-score values were obtained as in Figure 2.
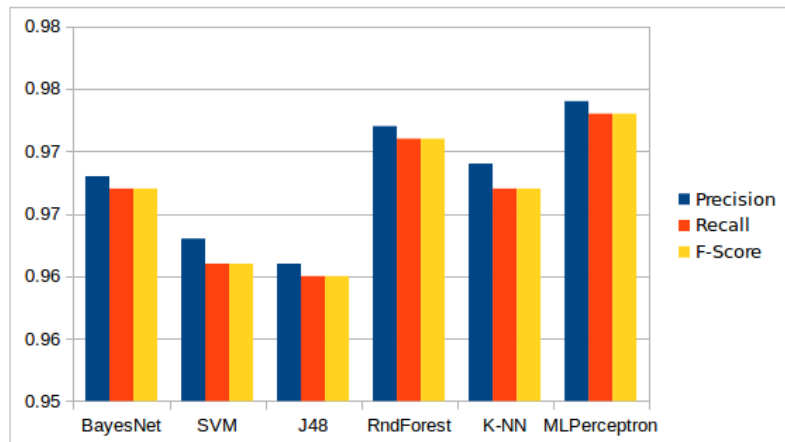
Figure 2. Test results

As seen in Figure 2, Multilayer Perceptron model has the best result. With this model, 973 of the 1000 test samples were classified correctly and 27 incorrect classifications were made. Accuracy and sensitivity were calculated as 0.974, and 0.973, respectively.

Tests were performed with Windows 7 operating system on a virtual machine running single core 1.5 GB RAM with i3 processor. The run time of the models are given in Table 1.

Table 1. Testing time

Model	Model Creation Time	Testing Time
Bayes Network	1.13 seconds	0.38 seconds
Support Vector Machine	5.31 seconds	1.13 seconds
J48 Decision Tree	1.75 seconds	0.06 seconds
Random Forest	3.33 seconds	0.2 seconds
K-Nearest Neighbor	0.01 seconds	1.42 seconds
Multilayer Perceptron	236.19 seconds	0.25 seconds

The timeframes given in Table 1 do not include the production of word vectors with the Skipgram model and feature extraction. It took 9 minutes and 20 seconds to create the Skipgram model and it took 46 seconds to create the feature vectors of the same set.

4. CONCLUSION AND FUTURE WORK

Phishing attacks are one of the major problems nowadays. These attacks can cause irreparable harm to people and, in particular, institutions if they do not take action against this problem. For institutions, even though it is an appropriate approach to train the staff to provide them with awareness of these attacks, it would still be necessary to use security programs as a more stringent prevention. In this study, an approach based on NLP and Machine Learning has been proposed for the detection of phishing attacks. The aim of the study is to show that the semantic

analysis of e-mail content can be effective for phishing detection. An acceptable detection rate and f-score were obtained in the study. The best result was obtained with the Multi Layer Perceptron model, but it takes a long time to train this model.

For more accurate results, the Skipgram model should be trained using a larger corpus and the size of the data set should be increased. There are some pre-trained models available for word representations. The relationships between words can be better captured by using word vectors in these models. The available data sets are actual e-mails, but they are not sufficiently comprehensive. It is appropriate to create or obtain more comprehensive data sets for future studies. In addition, only using semantic analysis may be insufficient to detect phishing attacks. Therefore, the method described in this study may give rise to more false positives in practice than the obtained test results. In order to solve this problem, it is aimed to get more realistic and better results by adding various URL features to semantic text classification features and by improving the data set as a future work.

ACKNOWLEDGMENT

REFERENCES

[1]. http://www.phishing.org/phishing-techniques, Available: 02.01.2019
[2]. FBI, IC3. (2017) Internet Crime Report, Url: https://pdf.ic3.gov/2017_IC3Report.pdf, Available: 02.01.2019
[3]. Bergholz, A., Chang, J. H., Paass, G., Reichartz, F., Strobel, S. , "Improved Phishing Detection using Model-Based Features", The Fifth Conference on Email and Anti-Spam (CEAS), California, USA, August 2008.
[4]. Weider, D. Y., Nargundkar, S., Tiruthani, N. , "PhishCatch-A Phishing Detection Tool", 33rd Annual IEEE International Computer Software and Applications Conference, Seattle, USA, July 2009.
[5]. Khonji, M., Iraqi, Y., Jones, A., "Lexical URL analysis for discriminating phishing and legitimate e-mail messages", International Conference for Internet Technology and Secured Transactions, United Arab Emirates , Dec 2011.
[6]. Kumar, B., Kumar, P., Mundra, A., Kabra, S., "DC scanner: Detecting phishing attack", Third International Conference on Image Information Processing (ICIIP), Waknaghat, India, Dec 2015.
[7]. Patil, P., Rane, R., Bhalekar, M., "Detecting spam and phishing mails using SVM and obfuscation URL detection algorithm", International Conference on Inventive Systems and Control (ICISC), Coimbatore, India, Jan 2017.
[8]. Peng, T., Harris, I., Sawa, Y., "Detecting Phishing Attacks Using Natural Language Processing and Machine Learning", IEEE 12th International Conference on Semantic Computing (ICSC), Laguna Hills, CA, USA, Jan 2018.
[9]. Miyamoto, D., Hazeyama, H., Kadobayashi, Y., "An Evaluation of Machine Learning-Based Methods for Detection of Phishing Sites", Advances in Neuro-Information Processing Lecture Notes in Computer Science, 539-546, 2008.
[10]. Kumaraguru, P., Rhee, Y., Acquisti, A., Cranor, L. F., Hong, J., Nunge, E., "Protecting people from phishing", Proceedings of the SIGCHI Conference on Human Factors in Computing Systems, 905-914, 2007.
[11]. Bojanowski, P., Grave, E., Joulin, A., Mikolov, T., "Enriching word vectors with subword information", Transactions of the Association for Computational Linguistics, 5, 135-146, 2017.
[12]. https://monkey.org/~jose/phishing/, Available: 02.01.2019
[13]. http://csmining.org/index.php/spam-email-datasets-.html, Available: 25.10.2017
[14]. https://fasttext.cc/, Available: 02.01.2019
[15]. Mikolov, T., Chen, K., Corrado, G., Dean, J., "Efficient estimation of word representations in vector space", arXiv preprint arXiv:1301.3781.s, 2013.
[16]. https://en.wikipedia.org/wiki/Word2vec, Available: 20.01.2019.
[17]. https://www.cs.waikato.ac.nz/ml/weka/, Available: 21.01.2019.

Particle Swarm Optimization Based Fuzzy Hyper Rectangular Composite Neural Networks: An Overview

Sibel Senan[1], Zeynep Orman[2], Nilay Salt Akkus[3]

Abstract

Particle Swarm Optimization Based Fuzzy Hyper Rectangular Composite Neural Network (PFHRCNN) combines three computational intelligence approaches including hyper-rectangular composite neural networks (HRCNN), fuzzy systems and Particle Swarm Optimization (PSO). This paper presents a detailed analysis of all PFHRCNNs related studies since the introduction of these studies in the literature up until today. In this context, feature extraction methods that are used in these studies are examined. Then, number of classes, features and samples used in these studies are determined. Finally, recognition success rates of PFHRCNN and other alternative methods are compared. Also, all studies in this area of interest are examined according to the computational results of PFHRCNN and HRCNN for computation time (complexity), recognition rate (success) and number of rule metrics. In the light of the proposed analysis, it can be concluded that the highest success rate is obtained by PFHRCNN approach compared to the other models. However, this approach might be considered as disadvantageous in terms of calculation time.

Keywords: Neural Networks, Fuzzy Hyper Rectangular Composite Neural Networks, Particle Swarm Optimization, Particle Swarm Optimization Based Fuzzy Hyper Rectangular Composite Neural Networks.

1. INTRODUCTION

Neural networks have taken intensive attention as one of the useful artificial intelligence approaches used in the various engineering applications. The power of neural networks rely on their ability of learning and therefore generalizing, forecasting, and classifying. Generating new models of neural networks to obtain more efficient results have always been the focus of interest for researchers in this field. Therefore, various classes of neural networks are introduced to the literature like Hyper-Rectangular Composite Neural Networks (HRCNNs) and Particle Swarm Optimization Based Fuzzy Hyper Rectangular Composite Neural Networks (PFHRCNNs). HRCNNs are where synaptic weights can be interpreted as clear If-Then rules [1]-[2]. However, a trained HRCNN may lead to some ineffective If-Then rules that gives a weak generalization capacity as a result. Fuzzy Hyper Rectangular Composite Neural Networks(FHRCNNs) have been introduced to handle this problem by transforming a clear If-Then rule into a fuzzy rule combined with a confidence factor [3]. Basically, the class of FHRCNNs is the fuzzified version of the class of HRCNNs. In FHRCNNs, the synaptic weights of a hidden layer define a hyperrectangle, which then corresponds to a fuzzy rule [4]-[6]. Due to their relaible results FHRCNNs have been used in various applicaitons recently [7]-[10]. Particle Swarm Optimization(PSO) based FHRCNNs are very new class of neural networks that have been introduced to literature to improve the effectiveness of the FHRCNNs by applying PSO method to the system[11]. In this system, optimization of the parameters is provided by PSO method. PFHRCNNs have been used in various fields like; removal of medical diagnosis rules for diseases such as breast cancer, Parkinson disease and liver disease [11], survival prediction of patients in the intensive care unit over the last 24 hours [12], postoperative recovery estimation [13], recognition of emotional content in music [14], and issuing rules for the detection of tax evasions [15].

[1] *Istanbul University-Cerrahpasa Department of Computer Engineering, 34320, Avcilar/Istanbul, Turkey.* ssenan@istanbul.edu.tr

[2] *Corresponding author: Istanbul University-Cerrahpasa, Department of Computer Engineering, 34320, Avcilar/Istanbul, Turkey.* ormanz@istanbul.edu.tr

[3]*Itelligence Turkey, Nidakule Atasehir Kuzey Is Merkezi, Barbaros Mah. Begonya Sok. No:3/A 34746 Atasehir/Istanbul, Turkey.* saltnilay@gmail.com

The purpose of this paper is to review all studies related to the PFHRCNNs since the introduction of PFHRCNNs into the literature up today. We will analyze all feature extraction methods that are used in these studies. Then, number of classes, features and samples used in these studies will be determined. Finally, recognition success rates of PFHRCNNs and other alternative methods will be compared. Also, all studies in this area of interest will be examined according to the computational results of PFHRCNNs and HRCNNs for computation time (complexity), recognition rate (success) and number of rule metrics. Hence, this survey paper will set light to researchers who consider to work in this field of area.

2. PARTICLE SWARM OPTIMIZATION BASED FUZZY HYPER RECTANGULAR COMPOSITE NEURAL NETWORK (PFHRCNN)

PFHRCNN combines three computational intelligence approaches that are HRCNNs, fuzzy systems and PSO method. PFHRCNNs overcome the disadvantages of HRCNNs. Mainly, PFHRCNN is a new model superior to FHRCNN by using PSO algorithm to optimize the parameters.

After training phase, HRCNNs give results as a set of clear If-Then rules. However, some of these generated crisp rules may be ineffective. Therefore, a crisp rule is transformed into a fuzzy rule incorporated with a confidence factor. Finally, PSO algorithm is used to trim the rules, search a set of good confidence factors, and fine-tune the locations of the selected hyper-rectangles to increase their effectiveness.

The PFHRCNN training algorithm consists of the following steps..

Step 1. *Generation of crisp rules*

For the classification of multi-class models, a HRCNN is created separately for each class. As a result of each trained HRCNN, a set of clear If-Then rules will occur. For k hidden nodes, the rules are presented by the form of H_k n-dimensional hyper-rectangles.

Step 2. *Optimization of fuzzy rules*

All crisp rules may not have a high recognition rate. To overcome this problem, confidence factor for each rule is used and incorporate some degree of fuzziness into class assignments.

Since the inclusion of fuzzy logic into the rules does not guarantee that the performance of the classification can certainly be improved, the location of the hyper-rectangle can be fine-tuned to increase its effectiveness. To achieve this purpose PSO algorithm is implemented.

The purpose of the PSO is to find the particle with the highest recognition rate. At the end, the best particle with the highest recognition performance is used to construct a PFHRCNN with the minimal number of fuzzy rules while the recognition performance is the highest one.

Step 3. *Classification*

After step 2, using a PSO, and a series of fuzzy rules PFHRCNN is constructed. Finally, an unknown data pattern is classified.

3. RESULTS AND DISCUSSION

We examined all studies about the PFHRCNNs in the literature. Since it is a new neural network model, we determined 5 papers in this topic. Table 1. shows the feature extraction method based analysis of these studies. Table 2. shows the numbers of classes, features and samples used in these studies. The comparison of recognition success rates of PFHRCNN and other alternative methods is given in Table 3. This paper also shows examination of all these studies according to the computational metricss of models PFHRCNN and HRCNN. These metrics are given as computation time (complexity), recognition rate (success) and number of rules used in these studies.

o *Feature Extraction Methods*

Feature extraction plays a very important role in the pattern recognition applications. It is better not to use more features than required based on the evaluation of calculation efficiency. The methods used in feature extraction in all studies related to PFHRCNNs are determined and given in Table 1. In some studies, no feature extraction method is used, instead feature extraction is made by taking advantage of expert knowledge. Some of the studies include various applications in them. We show the studies by their application contents.

Table 18. Feature Extraction Methods

Application	Feature extraction method
[11] Wisconsin Breast Cancer Diagnosis	-
[11] Liver Disorder Diagnosis	-
[11] Parkinson Diagnosis	-
[12] Survival Rate of the Intensive Care Unit Patients	Average Real Variability (ARV)
[13] Postoperative Recovery Rate	-
[14] Music Emotion Recognition	MIR Toolbox
[15] Detection of Tax Evasion	Fisher Ratios
	Principal components analysis, Pearson's correlation coefficients

o *Number of Classes/Features/Samples*

Different number of samples is used in the applications of all studies related to PFHRCNNs. Also, the features extracted from samples differ from each other. However, most of the class numbers are same. Table 2. shows the values of these numbers.

Table 2.Number of Classes/Features/Samples

Application	Number of classes	Number of features	Number of samples
[11] Wisconsin Breast Cancer Diagnosis	2	9	699
[11] Liver Disorder Diagnosis	2	6	345
[11] Parkinson Diagnosis	2	23	197
[12] Survival Rate of the Intensive Care Unit Patients	2	10	240
[13] Postoperative Recovery Rate	3	8	90
[14] Music Emotion Recognition	4	38	480
[15] Detection of Tax Evasion	2	13	35.582 (year 2011) 28.831 (year 2012)

o *Recognition Rates of Methods*

We determined all models which are compared with PHRCNN model in the studies. The comparison of recognition success rates of PFHRCNN and other alternative methods is given in Table 3. The results show that the highest success rate is obtained by the PHRCNN model in these applications. This table also can give researchers an idea of which methods PFHRCNN can be an alternative to.

Table 3.Recognition Rates

Application	PFHRCNN	HRCNN	MLP	RBF	SVM	SVM linear	SVM-RBF	SVM-Sigmoid	GP
[11] Wisconsin Breast Cancer Diagnosis	%97,5	%95	-	-	-	-	-	-	-
[11] Liver Disorder Diagnosis	%85,5	%82,5	-	-	-	-	-	-	-
[11] Parkinson Diagnosis	%87,5	%87,5	-	-	-	-	-	-	-
[12] Survival Rate of the Intensive Care Unit Patients	%91	%85	%82	%83	-	%49	%82	%68	-
[13] Postoperative Recovery Rate	%84	%82,5	-	-	-	-	-	-	-
[14] Music Emotion Recognition	%83,9	%77,5	%72,1	-	%75,8	-	-	-	%73,7
[15] Detection of Tax Evasion	%97,5	-	-	-	-	-	-	-	-

o   ***Computational Metrics of PFHRCNN and HRCNN***

The examination of all the studies according to the computational metrics of models PFHRCNN and HRCNN is given in Table 4. These metrics are given as computation time (complexity), recognition rate (success) and number of rules used in these studies.

Table 4. Metrics of PFHRCNN and HRCNN

Applications	PFHRCNN			HRCNN		
	Time(second)	Average number of rules	Recognation rate	Time(second)	Average number of rules	Recognation rate
[11] Wisconsin Breast Cancer Diagnosis	28,78	10	%97,5	0,7	16	%95
[11] Liver Disorder Diagnosis	24,20	24	%85,5	0,85	45	%82,5
[11] Parkinson Diagnosis	13,77	8	%87,5	0,68	15	%87,5
[12] Survival Rate of the Intensive Care Unit Patients	-	10	%91	-	16	%85
[13] Postoperative Recovery Rate	-	9,4	%84	-	13,1	%82,5
[14] Music Emotion Recognition	35,6	10	%83,9	0,52	19	%77,5
[15] Detection of Tax Evasion	-	-	%97,5	-	-	-

4.   CONCLUSIONS

Particle Swarm Optimization Based Fuzzy Hyper Rectangular Composite Neural Network (PFHRCNN) combines three computational intelligence approaches including hyper-rectangular composite neural networks (HRCNN), fuzzy systems and Particle Swarm Optimization (PSO). This paper surveyed all PFHRCNNs related studies since the introduction of these studies in the literature up until today. In this context, we examined all feature extraction methods and determined the number of classes, features and samples used in these studies. Finally, we compared recognition success rates of PFHRCNN and other alternative methods. Also, we gave the examination of all the studies in this area of interest according to the computational metrics of models PFHRCNN and HRCNN. The analysis we made reveal the effectiveness of PFHRCNNs in terms of success rate. This survey paper may set light to researchers who consider working in this field of interest.

ACKNOWLEDGMENT

REFERENCES

[1].   M. C. Su, A neural network approach to knowledge acquisition, PhD. Dissertation, University of Maryland, Aug. 1993.

[2].   M. C. Su, Use of neural networks as medical diagnosis expert systems, Computers in Biology and Medicine, vol. 24, Issue 6, Nov. 1994, pp. 419-429.

[3].   M. C. Su and C. J. Kao, Time Series Prediction Based on a Novel Neuro-Fuzzy System, Fourth Golden West Conference on Intelligent Systems, San Francisco, USA, pp. 229-232, 1995.

[4].   M. C. Su, Identification of singleton fuzzy models via fuzzy hyperrectangular composite NN, Fuzzy Model Identification-Selected Approach, In: H. Hellendoorn and D. Driankov (eds.), Berlin, Germany: Springer-Verlag, pp.193-212, 1997.

[5].   W. Liu, C. S. Chang, M. C. Su, Neuro fuzzy networks for voltage security monitoring based on synchronized phasor measurement, IEEE Trans. Power Syst., vol. 13, no. 2, pp. 326-332, May. 1998.

[6].   W. Liu, M. C. Su, S. S. Tsay, and Y. J. Wang, Application of a novel fuzzy neural network to real-time transient stability swings prediction based on synchronized phasor measurements, IEEE Trans. Power Syst., vol. 14, pp. 685–692, May. 1999.

[7].   M. C. Su, H. Huang, C. Lin, C. Huang, C. Lin, Application of neural networks in spatio temporal hand gesture recognition, Proceedings of the IEEE World Congress on Computational Intelligence, 1998.

[8].   S. Chang, Knowledge Discovery from Dynamic Data on a Nonlinear System, Open Journal of Applied Sciences, vol. 5, pp. 576-585, Oct. 2015.

[9]. G. C. Liao, T. P. Tsao, Application of fuzzy neural networks and artificial Intelligence for load forecasting, Electric Power Systems Research, vol. 70, Issue 3, pp. 237-244, Aug. 2004

[10]. M. C. Su, A fuzzy rule-based approach to spatio-temporal hand gesture recognition, IEEE Trans. Syst., Man, Cybern. C, Appl. Rev., vol. 30, pp. 276–281, 2000.

[11]. Y. Z. Hsieh, M. C. Su, P. C. Wang, A PSO-based Rule Extractor for Medical Diagnosis, Biomedical Informatics, vol. 49, pp. 53-60, 2014.

[12]. Y. Z. Hsieh, M. C. Su, C. H. Wang, P. C. Wang, Prediction of survival of ICU patients using computational intelligence, Computers in biology and medicine, vol. 47, pp. 13-19, 2014.

[13]. Y. Z. Hsieh, C. H. Wang, M. C. Su, C. H. Lu, J. C. Yu, Y. M. Chiang, Prediction of postoperative recovery based on a computational rules extractor, 2015 International Conference on Consumer Electronics-Taiwan (ICCE-TW), 2015.

[14]. Y. H. Chin, Y. Z. Hsieh, M. C. Su et al., Music emotion recognition using PSO-based fuzzy hyper-rectangular composite neural networks, IET Signal Process., vol. 11, no. 7, pp. 884-891, 2017.

[15]. Y. Z. Hsieh, M. C. Su, A. Y. S. Su, W. R. Shih, J. C Yu, C. Y. Huang, The computational rules extractor in the detection of tax evasion, 2015 International Carnahan Conference on Security Technology (ICCST), 2015.

Heat Transfer on an Insulated Plane Wall and Its Effect on Climate Change

Ali Can[1], Kamil Arslan[2]

Abstract

The climate change studies are getting important due to future considerations of earth and in environmental section of life.The road maps due to the mitigation action for decreasing the adverse effect of direct greenhouse gases emitted into the atmosphere are being important for future planning of earth. The climate change effect of building covering is not considered until now and this study will be the one for calculating the CO_2 equivalent emission decreasing with different type of insulator on a plane wall due to their carbon footprint. The theoretical energy saving is calculated according to the energy balance of heat transfer conduction rules.

The heat transfer is only energy interaction involved for this study and there is no heat generation. The steady energy balance for the wall with no change in the temperature of wall due to time at any point will be considered. Therefore, the rate of heat transfer into the wall must be equal to the rate of the heat transfer out of it. The wall thickness L, the average thermal conductivity k for concrete, the two surfaces of the wall are maintained at constant temperatures of T1 and T2 and one dimensional steady heat conduction through the wall is maintained. It is simply described by Fourier's law of heat conduction and the effect of insulator on the wall is determined as energy saving and its positive effect on consuming less energy. This causes decreasing GHGs emitted to the atmosphere due to less energy consumption on the buildings.

The best insulators are aluminium foil separating fluffy, silica powder and combination of aluminium foil and glass paper. These insulators are approximately decreasing $5.2*10^{-2}$ kg daily CO_2 eq. emission in case of hard coal, lignite, asphalt and second fuel coal used as fuels and $2.6*10^{-2}$ kg daily CO_2 eq. emission in case of natural gas consumptions.

Keywords: Heat Transfer, Plane wall, Energy Efficiency and CO_2 Equivalent GHGs Emission

1. INTRODUCTION

Heat transfer is the energy interaction involved in a layer which can be described by simple temperature changes within. The energy balance when there is no heat generation is simply the difference within the heat transfer in and out of layer [1]. The changes in the wall described the energy as the heat transfer through the wall, which is constant and the conduction through the wall changes in linear. That is, the temperature distribution in the wall under steady condition is a straight line [2].

In most of the research, the heat transfer is characterized by low emissions [3, 4]. In Saha and etc. [3], the heat transfer is studied with CO and NO_x emissions, and emissions are related with heat flux of different fuels. In another study done by Mishra, the NO and CO_2 emissions are studied, and it related with convection ratio and Reynolds Number [4]. CO is mostly an incomplete oxidation of hydrocarbon fuels. However, in some of industrial processes, it is desirable. CO is dangerous emission and it prevents complete oxidations [5]. The studies related to the heat transfer and emissions can be extended. However, the energy efficiency and heat transfer related to the Climate Change problem is unexpectedly not considered.

The energy efficiency for the sustainable development is one of the goals to design as architectural principles. The adaptable supports are developed due to the user's needs and environment [6]. The energy related design and

---

[1]*Corresponding author: Karabuk University, Department of Mechanical Engineering, 78050, Karabuk, Turkey. alican@karabuk.edu.tr*

[2]*Karabuk University, Department of Mechanical Engineering, 78050, Karabuk, Turkey. kamilarslan@karabuk.edu.tr*

systems are vital infrastructure to adapt climate change. Since the future impact assessment is highly uncertain as the global climate is continuously changing [7].

Climate Change is a global scale problem. The latest solution for this problem was putted into force by the agreement of countries. The countries' reduction target has to be achieved by governmental authorities. The main mitigation obligation is to adopt national strategies for decreasing GHGs emissions due to 1990's level [8]. The most important international instruments do decrease the GHGs emissions are the UNFCCC and Kyoto Protocol. Both are settings rules and procedure for countries [9]. With the Paris Agreement, all Parties have to put forward their best efforts through "nationally determined contributions" (NDCs) for sustaining low carbon future [10].

Within this study, the decreasing conduction heat transfer in a wall and keep energy within the inside is studied theoretically by using many insulators on the wall. The energy efficiency and high benefit of insulators within the climate change actions will be resulted. Therefore, the insulators on the wall are causing less consumption of fuels, which result as low emissions.

2. METHODOLOGY

Heat transfer is the energy interaction and energy balance [2] for the wall can be expressed as Eq.1.

$$\begin{pmatrix} Rate\ of\ heat \\ Transfer\ into\ the\ wall \end{pmatrix} - \begin{pmatrix} Rate\ of\ heat \\ Transfer\ out\ of\ the\ wall \end{pmatrix} = \begin{pmatrix} Rate\ of\ Change\ of \\ the\ energy\ of\ the\ wall \end{pmatrix} \quad (1)$$

or

$$\dot{Q}_{in} - \dot{Q}_{out} = \frac{dE_{wall}}{dt} \text{ for steady operation } dE_{wall}/dt = 0$$

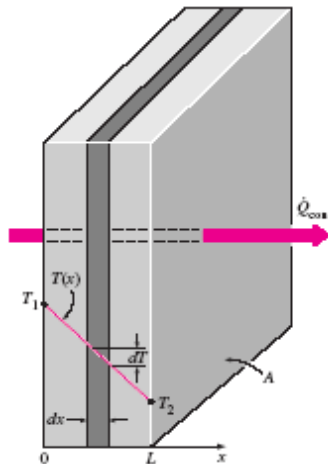*Figure19. Under steady condition, the temperature distribution in plane wall* [2]

The Fourier's law of heat conduction for the wall can be expressed as Eq.2.

$$\dot{Q}_{cond,wall} = -kA\frac{dT}{dx} \quad (2)$$

where

k: thermal conductivity (W/mK),
T_1 and T_2:wall temperatures (K),
L: Wall thickness (m),
A: Plane area (m^2)
Q: Heat Transfer (W)

The following insulation materialsare selected for the study (Table 1).

Table 1. Selected insulation materialsand theirthermal conductivity values

Insulation Material	k (W/m.K)	Insulation Material	k (W/m.K)
Glass Fiber	0.036	Mineral Fiber	0.042
Polystyrene	0.04	Cork	0.039
Polyurethane	0.023	Silica Powder	0.0017
		Aluminium Foil Aluminium Foil	
Perlite	0.052	seperating fluffy glass material	0.00016
Rubber	0.032000	Aluminium Foil and Glass Paper	0.000017

For heat conduction through a plane wall can be rearranged as Eq.3.

$$\dot{Q}_{cond,wall} = \frac{T_1 - T_2}{R_{wall}}; \qquad R_{wall} = \frac{L}{kA} \qquad (3)$$

Where,

R: Thermal resistance (K/W), The total thermal resistance can be considered as
$R_{total} = R_{wall} + R_{insulator}$

In calculating the CO_2, CH_4 and N_2O emissions,the (IPCC - Tier 1) methodology was used as given in the below Eq. 4 and Eq. 5. The general formula (Eq. 4) for the CO_2emission is given as [11, 12].

$$CO_2 Emiss. = \sum U_n * EF * CF * E * C\text{-}CO_2 \quad (4)$$

Where,

U_n: The fuel consumption quantity
CF: Conversion Factor
n: Fuel type
EF: Emission Factor (IPCC value)
E: Efficiency (95-99%)
$C\text{-}CO_2$: Carbon to CO_2 emission

And the general formula (Eq. 5) for the CH_4 and N_2O emissions is given by IPCC Guidelines [11], [12].

$$Non\text{-}CO_2 Emiss. = \sum U_n * EF * CF \quad (5)$$

For the GHGs emission calculations, the following steps are considered: The energy units are converted into Net Calorific Values (NCV) and the fuel data consumption of buildings are estimated according to the Can [13] studies.

3. RESULT AND DISCUSSION

The study as it was expected has shown that the best insulation material means the least thermal conductivity value. However, their climate change effect is not guessed due to carbon footprint.

Table 2. Calculated heat transfer properties of insulation materials

Insulation Material	Rin	Rtot	$\dot{Q}_{tot}$	$\dot{Q}_{con}$	$\dot{Q}_{diff}$ ($\dot{Q}_{con}$-$\dot{Q}_{tot}$)	Diff (%) ($\dot{Q}_{diff}/\dot{Q}_{con}$)*100
Glass Fiber	0.833	1.213	6.347	20.277	13.929	68.696
Polystyrene	0.750	1.130	6.816	20.277	13.461	66.387
Polyurethane	1.304	1.684	4.572	20.277	15.704	77.451
Perlite	0.577	0.957	8.049	20.277	12.228	60.305
Rubber	0.938	1.317	5.846	20.277	14.431	71.171
Mineral Fiber	0.714	1.094	7.038	20.277	13.238	65.289
Cork	0.769	1.149	6.702	20.277	13.575	66.949
Silica Powder	17.647	18.027	0.427	20.277	19.850	97.893
Aluminium Foil seperating fluffy glass material	187.500	187.880	0.041	20.277	20.236	99.798
Aluminium Foil and Glass Paper laminate	1764.706	1765.086	0.004	20.277	20.272	99.978

With this study, the cancelled direct greenhouse gases per meter square area, which concrete (thermal conductivity k= 0.79 W/mK) wall thickness (L) is just 30 cm and insulation material is 3 cm thickness, has been calculated. According to the study, the Table 2 was obtained for different type of insulation materials.

The T_2 (outside temperature) is taken as 13.3 °C. This value is the average value of provinces atmospheric temperatures of Turkey throughout the years between 1990 and 2016. The T_1 (inside temperature) is taken as 21 °C. The value is the average of indoor temperature of any types of house throughout the years.

It is seen that the best insulation material is the aluminum foil and glass paper laminate combination. With this material the heat transfer is decreased to the minimum level, which means the heat transfer is decreased to a level of 99.97%. Therefore, the less fuel will be consumed and high rate decreasing of CO_2 equivalent emission to the atmosphere.

By using many insulation materials, the decreasing of daily CO_2 equivalent emission to the atmosphere is given in the following Table 3. due to different type of fuels that could be used for heating purposes. If the used fuel is lignite, which means high rate GHGs emissions to the atmosphere, there will be approximately $5.6*10^{-2}$ kg daily CO_2 eq. emission will be decreased within 1 m^2 area wall of in a building in Turkey according to atmospheric conditions by using this best material as an insulator. The following Table 3. is given the CO_2 eq. GHGs decreasing by using different type of insulation materials.

Table 3. CO_2 eq. GHG decreasing by using different type of insulation material

Insulation Material	CO$_2$ eq. (ton)				
	Hard Coal	Lignite	Asphalt	Second Fuel Coal	Natural Gas
Glass Fiber	3.92E-05	4.13E-05	3.92E-05	3.92E-05	1.86E-05
Polystyrene	3.81E-05	4.02E-05	3.81E-05	3.81E-05	1.80E-05
Polyurethane	4.31E-05	4.56E-05	4.31E-05	4.31E-05	2.09E-05
Perlite	3.54E-05	3.73E-05	3.54E-05	3.54E-05	1.63E-05
Rubber	4.03E-05	4.25E-05	4.03E-05	4.03E-05	1.92E-05
Mineral Fiber	3.76E-05	3.97E-05	3.76E-05	3.76E-05	1.77E-05
Cork	3.84E-05	4.05E-05	3.84E-05	3.84E-05	1.81E-05
Silica Powder	5.24E-05	5.54E-05	5.24E-05	5.24E-05	2.64E-05
Aluminium Foil seperating fluffy	5.32E-05	5.64E-05	5.32E-05	5.32E-05	2.69E-05
Aluminium Foil and Glass Paper	5.33E-05	5.64E-05	5.33E-05	5.33E-05	2.70E-05

Figure 2 is also showing the different insulation materials and its effect on energy efficiency which is related to the final GHGs emission. The total GHGs emission as in unit CO_2 equivalent was given in this figure.
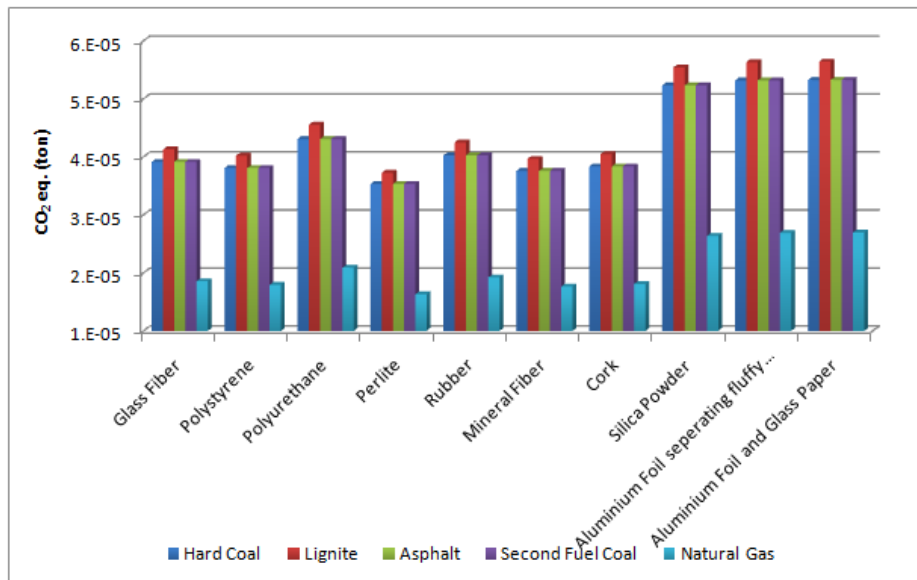
Figure 2. Different insulation materials and its effect on energy efficiency which is related to the final GHGs emission

The worst insulator in the selected insulation material is the perlite because the CO_2 eq. emission decrease is approximately $3.5*10^{-2}$ kg for hard coal, lignite, asphalt and second fuel coal. If the fuel is natural gas, then the total GHGs decrease will be just $1.6*10^{-2}$ kg daily CO_2 eq. emission. On the other side, the best insulatorsare aluminum foil separating fluffy, silica powder and combination of aluminum foil and glass paper. These

insulators are approximately decreasing $5.2*10^{-2}$ kg daily CO_2 eq. emission in case of hard coal, lignite, asphalt and second fuel coal used as fuels and $2.6*10^{-2}$ kg daily CO_2 eq. emission in case of natural gas consumptions.

CONCLUSION

The best insulators are aluminum foil separating fluffy, silica powder and combination of aluminum foil and glass paper. These insulators are approximately decreasing $5.2*10^{-2}$ kg daily CO_2 eq. emission in case of hard coal, lignite, asphalt and second fuel coal used as fuels and $2.6*10^{-2}$ kg daily CO_2 eq. emission in case of natural gas consumptions. In case of building covering, the best efficiency, means less energy consumption for heating purposes and less money spending,is obtained by aluminum foil and glass paper.

REFERENCES

[1]. Jackson E.G., Kilham J. K., 1956. Heat Transfer from Combustion by Forced Convection. Industrial Engineering Chemistry vol 48,11. p. 2077-2079

[2]. Cengel Y. A., Ghajar A. J., 2011. Heat and Mass Transfer, Fifth Edition in SI Units(book). Chapter 3.p.142-160.

[3]. Saha C., Ganguly R., Datta A., 2008. Heat Transfer and Emission Characteristics of Impinging Rich Methane and Ethylene Jet Flames. Experimental Heat Transfer. Volume 21. Issue 3.p.169-187.

[4]. Mishra D.P., 2003. Emission Studies of impinging premixed flames. Fuel. V.83.p.1743-1748.

[5]. Chien Y. C., Martin D. E., Rankin D. D., 2016. CO emission from an impinging non-premixed flame. Combustion and Flame. V.174. p.16-24.

[6]. Fakourian F., Asefi M., 2019. Environmentally Responsive Kinetic Facade For Educational Building. Journal of Green Building. Vol 14. P.165-186.

[7]. Emodi N.V., Chaiechi T., Beg. A., 2019. The Impact of Climate Variability and Change on the Energy System: A systematic scoping review. Science of the Total Environment. V. 676.p. 545-563.

[8]. IPCC, 2013. Climate Change 2013: The Physical Science Basis, Working Group I contribution to the Fifth Assessment Report of the Intergovernmental Panel on Climate Change, Cambridge University Press. www.ipcc.ch/report/ar5/. Date: 17.09.2016.

[9]. TurkStat, 2015. National Greenhouse Gas Inventory Report, 1990-2015. Annual Report submission under the "Framework Convention on Climate Change".

[10]. UNFCCC, 2016. United Nations Framework Convention on Climate Change web page: UNFCCC - https://unfccc.int/national_reports/annex_i_ghg_inventories/national_inventories_submissions/items/9492.phpdate:10. 09.2016.

[11]. IPCC 1996. Greenhouse Gas Inventory Reference Manual – Revised 1996 IPCC Guidelines for National Greenhouse Gas Inventories – Volume 3 – Intergovernmental Panel on Climate Change – Edited by Houghton J.T., et al. 1996.

[12]. IPCC 2006.Greenhouse Gas Inventory Reference Manual – IPCC Guidelines for National Greenhouse Gas Inventories - Intergovernmental Panel on Climate Change, 2006.

[13]. Can A., 2006. Investigation of Turkey's Carbon Dioxide Problem by Numerical Modeling. (Ph.D.Thesis) – METU.

Global Foreign Trade Performance of Turkish Textile and Clothing Sector

Seher Kanat[1], Turan Atilgan[2]

Abstract

Turkish textile and clothing sector has both socially and economically maintained its significance since the foundation of Turkish Republic and even since the last years of Ottoman Empire. The sector directly provides employment to one million people whereas it indirectly creates employment to two million people. Besides, the sector approximately gains 15 billion dollar net currency every year. The average unit export price per kilogram is found to be 1,4 dollar for Turkey whereas it ranges between 13 and 14 dollars with regard to textile and clothing sector. The sector is one of the leading sectors, which create added-value, due to this property.

However, the sectors have also undergone serious alterations and transformation in recent years just as the many fields in the globalizing world. Textile and clothing sector is one of these sectors which have been significantly affected from these alterations and transformation. On the one hand, these alterations and transformation have occurred due to the global rivals and on the other hand, they have existed because of the structural alterations and changes in consumer preferences. Sector demonstrates a production structure which changes from conventional textile products manufacturing to technical textile production and intense innovation and differentiation. Besides, it concentrates on fast fashion products, intense design and branding activities and multi-channel activities with respect to consumer preferences. In addition to these, new rival countries have been appeared instead of classic global rivals. Therefore, these alterations and transformation, which the sector has experienced in global foreign trade during the recent years, would be evaluated in this study and suggestions would be made.

Keywords: Foreign trade, Turkish textile and clothing sector, unit export price, net added-value

1. INTRODUCTION

Textile and clothing sector, which is one of the cornerstones of Turkey's economic development, has maintained its significance and place within the national economy for many years. Sector is one of the irreplaceable sectors of national economy due to its export potential, provided employment and created added-value.

According to the explained data of Turkish Exporters Assembly, clothing sector has become the second biggest exporter of Turkey after automotive industry with 17,6 billion dollars exports [1]. Besides, both textile and clothing sectors continue to have net foreign trade surplus. Unit export prices per kilogram are one of the indicators which prove the importance of the sector within the national economy.

According to the data of Turkish Exporters Assembly, unit export price of Turkey per kilogram has been actualized as 1,28 dollars in 2017. This figure has been occurred as 4,40 dollars in textile and its raw materials, whereas it has been actualized as 14,92 dollars in clothing [2]. Similarly, unit export price of Turkey per kilogram has been actualized as 1,29 dollars in 2018, whereas industry unit export price has been occurred as 1,73 dollar/kg [3]. Unit export price of clothing has been actualized as 15,36 dollar/kg in January-August 2018 period [4]. As it can be seen, sector significantly contributes to national economy with its created added- value.

2. THE PURPOSE AND THE METHOD OF THE RESEARCH

This research aims to analyze the last decadal global foreign trade performance of Turkish textile and clothing sector. In accordance with the aim of the research, the decadal (2009-2018) global foreign trade performance of

---

[1]Corresponding author: Assoc. Prof. Dr., Ege University, Department of Textile Engineering, 35100, Bornova/Izmir, Turkey, seher.kanat@ege.edu.tr

[2]Prof. Dr., Ege University, Department of Textile Engineering, 35100, Bornova/Izmir, Turkey, turan.atilgan@ege.edu.tr

Turkish textile and clothing sector is analyzed in detail. During the analysis; decadal foreign trade balances of sectors, annual percentage changes of export and import values, the shares of textile and clothing sectors within the global export and import values are calculated, shown in graphics and evaluated. In the second stage, the decadal (the kilogram based export values of 2018 has not been explained yet, therefore the decadal period has been changed as 2008-2017) global unit export prices of Turkey are calculated separately for each textile and clothing product group within the International Harmonized System Commodity Classification. According to the classification, there are 14 product groups and their explanations are shown in Table 1. Besides, the decadal unit export prices are also calculated for textile (whole product groups between 50 and 60) and clothing (whole product groups between 61 and 63) sectors. The obtained data is evaluated and interpreted via graphics.

Table 1. Distribution of textile and clothing products according to the International Harmonized System Commodity Classification Codes [5]

Hs Code	Explanation
50	Silk
51	Wool, Fine or Coarse Animal Hair; Horsehair Yarn and Woven Fabric
52	Cotton
53	Vegetable Textile Fibers; Paper Yarn and Woven Fabrics of Paper Yarn
54	Man-Made Filaments; Strip and The Like of Man-Made Textile Materials
55	Man-Made Staple Fibers
56	Wadding, Felt and Nonwovens, Special Yarns; Twine, Cordage, Ropes and Cables and Articles Thereof
57	Carpets and Other Textile Floor Coverings
58	Fabrics; Special Woven Fabrics, Tufted Textile Fabrics, Lace, Tapestries, Trimmings, Embroidery
59	Textile Fabrics; Impregnated, Coated, Covered or Laminated; Textile Articles of a Kind Suitable For Industrial Use
60	Fabrics; Knitted or Crocheted
61	Apparel and Clothing Accessories; Knitted or Crocheted
62	Apparel and Clothing Accessories; Not Knitted or Crocheted
63	Textiles, Made Up Articles; Sets; Worn Clothing and Worn Textile Articles; Rags

The export and import values and quantities, which are used in the calculations, are acquired from Trademap [6] and UN Comtrade Database [7]. The whole export and import values are acquired as US dollars, whereas all quantities are obtained as kilogram. The unit export price, which is chosen as one of the research methods, is calculated via dividing Turkey's annual global export value (US dollars) by its annual global export quantity (kg).

3. FINDINGS OF THE RESEARCH AND THEIR ANALYSIS

If Turkey's global textile and clothing trade is analyzed, it can be seen that Turkey maintains its importance in the global market and it possesses net foreign trade surplus in both sectors (Figure 1). Turkish textile sector possesses 1,9 billion dollars foreign trade surplus by 2018, whereas Turkish clothing sector has 15,5 billion dollars foreign trade surplus. Turkey's global textile export has increased from 6,5 billion dollars in 2009 to 10,5 billion dollars level in 2018 by demonstrating 63% increase. On the other hand, clothing export has decennially increased from 12,8 billion dollars to 17,4 billion dollars with 35% increase. Turkey's global textile import has increased from 6,4 billion dollars in 2009 to 8,6 billion dollars in 2018 by indicating 34% increase. However, its global clothing import has decennially decreased to 1,8 billion dollars from 2 billion dollars with 10% decrease. Turkish textile sector's global foreign trade surplus has decennially increased from 6 million dollars to 1,8 billion dollars, whereas Turkish clothing sector's global foreign trade surplus has decennially increased from 10,8 billion dollars to 15,5 billion dollars. Similarly, Turkish textile and clothing sector's global foreign trade surplus has decennially increased from 10,8 billion dollars to 17,4 billion dollars by demonstrating 61% increase.

Both decadal textile and clothing export values have usually demonstrated an increment tendency, whereas import values generally have shown a decline tendency (Figure 2 and 3). Turkey's global textile export has decennially increased 22% at most, whereas it has decreased 12% at the furthest. Besides, Turkey's global clothing export has decennially increased 10% at most, whereas it has decreased 9% at the furthest. On the other hand, global textile import has decennially increased 44% at most, whereas it has decreased 16% at the furthest. In addition, global clothing import has decennially increased 34% at most, whereas it has decreased 21% at the furthest. If textile and clothing sectors are evaluated jointly, it can be seen that, decadal textile and clothing export has increased 14% at most, whereas it has decreased 10% at the furthest. However, textile and clothing import has decennially increased 41% at most, whereas it has decreased 17% at the furthest.
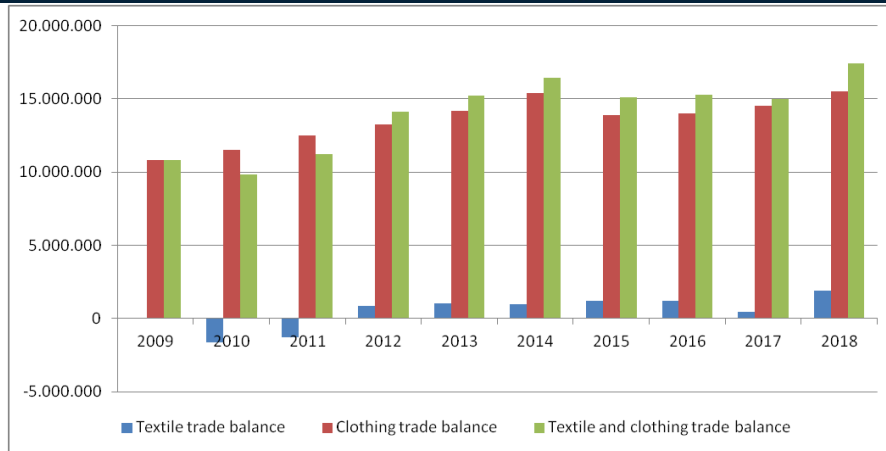
Figure 1. Turkey's global textile and clothing trade balance (US dollars)
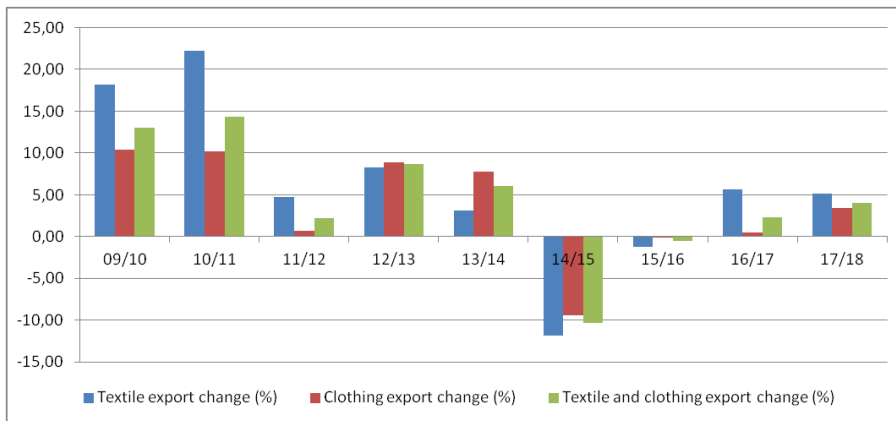
Figure 2. Annual percentage changes of Turkey's global textile and clothing exports

Figure 3. Annual percentage changes of Turkey's global textile and clothing imports

If Turkey's shares within global textile and clothing exports are analyzed; it is determined that Turkish textile and clothing export has taken 3,45% share from global textile and clothing export in 2009, whereas it has taken 3,34% share in 2018 (Figure 4). As it can be seen, the share of textile and clothing sector within the global textile

and clothing exports has decennially decreased 3%. However, sector has maintained its share in the global textile and clothing market during the determined period. On the other hand, Turkish textile sector has taken 3,21% share from the global textile export in 2009, whereas it has taken 3,65% share in 2018. Besides, Turkish clothing sector has taken 3,59% share from the global clothing export in 2009, whereas it has taken 3,17% share in 2018. Therefore, the share of Turkish textile exports within global textile exports has decennially increased 14%, whereas the share of Turkish clothing exports within global clothing exports has decennially decreased 12%.
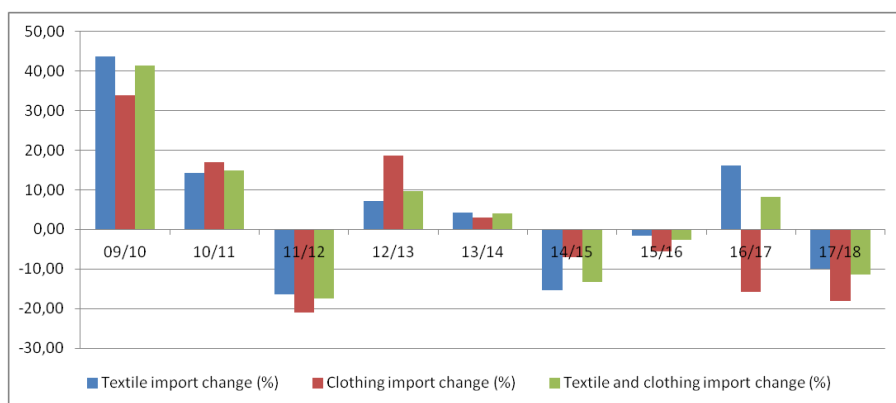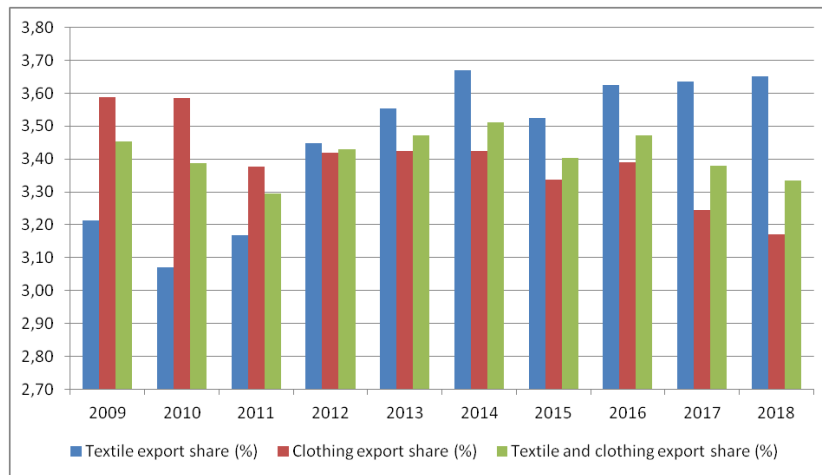

Figure 4. Annual shares of Turkish textile and clothing exports within the global textile and clothing exports

If Turkey's shares within global textile and clothing imports are analyzed; it is determined that Turkish textile and clothing import has taken 0,16% share from global textile and clothing import in 2009, whereas it has taken 0,14% share in 2018 (Figure 5). As it can be seen, the share of textile and clothing sector within the global textile and clothing imports has decennially decreased 12%. On the other hand, Turkish textile sector has taken 3,53% share from the global textile import in 2009, whereas it has taken 3,17% share in 2018. Besides, Turkish clothing sector has taken 0,57% share from the global clothing import in 2009, whereas it has taken 0,37% share in 2018. Therefore, the share of Turkish textile imports within global textile imports has decennially decreased 10%, whereas the share of Turkish clothing imports within global clothing imports has decennially decreased 35%.
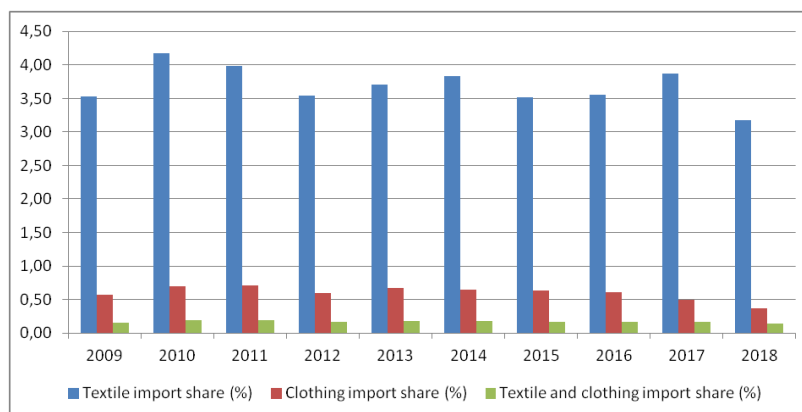
Figure 5. Annual shares of Turkish textile and clothing imports within the global textile and clothing imports

If the global unit export prices of Turkish textile and clothing sectors are analyzed; it can be seen that, textile sector's decadal unit export prices have altered between 6,30 and 8,81 dollars, whereas clothing sector's decadal unit export prices have changed between 15,09 and 19,91 dollars (Figure 6). The decadal global unit export price

of Turkish textile sector has been calculated as 7,63 dollar per kilogram, whereas it has been determined as 17,88 dollar per kilogram for Turkish clothing sector.
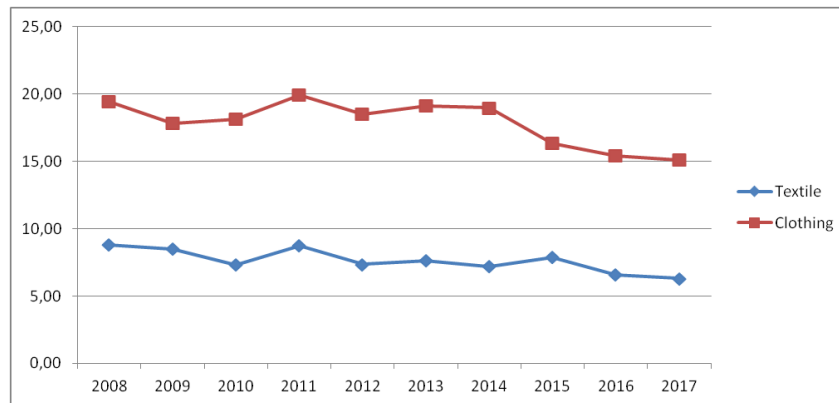
Figure 6. Global unit export prices of Turkish textile and clothing sectors (Dollar/kg)

If the global unit export prices of Turkish textile sector are analyzed on the basis of product groups, it can be seen that the highest unit export prices belong to silk group (Figure 7). The decadal average unit export price of silk group has been actualized as 27,30 dollar per kilogram. If the product groups, which raise the unit export prices per kilogram, are kept out, it can be seen that the decadal average unit export prices have altered between 3,04 dollars and 10,52 dollars (Figure 8). Silk group; special woven fabrics, tufted textile fabrics, embroideries; wool group and knitted or crocheted fabrics have possessed the highest decadal average unit export prices per kilogram (decadal average unit export prices have been calculated as 27,30; 10,52; 7,22; 6,77 dollar/kg respectively). On the other hand; wadding, felt and nonwovens; carpet and other textile floor coverings; vegetable textile fibers group and cotton group have owned the lowest decadal average unit export prices per kilogram (decadal average unit export prices have been calculated as 3,04; 3,49; 4,69; 4,91 dollar/kg respectively).
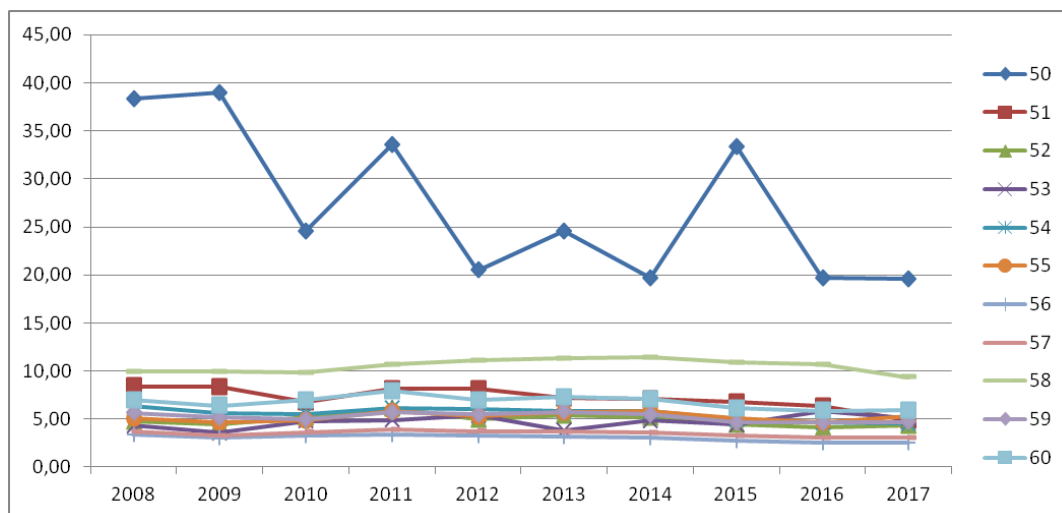

Figure 7. Global unit export prices of Turkish textile sector on the basis of product groups (Dollar/kg)
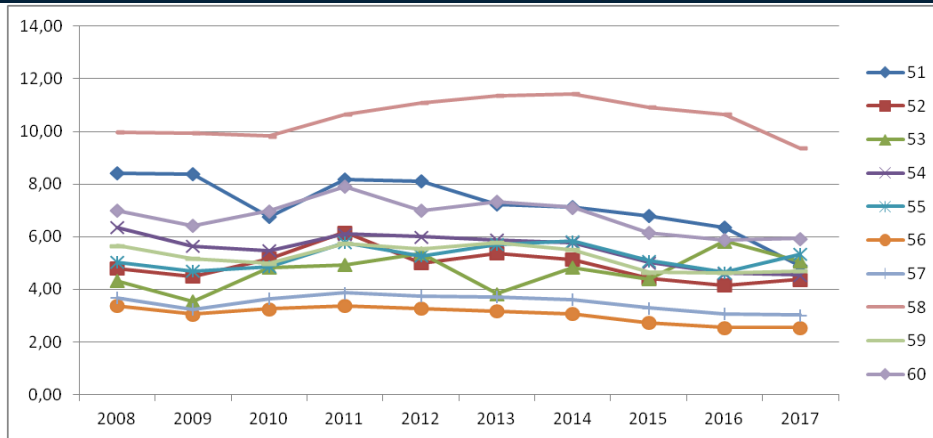
Figure 8. Global unit export prices of Turkish textile sector on the basis of product groups (except product group 50) (Dollar/kg)

If the global unit export prices of Turkish clothing sector are analyzed on the basis of product groups, it can be seen that the highest unit export prices belong to woven apparel and clothing accessories (Figure 9). The decadal average unit export price of woven apparel and clothing accessories has been actualized as 25,48 dollar per kilogram. Turkish clothing sector's decadal average unit export prices have altered between 6 dollars and 27,69 dollars. Woven apparel and clothing accessories and knitted apparel and clothing accessories have possessed the highest decadal average unit export prices per kilogram (decadal average unit export prices have been calculated as 25,48; 21,54 dollar/kg respectively), whereas home textile and used textile products category has owned the lowest decadal unit export prices per kilogram (decadal average unit export price has been calculated as 6,63 dollar/kg).
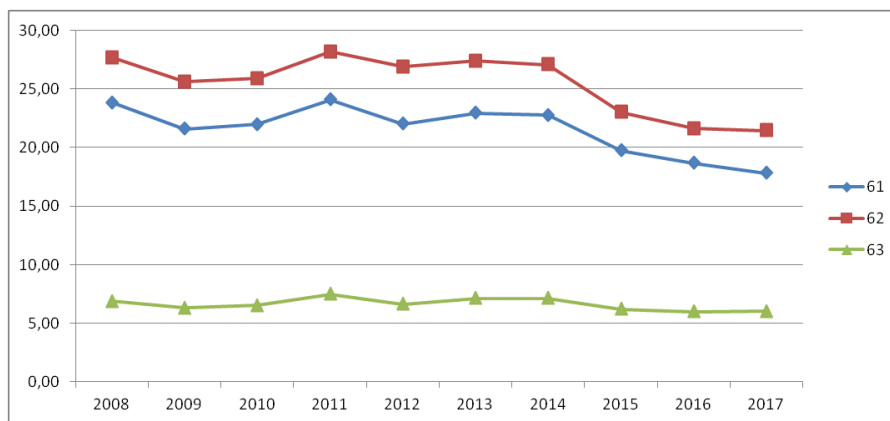
Figure 9. Global unit export prices of Turkish clothing sector on the basis of product groups (Dollar/kg)

4. CONCLUSIONS AND GENERAL EVALUATION

Turkish textile and clothing sector maintains its significance in the national economy and exports despite the increasing international competition. If Turkey's global textile and clothing trade is analyzed, it can be seen that, Turkey maintains its importance in the global market and both sectors possess net foreign trade surplus. Turkish textile sector possesses approximately 1,9 billion dollars foreign trade surplus by 2018, whereas Turkish clothing sector has 15,5 billion dollars foreign trade surplus. Turkish textile and clothing sector's global foreign trade surplus has decennially increased from 10,8 billion dollars to 17,4 billion dollars by demonstrating 61% increase.

According to the World Trade Organization data [8], Turkey is the fifth biggest textile exporter of the world, whereas it is the sixth biggest clothing exporter by 2017. Besides, as stated by this research, Turkey's global textile export has decennially increased from 6,5 billion dollars to 10,5 billion dollars by demonstrating 63% increase. On the other hand, Turkey's global clothing export has decennially increased from 12,8 billion dollars to 17,4 billion dollars with 35% increase. Turkish textile and clothing sector has taken 3,34% share from global textile and clothing exports by 2018.

Another indicator, which demonstrates that the sector maintains its place and significance in global textile and clothing market, is the unit export prices per kilogram. Global decadal average unit export price of Turkish textile sector has been actualized as 7,63 dollar per kilogram, whereas it has been determined as 17,88 dollar per kilogram for Turkish clothing sector. If Turkey's unit export price per kilogram (1,28 dollar/kg) is taken into consideration, the created net added-value of the sector can be seen explicitly.

According to another research result, the highest decadal average unit export prices belong to silk group; woven apparel and clothing accessories; knitted apparel and clothing accessories; special woven fabrics, tufted textile fabrics, embroideries; wool group and knitted or crocheted fabrics. On the other hand, wadding, felt and nonwovens; carpet and other textile floor coverings; vegetable textile fibers group and cotton group have owned the lowest decadal average unit export prices per kilogram. As it can be seen, clothing products possess the highest net added-value within the textile and clothing products.

To sum up, Turkish textile and clothing sector has decennially maintained its significance in global textile and clothing exports in spite of the increasing rivalry conditions and new rivals (Vietnam, Bangladesh etc.), which increase their global competitiveness. At this point, Turkey should export high value-added products (especially clothing products) and should increase these products' export amounts in order to compete against these rivals and increase its competitiveness. In this context, it should produce and export high-qualified products (branded clothing products, technical textiles etc.) with appropriate costs by using its knowledge, experience and expertness. Therefore, it should give great importance to research and development activities and design. Thus, it should both increase the export amounts and the average unit export prices.

REFERENCES

[1] Timeturk, 2019, 2018 Export Figures Are Announced, https://www.timeturk.com/2018-yili-ihracat-rakamlari-aciklandi/haber-1018646 (Date of Access: May 2019)

[2] Turkish Exporters Assembly, 2018, Kilogram Value is 28 Dollars in Exports, http://www.tim.org.tr/tr/inpressdt-72632d4f-51c2-416a-be51-df5b3970229e.html (Date of Access: May 2019)

[3] Turkish Exporters Assembly, 2019, 2019 Export Report, 70 p.

[4] Uludag Exporters' Association Research and Development Branch, 2018, Research and Development Bulletin, Issue: 21, 13 p.

[5] Foreign Trade Online, Harmonized System Codes, https://www.foreign-trade.com/reference/hscode.htm?cat=9 , (Date of Access: May 2019)

[6] Trademap, Trade Statistics for International Business Development, https://www.trademap.org/Index.aspx , (Date of Access: May 2019)

[7] United Nations Comtrade Database, https://comtrade.un.org/data/ , (Date of Access: May 2019)

[8] World Trade Organization, 2018, World Trade Statistical Review 2018, 213 p.

A New Paradigm in Clothing Sector: Marketing 3.0

Seher Kanat[1], Turan Atilgan[2]

Abstract

Global and technological improvements have affected the enterprises in many fields as well as marketing field. If the improvements in marketing are analyzed, it can be seen that marketing 1.0 has been evolved to marketing 2.0 and shortly afterwards it is evolved to marketing 3.0. Product focused marketing approach, in which real sector becomes prominent, has been dominated until 1960s. During this period, one-way communication from producer to consumer has been occurred and this communication has aimed to persuade the consumers to believe that product is good. Neither the consumers' desires nor their expectation are taken into consideration. Besides, customer satisfaction, customer loyalty, after sales services and communication with consumers are not taken into account in this period, which is also defined as mass production period. Instead of these, expressing product properties has become prominent during this period.

The rivalry between products has substantially given place to the competition between services in 1960s and 1970s. Service quality, quality standards and unconditional customer happiness have determined as the most significant subjects of this period. During this period, the consumers have gained more information about products and brands. Therefore, they have started to compare these products and brands. Consequently, the enterprises have tended towards customer services and customer relations.

Products and services have become the same in the later 1990s due to the rapid improvements in technology, internet, digitalization and social media tools. Besides, the consumers have been informed about everything in a short time. Therefore, the enterprises have tended towards new searches. Thus, marketing 3.0 period has begun. In this period, the consumers have started to desire more than good products and services from enterprises. The satisfaction of their spiritual needs has gained more importance rather than the fulfillment of their physical needs. Therefore, the consumers have started to give importance to a product's intangible value, perception, difference, personality and to the gained sense and experience besides its quality, proper price and services. Thus, this new marketing era has also named as values-driven era.

This new era also affects the clothing sector and the enterprises, which operate in this sector, as well as all other sectors and enterprises. On the other hand, Turkish clothing sector both economically and socio-culturally possesses a great significance for national economy. In this context, this study, analyzes the preparation of major Turkish clothing enterprises for this serious alteration and their progress and capabilities in terms of marketing 3.0.

Keywords: Marketing, marketing 3.0, clothing sector, values-driven era

1. INTRODUCTION

Enterprises have changed their marketing approaches due to increasing importance of consumer desires and expectations. Consumer desires and expectations have become the focal point of enterprises when product focused marketing approach has altered to consumer focused marketing approach. However, also consumers have been altered in rapidly changing and developing world. Nowadays, numerous consumers are interested in environmental, social and cultural issues and they want to show their awareness to their environment. At this point, the customers do not aim to find solutions to local and global environmental and social issues. They aim to contribute to the solutions of these issues and, in some ways, they want to unburden themselves.

At this point, marketing 3.0 approach, which handles consumer as a whole with its mind, spirit and heart, becomes prominent. Marketing 3.0 actualizes marketing activities by paying attention to the spiritual, collaborative,

---
[1]*Corresponding author: Assoc. Prof. Dr., Ege University, Department of Textile Engineering, 35100, Bornova/Izmir, Turkey, seher.kanat@ege.edu.tr*

[2]*Prof. Dr., Ege University, Department of Textile Engineering, 35100, Bornova/Izmir, Turkey, turan.atilgan@ege.edu.tr*

cultural, social and environmental desires of consumers. Therefore, it reaches consumers by using different channels, communicates continuously and mutually and includes the consumers in design and product development processes. In this context, this research focuses on marketing 3.0 paradigm and the marketing 3.0 implementations of major Turkish clothing enterprises.

2. MARKETING 3.0 CONCEPT AND ITS FEATURES

Marketing functions may be seen as having evolved through the ages to serve different needs. The first age of marketing (marketing 1.0) was product-centric, the second age during the information era (marketing 2.0) was consumer centric and the current age (marketing 3.0) is the values-driven era where consumers are not just seen as consumers but rather whole human beings with minds, hearts and spirits [1]. Marketing 3.0 represents the most recent marketing paradigm, with the key assumption that companies treat consumers as human beings with intelligence, heart, soul and spirit. As such, it is a prominent philosophy, gaining relevance among consumers who increasingly recognize the effects of unpredictable social, economic and environmental changes on them. Previous paradigms included marketing 1.0, which emerged during the industrial product-centric era and focused on mass sales of products based on functional value propositions, the marketing department's activities centered solely on the product or service for sale. An enhanced version, marketing 2.0, arose during the information age, such that companies adopted an emotional value proposition. That is, marketing 2.0 is based not on the product transactions but on the relationships that allow companies to engage consumers with messages and individualized services and products. Consumers differ in their preferences, so companies must segment the market and develop unique products for different consumers [2]. However, marketing 3.0 is a stage where retailers are shifting from consumer-centricity to human-centricity and this transformation is specifically visible for information goods which create opportunities for multichannel effects. Accordingly, recent advances in technology such as mobile communication technology have presented retailers with several opportunities to be knowledgably aware of their customers' characteristics, communicate with them and offer consumer-based products and services [3].

In other words; marketing 1.0 is product-centric, transaction and sales oriented whereas marketing 2.0 is consumer-centric and relationship oriented. Marketing 3.0 is human centric and value driven and it invites consumers to participate in the company's product development and communication [4]. Table 1 demonstrates the key features of marketing 1.0, 2.0 and 3.0.

Table 1. Comparison of marketing 1.0, 2.0 and 3.0 [5]

	Marketing 1.0 Product-centric marketing	Marketing 2.0 Consumer-oriented marketing	Marketing 3.0 Values-driven marketing
Objective	Sell products	Satisfy and retain the consumers	Make the world a better place
Enabling forces	Industrial revolution	Information technology	New wave technology
How companies see the market	Mass buyers with physical needs	Smarter consumer with mind and heart	Whole human with mind, heart and spirit
Key marketing concept	Product development	Differentiation	Values
Company marketing guidelines	Product specification	Corporate and product positioning	Corporate mission, vision and values
Value propositions	Functional	Functional and emotional	Functional, emotional and spiritual
Interaction with consumers	One-to-many transaction	One-to-one relationship	Many-to-many collaboration

The era of marketing 3.0 is the era where marketing practices are very much influenced by changes in consumer behavior and attitude. It is the more sophisticated form of the consumer-centric era where the consumer demands more collaborative, cultural and spiritual marketing approaches [5]. In this context, the components of marketing 3.0 can be listed as [5,6]:

1. Collaborative marketing means engaging consumers in the development of products.

2. Cultural marketing means attention to the social and cultural problems (such as social injustice, care of the environment, tolerant attitude to animals, protection of human rights).

3. Spiritual marketing means creative approach to products development, creation of the intangible values in the product, which allow satisfying creative and spiritual needs, providing impressions, emotions and meanings that affect the spirit of a person.

Marketing 3.0 is characterized by populations who want to satisfy functional, emotional and spiritual needs through their consumption [2]. In the values-driven era, people demand to be treated not as just simple consumers; instead they want to be treated as whole human beings with minds, hearts and spirits [7]. This evolution to more human-centric value propositions is shaping the future of marketing in three main ways. First, mass participation and co-creation through collaborative marketing reflect how modern social media and the internet have tapped into natural human desires for connectivity and interactivity. Companies thus seek collaborative marketing strategies, such as product or service co-creation, with consumers, employees, channel partners and other companies that have similar goals and values. Second, in the globalization paradox, technological advances have created truly global citizens who still want to be considered individuals. Accordingly, marketing needs to address both local and global communities simultaneously. Third, the rise of a creative society and human-spirit marketing encourages creative people, who tend to innovate, collaborate and express themselves more than others, to pursue their self-actualization but also demand originality and trendiness in the products and services they consume [2].

Therefore, the conceptual approach of marketing 3.0 entails a redefined triangle. Rather than brand, positioning and differentiation, it builds on this formula to suggest a 3-I model, encompassing identity, image and integrity. The first I, identity, reflects the relationship between positioning and brand and seeks to address the rational portion of the value proposition. Image instead lies at the juncture of differentiation and brand and strives to capture the emotions of the target audience. Finally, integrity represents the intersection of positioning and differentiation and it aims to fulfill the brand promise authentically while fostering trust, commitment and loyalty. This 3-I model demonstrates how more intangible and social factors can determine the real and perceived value created by a company [2,5].

Marketing 3.0 acknowledges that psycho-spiritual benefits are the most fundamental need of consumers and perhaps the ultimate differentiation a marketer can create [1]. Emotional involving as many consumers as possible, both while developing the product and at its consumption, the intention to touch consumers at a higher level has become the main marketing purpose. Now, marketers through the social communications associate products consumption to people's hopes that the world would change for the better by asserting that the creation and consumption of a certain product contribute to solving global social and environmental problems (for example, by asserting that the consumption of cosmetics made from the raw ingredients, which were purchased on the base of support community fair trade (The Body Shop) would help to eliminate social injustice problem) [6].

As it can be seen, marketing 3.0 includes issues such as supporting sustainability, green consumerism and marketing with an environmental outlook as its focus is on the whole person and perhaps society. It speaks about social justice, cause marketing for socio-cultural transformations and that businesses should be committed to reducing negative impacts on society and the environment, not just for public relations reasons, but rather as good corporate citizens [1]. Because, marketing 3.0 paradigm proffers the idea that customers are increasingly seeking solutions to their own concerns and are interested in building a better world. Such understanding involves purchase decisions on the basis of fulfilling social and ethical values (such as social justice, human welfare, and environmental sustainability). In other words, customers look to products and services to meet their own needs in parallel with fulfilling spiritual, social and moral values. The extent to which a product or service provides freedom of choice, independence as well as benevolence, social justice, equality and environmental responsibility is becoming more and more crucial for customers when making purchase choices, especially in a developed world, where consumption appears to have become an end in itself, through which customers find a voice to promote a better society. Furthermore, customers are increasingly showing concerns about the effects of their purchase choices not only for themselves but also for broader society, which represents a strong embracement of transcendent motives in their actions. In other words, in addition to making purchase decisions with an eye on external benefits gained or the pleasure acquired from the purchase decision itself, customers are more and more concerned about whether their purchase decisions contribute to solving the problems of someone else. In effect, customers are more and more worried about whether others, both known or unknown, meet human good, such as truth, beauty, work, friendship, life and dignity such that their purchase decisions' impact on others is carefully calculated [8].

3. THE PURPOSE AND THE METHOD OF THE RESEARCH

Marketing 3.0 paradigm considers the consumers as a whole with their minds, hearts and spirits. It actualizes the marketing activities by paying attention to consumers' approaches with regard to cultural, social and environmental issues. It aims continuous communication with consumers and their inclusion in the processes as far as possible.

In this context, this research aims to analyze the marketing 3.0 implementations of successful major Turkish clothing enterprises, which possess their own brands and operates in international markets. In accordance with the aim of the research, the data belonging to the marketing 3.0 implementations of chosen major Turkish clothing enterprises (Adil Isik Group, LC Waikiki, Mavi Jeans and Koton) are collected from secondary data resources and analyzed.

4. FINDINGS OF THE RESEARCH AND THEIR ANALYSIS

4.1 Adil Isik Group (adL and Love my body)

Adil Isik Group takes its strength from its customer focused system, product quality and fast supply system. It follows the global trends closely and swiftly puts them on market. The group possesses two brands which are named as adL and Love my body. adL focuses on the designs which highlights elegant and graceful woman, whereas Love my body gives prominence to the ageless fashionable collections with alternative sizes. adL brand is created in 1992, whereas Love my body brand has been operating since 2008 [9,10,11]. If Adil Isik Group's marketing implementations are analyzed, it can be seen that, the enterprise accommodates to value focused marketing 3.0 era and tries to implement all components of marketing 3.0.

Working women constitute the target market of adL brand. However, the brand has prepared sportive collections, which are named as codentery-line, in accordance with customer demands. Besides their staff (especially salespeople) personally communicate with customers. In order to achieve this, the brand gives special educations to their staff and customer desires and expectations are directly transferred to head office. In addition to these, the brand regularly conducts surveys every year and collects and evaluates customers' desires and complaints via these surveys. The brand prepares its collections by considering the customers', designers' and even interns' opinions [12]. New collection preparation with regard to customer demands and design process by considering the customers' and other shareholders' desires and complaints can be given as examples to collaborative marketing component of marketing 3.0.

The adL customers, who have been wearing the adL products since their youth, demand plus-size clothing products from the brand due to their increasing ages and being mothers and plus-size consumers. Therewith, Love my body brand is created [13]. Love my body, which is the other brand of the group, gives "love your body as is" message to their customers [14]. In this context, it represents the plus-size women consumers' desires and helps them.

Besides, Love my body does not define itself as a plus-size brand. It produces women clothes which are between 36 and 50 sizes and transmits the designs to upper-sizes by using colors and patterns. Therefore, it satisfies the colorful and fashionable dressing needs of plus-size women [14]. In other words, it defends that the world should accept plus-size women as they are and they also possess fashionable dressing rights. In this context, this approach of the group and its brand can be given as examples to collaborative and spiritual marketing components of marketing 3.0.

On the other hand, adL collaborates with TOCEV foundation within the context of a social responsibility project. The kids have drawn their dreams via paintings and brand's designers have transformed these paintings to scarf patterns. Revenue of these scarves are donated to the foundation [15,16]. In other words, the brand both socially reflects kids' dreams via its products and helps to children, who need financial support for their education. Therefore, this implementation can be given as an example to spiritual and cultural marketing components of marketing 3.0.

adL, also collaborates with Turkish Educational Foundation and prepares a collection by inspiring from Safiye Ayla's clothes. Revenue of this collection is donated to the foundation. This cooperation aims to memorialize Safiye Ayla and familiarize her to young generation. Safiye Ayla is the first singer of Turkey and also she is the first donor of Turkish Educational Foundation [16]. This cooperation reflects the cultural marketing component of marketing 3.0 in terms of helping the children, who need financial support for their education, and memorializing and familiarizing a singer, who belongs to republic culture.

4.2 LC Waikiki

LC Waikiki's brand journey has started in France in 1988 and it has continued to its way as a Turkish brand since 1997. The brand, which adopts "everyone deserves to dress well" philosophy, presents accessible fashion to its customers in 922 stores in 45 countries by providing qualified products at affordable prices [17]. The brand aims to dress people according to their styles and budgets and make them feel good via everyone deserves to dress well philosophy [18]. In this context, the brand's aim and philosophy conform with the spiritual and cultural

marketing components of marketing 3.0 due to their contributions to social justice and values, which affect the consumers' spirits.

LC Waikiki's LCW Sense is a mobile application, which is developed for visually impaired people. Products' color, pattern, size, fabric contents, washing instructions and price information are read aloud to users via this mobile application, which scans barcodes. Therefore, blind people can purchase clothes by themselves [19]. This support, which annihilates physically handicapped people's disadvantages with regard to clothes shopping, can be given as an example to spiritual and cultural marketing components of marketing 3.0.

4.3 Mavi Jeans

Mavi Jeans, which is established in Istanbul in 1991, has started to its international journey in 1996. Nowadays, it meets with consumers in 5.500 sales points in 35 countries. The brand, which takes its strength from denim roots, is transformed into an international clothing brand. It continues to produce high qualified products with "perfect fit" philosophy. Perfect fit philosophy, understands customers' needs, follows these needs closely and provides qualified products which deserve their prices [20]. Mavi Jeans designs its products according to their customers' bodies. Perfect fit philosophy means the appropriateness of products both to human body and life. The brand uses different pattern systems in different countries in order to provide perfect fit in terms of human body. Besides, it provides cultural and budgetary properness via perfect fit philosophy. Mavi Jeans is an unique Mediterranean brand, which possesses an identity and attitude in the sight of environment and society [21,22]. Thus, Mavi provides the collaborative component of marketing 3.0 by designing and producing fitting products. Besides, it presents the cultural marketing component of marketing 3.0 by addressing to consumers' cultures via perfect fit philosophy and it provides the spiritual marketing component of marketing 3.0 via affecting consumers' spirits with its brand identity, unique attitude and innovative product designs.

Mavi possesses a social responsibility project, which is named as "Indigo Turtles". The project takes inspiration from young people and aims to protect sea turtles, which are in danger of extinction, by providing support to the activities of Ecological Research Society [23]. The staff and customers of Mavi camp in beaches, where the sea turtles have spawned, and protect the baby turtles and help their arrival to the sea. Besides, a customer, who buys an Indigo Turtles t-shirt, provides protection to five baby sea turtles [24]. Mavi provides protection to animals, which are in danger of extinction, with this social responsibility project and also it touches to the spirits of people who loves and wants to protect the nature. In this context, it provides cultural and spiritual marketing components of marketing 3.0.

4.4 Koton

Koton, which is established in Istanbul in 1998, meets with its customers in more than 800 sales points throughout the world. Koton is a clothing brand, which presents women, men, children and baby clothes [25]. Brand has measured the customer experiences in its stores with the help of a consulting firm. It is revealed that 55% of the customers visit Koton stores in order to find new products due to the wide variety and fast product change. Therewith, the brand has enlarged its design team and has sent 45 new models to its stores each week. Besides, the brand aims to understand and satisfy the unspoken customer needs and desires. In this context, the trouser patterns are renewed according to the observations and measured customer experiences. New patterns provide spindly legs and tight and small hips. The trouser sales have increased 100% at this period in spite of the economic crises [26,27]. The brand has experienced and measured its customers' desires and expectations even without their awareness and has developed new products according to these measures. These implementations can be given as an example to collaborative marketing component of marketing 3.0. Besides, they provide spiritual marketing component of marketing 3.0 by positively addressing to woman spirit and emotions with product design.

Koton supports women employment by implementing positive discrimination principle with social responsibility projects and inclusionary business models. Koton approximately employs 7.000 women, which is over European Union's women employment average, and possesses 63% woman employee ratio and 50% woman manager ratio. Besides, the brand has signed the Women's Empowerment Principles and provides employment and regular income to 2.500 women, who lives in undeveloped provinces of Turkey (Mardin, Adiyaman, Batman, Sanliurfa etc.), with its Handicraft Project [28]. The brand fulfills the spiritual and cultural marketing components of marketing 3.0 by providing positive discrimination to women, supporting women employment and endeavoring for the protection of women's social and economical rights.

5. CONCLUSIONS AND GENERAL EVALUATION

Nowadays, consumers are the individuals, who are aware of their own identities and the surrounding world and who live according to this awareness. Therefore, most of the consumers demand spiritual satisfaction as well as high quality and proper price from the products that they bought. In this context, marketing 3.0, which is called as values-driven era and which handles consumers as a whole with their minds, spirits and hearts, implementations gain importance. Marketing 3.0 consists of collaborative marketing, which requires customers' involvements to product development and design processes; cultural marketing, which wants to attract attention to social and cultural problems of societies; and spiritual marketing, which satisfies consumers' spiritual needs by using creative approaches in product development and design.

In this context, clothing sector, which provides the clothes, which are one of the most significant ways of self-expression, gives the necessary importance to marketing 3.0 implementations in this values-driven era. Therefore, this research analyzes the marketing 3.0 implementations of successful major Turkish clothing enterprises, which possess their own brands and operates in international markets. According to the obtained research results, Turkish clothing brands successfully actualize all three components of marketing 3.0. Brands reflect consumers' desires and expectations to their products by including the consumers in their design and product development processes. Therefore, they successfully implement the collaborative component of marketing 3.0.

According to the other research results, brands both raise the awareness of the society and contribute to the solutions of social and cultural problems by attracting attention to these issues (education right, women rights, animals which are threatened with extinction, children rights etc.) of the society and even by reflecting these issues to their product designs. Besides, brands address to consumers' spirits with both their social responsibility projects and designed products and satisfy their spiritual needs. Therefore, Turkish clothing brands also successfully actualize the cultural and spiritual components of marketing 3.0.

As it can be seen, Turkish clothing brands have realized the importance of marketing 3.0 paradigm. These brands, which operate under intense national and international rivalry, accept the consumers as a whole with their minds, spirits and hearts in order to differentiate from their rivals and increase their competitiveness. In this context, they actualize marketing 3.0 implementations, which will satisfy consumers' spiritual needs and highlight their values.

REFERENCES

[1] Salimath M.S., Chandna V., 2018, Sustainable consumption and growth: examining complementary perspectives, Management Decision, https://doi.org/10.1108/MD-12-2016-0934

[2] Martinez-Canas R., Ruiz-Palomino P., Linuesa-Langreo J., Blazquez-Resino J.J., 2016, Consumer participation in co-creation: an enlightening model of causes and effects based on ethical values and transcendent motives, Frontiers in Psychology, Vol.7, p:1-17

[3] Rezaei S., Valaei N., 2017, Branding in a multichannel retail environment: online stores vs app stores and the effect of product type, Information Technology & People, Vol.30, No.4, p:853-886

[4] Liu Y.Y., Macerinskiene A., 2016, Managing the digital campaign process for sustainable tourism destinations, WIT Transactions on Ecology and The Environment, Vol.201, p:139-153

[5] Kotler P., Kartajaya H., Setiawan I., Marketing 3.0: From Products to Customers to the Human Spirit, 2010, John Wiley & Sons Inc., USA, 188 p.

[6] Voronov M., Chasovskikh V., 2018, Influence of Social Communications on Changes in Marketing Concept, The European Proceedings of Social & Behavioural Sciences, p:1404-1414, http://dx.doi.org/10.15405/epsbs.2018.02.164

[7] Gomez-Suarez M., Martinez-Ruiz M.P., Martinez-Caraballo N., 2017, Consumer-brand relationships under the marketing 3.0 paradigm: a literature review, Frontiers in Psychology, Vol.8, p:1-4

[8] Linuesa-Langreo J., Ruiz-Palomino P., Elche-Hortelano D., 2017, New strategies in the new millennium: servant leadership as enhancer of service climate and customer service performance, Frontiers in Psychology, Vol.8, p:1-14

[9] https://www.adilisikgroup.com/hakkimizda (Date of Access: May 2019)

[10] https://www.adl.com.tr/tr/t/hakkimizda (Date of Access: May 2019)

[11] https://www.lovemybody.com.tr/hakkimizda (Date of Access: May 2019)

[12] https://www.star.com.tr/cumartesi/demokratik-8200-3bmarka-8200-3badl-8200-3b-haber-1145740/ (Date of Access: May 2019)

[13] http://www.hurriyet.com.tr/ekonomi/marka-yolculugu-esiyle-basladi-30-u-rusya-da-148-magazayi-yakaladi-19398608 (Date of Access: May 2019)

[14] https://www.aksam.com.tr/cumartesi/uc-kusak-ayni-anda-ayni-magazadan-giyiniyor/haber-570460 (Date of Access: May 2019)

[15] http://www.pudra.com/yasam/gundem/tocev-cocuklarinin-hayalleri-adl-desenlerinde-27475.htm (Date of Access: May 2019)

[16] https://www.adilisikgroup.com/sosyal-sorumluluk (Date of Access: May 2019)

[17] http://corporate.lcwaikiki.com/hakkimizda (Date of Access: May 2019)

[18] http://corporate.lcwaikiki.com/kurumsal-politikalar (Date of Access: May 2019)

[19] http://www.bilisimdergisi.org.tr/yazarlar/roportajlar/lc-waikiki-kurumsal-iletisim-reklam-muduru-sevda-malkoc-toplumumuzdaki-dezavantajli-kesimlere-yonelik-sayisiz-calismalar-yurutuyoruz.html (Date of Access: May 2019)

[20] http://www.mavicompany.com/tr/mavi/hakkimizda (Date of Access: May 2019)
[21] https://www.posta.com.tr/isin-sirri-herkes-icin-olmasinda-9287 (Date of Access: May 2019)
[22] https://pazarlamasyon.com/turk-markalarinin-bir-felsefesi-var-mi/ (Date of Access: May 2019)
[23] http://www.mavicompany.com/tr/degerler/sosyal-sorumluluk (Date of Access: May 2019)
[24] https://www.mavi.com/indigo-turtles (Date of Access: May 2019)
[25] https://www.koton.com/tr/corporate/about-us (Date of Access: May 2019)
[26] http://www.hurriyet.com.tr/altinci-hissin-kerameti-12326833 (Date of Access: May 2019)
[27] https://www.kadinvekadin.net/iste-vucut-tiplerine-gore-tasarlanan-pantolonlar.html (Date of Access: May 2019)
[28]   http://www.aydinozel.net/koton-pozitif-ayrimcilik-ilkesiyle-binlerce-kadina-istihdam-sagliyor-3855h.htm   (Date   of
        Access: May 2019)

Utilization of Excess Activated Sludge and Yeast Residues as Alternative Substrate for Sulfate Reduction

Amine Yucel[1], Tulay Yilmaz[1], Yakup Cakmak[1], Deniz Ucar[1]

Abstract

Acidic mine drainage are characterized by high sulfate, metal and low pH. Generally, AMD is formed by the reaction of sulfur and metal containing minerals with oxygen and water. In the treatment of AMD, sulfate can be reduced to sulfide in the presence of an electron donor and produced sulfide could be used to precipitate metals in the AMD. In this process, alkalinity is also produced. In the literature ethanol, glucose, lactate, acetate are widely reported. However, in field applications, low cost electron and carbon sources were also used such as sawdust or manure. In this study, anaerobic digested activated sludge and yeast were used as substrate in sulfate reduction process as alternative carbon and electron sources. Excess activated sludge and yeast residues were fed to batch reactors (600 – 1400 mg COD/L equivalent) containing 2000 mg SO_4^{2-}/L and reduction performances were monitored by means of sulfate reduction, sulfide and alkalinity production. According to reduction performances, activated sludge and yeast residues were fed to continuous sulfidogenic reactors.

Keywords: *Excess activated sludge, yeast residues, sulfate reduction*

1. INTRODUCTION

Heavy metals are released into the environment by several anthropogenic and natural sources. Some of the anthropogenic sources are mining, fertilizers, tanneries, batteries, paper and electroplating industries[1]. In particular, metal finishing and electroplating industries generate large quantities of metal containing wastewaters[2]. In the environment, released heavy metals could result in significant problems. Such problems may cause both acute and chronic toxicities [3,4]. Some heavy metals are also carcinogenic and non-biodegradable.

One of the industries that discharge large volumes of heavy metals is the mining industry. Beside heavy metals, mining industry wastewaters also contain high concentrations of sulfate. In a study conducted in a mining area in Turkey, sulfate concentrations up to 3.34 g/L were reported[5].

Heavy metals could be precipitated as hydroxide or metal sulfide form. The metal sulfide form of precipitation is a fast and effective process and it has a low solubility over a wide range of pHs[6]. The only requirement of the mining industry wastewater is organic substrate to activate sulfate reducing bacteria. The sulfate is reduced to sulfide, which could be used to form metal sulfide precipitation, when organic substrate is added to wastewater[5,7–9]. Equations (1) and (2) show the sulfate reduction and metal precipitation respectively.
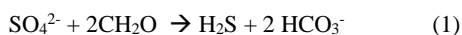
$$SO_4^{2-} + 2CH_2O \rightarrow H_2S + 2 HCO_3^- \qquad (1)$$

$$H_2S + M^{2+} \rightarrow MS + 2H^+ \qquad (2)$$

---

[1] *Corresponding author: Harran University, Gap Renewable Energy and Energy Efficiency Center, 63100, Haliliye/Sanliurfa, Turkey. denizucar@dharran.edu.tr*

Some commercial and efficient substrates such as ethanol[8,9], lactate[7] or acetate[10] could be used in sulfate reduction. For some economic reasons, some inexpensive substrates can also be used such as manure or saw dust.

In some experiments, excess activated sludge is also used for denitrification[11]. Dead regeneration model proves that some biodegradable substrate can be released by the excess sludge. Therefore the aim of this study is to investigate the usability of excess activate sludge and yeast residues as carbon sources.

2. MATERIAL AND METHOD

o   *Experimental Setup*

One laboratory scale column reactor and 7 sets of batch reactor were used in the study. Batch reactors are 150 ml opaque brown serum bottles. The reactors were inoculated with sludge from the continuous reactor and operated in a temperature controlled room at 30 ° C.

o   *Operational Conditions*

Batch reactors were installed after regular sulfate reduction in the continuous reactor was observed in the presence of ethanol. In the reactors, COD was provided with activated sludge and yeast residues. For this purpose, sludge taken from an activated sludge process in laboratory and an ethanol reactor was subjected to anaerobic digestion. The reactors were then installed with dissolved COD resulting from this digestion.. Accordingly, the sulfate concentration was kept at 2000 mg / L, while the COD concentration was varied between 600 and 1400 mg / L. After the installation of the reactors, sulfate, sulfur alkalinity and COD analyzes were performed regularly. In this way, the ability of excess activated sludge and yeast residue to reduce sulfate was revealed.

o   *Analytical Methods*

COD (closed flux method) sulfate and alkalinity were measured according to standard methods[12]. For COD tests, the sample pH first decreased to below 2 with concentrated H_2SO_4. It was then purged with N_2 gas for 5 min to remove H_2S[9]. Sulfate was measured according to a turbiditimetric method. A spectrophotometric method described by Cord-Ruwisch was used to measure sulfide[13]. A Hack – HQ 40d pH meter was used to measure pH.

3. RESULTS AND DISCUSSION

The variations of COD and sulfide for excess activated sludge are shown in Table 1. The initial COD was varied between 600 in reactor 1 and 1400 in reactor 5. There were also two control reactor one contains no COD and another contains no biomass.

According to Table 1., it could be seen that COD oxidation was performed in all reactors. For example, initial (0. Hour) and end (48. Hour) COD concentrations were 600 and 192 mg/L for reactor 1. Similarly the COD in the other reactors were also decreased to approximately 170 mg/L level.

As a result of COD oxidation, sulfate reduction was observed. As a proof of sulfate reduction, sulfide concentrations were monitored regularly and between 11.15 and 20.38 mg/L sulfide was produced as a result of sulfate reduction (Table 1).

Table 2 shows the similar data on yeast residues. When yeast residues were implemented to sulfidogenic reactors, COD oxidation was remained in a limited level. Although 600 mg/L COD containing reactor 1 was decreased to 284 mg/L in the end of 48 hours, the reactor containing 1400 mg/L was remained in the almost same level.

Although COD oxidation was remained in limited level, sulfide was observed in the end of reactors. The sulfide concentrations in the enf of 48 hour were varied between 6.12 to 8.83 mg/L.

Table 1. COD and Sulfide concentrations of excess activated sludge used reactors throughout the study.

Time / Reactor no	1	2	3	4	5	Control 1	Control 2
Excess Activated Sludge							
Chemical Oxygen Demand (COD)							
0	600	800	1000	1200	1400	1000	0
3	880	872	960	1240	1448	848	329,6
12	688	808	952	1168	1272	864	208
24	432	560	584	720	816	416	83,2
48	192	176	208	144	272	208	48
Sulfide							
0	0	0	0	0	0	0	0
3	7,63	7,9	9,995	10,23	14,8	3,41	0
12	2,785	3,56	5,655	6,895	7,6	1,7	0
24	7,98	9,14	10,305	10,77	12,86	6,04	3,56
48	11,155	14,1	13,95	14,72	20,38	8,06	2,2

Table 2. COD and Sulfide concentrations of excess activated sludge used reactors throughout the study.

Time / Reactor no	1	2	3	4	5	Control 1	Control 2
Excess Yeast Residues							
Chemical Oxygen Demand (COD)							
0	600	800	1000	1200	1400	1000	0
3	697,5	1094	1305	1529	1497	1574	48
12	828,5	1046	1286	1554,5	1638	1203	57
24	707,2	902,4	1141	1305,2	1484,5	1203	0
48	284,8	499,2	1027,2	1382,4	1484,8	1011	3,2
Sulfide							
0	0	0	0	0	0	0	0
3	7,2825	14,41	18,25	20,61	21,58	10,69	0,46
12	11,235	19,76	20,69	24,18	24,02	14,72	0,93
24	12,165	13,48	17,36	14,8	15,19	12,09	1,39
48	8,835	6,12	7,595	7,745	8,37	8,21	0,93

Although the batch reactors were not efficient and there was limited sulfide production, obtained COD (from excess activated sludge and excess yeast residues) was used to reduce sulfate in continuous reactors. The sulfate concentrations under ethanol fed, activated sludge fed and yeast residues fed periods were presented in Figure 1.
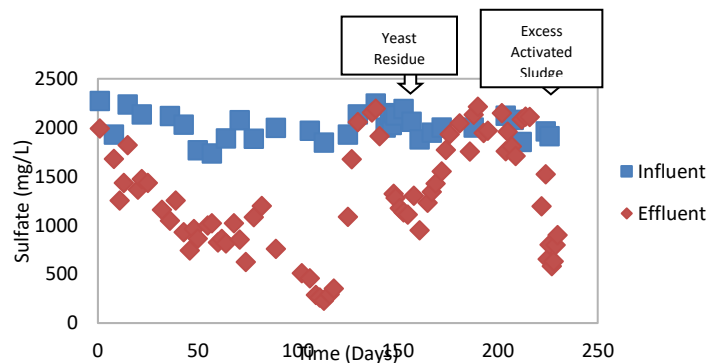

Figure 21. (a) Example of an unacceptable low-resolution image

REFERENCES

[1] F. Fu, Q. Wang, Removal of heavy metal ions from wastewaters: A review, J. Environ. Manage. 92 (2011) 407–418. doi:10.1016/j.jenvman.2010.11.011.

[2] K. Upadhyay, Solution for wastewater problem related to electroplating industry: an overview, J. Ind. Pollut. Control. 22 (2006) 59–66.

[3] R.M.M. Sampaio, R. a. Timmers, Y. Xu, K.J. Keesman, P.N.L. Lens, Selective precipitation of Cu from Zn in a pS controlled continuously stirred tank reactor, J. Hazard. Mater. 165 (2009) 256–265. doi:10.1016/j.jhazmat.2008.09.117.

[4] F. Glombitza, Treatment of acid lignite mine flooding water by means of microbial sulfate reduction, Waste Manag. 21 (2001) 197–203. doi:10.1016/S0956-053X(00)00061-1.

[5] E. Sahinkaya, F.M. Gunes, D. Ucar, A.H. Kaksonen, Sulfidogenic fluidized bed treatment of real acid mine drainage water, Bioresour. Technol. 102 (2011) 683–9. doi:10.1016/j.biortech.2010.08.042.

[6] D. Bhattacharya, A.B. Jumawan, G. Sun, C. Sund-Hagelberg, K. Schwitzgebel, Water 1980, in: AIChE Symp. Ser., New York, 1981: pp. 31–38.

[7] A. Bayrakdar, E. Sahinkaya, M. Gungor, S. Uyanik, A.D. Atasoy, Performance of sulfidogenic anaerobic baffled reactor (ABR) treating acidic and zinc-containing wastewater, Bioresour. Technol. 100 (2009) 4354–4360. doi:10.1016/j.biortech.2009.04.028.

[8] O.K. Bekmezci, D. Ucar, A.H. Kaksonen, E. Sahinkaya, Sulfidogenic biotreatment of synthetic acid mine drainage and sulfide oxidation in anaerobic baffled reactor, J. Hazard. Mater. 189 (2011) 670–676. doi:10.1016/j.jhazmat.2011.01.087.

[9] D. Ucar, O.K. Bekmezci, A.H. Kaksonen, E. Sahinkaya, Sequential precipitation of Cu and Fe using a three-stage sulfidogenic fluidized-bed reactor system, Miner. Eng. 24 (2011) 1100–1105. doi:10.1016/j.mineng.2011.02.005.

[10] M. Yildiz, T. Yilmaz, C.S. Arzum, A. Yurtsever, A.H. Kaksonen, D. Ucar, Sulfate reduction in acetate-and ethanol-fed bioreactors: Acidic mine drainage treatment and selective metal recovery, Miner. Eng. 133 (2019) 52–59.

[11] H. Sun, Q. Wu, P. Yu, L. Zhang, L. Ye, X.X. Zhang, H. Ren, Denitrification using excess activated sludge as carbon source: Performance and the microbial community dynamics, Bioresour. Technol. 238 (2017) 624–632. doi:10.1016/j.biortech.2017.04.105.

[12] APHA, AWWA, WEF, Standard Methods for the Examination of Water and Wastewater, 1999.

[13] R. Cord-ruwisch, A quick method for the determination of dissolved and precipitated sulfides in cultures of sulfate-reducing bacteria, J. Microbiol. Methods. 4 (1985) 33–36.

Bioreduction of Nitrate and Perchlorate in Thiosulfate Based Batch Bioreactor

Tulay Yilmaz[1], Amine Yucel[1], Erkan Sahinkaya[2], Deniz Ucar[1]

Abstract

Perchlorate (ClO_4^-) is salts derived from perchloric acid. Although formed by natural processes, perchlorate on earth is mainly produced commercially. Due to its low adsorption properties, it can easily reach to groundwater. Nitrate, on the other hand, is one of the most common pollutants and the most important sources of nitrate are domestic and industrial wastewater discharged without the use of agricultural fertilizers and nutrient removal. Nitrate causes a disease known as methemoglobinemia, which is characterized by higher than normal level of methemoglobin in blood (hemoglobin [Fe^{2+}] instead of nitrate oxidized methemoglobin [Fe^{3+}]). For these reasons, studies are carried out on the simultaneous removal of both pollutants. In this context present study aimed at investigating simultaneous reduction of nitrate and perchlorate in thiosulfate based denitrifying batch reactors. In this context a laboratory-scale 50 ml reactors were used to investigate the performance of 50 mg NO_3^--N/L reduction at varying perchlorate concentrations (50-2000 µg/L). The reactors were operated for 72 hours and regularly analyzed for nitrite, nitrate, perchlorate and sulfate. For all reactors, at the end of the 12th hour, high nitrate removal rates independent from influent perchlorate (over 90%) were observed. At the end of 24th hour, nitrate was completely removed in all reactors. Perchlorate in the reactors containing up to 50-300 µg/L and 500-1000 µg/L were completely removed within 48 and 72 hours, respectively. Sulfate was produced as a result of thiosulfate based denitrification and its concentration was varied between 512-792 mg SO_4^{2-}/L.

Keywords: *Perchlorate reduction, nitrate reduction, thiosulfate, autotrophic denitrification*

1. INTRODUCTION

Perchlorate (CIO_4^-) is the salt derived from perchloric acid. Perchlorate, which can contaminate drinking water sources via natural and anthropogenic sources, is used in the products such as air-bags, fireworks, military weapons such as missiles and rockets; and also pharmaceutical industries (such as the treatment of hyperthyroidism). It naturally forms from the chemical reaction between chlorine gas and ozone. Perchlorate can also be found in nitrate deposits in arid regions such as the Atacama Desert in Chile[1]. With the usage of these nitrates as fertilizer, perchlorate also can enter groundwater contaminated by nitrate fertilization[2].

Due to the high solubility and low adsorption properties of ammonium perchlorate, it can easily reach sources of drinking water. Perchlorate blocks the iodine uptake by the thyroid, decreasing the thyroid hormone (triiodothyronine-T3 and thyroxine-T4) concentrations in the body[3]. These hormones regulate basal metabolisms in adults and normal development processes in children. Therefore the presence of perchlorate in drinking water can trigger many diseases related to the basal metabolism.

Current remediation methods are classified into two sub-groups: removal or destruction[2]. While removal methods consist of ion exchange, membrane filtration and adsorption; destruction methods are chemical, electrochemical and biological reduction. Besides the additional chemical requirements for the reduction process, as well as the high costs and low efficiency that occur when other contaminants are present in the solution, the removal method has serious drawbacks, as concentrated brine is discharged. However, the biological reduction is the most common method, due to its fast reaction rate, not requiring expensive catalyst or chemicals. In many studies, CIO_4^- is biologically reduced to CI^- ions successfully[4].

---

[1] Corresponding author: Harran University, Gap Renewable Energy and Energy Efficiency Center, 63100, Haliliye/Sanliurfa, Turkey. denizucar@dharran.edu.tr

[2] Istanbul Medeniyet University, Bioengineering Department, Goztepe /Istanbul erkansahinkaya@gmail.com

Heterotrophic reduction of oxyanions is its fast and effective nature compared to autotrophic processes. Wang et al. (2013) compared the efficiency of hydrogen and acetate as electron donors for perchlorate reduction. For hydrogen and acetate, 15 and 8 days were required, respectively, for the reduction of 2.5 mg l^{-1} perchlorate[5]. However, If carbon is added at a concentration higher than the stoichiometric requirement, residual organic matter can stimulate bacterial growth in water distribution systems and contribute to the formation of disinfection byproducts during chlorination [6].

To overcome these problems, autotrophic perchlorate reducing bioreactors in which inorganic electron donors such as H_2 [7], Fe(0) [8] and elemental sulfur [6] have also been used as electron donors. Cao et al. (2005) investigated the perchlorate reduction with iron nanoparticles. The reaction was temperature dependent and the perchlorate reduction rate at 75°C was 1.52 mg perchlorate/(g nanoparticles.h). Although reaction is favorable in terms of thermodynamics (activation energy was calculated as 79.02 ± 7.75 kJ $mole^{-1}$), as authors noted, perchlorate reduction is limited by the slow kinetics [8]. Ju et al. (2008) tested the performances of various inoculums taken from aerobic or anaerobic environments with various electron donors. The reduction rate was 0.18 mM d^{-1} with S^0 and aerobic process sludge for electron donor and inoculum respectively. Reduction rates of Hydrogen and Fe^0 with the same inoculum were ≥ 0.37 mM d^{-1} on day 8 and 0.085 mM d^{-1} on day 37, respectively [6].

Another reduced sulfur compound is thiosulfate which is a water soluble compound. Studies also show that effective nitrate could be reduced by the thiosulfate based denitrification process. In this study, thiosulfate based simultaneous nitrate and perchlorate reduction were investigated.

2. MATERIAL AND METHOD

o **Experimental Setup**

In the study, a column reactor was operated under thiosulfate based denitrifying conditions. Before perchlorate to be added to column reactor, simultaneous nitrate and perchlorate reduction was investigated by batch reactors. To do that, eight set of reactor together with four control reactors were established. The reactors were 50 ml injectors equipped with 0.45 µm polyethersulfone injector filter to allow direct sampling from the reactor. The reactors were kept at 30 °C in temperature controlled room and sampled regularly. The sludge used in the reactors were taken from continuous column reactor.

o **Operational Conditions**

Each reactor was contained different concentrations of perchlorate. The concentrations were varied between 50 – 2000 µg/L. The operational conditions were presented in Table 1.

Table 1. The operational conditions.

Reactor No	Nitrate $(mg\ NO_3^--N/L)$	Perchlorate $(mg\ ClO_4^-)$	Inoculum	Electron Source (mg Na_2SO_3/L)
1	50	50	5 ml Sludge	744
2	50	100	5 ml Sludge	744
3	50	150	5 ml Sludge	744
4	50	200	5 ml Sludge	744
5	50	300	5 ml Sludge	744
6	50	500	5 ml Sludge	744
7	50	1000	5 ml Sludge	744
8	50	2000	5 ml Sludge	744
Control 1	50	-	5 ml Sludge	744
Control 2	0	5000	5 ml Sludge	744
Control 3	50	1000	-	744
Control 4	50	1000	5 ml Sludge	-

The reactors were sampled at the beginning of the study at the 6th, 12th, 24th, 48th and 72th hour intervals and nitrate, nitrite, perchlorate, sulfate analyzes were performed from these samples.

o *Analytical Conditions*

Nitrate, nitrite, sulfate and chloride, were analyzed by suppressed conductivity ion chromatography using Shimadzu HIC-SP system fitted with a DIONEX Ion-Pac AS9-HC column (4 mm x 250 mm). The chromatographic conditions were 1 ml/min flow rate, 50 µl injection volume, 40 °C column temperature. Perchlorate was measured by the same system (suppressed conductivity) with Ion-Pac AS20 column. The chromatographic conditions were 0.25 ml/min flow rate, 35 °C column temperature, 50 µl injection volume.

3. RESULTS AND DISCUSSION

Perchlorate concentrations are shown in Figure 1. In the end of 72-hour test, perchlorate concentration was below the measurable level in the first 7 reactors, while a 90% removal was observed for the reactor at an initial concentration of 2000 µg/L. In the reactor 1 having an influent concentration of 50 µg/L, 100% perchlorate removal was observed in 24 hours. Generally, after a period of 24 hours, the reactor containing 50 µg/ L perchlorate; At the end of 48 hours, 100% perchlorate removal was observed. In the end of 72 hours period, 90% removal in the reactors containing up to 1000 µg/ L perchlorate was observed. Inoculum-free and thiosulfate-free reactors indicate that the process is thiosulfate-based reduction.
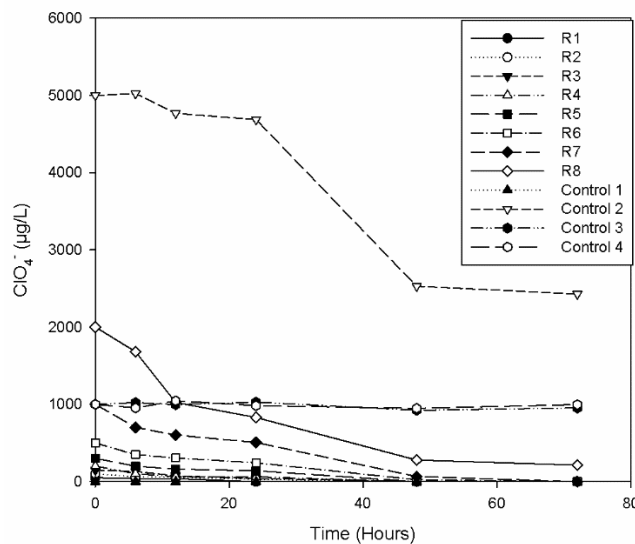

Figure 1. Perchlorate concentrations throughout the study

Nitrate reduction process is presented in Figure 2. In the experiments, no negative effect of perchlorate on nitrate removal was observed for thiosulfate based reactor. Nitrate removal rates were observed for all reactors at the end of 12 hours independent of the influent perchlorate concentration and 100% nitrate removal was observed at all reactors after 24 hours. A negligible nitrate removal in the control reactor without control sludge addition (Control 4) and a reduction of 20% in the control reactor without thiosulfate added (Control 3) indicates that the process is thiosulfate based and biological. The 20% treatment in the reactor without thiosulfate can be explained by the endogenous decay and biodegradable substrate release by the inoculum. In the reactors, 0 - 5 mg NO_2^--N/L concentration was observed during the first 12 hours and in other samples nitrite was below the measurable level.
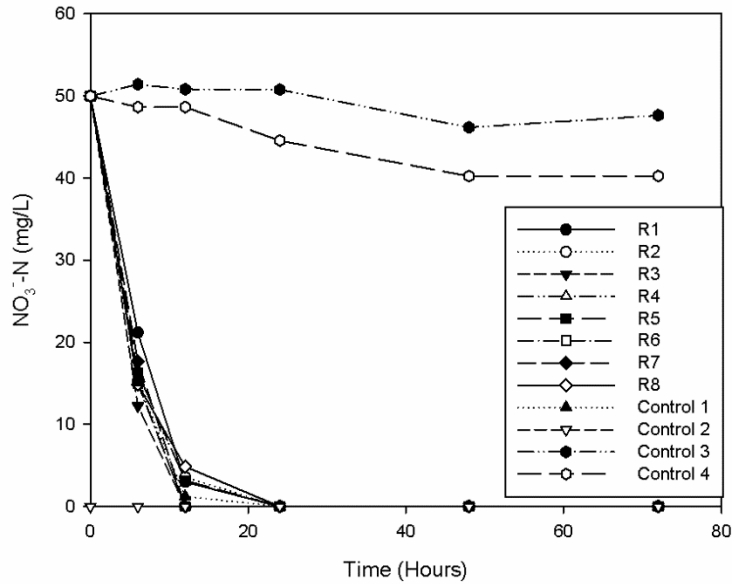
Figure 2. Nitrate concentrations throughout the study

Sulfate was produced as a result of thiosulfate based denitrification process. Simultanously with the nitrate reduction process, the concentration increased during the first 24 hours. No increase in sulfate concentration was observed in the nitrate-free control reactor. In the first 8 reactors, produced sulfate were between 512 to 792 mg SO_4^{2-}/. In the thiosulphate-based reduction process, considering that 11.06 g of sulfate is produced per gram of nitrate nitrogen, theoretically 553 mg/L sulfate is expected to form. Reactions such as sulfate reduction, oxidation of thiosulfate with oxygen in the reactors are factors that may produce slightly different results from the theoretical value.
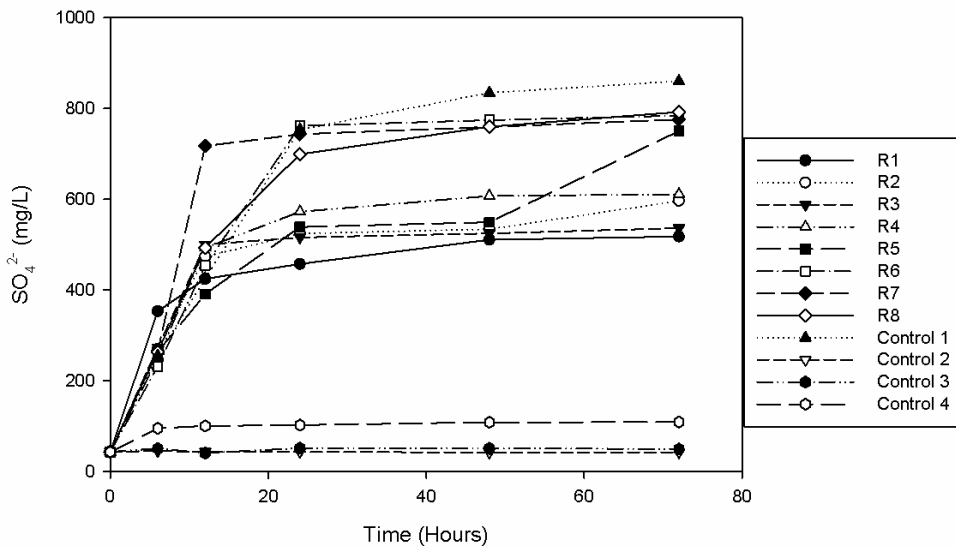

Figure 3. Sulfate concentrations throughout the study

ACKNOWLEDGMENT

REFERENCES

[1] D.C. Catling, M.W. Claire, K.J. Zahnle, R.C. Quinn, B.C. Clark, M.H. Hecht, S. Kounaves, Atmospheric origins of perchlorate on mars and in the atacama, J. Geophys. Res. E Planets. 115 (2010) 1–15. doi:10.1029/2009JE003425.

[2] R. Srinivasan, G.A. Sorial, Treatment of perchlorate in drinking water: A critical review, Sep. Purif. Technol. 69 (2009) 7–21. doi:10.1016/j.seppur.2009.06.025.

[3] M.A. Greer, G. Goodman, R.C. Pleus, S.E. Greer, Health effects assessment for environmental perchlorate contamination: the dose response for inhibition of thyroidal radioiodine uptake in humans., Environ. Health Perspect. 110 (2002) 927–37. http://www.pubmedcentral.nih.gov/articlerender.fcgi?artid=1240994&tool=pmcentrez&rendertype=abstract (accessed September 10, 2014).

[4] N. Bardiya, J.-H. Bae, Dissimilatory perchlorate reduction: a review., Microbiol. Res. 166 (2011) 237–54. doi:10.1016/j.micres.2010.11.005.

[5] R. Wang, M. Chen, J.W. Zhang, F. Liu, H.H. Chen, Microbial Perchlorate Reduction in Groundwater with Different Electron Donors, in: Appl. Mech. Mater., 2013: pp. 1402–1407.

[6] X. Ju, R. Sierra-Alvarez, J. a Field, D.J. Byrnes, H. Bentley, R. Bentley, Microbial perchlorate reduction with elemental sulfur and other inorganic electron donors., Chemosphere. 71 (2008) 114–22. doi:10.1016/j.chemosphere.2007.09.045.

[7] M.C. Ziv-El, B.E. Rittmann, Systematic evaluation of nitrate and perchlorate bioreduction kinetics in groundwater using a hydrogen-based membrane biofilm reactor, Water Res. 43 (2009) 173–81. doi:10.1016/j.watres.2008.09.035.

[8] J. Cao, D. Elliott, W. Zhang, Perchlorate Reduction by Nanoscale Iron Particles, J. Nanoparticle Res. 7 (2005) 499–506. doi:10.1007/s11051-005-4412-x.

Sol-Gel Synthesis And Characterization Of Titanium Dioxide Powder

Deniz Coban Ozkan[1], Salih Alper Akalin[2], Ahmet Turk[3], Erdal Celik[4]

Abstract

Titanium Dioxide is a semiconductor that widely used in many areas and has three different crystal structures with different properties. TiO_2 can be synthesized with many different methods. The aim of this study is to synthesize titanium oxide as nano powder by Sol-Gel method and characterize it with various methods.

Keywords: TiO2, Sol-Gel, Powder

1. INTRODUCTION

Titanium Dioxide (TiO_2) is a semiconductor with a wide range of usage areas. Due to its chemical and photochemical stability, photoactive properties, good optical transparency, low cost, high refractive index and non-toxicity properties, it is preferred for water purification, self-cleaning, non-fogging surfaces and solar cells. TiO_2 can be synthesized with many different methods such as Chemical Vapor Deposition (CVD), Sputtering, Pulsed Laser Deposition, Electron Beam Evaporation, Ion Beam Assisted Deposition and Sol-Gel. Sol-Gel, among these methods, is a technique used in the production of thin film and powder by the use of simple devices at low temperature. Although TiO2 has three different crystal structures: anatase, rutile and brookite, the photoactivity of the anatase phase is better than the others. The anatase phase of titanium oxide was synthesized as nano powder by Sol-Gel method which consists of three steps, these are solution, gelation and annealing. Titanium isopropoxide was used for precursor material which is added in ethanol while acetic acid was added to adjust ph value of solution then the solution was heated up for gelation on the heat plate. The gel was heated to 500oC to obtain crystalline structure according to the results of Differential Thermal / Thermogravimetric Analysis (DTA/TG). The structural and morphological properties of powder were characterized by X-ray Diffraction (XRD) and Scanning Electron Microscopy (SEM), respectively (1-6).
In this study, the anatase phase of titanium oxide was synthesized as nano powder by Sol-Gel method and and characterized by different methods.

2. TITANIUM DIOXIDE SYNTHESIS AND CHARACTERIZATION

The anatase phase of titanium oxide was synthesized as nano powder by Sol-Gel method which consists of three steps, these are solution, gelation and annealing.

Titanium (IV) isopropoxide was used as the source of titanium in the synthesis of titanium dioxide. Titanium (IV) isopropoxide, which is added to ethanol, is stirred in the magnetic stirrer for about 30 minutes, then acetic acid is added thereto and the mixture is stirred for a further 30 minutes (Fig 1).

---

[1] *Corresponding author: Manisa Celal Bayar University, The Institute Of Natural And Applied Sciences, Turkey.*
deniz.coban@cbu.edu.tr.
[2] *Dokuz Eylul University, Graduate School Of Natural And Applied Sciences, Izmir Turkey.*
[3] *Manisa Celal Bayar University, Metallurgy And Materials Engineerin, Turkey.*
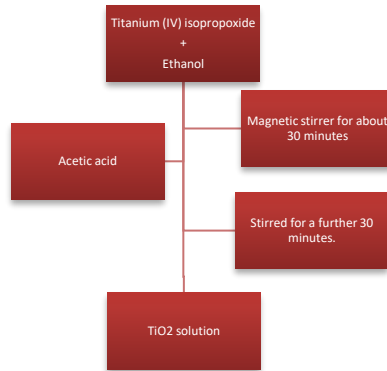[4] *Council of Higher Education, Bilkent, Ankara. Turkey.*

Figure 1. Synthesis steps of titanium dioxide.

When turbidity and pH values of the solution were checked after synthesis; turbidity value: 0.64 ntu and ph value: 5.5. These results indicate that the solution was successfully prepared.

In order to determine the bond structures in the prepared solution, fouirer transform infrared spectrography(FTIR) analysis was performed. As seen in figure 2, the material in the form of gel appears to have carbon and hydrogen bonds in the structure at about 1500 wavenumbers cm^{-1}.
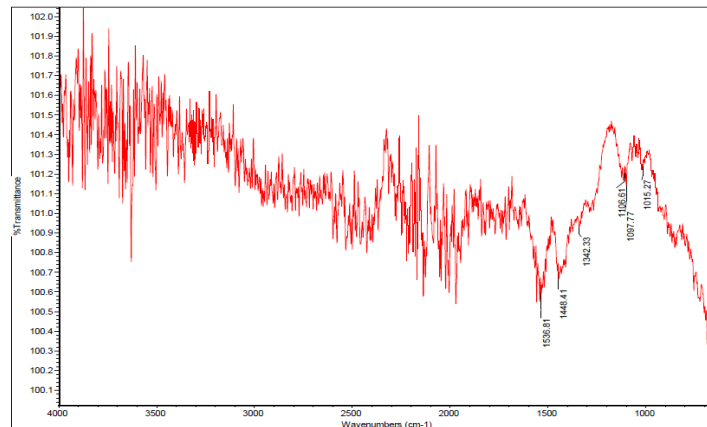

Figure 2. FTIR analysis of titanium dioxide before heat treatment.

In order to calculate the particle size of nano powder before heat treatment, scanning electron microscopy images of dried gel (about 100 degrees) are given. It is seen that the grain size of this roughly ground powder is around 200-400 nanometers (Fig 3).
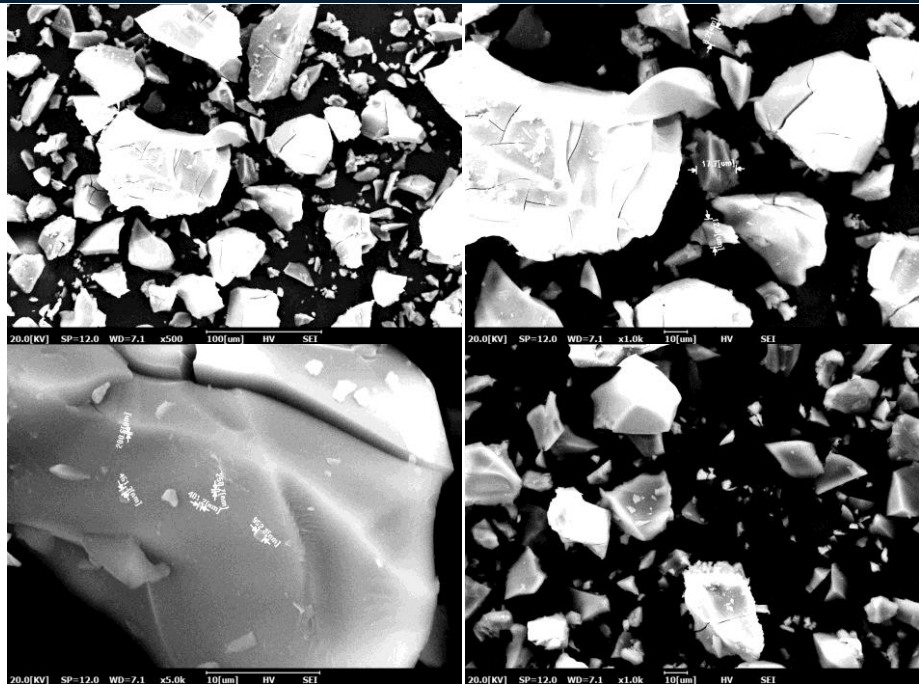
Figure 3. Scanning electron microscopy images of dried gel.

According to determine the heat treatment temperature of the gel, Differential Thermal / Thermogravimetric Analysis was performed. Exothermic peak is observed at about 450 degrees Celsius. Therefore gel was heated to 500°C to obtain crystalline structure according to the results of DTA/TG (Fig 4).
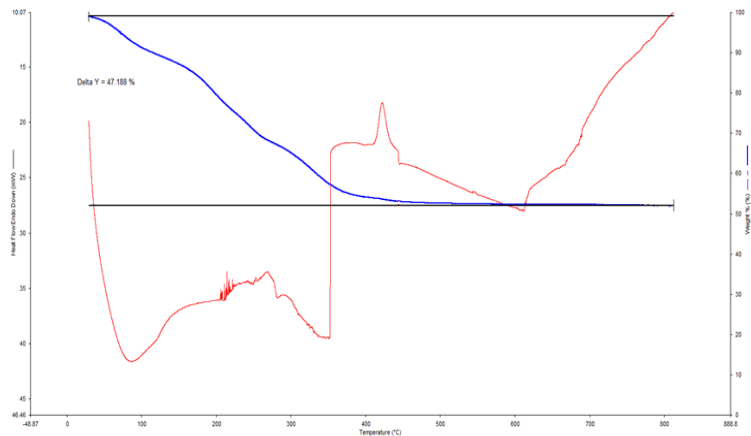

Figure 4. Differential Thermal / Thermogravimetric Analysis

After the heat treatment FTIR analysis was performed. As a result of the analysis, it is seen that undesirable bonds such as carbon and hydrogen are removed (Fig 5).
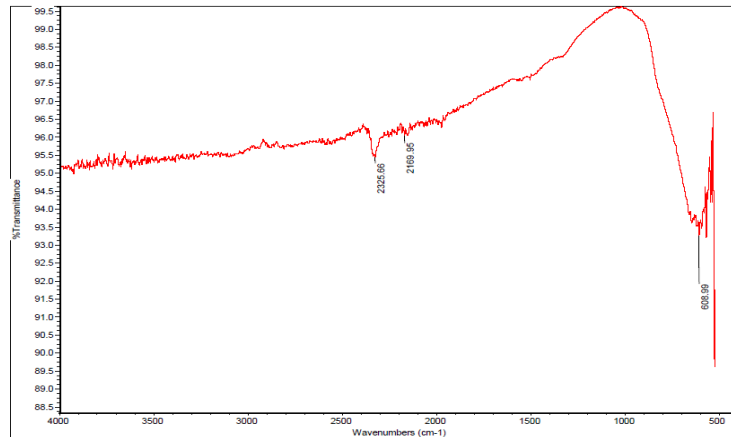
Figure 5. FTIR analysis of titanium dioxide.

Scanning electron microscopy images of powder are given. It is seen that the grain size of this roughly ground powder is not change and still around 200-400 nanometers.
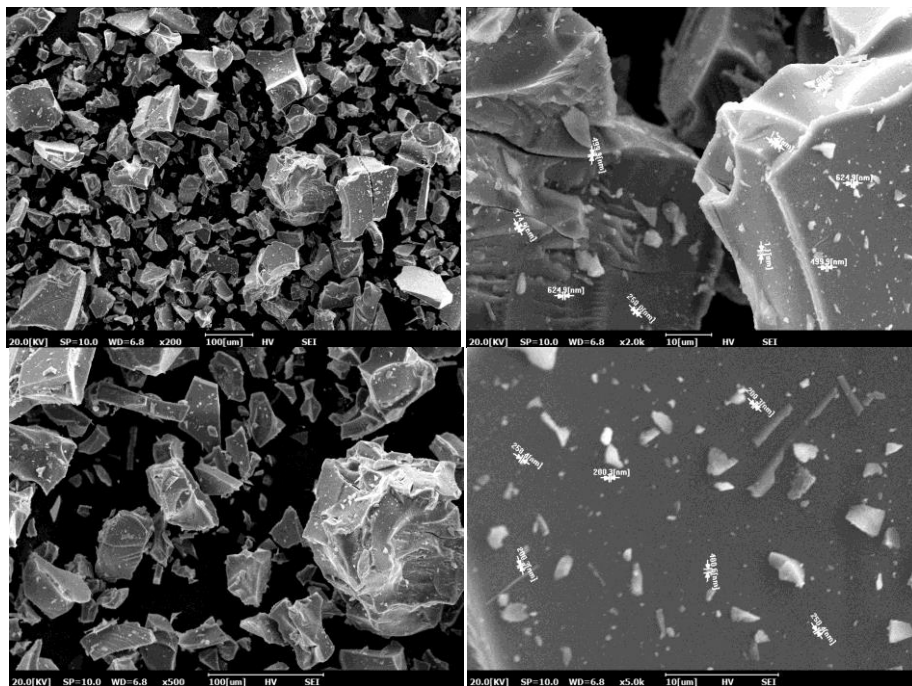
Figure 6. Scanning electron microscopy imags.

X-Ray Diffraction analysis was performed in order to check whether the titanium dioxide powders we synthesized are in the desired phase and structure. As a result of the search result of the material we synthesized, TiO_2 powders are in the anatase phase.

Figure 7. X-Ray Diffraction of TiO2.

CONCLUSION

The aim of this study was to obtain the anatase phase phase of titanium oxide and synthesis of the powder was carried out by sol-gel method. Solution passed to the gel form on a hot plate at about 100 degrees centigrade and was allowed to dry. Heat treatment was carried 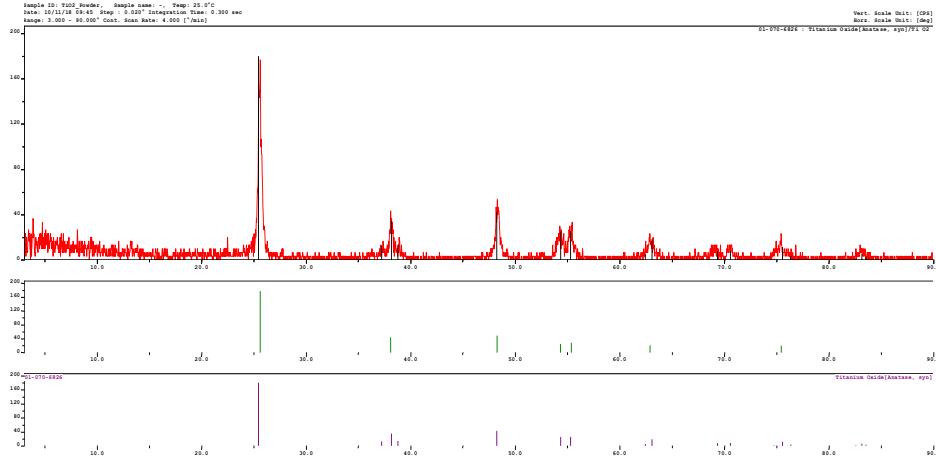out according to the result of DTA / TG. Before and after heat treatment, FTIR analysis and SEM images were taken and changes of the bonds in the structure and possible particle size changes were obtained. It has been proved that we obtain the anatase phase of TiO_2 after obtaining the XRD results of the synthesized powder.

REFERENCES

[1].   Nataraj, J. R., Bagali, P. Y., Krishna, M., Vijayakumar, M.N. Development of Silver Doped Titanium Oxide Thin films for Gas Sensor Applications, Materials Today: Proceedings, 5(4(3)), 10670-10680, 2018.
[2].   Kang, M., Kim, S. W., Park, H. Y., Optical properties of TiO2 thin films with crystal structure, Journal of Physics and Chemistry of Solids, 123, 266-270, 2018.
[3].   Pan, T., Cao, W., Wang, M. TiO2 thin film temperature sensor monitored by smartphone, Optical Fiber Technology, 45, 359-362, 2018.
[4].   Bian, L., Song, M., Zhaou, T., Zhao, X., Dai, Q. Band gap calculation and photo catalytic activity of rare earths doped rutile TiO2, Journal of Rare Earths, 27(3), 461-468, 2009.
[5].   Bogle, K. A., More, K. D., Dadge, J. W., Mahabole, M. P., Khairnar, R. S. Nano-crystalline TiO2 thin film: Synthesis and investigation of its optical switching characteristics, Thin Solid Films, 653, 62-66, 2018.
[6].   Demirci S., Dikici T., Yurddaskal M., Gultekin S., Toparli M., Celik E., Synthesis and characterization of Ag doped TiO2heterojunction films and their photocatalytic performances, Applied Surface Science 390 (2016), 591–601.

Investigation of the Coloration Processes of Hawthorn (*CrataegusMonogyna*) on Woolen Fabrics

Fazlihan Yilmaz[1], M.Ibrahim Bahtiyari[2], Huseyin Benli[3]

Abstract

The fruits of the hawthorn plant were selected as the source of natural dyestuff for wool fabrics in this study. The fruits of hawthorn have been firstly used in dyeings without use of any mordanting agents but in addition to the mordant-free dyeing processes, dyeings were also carried out by using different concentrations of FeSO4.7H2O or SnCl2.2H2O mordanting agents. After the dyeing processes; washing and light fastness of the dyed samples were tested and the obtained colors were measured by a spectrophotometer. Different color shades were found from the use of this natural dye source with the use of different mordanting agents and as a result, it was determined that hawthorn fruit can be a natural dye source.

Keywords: Wool, hawthorn fruit, mordant, dyeing, color

1. INTRODUCTION

Natural dyes, obtained from plants, insects/animals and minerals, are renewable and sustainable bioresource products with minimum environmental impact and known since antiquity for their use, not only in coloration of textiles [1]. Since natural dyes are biodegradable and less toxic and allergenic than synthetic dyes, they are considered to be environmentally friendly. Although synthetic dyeing methods have taken over in the last century, dyeing materials are still abundant in the natural world today. The global demand for natural dyes per year is about 10,000 tonnes, which is equivalent to 1% of the world synthetic dye consumption [2]. As the present trend throughout the world is shifting towards the use of ecofriendly and biodegradable commodities, the demand for natural dyes is increasing day by day [3].

In textile dyeing operations a re-introduction of natural dyes is of interest due to increased attention to water pollution, sustainability of raw materials and products, biodegradability and environmental aspects [4].

Hawthorn (Crataegus spp.), a member of the Rosaceae family, is a thorny shrub/small tree commonly found in hedgerows that produces pink or white flowers in spring and red berries in autumn [5]. Hawthorn (*Crataegus*), found in northern temperate regions such as East Asia, Europe, and Eastern North America, is a genus of the Rosaceae family [6].

2. MATERIALS AND METHODS

2.1. Materials

Wool fabrics, which were ready for coloration, with a weight of 160 g/m^2 was used in this study. Hawthorn was obtained from herbal markets. After the hawthorn supply, it was dried in the shade and milled in the mill. The milled part was used for dyeing.

[1]*Corresponding author: Erciyes University, Department of Textile Engineering, 38039, Kayseri, Turkey,* *fazlihanyilmaz@erciyes.edu.tr*

[2] *Erciyes University, Department of Textile Engineering, 38039, Kayseri, Turkey, ibahtiyari@yahoo.com*

[3] *Kayseri University, Mustafa Cikrikcioglu Vocational School, 38280, Kayseri, Turkey. hbenli@kayseri.edu.tr*

Figure 1. Dried *CrataegusMonogyna* fruit

Figure 2. Grinded *CrataegusMonogyna* fruit
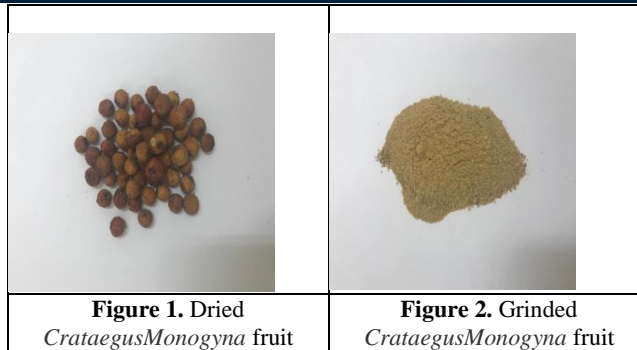
2.2. Method

Dyeing experiments with hawthorn fruit were carried out according to together mordant method. That is, the dyestuff source, fabric and mordant materials are all put into the dyeing bath and dyeing experiments were done. Dyeing experiments were also done without any mordant material. The ground plant dye source was used directly in dyeing processes. Iron (II) sulfate ($FeSO_4.7H_2O$) and Tin (II) chloride ($SnCl_2.2H_2O$) were used as mordant. These mordant materials were used in 3 different concentrations (1%, 3%, 5%) in proportion to the weight of the fabric. In dyeing experiments with mordant, an equal amount of plant dye source was used with the weight of fabric (1:1). In dyeing experiments without mordant, plant dyestuff were used in ratio of 1:1 and 1:3 in proportion to fabric weight. The fabric was treated in a dye bath for 15 minutes at 45°C and then the bath was heated to 100°C for 30 minutes. As a result, dyeing was carried out for 80 minutes at 100 degrees. After dyeing, the fabrics were washed and dried at room temperature.
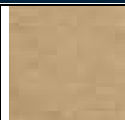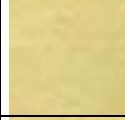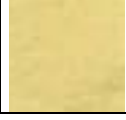
The dyed fabrics were analyzed in terms of color efficiencies (K/S) and color values (CIE L*a*b*) with the help of spectrophotometer. Moreover, the washing fastness with ISO 105-C10 standard in test condition of Test A (1) [7] and light fastness with ISO 105-B02 standard [8] were evaluated too.

3. RESULTS AND DISCUSSION

The K/S and CIE L*a*b* values of the dyed fabrics are shown in Table 1. The colors obtained are also presented in Table 1 too.

Table 1. CIELAB (L*, a*, b*, C*ve h°) and K/S values of the samples

Mordant type	CIE L*a*b* (D65)						Colors
	K/S	L*	a*	b*	C*	h⁰	
No mordant (1:1)	2.07	68.63	7.97	20.53	22.02	68.79	
No mordant (1:3)	3.9	61.68	10.96	24.2	26.57	65.63	
Iron (II) sulfate (%1)	2.14	67.58	7.62	19.87	21.28	69.02	
Iron (II) sulfate (%3)	2.13	66.75	5.45	18.19	18.99	73.33	

Iron (II) sulfate (%5)	2.05	67.99	6.19	18.95	19.93	71.89	
Tin (II) chloride (%1)	3.5	74.03	0.67	27.35	27.36	88.6	
Tin (II) chloride (%3)	3.09	81.13	-1.21	33.77	33.79	92.04	
Tin (II) chloride (%5)	3.44	80.39	-1.2	37.04	37.06	91.85	

When K/S values are examined, the lowest values are 2.05 and 2.07. The K/S:2.05 was achieved by using 5% iron (II) sulfate and the 2.07 value was obtained in a 1:1 dyeing experiment without the use of mordant. The highest K/S value is 3.9 which was reached by using plant dye source at a ratio of 1:3 without using mordant material. So it can be told that by the increase of the natural dye source concentration the color efficiencies of the samples can be increased. The K/S values of samples dyed with iron sulfate mordant showed that the color efficiencies were nearly same even in the use of different concentration of iron based mordant. This situation can also be said in dyeing experiments using tin (II) chloride mordant as well.

The colors obtained during the dyeing process using hawthorn fruit were also examined and it was also found that brown and yellow shades were obtained depending on the mordant. Brown tones were observed in dyeing experiments using without mordant material and also in dyeing experiments using iron (II) sulfate mordant however the color and shades of yellow were obtained in dyeing experiments in which tin (II) chloride were used as mordant. For example; in the experiments performed with 1:3 dyeing concentration without using any mordant, the values: $a^* = 10.96$, $b^* = 24.2$ and $h^o = 65.63$ were measured and the color is perceived as brown. But in the dyeing experiment using 5% tin (II) chloride mordant, the color is yellow and $a^* = -1.2$, $b^* = 37.04$ and $h^o = 91.85$.

Table 2. The fastnesses of the dyed samples

Mordant Agent	Light	Washing	
		C.C.	5
No mordant (1:1)	4	Sta.	5
	4-5	C.C.	5
No mordant (1:3)		Sta.	5
		C.C.	5
Iron (II) sulfate (%1)	4	Sta.	5
		C.C.	5
Iron (II) sulfate (%3)	4	Sta.	5
		C.C.	5
Iron (II) sulfate (%5)	4	Sta.	5
		C.C.	5
Tin (II) chloride (%1)	4	Sta.	5
		C.C.	5
Tin (II) chloride (%3)	3-4	Sta.	5
		C.C.	5
Tin (II) chloride (%5)	3-4	Sta.	5
***Sta.:** Staining on wool;* ***C.C.:** Color Change*			

When the light and wash fastness values in Table 2 are examined, it is possible to say that the washing fastness values are quite good/perfect. Because all values in terms of both the reference fabric contamination and color change were found minimum/limited so the fastness value was 5 however the light fastness values were moderate and it was seen that nearly similar values between the samples were obtained.

4. CONCLUSIONS

Nowadays, the popularity of environmentally friendly products has increased and the production of these products has gained importance. In this study, it was investigated whether it is possible to use hawthorn fruit as a source of natural dyestuff for woolen fabrics. It was determined that hawthorn fruit was able to color woolen fabrics and showed sufficient fastness to use.

REFERENCES

[1]. M. Shahid,S. U. Islam, F. Mohammad, "Recent advancements in natural dye applications: a review" Journal of Cleaner Production, vol. 53, pp. 310-331, 2013.

[2]. N. Punrattanasin, M. Nakpathom, B. Somboon, N. Narumol, N. Rungruangkitkrai, R. Mongkholrattanasit, "Silk fabric dyeing with natural dye from mangrove bark (rhizophoraapiculatablume) extract" Industrial Crops and Products, vol. 49, pp. 122-129, 2013.

[3]. S. Ali, T. Hussain, R. Nawaz," Optimization of alkaline extraction of natural dye from henna leaves and its dyeing on cotton by exhaust method" Journal of Cleaner Production, vol. 17, pp. 61-66, 2009.

[4]. S. Komboonchoo, T. Bechtold, "Natural dyeing of wool and hair with indigo carmine (c.i. natural blue 2), a renewable resource based blue dye" Journal of Cleaner Production, vol. 17, pp. 1487-1493, 2009.

[5].E. Shortle, M. N. O. Grady, D. Gilroy, A. Furey, N. Quinn, J. P. Kerry, "Influence of extraction technique on the anti-oxidative potential of hawthorn (crataegusmonogyna) extracts in bovine muscle homogenates" Meat Science, vol. 98, pp. 828-834, 2014.

[6].A. S. Jalali, S. Hasanzadeh, H. Malekinejad, "Crataegusmonogyna aqueous extract ameliorates cyclophosphamide – induced toxicity in rat testis: stereological evidences" ActaMedicaIranica, vol. 50 (1), pp. 1-7, 2012.

[7] ISO 105-C10:2006, Textiles–Tests for color fastness - Part C10: Color fastness to washing with soap or soap and soda, Test Condition: Test A (1), International Organization for Standardization, Geneva, Switzerland.

[8] ISO 105-B02:1994, Textiles–Tests for color fastness, Part B02: Color fastness to artificial light, International Organization for Standardization, Brussels, Belgium.

An Application for Performance Management in Construction Projects

Aynur Kazaz[1], Ersan Erkovan[2], Serdar Ulubeyli[3]

Abstract

In today's intense competition environment, businesses must always perform highly in order to achieve their goals. It is obvious that the monitoring, evaluation and measurement or management of the performances of both the enterprises and their employees will increase the performance of the enterprise in a positive way in the future. In particular, the construction projects in the construction sector, where competition is intense, and technology is advancing rapidly, need performance management due to their complex structure and intensive manpower. Monitoring, evaluating and measuring the performance of the construction projects is very important for the completion of the project in the desired success criteria. In this study, first of all, a literature study on performance management will be made and brief information will be given. Then, a web-based computer program, which is also a subject of academic study, will be presented as an application proposal for performance management of construction projects.

Keywords: Performance Management, Performance Evaluation, Performance Measurement.

1. INTRODUCTION

The construction sector is one of the fastest developing sectors. It is an important industry branch at the global and national level. Construction projects provide many investment opportunities to sectors such as tourism, industry and energy. Therefore, the construction sector is an important economic indicator for developing countries. In our country, the construction sector plays a vital role for the country both in economic growth and employment. Today, developments and innovations that occur in terms of technology and administration necessitate construction companies to manage their business processes much better. In order to evaluate these processes, companies should be able to see their own good and missing aspects.

With the establishment of performance management systems, it is ensured that these processes can be managed more effectively. Leading businesses know that the difference between success and failure is a powerful performance management system. Because, thanks to the performance management system, businesses can monitor how much they have reached their goals and objectives, create a quantitative decision-making environment, establish effective motivation systems by evaluating their employees more objectively, and increase quality and productivity by providing customer satisfaction. The establishment and execution of effective performance evaluation systems depend primarily on the human resources departments, including the managers, and the fulfillment of the responsibilities of those assessed [1].

Performance management is a systematic management tool consisting of phases which are agreed objectives, performance standards, targets, measurement, feedback, reward, etc. to aim that motivating employees to realize their own potential, to achieve more effective results from organizations, teams and employees [2].

In this study, first of all, a literature study on performance management will be made and brief information will be given. Then, a web-based computer program, which is also a subject of academic study, will be presented as an application proposal for performance management of construction projects.

[1] *Corresponding author: Akdeniz University, Department of Civil Engineering, 07070, Konyaalti/Antalya, Turkey.* akazaz@yahoo.com

[2] *Akdeniz University, Department of Civil Engineering, 07070, Konyaalti/Antalya, Turkey.* ersan_erkovan@yahoo.com

[3] *Bulent Ecevit University, Department of Civil Engineering, 67100, Zonguldak, Turkey.* ulubeyli@beun.edu.tr

2. PERFORMANCE CONCEPT

Performance is expressed as doing business, successful implementation in general terms. It is stated that performance, which is the main criterion in the measurement of success, is a broad concept that enables an organization to measure its success in achieving its objectives [3].

The development of the concept of performance is based on World War II. In order to meet the high demand in this period to a certain extent, it has necessitated a high rate of utilization of the resources. In this case, the importance of efficiency has come to the fore. It is suggested to offer the product or service to the customer at a lower cost [4]. Performance is a concept in which what is achieved in a planned way in a general sense is defined as a quantity or attribute [5]. It is possible to mention not only success but also failure with the concept of performance [6]. The concept of performance is closely related to the realization of a specific goal, the execution of a specific task or job. Performance is defined as the quantity or qualification of a planned activity [7].

The performance of any work refers to the result obtained from that work or output from that job within a specified period of time. This result is expressed as the proper implementation of the objectives of the institution. Therefore, the performance of a business can be defined as all efforts to achieve the objectives of the enterprise [8].

o *Performance Measurement*

Performance measurement in performing products, services or transactions, it is the method of measuring how tasks are performed objectively within a program [9]. Performance measurement, determination of the performance level of the organization, that is, in the activities of the organization and resource utilization, economy, efficiency, etc. measuring the extent to which the principles can be reached is a fundamental approach to identifying and taking the necessary measures to improve the problems.

Performance needs to be systematically measured and evaluated. For this purpose, firstly, objectives and optimum performance indicators and standards should be determined to allow an objective assessment based on comparison, data collection and measurement with these data [2].

The seven criteria to be used in the measurement of performance are described below [2].

- **Quality:** The following dimensions can be mentioned in the measurement of quality; quality of people, quality of management, quality of products and services. These specified quality dimensions can be further analyzed more specifically. For example, incorrect product rate, machine failure, returned product rate, delays in the delivery time of the product to the customer, service related complaints and so on can be taken into consideration in measuring the quality of the product.

- **Efficiency:** In general, productivity refers to the relationship between production outcome (output) and production factors (input). When efficiency is mentioned; labor productivity, capital efficiency, total factor productivity and so on efficiency dimensions need to be dealt with individually.

- **Profitability:** In the simplest terms, profitability is the ratio of earnings to the capital used to achieve this gain. The concept of profitability can also be divided into some sub-groups in technical terms. For example, sales profitability, equity, gross sales, net profit for the period, operating profit/loss, pre-tax/post-tax profit, etc. profitability dimensions can be considered and measured.

- **Cost:** Organizational performance can be measured by looking at some basic cost indicators in the organization. Labor cost, capital cost, production cost, financing cost, material cost, etc. can be shown as an example in this regard.

- **Innovation:** One of the criteria that can be used to measure organizational performance is innovation. New discoveries in the organization, new products, life cycle of products etc. On the basis of criteria, it can be determined to what extent innovation and creativity exist in the organization.

- **Customer Satisfaction:** In order to measure customer satisfaction, some criteria such as customer complaints, number of new customers, delivery time of orders, delivery of faulty goods can be taken as basis.

- **Employee Satisfaction:** In terms of employee satisfaction, performance indicators such as absenteeism, labor turnover rate can be looked at.

These performance criteria or performance indicators can also be sub-divided within themselves (Figure 1).
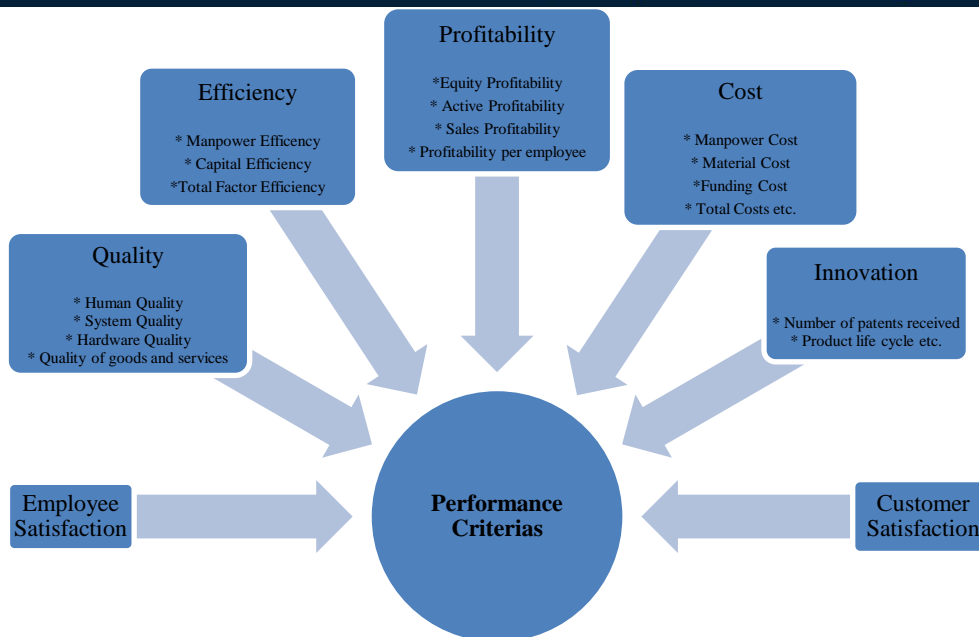
Figure 1. Main indicators for evaluating and measuring the performance of organizations

o **Performance Management**

Performance management is a process in which the results achieved by an organization are evaluated together by means of the way in which it achieves its predetermined objectives and targets [11]. According to another definition, performance management can be expressed as follows. Performance management for business is defined as a "strategic and integrated approach to increase the effectiveness of companies by improving the performance of the people who work in them and by developing the capabilities of teams and individual contributors [12].

For a successful performance management, the performance management process needs to be designed very well. It is useful to comply with the following principles in the processes related to performance evaluation and measurement in the organization [13].

- A plan for performance improvement in the organization should be developed.

- The objectives of the performance improvement plan should be determined.

- Existing performance in the organization should be evaluated and measured. Problems in performance should be identified. Information about quality should be collected in the organization.

- The gap between the current performance level and the desired performance level should be determined.

- Analysis should be made on how to evaluate the new information needed to improve performance and how to use the data effectively.

- The design and development of the knowledge possessed must be ensured.

- Methods and techniques for performance evaluation and measurement should be determined.

- Performance evaluation and measurement should be performed. In the context of the data obtained, the performance of the organization should be continuously improved.

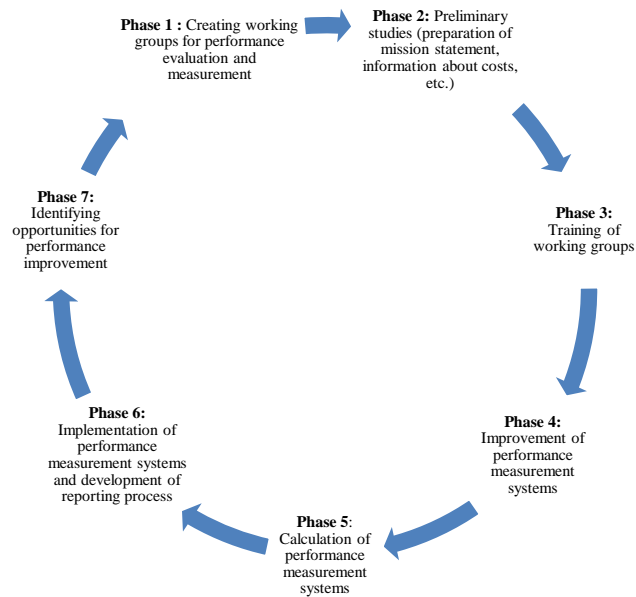The performance management process is shown below (Figure 2) [14].

Figure 2. The Performance management process

On the other hand, the organization needs to adopt some basic principles for the success of performance management systems. We can summarize the principles on this subject as follows [15]:

- The system should provide information about performance situations related to the internal and external environment of the enterprise.

- The system should create a motivation for the development of the enterprise. The system should be able to explain the behavior of executives, decision making and the relationship between objectives and functions in the management process. Measurement results should be communicated not only to the relevant managers but also to the employees and provide the opportunity to learn their accomplishments and correct themselves.

- The system should not contain too much or too little information that could lead to misunderstandings or missing important issues. Both are equally inconvenient.

- The information provided by the system must be easily understood and acceptable to the users. The same is true for those measured. For this purpose, all relevant segments should be included in the system design and implementation. As the level of participation increases quantitatively and qualitatively, approval and support also grow to that degree. Validation is the basic requirement for performance improvement purposes.

- The system should have the power to refute the defense and counter-arguments in the face of the adverse or unexpected results.

- The system must provide the information on time, provide sufficient time between the presentation of the information and the making and implementation of the necessary decisions. For this purpose, measurement systems should be provided to a regular and continuous structure.

- The system should have a structure that will determine the changes in the performance realistically. The selected indicators should really fit in the performance areas to be measured. Most of the indicators allow for partial measurements such as efficiency indicators. This leads to a one-way evaluation of events. Therefore, either a wide variety of indicators should be used in a holistic structure or total performance measurement methods should be used.

- Too much certainty to search for measurements can force the system. Working with average values can sometimes cause significant improvements to be overlooked. Measurements must be selected between these two extremes.

- Measurement systems must have a flexible and dynamic structure that is sensitive to changes in internal and external conditions. It should be known that the problem of the future cannot be solved with the methods of the past, the system should be constantly monitored. Instead of partial corrections in the system, new measurement systems should be developed in accordance with the changing conditions of the organization.

- An important condition in a performance measurement system is the definition unit. The information transmitted by the system should be perceived and interpreted in the same way in the internal and external environment. For example, the percentage of sales per employee should be determined precisely whether sales will be gross, taxed or discounted.

- Cost effectiveness of the system should be provided. For this purpose, it should be kept as simple as possible, and the existing facilities of the company should be utilized in measurement, recording and analysis. The effort, time and money required to provide data with measurements should be comparable to the validity and benefits of these data.

- In a measurement system, the definition of the "analysis unit" is very important. The limits of the unit to be measured should be determined. It may be possible to select the appropriate techniques and criteria for measurements under this condition.

- Measurement of all aspects of performance is impossible and subjective judgments can always be made in evaluations. The argument that everything can be measured may not always be appropriate in terms of cost. Therefore, it is necessary to acknowledge that performance measurement systems cannot be completely perfect.

- The way to achieve a good measurement system is through trial and error. It is not possible to capture perfection on paper. For this purpose, it should start with simple systems first and try to develop systems according to application results.

3. PERFORMANCE MANAGEMENT IN CONSTRUCTION SECTOR

In the construction sector, companies need to the performance measurement, especially on the basis of the project, find an answer to the question of the extent to which the objectives of those projects are fulfilled. These targets are project plans such as project schedule, project budget and work distribution.

The performance measurement in the projects shows how successful the project is in line with its objectives. In terms of traditional project management, success is achieved when project performance indicators are realized at optimal value in the execution of a project. In this context, in order for the projects to be successful, the project needs to be completed in the desired quality, the lowest possible cost and as soon as possible. Therefore, the first condition for a project to be successful is that its management plans the project in line with realistic objectives [16].

Deviations in project performance are either caused by unrealistic objectives of the project or inefficient management of the project [16]. If the reason for the deviation in performance is due to inefficiency management when analyzed, the project manager should take the necessary measures to bring the performance to the desired performance as close as possible. If the deviation is due to unrealistic targets, the historical database should be updated.

It can be said that many methods are used to measure project performance. These methods should provide project managers and stakeholders with the ability to answer the following questions [17].

- What is the current status of the project in terms of time and cost?

- How much will it cost to complete the project?

- When will the project be completed?

- Are there any potential problems to be identified now?

- What are the activities that can cause time and cost to be exceeded and where?

- What has been done with the money spent?

- If there is a cost overrun in the half way, can the budget overrun be estimated when the project is completed?

- Can potential problems be defined before they are too late to be corrected?

4. JOINT PROJECT MANAGEMENT PORTAL AS AN EXAMPLE FOR PERFORMANCE MANAGEMENT IMPLEMENTATION

Within the framework of general management, various performance measurement systems such as return on investment, customer value analysis, performance pyramid are used in order to measure the success of the activities performed. With these systems, it is possible to measure the performance of the projects. But the projects are quite different from ordinary organizations because of their nature. Therefore, measuring the performance of the project as an ordinary activity performance will not provide the correct data to the managers.

The performance of the projects should be measured in line with the specific objectives and objectives of the projects. For this reason, it is necessary to measure the performance of the projects which include activities for achieving a certain purpose within a pre-determined time, budget and quality constraint by taking into account the effective use of these constraints [18].

In the project performance measurement, the real success of the project can never be determined. However, it is possible to obtain the best results with the best measurements. In addition, measuring the performance of a project usually increases the performance of that project [19].

Naturally, the performance management process mentioned above needs to be assigned to the human resource. In construction companies, the need for solutions to reduce the human resources required for this job is emerging. The Joint Project Management Portal is structured as a web-based software to serve construction companies under the main headings of organization management, contract management, project management, process management, risk management, internal control management and performance management (Figure 3). In this way, all the required management work is done under a single software, labor and time savings will be provided, necessary intervention by the company management will be done in a timely and accurate way can be guaranteed.

Figure 3. Joint project management portal modules
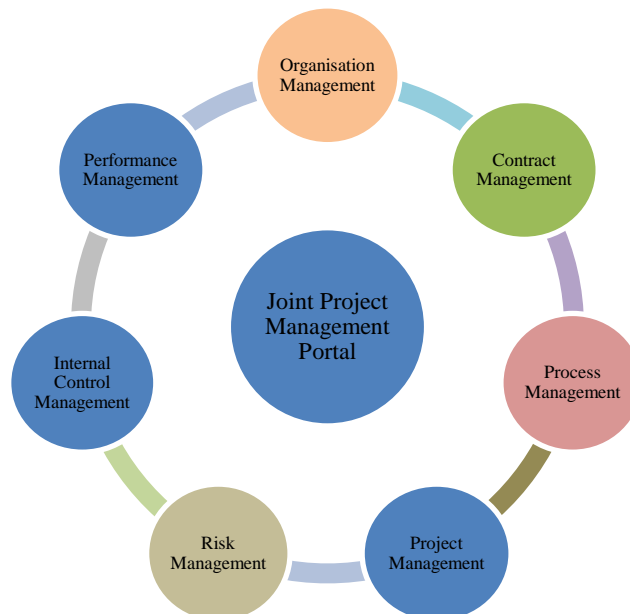
The main page of the Joint Project Management Portal is shown in figure 4. The Joint Project Management Portal consists of seven main modules: organization management, contract management, project management, process management, risk management, internal control management and performance management. And also screenshot of the performance management module is shown in figure 5.
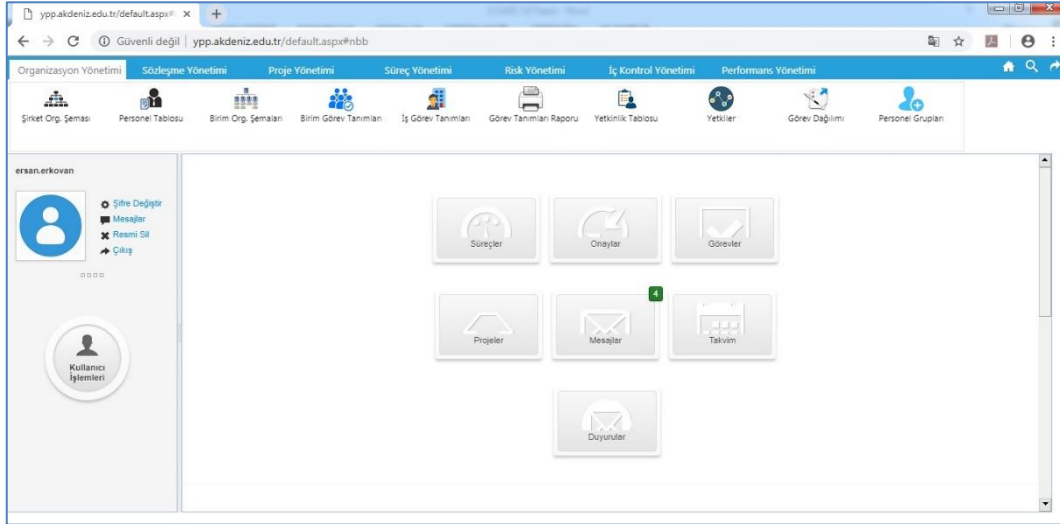
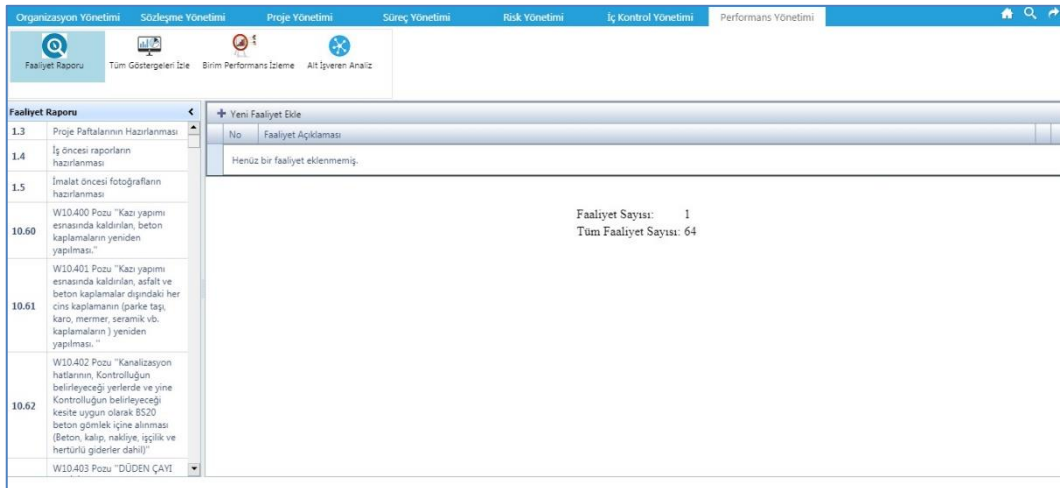*Figure 4. Main page of the joint project management portal*

Figure 5. Screenshot of the performance management module

5. CONCLUSION

Construction companies need a performance management system in order to adapt to the increasingly developing economic and technological developments and to survive in the competitive environment. It is obvious that the monitoring, evaluation and measurement or management of the performances of both the enterprises and their employees will increase the performance of the enterprise in a positive way in the future In particular, the importance of performance management in achieving the intended objectives of the projects carried out by construction companies is even more evident.

At this point; The Joint Project Management Portal is designed as a web-based computer software that provides the performance management system that the construction companies need thanks to its performance management module. JPMP, which started as an academic study, is intended to be an effective and dynamic application tool for all construction companies in the sector, which will be developed by means of data obtained from participating construction companies, in the fields of organization management, contract management, process management, project management, risk management, internal control management and performance management

ACKNOWLEDGMENT

REFERENCES

[1]. M. Akcakaya, "Performance management in public sector and problems encountered," *Journal of the Black Sea Studies*, vol. 32, pp. 171–202, 2012.

[2]. Uyargil, *Performans Yonetimi Sistemi Bireysel Performansin Planlanmasi Degerlendirilmesi ve Gelistirilmesi*, Istanbul, Turkey: Beta Basim A.S., 2013.

[3]. S. Sevimler, "Elements of total quality management and elements of the relationship between the education and business performance," M.Sc. thesis, Dumlupinar University, Kutahya, Turkey, Sep. 2010.

[4]. E. Celikdin, "Integrated usage of SWOT analysis and AHP with balanced scorecard system: An application in a feed mill," M.Sc. thesis, Aksaray University, Aksaray, Turkey, Mar. 2014.

[5]. M. Simsek, *Toplam Kalite Yonetimi*, Istanbul, Turkey: Alfa Yayinlari, 2007

[6]. O. Olcen, "Performance measurement in organizations and performance measurement process with balanced scorecard in a firm which is operating internationally," M.Sc. thesis, Anadolu University, Eskisehir, Turkey, Agu. 2012.

[7]. S. Yildiz, "The effect of intellectual capital on business performance: a research in banking sector," *Journal of Social Sciences*, vol. 11, pp. 11-28, 2011.

[8]. T. Bolat, *Toplam Kalite Yonetimi(Konaklama Isletmelerinde Uygulanmasi)*, Istanbul, Turkey: Beta Yayincilik, 2000

[9]. O. H. Yuregir and G. Nakiboglu, "Performans olcumu ve olcum sistemleri: genel bir bakis," *Journal of Cukurova University Institute of Social Sciences*, vol. 16, pp. 545-562, 2007.

[10]. C. Aktan, "Performance management: performance evaluation and measurement in organizations," *Journal of Organizations and Management Sciences*, vol. 1, pp. 25-49, 2009.

[11]. H. Ates and D. Cetin, "Performance management in public sector and performance-based budget," in: M. Acar and H. Ozgur, (Ed.), *Cagdas Kamu Yonetimi II*, Ankara, Turkey: Seckin Yayinlari, 2004

[12]. M. Armstrong and A. Baron, *Performance Management: The New Realities*, London, England: Institute of Personel and Development , 1998

[13]. S. Sink, "Development measurement systems for world class competition," in: W. F. Christopher and C. G. Thor, (Ed.), *Handbook for Productivity Measurement and Improvement*, Portland, The USA: Productivity Press, 1993.

[14]. G. L. Gass and C. Prince, "Family of measures: a tool for continuous improvement," in: W. F. Christopher and C. G. Thor, (Ed.), *Handbook for Productivity Measurement and Improvement*, Portland, The USA: Productivity Press, 1993.

[15]. Z. Akal, *Isletmelerde Performans Olcum ve Denetimi – Cok Yonlu Performans Gostergeleri*, Ankara, Turkey: MPM Yayini, 1992.

[16]. R. Navon and R. Sacks, "Assesing research issues in automated project (APPC)," *Automation in Construction*, vol. 16, pp. 474-484, 2007.

[17]. M. Bahar, "Earned value method and application in the service procurements contract type," M.Sc. thesis, Istanbul University, Istanbul, Turkey, Jul. 2008.

[18]. Z. Duran, "Earned value analysis as a project performance measurement system and a research," M.Sc. thesis, Pamukkale University, Denizli, Turkey, Jan. 2016

[19]. H. Kerzner, *Project Management Metrics, KPIs, and Dashboards*, New Jersey, The USA: John Wiley and Sons, 2013.

An Example of Internal Control Application for Contractor Companies in the Construction Sector

Aynur Kazaz[1], Ersan Erkovan[2], Serdar Ulubeyli[3]

Abstract

As a result of the intense competition environment in the construction sector and the complexity of the construction business depending on the developing technology, inadequacies in the monitoring of the activities of the enterprises have emerged with the classical control methods. As a solution to this new situation, COSO internal control model consisting of five independent professional organizations in the United States has emerged, which is a pioneer in the transformation of internal control into an important element in enterprises today. The internal control model, known today as the COSO model in the world, is the most widely accepted and continuously developed, updated and most comprehensive model, due to its level and scope to meet the needs of enterprises. The purpose of these model is to ensure compliance of business and activities in enterprises with legislation, the reliability of financial and managerial reporting, the effectiveness and efficiency of activities and the protection of assets. Similarly, it has become necessary to use an effective internal control model in order to maintain their development and to build their corporate structures for enterprises in construction sector which is one of the most important economic sectors. For this purpose, joint project management portal software which is considered to be used as a tool in the implementation of COSO internal control model in construction companies has been developed. With this web-based software, it is aimed that construction companies carry out their internal control activities effectively. In this study, first of all, general information about COSO internal control model will be given and joint project management portal will be introduced as an example of internal control model implementation in terms of construction sector.

Keywords: Internal Control, Construction Management, COSO Internal Control Model, Joint Project Management Portal

1. INTRODUCTION

As a result of the rapid increase in technology and globalization since the 80s; enterprises had to adapt to these economic and technological developments. This has led to a change in management understanding in public and private sector organizations. Structures belonging to the activities and management of enterprises have become more complex. In this process, while widespread communication, transparency and accountability have been highlighted, modern management practices such as strategic planning, performance management, risk management, internal control and internal audit have gained importance in order to manage the risks and opportunities of change.

All these developments have led to innovations in the task descriptions of business executives. The concepts of internal control, risk management and corporate governance have entered the field of activity of banks and insurance companies in the past and nowadays have been on the agenda of all private and public institutions.

At this point, for the need of a comprehensive and standardized internal control model mentioned above for businesses, Committee of Sponsoring Organizations (COSO), known as Treadway Commission, was established by five professional organizations (American Accounting Association, American Institute of Certified Public

---

[1] *Corresponding author: Akdeniz University, Department of Civil Engineering, 07070, Konyaalti/Antalya, Turkey. akazaz@yahoo.com*

[2] *Akdeniz University, Department of Civil Engineering, 07070, Konyaalti/Antalya, Turkey. ersan_erkovan@yahoo.com*

[3] *Bulent Ecevit University, Department of Civil Engineering, 67100, Zonguldak, Turkey. ulubeyli@beun.edu.tr*

Accountants, Financial Executives International, Institute of Internal Auditors, Institute of Management Accountants) operating in the United States in 1985.

The aim of COSO; to identify the causes of fraudulent financial reports issued by enterprises and to reduce the likelihood of occurrence. COSO published the first internal control model made by the committee members in 1992 and received great attention.

The renewed model, which was prepared taking into consideration the developing technology and which also regulates the five basic principles on which the system is based, emerged in 2013.The internal control model, known today as the COSO model in the world, is the most widely accepted and continuously developed, updated and most comprehensive model, due to its level and scope to meet the needs of enterprises.

2. COSO INTERNAL CONTROL MODEL

In the United States, the Watergate scandal in the mid-70s has a significant share in the importance of the concept of internal control. Internal control is a process, effected by an entity's board of directors, management and other personnel, designed to provide reasonable assurance regarding the achievement of objectives which are effectiveness and efficiency of operations, reliability of financial reporting and compliance with applicable laws and regulations [1].

According to another definition; Internal control includes all harmonized coordinated methods and organizational plan that encourage participation in the foreseen managerial policies, protection of business assets, control of the accuracy and reliability of accounting information [2].

What is intended with reasonable assurance is actually a high level of assurance. With reasonable assurance, it is never considered to be an absolute level of assurance. The reason for this is that the decision-making process is human-oriented and that there is always the possibility of a margin of error. Reasonable assurance is a fact that uncertainty and risk cannot be foreseen.

COSO aims to increase the quality of financial reports through the business ethics of financial reporting, effective internal controls and corporate governance and is formed by the gathering of voluntary organizations that are preparing regulations to realize the goals they set. The COSO model forms the basis of the standards for the internal control system. The main objectives of the COSO internal control system, an internal control model; to ensure that the activities are effective, to prepare reliable financial reports, to comply with laws and regulations, to comply with ethical values and to protect the assets. [3].

The elements that constitute the internal control process of the COSO internal control model were initially described as a pyramid. The internal control process is shown in Figure 1. In the COSO internal control structure, which was renewed in 2013, these elements were depicted as a three-dimensional cube (Figure 2). These elements; control environment, assessment of risks, control activities, information sharing and communication and monitoring.

There are three dimensions on the cube: "elements", "internal control purposes" and "organizational structure". The elements are composed of the five main categories mentioned above. The objectives of internal control are examined in three main categories: "activities", "financial reporting" and "compliance". In the organizational structure of the third dimension of the cube, the general institutional structure of the enterprise, its sub-divisions, if any, its affiliates and detail functions are included. The emphasis is that the controls that are designated for detail business functions should be in harmony with the controls that are designated for the whole business [4].
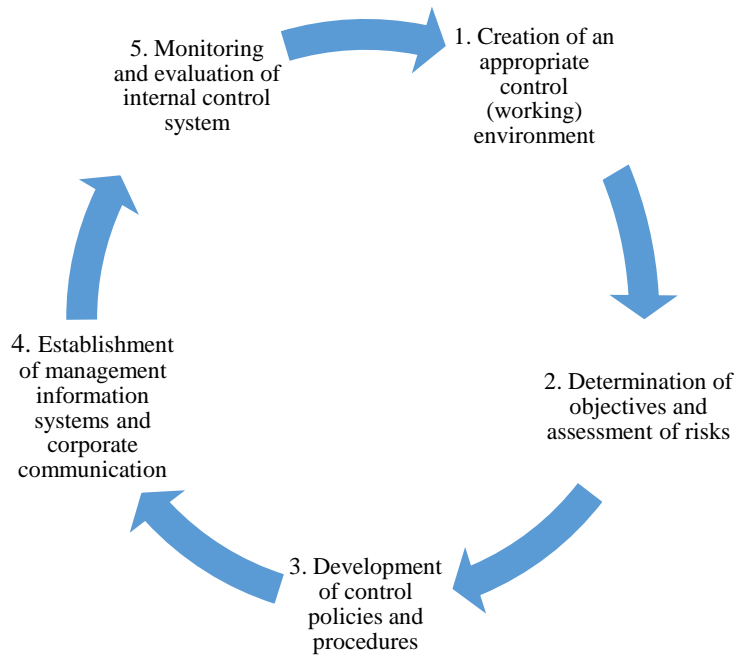
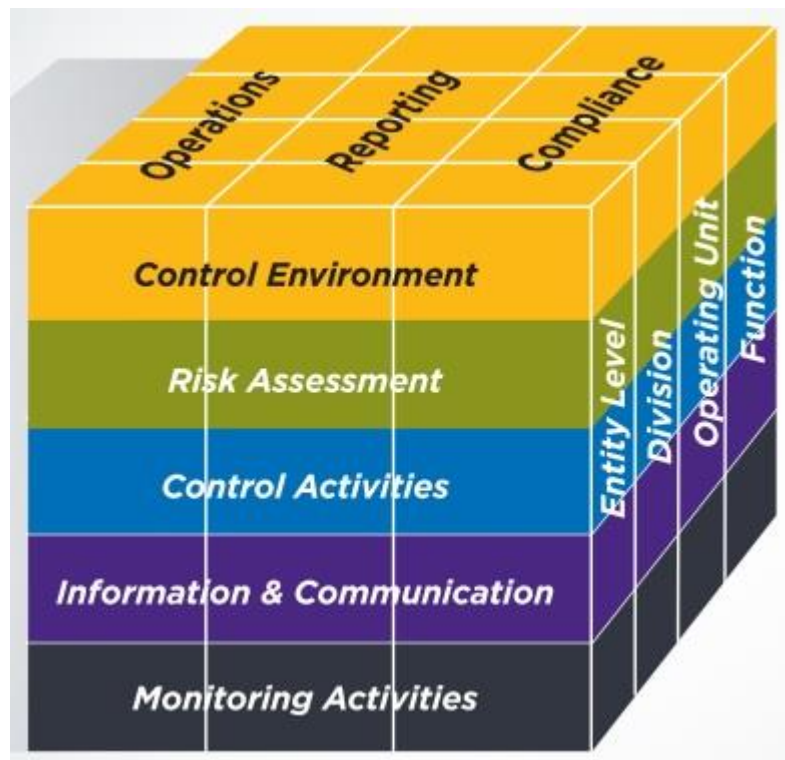Figure 1. COSO based internal control process

Figure 2. COSO cube

o   ***Structure of the COSO Internal Control Model***

Internal control structure, according to the essence of a structure connected to the human factor. Therefore, there is no guarantee that the internal control system will be effective in achieving the objectives of the enterprise.

Because human-specific deficiencies, defects, misunderstandings and misapplications, abuses or indifference can prevent the control structure from achieving the desired level of success. There is a misconception that the internal control structure is only related to financial issues. However, it is true that internal control is related to all activities of the institution. No unit, task or person is out of this process. The inclusion of all business elements in the internal control structure is not a bureaucratic obstacle in terms of the process. In other words, the scope of internal control does not cause bureaucracy, cumbersome structure or distraction of people. All business personnel should not consider internal control as additional work to the processes, but should perceive it as a part of the processes. The internal control structure is not a routine, static process but rather a system that can change and adapt to business structures [5].

o   ***Components of the COSO Internal Control Model***

In the COSO cube, the relationship between the elements of internal control and the objectives of internal control and its operation activities were shown. Within this framework, activities and units (departments), objectives and elements of internal control are integral to the different surfaces of a cube [6]. All activities and units in this cube benefit from the following five components of internal control aimed at the effectiveness and efficiency of activities, the reliability of the information and compliance with the legislation. These components are described below.

▪   *Control Environment*

The "control environment" component of the internal control structure has a more spiritual content rather than a material concept. The control environment influences, improves and provides a basis for systematic order control of company employees. When the control environment is mentioned, the environment in which the employees of the institution perform their activities and tasks should be considered [5]. The five principles that constitute the control environment are shown below.

- The organization demonstrates a commitment to integrity and ethical values.

- The board of directors demonstrates independence from management and exercises oversight of the development and performance of internal control.

- Management establishes, with board oversight, structures, reporting lines, and appropriate authorities and responsibilities in the pursuit of objectives.

- The organization demonstrates a commitment to attract, develop, and retain competent individuals in alignment with objectives.

- The organization holds individuals accountable for their internal control responsibilities in the pursuit of objectives.

▪   *Risk Assessment*

According to COSO, risk can be defined as events/events that can be encountered in the process of reaching their targets and that will adversely affect the process of reaching their targets. The four principles that constitute the risk assessment are shown below.

- The organization specifies objectives with sufficient clarity to enable the identification and assessment of risks relating to objectives.

- The organization identifies risks to the achievement of its objectives across the entity and analyzes risks as a basis for determining how the risks should be managed.

- The organization considers the potential for fraud in assessing risks to the achievement of objectives.

- The organization identifies and assesses changes that could significantly affect the system of internal control.

▪   *Control Activities*

Control activities are prevention, detection and guidance (compliance, approval, validation, reconciliation and review) within the business and it processes, including all employees of the business in terms of minimizing risks on the basis of policies and regulations established by the senior management in the business [7]. The three principles that constitute the control activities are shown below.

- The organization selects and develops control activities that contribute to the mitigation of risks to the achievement of objectives to acceptable levels.

- The organization selects and develops general control activities over technology to support the achievement of objectives.

- The organization deploys control activities through policies that establish what is expected and procedures that put policies into action.

- *Information and Communication*

Information and communication, one of the components of the internal control structure, provides the relationship between the four other elements through information sharing and communication. The internal control structure, which is seen as a tool for achieving corporate goals and targets by organizing the information flow across the enterprise, has an important role in increasing its ability to operate and implement. Communication refers to the transfer and transformation of information both horizontally and vertically within the enterprise and to persons, administrations and authorities concerned with the appropriate mechanisms outside the enterprise [8].

The three principles that constitute the information and communication are shown below.

- The organization obtains or generates and uses relevant, quality information to support the functioning of internal control.

- The organization internally communicates information, including objectives and responsibilities for internal control, necessary to support the functioning of internal control.

- The organization communicates with external parties regarding matters affecting the functioning of internal control.

- *Monitoring Activities*

Monitoring includes all review and follow-up activities carried out to evaluate the quality of internal control structure. Due to various internal and external factors, the effectiveness of the internal control structure may deteriorate over time. For this reason, internal control structure can be monitored by internal or independent audits at certain times and can be monitored continuously by the instructions of the management. Continuous monitoring usually by making comparisons by periods, by carrying out reconciling studies related to accounts, especially at high risk when needed it can be sustained in the form of an inventory of assets. As a result of both independent and continuous monitoring, measures should be taken by the management in order to strengthen the areas where the effectiveness of the internal control structure is reduced or weakened. Whether these measures are implemented should be monitored by the management [2]. The two principles that constitute the monitoring activities are shown below.

- The organization selects, develops, and performs ongoing and/or separate evaluations to ascertain whether the components of internal control are present and functioning.

- The organization evaluates and communicates internal control deficiencies in a timely manner to those parties responsible for taking corrective action, including senior management and the board of directors, as appropriate.

3. JOINT PROJECT MANAGEMENT PORTAL AS AN EXAMPLE OF INTERNAL CONTROL IMPLEMENTATION

The most important task in the establishment of internal control system in construction contracting enterprises is to board of directors. The board of directors, which is responsible for the establishment and supervision of the internal control system, should correctly check the risk areas that the construction contracting entity may face. It should test financial and managerial information in terms of accuracy, reliability and timing, and ensure that the business complies with laws, regulations, objectives, standards, policies and procedures [9].

Establishing the internal control system has the material cost to bring to the enterprise. This cost is directly proportional to the number and quality of personnel in the system and to the technical equipment used in the system to be installed also [10].

The implementation of internal control procedures and methods increases the existing bureaucracy within the enterprise. More documents and workforce are spent in the execution of transactions. In addition, the delay of business due to bureaucratic procedures, it causes profitability and loss of productivity may lead to loss.

Moreover, due to bureaucratic processes, the delay of business can be lost as it causes profitability and productivity to decrease. These losses and expenses that the company has incurred in the establishment and operation of the internal control system are the cost of the internal control system. In short, the cost of the internal control system increases as internal control procedures and methods are applied in the enterprise [11].

In order to prevent the above-mentioned bureaucracy and thus increasing the cost, the need for a software to reduce the workload of the business personnel is emerging. The Joint Project Management Portal is structured as a web-based software to serve construction companies under the main headings of organization management, contract management, project management, process management, risk management, internal control management and performance management. In this way, all the required management work is done under a single software, labor and time savings will be provided, necessary intervention by the company management will be done in a timely and accurate way can be guaranteed.

The main page of the Joint Project Management Portal is shown in figure 3. The Joint Project Management Portal consists of seven main modules: organization management, contract management, project management, process management, risk management, internal control management and performance management. The screenshots of some of these modules are shown below according to their order of appearance in the software.
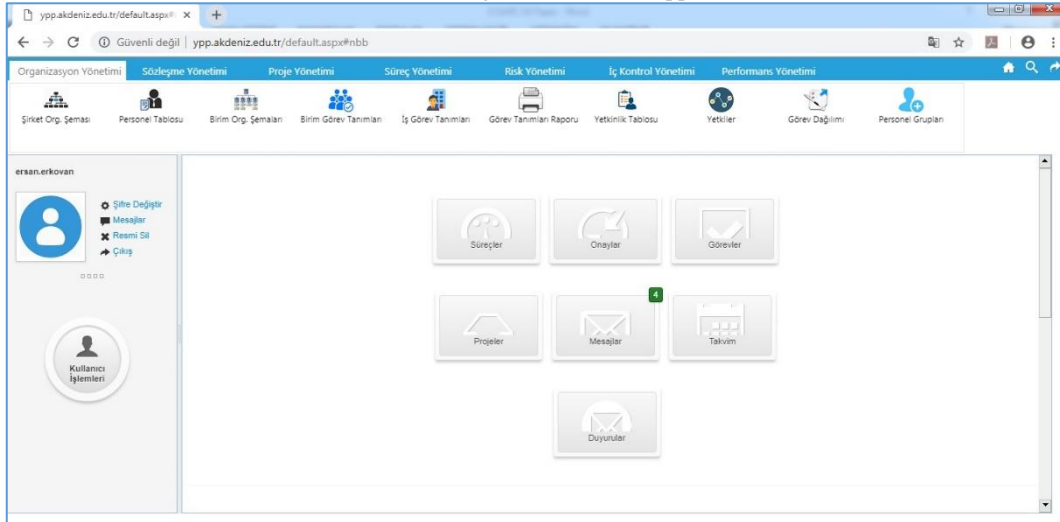

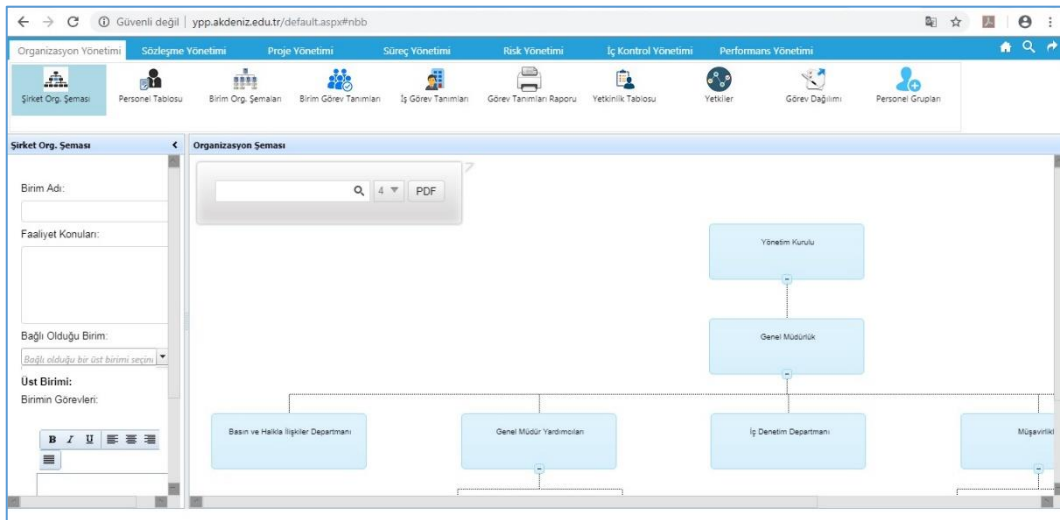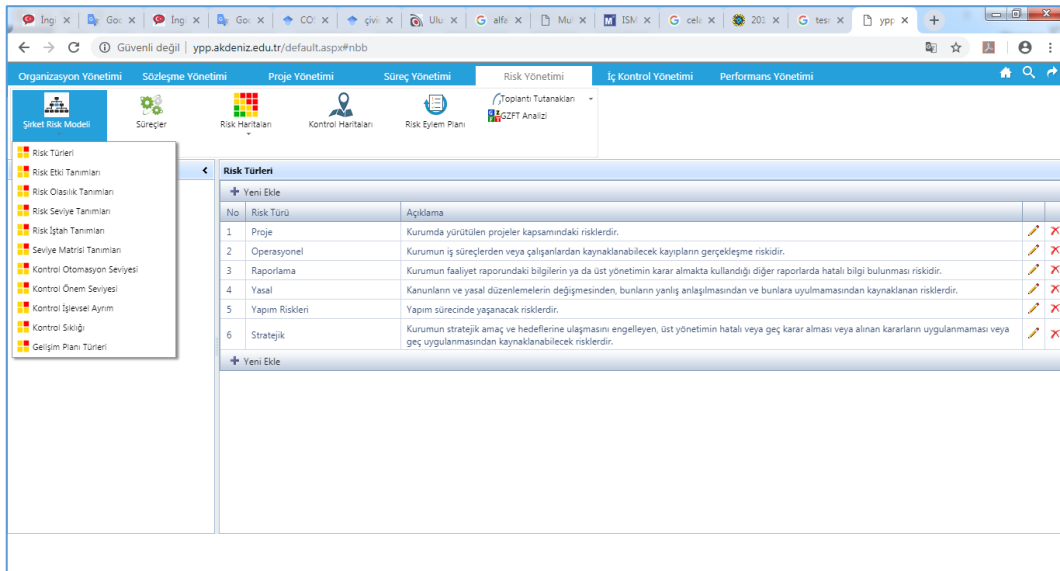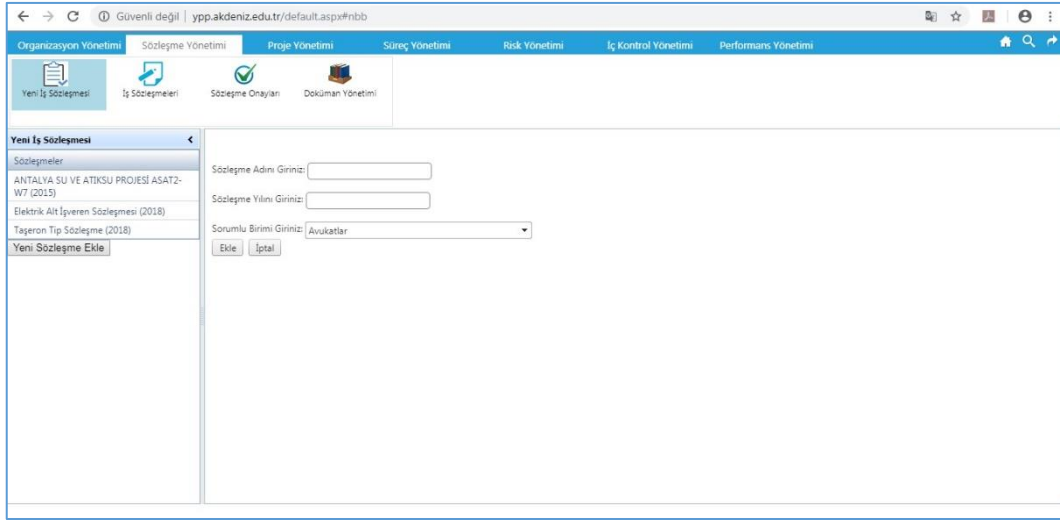*Figure 3. Main page of the joint project management portal*

Figure 4. Screenshot of the organization management module

502

Figure 5. Screenshot of the contract management module

Figure 6. Screenshot of the risk management module

Figure 7. Screenshot of the internal control management module

4. CONCLUSION

Nowadays, construction companies need an effective internal control model in order to adapt to the increasingly developing economic and technological developments and to survive in the competitive environment. The internal control model is a tool that will be used to achieve the objectives of construction companies. This model should be applied continuously, not in certain periods in order for companies to achieve their goals.

COSO internal control model is the most widely accepted model in today's internal control models thanks to its content, its application guide to enterprises and its features such as continuous updating. COSO is also a proactive tool with a holistic structure in terms of integration and synchronization of internal control mechanisms. The application of COSO internal control model as an internal control model of construction companies is a subject requiring high knowledge and skills. Applications without understanding and internalizing the logic of the model will not yield the desired benefits.

At this point; The Joint Project Management Portal is designed as a web-based computer software that provides the COSO internal control model that the construction companies need thanks to its internal control module. JPMP, which started as an academic study, is intended to be an effective and dynamic application tool for all construction companies in the sector, which will be developed by means of data obtained from participating construction companies, in the fields of organization management, contract management, process management, project management, risk management, internal control management and performance management.

ACKNOWLEDGMENT

REFERENCES

[1]. S. Pickett, *The Internal Auditing Handbook*, West Sussex, United Kingdom: John Wiley & Sons, 2003.
[2]. H. Turedi, "Restructing of the Turkish public finance management: internal control," *Journal of Management and Economics*, vol. 9, pp. 99–127, 2011.
[3]. Anil Keskin, "Internal control system and evaluation in public and private sector management," *Journal of Denetisim*, vol. 3, pp. 14–21, 2009.
[4]. H. Turedi, A. O. Koban and G. Karakaya, "Comparing COSO internal control (USA) model with the English (Turnbull) and Canada (COCO) models," *Journal of Sayistay*, vol. 99, pp. 95–115, 2015.
[5]. H. Turedi and G. Karakaya, "COSO internal control model and control environment," *Finance, Politics & Economic Reviews*, vol. 52, pp. 65–74, 2015.
[6]. G. Kurt and T. Ucma, "The innovations of COSO internal control-integrated framework update project," *Journal of the World of Accounting Science*, vol. 15, pp. 99–109, 2013.
[7]. Hasanefendioglu and M. Uzel, "COSO, the magic lamp of Aladdin? (COSO-based internal control system in all aspects)," *Journal of Financial Solution*, vol. 141, pp. 209–226, 2017.

[8]. (2019) Public Internal Control Guide. [Online]. Available: http:// www.bumko.gov.tr /
[9]. O. Odabas, "Internal control system in construction contract companies and an application," M.Sc. thesis, Marmara University, Istanbul, Turkey, Aug. 2010.
[10]. O. Duman, *Accounting Audit and Reporting*, Ankara, Turkey: TESMER, 2008.
[11]. Kepekci, *Internal Control System*, Ankara, Turkey: TESMER, 1994.

Antimicrobial Activities of Some Disinfectants Used in the Food Industry

Ozum Ozoglu[1], Esra Kocak[1], Seda Dundar[1], Hande Colak[1] And Mihriban Korukluoglu[1]

Abstract

Antimicrobial activities of some disinfectants used in the food industry on several microorganisms were searched in this study. Four different commercial disinfectants entitled as D1, D2, D3 and D4 which are used for CIP (Cleaning in Place), tools and equipment cleaning in the industry were investigated. They had various agent contents. Then, two yeasts (*Saccharomyces cerevisiae* and *Schizosaccharomyces pombe*), one mould (*Aspergillus niger*) and three bacteria (*Lactococcus lactis*, *Bacillus subtilis* and *Escherichia coli*) were chosen as test microorganisms. First of all, well diffusion method was followed to understand antimicrobial efficacy of the disinfectants. After that, showing antimicrobial activity ones were chosen testing to determine effect times of the disinfectants on the microorganisms for an hour with 30-minute intervals. In the meantime, the commercial disinfectants were supplied as the highest and the lowest concentrations that recommended on the manufacturer's label during the all experiments. While, both maximum and minimum concentration of D2 and D3 were shown antimicrobial activity on *S.cerevisiae* and *L.lactis*, only maximum concentration of D2, D3 and D4 were been effective on *B.subtilis*. Moreover, any disinfectants and any concentration were not prevailed on *S.pombe*, *A.niger* and *E.coli*. However, minimum and maximum concentrations of D2 and D3 were affected on *S.cerevisiae* and *L.lactis* in first and last 30 minutes even following few days, maximum concentration of them affected *B.subtilis* just a little in first 30 minutes. Consequently, struggled microorganisms and the applying time should be considered when using disinfectants in the food industry.

Key words: Disinfectant, antimicrobial activity, food industry

1. INTRODUCTION

Microbial contamination is one of the major problems in the food industry. Eliminate or minimize the sources of microbial contamination is required for providing quality and safety of products in the industry. Besides, it is important for consumers and regulatory bodies [1]–[3]. Disinfectants are commonly used for this aim in the food industry especially on equipments and food-conduct surfaces that are the source off cross-contamination [1], [2], [4], [5].

Disinfectants are chemical and antimicrobial agents used at disinfection processes for providing microbial safety of the products and/or maintaining standard hygiene conditions in the industry. Disinfectants are effected on microorganisms in the way inhibition or changing cell pore, nucleic acids, enzyme structure and spores of microorganisms Effectiveness of the disinfectants are consist in disinfectant concentration and chemical compounds, temperature, exposure time etc. [1], [2], [6], [7]. Thus, they can a microbicidal (killing microorganisms) or microbiostatic (inhibition growth of microorganism) effect on microorganisms in terms of these parameters [8]. Therefore, these effects of the disinfectants should be considered when choosing disinfectants in the industry for a suitable aim [2], [3]. In light with these information, antimicrobial activities of some disinfectants used in the food industry on several microorganisms were searched in this study.

2. MATERIALS AND METHODS

2.1. Test Microorganisms

---

[1] *Department of Food Engineering, Faculty of Agriculture, Bursa Uludag University, 16059 Bursa, Turkey*
***Corresponding Author:** E-mail: ozoglu@uludag.edu.tr*

Six different microorganisms (two yeasts, one mould and three bacteria) that were detailed below were chosen as test microorganisms in the study. Test microorganisms:

Yeasts; *Saccharomyces cerevisiae* ATCC 9763 and *Schizosaccharomyces pombe* (Bursa Uludag University Food Engineering Department), Mould; *Aspergillus niger* ATCC 16404 (*Aspergillus brasiliensis* Varga et al.), Bacteria; *Lactococcus lactis* (produced biofilm) (B.U.U. Food Eng. Dep.), *Bacillus subtilis* (Ankara University Biotechnology Institute) and *Escherichia coli* ATCC 25923

2.2. Commercial Disinfectants

Four different commercial disinfectants that are used in the food industry for CIP (Clean-in-Place) and equipment cleaning were studied. They were named as D1, D2, D3 and D4 which were explained to the contents on the below;

D1; Sodium hydroxide, D2; Sodium hydroxide, Surface-active and Foaming agent, D3; Sodium hydroxide, Sodium hypochlorite, Amines, C10-16 alkyl dimethyl and N-oxides, D4; Tetrasodium ethylenediaminetetraacetate, sodium carbonate and alkyl alcohol ethoxylate.

2.3. Antimicrobial Activity

Antimicrobial activities of the disinfectants were determined by Well-diffusion methods [9]–[11]. Minimum and maximum usage doses of the disinfectants recommended by producing company were studied for this aim. All microorganisms were inoculated as 6-7 logarithmic unit initial load on suitable media that were Malt Extract Agar/Broth (Merck) for yeasts and the mould, MRS Agar/Broth (Merck) for *Lactococcus lactis*, Tryptic Soy Agar/Broth (Oxoid) for *Bacillus subtilis* and *Escherichia coli*. All experiments were done in triplicate.

2.4. Treatment Time

Treatment time of the disinfectants were observed according to the method of Korukluoglu et al. (2006). The analyzes were performed on tubes and evaluated by turbidity. It was applied for 30th and 60th minutes. 60 minutes were chosen being the period selected as the max time for disinfection in the food industry [5]. The trial was done in triplicate.

2.5. Surface Plate Method

The method was followed for calculation initial amount of the test microorganisms and observing viability of the microorganisms after 30 and 60 minute-disinfectant treatments [12].

3. RESULTS AND DISCUSSION

3.1. Antimicrobial Activities of the Disinfectants

Zone diameters of the wells were measured after incubation on the Petri dishes observed zones. The results were shown on Table 1 given as mean values and Figure 1.

Table 1. Zone diameter of the wells (mm)

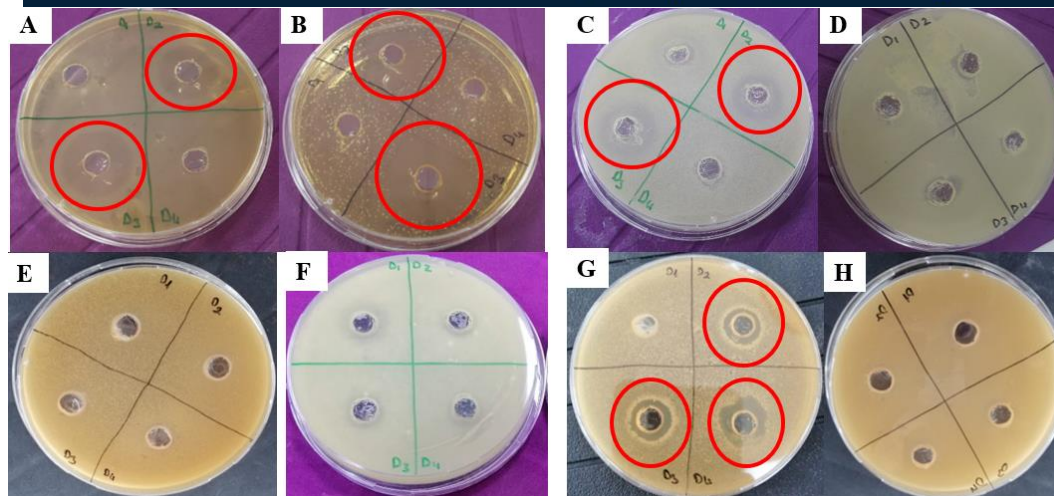| Disinfectants(%concentrations)/Test Microorganisms(6-7 log)	S. cerevisiae	S.pombe	A.niger	L. lactis	B.subtilis	E.coli
D1 min/max	-/-	-/-	-/-	-/-	-/-	-/-
D2 min/max	-/-	-/16.5	-/-	16/20.5	-/14	-/-
D3 min/max	-/-	-/19.5	-/-	15/23.5	-/14	-/-
D4 min/max	-/-	-/-	-/-	-/-	-/18.5	-/-

* Diameters of each well was 8 mm.

Figure 1. Zone formations: A: L.lactis with minimum disinfectant concentration, B: L.lactis with maximum disinfectant concentration, C: S.pombe with maximum disinfectant concentration, D: S.pombe with minimum disinfectant concentration, E: E.coli with maximum disinfectant concentration, F: A.niger with maximum disinfectant concentration, G: B.subtlis with maximum disinfectant concentration and H: B.subtlis with minimum disinfectant concentration.

It is clearly seen that on Table 1 and Figure 1, maximum and minimum concentration of disinfectant D2 and D3 were shown antimicrobial effect on *L.lactis* and *S.pombe*. Besides, maximum concentration of D2, D3 and D4 were been effected on *B.subtilis*. Moreover, any disinfectants with any concentration were not prevailed on *S. cerevisiae*, *E.coli*. and *A.niger*. Therefore, they showed resistance to the disinfectants.

This is known that disinfectants are more efficient on Gram (+) microorganisms than Gram (-) ones [13], [14]. So, this study was supported the issue due to fact that meanwhile *B.subtilis* and *L.lactis* are Gram (+), *E.coli* is Gram (-) bacteria [15]. Apart from these, even as *L.lactis* is produced biofilm, maximum and minimum concentration of D2 and D3 disinfectants were shown antimicrobial effect on it. It is a significant result by the reason of that biofilm structure is provided a resistance to antimicrobial agents. Biofilm is a structured form community of unicellular organisms enclosed in a self-produced extracellular matrix [16]–[18].

According to study was done for determining antifungal effects of eight commercial disinfectants namely alcohol, peracetic acid, iodophors, aldehydes, quaternary amine compounds (QAC, a, b and c), and a chlorine-based agent againsted *Saccharomyces cerevisiae*, *Saccharomyces uvarum*, *Kloeckera apiculata*, *Candida oleophila*, *Metschnikowia fructicola*, *Schizosaccharomyces pombe*, *Aspergillus niger* (5 strains) and *Penicillium roqueforti* (5 strains) by Korukluoglu et al. (2006), antifungal effects of the disinfectants were shown an alteration with regard to type of microorganisms and compound of disinfectants. When their studies' results were investigated it was seen that, *A.niger* was the most resistance one in generally. Also, *S.pombe* was more sensitive to the disinfectants than *S. cerevisiae* [5]. These results are similar to the current study.

Disinfectants contained quaternary ammonium compounds especially chain lengths between C12 and C16 ones are more stronger antimicrobial effects than other ones [19]–[22]. Thus, D3 could indicated wide spectrum antimicrobial effect because of its C10-16 alkyl dimethyl content.

3.2. Treatment Time

Showed antimicrobial activities disinfectants were practised with the activity concentration and been effective on microorganisms to figured out treatment time of the disinfectants. Survival microorganisms were checked with counting of the colonies on Petri dishes which were inoculated from not to shown visible turbidity on tubes after 30th and 60th minutes disinfectants treatments. Then, the results were given at Table 2 as mean values of triplicate trials.

Table 2. Number of colonies (Log) after 30 and 60 minutes disinfectants treatments

Disinfectants(%concentrations)/Test Microorganisms	S.pombe		L. lactis		B.subtilis	
	30 min.	60 min.	30 min.	60 min	30 min.	60 min
D1 min/max	-	-	-	-	/-	/-
D2 min/max	/-	/-	-/-	-/-	/2	/2.53
D3 min/max	/-	/-	-/-	-/-	/1.30	/1
D4 min/max	-	-	-	-	/-	/-

When looked at the Table 2, it is obviously seen that, minimum and maximum concentrations of D2 and D3 were affected on *S.pombe* and *L.lactis* in first and last 30 minutes like as microbicidal even following 30 minutes however, maximum concentration of them affected *B.subtilis* like as microbiostatic.. It may related with that pathogen microorganisms have more resistance to disinfectants than other microorgnisms [20], [21]. Also, D4 showed microbicidal effect on *B.subtilis*. Apart from these, maximum concetration of D2 and D3 disinfectants were dropped the growth of *B.subtilis* roughly 5 logarithmic units. Although D2 was much more effected on the beginning, D3 was become more effected with time.

4. CONCLUSIONS

Disinfectants are used in the food industry for microbiological safety. Then, antimicrobial activities of some disinfectants used in the food industry on several microorganisms were searched in this study. To do results, different concentration of disinfectant D2, D3 and D4 were been effected on some of the microorganisms to the contrary D1. May it can be deduced from that, only using of sodium hydroxide not to be efficiently effect on microorganisms like D1 instead of mixing various contents.

Any disinfectants and any concentration were not prevailed on *S. cerevisiae*, *E.coli*. and *A.niger*. It could be expected due to the fact that these microorganisms are more stable than others in their variety.

Minimum and maximum concentrations of D2 and D3 were showed antimicrobial effect on *S.pombe* and *L.lactis* in first and last 30 minutes as microbicidal even following few days, maximum concentration of them affected *B.subtilis* as microbiostatic.

To sum up, struggled microorganisms, the applying time, contents and concentration of the disinfectants should be considered when choosing disinfectants in the food industry.

REFERENCES

[1]   S. Langsrud, M. Singh, E. Heir, and A. L. Holck, "Bacterial disinfectant resistance a challenge for the food industry," *Int. Biodeterior. Biodegradation*, vol. 51, pp. 283–290, 2003.

[2]   I. Falcó, M. Verdeguer, R. Aznar, G. Sánchez, and W. Randazzo, "Sanitizing food contact surfaces by the use of essential oils," *Innov. Food Sci. Emerg. Technol.*, vol. 51, pp. 220–228, 2019.

[3]   A. Sener and A. Temiz, "Tavuk Kesimhane ve Isletmelerinde Kullanilan Ticari Dezenfektanlar ve Etkinlikleri," *Orlab On-Line Mikrobiyoloji Derg.*, vol. 2, no. 10, pp. 1–28, 2004.

[4]   G. Sundheim, S. Langsrud, E. Heir, and A. L. Holck, "Bacterial resistance to disinfectants containing quaternary ammonium compounds," *Int. Biodeterior. Biodegradation*, vol. 41, pp. 235–239, 1998.

[5]   M. Korukluoglu, Y. Sahan, and A. Yigit, "The fungicidal efficacy of various commercial disinfectants used in the food industry," *Ann. Microbiol.*, vol. 56, no. 4, pp. 325–330, 2006.

[6]   U. Abbasoglu, "Dezenfektanlar : Siniflama ve Amaca Uygun Kullanim Alanlari," in *6. Ulusal Sterilizasyon Dezenfeksiyon Kongresi*, 2009, pp. 109–120.

[7]   A. M. Janssen, A. B. S. Vendsen, and G. Laboratories, "Antimicrobial activities of essential oils A 1976-1986 literature review on possible applications," *Pharm. Weekbl. Sci. Ed.*, vol. 9, pp. 193–197, 1987.

[8]   B. Meyer, "Does microbial resistance to biocides create a hazard to food hygiene?," *Int. J. Food Microbiol.*, vol. 112, no. 3, pp. 275–279, Dec. 2006.

[9]   F. Lucke and U. Schillinger, "Antibacterial Activity of Lactobacillus sake Isolated from Meat," *Appl. Environ. Microbiol.*, vol. 55, no. 8, pp. 1901–1906, 1989.

[10] E. G. Altuntas, K. Ayhan, and G. Okcu, "Cig Sut Ve Peynir Orneklerinden Izole Edilen Laktik Asit Bakterilerinin Antimikrobiyel Aktiviteleri," vol. 35, no. 3, pp. 197–203, 2010.

[11] J. Bakht, A. Islam, and M. Shafi, "Antimicrobial Potentials Of Eclipta Alba By Well Diffusion Method," *Pakistan J. Bot.*, vol. 43, pp. 169–174, 2011.

[12] A. K. Halkman and K. Ayhan, "Mikroorganizma Sayimi," 2005, p. 18.

[13] W. A. Rutala and D. J. Weber, "Disinfection, Sterilization, and Control of Hospital Waste," *Mand. Douglas, Bennett's Princ. Pract. Infect. Dis.*, p. 3294–3309.e4, Jan. 2015.

[14] J. Fisher, "Cleaning Procedures in The Factory | Types of Disinfectant," *Encycl. Food Sci. Nutr.*, pp. 1382–1385, Jan. 2003.

[15] F. Lowy, "Bacterial Classification, Structure and Function," 2009.

[16] T. C. Mah and G. A. O. Toole, "Mechanisms of biofilm resistance to antimicrobial agents," *TRENDS Microbiol.*, vol. 9, no. 1, pp. 34–39, 2001.

[17] B. Carpentier and O. Cerf, "Biofilms and their consequences , with particular reference to hygiene in the food industry," *J. Appl. Bacteriol.*, vol. 75, pp. 499–511, 1993.

[18] C. Rodriguez-Melcon, R. Capita, J. J. Rodriguez-Jerez, J. V. Martinez-Suarez, and C. Alonso-Calleja, "Effect of Low Doses of Disinfectants on the Biofilm-Forming Ability of Listeria monocytogenes," *FOODBORNE Pathog. Dis.*, vol. 16, no. 4, pp. 262–268, 2019.

[19] E. Fu, K. McCue, and D. Boesenberg, "Chemical Disinfection of Hard Surfaces – Household, Industrial and Institutional Settings," in *Handbook for Cleaning/Decontamination of Surfaces*, Elsevier Science B.V., 2007, pp. 573–592.

[20] J. V Martínez-suárez, S. Ortiz, and V. López-alonso, "Potential Impact of the Resistance to Quaternary Ammonium Disinfectants on the Persistence of Listeria monocytogenes in Food Processing Environments," *Front. Microbiol.*, vol. 7, no. May, pp. 1–8, 2016.

[21] J. T. Holah, J. H. Taylor, D. J. Dawson, and K. E. Hall, "Biocide use in the food industry and the disinfectant resistance of persistent strains of Listeria monocytogenes and Escherichia coli," *J. Appl. Microbiol. Symp. Suppl.*, vol. 92, pp. 111–120, 2002.

[22] T. Møretrø, B. C. T. Schirmer, E. Heir, A. Fagerlund, P. Hjemli, and S. Langsrud, "Tolerance to quaternary ammonium compound disinfectants may enhance growth of Listeria monocytogenes in the food industry," *Int. J. Food Microbiol.*, vol. 241, pp. 215–224, 2017.

Microbiological Surveying of Some Probiotic Products on the Markets in Turkey

Mihriban Korukluoglu[1], Ozum Ozoglu[1], Rukiye Colak-Sasmazer [1]

Abstract

Recently, people tend to consume probiotic products cause of their health benefits. Therefore, many companies have produced various probiotic food products. Thus, 11 different probiotic products that are found on the markets in Turkey and bought in same time were surveying with regard to microorganism levels on bought and expire dates of each products. 4 probiotic dairy drinks (plain, strawberry, pineapple and apricot), 2 plain kefirs from manufactured different companies and 1 strawberry kefir, 1 probiotic strawberry kefir yogurt and 3 probiotic yogurts (plain, strawberry and infant-specific) by several companies were chosen for the study. Level of bifidobacteria, *Lactobacillus acidophilus*, total viable counts, mould and yeast were controlled on the products at bought and expire dates according to reference enumeration methods. The samples were investigated on different time of the storage process because of their production dates. When the results were evaluated, all products were generally saved their probiotics level. Just, roughly 1 log decreasing was observed on bifidobacteria and *Lactobacillus acidophilus* level in the infant-specific yogurt and the kefir 23-day stored respectively. Even, total viable counts reduced almost 1 log on the strawberry yogurt; not to change on the other samples. Yeasts were counted only the kefirs as expected, also a little bit on expiring dates of plain and strawberry yogurts. There were not found any mould on the all samples.

Key words: Probiotic products, bifidobacteria, Lactobacillus acidophilus, expire date

1. INTRODUCTION

Nowadays, people tend to consume probiotic products cause of their health benefits especially on gastrointestinal system. Name of Probiotics comes from a Greek word which is meaning 'for life' and it is referred to living microorganisms that have beneficial effects on human gut taken in adequate amounts [1]–[3]. Acceptance of a food product as probiotic, it has to contain at least 6 log viable probiotic microorganisms and protect the level during shelf-life. Besides, *Bifidobacterium*, *Lactobacillus* and non-pathogenic yeasts are most commonly used probiotic microorganisms [4]–[7].

Companies have produced various probiotic food products as a result of increasing the demand for probiotic products [8]–[10]. Many food matrices, especially dairy products especially yoghurt are used for producing probiotic food products. Dairy products are commonly chosen for providing probiotic food products because of their Lactic acid bacteria (LAB) content. LAB can produce several different antimicrobial compounds supporting probiotic characteristics of the products [5], [10]–[12].

In line with these information, 11 different probiotic products that are sold on the markets in Turkey and bought in same time were surveying with regard to bifidobacteria, *Lactobacillus acidophilus*, total viable counts, mould and yeast levels on bought and expire dates of each products.

2. MATERIALS AND METHODS

2.1. Probiotic Product Samples

Eleven different probiotic products that are found on the markets in Turkey and bought in same time were surveying with regard to microorganism levels on buying and expiration dates of each products. 4 probiotic dairy drinks (plain, strawberry, pineapple and apricot), 2 plain kefirs from manufactured different companies

---

[1] *Department of Food Engineering, Faculty of Agriculture, Bursa Uludag University, 16059 Bursa, Turkey*
Corresponding Author: *E-mail:* mihriban@uludag.edu.tr

and 1 strawberry kefir, 1 probiotic strawberry kefir yogurt and 3 probiotic yogurts (plain, strawberry and infant-specific) by several companies were chosen for the study (Shown on Table 1).

Table 1. Different studied probiotic products provided from the markets in Turkey

PRODUCT NAME	COMPANY	BUYING DATE	EXPIRATION DATE
Plain Probiotic Dairy Drinks	A	10.08.2018	30.08.2018
Strawberry Probiotic Dairy Drinks	A	10.08.2018	30.08.2018
Pineapple Probiotic Dairy Drinks	A	10.08.2018	30.08.2018
Apricot Probiotic Dairy Drinks	A	10.08.2018	30.08.2018
Plain Kefir	B	10.08.2018	02.09.2018
Probiotic Strawberry Kefir Yogurt	B	10.08.2018	16.08.2018
Plain Kefir	C	10.08.2018	12.08.2018
Strawberry Kefir	C	10.08.2018	29.08.2018
Plain Probiotic Yogurts	D	10.08.2018	25.08.2018
Strawberry Probiotic Yogurts	D	10.08.2018	17.08.2018
Infant-Specific Probiotic Yogurts	E	10.08.2018	23.08.2018

2.2. Enumeration of Bifidobacterium animalis ssp. lactis

ISO 29981|IDF 220:2010 Milk products - Enumeration of presumptive bifidobacteria – Colony count technique at 37℃ protocol was done in triplicate [13].

2.3. Enumeration of Lactobacillus acidophilus

ISO 20128, IDF 192: Milk products - Enumeration of presumptive *Lactobacillus acidophilus* on selective medium – Colony- count technique at 37℃ protocol was practiced in triplicate [14].

2.4. Enumeration of Mould and Yeast

ISO 6611 / IDF 094:2004 Milk and milk products - Enumeration of colony-forming units of yeasts and/or moulds - Colony-count technique at 25℃ method was applied in triplicate [15].

2.5. Total Viable Count

ISO 16297:2013 - Milk -- Bacterial count method was followed in triplicate for total viable count [16].

3. RESULTS AND DISCUSSION

3.1. Counting of Bifidobacterium animalis ssp. lactis and Lactobacillus acidophilus

Number of *Bifidobacterium animalis* ssp. *lactis* and *Lactobacillus acidophilus* on the probiotic samples at buying and expiration days at 4°C stored were shown as mean value of triplicate experiments in Table 2 and 3 respectively.

Table 2. Results of *Bifidobacterium animalis* ssp. *lactis* counting on buying (first day) and expiration day (Log)

PRODUCT NAME	COMPANY	BUYING DATE	EXPIRATION DATE
Plain Probiotic Dairy Drinks	A	7.64	7.60
Strawberry Probiotic Dairy Drinks	A	7.63	7.60
Pineapple Probiotic Dairy Drinks	A	7.52	7.46
Apricot Probiotic Dairy Drinks	A	7.49	7.43
Plain Kefir	B	7.64	7.04
Probiotic Strawberry Kefir Yogurt	B	7.93	7.86
Plain Kefir	C	6.49	6.51
Strawberry Kefir	C	6.56	6.46
Plain Probiotic Yogurts	D	6.51	6.32
Strawberry Probiotic Yogurts	D	6.52	6.48
Infant-Specific Probiotic Yogurts	E	7.78	6.62

Table 3. Results of *Lactobacillus acidophilus* counting on buying (first day) and expiration day (Log)

PRODUCT NAME	COMPANY	BUYING DATE	EXPIRATION DATE
Plain Probiotic Dairy Drinks	A	7.40	7.30
Strawberry Probiotic Dairy Drinks	A	7.62	7.60
Pineapple Probiotic Dairy Drinks	A	7.69	7.61
Apricot Probiotic Dairy Drinks	A	7.65	7.61
Plain Kefir	B	6.28	5.95
Probiotic Strawberry Kefir Yogurt	B	7.08	7.85

Plain Kefir	C	6.76	6.76
Strawberry Kefir	C	6.70	6.70
Plain Probiotic Yogurts	D	6.78	6.60
Strawberry Probiotic Yogurts	D	6.79	6.78
Infant-Specific Probiotic Yogurts	E	7.34	7.04

It is clearly seen that, all products were generally saved their probiotics levels as 6-7 log on Table 2 and Table 3. Just, roughly 1 log decreasing was observed on bifidobacteria and *Lactobacillus acidophilus* level in the infant-specific yogurt and the kefir 23-day stored respectively. Then, this dropping is not significant due to the fact that viable probiotic microorganisms level were protected for acceptance as probiotic product end of the shelf-life [4], [5], [17]. The results were seen similarity with study of Moreno et al.(2005) which done with 8 different commercial milk. Number of total LAB level was protected as acceptable as probiotic during 4°C storage times [18].

3.2. Counting of Total Viable Bacteria

Number of total viable bacteria on the probiotic samples at buying and expiration days at 4°C stored were shown as mean value of triplicate experiments at Table 4.

Table 4. Results of total viable bacteria counting on buying (first day) and expiration day (Log).

PRODUCT NAME	COMPANY	BUYING DATE	EXPIRATION DATE
Plain Probiotic Dairy Drinks	A	7.83	7.85
Strawberry Probiotic Dairy Drinks	A	7.90	7.91
Pineapple Probiotic Dairy Drinks	A	7.86	7.86
Apricot Probiotic Dairy Drinks	A	7.85	7.88
Plain Kefir	B	7.36	7.30
Probiotic Strawberry Kefir Yogurt	B	7.96	7.88
Plain Kefir	C	6.86	6.87
Strawberry Kefir	C	6.81	6.74
Plain Probiotic Yogurts	D	6.95	6.90

Strawberry Probiotic Yogurts	D	7.48	6.78
Infant-Specific Probiotic Yogurts	E	7.91	7.85

According to Table 4, number of total viable bacteria was almost stable at the end of expiration dates. Thus, it can be deduced that dedicated expiration dates by produced packaging company were optimum for these products [19].

3.3. Growth of Mould and Yeast

Growth of mould and yeast on the probiotic samples were observed at buying and expiration days and stored at 4°C. Then, the results were given as mean value of triplicate experiment at Table 5.

Table 5. Results of mould and yeast counting on buying (first day) and expiration day (Log).

PRODUCT NAME	COMPANY	BUYING DATE	EXPIRATION DATE
Plain Probiotic Dairy Drinks	A	<1	<1
Strawberry Probiotic Dairy Drinks	A	<1	<1
Pineapple Probiotic Dairy Drinks	A	<1	<1
Apricot Probiotic Dairy Drinks	A	<1	<1
Plain Kefir	B	4.60	4.91
Probiotic Strawberry Kefir Yogurt	B	4.72	4.76
Plain Kefir	C	3.00	3.08
Strawberry Kefir	C	3.34	3.43
Plain Probiotic Yogurts	D	<1	1.00
Strawberry Probiotic Yogurts	D	<1	1.30
Infant-Specific Probiotic Yogurts	E	<1	<1

* There was not observed any mould in the products (<1). Thus, results on the above are regard yeast observation.

Yeasts were counted only the kefir samples as expected due to fact that they content yeast in normally [20]. Also a little bit on expiring dates of plain and strawberry yogurts. However, they were not on the considering level that roughly 1 log. Besides, there were not found any mould on the all samples.

4. CONCLUSIONS

Many food companies have produced various probiotic food productsbecause of increasing the demand for

probiotic products by consumer. In this study, some of these products sold on the markets in Turkey were

investigated. To the results, all of the products were generally saved their probiotics level which is required acceptance as probiotic products (6 log<). Yeasts were counted only the kefir samples as expected. Moreover, there were not found any mould on the all samples.

Consequently, it could be deduced that, various probiotic products on the markets in Turkey safely consumed by taking into consideration expire dates.

REFERENCES

[1]   P. R. Lee, C. X. Boo, and S. Q. Liu, "Fermentation of coconut water by probiotic strains Lactobacillus acidophilus L10 and Lactobacillus casei L26," *Ann. Microbiol.*, vol. 63, no. 4, pp. 1441–1450, 2013.

[2]   K. R. Pandey, S. R. Naik, and B. V. Vakil, "Probiotics, prebiotics and synbiotics- a review," *J. Food Sci. Technol.*, vol. 52, no. 12, pp. 7577–7587, 2015.

[3]   C. Quin, M. Estaki, D. M. Vollman, J. A. Barnett, S. K. Gill, and D. L. Gibson, "Probiotic supplementation and associated infant gut microbiome and health: A cautionary retrospective clinical comparison," *Sci. Rep.*, vol. 8, no. 1, pp. 1–16, 2018.

[4]   O. Yerlikaya, "Starter cultures used in probiotic dairy product preparation and popular probiotic dairy drinks," *Food Sci. Technol.*, vol. 34, no. 2, pp. 221–229, 2014.

[5]   A. B. Shori, "The potential applications of probiotics on dairy and non-dairy foods focusing on viability during storage," *Biocatal. Agric. Biotechnol.*, vol. 4, no. 4, pp. 423–431, 2015.

[6]   T. R. Reid, G., Sanders, M. E., Gaskins, H. R., Gibson, G. R., Mercenier, A., Rastall, R., Roberfroid, M., Rowland, I., Cherbut, C., and Klaenhammer, "New scientific paradigms for probiotics and prebiotics," *J Clin Gastroenterol*, vol. 37, no. 2, pp. 105–118, 2003.

[7]   E. Isolauri, Y. Sutas, P. Kankaanpää, H. Arvilommi, and S. Salminen, "Probiotics: effects on immunity.," *Am. J. Clin. Nutr.*, vol. 73, no. 2 Suppl, p. 444S–450S, 2001.

[8]   O. Don, A. Niranjalie, H. Lunuwilage, D. Weerahewa, and S. Vidanagamage, "Role and Current Trends of Developing Fruit , Vegetable and Cereal based Probiotic Foods : A Role and Current Trends of Developing Fruit , Vegetable and Cereal based Probiotic Foods : A review," no. July 2018, 2017.

[9]   M. Daneshi, M. R. Ehsani, S. H. Razavi, and M. Labbafi, "Effect of refrigerated storage on the probiotic survival and sensory properties of milk/carrot juice mix drink," *Electron. J. Biotechnol.*, vol. 16, no. 5, 2013.

[10]   A. Annunziata and R. Vecchio, "Consumer perception of functional foods: A conjoint analysis with probiotics," *Food Qual. Prefer.*, vol. 28, no. 1, pp. 348–355, 2013.

[11]   F. Leroy and L. De Vuyst, "Lactic acid bacteria as functional starter cultures for the food fermentation industry," *Trends Food Sci. Technol.*, vol. 15, no. 2, pp. 67–78, 2004.

[12]   A. L. D. Batista *et al.*, "Quality parameters of probiotic yogurt added to glucose oxidase compared to commercial products through microbiological, physical-chemical and metabolic activity analyses," *Food Res. Int.*, vol. 77, pp. 627–635, 2015.

[13]   "ISO 29981:2010 - Milk products -- Enumeration of presumptive bifidobacteria -- Colony count technique at 37 degrees C." [Online]. Available: https://www.iso.org/standard/45765.html. [Accessed: 31-Aug-2018].

[14]   "ISO 20128:2006 - Milk products -- Enumeration of presumptive Lactobacillus acidophilus on a selective medium -- Colony-count technique at 37 degrees C." [Online]. Available: https://www.iso.org/standard/35292.html. [Accessed: 31-Aug-2018].

[15]   "ISO 6611:2004 - Milk and milk products -- Enumeration of colony-forming units of yeasts and/or moulds -- Colony-count technique at 25 degrees C." [Online]. Available: https://www.iso.org/standard/40473.html. [Accessed: 31-Aug-2018].

[16]   "ISO 16297:2013 - Milk -- Bacterial count -- Protocol for the evaluation of alternative methods." [Online]. Available: https://www.iso.org/standard/56110.html. [Accessed: 11-Jun-2019].

[17]   A. Terpou *et al.*, "Growth Capacity of a Novel Potential Probiotic Lactobacillus paracasei K5 Strain Incorporated in Industrial White Brined Cheese as an Adjunct Culture," *J. Food Sci.*, vol. 83, no. 3, pp. 723–731, 2018.

[18]   Y. Moreno, M. C. Collado, M. A. Ferrús, J. M. Cobo, E. Hernández, and M. Hernández, "Viability assessment of lactic acid bacteria in commercial dairy products stored at 4 °C using LIVE/DEAD® BacLight™ staining and conventional plate counts," *Int. J. Food Sci. Technol.*, vol. 41, no. 3, pp. 275–280, 2006.

[19]   "Tetra Top carton bottles for chilled and ambient products." [Online]. Available: https://www.tetrapak.com/packaging/tetra-top. [Accessed: 21-Sep-2018].

[20]   M. Ghasempour, S. A. l. A. Sefdgar, A. A. kba. Moghadamnia, R. Ghadimi, S. Gharekhani, and L. Shirkhani, "Comparative study of Kefir yogurt-drink and sodium fluoride mouth rinse on salivary mutans streptococci," *J. Contemp. Dent. Pract.*, vol. 15, no. 2, pp. 214–217, 2014.

Detection Of Vehicle License Plate Location Using Convolutional Neural Network

Muazzez Buket Darici[1], Furkan Kiraci[1] Atilla Ozmen[1], Metin Sengul[1]

Abstract

In recent years, the necessity of personal working in traffic control is increasing because of the increasing number of vehicles in traffic. To deal with this problem, computer based automatic control systems are being developed. One of these systems is automatic vehicle license plate recognition system. In this work, vehicle license plate location is presented by Convolutional Neural Network (CNN). In this system 144 vehicle images captured under several weather conditions were utilized. From these images it was obtained 1980 images which contain part of plate or not. The region of the vehicle license plate has been detected by using these images in CNN after a basic enhancement process. In this work, it has been reached the accuracy rate of 95.14% in detection of license plates and the success rate of 95.83% in CNN.

Keywords: personal working in traffic control;convolutional neural networks; vehicle license plate location

1. INTRODUCTION

Number plates are used for identification of vehicles all over the nations. Vehicles in each country have a unique license number, which is written on its license plate. This number distinguishes one vehicle from the other one. Many applications are used to determine exactly where the license plate is. Some challenging situations are encountered when the license plate is detected. These difficulties are listed by image blur, angle of photo, plate images that taken in bad weather conditions, etc. In the literature, many license plate detection algorithms have been proposed. Algorithms for license plate detection can be classified into two categories. The first one is to identify numbers/characters which are then grouped to produce license plate candidates. The other one is to find image regions that are license plate like and then refine those regions by removing unnecessary background. In [1], extraction of plate region was done using edge detection algorithms and smearing algorithms. The success rate for this work is 97.6% for the extraction of plate region, This system is only designed for the identification of Turkish license plates. In [2], mainly focused on Edge Detection(Sobel Edge Detection)technique and then filtering of noise by Median Filter, Smoothing, Connector, Masking, ,and then Color Conversation is done.In [2], it has been seen that the detection is not that clear and proper, which it was found, is due to improper light segment or varying illumination effects. Also, in recent years, some related works with CNN have been increased to detect license plate. In[3], recognition steps are as follow:(1)Image Enhancement: by histogram equalization method (2)Structuring Elements : by thickening, (3) Hat transformations: which is use for contrast, enhancement(top has & bottom has)setting (4) Morphological Operations like dilation and erosion (5) Plate region confirmation (6) Character Segmentation and Recognition by neuron implementation model .by this reference 250 color images were used for testing the technique, These results report a high accuracy rate of above 95%.Although the technique is quite efficient enough to work very well in the real time environment but currently the technique proposed lays more emphasis on the accuracy of the overall system, while the some more work is to be done to make the technique more efficient.

In [4], the images are partitioned in sub-region with overlapping grid. Each sub-region is independently fed to a CNN which produce for each sub-region a single value in the [0,1] range. The output is 1 when the sub-region contains a nearly centered license plate, and 0 when it contains less than half of a license plate with other

situations producing intermediate values. By analyzing, the outputs of neighboring sub-regions, it is estimated the location of each detected license plate. The proposed approach achieved a precision of 0.87 and recall of 0.83.

In this paper, the images have been partitioned in sub-region without overlapping. If the sub-region includes any part of the license plate without any restrictions, the output is 1; otherwise the output is 0. Then these sub-regions fed into CNN. After training, each image has been tested by overlapping at the step of finding location of the license plate. In [4], 1829 images were used to achieve a precision of 87%. In this paper by using only 144 pictures, the accuracy rate of 95.14% has been reached.

2. DEEP LEARNING

Deep learning was improved from artificial neural network, and now it is used as a common field of machine learning. The observation of artificial neural network began from 1940s. Deep learning models usually embark on hierarchical structures to connect their layers. The output of a lower layer can be regarded as the input of a higher layer via simple linear or nonlinear calculations. These models can transform low-level features of the data into high-level abstract features. Owning to this characteristic, deep learning models can be stronger than shallow machine learning models in feature representation. From the beginning to the present, there are many different types of deep learning models. The typical models include Auto-encoder (AE), Deep Belief Network (DBN), Convolutional Neural Network (CNN) and Recurrent Neural Network (RNN) [5].

Using CNNs for deep learning has become increasingly popular. The main factors of this popularity are:
- CNNs eliminate the need for manual feature extraction—the features are learned directly by the CNN.
- CNNs produce state-of-the-art recognition results.
- CNNs can be retrained for new recognition tasks, enabling you to build on pre-existing networks [6].

Convolutional Neural Network has had ground breaking results over the past decade in a variety of fields related to pattern recognition; from image processing to voice recognition. The most useful aspect of CNNs is decreasing the number of parameters in ANN [7].

The essence of CNN is a multi-layer perceptron. The key to its success lies in the local connection and the way of sharing weights. CNN is a kind of neural network, its weight sharing network structure makes it more similar to the biological neural network, reduces the complexity of the network model and the number of weights [8].

A Convolutional Neural Networks consists of multiple layers, such as convolutional layers, max-pooling or average-pooling layers, and fully-connected layers which their representations are shown in Figure 1. The neurons in each layer of a CNN are arranged in a 3-D manner, transforming a 3-D input to a 3-D output. For example, for an image input, the first layer (input layer) holds the images as 3-D inputs, with the dimensions being height, width, and the color channels of the image. The neurons in the first convolutional layer connect to the regions of these images and transform them into a 3-D output. The hidden units (neurons) in each layer learn nonlinear combinations of the original inputs, which is called feature extraction [9].
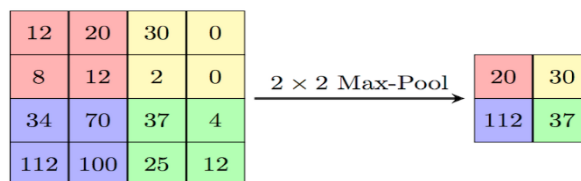
(a)
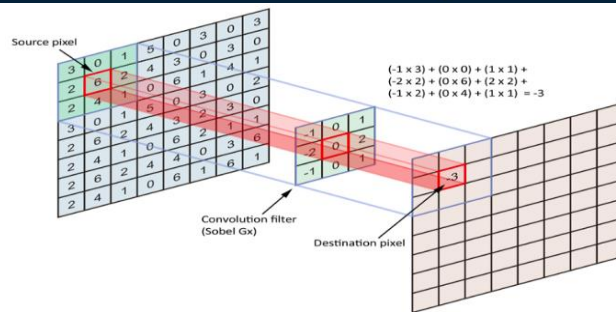
(b)
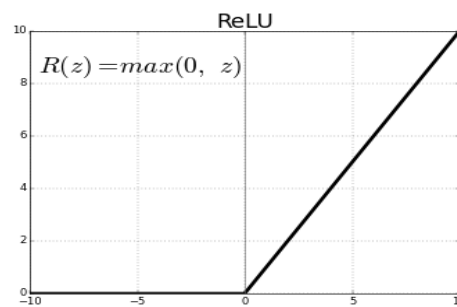
(c)

Figure 1. The representation of (a) Max-Pooling Layer, (b) Convolution Layer, (c) RELU layer[10].

3. METHODOLOGY

In this work, it has been tried to detect placement of a license plate in images with Convolutional Neutral Network. It was done by partitioning of images, training and testing for the detection of placement where the license plate is. In CNN part, 24x80 RGB images were used as an input layer. Hidden layers consists of Convolution, Batch Normalization, RELU and Max Pooling layer. In this algorithm, each layer has been utilized 4 times respectively.

o *Partition of Images*

It was created a matrix which consists of 0's and 1's by partitioning all images one by one without overlapping. The matrix representation of a vehicle is shown in Figure 2. The reason of non-overlapping is to provide the algorithm works faster and therefore save on time for this project. 0's means in this matrix there is no any part of the plates and 1's mean that blocks contain a part of the plates. The size of the blocks which are used for partition is 24x80.Since size of the all images which were used is 480x640, dimension of the created matrices is 20x8 after partition.

(a)

```
o    o    o    o    o    o    o    o
o    o    o    o    o    o    o    o
o    o    o    o    o    o    o    o
o    o    o    o    o    o    o    o
o    o    o    o    o    o    o    o
o    o    o    o    o    o    o    o
o    o    o    o    o    o    o    o
o    o    o    o    o    o    o    o
o    o    o    o    o    o    o    o
o    o    o    o    o    o    o    o
o    o    o    o    o    o    o    o
o    o    o    o    o    o    o    o
o    o    1    1    1    1    o    o
o    o    1    1    1    1    o    o
o    o    1    1    1    1    o    o
o    o    1    1    1    1    o    o
o    o    o    o    o    o    o    o
o    o    o    o    o    o    o    o
o    o    o    o    o    o    o    o
o    o    o    o    o    o    o    o
```
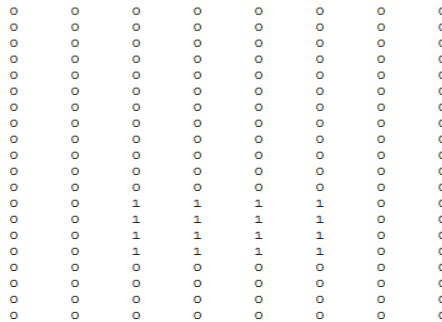
(b)

Figure 2. (a)The original image; (b) The matrix representation of image.

o *Training of the Plates*

The blocks which are in folders named as "0" and "1" have been trained and tested. It has been utilized 90% of these blocks to train process and rest of it to test. At this stage, blocks in the folders were reviewed because of some observed failures. For example, it was noticed that the algorithm perceives blocks which contains the white block of the white car as a plate. After that, it was added more blocks from different white cars to folder which does not contain plates to be able to increase the success rate of the algorithm. In the test stage, it was observed that success rate of some dirty plates is low. Therefore, it was applied a pre-process to enhance the original image by increasing the color contrast of the image. Thanks to this pre-process it was aimed to ensure the algorithm works successfully on vehicles which have a dirty plate because of some weather conditions or etc. In this process, it was used 24x80 RGB image as an input layer. Then Convolution, Batch Normalization, RELU and Max Pooling layer have been utilized respectively. The Convolution layer convolves the input by moving the filters along the input vertically and horizontally and computing the dot product of the weights and the input, and then adding a bias term [10]. A Batch Normalization layer normalizes each input channel across a mini-batch. It is used to speed up the training of convolutional neural network and reduce the sensitivity to network initialization [10]. RELU allows for faster and more effective training by mapping negative values to zero and maintaining positive values [10]. Max Pooling simplifies the output by performing nonlinear down sampling, reducing the number of parameters that the network needs to learn [10].

o *Testing of the Plates*

In this step of the work, it has been scanned the original image block by block by overlapping. The reason of overlapping unlike Section A. is to not miss any part of the license plate in image. It was tested whether each block contains a plate or not with the results obtained from Neural Network. After that, it has been held the region has the highest plate density and has been cleaned the rest by using Connected Component Analysis Method. It was found the size of the image that is scanned block by block by overlapping. An original image with a size of 480x640 has been a size of 23x112 after overlapping. It has been observed the density of plates in an image has the size of 23x112. Then, it was found a ratio to show the region perceived as plate in the original image has the size of 480x640. Using these information, it was aimed to enclose the region around the plate in a rectangle. The result after Connected Component Analysis and enclosing of region of plate can be seen in Figure 4,5. However, since the resolution of the image which was overlapped is low, this found ratio covered not only exact region of plate, but also some region around the plate.
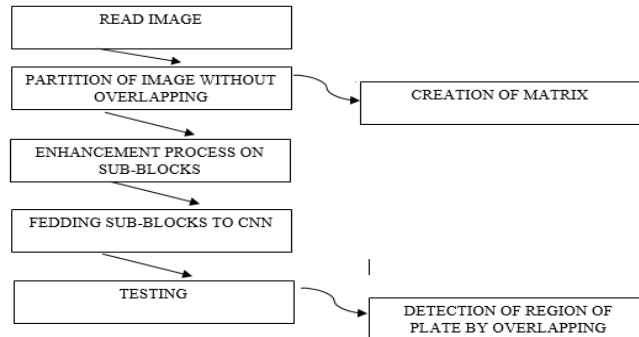
Figure 3. The block diagram for detection of license plate.
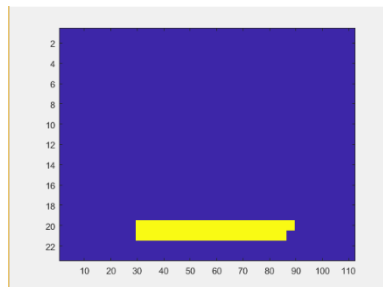
Figure 4. The result of the original image after overlapping and Connected Component Analysis

Figure 5. Enclosing of the region around the plate in a rectangle.

4. SIMULATIONS AND RESULTS

In this work, it has been used 144 vehicle images which their sizes are 480x640 captured generally from distance between 2 and 4 meters under different weather conditions. The accuracy rate of detection of license plates is 95.14%. This means that, the algorithm finds region of license plate of 128 vehicles out of 144. It has been obtained totally 1980 sub-images that their sizes are 24x80 from these images to be able to train in CNN. It has been achieved the success rate of 95.83% in the training process in CNN for these images as shown in Figure 6 .

Figure 6. The result of Training Process.

Figure 7. Some samples of results of algorithms

5.CONCLUSION

As a conclusion, in this paper it is aimed to find the location of vehicle license plates in images based on deep learning. Firstly, sub-images have been attained without overlapping from the original images to be able to use in deep learning.Then,it has been detected the location of license plate in original images with overlapping which is used to not to miss any part of the plates in images thanks to the results which were obtained from CNN. As mentioned before in sim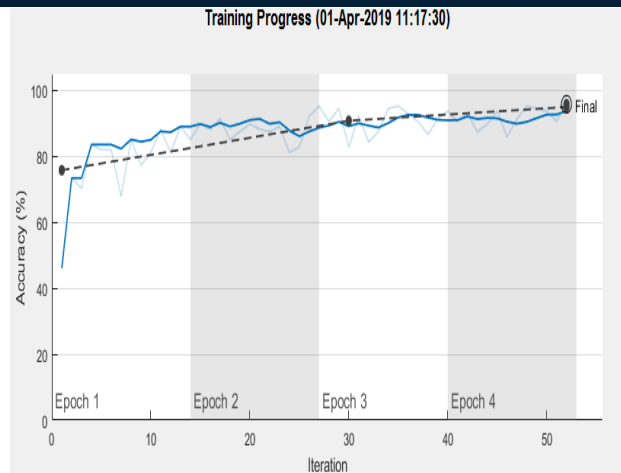ulations and results part, the used images were taken generally from distance between 2 and 4 meters. The algorithm is not very effective to detect the location of license plates in vehicle images taken from a long distance. Therefore, it is thought that the success rate will be increased by using only vehicle images taken at close range.Future work includes the incerase of vehicle images taken from close distance and character analysis of license plates by using different and more effective ways.

REFERENCES

[1]. S. Ozbay, and E. Ercelebi," Automatic Vehicle Identification by Plate Recognition", Processing of world academy of science engineering and technology vol9, ISSN 1307-6884, november 2005.

[2]. Z.X. Chen, C.Y. Liu, F.L. Chang, and G.Y. Wang," Automatic License-Plate Location and Recognition Based on Feature Salience", IEEE Transaction on vehicle technology, VOL. 58, NO. 7, september 2009.

[3]. Humayun Karim Sulehria, Ye Zhang, Danish Irfan, Atif Karim Sulehria," Vehicle Number Plate Recognition Using Mathematical Morphology and Neural Networks", WSEAS TRANSACTIONS on COMPUTERS, Volume 7,ISSN: 1109-2750, Issue 6, June

[4]. F. D. Kurpiel, R. Minetto, B.T. Nassu, "Convolutional Neural Networks For License Plate Detection in Images", IEEE International Conference on Image Processing (ICIP), 2017.

[5]. X. Du, Y. Cai, S. Wang, L. Zhang, "Overview of deep learning", IEEE 2016 31st Youth Academic Annual Conference of Chinese Association of Automation (YAC), january 2017.

[6]. https://www.mathworks.com/solutions/deep-learning/convolutional-neural-network.html.

5TH INTERNATIONAL CONFERENCE ON ENGINEERING AND NATURAL SCIENCE
12-16 June 2019 Prague

[7].   S. Albawi, T.A. Mohammed, S.A. Zawi, "Understanding of a convolutional neural network", IEEE 2017 International Conference on Engineering and Technology (ICET), march 2018.

[8].   J. Yang ; J.Li "Application of deep convolution neural network", 14th International Computer Conference on Wavelet Active Media Technology and Information Processing (ICCWAMTIP), 2017.

[9].   Murphy, K. P. Machine Learning: A Probabilistic Perspective. Cambridge, Massachusetts: The MIT Press, 2012.

[10].   https://www.mathworks.com

[11].   Karnik, "Performance of TCP congestion control with rate feedback: TCP/ABR and rate adaptive TCP/IP," M. Eng. thesis, Indian Institute of Science, Bangalore, India, Jan. 1999.

[12].   J. Padhye, V. Firoiu, and D. Towsley, "A stochastic model of TCP Reno congestion avoidance and control," Univ. of Massachusetts, Amherst, MA, CMPSCI Tech. Rep. 99-02, 1999.

[13].   *Wireless LAN Medium Access Control (MAC) and Physical Layer (PHY) Specification*, IEEE Std. 802.11, 1997.

Accelerated composting of cattle manure by using special bacteria and enzyme mixture

Cevat Yaman[1]

Abstract

Composting is one of the best options to dispose cattle manure which contains organic matter, N, P, K elements. The objective of this study was to investigate the use of specifically manufactured bacteria and enzyme mixture for composting cattle manure at a full-scale plant. Two trapezoid manure piles of 50 tons were placed at 1.7 m in height, 2.1 m in bottom width, 0.6 m in top width, and 54 m in length. A specifically manufactured bacteria and enzyme mixture was solubilized in 400 liters of clean tap water and applied to one of the compost piles by spraying the solution over the pile and while mixing the pile with a compost turner tractor. The second pile was used as a control; thus, solution of bacteria and enzyme was not applied. After 17 days, C:N ratio was reduced from 25.62 to 10.92, organic matter was reduced from 84.51% to 63.29%, and total nitrogen (TN) was increased from 1.89% to 3.36%. The control pile was not able to reach the same C:N and TN levels during the monitoring period.

Keywords: Composting, bacteria and enzyme, cattle manure, C:N ratio, windrow composting

1. INTRODUCTION

Extensive production of livestock can result in pollution problem causing the deterioration of air, water, and soil quality [1]. Excessive accumulation of manure will lead to nutrient surpluses in the farm areas especially when nutrient demand is greater than the fertilization requirements. The right management of nutrients must include the reduction of manure volume, properly designed and operated composting plant, and the environmentally friendly manure transportation systems. Composting must comply with all environmental regulations and problems during handling the manure from husbandry to the composting site. Composting process reduces the volume of the unprocessed manure through biological and chemical mineralization reactions under aerobic conditions. At the end, a useful end-product, compost, is produced [2] [3]. If this end-product (compost) is used for crop fertilization, the risk of spreading pathogens and weeds will be minimized as well as the soil quality will be improved [4]. The process of composting is usually adjusted by the C:N ratio of the compost materials. The recommended value of C:N ratio is from 25 to 35, in which C is the energy source and N is the nutrient source for microbial growth. If the C:N ratio is not balanced in a compost pile, it will either slow the compost process or cause N losses during the composting process. Bernal et al., (2009) [2] and Pardo et al. (2015) [5] reported that gaseous emissions account for up to 60 to 70% of the initial N and C content in manure, respectively. The most common way of losing N is due to ammonia volatilization, which usually takes place during the first few weeks of composting process [6-8].

The microorganisms are essential for transformation and transportation of nutrients in the compost. During the process of composting, different bacteria carry out to the nitrogen transformation and some fungi and bacteria favor the solubilization of phosphorus and potassium. Therefore, these microorganisms can help the enhancement of the availability of these nutrients in the soil [9]. Most of the composting bacteria are decomposers, which are also called saprophytes, belonging to the group of chemoorganotrophic microorganisms. Some examples of these bacteria are; *Pseudomonas, Burkholderia, Zymomonas,*

[1] *Environmental Engineering Department, College of Engineering A13, Imam Abdulrahman Bin Faisal University, Main Campus, Dammam, 1982, Saudi Arabia E mail: cevatyaman@yahoo.com Phone: 966550245937*

Xanthomonas, and nitrogen-fixing aerobic bacteria. Some chemolithotrophic bacteria (genera of *Nitrosomonas* and *Nitrospira*) are also involved in composting processes such as nitrification bacteria which converts ammonium to nitrite and nitrate [10-13]. Fungi are also involved in decomposing wastes during compost processes. Fungi are known as decomposers and they can be present in compost piles during the first and final phase of the composting process. The most representative genera of fungi are; *Aspergillus, Acremonium, Chrysosporium, Fusarium, Mortierella, Penicillium*, and *Trichoderma* [14], [15].

These types of bacteria and fungi contribute to the decomposition and transformation of nutrients. Therefore, it is important to offer alternatives for the enrichment of compost like providing high amounts of nutrients that are readily available for plants. One of the most promising methods is the introduction of special microbial organisms and enzymes into the compost pile to accelerate the composting process and increase the content of nutrients in the finished compost. This study investigates the effects of inoculating specifically produced compost activator bacteria on the acceleration of cattle manure compost process at a full-scale plant.

2. MATERIALS AND METHODS

Composting is the controlled natural decomposition of organic matter into usable humus for gardens, trees, shrubs and indoor plants. Most organic materials can compost naturally, but conditions can be variable, resulting in inconsistent, poor compost. An understanding of the composting process and proper management can improve composting, producing a uniform, high-quality product. Microorganisms use oxygen and water to decompose organic wastes. End products of this process include nutrient-rich compost, carbon dioxide (CO_2), heat and water (Figure 1).

o ***Composting Factors***

All natural organic materials eventually decompose. The length of the composting process depends on a number of factors:
- carbon and nitrogen ratio
- surface area
- aeration
- moisture
- pile temperatures
- the right microorganisms
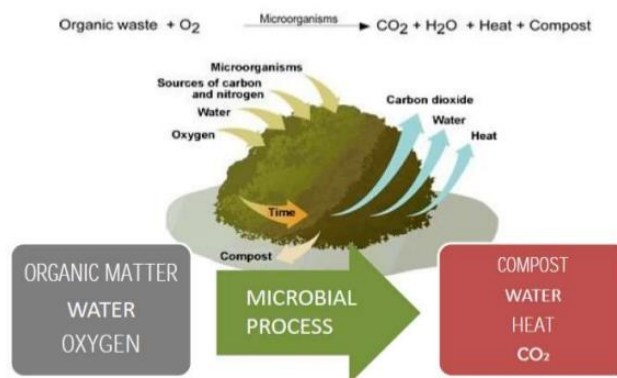
Figure 1. Composting process

o ***Carbon-to-Nitrogen Ratio***

Every living material has a C:N (carbon-to-nitrogen) ratio in its structure. C:N is an important parameter to consider for composting organic materials. Microorganisms consume carbon as an energy source, and nitrogen for protein synthesis. With the proper balance of C:N ratio, microorganisms can decompose organic material much faster. When there is not sufficient nitrogen (high C:N ratio), decomposition slows down. When there is

more nitrogen (low C:N), most of the nitrogen will be lost to the atmosphere as ammonia gas, which can create odor problems. For efficient composting, the optimum C:N should be approximately 26-35 by weight. Since most materials do not meet this ratio, different compost materials must be blended to meet the ratio. For instance, mixing two parts of lawn clippings with one-part leaves will result in a C:N of approximately 30:1. The C:N of some common compost materials are shown in Table 1.

Table 1. Carbon-to-Nitrogen ratios by weight

High N materials	
Composting material	**Carbon-to-Nitrogen ratio**
Vegetable waste	12-20:1
Grass clippings	12-25:1
Cow manure	20:1
High C materials	
Leaves	30-80:1
Paper	150-200:1
Wood chips	100-500:1

o   *Surface Area*

Most of the microbial activity occurs on the surface of particles. Thus, the more surface area exposed, the faster the decomposition. Although it is not required, compost materials should be shredded into small pieces to accelerate the process. For example, fallen leaves can be shredded by simply mowing them.

o   *Aeration*

Rapid decomposition of organic materials occurs most efficiently under aerobic conditions. Air movement in a compost pile depends on porosity and moisture content. Porosity is identified as the spaces between particles in a compost pile, which are filled with air. If the moisture content in the pile is too high, these spaces will be filled with water, decreasing porosity. Excessively small particle size will also decrease porosity. Adding coarse materials, regular turning of the pile, and proper moisture will improve aeration. Compost pile can be turned using a fork or shovel, or commercially available aeration tools.

o   *Moisture*

Microorganisms require moisture to decompose organic materials. The optimum moisture of compost piles without limiting aeration is around 40-60%. If the pile is too dry (not sufficient moisture), microbial decomposition will slow. If the pile is too wet (excess moisture), nutrients will leach out, oxygen will be depleted within the pile, and odors will be produced. An easy way of measuring the moisture is to squeeze a handful of compost material. The material should have a drop or two of liquid expelled when tightly squeezed in the hand. Excessively moist compost piles should be turned to allow air circulation and better drainage. Dry, fibrous materials such as sawdust can also be added to alleviate the problem. Excessively dry compost piles should be watered gradually either with a hose. Gradual watering is very important because some materials shed water or absorb it only on the surface.

o   *Temperature*

Microbiological activities during the composting process generate heat, which increase pile temperature. The process occurs in four steps, depending on the temperature fluctuations. The first step, the mesophilic stage, occurs when the pile temperature varies between ambient and 43.3°C. In this phase, microorganisms start to grow and decompose the organic matter, producing heat which increase the pile temperature. The thermophilic stage starts as the pile temperature rises above 43.3°C. Optimum decomposition occurs between 43.3°C and 60°C; thus, it is important to maintain the pile at this temperature range for a while. If pile temperature rises above 65.5°C, composting microorganisms will die. The cooling phase follows as microbial activity slows due to nutrient depletion, which decreases pile temperature. The compost at this stage is still not mature, containing phytotoxins that can inhibit plant growth. The final step of composting is called the maturation. In this stage, complex chemical reactions break down the phytotoxins. Mature compost contains no plant growth inhibitors, has a good earthy smell, and is nutrient balanced.

o   *Selection and preparation of the compost material*

Cattle manure is an excellent source of nutrients for crops and can improve soil quality. Properties of manure are affected from several factors such as diet, animal age, digestibility, fiber content; housing, and environment. The solid content (the percent of solids per unit of liquid) is an important parameter for composting. More precisely, the make-up of manure solids like fixed and volatile solids, suspended solids and dissolved solids also play an important role in composting. The content of nutrients (nitrogen, phosphorus, and potassium) is also important since it affects land application rates. The characteristics of the fresh manure used in this study are shown in Table 2. This study was carried out near a cattle barn where the fresh manure was first left under the sun for a few days to bring the moisture content down to about 70%. An impermeable concrete floor was prepared for the windrow composting process and the compost area was open to the atmosphere.

The waste manure was transported to the composting site in trucks. Once arrived at the site, the manure waste was dumped on the platform specifically prepared to achieve windrow composting. As manure accumulated, the previous load was turned to make sure that adequate mixing is achieved. Finally, 50 tons of manure was placed on the platform and mixed several times with a windrow compost tractor.

Table 2. Characteristics of the manure used in the study

Average weight of one cow (kg)	Total manure (kg/day)	Moisture content (%)	Density (kg/m^3)	TS (%)	VS (%)	TN (%)	P_2O_5 (%)	K_2 (%)	C:N Ratio
500	50	71	400	29	84	1.89	1.95	1.99	25.94

o   *Dimensions of the compost pile*

After the manure was ready for composting, 50 tons of cattle manure was transported to the compost area and piled in a trapezoidal shape as shown in Figure 2. The bottom length, the height, and the upper length of the trapezoidal piles were 2.1 m, 1.7 m, and 0.6 m, respectively. The dimensions of the piles were determined based on the available area and the amount of the manure (50 tons). The length of each pile, bacteria added pile and the control pile, was selected as 54 m as shown in Figure 3.
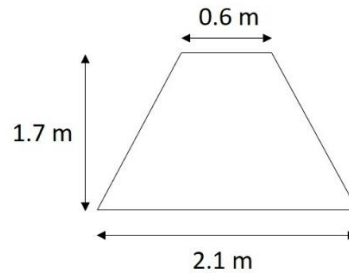
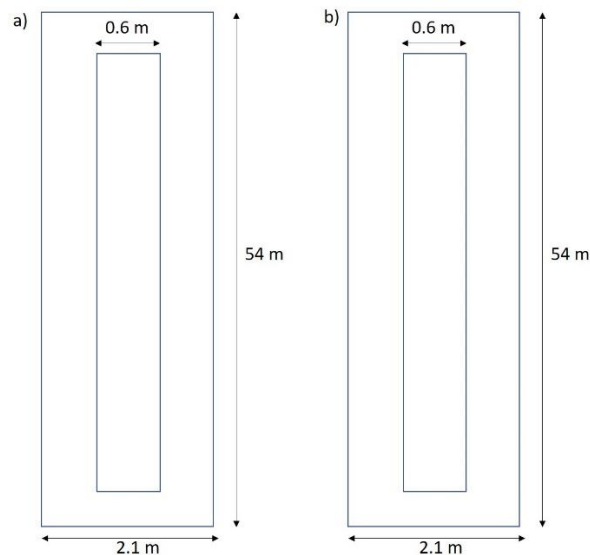*Figure 2. Cross section of the windrow compost pile*

Figure 3. Plan views of the windrow compost piles, a) compost bacteria added pile, b) control pile

o *Application of compost activator bacteria*

This product, compost activator, stimulates the composting process through the addition of concentrated bacteria and enzymes, the same bacteria and enzymes that occur in nature. This accelerated method of composting provides finished compost in the shortest time possible, as little as days. This abbreviated composting cycle saves time and money. The amount of compost activator is determined at a rate of one pound (454 gram) per 8 m3 of raw compost material. The volume of manure in this study is calculated as 50,000 kg/400 kg.m3-, which is equal to 125 m3. Then, the amount of compost activator needed is calculated as 125x454/8, which is equal to 7,093 grams (≈7 kg). How much water used is critical as that is what disperses the product into the matrix better. Compost activator bacteria is in powder form and needs to be dissolved in water before application to the pile. How much water is used depends on the starting moisture levels of the pile. The moisture content of the manure in this study is around 71%. Too much moisture causes problems, such as preventing adequate aeration. First, it is important to hydrate the microorganisms in compost activator to make sure that they will be ready to go when applied to the system. Therefore, a minimum amount of water is needed to completely dissolve the product and ensure the activity of the water is high enough to adequately hydrate the microorganisms. The excess water will be used as a carrier. This is where the amount of water used is important in some situations. For systems that are well mixed, the amount of carrier is not critical. In poorly mixed systems, more water is needed to allow for better dispersion. Usually by the time manure is being composted much of the moisture will be gone. Sampling will reveal the current moisture content at the start when building the pile and from that how much water is needed can be calculated to bring the moisture up to optimum levels. That is how much water needs to be used to dissolve the compost activator. It is usually better to try to have it

as large a volume as possible to get best dispersion of the bacteria solution. The prepared solution was dispersed over the pile by using a windrow machine. As the solution was sprayed over the pile, the windrow machine mixed the compost material to make sure that the bacteria solution was dispersed equally in the pile. A separate control pile was also used for comparison. Temperature, pH, moisture contents were monitored during the study.

3. RESULTS AND DISCUSSION

o *Variations of compost properties during composting*

The temperature of the compost core pile monitored over the one-month period (Figure 4) varied from 30 °C at the beginning to a maximum of 65 °C by day 6, with the thermophilic stage (≥50 °C) being achieved at day 5 for pile 1 and at day 10 for pile 2. The materials in both piles were exposed to temperatures greater than 65 °C for more than 3 consecutive days as suggested by the US composting council [16]. The pH value of the compost piles was slightly alkaline. In addition, temperatures of the piles were maintained higher than 50 °C for at least 15 consecutive days to reduce the potential for spreading infectious disease. The compost moisture for both piles generally declined during the entire composting process, from the initial 71% to the final 59%.
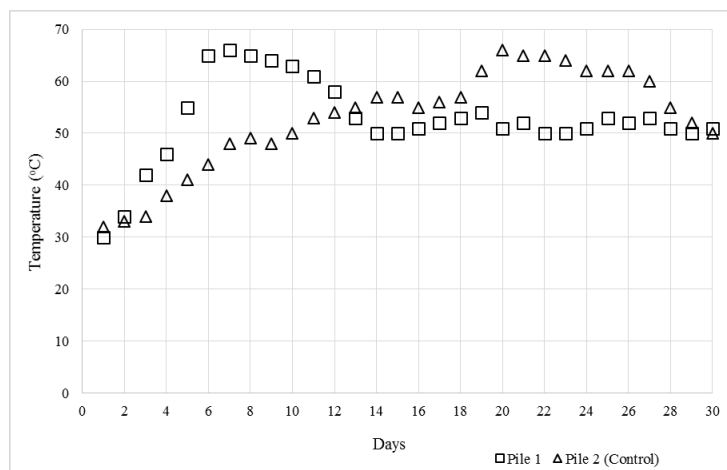
Figure 4. Changes in temperature during composting

The C:N value of the compost piles decreased from the initial 25.62 to the final 13.62 (Pile 1) and 20.1 (file 2), with a significant decrease from 4 to 12 days for pile 1(Figure 5). The changes in total nitrogen throughout the composting process are shown in Figure 6. Total nitrogen in pile 1 gradually increased from the initial 1.89% to 3.2% at day 19, followed by little variation to the end of composting. However, in pile 2, total nitrogen slowly increased from the initial 1.89% to 2.67% at day 25, followed by small variation to the end of the study. Total nitrogen in both piles increased especially after day 10 as percentages due to the reduction in carbon content. However, the rate of TN increase was much faster in pile 1.

Figure 5. Changes in C:N ratio during composting

Figure 6. Changes in total nitrogen during composting

o   ***Effect of compost activator bacteria on compost process***

It is clearly seen in Figures 4, 5, and 6 that the compost activator added pile (pile 1) performed much better than the control pile (pile 2) in terms of temperature increase, C:N ratio, and total nitrogen percentage in the final compost. Compost activator bacteria accelerated the compostin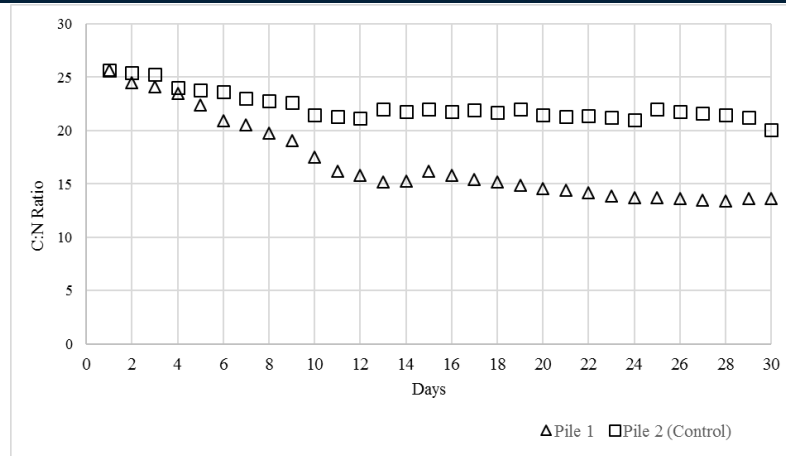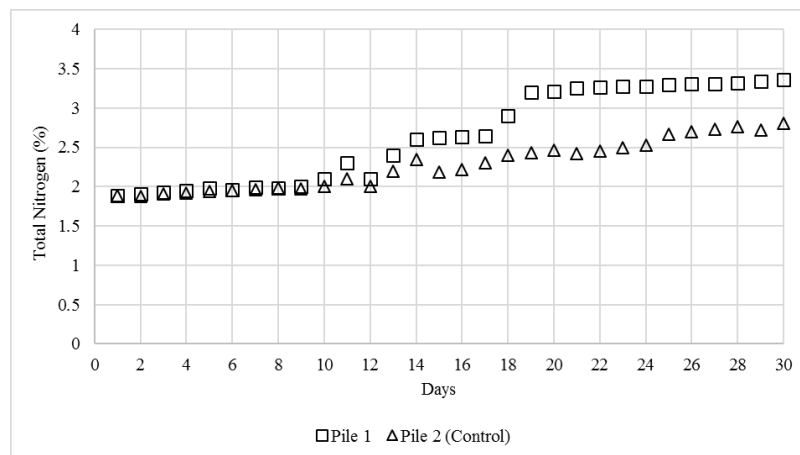g process. The C:N ratio in pile 1 dropped to less than 20 after day 8, while the C:N ratio was always above 20 during the study. After day 18, the C:N ratio was below 15 for pile 1, which shows the maturity of the compost.

CONCLUSIONS

This full-scale study demonstrated that composting duration can be shortened by applying compost activator bacteria. From the data obtained, it can be concluded that the windrow composting of cattle manure wastes by adding composting bacteria is an effective way to reduce the time for composting. Also, the waste compositions were optimum for the increase in temperature necessary to ensure the hygiene of the compost produced. Optimum C:N ratios were also achieved in bacteria added pile much faster than the control pile.

BIOGRAPHY: Dr. Yaman received his master and PhD degrees from Drexel University (USA) in Environmental Engineering. He worked at MT Associates (NJ, USA), Roux Associates (NJ, USA) and RT Environmental Services (PA, USA) as an engineer. After returning back to Turkey, Dr. Yaman worked as Deputy General Manager at the Ministry of Environment, as Head of Environmental Protection Department at

Istanbul Metropolitan Municipality and as a faculty member at Gebze Technical University. Dr. Yaman is currently working at Imam Abdulrahman Bin Faisal University, Saudi Arabia. His main research areas are waste management and bioremediation.

ACKNOWLEDGMENT

REFERENCES

[1]. Petersen, S.O., Sommer, S.G., Beline, F., Burton, C., Dach, J., Dourmad, J.Y., Leip, A., Misselbrook, T., Nicholson, F., Poulsen, H.D., Provolo, G., Sørensen, P., Vinner_ as, B., Weiske, A., Bernal, M.P., B€ohm, R., Juh_asz, C., Mihelic, R., 2007.

[2]. Bernal, M.P., Alburquerque, J.A., Moral, R., 2009. Composting of animal manures and chemical criteria for compost maturity assessment. A review. Bioresour. Technol. 100, 5444-5453.

[3]. Pardo, G., Moral, R., Aguilera, E., del Prado, A., 2015. Gaseous emissions from management of solid waste: a systematic review. Glob. Change Biol. 21, 1313-1327.

[4]. Onwosi, C.O., Igbokwe, V.C., Odimba, J.N., Eke, I.E., Nwankwoala, M.O., Iroh, I.N., Ezeogu, L.I., 2017. Composting technology in waste stabilization: on the methods, challenges and future prospects. J. Environ. Manage. 190, 140-157

[5]. Larney, F.J., Hao, X., 2007. A review of composting as a management alternative for beef cattle feedlot manure in southern Alberta, Canada. Bioresour. Technol. 98, 3221-3227.

[6]. Martins, O., Dewes, T., 1992. Loss of nitrogenous compounds during composting of animal wastes. Bioresour. Technol. 42, 103-111.

[7]. Parkinson, R., Gibbs, P., Burchett, S., Misselbrook, T., 2004. Effect of turning regime and seasonal weather conditions on nitrogen and phosphorus losses during aerobic composting of cattle manure. Bioresour. Technol. 91, 171-178.

[8]. Sommer, S.G., 2001. Effect of composting on nutrient loss and nitrogen availability of cattle deep litter. Eur. J. Agron. 14, 123-133.

[9]. Sanchez, Ó. J., Ospina, D. A., Montoya, S., 2017. Compost supplementation with nutrients and microorganisms in composting process. Waste Manage. 69, 136–153

[10]. Insam, H., de Bertoldi, M., 2007. Microbiology of the composting process. In: Diaz, L. F., de Bertoldi, M., Bidlingmaier, W., Golueke, C. (Eds.), Compost Science and Technology. Elsevier, pp. 25–48.

[11]. Madigan, M., Martinko, J., Dunlap, P., Clark, D., 2009. Brock. Biología de los Microorganismos. Pearson, Madrid.

[12]. Ryckeboer, J., Mergaert, J., Coosemans, J., Deprins, K., Swings, J., 2003a. Microbiological aspects of biowaste during composting in a monitored compost bin. J. Appl. Microbiol. 94, 127–137.

[13]. Ryckeboer, J., Mergaert, J., Vaes, K., Klammer, S., De Clercq, D., Coosemans, J., Insam, H., Swings, J., 2003b. A survey of bacteria and fungi occurring during composting and self-heating processes. Ann. Microbiol. 53, 349–410.

[14]. Anastasi, A., Varese, G., Marchisio, V., 2005. Isolation and identification of fungal communities in compost and vermicompost. Mycologia 97, 33–44.

[15]. Pérez, Y., Rebollido, R., Martínez, J., 2010. Aislamiento e identificación de hongos en compost elaborado a partir de residuos solidos urbanos (Isolation and identification of fungi in compost produced from municipal solid waste, in Spanish). Agro Sur 38, 1–7.

[16]. Thompson, W., Leege, P., Millner, P., Watson, M.E., 2003. Test Methods for the Examination of Composts and Composting. The US Composting Council, US Government Printing Office.

[17]. van Heerden, I., Cronje, C., Swart, S.H., Kotze, J.M., 2002. Microbial, chemical and physical aspects of citrus waste composting. Bioresource Technol. 81, 71–76.

[18]. Kim, J.-D., Park, J.-S., In, B.-H., Kim, D., Namkoong, W., 2008. Evaluation of pilot-scale in-vessel composting for food waste treatment. J. Hazard. Mater. 154, 272–277.

Optimization of hydrothermal synthesis of Ce³⁺ co-doped NaYF₄, Yb³⁺, Er³⁺upconversion nanoparticles and investigation of their size, morphology, and phase transitions.

Seda Demirel Topel[1]

Abstract

Herein, the synthesis of water-soluble polyethyleneimine (PEI) modified UCNPs which were prepared by a hydrothermal method have been reported. The resultant UCNPs were small size and hexagonal β-phase structure thanks to the Ce³⁺ co-doping effect. Without Ce³⁺ ion co-doping, NaYF₄,Yb³⁺,Er³⁺ (80% Y,18% Yb, 2% Er) UCNPs were micro-rods shape with ≈5 μm length and pure hexagonal phase. After introducing 3% of Ce³⁺ to the NaYF₄,Yb³⁺,Er³⁺ (72% Y,20% Yb, 5% Er) UCNPs, the sizes of the UCNPs have been reduced to 90 nm diameter with hexagonal phase and 30 nm diameter with cubic phase. The cubic-to-hexagonal phase transition process was approved by X-ray diffraction (XRD) and their sizes were also calculated from the Debye-Scherrer equation from the XRD data which are coherent with the particle size measured from transmission electron microscope (TEM). Additionally, the UCNPs display three emission bands at 520, 540 and 654 nm under 980 nm laser due to the 4f-4f transitions of Er³⁺ ions.

Keywords: upconversion, nanoparticle, X-Ray diffraction, Debye-Scherrer, TEM

1. INTRODUCTION

Upconversion nanoparticles (UCNPs) are an emerging class of nanomaterial made of a NaYF₄ host lattice including Yb³⁺ and Er³⁺ ions which act as an absorber and emitter ion, respectively [1]. Due to the Yb³⁺ ion embedded in host lattice of NaYF₄, the nanoparticle can absorb long wavelength near infrared (NIR) excitation and convert it into short wavelength ultraviolet (UV) and visible light [1]. This process has been known as upconversion process [1]. In the late of 1990s, Menyuk and Kano had been first introduced Yb³⁺ and Er³⁺ doped NaYF₄ which is the most efficient UCNP today [2,3]. After the discovery of this phenomenon, these nanomaterials have been became one of the most attractive research field within nanoscience community, and applied to bioimaging, drug delivery, photodynamic therapy, dye sensitized solar cells, detection sensors, 3D optical displays, security labeling and optical data storage [4]. Among all of these applications, it has gained immense interest in the biological applications due to their low toxicities and deep penetration ability of the excitation light [5]. Upon excitation with NIR light of the UCNPs, the absorption of blood components such as oxy-hemoglobin, deoxy-hemoglobin and water are at minimum which means that UCNPs have deeper penetration of light and have high signal to noise ratio [6].

In order to engineer an upconversion nanomaterial for a biological approach, three important parameters should be considered as follows *(i)* solubility, *(ii)* crystallinity, *(iii)* size of the UCNP [7]. Firstly, for a biological application, the synthesized UCNPs should be water dispersible. Therefore, the surface of UCNPs should be modified with a water soluble polymer such as polyacrylic acid (PAA), polyethyleneimine (PEI), polyethyleneglycol (PEG), and/or polyvinylpyrrolidone (PVP) [8]. The another important parameter for UCNP is its crystallinity. The upconversion luminescence efficiency of the hexagonal nanocrystals is much higher than that of the cubic phase NAYF₄ nanocrystal. Lastly, the UCNPs should be less than 50 nm diameter in size in order to penetrate through the cells for biological applications [8].

---

[1] *Antalya Bilim University, Faculty of Engineering, Department of Mat.Sci& Nanotech Eng. 07190, Antalya,Turkey*

On the other hand, the preparation technique effects the size of the UCNPs as well. A variety of techniques, including thermal decomposition, solvothermal, co-precipitation, sol-gel and hydrothermal method have been demonstrated to prepare the lanthanide doped UCNPs [9]. Between these techniques hydrothermal method is an environmental friendly, requires relatively low temperature and result in a good crystallinity with higher yields compared to the other methods. Hence, it is essential to produce UCNPs with higher yields, water soluble property, hexagonal phase and small size in order to apply to a biological field [10]. Keeping mind all of the mentioned requirements, we designed and synthesized water-soluble polyethyleneimine (PEI) modified UCNPs which were prepared by a hydrothermal method and produced in small size and hexagonal phase structure thanks to the Ce^{3+} co-doping effect.

2. MATERIALS AND METHOD

Materials: All the rare earth chloride ($RECl_3$) lanthanide salts ($YCl_3.6H_2O$, $YbCl_3.6H_2O$, $ErCl_3.6H_2O$ and $CeCl_3.6H_2O$), NaOH, NH_4F, PEI; MW 10.000 g/mol) and solvents were purchased from Sigma-Aldrich and Merck, and used without any further purification.

Characterization: The synthesized UCNPs were characterized by FEI, Tecnai G2F30 TEM and Rigaku, micromax 007HFDW XRD instrument. Optophysical properties and fluorescent measurements were obtained from Ocean Optics, USB4000-FL model spectrophotometer with an external 980 nm laser.

Methods: The UCNPs have been prepared by hydrothermal method. Firstly, $YCl_3.6H_2O$ (0.72 mmol), $YbCl_3.6H_2O$ (0.20 mmol), $ErCl_3.6H_2O$ (0.05 mmol) and $CeCl_3.6H_2O$ (0.03 mmol) were added into a Teflon beaker. Then, into this beaker NaCl (1 mmol) and 4 mL of d.d.H_2O were added and stirred at room temperature (r.t) until all the lanthanide salts dissolved. After solved all the salts, 50 mL of anhydrous ethanol were added and stirred further 5 minutes. The PEI (0.1 mmol) was dissolved in 20 mL of dd H_2O and 10 mL of this solution was introduced into the main solution. Last, NH_4F (5 mmol) were added to the Teflon beaker and for 20 minutes the resultant mixture was bubbled under $N_2(g)$ atm , and then sealed into a stainless steel autoclave reactor and heated to 200°C for 1-3 hours. When the reaction was completed, the autoclave was allowed to cool to r.t. All the white precipitates were separated with ultracentrifuge at 10.000 rpm for 15 min. For purification, all the UCNPs were washed 3 times with ethanol:H_2O (1:1) (50 mL) and dried in a vacuum oven at 40°C during a night. The prepared UCNPs were then characterized by TEM, TEM-EDX, TEM-mapping and XRD.

3. RESULTS AND DISCUSSION

In order to optimize the size of the UCNPs by hydrothermal method, different volumes of ethanol, different concentrations of PEI in aqueous solution and different ratios of Ce^{3+} ion in $RECl_3$ solution have been applied to different batches (1-4). The resultant sizes and surface morphology of the synthesized UCNPs from each batches have been determined by TEM. In the first batch, 0.2 M $RECl_3$ solutions were prepared and used in the ratio as follows 78:20:2 (Y: Yb: Er) and for water solubility of the UCNPs, 5% of PEI solution was added. The prepared solutions were transferred into the Teflon beaker. The reaction was carried out at 200°C for 2 hours. As a result of the batch-1, the UCNPs were obtained with 5μm rod shape and pure hexagonal phase.
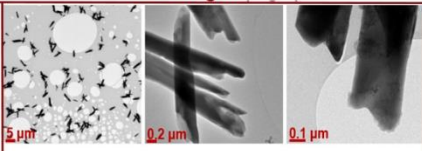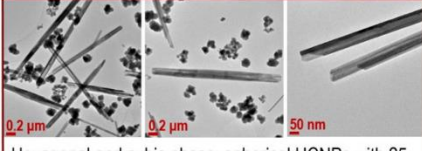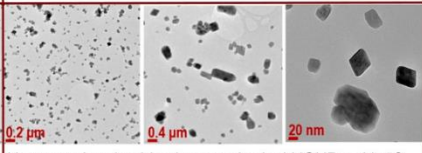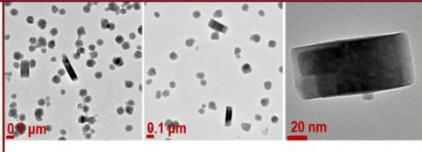
No	TEM Images	Reaction Conditions
1	Hexagonal phase: rod shape UCNPs with 5 μm length	0.2 M $RECl_3$ (No Ce^{3+}) Y: Yb: Er (%)= 78:20:2 $RECl_3$: NaCl = 1: 1.8 NaCl : NH_4F = 1: 1.1 PEI = % 5 (aq.) **Ethanol = 10 mL** Temperature = 200°C Time = 2 hours
2	Hexagonal and cubic phase: spherical UCNPs with 25 nm diameter and rod shape UCNPs with 1.5 μm length	0.5 M $RECl_3$ Y: Yb: Er:Ce (%)= 72:20:5:3 $RECl_3$: NaCl = 1: 0.5 NaCl : NH_4F = 1: 2.5 PEI = % 5 (aq.), 5 mL **Ethanol = 15 mL** Temperature = 200°C Time = 2 hours
3	Hexagonal and cubic phase: spherical UCNPs with 50 nm diameter and rod shape UCNPs with 100 nm length	0.5 M $RECl_3$ Y: Yb: Er:Ce (%)= 72:20:5:3 $RECl_3$: NaCl = 1: 0.5 NaCl : NH_4F = 1: 2.5 PEI = % 5 (aq.), 10 mL **Ethanol = 20 mL** Temperature = 200°C Time = 2 hours
4	Hexagonal and cubic phase: spherical UCNPs with 25 nm diameter and rod shape UCNPs with 80 nm	0.5 M $RECl_3$ Y: Yb: Er:Ce (%)= 72:20:5:3 $RECl_3$: NaCl = 1: 5 NaCl : NH_4F = 1: 2.5 PEI = % 5 (aq.), 10 mL **Ethanol = 30 mL** Temperature = 200°C Time = 2 hours

Figure 1. Reaction conditions and their corresponding TEM images of UCNP samples 1-4

Yu and co-workers were reported that the UCNPs doped with Group III (Ce and La) could induce anisotropic crystal growth to form $NaYF_4$ nanorods with reduced diameter. Therefore, in batch-2, we introduced 3% of Ce^{3+} ion to the $RECl_3$ solution while the percentage of PEI solution was kept constant and increased the volume of ethanol from 10 mL to 15 mL in the reaction vessel. TEM results show that the lengths of the rods were decreased from 5 μm to 1 μm compared to batch-1 and small spherical nanoparticles were appeared with 25 nm diameter. Increasing the volume of ethanol resulted the decreasing the particle size as well. Therefore, in batch-3, we increased the volume of ethanol to 20 mL while keeping the other parameters constant at batch-2. In this case, the length of the rod shape UCNPs were reduced to 100 nm and the spherical UCNPs are 50 nm. In the last batch-4, the volume of the ethanol was further increased to 30 mL, and showed that the length of the rod shape UCNPs were reduced to 80 nm. The results revealed that the addition of ethanol having such a low dielectric constant to the aqueous media may alter the thermodynamic of the hydrothermal reaction system. As a result of this changing in the thermodynamic, varying the dielectric property of ethanol/water may affect the colloidal interaction between solid particles which leads to the changing in the nucleation kinetics and all of the mentioned effects may result in reducing the particle size, and the size distribution of resultant UCNPs.

In order to prove the rare earth elements were dopped successfully in the upconversion nanocrystal, TEM-EDS (Energy Dispersive X-ray spectroscopy) mapping onto a selected nanoparticle was applied (Fig.2). In Fig. 2, the lighter areas on the nanoparticle represent the existence of the related elements on to UCNP. Hence, it shows that the nanoparticles were successfully doped with cerium, erbium, ytterbium and yttrium. Due to the branched PEI modification on the surface of UCNPs, there is a carbon mapping which covers the whole surface of UCNP (Fig.2).
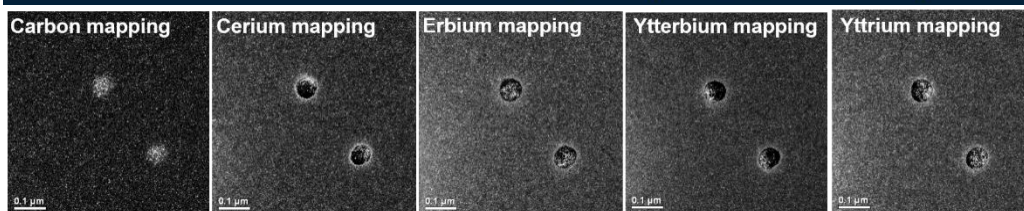
Figure 2. TEM-EDS mapping in Ce3+ co-doped NaYF$_4$:Yb^{3+}, Er^3 UCNPs

The crystallinity and phase transitions of the resultant UCNPs obtained from batches 1-4 were determined by XRD measurements (Fig.3). According to Chang H., the rate of homogeneous nucleation is strongly dependent on the degree of supersaturation. At lower ethanol volumes, the RECl$_3$ solution is more concentrated. Thus, the nucleation rate increases at concentrated solutions during the hydrothermal synthesis. As a result of this theorical assumption, upconversion nanocrystals should be grow through the hexagonal phase at micron size. XRD data prove this assumption and demonstrate that sample 1 and 2, prepared from batches 1 and 2, are all in pure hexagonal phase. After increasing the volume of ethanol in batch 3 and 4, their corresponding samples 3 and 4 have cubic and hexagonal phase as a mixture (Fig.3). XRD data reveals that increasing the ethanol volume not only effected the particle size, but also effected the phase transitions.
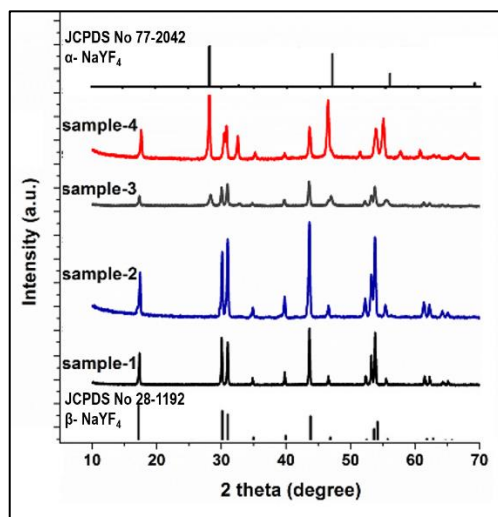
Figure 3. XRD data of UCNP sample 1-4

Fluorescence spectrum (FS) of Ce^{3+} co-doped NaYF$_4$:Yb^{3+}, Er^3 at the room temperature given in Fig. 4. FS shows the narrow emission bands corresponding to characteristic *4f–4f* transitions of Er^{3+} ions doped in the UCNPs. The green emission observed at 440, 520 and 540 nm originate from 2H$_{9/2} \rightarrow$ 4 I$_{15/2}$, 2H$_{11/2} \rightarrow$ 4 I$_{15/2}$, 4 S$_{3/2} \rightarrow$ 4 I$_{15/2}$ transition, respectively, whereas the red fluorescence at 658 nm is attributed to the 4F$_{9/2}$– 4 I$_{15/2}$ transition.
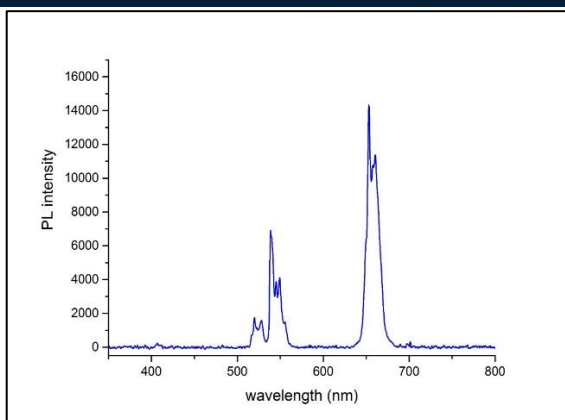
Figure 4. Fluorescence spectrum of the UCNP sample-4 under 980 nm laser excitation

4. CONCLUSION

As a conclusion, PEI coated and Ce^{3+} co-doped $NaYF_4$:Yb^{3+}, Er^{3+} UCNPs was synthesized via a hydrothermal method and four different reaction conditions have been tried to optimize the reaction in order to produce small size, hexagonal phase and water dispersible UCNPs. The results reveal that by increasing the volume of ethanol and introducing to Ce^{3+} ion as a co-dopant resulted in decreasing the sizes of hexagonal phased UCNPs from 1.5 μm to 80 nm, and the particles were also stabilized with PEI coating. The resultant solution of those nanoparticles in aqueous solution is very stable at room temperature and can keep without any precipitation for a month and also their luminescence properties are very stable as well.

ACKNOWLEDGMENT

REFERENCES

[1]. M. Haase, H. Schafer, "Upconverting nanoparticles", Angew. Int. Chem.Ed., vol.50, pp.5808-5829, 2011.

[2]. N. Menyuk, K. Dwight, J.W. Pierce, "$NaYF_4$:Yb, Er-An efficient upconversion phosphor", Appl. Phys. Lett., vol.21, pp.159-163, 1972.

[3]. T. Kano, T. Suzuki, A. Suzuki, S. Minagawa," Fabrication of efficient upconversion type green LED using $NaYF_4$-Yb, Er phosphor, J. Electrochem.Soc.,vol. 120, pp. C87, 1973.

[4]. L.Y. Ang, M.E. Lim, L.C. Ong, Y. Zhang, "Applications of upconversion nanoparticles in imaging, detection and therapy", Nanomed., vol.6, pp.1273-1288, 2011.

[5]. Gnach, T. Lipinski, A. Bednarkiewicz, J. Rybka, J.A. Capabianco, "Upconverting nanoparticles: assessing the toxicity", Chem. Soc.Rev., vol.44, pp. 1561-1584, 2015.

[6]. H. Qiu, M. Tan, T.Y. Ohulchanskyy, J.F. Lovell, G. Chen, "Recent progress in upconversion photodynamic therapy", Nanomaterials (Basel), vol. 8, pp. 344-362, 2018.

[7]. Gee, X.Xu, "Surface functionalization of upconversion nanoparticles with different moieties for biomedical applications" Surfaces, vol.1, 96-122, 2018.

[8]. Gulzar, J. Xu, P. Yang, F. He, L. Xu, "Upconversion process: versalite applications and biosafety", Nanoscale, vol.9, pp.12248-12282, 2017.

[9]. J. Chen, X. Zhao, "Upconversion nanomaterials: synthesis, mechanism, and applications in sensing" Sensors, vol.12, pp.2414-2435, 2012.

[10]. S. Demirel Topel, G. Turgut Cin, E.U. Akkaya, "Near IR excitation of heavy atom free Bodipy photosensitizers through the intermediacy of upconverting nanoparticles", Chem. Commun. vol. 50, pp.8896-8899, 2014.

BIOGRAPHY

Seda Demirel Topel has received her B.S degree in Chemistry (2006, Akdeniz University), her M.S degree in Organic Chemistry (2009, Akdeniz University) and her PhD degree in Organic Chemistry (2013, Akdeniz University and Bilkent University). In the first years of her PhD, she joined the Natural Products group as a researcher for 6 months at Lund Universty, Sweden, and then continued her PhD studies at National Nanotechnology Research Center (UNAM), Bilkent University in the field of organic-hybrid nanoparticles for photodynamic therapy (2010-2013). Then she continued her studies as Post-Doc fellows at the Department of Molecular Sciences, SLU, Sweden and at the Department of Material Science and

Engineering, Akdeniz University in 2013-2015 and 2015-2017, respectively. Now, she is working as Assist. Prof. at the Department of Material Science and Nanotechnology Engineering at Antalya Bilim University, since 2017. Her research interests include the synthesis and characterization of different types of nanoparticles (silicon dioxide, titanium dioxide, superparamagnetic iron oxide and upconversion nanoparticles) and their hybrid forms with organic ligands for biological (theranostic, bio-imaging, controlled drug delivery) and environmental applications (water treatment, sequestration of lanthanide elements from ores).

A Decision Framework for Sustainability Assessment of Energy Generation Technologies in India

Manju Pandey [1], Akshay Hinduja[1]

Abstract

Sustainability of energy sources have a major concern among the researchers and environmentalist across the world. Due to rapid growth of population, increasing economic developments, and rising living standard, the demand of energy has been escalating in India. However, the energy sources in India energy sector are mainly based on fossil fuels, which emit harmful gases and byproducts in the environment. Its consequences can easily be observed on climate. Besides, these resources are limited, and may be completely depleted in few decades. A balanced approach is required to solve the issue of environmental degradation as well as to supply expanding demand of energy. Deployment of sustainable energy sources can be one solution to this adverse situation as it prevents the environment from pollution as well as preserves the natural resources. The objective of this paper is to introduce a decision framework that prioritizes the sustainability indicators as well as evaluates the energy generation technologies for sustainability. The framework comprises three phases, identification of sustainability criteria and indicators, prioritization of sustainability indicator, and sustainability assessment of energy generation technologies. The paper identified 20 indicators and classified them into five criteria. The prioritization and evaluation phases encompasses intuitionistic fuzzy analytic hierarchy approach that effectively handles the uncertainty and hesitancy in the experts' opinions. The paper also adapted a case study to illustrate the working of the assessment framework.

Keywords: Sustainable energy, Sustainability Assessment, Multi Criteria Decision Making, Intuitionistic Fuzzy Analytic Hierarchy Process.

1. INTRODUCTION

Energy is an indispensable requirement to any country for its economic and social development. Energy has become an essential parts of businesses, industries, service sectors, and even domestic day-to-day works. With the rapid growth in population and swift rise in standard of living, the energy consumption is also increasing. The growing demands for energy is triggering the over utilization of the available natural resource and rising accumulation of the greenhouse gases in the atmosphere. Resulting climate changes as well as soil, air and water pollution are adversely affecting the quality of life and human health in a large part of the world population (Kan, Chen and Tong, 2012; Amutha and Juliet, 2017). Furthermore, the International energy agency (IEA) has predicted a 53% growth in energy consumption by 2030, which will lead to the extraction of available fuels at very faster rate and may result in deplete of their reservoir very soon.

The situation in Indian context is more critical as it is second most populated country with around 17.74% of the gross world population. With the massive growth in the population, India is seeing unprecedented rise in domestic and industrial consumption of energy. This premise causes overconsumption of available natural resources, which drives the fear of scarcity of those resources. In addition, India is largely dependent on fossil fuels as it 64% of total energy have been produced using coal, natural gases and oil (Ministry of Power, 2019). These fossil fuels have highest CO_2 emission per capita. However, due to their low cost and easy availability, these fossil fuels are still dominating in the energy generation in India. This state of energy generation and consumption in India is constantly polluting the environment and fuel exhaustion, which may further lead to

[1] *Corresponding author: National Institute of Technology, Department of Computer Applications, 492010, Raipur, India,* *manjutiwa@gmail.com*

the country to the state of fuel starvation in the not too distant future. Therefore, an urgent action plan is imperative to prevent the society from aforementioned harmful effects.
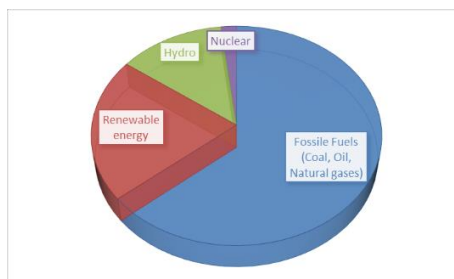

Figure 1: Power Sectors in India

With aforementioned issues in mind, many international and national organizations have realized the need to shift the energy generation program from conventional fuel system towards sustainable energy generation technologies. In a report, published by The World Commission on Environment and Development (WCED), the 'sustainability' is defined as "meeting the needs of the present without compromising the ability of future generations to meet their own needs"(WCED, 1987). Since then, the 'sustainability' has been extensively conversed topic in the society and incorporated into many sectors such as, purchasing, manufacturing, design and development, waste management and supply chain management (Yeh and Xu, 2013; Parezanovic et al., 2016; Chou et al., 2017; Kumar et al., 2017; Sakai et al., 2017). In recent time, a number of research works have been carried out regarding sustainability assessment in the energy sector. (Kumar et al., 2017) has carried out an extensive review regarding sustainability assessment. (Bhattacharyya, 2010) identified five strategies (Adaptation of best-practice technologies; Management of energy demand; Good Governance; Management of indigenous resources and Deployment of decentralized and distributed supply options) and four major challenges (Supply chain management, Resource management, Energy investment projects management and Environmental and social responsibility management) for sustainability in India. (Gallego Carrera and Mack, 2010) evaluated different energy technologies over nine indicators classified in four criteria. The researcher also concluded that each country has its different preference regarding energy technologies, which depends upon its geographical location, available energy sources, industries, and economy. (Doukas et al., 2012) employed Principal Component Analysis to assess the rural communities' energy sustainability based on outputs of two European projects. (Liu et al., 2013) evaluated the sustainability of a Hydroproject at China with respect to 10 economic, environmental and social indicators.(Liu, 2014) developed nine general indicators for sustainability assessment for renewable energy technologies.(Maxim, 2014) evaluated 13 energy technologies based on social, economic, environmental and technological indicators using weighted sum method (WSM) multi criteria decision making (MCDM) method. (Milutinović et al., 2014) developed an analytic hierarchy process (AHP) based framework to assess the sustainability of waste management models. (Luthra, Mangla and Kharb, 2015) employed Fuzzy AHP to evaluate 25 sustainability indicators divided into five major criteria and also performed sensitivity analysis with respect to different weights of environment criteria. In the study, Environment was assessed as most important criterion while Capacity utilization and effectiveness was ranked top among all the sustainability indicators. (Katre and Tozzi, 2018) developed an assessment framework consisting different analytical methods for Decentralized Renewable Energy (DRE) systems.

The literature survey indicates that sustainability of a process or system can be assessed with respect to a number of criteria and indicators. Existence of evaluating criteria and indicators implies that the multi criteria decision making approach can effectively address the issue of assessment of sustainability indictors and based on those indicators, assessment of different energy generation technologies. However, only few studies have applied MCDM methods for the sustainability assessment. The existing MCDM frameworks for the assessment of sustainability have used crisp or fuzzy values to extract judgments from experts, which are inadequate to register hesitancy or indeterminacy of experts' opinion (Atanassov, 2012). In addition, most of the studies have taken into account only social, environmental and economic criteria while technical and operational criteria are remained unaddressed. Furthermore, a number of studies have taken equal weights for all indicators while evaluating sustainability of any system, which can produce misleading results in general because each country has different preference towards these evaluating indicators based on the available energy resources and industries. The objective this paper is to propose a framework that prioritize the sustainability indicators and assess the energy generation technologies in Indian energy sector. The first phase of the framework encompasses the identification of all the aspects that can affect the sustainability of an energy generation technology and the energy technologies feasible in India. Then, the identified elements are organized into a

hierarchical structure. In the second phase, based on that hierarchy, the experts' opinions are collected using intuitionistic linguistic variables. Next, the experts' opinions are arranged in the form of preference relations and a distance based intuitionistic fuzzy AHP method is applied to prioritize the sustainability criteria. In the third phase, the identified energy generation technologies are evaluated using similar method and most sustainable alternative is selected.

The remaining paper is organized as follows: Section 2 provides prerequisites of proposed framework. Section 3 explains the methodology. An adapted case study is demonstrated as numerical example. The last section concludes the paper.

2. PRELIMINARIES

o *Intuitionistic Fuzzy Sets and Preference Relations*

Human mostly use linguistic phrases, such as 'better', 'similar' and 'inferior', to express their opinion. These linguistic phrases are imprecise and vague. In addition uncertainty an inseparable part of real-world problems. Human cognition is an essential part of MCDM and therefore, experts' opinions are also subject to imprecision and uncertainty (Mardani, Jusoh and Zavadskas, 2015). To overcome this issue, fuzzy sets theory(Zadeh, 1965) has been incorporated with MCDM methods, which allow the expert to provide their opinions in fuzzy linguistic variables. However, one shortcoming of the fuzzy sets is that it can only express degree of membership. Subsequently, degree of non-membership can be derived by subtracting degree of membership from one. Fuzzy sets is incapable to express "degree of abstention" or "hesitancy" of human opinions(Torra and Narukawa, 2009). In order to cope with this issue many advances fuzzy concepts have been developed, such as Intuitionistic Fuzzy Sets (IFSs)(Atanassov, 1986), Hesitant Fuzzy Sets(Torra and Narukawa, 2009) and Pythagorean Fuzzy Sets(Yager, 2013). However, due to its simplicity, less computation requirement, and effectiveness to depict abstention, IFSs have been very popular MCDM tool and applied to many real-world problems(Kaur and Kumar, 2012; Mou, Xu and Liao, 2016; Zhao and Xu, 2016; Hinduja and Pandey, 2017). An IFS can be formally defined as:

Definition 1: Let X be the universal set, an IFS A can be defined as:

$$A = \{ (x, \mu(x), v(x), \pi(x)) | \ x \in X \} \tag{1}$$

Where, for each element $x \in X$, $\mu(x) \in [0,1]$ denotes the degree of membership, $v(x) \in [0,1]$ denotes the degree of non-membership, and $\pi(x) \in [0,1]$ denotes the degree of hesitancy with respect to IFS A with the constraint, $\mu(x) + v(x) + \pi(x) = 1$. In practice, an IFS is denoted as $(\mu(x), v(x))$, also referred to as intuitionistic fuzzy value. The degree of hesitancy can be derived by subtracting $\mu(x)$ and $v(x)$ from one.

Definition 2: An intuitionistic fuzzy preference relation (IFPR) B on X can be defined as a matrix $B = (b_{ij})_{n \times n} \subset X \times X$, where b_{ij} represents a intuitionistic fuzzy value, $b_{ij} = (\mu(x_i), v(x_j))$, or simply $b_{ij} = (\mu_{ij}, v_{ij})$ for all $i, j = 1,2, \dots, n$. In IFPR, each intuitionistic fuzzy value b_{ij} expresses the a degree of certainty μ_{ij}, to which element x_i is preferred to element x_j, and a degree of certainty v_{ij}, to which element x_i is non-preferred to element x_j. A scale, analogous to Saaty's scale(Saaty, 2008), is presented in Table 1 that shows the intensities of support and objection of the preferences.

Table 20: Analogy of 0.1-09 scale with Saaty's 1-9 scale (Xu and Liao, 2013)

1-9 scale	Linguistic variables	0.1-0.9 scale
1/9	Extremely not Preferred	0.1
1/7	Very strongly not Preferred	0.2
1/5	Strongly not Preferred	0.3
1/3	Moderately not Preferred	0.4
1	Equally Preferred	0.5
3	Moderately Preferred	0.6
5	Strongly Preferred	0.7
7	Very strongly Preferred	0.8

9	Extremely Preferred	0.9

** Use of intermediate values is allowed in both scales to present compromise.

In addition, an IFPR satisfies following constraints:

$$0 \leq \mu_{ij} + \nu_{ij} \leq 1, \quad \text{for all } i,j = 1,2,\ldots\ldots.,n \tag{2}$$

$$\nu_{ji} = \mu_{ij}, \quad \text{for all } i,j = 1,2,\ldots\ldots.,n \tag{3}$$

and

$$\mu_{ii} = \nu_{jj} = 0.5, \quad \text{for all } i,j = 1,2,\ldots\ldots.,n \tag{4}$$

Definition 3: Let $b_{pq} = (\mu_{pq}, \nu_{rs})$ and $b_{rs} = (\mu_{rs}, \nu_{rs})$ be two intuitionistic fuzzy values, then primary operations between them can be defined as:

(1) $\bar{b}_{pq} = (\nu_{pq}, \mu_{pq})$.

(2) $b_{pq} + b_{rs} = (\mu_{pq} + \mu_{rs} - \mu_{pq} \cdot \mu_{rs}, \nu_{pq} \cdot \nu_{rs})$.

(3) $b_{pq} \cdot b_{rs} = (\mu_{pq} \cdot \mu_{rs}, \nu_{pq} + \nu_{rs} - \nu_{pq} \cdot \nu_{rs})$.

(4) $\lambda b_{pq} = \left(1 - \left(1 - \mu_{pq}\right)^{\lambda}, \nu_{pq}^{\lambda}\right), \lambda > 0$.

(5) $b_{pq}^{\lambda} = \left(\mu_{pq}^{\lambda}, 1 - \left(1 - \nu_{pq}\right)^{\lambda}\right), \lambda > 0$.

(6) $d(b_{pq}, b_{rs}) = \frac{1}{2}\left(|\mu_{pq} - \mu_{rs}| + |\nu_{pq} - \nu_{rs}| + |\pi_{pq} - \pi_{rs}|\right)$

o   *Analytic Hierarchy Process*

Analytic Hierarchy Process (AHP), developed by Saaty(Saaty, 2008), is one of the most prevalent MCDM methods. Since its inception, the AHP has been applied to numerous real-world decision problems, such as assessment of solid waste disposal, selection of green supply chain management, CRM partner selection, and assessment of advanced manufacturing systems (Subramanian and Ramanathan, 2012). Unlike other prevalent MCDM methods, AHP utilizes relative preference rather than absolute scores to derive final priorities and ranking. The AHP method can be summarized in three steps:

   i.Decomposition

   ii.Pairwise comparison and local priority derivation

   iii.Synthesis of local priorities

First, each element of the decision problem is identified and classified into different levels of a hierarchy, such as $Objective \rightarrow Criteria \rightarrow Subcriteria(optional) \rightarrow Alternatives$. Afterwards, elements of each level are pairwise compared and based on these pairwise comparisons, a preference relation is constructed for each level. Many method for deriving priorities from the preference relations have been proposed, however, Saaty's Eigenvector method have been widely applied by the Industries and government bodies. Next, the local priorities of different level, derived using Eigenvector method, are synthesized to produce global priorities of alternatives and subsequently, rankings.
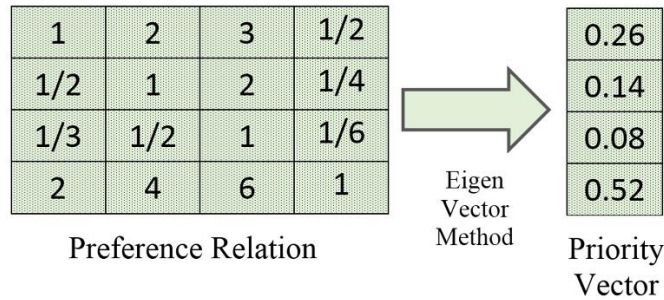
Figure 22: Priority Derivation in AHP

3. METHODOLOGY

Assessment of sustainability indicators and energy generation with respect to those indicators can be regarded as complex MCDM problem. In this section we introduce an Intuitionistic Fuzzy AHP based framework to prioritize the sustainability indicators and assessment of energy generation technologies. The framework is threefold: identification of sustainability indicators and energy generation alternatives, and construction of problem hierarchy; Prioritization of sustainability criteria; and evaluation of energy generation alternatives. The priority method of Intuitionistic Fuzzy AHP has been adapted from (Hinduja and Pandey, 2018). The detailed process is described as follows:

Step 1: With extensive literature survey, identify all the factors that affect sustainability of energy generation technologies and classify them into different clusters. Furthermore, identify energy generation alternatives that are feasible in Indian context.

Step 2: Organize identified decision elements into a problem hierarchy. Start with the objective as root, place clusters in the next level following by respective indicators. The alternative should be placed at the bottom level so that it can be evaluated with respect to all indicators.

Step 3: Based on the problem hierarchy, obtain experts' opinions using Table 2 and form IFPRs for each level of hierarchy.

Table 21: Assessment Scale used to collect opinions from decision makers (Hinduja and Pandey, 2018)

AHP/ANP Scale	Linguistic Terms	IFS
1	Equally Preferred (E)	[0.50, 0.50, 0.00]
3	Moderately Preferred (MP)	[0.60, 0.25, 0.15]
5	Strongly Preferred (SP)	[0.75, 0.15, 0.10]
7	Very Strongly Preferred (VP)	[0.90, 0.05, 0.05]
9	Extremely Preferred (EP)	[1.00, 0.00, 0.00]

** Use of intermediate values is allowed in both scales to present compromise.

Step 4: For each preference relation $A = (a_{ij})_{n \times n}$, construct a reference preference relation $R = (r_{ij})_{n \times n}$, which postulate the situation where each row contains "Extremely Preferred" intuitionistic values. The reference preference relation $R = (r_{ij})_{n \times n}$, where $r_{ij} = (\mu_{ij}^r, v_{ij}^r)$, can be defined as:

$$\mu_{ij}^r = \begin{cases} 0.5, & if\ i = j \\ 1.0, & otherwise \end{cases} \tag{5}$$

$$v_{ij}^r = \begin{cases} 0.5, & if\ i = j \\ 0, & otherwise \end{cases} \tag{6}$$

Step 5: For each preference relation $A = (a_{ij})_{n \times n}$, calculate similarity of each element of A with corresponding element in $R = (r_{ij})_{n \times n}$ using:

542

$$Sim(a_{ij}, r_{ij}) = \xi_{ij} = \frac{\rho \delta_{max}}{\delta_{ij} + \rho \delta_{max}}, \text{ for all } i, j = 1, 2, \dots n \tag{7}$$

Where, ξ_{ij}, similarity coefficient, represents similarity between a_{ij} and r_{ij}, for all $i, j = 1, 2, \dots n$ and $\delta_{max} = \max \{\delta_{ij}, i, j \in Mi, j = 1, 2, \dots n\}$. Symbol $\rho \in [0,1]$ denotes the distinguishing coefficient, which can be determined by decision makers. The smaller the ρ, the greater the distribution range. The output of this step is similarity matrix $(\xi_{ij})_{n \times n}$. The distance δ_{ij} can be calculated using:

$$\delta_{ij}(r_{ij}, a_{ij}) = \frac{1}{2}(|\mu_{ij}^r - \mu_{ij}^a| + |v_{ij}^r - v_{ij}^a| + |\pi_{ij}^r - \pi_{ij}^a|) \tag{8}$$

Step 6: Next, to obtain the priorities from the similarity matrix $(\xi_{ij})_{n \times n}$, similarity coefficients ξ_{ij} of each row are aggregated and normalized by matrix sum as:

$$\Upsilon_i = \frac{(\sum_{j=1}^n \xi_{ij}) - 1}{(\sum_{i=1}^n \sum_{j=1}^n \xi_{ij}) - n}, \text{ for all } i, j = 1, 2, \dots n. \tag{9}$$

The vector $(\Upsilon_i), i = 1, 2, \dots n$ denotes the local priorities.

Step 7: After deriving priorities from all the IFPRs, all the local priorities are synthesized to obtain the global priorities of energy generation technologies. The alternative with highest priority is regarded as most sustainable energy generation technology.

4. NUMERICAL EXAMPLE

The climate change and rapid fuel depletion have been major concern in India. Thus, many attempts have been made to encourage renewable energy technologies, and assess the sustainability and viability of them in India with respect to environmental as well as economic perspective (Bhattacharyya, 2010). In this section, we illustrate the working of the proposed framework. First, we identify sustainability indicators and energy generation alternative by an extensive literature survey and then, organize them in a hierarchical structure. Afterwards, we illustrate the priority derivation process using an adapted case study (Luthra, Mangla and Kharb, 2015). For the sake of simplicity, only prioritization of sustainable criteria are is presented in this section.

First, the sustainable criteria, their respective indicators and energy alternatives are extracted from the stock of existing literature(Pohekar and Ramachandran, 2004; Liu, 2014; Maxim, 2014; Santoyo-Castelazo and Azapagic, 2014; Luthra, Mangla and Kharb, 2015). We have identified 20 significant sustainability indicator and classified them into five main factors, Environmental, Economic, Social, Technological and Operational:

❖ **Environmental:** *Land use; Toxic gas emission; Waste reduction; Integration of environmental management systems.*

❖ **Economic:** *Payback period; Economic effectiveness; Capital cost; Investment opportunity.*

❖ **Social:** *Societal equity; Human health and safety; Social acceptability; Cultural heritage protection; Employment generation and increasing living standard.*

❖ **Technological:** *Capacity utilization; Ability to adopt smart technologies; Flexibility to update with technological advancement.*

❖ **Operational:** *Ability to respond increasing demands; Optimal resource allocation; Diversification of energy generating sources; Reliability; Reserve capacity.*

Besides, we have identified 9 energy generation technologies that are feasible in Indian context, which are listed below:

Table 22: Energy generation alternatives and their fuels

Energy generation Technology	Resource/ Fuel
Thermal Power	Coal
Natural Gases	Natural gases

Combined heat and power	Gas/Coal
Piston Engine	Diesel/Gas
Hydro	Water flow
Wind Power	Wind
Solar PV	Solar radiation
Biomass	Biomass
Nuclear	Nuclear fuel

Afterwards, all the decision elements are organized in a hierarchical structure, which represents the direction of assessment. The bottom level energy alternative are evaluated with respect to all sustainability indicators (sub-criteria), sub-criteria are evaluated with respect to respective factors, and all factors are assessed with respect to the goal that is "Selection of most sustainable energy alternative". Fig. 3 shows the hierarchy of the energy alternative selection problem.

For each non-terminal elements of the hierarchy, an IFPR is constructed by collecting experts' opinions. In the following, we illustrate an adapted case study (Luthra, Mangla and Kharb, 2015) as numerical example to demonstrate working of priority method described in previous section. The original case study used triangular fuzzy numbers to express preferences. We defuzzyfied them and determined equivalent intuitionistic fuzzy values. An equivalent IFPR corresponding to the case study is shown in the Table 4.
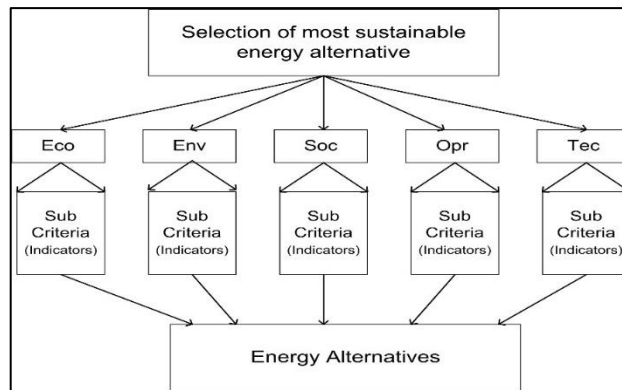
Figure 23: Problem Hierarchy

Table 23: IFPR showing relative preference of sustainability criteria

	Economic	Environmental	Social	Operational	Technical
Economic	(0.50,0.50)	(0.55,0.30)	(0.50,0.50)	(0.30,0.55)	(0.50,0.35)
Environmental	(0.30,0.55)	(0.50,0.50)	(0.55,0.30)	(0.70,0.20)	(0.30,0.55)
Social	(0.50,0.50)	(0.30,0.55)	(0.50,0.50)	(0.50,0.35)	(0.45,0.30)
Operational	(0.55,0.30)	(0.20,0.70)	(0.35,0.50)	(0.50,0.50)	(0.50,0.50)
Technical	(0.35,0.50)	(0.55,0.30)	(0.30,0.45)	(0.50,0.50,)	(0.50,0.50)

Using Eq. (5) and Eq. (6), described in step 4 of methodology, we constructed the reference preference relation (Table 5) corresponding to the IFPR shown in Table 4. Afterwards, a similarity matrix $(\xi_{ij})_{n \times n}$ is constructed using Eq. (7), which is shown in the Table 6. Then, the similarity coefficient of each row are aggregated and normalized using Eq. (9). The final priority scores are presented in the Table 7.

Table 24: Reference preference relation corresponding to the IFPR shown in the Table 5

	Economic	Environmental	Social	Operational	Technical
Economic	(0.50,0.50)	(1.0,0.0)	(1.0,0.0)	(1.0,0.0)	(1.0,0.0)
Environmental	(1.0,0.0)	(0.50,0.50)	(1.0,0.0)	(1.0,0.0)	(1.0,0.0)
Social	(1.0,0.0)	(1.0,0.0)	(0.50,0.50)	(1.0,0.0)	(1.0,0.0)
Operational	(1.0,0.0)	(1.0,0.0)	(1.0,0.0)	(0.50,0.50)	(1.0,0.0)
Technical	(1.0,0.0)	(1.0,0.0)	(1.0,0.0)	(1.0,0.0)	(0.50,0.50)

Table 25: Similarity matrix of the IFPR and corresponding reference preference relation

	Economic	Environmental	Social	Operational	Technical
Economic	1	0.151	0.138	0.102	0.138
Environmental	0.103	1	0.151	0.210	0.103
Social	0.138	0.103	1	0.138	0.127
Operational	0.151	0.09	0.11	1	0.138
Technical	0.11	0.151	0.103	0.138	1

Table 26: Final Preference Scores of Sustainability Criteria

Criteria	Final Preference
Economic	0.204
Environmental	0.219
Social	0.195
Operational	0.189
Technical	0.194

It can be observed that Environmental criterion is most critical criterion following by economic and social criterion. The priorities, derived in this paper are consistent with the results of original case study, and therefore, it can be concluded that the described method for deriving priorities from IFPRs effectively prioritizes the sustainability criteria and can rank the energy alternatives accurately. In a similar fashion, the sub-criteria can be prioritized with respect to their criteria in the next phase. Afterwards, all the energy alternatives can be assessed over all the sub-criteria. Subsequently, all the local priorities can be synthesized to produce final evaluation scores of alternatives. The alternative with highest score is regarded as the "most sustainable energy generation technology".

5. CONCLUSION

With the unprecedented growth in India population, the demand for residential and industrial energy is also increasing rapidly. This scenario is forcing the government produce and supply the energy accordingly. In order to supply required energy, many energy plants of different technology have been installed and most of them are driven by fossil fuels, which are not sustainable. The fossil fuel based plants have highest emission of harmful gases. Besides, the reserve of the fuels are also limited. Consequently, our environment is constantly getting polluted and the country can see a state of fuel starvation in the not too distant future. As a result, many

research bodies and industries have started working towards sustainable and renewable energy sources. It is imperative to evaluate the energy generation alternative based on sustainability criteria so that most sustainable alternative for a particular geography can be opted.

This paper proposes a decision making framework for prioritizing the sustainability criteria and indicators, and assessment of energy generation technologies based on those indicators. The framework first identified the relevant decision elements including sustainability criteria, indicators and alternatives; then, intuitionistic fuzzy AHP is used to prioritized the criteria and assess the energy generation technologies. Use of the intuitionistic fuzzy sets overcomes the fuzzy sets' incapability of dealing with hesitancy in decision makers' opinions. In addition, a case study is adapted to demonstrate the prioritization of sustainability criteria. The paper also comprehensively listed the factors that affects the sustainability, and all the energy generation technologies feasible in India. The paper will be helpful in assessment of potential energy plants and improving the sustainability of energy in India.

We have also identified the potential avenues, on which the present work can be expanded. One limitation of this methodology is that it assumes all the criteria and indicators completely independent, which is not always the case in real world decision problems. Analytic network process (ANP) can be applied to build a feedback network between decision elements, which will reflect the net influence of the criteria on each other. Besides, this study lack a full scale case study, which can impart many significant insights with the relevant industries and government bodies. In addition, hesitant fuzzy linguistic term set (HFLTS) can be used to obtain experts' preference(Rodriguez, Martinez and Herrera, 2012). The HFLTS is more powerful in dealing with uncertainty and indeterminacy of experts' opinions as it allows to express the preference with terms such as "at least good", and "between bad and medium".

REFERENCES

[1]. Amutha, D. and Juliet, M. (2017) 'Impact of Climate Changes on Human Health in India', in Ssrn. ssrn. doi: http://dx.doi.org/10.2139/ssrn.3071055.

[2]. Atanassov, K. T. (1986) 'Intuitionistic fuzzy sets', Fuzzy Sets and Systems, 20(1), pp. 87–96. doi: http://dx.doi.org/10.1016/S0165-0114(86)80034-3.

[3]. Atanassov, K. T. (2012) On Intuitionistic Fuzzy Sets Theory. 1st edn. Springer-Verlag Berlin Heidelberg. doi: 10.1007/978-3-642-29127-2.

[4]. Bhattacharyya, S. C. (2010) 'Shaping a sustainable energy future for India: Management challenges', Energy Policy. Elsevier, 38(8), pp. 4173–4185. doi: 10.1016/j.enpol.2010.03.045.

[5]. Chou, Y. C. et al. (2017) 'Building criteria for evaluating green project management: An integrated approach of DEMATEL and ANP', Sustainability (Switzerland), 9(5). doi: 10.3390/su9050740.

[6]. Doukas, H. et al. (2012) 'Assessing energy sustainability of rural communities using Principal Component Analysis', Renewable and Sustainable Energy Reviews. Elsevier Ltd, 16(4), pp. 1949–1957. doi: 10.1016/j.rser.2012.01.018.

[7]. Gallego Carrera, D. and Mack, A. (2010) 'Sustainability assessment of energy technologies via social indicators: Results of a survey among European energy experts', Energy Policy. Elsevier, 38(2), pp. 1030–1039. doi: 10.1016/j.enpol.2009.10.055.

[8]. Hinduja, A. and Pandey, M. (2017) 'Multicriteria Recommender System for Life Insurance Plans based on Utility Theory', Indian Journal of Science and Technology, 10(14), pp. 1–8. doi: 10.17485/ijst/2017/v10i14/111376.

[9]. Hinduja, A. and Pandey, M. (2018) 'Assessment of Healthcare Waste Treatment Alternatives Using an Integrated Decision Support Framework', International Journal of Computational Intelligence Systems, 12(1), pp. 318–333. Available at: https://www.atlantis-press.com/article/125905685.

[10]. Kan, H., Chen, R. and Tong, S. (2012) 'Ambient air pollution, climate change, and population health in China', Environment International. Elsevier Ltd, 42(1), pp. 10–19. doi: 10.1016/j.envint.2011.03.003.

[11]. Katre, A. and Tozzi, A. (2018) 'Assessing the sustainability of decentralized renewable energy systems: A comprehensive framework with analytical methods', Sustainability (Switzerland), 10(4). doi: 10.3390/su10041058.

[12]. Kaur, P. and Kumar, S. (2012) 'An intuitionistic fuzzy simple additive weighting (IFSAW) method for selection of vendor', Proceedings of the International Conference on Electronic Business (ICEB), 15(2), pp. 31–35.

[13]. Kumar, A. et al. (2017) 'A review of multi criteria decision making (MCDM) towards sustainable renewable energy development', Renewable and Sustainable Energy Reviews. Elsevier, 69(June 2016), pp. 596–609. doi: 10.1016/j.rser.2016.11.191.

[14]. Liu, G. (2014) 'Development of a general sustainability indicator for renewable energy systems: A review', Renewable and Sustainable Energy Reviews. Elsevier, 31, pp. 611–621. doi: 10.1016/j.rser.2013.12.038.

[15]. Liu, J. et al. (2013) 'Sustainability in hydropower development - A case study', Renewable and Sustainable Energy Reviews. Elsevier, 19, pp. 230–237. doi: 10.1016/j.rser.2012.11.036.

[16]. Luthra, S., Mangla, S. K. and Kharb, R. K. (2015) 'Sustainable assessment in energy planning and management in Indian perspective', Renewable and Sustainable Energy Reviews. Elsevier, 47, pp. 58–73. doi: 10.1016/j.rser.2015.03.007.

[17]. Mardani, A., Jusoh, A. and Zavadskas, E. K. (2015) 'Fuzzy multiple criteria decision-making techniques and applications - Two decades review from 1994 to 2014', Expert Systems with Applications. Elsevier Ltd, 42(8), pp.

4126–4148. doi: 10.1016/j.eswa.2015.01.003.

[18]. Maxim, A. (2014) 'Sustainability assessment of electricity generation technologies using weighted multi-criteria decision analysis', Energy Policy. Elsevier, 65, pp. 284–297. doi: 10.1016/j.enpol.2013.09.059.

[19]. Milutinović, B. et al. (2014) 'Multi-criteria analysis as a tool for sustainability assessment of a waste management model', Energy, 74(C), pp. 190–201. doi: 10.1016/j.energy.2014.05.056.

[20]. Ministry of Power, G. of I. (2019) Power Sector at a Glance ALL INDIA, Ministry of Power, Govt. of India. Available at: https://powermin.nic.in/en/content/power-sector-glance-all-india (Accessed: 12 March 2019).

[21]. Mou, Q., Xu, Z. and Liao, H. (2016) 'An Intuitionistic Fuzzy Multiplicative Best-Worst Method for Multi-Criteria Group Decision Making', Information Sciences. Elsevier Inc. doi: 10.1016/j.ins.2016.08.074.

[22]. Parezanovic, T. et al. (2016) 'Evaluation of Sustainable Mobility Measures Using Fuzzy COPRAS Method', Management - Journal for theory and practice of management, 21(78), pp. 53–62. doi: 10.7595/management.fon.2016.0006.

[23]. Pohekar, S. D. and Ramachandran, M. (2004) 'Application of multi-criteria decision making to sustainable energy planning - A review', Renewable and Sustainable Energy Reviews, 8(4), pp. 365–381. doi: 10.1016/j.rser.2003.12.007.

[24]. Rodriguez, R. M., Martinez, L. and Herrera, F. (2012) 'Hesitant fuzzy linguistic term sets for decision making', IEEE Transactions on Fuzzy Systems, 20(1), pp. 109–119. doi: 10.1109/TFUZZ.2011.2170076.

[25]. Saaty, T. L. (2008) 'Decision making with the analytic hierarchy process', International Journal Services Sciences, 1(1), pp. 83–98.

[26]. Sakai, S. et al. (2017) 'Waste prevention for sustainable resource and waste management', Journal of Material Cycles and Waste Management. Springer Japan, 19(4), pp. 1295–1313. doi: 10.1007/s10163-017-0586-4.

[27]. Santoyo-Castelazo, E. and Azapagic, A. (2014) 'Sustainability assessment of energy systems: Integrating environmental, economic and social aspects', Journal of Cleaner Production. Elsevier Ltd, 80(2014), pp. 119–138. doi: 10.1016/j.jclepro.2014.05.061.

[28]. Subramanian, N. and Ramanathan, R. (2012) 'A review of applications of Analytic Hierarchy Process in operations management', International Journal of Production Economics, 138(2), pp. 215–241. doi: http://dx.doi.org/10.1016/j.ijpe.2012.03.036.

[29]. Torra, V. and Narukawa, Y. (2009) 'On hesitant fuzzy sets and decision', in IEEE (ed.) IEEE International Conference on Fuzzy Systems. Jeju Island, South Korea, pp. 1378–1382. doi: 10.1109/FUZZY.2009.5276884.

[30]. WCED (1987) Our Common Future. London. Available at: http://www.un-documents.net/our-common-future.pdf.

[31]. Xu, Z. and Liao, H. (2013) 'Intuitionistic fuzzy analytic hierarchy process', IEEE Transactions on Fuzzy Systems, 22(4), pp. 749–761. doi: 10.1109/TFUZZ.2013.2272585.

[32]. Yager, R. R. (2013) 'Pythagorean fuzzy subsets', in Proceedings of the 2013 Joint IFSA World Congress and NAFIPS Annual Meeting, IFSA/NAFIPS 2013. Edmonton, AB, Canada: IEEE, pp. 57–61. doi: 10.1109/IFSA-NAFIPS.2013.6608375.

[33]. Yeh, C.-H. and Xu, Y. (2013) 'Sustainable planning of e-waste recycling activities using fuzzy multicriteria decision making', Journal of Cleaner Production. Elsevier Ltd, 52, pp. 194–204. doi: 10.1016/j.jclepro.2013.03.003.

[34]. Zadeh, L. A. (1965) 'Fuzzy sets', Information and Control, 8(3), pp. 338–353. doi: http://dx.doi.org/10.1016/S0019-9958(65)90241-X.

[35]. Zhao, H. and Xu, Z. (2016) 'Intuitionistic fuzzy multi-attribute decision making with ideal-point-based method and correlation measure', Journal of Intelligent & Fuzzy Systems, 30(2), pp. 747–757. doi: 10.3233/IFS-151795.

Bending Rigidity of Polyester Microfilament Woven Fabrics

Gulbin Fidan[1], Yasemin Korkmaz[2], H. Kubra Kaynak[3]

Abstract

Synthetic fiber industry has been enforced to make developments due to the increasing performance demand for textile products. One of the most important developments in synthetic fiber industry, is absolutely producing extremely fine fibers which are named as microfibers and nanofibers. Microfibers are defined as the fibers finer than 1 dtex or 1 denier. It is possible to obtain good level of water resistance by applying water repellency treatment to tightly woven microfilament fabrics. This type of fabrics are superior to coated or laminated fabrics in different end uses namely; tent, sleeping bag, raincoat and winter sport shell fabric, due to their light weight, durability, waterproofness, windproofness, breathability and drapeability. In this study, it is intended to investigate the effects of weft sett and filament fineness on bending rigidity of water repellent finished microfilament woven fabrics. For this purpose, 1/1 plain weave and 3/2 hopsack weave types were selected. Different weft sett values were selected for these weave types with the same warp sett. Different filament finenesses were applied as 1,14 dtex, 0,76 dtex, 0,57 dtex and 0,33 dtex in weft direction with 110 dtex yarn linear density. The woven samples were applied with water repellent finish at the same conditions and then, the effects of weft sett and filament fineness on the bending rigidity characteristic of these samples were determined.

Keywords: Microfilament, Woven Fabric, Bending Rigidity, Water Repellent, Polyester

1. INTRODUCTION

When the fiber types used throughout the world are examined, it is seen that the majority of them are composed of synthetic fibers. It is seen that per capita consumption of natural fiber is gradually decreasing, especially as the production amounts of natural fibers do not change much and the number of users is associated with increasing world penetration. The inability to increase the production of natural fibers and the increasing production of synthetic fibers and the increasing fiber quality in parallel with the technologies developed have made it easier for the synthetic fibers to find more place in the market. Among the synthetic fibers, polyester is the most widely used fiber.

One of the important developments in synthetic fibers is the reduction of fiber fineness to micro and nano dimensions. The importance of microfibers increases with each passing day as the fabric properties produced from microfibres have superior properties compared to fabrics produced from conventional fibers. Fiber fineness is one of the most important parameters affecting yarn and fabric properties. The increase in the number of fibers in the yarn cross-section, the decrease in fiber fineness, yarn strength, reduction in the amount of twist required for yarn formation, moisture absorption, air permeability, water repellency, fabric touch, wrinkle properties, affect of many properties such as bending resistance. From this point, it is inevitable that the usage areas of microfibers will increase. Microfibers have found use in many sectors such as cleaning cloths, medical textiles, synthetic leathers, filter fabrics, construction applications. When samples cleaning cloths are given as an example, dirt and dust are generally transported from place to place without being trapped inside in

---

[1] *Corresponding author: Gaziantep University, Naci Topcuoglu Vocational School, Textile and Carpet Machinery Department, Gaziantep, Turkey, gfidan@gantep.edu.tr*

[2] *Kahramanmaras Sutcu Imam University, Textile Engineering Department , Kahramanmaras, Turkey, ykorkmaz@ksu.edu.tr*

[3] *Gaziantep University, Textile Engineering Department, Gaziantep, Turkey, tuluce@gantep.edu.tr*

conventional cleaning cloths. Microfibers have very high surface areas and small diameters, which provide high absorption properties to fabrics made of these fibers. Cleaning cloths made of microfibers remove dirt from the surface and can keep dirt in the fabric structure until it is washed. They can also be cleaned with water without the need for any chemicals. In addition to attracting liquid, microfibrous fabrics also attract microbes and particles in the liquid. Therefore, increased surface area and absorption properties allow microfibers to draw up to many times the liquid of their own weight. The thinner the fiber, the greater the fiber per square centimeter, the more fibers come into contact with the surface to be cleaned. In this way, faster and more efficient results are obtained [1].

2. MICROFIBERS

Microfibers are called fibers with a diameter of 1.0 dtex or 1.0 denier thinner [2,3]. Figure 1 shows the fiber diameters of different fibers with microfibers.
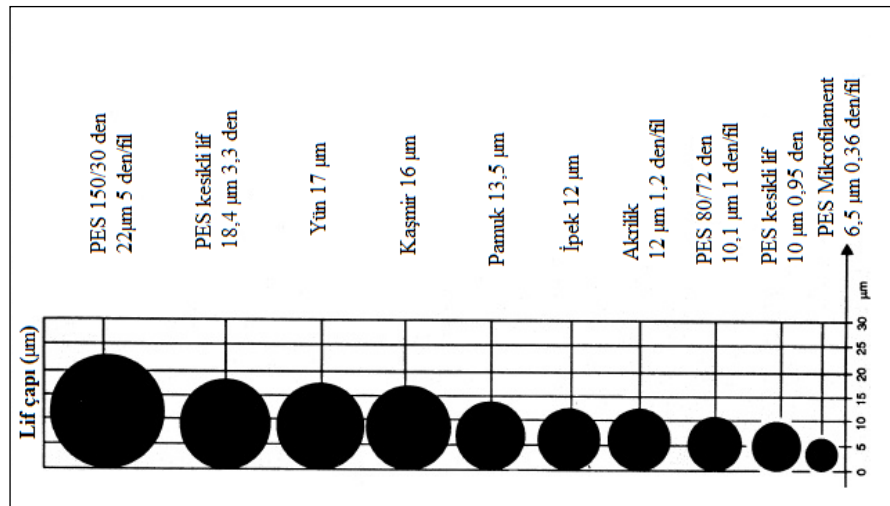

Figure 1. Comparison of the diameter of various types of fiber [4]

3. BENDING STRENGTH

Bending strength refers to the resistance of the textile to bending. Bending rigidity for woven fabrics can also be explain as the resistance of the textile product to be bended under its own weight to a certain extent rectangular cut. A high bending strength value indicates that the fabric is stiff and has a structure that is resistant to bending. Low bending strength value means that the fabric structure is soft and draped. Bending rigidity of a fabric is influenced by many parameters such as the fiber used, yarn count, yarn twist, yarn production method, woven fabric construction, fabric density and finishing processes applied to the fabric.

In this study, bending rigidity properties of woven fabrics produced from microfibers were investigated. It is thought that this study will contribute to the literature since there is no study on the effect of microfibers on the bending strength of fabrics as well as many other features added to the fabric properties.

4. MATERIAL AND METHOD

In this study, for weft direction, polyester yarn with 110 dtex linear density was produced by using microfilament fibers of 1.14 dtex, 0.76 dtex, 0.57 dtex and 0.33 dtex fineness. Figure 2 shows a cross-sectional view of yarns with different filament fineness.
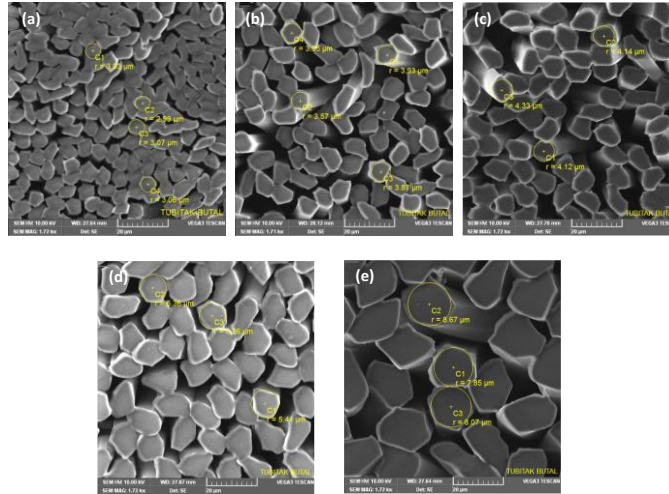
Figure 2. SEM views of filament yarns with different filament linear

(a) 0,33 dtex – 333 filament number, (b) 0,57 dtex - 192 filament number (c) 0,76 dtex - 144 filament number

(d) 1,14 dtex - 96 filament number , (e) 3,05 dtex [5]

Microfilament weft yarns produced by using 4 different microfibers were produced by woven fabrics in different weft densities with 1/1 plain and 3/2 hopsack weaves. For warp direction, warp yarns were constant and 55 dtex/72 filament yarns were used. Fabric production was done on Smith Textile GS940 (Italy) weaving loom at 445 rev / min at 220 cm reed width. All of the woven samples produced by changing only weft yarns. So the results were examined only on the basis of the weft direction. 21 samples were compared for fabric bending strength. Structural properties of sample fabrics were determined after water repellent finishing. All fabric samples were treated with water repellent finish, at the same conditions. Fluorocarbon based water repellency finish was applied to samples. 20 g/L softing agent and 40 g/L water repellent chemical was used in the solution. Wet pick-up of the fabric samples was about 10%, the squeezing pressure was 2.5 bar. The water repellency treatment was done at 20 m/min process speed. The drying temperature was 170ºC and drying speed was 20 m/min. Table 1 shows the distribution of samples according to weave type, weft sett and filament fineness.

Table 1. Sample properties

Weave Type	Weft Sett	Filament Fineness	Filament Numbers	Weave Type	Weft Sett	Filament Fineness	Filament Numbers
Hopsack Weave (3/2)	47	0.33	333	Plain Weave	34	0.33	333
		0.57	192			0.57	192
		0.76	144			1.14	96
	50	0.33	333		36	0.33	333
		0.57	192			0.57	192
		0.76	144			1.14	96
	53	0.33	333		38	0.33	333
		0.57	192			0.57	192
		0.76	144			1.14	96
					40	0.33	333
						0.57	192
						1.14	96

Fabric samples were subjected to bending strength test after conditioning for 8 hours at 20 ± 2 ° C and $65 \pm 2\%$ relative humidity [6]. The sample fabrics were then subjected to the Bending Strength Test Apparatus as shown in Figure 3. Bending resistance of fabrics was determined according to BS 3356: 1990 'Determination of bending length and flexural rigidity of fabrics' [7]. According to this standard, 2.5 cm x 20 cm dimensions of 3 weft and 3 warp test samples were prepared for each fabric sample. A total of 24 hanging length values were obtained at both ends of the front and back sides of the samples.
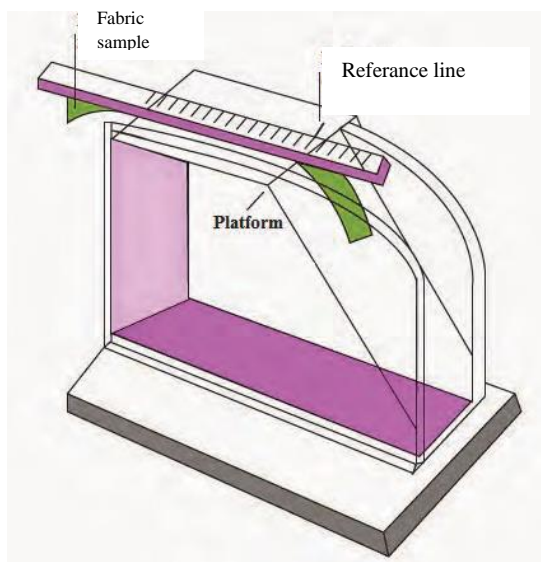

Figure 3. Bending rigidity test device [8]

Bending strength was calculated by using the related formulas over the hanging length values of the fabrics [9].

$$C_A = \frac{X_A}{2}$$

$$C_Ç = \frac{X_Ç}{2}$$

$$G_A = 0{,}1 * W * C_A^3 \quad \text{(mg.cm)}$$

$$G_Ç = 0{,}1 * W * C_Ç^3 \quad \text{(mg.cm)}$$

$$G_O = \sqrt{G_A} * \sqrt{G_Ç}$$

X_A: Weft Direction Hanging Length (cm)

X_C: Warp Direction Hanging Length (cm)

C_A: Weft Direction Bending Length (cm)

C_C: Warp Direction Bending Length (cm)

G_A: Weft Direction Bending Strength

G_C: Warp Direction Bending Strength

G_O: Fabric Bending Strength (mg.cm)

W = Avarage Weight (g/cm²) [9]

5. RESULTS

As a result of the study, fabric bending strength results were examined. Since there was no change in the warp direction, it was not subjected to a separate evaluation. The test results are shown in Table 2 and 3.

Table 2. Structural properties of hopsack weave sample fabrics

Weave type	Filament fineness (dtex)	Filament number	Weft sett	Fabric weigth	Bending stength on weft direction	Fabric bending strenth
3/2 hopsack	0.33	333	47	123	642.2	176.4
			50	127	727.1	232.1
			53	129	823.0	237.7
	0.57	192	47	117	869.4	152.4
			50	125	1180.7	260.4
			53	128	1525.2	387.8
	0.76	144	47	119	494.0	185.2
			50	123	552.2	192.8
			53	126	716.7	254.6

Table 3. Structural properties of plain weave sample fabrics

Weave type	Filament fineness (dtex)	Filament number	Weft sett	Fabric weigth	Bending stength on weft direction	Fabric bending strenth
1/1 plain	0.33	333	34	106	446.4	179.0
			36	109	501.5	182.9
			38	113	634.4	226.9
			40	117	779.6	244.4
	0.57	192	34	106	583.6	235.8
			36	109	682.5	260.9
			38	113	712.0	224.9
			40	118	911.2	325.0
	1.14	96	34	106	293.4	149.9
			36	110	352.1	141.5
			38	116	393.6	169.5
			40	118	546.7	195.3

The graphics are presented below for a better analysis of these results. Figures 4 and 5 show results for weft direction bending rigidity.
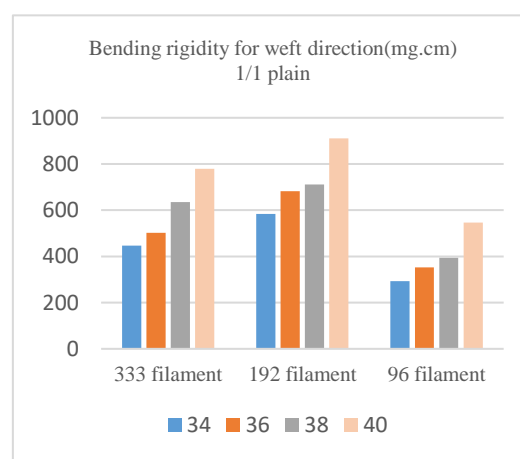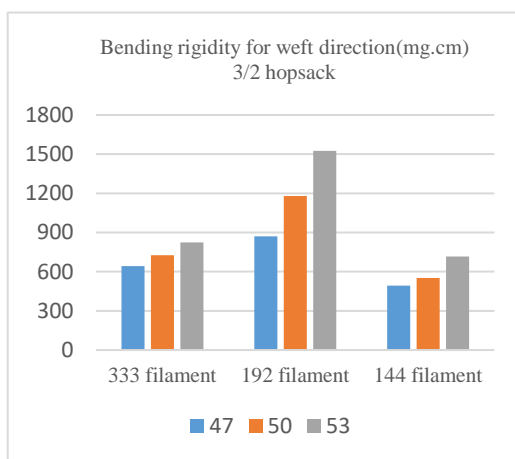

Figure 4. Bending rigidity for weft direction (3/2 hopsack)   *Figure 5. Bending rigidity for weft direction (1/1 plain)*

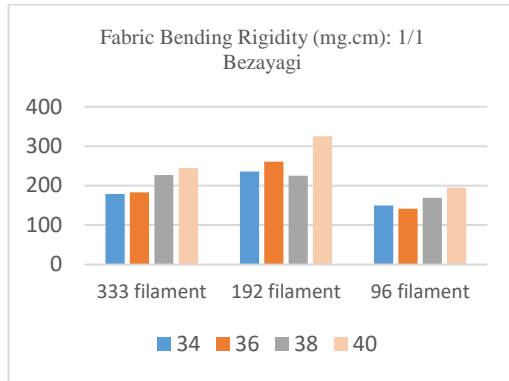Figures 6 and 7 show results for fabric bending rigidity.

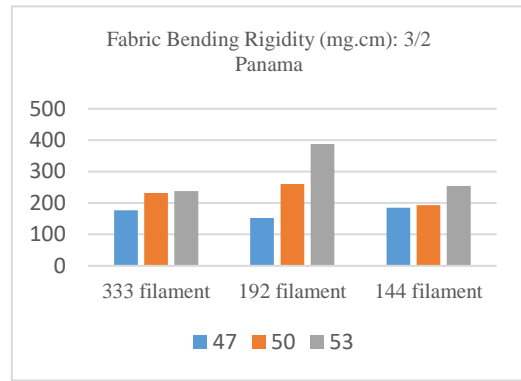*Figure 6. Fabric bending rigidity (3/2 hopsack)*   *Figure 7. Fabric bending rigidity (1/1 plain)*

When the bending strength results of the fabrics are examined, in both woven types it is seen that the bending rigidity increases with increasing weft sett in both filament number.

Table 4. ANOVA for bending rigidity of hopsack samples

Source	Sum of Squares	df	Mean Square	F	Sig.	Partial Eta Squared
Corrected Model	10215431.893ᵃ	8	1276928.987	60.480	0.000	0.830
Intercept	77139375.974	1	77139375.974	3653.620	0.000	0.974
weftsett	2174417.340	2	1087208.670	**51.494**	0.000	0.510
filfineness	7260612.669	2	3630306.335	**171.945**	0.000	0.776
weftsett * filfineness	780401.884	4	195100.471	9.241	0.000	0.272
Error	2090200.673	99	21113.138			
Total	89445008.540	108				
Corrected Total	12305632.566	107				
a. R Squared = 0.830 (Adjusted R Squared = 0.816)						

As seen from Table 4, number of filaments and weft sett have statistically significant effects on bending rigidity of hopsack samples. Also, it can be seen from F and Partial Eta squared values that the number of filaments is more effective on bending rigidity than weft sett for hopsack samples.

Table 5. ANOVA for bending rigidity of plain samples

Source	Sum of Squares	df	Mean Square	F	Sig.	Partial Eta Squared
Corrected Model	4535884.488ᵃ	11	412353.135	36.692	0.000	0.754
Intercept	47663605.080	1	47663605.080	4241.227	0.000	0.970
weftsett	1783315.755	3	594438.585	**52.895**	0.000	0.546
filfineness	2687965.730	2	1343982.865	**119.591**	0.000	0.644

weftsett * filfineness	64603.003	6	10767.167	0.958	0.456	0.042
Error	1483437.592	132	11238.164			
Total	53682927.160	144				
Corrected Total	6019322.080	143				
a. R Squared = 0.754 (Adjusted R Squared = 0.733)						

As seen from Table 5, number of filaments and weft sett have statistically significant effects on bending rigidity of plain samples. Also, it can be seen from F and Partial Eta squared values that the number of filaments is more effective on bending rigidity than weft sett for plain samples.

CONCLUSIONS

Microfibers have a wider usage area. Their ligth weigth and good drapeability properties are so important for customers. For determining these properties, bending rigidity is an important test method.

In this study it is seen that both hopsack and plain fabric samples, number of filaments and weft sett have statistically significant effects on bending rigidity. Also for all woven types, the number of filaments is more effective on bending rigidity than weft sett.

REFERENCES

[1]. Demiroz Gun, A., Demircan, B., Sevkan, A., 2011. Production Methods, Properties and Applications of Microfibers. The Journal of Textiles and Engineers, 18 (83): 38-46

[2]. Mukhopadhyay, S., 2002. Microfibers-An Overview. Indian Journal of Fiber and Textile Research, 27(3): 307-314.

[3]. Mukhopadhyay, S.,Ramakrishnan, G., 2008. Microfibers. Textile Progress, 40(1): 1-86.

[4]. Falkai, B.V., 1991. Production and Properties of Microfibers and Microfilaments. The Indian Textile Journal, 2: 62-70.

[5]. Kaynak H. K., 2013. Investigation of the performance properties of fabrics woven with microfilament yarns. University of Cukurova, Institute of Natural and Applied Science, Doctoral Thesis, Adana.

[6]. TS EN ISO 139 - Textiles - Standard atmospheres for conditioning and testing

[7]. BS 3356:1990 - Determination of bending length and flexural rigidity of fabrics

[8]. Turksoy H. G., Akkaya T., Ustuntag S., 2017. Evaluation of Woven Fabric Performances of Air-Jet Yarns. The Journal of Textiles and Engineers, 24 (107): 138-145.

[9]. Ak, F.N., 2006 The Effect Of Some Weaving Constructions On Fabric Performance Properties. University of Cukurova, Institute of Natural and Applied Science, MSc Thesis, Adana, 105 p.

On the Use of Human Body Models in Wireless Capsule Endoscopy Localization based on Ultra Wide Band Signaling

Memduh Suveren[1], Muzaffer Kanaan[2]

Abstract

Wireless Capsule Endoscopy (WCE) is a relatively pain-free medical imaging technique, especially in the small-intestine region of the human body. Many diseases of the gastro-intestinal (GI) tract, such as Crohn's disease, can be easily diagnosed with WCE. The recent trend is towards evolving WCE devices as remotely controllable devices, particularly with a view to replacing traditional colonoscopy (which is a more painful form of imaging the GI tract). An important problem in this space is the localization of the capsule endoscope inside the body, as this enables the medical specialist to make a more accurate diagnosis in an easier manner. In this study, we have obtained the estimation positions of the WCE capsule in the small intestine using the RSS based algorithm, sensors placed on the human body model and software that makes electromagnetic simulations. We have reached a total of 25.5 mm RMS distance estimation error in 3 axes.

Keywords: In-body Localization, RSS, Wireless Capsule Endoscopy

1. INTRODUCTION

Wireless capsule endoscopy is a non-invasive, painless imaging technique for parts of the gastrointestinal (GI) tract. WCE is particularly used to view the small intestine, which is very difficult to reach via conventional endoscopy techniques ([1, 2]). With this technique, the patient swallows a small pill-sized capsule, which is equipped with a camera and a wireless transmitter. When swallowed, the camera within the capsule starts taking pictures, while traveling through the GI tract, relaying the images via a wireless transmitter to an on-body receiver. The received images can then be analyzed by the specialist for diagnostic and treatment purposes.

An important problem for current and future WCE systems is accurate localization of the endoscopy capsule within the human body. If images obtained by the capsule can be correlated with a location, diagnosis and treatment can be accomplished much faster and in a more accurate manner.

An important factor that needs to be taken into account when studying localization systems for WCE is the complex, nonhomogeneous nature of the human body. Different tissue types (skin, muscle, and bone) all have propagation characteristics that are frequency-dependent, adversely affecting the transmission of RF signals [3]. It is, therefore, critical that effects of the human body on RF signals be quantified in order to come up with accurate localization systems for WCE. Standard procedure for quantifying propagation of wireless signals in different kinds of environments (indoor, for example), it is customary to take measurements. However, for ethical as well as technical reasons (i.e. non-repeatability of the results, as no two human bodies are exactly alike) it is not feasible to take measurements directly from actual human bodies. This is where computerized, 3-D models of the human body are of considerable importance.

Use of a 3-D human body model for WCE localization offers several advantages. First, a 3-D model offers results that can be more or less replicated (barring, of course, factors such as differences in algorithmic implementation or resolution). Second, computerized 3-D models can be easily manipulated to focus

---

[1] *Corresponding author: Erciyes University, Department of Mechatronic Engineering, 38038, Melikgazi/Kayseri, Turkey. msuveren@erciyes.edu.tr*

[2] *Erciyes University, Department of Mechatronic Engineering, 38038, Melikgazi/Kayseri, Turkey. mkanaan@erciyes.edu.tr*

investigations over a certain body region of interest, significantly lowering computation time. This is feasible principally because RF propagation for a WCE transmitter tends to be localized in the region where the capsule is (the small intestine, for instance), being significantly attenuated by body tissues outside this region. One can, therefore, come up with a truncated body model that includes only the region of interest, something that is very difficult with physical 3-D phantoms.

Ultra-Wide-Band (UWB) technology is being used for numerous different applications in wireless communication, ranging from accurate indoor localization for mentally ill and disabled patients ([4]) to precise wireless capsule endoscopy ([5]). The advantages of UWB for these scenarios include wide bandwidth and simple transceiver architectures enabling low-power consumption, resulting in communications at a higher data rate [5].

In this short paper, we summarize the results of our work focusing on in-body propagation and localization for WCE using a human body model. We focus specifically on WCE localization in the small intestine utilizing Ultra-Wide-Band technology as detailed in the next section.

2. SIMULATION ENVIRONMENT

An In the simulation stage, a 3-D voxel model of the human body developed under the Visible Human Project [6] as shown Figure 1 and software from Remcom which carried out the Finite Difference Time Domain (FDTD) electromagnetic simulations was used. FDTD techniques are suitable for UWB studies because a system's response to a broadband pulse can be easily captured in a single simulation. Therefore, UWB signals have been used in this study as in most of our previous studies [7-15].
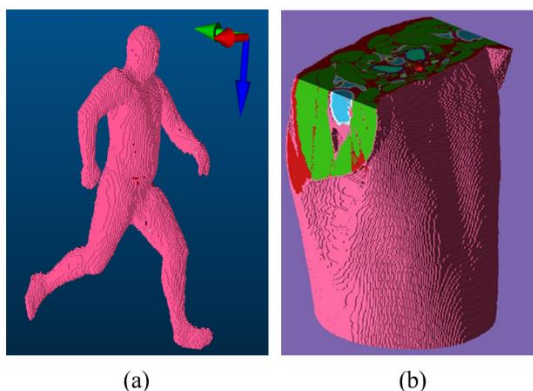

(a)   (b)

Figure 1. 3-D voxel models of the human body: a) the full body model, b) truncated voxel model

In the model shown in Figure 1-b, the organs such as head, arms and legs were not included in the model to reduce simulation times and mostly focus on the small intestine region. In FDTD simulations, the size of the cell was chosen to be 2 mm in the x and z direction and 0.5 mm in the y direction to satisfy the Courant Limit. The Perfectly Matching Layer (PML) boundary condition has also been used to limit the problem size and disregard the effects of body reflection [7]. After incorporating the 3-D human body model inside the simulation software, the elliptic disc dipole antenna [16], shown in Figure 2. was placed inside this structure.
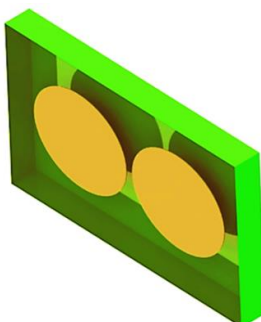

Figure 2. Elliptic dipole antenna [12]

This elliptic dipole antenna consists of two identical ellipse which are designed to have a large diameter of 8 mm, a small diameter of 7 mm, and is placed between a dielectric case for separation from body tissues. This antenna is fed from the gap between two ellipse and antenna dimensions are adjusted 2x20x12 mm. The signal power level at the antenna input was set to 1 mW from a 50Ω source situated in the feed point between the elliptical disks in the antenna structure [12].

The antenna is fed by a Modulated Gaussian wave with a center frequency of 4.1 GHz and a -10dB bandwidth of 1.4 GHz. With this parameter selection, most of the signal energy resides in the 3.4-4.8 GHz band (which is also known as the "UWB low band"[17]). The antenna was placed inside the small intestine to obtain data for wireless capsule endoscopy scenario. This scenario in which the position of the WCE is obtained by the point sensors placed on the body is similar to the structure shown in Figure 3.
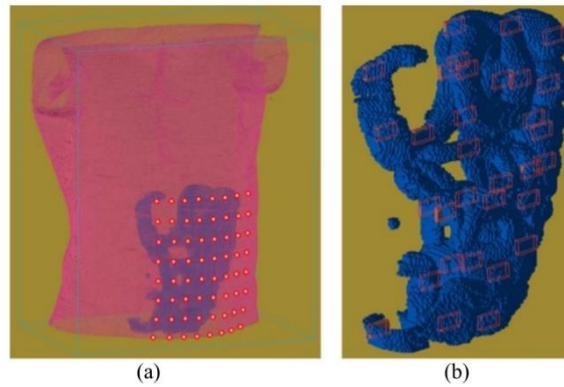

(a) (b)

Figure 3. a) Receiver sensor localization on the body, b) WCE positions in the intestine [15]

After the UWB signal is applied at the input of the implanted antenna, FDTD simulation results were used to obtain the magnitude of the Poynting vector data at distances on the body surface. The Poynting vector is defined as the vector product;

$$\mathbf{P}(t) = \mathbf{E}(t) \times \mathbf{H}(t)$$
(1)

where $\mathbf{E}(t)$ and $\mathbf{H}(t)$ are the values of the electric and magnetic field intensities, respectively. The magnitude of $\mathbf{P}(t)$ at each of the receive sensors on the body was calculated for every possible location of the WCE transmit antenna. For each of the 32 possible antenna locations within the small intestine, Poynting vector data at each of the 64 point sensor was collected and so a total of 32x64=2048 data sets were obtained. Each Poynting vector is then integrated to calculate the energy density (in J/m^2) of the receiving sensors as given by

$$E = \int_t |\mathbf{P}(t)| dt$$
(2)

As a result, with this calculated energy value (E), the substructure was prepared for 3-dimensional location estimation of WCE. These calculated energy values used for localization algorithm. Details of the localization algorithm are given in the next section.

3. LOCALIZATION ALGORITHM

In order to localize the WCE capsule, the energy density values of the sensors shown in Figure 3-a were used. These sensors are placed on the X and Z axis, respectively, with 8 columns and 8 rows on the body. Y axis is directed into the body. Here, only 10 sensors which have the highest energy value for each WCE positioning were used in the localization algorithm. The reason for using 10 sensors in the positioning algorithm was that the energy after the 10th sensor is less than 10% of the highest energy value and has little contribution. Figure 4. shows 10 sensors with the best energy value in 2-D for a random WCE position. In Figure 4, it is clear that the use of position and energy of the best sensors for WCE position estimation will greatly contribute to the positioning algorithm.
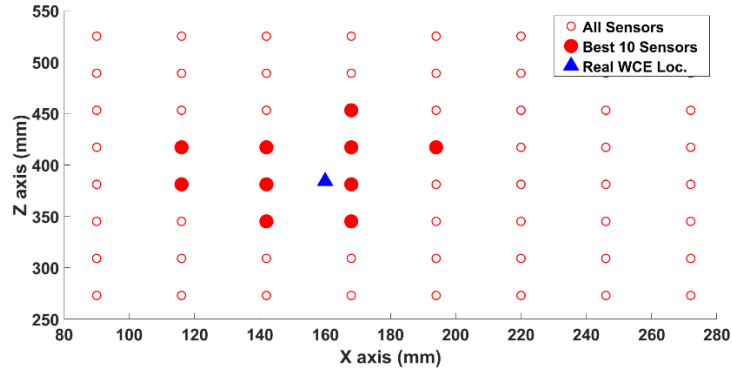
Figure 4. 2-Dimension sensor placement on the body and best 10 sensors for random WCE position

For this reason, the position and energy of the best sensors in the X and Z position estimation of the WCE were used as shown below,

$$\hat{X}_n = \sum_{i=1}^{10} X_i \tilde{E}_i,$$

$$\hat{Z}_n = \sum_{i=1}^{10} Z_i \tilde{E}_i \tag{3}$$

$$\tilde{E}_i = \frac{E_i}{\sum_{j=1}^{10}(E_j)}$$

Where $\hat{X}_n$ and $\hat{Z}_n$ estimated positions of the WCE (n=1,2,3…32), X_i and Z_i are the *i*-th sensor's position on the body and $\tilde{E}_i$ is normalization function that the ratio of the *i*-th sensor to sum of the all sensors. Although the sensors are evenly spaced in the X-Z plane on the body, the Y positions of the sensors depend entirely on the shape of the belly. Therefore, the position estimation of WCE cannot be made similar to X and Z. Here, the Y position was found by curve fitting with the least square method depending on the energy value of the best sensor as seen Figure 5.
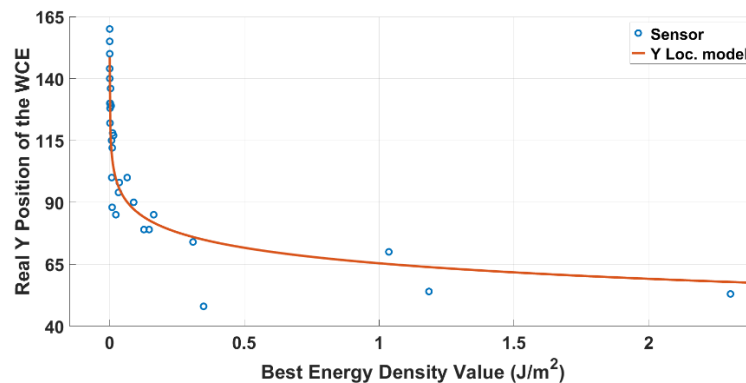

Figure 5. Curve fitting for Y position of the WCE

The model obtained to determine the position of the WCE on the Y axis is,

$$\hat{Y} = 65.39 - 20.82\log(E_1) \tag{4}$$

where $\hat{Y}$ is estimated position of the WCE on the Y axis and E_1 is the best energy density value obtained among all sensor.

4. RESULTS

The 3D position estimation of the WCE was performed by running the Localization algorithm in the previous section and Figure 6 was obtained.
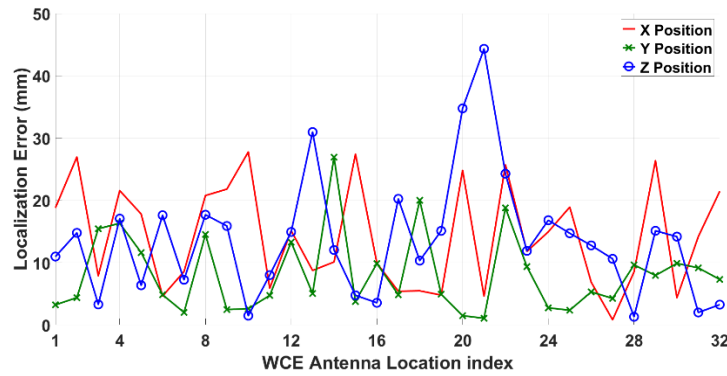

Figure 6. Localization error of WCE

Figure 6 shows the localization error between the known antenna positions and estimated positions for the 32 test locations within the small intestine. Here, RMS positioning error obtained in X, Y, and Z axes are 16.38 mm, 10.19 mm and 16.68 mm, respectively. By means of the error values obtained in each axis, the total localization estimation error is obtained by the following Equation.

$$\varepsilon_n = \sqrt{(\hat{X}_n - X_n)^2 + (\hat{Y}_n - Y_n)^2 + (\hat{Z}_n - Z_n)^2} \tag{5}$$

The RMS value of the total localization estimation error is 25.5 mm. Also, empirical CDF function of it, given at Figure 7.
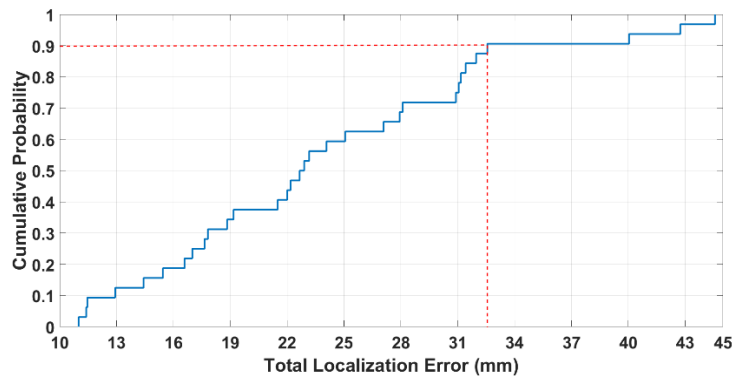

Figure 7. Empirical CDF of Total Localization Error

This graph shows that the total positioning error is less than or equal to 32.56 mm, with a probability of 90%. Thus, the position of a WCE antenna moving in the small intestine is precisely obtained by this study.

CONCLUSIONS

In this paper, we discussed the problem of localization of the WCE antenna in the small intestine using UWB signaling and proposed localization algorithm. The proposed positioning algorithm allowed for non-invasive WCE location estimation only through position and energy values of sensors placed on the body. Our results indicate the RMS value of the total localization estimation error is 25.5 mm. The results help to advance the state of the knowledge in the area of accurate UWB-based in-body WCE localization.

REFERENCES

[1] P. Swain, G. J. Iddan, G. Meron, and A. Glukhovsky, "Wireless capsule endoscopy of the small bowel: development, testing, and first human trials," in Biomonitoring and Endoscopy Technologies, 2001, pp. 19-24.
[2] G. Iddan, G. Meron, A. Glukhovsky, and P. Swain, "Wireless capsule endoscopy," Nature, vol. 405, p. 417, 2000.
[3] C. Gabriel, S. Gabriel, and y. E. Corthout, "The dielectric properties of biological tissues: I. Literature survey," Physics in medicine & biology, vol. 41, p. 2231, 1996.
[4] M. A. Stelios, A. D. Nick, M. T. Effie, K. M. Dimitris, and S. C. Thomopoulos, "An indoor localization platform for ambient assisted living using UWB," in Proceedings of the 6th international conference on advances in mobile computing and multimedia, 2008, pp. 178-182.
[5] A. Khaleghi, R. Chávez-Santiago, and I. Balasingham, "Ultra-wideband pulse-based data communications for medical implants," IET communications, vol. 4, pp. 1889-1897, 2010.
[6] M. J. Ackerman, " Viewpoint: The Visible Human Project, Journal Biocommunication, 18,2, p. 14.," 1991.
[7] M. Kanaan and M. Suveren, "In-body ranging for ultra-wide band wireless capsule endoscopy using a neural network architecture," in Medical Information and Communication Technology (ISMICT), 2016 10th International Symposium on, 2016, pp. 1-5.
[8] M. Kanaan, R. Akay, and M. Suveren, "In-body ranging for ultra-wide band wireless capsule endoscopy using neural networks based on particle swarm optimization," Selcuk Universitesi Muhendislik, Bilim ve Teknoloji Dergisi, vol. 6, pp. 207-217, 2018.
[9] M. Kanaan and M. Suveren, "In-Body Ranging with Ultra-Wideband Signals: Techniques and Modeling of the Ranging Error," Wireless Communications and Mobile Computing, vol. 2017, 2017.
[10] M. Suveren, M. Kanaan, and C. K. M. Bolumu, "Investigation of shadowing effects in ultra wide band implant Body Area Networks," in Signal Processing and Communications Applications Conference (SIU), 2014 22nd, 2014, pp. 874-877.
[11] M. Kanaan and M. Suveren, "A new propagation modeling technique for ultra-wideband implant body area networks based on a neural network architecture," Neural Computing and Applications, vol. 28, pp. 3603-3615, 2017.
[12] M. Kanaan and M. Suveren, "A novel frequency-dependent path loss model for ultra wideband implant body area networks," Measurement, vol. 68, pp. 117-127, 2015.
[13] M. Kanaan, M. Suveren, and O. G. Saracoğlu, "On the bandwidth dependency of near-field effects in UWB implant body area networks," in Proceedings of the 8th International Conference on Body Area Networks, 2013, pp. 553-557.
[14] M. Kanaan, C. Kocer, and M. Suveren, "On the relationship between antenna parameters and near-field effects for UWB implant body area networks," in Medical Information and Communication Technology (ISMICT), 2014 8th International Symposium on, 2014, pp. 1-5.
[15] M. Kanaan and M. Suveren, "Ranging for in-body localization of ultra wide band wireless endoscopy capsules using neural networks," in Signal Processing and Communication Application Conference (SIU), 2016 24th, 2016, pp. 717-720.
[16] A. Khaleghi and I. Balasingham, "Improving in-body ultra wideband communication using near-field coupling of the implanted antenna," Microwave and Optical Technology Letters, vol. 51, pp. 585-589, 2009.
[17] Q. Wang, K. Masami, and J. Wang, "Channel modeling and BER performance for wearable and implant UWB body area links on chest," in Ultra-Wideband, 2009. ICUWB 2009. IEEE International Conference on, 2009, pp. 316-320.

Investigation Of The Effects Of The Correlation Between The Closing Force And The Remaining Stress On Twin Tube Shock Absorber Performance

Abdurrahim Arkan[1]

Abstract

In this study, remaining stress on the inner tube of the shock absorber, which is a part of the vehicle suspension system, has been measured and the performance effects of the differences in remaining stress on shock absorber were investigated. During production, the damper outer tube is closed on the inner tube together with oil seal and this creates remaining stress on the inner tube. For this measurement, strain gauges were applied on the inner tube and the remaining stress value were collected via data acquisition device during the production and converted into force. The performance effects of difference remaining stresses on the damper were investigated by doing damping force and noise tests..

Keywords: strain gauges, shock absorber, remaining stress measurement

1. INTRODUCTION

A shock absorber is a mechanical device to damp shock impulse and convert kinetic energy into thermal energy. Shock absorbers improves handling and comfort by reducing the vibrations from the road. Basically, it has an oil filled cylinder group and a piston that can move in the vertical direction. The piston is connected to the vehicle chassis and the outer tube to the axle.
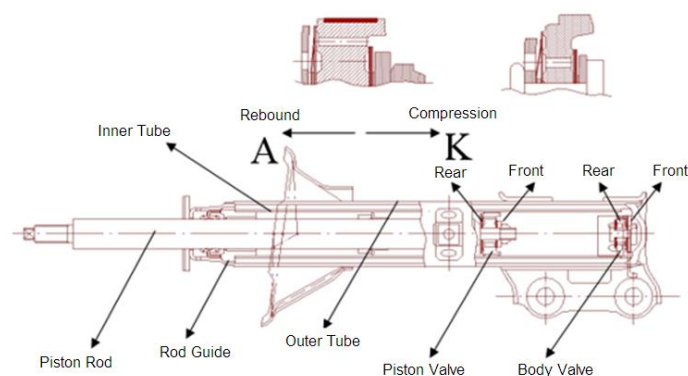

Figure 1. Shock absorber components

There are two valve group in the shock absorber that control the rebound and compression forces. When the car fall into the pothole the piston moves out of the inner tube(direction A) and the oil trapped between the rod

[1] *Maysan Mando A.S. Bursa, Turkiye,* *aarkan@maysanmando.com*

guide pass through the piston valve washers. The oil pass through the piston valve from the volume between piston and rod guide to the volume between piston and body valve by the rate of piston valve washers resistance. This resistance creates damping force effect at the rebound direction. Because of the piston moves out of the inner tube additional volume occurs. For filling the additional volume, the oil pass through the body valve from the volume between outer tube and inner tube to the volume between body valve and piston by stretching the body valve washers.

When the car bump into the speed bump the piston moves into the inner tube(direction K) and the oil pass through the piston valve from the volume body valve and piston to the volume rod guide and piston by the rate of piston valve washers resistance. Because of the piston moves into the cylinder additional rod volume occurs. This additional rod volume causes the oil, pass through the body valve from the volume between piston and body valve to the volume, between outer tube and inner tube. In the meantime, damping force effect occurs at the compression direction.

When we examine performance of the shock absorbers, we look at damping force graphs at certain speed.
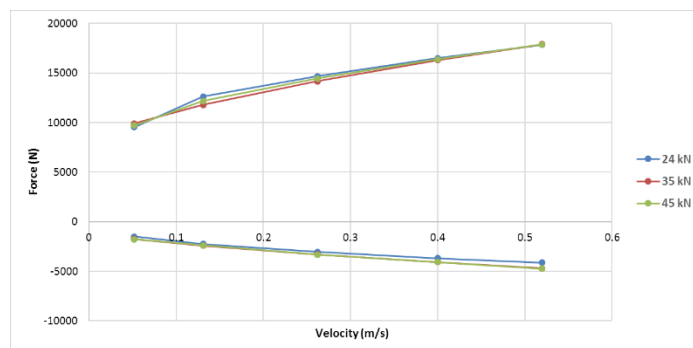
Figure 2. Damping force curves

2. INNER TUBE REMAINING STRESS MEASUREMENT

Before the remaining stress measurement, the inner tube should be placed in a v-block and the position should be adjusted. The location of the strain gauge should be marked by taking position of the knuckle bracket, stab bracket and spring seat into account.

o   ***Strain Gauge Selection***

The strain gauge is selected from the manufacturer's catalog according to the properties of the material to be bonded. In this study, TML type FLAB-6-350-11 strain gauge was selected.

Figure 3. Strain gauge

o   ***Preparation Of The Inner Tube Surface To Be Bonded With Strain Gauge***

First the area of strain gauge to be bonded with inner tube is cleaned with brake cleaner and sandpaper. A few drops of acidic solution are dropped to the cleaned area. After waiting for a few seconds, it is again wiped with cotton, a few drops from the neutralizing solution and after the surface has been wiped off, the surface is ready to glue the strain gauge.

Figure 4. Preparation of the strain gauge area

o **Bonding Strain Gauge to Inner Tube Surface**
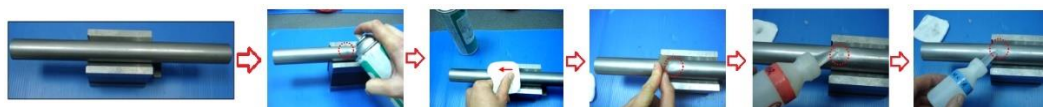
The strain gauge to be bonded to the prepared measurement surface is held with the aid of a pair of tweezers and placed opposite to a clean surface. The tape is placed to the center of the strain gauge. The upper surface of the tape is removed by gently pulling the bonded surface together with the attached strain gauge. The area under the strain gauge is expected to dry for a few seconds by applying very little from the catalyst. A small amount of adhesive applied to the area where the catalyst is applied, and pressure applied on the area of the strain gage. In this way the first strain gauge was bonded to the inner tube. The bonding of the strain gauge was completed by bonding the other 3 strain gauge with 90 degree angle between them.
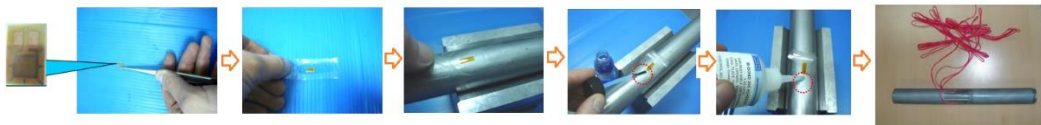

Figure 5. Bonding Strain Gauge to Inner Tube Surface

o **Preparation of Other Shock Absorber Parts**

Shock absorber outer tube is drilled and the strain gauge cables to be taken out. In this way, the strain gauge connection cables can be connected to the data acquisition device through the drilled outer tube. After that the piston rod is placed in to the inner tube without oil, together with the valve assembly.
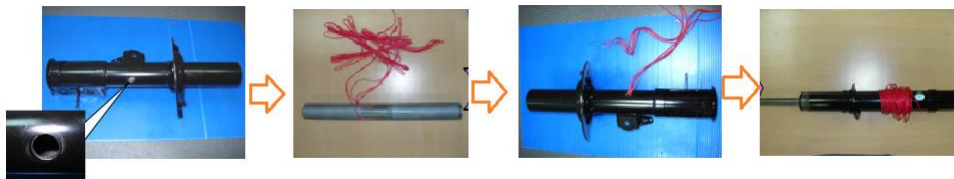
Figure 6. Inserting the inner tube into the outer tube

o **Preparation of Data Acquisition Device**

The cables coming out of the body pipe are connected to the data acquisition device with quarter bridge connection. Then the gauge factor specified in the strain gauge manufacturer's manual is entered in the corresponding field of the data acquisition device. Thus, the data acquisition device will be able to record the remaining stresses on the inner tube in the unit of micro-strain when the shock absorber is closed.

Figure 7. Preparation of Data Acquisition Device

o **Remaining Stress Test and Force Calculations**

After all these steps, the shock absorber is ready to close in mass production conditions. In this study, the effect of remaining stresses on the inner tube formed by 3 different closing forces examined. Shock absorbers are closed with 24 kN, second with 35 kN and 45 kN axial closing forces. Remaining stresses on the inner tube were recorded simultaneously. As shown in the figure below, the shock absorber outer tube is closed on the oil seal with 90 degree by doing like this permanent pressure is generated on the inner tube.
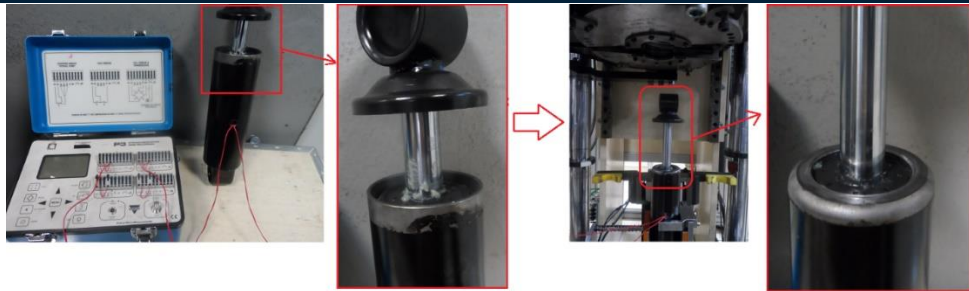
Figure 8. Shock Absorber Outer Tube End Closing

o   ***Stress to Force Calculations***

After the closing operation inner tube remaining stress was recorded as a unit of micro strain. These raw data need to be converted into kilogram force unit. Force transformation is done as follows.
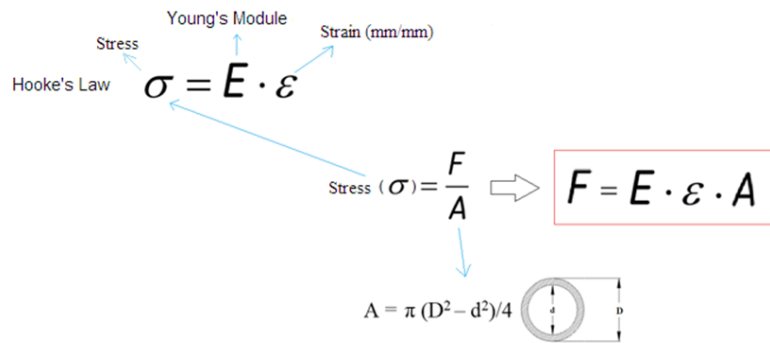
Figure 9. Stress - Force Conversion Calculations

For example, after closing operation inner tube remaining stress is 525 microstrain($\mu\varepsilon$), young's module is 210000 N/mm^2, outer tube diameter is 34 mm and inner tube diameter is 30 mm. According to this information calculations;

F= E . ε . A

A= 3.14(34^2 – 30^2)/4 = 200.96 mm^2

F= 210000 . 0.000525 . 200.96 =22156 Newton= 2261 kgf (remaining stress)

o   ***Remaining Stress Results According to Different Closing Forces***

According to three different axial closing forces, the inner tube permanent stresses were recorded with data acquisition device. Results of the inner tube remaining stress test with axial closing force of 24 kN are as follows;
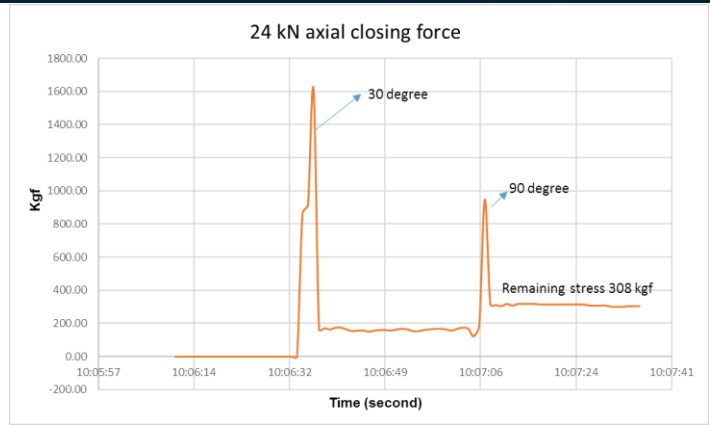
Figure 10. 24 kN axial closing operation inner tube stress graph

Results of the remaining stress test with axial closing force of 35 kN are as follows;
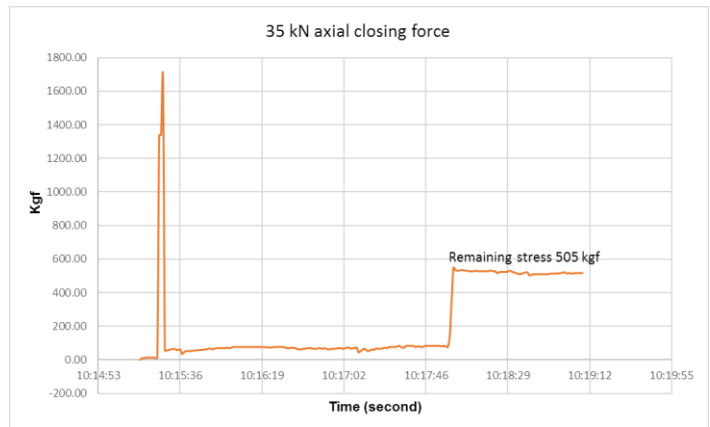
Figure 11. 35 kN axial closing operation inner tube stress graph

Results of the remaining stress test with axial closing force of 45 kN are as follows;

Figure 12. 45 kN axial closing operation inner tube stress graph

Measurements taken with three different closing forces the highest inner tube remaining stress is 1200 kgf with 45kN closing force and lowest remaining stress is 308 kgf with 24 kN closing force.
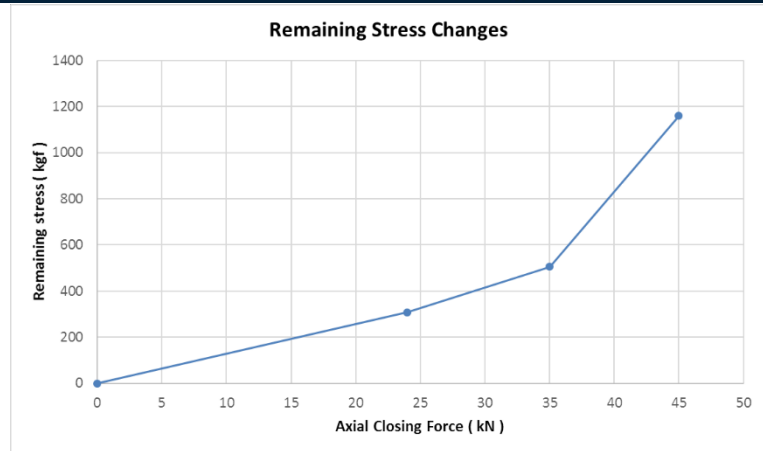
Figure 13. Axial closing force – Remaining stress graph

3. SHOCK ABSORBERS PERFORMANCE TESTS

Damping force measurement and vibration level tests were performed to examine the effect of different remaining stress on the shock absorbers performance.

By doing damping force measurement we can see the cavitation and damping force loss with the different remaining stress samples.

In the vibration level test, it is aimed to observe the noise effects by measuring the level of the vibrations transferred by the shock absorbers with different permanent stress to the chassis.

o *Damping Force Measurement*

With the damping force test, the damping performance of the shock absorber is tested. For this measurement, the damping curves are examined by running at different speeds in the servo hydraulic test machine (fig. 14).
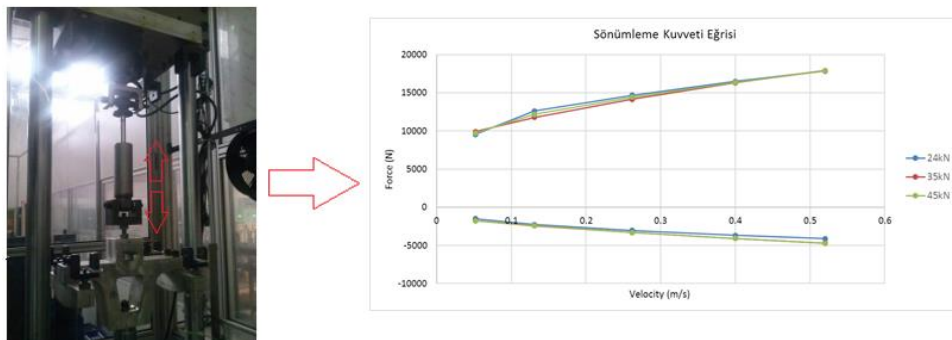
Figure 14. Damping force measurement

Damping force measurement with the 24kN, 35kN and 45kN axial closing force results as follows;
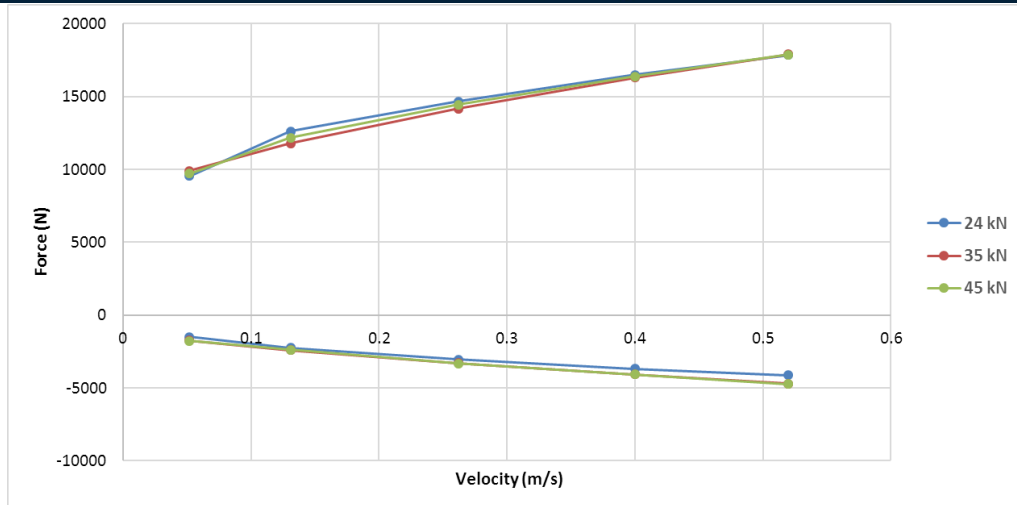
Figure 15. Damping force results

According to the results of the damping force test, there is no difference between the damping performance of the shock absorbers prepared at three different axial closing forces.

o   ***Vibration Level Test***

Vibration level testing is a test to measure the level of vibrations the shock absorber transfers to the chassis. In this test, acceleration sensor is mounted to the upper connection of the shock absorber and runs with ± 5mm, 10Hz. The result of vibration levels are displayed in the chart by scaling to 0 dB ref = 1.00 (m / s²) ² / Hz.
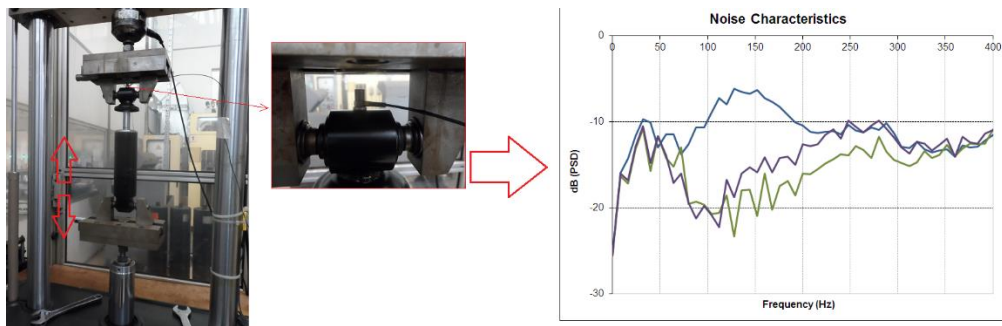
Figure 16. Vibration level testing

Vibration test results are as follows;
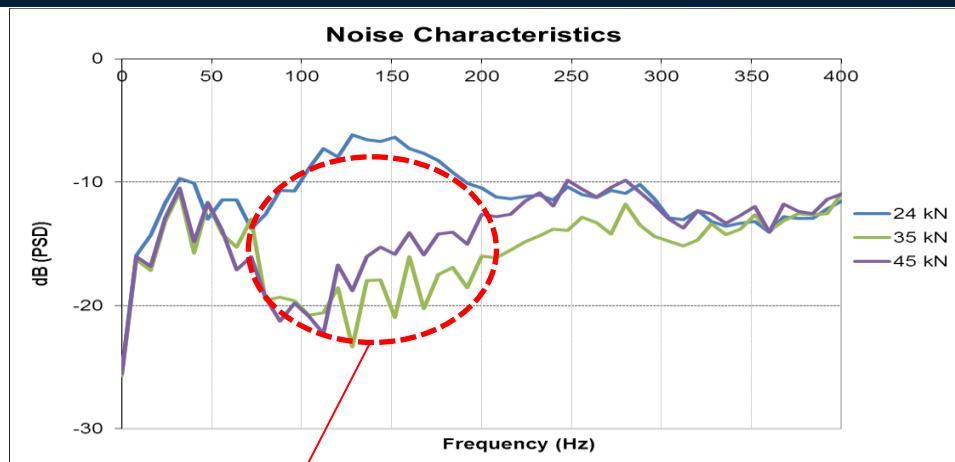
Figure 17. Vibration levels

At the 24kN sample, higher vibration level was measured between 100 Hz to 200 Hz unlike other two closing force samples. It was observed that the inner tube of the shock absorber was moving during the test and this made clanking noise.

4. CONCLUSIONS

In this study, remaining stress on the inner tube, has been measured and the performance effects of the differences in remaining stress on shock absorber were investigated.

As a result;

I.   As the axial closing force increased, It has been observed that the remaining stress of the inner tube increased logarithmically.

II.   It has been observed that remaining stress differences do not affect the damping performance in the samples produced with three different closing forces.

III.   In the vibration tests, it was observed that sample with 24 kN the inner tube is moving, thus creating clanking noise.

IV.   According to the results of the performance tests, it is seen that it is not applicable to do 24kN closing operation due to creating clanking noise.

REFERENCES

[1]. Dixon, J.J., (2001), "The Shock Absorber Handbook, Society of Automobile Engineers", UK.
[2]. Branislav Titurus et. al., "A method for the identification of hydraulic damper characteristics from steady velocity inputs" A Journal of "Mechanical Systems and Signal Processing"2010
[3]. D.N. Johnston, K.A. Edge, N.D. Vaughan. Experimental investigation of flow and force characteristics of hydraulic poppet and disc valves. Proceedings of the Institution of Mechanical Engineers, Part A: Journal of Power and Energy, 205(3): 161–171, 1991.
[4]. S.L. Ceccio, C.E. Brennen. Observations of the dynamics and acoustics of travelling bubble cavitation. Journal of Fluid Mechanics, 233: 633–660, 1991.
[5]. Piotr Czop, Jacek Gniłka,2016 "Reducing aeration and cavitation effect in shock absorbers using fluid-structure interaction simulation", Computer Assisted Methods in Engineering and Science, 23: 171–189, 2016
[6]. Sandip K. K., Milind S. M., 2014 "Experimental investigation of damping force of twin tube shock absorber" Int. Journal of Engineering Research and Applications Vol. 4, Issue 9, p.59-64
[7]. Vedat Temiz – "Makina Elemanlarinin Mukavemeti"
[8]. P. Czop, D. Slawik, P. Sliwa. Static validation of a model of a disc valve system used in shock absorbers.International Journal of Vehicle Design, 53(4): 317–342, 2010.
[9]. Adrian Simms and David Crolla, "The Influence of Damper Properties on Vehicle Dynamic Behavior" SAE Technical Paper Series, 2002-01-0319.

Evaluation of the Building Envelope to Achieve Comfort Standards in an Office Building in Izmir

Ayse Sena Cildir[1], Ayca Tokuc[2]

Abstract

Buildings consume about 40% of the world's energy, accounting for about 50% of carbon dioxide emissions. It is estimated that energy use in the built environment will increase by 34% over the next 20 years. In this context, the recast of the Directive on Energy Performance of Buildings (EPBD – 2017) establishes 'nearly zero energy building' as the target for all public buildings after 2018 and for all new buildings after 2020 at the European level.

The purpose of this study is to examine the effect a passive design strategy, the design of building envelope, in reaching thermal comfort standards for an office building located in Dokuz Eylul University, Izmir. The method is to investigate the effect of various variables on this office building within the context of reaching a nearly zero energy building via building energy simulation. The simulation model is validated and the addition of an outer facade element to generate a double skin scenario is modelled in the DesignBuilder software, i.e. the heating and cooling loads were calculated with the EnergyPlus simulation engine.

The variables of the scenario included changing double skin type, orientation, amount of space between the skins, ventilation, wall window ratio, glass type, shading and natural ventilation. The scenarios are discussed through yearly analyses of heating and cooling loads. The results show that reaching a nearly zero energy office building is not feasible with the evaluated passive design strategies; however they can play a significant role in decreasing the energy consumption of the building.

Keywords: Building energy simulation, DesignBuilder, Energy efficiency, nearly Zero Energy Buildings, Thermal comfort.

1. INTRODUCTION

The rapid increase in world energy use leads to the depletion of fossil based energy resources and has caused severe environmental impacts such as global warming and climate change. While buildings account for about 70% of sulfur oxides and 50% of carbon dioxide (CO_2) emissions, they consume about 40% of the world's energy consumption, 16% of the world's fresh water and 25% of the forest timber [1]. Energy use in the built environment is estimated to increase by 34% over the next 20 years. Also in 2030, the consumption attributed to houses and non-domestic sectors is expected to increase to 67% and 33%, respectively [2].

The concept of zero energy building (ZEB) is now perceived as a realistic solution to reduce CO_2 emissions and / or energy use in the construction sector, and not as a distant future concept. An increasing number of ZEB projects and research in this area highlight the increasing international interest in ZEBs. The objectives for the implementation of ZEBs are discussed at the European level within the recast of the Directive on Energy Performance of Buildings (EPBD) adopted in May 2010 [3]. As of 2018, the EPBD has set out to be a "nearly zero energy building" as a building target for all public buildings or public administration buildings of the public authorities and for all new buildings after 2020. Studies carried out to date define the concept of ZEB

with a wide variety of expressions, and different approaches to ZEB definitions can be seen. The lack of a generally accepted definition of ZEB is currently debated at the international level [4].

The building's facade affects its energy budget and comfort more than other systems in most buildings. In the design process of high-performance building facades, directives specific to climatic principles must be taken into account. The basic methods for designing high-performance building facades are: arranging building orientation according to the position of the sun; using natural ventilation to improve air quality and reduce cooling loads; minimizing the energy use of mechanical heating / cooling by optimizing the opaque components of the building shell with insulation material; increasing the use of daylight to minimize the use of artificial lighting and mechanical heating/cooling use by optimizing transparent components of the facade such as window / wall ratio (WWR), visible light transmission of glazing (VLT), U-value and solar heat gain coefficient (SHGC); and adding shading to control cooling loads and increase thermal comfort [5].

There are many studies on the optimization of building energy consumption through simulation programs in the literature. Boyanoa et al. [6], investigated the effect of different improvement scenarios on the energy consumption and economic performance of a building for three places representing three climatic regions of Europe. They had two scenarios with different lighting control systems, two scenarios for the improvement of glass and wall insulations, and two different building orientation variables. Yildiz et al. [7], investigated the effect of WWR on the building energy performance of an educational building in Izmir. They calculated that the eastern and western facades are the most effective and the northern facade has the least effect in terms of total energy consumption. When using low-e coated glass instead of double glazing (base case), they found that the same effects is obtained according to directions. Altan et al. [8], presented thermal balance and daylight level analysis of residential areas. In this context, they modelled four different hypothetical spaces with different windows. The parameters for evaluation are the thickness of the thermal insulation layer of the outer wall, and the type of window glazing. The outputs provided information about optimal facade design for energy efficiency and favorable daylight in buildings with temperate climates.

Early design phase decisions affect 80% of all design decisions [9], therefore the use of Building Performance Simulation (BPS) tools at the beginning of the design process is indispensable for assessing the challenges of energy efficient building design. Although there are similar scenarios in the literature, there is a lack of studies which use simulation programs as a decision support tool and aim to optimize environmental comfort, in terms of office buildings in the Mediterranean climate regions. The purpose of this study is to evaluate the parameters related to double skin facade (DSF) in Izmir, Turkiye climate for office buildings in terms of reaching nZEB standarts. In this context, DSF design parameters identified and examined comparatively. nZEB standarts require buildings to conform to thermal comfort standards, beside being very highly energy efficient [10]. Thus, DSF alternative's effect on the thermal comfort levels also examined.

2. METHODOLOGY

The methodology of the investigation is modelling of an existing office building and validating the model with measurements from inside and outside of the building, to calculate the annual total primary energy loads of the selected variables and the base case, and to compare the total and heating, cooling, lighting, room electricity, domestic hot water energy consumptions energy loads via building energy simulation. Also predicted mean vote (PMV) - predicted percentage dissatisfied (PPD) and discomfort hours are compared as thermal comfort parameters.

EnergyPlus is selected as the simulation engine for this study. It is a 3rd generation dynamic building energy simulation engine developed by the US Department of Energy to model building, heating, cooling, lighting, ventilation and other energy flows. DesignBuilder 5.5.0.012 [11], which is a graphical interface of EnergyPlus simulation engine, is used in this study.

2.1. Building Description and Building System

The office building is located in Tinaztepe Campus, at 38°21'57.91" North and 27°12'26.28" East with 194 m altitude. It has been in service since 2015 and comprises of 5-stories, 4 of which have the same open-plan office given in Figure 1. The structural system of the building is reinforced concrete frame and the slab is hollow-tile floor slab with 40 cm thickness. The floor height is 385 cm.
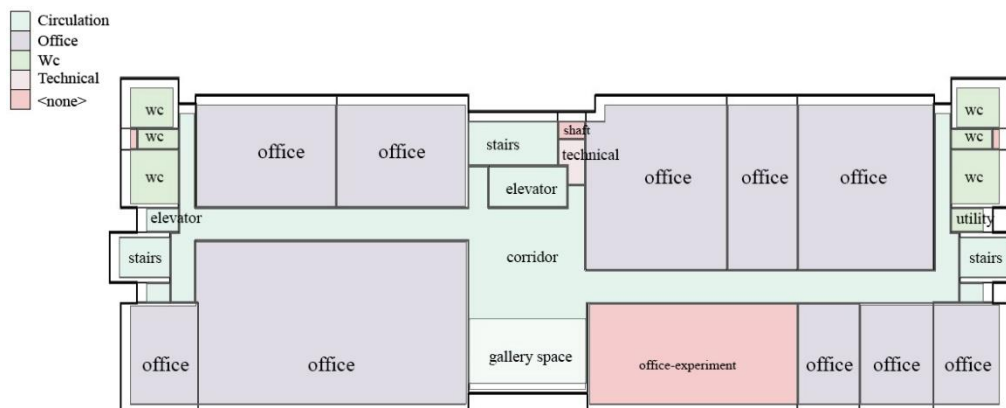
Figure 1. Model of the building's first floor

2.2. Building Elements

Four different wall sections are used in the building: basement wall with reinforced concrete curtain walls; exterior wall with brick wall, 40 cm gap, 6cm stone wool insulation material and aluminum composite coating; interior wall type 1 with panel system; and interior wall type 2 with brick wall. 3 different floor types are used in the building: basement floor with foundation, mezzanine floor, mezzanine floor wet space flooring. Two different roof types are used in the building: the biggest part of the roof is flat roof. Sandwich panel roof system with light steel structure is also used above the terrace. The U-values of the opaque building components are as follows: basement wall (0.621 W/m²K), exterior wall (0.451 W/m²K), interior wall type 1 (0.45 W/m²K), interior type 2 (2.196 W/m²K), basement floor (0.505 W/m²K), interior floor (0.252 W/m²K), flat roof (0.234 W/m²K) and sandwich panel roof (0.683 W/m²K). The infiltration rate of the building is 11.3 l/s-m² (0.6 ac/h).

Three facade types are used in the building. In the central of the south and north side of the building and in the office sections of the 3rd and 4th floors, a single layer aluminum curtain wall is used. This facade is fixed to the floors. The facade type used in the remaining office areas of the building consists of 245 cm single layer glass facade with 60 cm sill height and %48 WWR with exterior wall type as pre-described. Third one is the facade of the service areas on the east and west sides of the building with 6 cm stone wool thermal insulation material and brick wall. Double glazing windows with aluminium window frame with thermal breaks are used. U value of the glass is 2.34 W/m²K.

2.3. Validation of the Simulation

The office is open from 07:00 to 19:00 except for weekends and holidays. The office sschedule is fully occupied from 09:00 to 12:00 and 14:00 to 17:00. It is occupied by 75% between 12: 00-14: 00 due to lunch. HVAC elements do not work out of working hours. The heating/cooling energy of the building is supplied by 4 pipe fan coil unit, which works with natural gas, and air-cooled chiller. The heating performance coefficient (COP value) of the air conditioning system is 0.85, and the cooling COP value is 1.8. Mechanical heating/cooling elements of the building keep the building 22°C during the heating period and 24°C during the cooling period. Natural ventilation is provided when the indoor temperature of the building exceeds 24°C. Mechanical ventilation is activated when the building temperature drops below 10°C. The target illumination for the office space of the building is 500 lux, which is stated as the minimum value for office spaces in EN 12464-1.2009 [12]. There is no lighting control connected to any daylight sensor.

Inside and outside measurements are made to validate the model with actual data. Hourly data representing 7 days are obtained from 17.12.2018 to 24.12.2018. The interior measurements are carried out on the first floor of the building in a 121.6 m² office, which faces the south facade, and was not in use during the measurement period. Once the measuring instruments are installed, the space is completely closed for reliability. HIOKI 8421-51 datalogger is used to obtain indoor dry bulb temperature (°C) data with T-type thermocouples used to measure three points. PCE-FWS 20 meteorological station is used to obtain outdoor dry bulb temperature (°C), dew point temperature (°C), atmospheric pressure (kPa), and humidity (%).PCE-SPM-1 dosimeter is used to obtain the solar radiation data.

The obtained data are entered into Elements [13], which is an open source weather file generating software prepared with the contributions of Rocky Mountain Institute, and an EnergyPlus weather file (.epw) file is generated for use in the DesignBuilder software. Measured data and simulated data are compared to validate the model. Results are, root mean square error coefficient (CV (RMSE)) = 9.37% and mean bias error (MBE) =%0.51, which are within the validation range of AHSRAE Guideline 14 [14].

2.4. Energy Consumption of the Base Case

Detailed building energy consumption data of the current building are obtained based on the simulations made using the measured weather data on the verified model. The total annual primary energy per m² of the base case is 221.30 kWh/m². The energy loads included in the calculation are total heating, cooling, lighting, hot water and room electricity loads. Primary energy calculations are based on total site energy. The highest share in total annual energy consumption belongs to the cooling load with a rate of 39.5%. This is followed by room electricity and lighting loads with rates approaching 22%. The hot water energy load is 9.6% and the lowest energy load is heating with 5%.

Looking at the distribution of energy consumption by months, it is seen that the heating is zero summer months in accordance with the expectations. The cooling load is active between April and November and peaks in August. Due to heat gain from sunlight, lighting, computers, equipment and heat generated by users, the cooling load does not reach zero during the winter months. Hot water, lighting and room electricity loads show a linear distribution in all months. Room electricity includes consumptions related to user behavior, such as office equipment and computer use. Hot water use also depends on user behavior and occupancy density. As the facade design could not change the energy consumption of the room electricity and hot water, measures targeting to reduce the highest energy consumption, i.e. cooling and lighting, are taken.

All comfort calculations are carried out for the following conditions; clothing insulation is 1 clo in winter, 0.5 clo in summer, metabolic rate is 123 W/person in office areas, 140 W/person in circulation areas, toilets, utility rooms, 110 W/person in restaurant and 180 W/person in the kitchen. According to ASHRAE Standard 55, the relative humidity should be between 30% and 70%, -0.5 <PMV <0.5 and PPD <10. And the accepted operative temperature range is 20-23°C in summer and 23-26°C in winter [14]. In the base case, the humidity is in the range of 30-70% in all months and the annual average. The Fanger PMV index provides group B thermal comfort standarts with an annual average of -0.37 (Table 1). However, in winter months and April, the index approaches -1, indicating that some of the users feel cold. Operative temperature values are found to exceed the limits of the recommendations made by ASHRAE Standard 55 in both winter and summer months. The discomfort hours in winter are critically higher than in summer. During the year, 308.93 uncomfortable hours are experienced in the building. The average annual PPD index of the PMV value is 7.92 and complies with the Group B thermal comfort standards.

Table 1. Monthly and annual data for comfort variables of the base case

	Humidity	Fanger PMV	Air Temperature	Radiant Temperature	Operative Temperature	Discomfort hours	Outside dry bulb temperature
	%		°C	°C	°C	hour	°C
January	42.47	-0.71	19.98	20.15	20.07	68.15	8.91
February	36.36	-0.70	20.14	20.40	20.27	62.12	8.36
March	40.54	-0.44	20.99	21.41	21.20	50.20	10.65
April	47.93	-0.91	22.66	23.41	23.04	13.77	16.14
May	48.05	-0.48	23.93	24.86	24.39	1.82	20.96
June	50.08	-0.17	24.67	25.81	25.24	2.56	24.44
July	48.38	-0.02	25.14	26.29	25.72	0.95	25.82
August	52.93	-0.03	25.00	26.18	25.59	4.07	25.38
September	50.07	-0.19	24.62	25.78	25.20	2.97	23.03

October	45.30	0.15	23.06	23.90	23.48	3.33	16.95
November	37.84	-0.36	21.36	21.87	21.62	39.45	11.45
December	38.53	-0.65	20.23	20.55	20.39	59.55	8.87
Annual	44.92	-0.37	22.66	23.40	23.03	308.93	16.79

2.5. Scenarios

Within the framework of investigating the effect of building envelope elements and energy efficient building systems in achieving nZEB standards, the following variables are effective in creating scenarios for designing high performance building envelope. Aksamija [5] also mentioned these variables as:

- Minimizing the required energy for mechanical heating/cooling by optimizing the opaque components of the building envelope;

- To increase the use of daylight by optimizing the transparent components of the building envelope, such as WWR, visible light transmission (VLT), U-value and SHGC, thereby minimizing the energy used for artificial lighting and mechanical heating/cooling;

 - Using shading elements to control cooling loads and increase thermal comfort.

The possible contribution of eight main parameters with twenty different variables for different scenarios in reducing building energy consumption was evaluated. In order to compare the measures taken, each scenario will be implemented individually. Design variables are evaluated by simulation and the most energy efficient option is determined. However, the DSF is located only in the southern facade where office areas located. Although the addition of an external shading element also improves energy performance, the absence of external shading was chosen to in comparing the energy efficiency of the DSF design.

Four main parameters are about general spesifications of the DSF: Type of DSF, location of DSF, depth of cavity and ventilation of DSF. Four main parameters are about translucent elements of the DSF: WWR of the outer skin, glass type of the outer skin, internal shading and external shading. Two types of DSF are evaluated in the study; floor height DSF and building height DSF. In addition to southern located DSF, south and north, south and east, south and east and west location options are also evaluated. As cavity depth, 90 cm and 140 cm are reviewed. All day long ventilation in the summer and only night ventilation in the summer are simulated as DSF ventilation options. Three types of WWR of the outer skin are evaluated; %100, %70 and %52. Three types of glass used for the outer skin; 6 mm clear single glass, 6/12/4 argon gas double glass, and 3/13 triple glass. For internal shading, blind with low reflectivity slats or no shading options are evaluated. The last parameter is external shading, 50cm overhang and no shading options are simulated.

3. RESULTS AND DISCUSSION

The best results are obtained for the DSF facade option presented with the name DSF-1. Then fourteen alternative DSF designs are simulated by changing one variable at a time. Table 2 shows the annual energy consumption of resources per m², the annual primary energy per m² and the percentage of primary energy savings according to the base case of the building. The results are as follows:

- Building height DSF increased the cooling loads and decreased the lighting loads. Meanwhile the floor height DSF type has a positive effect on cooling and a negative effect on lighting energy loads due to the shading effect of the slabs between the floors. Since the cooling load has a higher overall effect, 0.13% more savings were achieved in the floor height DSF alternative.

- Adding DSF to the northern facade along with the south, increased cooling and lighting loads, reduced heating loads, and consequently reduced energy savings by almost 1%. Under the climatic conditions of Izmir where the cooling loads prevail, the DSF has a negative effect by increasing the cooling loads of the northern facade, which are relatively low compared to other facades. This result is compatible with the literature.

- Most of the east and west facade of the building has technical and circulation areas and is deaf. Only the 8 m part near the south facade contains office areas, on which DSF were added. Adding DSF to the eastern facade along with the southern facade reduced the heating loads. The effect on other sources is insignificant. This alternative is 0.21% more efficient.

- Adding DSF to the eastern and western facades along with the southern facade increased the cooling loads and reduced the heating loads. The effect on other sources is insignificant. This alternative is 0.09% more efficient. The lowering of the heating loads in the east and west facades shows that DSF will be more effective in cold climates where the heating load is dominant.

- Increasing the DSF cavity depth from 90 cm to 140 cm reduced the cooling loads by reducing the amount of heat gained through the window, but increased the lighting loads by increasing the shading effect. The percentage of savings remained unchanged.

- In the summer, using only night ventilation increased the cooling loads. The hot air collected in the DSF should be evacuated by ventilating through all day in summer, not only during the night hours when the temperature drops.

- Reducing the WWR on the outer skin of the DSF from 100% to 70%, reduced the cooling loads as the amount of heat gained from the window decreased, but increased the heating and lighting loads. 100% WWR is 0.11% more efficient than 70% WWR.

- Reducing the WWR from 100% to 52% on the outer skin of the DSF had similar effects. 100% WWR is 0.31% more efficient than 52% WWR.

- The same type of glass used in the building on the outer skin of the DSF has reduced cooling loads and increased heating loads. It also increased the lighting loads due to the film coating on the glass surface. The use of single clear glass is almost 1% more efficient than double glazing with 6/12/4 argon gas filling.

- The use of 3/13 air filled triple glazing on the outer skin of the DSF increased cooling and lighting loads, and reduced heating loads. Single layer clean glass usage is 0.7% more efficient.

- The use of blind with low reflective slats as internal shading on the inside of the outer skin of the DSF increased both the cooling and lighting loads. Using any internal shading element is 1.27% more efficient.

- The addition of 50 cm overhang as external shading element to the DSF reduced the cooling loads, and increased the heating and lighting loads. The alternative with the 50 cm overhang is 0.1% more efficient.

Table 2. Annual energy consumption of resources per m² according to the changed variables, annual primary energy per m² and the percentage of primary energy saving according to the base case (Variables used in DSF-1)*

		Cooling (kWh/m²y)	Heating (kWh/m²y)	Room electricity (kWh/m²y)	Lighting (kWh/m²y)	Domestic hot water (kWh/m²y)	Primary energy (kWh/m²y)	Percentage (%)
DSF type	Floor height DSF*	70.39	12.81	51.38	32.87	21.89	186.06	15.92
	Building height DSF	71.00	12.83	51.38	32.54	21.89	186.36	15.79
DSF location	South*	70.39	12.81	51.38	32.87	21.89	186.06	15.92
	South+North	72.01	11.79	51.69	34.16	21.84	188.22	14.95
	South+East	70.40	12.47	51.36	32.82	21.83	185.61	16.13
	South+East+ West	70.77	12.41	51.34	32.82	21.81	185.88	16.01
Cavity depth	90 cm*	70.39	12.81	51.38	32.87	21.89	186.06	15.92
	140 cm	70.09	12.81	51.38	33.14	21.89	186.08	15.92
DSF ventilation	Daylong in the summer*	70.39	12.81	51.38	32.87	21.89	186.06	15.92
	Night time in the summer	70.92	12.80	51.38	32.87	21.89	186.58	15.69
WWR	100%*	70.39	12.81	51.38	32.87	21.89	186.06	15.92
	70%	69.80	12.92	51.38	33.61	21.89	186.32	15.81
	52%	69.50	12.98	51.38	34.29	21.89	186.76	15.61
Glass type	6mm single clear glass*	70.39	12.81	51.38	32.87	21.89	186.06	15.92
	6/12/4 argon double glass	69.09	13.36	51.38	35.69	21.89	188.13	14.99

	3/13 triple glass	72.79	11.43	51.38	33.42	21.89	187.62	15.22
Internal shading	None*	70.39	12.81	51.38	32.87	21.89	186.06	15.92
	Blind with low reflect. slats	71.27	12.81	51.38	34.83	21.89	188.89	14.65
External shading	None*	70.39	12.81	51.38	32.87	21.89	186.06	15.92
	50 cm overhang	69.59	13.01	51.38	33.26	21.89	185.85	16.02

While the total annual primary energy per m² of the base case is 221.30 kWh/m², it is 186.06 kWh/m² for DSF-1. It is seen that a saving of 15.92% in total primary energy is achieved with DSF-1 (Table 3).

Table 3. Comparison of annual primary energy consumption of base case and DSF-1 (kWh/m²y)

	Cooling (kWh/m²y)	Heating (kWh/m²y)	Room electricity (kWh/m²y)	Lighting (kWh/m²y)	Domestic hot water (kWh/m²y)	Total primary energy (kWh/m²y)	Percentage (%)
Base case	88.78	11.72	51.32	50.98	21.77	221.30	100
DSF-1*	70.39	12.81	51.38	32.87	21.89	186.06	84.08

* In DSF-1, since the building area is taken 148 m² more than the base case, the total number of occupants is also calculated proportionally.

The two main saving factors are cooling and lighting energy. Since room electricity and hot water consumption depends on user behavior and occupancy density, they are not considered. In DSF-1, cooling energy requirement decreased by 20.7% and lighting requirement decreased by 35.5%.

Heating load increased in DSF-1. However, since the percentage of heating energy in the total energy is 5.2%, it did not have a noticeable affect on energy savings. Direct heat gain from the windows decreased due to the shading effect in DSF-1. Increase in the heating load shows that heating effect of the hot air collected in the cavity of DSF is less effective than getting direct heat gain from the window on the south facade in winter.

Monthly and annual comfort data of the DSF-1 alternative are summarized in Table 4. Humidity rate is between 30-70% in all months and annual average, in accordance with comfort standards. Fanger PMV index provides group B thermal comfort with an annual average of -0.46. The index is between -0.5 and -1 in winter and shows that some of the users feel cool in April and May. The operative temperature values are suitable for ASHRAE Standard 55 in summer and winter months except for January. The number of discomfort hours in winter is higher than in summer and 303.68 hours are experienced throughout the year in the building. The annual average PPD index of the DSF-1 is 9.49 and complies with the group B thermal comfort standards as it meets the PPD <10 criterion.

Table 4. Monthly and annual data for comfort variables of the DSF-1

	Humidity (%)	Fanger PMV	Air Temperature (°C)	Radiant Temperature (°C)	Operative Temperature (°C)	Discomfort hours (number)	Outside dry bulb temperature (°C)
January	42,57	-0,74	19,88	20,04	19,96	64,55	8,91
February	36,54	-0,74	19,99	20,23	20,11	61,53	8,36
March	40,79	-0,50	20,78	21,16	20,97	47,35	10,65
April	48,63	-1,00	22,42	23,12	22,77	16,03	16,14
May	49,03	-0,61	23,60	24,46	24,03	1,92	20,96
June	51,56	-0,30	24,34	25,39	24,87	3,32	24,44

July	49,86	-0,17	24,73	25,83	25,28	1,23	25,82
August	55,00	-0,17	24,61	25,72	25,17	6,80	25,38
September	51,93	-0,33	24,20	25,32	24,76	5,97	23,03
October	45,71	0,08	22,79	23,62	23,21	2,79	16,95
November	37,99	-0,42	21,15	21,65	21,40	35,87	11,45
December	38,66	-0,69	20,11	20,43	20,27	56,31	8,87
Annual	45,74	-0,46	22,40	23,10	22,75	303,68	16,79

4. CONCLUSIONS

In the scenario where DSF is added to the southern front, twenty different variables are identified under eight main parameters that affect the DSF design. The main parameters are as follows; type, location, cavity depth, ventilation of the DSF, WWR of the exterior skin, glass type of the exterior skin, internal and external shading. Variables were evaluated by simulation and the most energy efficient DSF design is determined and named as DSF-1. Accordingly, DSF-1 features are as follows; type of DSF is floor height, location of the DSF is southern facade, 90 cm cavity depth, all day long ventilation in summer, 100% WWR of exterior skin, 6 mm clear single glass for exterior skin, no internal or external shading. Total annual primary energy of the DSF-1 is 186.06 kWh/m²y. Cooling, room electricity, lighting, hot water and heating energy loads are 37%, 27%, 17.3%, 11.5% and 6.8% respectively. A thermal buffer of 90 cm is created in front of the southern facade of the existing structure with DSF-1. This buffer zone decreased the heating loads by storing heat energy in winter, and in the summer it reduced the cooling loads by providing shading effect and lowering the heat energy collected in the buffer zone by ventilation. With DSF-1 facade alternative, %15.92 energy saving is achieved in annual total primary energy. Beside the energy savings, building's comfort parameters are also investigated and annual discomfort hours are decreased by 5 hours with DSF-1. Although the average annual PMV value is within the limits of group B comfort standarts of ASHRAE Standart 55 in the DSF-1 alternative, it is closer to "0" value in the base case.

The optimized facade retrofit alternative is presented with DSF-1. Then to evaluate the effect of design variables to DSF's energy efficiency, fourteen alternative DSF design simulated by changing a variable each time and energy saving rates are calculated according to the base case. The results show that reaching a nearly zero energy office building is not feasible with the evaluated passive design strategies; however they can play a significant role in decreasing the energy consumption of the building. In future studies, the building facade will be redesigned and auxiliary systems in the building will be developed to meet nZEB criteria for non-residential buildings, as well as facade designs that meet the thermal comfort standards of PMV-PPD values and discomfort hour values.

ACKNOWLEDGMENT

REFERENCES

[1]. A. Bitan, "The high climatic quality of city of the future", *Atmospheric Environment,* Vol. 26(8), pp. 313-329, 1992.
[2]. L. Pérez-Lombard, J. Ortiz and C. Pout, "A review on buildings energy consumption information", *Energy and Buildings*, Vol. 40(3), pp. 394-398, 2008.
[3]. "E. P. B. D. Directive 2010/31/EU of the European Parliament and of the Council of 19 May 2010 on the energy performance of buildings (recast)", *Official Journal of the European Union*, Vol. 18(06), 2010.
[4]. A. J. Marszal, P. Heiselberg, J. S. Bourrelle, E. Musall, K. Voss, I. Sartori and A. Napolitano, "Zero energy building–a review of definitions and calculation methodologies", *Energy and Buildings*, Vol. 43(4), pp. 971-79, 2011.
[5]. A. Aksamija, "Design methods for sustainable, high-performance building facades", *Advances in Building Energy Research*, Vol. 10(2), pp. 240-62, 2016.
[6]. A. Boyano, P. Hernandez and O. Wolf, "Energy demands and potential savings in European office buildings: Case studies based on EnergyPlus simulations", *Energy and Buildings*, Vol. 65, pp. 19-28, 2013.

[7]. Y. Yildiz, T. G. Ozbalta and Z. D. Arsan, "Farkli cam turleri ve yonlere gore pencere/duvar alani oraninin bina enerji performansina etkisi: egitim binasi, Izmir", *Megaron*, Vol. 6(1), 2011.

[8]. H. Altan, J. Mohelnikova and P. Hofman, "Thermal and daylight evaluation of building zones", *Energy Procedia*, Vol. 78, pp. 2784-2789, 2015.

[9]. U. Bogenstätter, "Prediction and optimization of life-cycle costs in early design", *Building Research & Information*, Vol. 28(5-6), pp. 376-386, 2000.

[10]. "Towards nearly zero-energy buildings - Definition of common principles under the EPBD Final report - Executive Summary", 2013.

[11]. DesignBuilder Software Ltd. [Online]. Available: http://www.designbuilder.co.uk

[12]. *Light and Lighting – Lighting of Work Places – Part 1: Indoor Work Places*, EN 12464-1, 2009.

[13]. Elements 1.0.6, Rocky Mountain Institute, Big Ladder Software. [Online]. Avaliable: https://bigladdersoftware.com/projects/elements/

[14]. "American Society of Heating, Ventilating, and Air Conditioning Engineers (ASHRAE) Guideline 14, Measurement of Energy and Demand Savings", Atlanta, GA, USA, ASHRAE Tech. Rep. 2014.

BIOGRAPHY

Ayse Sena Cildir was born in 1991 in Izmir. She graduated from Istanbul Technical University, Department of Architecture in 2014. Currently she is working on her MSc thesis at the Structural Construction Design program of Dokuz Eylul University Faculty of Architecture.

Ayca Tokuc is an Associate Professor at the Faculty of Architecture, Dokuz Eylul University, Turkey. She is involved in a number of collaborative projects to enhance the built environment and health in the city. Her research examines energy efficient design as both a concept and in implementation in various scales including building and community scales. Her other interests lie in biodesign, regenerative design, innovative design, climate change, sustainable design and thermal energy storage.

Tensile Strength of Absorbable and Nonabsorbable Sutures

H. Kubra Kaynak[1], Gulsum Colak[1], Fatma Bes[1], Yunus Emre Acik[1]

Abstract

A suture is a thread that is a very old implantable medical material. For providing sufficient level of wound strength or compresses blood vessels in order to stop bleeding, sutures must provide many properties such as adequate tensile strength, elasticity, knot security, not cut through tissue, low tendency for infection, low memory and ease of handling. Among these properties tensile strength is the foremost property. In this study, it is intended to investigate the tensile strength of different absorbable and nonabsorbable suture types which are commercially produced in Turkey. For this aim, 11 different suture types; 6 of absorbable and 5 of nonabsorbable are tested to determine the tensile strength. All samples were conditioned according to ASTMD 1776 before the tests. Tensile strength tests were done according to ASTMD 2256.

Keywords: suture, tensile strength, extension, absorbable, non-absorbable

1. INTRODUCTION

A suture is a thread that both approximates and maintains tissues until the natural healing process has provided a sufficient level of wound strength or compresses blood vessels in order to stop bleeding [1]. Sutures must provide many properties such as adequate tensile strength, elasticity, increased knot security, not cut through tissue, low tendency for infection, low memory and ease of handling. All these properties are affected by structural properties of sutures namely; raw material, being monofilament or produced by braiding, coated or uncoated, being absorbable or nonabsorbable. Due to the developments in polymer technology different raw materials are used for suture production to determine the ideal suture material. Tensile strength and knot strength properties are the foremost properties of a suture and these properties provide information in vitro performance of the material such as durability while stretching and knotting during surgery, security of the knot after surgery and durability against fatigue in tissue exudates. So that, in the literature there are many studies on different performance properties of sutures [2-12]. Even though suture is a very old implantable medical material, due to providing different materials and different structural properties for sutures, even today there is still an ongoing research to develop and optimize this material.

2. MATERIAL AND METHOD

In this study, it is intended to investigate the tensile strength performance of different commercially available absorbable and nonabsorbable suture types in Turkey. All suture samples are 2.0 USP. For this aim, 11 different suture types; 6 of absorbable and 5 of nonabsorbable are tested to determine the tensile strength. Properties of the sample sutures are given in Table 1.

Table1. Properties of the samples

	Raw material	Structure	Sterilazation
Absorbab	Polyglactin 910-Poly (glcolide-co- lactide)	Multiflament - Braided	Etilen oxide
	Polyglactin 910-Poly (glcolide-co- lactide) RAPID	Multiflament - Braided	Gamma Rays
	Polyglcolic acid - PGA	Multiflament - Braided	Etilen oxide

---

[1] *Corresponding author: * Gaziantep University, Textile Engineering Department, Gaziantep, Turkey, tuluce@gantep.edu.tr*

	Polyglcolic acid PGA-RAPID	Multiflament - Braided	Gamma Rays
	Polyglecaprone 25- Poly (glycolide-co-caprolactone)	Monofilament	Etilen oxide
	Polydiaxonano - PDO	Monofilament	Etilen oxide
Non-absorbabl	Polyamide	Monofilament	Etilen oxide
	Polypropylene	Monofilament	Etilen oxide
	Polyester	Multiflament - Braided	Etilen oxide
	Silk	Multiflament - Braided	Etilen oxide
	Polyvinylidene Flouride	Monofilament	Etilen oxide
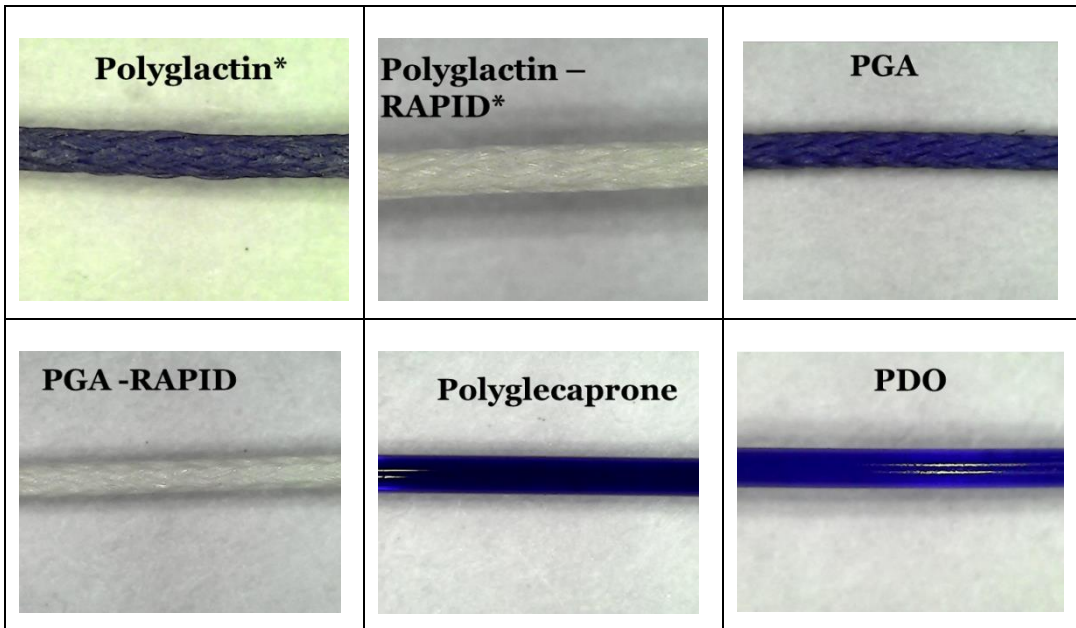
Figure 1. Microscobic views of absorbable sutures
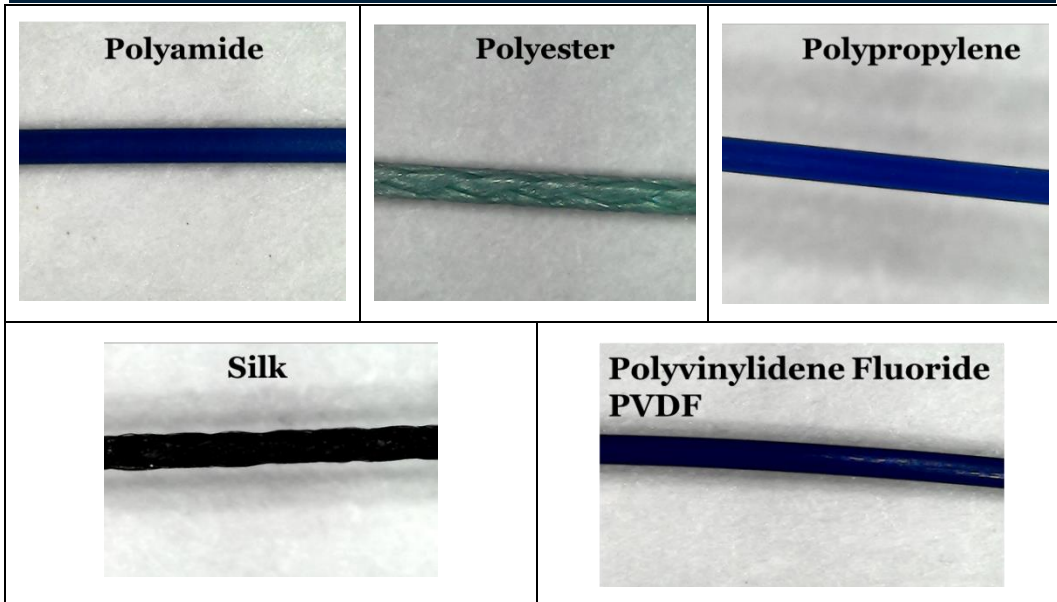
Figure 2. Microscobic views of non-absorbable sutures

All samples were conditioned according to ASTMD 1776 before the tests. Tensile strength tests were done according to ASTMD 2256 by TITAN test device. Tensile strength and elongation was detected as a result of tensile strength test.

3. RESULTS

o   ***Tensile strength of Absorbable Sutures***

Tensile strength results of absorbable suture samples are given in Figure 3 and extension results are given in Figure 4. In addition, microscopic views of the samples are taken at breaking regions to examine the failure effect of the absorbable sutures and are given in Figure 5.
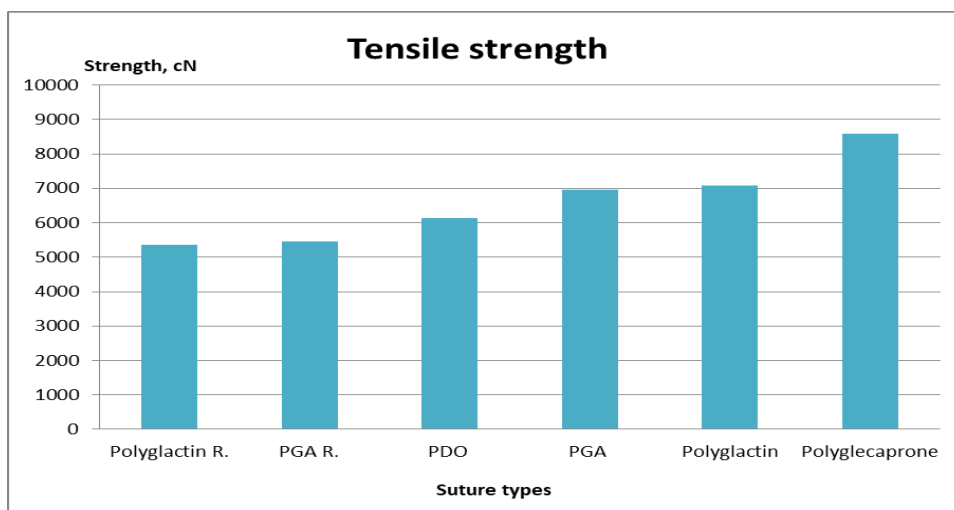
Figure 3. Tensile strength of absorbable sutures
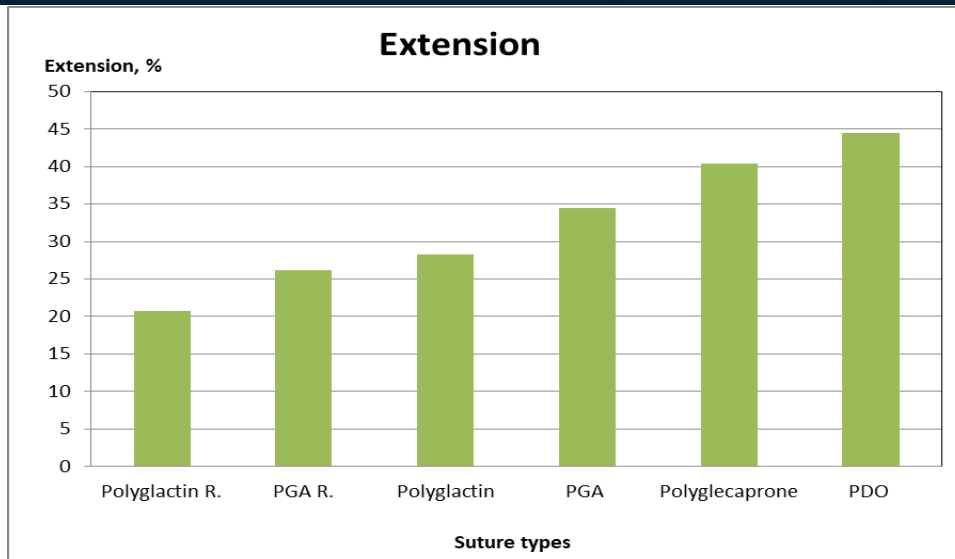
Figure 4. Extension of absorbable sutures

As it can be seen from graphical representations, PDO sample has the highest tensile strength but a moderate extension level. Besides, polyglecaprone sample has a high level of tensile strength and extension. On the other hand, polyglecaprone rapid sample has the lowest tensile strength and extension. It should be considered that the only difference between these two samples is the sterilization process. For a higher absorption speed rapid sample was sterilized by Gamma rays. This situation provides a better biodegradability from the producer side. But also, it causes a lower tensile strength and extension. The similar situation is also observed for PGA sample.
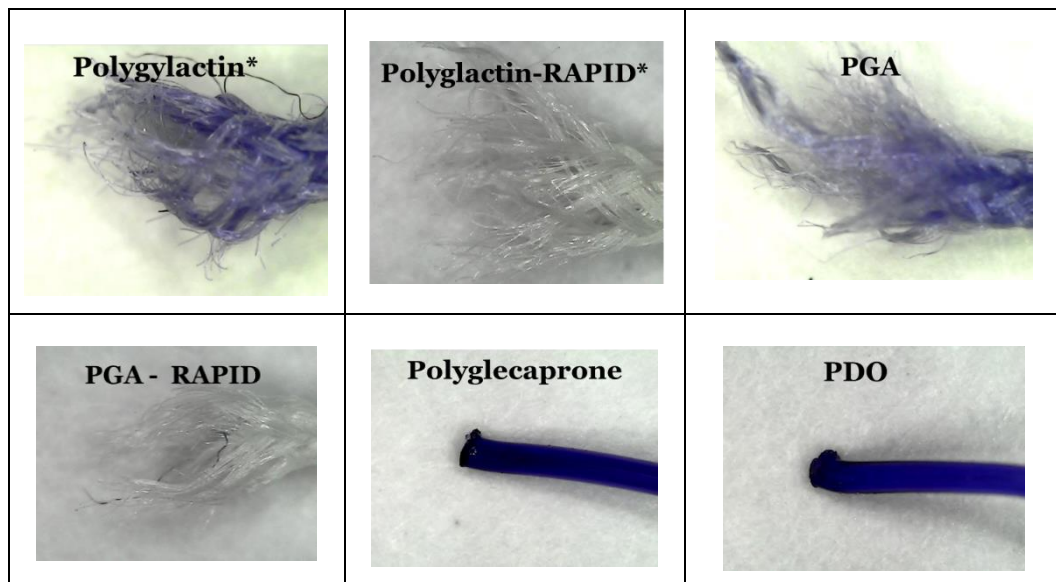
Figure 5. Microscopic views absorbable sutures after breaking

o   *Tensile strength of Nonabsorbable Sutures*

Tensile strength results, extension results and microscopic views of the samples are taken at breaking regions are given in Figures 6, 7 and 8, respectively.
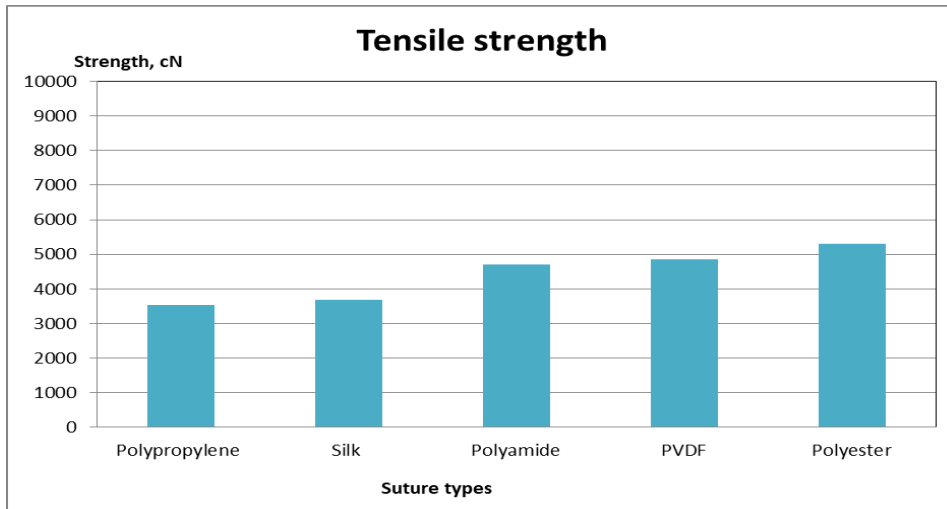
Figure 6. Tensile strength of non-absorbable sutures
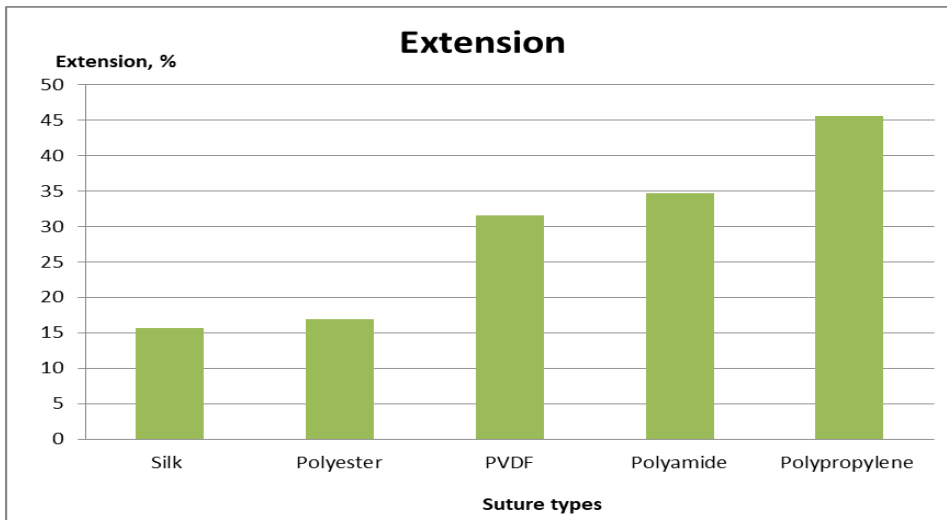
Figure 7. Extension of non-absorbable sutures

It can be seen from Figures 3 and 6, absorbable suture samples has considerably higher tensile strength values than non-absorbable ones. On the other hand, among non-absorbable suture samples polyester has the highest tensile strength but a very low level of extension. Also, polypropylene has the lowest tensile strength but the highest extension. Silk suture sample has low level of strength and also extension.
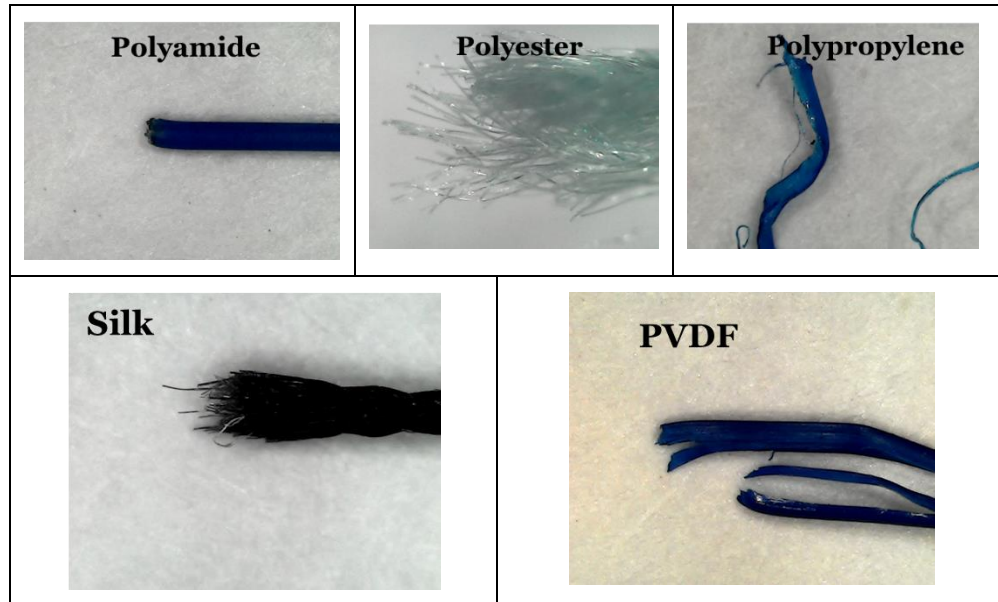
Figure 8. Microscopic views non-absorbable sutures after breaking

CONCLUSIONS

When examining the tensile property of sutures it should be considered that;

- Higher biodegredability can be obtained by using different polymeric materials and sterilization process. But, higher biodegredability cause the tensile strength to reduce.

- Different suture types are convenient for different tissue types. So, the choice should be done considering this criteria.

- For future study, the vitro tensile and knot strength performance of sutures must be studied by simulating the tissue exudates.

REFERENCES

[1] Gupta, B., Grover, N., Viju S. and Saxena, S., 2008, Polyester and naylon based textiles in biomedical engineering in: Polyesters and Polyamids, Woodhead Publishing.
[2] Carr, D. J., Heward, A. G., Laing, R. M. and Niven, B. E., 2009, Measuring the strength of knotted suture materials, Journal of the Textile Institute,100:1,51-56.
[3] Avcioglu Kalebek, N., Erol Konur, E., Ozdinc, O., 2016, Tensile and Knot Performance of Polyester, Silk, Polypropylene and Polydioxanone Sutures, Tekstil ve Muhendis, 23: 103, 172-181.
[4] Abdessalem, S.B., Debbabi, F., Jedda, H., Elmarzougui, S., Mokhtar, S. , 2009, Tensile And Knot Performance of Polyester Braided Sutures, Textile Research Journal, Vol:79 (3), pp.247-252, 2009.
[5] Bayraktar E.K., Hockenberger, A.S., 2001, Investigating the knot performance of silk, polyamide, polyester and polypropylene sutures, Texile Research Journal, 71 (5), 435-440.
[6] Debbabi, F., Abdessalem, S.B., Limem, S., 2011, New test methods to evaluate the performance of dermatological braided sutures from both the doctor and the patient sides, Journal of the Textile Institute, 102: 6, 548-557.

[7] Kim, J., Lee, Y., Lim, B., Rhee, S. Yang, H., 2007, Comparison of tensile and knot security properties of surgical sutures, J Mater Sci: Mater Med, 18:2363–2369.

[8] Debbabi, F., Abdessalem, S.B., 2014, Simultaneous optimization of mechanical properties of braided polyethylene terephthalate suture subjected to hot-stretching treatment, Journal of Industrial Textiles, DOI: 10.1177/1528083714560256.

[9] Gemci, R., Ulcay, Y., 2004, Ameliyat Iplikleri Tipleri Ozellikleri Ve Krome Katgut Ile Normal Katgut Arasindaki Mukavemet Farklari, Uludag Universitesi Muhendislik Mimarlik Fakultesi Dergisi, Cilt 9, Sayi 2, 95-105.

[10] Tiyek, I., Gemci, R., Turkoglu, S., 2011, Comparison of physical properties of sutures in medical liquids, International Journal of the Physical Sciences Vol. 6(8), pp. 2158-2168.

[11] Karaca, E., Hockenberger, A.S. and Yildiz, H., 2005, Investigation Changes in Mechanical Properties and Tissue Reaction of Silk, Polyester, Polyamide, and Polypropylene Sutures in Vivo", Textile Research Journal, Vol:75 (4), pp.297-303.

[12] Marturello, D.M., Fadden, M.S., Bennett, R.A., Ragetly, G.R., Horn, G., 2014, "Knot Security and Tensile Strength of Suture Materials", Veterinary Surgery, Vol:43, pp.73-79.

Study of a proposal for the development of a water supply network for Irbid City, Jordan

Lamis Sayed Abdelkader[1], Tema Otoum[2], Rawan Alali[3]

Abstract

A water distribution network is the means of getting water from the source to the consumer. It serves to convey the water from the water source and treatment works where necessary to the point where it is delivered to the consumer. The distribution system of a water works consists of the pipes, valves, hydrants and appurtenances used for distributing the water, the elevated tank and reservoir used for fire protection and for equalizing pressures and pump discharges and meters. Water distribution networks is an important component of any water supply system accounting for up to 80% of the total cost of the system and as a result operation and maintenance cost may soar higher if they are poorly designed, hence the need to have a well planned, designed and constructed water distribution network cannot be over emphasized especially because of its importance to industrial growth and water's crucial role in society for health, fire fighting and quality of life.

Keywords: Water distribution network, water supply network, Irbid City, Water management, Water network

1. INTRODUCTION

Jordan faces a complex set of development challenges stemmed from the chronic water scarcity. The situation is aggravated by climatic conditions, geography and, region's geopolitical environment. Water scarcity poses a serious challenge that affects the well King Abdul being, security and economic future of all Jordanians.

Water management in Jordan has focused on supplying water for human consumption. However, increasing demands on the country to be more resilient and better prepared for future pressures on its water supply, as well as the urgent need to enhance sanitation coverage, trigger the need to review Jordan's development plans and strategic options. Water needs to be considered in the context of other crucial resources, i.e., the production of food and generation of energy, hence the need for a better understanding of the water-food-energy.

2. BACKGROUND

WaterCAD is a specialized and specialized water network design program because the program is run using -1 Windows. It is able to shorten the time in the network component audit and design test. It also gives us important reports about the elements of the network and the design modification process. Which is easy to

---

[1] *Corresponding author: Assistant Professor, Yarmouk University, Department of Architecture Engineering, Jordan.*

Beni-Suef University , Faculty of Industrial Education, Egypt, lamisabdelkader@hotmail.com

[2] *Second Author: Civil Engineer, Yarmouk University, Civil Engineering Department, Jordan.*

[3] *Third Author: Architect Engineer, Yarmouk University, , Department of Architecture Engineering, Jordan.*

deal with by this program that we can modify an element and see its impact on the rest of the elements in a simple and fast.

3. THE PROGRAM IS CHARACTERIZED BY:

- Possibility of drawing and design.
- The possibility of dealing with other computer programs and the exchange of graphics and data and results, such as programs (AutoCAD-GIS).
- Ease of dealing with specialized data entry programs such as Excel – Access.
- Flexibility and high-end capabilities as well as ease of data entry and review and evaluation of results.
- Easy to make adjustments to the input and re-analysis of hydraulic in a simple and fast.
- Shorten a lot of time in checking network elements and design testing.
- High possibility of reviewing results and reporting to all network elements.
- Ability to test design for different design situations and see effects on network elements such as changes in speeds and pressures.[9]

4. SURFACE WATER

Surface water in Jordan contributes about 28% of the total water supply in the country. The country's three main rivers, the Jordan, Yarmouk and Zarqa, are a major part of the country's surface water system. However, the available water supply from each has become highly unreliable. Upstream diversion and over-pumping in Syria (Yarmouk River and its tributaries) and Palestine (Jordan River) directly affects water availability in Jordan. In the past, one of the main water resources in Jordan was the Jordan River, with a flow of 1.3 billion m3 per year (BCM/yr). A 2010 study found that the Lower Jordan River has been reduced to 2% of its historic flow.
 Water quality has also deteriorated sharply, with high levels of salinity and pollution from agricultural fertilizer and untreated wastewater upstream in Israel and the West

Objectives

To Designing a water network for Huwara in Irbid for 20 years , is to determine the flow of water and velocity in all the pipes in the network and the pressure at all junctions of the pipe system.

Study area

On which the network is designed. our studied area located about 4 miles east of the center of Irbid governorate at Petra street and covers an area of 2.1345 m^2, the highest elevation is 577 m above sea level and the lowest elevation is 553 m above sea level.[10]
There are different buildings in the area where each building has a certain population, so we have to count the population on the organization's map to find out the water they need.

Methodology

Before starting the hydraulic analysis process on WaterCAD program , we have to collect the information which was needed for analysis such as : study area and population regulation , flow calculation and street map.

Population

Before starting the hydraulic analysis process, we must collect the information we need for analysis, the most important of which is the flow calculation.
This network is supposed to serve the region for 20 years and therefore it is important to calculate the population increase, so we should know the rate of population increase in Jordan.
The rate of population increase varies each year according to the circumstances surrounding the region. Therefore, we calculated the average of increase rate for 5 years ago and obtained an increase rate of **2.5%**.[6]
Now that we know the rate of population increase, we must calculate the current and expected population through the map of the organization, which shows the type of buildings .[11]In general we relied on the estimate of the population in each building through a] **German study** on Jordan, this study shows the type of each building and the average population They live in every building.[12]

Figure (1): Huwara location

Figure (2): Population organization map

Table (1) : Current population (P_o) for each type of building

Land type	A	B	Private B	C	
Avg. # people residents of the building (P_o)	4	4	4	5	
# buildings in study area	302	1250 *5	127	66	
Sum of people (P_o)	**1208**	**25000**	**508**	**330**	**27046**

The population is calculated in 50 years according to the following equation:

$P_n = P_o (1 + K_a (T))$

Where :

P_n : Population after T years .

P_o : Current population .

K_a : The rate of population increase which equal to 2.5% .

T : # of years.[6]

From the above equation, we will calculate the population after 20 years for each building, because the per capita share varies according to the type of building.

Table (2): Population after 20 years for each type of building

Land type	A	B	Private B	C	
Avg. # people residents of the building (P_n)	6	6	6	8	
# buildings in study area	302	1250 *5	127	66	
Sum of people (P_n)	**1812**	**37500**	**762**	**528**	**40602**

We know that when hydraulics analysis is done, several data are needed. The most important of these is the amount of water demand by the area served by the network to be designed.

CONSUMPTION OF WATER

To calculate the amount of flow, we must know the per capita daily consumption in addition to the number and type of buildings as calculated in advance as the amount of water consumed varies according to the type of building.

As we know that the per capita daily consumption is different from world, where in Jordan the average consumption per capita (70-90) liters per person per day, a small amount compared to the countries rich in water.

We relied on a German study on buildings in Jordan to determine the amount of water needed in a building.

Once we know the per capita share and the population, we can't calculate the amount of flow because in the design process we can't take average consumption but we must take the peak value per capita consumption.

Table (3) : Quantity of daily consumption per capita by types of land .

Land type	Number of people or visitors (P_n)	Number building in study area	Peak per capita consumption(m^3)	Daily consumption rate (m^3)
A	6	302	0.145	**263**
B	6	1250 * 5	0.126	**4725**
Private (B)	6	127	0.126	**97**
C	8	66	0.126	**67**
Garden	100	1	0.05	**5**
Services	100	13	0.04	**52**
Trade shows	100	215	0.02	**430**
Public	200	4	0.05	**40**
Sum				**5679**

It is known that Jordan is a poor country with water, so the water deliveries to citizens are not continuous, but the process of flow once a week for only one day, so we must calculate the quantities of water per week. Then the amount of water within a week is **39753** m^3.

Modeling structure

Through which the map of the area is introduced and the location of the streets where the pipes will be drawn and then exported to the WaterCAD program.

Figure (3): map of area.

The following data is essential for building up a decent hydraulic model of the Water Distribution Network, To analyze the network of the pipe line, the following input data is mandatory.

Reservoirs

The nodes where the volume of stored water that vary with time during a simulation is reservoir data ,the primary input property for reservoir is **elevation** ,where the water comes to network from two main reservoirs, Houfa and Zubda, which will be placed on both ends of the network, Assuming that the water in both tanks is 15 meters high, the water surface in both tanks is 585 and 590 m respectively.[10]

Pipes

Pipes are the links that allows the water to flow from one point to other in the allowed network, The hydraulic input variable for pipes include material, length, fraction factor coefficient and diameter .

Pipe material

From about material we will use **Ductile iron** because it has Long life, ability to withstand internal pressure and external loads, available in Jordan at a reasonable price and toughness and imperviousness.

Pipe length

The length of the pipe is not computed arithmetically, but when drawing the network for the street plan, the length of the pipe is ready in the program and represents the length of the real street through which the pipe passes.

Fraction Factor Coefficient

The **Hazen–Williams** equation is an empirical relationship which relates the flow of water in a pipe with the physical properties of the pipe and the pressure drop caused by friction. It is used in the design of water pipe systems. such as fire sprinkler systems, water supply networks, and irrigation systems.
The **Hazen–Williams** fraction factor coefficient of Ductile Iron **C = 130** .[8]

Pipe diameter

All water pipes and water mains must be sized to meet the flow demands and pressure requirements But the information was not enough to use the equation of diameter but Estimate the pipe sizes on the basis of water demand, and local code requirements, we use 4 in diameter for all pipes.

Junction

These are the points in the network, where the links join together and at which, the water enters and leaves the network. The input data required for the junctions are:

Elevation

Google earth Is a mapping and geographic information program. The program raws a map of the earth by installing images obtained from satellite imagery, aerial photography and 3D geospatial information systems
The main purpose of using Google Earth is to know the heights that we need in the process of input the data for each junction, reservoir and others.

Water demand

To calculate the amount of water required, we perform a rough calculation for each node according to the surrounding buildings, the calculation method is as follows:
WD =Σ(# of visitors by type of building * share per person * 7days a week) *(Building number of the same type))

Table (4):Elevation and demand of some of junction

Demand (m³/week)	Elevation (m)	Label		Demand (m³/week)	Elevation (m)	Label
250	563	J-57		120	570	J-24
250	566	J-43		98	570	J-284
344	562	J-60		148	569	J-25
265	555	J-173		678	569	J-240
104	562	J-32		124	569	J-293
254	566	J-40		200	566	J-26
475	559	J-304		100	566	J-29
159	555	J-101		244	566	J-28
872	561	J-232		118	568	J-299
122	570	J-194		366	566	J-54
927	558	J-61		170	567	J-30
146	568	J-195		120	561	J-300

Calibration

After the data is entered as in the previous chapter, we must start the hydraulic analysis process through the WaterCAD program.
After the results are shown we perform the calibration process to reach the ideal values.

Standard value for Pressure and Velocity:

Velocities **above 3 ft/sec** help keep any solids from depositing in the pipeline.
Velocities **over 10 ft/sec** may erode the pipe lining and damage valves.
Typical Pressure in a distribution system is (**450-520**) **KPa** .
Maximum allowable pressure is **1030 KPa** .[7]

Preliminary Analysis Results :

We will initially set values for the results of the initial analysis. Values are the highest value and lowest value for both pressure and velocity.

Table (5): Max. & Min. Value for Pressure and Velocity after preliminary analysis .

	Pressure in Junction (KPa)	Velocity in Pipe (ft/s)
Maximum Value	- 4,178	97.15
Minimum Value	- 7,362	0.00

We also note that the results of the analysis showed irrational values and cannot be applied to reality, and this is due to several problems, the most important of which is the existence of negative pressure and the use of one diameter for all the tubes. The following is a solution to these problems.

Negative Pressure

Negative pressures are generated in the hydraulic simulation any time that the hydraulic grade dips below the nodal elevation.

1) Too high elevations at As such, negative pressures could be the result of a number of different things :
certain nodes.

2) Too high a head loss in the system (caused by high pipe velocities or high pipe roughness).

3) Too high a demand in the system.

4) System disconnections .

Knowing the causes of negative pressure helps us solve this problem, so we will start to solve these reasons gradually and will start by adding pumps to the network.[8]

Pumping

Introduction

Pump, a device that expends energy in order to raise, transport, or compress fluids.

Pumps that increase the pressure within the distribution system or raise water into an elevated storage tank are called booster pumps. most water distribution pumps are of the centrifugal type, in which a rapidly rotating impeller adds energy to the water and raises the pressure inside the pump casing.[8]

Definition Pump in WaterCAD

To solve the negative pressure problem we will start with the easiest solution is adding pumps to the network, to define the pump on the WaterCAD program must be two important elements are the amount of flow on the system in addition to the head provided by the pump to the system .

In Jordan, pumps can be used up to 100 m. As for the flow, we have already learned that the total flow is about 40,000 m^3 during the day of pumping.

This amount will be divided equally between the two reservoirs, meaning that in each tank will be put a number of pumps carrying 20,000 m^3 and raise the head hundred meters.

We will put two pumps on series in each reservoir, the system will consist of 4 pumps, and the following table and figure shows the pump information:

Table (6) : Pump information , Flow & Head .

	Flow (m³/day)	Head (m)
Shutoff	0	133.33
Design	20,000	100.00
Max. Operating	40,000	0.00

After adding pumps to the network and with several attempts to change the head of pumps and increasing the number of pumps results were unsatisfactory, where it remained negative pressure problem, the following table shows the results after the addition of pumps.

Table (7) : Max. & Min. Value for Pressure and Velocity after adding pump .

	Pressure in Junction (KPa)	Velocity in Pipe (ft/s)
Maximum Value	- 2,278	96.73

Minimum Value	- 5,432	0.05

So we will solve the second problem to get rid of the negative pressure is the presence of pipes with high speeds.

Pressure and Velocities Calibration

We also know that the pipes near the reservoir have high speeds and vice versa, to reduce this speed through the **Hazen- Williams equation** with the same height stability is increasing the diameter of the tube.

At the same time and with the results of the preliminary analysis there are speeds of not more than **3 ft/sec** second so we reduce the diameter of the tube to increase speed in this solution we can solve the problems of speed and negative pressure.

$V = 0.849\ C_{HW}\ R_h^{0.63}\ S^{0.54}$

C_{HW} : Hazen- Williams Coefficient .

R_h : hydraulic radius ($R_h = A/P = D/4$).

S : slope of EGL or head loss per unit length ($S = h_f / L$) .

$H_f = (KQ^m)$,($K= 4.73L/D^{4.87}C_{HW}^{1.5}$) , m=1.85 .[8]

The Hazen- Williams equation shows that the velocities depend on several factors the Hazen- Williams Coefficient, which is directly proportional to the velocity, in addition to the diameter of the tube.

After several attempts to modify the velocities by changing the pipe diameters based on the amount of flow and the location of the pipes. The increase of pipe diameters is in the vicinity of the reservoir and the reduction of the diameters is in the center of the network and the areas with low speeds

Table (8) : pipe diameter and place of them.

Diameter of pipes	Place of pipes	Number of pipes
12	Pipes out of tanks	14
8	High speed pipes	10
6	Normal speed pipes	19
4		89
2	Low speed pipes	120

Changing the type of material made from the pipes such as the PVC, which has Hazen- Williams Coefficient =150 .[8]

The following table shows the change in velocities after changing the type of material from ductile iron to PVC in pipes with a speed of less than 3 ft/s .

Table (9) : Pipe speeds after use PVC

Pipes	Pipe using ductile iron (ft/s)	Pipe after using PVC (ft/s)
P-82	1.89	2.18
P-105	1.09	1.26
P-388	1.76	2.03
P-504	1.91	2.20
P-566	1.00	1.15

4.6 The Final Results :   -2

To obtain optimal values for pressure in the pipes and at the junction with a maximum value equal to (931 KPa) , and a small value equal to (521 KPa), these values are within the permissible values (450-1030) KPa.

Table (10) : final pressure of some of junction.

Pressure (kPa)	Hydraulic Grade (m)	Demand (m³/day)	Elevation (m)	Label
931	653.08	369	558	J-292
914	651.36	80	558	J-287

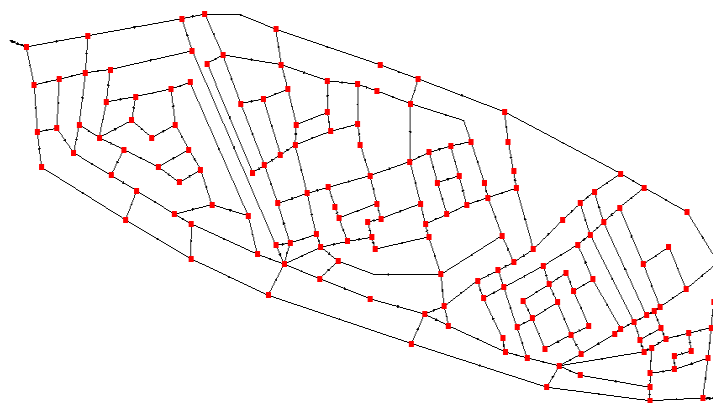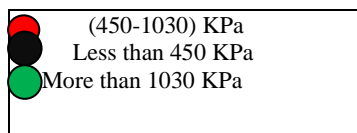| 914	653.35	129	560	J-298
908	652.73	173	560	J-289
906	658.55	200	566	J-26
905	653.47	120	561	J-300
895	651.5	185	560	J-290
889	651.8	173	561	J-288
885	656.44	366	566	J-54
882	649.16	475	559	J-304
882	656.14	100	566	J-29
880	652.94	420	563	J-49
879	658.86	148	569	J-25
878	649.75	230	560	J-35
878	655.68	244	566	J-28
877	659.65	120	570	J-24

Figure (4): pressure of junction

In addition to the use of two pumps in each reservoir, each pump with a flow of 20,000 cubic meters and a 35 meter head.

Table (10) : Final Pump information , Flow & Head .

	Flow (m³/day)	Head (m)
Shutoff	**0**	**46.67**
Design	**20,000**	**35.00**
Max. Operating	**40,000**	**0.00**

The velocities have obtained good values in most of the network, but in some pipes the speeds of ideal values have not reached due to several factors, including the large number of pipes and the different heights within the network.

The velocities calibration process may affect compression values if ideal values are to be obtained across the entire network.

Table (11) : final flow and velocity of some of pipes

Velocity (ft/s)	Flow (m³/day)	Diameter (in)	Length (m)	Label
10.39	19958	12	3	P-562
9.78	2088	4	27	P-421
9.74	-2079	4	8	P-501
9.72	4668	6	113	P-558
9.67	-8260	8	32	P-381
9.44	-8064	8	10	P-524
9.35	-499	2	41	P-321
9.07	4359	6	28	P-132
8.96	7652	8	29	P-331
8.79	-4222	6	35	P-372
8.73	-466	2	31	P-114
8.61	-460	2	28	P-396
8.55	-1826	4	17	P-229
8.3	-3985	6	13	P-506
8.27	-442	2	64	P-553
8.13	3907	6	101	P-514
8.12	3902	6	39	P-420
8.11	-1731	4	56	P-559
7.92	423	2	14	P-183
7.87	-3781	6	40	P-512
7.72	3711	6	19	P-505
7.65	3674	6	43	P-42
7.64	19994	12	6	P-551

Figure (5): velocity of pipe

.

12 in ⬤ 8 in ⬤ in ⬤ in ⬤ ⬤
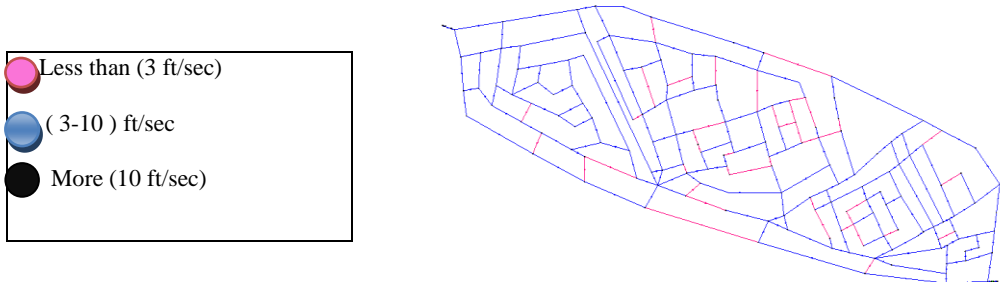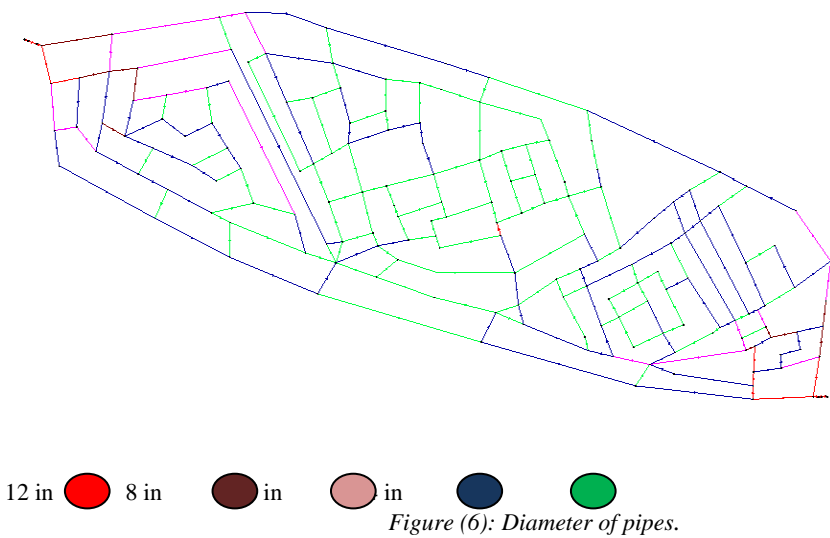
Figure (6): Diameter of pipes.

REFERENCES

[1]. EPANET Methodology, (1999). Water Supply and Water Resources. Division of the U.S. Environmental Protection Agency's National Risk Management Research Laboratory.

[2]. Cullinane, M.J., Lansey, K.E. and Mays, L.W., (1992). "Optimization Availability-based Design of Water Distribution Networks." ASCE J. Hydraulic Eng., Vol.118, No. 3, pp. 420-441.

[3]. Rossman, L., (2000). EPANET User's Manual. Risk Reduction Engineering Laboratory, U.S. Environmental Protection Agency, Cincinnati, Ohio

[4]. J. Van Zyl, and Y. Chang, (2010). " Programming styles for an open source EPANET Project". Water Distribution Systems Analysis, pp. 29-36.

[5]. "MIDDLE EAST :: JORDAN", www.cia.gov,2-4-2018 ،Retrieved 11-4-2018.

[6]. "World Population Prospects - Population Division - United Nations".

[7]. "Water and Wastewater Technology, 6th edition, Hammer and Hammer, Jr, Prentice-Hall, Inc., 2007 "

[8]. "Fundamentals of Hydraulic Engineering Systems-4 ed-R. Houghtalen"

[9]. " INMA Kingdom training and development center"

[10].Google earth program

[11]. Grater Irbid municipality

[12]. German Intentional Cooperation (GIZ) --- www.mwi.gov.jo .

The Affection of Concrete Recycling Technology and Achieving Sustainability in Construction

Lamis Abdelkader[1]

Abstract

Because of the global impacts of environmental issues, there is a general orientation for sustainable development to overcome these issues in all sectors around the world. It is common knowledge that construction is not environmentally friendly, so the recycling of building waste is very effective in improving this problem and it offers many advantages:

  Reduced demand for new resources.
  Reduction of associated transport and production expenses.
  Reducing the area of landfills.

The waste resulting from the construction and demolition processes represents 10 to 15 percent of the total waste in the developed countries. [1], Waste from construction and demolition includes concrete, bricks, wood, glass, insulating materials, ceilings, wires, pipes, gravel and dust. Concrete is the most common waste and constitutes about 50 percent of the total waste [2]. In this research the possibility of recycling the concrete will be explored.

Keywords: Concrete, Recycling concrete, Recycling Technology, Construction Sustainability, Environmental Friendly.

1. RECYCLING CONCRETE

EFFECT OF PHYSICAL RECYCLING OF CONCRETE:

Construction waste is disposed of in landfills, and new quarry products are procured and supplied to the site for new concrete production. Energy is used to dispose of these wastes and produce new materials for construction. By recycling, construction waste can be used to produce new concrete, thus reducing the waste of more natural resources, as well as the cost and energy needed to transport materials.

The profitability and cost-effectiveness of the concrete recycling process can be determined by the following key variables:

The price of new rickham and the extent of its proximity, which affects the cost of transportation.
Prices of recycled aggregates and proximity.
Quality of construction, demolition waste, and level of pollution.
Government incentives related to procurement.

---

[1] *Corresponding author: Assistant Professor, Yarmouk University, Department of Architecture Engineering, Jordan. Beni-Suef University , Faculty of Industrial Education, Egypt, lamisabdelkader@hotmail.com*

Costs associated with waste disposal in **.a** landfills (taxes, transport, shipping and unloading).Demand for recycled concrete products, which rely largely on public opinion for recycled aggregates.Residues of industrial construction are not contaminated with other types of waste during the process of sorting, and there is no need for decontamination.Industrial waste should preferably be placed close to concrete treatment sites, thus reducing transport costs.

Reusing concrete can a good way to reduce construction costs while providing some benefits to the environment. [10]

There are many examples of achieving a high saving ratio through the implementation of concrete recycling. Some are mentioned below:

In the United States, many states have achieved savings of up to 60 percent through the use of recycled aggregates rather than new aggregates in public construction projects. [4] Forty-one million tons of concrete are recycled annually in the United States [3]. It is currently being used in concrete and asphalt products with better performance compared to new aggregates. Recycled aggregates are less in material, time and gross cost of the project and less weight per unit by 10 to 15% compared to new quarries.In Queensland, Australia, and annual costs have fallen by 85 percent when used for recycled aggregates instead of the new rubble, dueto the cancellation of landfill fees, abstraction and detonation, lower associated costs and lower costs [2].In Europe, recycled concrete rubble can be sold at 3 to 12 euro per ton and at a production cost of 2.5 to 10 euro per ton. The highest selling price is obtained at sites where all construction and construction waste has been recycled and maximized. This can be easily achieved with industrial waste.When it comes to least developed countries, a study was conducted in Thailand showing that the use of 100 percent of the rubble of concrete waste can lead to the production of hollow concrete blocks with good properties. Thus, the cost per concrete block is reduced to 70 percent compared to the normal price of the concrete block on the Thai market [5]

Concrete Rubble:**Concrete Recycling Process:**

Concrete recycling processes vary depending on the sources of recycled aggregates. If the concrete source is demolished, the necessary processes are to sort the material according to their type. But if the source is industrial waste, there is no need for sorting.

The concrete aggregates collected from the demolition sites are subjected to crushing, crushing and sifting. These systems start with the first jaw process, for the large aggregates of aggregates of different directions, to the size of the aggregates from 800 to 1200 mm. Followed by primary and secondary cutters, and determine their use or non- dependence on the final product required. . Rubbing heads are needed if the dirt and foreign parts should be removed. We also find that the screens of the fine surface remove the fine materials from the rough rubble. And then if some of the dirt, mud, wood, plastics and organic materials are applied additional processes. This is done by floating in water, picking by hand, separating air, and using electromagnetic separators. With control and quality inspection, materials can be produced without the need for washing, as with new aggregates, which may be mixed with clay and silt [7].

Recycled aggregates are smaller in size and usually range in size from 0-12 mm and are usually used in construction activities, such as the construction of interlocking concrete blocks, replacement of substrates such as base gravel, etc. For the production of specific elements, recycled aggregates are mixed with quantities Suitable for cement, water, and sometimes other additions. The most common treatment period is 28 days.
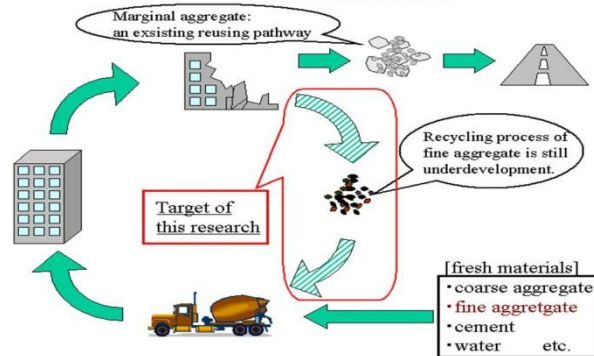
Material for building new oceanic reef habitats: Large pieces of concrete carefully positioned offshore can form the foundation ~~for new to build a new reef [10]~~

The MILL TRACK M 5000 is a compact crusher with a hammer and a slot of mm.450x 300 powered by Isuzu diesel engine (21.5 kW). It features a mill with swing hammers, a portable conveyor belt and a feeder that has been built into a large box for loading. . The Mill Track MT 5000 can handle aggregates and concrete (except reinforcing steel), marble, gypsum, glass and others, and convert waste into good reusable materials. MILL TRACK M 5000 is controlled remotely. Through the screens available. This crusher can produce gravel from recycled concrete and construction debris in sizes ranging from 10-30mm, allowing the use of aggregates in various applications.

Developed countries strongly support mobile crushers, due to the possibility of crushing waste on site, thereby avoiding transport to recycling sites. The right size of the TRACK MIL 5000 make it the perfect choice to be used directly at the site to handle the components of aggregates and stones from construction residues. Ideally, the contractor will have an effective waste management system resulting from the demolition and construction process that will reduce the complexity of the operation. Through intelligent planning some construction waste can already be used in situ as packing materials. In addition, we find that the treatment of debris in the site facilitates the process of transport.

Concrete Mixer Trucks Working:
Technical possibilities for recycling of concrete:

There are many successful experiments in the use of aggregates in the production of component elements of concrete. Good compressive strength is achieved with different types of recycled aggregates, *at different rates. Here are some of them.*

In Lebanon, P. succeeded. Matar and R. El Dalati in obtaining Hollow blocks containing a certain proportion of recycled aggregates, which was compressive strength higher than the masses of natural aggregates. The recycled aggregate was obtained by crushing the debris of the structural concrete, ranging in size from 6-12 mm. The compressive strength of the concrete blocks produced from the aggregates was higher than 7 to 38 percent, depending on the rate of the added components (recycled aggregates, water, cement, and superior cities). In Belgium, concrete blocks with a high proportion of recycled aggregates were produced under the trade name RecyMblock. Thus, a total mass containing 95% recycled aggregate was presented. While the hollow mass contained 75% recycled materials and no damage was detected after 14 cycles of freeze and melting test. However, further tests are needed to ascertain the suitability of this concrete block to meet construction or external work in case of continuous contact with water. In Japan, the concrete consists of 30% of the weight of recycled rubble instead of the natural aggregate, as it has the same compressive strength compared to the similar materials as it has the same (the dose of cement, W / C and its initial efficiency), which was achieved only with the natural debris. The recycled aggregate of the returned concrete (used concrete from the factory in the concrete truck as the excess material) was provided. The design of a new concrete mix included the replacement of the rough natural aggregates with the new aggregates (replacement by 30%) and the replacement of fine aggregates with smelting smelting Copper (replacement by 36 percent). The total diameter had a maximum of 25 mm. The water permeability, frost resistance and penetration resistance tests chlorine confirm that concrete made of new aggregates.

Equipment should have a powerful electromagnet or water flotation or an air separator system that can pull steel from concrete. [11]

In China, recycled concrete blocks have been produced by adding concrete blocks, ranging in size from 5-40mm. With different percentages of recycled aggregates added, and the pressure strength was higher than the concrete containing the natural aggregate alone. The highest compressive strength was reached when 70 percent of recycled aggregates were added. But when the rate of recycled rubella was 100 percent, the pressure strength was a little lower but still good.In Kuwait, al-Mutairi used an old concrete with a size of 0-19 mm to replace 50% and 100% of the rough aggregate required, and used saltwater instead of fresh water to obtain reasonable concrete strength. Recycled concrete treatment in seawater For 28 days. The results indicated that even with me using 100 percent of the total recycled concrete can achieve a design with a strong 35 Mp. The highest resistance is obtained when 25 percent of the sea water is mixed and 75 percent of the water is fertilized [9].

RESULTS

If recycled aggregates are provided in large quantities and high quality, this offers different opportunities in use and in the trade. There are some examples of such applications: paving applications, concrete elements and dirt walls (in the case of large parts), stone landscapes, paving, roadblocks, noise barriers, interstitial walls, road barriers, etc.There is still a widespread view that concrete containing recycled aggregates has less compressive strength than new concrete. However, there are many cases where recycled concrete has shown an equal or higher strength than the new one.There are also some benefits to recycling on natural aggregates. Recycled aggregates contain better thermal insulation properties and concrete insulation capacity proportional to the proportion of recycled aggregate [10]. Where recycled rubble often has better compression properties and is the preferred material for applications such as road base and layer under foundation [4]. Less cement can also be used in layers under the foundation. Another benefit is the low weight of the unit of recycled aggregates which makes dealing with it cheaper.The recycling of concrete is particularly interesting for oil-rich countries, as these countries usually have a decline in the prices of diesel and crackers usually work with diesel.

Recommendations.

Recycling of demolition and construction waste has tangible and measurable benefits. In the GCC region there are two factors that increase the possibility of recycling. First factor costs are very low, reducing the cost of energy-intensive processes such as stone cracking. Second, because of the scarcity of water and the ability to use seawater in the treatment process, it reduces costs and even more. This is achieved in particular and from an economic point of view not only savings to the concrete manufacturer but also to society by reducing the use of subsidized goods.

REFERENCES

[1]. United Nations Environment Program: Waste – Investing in energy and resource efficiency, 2011 Tam VWY.: Economic comparison of concrete recycling: A case study approach. Resources, Conservation and Recycling 2008; 52: p. 821–828
[2]. US EPA: WARM Version 12, Chapter Concrete, 2012
[3]. World Business Council for Sustainable Development: Recycling Concrete, 2009
[4]. Kaosol T.: Reuse Concrete Waste as Crushed Stone for Hollow Concrete Masonry Units, The 3rd Technology and Innovation for Sustainable Development International Conference, Faculty of Engineering, Khon Kaen University, Thailand, 4-6 March 2010
[5]. Matar P., El Dalati R.: Using recycled concrete aggregates in precast concrete hollow blocks, Mat.-wiss. u. Werkstofftech. 2012, 43, No. 5
[6]. Ganiron Jr TU.: Recycling Concrete Debris from Construction and Demolition Waste, International Journal of Advanced Science and Technology 2015, Vol.77, p.7-24
[7]. Ferrari G et al. New sustainable technology for recycling returned concrete. Constr Build Mater 2014, http://dx.doi.org/10.1016/j.conbuildmat.2014.01.008
[8]. Al-Mutairi N. and Haque M. N.: Strength and durability of concrete made with crushed concrete as coarse aggregates, Proceedings of the International Symposium on Recycling and Reuse of Waste Materials, p. 499–506, Scotland, UK, 2003.
[9]. Zhu L., Dai J., Bai G., Zhang F.: Study on thermal properties of recycled aggregate concrete and recycled concrete blocks, Construction and Building Materials 2015; Volume 94, p. 620–628.
[10]. https://www.thebalancesmb.com/recycling-concrete-how-and-where-to-reuse-old-concrete-844944
[11]. https://www.environmentalleader.com/2017/01/manufacturers-get-new-standard-for-recycling-concrete/

The Importance of Blowing Angle While Designing an Active Blowing System

Tugrul Oktay[1], Ozturk Ozdemir Kanat[2]

Abstract

In this study, it is studied to improve the vortex due to flow separation over the wing upper surface caused by pressure difference between the wing surfaces based on wing profile structure in the straight flight of an UAVs by using active blowing method. It is investigated to obtain the best efficiency from the compressed air blown into the flow. For this reason, the output angle of the air blown according to the flow is changed and the optimum blowing angle is decided. The position, area and pressure outlet magnitude of the air used for active blowing over the wing upper surface are kept constant. On the contrary, only the outlet angle of the compressed air is changed according to the top surface of the wing. The analyses are performed for the negative and positive different angles of attack of the UAVs. Thus, the effect of the blowing angle which is used as a variable on the performance has been tried to be evaluated. It is observed that the increase of the blowing angle causes a reverse flow on the wing after a certain size. In addition to this, this study shows that the change in the blowing angle alone does not cause much change in the performance of the UAVs, which has a low pressure outlet value.

Keywords: Blowing angle, active flow control

1. INTRODUCTION

The usage of unmanned aerial vehicles is increasing day by day. For example, defense industry, agricultural spraying, cargo transportation, film sets can be shown in many areas of our lives. In [1], more detailed applications of UAV can be found. Studies about unmanned aerial vehicles are examined and the literature is researched [2,3].

Flow separation occurs due to the pressure difference in the external flow over the aircraft' s wing lower and upper surfaces. Due to this flow separation, while the drag and noise increase, the lift force decrease. Therefore, direct flight performance is affected. In previous periods, to reduce or eliminate this negative impact, as aerodynamic design change, blowing or suction channels, vortex generators different methods have been tried [4]. Particularly on high-speed flights shock waves occur on the upper surface of the wing due to the interaction of the boundary layer and the outer flow area [5].

Flow control can be described as interfering with flow to increase the yield or performance of a fluid. Flow control has become an important research area in recent years [6]. The flow control, together with its aerodynamic effects, also provides positive contributions to aircraft control. Shmilovich and Vatsa [7] in their study as an example of the flow control applications, they stated that adequate control of the vertical stability of the aircraft, which is not running an engine, provides sufficient directional controllability. Xu and Zhou [8] conducted a study on the improvement of the longitudinal stability of aircraft using the synthetic jet flow control method. When previous studies about active flow control are examined, different techniques are used. Most of these are blowing or suction techniques for existing aircrafts. Again, the upper surface blowing method is a

---

[1] *Aeronautical Engineering, Faculty of Aeronautics and Astronautics, Erciyes University, Kayseri, 38039, Turkey.*
tugruloktay52@gmail.com

[2] *Corresponding author: PhD. Candidate, Department of Civil Aviation, Graduate School of Natural and Applied Sciences, Erciyes University, Kayseri, 38039, Turkey / Research Assistant, Department of Airframe and Powerplant Maintenance, School of Civil Aviation, Kastamonu University, Turkey, ozturkkanat@gmail.com*

flow control technique used to increase the landing and takeoff capabilities of the aircraft. By using this method, it is aimed to increase the landing and takeoff capabilities of the aircrafts for shorter runways [9]

In this study, blowing that is one of the active flow control methods, is used. In this method, compressed air is transferred to the upper surface of the wing by using an external air source. When previous studies about blowing are reviewed, it is observed that there is no study about blowing angle in the literature. Therefore, this conference paper is a first in this aspect.

2. NUMERICAL METHOD

Firstly, blowing areas are formed in order to decrease drag while increasing lift over the wing of the unmanned aerial vehicle. These blowing areas are located on the wing and are shown in Fig 1f. The location, diameter and size of the blowing areas are kept constant in this study. As a variable only the blowing angle is given. 3 different blowing angle values are used. These are:

- 0°
- 45°
- 90°

The numerical analysis of these 3 different angle of attack and parallel to external flow direction are obtained and the values of lift and drag coefficients are compared in the results section.

Ansys Fluent program was used to calculate numerically the external flow coefficients. For this purpose, firstly boundary region is created. In Fig 1a shows the boundary and the UAV. Once sufficient size boundary is designed, the interior of the boundary is divided into different sized control volumes. Hybrid control volumes method is used. Therefore, the aircraft surface is covered with inflation layers. The remaining interior of boundary is created by prism method. After making the necessary verifications, control volumes are obtained as in Figure 1 [10].

a   b
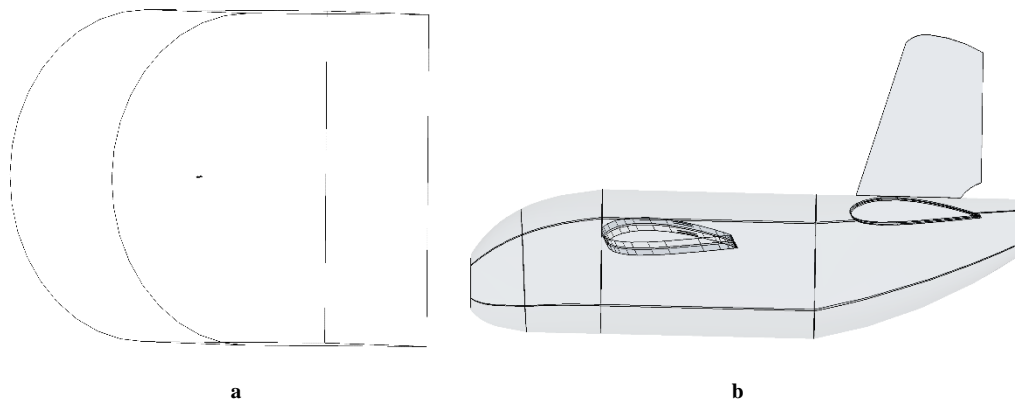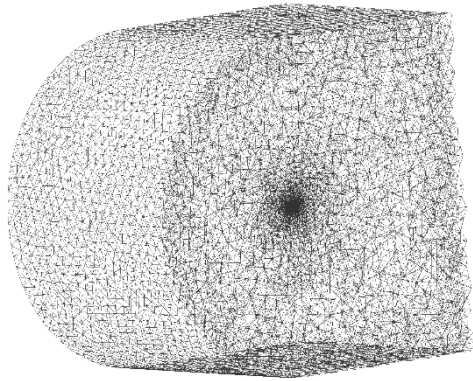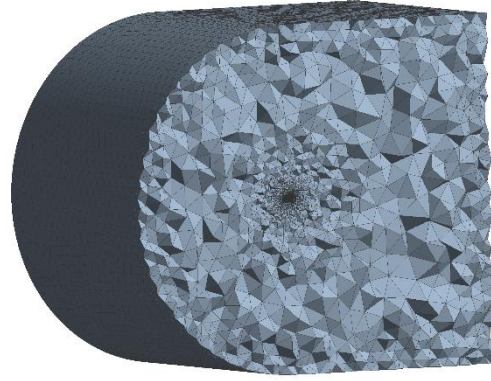
c   d

e   f

Figure 1. Control Volumes

Another step required for the solution is to calculate the solution with the right method and model. For this reason, it is used with co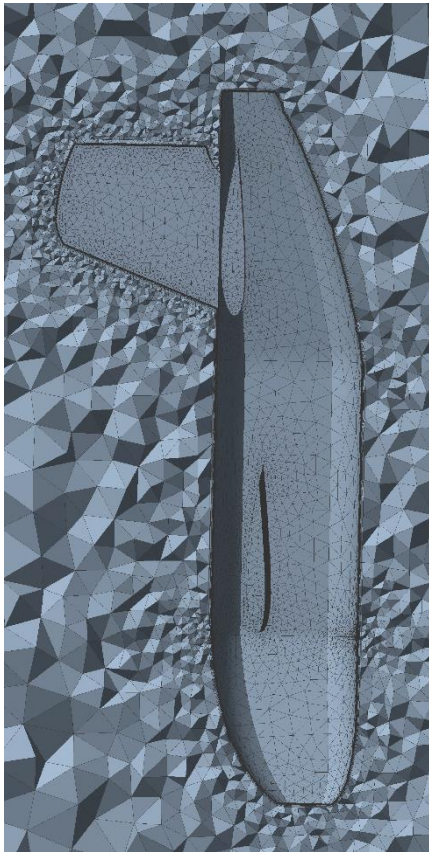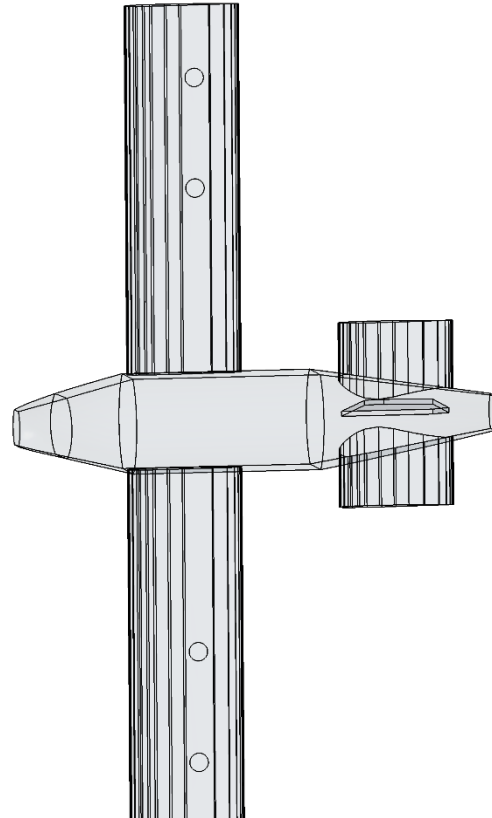upled method to obtain more accurate results using parallel processing. As the turbulence model kw-SST is also used [11].

RESULTS

The calculated values for the lift coefficient are shown in Figure 2. When the results are examined, it is seen that the change in blowing angle has little effect on the lift coefficient. This effect was limited to one ten-thousandth. 90º was analyzed as the highest blowing angle. This blowing angle is positioned perpendicular to the external flow. At higher blowing angles it is estimated that reverse flow may occur in the external flow.

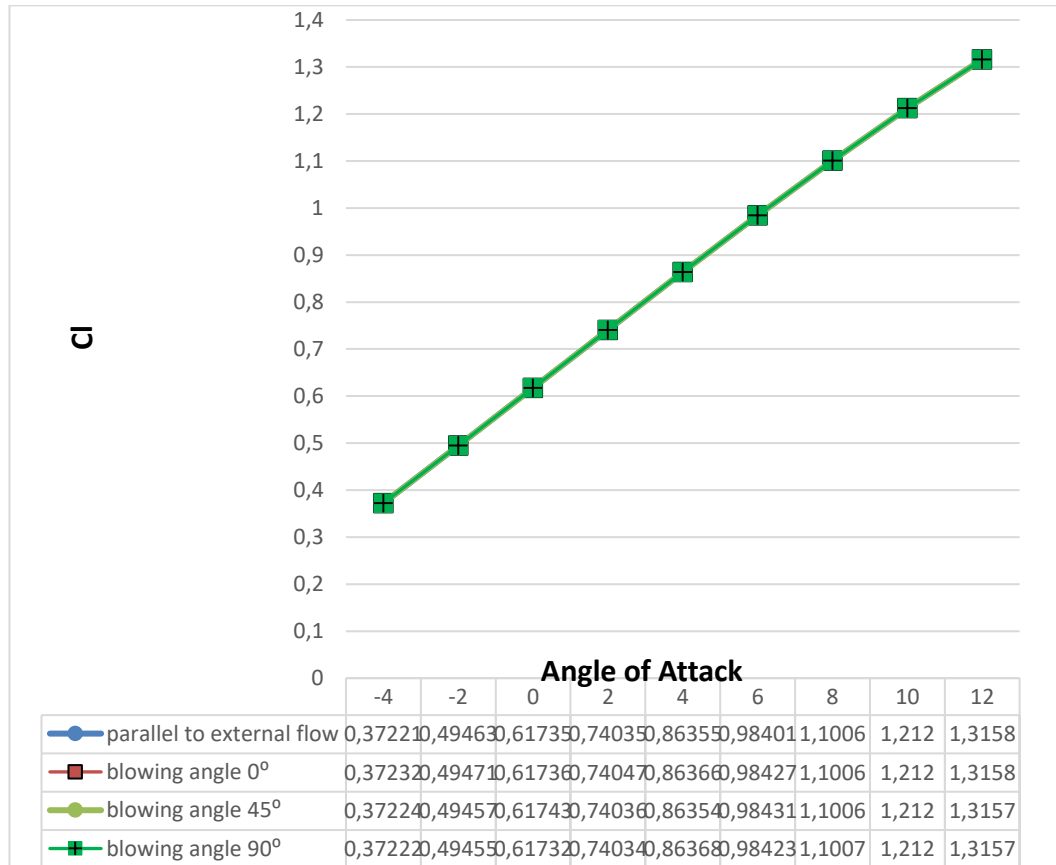|	-4	-2	0	2	4	6	8	10	12
parallel to external flow	0,37221	0,49463	0,61735	0,74035	0,86355	0,98401	1,1006	1,212	1,3158
blowing angle 0º	0,37232	0,49471	0,61736	0,74047	0,86366	0,98427	1,1006	1,212	1,3158
blowing angle 45º	0,37224	0,49457	0,61743	0,74036	0,86354	0,98431	1,1006	1,212	1,3157
blowing angle 90º	0,37222	0,49455	0,61732	0,74034	0,86368	0,98423	1,1007	1,212	1,3157

Figure 2. C_L coefficients

The calculated results for the drag coefficient are shown in Figure 3. It is observed that the changes in the blowing angle are not a big factor in the variation of drag coefficient as in the lift coefficient and the drag coefficient values are the same in some angles of attack. Moreover, it is seen that the changes are one ten-thousandth.

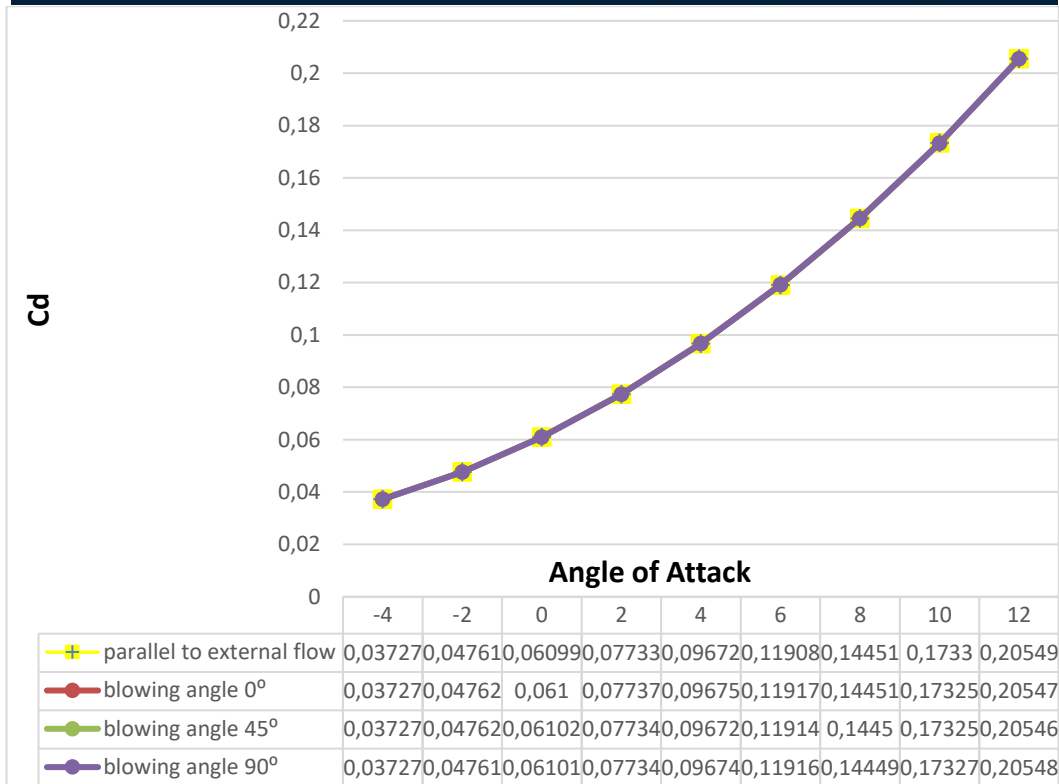|	-4	-2	0	2	4	6	8	10	12
parallel to external flow	0,03727	0,04761	0,06099	0,07733	0,09672	0,11908	0,14451	0,1733	0,20549
blowing angle 0°	0,03727	0,04762	0,061	0,07737	0,09675	0,11917	0,14451	0,17325	0,20547
blowing angle 45°	0,03727	0,04762	0,06102	0,07734	0,09672	0,11914	0,1445	0,17325	0,20546
blowing angle 90°	0,03727	0,04761	0,06101	0,07734	0,09674	0,11916	0,14449	0,17327	0,20548

Figure 3. C_D coefficients

Figure 4 shows the E_{max} values that represent the total performance. According to these results, the highest performance was obtained with 45° blowing angle. Accordingly, a performance improvement of 0.18 percent was calculated.
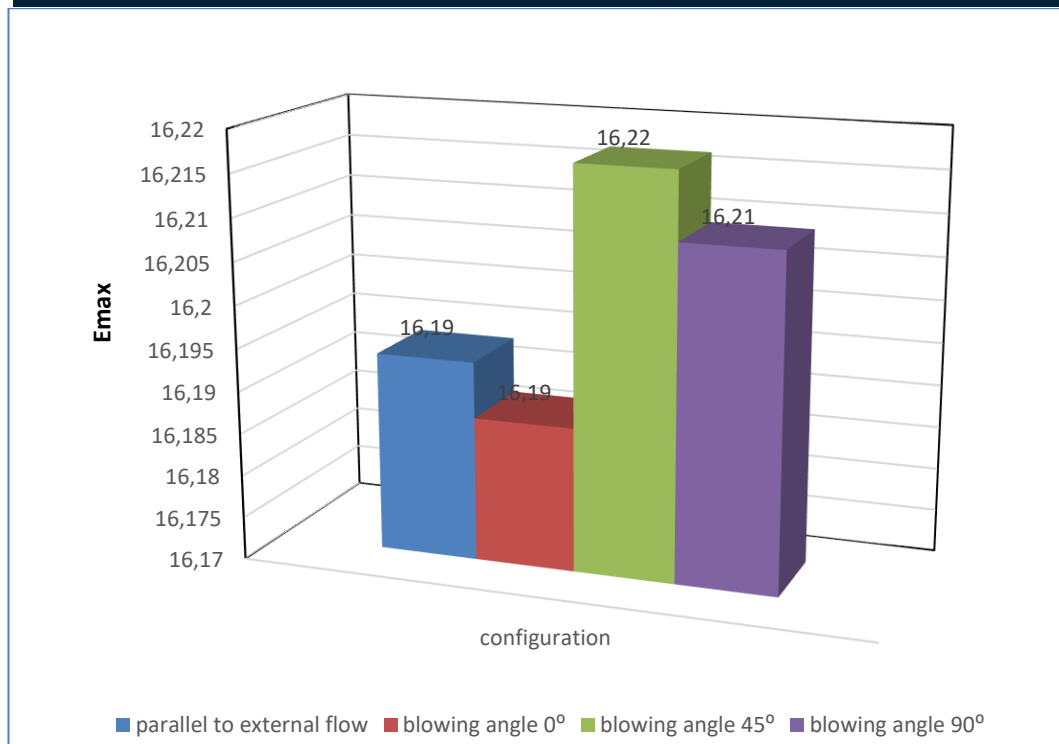
Figure 4. E_{max}

CONCLUSIONS

With this study, it is calculated that a change in the blowing angle has no significant effect on the aircraft lift and drag coefficients. Therefore, the effect on total performance is limited. In subsequent studies, a common evaluation of studies with other variables, such as the location, blowing angle and blowing size, will make a significant contribution to the literature.

ACKNOWLEDGMENT

REFERENCES

[1]. R. Austin, ''*Unmanned Aircraft System*s,'' Wiley, 2010.

[2]. O. O. Kanat., E. Karatay, O. Kose and T. Oktay, ''Combined active flow and flight control systems design for morphing unmanned aerial vehicles'', *Proceedings of the Institution of Mechanical Engineers Part-G Journal of Aerospace Engineering*, vol. 233, pp. 1-20, May 2019.

[3]. T. Oktay, O. O. Kanat and A. Ceyhan, ''Improvement of wingtip vortices with active flow controller having several blowing points'', *8th International Advanced Technologies Symposium (IATS'17),* October 19-21, 2017, Elazig, Turkey.

[4]. H. Shan, L. Jiang, C. Liu, M. Love and B. Maines, ''Numerical study of passive and active flow separation control over a NACA0012 airfoil,'' *Computers and Fluid*s, vol. 37, pp. 975-992, 2008.

[5]. E. Stanewsky, ''Adaptive wing and flow control technology,'' *Progress in Aerospace Sciences*, vol. 37(7), pp. 583-667, 2001.

a. Yagiz, O. Kandil and Y. V. Pehlivanoglu, ''Drag minimization using active and passive flow control technique,'' *Aerospace Science and Technology*, vol. 17, pp. 21-31, 2012.

b. Schmilovich and V. N. Vatsa, ''Practical computational methods for airplanes with flow-control systems,'' *American Institute of Aeronautics and Astronautics,* vol. 57(5), pp. 35-52, 2019.

[6]. X. Xu and Z. Zhou, ''Study on longitudinal stability improvement of flying wing aircraft based on synthetic jet flow control,'' *Aerospace Science and Technology*, vol. 46, pp. 287-298, 2015.

[7]. Y. Yadlin and A. Schmilovich, ''Lift enhancement for upper surface blowing airplanes,'' *31*[st] *American Institute of Aeronautics and Astronautics Applied Aerodynamics Conference,* 2013.

[8]. O. O. Kanat, D. S. Korpe and A. O. Kurban, ''Yatay Kuyruklarda Kivrik Kanat Ucu Kullaniminin Aerodinamik Etkileri,'' *Journal of Aviation*, vol. 1(2), pp. 87-98, 2017.

[9]. Ansys Fluent Theory Guide 2013.

The Aerodynamic Effects of Pressure Magnitude and Blowing Angle on Lateral Autonomous Performance of UAVs

Tugrul Oktay[1], Ozturk Ozdemir Kanat[2]

Abstract

In this study, the effects on the lateral flight control system of the UAVs are investigated by improving using active flow control technique the vortex occurring on the upper surface of the UAVs' wing during the straight flight. Blowing which is one of the flow control methods for an aircraft is preferred for this study. In order to obtain the best blowing data, carrying out numerical analysis of different angles of attack the effects of blowing angle and different pressure magnitude on the aerodynamic performance of the UAV are evaluated. In order to evaluate the aerodynamic performance, changes in the lift and drag coefficient values on the aircraft were considered. Lateral flight performance of UAVs is analyzed with MATLAB/Simulink program according to the pressure and blowing angle values at which aerodynamic performance is highest. As a result, it has been observed that there are significant improvements in UAV's lateral autonomous flight performance compared to the initial values.

Keywords: Blowing angle, blowing magnitude, AFC, lateral autonomous control

1. INTRODUCTION

The use of unmanned aerial vehicles is increasing day by day in many fields such as civil, military, commercial, agricultural. The main reason for this situation is that the usage, production and operating costs are much lower compared to manned aircraft. For many other UAV applications [1] can be visited. The purpose of this numerical study, previously an UAV the name of ZANKA-IIB was produced at Erciyes University, Faculty of Aeronautics and Astronautics, Model Aircraft Laboratory, to improve flight performance the UAV by using active flow control system (AFC).

The ability of an aircraft to maintain or protect its balance position is known as stability. Controllability is known as the effect created by the pilot or by the control systems on the balance. Automatic control for aircrafts is to ensure that any desired flight parameters can be kept at that value without human impact. In this direction, feedback automatic control systems are used. Controllers in feedback automatic control systems are especially converters used to improve system dynamics [2]. The PID-based hierarchical autopilot system is designed simultaneously with the active flow control method in order to improve lateral performance and compressed air outlet channels at the same points on the wing. P, I, D parameters in order to minimize a cost function consisting of performance parameters, i.e. maximum overshoot, rise time and settling time during trajectory tracking.

Computational flow dynamics (CFD) is a branch of fluid mechanics, where problems with fluid behavior are fundamentally solved and analyzed on the computer by numerical methods and algorithms. The use of computational fluid dynamics by the aerospace industry is a result of cost reduction. Nowadays, the design process of an aircraft consists of 3 phases: conceptual, preliminary and detailed design. Preliminary design phase is also included computational simulations. In this way, the cost of the design can be calculated optimally

[1] *Aeronautical Engineering, Faculty of Aeronautics and Astronautics, Erciyes University, Kayseri, 38039, Turkey. tugruloktay52@gmail.com*

[2] *Corresponding author: PhD. Candidate, Department of Civil Aviation, Graduate School of Natural and Applied Sciences, Erciyes University, Kayseri, 38039, Turkey / Research Assistant, Department of Airframe and Powerplant Maintenance, School of Civil Aviation, Kastamonu University, Turkey, ozturkkanat@gmail.com*

before going into production. ANSYS Fluent, a famous CFD software, is used for this numerical study. It is based upon finite volume method approach [3].

Especially for aircrafts, flow control is carried out in two ways. These are active flow control and passive flow control. Passive control can usually be explained as aerodynamic improvements made on the aircraft design. Today, the best examples of these are curved wing tips (i.e. winglets, sharklets, split scimitar winglets) can be shown. Their most obvious characteristics compared to active flow control systems are that they are not variable due to their constant construction during the all flight [4]. For this reason, they provide a positive contribution at some stages of the flight and cause a negative effect at other times. 45% to 35% of the drag forces occurring of carrying passenger for commercial purposes aircraft on the straight flights are respectively skin friction and induced drag. For longer straight flight time, the smaller improvements that can be made in these types of drag will lead to large gains in cost. The development of flow control systems has become a necessity since a laminar flow zone cannot be created over the aircraft. Using various flow control systems on aircraft, it is aimed to weaken the vortex due to reducing the drag. Wygnanski [5] conducted a review of flow control applications. One of the flow control methods is blowing. With this method, it is tried to reduce the distortion in the flow by transferring compressed air to the point where the distortion in the flow occurred.

In order to increase the aerodynamic performance of ZANKA-IIB with this numerical study, blowing points are designed over the wing. Two variables are determined for blowing points. These variables are magnitude of blowing pressure and blowing angle. Numerical analysis is performed according to these variables and as a result, the changes in lateral autonomous performance of the UAVs according to the best aerodynamic performance value are calculated.

2. ANALYSIS MODEL

The most important difference of the blowing method used in this study is the simultaneous designing of the change in pressure magnitude with blowing angle. For this purpose, a total of 4 blowing zones are designed, two of which are on the upper surface of each wing of our unmanned aerial. The top view of our unmanned aerial vehicle is as in Figure 1. In addition to this, Figure 1 also shows circular blowing zones on the upper surfaces of the wings.
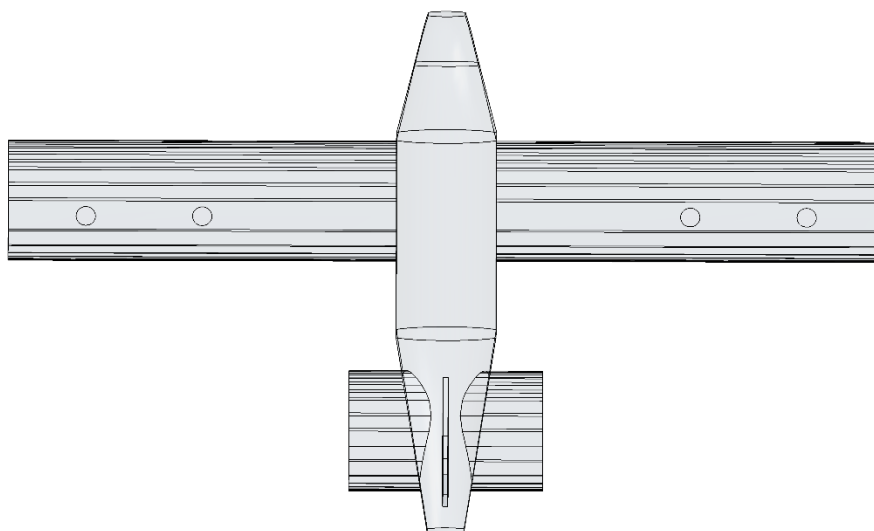
Figure 1. Top view of the UAVs

[6] and [7] can be given as an example of researches to improve the performance of aircraft using active blowing method. A total of 240 hours computerized numerical analysis is studied for 10 different attack angles (-6, -4, -2, 0, 2, 4, 6, 8,10, 12), 3 different blowing angle (0º, 45º, 90º) and 3 different pressure magnitude (10000 P, 25000 P, 50000 P). Ansys Fluent program is used for numerical analysis. After the sufficiently large boundary is created, the control volumes are created using the cells in Table 1 [8-9].

Table 27. Detail of Cells

Property	Sizing
Minimum Element Size	0.005 m
Proximity Minimum Size	0.005 m
Maximum Size	1.6 m
Maximum Face Size	3.20 m
Growth Rate	1.20
Curvature Normal Angle	18º
Mesh Method	Hybrid (Prism-inflation)

Figure 2 shows the used control volumes.

(a)

(b)

(c)

(d)

(e)   (f)
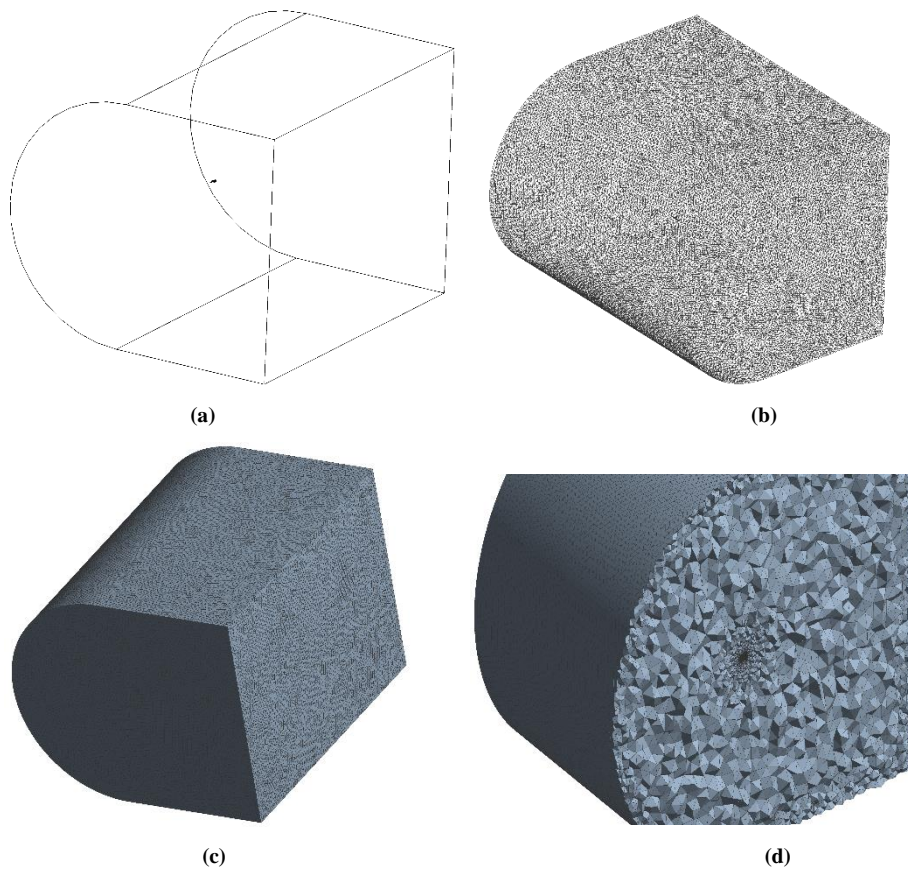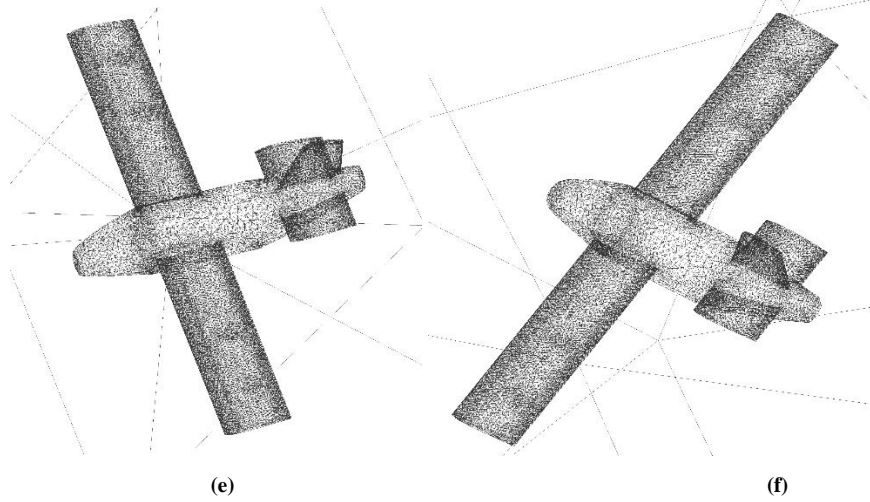
Figure 2. Control volumes

After obtaining control volumes, numerical analyzes are calculated according to different blowing angle and different pressure magnitudes. To calculate the solution kw-SST turbulence model is also used [10-11]. These analyzes are carried out according to the analysis flow chart in Figure 3. The using configuration names are B_1, B_2, B_3, B_4, B_5, B_6, B_7, B_8, B_9, B_{10}, B_{11}, B_{12}
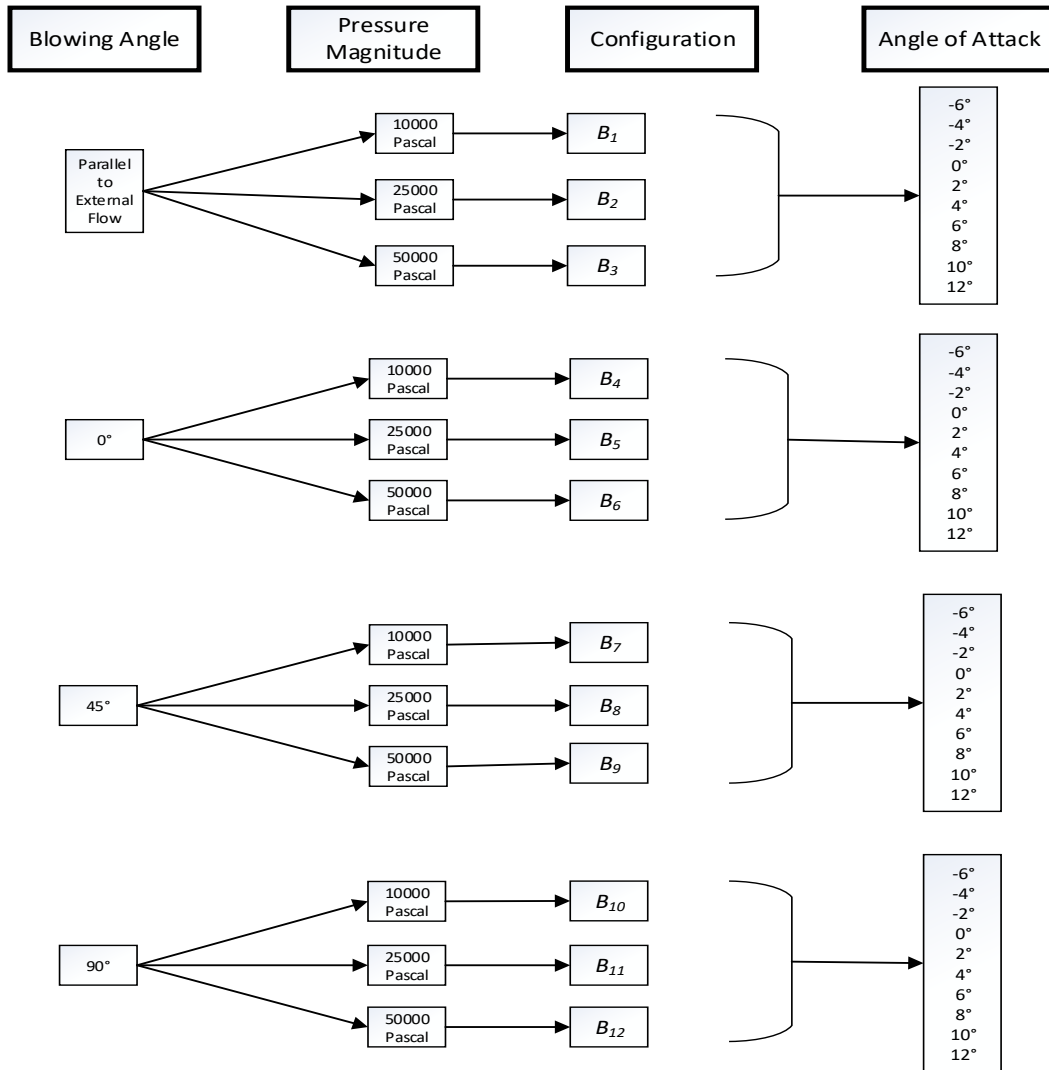
Figure 3. Analysis flow chart

The effect of blowing on total performance is calculated according to the drag and lift coefficient data obtained as a result of the analysis. For this purpose, equation 1 is used. This equation is known as E_{max} (refers to maximum lift / drag). The lateral autonomous flight performance of the aircraft is calculated according to the highest E_{max} value which is calculated using equation 1 [12].

$$E_{max} = \frac{1}{2\sqrt{K \times C_{D_0}}} \qquad\qquad 1$$

SIMULATION MODEL

When the longitudinal and lateral motion dynamics of the constant wing aircrafts are observed, the relationships with each other are negligible. In addition to this, the effect of aircraft dynamics in the vertical axis motion is ignored. In brief, lateral and longitudinal movement can be examined independently of each other. According to this information, only lateral movement is examined in the control part of this study. In equation 2, a lateral state space model is given [13].

$$\begin{bmatrix} \Delta\dot\beta \\ \Delta\dot p \\ \Delta\dot r \\ \Delta\dot\phi \\ \Delta\dot\psi \end{bmatrix} = \overbrace{\begin{bmatrix} \dfrac{Y_\beta}{u_0} & \dfrac{Y_p}{u_0} & -\left(1-\dfrac{Y_r}{u_0}\right) & -\dfrac{g}{u_0}\cos(\theta_0) & 0 \\[2mm] L_\beta^*+\dfrac{I_{xz}}{I_{xx}}N_\beta^* & L_p^*+\dfrac{I_{xz}}{I_{xx}}N_p^* & L_r^*+\dfrac{I_{xz}}{I_{xx}}N_r^* & 0 & 0 \\[2mm] N_v^*+\dfrac{I_{xz}}{I_z}L_v^* & N_p^*+\dfrac{I_{xz}}{I_z}L_p^* & N_r^*+\dfrac{I_{xz}}{I_z}L_r^* & 0 & 0 \\[2mm] 0 & 1 & 0 & 0 & 0 \\[1mm] 0 & 0 & \sec(\theta_0) & 0 & 0 \end{bmatrix}}^{A_{la}} \begin{bmatrix} \Delta\beta \\ \Delta p \\ \Delta r \\ \Delta\phi \\ \Delta\psi \end{bmatrix} + \overbrace{\begin{bmatrix} 0 & \dfrac{Y_{\delta_r}}{u_0} \\[2mm] L_{\delta_a}^*+\dfrac{I_{xz}}{I_{xx}}N_{\delta_a}^* & L_{\delta_r}^*+\dfrac{I_{xz}}{I_x}N_{\delta_r}^* \\[2mm] N_{\delta_a}^*+\dfrac{I_{xz}}{I_z}L_{\delta_a}^* & N_{\delta_r}^*+\dfrac{I_{xz}}{I_z}L_{\delta_r}^* \\[1mm] 0 & 0 \\ 0 & 0 \end{bmatrix}}^{B_{la}} \begin{bmatrix} \Delta\delta_a \\ \Delta\delta_r \end{bmatrix} \qquad (2)$$

The lateral state space model, which is exposed to a wind and when the turbulence is added, is given in equation 3. The turbulence model in here is the Von-Karman model [14].

$$\begin{bmatrix} \Delta\dot\beta \\ \Delta\dot p \\ \Delta\dot r \\ \Delta\dot\phi \end{bmatrix} = \overbrace{\begin{bmatrix} \dfrac{Y_\beta}{u_0} & \dfrac{Y_p}{u_0} & -\left(1-\dfrac{Y_r}{u_0}\right) & -\dfrac{g}{u_0}\cos(\theta_0) \\[2mm] L_\beta^*+\dfrac{I_{xz}}{I_{xx}}N_\beta^* & L_p^*+\dfrac{I_{xz}}{I_{xx}}N_p^* & L_r^*+\dfrac{I_{xz}}{I_{xx}}N_r^* & 0 \\[2mm] N_v^*+\dfrac{I_{xz}}{I_z}L_v^* & N_p^*+\dfrac{I_{xz}}{I_z}L_p^* & N_r^*+\dfrac{I_{xz}}{I_z}L_r^* & 0 \\[1mm] 0 & 1 & 0 & 0 \end{bmatrix}}^{A_{la}} \begin{bmatrix} \Delta\beta \\ \Delta p \\ \Delta r \\ \Delta\phi \end{bmatrix} + \overbrace{\begin{bmatrix} 0 & \dfrac{Y_{\delta_r}}{u_0} \\[2mm] L_{\delta_a}^*+\dfrac{I_{xz}}{I_{xx}}N_{\delta_a}^* & L_{\delta_r}^*+\dfrac{I_{xz}}{I_x}N_{\delta_r}^* \\[2mm] N_{\delta_a}^*+\dfrac{I_{xz}}{I_z}L_{\delta_a}^* & N_{\delta_r}^*+\dfrac{I_{xz}}{I_z}L_{\delta_r}^* \\[1mm] 0 & 0 \end{bmatrix}}^{B_{la}} \begin{bmatrix} \Delta\delta_a \\ \Delta\delta_r \end{bmatrix} + \overbrace{\begin{bmatrix} \dfrac{Y_\beta}{u_0} & 0 & 0 \\[2mm] -L_\beta^*\dfrac{I_{xz}}{I_{xx}}N_\beta^* & -L_p^*\dfrac{I_{xz}}{I_{xx}}N_p^* & -L_r^*\dfrac{I_{xz}}{I_{xx}}N_r^* \\[2mm] -N_v^*\dfrac{I_{xz}}{I_z}L_v^* & -N_p^*\dfrac{I_{xz}}{I_z}L_p^* & -N_r^*\dfrac{I_{xz}}{I_z}L_r^* \\[1mm] 0 & 0 & 0 \end{bmatrix}}^{B_{la_{gust}}} \begin{bmatrix} v_g/u_0 \\ p_g \\ r_g \end{bmatrix} \qquad (3)$$

One of the most important issues in the design of an automatic control system is the effect of the control system on the stability of the aircraft. In automatic control systems with feedback, PID controllers take error signals and try to reach the desired setting level. Nowadays PID (Proportional-Integral-Derivative), it is a commonly used control method. In our study, 3-layer PID controller is used. These layers are outer loop, middle loop and inner loop. In Figure 4, using PID-based auto pilot system is shown.
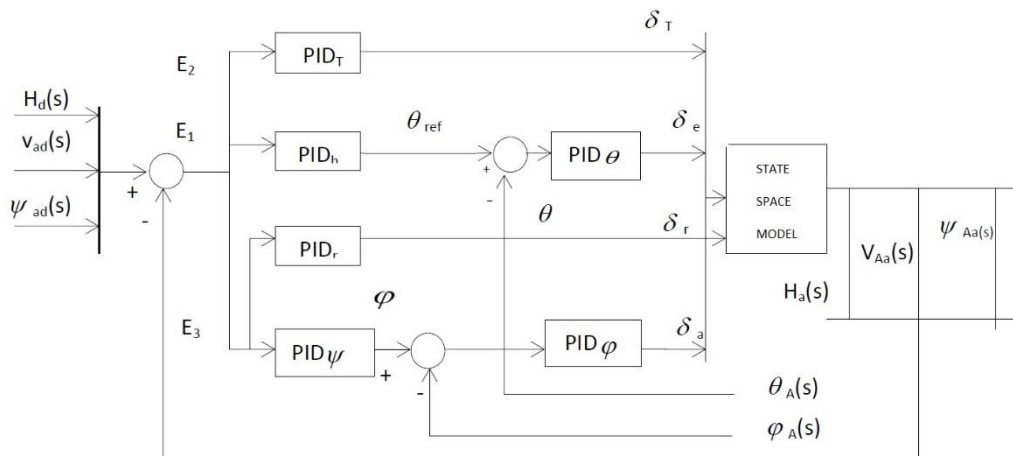
Figure 4. PID Based Autopilot Structure

Due to the high number of variables used for both autopilot and flow control, it is necessary to use an optimization method. For this reason, SPSA (Simultaneous Perturbation Stochastic Approximation) method, which is considered to be more effective, is used. More information about this method is given in previous studies [15, 16].

RESULTS

Lift coefficients obtained as a result of the calculation are given in Figure 5. According to these values, changes in some blowing angle and pressure values are positively reflected on the lift. This positive effect seems to be limited.
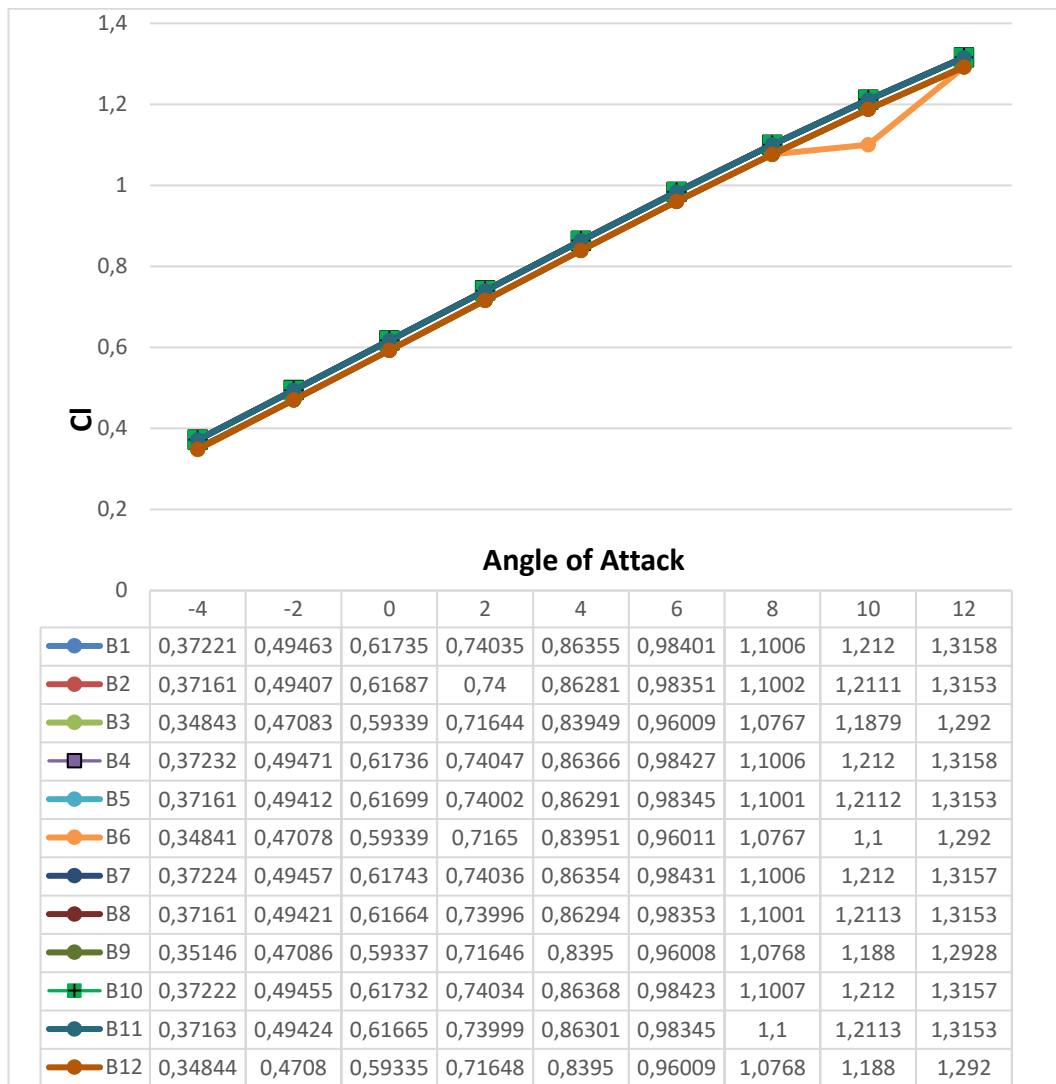
Angle of Attack	-4	-2	0	2	4	6	8	10	12
B1	0,37221	0,49463	0,61735	0,74035	0,86355	0,98401	1,1006	1,212	1,3158
B2	0,37161	0,49407	0,61687	0,74	0,86281	0,98351	1,1002	1,2111	1,3153
B3	0,34843	0,47083	0,59339	0,71644	0,83949	0,96009	1,0767	1,1879	1,292
B4	0,37232	0,49471	0,61736	0,74047	0,86366	0,98427	1,1006	1,212	1,3158
B5	0,37161	0,49412	0,61699	0,74002	0,86291	0,98345	1,1001	1,2112	1,3153
B6	0,34841	0,47078	0,59339	0,7165	0,83951	0,96011	1,0767	1,1	1,292
B7	0,37224	0,49457	0,61743	0,74036	0,86354	0,98431	1,1006	1,212	1,3157
B8	0,37161	0,49421	0,61664	0,73996	0,86294	0,98353	1,1001	1,2113	1,3153
B9	0,35146	0,47086	0,59337	0,71646	0,8395	0,96008	1,0768	1,188	1,2928
B10	0,37222	0,49455	0,61732	0,74034	0,86368	0,98423	1,1007	1,212	1,3157
B11	0,37163	0,49424	0,61665	0,73999	0,86301	0,98345	1,1	1,2113	1,3153
B12	0,34844	0,4708	0,59335	0,71648	0,8395	0,96009	1,0768	1,188	1,292

Figure 5. C_l coefficient

In Figure 6, the variation of the drag coefficients with used the configurations are given. When the figure is examined in detail, it is understood that the difference between the configurations at low angles of attack is very small. On the contrary, as the angle of attack increases, negative disintegrations are more pronounced.
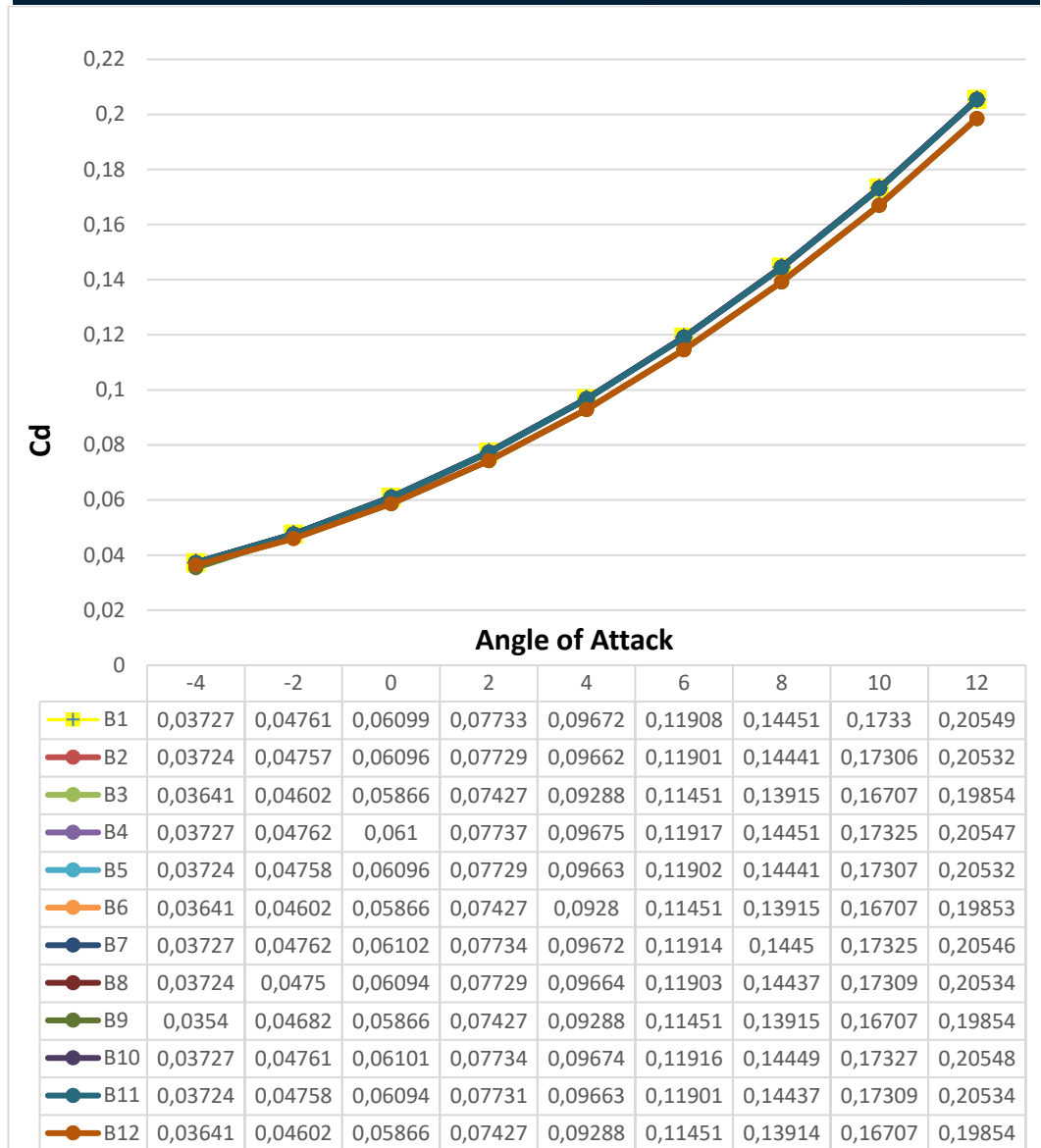
		-4	-2	0	2	4	6	8	10	12
+	B1	0,03727	0,04761	0,06099	0,07733	0,09672	0,11908	0,14451	0,1733	0,20549
	B2	0,03724	0,04757	0,06096	0,07729	0,09662	0,11901	0,14441	0,17306	0,20532
	B3	0,03641	0,04602	0,05866	0,07427	0,09288	0,11451	0,13915	0,16707	0,19854
	B4	0,03727	0,04762	0,061	0,07737	0,09675	0,11917	0,14451	0,17325	0,20547
	B5	0,03724	0,04758	0,06096	0,07729	0,09663	0,11902	0,14441	0,17307	0,20532
	B6	0,03641	0,04602	0,05866	0,07427	0,0928	0,11451	0,13915	0,16707	0,19853
	B7	0,03727	0,04762	0,06102	0,07734	0,09672	0,11914	0,1445	0,17325	0,20546
	B8	0,03724	0,0475	0,06094	0,07729	0,09664	0,11903	0,14437	0,17309	0,20534
	B9	0,0354	0,04682	0,05866	0,07427	0,09288	0,11451	0,13915	0,16707	0,19854
	B10	0,03727	0,04761	0,06101	0,07734	0,09674	0,11916	0,14449	0,17327	0,20548
	B11	0,03724	0,04758	0,06094	0,07731	0,09663	0,11901	0,14437	0,17309	0,20534
	B12	0,03641	0,04602	0,05866	0,07427	0,09288	0,11451	0,13914	0,16707	0,19854

Figure 6. C_d coefficient

E_{max} values which are calculated according to the lift and drag coefficients obtained as a result of numerical analyzes and expressing the change in the performance of our aircraft, are given in Figure 7. According to this figure, the highest performance is obtained for the B_9 configuration.
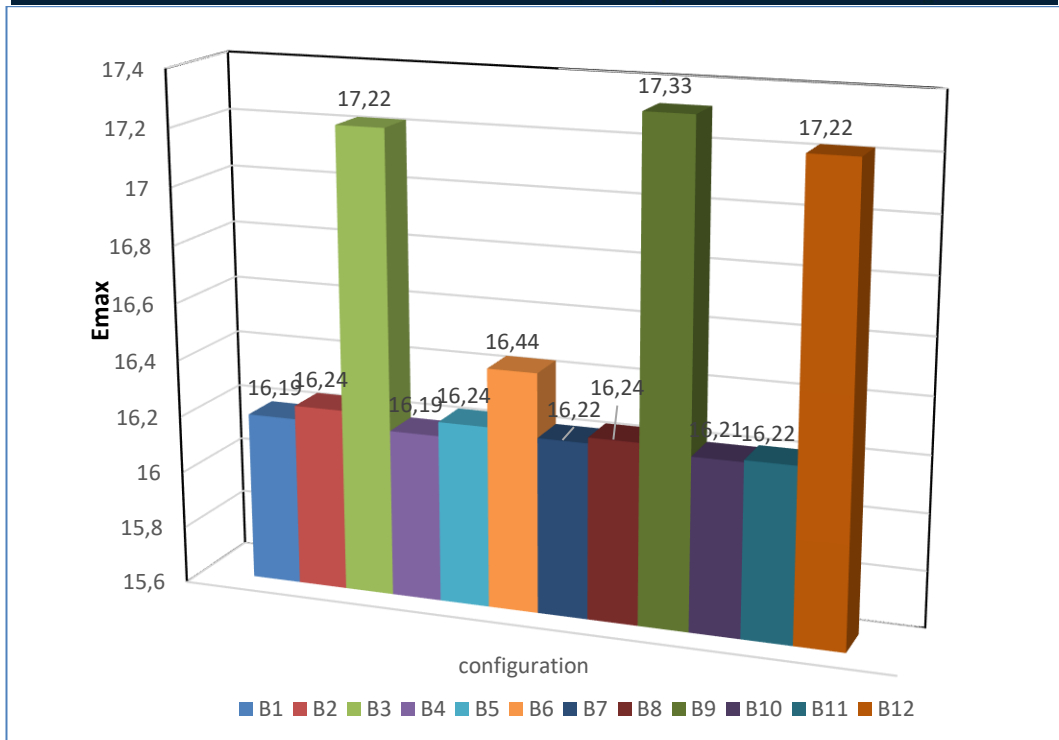
Figure 7. E$_{max}$

The cost analysis for the B_9 configuration, in which the highest E_{max} value is obtained, is shown in Figure 8. Simultaneous design resulted in about 5 percent improvement in rise and settling time and overshoot autonomous performance parameters when compared to the initial configuration.
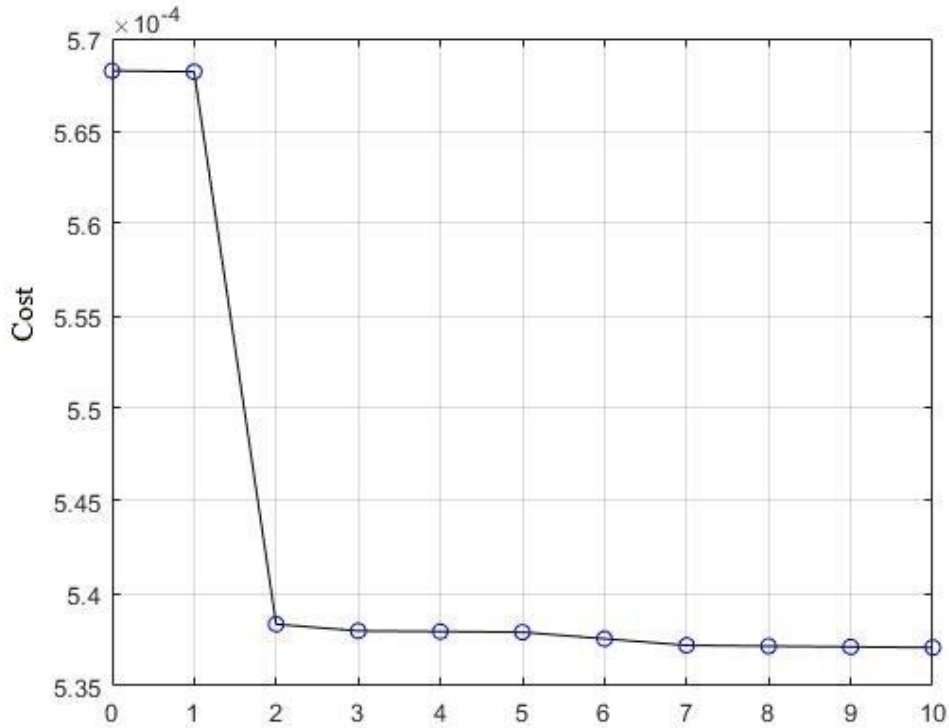
Figure 8. Cost Function

CONCLUSIONS

As a result, a simultaneous autopilot system design has been realized with active flow control for ZANKA-IIB. For this purpose, the lateral autonomous flight performance cost index was recalculated according to the highest E_{max} value obtained by active flow control and it was determined that the improvement was about 5 percent.

ACKNOWLEDGMENT

REFERENCES

[1]. R. Austin, "*Unmanned Aircraft Systems*," Wiley, 2010.

[2]. R. C. Nelson, ''*Flight Stability and Automatic Control*. 2nd ed.,'' McGraw-Hill, New York, chapters 2-6, 2007.

[3]. O. O. Kanat., E. Karatay, O. Kose and T. Oktay, ''Combined active flow and flight control systems design for morphing unmanned aerial vehicles'', *Proceedings of the Institution of Mechanical Engineers Part-G Journal of Aerospace Engineering*, vol. 233, pp. 1-20, May 2019.

[4]. T. Oktay and O. O. Kanat, ''A review of aerodynamic active flow control,'' *8th International Advanced Technologies Symposium (IATS'17)*, October 19-21, 2017, Elazig, Turkey.

I. Wygnanski, ''The variables affecting the control of separation by periodic excitation,'' *American Institute of Aeronautics and Astronautics,* paper 2004-2622, 2004.

[5]. T. Oktay, O. O. Kanat and A. Ceyhan, ''Improvement of wingtip vortices with active flow controller having several blowing points'', *8th International Advanced Technologies Symposium (IATS'17)*, October 19-21, 2017, Elazig, Turkey.

[6]. O. O. Kanat and T. Oktay, ''Effect of blower location and radius on lateral flight control system of UAVs,'' *2nd International Congress of Multidisciplinary Studies*, 4-5 May 2018, Adana, Turkey.

[7]. Thomas, J.L. and Salas, M.D., 1986. Far-Field Boundary Conditions for Transonic Lifting Solutions to the Euler Equations. AIAA Journal, vol. 24(7), pp. 1074-1080.]

[8]. ANSYS Fluent Theory Guide, 2013.

[9]. Menter, F. R., Kuntz, M., & Langtry, R. (2003). Ten years of industrial experience with the SST turbulence model. Turbulence, heat and mass transfer, 4(1), 625-632.

[10]. Abbott.I.H,'Theory of wing section, including a summary of airfoil data", Dover book on Physics, 1995

[11]. N. X. Vinh, ''Flight mechanics of high-performance aircraft'', *Cambridge University Press*, Cambridge, pp. 55, 1993.

[12]. T. Oktay, M. Konar, M. A. Mohamed, M. Aydin, F. Sal and M. Onay, ''Autonomous flight performance improvement of load-carrying unmanned aerial vehicles by active morphing,'' *International Journal of Mechanical, Aerospace, Industrial, Mechatronic and Manufacturing Engineering,* vol.10(1), pp.123-132, 2016.

[13]. U.S. Military Handbook MIL-HDBK-1797, 1997.

I. J. Wang and J. C. Spall, ''Stochastic optimization with inequality constraints using simultaneous perturbations and penalty functions,'' In Decision and Control, 2003. *Proceedings 42 nd TEEE Conference* on (Vol. 4, pp. 3808-3813). IEEE, 2003.

[14]. P. Sadegh and J. C. Spall, "Optimal random perturbations for multivariable stochastic approximation using a simultaneous perturbation gradient approximation", *IEEE Transactions on Automatic Control*, 43(10), pp. 1480-1484, 1998.

Sustainable and Cleaner Textile Production: Reducing Consumptions and Emissions in a Textile Mill by Application of Best Available Techniques

Emrah Ozturk[1], Mustafa Karaboyaci[2], Mehmet Kitis[3]

Abstract

A cleaner production study was carried out in a textile mill which mainly includes woven and knitted cotton fabric dyeing-finishing. According to cleaner production application methodology, basic production and auxiliary processes were defined in terms of inputs (raw material, water, energy, steam, chemicals etc.) and outputs (wastewater, emissions, wastes etc.) by detailed onsite investigations and data collection/analysis. Specific amounts of inputs and outputs were calculated according to mass and energy balances. In addition, a chemical inventory study for all chemicals (dyestuffs and auxiliary chemicals) used in the mill was carried out. In this context, material safety data sheets (MSDS) of a total of 198 chemicals were investigated for biodegradability and toxicity aspects. A total of 25 chemicals (10 auxiliary and 15 dyestuffs) was proposed to be replaced by the environmentally friendly substitutes. Raw groundwater and softened water (process water) samples were collected at different periods and analyzed in terms of pH, conductivity, total dissolved solids (TDS), hardness, iron, sulfate, total organic carbon (TOC), and total nitrogen (TN) parameters. Thus, the performance of water softening system was evaluated. In addition, wastewater samples were collected at different periods from various wastewater generation points and composite wastewater and these samples were analyzed in terms of pH, conductivity, chemical oxygen demand (COD), total suspended solids (TSS), color, and other parameters. Wastewater reuse possibilities with or without treatment were evaluated. Besides, potential savings and reductions were calculated by comparing the specific consumption values of the mill with those reported in the European Commission (EC) Integrated Pollution Prevention and Control (IPPC), Textile Sector Best Available Techniques (BAT) Reference document (BREF) and literature (data from similar textile mills). Consequently, a total of 14 BATs were determined working with mill management, technical staff and experts by employing a systematic and analytic decision making method. These BAT suggestions include establishment of sustainable and cleaner production policy in the mill, monitoring of all process inputs and outputs in terms of amounts and qualities, avoiding overflow and unnecessary rinsing, optimization of water softening unit, reuse of suitable process wastewaters, reduction of flotte ratios in jet dyeing machines, chemical substitutions, improving coordination among dyehouse and laboratory, optimization of dyeing recipes, use of more energy efficient lighting equipment, preheating of combustion air and feedwater in steam boilers, and installation of automatic chemical dosing system. After the implementation of these BATs in the mill, the following reductions can be potentially achieved; 40-45% in water consumption, 19-26% in energy consumption, 26-36% in chemical consumption, 44-51% in wastewater amounts, 52-72% in wastewater COD load, 24-27% in waste gas emissions, and 13-20% in solid wastes. It was found that potential payback periods of these BATs may range from 4 to 36 months.

Keywords: Best available techniques, chemical, cleaner production, energy, reduction, saving, textile, water.

---

[1]Corresponding author: Isparta University of Applied Sciences, Dept. of Environmental Protection Technologies, 32510, Aksu/Isparta, Turkey. emrahozturk@isparta.edu.tr

[2]Suleyman Demirel University, Dept. of Chemical Engineering, 32260, Cunur/Isparta, Turkey. mustafakaraboyaci@sdu.edu.tr

[3]Suleyman Demirel Univesity, Dept. of Environmental Engineering, 32260, Cunur/Isparta, Turkey. mehmetkitis@sdu.edu.tr

1. INTRODUCTION

Cleaner production is defined as the continual application of an integrated preventive environmental strategy in processes, products and services, to increase of productivity and competitiveness, and reducing the risks on the environment and human [1]. The clean production approach has become increasingly popular since the mid-1990s and is still popular today. The clean production approach has begun to take its place in the environmental policies of the countries since the mid-1990s. The European Commission adopted the Integrated Pollution Prevention and Control (IPPC) Directive and enacted in 1996 for the first time [2]. In order to facilitate the applicability of clean production in industries by the European Commission IPPC Bureau, the Best Available Techniques (BAT) were defined and sectoral reference documents (BREF) were prepared [3]. In 2010, the IPPC Directive was included in the scope of the Industrial Emissions Directive (IED, 2010/75/EU) [4]. In addition, BAT-based emission limit values (ELV) were defined. IED has not yet been introduced to the Turkish legislation but the first step has been taken with the publication of a Communique entitled "Integrated Pollution Prevention and Control in the Textile Sector" (Turkish Communique) in 2011 [5]. Textile mills which are over 10 tons/day installed capacity (employing washing, bleaching, mercerizing, sizing, printing, desizing and similar pretreatment, dyeing and finishing) were included in the scope of the Communique. Regulation of procedures and principles that minimize negative effects of textile sector activities, control of discharges to water, air and soil environments, efficient usage of raw materials/energy, and usage of cleaner production technologies can be listed as the general aims of Turkish Communique [5]. In 2013, The Turkish Scientific and Technological Research Council of Turkey (TUBITAK) Marmara Research Center (MRC) Environment and Cleaner Production Institute was established and became the national cleaner production center. Moreover, cleaner production studies and projects in various industrial sectors have been accelerated between the years 2011-2019 in Turkey. In addition, many R&D projects have been carried out and/or still ongoing in order to support the transition process to clean production in the industries by the Ministry of Environment and Urbanization, the Ministry of Forestry and Water Affairs and the Ministry of Science, Industry and Technology in Turkey.

In this study, a cleaner production study was carried out in a textile mill employing cotton and polyester (PES) fabric dyeing-finishing in accordance with the clean production application methodology. This study may be provided a roadmap for clean production studies of similar textile enterprises and their performance assessments. In addition, the existence of real-scale studies in the sector can be make significant contributions to researchers and similar facilities working on this field.

1.1. Textile Industry

Textile industry has met one of the most basic needs of humanity and today more than 150 countries are textile supplier [6]. In many countries, the textile sector is a locomotive sector due to creation of employment opportunities, high export incomes and high share of gross national product (GNP) [7]. The textile industry is one of the industrial sectors consisting of a large number of sub-sectors and complex production processes. Generally, textile production processes can be classified as wet and dry processes [8]. Water consumption is intensive in wet processes, while energy consumption is more intensive in dry processes. Resource usage and waste/emission amounts in the sub-sectors of the textile industry are variable depending on process properties, applied recipes, utilized techniques and technologies. The specific water consumption ranges between 70 and 250 L/kg product [9] and the energy consumption varies from 10 to 80 MJ/kg product especially in cotton/PES fabric finishing and dyeing facilities [10]. Also chemical consumption varies between 10 and 100% of the fiber weight [9]. Typically 40-60% of the chemicals used in production process are discharged by wastewater streams. Therefore, the environmental problems causing from the textile industry are mainly due to the high amount of wastewater generation and the chemical loads carried by the wastewater [11]. In textile industry, CO, CO_2, NO_x and SO_x emissions are also formed as a result of the burning of fossil fuels used in the production of thermal energy [3]. Solid wastes with different characters (such as recoverable, contaminated waste, hazardous wastes and textile wastes) are formed in the textile industry as in other industries [3]. In the textile industry, both resource uses and wastes/emissions can be avoided at the source by applying the appropriate BAT. Thus, the pressures of the industry on the environment and natural resources can be reduced.

2. MATERIAL and METHOD

2.1. Studied Textile Mill

The studied textile mill was located in Denizli province and it mainly produced cotton/PES woven and knitting fabric dyeing-finishing. It has 7067 tons/year fabric bleaching and 8797 tons/year fabric dyeing capacity. The textile mill has a semi-batch production line in terms of its production structure and dyeing processes were carried out according to the exhaust dyeing method in high temperature (HT) jet dyeing machines. HT Jet

dyeing machines operate at moderate liquor ratios (1:10-1:12 liquor ratios) in the mill. Total water demand flow rate of the mill was 1500-2000 m^3/day and it was supplied from underground water resources. The supplied raw water was softened in ion exchangers before using in production processes as process water in the mill. Industrial and domestic wastewater were generated in the mill and they were separately collected and then discharged to wastewater treatment plant channel system. The average wastewater flow rate was 1800-2000 m^3/day in the mill.

Thermal energy (steam and hot-oil) and electricity were consumed in the mill. The average electricity and coal consumptions were 5000 MWh/year and 7500 tons/year, respectively. Thermal energy was produced from coal and it was transported to production processes by steam and hot-oil. Steam and hot oil were used in indirect dryers. Besides natural gas was used in stenter and singeing processes especially. Many kind of chemical (dyestuff and auxiliaries chemical) were also used in production and auxiliary processes of the mill. Almost all chemicals were used especially in finishing-dyeing processes. There was no automatic chemical dosing system in the mill. Waste flue gas emissions occur at a total of 7 points in the mil. However, the most important emission source was steam boilers in the mill. The steam boiler chimney has a wet filter and a heat recovery system (economizer) to reduce emissions. In addition, there were plate heat exchangers for the recovery of waste heat from wastewater streams.

2.2. Applied Methodology

Data collection and analysis were conducted in order to evaluate the resource efficiency and environmental performance of the mill. Specific resource uses (water, energy, chemical, etc.) and wastes/emissions (wastewater, waste gas emission, solid wastes, waste heat etc.) were calculated on the basis of processes. In addition, raw water and process water samples were collected at different periods and pH, conductivity, hardness, turbidity, iron, sulfate and total nitrogen (TN) parameters were analyzed. Thus, the performance of the water softening unit was evaluated. Specific thermal energy and electricity consumption were calculated on the basis of the production processes. Specific dyestuff and auxiliary chemical uses were calculated on the basis of the processes. Moreover, a chemical inventory study was conducted by examining the Material Safety Data Sheets (MSDS) of 198 chemicals used in the mill. Biodegradability and elimination of each chemical, toxic properties (lethal concentration (LC_{50}), lethal dose (LD_{50}), effective concentration (EC_{50}) and inhibitory concentration (IC_{50})) were investigated. According to the IPPC textile BREF, chemicals with low biologic degradation/elimination (<70%) and toxic character were identified. It was proposed to substitute the determined toxic chemicals with their environmentally friendly counterparts.

Composite wastewater and process wastewater samples were collected at different periods and analyzed. In the samples collected from composite wastewater, the parameters of pH, conductivity, chemical oxygen demand (COD), total suspended solids (TSS), color and oil-grease, free chlorine, phenol, chromium (Cr^{+6}), sulfate, sulfur, total nitrogen and phosphorus were analyzed. Thus, composite wastewater loads were calculated and reuse potentials were evaluated. In addition, pH, conductivity, COD, TSS and color parameters were analyzed in collected process wastewater samples. Thus, reuse potentials of process wastewater with treatment (WT) or without treatment (direct reuse (DR)) were evaluated. Water and wastewater analysis were conducted according to Standard Methods [12]. Textile wastes, recyclable wastes, hazardous wastes, contaminated wastes and waste mineral oil were determined on the basis of processes/units. The official waste declaration forms were used to determine the amount of solid waste. The amounts of waste gas emissions were compiled from official emission reports. Also, waste heat lost from waste flue emissions, hot surfaces and hot wastewater streams were calculated.

The current resource efficiency and environmental performance of the mill were compared with the similar textile mill in the literature and IPPC BREF document. Thus, potential savings/reductions that can be achieved in the mill were calculated. A BAT list which including total 117 BAT were prepared for the mill. These BAT suggestion were evaluated by using a combination of criteria weighting method (CWM), weighted sum method (WSM) and simple ranking method (SRM). In this context, each suggested BAT was weighted according to economic saving potential, environmental benefit potential, technical applicability and positive or negative side interactions criteria. The suggested BATs were weighted by expert, technical employers and mill management. Thus, various technical opinions were included in the decision-making process. In addition, total priority scores were calculated for each BAT and ranked according to the calculated priority scores. Potential savings/reductions were calculated after the implementation of each determined priority BAT. The potential payback periods were also calculated for the priority BATs.

3. RESULTS and DISCUSSION

3.1. Water Consumption and Wastewater Generation

A total of 719,395 m^3/year water was consumed in the facility and it was supplied from groundwater. Only 0.7% of the raw water was used directly (without hardness removal) in plant cleaning processes that do not require high water quality. In the regeneration of cationic ion-exchange resins, 7% of total water was consumed. In the mill, 99% of the raw material was used in the production process after hardness removal in the water softening system consisting of sand filter and cationic ion exchange resins. 91% of the softened water was consumed in the finishing and dyeing processes. Finishing and dyeing processes have share of 36 and 55% in total water consumption, respectively. In addition, 1% of softened water was used as boiler feed water after the additional hardness removal in RO processes. In the mill, 0.3% of the total water consumption was consumed for domestic needs. Average water consumption, distribution of total water consumption and specific water consumption values can be seen in Table 1.

Table 28. Specific water consumption and distribution in production processes

Process	Average water consumption (m^3/year)	Distribution (%)	Average specific water consumption
Raw water consumption	719,395	100	115 L/kg product
Facility cleaning	4,709	0.7	1.5 L/m^2-day
Softened water consumption	714,687	99	115 L/kg product
Finishing	261,984	36	42 L/kg product
Dyeing	392,967	55	63 L/kg product
Steam production	5,039	1	0,8 L/kg product
Regeneration	52,799	7	9 L/kg product
Domestic water consumption	1,904	0.3	42 L/person-day

Specific water consumption values were calculated on the basis of processes in cleaner production studies carried out in the mill. Accordingly, specific raw and softened water consumptions were 115 L/kg product in the mill. The specific softened water consumption in pre-finishing and dyeing/finishing processes were 42 and 63 L/kg, respectively. The use of overflow washing/rinsing in finishing and using high flotte ratio dyeing machine in dyeing were increased specific water consumption in the mill. The specific softened water consumption values in the regeneration of ion exchangers resins and boiler feed water in steam production were 0.8 and 9 L/kg, respectively. It is seen that the specific amounts of boiler feed water are quite low in steam production due to use of closed steam system and reuse of steam condensate in the mill. The specific process water consumption in the finishing and dyeing of cotton and PES woven-knitted fabrics were 94 and 152 L/kg product, respectively. Reducing flotte ratio in dyeing machine and reuse of suitable wastewater (especially rinsing and washing processes) can be performed to decrease of water consumption in the mill.

Raw and softened water samples were collected at different periods and pH, conductivity, turbidity, total dissolved solids (TDS), hardness, iron, sulfate and TN parameters were analyzed (Table 2). Thus, the water quality requirement of the mill and the performance of the softening system were evaluated. In the mill, water softening system can be optimized and regeneration and/or resin rinsing water can be reused in order to minimize water consumption.

Table 2. Analysis results of raw and softened water

Parameter	Unit	Raw water	Softened water
pH	-	7.9	7.6
Conductivity	µS/cm	1627	1704
Turbidity	NTU	1.5	1
TDS	mg/L	814	853
Hardness	mg/L CaCO$_3$	392	18
Iron	mg/L	0.2	<0.1
Sulphate	mg/L	113	111
TN	mg/L	0.05	0.05

In the mill, the amount of composite wastewater was monitored by wastewater meters and flowmeters. However, the amount of wastewater was not monitored on the basis of processes. The total amount of composite wastewater generated in the mill was 714,363 m^3/year. The process wastewater generated in the HT finishing-dyeing process constitutes 91% of the composite wastewater. The share of pre-treatment and finishing wastewater in the amount of composite were 37 and 55%, respectively. Regeneration and facility cleaning

wastewater have a share of 7 and 0.7% in composite wastewater, respectively. The specific wastewater values were the same as the specific water consumption values presented in Table 1.

The main factors that determine the characterization of process and composite wastewater in the mill were the fiber type, the color shade, the fixation ratios of the dyestuffs and the applied production program. Considering these factors, 2-hours composite samples were collected from process and composite wastewater and pH, electrical conductivity, COD, ammonium-N, TSS, oil-grease, sulfur, free chlorine, sulfite and color parameters of the wastewater samples were analyzed (Table 3). In addition, process wastewater samples were analyzed for pH, conductivity, COD, TSS and color parameters (Table 4). Thus, the potential of reuse of process wastewater with treatment (WT) or without treatment (direct reuse (DR)) were evaluated. Specific wastewater pollution loads were also calculated by using process and composite wastewater analysis results. According to this, specific COD and TSS loads in composite wastewater were 155 and 21 g/kg product, respectively.

Table 3. Composite wastewater characterization results

Parameter	Unit	Value
pH	-	9
Conductivity	μS/cm	6595
COD	mg/L	886
Ammonium-N	mg/L	<0,5
TSS	mg/L	124
Oil-grease	mg/L	<10
Sulphur	mg/L	<0,1
Free chlorine	mg/L	<0,1
Sulfite	mg/L	<1
Color	Pt-Co	190

Table 4. Process wastewater analysis results

Sample No.	Process	Color shade	pH	Conductivity (μS/cm)	COD (mg/L)	TSS (mg/L)	Color (Pt-Co)	Reuse potential
1	Rinse water after bleaching	Dark/Light	10.2	3240	3468	1340	512	WT[b]
2	Bleaching	Dark/Light	11.1	6000	11220	7660	1658	WT
3	Acid and enzyme	Dark	-[a]	-	2295	48	76	WT/DR[c]
4	Washing/rinsing	Dark	-	-	1530	126	46	WT/DR
5	Bleaching	Light	-	-	1836	260	179	WT
6	Washing/rinsing	Dark	-	-	612	120	37	WT/DR
7	Neutralization after dyeing	Dark	-	-	816	76	3174	WT
8	Neutralization	Light	-	-	1122	38	602	WT/DR
9	Dyeing	Dark	-	-	3765	65	3822	WT
10	Dyeing (80 ºC)	Light	10.2	61000	714	540	2014	WT
11	Rinsing after dyeing	Dark	10.2	33000	1428	52	3417	WT
12	Rinsing after dyeing	Light	10.5	37400	326	86	1007	WT/DR
13	Hot rinsing/washing (95 ºC)	Light	10.2	23900	714	218	683	WT
14	Hot washing/rinsing (70 ºC)	Light	-	-	510	230	350	WT
15	Rinsing	Dark/Light	-	-	179	60	86	DR
16	Hot washing/rinsing (95 ºC)	Dark	9.5	3270	1122	136	2558	WT
17	Hot washing/rinsing (95 ºC)	Dark	9	6300	1530	140	1911	WT
18	Hot washing/rinsing (95 ºC)	Dark	-	-	796	76	1076	WT
19	Hot washing/rinsing (80 ºC)	Dark	9	4.800	224	44	570	WT/DR

20	Rinsing	Dark	9.4	12510	107	16	1137	WT/DR
21	Rinsing	Dark	-	-	61	20	366	DR
22	Softening	Dark	6	1803	230	30	62	DR
23	Softening	Light	8.4	6050	1275	112	<20	DR

[a]Data not available; [b]WT: reuse after treatment; [c]DR: Direct reuse (without treatment)

3.2. Energy Consumption and Waste Flue Gas Emissions

Coal was used as the primary energy source in steam and hot oil boilers to meet the thermal energy required in the mill. Hot oil was mostly used in contact dryers and steam especially in finishing-dyeing processes. In addition, the natural gas was generally used in singeing machines and stenters. Electricity was used to operate pumps, machines, compressors, electric motors and devices, lighting and office devices in the mill. Total coal consumption in the mill was 7886 tons/year and 66 and 34% of total coal were consumed in steam and hot oil boilers, respectively. An average of 2210 tons steam/month of steam is consumed in the mill. 90-95% of the steam was used in finishing-dyeing processes, 5-10% in drying processes and 1% in building heating. The specific coal and steam consumption in the mill were 1.46 kg coal/kg product and 4.5 kg steam/kg product. Moreover, the specific coal consumption in steam and hot oil boilers were 0.95 and 0.5 kg coal/kg, respectively.

The average electricity consumption was 5,126,128 kWh/year. 31 and 56% share of the total electricity were consumed in HT dyeing machines and stenters, respectively. 1 and 8% share of the total electricity were consumed in water softening unit and boilers, respectively. Specific energy consumptions were also calculated on the basis of production processes. Specific electricity consumption was 0.82 kWh/kg product in overall the mill. The specific electricity consumption in dyeing and finishing processes were 0.25 kWh/kg product. Specific total energy consumption (electricity and thermal) of the mill was also calculated. Accordingly, specific total energy consumption was 30 MJ/kg product in the mill. Only specific thermal energy consumption was 27 MJ/kg product. Energy losses were also calculated theoretically. Accordingly, 0.44, 0.15 and 0.12 MJ/kg product energy were lost from waste flue gases, wastewater streams and electric motors, respectively.

The main waste flue gas emissions in the mill were caused by steam and hot oil boilers, dryers (stenters, pre-dryer, singeing machines and free desiccant) chimneys. It was determined that the total mass flow rate of the total flue gas emissions was 29.4 m^3/hour in the mill. The main waste flue gas emissions from the mill were CO, NO$_x$, SO$_2$, dust and VOCs. Specific emission values were calculated by utilizing the values of mass flow rates of waste flue gas emissions. Accordingly, specific CO, SO$_2$ and NO$_x$ values in the mill were 4.3, 28.1 and 13.4 g/kg product.

3.3. Chemical Consumption and Chemical Inventory Study

High amount of chemical were consumed in dyeing and finishing processes of the mill. Besides various chemical were consumed in facility cleaning, boilers, air conditioning system, water softening unit etc. Softeners, wetting agent, leveling agent, caustic, pH-adjusting agent, beaching agent, acids, dispersing agent, carriers, peroxide, antifoaming agent, lubricant agent, stabilizer, degreaser and beam bender agent were intensively consumed in the finishing and dyeing processes. In addition, indanthrene, disperse and reactive dyestuffs were consumed in dyeing processes. In the mill, total auxiliary chemical and dyestuff consumption were 1445 and 41 tons/year, respectively. Specific auxiliary chemical and dyestuff consumption were 233 and 9 g/kg product in the mill, respectively.

A chemical inventory were carried out in the mill. In this context, total 198 chemical MSDSs were investigated in terms of toxicity and biodegradability properties. Chemical substitutions with environmental friendly counterparts were suggested for total of 25 chemicals (10 auxiliary chemicals and 15 dyestuffs) which have lower biodegradable and toxic. Thus, biological degradation of process wastewater can be increased and toxicity can be reduced.

3.4. Solid Waste Generation

In the mill, solid wastes and their specific amounts were determined. The specific hazardous waste and recyclable waste amount of the mill were 0.49 and 1.12 g/kg product, respectively. In addition, the specific domestic solid waste and waste oil produced in the plant were 1.15 g/person and 0.02 g/kg product, respectively. The solid wastes generated in the mill were separately collected and disposed according to existing environmental legislation. Hazardous wastes were collected at waste collection sites built according to standards and disposed by licensed organization.

3.5. Potential Saving and Reduction Ratios

Specific consumptions and specific waste/emission values of the mill were compared with similar textile mills data in literature and IPPC textile BREF document (Table 5). Thus, saving and reduction potentials were calculated. Generally, specific values of the mill were between reference ranges however there were important saving and reduction potential of the mill when the minimum reference values were based.

Table 5. Potential saving and reduction ratios

Parameter	Studied textile mill	Literature	IPPC Textile BREF	Potential savings/reduction ratios (%)	References
Specific water consumption (L/kg product)	115	70-250	60-230	39-48	[3], [7], [9], [11]
Specific electricity consumption (kWh/kg product)	0.82	0.1-7.3	0.5-3	40	[10], [13]
Specific total energy consumption (MJ/kg product)	30	10-80	13-72	56-65	[3], [10], [13]
Specific steam consumption (kg steam/kg product)	4.5	4-9	1.5	12-65	[3], [14]-[16]
Specific auxiliary chemicals consumption (g/kg product)	233	151-383	95-670	35-60	[3], [11]
Specific dyestuff consumption (g/kg product)	9	7-10	10-20	22	
Specific wastewater generation (L/kg product)	115	70-250	60-230	39-48	[3], [7], [9], [11]
Specific wastewater COD loads (g/kg product)	155	43-303	14-618	72-90	[3], [7], [11]
Specific waste flue gas emissions (g/kg product)	CO:4.3 SO$_2$:28 NO$_x$:13.4	CO:0.28 SO$_2$:0.12 NO$_x$:0.3	-	56-98	[7], [17]-[19]
Specific solid waste generation (g/kg product)	1.5	1.5-36	11-21	under reference values	[3], [7], [20]

3.6. Determination of Priority BATs for the Mill

A list, including of 117 BAT, was prepared in order to improve resource efficiency and environmental performance by using the data obtained from the clean production analysis studies carried out in the mill. Each BAT was evaluated with technic personals, experts and mill management in terms of techno-economic applicability, saving/reduction opportunities, environmental benefits and economic aspects. Ultimately, 14 BATs were determined as priority and savings/reductions were calculated for the each priority BATs.

3.7. Savings and Reductions Ratios

The potential savings and reductions in consumption and environmental performance with the implementation of each of the priority BATs in the mill were calculated. Also, potential payback periods for each priority BAT were calculated (Table 6). After the implementation of the priority BATs in the future, it can be achieved 40-45% savings in water consumption, 19-26% savings in energy consumption, 26-36% savings in chemical consumption, 44-51% reduction in wastewater amounts, 52-72% reduction in wastewater COD load, 24-27% reduction in flue gas emissions and 13-20% reduction in solid waste amounts. The payback period of a significant part of the priority BATs can be shorter than 1 year. However, in general, the payback period of priority BATs may vary from 4 to 36 months.

Table 6. Priority BATs and calculated savings/reductions

Priority BATs	Reduction ratios (%)							Payback period (year)
	Water	Energy	Chemical	Wastewater	COD load	Flue gas emission	Solid waste	
Establishing a sustainable production policy and setting targets Monitoring of inputs and outputs in the production processes (in terms of quantity and quality) and reporting	4-9	3-5	4-6	4-9	6-8	2-4	4-8	1-3

Avoiding overflow rinsing and unnecessary washing	10-15	2	2-4	11-16	3-8			<1
Optimization of water softening unit	6-10			8-12	1-3			<1
Reducing of water and chemical consumption by reuse of separate process wastewater	9-13	2-5	2-5	10-14	7-10	2-3		1-2
Reuse of relatively clean wastewater in areas that do not require high water quality	1-2			1,5-3				<1
Reduction of flotte ratios and/or use of machines with lower flotte ratio	16-20	8-10	16-18	16-20	15-25	7-9	8-9	2-3
Replacement of toxic chemicals with environmental friendly counterparts								
Using automatically chemical preparation and dosing system			11-20		25-45			2-3
Improvement of coordination between laboratory-dyehouse and reducing reprocesses	3-8	3-8	3-8	3-8	3-8	3-8	3-8	1-2
Applied thermofixing before washing		3-6				3-6		1-2
Modification of air conditioning and humidification system fans and motors		3-5						<1
Using more efficient lighting system		4-6						1-2
Preheating combustion air and feed water in steam boiler with hot flue gas emission		3-6				3-6		1-2
Total reduction ratios (cross media effects considered)	40-45	19-26	26-36	44-51	52-72	24-27	13-20	-

4. CONCLUSIONS

A cleaner production study was carried out in a textile mill employing cotton-PES fabric weaving-knitting subsequent dyeing-finishing. Environmental and technical performance of the mill were evaluated according to cleaner production methodology. A list of BAT was suggested to the studied textile mill. It was found that some separate wastewater streams from wet processes could be directly reused in dyeing-finishing processes and facility cleaning even without treatment. Energy consumption can be reduced by implementation of reducing reprocess ratio, modification of process and steam boilers, using more efficient lighting system, avoiding of overflow rinsing and reducing flotte ratios in HT dyeing machines. A company-wide chemical inventory study indicated that 198 chemicals (10 auxiliaries and 15 dyestuffs) should be replaced with less toxic and more biodegradable counterparts. After the implementation of determined priority 14 BATs the following reductions/savings could be achieved; water consumption: 40-45%, energy consumption: 19-26%, chemical consumption: 26-36%, total wastewater flowrate: 44-51%, COD load of composite wastewater: 52-72%, waste flue gas emissions: 24-27% and solid wastes: 13-20%. It was found that payback period of such investment ranges from 4 to 36 months by the application of priority BATs in the studied textile mill.

REFERENCES

[1]. *United Nations Environment Programme (UNEP). Cleaner Production: A Training Resource Package, Industry and Environment. UNEP Division of Technology, Industry, and Economics Sustainable Consumption and Production Branch,* ISBN 9280716050, 1996.

[2]. *European Commission Integrated Pollution Prevention and Control (IPPC) Directive. Council Directive 96/61/EC of 24 September 1996 Concerning Integrated Pollution Prevention and Control,* 1996.

[3]. *European Commission (EC). Integrated Pollution Prevention and Control (IPPC) Reference Document on Best Available Techniques for the Textile Industry (BREF). European Commission IPPC Bureau,* Seville, 2003.

[4]. *Industrial Emissions Directive (IED). Directive 2010/75/EU of the European Parliament and of the Council, of 24 November 2010, on Industrial Emissions (Integrated Pollution Prevention and Control-recast),* 2010.

[5]. Turkish Ministry of Environment and Urbanization (TMEU). Integrated Pollution Prevention and Control in Textile Sector, 2011, Available: http://www.resmigazete.gov.tr

[6]. *World Trade Organization (WTO). World Trade Statistical Review*, 2018. Available: https://www.wto.org/

[7]. Ozturk, "Applications of Integrated Pollution Prevention and Control and Clean Production in Textile Industry," Ph.D. thesis, Suleyman Demirel University Environmental Engineering Dept., Isparta, July, 2014.

[8]. E. Ozturk, M. Karaboyaci, U. Yetis, N.O. Yigit, M. Kitis, "Evaluation of integrated pollution prevention control in a textile fiber production and dyeing mill," *J. Clean. Prod.* vol. 88, pp. 116-124, 2015.

[9]. E. Ozturk, U. Yetis, F.B. Dilek, G.N. Demirer, "A chemical substitution study for a wet processing textile mill in Turkey," *J. Clean. Prod.* vol. 17, pp. 239-247, 2009.

[10]. S. Palamutcu, "Electric energy consumption in the cotton textile processing stages," *Energy* 35, pp. 2945-2952, 2011.

[11]. E. Ozturk, H. Koseoglu, M. Karaboyaci, N.O. Yigit, U. Yetis, M. Kitis, "Minimization of water and chemical use in a cotton/polyester fabric dyeing textile mill," *J. Clean. Prod.* vol. 130, pp. 92-102, 2016.

[12]. American Public Health Association (APHA), *Standard Methods for the Examination of Water and Wastewater, nineteenth Ed. American Public Health Association*, Washington, DC, 1997.

a. Hasanbeigi, "Energy-Efficiency Improvement Opportunities for the Textile Industry," China Energy Group Energy Analysis Department Environmental Energy Technologies Division, Ernest Orlando Lawrence Berkeley National Laboratory, LBNL-3970E, 2010.

[13]. S. Swaminathan, R. Rudramoorthy, "New technologies are viable but capital investment could be high," *Express Textile*, September, 2004.

[14]. Intelligent Energy Europe (IEE), "EMS-Textile Project: Promotion of Energy Management Practices in the Textile Industries of Greece, Portugal, Spain and Bulgaria," Benchmarking Information V.4. (IEE/04/113/S07.38648). European Commission, Brussels, 2006.

[15]. S. Purohit, "Energy conservation in textile industry," *Textile Magazine*, vol. 49, pp. 245-274, 2007.

[16]. M. Aysen, "Air pollutant emission potentials of cotton textile manufacturing industry," *J. Clean. Prod.*, vol. 6, pp. 339-347, 1998.

[17]. E. Kalliala,, P. Talvenmaa, "The Finnish Background Report for the EC Documentation of Best Available Techniques for Wet Processing in Textile Industry," The Finnish Environment Institute ISBN 952-11- 0753-7, 2000.

[18]. V.N. Thai, A. Tokai, Y. Yamamoto, D.T. Nguyen, "Eco-Labeling criteria for textile products with the support of textile flows: a case study of the Vietnamese textile industry," *Journal of Sustainable Energy and Environment*, vol. 2, pp. 105-115, 2011.

[19]. E. Ozturk, H. Koseoglu, M. Karaboyaci, N.O. Yigit, U. Yetis, M. Kitis, "Sustainable textile production: cleaner production assessment/eco-efficiency analysis study in a textile mill," *J. Clean. Prod.* vol. 138, pp. 248-265, 2016.

The Methods for Prevention of Corrosion: Use of Inhibitors

Semra Bilgic[1]

Abstract

Corrosion is defined as the deteoration of metals and alloys by chemical and electrochemical reactions. Corrosion is unwanted phenomenon because of harmful effects for human health, environment and economic losses. Therefore, there are several methods to prevent or reduce the corrosion.

Use of inhibitors is one of the most effective methods for the protection of many metals and alloys against corrosion.

Inhibitors are chemical compounds, added several systems, chemical processes, vapour generators, petroleum gas pipelines. Inhibitors prevent corrosion either by being adsorbed on the surface of metals and alloys, or by forming a protective layer or by causing the formation of unsoluble complex. These compounds can be organic or inorganic compounds organic inhibitors contain oxygen, nitrogen, sulphur and heterocyclic compounds such as amines, aldehydes, heterocyclic nitrogen compounds, sulphur-containing compounds. Inorganic inhibitors contain inorganic ions such as NO_2^-, CrO_4^-

Another classification of inhibitors is as follows:

1) Anodic inhibitors
2) Cathodic inhibitors
3) Mixed inhibitors

Anodic inhibitors prevent or reduce anodic corrosion. These inhibitors are generally anions. Cathodic inhibitors cause to prevent or decrease cathodic corrosion, they are cations. Mixed inhibitors reduce the corrosion rates of both anodic and cathodic reactions. They are organic compounds.

Keywords: *Corrosion, anodic inhibitors, cathodic inhibitors, mixed inhibitors.*

1. WHAT IS CORROSION?

The term of corrosion can be defined as the interaction of metals and alloys with surrounding environments. Corrosion is an electrochemical process it involves the transfer of electrons between a metal surface and aqueous electrolyte solution. Formation of rust on iron and steel and other corrosion products, darkness on silver, the formation of green patina on copper and brass, cracks in aircraft, automobiles, boats, gutters, ships can be given as a few examples.

The problem of corrosion is common and dangerous phenomenon in various sectors, such as chemical industry, petrochemical, shipbuilding construction, automotive, aviation, railway, maritime and others.

Corrosion wastes the sources and products, stops production and causes various accidents. Corrosion causes important economical losses.

Corrosion is a major factor in the investment and production of the industry. According to some estimations, the cost of corrosion to a national reaches to 3.5–5.5% of the gross national products.

It is predicted that twenty percent of iron produced is lost by corrosion every year.

Due to its different harmful effects, corrosion is unwanted phenomenon, it is important to minimize or control metals and alloys against corrosion. Corrosion is a major industrial problem and its effect is important technically, economically and environmentally. There are several methods to prevent or reduce corrosion such as

➢ paintings,
➢ coatings,
➢ cathodic
➢ protection,
➢ anodic production and
➢ adding chemical

substances as called inhibitor.

2. INHIBITORS

The use of corrosion inhibitors can be considered as one of the best effective methods of the protection of many metals and alloys against corrosion.

Inhibitors are added in several systems such as cooling systems, chemical processes, vapour generators, petroleum pipe lines.

Inhibitors prevent corrosion either by being adsorbed on the surface of metals and alloys, or by forming a protective layer or by causing the formation of insoluble complex.

Corrosion inhibitors decrease the rate of corrosion when added in relatively small quantities to the system under corrosion. Corrosion inhibitors can be classified into the following categories:

1) Anodic inhibitors

2) Cathodic inhibitors

3) Mixed inhibitors

• Anodic inhibitors which retard the anodic corrosion reactions by forming passive films.

1) Anodic inhibitors are chemical substances that form a protective layer of oxide film on the surface of metal causing resistance to corrosion. These inhibitors are generally anions.

As the concentration of these inhibitors increases, inhibitors react with the anodes, forming a passive layer.

Therefore, these inhibitors are also known as passivators.

Anodic inhibitors act by a reducing anodic reaction, that is, blocks the anode reaction and supports the natural reaction of passivation metal surface, also, due to the forming a film adsorbed on the metal.
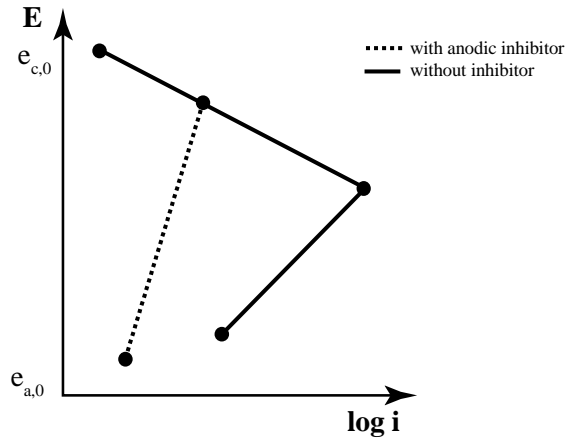
Anodic inhibitors: chromate (CrO_4^-), molybdate (MoO_4^-), benzoate ($C_7H_5O_2^-$), silicate (SiO_4^{4-}), nitrate (NO_3^-)
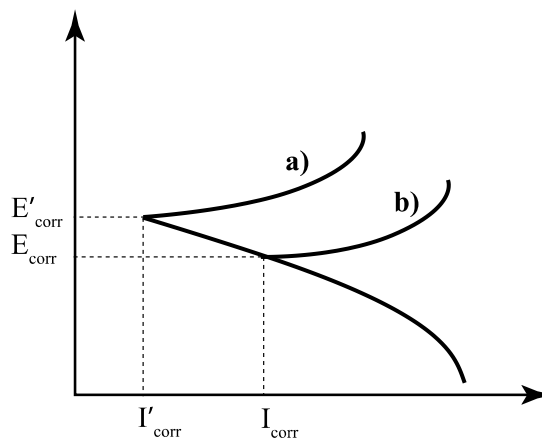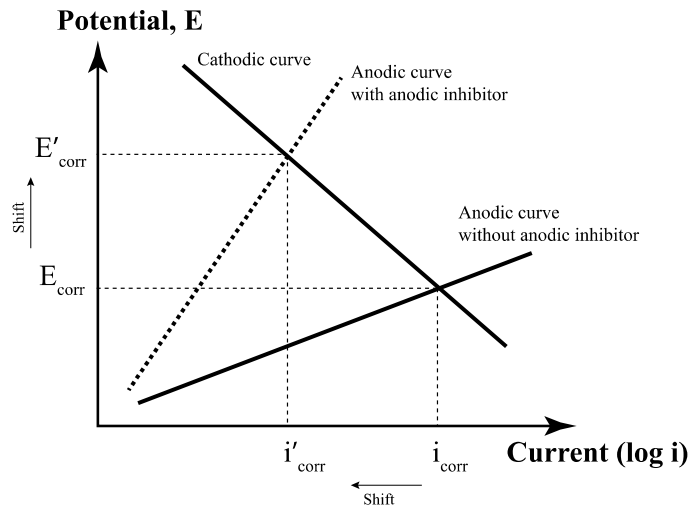
Potentiostatic polarization diagram: electrochemical behavior of a metal in a solution with anodic inhibitor (a) versus without inhibitor (b).

This graph shows a potentiostatic polarization diagram of a solution with behavior inhibitor anodic. The anodic reaction is affected by the corrosion inhibitors and the corrosion potential.

As can be seen from these graphs, anodic inhibitor causes to shift the corrosion potential towards to positive value. When the presence of anodic inhibitor corrosion current density reduces.

• Cathodic inhibitors that suppress cathodic reaction, such as reduction of dissolved oxygen.

2) Cathodic inhibitors: Cathodic inhibitors show the reaction at the cathode. Generally cathodic inhibitors are cations.

During the corrosion process, the cathodic corrosion inhibitors prevent the occurrence of the cathodic reaction of the metal.

These inhibitors slows down the cathodic reaction to limit the diffusion of reducing species to the metal surface.

These inhibitors affect the reduction of hydrogen in acidic media or the reduction of oxygen in neutral and/or alkali media.

The cathodic inhibitors form a barrier of insoluble precipitates over the metal, covering it. Thus, restricts the metal contact with the environment, even if it is completely immersed, preventing the occurrence of the corrosion reaction.

Cathodic inhibitor also changes corrosion potential and corrosion current density, such as anodic inhibitors.

Cathodic inhibitor reduces corrosion current density, in other words corrosion rate, while shifting corrosion potential to cathode.
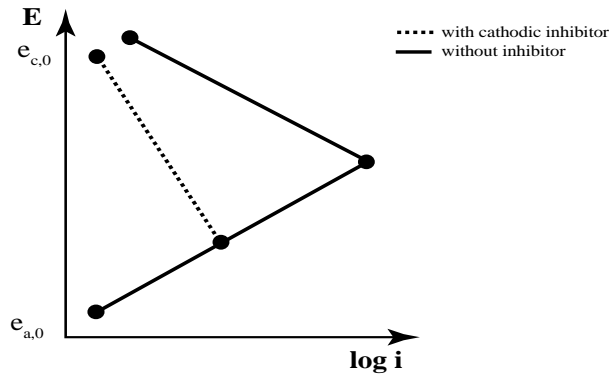
Cathodic inhibitors: calcium bicarbonate ($Ca(HO_3)_2$), Antimon (Sb^{3+}), (on iron)
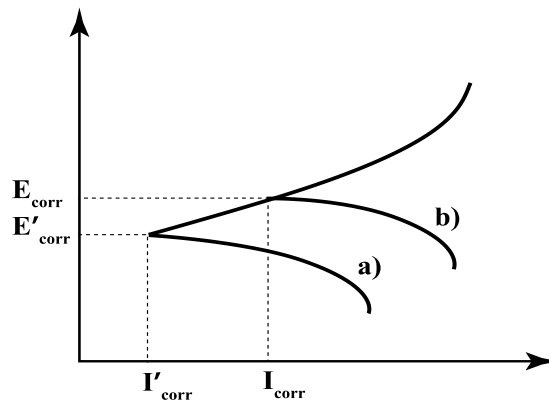
Potentiostatic polarization diagram: electrochemical behavior of the metal in a cathodic inhibitors solution (a), as compared to the same solution, without inhibitor (b)

As can be seen from the above graphs when the presence of cathodic inhibitor the cathodic reaction is affected the corrosion potential is shifted to more negative values.

Some examples of inorganic cathodic inhibitors are the ions of the magnesium, zinc, and nickel that react with the hydroxyl (OH^-) of the water forming the insoluble hydroxides as ($Mg(OH)_2$, $Zn(OH)_2$, $Ni(OH)_2$ which are deposited on the cathodic site of the metal surface, protecting it.

For example it seen in hard waters a kind of this mechanism of inhibiting, due to the effect of the magnesium or calcium bicarbonate on it. When temporary hard water flows over the metal it can assist on the nucleation of carbonates, allowing the reactions near to the equilibrium and forming precipitations on the metal surface. These precipitations, like a $CaCO_2$, cover the cathodic area, protecting the metal. So these cathodic inhibitors depend only on the chemistry of the water, are not due the metal composition.

• Mixed inhibitors that interacts with both anodic and cathodic reactions.

3) Mixed inhibitors: Mixed inhibitors are usually organic compounds containing nitrogen and sulfur.

These are film–forming compounds that reduce both the cathodic and anodic reactions.

Naturally the occurrence of molecules exhibiting a strong affinity for metal surfaces compounds showing good inhibition efficiency and low environmental risk. These inhibitors bound up a protective hydrophobic film adsorbed molecules on the metal surface, which provides a barrier to the dissolution of the metal in the electrolyte. They must be soluble or dispersible in the medium surrounding the metal.

The most commonly used mixed inhibitors are silicates and phosphates used in domestic water softeners to prevent the formation of rust water.

Mixed inhibitors reduce the corrosion rates both anodic and cathodic reactions.
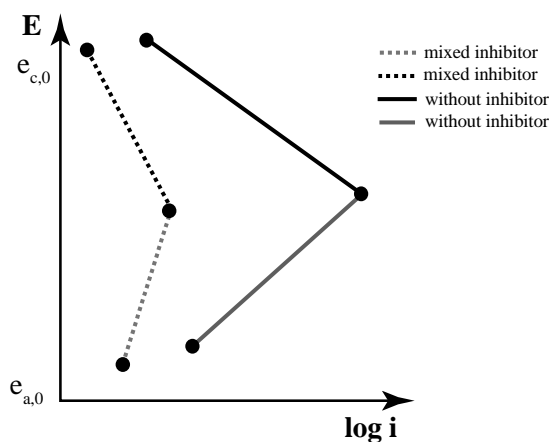
Mixed inhibitors are organic compounds (contain nitrogen and sulphur)

Potential, E
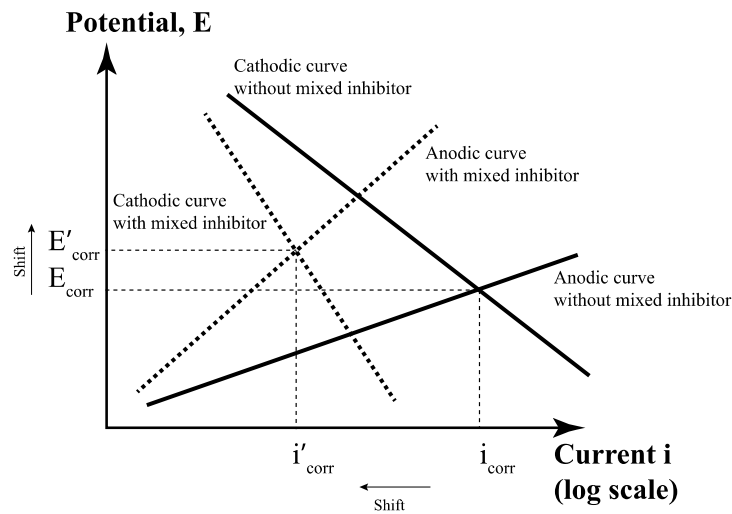
The inhibitor efficiency could be calculated by the following equation

$$\eta \% = \frac{i_0 - i_1}{i_0} \times 100$$

η: inhibitor efficiency

i_0: corrosion rate of metal without inhibitor

i_1: corrosion rate of metal with inhibitor

Another classification is as follow:

i) Inorganic inhibitors

ii) Organic inhibitors

i) Inorganic inhibitors contain inorganic ions such as NO_2^-, CrO_4^-

ii) Organic inhibitors contain oxygen nitrogen sulphur and heterocyclic compounds.
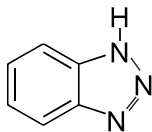
 Benzotriazole

These inhibitors are adsorbed on the metal surface blocking the active corrosion sites.

Some examples are amines, aldehydes, heterocyclic nitrogen compounds, sulphur–containing compounds.

The efficiency of organic inhibitors depends on

• the chemical structure, like the size of organic molecule

• aromacity and conjugated bonding and the carbon chain length

• type and number of bonding atoms or groups in the molecule (π or σ bonds)

• nature and the charges of the metal surface of adsorption mode like bonding strength to metal substrate

• ability for a layer to become compact or cross–linked

• capability to form a complex with the atom as a solid within the metal lattice

• type of electrolyte solution like adequate solubility in the environment.

The efficiency of these organic corrosion inhibitors is related to the presence of polar functional groups with S, O or N atoms in the molecule, heterocyclic compounds and pi (π) electrons, generally have hydrophilic or hydrophobic parts ionizable. The polar function is usually regarded as the reaction center for the establishment of the adsorption process.

Inhibitor which is effective for a metal or corrosion media does not affect the at same corrosion environment for another metal. Therefore, it is necessary to make experimental studies on the selection of corrosion inhibitors for each metal or alloy and corrosion environment.

Several corrosion inhibitors have been developed from natural raw materials, to protect different metals that are used in quotidian life. Eventually, collaborations of research groups have been investigated about the mechanisms of the corrosion inhibition processes, the optimum operation conditions of corrosion inhibitors, as well as the most appropriate type of molecule for each metal and corrosive media system.

For all types of inhibitors, we should consider some environmental actions factors because some elements such as metals, pH, composition, impurities, agitation, temperature, geometry of the system, the concentration of inhibitor and the mixture of one or more inhibitors may change the anti-corrosive mechanism.

INDUSTRIAL APPLICATIONS

There are several industrial applications of inhibitors. These are follows:

1) Acid pickling: Prevent the attack in the metal due to the acid solution in which metal gets cleaned of mill scale (bark lamination), and also prevented the subsequent hydrogen evolution inhibitors are added, typically organic, must be soluble or dispersed in the solution. Examples: thiourea and amino and its derivatives, propargyl alcohol.

2) Oil industry: sodium carbonates or organic amines complex are employed to reduce the corrosive effect of CO_2, H_2S and organic acids, enabling the use of more cheaper materials and less resistant to corrosion in wells extracting crude oil. Pipes for gasoline and kerosene are employed sulphonated oils, sodium nitrite. Oil well uses up fatty amines, fatty acids, imidazolines and quaternary ammonium salts. Internal pipe corrosion occurs in wet gas transportation due to condensation of water containing dissolved corrosive gases. Corrosion is caused by the dissolution of the corrosive gases, such as carbon dioxide and hydrogen sulfide as well as condensation of acid vapors.

3) Water transmission and distribution systems: is used corrosion inhibitor in combination with pH adjusters and alkalinity control towards an efficient protection. The most common inhibitors are phosphates, amines volatiles (Cyclohexylamine, morphine).

4) Concrete: To improve the durability of reinforced concrete structures, which are impaired due the high alkalinity, are used corrosion inhibitors, mixed with cement or concrete paste. An example is phosphate ion.

5) Boiler: Thermoelectric use, in general, Ammonia, Cyclohexyl-amine, alkanol and Morpholine as inhibitors in boilers in various processes. The inhibitors, also, are added by the hydrochloric acid used for the solubilization of limescale to prevent the attack on pipes.

In spite of many corrosion inhibitors have high inhibition efficiencies, several have undesirable side effects even at very low concentrations, due to their toxicity to humans, deleterious environmental effects and high costs. The toxicity of these compounds is the first dangerous problem. Therefore scientists investigate the use of non-toxic natural products as inhibitors that are eco-friendly. In recent years plant extracts are used as corrosion inhibitors, these compounds also show some good properties such as cheap, biodegradable and renewable.

REFERENCES

[1] V.E. Carter, *"Metallic Coatings for Corrosion Control"*, 1st Edition, 1977.
[2] A. Vimalanandan, A. Bashir and M. Rohwerder, *Materials and Corrosion*, 54(2014), 392.
[3] P.P. Behnam, *Anti–Corrosion Methods and Materials*, 9(1962), 365.
[4] R. Hasanov, S. Bilgic, G. Gece, *Journal of Solid State Electrochemistry*, 15(2011), 1063.
[5] E.C. Gomes, M.A.S. Oliveira, *Surface Coat. Tech.*, 205(2011), 2857.
[6] M. Shabani–Nooshabadi, S.M. Ghoreishi, M. Behpour, *Electrochim. Acta*, 54(2009), 6989.
[7] S. Uneri, *"Korozyon ve Onlenmesi"*, 2nd Edition, 2011, Ankara.
[8] M. Doruk, *"Metalik Malzemeler ve Korozyon"*, 1st Edition, 2014, Ankara.
[9] S.K. Shukla, A.K. Singh and M.A. Quraishi, *Int. J. Electrochem. Sci.*, 7(2012), 3371.
[10] M. Finggar and J. Jackson, *Corros. Sci.*, 2009, 51, 868.

[11] G.S. Oz and S. Bilgic, *Int. J. Corros. and Scale Inh.*, 7(2018), 390.

[12] O.C. Akalezi, E.E. Oguzie, Evaluation of anticorrosion properties of Chrysophyllum albidum leaves extract for mild steel protection in acidic media. *Int. J. Ind. Chem.*, 7(2016), 81–92.

[13] G. Ji, S. Anjum, S. Sundaraun and R. Prokash, Musa paradisica peel extract as green corrosion inhibitor for mild steel in HCl solution, *Corros. Sci.*, 90(2015), 107–117.

[14] S. Deng, X, Li, Inhibition by Ginkgo leaves extract of the corrosion of steel in HCl and H_2SO_4 solutions, *Corros. Sci.*, 55(2012), 407–415.

The Concentration Dependence of the Inhibition Efficiency of Sodium Tetraborate for Steel Corrosion in Alkaline Media

Gul Seda Oz[1], Semra Bilgic[1]

Abstract

Corrosion is the deteoration of metals and alloys as a result of chemical and electrochemical reactions between them and surrounding environment. Corrosion is unwanted phenomenon. Because it has harmful effects for human health and it causes several accidents and great losses in the economies. Harmful effects of corrosion can be prevented in several ways such as metallic coatings, non-metallic coatings, anodic and cathodic protection of metals and use of chemical compounds called inhibitors.

Inhibitors can be organic and inorganic compounds. Organic inhibitors contain oxygen, nitrogen, sulphur and heterocyclic compounds. Inorganic inhibitors contain inorganic ions such as NO_2^-, CrO_4^-. Studies with inorganic inhibitors are quite rare.

In this study the inhibition effect of sodium tetraborate ($Na_2B_4O_7.10H_2O$) on the corrosion of steel has been investigated in 3% and 5% KOH. Corrosion parameters have been determined using Tafel extrapolation and impedance spectroscopy methods by the adding of 1%-7% $Na_2B_4O_7$ in two KOH concentrations. According to the experimental findings the inhibition efficiency of $Na_2B_4O_7$ in both KOH media increases in 1%-4% concentration range whereas it decreases in 5%-7% concentration range. However, in this concentration range of sodium tetraborate, corrosion rates are less than those without inhibitor.

Keywords: Corrosion, inhibitor, sodium tetraborate.

1. DEFINITION OF CORROSION

The term of corrosion can be defined as the interaction of metals and alloys with surrounding environments.

Corrosion is an electrochemical process it involves the transfer of electrons between a metal surface and aqueous electrolyte solution. Formation of rust on iron and steel and other corrosion products, darkness on silver, the formation of green patina on copper and brass, cracks in aircraft, automobiles, boats, gutters, ships can be given as a few examples.

The problem of corrosion is common and dangerous phenomenon in various sectors, such as chemical industry, petrochemical, shipbuilding construction, automotive, aviation, railway, maritime and others.

Corrosion wastes the sources and products, stops production and causes various accidents. Corrosion causes important economical losses.

Corrosion is a major factor in the investment and production of the industry. According to some estimations, the cost of corrosion to a national reaches to 3.5–5.5% of the gross national products.

It is predicted that twenty percent of iron produced is lost by corrosion every year.

Due to its different harmful effects, corrosion is unwanted phenomenon, it is important to minimize or control metals and alloys corrosion technically, economically, environmentally which corrosion is a major industrial problem. There are several methods to prevent or reduce corrosion such as

➢ paintings,
➢ coatings,
➢ cathodic
➢ protection,
➢ anodic production and
➢ adding chemical

substances as called inhibitor.

The use of inhibitors can be considered as one of the best methods to prevent metals and alloys against corrosion.

A corrosion inhibitor is a chemical substance added in small concentrations in corrosive medium or an environment, effectively decreases the corrosion rate. These compounds prevent corrosion either by being adsorbed on metals and alloys or by forming a protective layer or by causing the formation of unsoluble complex on the surface of metals and alloys. These compounds are

i) inorganic compounds
ii) organic compounds

2. EXPERIMENTAL METHOD
Electrochemical experiments were carried out in a pyrex cell.

Experimental cell

Table 1. The chemical composition (wt %) of steel used in the study

C	Si	Mn	P	S	Cr	Ni	Fe
0.03	1.01	2.03	0.042	0.03	18.76	8.58	69.52

This steel, 5 mm in diameter was embedded in methyl metacrylate, mechanically polished with 1200 grit emery paper. Later it was washed with bidistilled water then placed in the test solutions.

All solutions were de-aerated with nitrogen for 30 minutes in the cell prior to each experiment.

The nitrogen was throughly purified from oxygen using BASF Catalyst R–311. During each experiment, solutions were mixed with a magnetic stirrer.

Saturated calomel electrode (SCE) was used as reference electrode and platinum foil was used as counter electrode.

All potentials were measured versus SCE.

The experiments were carried out using the combined system Wenking LB 75 L laboratory model potentiometer, Wenking VSG 72 model voltage-scan generator, Yokogawa Technicorder Type 3077 recorder, BM 101 thermostat.

The scan rate was chosen as 2.5 mVs^{-1}.

Bidistilled water was used to prepare the solutions. The concentrations of KOH were selected as 3% and 5%. The concentrations of sodium tetraborate were chosen as 1% – 7%. The inhibition efficiencies of temperature were also investigated from 25°C to 70°C from 15°C increments.

In this study, the experiments were repeated at least three times and the average values are given.

In this study to determine the corrosion rates the anodic and cathodic Tafel regions extrapolating to corrosion potential was used.

There are several methods to determine the corrosion rates.

These are

 i) Mass loss method

 ii) Tafel extrapolation method

iii) Impedance spectroscopy method

Tafel extrapolation method: If the applied external current exceeds 10 times than the corrosion current polarization curves show a breaking. After this breaking point a linear region begins in the polarization curve (E–log i). This region is called Tafel region and the slope is called Tafel slope.

$\eta = a + b \log i$ Tafel equation

where η is over voltage (over potential), i is corrosion current density, a and b are constants.

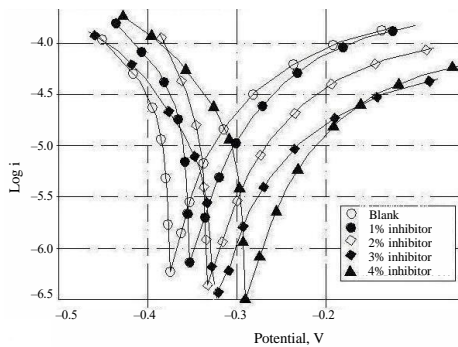*(a)*   *(b)*
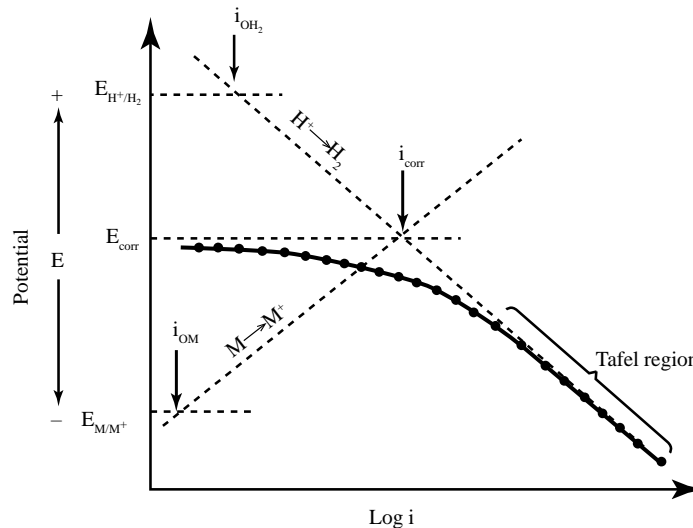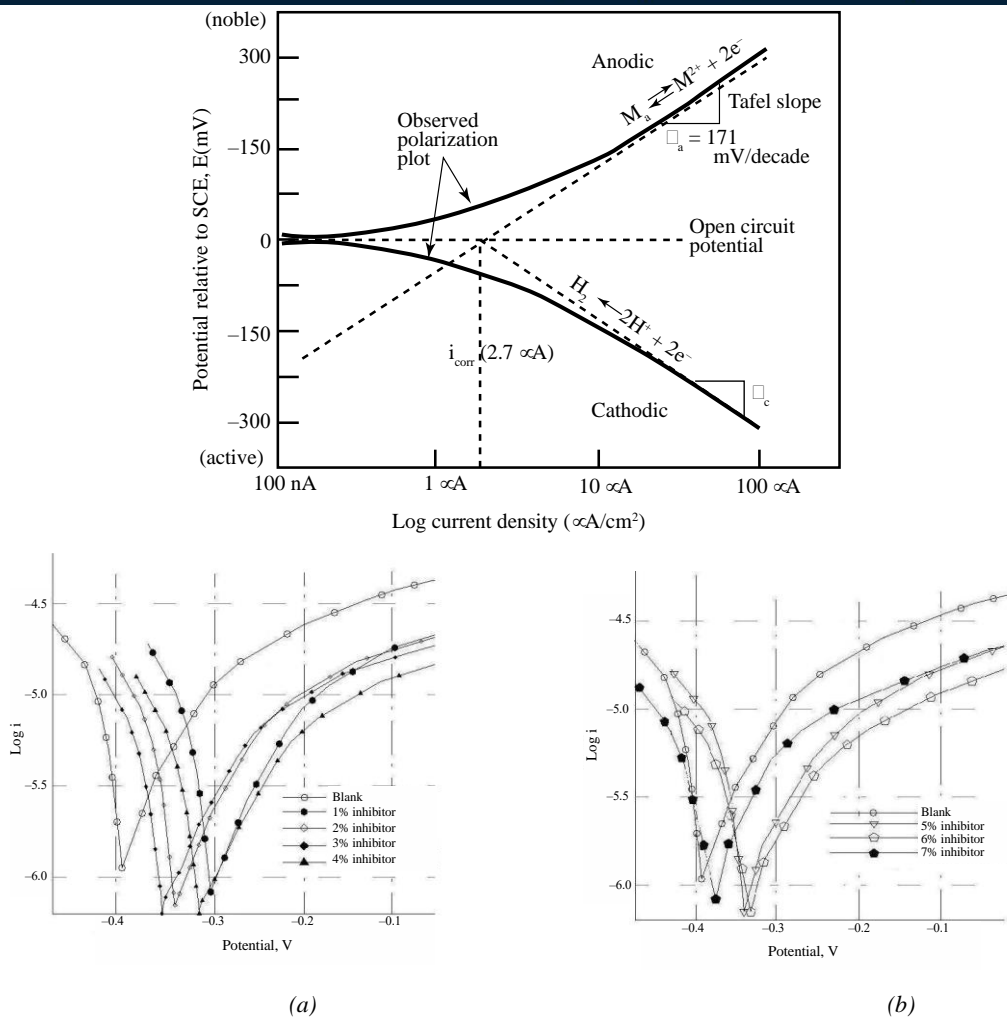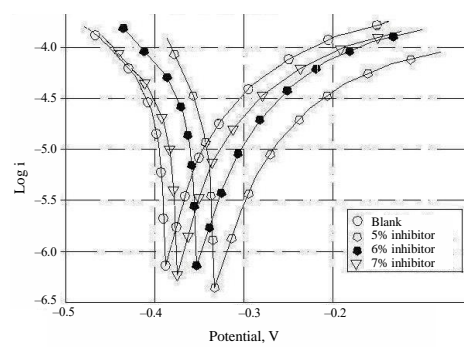
Fig. 1a. The anodic and cathodic polarization curves in 3% KOH in the absence and presence of various concentrations of Na₂B₄O₇ at 25ºC.
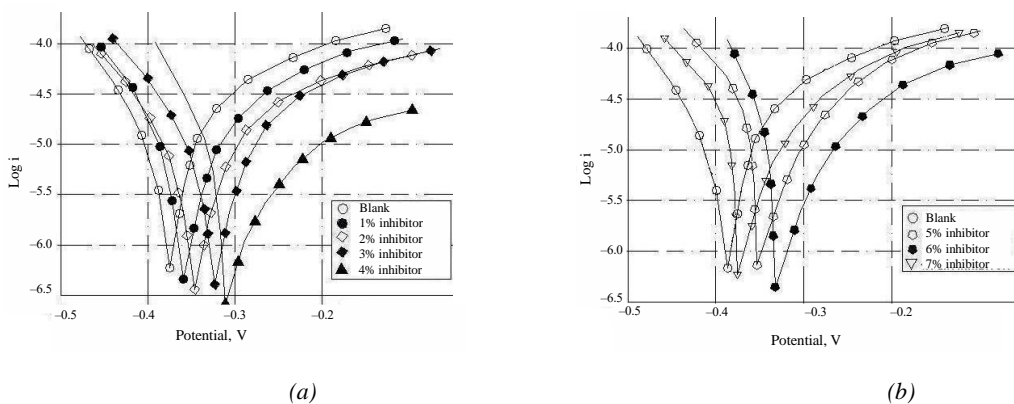
Fig. 1b. The anodic and cathodic polarization curves in 3% KOH in the absence and presence of various concentrations of Na₂B₄O₇ at 25ºC
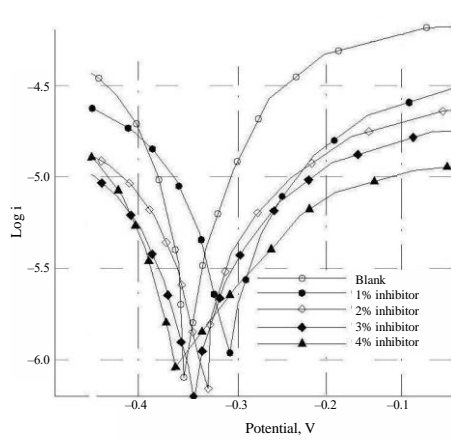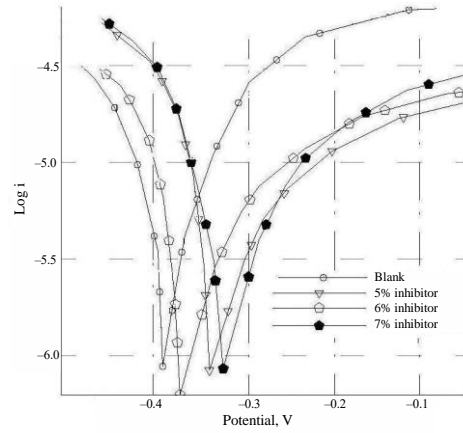
(a)   *(b)*

Fig. 2a. The anodic and cathodic polarization curves in 3% KOH in the absence and presence of various concentrations of Na$_2$B$_4$O$_7$ at 55°C.

Fig. 2b. The anodic and cathodic polarization curves in 3% KOH in the absence and presence of various concentrations of Na$_2$B$_4$O$_7$ at 55°C

(a)   *(b)*

Fig. 3a. The anodic and cathodic polarization curves in 5% KOH in the absence and presence of various concentrations of Na$_2$B$_4$O$_7$ at 25°C.

Fig. 3b. The anodic and cathodic polarization curves in 5% KOH in the absence and presence of various concentrations of Na$_2$B$_4$O$_7$ at 25°C

(a)   *(b)*

Fig. 4a. The anodic and cathodic polarization curves in 5% KOH in the absence and presence of various concentrations of Na₂B₄O₇ at 55ºC.

Fig. 4b. The anodic and cathodic polarization curves in 5% KOH in the absence and presence of various concentrations of Na₂B₄O₇ at 55ºC

Table 2a. Corrosion parameters such as corrosion potentials (E_cor) anodic and cathodic Tafel slopes (β_a and β_c), corrosion current densities (i_cor) and percentage inhibition efficiencies (η%) in various concentrations of Na₂B₄O₇ in 3% KOH at 25ºC.

Inhibitor concentration (%)	E_{cor} (mV)	β_a	β_c	i_{cor} ($\mu A/cm^2$)	η %
3% KOH (blank)	−379	43	110	2.77	−
1	−366	38	107	1.99	28
2	−353	35	106	1.79	35
3	−359	41	108	1.58	43
4	−347	17	143	1.35	51
5	−361	41	103	1.44	48
6	−353	44	112	1.80	35
7	−376	46	109	1.94	30

The percentage inhibition efficiency (η%) is calculated from the following equation

$$\eta\% = \frac{i_0 - i_1}{i_0} \times 100$$

where i_0 and i_1 are the corrosion current densities without and with inhibitor.

Table 2b. Corrosion parameters such as corrosion potentials (E_cor) anodic and cathodic Tafel slopes (β_a and β_c), corrosion current densities (i_cor) and percentage inhibition efficiencies (η%) in various concentrations of Na₂B₄O₇ in 3% KOH at 40ºC.

Inhibitor concentration (%)	E_{cor} (mV)	β_a	β_c	i_{cor} ($\mu A/cm^2$)	η %
3% KOH (blank)	−347	51	118	3.80	−
1	−357	43	106	2.29	40
2	−354	38	102	2.09	45
3	−343	41	110	1.66	56
4	−355	39	112	1.41	63
5	−348	44	118	1.87	50
6	−359	46	120	2.20	42
7	−367	49	119	2.29	39

Table 2c. Corrosion parameters such as corrosion potentials (E_{cor}) anodic and cathodic Tafel slopes (β_a and β_c), corrosion current densities (i_{cor}) and percentage inhibition efficiencies ($\eta\%$) in various concentrations of $Na_2B_4O_7$ in 3% KOH at 55ºC.

Inhibitor concentration (%)	E_{cor} (mV)	β_a	β_c	i_{cor} (µA/cm²)	η %
3% KOH (blank)	−343	61	119	5.01	–
1	−328	54	116	2.95	41
2	−347	50	114	2.29	54
3	−350	48	116	1.82	64
4	−356	41	108	1.48	70
5	−340	49	103	2.88	42
6	−351	48	110	3.31	33
7	−338	47	107	3.54	29

Table 2d. Corrosion parameters such as corrosion potentials (E_{cor}) anodic and cathodic Tafel slopes (β_a and β_c), corrosion current densities (i_{cor}) and percentage inhibition efficiencies ($\eta\%$) in various concentrations of $Na_2B_4O_7$ in 3% KOH at 70ºC.

Inhibitor concentration (%)	E_{cor} (mV)	β_a	β_c	i_{cor} (µA/cm²)	η %
3% KOH (blank)	−353	64	118	5.49	–
1	−368	53	120	3.55	35
2	−371	51	116	2.63	52
3	−360	47	109	1.90	65
4	−355	43	108	1.51	72
5	−349	51	117	3.54	35
6	−362	56	118	4.36	20
7	−356	53	106	4.78	12

Table 3a. Corrosion parameters such as corrosion potentials (E_{cor}) anodic and cathodic Tafel slopes (β_a and β_c), corrosion current densities (i_{cor}) and percentage inhibition efficiencies ($\eta\%$) in various concentrations of $Na_2B_4O_7$ in 5% KOH at 25ºC.

Inhibitor concentration (%)	E_{cor} (mV)	β_a	β_c	i_{cor} (µA/cm²)	η %
5% KOH (blank)	−380	56	109	3.89	–
1	−371	44	104	2.51	35
2	−374	41	112	2.24	42
3	−369	47	107	2.14	45
4	−372	49	110	1.38	64
5	−384	50	111	1.47	62
6	−381	58	107	1.66	57
7	−390	43	116	1.90	51

Table 3b. Corrosion parameters such as corrosion potentials (E_{cor}) anodic and cathodic Tafel slopes (β_a and β_c), corrosion current densities (i_{cor}) and percentage inhibition efficiencies ($\eta\%$) in various concentrations of $Na_2B_4O_7$ in 5% KOH at 40ºC.

Inhibitor concentration (%)	E_{cor} (mV)	β_a	β_c	i_{cor} (µA/cm²)	η %
5% KOH (blank)	−379	66	116	4.23	–
1	−369	61	109	2.41	43
2	−360	57	112	2.19	48
3	−358	51	107	1.77	58
4	−366	44	103	1.69	60
5	−380	49	119	1.81	57

| 6 | −375 | 51 | 120 | 2.32 | 45 |
| 7 | −379 | 47 | 108 | 2.45 | 42 |

Table 3c. Corrosion parameters such as corrosion potentials (E_{cor}) anodic and cathodic Tafel slopes (β_a and β_c), corrosion current densities (i_{cor}) and percentage inhibition efficiencies ($\eta\%$) in various concentrations of $Na_2B_4O_7$ in 5% KOH at 55ºC.

Inhibitor concentration (%)	E_{cor} (mV)	β_a	β_c	i_{cor} ($\mu A/cm^2$)	η %
5% KOH (blank)	−368	77	121	5.60	−
1	−369	64	118	3.24	42
2	−371	63	120	2.46	56
3	−374	60	119	1.96	65
4	−372	58	106	1.62	71
5	−380	53	117	2.91	48
6	−383	48	112	3.47	38
7	−381	43	116	3.64	35

Table 3d. Corrosion parameters such as corrosion potentials (E_{cor}) anodic and cathodic Tafel slopes (β_a and β_c), corrosion current densities (i_{cor}) and percentage inhibition efficiencies ($\eta\%$) in various concentrations of $Na_2B_4O_7$ in 5% KOH at 70ºC.

Inhibitor concentration (%)	E_{cor} (mV)	β_a	β_c	i_{cor} ($\mu A/cm^2$)	η %
5% KOH (blank)	−384	77	121	5.60	−
1	−393	64	118	3.72	33
2	−391	63	120	2.51	55
3	−396	60	119	2.14	61
4	−401	58	106	1.51	73
5	−400	53	117	3.08	45
6	−399	48	112	3.58	36
7	−403	43	116	3.81	32

According to the results obtained in 3% and 5% KOH media, sodium tetraborate acts as an inorganic inhibitor.

The corrosion rates at 1% – 4% $Na_2B_4O_7$ concentration in both KOH environments gradually decrease but increase somewhat in the range of 5% – 7% concentrations of $Na_2B_4O_7$.

Corrosion rates in this range are although slightly less than those in the uninhibited medium in 5% – 7% inhibitor range.

This is probably due to the presence of more active sites on the steel surface at low concentration of inhibitor, and formation of a insoluble complex on the surface with a slight increase in its concentration. By the coverage of the surface, the inhibitor efficiency is gradually decreasing.

Accordingly, borate shows a better inhibition property in 5% KOH medium compared to that in 3% KOH medium.

We can explain these findings according to the chemical structure of $Na_2B_4O_7$.

As seen from the structure, the compound has the properties of both Lewis acid and Lewis base.
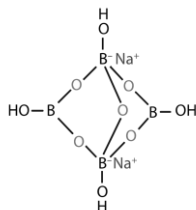
The chemical structure of sodium tetraborate ($Na_2B_4O_7$)

The increase in the inhibition effect in the 1% – 4% concentration range in both percentage KOH media may be considered to be due to the negatively charged boron atom, which gives a basic characteristic to the molecule, and the surface-coverage effect of $Na_2B_4O_7$ is apparent in the mentioned concentration range. However, at a concentration range of 5% – 7%, the compound combines with KOH and losses its protective properties. As the concentration of $Na_2B_4O_7$ increases, Fe^{2+} ions are retained by borax and Fe^{2+} replaces Na^+ in the complex.

The surface is blocked by the coverage of $B_4O_7^{2-}$ ions on the steel surface and the formation of a protective layer of Fe_2O_3 oxide. Experimental results also support this view.

Conclusion

As a result it can be said that sodium tetraborate acts as corrosion inhibitor for the steel in both 3% KOH and 5% KOH.

The corrosion rates reduce with increasing concentrations of inhibitor in both 3% KOH and 5% KOH media.

It has been determined that inhibition efficiencies for the same concentrations increase with increasing the temperature. These findings have been determined for both KOH media.

REFERENCES

[1] Abd El Haleem, S.M., Abd El Wanees, S., Abd El Aal, E.E., Diab, A. 2010. Electrochemical behaviour of organic and inorganic complexes of Zn(II) as corrosion inhibitors for mild steel: Solution phase study. *Corros. Sci.*, 292–302.
[2] Amer, M.A., Khamis, E. and El–Sesani, G. 2002. Effect of temperature on stability of adsorbed inhibitors on steel in phosphoric acid solutions. *J. Appl. Electrochem.*, 32, 149–156.
[3] El-Sherbini, S.M., Abd-El-Wahab, M.A., Amin, M., Amin, A., Deyab, M.A. 2006. Electrochemical behaviour of tin in sodium borate solutions and the effect of halide ions and some inorganic inhibitors. *Corros. Sci.*, 48, 1885–1898.
[4] Ilevbare, G.O., Burstein, G.T. 2003. The inhibition of pitting corrosion of stainless steels by chromate and molybdate ions. *Corros. Sci.*, 45, 1545–1569.
[5] Królikowski, A., Kuziak, J. 2011. Impedance study on calcium nitrite as a penetrating corrosion inhibitor for steel in concrete. *Electrochim Acta.*, DOI: doi: 10.1016/jelectata. 2011.01.069.
[6] Lugi, C., Dell'Era, A., Pasquali, M. 2009. Nickel–cobalt electrodeposited alloys for hydrogen evaluation in alkaline media. *Int. J. Hyd. Ener.*, 34, 2101–2106.
[7] Patel, N., Patton, B., Zanchetta, C., Fernandes, R., Guella, G., Kale, A., Miotello, A. 2008. Pd–C powder and thin film catalyst for hydrogen production by hidrolysis of sodium borohydride. *Int. J. Hyd. Ener.*, 33, 287–292.
[8] Urgen, M., Cakir, A.F. 1991. The effect of molybdate ions on the temperature dependent pitting potential of austenitic stainless steel in neutral chloride solutions. *Corros. Sci.*, Vol: 32, 835–852.

Retrofitting of Modern Heritage Masonry Infilled RC Buildings

T.Serhat Bozkurt[1], Baris Sayin[2], A.Sertac Karakas[3], Cemil Akcay[4]

Abstract

In retrofitting applications of historical buildings, it is considered that preserving historical heritage is an important factor. However, to perform such applications within the scope of retrofitting of the buildings should be carried out in such a way that it should not lose integrity with the originality of the buildings by employing an interdisciplinary approach. This study focuses on rehabilitation studies of a historical masonry infilled RC building; and thus, the study aims to be a reference for retrofitting of the structures. In the present study, a block building at the Faculty of Science and Literature located in Istanbul University registered as a cultural asset to be protected by the Regional Board of Protection of Cultural Heritage is investigated. In the scope of the study, it is presented that retrofitting techniques applied using carbon fiber, steel mesh, steel profile and shotcrete over structural members such as external walls, infilled walls, columns, beams and foundation in the block building.

Keywords: Historical structure, RC building, Retrofitting

1. INTRODUCTION

The need for repair and renovation arises due to the end of useful life of the materials which constitute a historical structure and in this respect it is of great necessity that all the other factors that threaten the integrity of the structure should be made clear along with the structural members and materials which come to the end of their useful life [1]. In this context, performed rehabilitation applications to restoration of historical structures are regarded as a significant factor in handing cultural heritage down next generations and keeping them alive by preservation. However, it is known that such practices in the above mentioned structures should be carried out in such a way that they do not violate the originality of the structure through an interdisciplinary approach.

Rehabilitation is defined as repair of a cultural asset by preserving its characteristics which constitute its historical identity, cultural values and changing it in such a way that it meets today's needs, and thus, making it functional. Increasing the strength of a structure against damages through interferences which were carried out by repair applications such as strengthening and renovation or decreasing the problems of a structure are regarded among rehabilitation applications. Repair which takes an important and a great role in preserving is one of the significant pillars of restoration. In conserving an architectural work, the act of repairing which includes strengthening, reintegration and renovation plays a key role in maintaining the originality value. Repair of a structure is explained as any kind of intervention which aims to rehabilitate it, recover the damage or breakdown the structure that it has undergone [1].

To make a decision regarding intervention in the restoration of historical buildings is a crucial issue. Before intervention, it is important to choose new material to be used in the applications in accordance with the existing material of the building and to use suitable new materials in the restoration which are appropriate for the

---

[1] *Istanbul University, Department of Construction and Technical Affairs, 34116, Fatih/Istanbul, Turkey. bozkurtt@itu.edu.tr*

[2] *Corresponding author: Istanbul University-Cerrahpasa, Department of Civil Engineering, 34320, Avcilar/Istanbul, Turkey. barsayin@istanbul.edu.tr*

[3] *Istanbul University, Department of Construction and Technical Affairs, 34116, Fatih/Istanbul, Turkey. skarakas@istanbul.edu.tr*

[4] *Istanbul University, Department of Architecture, 34116, Fatih/Istanbul, Turkey. cakcay@istanbul.edu.tr*

building's material disposition and chemistry. In this scope, generally two types of binder are used in structures: portland cement and lime. The structural characteristics of portland cement and lime are quite different from each other. This is because the difference between the thermal expansion coefficients of lime mortar and portland cement mortar leads to condensation differences, the mechanical strength and young's modulus of cement mortar is higher than those of lime mortar, and there are more micro spaces in portland cement compared to macro spaces in lime. It is significant to choose the mortar type which is similar to the original building structure in restoration applications due to the differences in the material behavior of the binders in question. For instance, in the restoration applications of masonry buildings where lime binder is used, if cement binder is used, the evaporation of the existing moisture in the structure gets hard because the pores of this type of mortar are too small. Since there becomes freezing in low temperature and evaporation in high temperature in this type of buildings, the repair plaster of cement comes off easily from the building or the moisture of the building increases. For this reason, it is a necessity to use lime binder mortar which is appropriate for the original material and in accordance with the physics of the building in masonry buildings constructed with lime binder mortar. Accordingly, it is thought that it is important to use cement based mortar which suitably works with the original material in applications to original, historical, RC concrete buildings [2-4].

The present study is mainly concerned with the restoration practices of a building which include foundation rehabilitation and strengthening applications of columns and infilled walls carried out without damaging the original structure of the cultural asset. In the study, the need for strengthening by determining the present condition of the building and the details of the strengthening technique to be used were determined by using SAP2000 software [5]. To do this, 16th block building at the Faculty of Science and Literature of Istanbul University was chosen as a case study. The details regarding steel mesh and carbon fiber fabric applications on the interior walls of the building, steel mesh and shotcrete application in the facade, rehabilitation applications including strengthening the RC columns, RC beams and RC slabs were given in this study.

2. HISTORICAL PROCESS

Being one of the outstanding structures of the Republic Period, the block buildings at the Faculty of Science and Literature of Istanbul University located in Vezneciler, Fatih, Istanbul, have been registered as a cultural asset to be preserved by Istanbul, no. IV Regional Board of Protection of Cultural Heritages. Designed by Architect Sedat Hakki Eldem and Emin Onat, the buildings of the Faculty of Science and Literature consist of 21 blocks and has 69200 m^2 closed area. The buildings reflect the architectural characteristics of the period in the city and thus has a monumental outlook (Fig. 1).
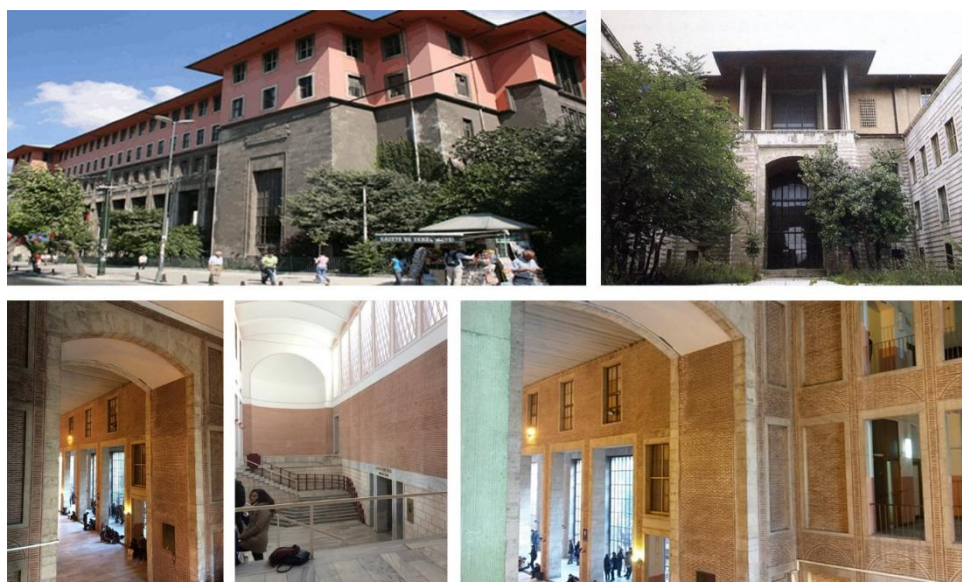

Figure 1. Facade and indoor views of the building at the Faculty of Science and Literature of Istanbul University

The building, used as the Faculty of Science and Literature of Istanbul University, has members such as fenestrations and eaves formings of the traditional Ottoman domestic architecture in the history of Turkish Architecture. In the building designed by Architecture Sedat Hakki Eldem there are rectangular and square courts surrounded by monumental and stone facade buildings. As the building was constructed at the beginning of the 1940s and cement was started to be used commonly at the time, the indoor shell forms (vaults, arcades, hemidomes, etc.) which have references of the Turkish architecture history were made by using RC material. Furthermore, with the help of RC load-bearing system the use of the eave forming, which is a feature of the Ottoman domestic architecture, provided a larger space in this building. The use of RC load-bearing system has a great contribution to the magnificence, high ceilings and greatness of the building entrances. Additionally, the spacious interior spaces with high ceilings via the use of RC load-bearing system enrich the monumental value of the building with its amazing perspective views.

3. REHABILITATION APPLICATIONS

Strengthening the foundation, columns, beams and wall members was carried out in the rehabilitation process of the 16th block at the Faculty of Science and Literature of Istanbul University (Fig. 2). Being one of the environmental factors, the groundwater had penetrated into the building foundation and the basement floor had foundered, so that the building was exposed to moisture and dampness for a long time, which has influenced the building physics statically. The intervention decisions for strengthening were made carefully so that they would not violate the space organization and the original plan of the building. The cement based strengthening binder was used in order to work in harmony with the present RC members as far as the material behavior is concerned in the strengthening applications of the building. The carbon fiber applications which were able to integrate with the load-bearing system were carried out in the 16th block building, and also steel profile strengthening applications in the columns, beams and ceilings at the basement floor to go with the existing RC system were performed. On the ground floor the columns were strengthened via jacketing applications.
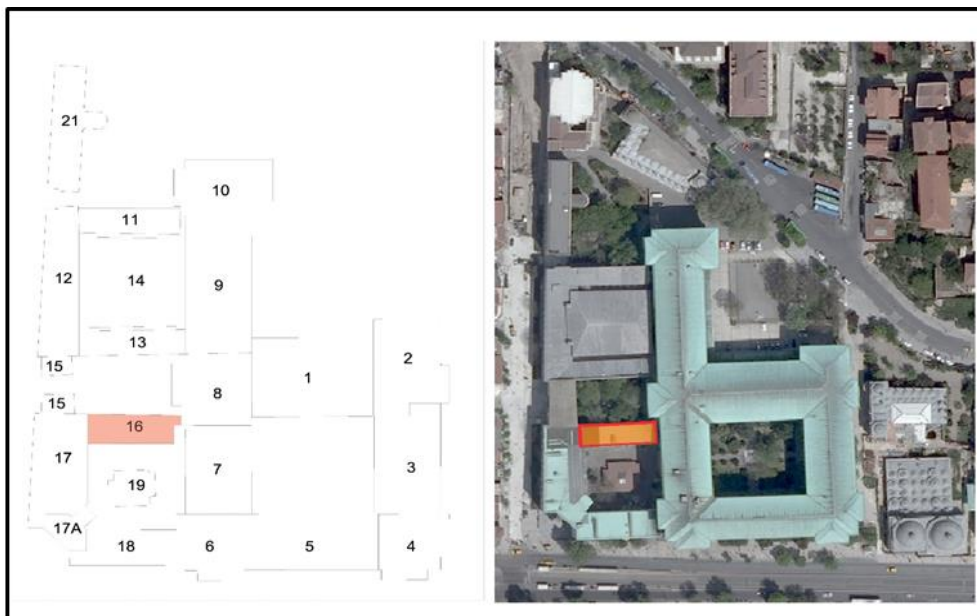
Figure 2. The layout plan and satellite photograph of the 16th block

3.1. Strengthening Applications in the Foundation and on the Basement Floor

Before the restoration applications in the 16th block of the Faculty of Science and Literature, it was determined that the below of the foundation was filled with water, and due to the effect of the groundwater, under the foundation there was disintegration and deterioration in the concrete of the columns and beams (Fig. 3). For this reason, first the groundwater under the foundation was drained. After the most of the groundwater under the foundation was drained, well points under the foundation were determined. In the well points of the lowest grade was gathered the groundwater and it was directed towards the sewage drain through a water pump. Thereby, the negative effects of the groundwater in the foundation on the present load-bearing system were eliminated.

Figure 3. The groundwater and the situation of load-bearing members in the foundation level

First the groundwater in the foundation had been drained. Following this it was determined that there was no deterioration in the foundation members that had been under water for a long time. As for the columns and beams which had not been exposed to the water effect, the steel bar which came out due to the break-off of the cover concrete were dyed with antirust; and thus they were put under protection.

After the existing negative conditions were restored, the next step was to implement the intervention decisions made about the building. They were carried out in accordance with the strengthening project approved by Istanbul IV Regional Board of Protection of Cultural Heritage [6]. Fig. 4 shows the application plan and details regarding the foundation construction of the design project approved by the above mentioned board.
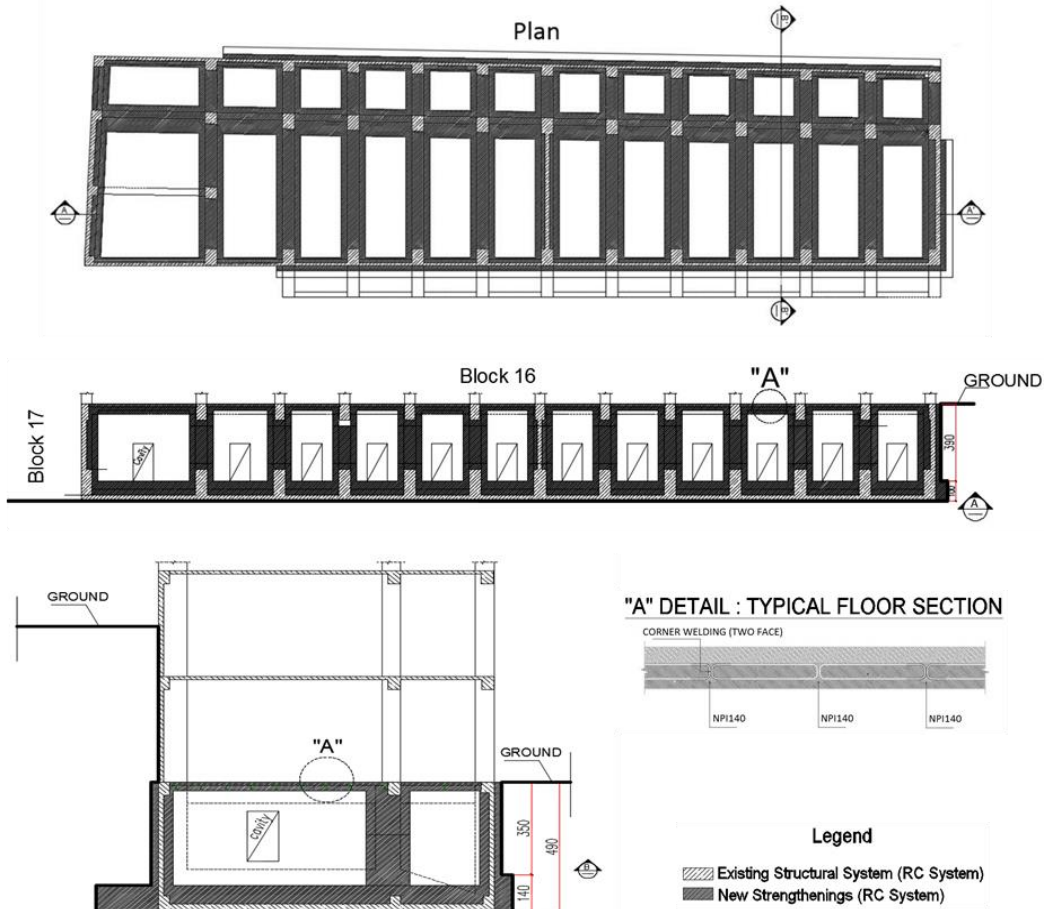
Figure 4. The plan and section details regarding the foundation construction

In addition to the shear wall under the soil, a 0.25 m. thick shear wall to strengthen was constructed and a well foundation construction was carried out by using wooden formworks. Since the building is located in the historical peninsula, the well foundation excavations were fulfilled with the consent and under the supervision of the Archeology Directorate. Considering the need that the well foundation construction should be at – 12.80 m. depth, the difficulty of removing the formworks which bear the soil load and the decay period of time of the materials under the soil, a wooden formwork system which breakdowns faster than plastic and steel material was chosen (Fig. 5). When the excavations and the construction of the strengthening wall on the exterior surface finished, a drain to prevent rain and underground water to be exposed was built in the lowest level of the building in order to preserve the building from underground water.

Figure 5. Well foundation construction (Excavation works at –12.80 m.)

Later on the strengthening works on the exterior surfaces of the building facing the court, the strengthening constructions on the lowest basement floor which is inside and not used were started. The dimension of the foundation, columns, beams and shear walls on the basement floor was increased, but as a result of this the space is narrowed. Due to the fact that, since the basement floor is not serviced, this situation was approved by the Protection Board. The application project of the above mentioned constructions is given in Fig. 6.
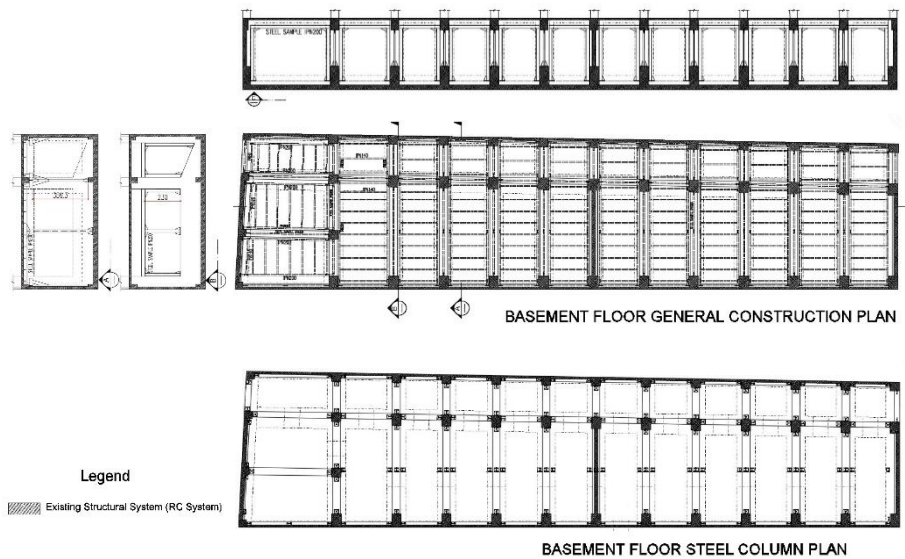
Figure 6. The design project regarding the steel constructions made in the strengthening of the basement floor

Anchor holes were made in the RC members and connecting rods were fixed in these holes by means of epoxy in order that jacketing in the strengthening of the lowest basement floor and the new shear walls would be integrated into the existing RC system. Once the building-up and the connections of the connecting rods were finished, the steel reinforcement connections of the shear walls, columns, beams and foundation were carried out. Because of the narrow working spaces, the existing columns and beams, the ineffective performance of the vibrator due to the large sections of the strengthened RC members, the self-compacting concrete was chosen. Therefore, before the wood formwork system was built in order to pour the self-compacting concrete, the connection of the steel reinforcement was finished. The strengthening applications were placed in the RC columns and beams. Fig. 7 shows the stages of the applications in the inner space of the basement floor.

Figure 7. Strengthening applications on the basement floor: (a) The drainage of the existing water, (b) The application of the steel profile columns and beams, (c) The anchor holes in the existing RC system and the connections of the rods via epoxy, (d) The connections of the steel bar in the foundation, columns and beams, (e) The connections of the shear walls between the columns, (f) The building-up the wooden formworks and the construction of the self-compacting concrete.

3.2. Strengthening Applications on the Ground and Typical Floors

In the strengthening applications on the typical floors apart from the basement floor, since these floors are actively being serviced, it was aimed to maintain the original structure of the building, and not to violate the space organization and the interior space. In the strengthening of the historical building, the rehabilitation applications were carried out only in the cement rendering layers and any new shear wall, column or beam was not built inside the building. There was not a serious deterioration in the load-bearing system because of the water effect and this became a significant factor in determining the constructions to be made. On the ground floor, jacketing application was fulfilled on the columns. On the interior walls, first steel meshing application was carried out, and then carbon fiber fabric was used to strengthen whereas on the external facade steel meshing application was fulfilled.

3.2.1 Jacketing Application

Anchor holes were made in the columns on the ground floor and connecting rods were fixed in these holes by means of epoxy. Firstly, the building-up and connections of the connecting rods were finished, secondly, the formwork was built, and finally the concrete was poured and jacketing application was carried out. Fig. 8 shows that performed jacketing application in the columns.

Figure 8. Jacketing application process on the ground floor (a-d)

3.2.2 Steel Meshing Application

The interior and external walls of the building were peeled and the original masonry brick layer was reached. After the plaster of the walls was ripped off, anchor holes were opened in the joint gaps of the masonry bricks and four connecting rods in a square meter were fixed. The anchor holes were filled with epoxy. When the connecting rods were fixed, the steel meshes were applied on the wall surfaces (Fig. 9). Following the steel meshing, shotcrete was applied on the surfaces, and therefore the whole wall surfaces were strengthened.

Figure 9. The using of the steel meshing in the wall strengthening

3.2.3 Carbon Fiber Applications

According to the design project of the building, the steel meshing was applied on the surfaces of the interior walls and then the carbon fibers were applied in crosswise in the carbon fiber application. The cement based strengthening mortar was used on the surfaces on which cross fibers were going to be applied in order to obtain a clean surface and the cross fibers were used on this surface. The cross carbon fibers were fixed and fastened on the wall surfaces with double component epoxy. The mineral based rendering was applied via epoxy on the carbon surfaces so that rendering could be used (Fig. 10).

Figure 10. The using of carbon fiber in the wall strengthening

CONCLUSIONS

16th block building at the Faculty of Science and Literature of Istanbul University was dealt with in this study which was carried out as the restoration project. Before the restoration, the groundwater on the basement floor was drained through pumps. By this way, the negative effects of groundwater in the foundation on the building physics were eliminated.

The applications which were carried out in the restoration of the building were as follows:

- The steel members were put in parallel with the RC columns and beams on the basement floor as a strengthening application.
- The columns were strengthened by converting them to shear walls on the basement floor.
- The steel bar was applied in both directions in the areas between the strip foundations on the basement floor. Then the concrete was poured, and thus the foundation was strengthened.
- The columns on the ground floor were strengthened by using the jacketing technique.
- The steel meshing and cross carbon fiber fabric were used on the interior walls of the typical floor, and thus the walls were strengthened.
- The exterior walls were strengthened by using the steel meshing on the external facade of the building.

As a result of the above mentioned rehabilitation applications, the building was strengthened against vertical load and lateral effects.

ACKNOWLEDGEMENTS

REFERENCES

[1] Zakar L. and Eyupgiller K.K. *Contemporary techniques in architectural restoration practices (Restorasyon uygulamalarinda cagdas teknikler*, Omur publication, Istanbul, 2015, (in Turkish).

[2] Kozlu H.H. *Characterization of historical mortars and features of restoration mortars in Kayseri district (Kayseri yoresindeki tarihi harclarin karakterizasyonu ve onarim harclarinin ozellikleri*, PhD thesis, Istanbul Technical University, 2010, (in Turkish).

[3] Gurdal E. and Ozgunler S.A. *Report: Traditional mortars and conservation mortars (Geleneksel Harclar ve koruma harclari*, Journal Restoration & Conservation (Restorasyon & Konservasyon), vol.2013, iss.16, Editors: Alkan N., Atay R.F. 2013, (in Turkish).

[4] Gulec A. *Characterization of mortars and plasters of some historic monuments (Bazi tarihi anit harc ve sivalarinin incelenmesi*, PhD thesis, Istanbul Technical University, 1992, (in Turkish).

[5] SAP2000 *Structural Analysis Program, Computers & Structures Inc.*, University Avenue, Berkeley, California, USA. 1984-2015.

[6] Republic of Turkey Ministry of Culture and Tourism, 4nd Istanbul Regional Board of Protection of Cultural Heritages, Decision no.107 of 05.06.2013.

Investigation on the Local Failure Mechanisms of an Existing Seven-story Masonry Structure

Baris Gunes[1], Betul Ertekin[2], Baris Sayin[3]

Abstract

In common earthquake engineering practice, normal, shear and tensile stresses governed on the masonry walls are checked under the seismic loads calculated from the modal analysis of the structure where the maximum excited mass is achieved in the seismic performance assessment procedures. However, various local failure mechanisms may occur under the modes which have lower excited mass ratio until reaching the main collapse mechanism. These mechanisms are directly related to the factors such as the geometry of the structure's layout, rigidity of the masonry walls, connection type of the slabs and distribution of the loads. Notably, these mechanisms become more critical in the medium-rise masonry buildings (having equal and more than four floors) and should be taken into consideration. In this study, kinematic limit analyses were done to investigate the local failure mechanisms that may occur on a seven-storey masonry building. As a result of the analyses, it has been observed that local failure mechanisms were governed far below the predicted loading level. It is emphasised that local failure mechanisms must be considered in the determination of the most appropriate strengthening method for the retrofit of this kind of masonry structures.

Keywords: Masonry buildings, kinematic limit analyses, local failure mechanisms

1. INTRODUCTION

Masonry buildings differ from the other type of buildings in terms of construction techniques and structural system properties. Although the in-plane stiffness and strength of the structural walls in masonry buildings are relatively high, they may have inadequacies under out-of-plane effects in terms of stiffness and strength. Thus, the structural safety of masonry buildings can be critical due to the seismic loads acting perpendicular to the structural walls. Besides, the increase in the distribution of principal stresses especially on the wall joints and the edges of the window and door openings is effective in the lateral structural behaviour depending on the total cross-sectional area of the walls. One of the essential steps in a more realistic representation of structural behaviour in the seismic analysis of masonry structures is to adopt the most convenient material behaviour and formulation in the finite element modelling. Various analysis methods are preferred in the determination of the linear and non-linear behaviour of masonry structures in terms of geometric considerations and material properties. In this context, sophisticated mathematical methods adopting geometric and material nonlinearity are used in the numerical analyses as well as simple methods and stress calculations in order to determine the seismic behaviour of masonry structures. The determination of adopting an appropriate methodology is vital, and each building should be evaluated considering their unique properties [1].

[1] Istanbul University-Cerrahpasa, Department of Civil Engineering, 34320, Avcilar/Istanbul, Turkey. bgunes@istanbul.edu.tr

[2] Istanbul University-Cerrahpasa, Institute of Graduate Studies in Sciences and Engineering, Istanbul, Turkey, betulertekin14@gmail.com

[3] Corresponding author: Istanbul University-Cerrahpasa, Department of Civil Engineering, 34320, Istanbul, Turkey. barsayin@istanbul.edu.tr

Although the finite element method, which is one of the widely used methods, is an effective analysis method in the determination of seismic performance level structures under the vertical and seismic loads, adopting a proper structural modelling should be considered as an important step in determining the actual behaviour of the related structures. In the evaluation of the seismic performance of masonry buildings; the necessary controls are made for compressive, tensile and shear stresses that are governed on the walls under primary load cases which have high modal participation rates. However, different local failure mechanisms can be activated under the modes with low modal participation rates before reaching the primary collapse mechanism due to some factors such as the geometric layout of the structural system, wall stiffnesses, the type of connections between the slabs and the walls, distribution of loads, etc. These local failure mechanisms become more critical in the multi-storey masonry buildings. In this study, kinematic limit analyses were conducted to evaluate these local failure mechanisms on an example masonry building.

In the literature, many methods have been presented, such as limit analysis, kinematic analysis, pushover analysis, finite element analysis and diagnostic analysis, for determining the seismic performance of masonry structures [2-14]. For example, Milani and Valente performed on the analysis of seven masonry churches that suffered damage during a seismic event. The broad set of examples considered in the study allows a comparative analysis of the pros and cons linked with the practical application of the different procedures. In particular, global FE pushover and limit analyses, combined with a plate and shell discretisation, are adopted to have an insight into i. Active failure mechanisms and ii. Accelerations associated with the formation of partial collapses. It is found that FE limit analysis may provide reliable failure mechanisms – when compared with the other approaches discussed – but requiring a reduced processing time, without the need to adopt questionable choices on the macro-blocks active at collapse [4]. In another study, Cecchi et al. developed a simplified micro-mechanical model for the kinematic limit analysis of masonry walls under Reissner–Mindlin plate hypotheses. A limit analysis model based on a compatible identification procedure has been presented for the out-of-plane loaded masonry walls under Reissner–Mindlin plate hypotheses. The model is applied to two meaningful structural examples. The first concerns a masonry wall under cylindrical flexion, whereas the second consists of an out-of-plane loaded rectangular plate with a central opening. For both cases, the influence of the shear strength on the collapse load is estimated varying panel slenderness [5]. Milani and Venturini proposed a 3D homogenized FE limit analysis software for the fragility curve evaluation of entire existing masonry churches. In the first phase, homogenised masonry strength domains are obtained using a simplified kinematic procedure applied on a three-leaf unitary cell. In the second phase, homogenised domains are implemented at a structural level on a plate and cell kinematic FE software [7]. Milani et al. presented a kinematic FE limit analysis approach for the 3D analysis of masonry buildings subjected to horizontal actions. In the study, both in- and out-of-plane failures are taken into account in the evaluation of the total internal power dissipated. The main conclusions are i. The proposed approach allows us to obtain failure mechanisms and collapse loads, provides similar results to more sophisticated approaches based on nonlinear increments and iterative finite element simulations, ii. The carried-out sensitivity analysis indicates that different predominant failure mechanisms can be obtained in the analysis after a moderate change in the material parameters [13].

Also, there are developed models and methods for seismic evaluation of masonry structures [15-23]. Chiozzi et al. presented an automatic computational procedure, starting from a 3D CAD model of the whole structure used as a basis for FE kinematic limit analysis computations and ending with a mesh adaptation process by means of a meta-heuristic approach, is able to furnish precise information on the most vulnerable parts and realistically predicts the acceleration activating the collapse [15]. Casapulla and Argiello developed a limit analysis of a simple out-of-plane failure mechanism of a laterally weakly connected masonry wall involving frictional resistances according to the displacement-based approach. The pushover analysis is made considering geometric nonlinearity, i.e. by evaluating the static multiplier for varied kinematic configurations, as a function of the displacement of a control point. Comparative results and pushover curves are developed to evaluate the displacement capacities for each case analysed [16]. Milani et al. Presented a micro-mechanical model presented for the limit analysis of respectively in- and out-of-plane loaded masonry walls are utilised in the presence of coupled membrane and flexural effects [17]. Panto et al. proposed a discrete-modelling approach for the simulation of both the in-plane and out-of-plane response of masonry structures. The method is applied to a basilica, which has been partially investigated in the literature. The results show the capability of the proposed discrete element approach to simulate the nonlinear response of monumental structures also for those cases in which the 'in' and the 'out' of plane response cannot be decoupled, as it happens for many structural layouts typical of churches, ancient palaces and several other monumental structures [18]. Betti and Galano evaluated the seismic behaviour by the pushover method, according to the Italian Technical Recommendations. The results were compared with the ones obtained by a simplified approach based on the kinematic theorem of

limit analysis. Comparisons of the expected seismic demand vs the seismic capacity of the Palace confirm the weakness of this building to suffer extensive damage under earthquakes, as frequently observed in similar construction typologies. Additionally, the comprehension of the structural behaviour under seismic loading allows the identification of a proper retrofitting strategy [21]. Palazzi et al. investigated the seismic behaviour of the church through the kinematic limit analyses. For this purpose, the main collapse mechanisms have been identified and analysed. The results show that the seismic response is unsatisfactory and shows the inadequacy of the seismic performance of this construction typology under high seismic activity, due to the extreme slenderness of the structural elements and to the absence of box-like-behaviour, making it particularly sensitive to earthquake loading [22].

The present study covers kinematic limit analyses performed to investigate the local failure mechanisms that may occur on a seven-storey masonry building. It is believed that the local failure mechanisms should be considered in the determination of the most appropriate strengthening method for the retrofit of masonry structures.

2. DESCRIPTION OF STRUCTURE

The investigated masonry building in this study is composed of seven storeys. These stories are named as the basement floor, ground floor and five standard floors. Story heights vary between 2.6 m. and 3.6 m. The structural system of the building resides on a regular layout which covers 199 m^2 area. The plan dimensions are 9.9 m. in the x-direction and 20.1 m. in the y-direction. Although the masonry walls located around the perimeter of the building have vertical continuity in general, the interior walls have vertical discontinuities which have been observed on some floors. Jack-arch slabs are used as the slab system in the building. The masonry wall thicknesses for the outer walls differ from 15 to 70 cm. The thickness of the inner walls varies between 15-45 cm. Unlike the other floors, some column-like masonry vertical structural members are observed in the interior of the basement floor. It is believed that these members with 33×40, 33×42, 35×41 and 85×93 cm. dimensions are formed as a result of removing some parts of the inner walls for architectural reasons in time. The overview of the building and plan of some floors are presented in Figure 1. The facade and the sectional elevation of the building are shown in Figure 2.
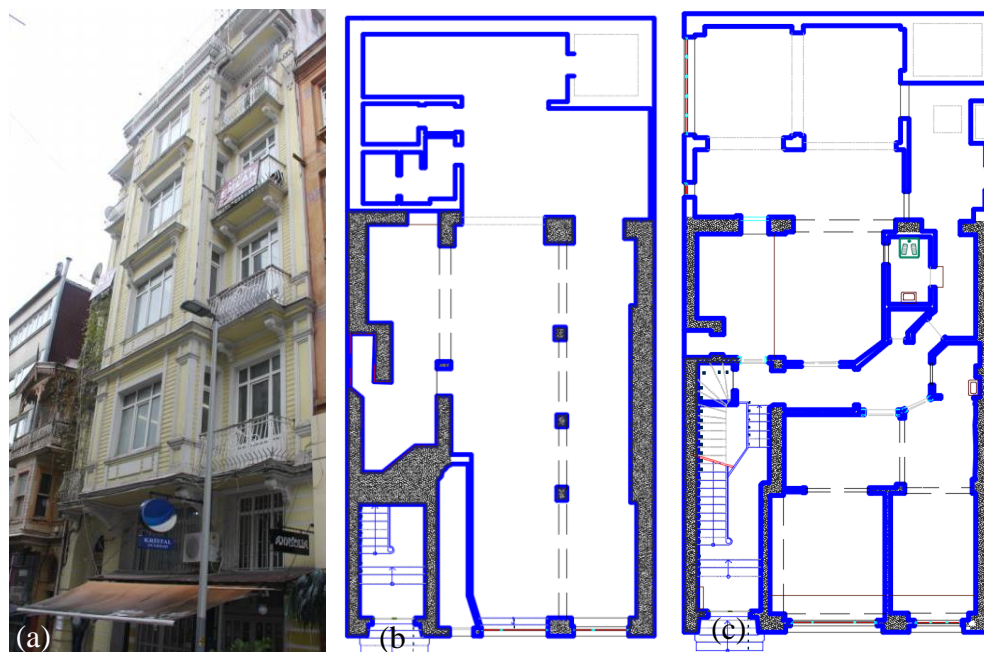
Figure 1. The building: (a) Overview, (b) Basement plan, (c) Ground plan
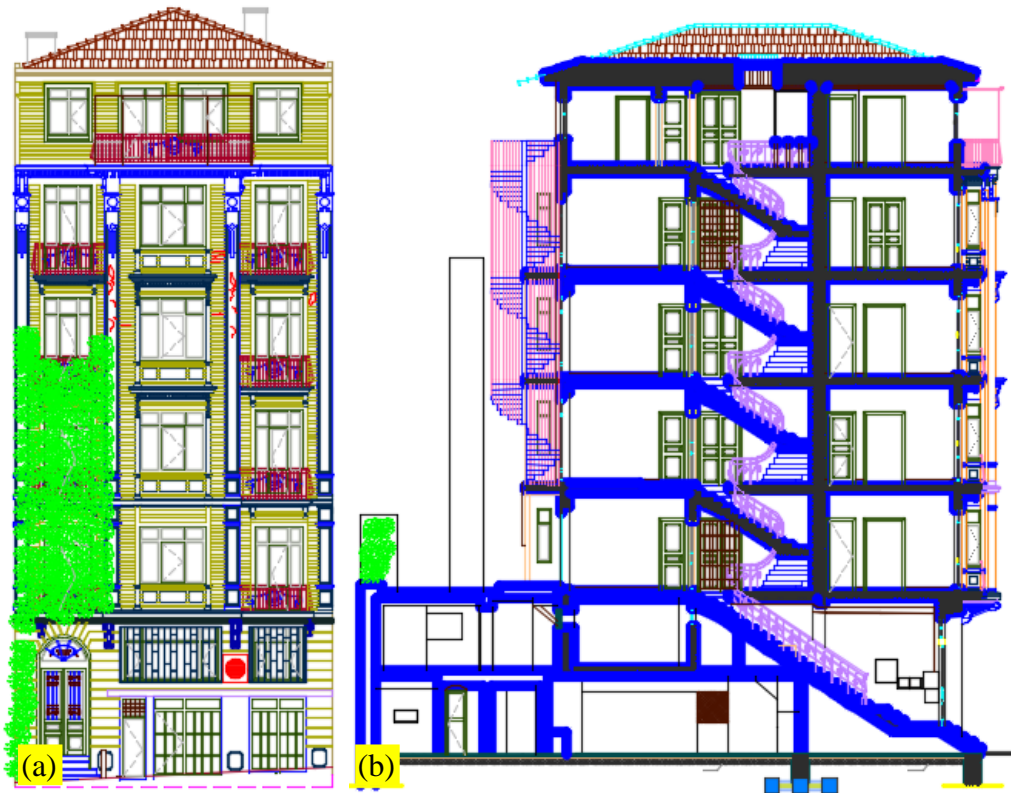
Figure 2. The building: (a) Facade, (b) Sectional elevation

3. KINEMATIC LIMIT ANALYSIS

The kinematic limit analysis is an important method which is used to determine the seismic safety of masonry structures. Kinematic analysis can be defined as; (i) evaluation of possible failure mechanism, (ii) calculation of the lateral force activating each mechanism type and the necessary seismic acceleration that forms this force, (iii) determination of the lateral seismic acceleration demand and finding the possible failure mechanism by comparing this determined demand with the capacity [24]. Most of the historic masonry structures have considerable vulnerabilities because of the lack of horizontal diaphragms and insufficient material strength, particularly under tensile effects. As a result of this, most of the failure mechanisms under the seismic loads occur from the local out-of-plane behaviour [25]. The kinematic limit analysis was first applied to masonry structures by Heyman [26, 27]. The assumptions made for the hypotheses on the masonry behaviour assume no tensile strength, infinite compression strength and the absence of sliding at failure, as presented by Heyman [26]. The kinematic limit analysis is based on the virtual work principle and relates the overturn work of the equivalent inertia force applied at the centroid of the element and horizontally oriented with the resistant moment calculated from the gravity loads. For each acceptable kinematic mechanism, the kinematic analysis aims to designate the activation coefficient α_0, defined as a multiplier of the normalised seismic acceleration [28].

In the kinematic limit analysis, the virtual work principal given by Eq. (1) is applied where F_i represents the generic concentrated load, and W_i represents the weight of every single part forming the failure mechanism. $\delta_{x,i}$ and $\delta_{y,i}$ are the horizontal and vertical virtual displacement components of the F_i and W_i. L_{fi} is the virtual work of the internal forces.

$$\alpha_0 \left(\sum_{i=1}^{n} W_i \cdot \delta_{x,i} + \sum_{i=1}^{n} F_i \cdot \delta_{x,i} \right) - \sum_{i=1}^{n} W_i \cdot \delta_{y,i} - \sum_{i=1}^{n} F_i \cdot \delta_{y,i} = L_{fi}$$

(34)

Finally, the calculations related to the spectral acceleration of the mechanism's activation a_0^* is given in Eq. (2). In this equation, M^* represents the effective participating mass and g represents the gravity acceleration.

$$a_0^* = \frac{\alpha_o \sum_{i=1}^{n} W_i + F_i}{M^*}, \qquad M^* = \frac{\left[\sum_{i=1}^{n} \left(W_i \, \delta_{x,i} + F_i \, \delta_{x,i} \right) \right]^2}{g \sum_{i=1}^{n} \left(W_i \, \delta^2_{x,i} + F_i \, \delta^2_{x,i} \right)}$$

(35)

The activation of the analysed mechanism will not be possible under the design earthquake if the condition presented in Eq (3) is valid.

$$a_0^* \geq a_c^* = \frac{a_g \times S}{q} \cdot \left(1 + 1.5 \cdot \frac{Z}{H} \right)$$

(36)

In this equation, a_gS is the design elastic spectral acceleration, q is the behaviour factor, Z is the height to the ground distance of the mechanism's linear hinge, H is the facade's total height.

The static analysis and seismic parameters used for the example building investigated in this study are given in Table 1. Acceleration coefficient used for this structure in the kinematic analyses is found by the data presented in this table. It is determined that, in the masonry building's structural walls, solid bricks with cement reinforced lime-based mortar are used. Based on TEC-2007 [29], the allowable compressive and shear stresses for these walls are specified as 0.8 and 0.15 (MPa), respectively.

Table 1. The seismic and soil parameters used in the numerical analyses

Parameter	Definition	Value/Class
A_o^*	Effective ground acceleration coefficient	0.30
I	Building importance factor	1.0
T_A, T_B^{**}	Spectrum characteristic periods	T_A=0.15 s., T_B=0.40 s.
$S(T_1)$	Spectrum coefficient	2.5
$R_a(T_1)$	Seismic load reduction factor	2.0

The kinematic analysis is done on the frontal facade wall of the building, and possible local failure mechanisms of this wall are evaluated. The investigated wall is 4.25 m wide and has 3.55 m height on each floor. The wall

thickness is 25 cm. There are window openings with 3.0x1.9 m. dimensions on the wall surface. The related wall is shown in Figure 3.

Figure 3. Investigated frontal facade wall of the building

In this study, three different failure mechanisms are evaluated for the masonry wall located at the facade of the building (Figure 4, Figure 5, Figure 6) which are; overturning (out-of-plane) failure, vertical bending failure and lateral bending failure of the wall. Related failure mechanisms can be activated by several reasons and primarily related to the thickness and height of the masonry wall, connection details on each floor level and the excited mass of the wall. PRO_CINEM [30] software is used to conduct the kinematic limit analyses in this study.

The controls made for the overturning failure mechanism of the investigated masonry wall are shown in Figure 4 and Table 2. It can be concluded that the out-of-plane overturning failure mechanism is activated for all of the wall parts forming this investigated facade wall. The structure does not provide necessary conditions to prevent overturning failure mechanism due to the lack of sufficient connection detailing applied to the structure to avoid this kind of failure mechanism.
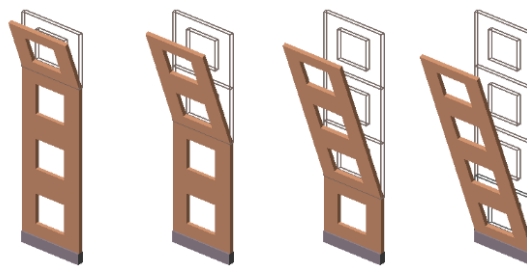
Figure 4. Overturning (out-of-plane) failure mechanism of masonry walls

Table 2. The controls made for the walls' overturning failure mechanism

Story	a_0	a_0^*	a_c	a_c/a_0^*	Check (a_c/a_0^*)
Story-4	0.058	0.064	0.509	7.90	No
Story-3	0.029	0.073	0.340	4.65	No
Story-2	0.018	0.023	0.170	7.40	No
Story-1	0.012	0.016	0.200	12.90	No

The controls made for the vertical bending failure mechanism of the investigated masonry wall are shown in Figure 5 and Table 3. It can be concluded that the vertical bending failure mechanism is activated for some of the wall parts forming this investigated facade wall in some stories.

Figure 5. Vertical bending failure mechanism of masonry walls

Table 3. The controls made for the walls' vertical bending failure mechanism

Story	a_0	a_0^*	a_c	a_c/a_0^*	Check (a_c/a_0^*)
Story-4	0.311	0.388	2.012	5.18	No
Story-3	0.932	1.162	1.341	1.15	No
Story-2	1.514	1.888	0.671	0.36	Yes
Story-1	2.094	2.611	0.200	0.08	Yes

The controls made for the lateral bending failure mechanism of the investigated masonry wall are shown in Figure 6 and Table 4. It can be concluded that the lateral bending failure mechanism is not activated for all of the wall parts forming this investigated facade wall.

Figure 6. Lateral bending failure mechanism of masonry walls

Table 4. The controls made for the walls' lateral bending failure mechanism

Story	a_0	a_0^*	a_c	a_c/a_0^*	Check (a_c/a_0^*)
Story-4	1.469	1.482	0.610	0.41	Yes
Story-3	1.469	1.482	0.440	0.30	Yes
Story-2	1.469	1.482	0.270	0.18	Yes
Story-1	1.469	1.482	0.200	0.13	Yes

4. CONCLUSIONS

In this study, kinematic limit analyses were conducted to evaluate possible local failure mechanisms of an existing seven-storey masonry building. The performance of the masonry buildings under the seismic loads is generally controlled according to the stresses governed on the masonry walls under the primary loads with high modal participation rates. However, different local failure mechanisms can be activated under the modes with low modal participation rates before reaching the primary collapse mechanism due to some factors such as the

geometric layout of the structural system, wall stiffnesses, the type of connections between the slabs and the walls, distribution of loads, etc. These local failure mechanisms become more critical in the multi-storey masonry buildings and definitely must be controlled.

The vulnerability against three different types of local mechanisms, namely, overturning (out-of-plane) failure, vertical bending failure and lateral bending failure is evaluated for a selected primary structural wall of the building in this study. It has been concluded that the necessary conditions were not satisfied for the first two types of local failure mechanisms (overturning (out-of-plane) failure and vertical bending failure), and were satisfied for the third type of local failure mechanism (lateral bending failure). In case of the first two local mechanisms' occurrence, the mechanisms were observed at much lower load levels than the predicted ones until reaching the global behaviour. It is emphasised by this study that these local failure mechanisms should be taken into consideration and prevented during the determination of the most appropriate strengthening method for the masonry structures.

REFERENCES

[1]. Z. Celep, K. Guler and F. Pakdamar, "Application of the finite element method in structural evaluation of historical buildings," in Restoration implementations from Turkey and Italy, Directorate General of Foundations Publications, 2016, p. 122.

[2]. G. Barbieri, L. Biolzi, M. Bocciarelli, L. Fregonese, and A. Frigeri, "Assessing the seismic vulnerability of a historical building," Engineering Structures, 57, 523-35, 2013.

[3]. S. Casolo, G. Milani, G. Uva and C. Alessandri, "Comparative seismic vulnerability analysis on ten masonry towers in the coastal Po Valley in Italy," *Engineering Structures* 49 465–490, 2013.

[4]. G. Milani and M. Valente, "Comparative pushover and limit analyses on seven masonry churches damaged by the 2012 Emilia-Romagna (Italy) seismic events: Possibilities of non-linear finite elements compared with pre-assigned failure mechanisms," *Engineering Failure Analysis* 47, 129–161, 2015.

[5]. A. Cecchi, G. Milani and A. Tralli, "A Reissner–Mindlin limit analysis model for out-of-plane loaded running bond masonry walls," *International Journal of Solids and Structures* 44, 1438–1460, 2007.

[6]. A. Cecchi and G. Milani, "A kinematic FE limit analysis model for thick English bond masonry walls," *International Journal of Solids and Structures* 45, 1302–1331, 2008.

[7]. Milani G. and Venturini G. "Automatic fragility curve evaluation of masonry churches accounting for partial collapses by means of 3D FE homogenized limit analysis," *Computers and Structures* 89, 1628–1648, 2011.

[8]. S. De Silva, G. H. M. J. S. De Silva and H. M. S. S. Padmal, "Assessment Method for Seismic Vulnerability of Old Masonry Buildings in Sri Lanka," *Procedia Engineering*, 212, 61-68, 2018.

[9]. F. Clementi, V. Gazzani, M. Poiani and S. Lenci, "Assessment of seismic behaviour of heritage masonry buildings using numerical modelling," *Journal of Building Engineering*, 8, 29-47, 2016.

[10]. G. Castori, A. Borri, A. De Maria, Corradi M. and R. Sisti, "Seismic vulnerability assessment of a monumental masonry building," *Engineering Structures*, 136, 454-465, 2017.

[11]. P. G. Asteris, M. P. Chronopoulos, C. Z. Chrysostomou, H. Varum, V. Plevris, N. Kyriakides and V. Silva "Seismic vulnerabilty assessment of historical masonry structural systems," *Engineering Structures*, 62-63; 118-134, 2014.

[12]. G. Fortunato, M. F. Funari and P. Lonetti "Survey and seismic vulnerability assessment of the Baptistery of San Giovanni in Tumba (Italy)" *Journal of Cultural Heritage*, 26, 64-78, 2017.

[13]. G. Milani, P.B. Lourenco and A. Tralli, "3D homogenized limit analysis of masonry buildings under horizontal loads" *Engineering Structures* 29, 3134–3148, 2007.

[14]. M. Gilbert, H. M. Ahmed and C. Casapulla, "Computational limit analysis of masonry structures in the presence of non-associative friction" *6th International Symposium in Computer Methods in Structural Masonry*, Rome, p. 1-8, 2003.

[15]. A. Chiozzi, N. Grillanda, G. Milani and A. Tralli, "UB-ALMANAC: An adaptive limit analysis NURBS-based program for the automatic assessment of partial failure mechanisms in masonry churches," *Engineering Failure Analysis*, 85, 201–220, 2018.

[16]. C. Casapulla and L. U. Argiento, "Non-linear kinematic analysis of masonry walls out of-plane loaded. The comparative role of friction between interlocked walls," *COMPDYN 2017: 6th ECCOMAS Thematic Conference on Computational Methods in Structural Dynamics and Earthquake Engineering*, M. Papadrakakis, M. Fragiadakis (eds.) Rhodes Island, Greece, 15–17 June 2017.

[17]. G. Milani, P. B. Lourenco and A. Tralli, "A kinematic limit analysis approach for masonry buildings: in- and out-of-plane failure mechanisms," *GIMC 2006: Convegno Italiano Di Meccanica Computazionale, 16*, Bolonha, Itália, 2006.

[18]. B. Pantò, F. Cannizzaro, S. Caddemi and I. Caliò, "3D macro-element modelling approach for seismic assessment of historical masonry churches," *Advances in Engineering Software* 97, 40–59, 2016.

[19]. G. Milani, P.B. Lourenco and A. Tralli, "Homogenised limit analysis of masonry walls, Part I: Failure surfaces," *Computers and Structures* 84, 166–180, 2006.

[20]. S. Caddemi, I. Caliò, F. Cannizzaro and B. Pantò, "New frontiers on Seismic modeling of Masonry structures, *Frontiers in Built Environment*," 3:39. doi: 10.3389/fbuil.2017.00039, 2017.

[21] M. Betti and L. Galano, "Seismic Analysis of Historic Masonry Buildings: The Vicarious Palace in Pescia (Italy)," *Buildings*, 2, 63-82, 2012.

[22]. N. C. Palazzi, L. Rovero, U. Tonietti and J. C. De la LIera, "Kinematic limit analysis of Basilica del Salvador, A significant example of neo-gothic architecture in Santiago, Chile," *16th European Conference on Earthquake Engineering*, Thessaloniki, Greece, 2018.

[23]. L. Giresini, M. Fragiacomo and M. Sassu, "Rocking analysis of masonry walls interacting with roofs," *Engineering Structures*, 116, 107–120, 2016.

[24]. HSG, "The guide of management of earthquake risks for historic structures," Directorate General of Foundations, 2017.

[25]. A. Giuffrè, "Letture sulla meccanica delle murature storiche", Kappa, Roma, 1991.

[26]. J. Heyman, "The stone skeleton," International Journal of Solids Structures, vol. 2, pp. 249-279, 1966.

[27]. J. Heyman, "The safety of masonry arches," International Journal of Mechanical Science, vol. 11, pp. 363-385, 1969.

[28]. A. Giuffrè, "Sicurezza e conservazione dei centri storici, II caso Ortigia", laterza, Bari, 1993.

[29]. TEC, "Turkish Earthquake Code: Specification for buildings to be built in earthquake regions," Ministry of Public Works and Settlement, Government of the Republic of Turkey, Ankara, 2007.

[30]. Pro_Cinem, "Pro_Cinem Software Manual," 2019.

Electro-oxidation process for the treatment of reactive blue 221

Gulin Bice Yildirim[1], Fatih Ilhan[1], Kubra Ulucan-Altuntas[1], Amar Ćemanović[2], Sevval Eyri[1], Ozer Cinar[1], [3]

Abstract

High concentration of color, make textile wastewaters as a major source of contamination. While physicochemical processes (adsorption and chemical coagulation) and biological processes (biological treatment/membrane bioreactor) were the most applied treatment method for textile wastewater, compared to these conventional treatment methods, advanced oxidation process produces less sludge with high removal efficiencies. The electrooxidation process is a treatment method which has increased in popularity in recent years because it does not imply sludge formation nor electrode consumption. In short, it is a process in which purification is carried out by providing electric current to an electrode without any chemical addition. In this study, general information about the electrooxidation process is given, as well as its use in water/wastewater treatment. As a sample study, the removal of Reactive blue 221 dye was determined with the use of a Ti/RuO_2 anode and a Titanium cathode. The most successful results were achieved with 30 mA/cm2 current density, 13 minutes reaction time, pH 3.8 and dye concentration of 60 mg/L, amounting to a reactive blue 221 treatment efficiency of 97.5%.

Keywords: electrochemical, oxidation, electro-oxidation, dye removal

1. INTRODUCTION

Wastewater treatment is always an up-to-date issue, hence there is always the need for state-of-the-art methods. Current advanced treatment methods are open to development, and electrochemical methods have an important place among them.

The basic principle of electrochemical oxidation is to generate electric current between two electrodes placed in a conductive solution medium and to initiate and accelerate electrochemical reactions with the help of the passing current. Electrochemical methods are preferred because of the low sludge formation and effective removal potential. This treatment method has recently started to be used for metal recovery purposes. In principle, this method relies on insoluble electrodes (Ru, Ti, stainless steel, Pt, etc.), and desired oxidation is achieved with gases such as Cl_2 and O_2 separated from the anode region and newly formed OH. and H_2O_2. This process may contribute to the oxidation of many substances. However, compounds with very low biodegradability are converted to end products such as CO_2 and H_2O or to biodegradable organic compounds [1].

The anode plays the active role in the electrooxidation process [1]. Electrochemical oxidation often depends on the characteristics of the wastewater, the type of anode used and the process conditions [2]. A wide variety of materials are used as the anode, which is one of the main factors affecting the process. These include: Ti/SnO_2, Ti/PbO_2, Ti/IrO_2, iron, aluminum, nickel, graphite, glass carbon electrodes. In addition, BDD (Borondoped diamond), which is produced from silicon coated with synthetic diamonds, has been used recently to gain conductivity [3].

[1] *Yildiz Technical University, Department of Environmental Engineering, 34220, Esenler/İstanbul, Turkey.*

[2] *Istanbul Technical University, Department of Environmental Engineering, Maslak/Istanbul, Turkey.*

[3] *Corresponding author: Yildiz Technical University, Department of Environmental Engineering, 34220, Esenler/İstanbul, Turkey. ocinar@yildiz.edu.tr*

2. ELECTROOXIDATION PRINCIPLE

The electrochemical oxidation process proceeds in two ways. One of these is direct oxidation at the anode surface, and the other is indirect oxidation in solution with the appropriate oxidants formed in the anode [4].

2.1. Direct Oxidation

The direct oxidation of the pollutants is carried out in 2 stages (Figure 1):

(1) Diffusion of pollutants from solution to anode surface
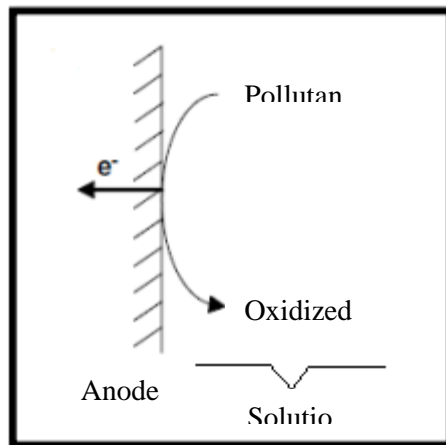
(2) Oxidation of pollutants on the anode surface

Figure 1: Direct oxidation

During the anodic oxidation of organic pollutants, two different paths can be followed:

1) Electrochemical conversion: The conversion of toxic pollution loads which are not biodegradable to biologically degradable organic compounds. In this way, organic compounds are only partially oxidized and may therefore require a second treatment (Equation 1).

$$R + MOx+1 \rightarrow RO + MOx \quad (1.10) \tag{1}$$

2) Electrochemical Degradation: Organic compounds are converted to carbon dioxide, water and other inorganic components. Complete treatment is achieved (Equation 2).

$$R + MOx(OH·)z \rightarrow CO_2 + zH + + ze + MOx \tag{2}$$

In the above equations;
MOx: Oxidized anode,
MOx + 1: Active oxygen,
R: Organic compound
Z: Number of adsorbed hydroxyl radicals in the anode.

Electrochemical oxidation of organic matter occurs at the potential site where water is broken down to produce oxygen. The initial step in the formation of oxygen (Equation 1) is the formation of adsorbed hydroxyl radicals which play an important role in the anodic decomposition of water molecules and the disintegration of organic pollutants. Oxygen conversion takes place either by the release of the chemically adsorbed oxygen molecule or by electrochemical oxidation of physically adsorbed hydroxyl radicals at the surface by electrochemical oxidation.

The active surface ($M = RuO_2$, Pt, IrO_2) is useful at the low potential where the M / MO redox pair is present, while the inert surface requires the potential of the H_2O / H_2O_2 redox pair.

Metal oxides (PbO_2, SbO_2) and diamond exhibit only inert surfaces [4].

The efficiency of direct oxidation depends on the amount of diffusion of the organic compounds to the anode surface, the activity of the anode and the current density applied [5].

2.2. *Indirect Oxidation*

In indirect oxidation, an electrochemically generated mediator is required for the oxidation to take place. Indirect oxidation agents produced anodically are responsible for the oxidation of inorganic-organic pollutants [5]. Chlorine (Cl), possibly caused by chloride oxidation at the anode, is the most common electrochemical oxidant.

Although it is not clear whether Cl has an active role in the oxidation of organic pollutants, ammonia oxidation often occurs through this mechanism. Common use of Cl in wastewater is due to the fact that it is a ubiquitous compound and is highly effective. Other common oxidants include hydrogen peroxide (H_2O_2), ozone (O_3) and hypochlorite (OCl^-), which can be produced through electrochemical processes. Metal catalytic agents (Fe $^{+3}$, Co $^{+3}$, Ag $^{+2}$, etc.) are also used for the production of hydroxyl radicals. However, the use of metal ions can result in generation of wastewater with a higher toxicity than the initial [6].

Indirect oxidation efficiency depends on reaction temperature, amount of diffused secondary oxidants in solution and pH values [7]. The resulting reactions are schematized in Figure 2.
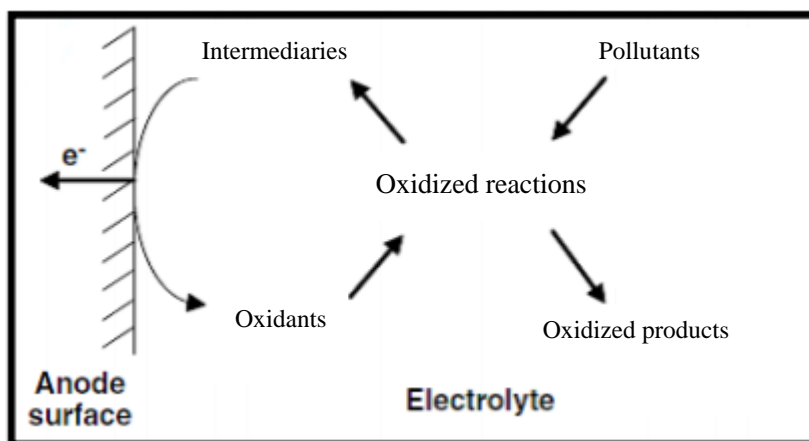
Figure 2: Indirect oxidation

Equations occurring during indirect electrooxidation are given in equations 3-9 and Figure 3. [7]

Anodic reactions:

$$2Cl^- \rightarrow Cl_2 + 2e^- \tag{3}$$

$$6HOCl + 3H_2O \rightarrow 2ClO_3^- + 4Cl^- + 1,5O_2 + 12H^+ + 6e^- \tag{4}$$

$$2H_2O \rightarrow O_2 + 4H^+ + 4e^- \tag{5}$$

Overall reactions:

$$Cl_2 + H_2O \rightarrow HOCl + Cl^- + H+ \tag{6}$$

$$HOCl \rightarrow H^+ + OCl^- \tag{7}$$

Cathodic reactions:

$$2H_2O + 2e^- \rightarrow 2OH\bullet + H_2 \tag{8}$$

$$OCl^- + H_2O + 2e^- \rightarrow Cl^- + 2OH\bullet \tag{9}$$
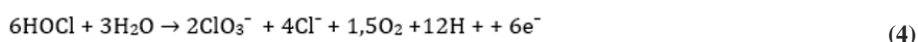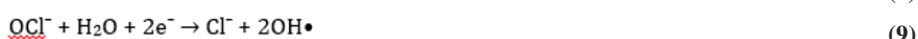
Figure 3: Indirect electrochemical oxidation equations

3. WORKING CONDITIONS OF ELECTROCHEMICAL OXIDATION AND FACTORS AFFECTING THE SYSTEM

The effect of active factors such as electrolyte, current density, electrode material, pH on electrochemical oxidation has been investigated. It is known that they affect the current efficiency, pollutant-removing efficiency and energy consumption [8].

3.1. Current Density

Optimizing the current density among the parameters in electrochemical oxidation processes is one of the most frequently mentioned terms in order to control the reaction rate. The effect of flow density on treatment efficiency varies depending on the characteristics of the wastewater to be treated. However, working with higher current densities usually requires higher energy consumption. As a result, cost increases [9].

Moraes and Bertazzoli (2005) found in their study that color removal from leachate is strongly dependent on current density. In this study, the authors obtained 5 times more color removal efficiency with a current density of 116 mA/cm² compared to 13 mA/cm² current density with an electrochemical process of 180 minutes [10].

3.2. Temperature

There is general belief that direct oxidation processes are not affected by temperature. Although they can operate at lower temperatures compared to other electrochemical treatment methods, ambient temperature is generally preferred for operation [9].

3.3. pH

As a result of the studies carried out, there is no clear indication as to whether the increase in pH will have an increasing or decreasing effect on the yield [9].

3.4. Electrolyte

Electrolyte is added to the test system in order to increase the conductivity of the electrochemical oxidation system, increase the current passing through the system and support indirect oxidation. The amount of electrolyte is one of the parameters that affect the process since it affects COD removal [11]. Various electrolytes (such as sulfate, iron ion and hydrogen peroxide) can be added to the system. The sulfate itself does not take part in the oxidation reactions on the electrodes, but it can increase electrochemical oxidation as a support electrolyte [8]. During electrooxidation, H_2O_2 may decompose into hydroxyl radicals [12].

3.5. Electrode material

The selection of the electrode material directly affects the process efficiency. The selected electrode material must have the following properties:

- Electrical conductivity should be high

- Must possess properties such as catalytic activity and selectivity

- High physical and chemical stability, corrosion resistance

- Low cost and durability [9].

Table 1 shows the recoveries and COD removal results of some anode electrodes.

Bejankiwar (2002) investigated the effects of anode surface area during electrochemical oxidation. As a result of the studies, it has been determined that with increasing electrode surface area the following can be observed: increase in the current intensity, increase in COD removal, constant value of current density, decrease in reaction time and decrease in energy demand. When Pt and Ti electrodes are used, large surface areas are provided with high mass transfers with ease of control and no solid waste problem [13].

Table 1: Color and COD removal results of some anode electrodes [14]
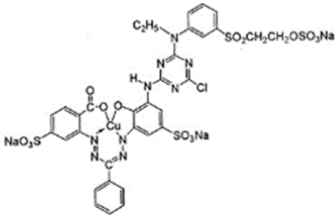
Anode material	Color removal (%)	COD removal (%)
Ti/Pt	40	9
Ti/RuO$_2$-TiO$_2$	42	26
Ti/SnO$_2$-Sb$_2$O$_5$	45	23
Ti/Pt-Ir	50	39
Ti/MnO$_2$-RuO$_2$	46	10
TiRhOx-TiO$_2$	47	29
TiPdO-Co$_3$O$_4$	48	25
Ti/RuO$_2$	99	90
Ti/Pt	99	99
Ti/Pt/Ir	99	82

4. CASE STUDY: REMOVAL OF TEXTILE DYES BY EO PROCESS

For this purpose, the elimination of Reactive Blue 226 dye by electrooxidation process using Ti/RuO$_2$ was investigated.

The data related to the dye used are outlined in Table 2.

Table 2: General information about Reactive blue 226.

Chemical structure	
Molecular structure	Formazan, metal complexes
Molecular formula	C$_{33}$H$_{24}$ClCuN$_9$Na$_3$O$_{15}$S$_4$
Molecular weight	1082,83

The results obtained in the electrooxidation process studies with this type of dye feature a very high yield efficiency of 97% at pH 3.8, at a low current such as 30 mA/cm^2 when the dye concentration was 60 mg/L and in as little as 13 minutes.

4.1. Evaluation

The aim of this study was to introduce electrochemical oxidation, a process which is rapidly increasing in popularity in recent years. For this purpose, reaction-based as well as application-based information is provided. In addition, a problem related to textile industry, one of the most wastewater producing industries, is evaluated. This problem is the removal of color stemming from a dye which is used extensively in the industry. In this study, it has been observed that the applied method is fast and efficient, with no sludge formation observed. Considering the results of the sample study, 97% removal was achieved with a current of 0.2 A in only 13 minutes. This demonstrates that the process is fast as well as feasible in terms of operating costs.

ACKNOWLEDGMENTS

REFERENCES

[1]. F. İlhan, U. Kurt, Ö. Apaydin, E. Arslankaya, and M.T. Gönüllü, "Elektrokimyasal aritim ve uygulamalari: kati atik sizinti suyu çalişmasi." Solid Waste Management and Environmental Problems Symposium in Turkey in the EU Process, Türkay, İstanbul, 1-16, 2007.

[2]. P. Canizares, C. Jimenez, F. Martinez, C. Saez, and M.A. Rodrigo, "Study of the Electrocoagulation Process Using Aluminum and Iron Electrodes." Ind. Eng. Chem Res.,46, 6189-6195, 2007.

[3]. A.M. Polcaro, S. Palmas, F. Renoldi, and M. Mascia, "On the performance of Ti/SnO2 and Ti/PbO2 anodes in electrochemical degradation of 2chlorophenol for wastewater treatment." J. Appl. Electrochemic., 29, 147-151, 1999.

[4]. V. Hege, "Bottlenecks of Sustainable Water Reuse." Advanced Treatment of Municipal Wastewater And Membrane Concentrates, 2002.

[5]. M. Gotsi, N. Kalogerakis, E. Psillakis, P. Samaras and D. Mantzavinos, "Electrochemical oxidation of olive oil mill wastewaters." Water Res. 39(17):4177-87, 2005.

[6]. M.F. Şen, "Kati Atik Sizinti Sularinin Elektrokimyasal Yöntemlerle Aritilabilirliğinin İncelenmesi (İzaydaş Tesisleri)." Master thesis, Gebze Yüksek Teknoloji Enstitüsü Mühendislik ve Fen Bilimleri Enstitüsü, Gebze, 2007.

[7]. C.A. Martinez-Huitle and S. Ferro, "Electrochemical Oxidation Of Organic Pollutants for The Wastewater Treatment, Direct and İndirect Processes." Chem Soc Rev 35:1324– 1340, 2006.

[8]. Y. Deng and D. Englehardt, "Electrochemical Oxidation for Landfill Leachate Treatment.", Waste Manag. 27(3):380-8, 2007.

[9]. A. Anglada, A. Urtiaga, and I. Ortiz, "Contributions Of Electrochemical Oxidation To Waste-water Treatment: Fundamentals and Review Of Applications." J Chem Technol Biotechnol; 84: 1747–1755, 2009.

[10]. P.B. Moreos, R. Bertazolli, "Electrodegradation of Landfill leachate in a flow electorchemical reactor." Chemosphere ; 58;1 ; 41-46, 2005.

[11]. M. Uğurlu, "The Removal of Some İnorganic Compounds from Paper Mill Effluents by The Electrocoagulation Method." G.U. Journal of Science, 17(3), 85-99, 2004.

[12]. P. Wang, W.C.I. Lau and H.P.H. Fang, "Landfill Leachate Treatment by Anaerobic Process and Electrochemical Oxidation." Environmental Science, 22,(5): 70, 2001.

[13]. R.S. Bejankiwar, "Electrochemical treatment of cigarette industry wastewater : feasibiltiy study." Water Research, 36 (17), 4386 -4390, 2002.

[14]. T. Kaygusuz, "Elektrokimyasal oksidasyon yönteminin tekstil atiksualarinin aritilabilirliğine etkilerinin tam ölçekli araştirilmasi." Namik Kemal Universitesi, FBE, Master thesis, 2013.

Numerical Investigation on Heat Transfer Enhancement and Flow Characteristics in a Tube Equipped by Twisted tape with Alternate Axis

Toygun Dagdevir[1], Orhan Keklikcioglu[2], Veysel Ozceyhan[3] and Ferdi Yologlu[4]

Abstract

In this study, effects of inserting twisted tape to a horizontal tube on heat transfer enhancement performance and flow characteristics is investigated with using a CFD program. The CFD program is based on finite volume technique to solve differential equations. The continuity, momentum and energy equations are discretized and Simple algorithm scheme is applied to link the pressure and velocity fields inside the solution domain. Analyses are carried out with Reynolds number of in range from 10,000 to 30,000, and constant heat flux is applied to wall of the tube. In order to simulate turbulent nanofluid flow k-ω standard turbulent model is applied for all cases. The numerical methodology is validated with literature in order to prove the accuracy of the study. The twisted tape configurations consist with various alternate axis. The results show that increase in turn amount of alternate axis provides higher heat transfer enhancement compared to typical twisted tape. However, used of the twisted tape with alternate axis more increase pressure drop penalty compared to typical twisted tape.

Keywords: Twisted tape, Heat transfer enhancement, Pressure drop, Performance evaluation criteria

1. INTRODUCTION

At last decade, energy costs dramatically rise up day by day, since human population increase and energy sources are consumed. Using the energy efficiently is significantly important for countries that import energy, especially. Heating or cooling systems need so much energy input such as pumping power and electrical resistant for heating, and compressor power for cooling. Within this scope, heat transfer enhanced methods are used and investigated methods. The heat transfer enhancement methods are divided in two groups: active methods and passive methods. Active methods require an input power to the system, but passive methods do not. The inserted twisted tape in a tube is commonly used method in industry as a passive method. Many researchers have been investigated twisted tape effects on heat transfer performance and flow characteristics since 60s. Some researches about the heat transfer enhancement by using various twisted tape configurations are given in Table 2.
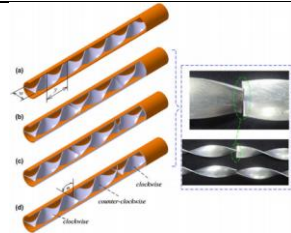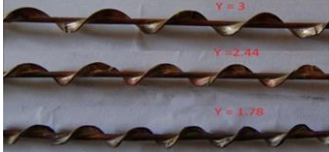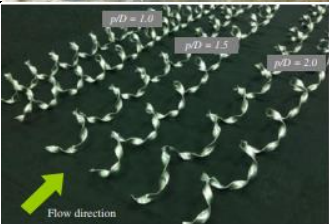
---

[1] Corresponding author: Erciyes University, Department of Mechanical Engineering, 38039, Melikgazi/Kayseri, Turkey. toygun@erciyes.edu.tr
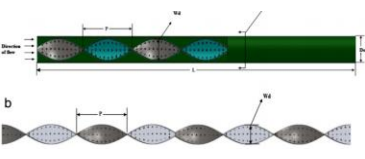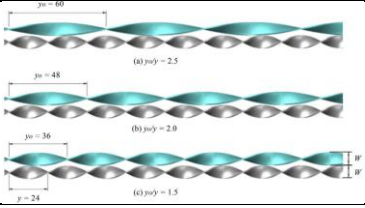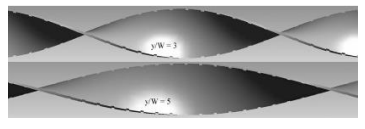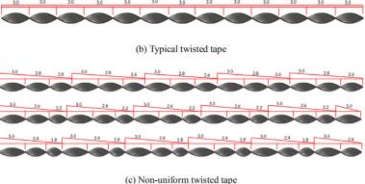
[2] Erciyes University, Department of Mechanical Engineering, 38039, Melikgazi/Kayseri, Turkey, keklikcioglu@erciyes.edu.tr

[3] Erciyes University, Department of Mechanical Engineering, 38039, Melikgazi/Kayseri, Turkey, ozceyhan@erciyes.edu.tr

[4] Erciyes University, Department of Mechanical Engineering, 38039, Melikgazi/Kayseri, Turkey, ferdi.ylgl41@gmail.com

Table 1. Literature review on heat transfer enhancement investigation by using twisted tape inserts.

No	Year	Authors	Insert type	Illustration	Operating conditions	Best PEC/ η	Observation
1	2010	S. Eiamsa-ard and P. Promvonge [1]	Alternate clockwise and counter-clockwise twisted tape		Working fluid: Water $3000 \leq Re \leq 27000$ $3 \leq TR \leq 5$	**η=1.4** for Re=3000, counterclockwise, θ=90°, TR = 3	The periodic change of swirl direction from clockwise to counterclockwise directions and vice versa, causes the sudden change of fluid arrangement, giving better fluid mixing and uniform temperature. The higher twist angle offers the larger difference of plane direction for the adjacent twist lengths, providing more effective disturbance to the flowing fluid.
2	2011	S. Suresh, K.P. Venkitaraj, P. Selvakumar [2]	Helical screw tape		Working fluid: Al_2O_3/water and CuO/water nanofluid $4900 \leq Pe \leq 13500$ $1.78 \leq TR \leq 3$ $\varphi=0.1\%$	**η=2.34** for Pe=4900 TR=1.78 CuO/water φ=0.1%	Insertion of helical screw tape causes to excellent fluid mixing and an efficient redevelopment of the thermal/hydrodynamic boundary layer.
3	2012	H. Bas and V. Ozceyhan [3]	Twisted tape inserts placed separately from the tube wall		Working fluid: Air $5132 \leq Re \leq 24989$ $2 \leq TR \leq 4$ $0 \leq$ Clearance ratio (c/D) $\leq$ 0.0357	**PEC=1.756** for Re=5183 TR=2 c/D=0.0178	The twist ratio is more effective on heat transfer enhancement than the clearance ratio. The twisted tapes are placed separately from the tube wall to obtain only heat transfer increase depending on laminar sublayer destruction near the tube wall. So, the effect of increased heat transfer surface area is eliminated.
4	2013	K. Nanan, K. Yongsiri, K. Wongcharee, C. Thianpong, S. Eiamsa-ard [4]	Helically twisted tapes		Working fluid: Air $6000 \leq Re \leq 20000$ TR=3 $1 \leq$ Pitch Ratio (PR) ≤ 2	**η=1.29** for co-swirl flow helically twisted tape PR=2 Re=6000	Using helically twisted tape enhance the heat transfer considerably. Because the effect of the secondary flow–induced inserts, leading to the better mixing between the fluids near the tube wall and the core region.

5	2013	M.M.K. Bhuiya, M.S.U. Chowdhury, M. Saha, M.T. Islam [5]	Perforated twisted tape		Working fluid: Air $7200 \leq Re \leq 49800$ TR=3 $1.6\% \leq$ Porosity $(R_p) \leq 14.7\%$	**PEC=1.59** for Re=7200 R_p=4.5%	The perforated twisted tape inserts generated swirl flow or secondary flow offering a longer flowing path of fluid flow through the tube; intensive mixing of fluid and pressure gradient might be created along the radial direction. Due to the tangential velocity component and lower flow cross-sectional area, the mixing of fluid between the fluids at the wall region and fluid at the core region was induced by the generated centrifugal force had significant ability to enhance the heat transfer rate.
6	2015	S. Eiamsa-ard, K. Kiatkittipong, W. Jedsadaratanachai [6]	Overlapped dual twisted-tapes		Working fluid: TiO$_2$/water nanofluid $5400 \leq Re \leq 15200$ $1.5 \leq y_o/y \leq 2.5$ $0.07\% \leq \varphi \leq 0.21\%$	**η=1.13** for Re=5400 TR=1.5 TiO$_2$/water φ=0.21%	Thermal performance factor increased as yo/y of O-DTs decreased. This implies that by decreasing yo/y, the augmentation of the heat transfer was more pronounced than pressure drop penalty. The thermal performance factor of O-DTs tended to decrease with the increase of Reynolds number.
7	2018	R.M. Sarviya and V. Fuskele [7]	Twisted tape insert having continuous cut edges		Working fluid: Water $3000 \leq Re \leq 19000$ $3 \leq y/W \leq 5$	**PEC=1.56** for Re=3000 y/W=3	The continuous cut edges cause the flow to spiral along the tube length and disturb the entire flow field that leads to higher heat transfer rate. removal of viscous sub-layer near tube wall is presumed to take place due to the additional turbulence generated by the continuous cut edges of R-CCTT and thus leading to a superior heat transfer improvement than TT.
8	2018	S. Eiamsa-arda, K. Wongcharee [8]	Non-uniform twisted tape		Working fluid: Ag/Water nanofluid $5210 \leq Re \leq 18000$ $1.8 \leq y/W \leq 3.010$ $0.007\% \leq \varphi \leq 0.03\%$	**PEC=1.62** **η=1.125** for Re=5210 y/W=3.0>2.4>1.8 φ=0.03%	The enhancing devices are more promising for energy saving at lower Reynolds numbers. The thermal performance factors associated with the use of non-uniform twisted-tapes (N-TT) with twist ratios (y/W) in series of 3.0>2.8>2.6, 3.0>2.6>2.2 and 3.0>2.4>1.8 were higher than those associated with the use of the typical twisted tape by around 1.3%, 3.0% and 4.6%, respectively.

2. NUMERICAL INVESTIGATION

2.1. Solution Domain

In this study, thermal performance of twisted tape with alternate axis inserted in a horizontal straight tube under constant heat flux is numerically investigated via a CFD program. Working fluid is selected as water. Solution domain that is modelled as 3D is schematically described as in Fig. 1. Mesh structures of the tube and the twisted tape are illustrated in Fig 2. The twisted tape has y/w ratio of 3.0. y and w represent the pitch length of twisted tape and width of the tape, respectively.
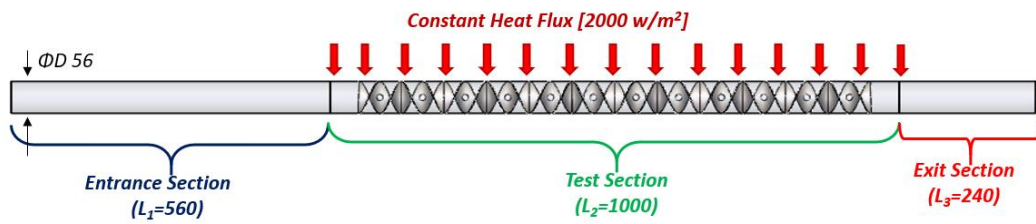
Figure 1. Solution domain and boundary types
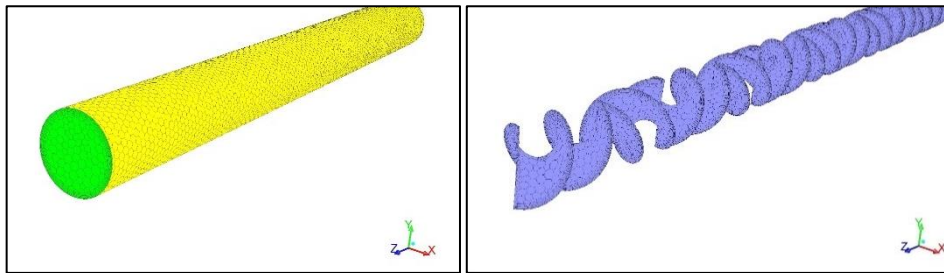
Figure 2. Mesh structures of the solution domain

The twisted tape comigrations are illustrated in Figure 3. Two periods length of the twisted tapes are selected as 75 mm. Three configurations are considered according to axis rotation direction. The configurations are named as AC, AACC and AAACCC.
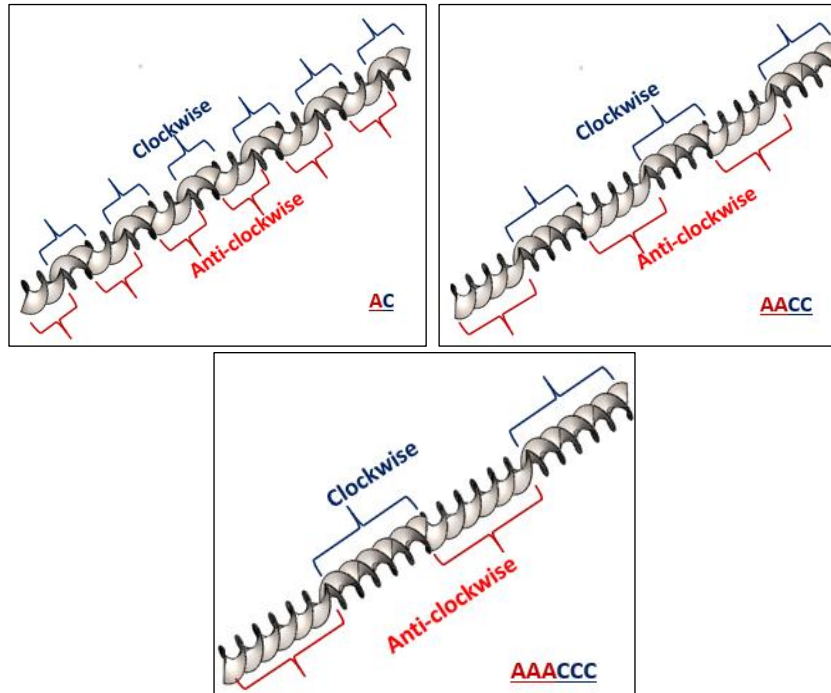
Figure 3. Configurations of the considered twisted tapes

2.2. Data Reduction

The CFD program uses differential equation to simulate and calculate flow characteristic and thermal occurrences. Used conversation equations in CFD program are as follows:

Conservation of mass equation [9]*:*

$$\frac{\partial \rho}{\partial t} + \nabla.(\rho u) = 0 \tag{1}$$

Conservation of momentum equation [9]:

$$\frac{\partial}{\partial t}(\rho \vec{v}) + \nabla(\rho \vec{v}\vec{v}) = -\nabla P + \nabla(\bar{\bar{\tau}}) + \rho \vec{g} + \vec{F} \tag{2}$$

Energy equation [15]:

$$\frac{\partial}{\partial t}(\rho E) + \nabla(\vec{v}(\rho E + p)) = \nabla\left(k_{eff}\nabla T - \sum_j h_j \vec{J}_i + (\bar{\bar{\tau}}_{eff}.\vec{v})\right) + S_h \tag{3}$$

The results were compared with S. Eimsa-ard [10] et al. and commonly used equations that are Gnielinski Eq. (6) and Blasius Eq. (7) in terms of Nusselt number (4) and friction factor (5), respectively.

Gnielinski Equation [11]:

$$Nu = \frac{hD}{k} \tag{4}$$

$$f = \frac{\Delta P}{\frac{1}{2}\rho V^2 \frac{L}{D}} \tag{5}$$

$$Nu = \frac{\left(\frac{f}{8}\right)(Re-1000)Pr}{1+\left[12.7\left(\frac{f}{8}\right)^{0.5}(Pr^{2/3}-1)\right]}$$
(6)

Blaisus Eq. [12]:

$$f = 0.316Re^{-0.25}$$
(7)

2.3. *Validation of the numerical methodology*

Different turbulence models are tested and k-w standard model is most matching model with reference results. Validation of the numerical study for smooth tube and water is given in Fig 4 in terms of Nusselt number and friction factor, respectively. As can be seen in these figures, a good agreement is ensured for proving accuracy of numerical methodology.
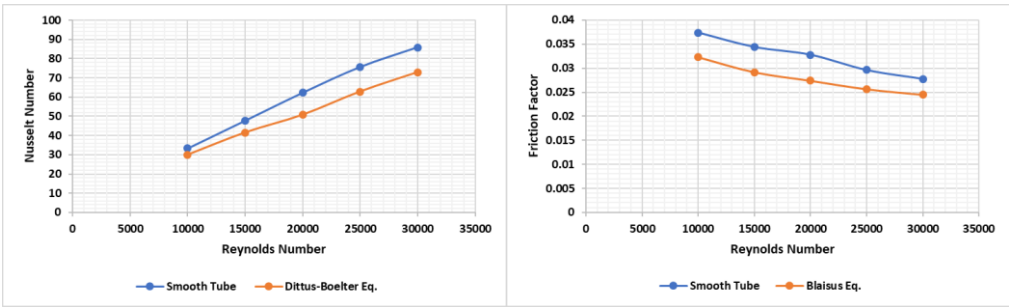
Figure 4. Validation of the numerical results for smooth tube according to (a) Nusselt number and (b) friction factor versus Reynolds number

3. RESULTS AND DISCUSSIONS

Using twisted tape enhance the heat transfer performance as can be seen in literature. The originality of this study which is twisted tape with alternate axis showed a good heat transfer enhancement. However, pressure drop penalty is higher than smooth tube.

Main reason of the enhancing heat transfer is that the twisted tapes destruct the thermal boundary layer as can be seen in Figure 5. Moreover, using twisted tape with alternate axis generates secondary flow through the flow by mixing the flow consecutively among the alternate axis rotation directions (Fig. 6). As mentioned before, using twisted tapes with alternate axis blocks the flow, and so the fluid friction and pressure drop penalty increase, as can be seen in Fig 7.
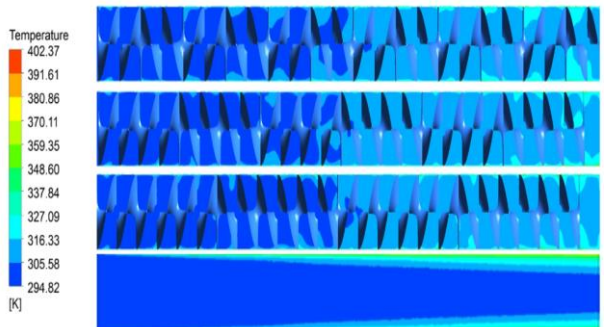
Figure 5. Temperature contours of the considered twisted tape inserted tubes and the smooth tube
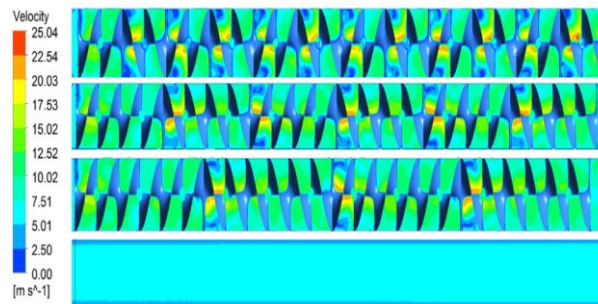
Figure 6. Velocity contours of the considered twisted tape inserted tubes and the smooth tube
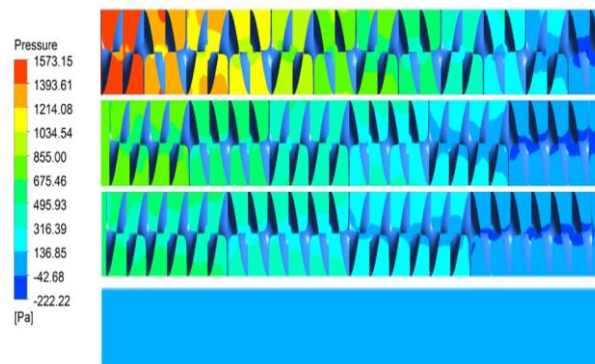
Figure 7. Pressure contours of the considered twisted tape inserted tubes and the smooth tube

4. CONCLUSION

Consequently, the used twisted tape increases the heat transfer performance. Furthermore, Fig. 8 shows that the more alternate axis (AC to AAACCC) increase heat transfer performance. However, AC twisted tape comigration dramatically increases the friction factor compared the smooth tube among the other twisted tapes, in Fig. 9. Performance evaluation criteria (PEC) is useful, when thermal and hydraulic performance are examined together. Fig. 10 shows that the AAACCC twisted tape is the best configuration according to PEC.

The results can be summarized in three items.

- Using twisted tape in a tube provides high heat transfer performance, but high friction. Number of different alternate axis rotation, heat transfer enhances significantly, but at this time, pressure drop penalty increases due to friction.

- Performance evaluation criteria (PEC) is used to determine the heat transfer performance and hydraulic performance. The PEC results of the study are lower than 1.0. It means that pumping power cost has to consider when using these twisted tapes in a heat exchanger system.

- When the pumping power does not matter, thermal efficiency (η) is obtained as about 3.5 times greater than smooth tube for AC configuration at Reynolds number of 10,000.
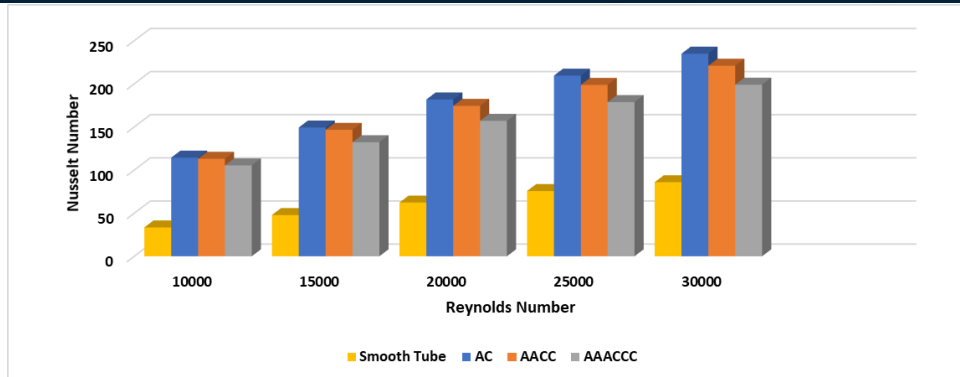
Figure 8. Nusslet number versus Reynolds number results of the considered twisted tape configrations.
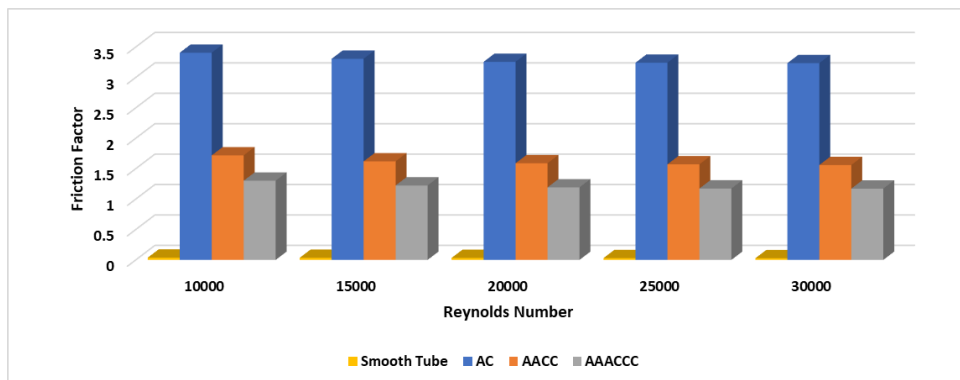
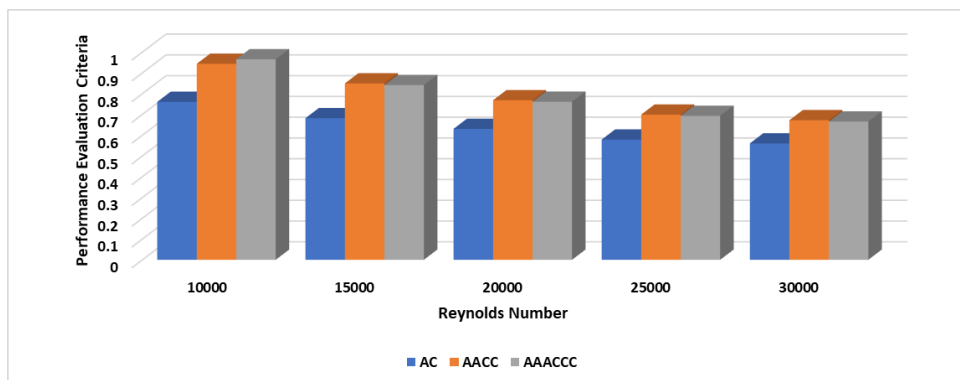*Figure 9. Friction factor versus Reynolds number results of the considered twisted tape configrations.*

Figure 10. Performance evaluation critera (PEC) number versus Reynolds number results of the considered twisted tape configrations.

ADKNOWLEDGEMENT

REFERENCES

[1]   S. Eiamsa-ard and P. Promvonge, "Performance assessment in a heat exchanger tube with alternate clockwise and counter-clockwise twisted-tape inserts", *International Journal of Heat and Mass Transfer*, vol. 53, pp. 1364-1372, 2010.

[2]   S. Suresh, K.P. Venkitaraj, P. Selvakumar, "Comparative study on thermal performance of helical screw tape inserts in laminar flow using Al2O3/water and CuO/water nanofluids", *Superlattices and Microstructures*, vol. 49, pp. 608-622, 2011.

[3]   H. Bas and V. Ozceyhan, "Heat transfer enhancement in a tube with twisted tape inserts placed separately from the tube wall", *Experimental Thermal and Fluid Science*, vol. 41, pp. 51-58, 2012.

[4]   K. Nanan, K. Yongsiri, K. Wongcharee, C. Thianpong, S. Eiamsa-ard, "Heat transfer enhancement by helically twisted tapes inducing co- and counter-swirl flows", *International Communications in Heat and Mass Transfer*, vol. 46, pp. 67-73, 2013.

[5]   M.M.K. Bhuiya, M.S.U. Chowdhury, M. Saha, M.T. Islam, "Heat transfer and friction factor characteristics in turbulent flow through a tube fitted with perforated twisted tape inserts", *International Communications in Heat and Mass Transfer,* vol. 46, pp. 49-57, 2013.

[6]   S. Eiamsa-ard, K. Kiatkittipong, W. Jedsadaratanachai, "Heat transfer enhancement of TiO2/water nanofluid in a heat exchanger tube equipped with overlapped dual twisted-tapes, *Engineering Science and Technology, an International Journal*, vol. 18, pp. 336-350, 2015.

[7]   R.M. Sarviya, Veeresh Fuskel, "Heat Transfer and Pressure Dropina Circular Tube Fitted with Twisted Tape Insert Having Continuous Cut Edges", *Journal of Energy Storage*, vol. 19, pp. 10-14, 2018.

[8]   S. Eiamsa-arda, K. Wongcharee, "Convective heat transfer enhancement using Ag-water nanofluid in a micro-fin tube combined with non-uniform twisted tape", *International Journal of Mechanical Sciences,* vol. 146, pp. 337-354, 2018.

[9]   *Fluent v.6.3 User Guide*, Fluent Corporation, Lebanon, New Hampshire, 2006.

[10] S. Eimsa-ard, P. Seemawute, K. Wongcharee, Influences of peripherally-cut twisted tape insert on heat transfer and thermal performance characteristics in laminar and turbulent tube flows, Experimental Thermal and Fluid Science, 2010, vol. 34, pp. 711-719.

[11] F.P. Incropera, P.D. Witt, T.L. Bergman, A.S. Lavine, *Fundamental of Heat and Mass Transfer*, John-Wiley & Sons, 2006.

[12] Petukhov BS: Heat transfer and friction in turbulent pipe flow with variable physical properties. *In Advances in Heat Transfer*. Edited by: Hartnett JP, Irvine TS. New York: Academic Press; 1970.

Investigation of Solar Energy Potential in the Southeastern Anatolia

Fevzi Onen[1]

Abstract

In parallel with the increase of Turkey's population and growing economy, consumption of energy resources has also increased in recent years. Turkey is dependent on foreign supplies by 73% in the current situation. In order to reduce this rate, it is carrying out studies on the determination of the potential of renewable energy sources while carrying out exploration works of fossil energy sources. Southeastern Anatolia Region of Turkey with economic and cultural wealth, which is a geographical and historical significance, has hosted many civilizations. In the Southeastern Anatolia Region, electricity generation from solar energy systems is expected to be one of the important investment opportunities of the future.

Compared to other regions of Turkey, most of the solar fields are located in the Southeastern Anatolia Region. Considering the average sunshine duration and Global Radiation Values in the Solar Energy Potential Map (GEPA), it is observed that the Southeastern Anatolia Region is rich in Solar Energy. In Şanliurfa, Gaziantep, Diyarbakir and other provinces, where the number of annual sunbathing days is high, investors started to operate many large and small solar power plants with the support of the state. A 250 kilowatt solar power plant was established in 3 thousand decares of land within the GAP International Agricultural Research and Training Center in Diyarbakir. In addition, the largest investment in the Southeastern Anatolia Region is the power plant with an annual capacity of 24 million kilowatt-hours, which consists of 40 thousand solar panels in Sanliurfa.

Keywords: Renewable Energy Sources, Solar Energy, Southeastern Anatolia Region, Diyarbakir

1. INTRODUCTION

In parallel with the increase of Turkey's population and growing economy, consumption of energy resources has also increased in recent years. Turkey is dependent on foreign supplies by 73% in the current situation. In order to reduce this rate, it is carrying out studies on the determination of the potential of renewable energy sources [1]. Turkey is in a very fortunate situation compared to many countries in terms of solar energy potential. Turkey is a country with a very high potential of solar energy as the average of **110 days**. The highest and lowest months in which solar energy is produced are **June and December**

Solar energy is one of the renewable energy sources that are becoming more and more popular every day. Southeastern Anatolia Region of Turkey, which has historical importance and cultural richness and economic geography, has hosted many civilizations. Electricity generation from solar energy systems in the Southeastern Anatolia Region is expected to be one of the major investment opportunities of the future.

Southeastern Anatolia Region is a very rich place in terms of solar energy from renewable energy sources. **Southeast Anatolia** and **Mediterranean region** are the highest region in terms of sunshine duration, while the **Black Sea** region is the lowest region (Table 1).

Table 1. Sunshine duration of regions [2]

Region name	Southeastern Anatolia	Mediterranean	Aegean	Eastern Anatolia	Central Anatolia	Marmara	Black Sea
Sunshine duration (hours / year)	2993	2956	2738	2664	2628	2409	1971

[1] *Dicle University, Department of Civil Engineering, 21280, Sur/Diyarbakir, Turkey. fonen@dicle.edu.tr*

As can be seen from the annual solar energy potential map of Turkey, the Mediterranean region and southeast are the most efficient in terms of solar energy potential (Figure 1).
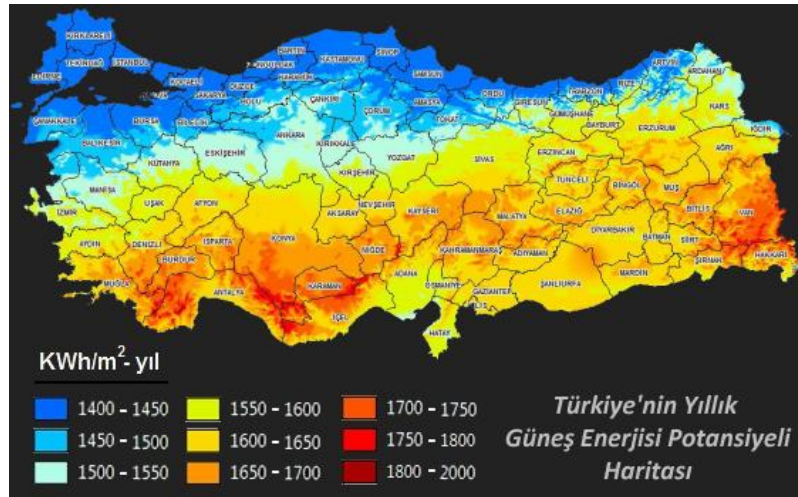

Figure 1. Turkey's annual solar energy potential map [3]

Profile of Solar Power Plants in Turkey:

- There is 1644 Solar Power Plant in Turkey. Total installed capacity is 1362.60 MW. In 2016, 1 020 000 000 kilowatt-hours of electricity were generated by the Solar Power Plants.

- Solar Power Plants are available in two different ways as **photovoltaic system** and **thermal systems.**

- **In the photovoltaic system**, radiation from the sun is converted into energy by means of panels.

- **Photovoltaic systems** are used more widely in Turkey.

2. MATERIALS AND METHODS

Solar Energy Potential of Southeastern Anatolia Region

Şanliurfa and Mardin are the highest provinces in terms of sunshine duration, while Diyarbakir is the lowest province (Table 2).

Table 2. Sunshine duration according to the Southeastern Anatolia Region provinces

Province	Sunshine duration (hours / year)
Adiyaman	2961
Gaziantep	2978
Şanliurfa	3033
Mardin	3033
Diyarbakir	2613
Şirnak	2975
Batman	2873
Siirt	2828
Kilis	2975

The solar energy potential maps and the existing solar power plants of the provinces in the Southeastern Anatolia region, the solar power plants under construction, and the solar power plants obtained from the pre-license and the planned solar power plants are given below [4].

Active, under construction, pre-license and planned solar energy investments in Adiyaman:

Active Solar Power Plants: **9.36** MW (12 units)
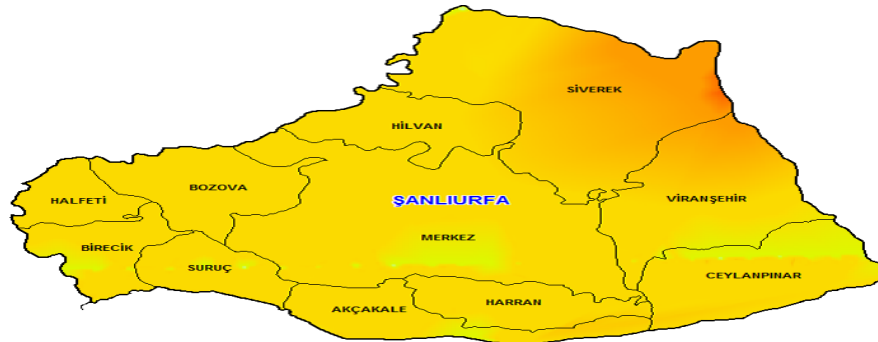
Solar Power Plants Under Construction: **1.28** MW (2 units)

Prequalification received: **10 MW** (1 unit)

Planned Solar Power Plants: **2.05** MW (1 unit)
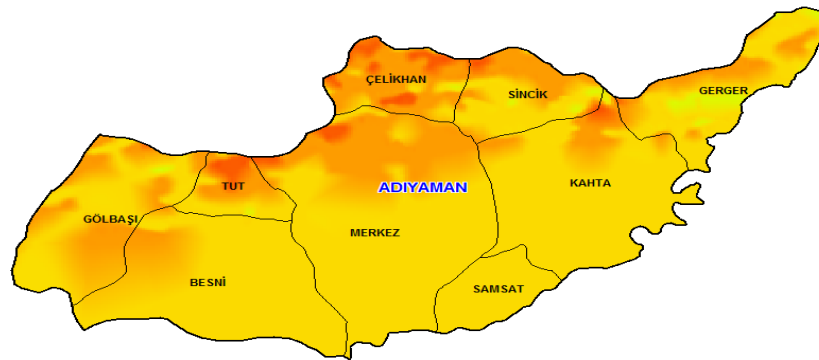
Figure 2. Adiyaman Solar Energy Potential Map

Active, under construction, pre-license and planned solar energy investments in Şanliurfa:

Active Solar Power Plants: **9.32** MW (3 units)

Solar Power Plants Under Construction: **46** MW (3 units)

Figure 3. Şanliurfa Solar Energy Potential Map

Active, under construction, pre-license and planned solar energy investments in Diyarbakir:

Active Solar Power Plants: **2.54** MW (5 units)

Solar Power Plants Under Construction: **2.23** MW (3 units)

Figure 4. Diyarbakir Solar Energy Potential Map

Active, under construction, pre-license and planned solar energy investments in Kilis:

Active Solar Power Plants: **7.74** MW (5 units)

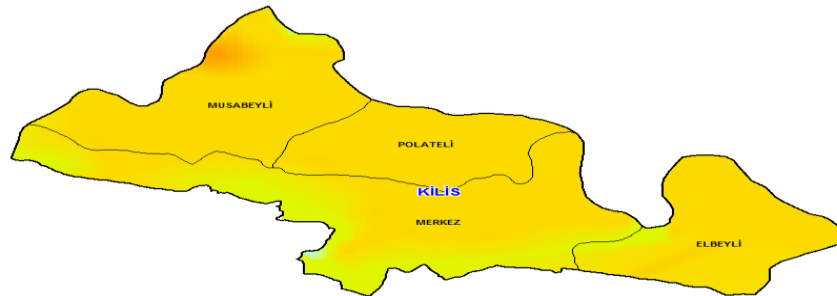Solar Power Plants Under Construction: **13.90** MW   (5 units)

Figure 5. Kilis Solar Energy Potential Map

Active, under construction, pre-license and planned solar energy investments in Gaziantep:

Active Solar Power Plants: **85.16** MW (20 units)

Solar Power Plants Under Construction: **40.21** MW (5 units)

Active, under construction, pre-license and planned solar energy investments in Mardin:

Active Solar Power Plants: **0.335** MW (2 units)

Prequalification received: **9 MW** (1 unit)

Active, under construction, pre-license and planned solar energy investments in Şirnak:

Solar Power Plants Under Construction: **0.3** MW (1 units)

Prequalification received: **7** MW (1 unit)

Active, under construction, pre-license and planned solar energy investments in Batman:

Active Solar Power Plants: **6** MW (1 units)

Solar Power Plants Under Construction: **1** MW (1 units)

Active, under construction, pre-license and planned solar energy investments in Batman:

Active Solar Power Plants: **0.20** MW (1 units)

Solar Power Plants Under Construction: **0.48** MW (1 units)

Dicle University Faculty of Engineering Solar Power Plant:

- Installed Power: 0,250 MW (250 kW)

- Number of Panels: 1000

Figure 6. View of solar energy panels at Dicle University.

CONCLUSION

When the Southeastern Anatolia Region of Turkey evaluated in terms of the direction of the Renewable Energy Sources Solar Energy it has a production capacity above the average.

The installation of Solar Power Plants has been accelerating in recent years.

Gaziantep province has the highest number of solar power plant investments. This province is followed by Şanliurfa and Adiyaman.

REFERENCES

[1]. H.Gülşen, C.Çiftçi, Güneydoğu Anadolu Bölgesinin Yenilenebilir Enerji Kaynaklari Bakimindan Potansiyelinin Araştirilmasi, Academia Journal of Engineering and Applied Sciences, Vol. 1, Issue 3, pp.48-56. 2017
[2]. Elektrik işleri Etüd idaresi www.eie.gov.tr
[3]. www.solar-med-atlas.org
[4]. www.enerjiatlasi.com/gunes-enerjisi

Prediction of Scour around a Side Weir in Linear Channel with GEP Model

Hayrettin Kaya[1], Fevzi Onen[2]

Abstract

Side-weirs have been widely used in hydraulic and environmental engineering applications. Side-weir is known as a lateral intake structure, which are significant parts of the distribution channel in irrigation, land drainage, and urban sewerage system, by flow diversion device. Local scour involves the removal of material around piers, abutments, side-weir, spurs, and embankments. Scour depth (H_d/p) based on four dimensionless parameters: approach flow velocity (V_1/V_c), water head ratio ($h_1 − p$)/h_1, side-weir length (L/b) and sediment size (d_{50}/p). The aim of this study is to develop a new formulation for prediction scour of side-weir intersection along the linear channel using Genetic Expression Programming (GEP) which is an algorithm based on genetic algorithms (GA) and genetic programming (GP). In addition, by looking at the Determination Coefficient (R^2) and the Mean Squared Error (RMSE), the predicted values obtained from the model were compared with the measured values. Sensitivity analysis is performed for GEP, and it is found that approach flow velocity (V_1/V_c) and water head ratio ($h_1 − p$)/h_1 are the most effective parameters on the scour depth.

Keywords: Side-weir, Scour depth, Genetic expression programming, Determination coefficient

1. INTRODUCTION

Side-weirs have been widely used in hydraulic and environmental engineering applications. Side-weir is known as a lateral intake structure, which are significant parts of the distribution channel in irrigation, land drainage and urban sewerage system. Side weirs are also used as an emergency structure in many hydraulic structures.

Onen and Agaccioglu [1] provided the expression of the change of the water surface along the side weir in a prismatic, horizontal and frictionless channel with a rectangular cross-section.

$$\frac{dh}{dx} = \frac{Qh\left\{-\dfrac{dQ}{dx}\right\}}{gb^2h^3 - Q^2} \qquad (1)$$

where; dh/dx=Change of water profile, Q=Main channel discharge rate (m^3/s), h=flow depth (m), b=main channel width (m), g=gravitational acceleration (m^2/h) and dQ/dx is given as flow rate (m^3/s.m) from unit length (Fig. 1). The water level rises from the upstream end of the side-weir towards the downstream end of the side-weir in the main channel in accordance with Equation (1) for subcritical flow conditions in the main channel (Figure 1).

---

[1] *DSİ, 21280, Sur/Diyarbakir, Turkey., h-kaya@dsi.gov.tr*

[2] *Corresponding author: Dicle University, Department of Civil Engineering, 21280, Sur/Diyarbakir, Turkey. fonen@dicle.edu.tr*
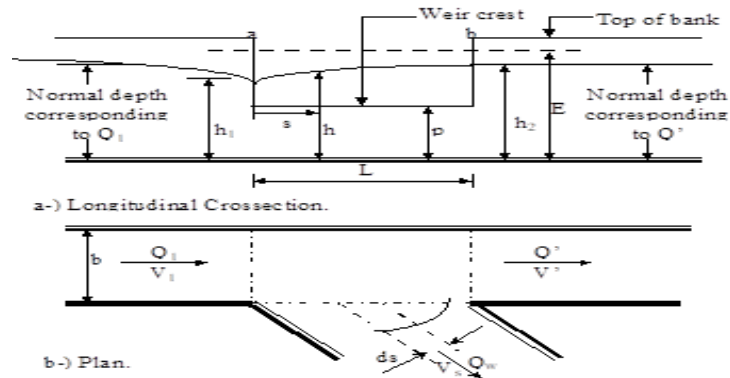
Figure 1. Definition sketch of subcritical flow over a rectangular side-weir [4]

According to Subramanya and Awasthy [2], El-Khashab [3], Agaccioglu and Yüksel [4] and Agaccioglu and Cosar [5], the location and size of the separation zone and reverse flow area depend on the intensity of secondary flow (Figure 2). When the flow velocity or remaining momentum towards the downstream direction in the main channel increases then the reverse flow area and the separation zone move towards the downstream end of the side weir.
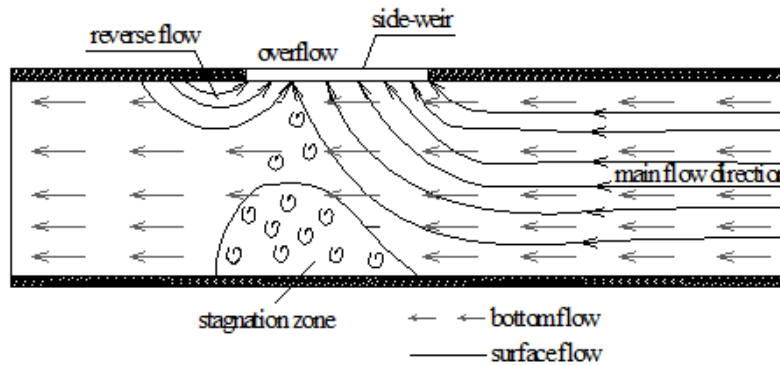

Figure 2. The position of the stagnation zone and reverse flow [5]

Chiew [6] mentioned that

- Clear-water scour occurs if the flow velocity is less than the critical speed (V<Vc)

- Live bed scour occurs If the flow velocity is greater than the critical velocity (V>Vc),

- The maximum depth of scour occurs at $V=V_c$

The changes in the main channel bottom topography around side-weirs are briefly mentioned according to flow visualization and the obtained bottom topography as given in Figure 3. According to observations during experiments, the location of maximum scour hole moves toward the downstream with an increasing of the dimensionless parameters of approach flow velocity V_1/V_c and water head ratio $(h_1-p)/h_1$ [7].
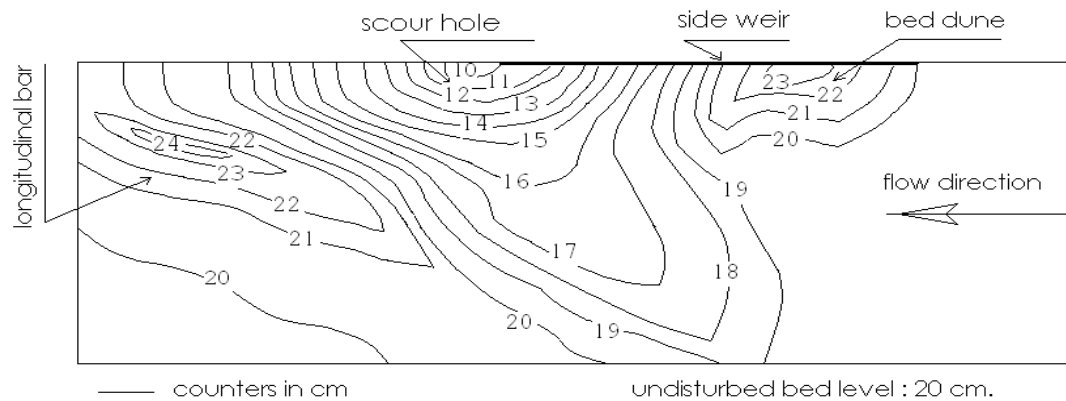
Figure 3. Bed topography at a side-weir.

Onen and Agaccioglu [8] experimentally investigated scour at side-weir intersection located on an alluvial river. Authors presented dimensionless parameters affected to the scour as follows:

$$H_d/p = f(V_1/V_c, L/b, h_1\text{-}p/h_1, d_{50}/p) \tag{2}$$

Where: the dimensionless parameters of V_1/V_c, L/b, $(h_1\text{-}p/h_1)$, d_{50}/p represent respectively, approach flow velocity, the water head ratio, the side-weir length and sediment size.

2. EXPERIMENTAL SETUP

- Experiments for studying the development of the scour depth both of clear-water and live bed scour at a side-weir intersection located on a straight alluvial channel are carried out with a model on a rectangular Plexiglas flume at the Hydraulic Laboratory of Yildiz Technical University, Istanbul, Turkey.

- The main flume is 40 cm wide with a 55 cm depth and a well-finished aluminum bottom. The discharge collection flume is 55 cm depth, 50 cm width and situated parallel to the main flume. Details of flume are shown in Figure 4.

- Side-weirs were located at the mid of the straight part of main channel. Three different lengths (25, 40 and 50 cm) and three different weir crest height (7, 12 and 17 cm) of the side-weir were placed on the side-weir station.

- Uniform bed materials are placed on a 20 cm thick layer in the flume with a bed slope of 0.001. The bed of the flume is firstly mixed to prevent sediment grading and layering, and then flattened before each run.

- No sediment inflow is allowed from the upstream end for clear-water conditions. Sediment discharges are first determined in the variable flow condition with prior experiments for live bed scours. The sediment is subsequently fed from a hopper-feeder arrangement the sediment feeding equipment is fitted with controllable vibrators that maintained a steady outflow rate of sediment. Then, the determined sediment quantities are fed from the upstream end of the main channel through the period of experiment for each of experiments. Live bed scour experiments are carried out for between 15 and 90min and for each experiment it has been continued in order to allow a minimum of four to five bed dunes to pass from the side-weir location. Besides, the live bed scour experiment was stopped before filling the scour hole with coming a new dune in the point of losing the effect of the bed dune which fills the scour hole.
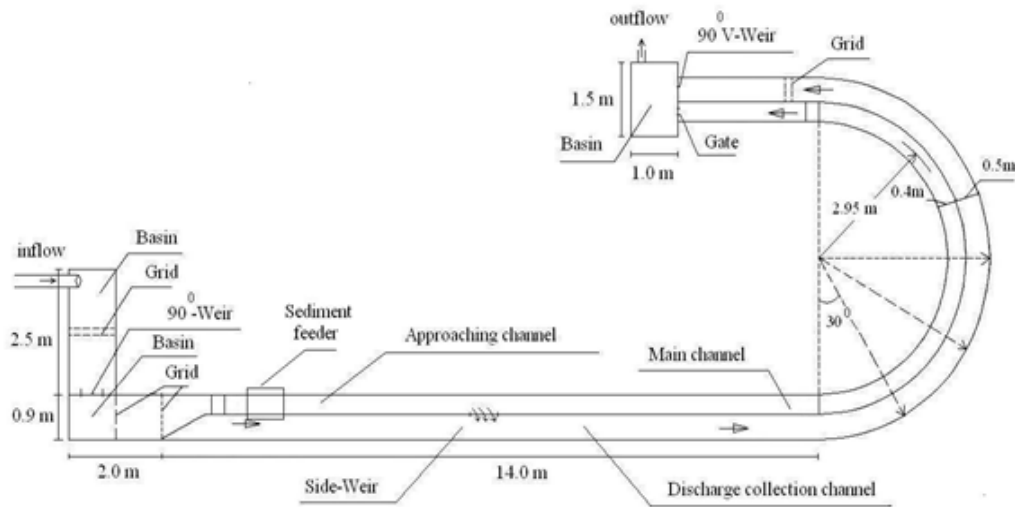
Figure 4. Plan of test flume

3. GENETİC EXPRESSİON PROGRAMMİNG

Gene expression programming (GEP) is an algorithm based on genetic algorithms (GA) and genetic programming (GP). This algorithm develops a computer program encoded in linear chromosomes of fixed-length. The main aim of GEP is to develop a mathematical function using a set of data presented to GEP model. For the mathematical equation the GEP process performs the symbolic regression by means of the most of the genetic operators of GA. The process starts with the generation of the chromosomes of a certain number of individuals (initial population). Then these chromosomes are expressed and the fitness of each individual is evaluated against a set of fitness cases. Then, the individuals are selected according to their fitness to reproduce with modification. These new individuals are subjected to the same developmental processes such as expression of the genomes, confrontation of the selection environment, selection, and reproduction with modification. The process is repeated for a certain number of generations or until a good solution is found [9].

The two main elements of GEP are the chromosomes and expression trees (ETs). The chromosomes may be consisted of one or more genes which represents a mathematical expression. The mathematical code of a gene is expressed in two different languages called Karva Language such as the language of the genes and the language of the expression trees (ET). The flowchart of GEP is given in Figure 5 [10].
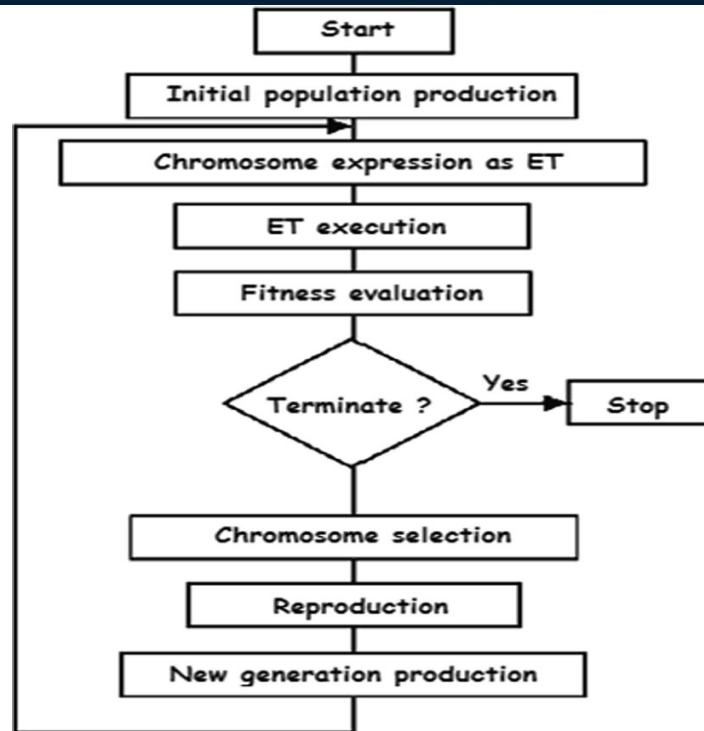
Figure 5. Genetic-expression programming (GEP) algorithm

Genetic expression programming (GEP) is an algorithm based on genetic algorithms (GA) and genetic programming (GP). The main aim of GEP is to develop a mathematical function using a set of data presented to GEP model. The two main elements of GEP are the chromosomes and expression trees (ETs). The GEP model has four input parameters (V_1/V_c, L/b, (h_1-p/h_1), d_{50}/p).

There are five major steps in preparing to use genetic expression programming. The selection of the fitness function. The second major step consists in choosing the set of terminals T and the set of function F to create the chromosomes. The third major step is to choose the chromosomal architecture, i.e. the length of the head and the number of genes. The fourth major step is to choose the linking function. And finally, the fifth major step is to choose the set of genetic operators that cause variation and their rates. Parameters of the training of the GEP models are given in Table 1.

Table 1. *Parameters of the optimized GEP model*

Parameter	Description of parameter	Setting of parameter
P_1	Chromosomes	30
P_2	Fitness function error type	R^2
P_3	Number of the genes	3
P_4	Head size	8
P_5	Linking function	*
P_6	Function set	+, -, *, /,1/X, $X^{1/2}$, $X^{1/3}$, X^2, X^3
P_7	Mutation rate	0.044
P_8	One-point recombination rate	0.3
P_9	Two-point recombination rate	0.3
P_{10}	Inversion rate	0.1
P_{11}	Transposition rate	0.1

The performance of GEP model is validated in terms of the common statistical measures coefficient of determination (R^2) and root-mean-square error (RMSE).

4. CREATION OF GEP MODEL

In the proposed models, the input parameters V/V_c, L/b, $(h_1\text{-}p)/h_1$, d_{50}/p and output H_d/p parameters are used. All the parameters are defined and then the models are simulated. GeneXproTools 5.0, a powerful soft computing software package was used to create GEP models. This program provides a compact and clear mathematical expression. The termination criterion was the maximum average fitness function, which is the mean square root error (RMSE) function. The program is run for a number of generations and is stopped if there is no improvement in the fitness function value or coefficient of determination (R^2).

In this study, 235 data of four independent parameters were used to construct GEP model. A total of 235 data, 80% (188) was used for training purposes and 20% (47) was used for testing purposes. Training data (188) was first used to construct the model. Other 47 data models were used to test/validation.

The GEP formulation model based on ET is developed as:

```
y = (((((d[2]+d[1])+d[0])+d[2])*((d[2]+d[1])*(d[2]-d[3])))        *
(((((d[0]*d[0])*(G2C7*d[3]))*pow((d[2]*d[1]),3))+d[2]);
*((sqrt((d[3]*G3C3))+pow(d[2],3))-((d[3]*d[3])-(d[1]*d[3])));          (10)
```

where the constants in the formulation are G2C7=-15.06 ve G3C3=10.63 and the actual parameters are d[0]=V1/Vc, d[1]=L/b, d[2]=(h1-p)/h1 and d[3]=d50/p. After putting the corresponding values, the final equation becomes

$$
Hd/p =
$$
$$
\left((V/V_{kr} + L/b + 2\,(h_1{-}p)/h_1) * (L/b + (h_1{-}p)/h_1) * ((h_1{-}p)/h_1 - d_{50}/p) \right) *
$$
$$
\left((V/V_{kr})^2 * (d_{50}/p * -15.06) * \left(((h_1{-}p)/h_1 * L/b)^3) + (h_1{-}p)/h_1 \right) \right) *
$$
$$
\left(\left(\sqrt{d_{50}/p * 10.63} + ((h_1{-}p)/h_1)^3 \right) - \left((d_{50}/p)^3 - (L/b * (d_{50}/p)) \right) \right)
$$

The training performance of proposed GEP model showed a high generalization capacity with $R^2 = 0.864$ and RMSE = 0.154 for maximum scour depth Figure 6.
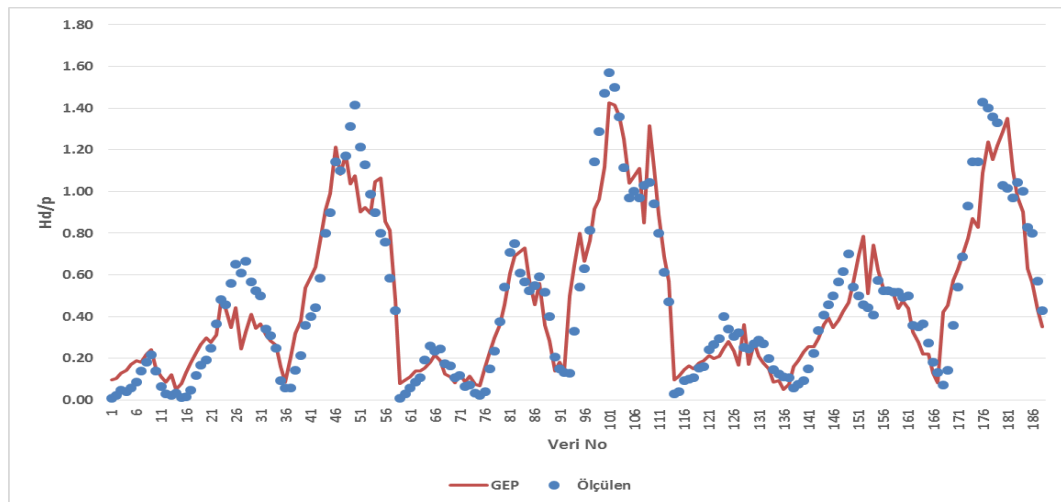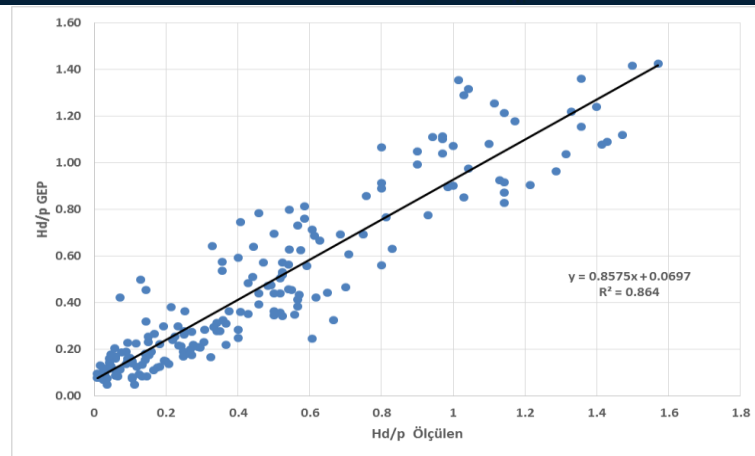
Figure 6. GEP estimations of Hd/p versus measured ones for train set

5. CONCLUSION

Scour depth based on four dimensional parameters: approach flow velocity (V_1/V_c), water head ratio (h_1-p)/h_1, side-weir length (L/b) and sediment size (d_{50}/p).

The explicit formulations of the developed GEP models are presented.

The testing performance of proposed GEP model showed a high generalization capacity with $R^2 = 0.864$ and RMSE = 0.154 for maximum scour depth.

As a result of the study, it is determined that the model performs well by comparing the values calculated in the mathematical modeling with the values measured in the physical model.

Additionally, sensitivity analysis is performed and it is found that V/Vc and sediment size (d_{50}/p) is the most effective parameter on scour depth.

ACKNOWLEDGEMENT

REFERENCES

[1]. Onen, F., Agaccioglu, H. Live bed scour at a side-weir intersection located on an alluvial channel. *Irrigation and Drainage*, *62*(4), pp.488-500. 2013.

[2]. Subramanya K, Awasthy SC. Spatially varied flow over side-weirs. Journal of Hydraulic Engineering ASCE 98(1): 1–10. Yu-TechL.1972.Discussionofspatiallyvariedflowoverside-weirs.Journal of the Hydraulic Division, ASCE 9(11): pp.2046–2048. 1972

[3]. El-Khashab AMM.. Hydraulics of flow over side-weirs PhD thesis, presented to the University of Southampton, England. Emiroglu ME, Kaya N. 2011. Discharge coefficient for trapezoidal labyrinth side weir in subcritical flow.

[4]. Agaccioglu H, Yuksel Y. 1998. Side-weir flow in curved channel. Journal of Irrigation and Drainage Engineering, ASCE 124(3): pp.163–175. 1975

[5]. Cosar A, Agaccioglu H.. Discharge coefficient of a triangular side weir located on a curved channel. Journal of Irrigation and Drainage Engineering, ASCE 130(5): pp.410–423. 2004

[6]. Chiew YM.. Local scour at bridge piers PhD thesis, University of Auckland, NZ, School of Eng., Rept.. No. 355. Chow VT. 1959. Open Channel Hydraulics. McGraw-Hill: New York; ch. 16, pp.439–460. 1984

[7]. Agaccioglu H, Onen F. Clear-water scour at a side-weir intersection along the bend. Irrigation and Drainage 54(5): pp.553–569. 2005.

[8]. Önen, F., Agaçcioglu, H. Scour at a side-weir intersection located on an alluvial river. *Hydrology Research*, *38*(2), pp.165-176. (2007).

[9]. Onen, F. Prediction of scour at a side-weir with GEP, ANN and regression models. *Arabian Journal for Science and Engineering*, *39*(8), pp.6031-6041. 2014

[10]. Onen, F. GEP prediction of scour around a side weir in curved channel. *Journal of Environmental Engineering and Landscape Management*, *22*(3), pp.161-170. 2014

Cloud-Based Speech Recognition Approach for Smart Home Systems

Saadin Oyucu[1], Ahmet Aksoz[2], Hüseyin Polat[3], Hayri Sever[4]

Abstract

Technologies that support people's communication with each other have changed structurally over time and human-machine interaction has emerged. One of the technologies that support human-machine interaction is the Internet of objects. With the Internet of objects, it is ensured that not only people communicate with themselves, but also with computers and other electronic devices. One of the applications of the Internet of Things is smart home systems. Smart home systems lighting, security, ventilation, temperature, etc. It allows users to control and track the systems more easily. Smart home users want to establish the communication they manage to their mother tongue by using the same devices that make up the smart home system. User rating communicating with the devices that make up the smart home system, allowing the machine and electronic devices to operate the command and control mechanism more quickly. For this reason, the requirements for a smart home system to work with voice commands and the advantages of speech recognition technologies are investigated. Cloud-based solutions were concluded that in more advantageous for Speech recognition technology. At the end of the study, a Turkish automatic speech recognition system was developed and presented via the cloud platform. A smart home system was also prepared as a model. Speech recognition requests from the smart home system were resolved on the cloud platform and transferred back to the smart home system. Thus, the processing power required for speech recognition was transferred to the cloud. The devices that make up the smart home system are only given the task of executing commands.

Keywords: Speech Recognition, Smart Home, Cloud Computing

1. INTRODUCTION

Automatic Speech Recognition (ASR) is defined as an intelligent system that can automatically translate phoneme or phoneme arrays from speech functions into text [1]. In other words, ASR, microphone or telephone input by the words spoken by the people is expressed as a machine-readable technology that transcribe [2].

ASR systems are developed by using different disciplines together. The overall structure of the ASR is also very complex. [3]. Therefore, although many studies have been made on ASR systems, the desired performance level has not been reached yet. In recent years, especially fast, high-capacity processor and memory technologies are becoming widespread, their performance is constantly increasing, allowing the creation of complex and powerful models required for ASR systems [4].

Mainly used in two different models of the ASR system. The first is the acoustic model from which acoustic information is obtained [5]. The second is the language model used to support acoustic knowledge and to express the language structure mathematically [6]. The division of acoustic modeling and language modeling used in ASR systems defines statistical speech recognition systems as in equation 1 [7].

[1] *Corresponding author: Gazi University, Department of Computer Engineering, 06500, Teknikokullar/Ankara, Turkey.* soyucu@gazi.edu.tr

[2] *Sivas Cumhuriyet University, Department of Mechatronics Engineering, 58500, Merkez/Sivas, Turkey.* aaksoz@cumhuriyet.edu.tr

[3] *Gazi University, Department of Computer Engineering, 06500, Teknikokullar/Ankara, Turkey.* hpolat@gazi.edu.tr

[4] *Çankaya University, Department of Computer Engineering, 06120, Çayyolu/İstanbul,* Turkey.sever@cankaya.edu.tr

$$W = \arg max P(W \mid A) = \arg max \frac{P(W)P(A|W)}{P(A)}$$

(1)

In Equation 1, the acoustic phoneme or feature vector sequence gives the corresponding word sequence in the speech recognition system for X = X1, X2,…, Xn. The maximization of the equation is directly dependent on the maximization of the share since it is performed with constant X observation. P (W) and P (X | W) components constitute the probabilistic quantities calculated by language modeling and acoustic modeling.

Basically, the austonic model calculates the posterior probability of the phoneme within a given time signal frame. Hidden Markov Models (HMM) are generally used to determine phoneme order [8]. Alignment of phonemes Gaussian Mixture Model (GMM: Gaussian Mixed Model) (HMM / GMM) using the distribution [9]. In HMM, Markov assumptions are made during the transition between the states and only the previous state is taken into consideration in the transition from one state to another.

Macinar the scope of this ISBN and electronic device for faster execution command and control mechanisms intended to communicate with the device that generates the intelligent home. Studies were carried out to make communication with speeches. Therefore, the smart home system works with voice commands and the advantages of speech recognition technologies have been examined. It has been concluded that cloud-based solutions are more advantageous, especially for embedded devices with limited resources.

At the end of the study, a Turkish automatic speech recognition system was developed. A ready set of data was used for this system. The developed system is presented via cloud platform. A scenario was prepared as an example in the smart home system. Speech recognition requests from the smart home system were resolved on the cloud platform and transferred back to the smart home system. Thus, the processing power required for speech recognition was transferred to the cloud. Only devices that make up the smart home system are assigned to run commands.

The speech parts obtained using the proposed method are used as separate inputs and sent to the cloud. The text data corresponding to the speech parts provided as input are sent back to the devices that comprise the smart home system. It is clear from the experiments that this approach increases the performance of the ASR system used in smart home systems. It also reduced the processing load on resource-constrained devices.

2. MATERIALS AND METHOD

Speech information to be sent to the cloud structure is expected to be lossless. Therefore speech data should be separated into parts at the right time. If the components are large, both the transmission time in the network and the solution time in the ASR system will be large. This is undesirable. The materials and methods to be used are important in this respect and should be handled with care. In this section, the ASR system of the whole material and methods for bridging the data set used in development are described in detail.

2.1. Turkish Automatic Speech Recognition System

The voice command files received via electronic devices must be transferred to the Turkish ASR system to be transferred to the text. Therefore, a basic Turkish ASR system was developed in the study. The Kaldi toolkit was used to develop the ASR system. Kaldi is an open source toolkit for speech recognition applications written in C ++ and licensed under "Apache License v2.0" [10]. Figure 1 shows a schematic overview is given Remove the toolkit.
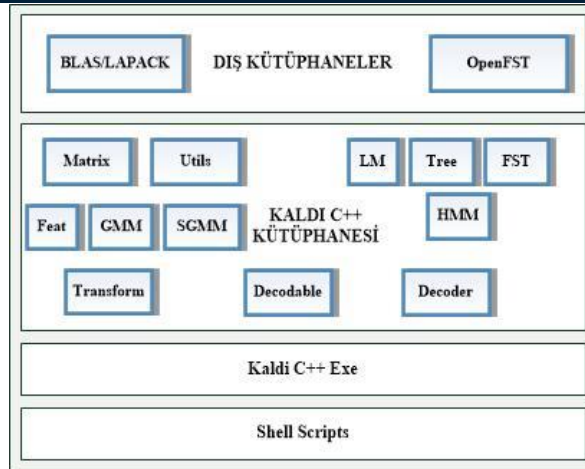
Figure 1. Kaldi tool set [10]

The toolkit is basically connected to two external libraries. The first end la which is used to condition frame "openfst" is another of the library is to numerical linear algebra. Numerical linear algebra library "BLAS" and "milksop" as is divided into two parts. Remaining library modules, each connected to only one of the external libraries it is positioned.

2.1.1. Feature Extraction

Feature extraction is one of the most important steps in speech recognition. Feature extraction plays an important role in separating a conversation from other conversations. Due to the nature of speech action, each speech has different individual characteristics integrated into speech knowledge [11]. These properties are obtained by different feature extraction techniques which are recommended for ASR systems and used successfully. Kaldi, standard Mel Frequency Cepstral Coefficients for reading feature extraction and waveform (MFCC: Mel-Frequency Cepstrum Coefficient) [12]. The technique of MFCC calculation is mainly based on short-term analysis. Therefore, an MFCC vector is calculated from each frame.

2.1.2. Acoustics and Language Modeling

Acoustic modeling of a speech process is the process of generating statistical information for feature vector sequences typically calculated from speech waveform [13]. Remained supporting numerous infrastructure for acoustic modeling. Classic Gaussian Mixed Model (GMM: Gaussian Mixed Model) and Subspace Gaussian Mixed Models (SGMM: Subspace Gaussian Mixed Model) can be easily developed with Kaldi [5]. Personal data are shown separately instead of Gaussian intensity is applied directly to the GMM class with natural parameters.

Language modeling models the arrangement of words in the language completely independent of its acoustic properties. [4]. It generally uses n-gram based modeling method. In these models, the probability calculations are performed by finding Markov's assumption and taking into consideration the word order of 2 to 4 in the past [14]. Therefore, it is not possible to model the order of words in a long sentence with n-grams, but only limited word history can be modeled. Since there is no Markov assumption in language models using feedforward neural networks, long dependencies in words can be modeled with these models [15].

2.1.3. Decoding

Kaldi education and decoding in the Weighted Finite State Transducers (WFST: Weight Finite State Transducer) is used. The input symbols in Kaldi are kept numerically. However, some problems arise in this approach since different phonemes are allowed to share the same data. The first of them is unable to identify the FST. Second is not have enough data to operate on the Viterbi. The Viterbi decoding algorithm is the most commonly used decoding algorithm for overlay codes and uses the maximum likelihood (ML: Maximum Likelihood) decoding technique [16].

3. APPLICATION DEVELOPMENT

In this part of the study, the system architecture of the proposed method and application is given. The structure of some classes and variables in the proposed method is explained. Java and C ++ are used to develop software codes.

3.1. General Architecture of the System

The general architecture of the system consists of three basic modules: pre-processing, ASR and post-processing. These modules operate sequentially. Figure 2 shows the overall architecture of the system.

Figure 2. General architecture of the system

As shown in FIG. a speech recording is provided as input. Speech information was taken from smart home devices. Each conversation piece is given in sequence to the individual ASR module. Communication between them is provided by internet infrastructure.

In the Smart home devices module, firstly speech information with a certain frequency is received. An ASR system was developed using version 5.0 of the Kaldi toolkit. The Turkish speech data set prepared by Boğaziçi University in 2012 and presented by the Linguistic Data Consortium (LDC) was used in the development of the ASR system [17]. This data set contains approximately 91.44 hours of actual speech data. Speech files have a sampling frequency of 16 KHz. The acoustic meta-data of each speaker used to train and test acoustic models were generated. The data is divided into two parts as acoustic data and language data reserved.

Mel frequency scale private-definable attributes are used for mining operations. Mel frequency scale is a scale that shows the perception of the change in the sound frequencies of the human ear. While the detection of sounds up to 1000 Hz is linear, the detection of change becomes logarithmic as the frequency increases. MFCC is the expression of the short-time power spectrum of the audio signal on the Mel scale. 25 ms squares were removed by observing the properties of strength spectrum separated audio file.

The ASR system was developed based on GMM-HMM. In the ASR system developed using the classic GMM-HMM, the probability of observation of each HMM situation is calculated by using bj (x) Gaussian mixtures. Technically, while training GMM-HMM system, monophone model expression level transcripts were used. In the last smart home devices module , the text data obtained from the ASR system is transmitted back to the electronic device in the order of the speech pieces entering the ASR system .

4. EXPERIMENTAL RESULTS

The results obtained in this study are expressed as Word Error Rate (WER) for different experiments. WER is a performance calculation metric that gives the most reliable result known for speech recognition [5]. It works at word level instead of phoneme level. The words in the text data obtained at the output of the ASR system is discussed individually. Each word is compared to the state it should be. Any discrepancy is considered to be incorrect. The performance of the classic GMM-HMM based ASR system is given in Table 1.

Table 1. GMM-HMM based Turkish ASR system

Education data set	Test data set	WER(%)	Sampling frequency
Boğaziçi data set	Boğaziçi data set	27.70	16 KHz

Table 1 provides the data set information used in the development and testing of the ASR system. Training and testing data set in 1/3 are reserved for testing purposes. Test procedures of the part of the Boğaziçi data set reserved for the test procedures was used. It was good to have the smart home device command detection to the network here. Otherwise, add that much bigger system wouldn't work on the device alone.

5. CONCLUSIONS AND RECOMMENDATIONS

Technologies that support people's communication with each other have changed structurally over time and human-machine interaction has emerged. One of the technologies that support human-machine interaction is the Internet of objects. With the Internet of objects, it is ensured that not only people communicate with themselves, but also with computers and other electronic devices. One of the applications of the Internet of Things is smart home systems. Smart home systems lighting, security, ventilation, temperature, etc. It allows users to control and track the systems more easily. Smart home users want to establish the communication they manage to their mother tongue by using the same devices that make up the smart home system. User rating communicating with the devices that make up the smart home system, allowing the machine and electronic devices to operate the command and control mechanism more quickly. For this reason, the requirements for a smart home system to work with voice commands and the advantages of speech recognition technologies are investigated. Cloud-based solutions were concluded that in more advantageous for Speech recognition technology. At the end of the study, a Turkish automatic speech recognition system was developed and presented via the cloud platform. A smart home system was also prepared as a model. Speech recognition requests from the smart home system were resolved on the cloud platform and transferred back to the smart home system. Thus, the processing power required for speech recognition was transferred to the cloud. The devices that make up the smart home system are only given the task of executing commands.

ACKNOWLEDGMENT

REFERENCES

[1]. A. A. M. Abushariah, T. S. Gunawan, O. O. Khalifa, and M. A. M. Abushariah, *English digits speech recognition system based on Hidden Markov Models*, Proc. Int. Conf. Comput. Commun. Eng., no. May, pp. 1–5, 2010.

[2]. H. Prakoso, R. Ferdiana, and R. Hartanto, *Indonesian Automatic Speech Recognition system using CMUSphinx toolkit and limited dataset,* 2016 Int. Symp. Electron. Smart Devices, ISESD 2016, pp. 283–286, 2017.

[3]. J. M. Baker et al., *Speech Recognition*, 5.1, pp. 75–80, 2009.

[4]. D. Amodei et al., *Deep Speech 2 : End-to-End Speech Recognition*, English and Mandarin archive : 1512 . 02595v1 [cs . CL] 8 Dec 2015', pp. 1–28.

[5]. Y. G. Thimmaraja and H. S. Jayanna, *Creating language and acoustic models using Kaldi to build an automatic speech recognition system for Kannada language*, 2nd IEEE Int. Conf. Recent Trends Electron. Inf. Commun. Technol., pp. 161–165, 2017.

[6]. E. Bocchieri and D. Caseiro, *Use of geographical meta-data in ASR language and acoustic models*, ICASSP, IEEE Int. Conf. Acoust. Speech Signal Process. - Proc., pp. 5118–5121, 2010.

[7]. X. Huang and L. Deng, *An overview of modern speech recognition*, Handb. Nat. Lang. Process., pp. 339–367, 2010.

[8]. J. Neto et al., *Speaker-Adaptation for Hybrid HMM-ANN Continuous Speech Recognition System*, Eurospeech, pp. 2171–2174, 1995.

[9]. G. Hinton et al., *Deep Neural Networks for Acoustic Modeling in Speech Recognition*, IEEE Signal Process. Mag., vol. 29, no. 6, pp. 82–97, 2012.

[10]. D. Povey et al., *The Kaldi speech recognition toolkit*, IEEE Work. Autom. Speech Recognit. Underst., no. June 2014, pp. 1–4, 2011.

[11]. S. Narang and M. Divya Gupta, *International Journal of Computer Science and Mobile Computing Speech Feature Extraction Techniques: A Review*, Int. J. Comput. Sci. Mob. Comput., vol. 4, no. 3, pp. 107–114, 2015.

[12]. A. N. Guglani, J., & Mishra, *Continuous Punjabi speech recognition model based on Kaldi ASR toolkit*, Int. J. Speech Technol., pp. 1–6, 2018.

[13]. A. V. Haridas, R. Marimuthu, and V. G. Sivakumar, *A critical review and analysis on techniques of speech recognition: The road ahead*, Int. J. Knowledge-Based Intell. Eng. Syst., vol. 22, no. 1, pp. 39–57, 2018.

[14]. L. Saul and F. Pereira, *Aggregate and mixed-order Markov models for statistical language processing*, 1997.

[15]. M. Karafi and J. H. Cernock, *a S a S*, no. September, pp. 1045–1048, 2010.

[16]. V. Shah, R. Anstotz, I. Obeid, and J. Picone, *Adapting an Automatic Speech Recognition System to Event Classification of Electroencephalograms 1*, 2018 IEEE Signal Process. Med. Biol. Symp. SPMB 2018 - Proc., pp. 1–5, 2019.

[17]. E. Arisoy, D. Can, S. Parlak, M. Saraçlar, and H. Sak, *Turkish Broadcast News Transcription and Retrieval*, IEEE Trans. Audio, Speech Lang. Process., vol. 17, no. 5, pp. 874–883, 2009.

Collecting the Data Required to Develop a Personalized Speech Recognition System to be used in the Internet of Things Ecosystem

Ali Saygin[1], Hüseyin Polat[2], Ahmet Aksoz[3], Saadin Oyucu[4]

Abstract

Internet of Things, which is defined as the objects connected with the internet network, provides the interaction between the objects and also the interaction between the human-object and the machine. While interconnected devices, machines or objects are communicating among themselves, it is also possible for people to manage, interact and command these devices. Lighting, heating, security, alarm, white goods and so on. Internet of Things technologies is used in smart home concepts where many objects are used. At this point, making the commands through speech recognition systems facilitates the interaction. But there are certain challenges for speech recognition. Speech recognition systems are based on statistical pattern recognition and classification approaches. Machine learning algorithms to train the necessary models in speech recognition systems are used. Machine learning scope, there are two main approaches to the development of statistical pattern classifiers. These are supervised learning and unsupervised learning methods d. In speech recognition, the controlled learning method is used to train speech classifiers such as Hidden Markov Models. A large speech data set is needed for the training of Hidden Markov Mode based classifiers. This training set should be based on the acoustics in the environment where the speech recognition system will be used, the amount of noise in the environment, the user, the voice characteristics of the user and the quality of the microphone. For this reason, it is aimed to obtain a data set from an environment where the Internet of Things ecosystem will be controlled. An Internet of Things platform is prepared for this purpose and the collected data is prepared for audio-text matching to be used in the development of a speech recognition system. An electronic device and a mobile application that will collect information on the user's speech will collect acoustic information in the media have been developed for this purpose. The data obtained will be used in the development of a personalized speech recognition system in the Internet of Things ecosystem.

Keywords: IoT, Data collection, Speech recognition

1. INTRODUCTION

Technologies that support people's communication with each other have changed structurally over time and the concept of human-machine interaction has emerged [1]. In the early stages, human machine or electronic device interaction realized with simple key systems has now been replaced by touch systems [2]. But even this situation allows people to communicate with machines or electronic devices to a limited extent. People communicate with their mother tongue by communicating with machines or electronic devices, enabling the command and control mechanism of machines or electronic devices to operate more quickly [3]. Therefore Automatic Speech Recognition (ASR: Automatic Speech Recognition) systems are improved and its use is increasing every day [4].

Electronic devices between communication as defined objects Internet (IoT: Internet of Thing), Big data and cloud it as new of technology out with the advent together completely automatic and from each other independent as can be improved. IoT business life, social life vehicles using, communication setup and purchase

[1] *Gazi University, Department of Electrical and Electronics Engineering, 06500, Teknikokullar/Ankara, Turkey.*
 asaygin@gazi.edu.tr

[2] *Gazi University, Department of Computer Engineering, 06500, Teknikokullar/Ankara, Turkey. hpolat@gazi.edu.tr*

[3] *Sivas Cumhuriyet University, Department of Mechatronics Engineering, 58500, Merkez/Sivas, Turkey.*
 aaksoz@cumhuriyet.edu.tr

[4] *Corresponding author: Gazi University, Department of Computer Engineering, 06500, Teknikokullar/Ankara, Turkey.*
 soyucu@gazi.edu.tr

etc. in process big amenities are provided. In short IoT many in the area life format affecting and is changing. Marketing to each individual in the field behavior and purchasing habits rune by personalized products are offered. Transportation in the area automatic as without driver and accident-free one the way shipping true quickly progress seen. Nowadays, technology in all areas our lives improve for important one role playing. Life improve devices with interaction establish for most good don't natural speech. At this point, ASR systems big task falls [5].

ASR relies heavily on statistical pattern recognition and classification and uses machine learning algorithms to train the necessary models. Within the scope of machine learning, there are two main approaches to developing statistical pattern classifiers: supervised learning and unsupervised learning methods. In ASR, supervised learning is used to train speech classifiers such as hidden Markov models (HMMs). HMM-based classifiers require a large speech corpus .Therefore, to develop high-performance ASR independent of a speaker, it is necessary to collect a wide range of speech samples from various speakers as well as transcriptions in these conversations [6].

As a result, it is important to develop a data set with voice and text data in order to develop the speech recognition system required for said IoT. The biggest problem with the commonly used methodologies for collecting written speech data is that the process is often costly and cumbersome, both in terms of time and budget. In the classical approach, pre-recorded speech documents are written by people for a particular language. Unfortunately, most of the spoken languages, including all Asian languages, are classified as insufficient resources for ASR applications. The main reason for this is the limited number of available written conversations required for training acoustic models (AMs) and language models (LMs). In this paper, a data set has been prepared to develop the speech recognition system required for IoT. Mobil application and the web page was collected by the speech information spoken by real people. Moreover, the obtained Turkish speaking corpus was presented to the approval of real users. Thus, healthier data were obtained.

2. DESCRIPTION OF THE CORPUS AND THE PROCESS

It is aimed to develop ASR system to enable speech control of devices in IoT ecosystem. The biggest obstacle is the lack of data on the Turkish language. In order to develop a system that is particularly personalized and capable of taking commands into account, a speech data set with special commands is required. Necessary data were collected by mobile application method. It was checked by real users. The use of these methods is explained in detail under separate headings.

2.1. Obtaining Corpus with Mobile Application

Data set required for training the ASR system the performance of all the words of the language in which the ASR operation is performed will improve performance. However, in this study, the words that can be used especially for IoT are spoken. These words yes, no, up, down, right, left, open, close, stop, back, forward and so on. Commands include commonly used conversations. Since Turkish is an additive language, its vocabulary is quite wide. This is a very challenging task when it is desired to obtain the acoustic structure of each word. Talk to the K-text data on a mobile application has been developed to achieve. Figure 1 shows a block diagram of the main modules for data collection with the mobile application presented in this study.
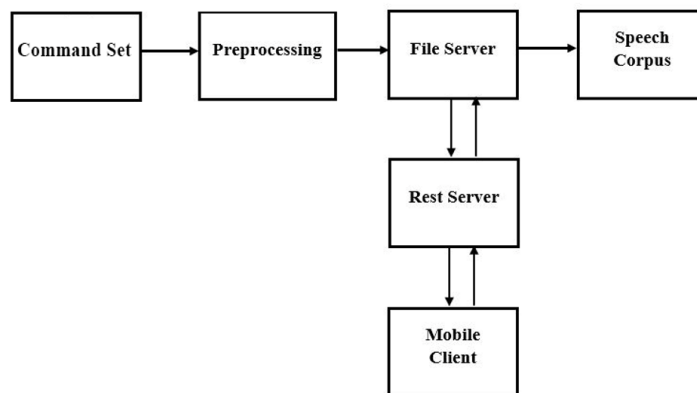

Fig 1. CORPUS Obtaining with mobile application

Command set module contains pre-defined commands and expressions that need to be spoken. Pre-processing module expressions obtained by the instruction set are broken so that a word or phrase. The texts separated as sentences or words in the pre-processor module are identified and uploaded to the file server. The statements prepared previously are sent to a mobile client via a Rest a PI running on the rest server. The mobile client shows the text received to the user and expects it to speak. The audio file of the text that the user voices is identified and stored on the file server. The screenshot of the mobile application developed for use in this study is given in Figure 2.
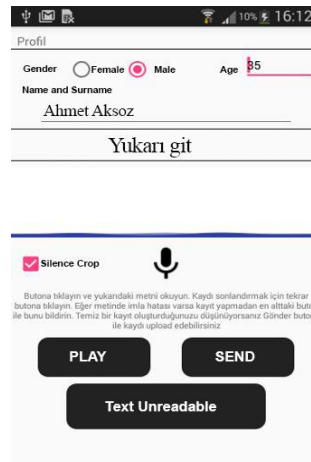

Figure 2. Mobil application

In the developed application, the user is provided with the necessary text information for vocalization. However, the user was asked to enter some information before starting the voiceover process. This information is gender, age and name. The information obtained is necessary for the gender distribution to be proportional when preparing data.

2.2. Data obtaining with web application

The data obtained by the two different methods mentioned in the study were voiced by real users. It has also been manually verified with the same users. A web interface has been created for this process. The process was performed in a similar manner to the mobile application block diagram of FIG. The texts on the file server are taken one by one with the help of a Rest web service. These received text matches are transferred to a web interface again with the help of Rest web service. Real users log in to the web interface and speak the text information received. It also controls the audio-text information received. In this control process, users can listen to the audio data that comes to them and at the same time, they can control the text information that comes with the audio file. The web interface for the web application is shown in Figure 3.

Figure 3. Web interface for the web application

Figure 3 checks the user text information e as shown is able to perform voice processing. If there is a mistake in the text, it can be corrected and sent back to the file server. Furthermore, if there is noise, overlap and uncertainty in the audio data, it can label this data according to the specified situation.

3. CONCLUSION

In this study, the data set required for the development of a speech recognition system intended for use in IoT applications was prepared. Two different approaches are presented for this data set. The first one is the mobile application and the other is the web interface. Data sets were collected with these two different approaches. The data obtained is sufficient for the development of speech recognition system.

In addition to the commands that will be used frequently in IoT, a data set including daily conversations has been prepared. Dependence on the speaker was eliminated by taking records from more than one person. The resulting data is verified by a real people. Thus, situations that would adversely affect the performance of speech recognition system were prevented. The next study will develop a speech recognition system and test its usability for IoT applications. In addition, due to the difficult nature of the Turkish language and vocabulary is wide, a research on Turkish speech recognition systems will be conducted.

REFERENCES

[1]. T. Song, et al. *Survey of Security Advances in Smart Grid: A Data Driven Approach*, IEEE Communications Surveys & Tutorials 19.1, 2017, pp: 397-422.
[2]. K. Susanne, et al. *Comparison of smart grid architectures for monitoring and analyzing power grid data via Modbus and REST*, EURASIP Journal on Embedded Systems 2017.1, 2017, vol. 12.
[3]. M. H. Yaghmaee, A. Leon-Garcia, and M. Moghaddassian, *On the Performance of Distributed and Cloud-Based Demand Response in Smart Grid*, IEEE Transactions on Smart Grid (2017).
[4]. H. Polat, and S. Oyucu, *Token-based authentication method for M2M platforms*, Turkish Journal of Electrical Engineering & Computer Sciences 25(4), 2017, pp: 2956-2967.
[5]. W. Yang, et al. *Robust data-driven state estimation for smart grid* IEEE Transactions on Smart Grid 8.4, 2017, pp: 1956-1967.
[6]. S. Oyucu, and H. POLAT. *M2M Sistemlerin, Akilli Şebekeler Üzerine Uygulanabilirliği*, El-Cezeri Journal of Science and Engineering 3(1), 2016.

Analysis of magnetic properties of a geothermal site and a case study

Cagatay Pamukcu[1], Oya Pamukcu[2], Ayca Cirmik[2]

Abstract

The application of geophysical methods is widely used in geothermal fields. Due to the fact that Turkey has a large geothermal field derived from geological and tectonic properties and needs of energy, geothermal field research is increasing in many regions. Geophysical searches are aimed at finding the physical parameters of geothermal systems by measurements from the surface. In recent days, many geophysical methods are applied for exploration in geothermal fields. Magnetic research, also known as the investigation of potential fields, examines the changes in the underground physical properties such as magnetization of rocks. Magnetic research helps to identify groundwater reservoirs, geothermal and petroleum sources, mines and faults. Magnetic measurements have an important role in finding areas where magnetization decreases due to thermal activity. In this study, the magnetic properties of a geothermal system and the magnetic data results of the field studies for investigating the geothermal potential in northern Aegean region were evaluated. There are metamorphic rocks of Sakarya zone, Ezine zone metamorphic rocks, Cetmi ophiolite Melani, upper Oligosen-lower Myosen aged Granitoids, Küçükkuyu formation, Gülpinar formation in and around the study area. The potential geothermal properties of the study area were interpreted by applying data processing techniques to magnetic data of the area containing these rocks.

Keywords: Geothermal field, magnetic, Northern Aegean Region

1. INTRODUCTION

Geothermal energy can be defined as hot water and steam which is formed by accumulated heat to create anomalies at various depths of the earth's crust and whose temperatures are continuously above the regional atmospheric average temperature and contain more molten minerals, various salts and gases than the groundwater and surface waters around it. Hydrothermal, magma and hot dry rock energy fields are formed according to the geological character of the environment in these areas formed by anomalies due to the mentioned geological events. Heat source, water source, reservoir and cover rock are the main components of geothermal systems. The geological conditions of the underground should have porosity and permeability properties where water can be accumulated and poured into a well without resistance. These conditions are provided in specific geological environments. Sedimentary basins are filled with high porosity and permeability materials; therefore, they form productive aquifers. If these basins are located around volcanic centres, if tectonic properties are appropriate, if there are processes required to transfer heat to the above mentioned environment, hydrothermal reservoir may be formed in these environments.

In recent days, due to the limited and gradually depleted energy resources, the trend towards alternative energy sources has increased. Geothermal energy is one of the alternative energy sources. Geothermal field research is increasing in many regions due to the fact that our country has a large geothermal field as a result of its geological and tectonic properties and it is needed to provide the energy needs of our country. The magnetic application, which is one of the many methods used in the investigation of geothermal systems, is realized to

find an answer to the geological structure and tectonic features of the existing system. In this study, the magnetic data of a geothermal basin in northwestern Anatolia was interpreted.

2. METHODS AND APPLICATIONS

Magnetic method is widely used for geothermal exploration and geological mapping of structures. The magnetic anomaly is caused by a change in the magnetization locally or regionally. The location, position, age, direction and size of the mass can be obtained by magnetization anomaly. The magnetic field strength is measured by the magnetometer and usually indicated by γ (gamma) or nT (nanoteslas). In geothermal areas, magnetic measurements are generally used to detect buried sources and faults and to estimate their probable depths. In terms of magnetic properties, the materials are grouped into three groups as diamagnetic, paramagnetic and ferromagnetic. Minerals are also investigated in three groups as ferromagnetic, antiferromagnetic and ferrimagnetic depending on the position of magnetic domains. Most of the minerals that form the rocks have paramagnetic and diamagnetic properties, while only a few have ferritic or antiferromagnetic properties. When ferromagnetic materials are heated to Curie temperature (point), the atoms forming the material vibrate at a greater frequency and amplitude than the normal temperature. During these movements of the atoms, the spin moments receive random directions. Ferromagnetic materials present paramagnetic behaviours above Curie temperature. Magnetic properties of antiferromagnetic materials also vary due to the temperature. However, these materials behave as paramagnetic above the temperature called as Neel temperature. The heat flow is the main quantity which can be observed and determines the changes of the temperature.

Many researchers ([1], [2], [3], [4], [5], [6], [7]) obtained the heat flow values by using magnetic anomalies or using the Curie depths obtained from magnetic anomalies, therefore, the crust and geothermal areas were interpreted. Many heat flow observations are obtained from land drilling and deep sea probes ([8]). The obtained heat flow values are generally insufficient to define the regional thermal structures because the heat flow values point to the local thermal anomalies and their measurements are geographically irregular. For this reason, determining the Curie depth based on the spectrum analysis of magnetic anomalies is valuable. This method determines the depth at which magnetite passes from a ferromagnetic state to a paramagnetic state. The bottom depth of such a magnetic source is assumed to be Curie point depth. The depth of the temperature source can be monitored with the methodology used to determine the depth of magnetic sources. In this context, depth approaches to geothermal fields can be done.

In this study, in the scope of the magnetic study realized in northern Aegean Region (Figure 1), the heat flow map of the study area (Figure 2) was examined and the heat flow anomalies with high amplitude were noticed. In the Marmara region located in North Aegean, there are geothermal areas which are important in the regions where the fault zones are concentrated especially in the south and southeast parts. These fields are Balikesir, Bursa, Çanakkale, Kocaeli, Sakarya and Yalova. The study area in Figure 3 is located within the borders of Çanakkale. In this context, magnetic anomalies measured in the region are presented in Figure 3. In the interpretation part of the study, the anomalies (Figure 3) were interpreted after applying baseline correction and reduction to the pole method.

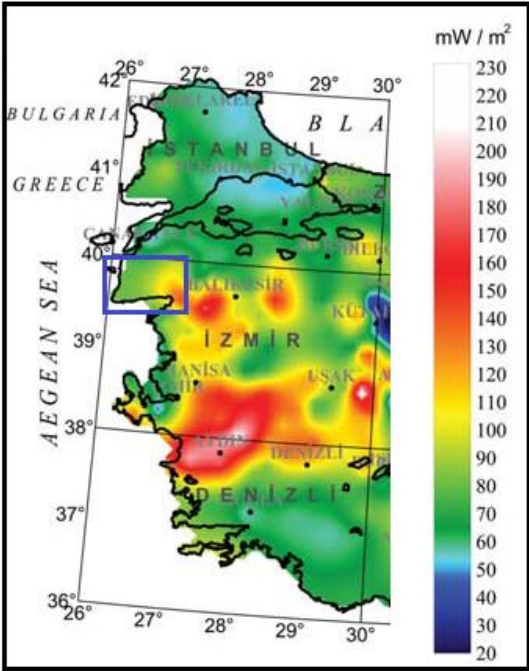*Figure 1. The view of the study area. This figure is created by using Google Earth [9].*

Figure 2. The heat flow map of the study area and its surroundings. Blue rectangle represents the study area.
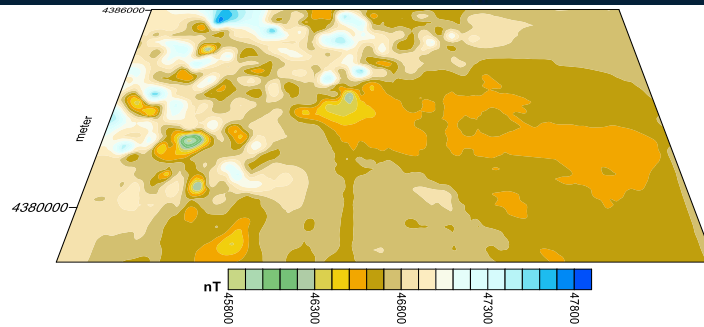*This figure is modified from [10].*

Figure 3. The obtained raw magnetic anomaly values of the study area.

3. RESULTS

Marmara region is rich in terms of geothermal potential. The geothermal system of the region is thought to have developed with North Anatolian Fault which is one of the important tectonic structures ([11]). In the study, as the first step, the baseline correction and reduce to the pole methods were applied the magnetic anomalies shown in Figure 3. Then, it is noticed that the anomalies with the low amplitude was fitted the regions which have higher heat flow values (Figure 2). Therefore, these regions are probably the parts which have geothermal potential. It is necessary to take advantage of the potential of compatible with environment, renewable and inexpensive geothermal resource on the basis of scientific, technical and economic principles. In this context, the studies based on the exploration, development, protection, production and the use of these resources should be supported in an efficient and sustainable way, especially in order to benefit from the production of electricity. One of the reasons for determining low amplitude values in magnetic and gravity applications applied in the study area is the presence of geothermal potential in the region. Consequently, it is recommended to apply the magnetic and gravity method from the geophysical methods at the beginning of the geothermal studies and to interpret them well.

REFERENCES

[1]. A., Tanaka, Y., Okubo, Y., O., Matsubayashi, Curie point depth based on spectrum analysis of the magnetic anomaly data in East and Southeast Asia, Tectonophysics, 306(3-4), 461-470, 1999.

[2]. Y., Okubo, R.J, Graf, R.O., Hansen, K., Ogawa, H., Tsu, Curie point depths of the island of Kyushu and surrounding areas, Japan, Geophysics, 50(3), 481-494, 1985.

[3]. M., Manea and V.C., Manea, Curie point depth estimates and correlation with subduction in Mexico, Pure and applied geophysics, 168(8-9), 1489-1499, 2011.

[4]. L.I., Nwankwo, P.I., Olasehinde, C.O., Akoshile, Heat flow anomalies from the spectral analysis of airborne magnetic data of Nupe Basin, Nigeria, Asian Journal of Earth Sciences, 4(1), 20-28, 2011.

[5]. O., Pamukçu, Z., Akçiğ, M., Hisarli, S., Tosun, Curie Point depths and heat flow of eastern Anatolia (Turkey), Energy

[6]. Sources, Part A: Recovery, Utilization, and Environmental Effects, 36(24), 2699-2706, 2014.

[7]. T., Gonenc, O., Pamukcu, C., Pamukcu, A. H., Deliormanli, The investigation of hot spots in western Anatolia by geophysical and mining approaches, Energy Sources, Part A: Recovery, Utilization, and Environmental Effects, 34(9), 775-792, 2012.

[8]. O., Pamukçu, T., Gönenç, A.Y., Çirmik, Ş., Demirbaş, S., Tosun, Vertical and horizontal analysis of crustal structure in eastern Anatolia region. Bulletin Of The Mineral Research and Exploration, (151), 217-229, 2015.

[9]. H.N., Pollack, S.J., Hurter, J.R., Johnson, Heat flow from the Earth's interior: analysis of the global data set, Reviews of Geophysics, 31(3), 267-280, 1993. http://www.earth.google.com

[10]. U., Akin, E.U., Ulugergerli, S., Kutlu, The assessment of geothermal potential of Turkey by means of heat flow estimation, Bulletin Of The Mineral Research and Exploration, 149(149), 201-210, 2014.

[11]. H. Dağistan, Yenilenebilir enerji ve jeotermal kaynaklarimi, Dunya Enerji Konseyi Turk Milli Komitesi, Turkiye, vol. 10, 2006.

ICENS

5TH INTERNATIONAL CONFERENCE ON ENGINEERING AND NATURAL SCIENCES

www.icens.eu

WESTERN MICHIGAN UNIVERSITY

NATIONAL UNIVERSITY OF PUBLIC SERVICE

University of CINCINNATI

INTERNATIONAL UNIVERSITY OF SARAJEVO IUS

TURKISH AIRLINES

EUROPE CONGRESS
www.europecongress.org